FG21-88MC11091
CONF-891167--

PROCEEDINGS

1989 Eastern Oil Shale Symposium

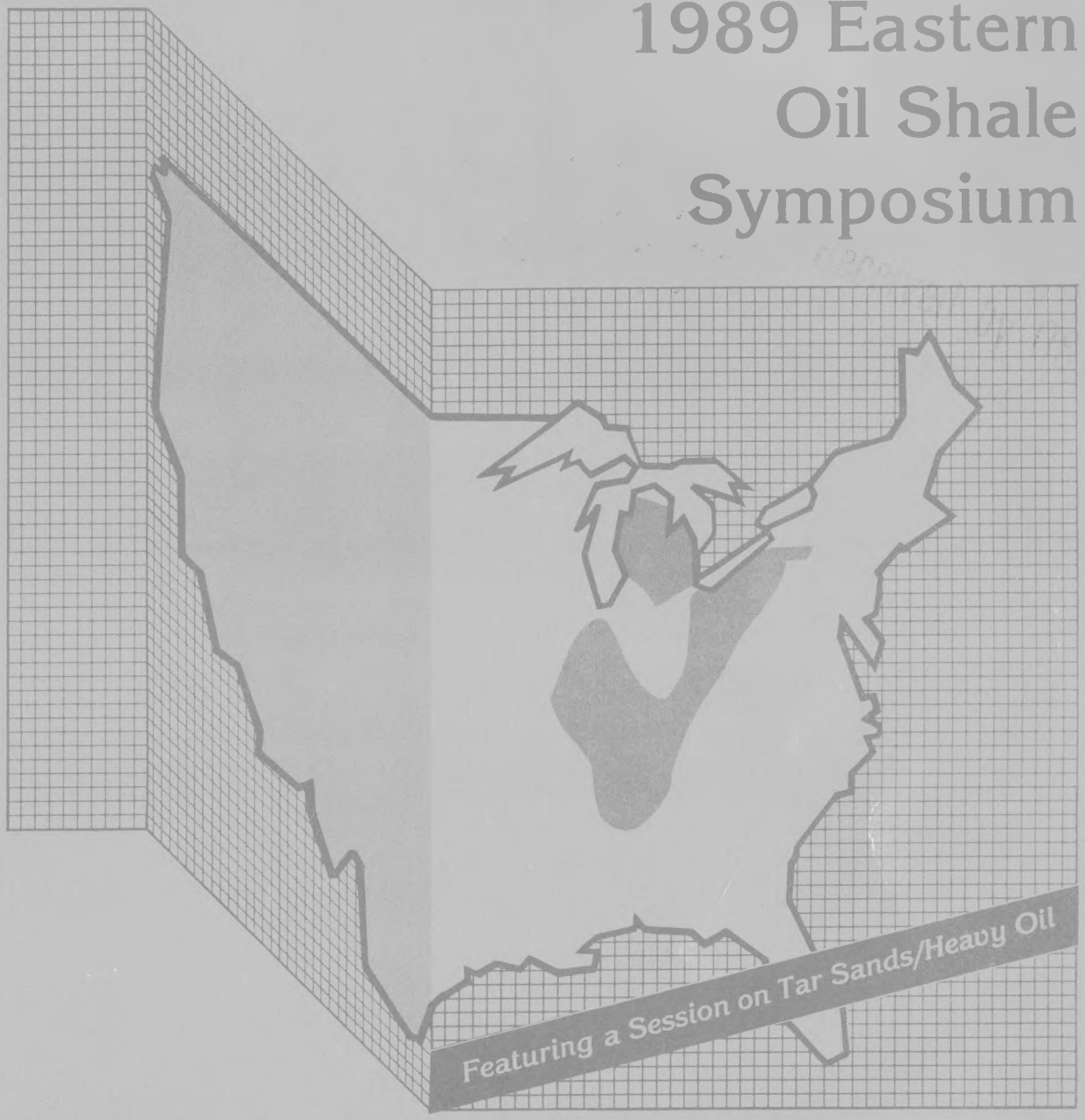

November 15-17, 1989
Marriott Griffin Gate Resort
Lexington, Kentucky

Sponsored By:
UNIVERSITY OF KENTUCKY
Institute for Mining and Minerals Research
Center for Applied Energy Research

and

UNITED STATES DEPARTMENT OF ENERGY

and

COMMONWEALTH OF KENTUCKY
Governor's Office for Coal and Energy Policy

DISCLAIMER

This report was prepared as an account of work sponsored by an agency of the United States Government. Neither the United States Government nor any agency thereof, nor any of their employees, makes any warranty, express or implied, or assumes any legal liability or responsibility for the accuracy, completeness, or usefulness of any information, apparatus, product, or process disclosed, or represents that its use would not infringe privately owned rights. Reference herein to any specific commercial product, process, or service by trade name, trademark, manufacturer, or otherwise does not necessarily constitute or imply its endorsement, recommendation, or favoring by the United States Government or any agency thereof. The views and opinions of authors expressed herein do not necessarily state or reflect those of the United States Government or any agency thereof.

DISCLAIMER

Portions of this document may be illegible in electronic image products. Images are produced from the best available original document.

1989 Eastern Oil Shale Symposium Program Technical Advisory Committee

Mr. Dharam V. Punwani
Technical Program Chairman
Institute of Gas Technology
Chicago, Illinois

Ms. Geaunita H. Caylor
Symposium Coordinator
Institute for Mining and Minerals Research
University of Kentucky
Lexington, Kentucky

Mr. Gary D. Aho
Cliffs Engineering, Inc.
Rifle, Colorado

Mr. Edward R. Bates
U.S. Environmental Protection Agency
Cincinnati, Ohio

Mr. Victor H. Carr
Eastern Shale Research Corp.
Shelbyville, Indiana

Mr. John R. Dyni
U.S. Geological Survey
Denver, Colorado

Dr. James Drahovzal
Kentucky Geological Survey
Lexington, Kentucky

Mr. Eddie J. French
U.S. Department of Defense
Alexandria, Virginia

Ms. Nancy R. Hasenmueller
Indiana Geological Survey
Bloomington, Indiana

Dr. Roy C. Kepferle
Eastern Kentucky University
Richmond, Kentucky

Mr. Francis S. Lau
Institute of Gas Technology
Chicago, Illinois

Mr. David Lazar
Institute for Mining and Minerals Research
University of Kentucky
Lexington, Kentucky

Dr. Larry A. Lukens
The New Paraho Corporation
Aurora, Colorado

Ms. Shiela Shelton Medina
East Kentucky Power Cooperative
Winchester, Kentucky

Dr. Francis P. Miknis
Western Research Institute
University of Wyoming Research Corp.
Laramie, Wyoming

Mr. Martin C. Noger
Kentucky Geological Survey
Lexington, Kentucky

Mr. Paul A. Petzrick
Oil Shale Association
Annapolis, Maryland

Mr. Edwin M. Piper
Stone & Webster Engineering Corp.
Denver, Colorado

Dr. John G. Reynolds
Lawrence Livermore National Laboratory
University of California
Livermore, California

Dr. Thomas L. Robl
Center for Applied Energy Research
University of Kentucky
Lexington, Kentucky

Mr. Carl E. Roosmagi
U.S. Department of Energy
Laramie, Wyoming

Ms. Aurora M. Rubel
Center for Applied Energy Research
University of Kentucky
Lexington, Kentucky

Dr. Cliff Schultz
Mineral Resources Institute
The University of Alabama
Tuscaloosa, Alabama

Dr. Lyle V.A. Sendlein
Institute for Mining and Minerals Research
University of Kentucky
Lexington, Kentucky

Mr. Jerry E. Sinor
J.E. Sinor Consultants Inc.
Niwot, Colorado

Mr. Gene E. Tampa
AMOCO Corporation
Naperville, Illinois

Mr. Fred H. Zerkel
Institute of Gas Technology
Washington, DC

David J. Lazar, Proceedings Editor
Institute for Mining and Minerals Research
University of Kentucky
Lexington, Kentucky

IMMR--89/201

DE91 008080

P · R · O · C · E · E · D · I · N · G · S

1989 EASTERN OIL SHALE SYMPOSIUM

November 15-17, 1989
Marriott Griffin Gate Resort
Lexington, Kentucky

Sponsors:

UNIVERSITY OF KENTUCKY
Institute for Mining and Minerals Research
Center for Applied Energy Research
UNITED STATES DEPARTMENT OF ENERGY
KENTUCKY ENERGY CABINET

Proceedings Publisher

INSTITUTE FOR MINING
AND MINERALS RESEARCH

MASTER

DISTRIBUTION OF THIS DOCUMENT IS UNLIMITED

April 1990. The opinions expressed in and the responsibility for the contents of the articles published in **Proceedings, 1989 Eastern Oil Shale Symposium** are those of the authors. They are not to be construed as the opinions of the Institute for Mining and Minerals Research or the University of Kentucky. All rights reserved except those granted to the individual authors and/or the employees thereof, and the U.S. Department of Energy.

EASTERN OIL SHALE SYMPOSIUM PROCEEDINGS

Publications in This Series:

IMMR82/066	**1981 Eastern Oil Shale Symposium Proceedings** - $25.
IMMR82/075	**1982 Eastern Oil Shale Symposium Proceedings** - $25.
IMMR83/089	**1983 Eastern Oil Shale Symposium Proceedings** - $25.
IMMR84/124	**1984 Eastern Oil Shale Symposium Proceedings** - $25.
KCERL85/147	**1985 Eastern Oil Shale Symposium Proceedings** - $25.
KECL86/158	**1986 Eastern Oil Shale Symposium Proceedings** - $25.
KECL87/175	**1987 Eastern Oil Shale Symposium Proceedings** - $25.
IMMR88/101	**1988 Eastern Oil Shale Symposium Proceedings** - $25.

DISCLAIMER

This report was prepared as an account of work sponsored by an agency of the United States Government. Neither the United States Government nor any agency thereof, nor any of their employees, makes any warranty, express or implied, or assumes any legal liability or responsibility for the accuracy, completeness, or usefulness of any information, apparatus, product, or process disclosed, or represents that its use would not infringe privately owned rights. Reference herein to any specific commercial product, process, or service by trade name, trademark, manufacturer, or otherwise does not necessarily constitute or imply its endorsement, recommendation, or favoring by the United States Government or any agency thereof. The views and opinions of authors expressed herein do not necessarily state or reflect those of the United States Government or any agency thereof.

CONTENTS

INTRODUCTION
Dharam V. Punwani, Symposium Chairman 1

TAR SANDS/HEAVY OIL

Experience in the Beneficiation of Two Alabama Tar Sands
C.W. Schultz, J.B. Cardoso, and G. Daniel Irvin, Mineral Resources Institute, University of Alabama 5

Extraction of Alabama Tar Sands with Heptane and Carboxylic Acid Mixtures and Using a Saponification Cycle
Richard K. Ulrich, Muddu K. Koppaiah, Vineet K. Majmudar
Department of Chemical Engineering, University of Arkansas 11

Uses of Generated Surfactants from a New Tar Sand Process for Extracting Hydrocarbons from Natural and Man-Made Materials
Kazem M. Sadeghi, Mohammed-Ali Sadeghi, and Teh Fu Yen,
Department of Civil and Environmental Engineering, University of Southern California 18

Selection, Design, and Scale-Up of Equipment to Extract Bitumen from Tar Sands
W. Roy Penney and Richard Ulrich, Department of Chemical Engineering, University of Arkansas 26

The Role of Organic Matter Complexes In Oil Sand Processability and Sludge Formation
L.S. Kotlyar and B.D. Sparks, Division of Chemistry, National Research Council 40

Low Temperature Oxidation Strategy for Increasing the Effectiveness of Hot Fluid Recoveryof Bitumen — An Experimental Study
John Ivory, Peter Toma, Roy Coates, and Mario DeRocco, Alberta Research Council — Oil Sands and Hydrocarbon Recovery Department
Declan Livesay, Esso Resources Canada, Ltd 50

Effect of Horizontal Wells on Sweep Efficiencies When Practicing Enhanced Oil Recovery in Heavy Oil Reservoirs
J.A. Lane, Terry Strickland, and Paul B. Crawford,
Petroleum Engineering Department, Texas A&M University 62

Properties of GPC Separated Maltene Fractions Derived from Utah and Athabasca Bitumen
L.S. Kotlyar, D.S. Montgomery, J.R. Woods, B.D. Sparks, and J.A. Ripmeester,
National Research Council — Division of Chemistry 68

Asphalt from Utah Tar Sands — A JWBA Project Sponsored by the U.S. Department of Energy
James W. Bunger, Jerry W. Wiser, Christopher P. Russell, and Prasad A.V. Devineni
James W. Bunger and Associates, Inc 79

Volatile Compound Evolution From Programmed Temperature Pyrolysis of Big Clifty and McKittrick Tar Sands at 10 C/Min Heating Rate
John G. Reynolds, Lawrence Livermore National Laboratory, University of California 86

The Chemical Aspects of Alberta Tar Sand Bitumens

O.P. Strausz, T.W. Mojelsky, T.M. Ignasiak, Z. Frakman, J.D. Payzant, and E.M. Lown, Department of Chemistry, University of Alberta..... 98

Use of Biomarkers, Including Aromatic Steroids, to Indicate Relationships Between Oil Sands/Heavy Oils/Bitumens and Conventional Oils, Western Canada Basin

P.W. Brooks, M.G. Fowler, and R.W. Macqueen, Institute of Sedimentary and Petroleum Geology, Geological Survey of Canada.....104

Relationship of Chemical Type Composition with Rheological Properties of Asphalts

M.A. Poirier, Esso Petroleum Canada
H. Sawatzky, Energy Research Laboratories, CANMET.....112

Tar Sands and Their Water Content

Costi A. Audeh, Mobil Research and Development Corporation, Central Research Laboratory.....119

Definition and World Resources of Natural Bitumen

Richard R. Meyer, U.S. Geological Survey.....124

The Orinoco Delta, A Future Exploratory Province for Heavy and Extra Heavy Oils

Lucas G. Zamora, Luis Gonzalez S., and Luz M. Linares, Lagoven, S.A.....125

Heavy-Oil Resource Potential of Southwest Missouri

Bruce W. Netzler, Missouri Department of Natural Resources, Division of Geology and Land Survey.....134

Athabasca South: Resource Characterization of an Active In Situ Pilot Area

J.R. MacGillivray,, D.A. Wynne, D.A.W. Keith, T. Berezniuk, D.M. Wightman and H. Berhane, Alberta Research Council, Alberta Geological Survey.....145

Heavy Crude and Tar Sand Resources in the Soviet Union

Gerard S. Medaisko, UNITAR/UNDP Information Centre for Heavy Crude and Tar Sands, United Nations.....159

Characterization of Heavy Oil Produced from the Wolf Lake In Situ Combustion Project

R.F. Alex, B. Fuhr, and C. Reichert, Alberta Research Council
H. Sawatzky and K. Jha, Energy Mines and Resources, CANMET
M. Polikar, BP Resources Canada, Ltd.....174

GEOLOGY, GEOCHEMISTRY, AND RESOURCE CHARACTERIZATION

Western Oil Shales Attrition and Breakage: Testing and Mineral Characterization

Ulrich Grimm and Glenn Swaney, U.S. Department of Energy, Morgantown Energy Technology Center.....205

Changes In the Clay Mineralogy of Eastern Oil Shale Induced by Retorting

T.L. Robl and A.M. Rubel, University of Kentucky, Center for Applied Energy Research
R.I. Barnhisel, Department of Agronomy, University of Kentucky.....212

Morphology of Sulfide Minerals in Eastern Oil Shale

Glenn M. Mason, Western Research Institute, University of Wyoming Research Corporation.....219

Organic Geochemistry, Petrography, and Maturation Trends of the Ohio Shale in Eastern Kentucky

Susan M. Rimmer and D.J. Cantrell, Department of Geological Sciences, University of Kentucky
Patrick J. Gooding, Kentucky Geological Survey, University of Kentucky.....232

Organic Geochemistry and Organic Petrology of Paleozoic Oil Shales In Canada

F. Goodarzi, M.G. Fowler, and W.W. Nassichuk, Institute of Sedimentary and Petroleum Geology, Geological Survey of Canada.....233

Directions and Characteristics of Jointing in the New Albany Shale (Devonian-Mississippian) of Southeastern Indiana

Curtis H. Ault, Indiana Geological Survey.....239

Pyroclastic Mineral Euhedral Horizons in Eastern United States Devonian Oil Shales

James E. Conkin, Department of Geology, University of Louisville.....253

Development of a Coking Indicator for Oil Shales

F.P. Miknis, Western Research Institute, University of Wyoming Research Corporation.....269

Comparison of Hydroretorting, Fischer Assay and Rock-Eval Analyses of Some World Oil Shales

John R. Dyni and Donald E. Anders, U.S. Geological Survey
Raymond C. Rex, Jr., Environmental Technology Transfer, Ltd.....270

Microscopic Characterization of Emulsion Interfaces

R.J. Mikula, V.A. Munoz, and W.W. Lam, Department of Energy, Mines and Resources, CANMET.....287

Examination of Wet- and Dry-Sieved Eastern Oil Shale and Microbial Reduction in Its Sulfur Content

E.J. Krieger, R.M. Pfister, and J.R. Ridge,
Department of Microbiology, The Ohio State University.....293

Water-Jet Assisted Mechanized Oil Shale Mining Factory Tests

Wilhelm J. Kogelmann, Alpine Equipment Corporation
Edward D. Thimons, U.S. Bureau of Mines
Joseph E. Virgona, U.S. Department of Energy
L. Alan Weakly, Exxon Company, USA.....303

Eastern Oil Shale Attrition and Breakage: Testing and Modeling

Ulrich Grimm and Glenn Swaney, U.S. Department of Energy, Morgantown Energy Technology Center.....316

ENVIRONMENTAL AND RECLAMATION RESEARCH

Chemical Equilibria Model Analysis of Hope Creek Eastern Oil Shale Lysimeter Leachate Data

Michael E. Essington, Western Research Institute,
University of Wyoming Research Corporation.....326

The Use of Activated Carbon in the Treatment of a Synthetic Oil Shale Processing Wastewater

Ronald W. Ballard, William P. Bonner, Rafael Bustamante, Sachin V. Prabhu,
Department of Civil Engineering, Tennessee Technological University.....339

Biological Treatability of Selected Organic Components of an Oil Shale Processing Wastewater

Sandra Miles, Rafael Bustamante, William P. Bonner,
Department of Civil Engineering, Tennessee Technological University.....348

Kinetics of Selected Heavy Metal Dissolution from Shale

Eric A. Robertson III, H. Scott Fogler, and John J. Gyenese, Department of Chemical Engineering,
The University of Michigan.....360

Evaluation of Oil Shale Solid Waste for Soil Stabilization

John P. Turner, Department of Civil Engineering, University of Wyoming
Kunal J. Suryavanshi, Ground Engineering Consultants.....365

Environmental and Health Surveillance Monitoring Results at Parachute Creek Shale Oil Project, 1988 and 1989

Janie B. Benton, Office of Synthetic Fuels Projects, U.S. Department of Treasury.....370

Simulated Climate and Shale Pile Response Within a Large Scale Environmental Chamber Developed in Wyoming

Quentin D. Skinner, Range Management Department, University of Wyoming
Tim L. Reeves, John R. Turner, and Victor Hasfurther, Department of Civil Engineering, University of Wyoming....386

Rainfall Simulation and Hydrologic Monitoring of a Combusted Western Oil Shale in Large Scale Lysimeters

Tim L. Reeves, Department of Civil Engineering, University of Wyoming.....394

PROJECTS AND PROCESS TECHNOLOGY

Prediction of Particle Size Distribution for Eastern Oil Shales Using the Self Similarity Approach

R.K. Mehta and C.W. Schultz, G.D. Irvin and J.B. Bates,
Mineral Resources Institute, University of Alabama.....405

Pressure Cycle Comminution of Eastern Oil Shale

M. Misra and M. Paoli, Mackay School of Mines, University of Nevada-Reno
M. Rao, Department of Electrical Engineering/Computer Science, University of Nevada-Reno.....411

Application of Licado Process to Eastern Oil Shale

R. Venkatadri, B.I. Morsi, and S.H. Chiang,
Department of Chemical and Petroleum Engineering, University of Pittsburgh.....417

Column Flotation of Eastern Oil Shales

C.W. Schultz, J.B. Bates, and W.E. Lamont,
Mineral Resources Institute, University of Alabama.....425

Beginning of an Oil Shale Industry in Australia

Bruce C. Wright, Southern Pacific Petroleum N.L. & Central Pacific Minerals N.L.....431

Niche Market Assessment for Eastern Oil Shale

Jerry E. Sinor, J.E. Sinor Consultants Inc.....440

PETROBRAS Boosts Oil Shale Fines Processing

Antonio Carlso Lisboa and Rubens E. Novicki, Petroleo Brasileiro, S.A.
Edwin M. Piper, Stone & Webster Engineering Corporation.....447

Application of Loc-Cat (R) Chelated Iron Scrubbers to Retort Gases

Donald Chapman, ARI Technologies, Inc.....458

Removal of Hydrogen Sulfide by Combusted Rundle Oil Shale: Sulfidation of Iron Oxides

John S. Killingley, D. Glenn Callaghan and Stuart J. Day, CSIRO Division of Fuel Technology.....465

Microbial Desulfurization of Eastern Oil Shale: Bioreactor Studies

A. Maka, C. Akin, F. Lau, V. Srivastava, and D.V. Punwani, Institute of Gas Technology.....471

Nitrogen Chemistry During Oil Shale Pyrolysis

Myongsook S. Oh, Kenneth G. Foster, Armando Alcaraz, and Richard W. Crawford,
Lawrence Livermore National Laboratory.....480

Pressurized Fluidized-Bed Hydroretorting of Indiana New Albany Shale in Batch and Continuous Reactors

Michael J. Roberts, David M. Rue, and Francis S. Lau, Institute of Gas Technology
Carl Roosmagi, U.S. Department of Energy.....487

Fluidized-Bed Retorting of Eastern Oil Shale

R.J. Gaire and G. Mazzella, Foster Wheeler USA Corporation
T.J. Hand, U.S. Department of Energy, Morgantown Energy Technology Center.....499

Operation of the 5-lb/hr KENTORT II Reactor in the Solid Recirculation Mode

S.D. Carter and D.N. Taulbee,
Center for Applied Energy Research, University of Kentucky.....511

Characterization of Liquid and Gaseous Products from the KENTORT II Fluidized Bed Retort/Gasifier

D.N. Taulbee and S.D. Carter,
Center for Applied Energy Research, University of Kentucky.....519

POSTER SESSION

Specific Gravity-Fisher Assay Relationships Among Eastern Oil Shales

C.W. Schultz and J.B. Bates, Mineral Resources Institute, University of Alabama.....533

Relationship of New Albany Shale (Devonian-Mississippian) and Rockford Limestones Mississippian to Silurian in Greene County, Indiana

Nancy R. Hasenmueller, Indiana Geological Survey.....539

Laboratory Furnace Design for Programmed Temperature Pyrolysis of Fossill Fuels

Kenneth G. Foster, Eugene J. Frohwien, Robert W. Taylor and David W. Bowen,
Lawrence Livermore National Laboratory, University of California.....540

Characterization of Particulates in Oil Sands Processing Streams

R.J. Mikula, W.W. Lam, and V.A. V.A. Munoz,
Department of Energy, Mines and Resources, CANMET.....541

Microscopic Techniques for Identification of Coke

V.A. Munoz, R.J. Mikula, and W.W. Lam,
Department of Energy, Mines and Resources, CANMET.....542

Application of Synchrotron Readiation for Analysis of Oil Shale and Shale Derived Products

Muthu S. Sundaram, Brookhaven National Laboratory
Lawrence J. Shadle, U.S. Department of Energy, Morgantown Energy Technology Center.....543

INTRODUCTION

by

Dharam V. Punwani
1989 Eastern Oil Shale Symposium Chairman

The 1989 Eastern Oil Shale Symposium, for the ninth consecutive year, continues the tradition of addressing the latest developments in all aspects of research in process technologies, environmental sciences, geology, geochemistry and reclamation technologies relevant to this vast resource, as well as tar sands and heavy oil.

In these days of plentiful energy, interest in synthetic fuels has decreased. I am among those who believe, however, that the U.S. has not yet won the energy war. There are still some serious questions about our long-term energy supply. A country that imports about 50% of its transportation fuel should not significantly reduce its efforts to develop synthetic fuels. No energy statistics could have predicted the extent of the energy crisis of the early '70's, and no statistics can predict when the next crisis might occur. Many believe that the U.S. will face another energy crisis; what is hard to predict is when that might happen.

We should use this window of opportunity during the non-crisis period to develop new and improved technologies that will lower the cost of producing synthetic fuels. Reducing the cost of producing synthetic fuels will benefit us long before we actually build commercial plants because it puts a cap on the maximum price of oil in the world market.

We should also remember that the real cost of importing oil is significantly higher that its market price because reliance on imports increases defense costs and the trade deficit, and reduces domestic jobs.

The United States needs a national energy strategy. Fortunately, efforts are now (November, 1989) under way to develop such a strategy. Eastern oil shale is a very significant resource for liquid transportation fuels. According to the U.S. Geological Survey, the extent of this resource is estimated to be equivilant to about one trillion barrels of oil. For this reason alone, the eastern oil shale resource deserves to be included in our national energy strategy. Furthermore, this resource is located in areas where the infrastructure for mining is well developed and is already available. If we want to see eastern oil shale become a part of a national energy strategy, we will all have to work together, and work hard, to disseminate the merits of this resource to our congressmen and senators. Discussing technical developments and research results for this resource at symposia like this is valuable, but is not adequate. The information must reach the policymakers in Washington, D.C.

I want to thank the University of Kentucky and the U.S. Department of Energy for their role as the major sponsors of this symposium. Thanks also to Mr. Hugh D. Guthrie (Director, Extraction Projects Management, U.S. Department of Energy, Morgantown Energy Technology Center) for delivering the banquet address and the University of Kentucky's Center for Applied Energy Research, Stone and Webster Corporation, and the Institute of Gas Technology for their contributions. Finally thanks to all of the Advisory Committee members and the University of Kentucky's Institute for Mining and Minerals Research staff for their efforts in ensuring smooth operations during the symposium and for compiling and producing this publication.

TAR SANDS/HEAVY OIL

Experience in the Beneficiation of Two Alabama Tar Sands

by

C.W. Schultz, J.B. Cardoso, and G. Daniel Irvin
Mineral Resources Institute, University of Alabama
Tuscaloosa, Alabama 35487

Abstract. Tar sand samples were collected from sites in Colbert and Lawrence counties in northern Alabama at sites known as Spring Creek and Black Wax Hill. Toluene extractions indicated bitumen contents of 8.3 and 8.6 percent respectively. Further characterization revealed that the Black Wax Hill sample had a higher clay content and a finer mineral matter matrix.

The Spring Creek tar sand responded better to flotation than did the Black Wax Hill sample. At all conditions tested, the Spring Creek sand yielded concentrates of higher bitumen content and higher bitumen recovery. The difference in response is attributed to the differences in physical characteristics.

Process optimization studies showed that an attrition scrubbing step, between grinding and flotation, markedly improved both the quality of concentrate and the recovery of bitumen. Concentrates containing 31 percent bitumen with 87 percent bitumen recovery were achieved.

Introduction

The Mineral Resources Institute, The University of Alabama, as a subcontractor to the University of Arkansas-Fayetteville has conducted a DOE sponsored investigation of the beneficiation of southern tar sands. The objectives of the investigation were; to develop a physical means of separating bitumen from associated mineral matter; and to produce a small lot of bitumen concentrate for extraction tests at the University of Arkansas. The investigation was limited to two Alabama tar sands. The samples, known as Spring Creek and Black Wax Hill, are both from the Hartselle sandstone formation. The samples are however distinctly different on both their physical characteristics and on the character of the contained bitumen.

This paper describes, sequentially, the steps taken on developing a system for concentrating bitumen from the subject tar sands. The system includes grinding, attrition scrubbing and froth flotation.

Sample Description

The tar sand samples used in this investigation are both from the Hartselle sandstone formation. One sample was taken from an outcrop on Spring Creek in Colbert County, AL. The second sample was taken from a site known as Black Wax Hill in Lawrence County. Both samples are referred to by these site names in this paper.

Dean-Starke extractions indicated bitumen contents of 8.3 % and 8.6 %, respectively for the Spring Creek and Black Wax Hill samples. In both samples the mineral matter was predominantly monocrystalline quartz. The Black Wax Hill sample did however contain pebble size lenses of unintruded clays.

The size distribution of the framework sands, (after extraction of the interstitial bitumen) are shown in figure 1. Note that the Spring Creek is much coarser, having a mean particle size of

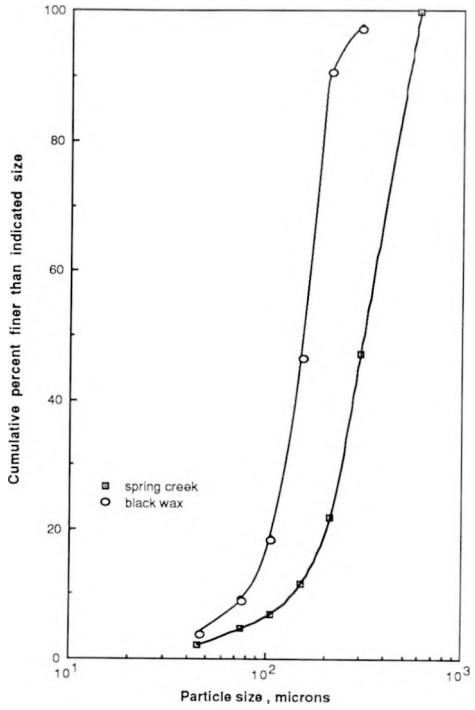

Figure 1. Size analysis of Alabama tar sand head sample extracted sands.

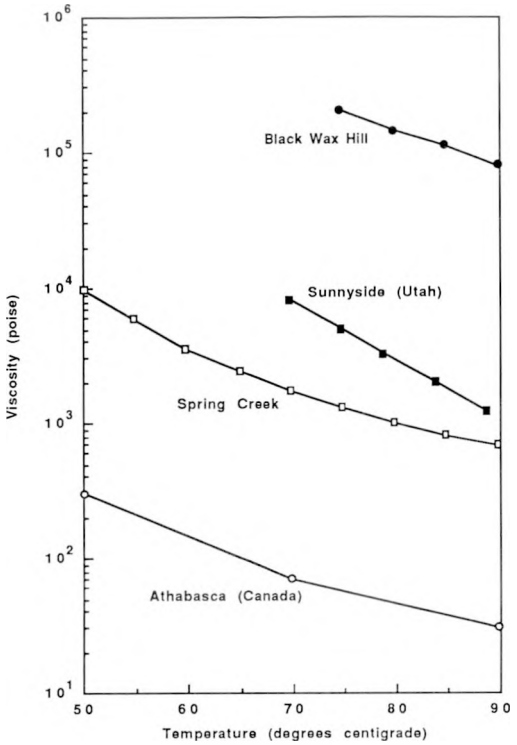

Figure 2. Comparison of tar sand viscosities.

300 microns, compared with the Black Wax Hill having a mean particle size of 150 microns.

A distinct difference also exists in the physical character of the contained bitumen in the two tar sands. The viscosities of the Spring Creek and Black Wax Hill bitumens are shown as a function of temperature in figure 2. Similar data for the Sunnyside, Utah and Atwabasca, Canada tar sands are also presented for purposes of comparison.

Fourier Transform Infrared (FTIR) analyses and Nuclear Magnetic Resonance (NMR) analyses indicate that the bitumens contained in both samples are composed mainly of primary and secondary aliphatic compounds with lesser amounts of tertiary aliphatics. CHN analyses show that the Spring Creek bitumen has a slightly higher ratio of hydrogen to carbon than does the Black Wax Hill bitumen.

Preliminary Beneficiation Tests

Grinding tests were performed on minus 4 mesh samples of both tar sands to establish the relationship between grinding time and product size distribution. The results of those tests are shown in figures 3 and 4. The data show that the coarse sample can be broken down to a size distribution approximating that of the extracted sands in relatively short time (approximately four minutes).

Heavy liquid tests were performed on samples of Spring Creek and Black Wax Hill tar sands which had been ground for thirty minutes in a laboratory rod mill. Mean particle sizes for the samples were, respectively, 53 and 48 microns. The tests were performed in aqueous salt solutions over a range of specific gravities from 1.4 to 2.3.

The liberation curves resulting from the heavy liquid tests are presented in figures 5 and 6. Note that the Spring Creek sample (figure 5) shows a higher degree of liberation than does the Black Wax Hill sample (figure 6) at essentially the same size. The difference in liberation is probably attributable to the finer size distribution of the original framework sands in the Black Wax Hill sample.

Froth flotation is a natural means of effecting a separation of bitumen from quartz grains. Bitumen, being naturally hydrophobic, readily attaches to air bubbles when presented with the opportunity. In contrast, quartz can be made hydrophobic only by the adsorption of a suitable heteropolar organic compound under closely controlled conditions of pH and metal ion concentration.

Preliminary flotation tests were conducted to assess the quality of separation which could be achieved under a variety of conditions. Variables investigated were; grinding time, frother type and dosage, dispersant addition and concentrate regrinding.

Test conditions and results of the tests performed on Spring Creek and Black

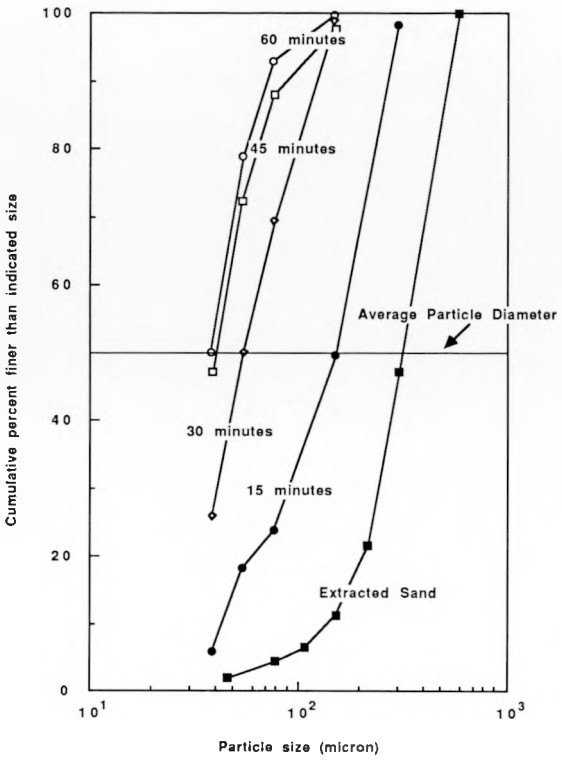

Figure 3. Size analysis of rod mill ground Spring Creek tar sand .

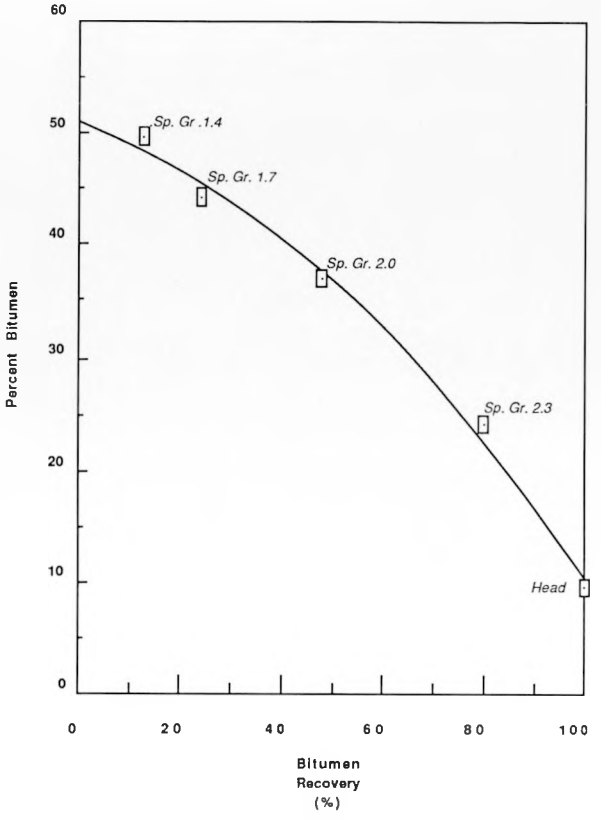

Figure 5. Spring Creek tar sand liberation

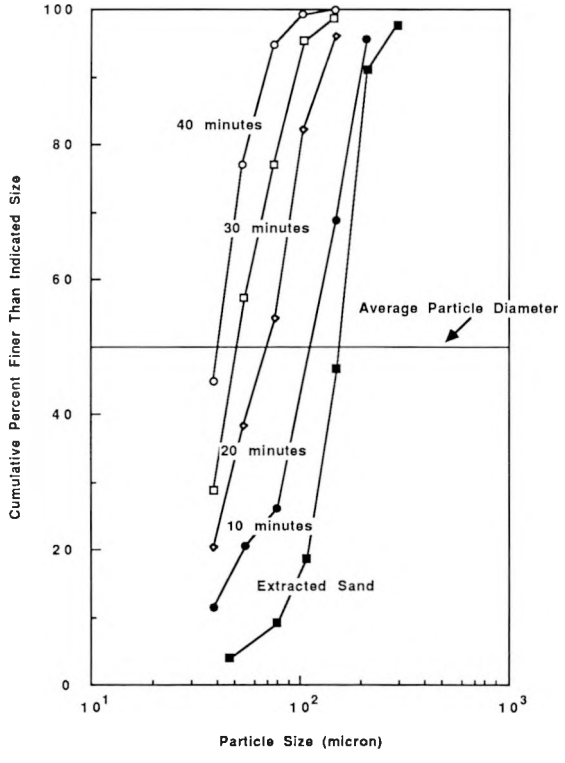

Figure 4. Size analysis of rod mill ground Black Wax Hill tar sand.

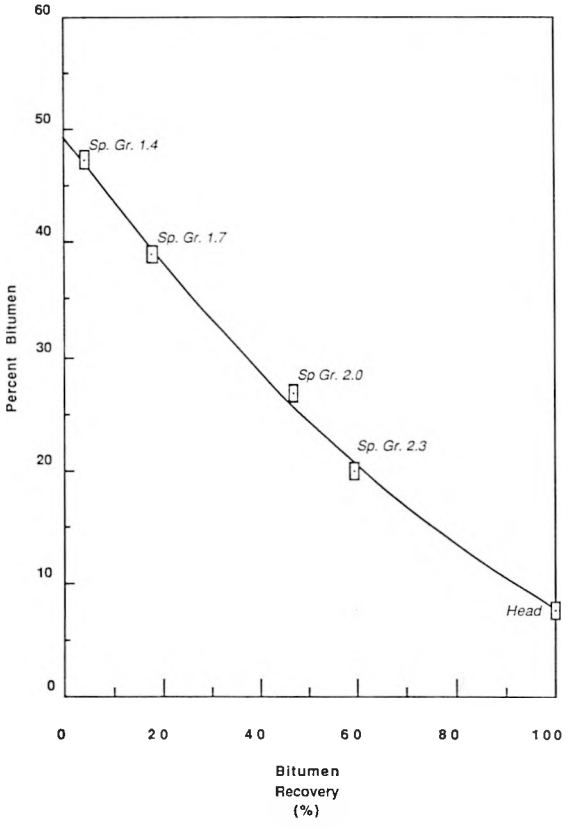

Figure 6. Black Wax tar sand liberation

Table 1. Effect of Grinding Time on Flotation Performance. Spring Creek Tar Sand.

Test Conditions				Results	
Grinding Time (Minutes)	Average Particle (Micron)	Reagent	Dosage (Pounds / Ton)	Concentrate Grade (% Bitumen)	Bitumen Recovery (%)
5	400	M-150 (1)	0.76	8.2	83.0
10	250	M-150 (1)	0.76	7.9	61.0
15	150	M-150 (1)	0.70	9.8	60.0
20	130	M-150 (1)	0.70	9.8	40.0
25	80	M-150 (1)	0.56	15.0	71.0
30	50	D-250 (2)	0.63	20.0	95.0
45	37	M-150 (1)	0.56	15.0	69.0
60	34	MIBC (3)	0.70	19.0	56.0

(1) M-150 - A polyglycol based compound plus fuel - oil , manfactured by Dow Chemical Co.
(2) D-250 - A polyethylene glycol compound , manfactured by Dow Chemical Co.
(3) MIBC - A methyl- isobutyl carbinol compound manafactured by Union Carbide Co.

Table 2. Effect of Grinding Time on Flotation Performance. Black Wax Hill Tar Sand.

Test Conditions				Results	
Grinding Time (Minutes)	Average Particle (Micron)	Reagent	Dosage (Pounds / Ton)	Concentrate Grade (% Bitumen)	Bitumen Recovery (%)
10	115	M-150 (1)	1.05	8.6	78.0
15	80	D-250 (2)	1.26	9.9	70.3
30	47	D-250 (2) Polyglycol	1.12 4.00	13.0	73.0
40	38	D-250 (2) Sodium Silicate	0.84 4.00	17.0	18.0
45	25	D-250 (2) Polyglycol	1.12 2.00	14.0	62.0
60	20	D-250 (2)	1.26	11.0	22.2
120	8	D-250 (2)	1.12	10.0	14.0

(1) M-150 - A polyglycol based compound plus fuel - oil , manfactured by Dow Chemical Co.
(2) D-250 - A polyethylene glycol compound , manfactured by Dow Chemical Co.

Wax Hill tar sands are presented in tables 1 and 2 respectively.

The data show that grinding time (i.e. feed size) is the dominant factor in the flotation of these materials. The optimum grinding time appears to be approximately 30 minutes, after which further grinding results in diminution of both concentrate grade and bitumen recovery. This is illustrated quite graphically in figure 7 where selected data for the Spring Creek tar sand flotation are plotted as a function of the percent of feed finer than 53 microns.

At this point in the investigation it was clear that conventional grinding is not an efficient means of effecting disengagement of bitumen from individual sand grains. Because bitumen is plastic, it yields readily under the impact loading supplied by a rod or ball mill. The fracture which occurs is almost entirely

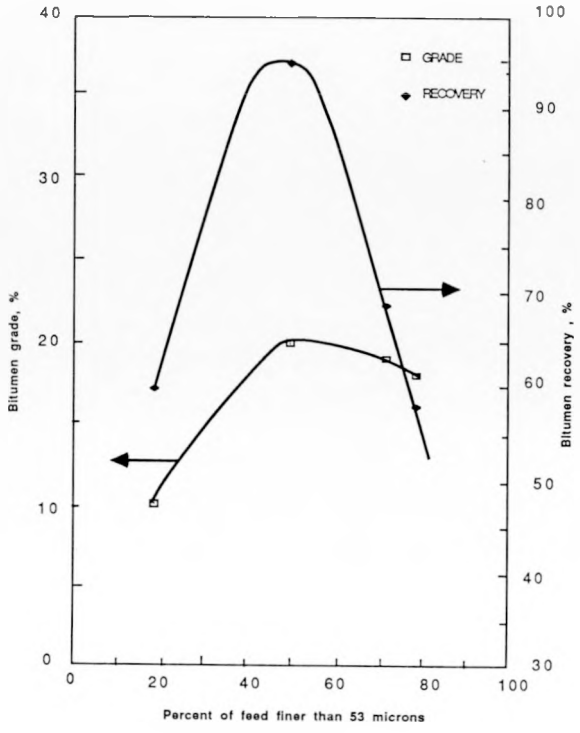

Figure 7. Effect of feed size on flotation of Spring Creek tar sand.

within the sand grains (transgranular) with virtually no fracture occurring at the sand-bitumen interface (intergranular). The foregoing data indicates that prolonged conventional grinding appears to actually reverse the process of liberation (sand-bitumen detachment). It was decided therefore, to investigate the possibility of attrition scrubbing whereby the sand-bitumen particles are subjected to high shear forces rather than impact forces.

Process Development

Because the "problem" in tar sand beneficiation is to shear the adhering bitumen off the surfaces of sand grains, there would appear to be no advantage in grinding a tar sand to a size finer than that of the matrix sand grains.

Attrition scrubbing tests were performed on samples of Spring Creek tar sand which had been ground to a size approximating the size distribution of the matrix grains. The ground product was filtered then diluted with fresh water to 75% solids. Scrubbing was carried out in a Denver conditioner which is equipped with two flights of opposed impellers. The conditioner is capable of operating at speeds of rotation from 1000 to 4000 rpm. In this investigation all scrubbing was done at 2100 rpm for periods of fifteen minutes. After scrubbing the slurry was transferred to a Denver flotation cell, diluted and floated. Visual examination of the flotation products indicated that very little detachment of bitumen from sand grains had been achieved at this relatively coarse size.

A series of tests were carried out to determine the degree of grinding required prior to scrubbing to yield an acceptable separation. Tests were performed at grinding times ranging from five to fifty minutes. In all tests the slurries were scrubbed for 15 minutes prior to flotation. The results of this series of tests, together with test conditions are tabulated in table 3 and presented graphically in figure 8. The data show a distinct optimum in terms of bitumen recovery after a thirty minute grinding period. The grade of concentrate achieved, however, continued to increase with increased grinding times. It should be noted that

Table 3. Effect of Feed Size on Tar Sand Flotation.

Test Conditions						Results	
Grinding		Scrubbing			Flotation	Concentrate	
Time (Mins)	Percent minus 53 (microns)	Time (Mins)	Reagent	Dosage (lbs/ton)	Dow Froth 250 (lbs / ton)	Bitumen Content (Percent)	Bitumen Recovery (Percent)
5	3.0	15	Sod. Silicate	1.4	0.2	8.2	83.0
15	20.0	15	Sod. Silicate	2.7	---	12.0	87.0
20	29.0	15	Sod. Silicate	2.7	0.05	15.0	68.0
30	42.0	15	Sod. Silicate	3.0	0.2	31.0	87.0
40	67.0	15	Sod. Silicate	2.7	---	33.0	69.0
50	100.0	15	Sod. Silicate	2.7	0.1	39.6	39.2

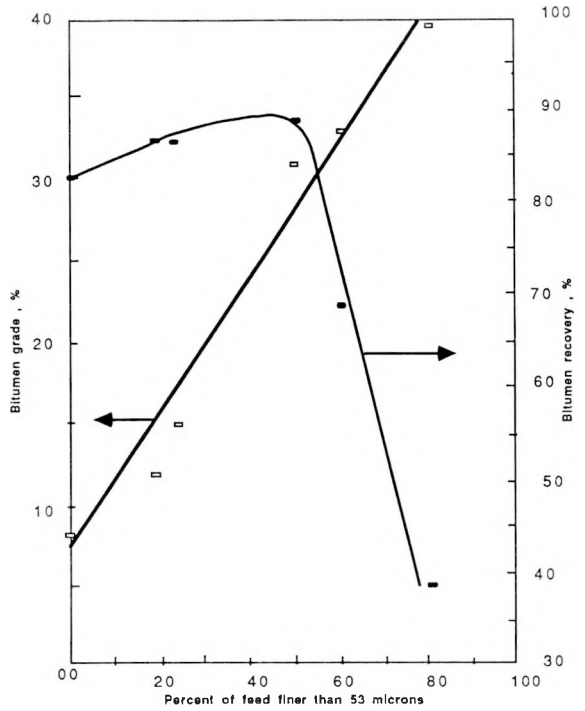

Figure 8. Effect of feed size on tar sand flotation.

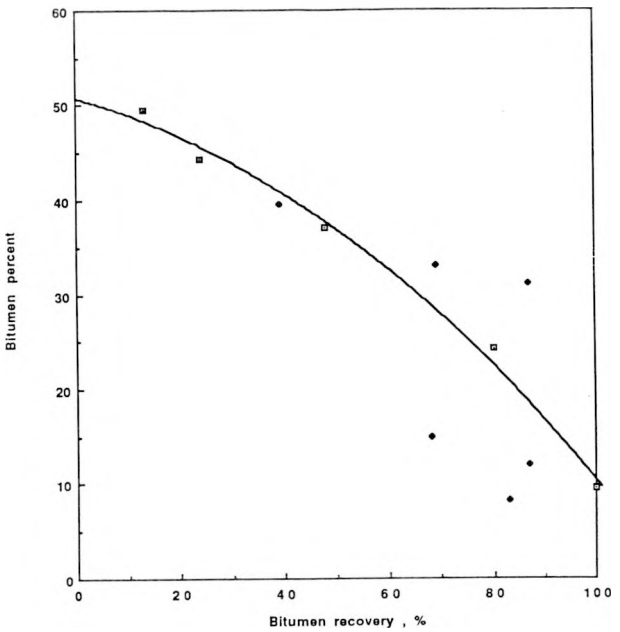

Figure 9. Effect of attrition scrubbing on bitumen liberation.

both concentrate grade and bitumen recovery were markedly higher than in previous tests in which the slurry was not scrubbed prior to flotation.

These data also show that a substantial increase in liberation is achieved by scrubbing. Figure 9 shows the data from table 3 plotted with the liberation curve for a sample which had been ground for 30 minutes. Note that all points in this series lie above the liberation curve indicating an increase in the degree of liberation.

The data again show that overgrinding is detrimental to the quality of separation which can be achieved. It might be inferred that a certain level of grinding is necessary to provide clean quartz surfaces which act as scrubbing media and that prolonged grinding tends to amalgamate fine mineral particles into the bitumen.

Conclusions

The authors believe that the data presented here represent substantial progress toward development of a physical beneficiation system for the Alabama tar sands. We acknowledge however that considerable work remains to be done in developing this process.

The data presented here indicate that neither grinding (i.e. conventional comminution) nor scrubbing alone can achieve a satisfactory level of bitumen-sand disengagement. A combination of grinding and attrition scrubbing appears to be the most favorable approach for process optimization. Further work in that direction is recommended.

Acknowledgements

The authors are indebted to the Department of Energy for the financial support of this project and to the University of Arkansas-Fayetteville, through whom that support was received.

Extraction of Alabama Tar Sands with Heptane and Carboxylic Acid Mixtures and Using a Saponification Cycle

by

Richard K. Ulrich, Muddu K. Koppaiah, Vineet K. Majmudar
Department of Chemical Engineering, University of Arkansas
Fayetteville, Arkansas 72701

Abstract. A tar sands extraction process is being developed that requires a heptane/oleic acid mixture to be used as the solvent. This paper is a description of the issues and problems involved in using this mixture in the contactor and the sand cleanup units of a generic tar sands processing plant. The optimal solvent composition was determined to be 70 vol % heptane and 30% oleic acid. A rotating disk method was used to determine that the solvation rate of bitumen into this solvent was sufficient for use in conventional contacting schemes. Spring Creek bitumen was 96 wt % soluble in this mixture. The phase behavior of a saponification cycle for sand cleanup was investigated and the reagent streams optimized.

Introduction

A solvent-based tar sands extraction process will consist of three main units regardless of the type of solvent used:

- A contactor where bitumen is dissolved off the sand.
- A sand cleanup unit for removing residual solvent and bitumen from the sand, thus recovering the chemicals and leaving a clean solid for burial.
- A bitumen recovery unit which isolates bitumen product and produces fresh solvent for recycling back to the contactor.

The usual method of bitumen recovery from the solvated bitumen stream is by thermal evaporation of the solvent. A non-thermal alternative to this is being investigated at the University of Arkansas in which the bitumen falls out by an induced phase separation. In order for this phase separation to work, specific components must be present in the solvent.

In one series of studies, a mixture of heptane and a carboxylic acid (oleic acid) was specified. Although the exact ratio of heptane and oleic acid is not tightly constrained in order to accomplish the bitumen recovery by phase separation, the solvent must consist exclusively of these two components. For the purposes of laboratory investigations, a commercial brand of oleic acid marketed under the name Xtol™ was used.[1] Xtol consists of approximately 90 wt % oleic acid with the balance being linoleic acid and various resins.

Scope of This Study

The purpose of the work presented here was to investigate the feasibility of using a heptane/Xtol solvent mixture in the contactor and sand cleanup sections of a generic solvent-based tar sand process. There were three tasks to this study:

1. Compare the dissolution rate and solubility of bitumen in this mixture to that of dissolution into pure aliphatic, aromatic and carboxylic acid solvents.

2. Determine the optimal ratio of heptane and Xtol for these two units. The important considerations included bitumen solubility, dissolution rate, and solution viscosity.

3. Determine the feasibility of employing a saponification cycle using the Xtol to accomplish the sand cleanup step. Since a carboxylic acid will be present in the

solvent, it should be able to act as a reversibly saponifiable species. The solvent composition used for this task is the optimal ratio determined from task 2.

Properties of the Tar Sands

Spring Creek sand from Alabama was chosen as the standard feed for the experimentation. The composition of the raw material in wt % was:

Bitumen:	7.4%
Water:	1.6%
Sand:	91.0%
Total:	100.0%

The weight percent of bitumen was determined by toluene extraction. This material is referred to as "bitumen" here even though it may contain entrained clays. The percent water was determined from weight loss at 60° C until the sample achieved constant weight. Following bitumen extraction by toluene, examination of the remaining solids under the microscope revealed that all traces of bitumen and water were removed leaving transparent, rounded quartz grains. The raw tar sand was used for some experiments and extracted bitumen was used for others.

The average equivalent-sphere grain diameter for the Spring Creek material was 13 microns based on a BET average surface area of 0.19 m^2/gm. On average, each raw tar sand grain had a coating 0.4 microns thick of bitumen and water. This layer amounts to about 6% of the clean sand grain radius. The void volume of the cleaned sand was 30%.

Solvent Evaluation for the Contactor

Solubility of Bitumen

The solubility of Spring Creek bitumen were measured as a function of the heptane/Xtol ratio in the solvent. Two grams of bitumen was dissolved in 100 grams of agitated solvent at room temperature. The resulting solution was filtered through fine paper with a vacuum funnel and the insoluble portion determined by the weight difference of the filter paper. The results are shown in Figure 1.

The insoluble fraction in heptane was 23 wt % and in pentane it was 34%. Only 6% was insoluble in pure Xtol and this value was found to be constant down to 30 vol % Xtol in heptane. Therefore, Xtol in the solvent exerts a beneficial influence on the amount of product that can be recovered relative to pure heptane.

Dissolution Rate of Bitumen

The dissolution rate of Spring Creek bitumen was measured into various mixtures of heptane and Xtol with the rotating disk system. The results were compared to pure aliphatic and aromatic solvents.

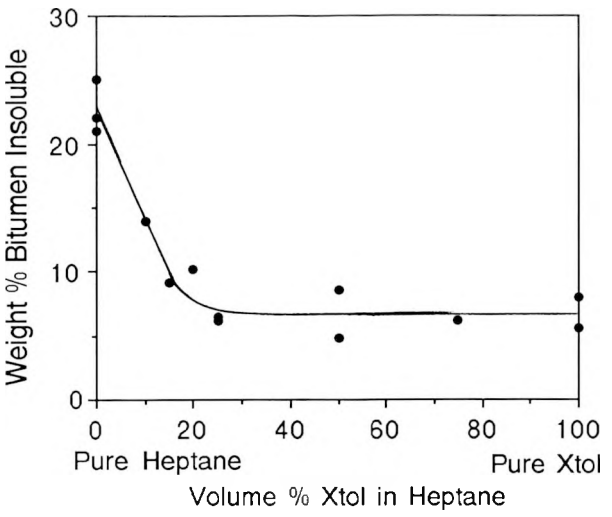

Figure 1. Solubility of bitumen in heptane/Xtol solvent mixtures.

Previous Bench-Scale Studies. Cormack and his co-workers have studied the dissolution of tar sand bitumen in various solvents and under various conditions of agitation using baffled and unbaffled stirred tanks.[2] Their results indicate that the ease of bitumen removal from raw tar sand is affected by the solid-solid interactions which increase at higher sand-to-solvent ratios. They also suggest that the diffusion of solvent into the bitumen produces a region of reduced viscosity and the stirring action is then able to shear off the bitumen, thus producing a strong dependence of dissolution rate on stirrer speed. Solvents with a higher aromatic content or with lower boiling points dissolve bitumen at a higher rate.[3, 4]

These and other conventional bench-scale contacting methods cited in the literature have limitations which make their dissolution studies difficult to port to systems that are not identical to that of the original investigations. Tar sand particles are irregular in shape and size and clumps of sands tend to break up during the contacting time. As a result, new surfaces are continuously exposed and old ones are cleaned to completion so that there is a continuum of bitumen coating thicknesses and exposure times in these contactors. As the clumps break up, the local mass transfer coefficients change and particle-particle collisions increase in frequency. In a continuous stirred tank reactor (CSTR) the mass transfer coefficient varies with location and cannot be accurately predicted from first principles. For most bench-scale apparatuses which have been used to study bitumen dissolution, the hydrodynamic and mass transfer conditions are varying with time and position throughout the experiment in an unpredictable manner.

The Rotating Disk Method. The surface of a rotating disk immersed in a fluid is one of the very few geometries where hydrodynamics and mass transfer characteristics are constant with both time and position and can be predicted quantitatively from first principles.[5, 6] The rotating disk can therefore be used as a technique for comparative and absolute studies of bitumen dissolution into various solvents under a variety of hydrodynamic and thermal conditions.

The rotating disk technique has been used extensively in electrochemistry for mass transfer studies.[5, 7, 8] The free dissolution of a number of metals in corrosive media and their cathodic protection have also been investigated by this method.[9, 10] The system has also been used to study the incorporation of solute elements into single crystals grown from a melt.[11, 12] A theory has been developed for the case of film condensation on a disk rotating in a large volume of saturated vapor.[13] It has also been suggested that the rotating disk would form a suitable tool for the study of the mechanics of rarified gases due to the well-characterized hydrodynamic conditions surrounding the disk.[14]

Application of the Rotating Disk to Bitumen Studies. In a CSTR or screw contactor there are three mechanisms of bitumen removal from the surface of sand grains: molecular diffusion across a mass transfer boundary layer, shearing away of solid particles by fluid action at the surface, and dislocation of bitumen by particle impact. The rotating disk method allows diffusional mass transfer effects to be modeled quantitatively since the mass transfer coefficient can be predicted from first principles. Fluid shear may be determined from the velocity distributions near the surface of the disk and the effects of particle impacts may be removed if there is no sand in the system. The rotating disk technique provides for relative comparison of bitumen dissolution into different solvents under identical and reproducible conditions and, with some development, may become a tool for the study of fundamental bitumen dissolution mechanisms.

Funk has studied the dissolution of bitumen in paraffinic solvents by using the rotating disk, liquid-fluidized beds, and direct particle-size analysis of the insolubles.[15] His work was performed at very low disk rotation rates and, as a result, mass transfer was dominated by diffusion across a thin layer of insoluble material which was left behind on the bitumen surface.

For the present study, a 5 cm diameter stainless steel disk was fabricated and set on the end of a mixer shaft. The surface of this disk was coated with a smooth layer of bitumen about 2 mm thick. The disk was immersed into the solvent being studied and rotated at 0 to 500 rpm for a specified amount of time. The rate of dissolution was then determined by the weight difference of the bitumen and the disk.

The dissolution flux from the rotating disk as a function of disk rpm is shown in Figure 2 and as a function of the heptane/Xtol ratio at 200 rpm in Figure 3. The data in Figure 3 are the slice out of Figure 2 along the dotted vertical line. The dissolution rate of pure Spring Creek bitumen into heptane was about two orders of magnitude higher than dissolution into Xtol under a wide range of hydrodynamic conditions. These rates are the combined effects of molecular diffusion and fluid shear; no sand particles were present in the system. During dissolution it was observed that particles are sheared off the bitumen surface. Some of these particles subsequently dissolve and others remain as insolubles.

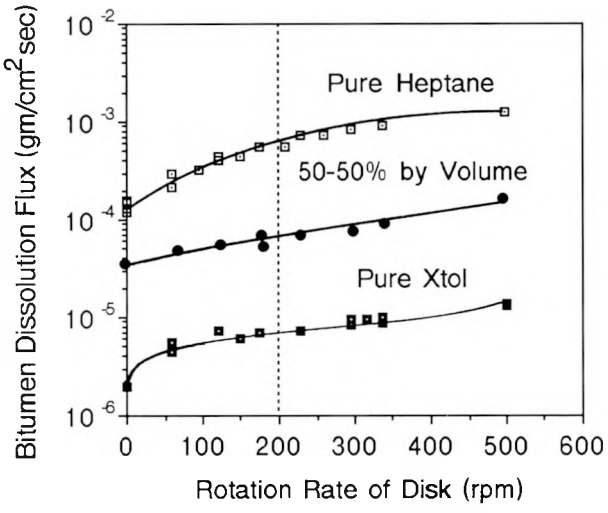

Figure 2. Dissolution rate of bitumen into heptane/Xtol solvent mixtures from the rotating disk as a function of disk rpm.

The dissolution flux was found to be constant over the entire face of the disk, since the bitumen layer remained flat during dissolution until the metal substrate was exposed. Hydrodynamic and mass transfer analysis of rotating disks leads to the conclusion that the mass transfer coefficient should be constant with position on the disk.[5, 6] This behavior indicates that diffusional mass transfer is probably an important dissolution mechanism compared to removal by fluid shear. The dissolution rate into heptane was greater than the rate into Xtol even though the bitumen is more soluble in pure Xtol. This reversal of solubility and removal rates are probably

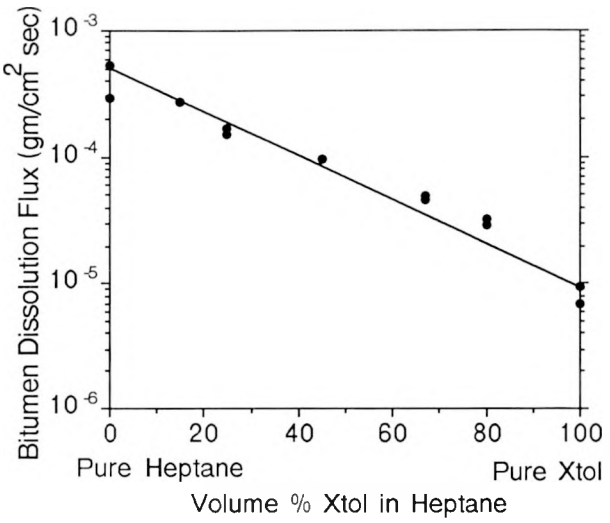

Figure 3. Dissolution rate of bitumen into heptane/ Xtol solvent mixtures using the rotating disk at 200 rpm.

related to solution viscosity effects on the diffusivities and mass transfer boundary layer thicknesses. Dissolution into pure toluene at 200 rpm was 8.8×10^{-4} gm/cm^2 sec, about twice that of the flux into pure heptane.

Since the density of bitumen is on the order of 1 gm/cm^3, the velocity at which the bitumen layer is thinned is given in cm/sec by the numbers on the ordinate of Figures 2 and 3. Therefore, a 1 micron bitumen layer would be removed by pure heptane at 200 rpm in less than one second while pure Xtol would require some tens of seconds. These results must be extrapolated cautiously from the well-defined rotating disk to the case of bitumen on a sand particle in a CSTR, but the relative results should be valid.

Bitumen dissolution rates from raw Spring Creek tar sands were also measured in a modified leaf test for comparison to the rotating disk work. Five grams of raw sand were ground to single particles and placed on course filter paper in a dry vacuum funnel. At the start of the test, 5 grams of 30 vol % Xtol in heptane were added to the sand and the solid phase was slowly agitated to simulate the action of an agitator in a stirred tank contactor. After some time, the vacuum was turned on to remove the solvated bitumen and, simultaneously, about 100 grams of IPA was added to quench the mass transfer and to reduce the solution viscosity for faster solvent removal by the vacuum.

The results indicated that total dissolution occurred from the sands in some time less than 5 minutes. It was impossible to determine the time to complete dissolution very well because of the rapid rate of bitumen removal; at least an additional 5 minutes were required to remove the solvent and quench the process after the end of the dissolution phase and this set a minimum temporal resolution on the experiment. These results are in general agreement with the rotating disk work which indicated that total dissolution would be achieved in under a few minutes. The rotating disk method was able to measure dissolution rates in regimes where leaf tests of this sort were too slow to resolve the rapid fluxes.

Optimal Solvent Composition

Based on solubility and dissolution rate studies, it was determined that 30 vol % Xtol in heptane is an optimal composition for the contactor. This mixture has the following advantages:

(1) Low viscosity. The viscosity of the mixture is much lower than the mass or volume weighted average. This is an important issue for reducing the amount of sand fines in the process loop since they will settle out faster at the lower viscosities.

- Pure heptane: 0.9 cp
- 30% Xtol: 7 cp
- Pure Xtol: 125 cp

(2) High bitumen solubility.

- Pure heptane: 77 wt %
- 30% Xtol: 94 wt %
- Pure Xtol: 94 wt %

(3) High dissolution rate, as measured on the rotating disk at 200 rpm.

- Pure heptane: 4×10^{-4} gm/cm^2 sec. A 1 micron bitumen layer would be removed in 0.25 seconds
- 30% Xtol: 1×10^{-4} gm/cm^2 sec. A 1 micron bitumen layer would be removed in 1 second
- Pure Xtol: 9×10^{-6} gm/cm^2 sec. A 1 micron bitumen layer would be removed in 11 seconds

This 70 vol % heptane + 30% Xtol mixture ("70/30") was used for the saponification studies for the sand cleanup unit.

Solvent Evaluation for the Sand Cleanup Unit

Saponification Cycles for Sand Cleanup

Sand from the contactor will be saturated with a mixture of heptane, Xtol, and bitumen. The carboxylic acid in the solvent is a reversibly saponifiable species and it might be possible to take advantage of this to form an in-situ soap to aid in the removal and recovery of the organic species from the sand prior to sand disposal. The addition of caustic to the sand-solvent-bitumen mixture would convert some of the oleic acid to soap, which would aid a subsequent water wash to

remove and recover the organics.[16, 17] The soap would be converted back to carboxylic acid by the addition of an acid stream. High removals of organic contaminants should be achievable in this manner. However, some disadvantages include the need for solids filtering during the wash and the production of a brine waste stream.

Batch saponification and desaponification studies were performed on matrix combinations of heptane and Xtol with various concentrations of caustic and acid streams in order to characterize the chemistry and phase behavior of these systems.

Saponification Studies

The saponification behavior of the base case solvent of 70 vol % heptane and 30% Xtol ("70/30") was studied without bitumen or sand present. The saponification was carried out with sodium hydroxide solutions of 0.2 to 5 M. Caustic solution was mixed with the 70/30 solvent in the presence of a pH indicator (phenylphthalene) in order to determine the percent total saponification as a function of the amount of caustic added. One ml of 70/30 solvent contains 9.76×10^{-4} moles of oleic acid based on the assumption that Xtol is 100% oleic acid (MW = 282.5). Theoretically, it would take the same number of moles of NaOH to completely saponify this amount of carboxylic acid and the pH indicator should indicate an endpoint once excess base is beginning to be added. However, there is about 5 to 10% inerts in the Xtol with the remainder being a mixture of oleic and linoleic acid, so the actual moles/ml of saponifiable material is probably less than the theoretical amount of 9.76×10^{-4} moles. The approach to this theoretical value is reported below as "percent theoretical saponification" with the understanding that this will be revised when the actual amount of saponifiable material in Xtol is determined.

Figures 4 and 5 show the results of saponifying the 70/30 solvent with various concentrations of caustic solution. Figure 4 shows the ml of caustic added per ml of 70/30 until one of two things happen: at less than 0.6 M NaOH the pH endpoint is reached or, at greater than 0.6 M caustic, the solution turns into a gel and the pH endpoint is not reached. This gel is stiff, non-liquid and does not liquify over a period of days. The volume of caustic needed to reach full theoretical saponification is shown as the curved line on top in Figure 4.

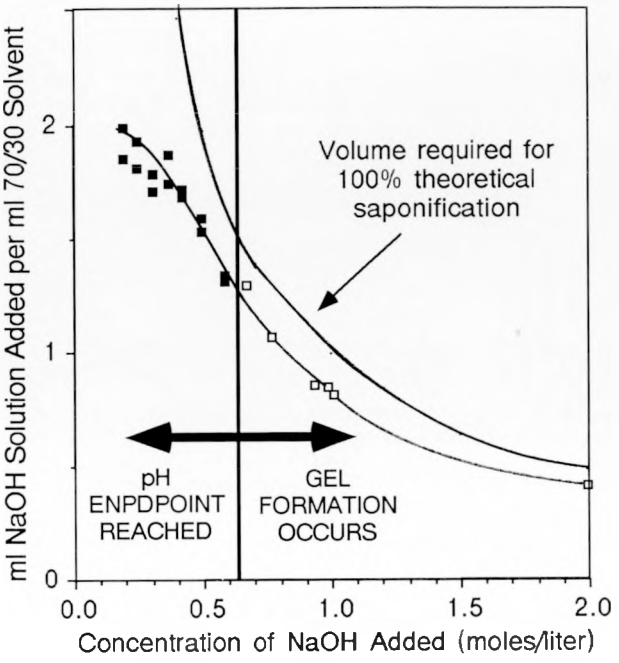

Figure 4. Saponification behavior of 70% (vol) heptane + 30% Xtol.

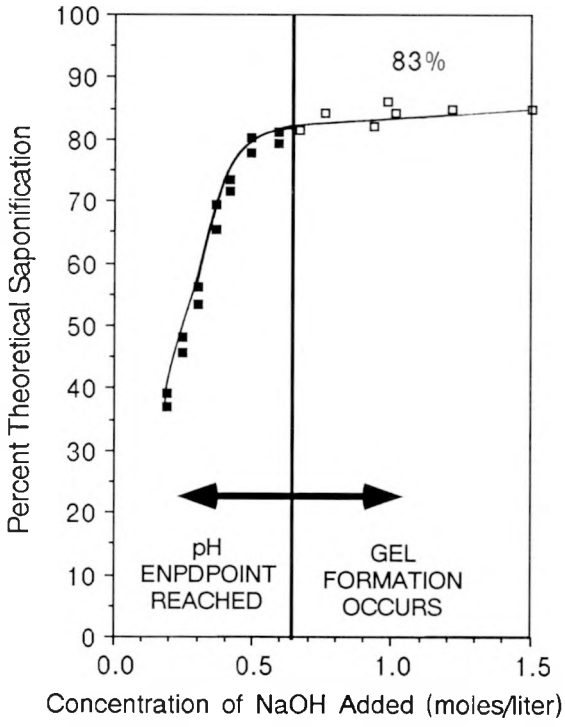

Figure 5. Percent theoretical saponification of 70% (vol) heptane and 30% Xtol.

Figure 5 is the percent theoretical saponification obtained vs. the normality of the caustic solution used for the saponification step. These results show that full theoretical saponification is never achieved, even with up to 5 M NaOH (not shown). The observed maximum is 83% of theoretical maximum. This may represent the complete conversion of all carboxylic acids in Xtol.

The tentative conclusion from this work is that a caustic solution of about 0.5 M is optimal for achieving a high degree of saponification (83 mol %) while avoiding gel formation when using the 70/30 solvent.

The phase behavior of 70/30 solvent was investigated as 0.5 M NaOH was added to the mixture (Figure 6). Initially, a three phase system is obtained as the caustic is added. Once 0.4 ml/ml of 0.5 M caustic has been added, the solvent phase disappears leaving a two-phase mixture. The top phase is a stable organic emulsion containing the heptane and the bottom phase is a soapy aqueous solution. At a point near the maximum obtainable saponification, 83 mol % for this case, the emulsion begins to shrink and the aqueous phase increases. Eventually, a one-phase aqueous mixture is obtained.

Desaponification Studies

The desaponification of the two-phase mixtures formed from 70/30 solvent and 0.5 M NaOH was easily and rapidly accomplished with HCl solutions under moderate agitation at room temperature. The recovered solvent could be cycled through the saponification-desaponification steps several times with no appreciable loss of volume.

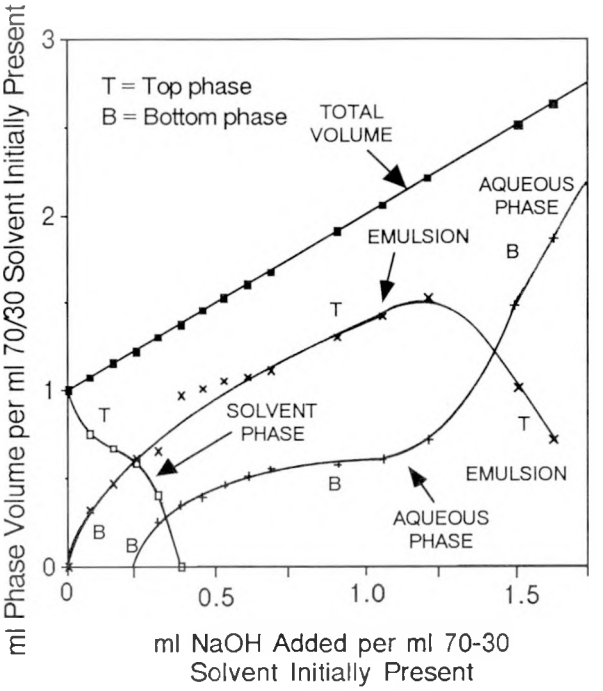

Figure 6. Phase behavior during saponification of 70% (vol) heptane and 30% Xtol with 0.5 M NaOH solution.

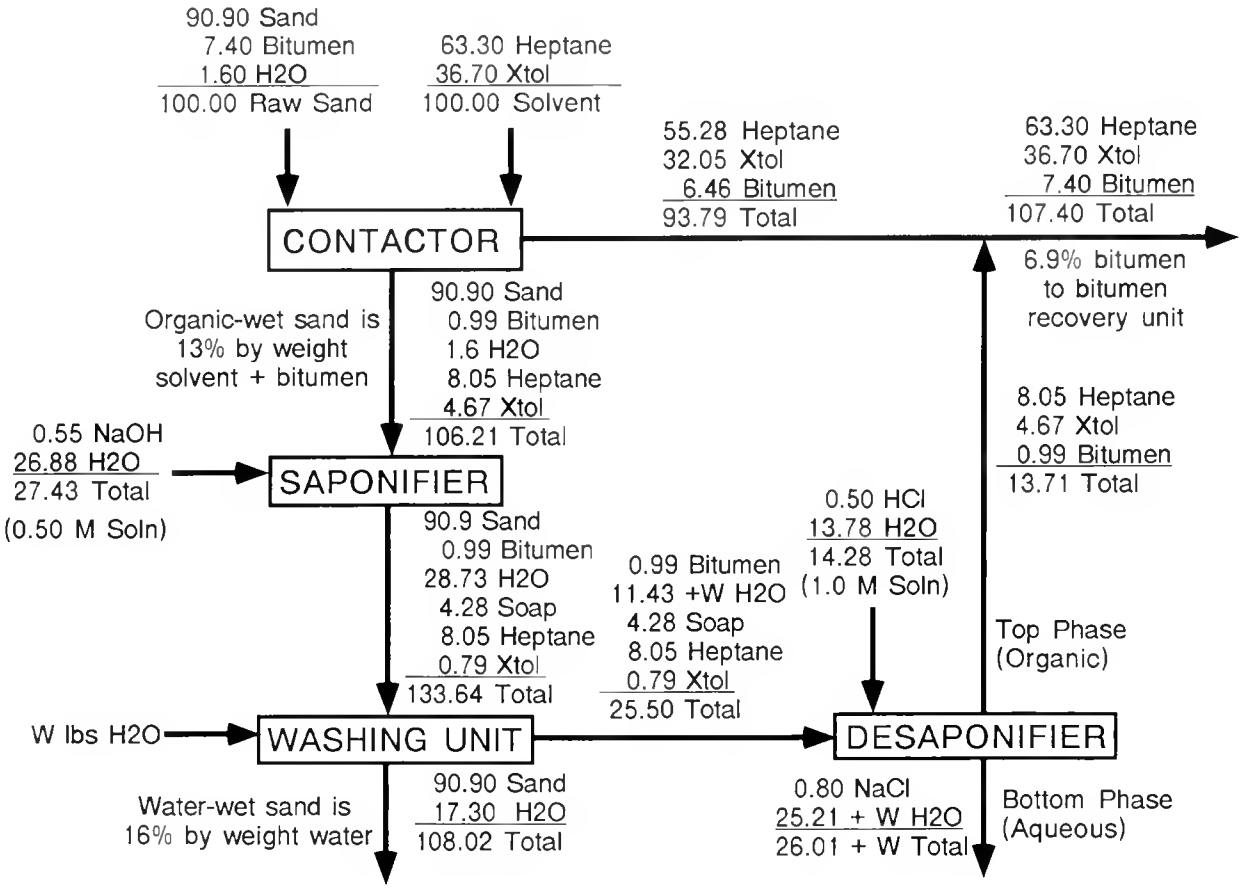

Figure 7. Mass balance for sand cleanup by saponification/desaponification cycles.

A Saponification-Desaponification Unit for Sand Cleanup

Figure 7 shows an idealized flowsheet for a sand cleanup unit employing a saponification cycle based on the results given above. This flowsheet was established with the following assumptions:

- A 1 to 1 weight ratio of solvent to raw tar sand.
- The weight percent of saturated clean sand is 16% for water and 13% for 70/30 solvent based on 30% void volume of the sand.
- All water from the contactor goes to the saponifier.
- 83 mol % of the Xtol is saponifiable, based on the assuming that Xtol is 100% oleic acid.

Both phases from the saponifier are sent to the sand washing unit, since each phase contains both organics and soap. The washing unit is non-specific in this flowsheet so the amount of water required to achieve sufficient organic removal is designated by "W." For every pound of bitumen produced, 0.108 lbs of salt would have to be disposed of, but this amount could be reduced by saponifying a smaller fraction of the carboxylic acid. Additionally, a more efficient wash unit would reduce the amount of water in the system, giving a more concentrated waste brine stream.

Conclusions

1. Bitumen would be removed quickly and easily from tar sands by heptane-Xtol mixtures due to the thin distribution of bitumen over the sand's surface combined with the inherently rapid solubilization into this organic solvent mixture.

2. A mixture of 70 vol % heptane and 30% Xtol was found to be optimal for the contactor with regard to bitumen solubility, dissolution rate, and solvent viscosity.

3. The optimal caustic concentration for the saponification cycle is 0.5 M NaOH with 70/30 solvent since it avoids gel formation and also achieves the maximum possible saponification of Xtol at about 83 mol %.

4. Desaponification is accomplished fully and rapidly with aqueous HCl.

References

1. Xtol is a registered trademark of Georgia Pacific.

2. D. Cormack, J. Kenchington, C. Phillips, and P. LeBlanc, Canadian Journal of Chemical Engineering, Vol. 55, pp. 572-580, Oct. 1977.

3. D. Mitchell, and J. Speight, Fuel, Vol. 52, pp.149, 1973.

4. H. Leung, and C. Phillips, Ind. Eng. Chem. Fundam., Vol. 24, pp.373, 1985.

5. A. Riddiford, Advances in Electrochemistry and Electrochemical Engineering," Vol. 4, pp.47, 1966.

6. V. Levich, Physicochemical Hydrodynamics, Prentice-Hall, 1962.

7. S. Beacom, and R. Hollyer, Journal of the Electrochemical Society, Vol. 109, pp. 495, 1962.

8. G. Johnson, and D. Turner, Journal of the Electrochemical Society, Vol.109, pp. 918, 1962.

9. D. Gregory, and A. Riddiford, Journal of the Chemical Society, pp. 375, 1956.

10. D. Gregory, and A. Riddiford, Journal of the Electrochemical Society, Vol.107, pp. 950, 1960.

11. J. Burton, R. Prim, and W. Slichter, J. Chem. Phys., Vol. 21, pp. 1987, 1953.

12. J. Burton, E.Kolb, W. Slichter, and J. Struthers, J. Chem. Phys., Vol. 21, pp. 1991, 1953.

13. E. Sparrow, and J. Gregg, Journal of Heat Transfer, Vol. 81, pp. 113, 1959.

14. S. Soo, Journal of Basic Eng., Vol. 83, pp. 423, 1961.

15. E. Funk, Canadian Journal of Chemical Engineering, Vol. 57, pp.333, June 1979.

16. H. Beaver, "Recovery of Fatty Acid from a Solvated Hydrocarbon Mixture," Doctoral Dissertation, University of Arkansas, 1985.

17. W. Munns, S. Kainys, and M. Dilys, Journal of the Americal Oil Chemistry Society, Vol. 39, pp. 189, 1962.

Uses of Generated Surfactants from a New Tar Sand Process for Extracting Hydrocarbons from Natural and Man-Made Materials

by

Kazem M. Sadeghi, Mohammed-Ali Sadeghi, and Teh Fu Yen
Department of Civil and Environmental Engineering
University of Southern California
Los Angeles, California 90089-0231

ABSTRACT

A process has been developed to generate self-propagated surfactants during bitumen recovery from tar sand using alkaline solution under ultrasonic energy. During the process, bitumen that floated to the top of the solution was found to be upgraded and free of asphaltene and pre-asphaltenes. The asphaltic part of the bitumen was shown to have dissociated into the solution in the form of vesicles due to interaction with amphiphiles. The multi-lamellar surfactant vesicles, which remain very stable for many years, have the capacity to extract hydrocarbons from virtually any source. This papers illustrates that these highly-efficient surfactants can remove bitumen from tar sand (Kentucky, California, Athabasca) and hydrocarbons from oil spills on land (Valdez oil spills), as well as clean oily soil (petroleum-contaminated soils). These data show a high efficiency in extracting hydrocarbon within minutes under sonication in an alkaline solution with addition of a trace free radical (H_2O_2). The mechanisms are related to membrane-mimetic chemistry.

INTRODUCTION

The study of the reactions initiated by ultrasonic energy in this country began 50 years ago. Since then, the mechanism of acoustic-chemical reactions remains poorly understood, thus limiting its practical application. Yet, in recent years, some considerable advances have been made in the technological generation of newer, higher intensity ultrasonic generators. Advances in ultrasonic waves are also becoming more successful in enhancing chemical processing operations by increasing the rates of individual transport phenomena involved in the overall operation.

In recent years, this problem has been reexamined, especially involving the application of cavitation in a microenvironment. For example, in aqueous solution, the instantaneous pressure at the center of a collapsing bubble has been estimated from theoretical considerations to be about 75,000 psi (5,100 atm). The temperature has been similarly estimated to reach values as high as 13,000^{o}F (7,200^{o}C) [14,15]. Therefore industry has slowly been awakened to this powerful and unique manner and feasibility for large scale process [21].

We have studied membrane-mimetic chemistry and applied the principles to sonochemistry. In addition, we have developed a new process for extracting and upgrading bitumens from tar sand [1,20] and also applied it to the refining of heavy crude oil [8]. In both cases, self-induces, in-situ surfactants are generated in excess quantities above that of separation or upgrading. This surplus amount of surfactant could very well be used for cleaning up environmental contaminations.

EXPERIMENTAL

We have reported the detailed experimental procedures for extracting bitumen from Athabasca tar sands in previous publications [1,2,5,6,20]. The methodology uses an alkaline solution with the aid of sonication. Stirring is applied only to help mix the solution with the sample and is not a major factor in the extraction. Two different alkalies were used to extract the bitumen: (1) 20:1 by volume distilled water to sodium silicate [wt. ratio SiO_2/Na_2O = 1.80) (PQ Corporation) and (2) 0.02 Molar NaOH (J.T. Baker Chemical Co.) solution. The stirrer operates at 320 rpm with the blade at 2 cm above the sample. Sonication was performed in a 10-gallon 40 kHz transducerized tank (Branson model ATH610-6) with a companion generator (Branson model EMA30-6). Six piezoelectric transducers, made from lead zirconate titanate ceramic, were bonded to an area of about 350 cm^2 directly at the bottom of the tank. The six transducers consume a total power of 180 Watts/cm^2 and deliver approximately 2.0 Watts/cm^2 acoustic intensity at the transducer surface. Ultrasonic energy was directed upward through the tank. The schematic design of the experimental apparatus is shown in Figure 1.

The bitumen extracted from tar sand (High Grade Athabasca tar sand, Sample No. 1981 HG) is given in Tables 1 and 2. The three experiments were carried out at an average temperature of 45^{o}C. 200g of tar sand was applied to 1000 ml of alkaline solution and sonicated for 6 hrs (Table 1, Figure 1) and 20 minutes with addition of free-radical initiators (Table 2). The bitumen was skimmed from the surface solution at intervals and oven

dried overnight under a vacuum at 50°C. The radical used in this work is a 30% hydrogen peroxide H_2O_2 from Fisher Scientific.

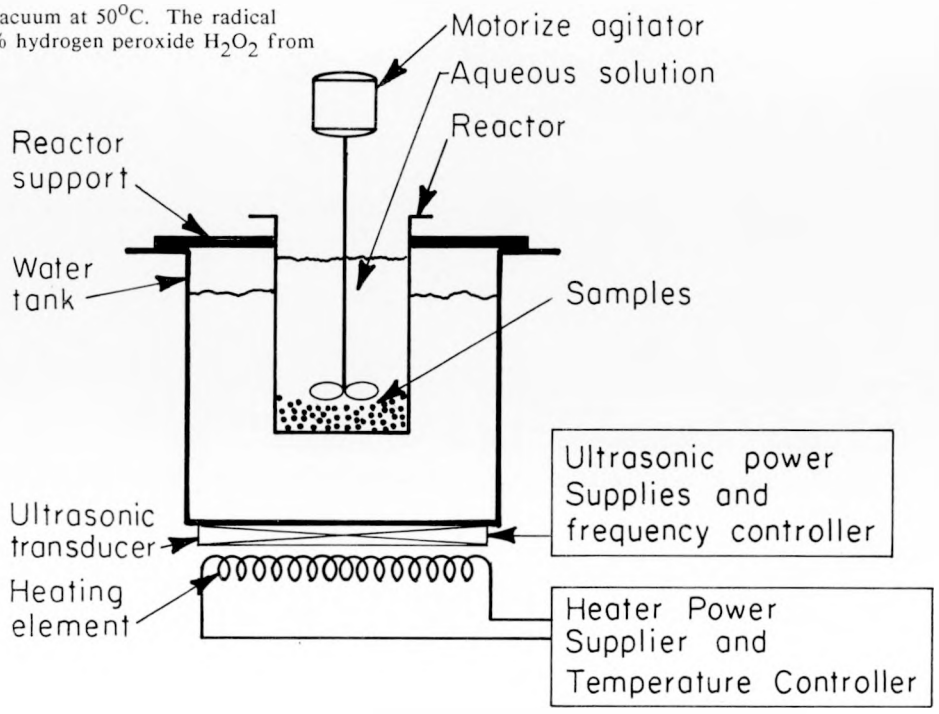

Figure 1. Laboratory set-up of the sonochemical process for recovery of hydrocarbon in natural and man-made materials.

Surfactant Formation

Tar sand samples (High Grade Athabasca Tar Sand, Sample No. 88-12, Location 23-92-10-W4M) used to make the surfactants originated from Athabasca, Alberta, Canada. The bitumen content was determined by Soxhlet extraction to be 14.5% by weight of tar sand. This surfactant was formed by using a 0.02 M NaOH solution with 5 drops of H_2O_2 to produce recovery at 20 minutes sonication time. A 90% bitumen recovery was obtained on top of the solution. The concentration of the solution was 7% organic content using the absorption technique reported previously [2]. The surfactant solution was used to recover hydrocarbon from the sources as reported below.

Sample Sources

The natural materials used in this study are as follows: Athabasca tar sand (sample No. 88-12) as previously mentioned was used again with the surfactants. Kentucky tar sand was from Logan County and California tar sand (Sisquoe) was from Santa Maria. Their bitumen/sand/water contents using Soxhlet extration with toluene are given in Figure 3. The man-made materials used are as follows: Exxon-Valdez oil spill in Prince William Sound, sample taken July 27, 1989. The soil/sand sample were from 16-20 mm deep in upper part, inner tidal zone and the other sample is contaminated plants/biomass. The last source is a contaminated soil from Company X (confidential) with petroleum. Figure 4 gives the oil/sand/water contents using Soxhlet extraction with toluene.

Experimental Runs

A control set of experiments were performed on the samples to determine the sonication time and yield of hydrocarbon recovered from each sample source. 25 g of sample were used with 100 ml of surfactants from the Athabasca tar sand (Sample No. 88-12) recovery process using NaOH solution (mentioned in the Surfactant Formation section. Also, 5 drops of H_2O_2 were added to speed the recovery rate. The temperature of solution was at 45°C with stirring at 320 rpm as shown in Figure 1.

The results are shown in Table 3, where the sonication time and recovery amount based on the organic are different for each sample. Table 4 shows where the fresh samples for Athabasca and Kentucky were soaked in the surfactant at room temperature (25°C) for 12 hours before sonication. All the samples were used as received except for the Kentucky and California tar sand. The Kentucky was sieved at 5 U.S. mesh size and the California at 20 U.S. mesh size.

In all the recovery runs, the amount of hydrocarbons floating on the surface and dissolving in the solution were taken into the total measurement. The skimmed oil from the surface of the solution was vacuum oven-dried at 50°C and weighed, while the solution concentration was measured after subtracting the initial amount of bitumen in place by using the absorption technique with a UV/visible Beckman Model 25 [1,2,6].

Light Microscopy

A Leitz SM-Lux-Pol cross polarizing microscopy was used to observe the surfactant vesicles (liquid crystal formation). The photomicrographs were taken (equipped with a high speed camera and color film using WILD MP515 Semiphotomat) of both reflection polarized light and transmittance of the incident light upon the sample. A more detailed experimental work is described elsewhere [5].

Table 1. The History of Bitumen Recovery from Athabasca Tar Sand Using Sodium Silicate Solution.

Time (hrs)	Bitumen (g)	Recovery (%)	Cum. Recovery (%)	pH	Temp. (^{o}C)
0.00	0.0000	0.00	0.00	12.05	50.0
0.50	0.4473	1.50	1.50	-	47.0
1.00	8.2402	27.65	29.15	-	40.0
1.50	0.4600	1.54	30.69	-	40.0
2.00	1.0660	3.58	34.27	-	44.0
2.50	2.4770	8.31	42.58	-	45.0
3.50	7.8600	26.38	68.96	-	47.0
4.50	5.9070	19.82	88.78	12.00	49.0
5.00	1.7062	5.73	94.51	-	50.0

* Amount of Bituminous Sand Used: 200.1g

RESULTS AND DISCUSSION

This new extraction technology is unique in that as bitumen separates from tar sand, it forms many useful by-products [1,3,5,6]. This paper discusses the uses of the self-propagated surfactants formed during the process. As shown in Figure 5, the Athabasca tar sand is a water wet sample and when sonication (rf) and alkaline solution are utilized, an upgraded bitumen, agglomerates, clean sand and clay, and surfactants are formed. For the upgraded bitumen, the average gravity of 15^{o}API is found, based on 95% cumulative recovery in the bitumen in Table 1. The Athabasca bitumen has an average value of 8^{o} API in its raw state. Agglomerates are the heavier asphaltenes and preasphaltenes that couple with the metals (Ti, V, etc.) to form charcoal-like materials that precipitate to the bottom. The clean sand and clay are both of commerical value. And last, the microemulsion of micelles to form surfactants (used in this work) have been reported previously to be stable for many years [5].

Surfactant Formation Mechanism

This process is unique in separating the asphaltene and preasphaltene from bitumen to form the upgraded asphaltene-free fractions from tar sand. Our group has previously reported (up to 50% by weight) of heavy asphaltic fractions removed from heavy crude oil using the same process described here [8]. The experimental results indicate that the surfactant formation is by specific chemical components in the bitumen that react with the base in the presence of sonication. The formation of surfactants is believed to follow a membrane mimetic mechanism [9-11,18]. The Athabasca tar sand contains bitumen that is rich in polar resin and asphaltene molecules [12]. These are "water wet" samples. These characteristics make the tar sand a perfect molecular configuration for the formation of these super-surfactants. Because the Kentucky and California tar sands are not water wet samples, surfactant formation is very slow compared to the Athabasca sample driving the process. The oil and petroleum molecules have much lower heteroatoms compared to bitumen and make it almost impossible to form surfactants with a short sonication time.

Athabasca tar sand contains about 6% heteroatoms (N,O,S) to the total bitumen. Asphaltenes in their natural state exist in micelle form, peptized with resin molecules. The center of this micelle can be either silica (or clay), or trace water, or metal (V, Ni, Fe, etc.). The important feature is that the polar groups are concentrated toward the center (oil external-water internal, or "reversed micelle"). Caviation induced by the sonication emulsification of the asphaltene and resin molecules can reorganize metal, polar and non-polar components into a continuous single phase micelle of the polar external form [13]. In membrane-mimetic fashion, a selective cation (e.g., sodium) present in the alkaline solution associates with the heterocycle center. The counter anion (e.g., hydroxide silicate) is activated and dissolves in the oil phase. In this manner, the molecule containing the heterocycle center is dissociated and any ionizable proton, such as in COOH, SH or NH, is replaced with the cation. When the surfactant migrates into the micelle, it disrupts the polar structure to form a Hartley micelle or polar-external micelle or gel or liquid crystal (Figure 6). With the aid of sonication energy, monolamellar vesicles are formed. Separation results as the micelles containing the lighter components rise to the top of the aqueous phase and release the lighter components to form a layer. The heavier asphaltenes and preasphaltenes complexed with the metals precipitate and agglomerate to form charcoal-like materials.

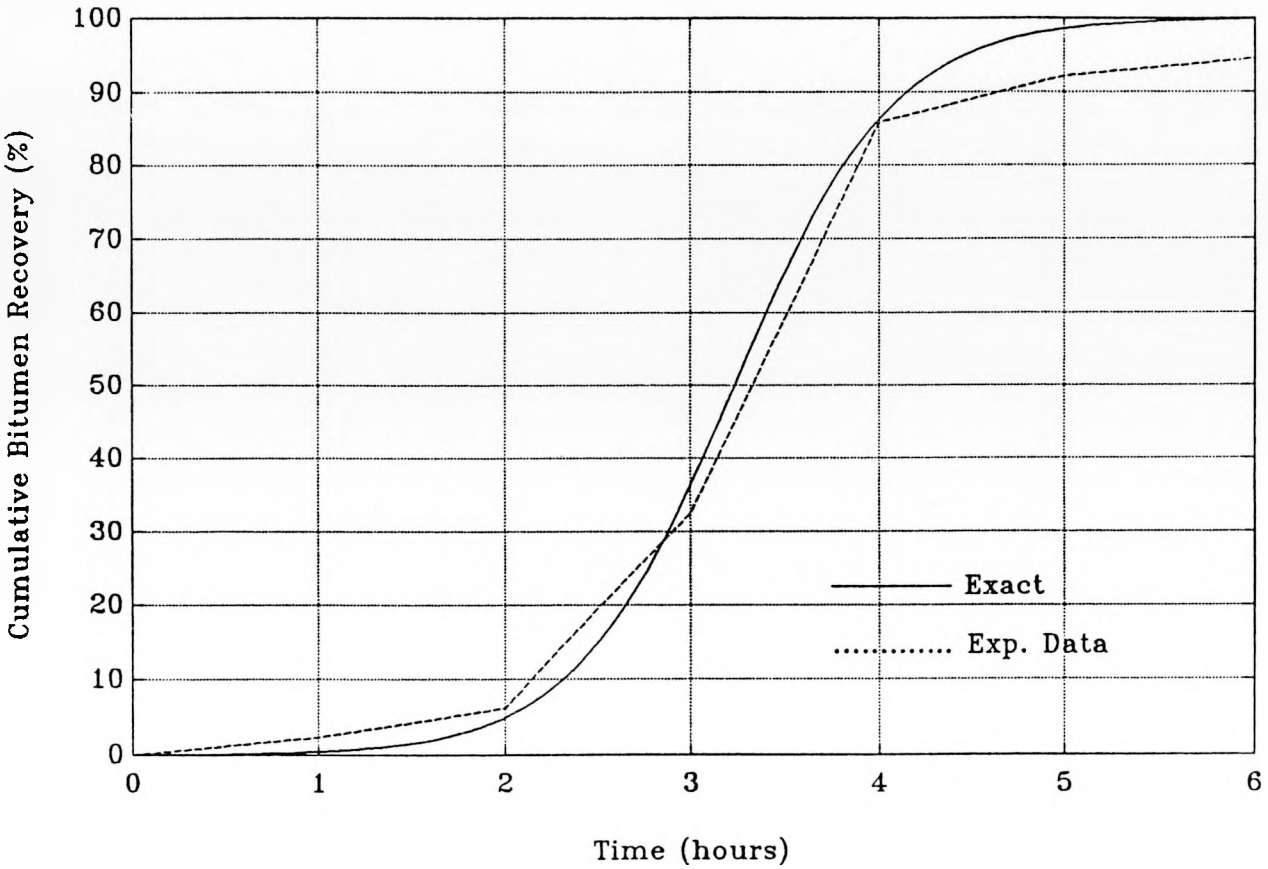

Figure 2. Recovery vs. time curve for sonochemical tar sand production process.

Sonication Phenomena

The ultrasonic vibration raises the solution temperature to 45°C [13,14], but the temperature raised has little effect on bitumen recovery [6]. A monotonic decrease in sonochemical yield is reported with increasing temperature [16]. Because sonication produces radicals, the addition of radicals (e.g., H_2O_2) enhances the reaction compared to the controlled run as shown in Table 2. In fact, the addition of a radical inhibitor (e.g., hydroquinone) slows the reaction [2]. Del Duca et al. [17] using isotopic exchange techniques, were able to establish that the water vapor molecules in a cavitation bubble were dissociated into atomic ($H^{\cdot}$) and ($^{\cdot}OH$) radicals. The monolamellar vesicles work as catalysts in carrying free radicals, such as hydrogen atoms and hydrated electrons. These radicals activate hydrogenation in the surfactant vesicle and, in turn, upgrade the bitumen to be recovered. The hydrogen formation ($H^{\cdot}$) from water be a hydrogenation process. In addition, the very low energy consumption makes sonication a new technology in fossil fuels.

Kinetic Study

To understand the rate variation of hydrocarbon separation from different sources, kinetic studies were conducted. The cumulative bitumen recovery from tar sand performed so far resembles the S-shape characteric rate curve (Figure 2). These curves refer to the amount of reagent reacted versus time in a typical autocatalytic reaction. The tow kinetic constants are the first order reaction constant and the second order autocatalytic reaction. The differential rate equation for the autocatalytic reaction can be expressed as:

$$(dX/dt) = k_1(C_0 - X) + k_2(C_0 - X)X$$

In this process, X is the amount of bitumen recovered, C_0 is the total amount of recoverable bitumen (total organics) initially present in the tar sand, and k_1 and k_2 are the two reaction rate constants. The first term on the right hand side of the above equation is the elementary first-order equation. The second term describes the autocatalytic reaction as the product of the second rate constant (k_2), the remaining bitumen in the tar sand (C_0 - X) and the amount of bitumen recovered (X). The value of the second order reaction constant (k_2) is larger than the first order reaction constant (k_1) [7]. It may be interpreted that the rate of autocatalytic reaction is quick once it begins. In other words, the first order reaction is rate-limiting. Therefore, increasing the k_1 value should lead to faster initiation and recovery of bitumen. A set of experimental data was randomly selected to do the mathematical model fitting. The reaction rate constant parameters were obtained via a minimization technique [7] and Table 1 reports the values as k_1 = 0.00104 and k_2 = 0.0803. In Figure 2, the experiment figure and the exact model curve do not fit toward the end because the solid agglomerates which were formed at the bottom of the solution were not incorporated into the recovered bitumen (surface skimmed) weight.

Table 2. The History of Bitumen Recovery from Athabasca Tar Sand Using Sodium Hydroxide and H_2O_2 Free-Radical Initiators.

Time (min.)	Control	H_2O_2 (wt. %)
0	0	0
4	6.0	28.9
8	12.3	81.1
12	26.2	86.8
16	32.3	92.0
20	37.0	94.4

Table 3. Recovery Results of this Process Applied to a Variety of Sources*.

Sample	Sonication Time	Recovery (%)
Athabasca Tar Sand (McMurray)	6 min	94
Kentucky Tar Sand (Edmonson)	2.5 hr	96
California Tar Sand (Sisquoc)	6 hr	44
Valdez Oil Spill (Soil/Sand)	10 min	95
Valdez Oil Spill (Plants)	30 min	62
Contaminated Soil (Company X)	1 hr	92

* Using Surfactants Formed from the Athabasca Tar Sand

NATURAL MATERIALS

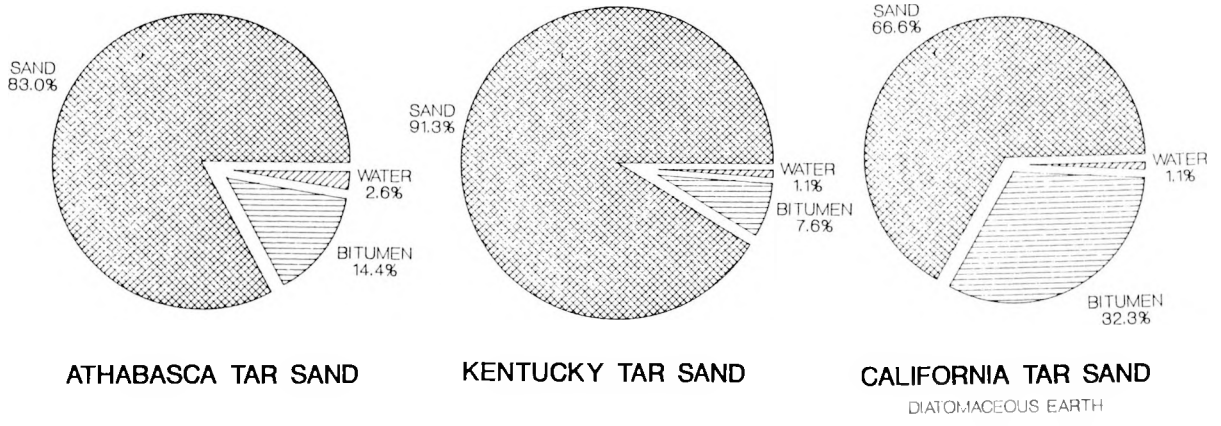

Figure 3. Composition of three natural tar sands: a) Athabasca, McMurray; b) Kentucky, Edmonson; c) California, Sisquoc.

MAN-MADE MATERIALS

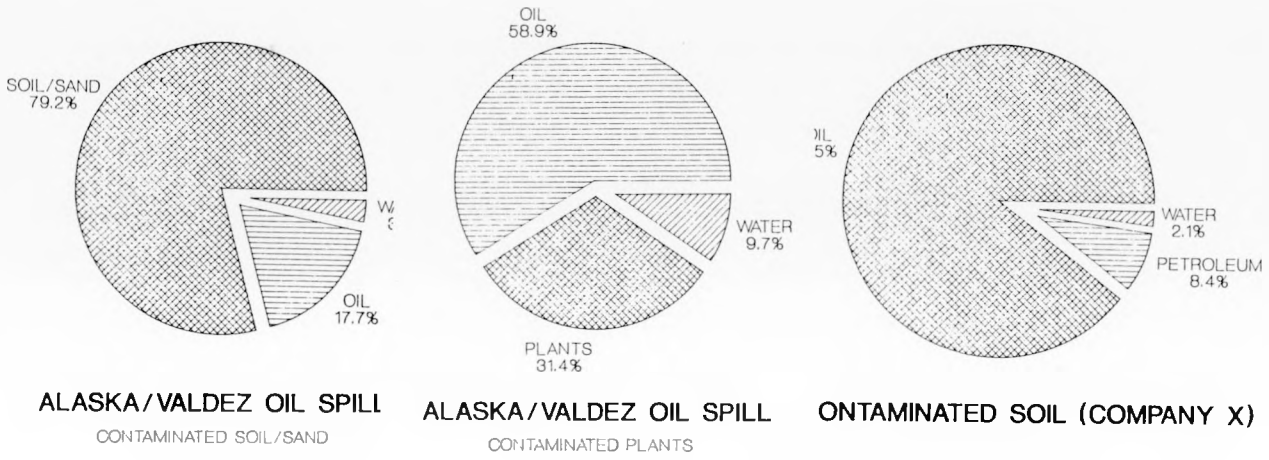

Figure 4. Composition of three man-made materials: a) oil spilled sand; b) oil soaked biomass; c) oil contaminated soil.

EXTRACTION DIAGRAM

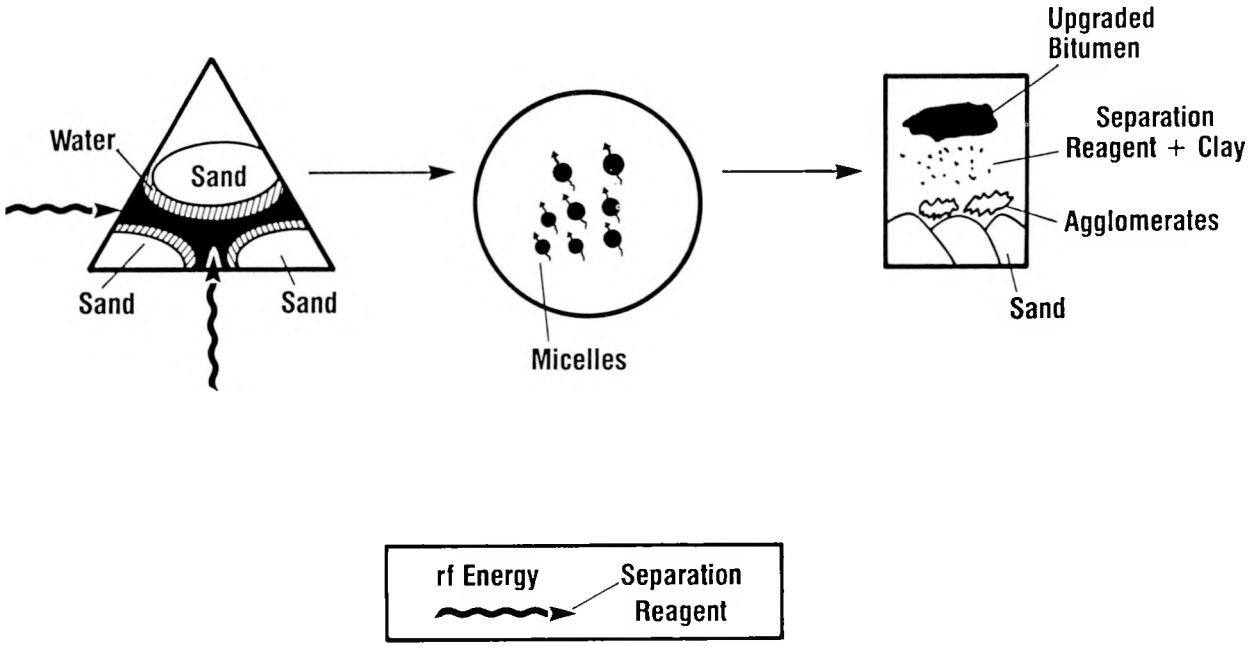

Figure 5. A sonochemical process for recovery of hydrocarbons from tar sand.

Recovery Results

Table 3 shows the results of the samples used to recover the hydrocarbons. When using the surfactants formed from the Athabasca tar sand, the recovery of the raw Athabasca tar sand reduced from 20 min (Table 2) to only 6 min (Table 3) time when sonication and H_2O_2 were applied. This shows the effects of the vesicles. To show that the optical activity and the liquid crystals formed during this process are valid, light microscopy was employed. Figure 7a (transmittance) and 7b (reflectance) show the completion of the process after 6 hours of sonication time. The emulsions are all optically active under polarized light (reflectant) showing a sign for surfactant activity. Even 4 months after the processing, the membrane-mimetic agents are osmotically active as shown in Figures 8a and 8b.

When the surfactants are utilized to extract bitumen from Kentucky tar sand, the recovery rate increases due to the sample being "oil wet". However, as shown in Figure 9a and 9b, the optical activity is still visible after the 2.5 hours of sonication. The California sample is even harder to separate due to its time in geological time of formation and the adhesive effects of the sand.

The Valdez spill (soil/sand) shows some very interesting results. Figure 10 shows the micrographs of the transmittance light on the sample after 10 min of sonication. The tremendous effect of formation of liquid crystals is evident. Very few liquid crystals were seen after hours of sonication with only 0.02 NaOH and the Valdez sample. The plant sample is harder to separate because of the adsorption of the oil to the biomass. The contaminated soil was a dry sample and the recovery rate was increased for this reason.

Table 4 shows the main body of this work, i.e., when the surfactants are made to be soaked with samples for 12 hours before sonication. As a comparison to Table 3, the time factor is reduced a great deal. This event is due in part to the generation of multiple-layered or multi-compartment surfactant vesicles (Figure 6), which aid in the separation of any hydrocarbon from adsorbed sources.

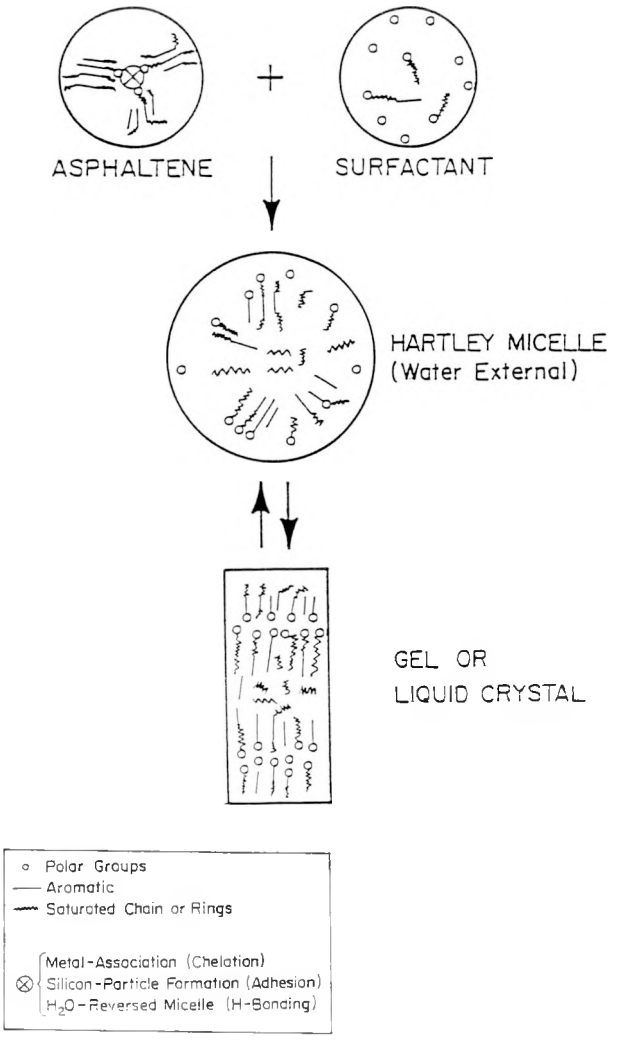

Figure 6. Rearrangement of the asphaltene micelle and the formulation of gel.

Table 4. Shortening of Treatment Time after Pretreatment*.

Sample	Sonication Time	Recovery (%)
Athabasca Tar Sand	2 min	96
Kentucky Tar Sand	20 min	94

* Soaking with Surfactant for 12 hr

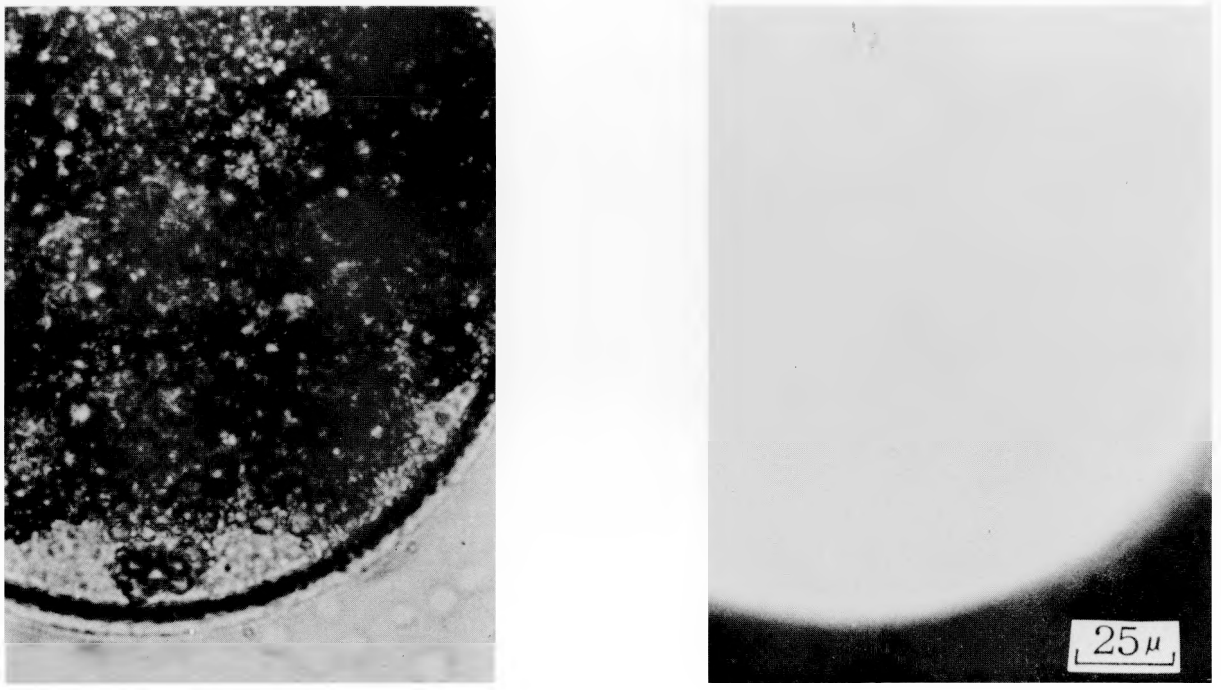

Figure 7. Liquid crystals formed after the addition of spent surfactant from raw Athabasca tar sand. a) Transmittance; b) Reflectance.

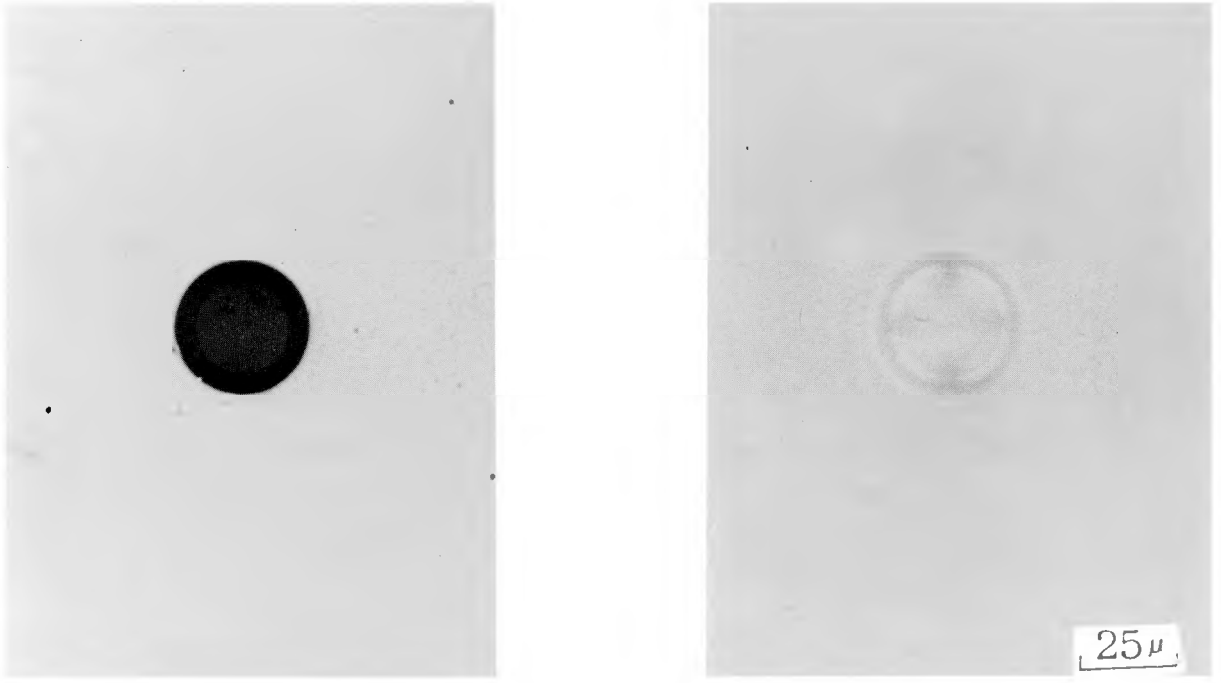

Figure 8. Liquid crystals in the suspension of the sample from Figure 7 after 4 months. a) Transmittance; b) Reflectance.

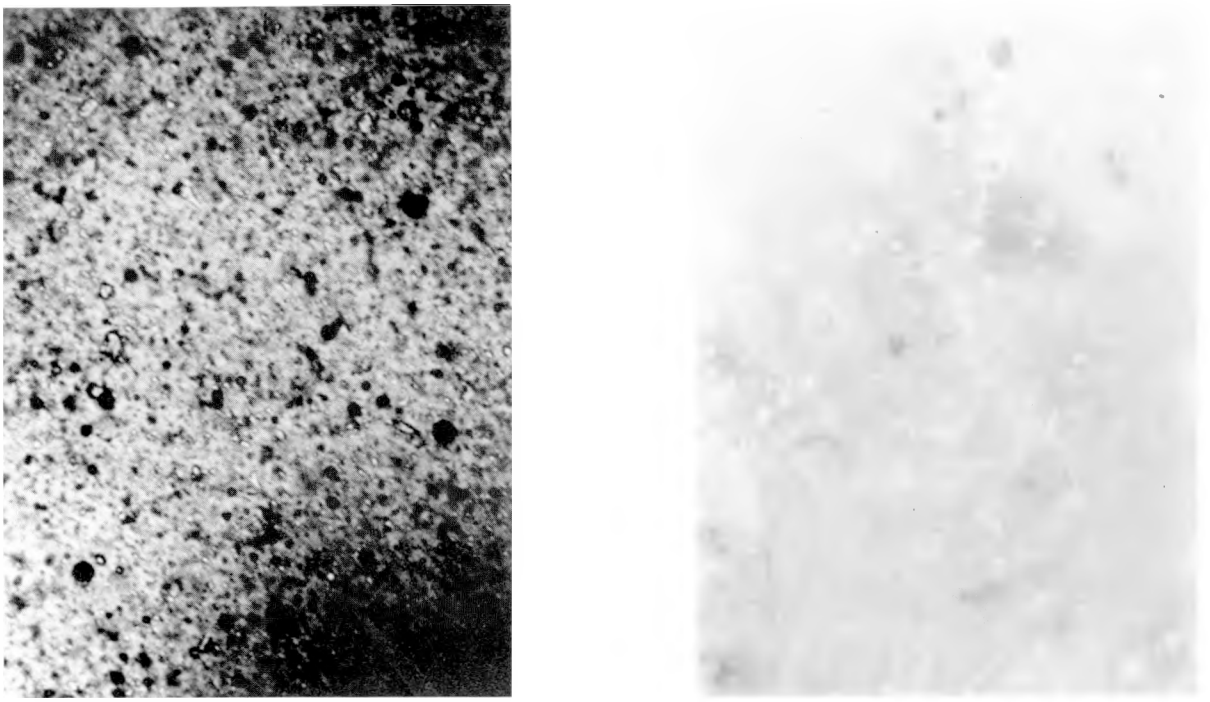

Figure 9. Optical activity for liquid crystal as found by light microscopy of a Kentucky tar sand from Logan County treated with spent surfactant. a) Transmittance; b) Reflectance.

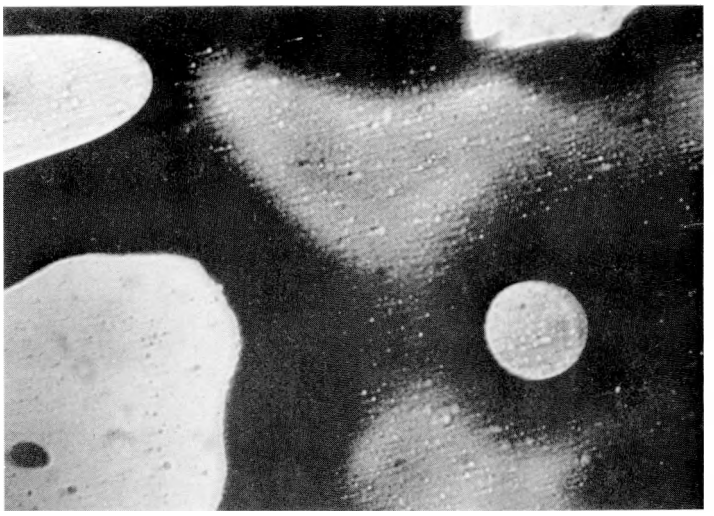

Figure 10. Liquid crystal formation of a Valdez oil spill soil sand sample after treatment with spent surfactant. (Sonication time, 10 mins.) Sample collected in Prince William Sound, Alaska.

CONCLUSION

This new process demonstrates that the application of alkaline solution medic (i.e., pH > 10) and sonication in the presence of free radical initiator (H_2O_2) will induce generations of self-propagating surfactants which could effectively extract bitumen from tar sand deposits.

ACKNOWLEDGEMENTS

We would like to thank Energy and Environment Research Laboratories, Inc., for financial support. We also acknowledge Dr. John G. Reynolds for supplying the Kentucky tar sand and Ms. Pam Grunwald for assistance with the two Valdez oil-contaminated samples.

REFERENCES

1. M.-A. Sadeghi, K.M. Sadeghi, J.-F. Kuo, L.-K. Jang and T.F. Yen, "Treatment of Carbonaceous Materials," U.S. Patent 4,765,885, August 23, 1988 (22 claims).

2. J.-F. Kuo, K.M. Sadeghi, L.-K. Jang, M.-A. Sadeghi and T.F. Yen, "Enhancement of Bitumen Separation from Tar Sand by Radicals in Ultrasonic Irradiation," Appl. Phys. Comm., 6(2), 205-212 (1986).

3. M.-A. Sadeghi, L.-K. Jang, J.-F. Kuo, K.M. Sadeghi, R.B. Palmer and T.F. Yen, "A New Extraction Technology for Tar Sand Production," The 3rd UNITAR/UNDP International Conference on Heavy Crude and Tar Sands, AOSTRA, Edmonton, Alberta, pp. 739-747, Chapter 70 (1988).

4. K.M. Sadeghi, M.-A. Sadeghi, G.V. Chilingarian and T.F. Yen, "Extraction of Bitumen from Bituminous Sands Using Ultrasound and Sodium Silicate," Khimiya i Tekhnologiya Topliv i Masel/(Chemistry and Technology of Fuels and Oils), 8, 24-28 (1988) in Russian.

5. M.-A. Sadeghi, K.M. Sadeghi, D. Momeni and T.F. Yen, "Microscopic Studies of Surfactant Vesicles Formed in Tar Sand Recovery," Oil Field Chemistry: Enhanced Recovery and Production Stimulation, ACS Symp. Ser. No. 396, Chapter 21, 393-409 (1989).

6. K.M. Sadeghi, M.-A. Sadeghi, J.-F. Kuo, L.-K. Jang and T.F. Yen, "A New Tar Sand Recovery Process: Recovery Methods and Characterization of Products," Energy Sources, 12(2) (1990).

7. R.S. Esfandiari, J.M. Sloss, K.M. Sadeghi and T.F. Yen, "Determination of Optimum Rate Constants for Autocatalytic Reaction of Tar Sand Recovery Process," (to be published).

8. A.S. Lee, X.W. Xu and T.F. Yen, "Upgrading of Heavy Crude at Low-Temperature and Ambient Atmosphere," Proceedings, The 4th UNITAR/UNDP International Conference on Heavy Crude and Tar Sand, Edmonton, Alberta, Paper No. 135 (1988).

9. J.H. Fendler, Membrane Mimetic Chemistry, John Wiley & Sons, New York, 1982.

10. T.F. Tadros, Surfactants, Academic Press, 1984.

11. J.H. Fendler, "Microemulsions, Micelles and Vesicles as Media for Membrane Mimetic Photochemistry," J. Phys. Chem., 84, p. 1485 (1980).

12. C.S. Wen, G.V. Chilingarian and T.F. Yen, "Properties and Structure of Bitumen," in Bitumens, Asphalts and Tar Sands, (G.V. Chilingarian and T.F. Yen, eds.), Elsevier Publishing Company, New York, NY, 7, p 155, (1978).

13. A.S. Lee, M.-A. Sadeghi and T.F. Yen, "The Role of Peroxides Reacting with Asphaltic Oil in Micellar Inversion Process," Preprint, ACS 21st IECEC, San Diego, CA, Aug. 25-29, 1986.

14. K.S. Suslick, Ultrasound, Its Chemical, Physical and Biological Effects, VCH Publishers, Inc., 1988.

15. J.R. Frederick, Ultrasonic Engineering, John Wiley and Sons, New York, 1965.

16. M. Ibishi and B. Brown, J. Acoustic Society of America, 41, p 3, (1967).

17. M. Del Duca, E. Yeager, M.O. Davis and F. Hovorka, "Isotopic Techniques in the Study of the Sonochemical Formation of Hydrogen Peroxide," J. Acoustic Society of America, 30(4), p 301, (1958).

18. T.F. Yen, "Application of Membrane-Mimetic Chemistry to Fossil Fuel Coversion," ACS 20th Central Regional Conference, West Virginia University, Morgantown, June, 1988.

19. A.S. Lee, M.-A. Sadeghi and T.F. Yen, "Microscopic Studies of Bitumen Derived Surfactant Vesicles," Pacific Conference on Chemistry and Spectroscopy, Irvine, October, 1987.

20. M.-A. Sadeghi, K.M. Sadeghi, J.F. Kuo, L.-K. Jang and T.F. Yen, "Sonication Method and Reagent for Treatment of Carbonaceous Materials, U.S. Patent 4,841,131, Jan. 2, 1990 (38 claims).

21. R.S. Ramalho, Introduction to Wastewater Treatment Process, 2nd ed., Academic Press, 1983, p. 566.

Selection, Design, and Scale-Up of Equipment to Extract Bitumen from Tar Sands

by

W. Roy Penney and Richard Ulrich
Department of Chemical Engineering
University of Arkansas
Fayetteville, Arkansas 72701

Abstract. Extraction equipment for solvating bitumen from tar sands must satisfy certain process requirements, including:

- agitation of solids (fed from the mining and the crushing operations) to effect dissolution of interstitial bitumen and release individual grains of sand,
- wash the sand free of bitumen to prepare the sand for solvent recovery, and
- isolate any fines from the solvated bitumen phase and wash them in preparation for solvent recovery and eventual environmentally acceptable disposal, either alone or with the clean sand.

Many different processing schemes have been proposed for solvent extraction of the bitumen and all of them in some fashion effect countercurrent flow of the solvent and sand. These schemes include:

- a series of sloped vessels containing augers,
- a series of rod or ball mills,
- a countercurrent moving bed in a vertical vessel,
- a compartmented, agitated, vertical vessel,
- rotary drum mixer followed by countercurrent washing of sand in moving beds,
- a series of agitated vessels and screens,
- an agitated vessel followed by a countercurrent wash in a series of hydroclones.

The potential advantages and disadvantages of all these are discussed along with selected other schemes.

The handling of fines which could remain with the solvent-bitumen phase is an important consideration. An inclined plate gravity settler or a disk centrifuge are logical choices to contain fines within the extraction system. Means of handling fines, either for separate discharge or co-discharge with the sand, are discussed.

Introduction

A Process Flow Schematic of a process for solvent extraction of bitumen from tar sands, which produces a solvated bitumen stream and a clean sand stream, is presented as Figure 1. Other processes using other equipment can be utilized to produce equivalent results; however, most of the processing requirements will be independent of the processing scheme or the processing equipment. For purposes of establishing a benchmark process it will be helpful to briefly describe the process depicted in Figure 1. A description of the process follows:

1. The crushed sand is auger-fed from a surge bin into the extraction vessel.

2. The crushed sand is dropped from the surge bin through an inerted purge column to prevent explosive air-hydrocarbon mixtures in the extraction vessel headspace.

3. The bitumen is solvent extracted from the tar sand in the agitated extraction vessel.

4. The sand-solvated bitumen slurry is pumped to the gravity wash column where a countercurrent flow of clean solvent washes essentially all the bitumen from the sand.

5. The compacted mixture of sand and solvent in the bottom of the wash column is auger fed to a flash dryer where the solvent is vaporized from the clean sand.

6. The sand from the flash dryer is discharged through an inerted purge column to prevent organic vapors from exiting the dryer system with the sand.

7. Any sand fines are kept within the wash column by use of an inclined plate solid-liquid separator installed on the solvated bitumen stream exiting the washing system.

Let's now consider the process requirements for any system which produces both a solvated bitumen stream and a clean sand stream in a safe and environmentally acceptable manner.

Process Requirement for Extraction and Sand Washing Systems

A successful system should satisfy several process requirements:

1. Allow the crushed tar sand to enter the system while controlling atmospheric emissions of controlled pollutants below allowable limits.

2. Dissolve the interstitial bitumen and release individual sand particles.

3. Agitate tar sand particulate feed while the bitumen is being dissolved to prevent clogging of the extractor with the tar sand feed.

4. Wash the sand free of bitumen to maximize bitumen yield and minimize the handling and environmental problems inherent in effluent sand which has a significant bitumen coating.

5. Prevent the fine solids from contaminating the bitumen product by (a) keeping the fine solids within the extraction system so that they exit with the sand or (b) separate the fines in a separate step and dispose of them separate from the sand.

6. Remove the solvent from the sand after the solvent-sand mixture is discharged from the washing system.

7. Discharge the clean sand from the solvent removal system while minimizing emissions of controlled pollutants to the atmosphere.

8. Handle the abrasive sand solids successfully.

9. Maintain a pumpable slurry in the extraction vessel.

Equipment Utilized for Extraction (i.e., dissolution) of Bitumen from Sand

Typical extraction equipment is:

1. Ball or Rod mills (Figure 3).

2. Augers in Tubes (Figures 7, 8 & 10; appendix A - Hildebrandt & Screw Conveyor type).

3. Agitated Vessels (Figures 1, 3a, 6 & 8).

4. Trayed Towers with Rotating Scraper Blades (Appendix A - Bonnoto type).

5. Vertical Towers with Liquid Fluidized Beds of Solids (Figures 9 & 10).

6. Moving Basket Extractors (Appendix A - Bollmann type & Appendix B - Rotocel unit).

A key economic consideration is the crushing requirements for the feed. Grinding expense rises rapidly as the particle size goes below 1/2 inch. The ability to handle large particles of feed probably decreases from equipment items 1 to 6 with mills able to handle about 2" size, augers about 1" size, agitated vessels about 1/2" size, with grinding below 1/2" necessary for 4, 5 and 6. Grinding requirements must not be ignored in selection of the extraction equipment.

Mechanical integrity of the equipment is a key consideration. The sand is very abrasive and chunks of bitumen could easily damage an agitator, auger or scraper blade. Agitated vessels can be obtained with elastometric linings and with elastometric coatings on agitators; such linings and coatings help considerably to minimize abrasion damage. The vertical towers could be prone to pugging because certain tar sands are sticky and tend to agglomerate when the bitumen is partially solvated.

Equipment Utilized for Washing of Sand

After the bitumen is dissolved by the solvent from the sand, the sand must be separated from the solvated bitumen. For most tar sands the sand particles are so small that washing on solid-liquid separation equipment such as belt filters and sold-bowl centrifuges is not a practical means of removing the dissolved bitumen from the sand particles. The practical alternative for tar sand solids is to use a washing system where the sand solids flow counter-current to a fresh stream of solvent. The fresh solvent then washes the sand essentially free of bitumen and the sand exits the washing system wetted with fresh solvent. The solvent can then be removed from the sand in a solvent dryer.

Equipment which will provide counter-current washing is:

1. Ball mills in Series (Figure 3).
2. Hydroclones in Series (Figures 4, 5 & 6).
3. Series of Slanted Augers in Tubes (Figures 7, 8 & 10; Appendices A - Hildebrandt and Screw Conveyor type and Appendix D).
4. Trayed, Scraper Type (Appendix A - Bonnoto).
5. Moving Basket (Appendix A - Bollmann & Appendix B - Rotocel).
6. Vertical Towers (Figures 9 & 10).

Each of these alternates will provide counter-current washing, which is necessary to remove the bitumen (1). There are two key considerations for selection, scaleup and design:

1. The efficiency of washing, i.e., how much clean solvent is required to achieve a given level of bitumen removal? and
2. Difficulty of scaleup. Stated another way - how predicable is scaleup?

At present the technology does not exist to predict either efficiency or scaleup for 4, 5 or 6 above. Consequently, extensive experimental work will be required. Preliminary design can be done for 1, 2 and 3. From qualitative considerations the following will give guidance in selecting the best washing system;

- Ball mills in series can handle large particulate feed, the washing efficiency can be predicted; but the equipment is inherently expensive and requires maintenance.
- Hydroclones are used extensively for washing solids in a very predicable fashion; they can be obtained with rubber linings; but the pumping requirements are relatively great.
- A series of slanted augers in tubes will perform predicably but abrasion could cause maintenance problems.
- The trayed scraper types are mechanically complex, could abrade rapidly and prediction of the effect of interstage backmixing on washing efficiency during scaleup is difficult.
- Moving basket types perform very well for flaked oilseeds but the sticky tar sand might cause plugging problems.
- Vertical towers are difficult to scaleup from a backmixing standpoint.

Control of Air Emissions

For any hydrocarbon-based solvent extraction process air emissions control is going to be a key consideration affecting both design and operation of the facility.

Fugitive emissions from pipe flanges, rotating shaft seals, etc. can be handled with well-known and widely-used design and operational techniques. However, the point source emissions as the tar sands feed enters the extraction system and as the clean, spent sand exits it are particularly troublesome because the control techniques are not well established and the applicable techniques vary with the handling characteristics of the solids.

Volatility of Solvent. The volatility of the solvent has a large impact on the potential organic emissions to the atmosphere, the inherent safety of the process and on the energy requirements for the process. For safest operation and easiest emissions control a solvent of low volatility is desired, especially in the extraction portion of the process. But, for easiest solvent removal from the sand (and, consequently, minimum energy usage) a solvent of high volatility is desired. To determine the best solvent requires careful analysis; however, qualitatively it is probably best to select a pure solvent (with very few high boiling impurities) with a saturation temperature between 200 and 300°F at standard conditions.

Emissions Control at the Solids Feed End of the Process. Without going into much detail, some common control techniques are:

1. Auger the feed from a surge bin into extraction:

   - Purge the interstitial air entering the extraction vessel through a condenser, scrubber, adsorber, incinerator (perhaps a power boiler) etc. Air then exists in the vapor space within the extraction system; this creates potential explosion hazards.

   - Place a purge column between the feed surge bin and the extraction vessel. Use augers or rotary valves to isolate the purge column from the surge bin and the extraction vessel. Introduce an inert gas at the bottom of the column and take it out the top. By this means air can reasonably be excluded from the extraction system (see Figure 1).

   - Enter the feed through a purged lock-hopper.

Emissions Control Where Spent Sand Exits. The problem of control is different here than at the solid feed entrance because the interstitial spaces within the bulk solids contain hydrocarbon vapors; thus the gas phase within the solids must be replaced with an environmentally acceptable gas prior to discharge to the atmosphere. Some alternates for accomplishing this are:

1. Drop the sand through a purge column. The inert gas purge sweeps the hydrocarbons out the top of the column to an emissions control system.

2. Purge the center of an auger conveyor to sweep the hydrocarbon vapor back into the process.

3. Use a flip-flop valve with a purge between upper and lower butterfly valves.

4. Convey the solids with air to dilute the hydrocarbons. Separate the air and send it to an incinerator, preferably a power boiler.

5. Use steam to strip the hydrocarbons from the sand, condense the steam and separate the hydrocarbon from the condensate. This scheme is normally most economical if the hydrocarbon is almost insoluble in water so that a phase separation can be used to separate organic from water.

Sand Cleanup

Reasonable alternates for removing the last solvent from the sand are:

1. Indirectly heated units (Figure 6),
   a. a flash dryer (Figures 1, 10),
   b. a dilute-phase, mechanically-agitated unit such as a Solidaire unit,
   c. a dense-phase, mechanically agitated unit such as a Holoflight processor.

2. A steam stripper (Figures 2, 7 & 9; Appendices C & D).

3. Displacement of the organic from the sand by washing with water.

In the literature steam stripping is the most prevelant method mentioned to remove the hydrocarbon from the sand. Steam stripping has an advantage in that the steam can be condensed and, provided the solvent is sparingly soluble in sand, a simple phase separation will ready the water for feed to the steam generation system. The use of steam is ideal for discharging the solids directly to the atmosphere without any inert purge. With dryers which contain essentially a pure solvent atmosphere, the solids must be purged with inerts (as indicated earlier, steam is a good choice) prior to exiting the drying system.

Keep Sand Fines Out of Bitumen Product

As the solvent exits the extraction system to go to solvent recovery the fines must be removed. Parallel plate gravity settlers or disk centrifuges are probably the equipment of choice. With parallel plate gravity separators the solids will be kept within the extractor/washer and will exit with the sand. With centrifuges the fines can be concentrated to the point that they could be sent to a separate drying system or could logically be sent to a power boiler for inceneration.

References

1. Kenchington, Jim and C. R. Phillips, "Operating Cost Parameters in Solvent Extraction of Bitumen from Oil Sand Mineral Deposits," Vol. 5, No. 4, p. 317, Energy Sources (1981).

2. Sparks, B. D. and F. W. Meadus, "Combined Solvent Extraction and Agglomeration Techniques for the Recovery of Bitumen from Tar Sands," p. 55, Energy Processing (Canada) Sept.-Oct. (1979).

3. U.S. Patent Numbers are given on Figures 7, 8, 9 & 10.

4. Appendices Material taken from:

   Appendix A - Encyclopedia of Chemical Technology (see page A-1),

   Appendix B - Chemical Engineering Magazine (see page B-1),

   Appendix C - Cresset Corporation Brochure (see page C-1),

   Appendix D - Paper by K. O. Graves and L. Hastings (see page D-1).

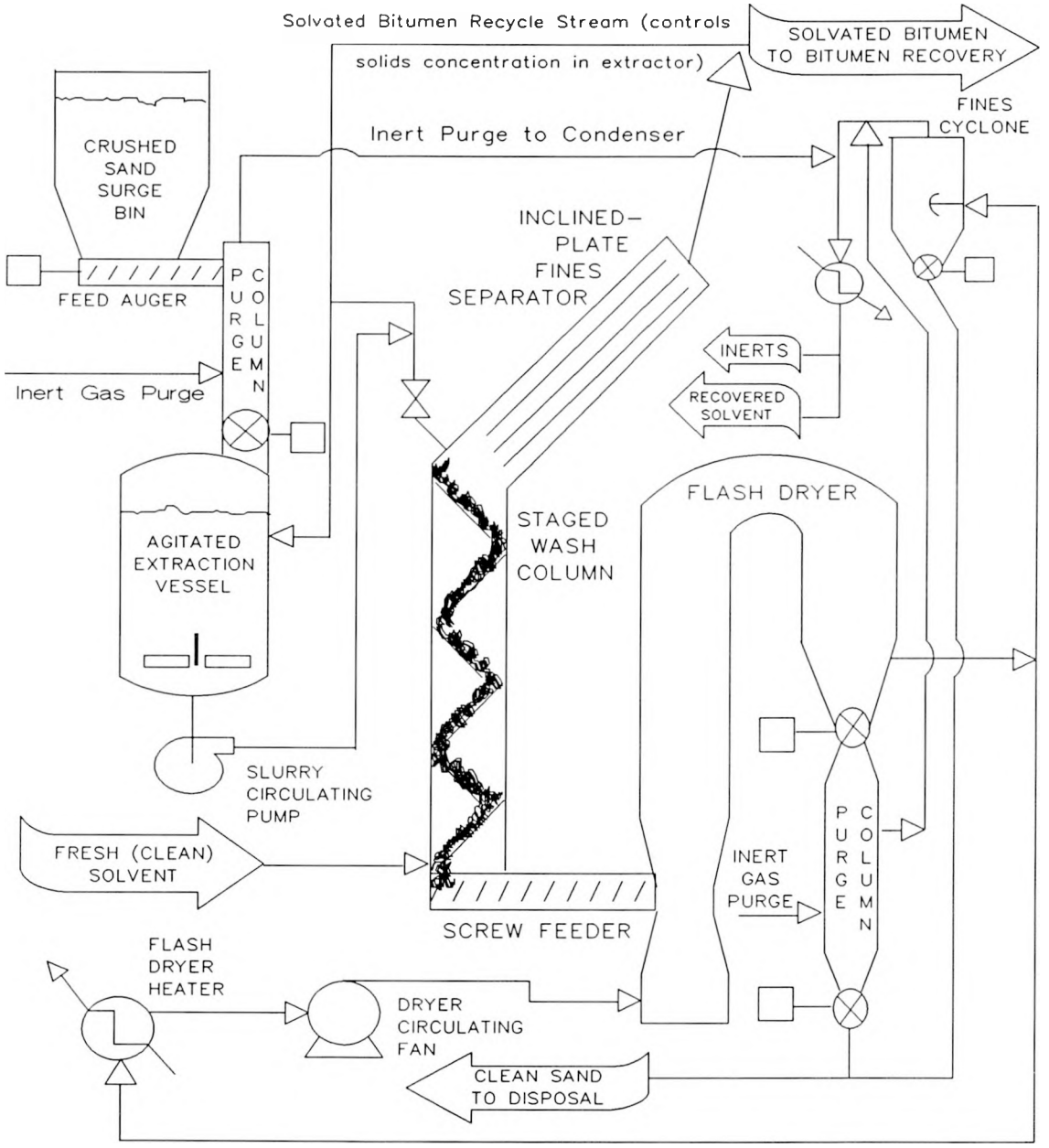

Figure 1. Illustrative Process Flow Scheme of an Extraction System for Recovering Bitumen from Tar Sand and Producing Clean Sand for Disposal

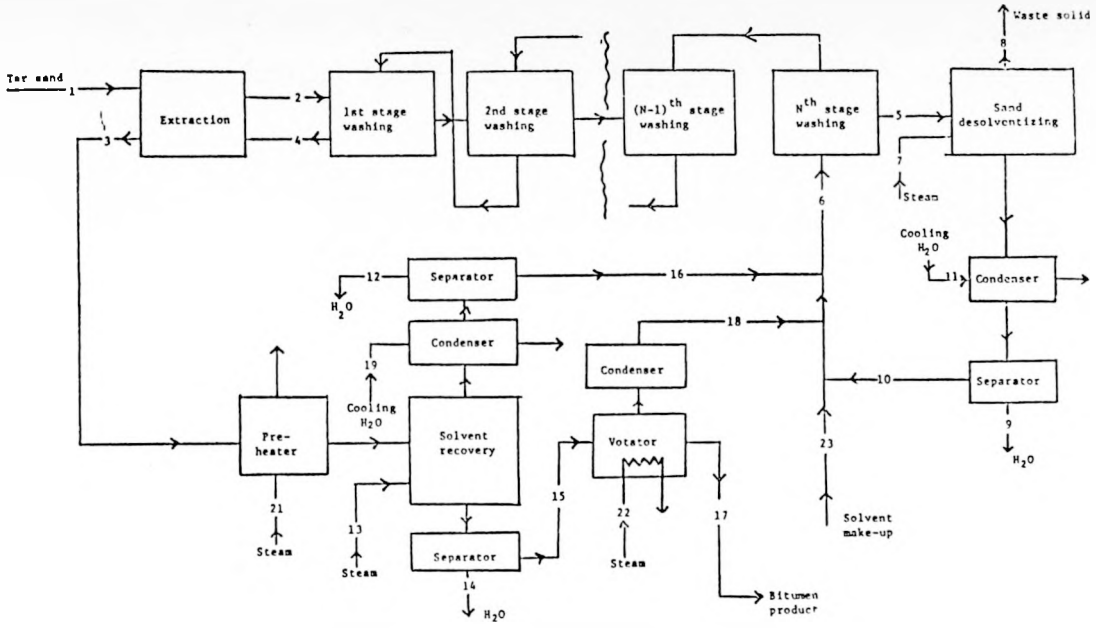

FIGURE 2. Flow sheet of proposed solvent extraction process.

Figure 2. Flow Sheet Illustrating Extraction, Counter-Current Multi-Stage Washing and Sand Desolventizing (from Ref. 1)

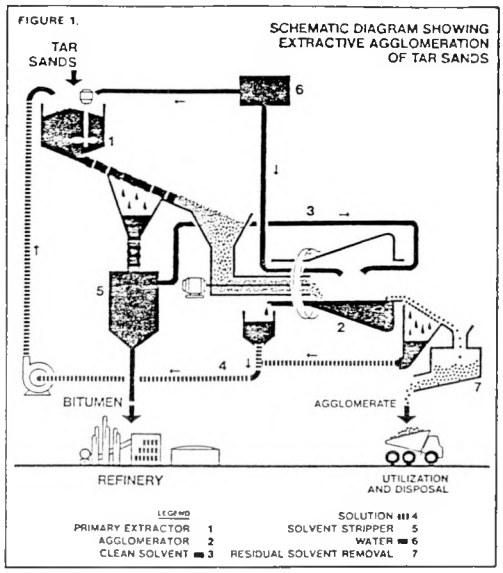

3a. Two-stage w/mixer and rotary drum.

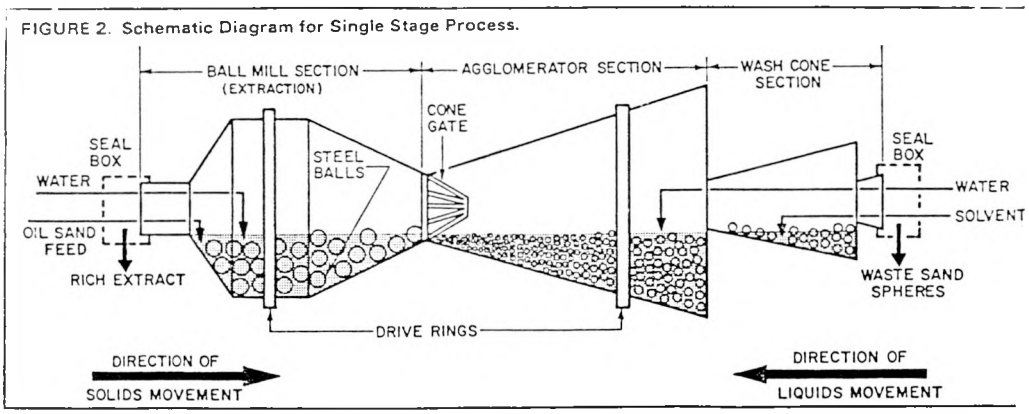

3b. Single-stage with sequential rotary drums.

Figure 3. Solvent Extraction Processes Using Agitated Vessels, Screens, and Ball Mills (from Ref. 2)

A SOHIO COMPANY
DORR-OLIVER
A step ahead in process equipment

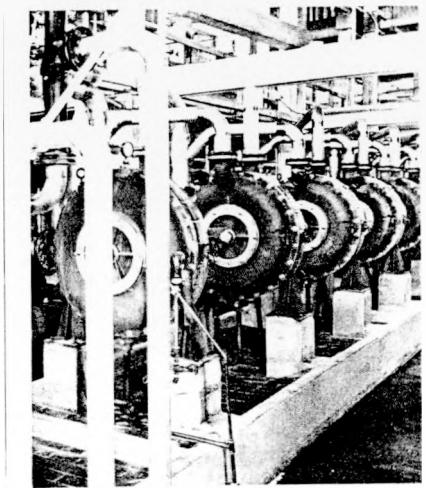

Countercurrent washing.

Definition. Removal of solubles from a slurry.

Range of Application. Slurry is concentrated. Then diluted with liquid containing a lesser concentration of solubles. And then reconcentrated. This process is repeated in several stages to remove the bulk of the soluble bearing liquor.

Majority of washing operations are accomplished in 3 to 20 stages countercurrently. Overflow from each following stage is used as dilution for the feed in the preceding stage. Wash liquid is introduced at the end of the process to provide last stage with cleanest wash. And works its way through the system to discharge with maximum solubles in the first stage overflow.

This process may also be used to eliminate traces of fines or contaminating solids.

Advantages. More economical than costly centrifuge stations. Easily controlled. Can be designed for optimum performance using computer program.

Limitations. Virtually none. Extreme effectiveness is possible with sufficient stages.

Typical materials processed.

Starches, including modified high purity gypsum from phosphoric acid, citric acid or titanium dioxide
Salt from brine
Crystals
Kaolin

BULLETIN DC-2

Typical flow sheets

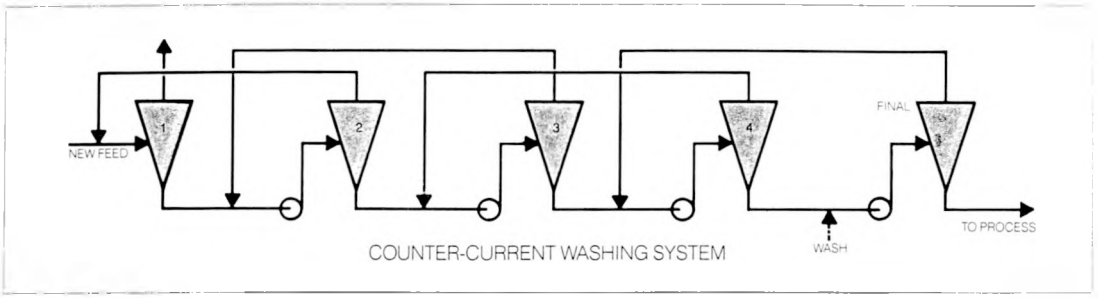

Figure 4. Counter-Current Solids Washing System Using Hydroclone Stages in Series

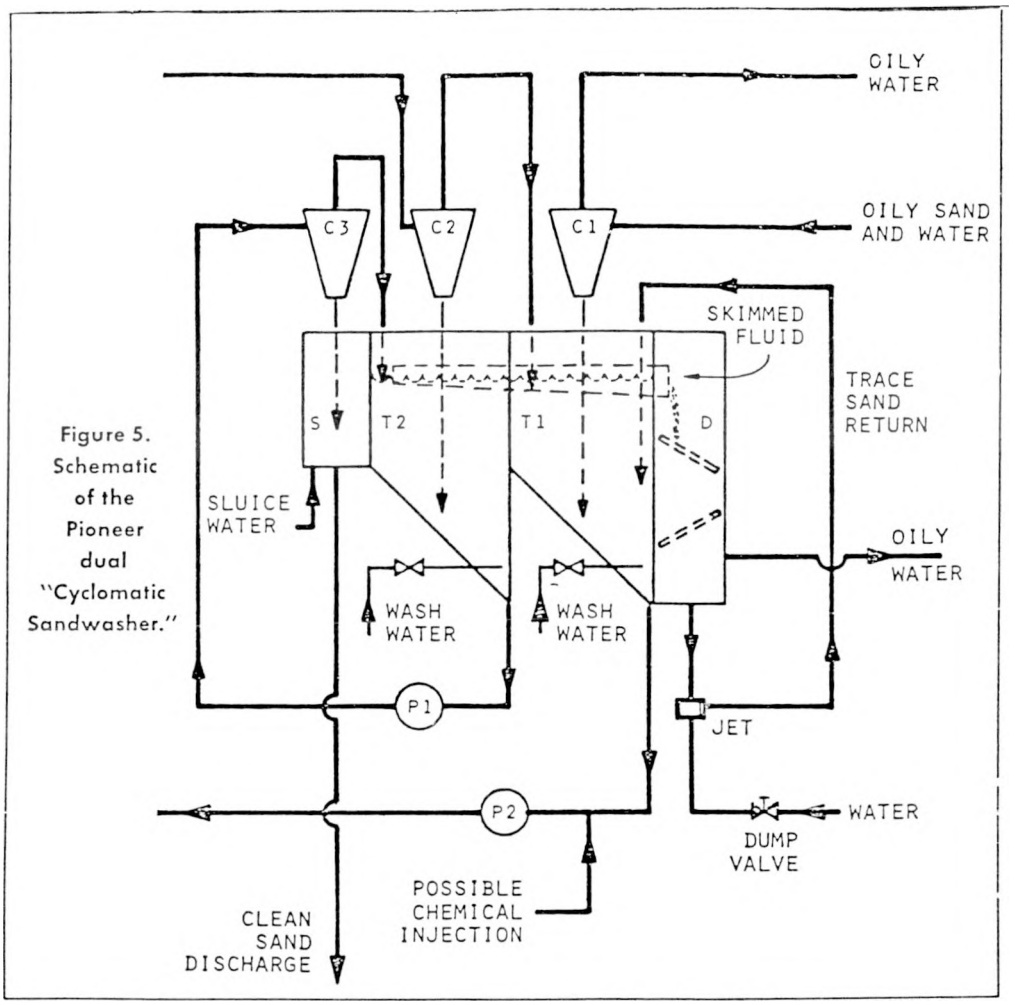

Figure 5. Schematic of the Pioneer dual "Cyclomatic Sandwasher."

Figure 5. Counter-Current Sand Washer Using Hydroclones "Cyclomatic Sandwasher" by Pioneer Centrifuging Co., Houston, TX

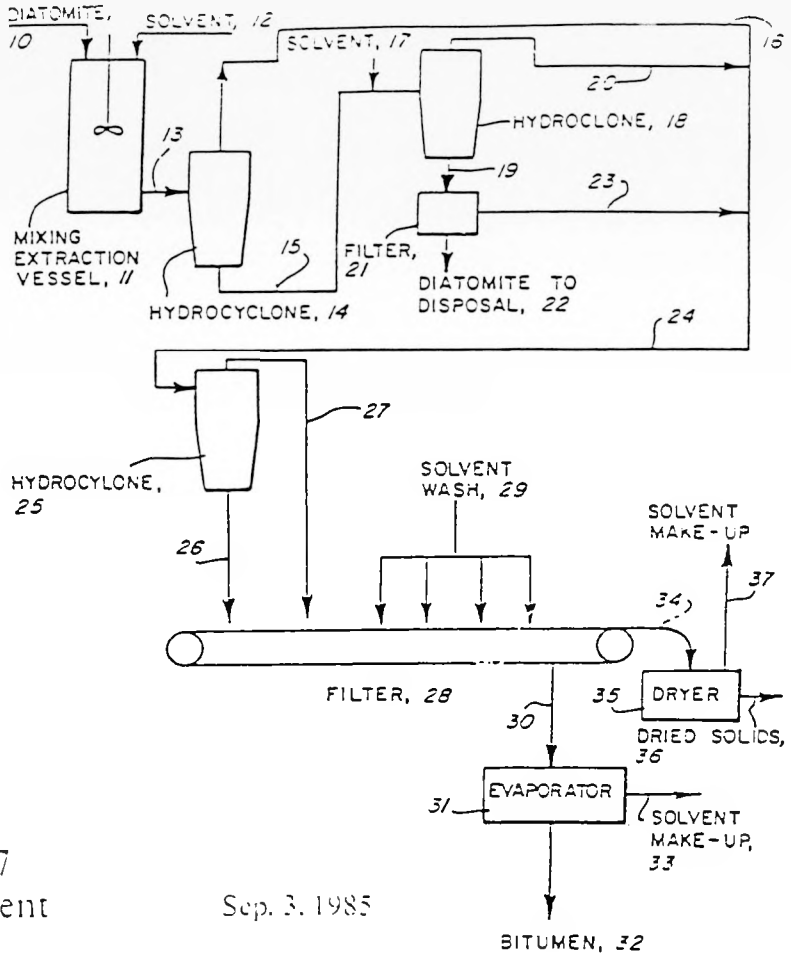

4.539.097
U.S. Patent Sep. 3, 1985

NOTES:
1. Mixing vessel used as primary extractor.
2. Dryer used to remove solvent from spent solids.

Figure 6. Extraction System Making Use of Hydroclones and Wash on Belt Filter for Counter-Current Extraction

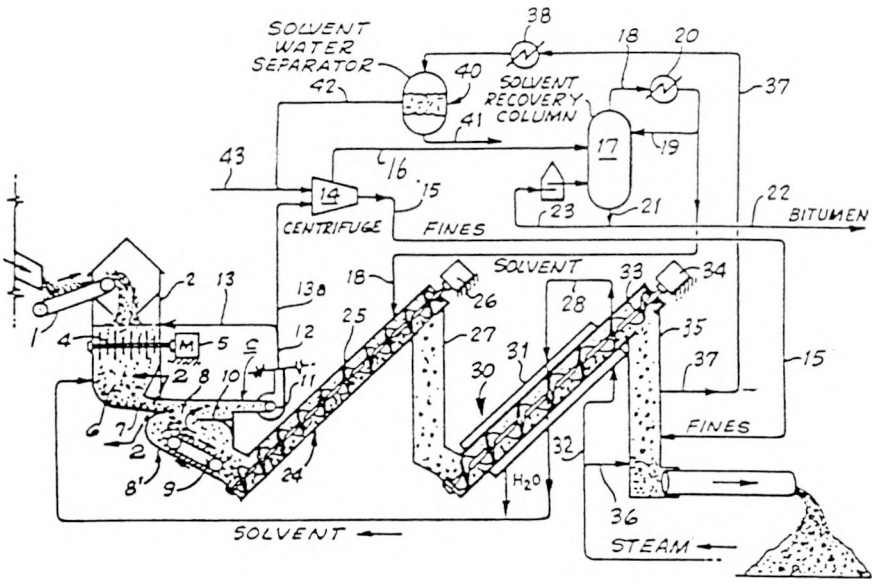

Notes:
1. Sand is made solvent-free by stripping with steam.
2. A centrifuge is used to separate the fines from the rich solvent stream.
3. No means shown to limit emissions to the atmosphere.

Figure 7. Counter-Current Extractor Using Slanted Augers to Move Solids Counter to Solvent

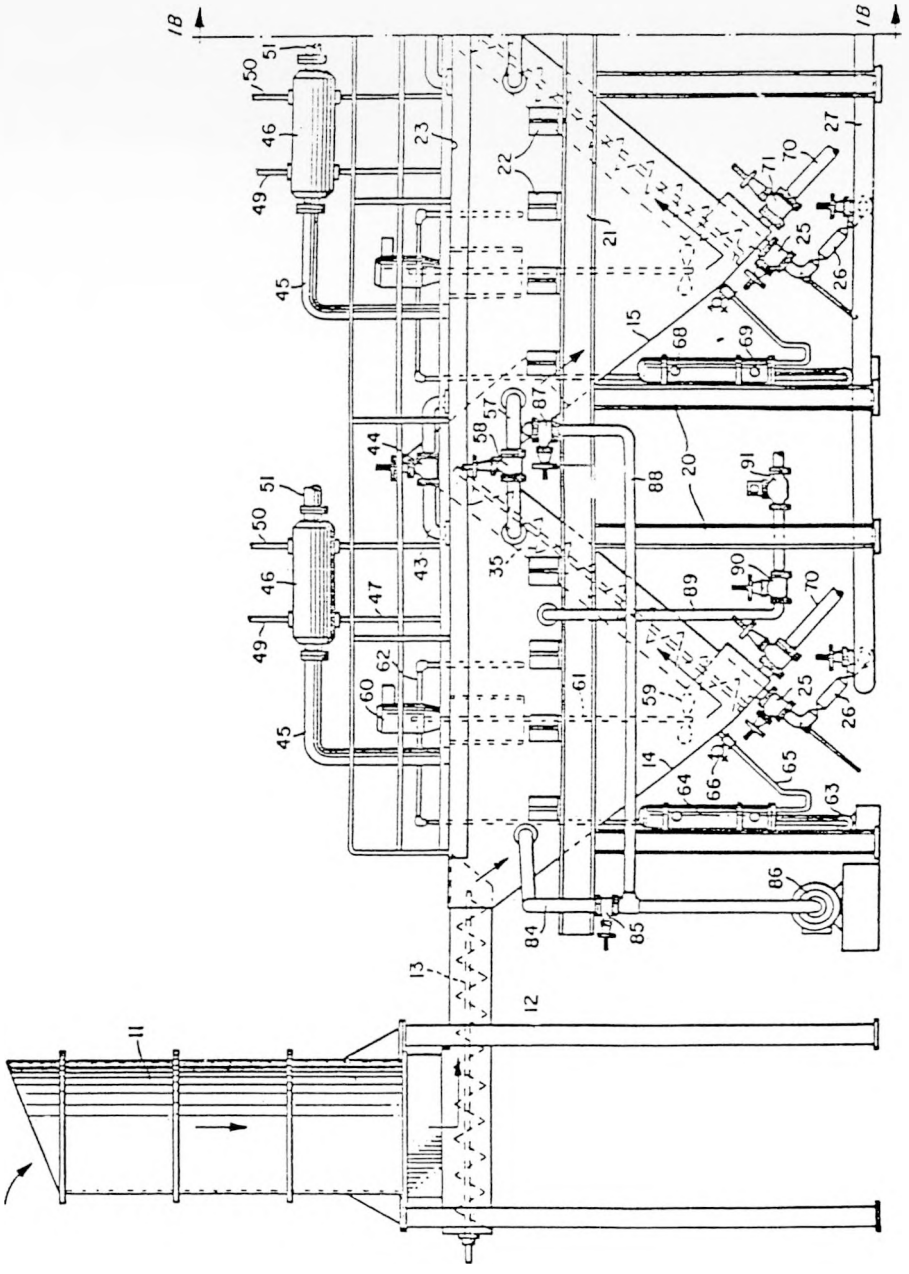

Figure 8. Counter-Current Extraction by Sloped Augers Conveying Solids Out of Vessel Counter to Solvent Flow

NOTES:
1. Auger Feed of Tar Sand.
2. Auger Discharge of Clean Sand
3. Steam Stripping of Solvent from Sand in the Bottom of the Column.

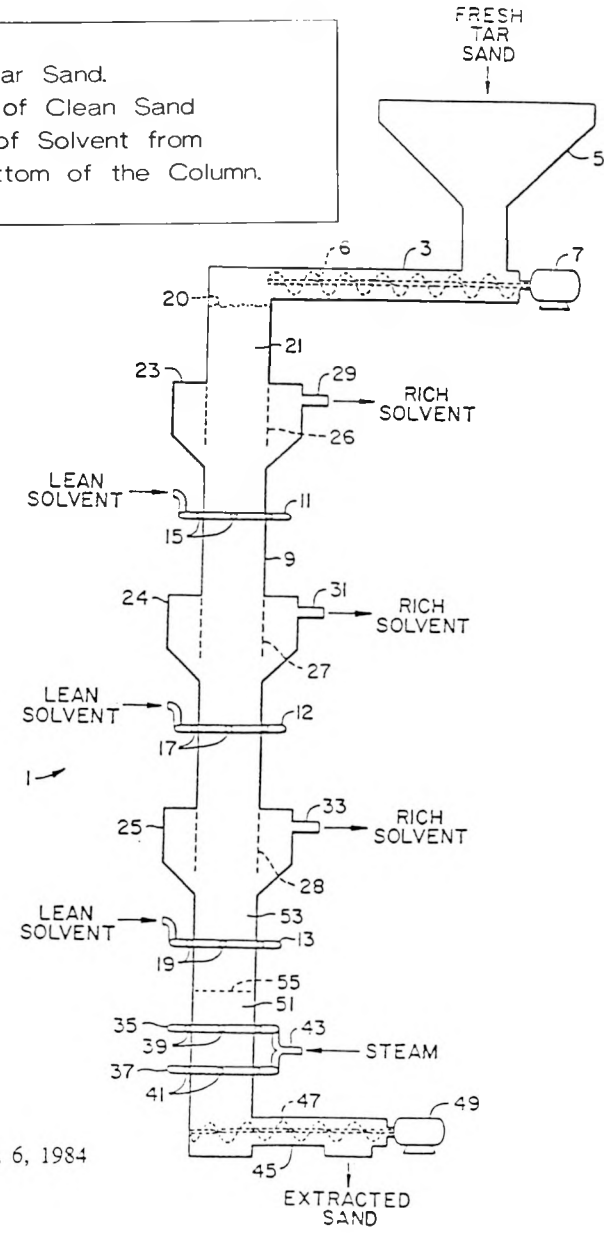

U.S. Patent Nov. 6, 1984 4,481,099

Figure 9. Vertical Tower Extractor. Gravity Downflow of Sand Fluidized by Solvent Flow.

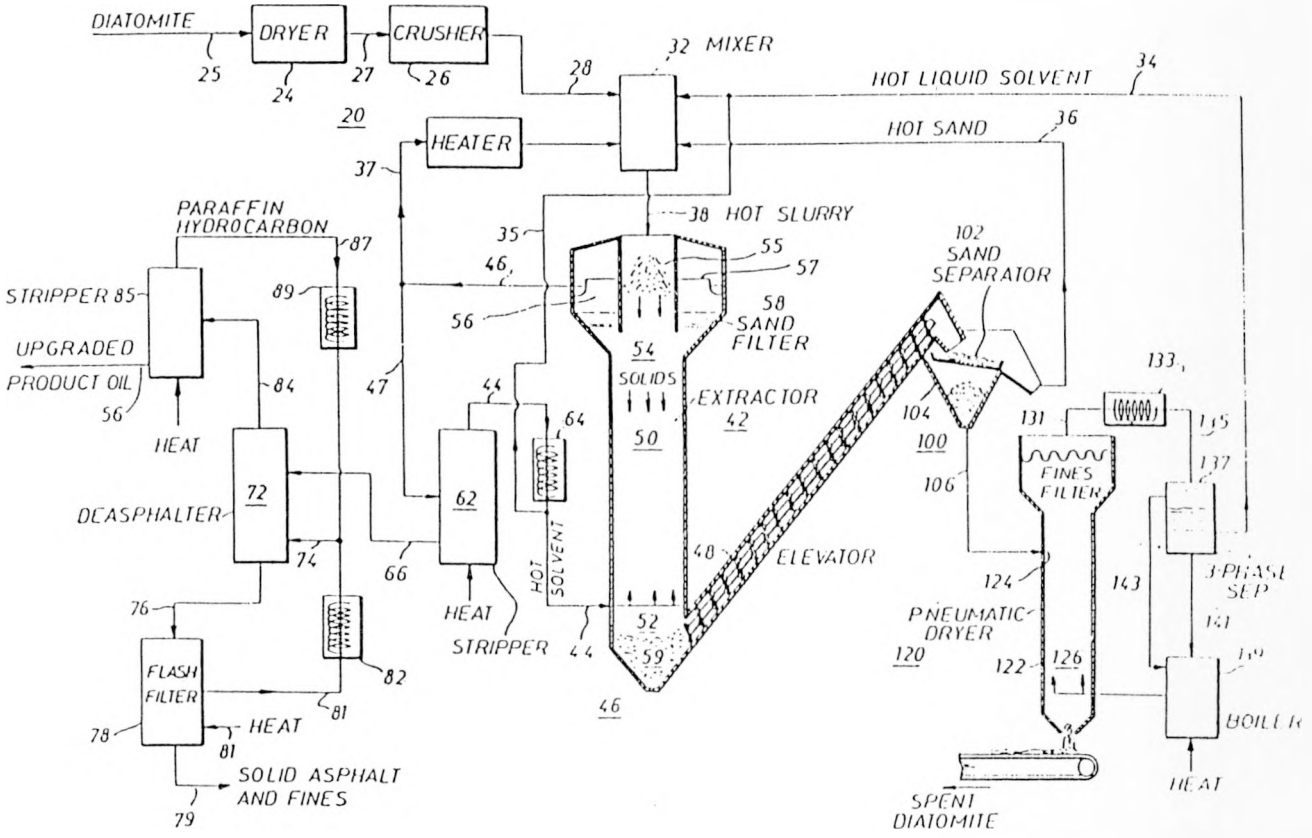

Figure 10. Counter-Current Extraction by Gravity Flow of Solids Down Vertical Vessel. Solids Conveyed Out Above Solvent Level in the Extractor

The Role of Organic Matter Complexes In Oil Sand Processability and Sludge Formation

by

L.S. Kotlyar and B.D. Sparks
Division of Chemistry, National Research Council
Ottawa, Ontario CANADA K1A 0R9

Abstract. Presently hot water extraction technology is being used in Canada to separate bitumen from oil sands recovered by strip mining. Unfortunately, Canadian oil sands deposits contain appreciable amounts of fine solids which, during processing, form an aqueous dispersion containing a significant amount of bitumen. This dispersion eventually stabilizes as a highly structured sludge which resists compaction, even during prolonged storage. It has been observed that considerable quantities of strongly bound organic matter (SOM) are associated with certain well defined solids fractions that can be separated from the sludge. These fractions which have also been observed in unprocessed oil sand feed samples are believed to play a role, not only in the processability of oil sands feed, but also in the intractability of sludge with respect to its compaction and settling properties. Consequently, it is desirable to gain a deeper insight into the nature of these components in both oil sand feed and sludge, in order to better understand their involvement in sludge build-up.

Introduction

The ease of bitumen recovery from oil sands by Hot Water Extraction depends upon the surface properties of the components, especially the water wet character of the clay and sand particles[1-3]. Oil wetting of some of the oil sands solids is caused by the presence of strongly bound organic matter (SOM) which cannot be removed by extraction with good solvents for bitumen such as toluene or dichloromethane. The presence of the SOM could also be responsible for the intractable behavior of the highly structured sludge generated in the Athabasca region after hot water extraction[4]. The toxicity of the water together with loss of bitumen, diluent naphtha and process water are among the most serious problems associated with the build-up of clay sludges in storage ponds[4,5].

In order to gain a deeper insight into the problems of oil sands processability as well as settling and compaction of tailings pond sludge an understanding of the forces involved in the bonding between inorganic matter, strongly bound organic matter and bitumen in both sludge and original oil sands feed is required. To this end it is necessary to liberate the organic rich solids (i.e. solids fractions enriched with SOM) from the rest of the solids and to be able to analyze them further. In earlier work[6,7] these solids were separated from the bulk of Athabasca oil sands using the cold water agitation test (CWAT). The purpose of this current work was: 1) to isolate the organic rich solids from the bulk of the sludge and to examine it by different techniques; 2) to discuss the differences and similarities between the properties of sludge solids fractions and those for medium grade oil sands of estuarine and marine origin from the same Athabasca quarry[6,7]. These oil sands were selected because they displayed different bitumen recovery behaviour using water based extraction techniques[7,8].

Experimental

The tailing pond sludge sample was supplied by Syncrude Research Ltd and was taken from a small sludge containment pond which had been filled with sludge pumped from the 17 m level of the main tailing pond. The composition of the sludge was determined by the classical technique using Soxhlet extractors in conjunction with Dean and Stark separators[9]. The sludge contained water (71.2%), solids (28.0%) and bitumen (0.8%). Sludge solids were 98% less than than 38 μm.

The procedure for isolation of organic rich solids from sludge by CWAT (Figure 1) is described in detail elsewhere[10] and is briefly as follows: distilled water was added to unextracted samples from which about 30% of the water was removed by centrifugation. Samples were agitated in sealed glass jars, using a high intensity Spex mixer, followed by centrifugation. As a result of this treatment the following layers were formed (from top to bottom): a colloidal suspension layer (A) and two compact solids layers RS-I and RS-II each distinguished by a significant colour difference. Toluene was added to each layer to dissolve bitumen. The bitumen concentrations for the toluene solutions produced from each layer were determined photometrically by measurements of absorption at 530 nm in comparison to standard solutions of bitumen. The solids content of the bitumen free layers was estimated gravimetrically after drying the samples at 110°C. Acetone solubles were isolated from the bitumen free RS-I fraction by refluxing it with acetone for 48 hours.

The elemental analysis (C,H,N) were performed using a Perkin-Elmer model 240 CHN analyzer. The insoluble organic carbon content (IOCC) of all solid fractions was obtained by subtracting carbonate carbon from the total carbon. Carbonate carbon was analyzed titrimetrically after acid digestion using a Carbon Dioxide Coulometer Model 5011. Metals were determined semiquantitatively by DC arc emission spectrometry.

Scanning electron microscopic (SEM) observations were made using a Cambridge Stereoscan-S250 with an energy dispersive X-ray analyzer attachment (Tracor Northern TN 5500).

Infrared spectra were recorded from solvent casts using a Perkin-Elmer model 683 i.r. spectrometer.

Solution ^{13}C NMR spectra were obtained on a Bruker MSL-300 spectrometer, set to a sweepwidth of 20 kHz with inverse gated proton decoupling to suppress nuclear Overhauser effects (NOE). A pulse flip angle of 45° was used with a pulse repetition time of 2 s. A paramagnetic relaxation agent chromium (III) acetylacetonate was added to the solutions of organic matter in $CDCl_3$ to allow for a short delay time between pulses in the carbon-13 channel.

Results

Treatment of sludge with CWAT produced an aqueous colloidal suspension (A) of poorly-crystalline[10] solids and two distinct compact solids layers RS-I and RS-II. The solids distribution by layers and the insoluble organic carbon content (IOCC) of the different fractions are given in Table 1. The solids in layer A represented 18.6% of the sludge (dry, bitumen free basis), solids in layer RS-I accounted for 4.7%, while the majority of the solids reported to layer RS-II. It can be seen from Table 1 that the IOCC of the solids fractions was markedly different. The RS-I fraction had the highest IOCC of 14.6% followed by the A fraction with an IOCC of 3.7% and the RS-II with an IOCC of 1.3%.

Table 1. Analysis of various layers

Fraction	Solids distribution by layer, % of total	Insoluble organic carbon content, wt%	Bitumen content per unit weight
RS-I	4.7	14.6	6.0
A	18.6	3.7	3.0
RS-II	76.7	1.3	0.8

Results showing metal contents of the solids fractions are given in Table 2. It can be seen that the metals (except Al) are primarily associated with the the RS-I solids. For solids derived from the colloidal suspension (A) Al was the most abundant element. Table 2 also includes results for carbonate carbon (C_{inorg}) distribution. The amount of C_{inorg} was highest in the RS-I fraction.

Table 2. Metal and carbonate carbon analysis of various solids fraction from sludge

Layer	Metal content, %						C_{inorg}, wt%
	Fe	Al	Ti	Zr[a]	Ni[a]	V[a]	
RS-I	10.3	7.6	2.1	980	125	240	2.0
A	3.0	11.1	0.4	300	70	210	0.2
RS-II	1.7	6.7	0.5	120	37	100	0.3

[a] ppm

Representative scanning electron micrographs of the RS-I solids are given in Figure 2 and show that this fraction consisted largely of globules made of fine particles. As indicated by the results of energy dispersive X-ray analysis, the main inorganic components of the globules were quartz, kaolinite, hydrous iron oxides and siderite. Titanium-minerals were relatively abundant in RS-I.

Discussion

The results presented in Table 1 indicate that; first, the CWAT can be used to isolate solids enriched with organic matter from the bulk of solids represented by the RS-II and second, based on IOCC, two different fractions of organic rich solids can be distinguished in sludge, namely, solids separated in the form of aqueous colloidal suspension (A) and compact layer RS-I.

The presence of the poorly-crystalline solids (A) is a common phenomenon for Athabasca oil sands of different grades and geological origin[6,7]. Examination of these solids using ^{29}Si NMR in conjunction with IR and transmission microscopy has shown that the poorly-crystalline inorganic matter is comprised of disordered aluminosilicate clays, most probably allophane[11]. A relatively high IOCC indicates that the inorganic components in these solids occur in some kind of association with strongly bound organic matter. The latter could interact[12] with those sites on allophane surfaces which arise from hydroxyl groups associated with metal ions such as Al^{+3}, Si^{+4} and Fe^{+2}. This interaction has a significant impact on the ultimate fate of the poorly-crystalline minerals by preserving them from crystallization. In the absence of a high concentration of flocculating cations (as in the case of estuarine oil sands) these inorganic matter-organic complexes, with their very fine particle sizes[11] and relatively low density are expected to possess a high colloidal stability in the sediment water. Increased ionic concentration of Mg, Ca, K (as noted for marine oil sands) could be responsible for the flocculation and precipitation of these partially oil wet[13] particles on the surfaces of crystalline minerals. The precipitated particles are likely to facilitate the formation of a hydrophobic solids phase. The schematic diagrams given in Figure 3 illustrate two different conditions of the (A) solids with respect to the solids, water and bitumen in oil sands[14]. Figure 3a shows the disposition of colloidally stable complexes in the connate water phase of estuarine oil sands. In this case the surfaces of most of the crystalline minerals are not contaminated with SOM and are separated from bitumen by a water envelope in accordance with the model generally accepted for Athabasca oil sands[15]. During bitumen extraction these solids do not report with the hydrocarbon phase (thereby facilitating a density separation as in the Hot Water Process) and are expected to be discharged to primary tailings. Figure 3b illustrates the case where the A particles affect the wettability of some oil sands solids by participating in the formation of a hydrophobic solids phase. Adhesion of bitumen to surfaces of such hydrophobic solids is thus facilitated which, in turn, creates problems for bitumen extraction by water based processes. During hot water extraction some of these hydrophobic solids together with associated bitumen could end up with the primary tailings. It is also likely that the presence of NaOH would partially clean mineral surfaces by releasing inorganic matter-organic complexes. As in the case for estuarine oil sands the latter will be disharged to primary tailings in the form of a stable colloidal suspension.

The RS-I solids had a relatively high IOCC of 14.6% which is significantly higher than the IOCC of 1.3% for the bulk solids fraction RS-II (Table 1). An important characteristic of the RS-I fraction was a relatively high capacity to retain bitumen. This is evident from the results presented in Table 1 which show that, in terms of bitumen content per unit weight of solids, the RS-I was enriched as compared with the RS-II. The presence of residual solids as two distinct layers with markedly different IOCC and different capacity to hold bitumen has also been detected in marine oil sands[7]. Another feature common to marine oil sands and sludge is that the RS-I fractions in both materials are largely in the form of "globule"-like particles (Figure 2). The metals, Ti and especially Fe, were associated primarily with these solids (Table 2). Iron, which is a common component of Athabasca oil sands, is considered to be present as iron hydroxides (mainly as grain surface staining[16]), siderite and as an integral part of the clay structure. As iron is known to play an active role in interaction with strongly bound organic matter, it is suggested that some of the SOM is present in the globules in the form of complexes with iron bearing minerals. Also, some SOM could occur in association with poorly-crystalline aluminosilicates. This suggestion is based on the results of X-ray diffraction analysis[10] which indicate the presence of a substantial amount of poorly-crystalline minerals in the RS-I fraction.

The "globules" of various sizes with their extremely heterogeneous surfaces in terms of wettability are considered to be the most active structure-forming agents in sludge. They appear capable of creating a three dimensional network through direct association with each other, and also through the residual bitumen and water soluble organic matter. Numerous cells or "pockets" occurring within this loose network are expected to be filled with water containing colloidally suspended, poorly-crystalline particles (fraction A). This would account for the significant water retention by the structured sludge. Also the structure is strong enough to accommodate larger clay and sand particles in the pockets[17].

The strength of the sludge structure can be partially attributed to the presence of organic matter extractable with acetone[18]. A high resolution ^{13}C NMR spectrum of acetone solubles derived from the RS-I fraction is presented in Figure 4. Chemical shifts were assigned based on the results reported by Suzuki et al.[19] and Thiel and Gray[20]. This spectrum in general resembles those for Athabasca asphaltenes and maltenes. The straight alkyl chains are represented as a set of signals at 14.1, 22.7, 32.2 and 29.7 ppm assigned to C_1 (terminal), C_2, C_3 and central methylene group (C_n), respectively. The average chain length (L) estimated from the ratio of the signals at 29.7 ppm and 14.1 ppm plus 5, plus the area of the branched methyl (19.7 ppm)[21] is given in Table 3 in comparison with those for Athabasca asphaltene and maltene. The aromatic carbon in the spectrum is represented by broad peaks in the range from 118 to 160 ppm. The carbon aromaticity (percent of aromatic carbon to total carbon, Table 3) of acetone solubles is only slightly

Table 3. Aromaticity and average aliphatic chain lengths (^{13}C NMR analysis).

Fraction	Aromaticity, %	Average aliphatic chain length (L)
Acetone solubles	39.6	12.7
Asphaltene	43.0	12.8
Maltene	23.0	10.8

lower than that of asphaltene and the average chain length is the same as for asphaltene from the oil sand feed. This, in conjunction with a molecular weight of 800 (vapor pressure osmometry) suggested that the lowest molecular weight fraction of asphaltene could report as acetone soluble material[22]. Spectra for bitumen fractions and that for acetone solubles differ in that the latter displays the resonances in the 173-180 ppm area which are most likely those of carboxylic functional groups. These resonances in conjunction with the presence of long aliphatic chains point to long chain fatty acids as possible constituents of the acetone solubles[23]. The latter type of compound is virtually absent in bitumen but occurs as a portion of the insoluble organic matter chemisorbed to the inorganic matrix in oil sands.

The NMR spectrum in Figure 4 is complemented by the results of infrared analysis (Figure 5). The presence of bonded carboxylic acids is suggested by a broad band in the region 3600-2000 cm^{-1} and by the peak at 1710 cm^{-1}. Polymeric phenols, alcohols and chelated ketones could also be present as indicated by the bands at 1710 cm^{-1}, 1610 cm^{-1} and 1040 cm^{-1}. The absorption band at 1040 cm^{-1} may be assigned to esters, sulfoxides, and various metal oxides[24].

It is likely, that due to their polarity, acetone solubles could act as a cementing agent between solids particles, coated to different extents with SOM, by adhering to the surfaces of both inorganic minerals as well as SOM. The polar character of this material will also permit it to adhere to the polar constituents in the bitumen thus facilitating the wetting of the solids by bitumen.

Conclusion

A cold water agitation test allowed solids fractions enriched with insoluble organic matter to be separated from the bulk of Syncrude tailings pond sludge. The results for sludge solids fractions were compared with those for medium grade oil sands of estuarine and marine origin. It appears that the presence of poorly crystalline aluminosilicate is a common phenomenon for both sludge and oil sands feed. Most of this material, especially for estuarine oil sands, is expected to be colloidally dispersed at the conditioning stage of the Hot Water Extraction process and to be discharged to primary tailings. It is likely that most of the "globule"-like organic rich solids found in sludge originated from oil sands displaying poor bitumen recovery, such as those of marine origin. These solids with their wettability intermediate between bitumen and water will be expected to have a tendency to accumulate at the oil-water interfaces, stabilizing various types of emulsions and also playing an active role in the formation and stability of the gel-like structure of sludge.

^{13}C NMR and IR characterization of the acetone solubles extracted from the RS-I fraction indicate a highly polar character for this material.

Acknowledgements

We thank Dr. P.E. Grattan-Bellew who kindly examined samples by scanning electrone microscopy and also the Chemistry Division, in particular V. Boyko (heavy elements determination) and V. Clancy (carbonate carbon analysis).

References

1. Sanford, E.C., Can. J. Chem. Eng., 1983, 61, 554.

2. "Guide to the Athabasca Oil Sands Area", Carrigy, M.A. and Kramers, J.W., Eds., Can. Soc. Petrol. Geol., Oil Sands Symposium, 1973, p.213.

3. "Oil Sands-Fuel of the Future", Hills, L.V., Ed., Calgary Soc. Petrol. Geol. Mem., 1974, 3, p. 263.

4. Kessick, M.A., "Clay tailing from Alberta Oil Sands and other sources. A review.", Alberta Environment Report, 1978/2, Edmonton, Alberta, Canada.

5. Camp, F.W., Processing Athabasca tar sand-tailing disposal, Can. J. Chem. Eng., 1977, 54, 581.

6. Kotlyar, L.S., Ripmeester, J.A., Sparks, B. D. and Montgomery, D.S., Fuel, 1988, 67, 808.

7. L.S. Kotlyar, H. Kodama, B.D. Sparks and P.E.Grattan-Bellew, Applied Clay Sci., 1987, 2, 253.

8. M.M Smith, R. Ehrlich and A. Hardin, AOSTRA, J.Res., 1985, 1, 245.

9. Syncrude Canada Ltd., 1979. Syncrude analytical methods for oil sand and bitumen processing. Edmonton, Alberta, p. 58

10. Kotlyar, L.S., Sparks, B.D and Kodama H., AOSTRA J. Res., in press.

11. L.S. Kotlyar, H. Kodama and J.A. Ripmeester, Applied Clay Science, in press.

12. Mortland, M.M., 1986. Mechanism of adsorption of nonhumic organic species by clays. In "Interactions of Soil Minerals with Natural Organics and Microbes", Ed. P.M. Huang and M.Schnitzer. Proc. Symp. Soil Sci Soc. Am., Washington, DC, Aug, 1983, p.59-74.

13. K.Darcovich, L.S. Kotlyar, W.C. Tse, J.A. Ripmeester, C.E. Capes and B.D. Sparks, Energy and Fuels, 1989, 3, 386.

14. Kotlyar, L.S., Sparks, B.D. and Kodama, H., AOSTRA J. Res., 1988, 4, 277.

15. K. Takamura, Can. J. Chem. Eng., 1982, 60, 538.

16. Ignasiak, T.M., Zhang, Q, Kratochvil, B., Maitra, C., Montgomery, D.S., AOSTRA J. Res., 1985, 2, 21.

17. J.D. Scott, M.B. Dusseault and W.D. Carrier III, Applied Clay Science, 1985, 1, 207.

18. Kotlyar, L.S. and Sparks, B.D, NRC Internal Report No. C-1182-89S, 1989.

19. Suzuki, T., Iton, M., Takegami, Y. and Watanabe, Y., Fuel, 1982, 61, 402.

20. Thiel, J. and Gray, M.R, AOSTRA J.Res., 1988, 4, 63.

21. Cyr, N., McInture, D.D., Toth, G. and Strausz, O.P., Fuel, 1987, 66, 1709.

22. Strausz, O.P, Fourth UNITAR Conference on Heavy Crude and Tar Sands, 1988, paper No. 96

23. Cyr, T.D. and Strausz, O.P., Org. Geochem., 1984, 7, 127.

24. Strausz, O.P., Berlozescki, S. and Ignasiak, T., "Chemical Studies on Resins", AOSTRA Agreement, #142, Final Report to Alberta Oil Sands Technology and Research Authority, June 30, 1982.

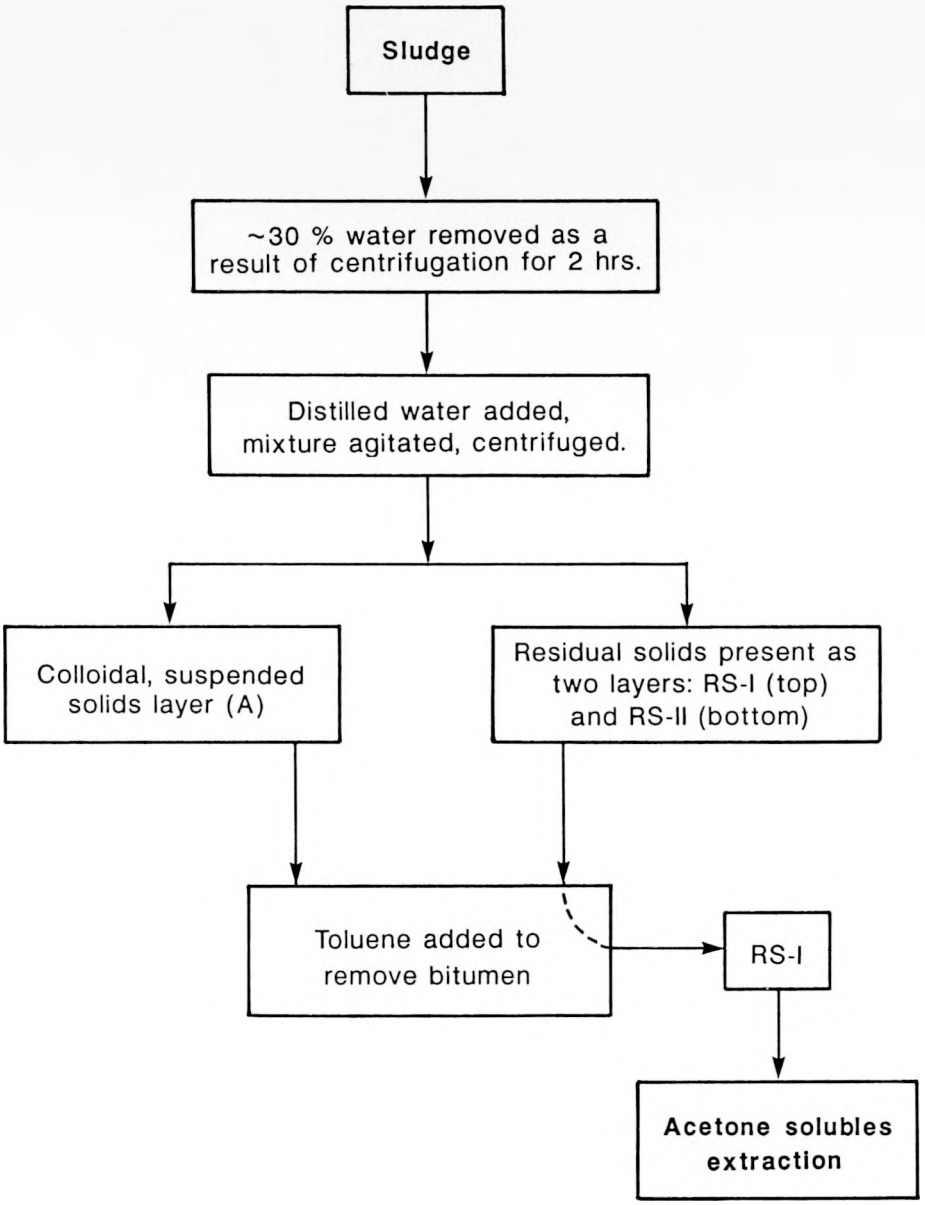

Fig.1 Treatment scheme for sludge.

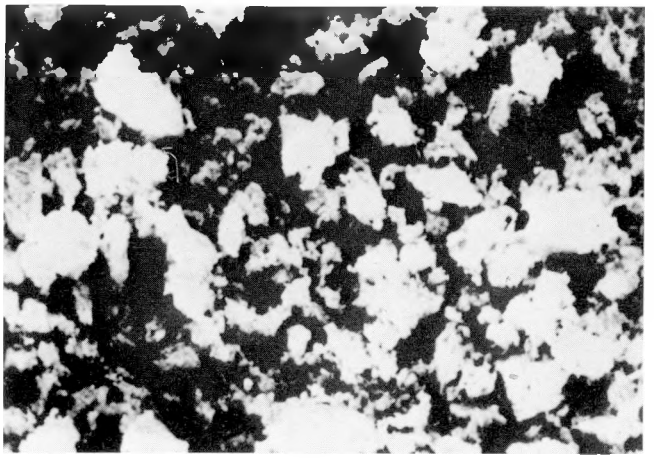

Fig. 2 SEM of the RS-I fraction from sludge.

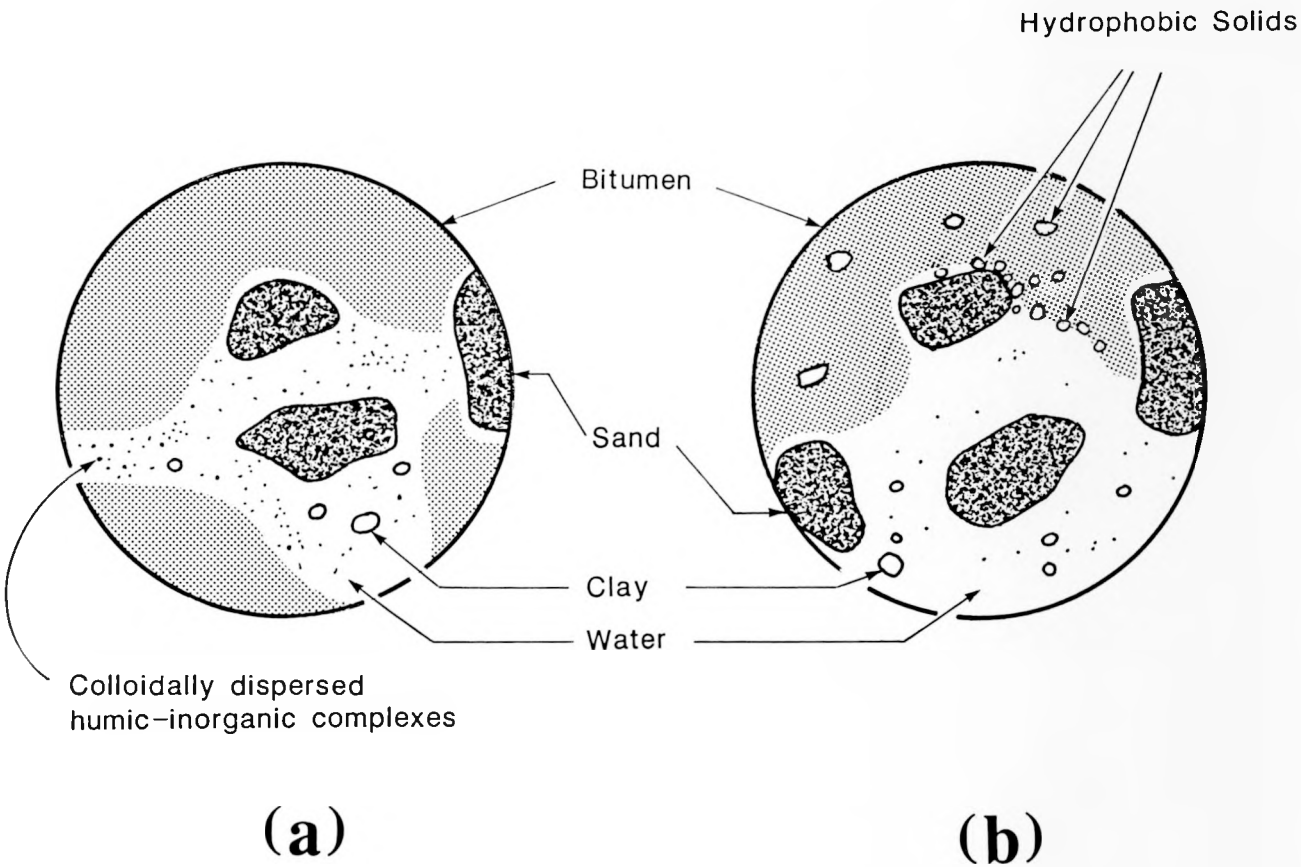

Fig.3 Schematic diagram illustrating differences between estuarine (a) and marine (b) oil sands.

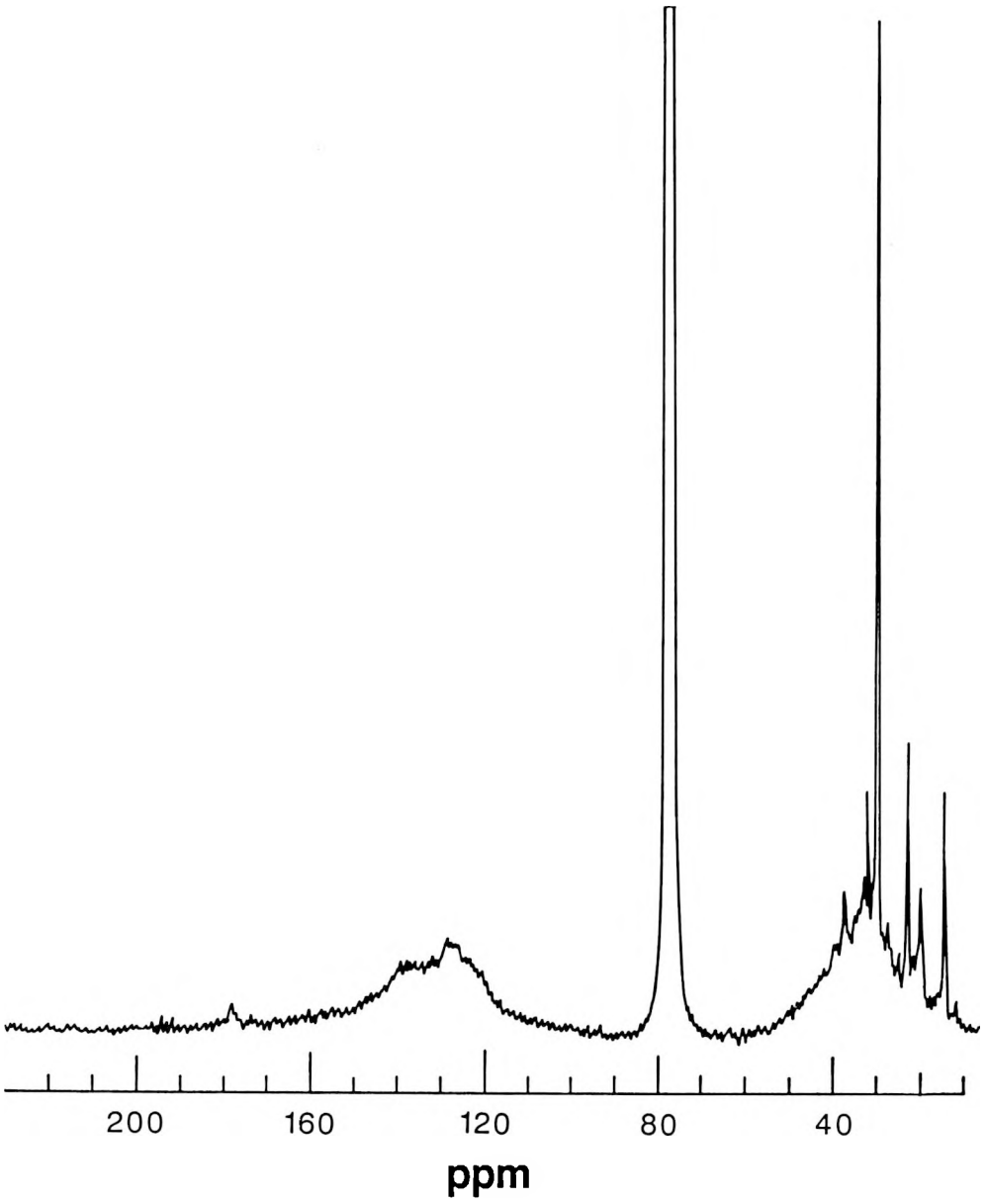

Fig.4 ^{13}C NMR spectrum of acetone solubles from sludge.

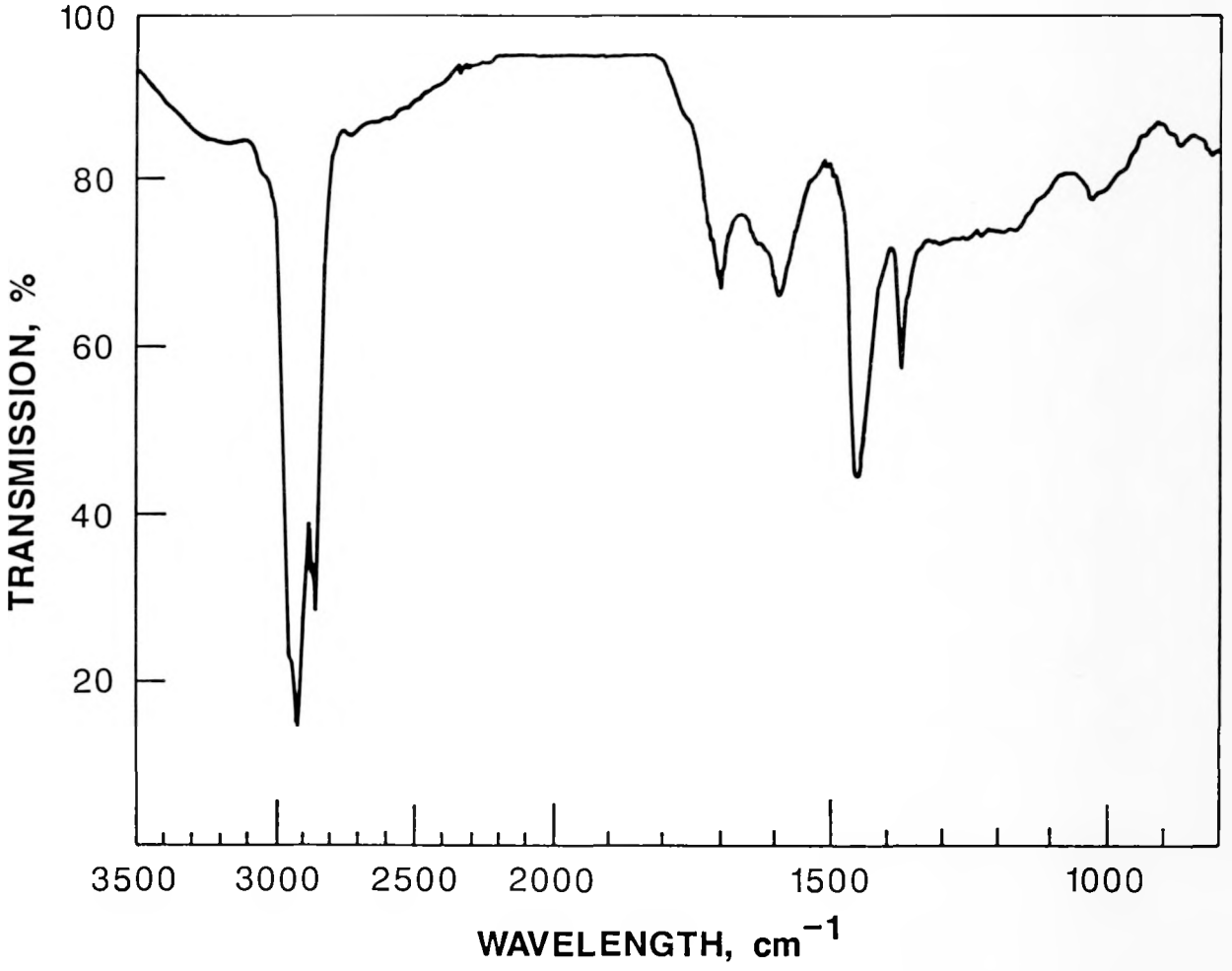

Fig.5 IR spectrum of acetone solubles derived from sludge.

Low Temperature Oxidation Strategy for Increasing the Effectiveness of Hot Fluid Recovery of Bitumen — An Experimental Study

by

John Ivory, Peter Toma, Roy Coates, and Mario DeRocco
Alberta Research Council — Oil Sands and Hydrocarbon Recovery Department
Edmonton, Alberta CANADA T6H 5X2
Declan Livesay
Esso Resources Canada, Ltd.

Abstract

This paper presents results from laboratory experiments which involved the recovery of bitumen by the injection of hot water and air.

Air commingled with hot water was injected continuously or in slugs. The effectiveness of air in enhancing the hot water recovery process and the major mechanisms involved in the recovery process were assessed using oil production, pressure drop and pH data as well as temperature distributions. Properties of produced fluids and residual oil were monitored including viscosities, asphaltene, sulfate, acetate and total inorganic carbon content.

An oil sand pack, which had a diameter of 0.25 m and was 1 m long and contained an axial communication path, was used during this study. In addition, core size experiments were performed. A substantial increase in final oil recovery from 13 to 58% of the initial oil in place was detected in the 1 m long oil sand pack. In the core experiments, air reduced the residual oil saturation from 34% to 16%.

The experiments indicated that: (1) low temperature oxidation was active at the edge of the recovery front where a significant temperature increase was observed during air injection, (2) because of changes resulting from low temperature oxidation reactions, the resistance to fluid flow through pore throats was increased and resulted in an increased pressure drop, (3) increased flow resistance in the communication path or bypass zones resulted in the diversion of hot fluids and enhanced bitumen production, (4) if air is injected too late, i.e. when the water-only recovery process is declining, its effect is less significant.

Introduction

The Athabasca, Cold Lake, Peace River, and Wabasca oil sand deposits in Northern Alberta, Canada cover an area of more than 7 million ha and contain approximately 215 billion m^3 of bitumen[1]. More than 200 billion m^3 of bitumen are too deep to be economically mined. The injection of steam or hot water may be used to supply heat (to reduce the bitumen viscosity and make it mobile) and a pressure differential to cause the bitumen to flow to a production well. The use of air as an injection fluid additive has been investigated at the Alberta Research Council. The temperature of the process is kept below 220°C so that that the more easily controlled low temperature oxidation (LTO) reactions predominate over combustion reactions.

Previous physical simulator tests at 216°C[1] have demonstrated that air injection with steam dramatically increases the bitumen recovery rate. The mechanisms involved in the enhanced recovery are considered to be:

1. Steam diversion due to increased flow resistance in the communication path. The increased resistance is caused by (a) rapid movement of cold bitumen into the communication path, (b) reduced absolute permeability of the communication path due to coke formation and asphaltene precipitation, (c) change in sand wettability (from water-wet to oil-wet) due to the low pH conditions produced by low temperature oxidation (LTO) reactions, and (d) increase in the volumetric flow rate due to the presence of incompressible gases (N_2, O_2, CO, CO_2, H_2S).
2. Heat produced by oxidation reactions.
3. In-situ production of CO and CO_2.

This paper summarizes the results which have been obtained from experiments, which were designed to determine if air would also improve recovery from a hot water process. One series of experiments was carried out on a small oil sand core (3.8 cm diameter, 22.5 cm long) to examine small scale effects of the water-air process and specifically to determine how air injection would affect the pressure drop across the core, the post-run oil saturation, bitumen properties, and produced aqueous phase properties. A second series of experiments was performed in an oil sand test bed which had a diameter of 25 cm and was 100 cm long. These latter experiments were designed to investigate the effect of air injection on the bitumen recovery versus time curve, the pressure drop across the communication path, and the temperature contours in the test bed. Through the temperature contours, the big cell offered the opportunity to evaluate the ability of air to affect conformance.

Background

The data from a number of kinetic studies[2-6] of the LTO process fit an equation of the form:

$$r = k_0 * \exp(-E/RT) * Po_2^n$$

Babu and Cormack[3] observed a decline in reaction rate when 50 g of O_2/kg of bitumen had been consumed. This occurred after the most reactive bonds and molecules had been oxidized. Phillips and Hsieh[4] considered two reaction schemes. In the first scheme, bitumen was considered to be oxidized in a single irreversible reaction to produce CO, CO_2, H_2O, and oxygenated hydrocarbons. The second reaction scheme involved the parallel formation of water and oxygenated hydrocarbons by one reaction pathway and carbon oxide gases by another.

Based on an analysis of combustion experiments, Burger and Sahuquet[7] concluded that clay or metallic derivatives (e.g. copper, iron, nickel, and vanadium) in the oil or solid matrix would catalyze oxidation reactions. In addition, Urban and Udell[8] showed that the oxidation of a 21°API oil in the presence of a complex sand (containing montmorillonite, kaolinite, mica, calcite, quartz, and feldspar) had a faster reaction rate than did oil oxidation in a quartz sand medium. They also showed that steam reduced the rate of O_2 consumption. However, the results of some experiments[3, 5, 9, 10] have indicated that oil sand solids did not have a strong catalytic effect on oxidation kinetics.

Coke Formation

The amount of coke produced during pyrolysis of Athabasca bitumen increases linearly with the extent to which the bitumen has been oxidized[11]. Initially during LTO maltenes are converted to asphaltenes and essentially no coke is formed[9]. Then at oxygen uptakes greater than 40 g/kg of bitumen, coke is formed from both asphaltenes and maltenes. Above 200 g/kg maltenes are converted directly to coke from which carbon oxide gases may be produced.

Bitumen Viscosity

The viscosity of Athabasca bitumen (measured at 78°C) increases with extent of oxidation up to 35 g O_2/kg of bitumen[12]. The viscosity increases even more dramatically at higher O_2 consumption (see Figure 1).

Experimental Procedures

The two facilities have previously been described in detail[13,14] and only the more salient features will be described here. Figure 2 is a flow diagram for the facility in which the core experiments were performed. Figure 3 shows a schematic of the 1-m cell.

Core Test Facility

Coreholder. A double wall Hassler setup was used in both facilities. In the core experiments, high grade Athabasca oil sand (13.2% bitumen) was tamped into a copper sleeve which was then inserted into a pressure vessel. The vessel was then installed in a Blue M mechanical convection oven. The latter was maintained at the desired operating temperature as these experiments were isothermal.

Injection. 96 g/h of MilliQ water and 4 g/h of air were pumped using piston displacement pumps (Ruska and ISCO). They were heated while flowing through the convection oven. The two fluids were then injected into the top (Runs CS-1 to CS-6) or bottom (CS-7 to CS-9) of the core. Flow direction was in the vertical direction. Because

of the high pressure drops caused by fluid flow the effect of gravity was negligible and the results were independent of flow direction.

Production. The produced fluid flowed into a network of three accumulators maintained at constant pressure (i.e. there were no pressure drawdowns) by means of a N_2 gas-Mighty Mite backpressure regulator system. The three accumulators were filled sequentially.

Data Acquisition. A DEC PDP11/44 computer was used to record data during the experiment. The location of most of the variable measurements can be seen in Figure 2. All of the injection and production stream temperatures were recorded. In addition, core temperatures 5.6 cm from each endcap were measured. Taps for the pressure drop across the central 12.5 cm of the core were located at a distance of 5 cm from each endcap.

Sample Analysis. The produced liquids in the three accumulators and in the production lines were analyzed for bitumen and water content. The pH, total inorganic carbon (Dohrman carbon analyzer), sulfate content (ion chromatography) and acetate content (ion exclusion chromatography) of the water in the three production accumulators were also measured.

The depleted core was analyzed for bitumen, water and solid contents. The mass percentage of coke (toluene insolubles) in the extracted sand was determined by measuring the change in mass of an extracted sand sample after heating it overnight at 540°C. The viscosity of the post-run bitumen was measured at 75°C and 125°C (Brookfield cone and plate viscometer). The acid number and asphaltene content of the depleted bitumen were also obtained. The acid number is the number of mg of KOH required to neutralize the acids in 1 g of oil.

1-m Cell

Coreholder. In the 1-m cell, a lead sleeve was utilized. After packing high grade Athabasca oil sand (12.1% bitumen), a 2.1 cm diameter cylindrical communication path was inserted along the central axis. This path was packed with water saturated 20-24 frac sand which had an absolute permeability of 205 $(\mu m)^2$. Insulation was placed between the lead sleeve and the pressure vessel. As it was desired to observe the development of temperature profiles in the test bed which resulted from hot water-air injection, the outside of the pressure vessel was not heated and the cell was not operated isothermally.

Injection. Flow was in the horizontal direction in all of the 1-m cell experiments. The water injection conditions (flow rate, temperature and pressure) were controlled by a mass flow meter, a control valve and an immersion heater. The air was injected into the water flow from a gas cylinder which had a pressure reducing regulator. The air was preheated by means of a steam jacket. The air flow rate was measured by a mass flow meter and adjusted by a control valve.

Production. Produced gas and liquid flowed into a high pressure vessel. Liquid was collected through a valve from the bottom of this vessel. Gas exited from the top of the high pressure vessel.

Data Acquisition and Control. The experiments were controlled by a combination of electronic controllers and a MACSYM II computer. All the measured variables were scanned by a Fluke data logger and recorded on magnetic tape. In addition, data required by the operator were scanned, processed, printed out, and stored on magnetic tape by the MACSYM II computer.

Sample Analysis. The produced liquid was collected at 10 minute intervals. Using the Dean Stark procedure, the samples were analyzed for bitumen, water, and sand content. This data was then used to produce bitumen recovery curves. The pH of the produced aqueous phase was also measured.

Operating Procedures

The experimental conditions and injection strategies are outlined in Tables 1 to 4.

Core Test Facility

Water was injected for at least 2 hours in order to deplete the core before injecting the air. In addition, it was desired to obtain a stable pressure drop before air injection so that its effect on this variable would be apparent. At the end of water-air injection, water-only injection was resumed to determine if any pressure drop changes persisted when air injection was stopped. During an experiment, the overburden pressure was maintained at 3.5 MPa above the production pressure.

Table 1. Experimental Conditions for Core Test Facility

Core Orientation:	Vertical
Flow Direction:	Downward (CS-1 to CS-6) Upward (CS-7 to CS-9)
Water Flow Rate:	96 g/h (1 PV/h)
Air Flow Rate:	4 g/h
Production Pressure:	2.16 MPa (CS-1 to CS-6) 2.45 MPa (CS-7) 4.23 MPa (CS-8 and CS-9)
Core Temperature:	211°C (CS-1 to CS-4) 219°C (CS-5 to CS-9)
Core Diameter and Length:	3.81 cm and 22.5 cm
Porosity and Pore Volume:	35% and 94 cm^3
Oil Sand Density:	2.09 g/cm^3
Mass of Core:	550 g

1-m Cell

Except for Runs 1m-1 and 1m-2, air was injected throughout each experiment. Run 1m-1 was a water-only baseline experiment. In Run 1m-2, 3.3 hours of water-only injection preceded water-air injection. A fresh oil sand pack was used in every run except 1m-4. The depleted pack

from the water-only run 1m-1 was used in that experiment.

Table 2. Experimental Conditions for 1-m Cell

Diameter	24.9 cm
Length	99.6 cm
Mass	94 kg
Initial Oil	12.1% by mass 85.2% saturation 11.4 kg
Initial Water	2.1% by mass 14.8% saturation
Porosity	37%
Density	1.95 g/cm^3
Comm. Path Sand	20-24
Comm. Path Diameter	2.15 cm
Comm. Path Perm.	205 (μm)^2

Experimental Strategy

Core Test Facility

The first nine experiments (three hot water-only and six water-air) were designed to determine the effect of the water-air process on the pressure drop and residual oil saturation in small cores (3.8 cm diameter, 22.5 cm long) which had been partially depleted by a waterflood. The effect of air injection on the properties viscosity, asphaltene content, and acid number of the residual bitumen was measured. In addition, changes caused by LTO reactions to the produced aqueous phase (sulfate, acetate, total inorganic carbon, and pH) and to the coke content of the post-run solids were determined. The experimental strategy used in these experiments is summarized in Table 3.

Table 3. Injection Strategy for Core Size Experiments

Run	Injection Strategy
CS-1	8 h water-only (h = hours)
CS-2	9 h water-only
CS-3	2 h water-only, 4 h water-air, 3 h water-only
CS-4	2 h water-only, 4 h water-air, 3 h water-only
CS-5	2 h water-only, 5.8 h water-air, 2.1 h water-only
CS-6	10 h water-only
CS-7	2.23 h water-only, 10.3 h water-air, 11.3 h water-only
CS-8	2 h water-only, 10.8 h water-air, 0.9 h water-only
CS-9	2 h water-only, 10.5 h water-air, 11.5 h water-only

1-m Cell

One water-only and six water-air experiments were performed. With the exception of 1m-7 which had a temperature of 170°C, an injection temperature of 200°C was used in all of the experiments. The experiments are summarized in Table 4. They were designed to investigate how air injection affects: (1) the rate of bitumen recovery, (2) the pressure drop across the communication path, and (3) the temperature profile in the test bed.

Table 4. 1-m Cell Experiments

1m-1: 29.1 hours of water-only injection at 200°C.
Water flow rate = 10 kg/h (0.55 test bed PV/h).

1m-2: Low concentration water-air injection at 200°C.

0 - 3.33 hours water-only injection at 10 kg/h.
3.33 - 29.83 hours water-air
Water: 10 kg/h. Air: 0.13 kg/h (1.3 mass%).

1m-3: Variable concentration water-air injection at 200°C. Water flow rate = 10 kg/h.

Time (hours)	Air (kg/h)	Concentration (mass%)
0-1.17	1.08	9.7
1.17-3.50	1.08 0.43	9.7 4.1
3.50-7.37	0.22	2.2
7.37-20.27	0.15	1.5

1m-4: Water-air injection at 200°C on depleted pack from 1m-1.

Time (hours)	Water (kg/h)	Air (kg/h)	Concentration (mass%)
0.-1.42	10	1.08	9.75
1.42-4.0	10	0.87	8.00
4.0-5.89	10	1.08	9.75
5.89-6.58	10	0.54	5.12
6.58-9.25	10	0.33	3.19
9.25-11.3	5	0.33	6.19

1m-5: Water-air injection at 200°C for 37.2 hours. Air injected midway between water injection well and production well for first 10.7 hours.

Water: 10 kg/h. Air: 0.22 kg/h (2.2 mass%).

1m-6: Water-air injection at 200°C for 34.2 hours.
Water: 10 kg/h. Air 0.22 kg/h (2.2 mass%).

1m-7: Water-air injection at 170°C for 36.5 hours.
Water: 10 kg/h. Air 0.22 kg/h (2.2 mass%).

The first test (1m-1) was a water-only baseline experiment. Run 1m-2 was a water-air experiment in which air was coinjected with water at a low concentration (1.3 mass%) into an oil sand bed which had already been flooded with water for 3.33 hours. In all of the other water-air experiments, air and water injection started

simultaneously.

Run 1m-3 involved a systematic reduction of the air concentration from an initial high value of 9.7% to 1.5% (by mass). This strategy was adapted in an attempt to optimize bitumen recovery whilst limiting pressure drop increases across the communication path.

The purpose of 1m-4 was to determine the effect which water-air injection would have on oil sand which had previously been subjected to a waterflood. The depleted test bed from 1m-1 was used in this experiment. Higher air concentrations were utilized in 1m-4 than in 1m-2 which had also examined water-air injection following water-only injection.

In Run 1m-5 the air was injected into the communication path midway between the water injection well and the production well for the first 10.7 hours of the run. For the rest of the experiment, it was coinjected with the water. The purpose of this test was to examine the process of confining the high pressure drop caused by LTO reactions to a limited zone. It should be noted that in all other tests in this series the air was coinjected with the water.

1m-6 had the same operating conditions as 1m-5 except that air was coinjected with the water throughout the experiment. It was designed as a baseline run to determine how injecting air at an intermediate position affected the results in 1m-5.

The effect of temperature was investigated by performing one experiment (1m-7) at an injection temperature of 170°C instead of 200°C as was used in all of the other experiments.

Experimental Results

Core Test Facility

Pressure Drop Results. In Figure 4, a typical water-air run CS-9 is compared to the water-only experiment CS-2. Initially there was a dramatic increase in pressure drop as a result of air injection. However, this increased pressure drop was not maintained and the pressure drop reached a maximum at a run time of 4 hours. It then started to fall even when water-air injection was maintained. Figure 4 shows that the pressure drop declined substantially after the maximum value had been obtained. As discussed later, air injection caused a reduction in the post-run oil saturation from 34% to 16%. This reduction results in a decreased resistance to fluid flow and was probably responsible for the decrease in pressure drop from its maximum value. The pressure drop also fell abruptly (at a run time of 12 hours) when air injection was stopped because of the change to a one phase flow situation.

Post-Run Oil Saturation. The initial oil saturation was approximately 80% for all of the experiments. The post-run oil saturations are summarized in Table 5. For 8 to 10 hour experiments (CS-1 to CS-6), the post-run oil saturation was significantly lower in the water-air experiments as compared to the water-only runs (23.1% to 25.0% versus 32.4% to 35.2%). When the length of water-air injection was increased from 4.0 to 10.5 hours (CS-7 to CS-9) and the total run time was extended from 10 to 24 hours, the post-run bitumen saturation was reduced to between 14.8% and 17.4%.

Table 5. Summary of Post-Run Oil Saturations

WATER-ONLY EXPERIMENTS		WATER-AIR EXPERIMENTS	
CS-1	33.0%	CS-3	23.1%
CS-2	32.4%	CS-4	23.2%
CS-6	35.2%	CS-5	25.0%
		CS-7	17.4%
		CS-8	15.8%
		CS-9	14.8%

Bitumen Properties. The viscosity data for the residual bitumen (i.e. the bitumen left in the core following an experiment) are summarized in Table 6. Air increased the bitumen viscosity by a factor between 3 and 10.

Table 6. Residual Bitumen and Solids Properties

	VISCOSITY @ 125°C (cP)	ASPHALTENE (%)	COKE (%)
PRE-RUN	60	11.2-18.1	0.63-1.85
	WATER-ONLY EXPERIMENT		
CS-2	73	16.2	0.65
	WATER-AIR EXPERIMENTS		
CS-4	587	28.3	-
CS-7	-	-	2.32
CS-8	-	-	1.54
CS-9	182	25.2	2.63

The asphaltene content of the post-run bitumen from water-only experiments was less than 20% and was similar to that of an unprocessed Athabasca bitumen. In contrast, the asphaltene content of the water-air residual bitumen ranged between 25% and 28%. Table 7 shows that the acid number of the post-run bitumen was approximately doubled by water-air injection.

Table 7. Summary of Residual Bitumen Acid Numbers

	Strong Acids	Total Acids
	PRE-RUN	
#1	2.68	3.29
#2	2.60	3.16
#3	2.47	2.99
	WATER-ONLY EXPERIMENTS	
CS-2	2.05	2.56
CS-6	2.95	3.43
	WATER-AIR EXPERIMENTS	
CS-4	7.65	7.94
CS-5	3.50	5.51
CS-7	3.61	3.94
CS-8	4.51	5.19
CS-9	6.46	7.08

Sand Properties. The average coke content of the

water-air experiments was three times that of a water-only experiment (Table 6). The coke particles which are formed have a profound and lasting effect on the absolute permeability by impeding fluid flow through pore throats.

Produced Water Analysis. The pH, sulfate, acetate, and total inorganic carbon contents of the produced water are summarized in Table 8. Air injection reduced the pH to 3. This pH reduction primarily resulted from the production of sulfate by the oxidation reactions. Air injection increased the sulfate content by an order of magnitude. The acetate content was also dramatically increased whereas any changes to the total inorganic carbon content were minimal.

Table 8. Properties of Produced Aqueous Phase

RUN	TIME (h)	pH[1]	SULFATE[2] (mg/l)	ACETATE[2] (mg/l)	TIC[1] (mg/l)
		WATER-ONLY INJECTION			
CS-2	0-1.8	7.98	67.	59.	25.5
CS-2	1.8-5.8	7.62	11.8	3.5	17.8
CS-2	5.8-9	7.96	12.4	3.9	12.0
		WATER-AIR INJECTION			
CS-4	0-1.8	6.89	67.	98.	8.5
CS-4	1.8-5.8	3.03	618.	608.	21.7
CS-4	5.8-9	3.58	165.	6.0	1.1
CS-9	0-1.8	6.86	80.2	177.	18.9
CS-9	1.8-8	3.27	480.	140.	50.5
CS-9	8-24	3.60	236.	53.	36.7

[1] pH and total inorganic carbon (TIC) of unfiltered water emulsion.
[2] sulfate and acetate concentrations of filtered water emulsion.

Produced Gas Composition. The composition of the produced gas (collected from a run time of 2 hours to a run time of 6 - 8 hours) are listed in Table 9. Essentially all of the injected O_2 was consumed in the water-air experiments.

Table 9. Properties of Production Gas

	CS-3	CS-4	CS-7	CS-8	CS-9
	Water -Air	Water -Air	Water -Air	Water -Air	Water -Air
Run Time (h)	1.8-5.8	1.8-5.8	1.8-8	1.8-8	1.8-8
H	0.0	0.0	0.4	0.3	0.2
O_2	0.95	0.32	0.5	0.2	0.2
N_2	94.6	94.7	91.1	90.9	91.3
CH_4	0.02	0.02	< 0.1	0.3	0.1
CO_2	0.83	1.00	1.5	1.5	1.3
CO	3.59	3.99	5.6	5.6	6.6
C_2H_4	0.0	0.0	0.2	0.2	< 0.1
C_2H_6	0.01	0.01	0.2	0.3	0.1
iC_3H_8	0.0	0.0	0.1	0.1	< 0.1
nC_4H_{10}	0.0	0.0	0.2	0.2	< 0.1
iC_4H_{10}	0.0	0.0	0.1	0.1	0.1
nC_5H_{12}	0.0	0.0	0.2	0.2	0.1
CO/CO_2	4.31	4.00	3.73	3.73	5.08

The ratio of CO_2 to CO in the water-air experiments was about 4. The H_2S concentration of the produced gas was of the order of 0.02 mass% in the water-air experiments. SO_2 was not detected in any of the experiments.

1-m Cell

Bitumen Recovery and Pressure Drop. The bitumen recovery data are summarized in Figure 5 and Table 10. The pressure drop results are given in Figures 6 to 9.

Table 10. Bitumen Recovery Results from 1-m Cell

	Time to Recover 15% of OOIP (hours)	Final Recovery (%)
1m-1	22.1	19.3
1m-2	21.4	20.4
1m-3	4.0	57.5
1m-4	12.8	29.6[1]
1m-5	12.2	49.4
1m-6	6.9	57.8
1m-7	10.1	62.4

[1] Based on initial bitumen in pack at start of 1m-4.

Very poor recovery was obtained from the

initial water-air experiment 1m-2. In fact, in terms of bitumen recovery and pressure drop characteristics (Figure 6) its behaviour was similar to that of the water-only experiment 1m-1. There are two apparent reasons for this poor performance. Firstly, the air concentration used was low (1.3 mass%). Apparently too much of it was entrained in the water and flowed straight through the communication path without reacting with the bitumen. This conclusion is supported by the fact that the produced aqueous phase was basic and had a pH of 8. Secondly, water-air injection was preceded by 3.3 hours of water-only injection which cleaned out much of the bitumen which entered the communication path during initial heating of the test bed. Thus, there was less bitumen in the communication path for the air to oxidize when it was eventually injected. In contrast in run 1m-4, injection of water and air into an oil sand which had been previously depleted in a waterflood (1m-1) resulted in the recovery of a significant amount of bitumen. In fact, 29.6% of the bitumen remaining from run 1m-1 was recovered as a result of water-air injection. The essential differences in run 1m-4 were: (1) the air concentration was much higher (initially at 9.75 mass%), and (2) the communication path probably contained more bitumen as a result of bitumen drainage between the two experiments 1m-1 and 1m-4.

Run 1m-3 was the most effective experiment in terms of bitumen recovery because it had the highest air injection rates. Figure 5 shows the high recovery rates which were obtained. However, as shown in Figure 6, the cost of this increased recovery was a much higher pressure drop than for water-only injection. Although the pressure drop declined with bitumen production, the final pressure drop was about four times that obtained in the water-only experiment. This was probably a result of permanent permeability changes caused by carbonaceous solids (precipitated asphaltene and coke) interfering with flow through pore throats in the communication path.

Figure 5 shows that in Run 1m-4 coinjection of water and air into a depleted test bed (from 1m-1) resulted in relatively high bitumen recovery rates. This was in contrast to run 1m-2 where air injection into a partially depleted oil sand had little effect on recovery. It therefore appears that the poor behaviour of air in 1m-2 was due to the low concentration used (1.3 mass%) or to the low bitumen saturation in the communication path at the time of air injection. Although lower than those obtained in Run 1m-3, pressure drops for run 1m-4 were much higher than for the water-only test 1m-1 (see Figure 7).

Faster recovery was obtained when air was injected with the water (1m-6) rather than at an intermediate point between the water injection well and production well (1m-5). The pressure drop was initially higher in 1m-6 than in 1m-5 but was subsequently lower (see Figure 8). The high pressure drop at the end of 1m-5 probably results from the coinjection of air with the water after a run time of 10.7 hours.

A comparison of the recovery curves for runs 1m-6 and 1m-7 shows that initially because of the lower oil sand temperature, the bitumen recovery was less in the 170°C experiment. However, after about 10 hours, the bitumen recovery rate started to increase dramatically in 1m-7. In this experiment, the pressure drop increased over the first two hours. However, after staying constant for about two hours, it started to increase again. This latter increase was a result of the low temperature oxidation reactions which took a few hours to have an effect because of the slow kinetics at 170°C.

Temperature Profiles. Figures 10 and 11 show the temperature contours for five of the seven experiments at run times of 5 hours and 10 hours. The temperature profiles for 1m-2 were essentially the same as for the water-only experiment 1m-1 and consequently they were not included. The profiles for 1m-7 were omitted as the bed temperatures were much lower than the other experiments because of the 170°C injection temperature. The profiles in the 170°C experiment were symmetrical about the communication path.

It is apparent from Figure 10 that at 5 hours the test bed was much hotter in Run 1m-3 than in any other experiment. This was a result of the high recovery rates which were obtained from the beginning of that experiment. Thus, as the bitumen was recovered, the hot water was able to penetrate into the oil sand rather than simply flowing through the communication path. As a result the oil sand was heated more quickly which in turn accelerated bitumen production.

The contours for four of the experiments in Figure 10, show conduction heating from the communication path. Essentially the hot water flowed through the communication path transporting hot bitumen which was sheared from the edge of the water zone. The run 1m-4 which used the depleted bed from 1m-1 is an exception. In that experiment the temperature contours indicate that a more pistonlike displacement occurred. Thus, the oil sand was heated by convection rather than conduction. The pistonlike displacement likely resulted from flow resistance caused by bitumen entering the communication path during and following 1m-1.

The oil sand in the experiment 1m-5 developed an interesting lower temperature region at the top of the bed above where the air was introduced. Also, temperatures were lower at the water injection well than in run 1m-6 where the operating conditions were similar except that the air was injected with the water.

Figure 11 shows that at 10 hours the test bed was still much hotter in 1m-3 than in the other experiments. In addition, the test bed continued to be hotter in 1m-6 than in 1m-5. Also, 1m-4 maintained its pistonlike displacement.

At 9.25 hours into run 1m-4, the water flow rate was reduced from 10 kg/h to 5 kg/h whilst the air flow rate was maintained at 0.33 kg/h. This caused the air concentration to increase from 3.2% to 6.2% (by mass). Although the rate of energy input was decreased, an increased dispersion of heat in the bulk of the oil sands was recorded (see Figure 12). This behaviour is explained as follows:

- By reducing the flow of hot water, and maintaining the air mass flow, the quantity of air entrained by water flowing through the communication path was reduced. More air was available for dispersion into the oil sand.

- An oxidation reaction was intensified near the injection well between 160°C and 170°C, especially in the regions of higher oil saturation.

pH Results. The pH and bitumen recovery rate data for runs 1m-3 are displayed in Figure 13. It is apparent from this graph that the pH of the produced aqueous phase decines rapidly at the same time as the bitumen production rate is increasing. However, the pH remains at a low value even when the bitumen production rate has fallen to a low value. Figure 14 shows similar data for run 1m-7. In this 170°C experiment, the production rate shows a sharp increase and the pH a rapid decrease after about 10 hours of water-air injection. The delay in this experiment was due to the slower kinetics at 170°C. These results indicate that the higher bitumen production rates and low pH both simultaneously result from the LTO reactions.

Discussion

The core experimental results showed that when air was injected with water a very high pressure drop was initially obtained. However, because air injection reduced the oil saturation in the core (from 34% to 24%), the increased pressure drop was not maintained. In the only 1-m cell experiment in which water-air injection immediately followed a waterflood, the air had little effect on the pressure drop across the communication path. Because of the low bitumen saturation in the communication path the bitumen essentially existed as an oil in water emulsion. In addition, the low air concentration in the injection fluid minimized contact between the dispersed bitumen droplets and the air thereby severely limiting the opportunities for oxidation reactions to occur.

The reduced post-run oil saturation brought about by air injection in the core experiments indicated that air had potential as an oil scavenger from a depleted zone. Because the gas phase is nonwetting the air flows primarily through the large pore network whereas water flows mainly through the small pores. Thus, the large pores undergo more oxidation and consequently, more plugging than do the small ones. As a result, more of the fluid flow is diverted to the small pore network. This is the mechanism by which air recovers bitumen from a depleted zone and reduces the residual oil saturation. In addition to the pore scale diversion, the larger scale diversion of injection fluid from the communication path to the oil sand was responsible for the high bitumen recoveries obtained in the 1-m cell experiments. These latter experiments indicated that it was important that there be sufficient bitumen in the communication path (in the form of water in oil emulsion or free bitumen) and a high enough air concentration in the injection fluid if the bitumen recovery rate was to be significantly increased.

Injection of air at an intermediate point between water injection and production wells resulted in a lower initial pressure drop and minimized the possibility of plugging occurring. However, the reduced pressure drop was accompanied by a lower oil production. Thus, the reservoir injectivity will determine whether the use of an intermediate air injection well is appropriate for a particular field situation.

Temperature is another variable which influences the amount of fluid diversion which occurs. At the lower temperature of 170°C, it took longer for the LTO reactions to have an effect and increase recovery. However, higher ultimate pressure drops and a similar bitumen recovery was obtained at 170°C (as compared to 200°C) when the LTO reactions eventually caused hot fluid diversion.

The best air injection strategy (run 1m-3) resulted in both the fastest recovery of bitumen and in the hottest test bed. A cascading effect occurred. The initial high concentration of air in the injection fluid caused bitumen to be produced rapidly. The hot injection fluid penetrated more easily into the oil sand which now had less bitumen. The oil sand became hotter and allowed the bitumen to be produced even more quickly etc.

In run 1m-4, increasing the air concentration from 3.2% to 6.2%, by halving the water injection rate whilst maintaining the air flow rate, increased the rate at which heat was dispersed in the oil sand. This was a probably a result of a partial blockage of the bypass zone. The greatest movement was seen in the 165°C contour which indicates that heat output was greatest for the LTO reactions which occurred around 165°C.

The addition of air increased the asphaltene content of the post-run bitumen in the core experiments from a value of 16% to between 25% and 28%. This is in agreement with the expected trend whereby oils and resins are converted to asphaltenes as a result of LTO reactions. Air injection also resulted in an increased bitumen viscosity. The acid number appears to be a consistent indicator of bitumen oxidation. As a result of the formation of acid groups in the bitumen, the acid number was always increased and typically was doubled by the LTO reactions.

Coke formation increased the solids mass by 1% and, by causing increased flow resistance, contributed to the increased pressure drop which resulted from air injection. On the other hand, the amount of air injected in the water-air process should be not be so extreme that a significant percentage of recoverable bitumen is "lost" to coke formation. Thus, when diversion has been successfully obtained, air injection should be stopped. As coke formation starts at an oxygen uptake of approximately 40 g/kg of bitumen [11], this should occur when about 100 g of air per kg of bitumen in the zone where the bypass is to occur has been injected.

The ratio of CO_2 to CO in the produced gas from the water-air experiments was about 4 and this implies that most of the combustion reactions were complete. It is also possible

that some CO was consumed in the water-gas shift reaction:

$$CO + H_2O = CO_2 + H_2$$

However, the H_2 concentration in the produced gas was very low.

H_2S was detected in the water-air experiments but not in the water-only experiments. The H_2S was likely produced by reactions subsequent to the LTO reactions. These reactions may have involved H_2 which was produced in the water-gas shift reaction.

CONCLUSIONS

1. Air injection with water reduces the residual oil saturation from a zone which has previously been depleted by a waterflood. This reduced oil saturation is a result of both an increased bitumen production and the formation of coke and carbon oxide gases from the bitumen.

2. As a result of water diversion from the communication path (horizontal fracture, high permeability channel, or underlying water layer) to the oil bearing zone, coinjection of air can dramatically increase bitumen recovery from a waterflood.

3. Air injection with water results in a more rapid transmission of heat through the oil bearing zone due to faster displacement of bitumen and to heat produced by oxidation reactions.

4. A substantial percentage of the residual bitumen is converted to coke and this results in a permanently reduced absolute permeability of the depleted zone. This effect enhances diversion to oil rich regions.

5. Air injection alters the properties of the residual oil (e.g. viscosity, asphaltene content, and acid number) and creates an acidic aqueous phase, which is due primarily to the production of sulfate ions.

6. The LTO and subsequent reactions produce CO_2, CO, H_2, and H_2S.

Nomenclature

E = activation energy J/kg-mole.
k_0 = reaction rate constant, m^3/k-mole/s.
n = reaction order
Po_2 = O_2 partial pressure in gas phase, kPa.
PV = pore volume
OOIP = original oil in place
r = reaction rate, k-mole/m^3-s.
R = Universal gas law constant = 8314 J/(kg-mole K).
T = absolute temperature (K).

Acknowledgements

Some of this work was carried out as part of the Alberta Oil Sands Technology and Research Authority (AOSTRA) and Alberta Research Council (ARC) Core Research Program. Considerable input was obtained from the industrial participants in this program. Experimental work performed as a part of the TEXACO Canada Resources - Alberta Research Council long-term cooperation is also included.

The authors wish to thank Mr. G. Korpany and Mr. S. Rabeeh for performing pilot plant and data processing operations. The contribution of Ms. C. Hopper in handling the word processing must also be acknowledged.

References

1. Cram, P.J., and Redford, D.A., "Low Temperature Oxidation Process for the Recovery of Bitumen." JCPT, p 72-83, (July-Sept.), 1977.

2. Zhang, Z., Barta, L., and Hepler, L.G., "Calorimetric Method for Measuring Rates of Oxidation of Bitumen in a Porous Medium", AOSTRA J. of Res., 3, No. 4 p 249-258, Fall, 1987.

3. Babu, D.R., and Cormack, D.E., "Low Temperature Oxidation of Athabasca Bitumen." Can. J. Chem. Eng., 61, p 575-580, Aug. 1983.

4. Phillips, C.R., and Hsieh, I.C., "Oxidation Reaction Kinetics of Athabasca Bitumen." FUEL, 64, p 985-989, July 1985.

5. Adegbesan, K.O., Donnelly, J.K., Moore, R.G., and Bennion, D.W., "Low-Temperature-Oxidation Kinetic Parameters for In-Situ Combustion: Numerical Simulation", SPE Res. Eng., p 573-582, Vol 2 No. 4, Nov. 1984.

6. Dabbous, K.D., and Fulton, P.F., "Low-Temperature-Oxidation Reaction Kinetics and Effects on the In-Situ Combustion Process." SPEJ, p 253-262, June 1974.

7. Burger, J.G., and Sahuquet, B.C., "Chemical Aspects of In-Situ Combustion-Heat of Combustion and Kinetics", SPEJ, p 410-422, Oct. 1972.

8. Urban, D.L., and Udell, K.S., "The Effects of Steam on the Combustion of Oil Sand", 63rd Annual Technical Conference and Exhibition of SPE, Houston, Texas, Oct. 2-5, 1988.

9. Millour, J.P., Moore, R.G., Bennion,D.W., Ursenbach, M.G. "An Expanded Compositional Model for the Low Temperature Oxidation of Athabasca Bitumen", JCPT, 26, No. 3, p 24-32, (May-June), 1987.

10. Moore, R.G., Bennion, D.W., and Ursenbach, M.G., "A Review of In-Situ Combustion Mechanisms", Paper No. 50, Fourth UNITAR/UNDP Conference on Heavy Crude and Tar Sands, Edmonton, Canada, August 7-12, 1988.

11. Babu, D.R., and Cormack, D.E., "Coking of Athabasca Bitumen: Effect of Oxidation and Sand." FUEL, 62, p 350-352, March 1983.

12. Babu, D.R., and Cormack, D.E., "Effect of Oxidation on the Viscosity of Athabasca

Bitumen." Can. J. Chem. Eng., 62, p 562-564, Aug. 1984.

13. Ivory, J., De Rocco, M., and Paradis, N., "Investigation of the Mechanisms Involved in the Steam-Air Injection Process", Petroleum Society of CIM, Saskatchewan Petroleum Conference, Sept. 25-27, 1989.

14. Coates, R., "Physical Simulator for Horizontal Well", WRI-DOE Tar Sand Symp., June 1985, Vail, Co.

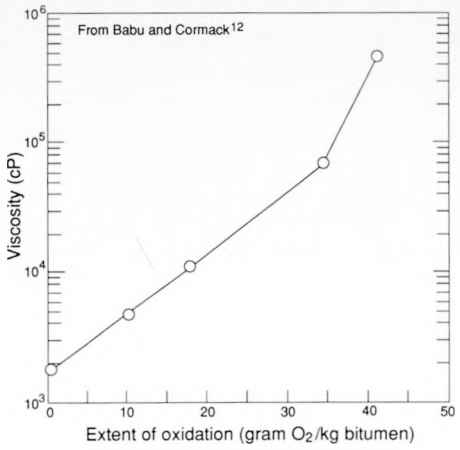

Figure 1. Bitumen viscosity at 78°C versus extent of oxidation.

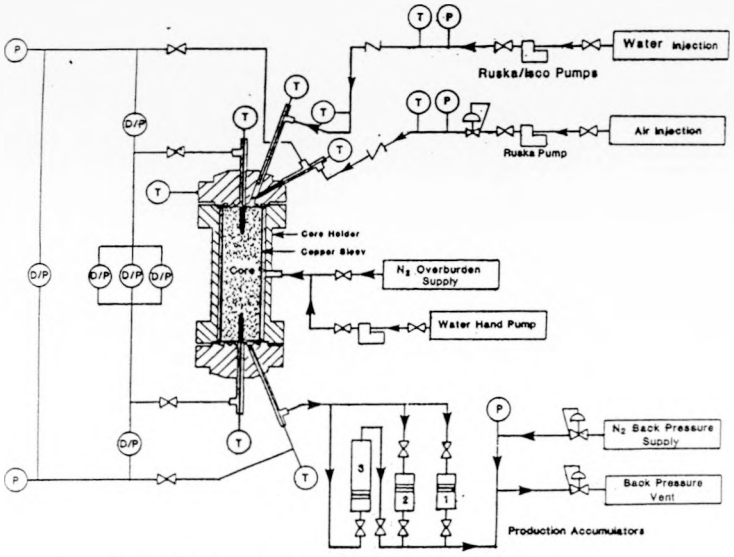

Figure 2 : Flow Diagram For Core Test Facility

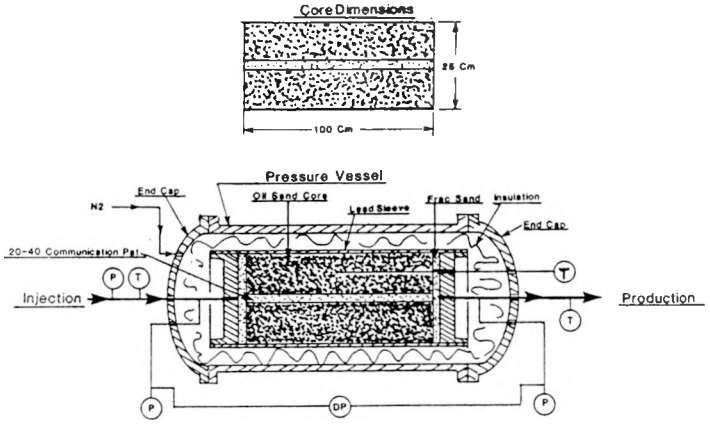

Figure 3. 1-m Cell Configuration

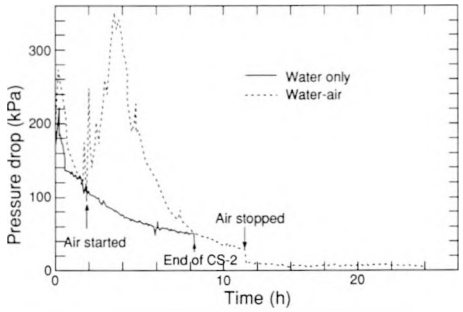

Figure 4. Pressure drop versus time for water-only run CS-2 and water-air run CS-9.

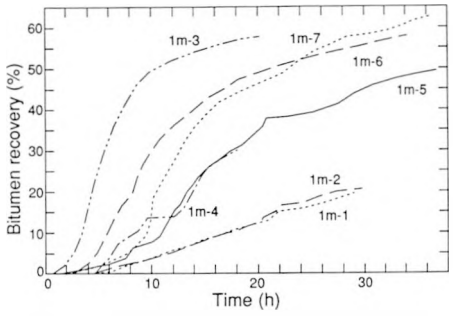

Figure 5. Percent bitumen recovery versus time for hot water run 1m-1 and hot water-air runs 1m-2 to 1m-7.

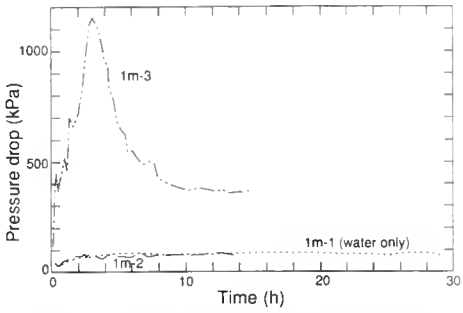

Figure 6. Pressure drop versus time for water only (1m-1) and water-air (1m-2 and 1m-3) experiments.

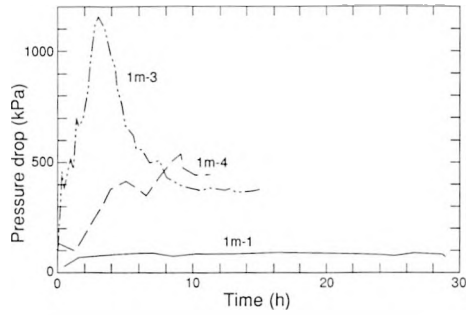

Figure 7. Pressure drop versus time for hot water run 1m-1 and water-air runs 1m-3 and 1m-4.

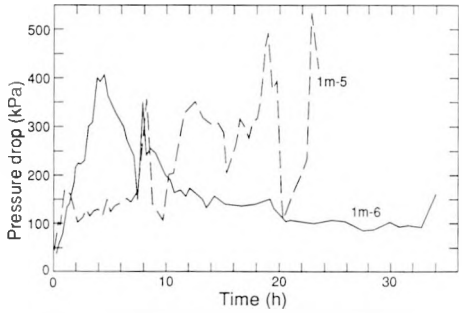

Figure 8. Pressure drop versus time for hot water-air experiments 1m-5 and 1m-6.

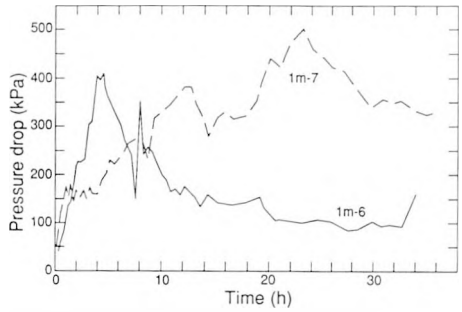

Figure 9. Pressure drop versus time for hot water-air experiments 1m-6 and 1m-7.

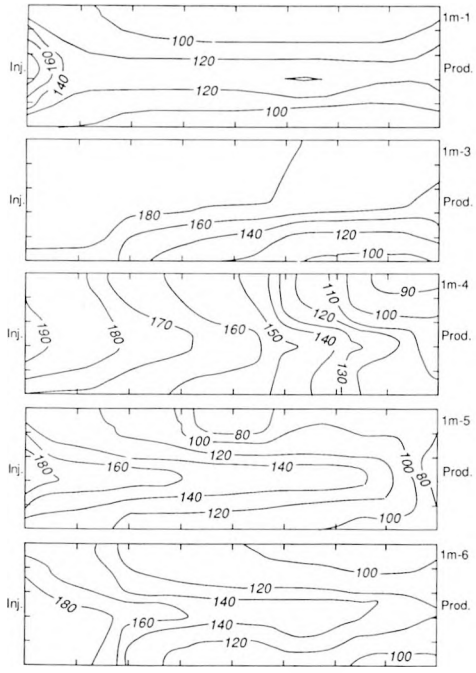

Figure 10. Temperature profiles at 5 hours.

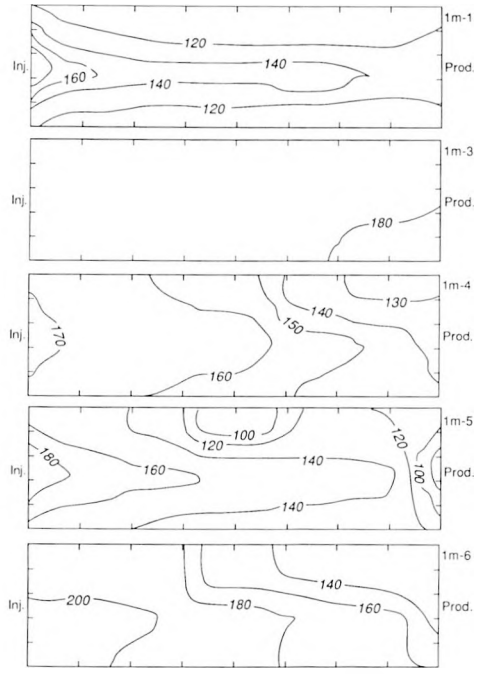

Figure 11. Temperature profiles at 10 hours (1m-4 is at 8.33 hours).

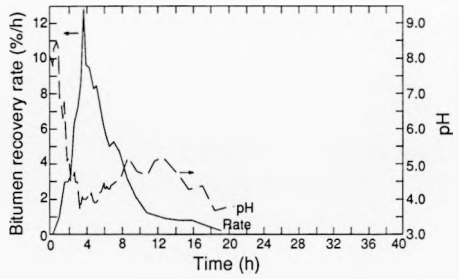

Figure 13. Bitumen recovery rate and pH vs time for run 1m-3.

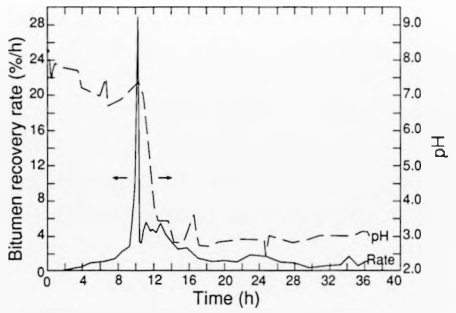

Figure 14. Bitumen recovery rate and pH vs time for run 1m-7.

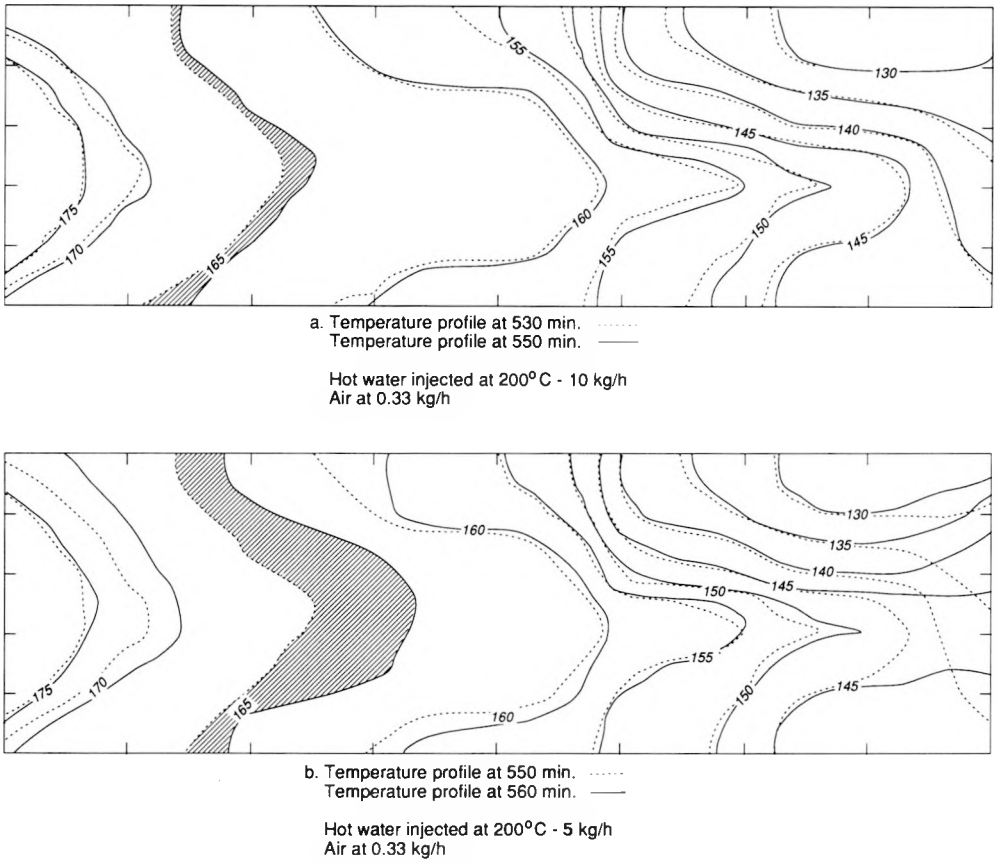

Figure 12. Temperature profiles before and after a step increase of air concentration in run 1m-4.

Effect of Horizontal Wells on Sweep Efficiencies When Practicing Enhanced Oil Recovery in Heavy Oil Reservoirs

by

J.A. Lane, Terry Strickland, and Paul B. Crawford
Petroleum Engineering Department
Texas A&M University
College Station, Texas 77843

Abstract. It has been estimated that slightly more than 500 billion barrels of oil were originally in place in reservoirs which have been discovered today. Of this amount, approximately one-third (170 billion barrels) of this oil has been produced. This leaves approximately 350 billion barrels of the oil underground, and much of this oil is heavy oil.

Studies were also made for direct line drive patterns in which horizontal wells were positioned at both production and injection wells. This system can lead to the highest achievable sweep efficiencies. The approximate cost for horizontal wells is given. These costs include approximate cost for preparing the old well, for drilling, and for completion.

Horizontal drilling is now finding applications in many oil producing provinces of the world. The length of the horizontal leg may vary from a few hundred feet to a few thousand feet. Under conventional producing methods, most of the heavy oil remains in the reservoir at abandonment. If water flooding is initiated, the viscosity ratios are so unfavorable that little additional oil can be expected in most cases. It was believed that horizontal wells might substantially increase the sweep efficiencies in heavy oil reservoirs. This paper reports on the greatly improved sweep efficiencies which may be possible when using properly oriented horizontal wells in heavy oil reservoirs. Studies were also made of areal sweep efficiencies which may result if a horizontal well were drilled in an unfavorable direction, that is a horizontal well that is parallel to flow between injection and producing wells.

Introduction

Horizontal drilling is in its infancy, but it appears to represent a very significant technical achievement. Horizontal wells are normally drilled for additional primary recovery. Many horizontal wells have provided greatly increased oil production rates over conventional oil rates using vertical wells. This has generated considerable interest in horizontal drilling. The technology of drilling horizontal wells has improved, and this has led to lower costs and faster payout. Directional measurement and control has greatly improved and led to greater confidence in horizontal drilling. Horizontal wells are being drilled with considerable confidence having lateral lengths in excess of one thousand feet. Success at the shorter lengths has led to the conceptual considerations of horizontal reaches of a few miles. Horizontal wells change the pressure gradient about the well bore. For a given draw-down the total flow rate may be much greater than a vertical well and, in addition, coning pressure gradients are greatly reduced.

Eventually we can expect to see horizontal wells being drilled for improved enhanced oil recovery programs. In some cases it will be desired to study the prospects of enhanced oil recovery in oil fields that have been developed using horizontal wells. Since the effect of horizontal wells on areal sweep efficiencies has not been reported on, it was believed desirable that such a study be made.

Results

Figure 1 illustrates a single horizontal well. With short, medium, and long turning radii, the horizontal reach may extend for only a few hundred feet to several thousand feet. Directional control is reasonably accurate. Initially the wells are usually drilled for improved rate of production; however, it is likely that an enhanced oil recovery program may be practiced at a later time. It was believed that well orientation could have a very large effect on the enhanced oil recovery program; so well orientation was studied.

The first orientation studied was for the case when the horizontal well was drilled directly from an injection well toward a producing well. Much of the reservoir will be by-passed, and it was desired to study this effect. The results apply for the case of direct line drive patterns with length to width ratios of 1.5 to one.

Unfavorably Positioned Horizontal Wells

Figure 2 was developed to show the areal sweep efficiency when the horizontal well was oriented in an unfavorable direction. The horizontal well was drilled from an injection well directly toward a producing well. It will be seen that the areal sweep efficiency would be 70.6 percent if no horizontal extension existed at the injection well. If the length of the horizontal leg were only 100 feet, the the swept area would be

reduced to near 50 percent of the pattern area. If the horizontal well was 200 feet long, the swept area at breakthrough would be reduced to only 30 percent of the pattern area. If the horizontal well were over 350 feet long, the swept area would approach zero percent at breakthrough.

Injection Wells With Favorable Horizontal Wells

It may be that only the injection wells have horizontal wells and these horizontal wells are all oriented in a favorable direction. A favorable direction would be a horizontal well drilled at one injection well toward the adjacent injection well. Such a horizontal extension would also be perpendicular to a line connecting the injection and producing well.

Information was also developed to show the area swept when only one class of well, injection or producing, had horizontal wells. Without horizontal legs the area swept would be 70.6 percent. If the length of the horizontal well were 135 feet, then the area swept at breakthrough would be near 85 percent of the pattern area. By increasing the length of the horizontal well to near 270 feet, the area swept would only be near 88 percent of the pattern area.

Ideally Positioned Horizontal Wells

If both injection and producing wells were drilled with horizontal extensions it would be possible to develop the ideal system. In this case a line of injection wells would be connected by their horizontal wells, and the line of producing wells would be connected by their own horizontal wells. Flow would be perpendicular to the horizontal wells. Breakthrough would occur at one pore volume of displaceable fluid injected and the area swept would be 100 percent. This represents the target for enhanced oil recovery.

Discussion and Conclusions

The technology of drilling horizontal wells has evolved into a reasonably accepted practice. Although only a limited data base is now available, previous success has been sufficient to expect a fairly wide-spread use of the method. Initial rates of production have been exceedingly good in some instances. Such results will drive the process, and we can soon expect to explore the prospects of applying enhanced oil recovery in oil fields in which horizontal wells have been drilled. Hence, it is necessary that the effect of horizontal wells on enhanced oil recovery be studied.

Laboratory studies indicated that the injectivity of horizontal wells may be several times greater than that of conventional vertical wells. It was also found that horizontal wells can either increase or decrease the areal sweep efficiency. The results depend largely on the orientation.

Increased areal sweeps were observed when the horizontal wells were drilled perpendicular to the direction of the flood or flow of fluid in the enhanced oil recovery

program. If both input and output wells had horizontal wells, it is possible to approach an areal sweep of near 100 percent. An improvement was noted if only one well had a horizontal well.

Decreased areal sweeps were observed when the horizontal well was drilled in a direction parallel to the direction of the flood. It is imperative that this procedure be guarded against.

In practicing enhanced oil recovery in viscous oil reserves, it is anticipated that the injected fluid will breakthrough when about half of the pattern has been swept. Horizontal wells have the potential of increasing the swept area to near 100 percent.

Horizontal wells have increased rates of production and injection. When properly applied, increased areal sweeps can result. Fields being developed using horizontal wells for increased primary recovery should surely consider and select orientations favorable for enhanced oil recovery. Significant benefits may be possible for heavy viscous oil reservoirs.

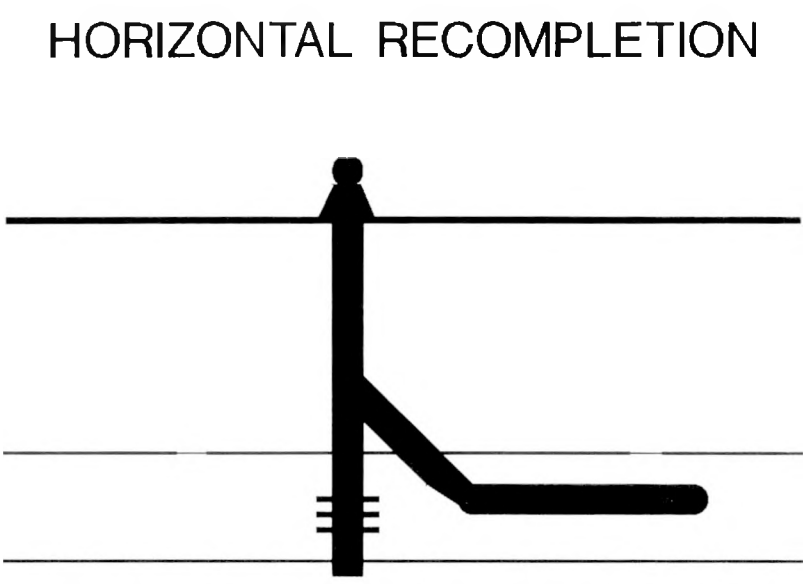

Figure 1. An artist's rendering of a horizontal well.

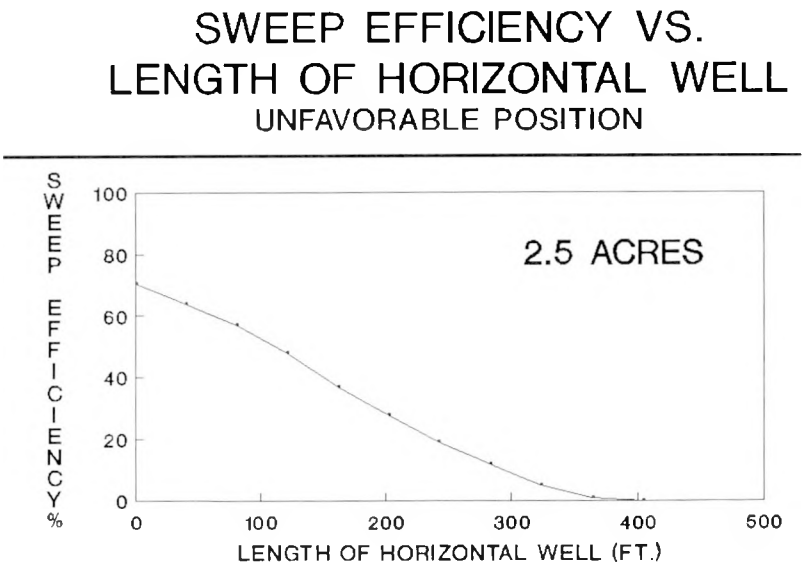

Figure 2. Sweep efficiency as a function of the length of a horizontal well located in an unfavorable position.

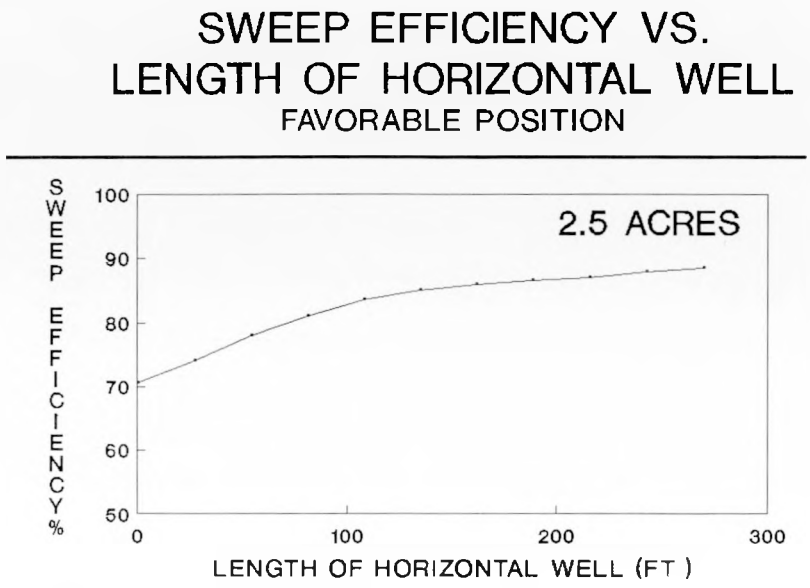

Figure 3. Sweep efficiency as a function of the length for horizontal wells located in a favorable position at the injection well.

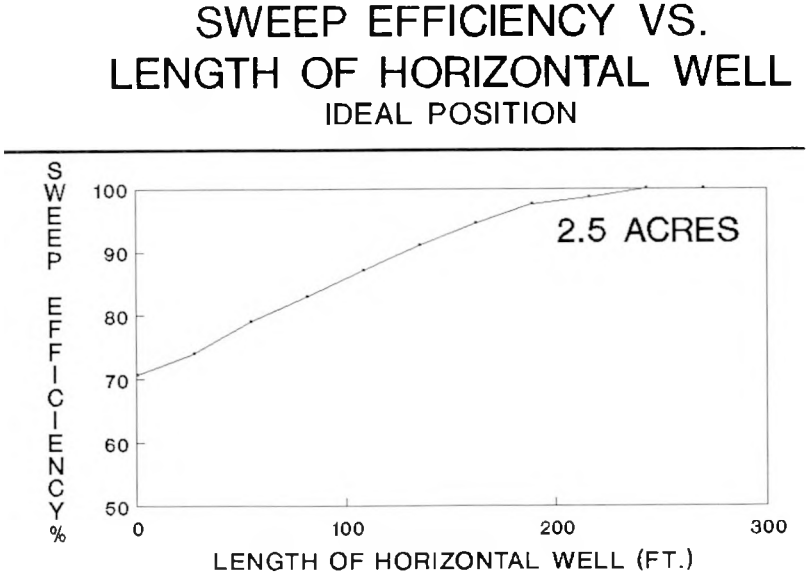

Figure 4. Sweep efficiency as a function of the length for horizontal wells located in a favorable position at both the producing and injection wells.

Properties of GPC Separated Maltene Fractions Derived from Utah and Athabasca Bitumen

by

L.S. Kotlyar, D.S. Montgomery, J.R. Woods, B.D. Sparks, and J.A. Ripmeester
National Research Council — Division of Chemistry
Ottawa, Ontario CANADA K1A 0R9

Abstract. This work deals with bitumens derived from two different types of oil sands: 1) Athabasca from the McMurray formation in Alberta, Canada and 2) from the Unita basin in the green River formation, Utah, USA. Maltenes separated from these two bitumen were fractionated by Gel Permeation Chromatography (GPC) into fractions having number average molecular weights in the range from 289 to 5831 for Athabasca and from 300 to 11985 for Utah maltenes. The fractions obtained were examined by vapor pressure osmometry, absorption spectrometry in the visible region as well as proton and ^{13}C NMR. Utah fractions were more aliphatic with longer average aliphatic chain length. Branched and alicyclic types were more abundant in the Utah samples, especially those of low MW. There was an apparent difference in the hydrocarbon structure of both maltene GPC fractions at MW approximating 800. An abrupt change in the correlation between the light absorbing parameter K_{500}/K_{600} and molecular weight at MW approximating 800 was also observed. It is suggested that these rapid changes provide a convenient means of dividing the maltenes into two classes which may be used to characterize the maltenes of heavy oils and bitumens derived from various sources.

Introduction

The dependence of the world oil supply upon middle East reserves has encouraged the development of processes to extract the bitumen from oil sands and to convert the bitumen into synthetic crude oil. Associated with this development there has been a perceived need to constantly improve the methods of characterizing the bitumen for resource evaluation and for estimating the influence of variations in the quality of the feedstocks upon the various upgrading processes. Frequently a specific application such as the selection of feedstocks suitable for the production of carbon fibres will focus on a rather narrow class of compounds in the crude oil. For example, the class of compounds which on pyrolysis will yield mesophase coke with large flow type structure. The work of Wong and Yen[1] has shown that the asphaltene gives "fine-grained mosaic structure" coke on pyrolysis and is therefore unsuitable. Nomura et al.[2] showed that fractionation on a magnesium silicate column produced a benzene eluate which had the required properties. Wong and Yen[1] fractionated the maltene on silica gel and identified the toluene eluate as being the most promising fraction in terms of giving the required "coarse-grained mosaic structure" on pyrolysis. Greinke[3] studied the thermal polymerization of pitch molecules using Gel Permeation Chromatography (GPC) and reported that molecules in the molecular weight (MW) range 400-700 daltons were the most reactive, i.e. produce mesophase with large flow structure, while those with MW higher than 1200 were essentially unreactive. If this were so, it may be a better strategy to bring about the initial separation of the maltene fractions lying within the molecular weight range of interest using relatively simple and rapid GPC method and then, if necessary, re-fractionate the fractions by chemical type. As a first step toward clarifying this issue the maltene fractions of two contrasting types of bitumen such as Athabasca and Utah, were fractionated by GPC on a preparative scale and the variations that occurred in the elemental composition were monitored as well as changes in the structural types by NMR. For convenience in determining the appropriate cut points during the fractionation by GPC the absorption spectra in the visible region of the various fractions were also monitored.

Experimental

The oil sands samples used in this work were obtained from the Suncor quarry in Fort McMurray, Alberta, Canada, and from the Unita Basin in the Green River Formation, Utah, USA.

The separation and analysis of oil sands was performed using the Soxhlet extraction-Dean and Stark method with toluene as the solvent[4]. The solvent was removed first at 80°C in a Brinkman rotary evaporator under reduced pressure and finally in a Brinkman SC/24 R sample concentrator at 90°C under nitrogen. Asphaltenes were separated by a standardized procedure which involved dissolution of the sample in an equal volume of benzene followed by subsequent dilution of the solution with ~40 volumes of n-pentane.[5] Maltenes were then obtained by evaporation of the filtrate. The yields of Utah and Athabasca asphaltenes were 16.2% and 14.0% respectively.

Table 1. Conditions for Preparative and Analytical GPC Separations

	PREPARATIVE	ANALYTICAL
Pump	P.E. Series 3B	P.E. Series 3B
Solvent	Toluene (Anechemia)	Chloroform (Fisher)
Column	Waters Styragel 500Å (2cmx122cm)	Waters Ultrastyragel Set: 1000, 500, 100Å (7.8mmx30cm)
Flowrate	9.9 ml/min	1 ml/min
Temperature	22°C	40°C
Pressure	3 Mpa	7 Mpa
Sample loop volume	5 ml	0.2 ml
Sample loading	0.2 g (2 ml injected)	0.2 mg (5 ml injected)
Valve description	Rheodyne 7125	P.E. ISS100 Autosampler
Detector(s)	Waters R401 R.I.	P.E. LC 25 R.I.
Interface	P.E. Chromatography	Nelson Analytical 900
Computer	Model 3600 P.E.	IBM AT Compatible
Software	P.E. Chromatographics 2	Nelson Analytical 2600 & 2900

The elemental analysis (C,H,N) was performed using a Perkin-Elmer model 240 CHN analyser. Sulfur was analysed by a titrimetric oxygen flask combustion method, using a Schöniger type combustion apparatus[6]. Preparative GPC separation was performed under the conditions outlined in Table 1. All samples and the mobile phase were first filtered through 0.45 μm membrane filters. Ten GPC effluent fractions (1 through 10) were collected on a time basis (1.5 min/sample) and evaporated in vacuo at 100°C in a Brinkman SC/24R sample concentrator. The maltenes were also subjected to an analytical GPC separation under the conditions given in Table 1.

The number average molecular weights of the preparative scale fractions were determined by vapor pressure osmometry (VPO) using a Wescan Model 232A instrument. The determinations were carried out in toluene at four or five concentrations (C) at room temperature.

Light absorbance measurements were made in the visible range of wavelengths using a Milton Roy Spectronic 501 spectrophotometer equipped with a 10 mm pathlength cell and a Mr. Sipper peristaltic pump. The maltenes fractions were dissolved in toluene for absorption measurements. The concentrations were expressed as g/100 mL. The error in light absorbance determinations on separate samples was ±2%.

Proton NMR measurements were performed on a Bruker MSL 300 spectrometer. Spectra were recorded in solution in $CDCL_3$. The ^{13}C NMR spectra were run using the same instrument. A paramagnetic relaxation agent, chromium (III) acetylacetonate was added to the solutions of bitumen fractions in deuterochloroform to allow for a short delay time between pulses in the carbon-13 channel. Data was collected at a sweepwidth setting of 20 kHz with inverse gated proton decoupling to suppress the nuclear Overhouser effect (nOe). A pulse flip angle of 45° was used with a pulse repetition time of 2 sec. Between 10000 and 20000 transients were collected in order to obtain an adequate signal to noise ratio.

RESULTS

Yields and molecular weights Maltenes were arbitrarily separated by preparative GPC into 10 fractions. The VPO number average molecular weights (MW) of the Utah and Athabasca maltenes GPC fractions eluted from the column are listed in Table 2. The molecular weight distributions of these fractions are shown in Figure 1. The results are expressed as cumulative weight percent, normalized for experimental losses vs molecular weights. It can be seen that the molecular weights of the various GPC fractions separated from Utah maltenes lie in a very broad range from 300 to 11985. This range is broader than that for the corresponding fractions derived from Athabasca maltenes (289 to 5831). It is also apparent that the weight percentage contribution of the high molecular weight fraction of the Utah maltenes is far greater than that for the Athabasca maltene.

Table 2 Molecular weights and light absorbance data for Utah GPC maltenes fractions

GPC Fraction	MW (VPO) Utah	MW (VPO) Athabasca	K_{400}/K_{600} [b] Utah	K_{400}/K_{600} [b] Athabasca
1	11985[a]	5831[a]	1.9	n.e.
2	8322	5735	2.1	n.e.
3	4315	3696	2.4	2.7
4	2115	2385	3.0	3.1
5	1223	1402	4.2	3.6
6	737	800	5.2	4.0
7	494	568	5.0	5.0
8	365	365	5.0	6.0
9	330	315	4.8	5.3
10	300	289[c]	n.e	4.8

[a]insufficient amount for carbon and proton NMR analysis
[b]measured at a concentration C = 0.17 g/100 mL
[c]sample size insufficient for carbon NMR examination
n.e. insufficient amount

Table 3. Elemental analysis of GPC fractions

GPC fraction #	Elemental analysis % C	H	N	S	O(dif)	H/C
Athabasca						
1	79.8	9.7	0.74	5.3	4.5	1.45
2	79.0	10.0	0.65	5.1	5.2	1.52
3	79.7	10.1	0.50	4.9	4.8	1.52
4	78.1	10.0	0.44	5.1	6.4	1.54
5	79.9	10.4	0.34	5.4	4.0	1.56
6	80.5	10.5	0.31	5.8	2.9	1.56
7	80.1	10.6	0.26	5.7	3.3	1.59
8	81.0	10.6	0.14	5.0	3.3	1.57
9	81.2	9.2	0.18	6.1	3.3	1.35
10	86.6	9.6	0.72	2.2	0.9	1.33
Utah						
1	85.5	10.1	1.37	tr	3.0	1.42
2	85.1	11.5	0.89	tr	2.5	1.62
3	85.4	11.8	0.67	tr	2.1	1.66
4	85.3	11.9	0.59	tr	2.2	1.67
5	85.7	12.0	0.48	tr	1.8	1.68
6	85.9	12.1	0.31	tr	1.7	1.69
7	85.8	11.7	0.28	tr	2.2	1.64
8	85.6	11.4	0.20	tr	2.8	1.60
9	85.4	11.3	0.20	tr	3.1	1.59
10	85.4	10.2	0.20	tr	4.2	1.43

Elemental analysis Elemental compositions and atomic H/C ratios of Utah and Athabasca maltenes GPC fractions are given in Table 3. It can be seen that nitrogen contents of Utah fractions 1 through 8 were higher compared to those determined for the corresponding Athabasca samples (with the exception of fraction 6). Athabasca maltenes fractions 9 and 10 were more abundant in nitrogen that those of Utah oil sands. Sulfur was present in Utah oil sands only in trace amounts. The H/C ratios of Athabasca maltene fractions were lower than the corresponding fractions of Utah maltenes (with the exception of fraction 1) indicating that the former have more aromatic character than the latter. It will be noted that as the molecular weight of the Utah fractions decreases the H/C ratio goes through a maximum value of 1.69 corresponding to fraction 6. This type of correspondence between MW and H/C was observed for Athabasca fractions and seems to be a common phenomenon for maltenes fractionated in this manner[7]. This result will be discussed more fully later.

Absorption spectroscopy The absorption of light by bitumen and bitumen fractions such as the asphaltenes and maltenes follows the Beer-Lambert law:

$$A = \text{Log } P_o/P = ecd \qquad (1)$$

where

A is absorbance.
Po is intensity of incident radiation
P is the transmitted radiation.
c is the concentration of solute in mol/L
d is the cell thickness in cm
e is molar absorptivity (molar extinction coefficient) of the solution at wavelength l.

In complex naturally occurring substances such as bitumens and humic acids, which possess a wide molecular weight distribution, the measurement of molecular weight introduces some uncertainties. It is therefore convenient to follow Flaig et al.,[8] and to change the units of measurement of concentration from c=mol/L to C=mg/100 ml so that Equation (1) assumes the following form:

$$A = \text{Log } P_o/P = ecd = (0.01e/M)Cd \qquad (2)$$

where M is the molecular weight of the substance. For a cell path length of 1 cm Equation (2) becomes:

$$A = \text{Log } P_o/P = (0.01e/M)C = K \qquad (3)$$

The quantity K, defined as the extinction coefficient[8a] is then directly proportional to the concentration C. It has been demonstrated that for a series of solutions of different concentrations of a bituminous substance with a given average molecular weight, that when log K is plotted against the wavelength of light a series of parallel lines is obtained, each associated with a given concentration. These lines are approximately straight over a considerable range of wavelength. These lines differ in their intercepts on the axes depending on the concentrations and the average molecular weight of the sample. This leads to the possibility of characterizing the chemical nature of the molecules which compose the bitumen fractions, by colour type, through the determination of the slope of any of these lines.

In this work the slopes of the absorption curves for Utah and Athabasca maltenes GPC fractions were characterized by the ratios of absorption at 500 nm to that at 600 nm and this function was plotted against MW (VPO) (Figure 2).

Several conclusions may be derived from the results presented in Figure 2: 1) the highest MW maltene fractions which possess the most intense color have the lowest K_{500}/K_{600} ratio and hence the lowest slope of absorption curve; 2) with decrease in MW down to 737 the value of K_{500}/K_{600} increases almost linearly, suggesting that the number of the light absorbing chromophors is proportional to their MW as was found for Athabasca asphaltenes;[9,10] 3) the observation that similar MW Athabasca and Utah maltenes GPC fractions have similar K_{500}/K_{600} suggests similarity in nature and number of their light absorbing chromophors.

Proton NMR Proton NMR spectra of the GPC separated Utah and Athabasca maltenes resemble each other with the main difference being the relative concentrations of the various structural groups indicated by the peak intensities in specific chemical shift ranges. On the basis of these data the distributions of different types of protons in the spectra were calculated. Assignments for the chemical shifts are given in Table 4.[11] The results obtained plotted against MW for different GPC fractions are presented in Figures 3-5. As can be seen from Figure 3 that proton aromaticities (percent of aromatic proton per total proton, H_{ar}, 8.7-6.0 ppm chemical shift region) of all fractions are low, which point to a high degree of aromatic substitution by aliphatic chains and rings. In both the Athabasca and Utah maltenes the lowest MW fractions have the highest proton aromaticity. H_{ar} decreases rapidly while going from fractions 10 to 8 and then changes are less pronounced especially for Utah maltenes. It also follows from Figure 3 that for a given molecular weight the Athabasca fractions contain a higher concentration of aromatic protons as compared to the corresponding Utah samples. A common feature for both Utah and Athabasca maltenes is that the signals due to methylene hydrogens in long-chain or branched hydrocarbons (H_β, 1.5 -1.0 ppm) are the least prominent in the lowest MW fractions. From fraction 10 to 6 the H_β content increases rapidly (Figure 3). For fractions with MW >800 changes in H_β are not as pronounced. It is apparent that the concentration of methylene hydrogen is greater for the Utah maltenes as compared to Athabasca maltenes fractions of corresponding molecular weight.

Table 4 Assignment for chemical shifts in ^1H spectra

Hydrogen type	Symbol	Chemical shift, ppm
Aromatic	H_{ar}	6.0-8.7
CH_3, CH_2 and CH α to an aromatic ring	H_α	2.0-3.4
CH_2 and CH ß to an aromatic ring and in naphthenic rings	H_n	1.5-2.0
ß-CH_3, CH_2 and CH or further from an aromatic ring	H_β	1.0-1.5
CH_3 γ or further from an aromatic ring	$H\gamma$	0.5-1.0

The Utah maltene fractions also appear to have higher degrees of branching (estimated as the ratio $H\gamma/H_\beta$) than the corresponding Athabasca samples (Figure 4). In the maltene fractions from both Athabasca and Utah the degree of branching decreases rapidly with increase in MW for fractions with MW below 800. The concentration of alkyl groups or saturated bridges attached to aromatic rings is indicated by the magnitude of H_α (3.4 -2.0 ppm). Similar to the Athabasca maltenes the Utah H_α content is the highest in the lowest MW fractions and decrease noticeably in the range of from 300 to 737 (Figure 5). Changes in H_α for higher MW samples are slight. For any given molecular weight the concentration of H_α is greater in Athabasca maltenes fractions than in the Utah maltenes.

Carbon-13 NMR Typical ^{13}C NMR spectra for maltenes GPC fractions are presented in Figure 6 (results for Utah maltene). Chemical shifts were assigned based on the results reported by Suzuki et al.[12] and Thiel and Gray[13]. The aromatic carbons in the spectra are represented by broad peaks in the range from 118 to 160 ppm. The carbon aromaticity (C_{ar}, percent of aromatic carbon to total carbon) calculated for various fractions are plotted against MW in Figure 7. The common feature for both maltenes is that 1) the lowest MW fractions possess highest C_{ar} 2) in the range of MW from 800 to 300 C_{ar} increases rather rapidly with decreasing molecular weights and 3) for fractions with MW >800 changes in C_{ar} are relatively slight but C_{ar} increases with increasing MW. The obvious factor differentiating maltenes was that the aromaticities of Athabasca fractions were higher then the Utah maltene fractions of corresponding molecular weight.

The straight alkyl chains are represented in the spectra as a set of signals at 14.1, 22.7, 32, and 29.7 ppm assigned to C_1 (terminal), C_2, C_3 and central methylene groups (C_n), respectively. The main feature of the spectra in Figure 6 is that the signals at 29.7 ppm were the strongest in the highest molecular weight fraction. For the low MW fractions intensity of central methylene groups decreased dramatically.

The average chain lengths were estimated knowing the ratio of the signals at 29.7 ppm to 14.1 ppm plus 5 plus the area of the branched methyl (19.7 ppm).[14] The results obtained plotted against MW in Fig. 8 indicate that (1) for both Athabasca and Utah maltenes the average chain lengths increase with increase in MW, (2) aliphatic chains of Utah fractions are longer compared with the corresponding fractions separated from Athabasca maltenes, (3) the most significant increase in the average chain lengths takes place in the range of MW from 300 to 800.

The featureless hump in the chemical shift range of about 55-25 ppm in the carbon spectra is associated with carbons of fused -ring/naphthenic cycloalkanes, branched paraffinic carbon and (or) short alkyl substituents on the aromatic rings. These structures seem to be more abundant in low MW fractions since more pronounced unresolved

envelopes are observed for samples 8 through 10 in Figure 6. Higher concentrations of alicyclic structures in the spectra of low MW GPC fractions is also indicated by more pronounced broad signal at 42.2-42.4 ppm[13]. The proportion of these structures was higher in Utah fractions as compared with the Athabasca fractions of corresponding MW. In summary, results of proton and carbon-13 NMR examination suggest that: (1) Utah maltenes fractions are more aliphatic with the average length of aliphatic chains longer as compared to corresponding fractions separated from Athabasca bitumens. Branched and alicyclic structures are more abundant in Utah fractions, especially those of low MW; (2) in maltenes from both sources the lowest MW fractions have highest aromaticity, lowest average aliphatic chain length and are more abundant in alicyclic and branched structures.

Discussion

As a result of GPC separation of Utah maltenes, fractions 1 through 10 were obtained with number average molecular weight ranging from 300 to 11985 (VPO). Similar to the results of fractionating Athabasca maltenes by GPC there was a break in the properties of GPC Utah maltene fractions at a MW of 737. Therefore we may divide the fractions into two groups: 1) MW ≤737 and 2) MW >737. Group 1 includes fractions 6 through 10 accounting for 55 % of Utah maltenes. This percentage yield is considerably less than that of fractions 6 through 10 of Athabasca maltenes (73,5 %). Group 2, fractions 1 through 5 constitute 45 % of the Utah maltenes.

The lowest MW fraction 10 is highly aromatic and as the MW increases from 300 to 737, C_{ar} decreases rapidly (Figure 7) while H/C ratio increases (Table 3). The presence of a high proportion of mono, di and tri aromatics could be responsible for the high value of C_{ar} and, consequently, the low H/C atomic ratio of this fraction[15]. The results of NMR analysis indicate that the aromatic rings present in the lowest MW fraction contain a substantial proportion of methyl, alicyclic and branched structures as substituents on the aromatic rings which suggests a significant concentration of alkyl groups or saturated bridges.[13] With increase in the maltene MW the contribution of longer side chains as substituents and the concentration of the saturate class becomes apparent. For example, fraction 6 (MW=737) has the lowest value of C_{ar} and the highest value of H/C. This suggests that similar to Athabasca maltenes this fraction may be enriched with the saturate class which effectively reduces the concentration of C_{ar}.

Similar to the Athabasca maltenes the degree of aromatic ring condensation (DARC) estimated from IR in low molecular weight Utah fractions is low.[7] Since polycondensed aromatic rings are considered to be a major source of light absorbing chromophores in bitumens, a low DARC would suggest a low number of chromophores. This suggestion is in accord with high K_{500}/K_{600} determined for these fractions (Table 2).

Group 2 GPC fractions 1 through 5 have molecular weights greater than 737. Carbon aromaticities of these samples are relatively low and change relatively slightly only from 16.7% to 21 % with increase in MW from 1223 (fraction 5) to 8322 (fraction 2) (Figure 7). Aromatic hydrogen content of the fractions in this range of MW are low indicating a high degree of aromatic ring substitution. As in the case of similar MW Athabasca fractions the major substituents are long aliphatic hydrocarbon chains. There is an indication that the high MW maltene GPC fractions have a high degree of aromatic ring condensation (DARC)[16] so the presence of long aliphatic hydrocarbon chains could be necessary in order to facilitate the solubilization of such polycyclic systems in n-pentane. It may be suggested on this basis that the solubility of the fractions having large clusters of condensed aromatic rings may be easily influenced by relatively small changes in the average aliphatic structures. This could explain why a slight increase in the average chain length from 18.7 to 20.2 carbon atoms per molecule (Figure 8) is associated with a dramatic increase in MW from 737 to 8322 and that the high MW fractions remain soluble in n-pentane in spite of an increase in C_{ar}. As indicated in Figure 7 the Utah fractions are more aliphatic as compared to Athabasca. This could also account for the fact that the weight percentage contribution of the high molecular weight fraction of the Utah maltenes is far greater than that of the Athabasca maltene. As was demonstrated by the results presented in Figure 2, Utah and Athabasca maltenes fractions of similar MW have similar K_{500}/K_{600}. This observation suggests that the nature and number of the light absorbing chromophors present in these fractions and consequently their DARC values are similar.

Conclusion

The separation of Utah maltenes by gel permeation chromatography using Styragel on a preparative scale resulted in the fractionation according to molecular weight extending from 300 to 11985 daltons as measured by vapor pressure osmometry. Utah maltenes fractions, compared with Athabasca maltenes of the same molecular weight, were more aliphatic with an average aliphatic chain length longer than those found in similar MW fractions separated from Athabasca bitumens. Branched and alicyclic structures are more abundant in Utah fractions, especially those of low MW. In the case of both Athabasca and Utah maltenes the lowest MW fractions have the highest percentage of aromatic carbon atoms, the lowest average chain length and a greater abundance of alicyclic and branched structures. As indicated by the results of the NMR examination there is an apparent difference in the hydrocarbon structure of both Utah and Athabasca maltenes GPC fractions at MW approximating 800. It was concluded that the rapid change of hydrocarbon type with respect to MW provides a convenient means of dividing the maltenes into two classes which may be used to characterize the maltenes of heavy oils and bitumens. There was also an abrupt change in the correlation between the light absorbing parameters K_{500}/K_{600} and molecular weight of GPC fractions at MW approximating 800. This provides a second method of dividing the maltenes into two classes based on light absorption data that are sensitive to the presence of condensed aromatic systems.

Acknowledgement

We would like to acknowledge the help of J.R.H. Séguin (elemental analysis).

References

1. Wong, E. and Yen, T.F. Energy Sources, 1988, 10, 201.

2. Nomura, M., Ida, T., Shimatani, T. and Notsu, S., AOSTRA J. Res., 1988, 4, 287.

3. Greinke, R.A., Carbon, 1986, 24, 677.

4. Syncrude Analytical Methods for Oil Sand and Bitumen Processing, Syncrude Canada Ltd., Edmonton, Alberta, August 1979, p. 58.

5. Mitchell D.L. and Speight, J.G., Fuel, 1973, 52, 149.

6. Schöniger, W., in "Proceedings of the International symposium on Microchemistry, 1958", Pergamon, N.Y. , 1960, p. 93.

7. Yang, P.W., Mantsch, H.H., Kotlyar, L.S. and Woods, J.R., Energy and Fuels, 1988, 2, 26.

8. (a) Flaig, W., Beutelspacher, H. and Rietz, E. "Chemical composition and physical properties of humic substances" in "Soil Components" volume I, ed by J.E. Gieseking, N.Y., 1975, p. 97; (b) ibid p. 98, 102.

9. Yokota, T., Scriven, F., Montgomery, D.S. and Strausz, O.P. Fuel, 1986, 65, 1142.

10. Kotlyar, L.S., Ripmeester, J.A., Sparks, B.D., Woods, J.A., Fuel, 1988, 67, 1529.

11. Bartle K.D., Ladner, W.R., Martin, T.G., Snape, C.E. and Williams, D.F., Fuel, 1979, 58, 413.

12. Suzuki, T., Iton, M., Takegami, Y. and Watanabe, Y., Fuel, 1982, 61, 402.

13. Thiel, J. and Gray, M.R., AOSTRA J. Res., 1988, 4, 63.

14. Cyr, N., McIntyre, D.D., Toth, G. and Strausz, O.P., Fuel, 1987, 66, 1709.

15. Payzant, J.D., Hogg, A.M., Montgomery D.S. and Strausz, O.P. AOSTRA J. Res., 1985, 1, 175; 1985, 1, 183; 1985, 1, 201.

16. Yang, P.W., Private communication, 1988.

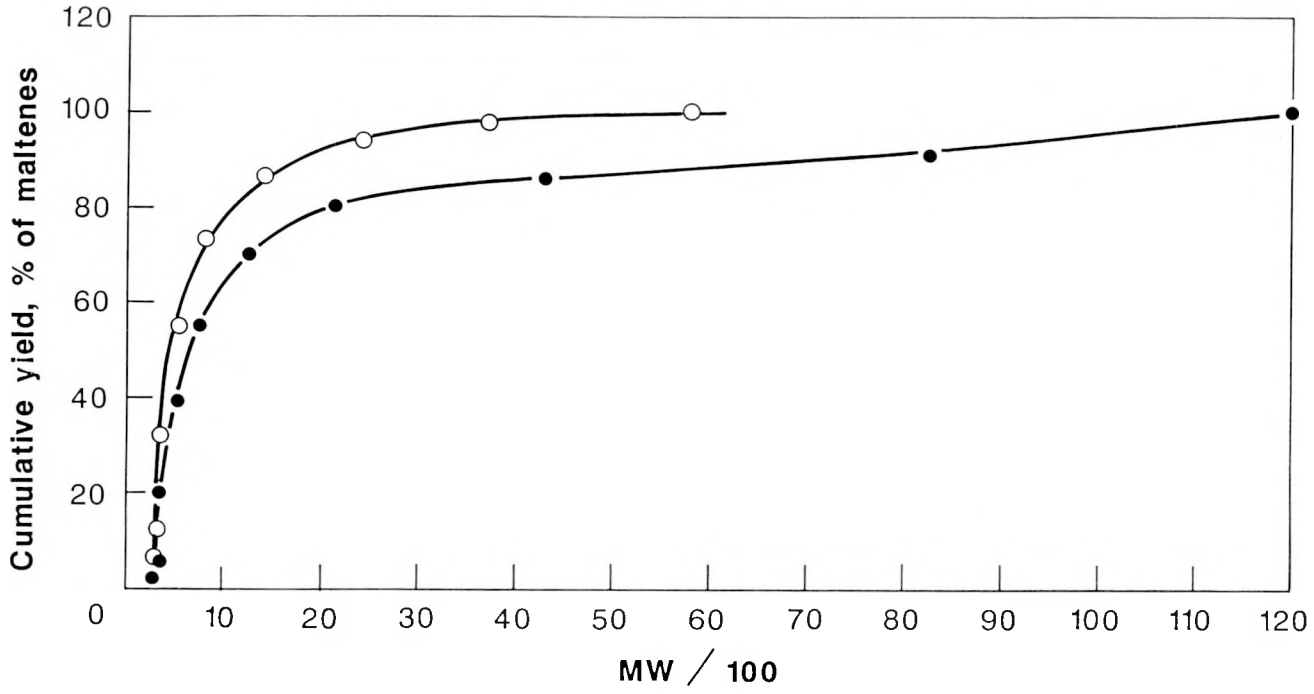

Fig.1 Yield of various fractions separated from Utah (●) and Athabasca (○) maltenes by GPC vs. number average molecular weight.

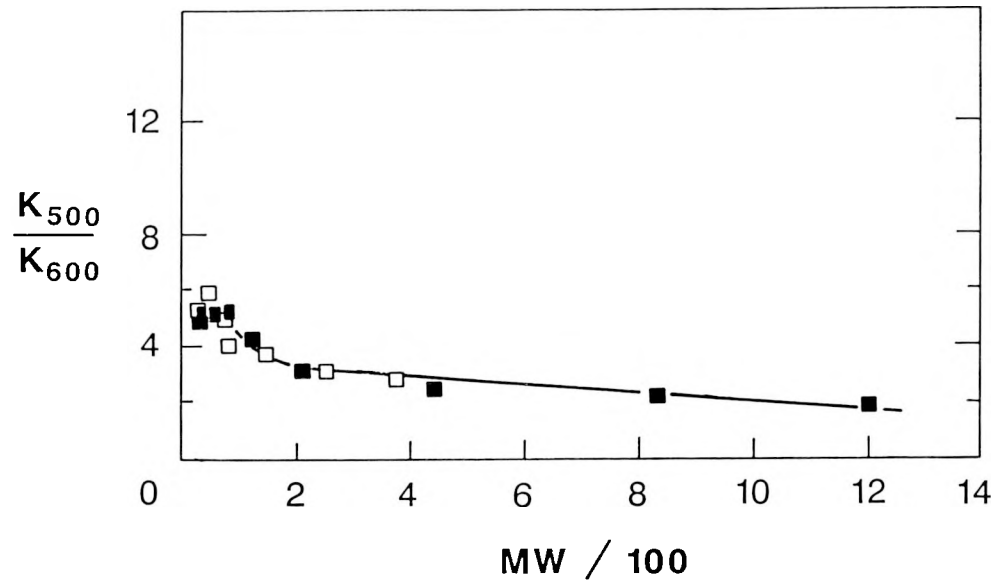

Fig.2 K_{500}/K_{600} for maltenes GPC fractions separated from Utah (■) and Athabasca (□) bitumen.

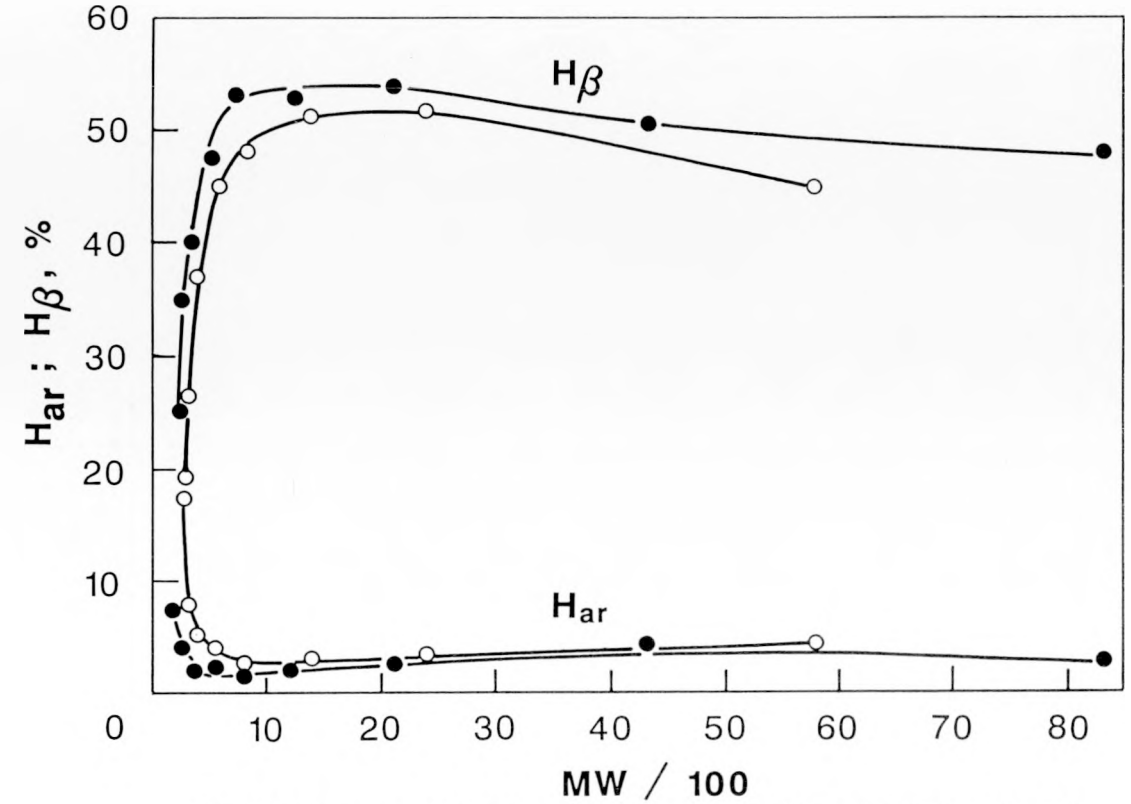

Fig.3 H_{ar} and H_β distribution vs. MW for Utah (●) and Athabasca (○) maltenes GPC fractions.

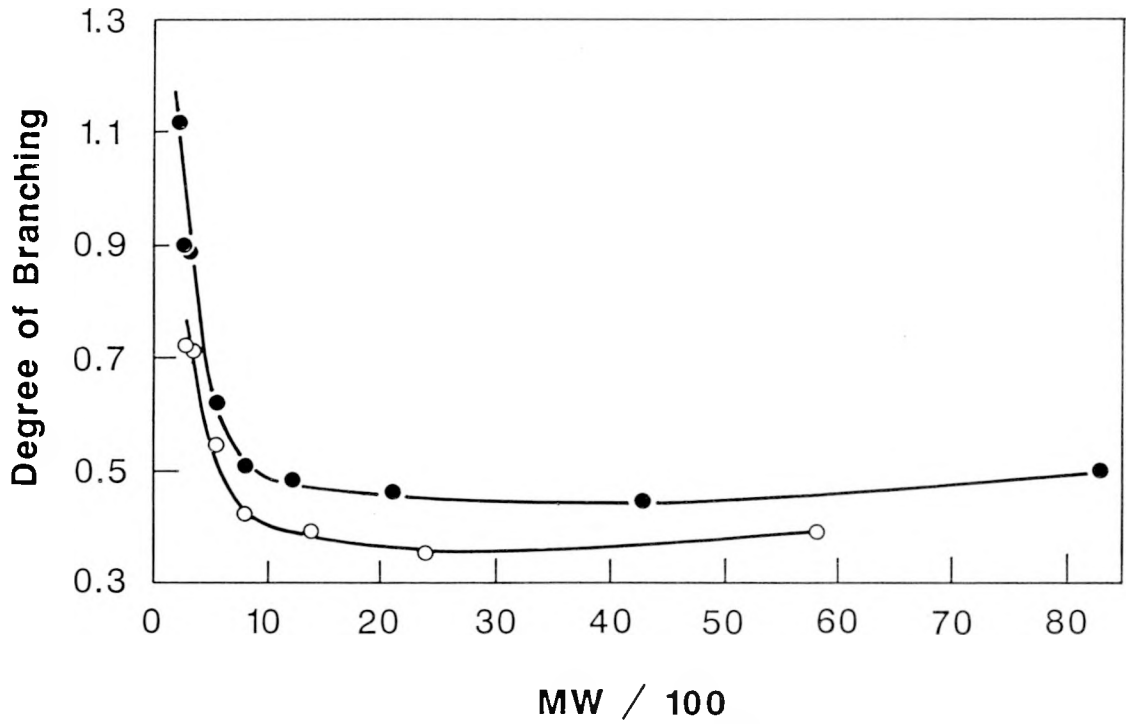

Fig.4 Degree of branching vs. MW for Utah (●) and Athabasca (○) maltenes GPC fractions.

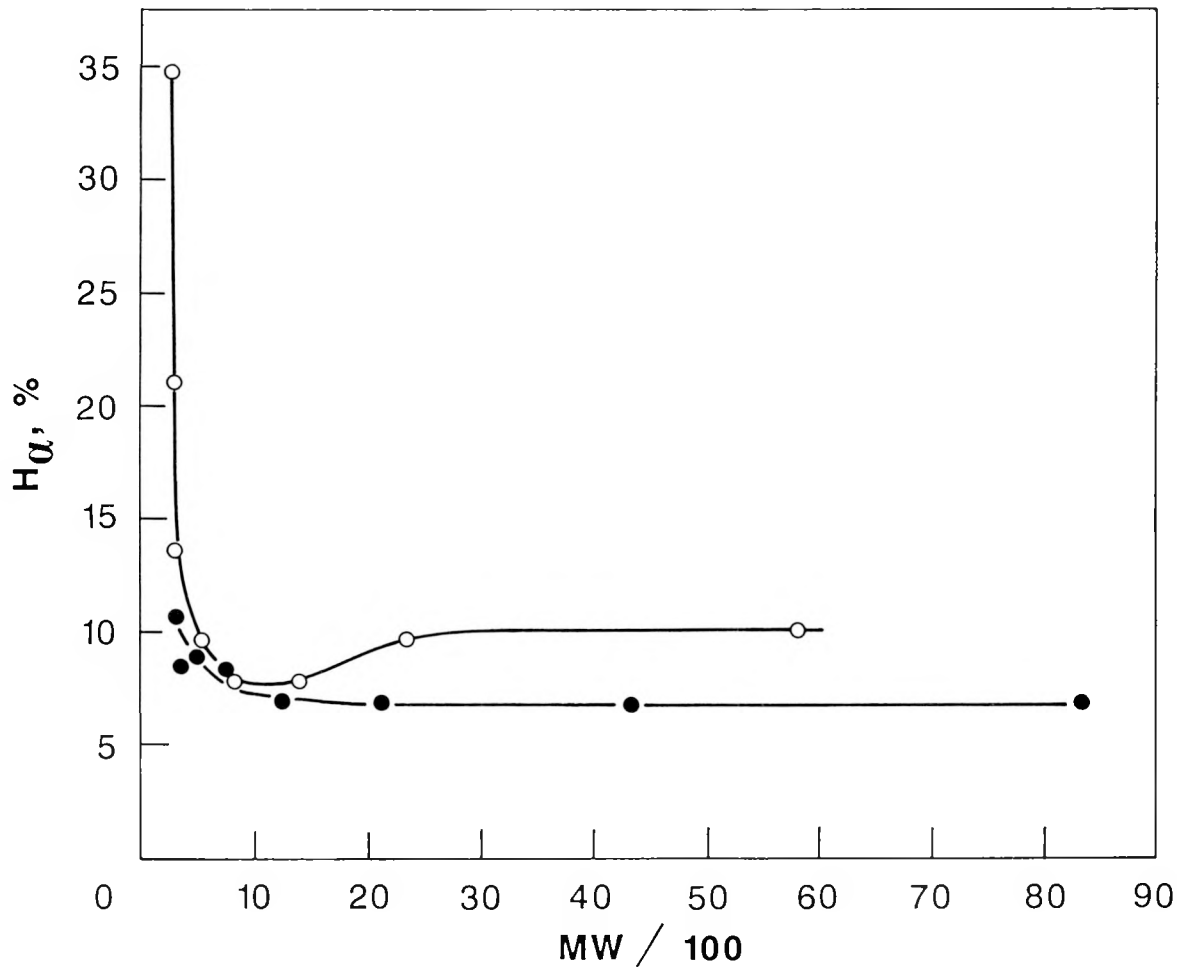

Fig.5 Distribution of H_α against MW for Utah (●) and Athabasca (○) maltenes GPC fractions.

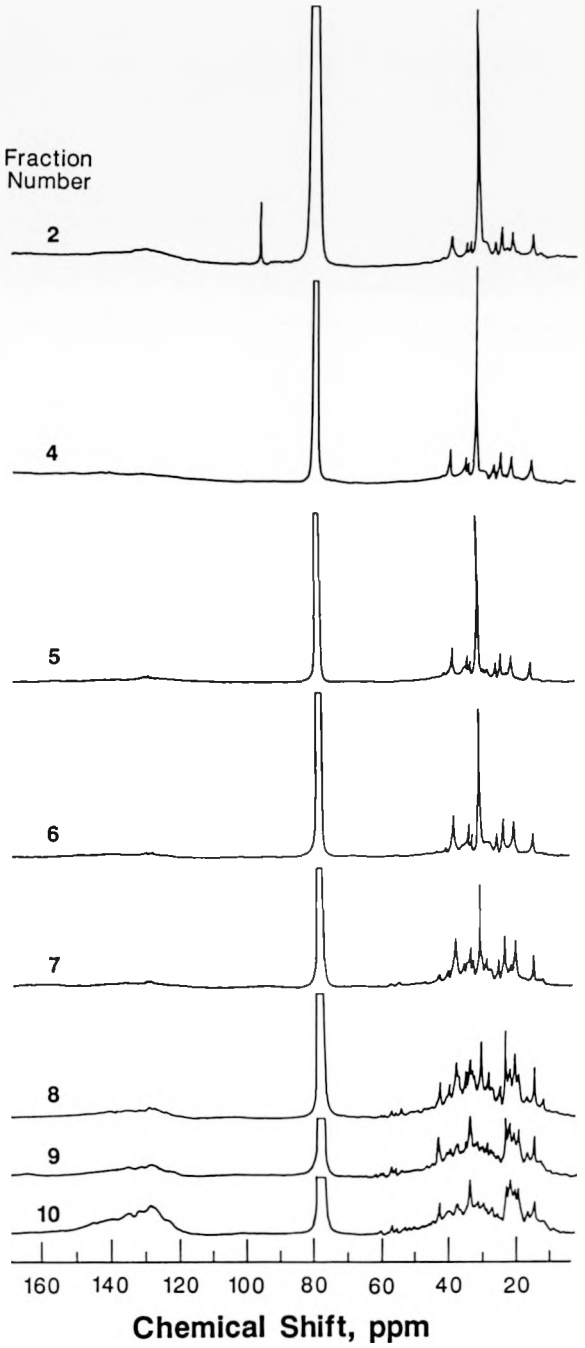

Fig.6 ^{13}C NMR spectra for GPC fractions derived from Utah maltene.

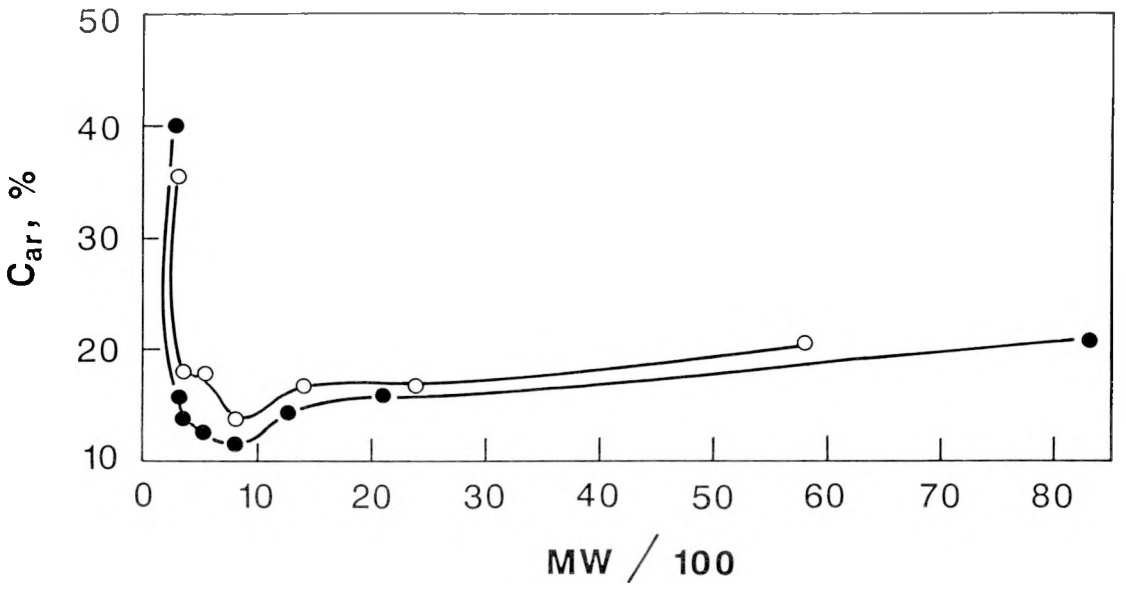

Fig.7 Carbon aromaticities (C_{ar}) of Utah (●) and Athabasca (○) maltenes GPC fractions vs. MW.

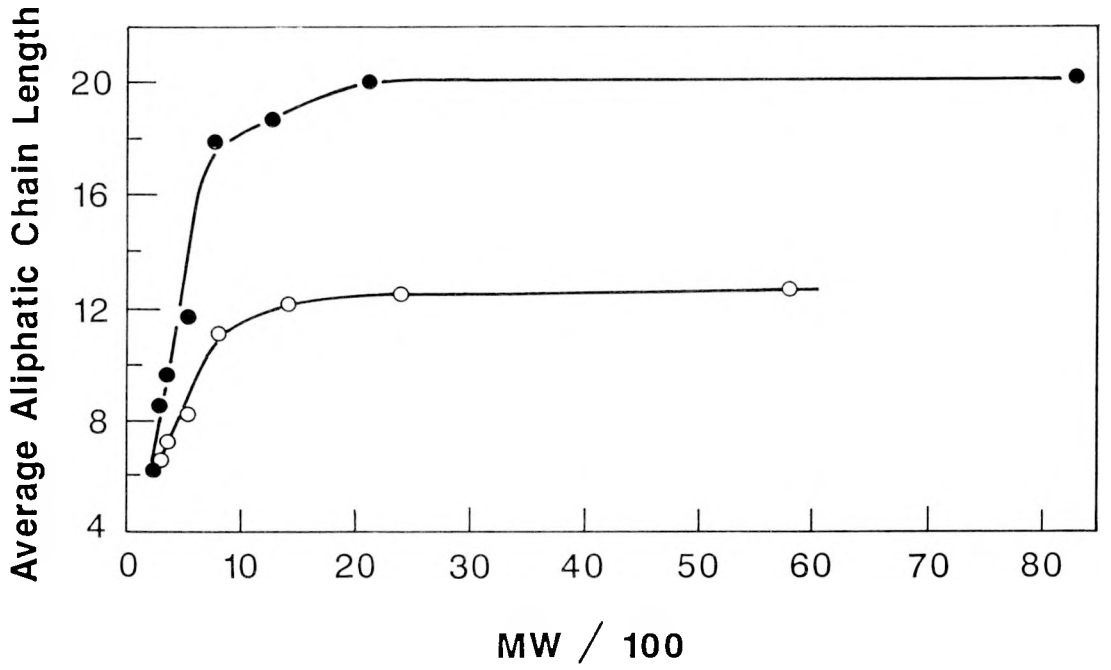

Fig.8 The average chain lengths of Utah (●) and Athabasca (○) maltenes GPC fractions against MW.

Asphalt from Utah Tar Sands — A JWBA Project Sponsored by the U.S. Department of Energy

by

James W. Bunger, Jerry W. Wiser, Christopher P. Russell, and Prasad A.V. Devineni
James W. Bunger and Associates, Inc.
Salt Lake City, Utah 84108

Abstract

JWBA has initiated a project for development of Utah's tar sands for production of specification-grade asphalt. Projected prices and costs strongly indicate economic viability within the market limitations. JWBA has licensed the water extraction technology developed at the University of Utah and has received both Phase-I and Phase-II funding from the U.S. Department of Energy SBIR program for development of the technology and project. The project calls for technology R&D, resource evaluation, market and transportation assessment, engineering and project optimization. Private funding will be used for commercial development activities related to resource acquisition, patent and market development and permitting. A 100 lb/hr process development unit (PDU) has been designed and construction is 50% complete. The PDU consists of three principal modules: extraction, cleaning and distillation. Start-up is anticipated for January, 1990. All of the major candidate deposits will be considered. The project will develop the engineering data, resource data and commercial information required for a major investment.

Introduction

The prospect of developing Utah tar sands for the production of specification-grade asphalt was first reported in 1976, by Bunger and Oblad. [1] Since that time, extensive research and development has been conducted to develop the technology necessary for efficient and environmentally-acceptable extraction technology. Over the past 13 years, economics of production of energy-related products has changed substantially. Today, and throughout the foreseeable future, conditions exist which strongly suggest economic potential for production of specification-grade asphalt from tar sands.

Asphalt is a commodity which is commonly derived from petroleum resid. With the advancements in resid upgrading and the high-capacity utilization of refineries, asphalt production has fallen sufficiently to support prices substantially above the current cost of crude. Prices for asphalt are expected to remain higher than the cost of crude over the foreseeable future.

Costs for production of asphalt from tar sands are estimated to be approximately two-thirds that of the cost of producing syncrude from tar sands. Thus, within the market volume limitations which will effect

the scale of the plant, there is a gross profit margin which promises economic viability with today's prices and costs.

In 1988, J. W. Bunger and Associates, Inc., (JWBA) proposed development of this concept to the U.S. Department of Energy under their Small Business Innovation Research program (SBIR). The Company received a Phase-I award in 1988, and based on the successful results of the feasibility study and the Company's proposal a Phase-II award was made in 1989. The current project consists of technology R&D, mine design and resource assessment, marketing costs assessment, process simulation and project economic analysis. The Phase-II project is designed to attract private capital for the large-scale development of the project. This manuscript is a description and progress report on the project.

Results of Feasibility Study

Results of the Phase-I Feasibility Study consist of four central components. These are: the technology, the resource, the market and the financial analysis.

Technology: The process concept is based on patented University of Utah hot water-extraction technology.[2] This technology has been developed over the past 15 years along with companion technology in thermal recovery and bitumen upgrading. A recent review of the University of Utah tar sand research and development effort has been published and contains a complete bibliography of this work. [3] JWBA has purchased license to the hot-water extraction technology embodied in the referenced patents.[2]

Beginning with the information contained in the literature and the patents, a process-flow diagram has been constructed and material balances have been estimated. The overall results are shown in Figure 1. The results reveal that high recoveries, as well as high thermal effeciencies, can be expected from a continuous process unit. Primary energy requirements are found in water heat-up and distillation steps. The thermal efficiency of this process is estimated to be 95%. Study level cost estimates were performed and revealed capital + operating costs of 16-19 $/bbl.

A sample of Asphalt Ridge Tar Sand was extracted and processed. Concentrates from 18 batch-type runs were combined and diluted with a hydrocarbon solvent, centrifuged and subjected to thin-film distillation. Three samples of differing initial boiling points were produced. Analysis of these samples shows that, as expected, viscosity increases and penetration decreases with increasing initial boiling point. Differing grades of asphalt, mainly AC-20 type, can be produced by varying the distillation conditions. Summary results are shown in Table 1. These results show that both an AC-20 and AC-10 meet viscosity-graded specifications.

Table #1

Results of Specification Testing

Property	Tar Sand Bitumen AC-20 Sample	AC-20 Spec.	Tar Sand Bitumen AC-10 Sample	AC-10 Spec.
Viscosity				
abs-poise (140° F)	1947	2000±400	917	1000±200
kin-cs (275° F)	316	300 min	300	250 min
Penetration				
1/10 mm @ 77° F	76	60 min	153	80 min
Ductility	100+	5+	115+	15+
PEN/VIS	-0.874	(a)	-0.155	(a)
Marshall Stability (lb)	1700	1200 min	ND	1100 min

(a) No standard specification exists but values between 0.0 and -0.5 are considered to be premium.

Resource: Information has been gathered on four Uinta Basin deposits namely: P.R. Spring, Sunnyside, Whiterocks and Asphalt Ridge. Both the literature and state agency files have been searched for information pertaining to previous companies' activities on the various deposits. Lease holders and operators have been contacted. The information on the general characteristics of each of the four deposits show that any of these four deposits would contain sufficient material for asphalt production over the life of a project. Some of these could support expansion to a larger synthetic fuel plant if future prices warrant.

Preliminary mine design and cost estimation was conducted by a model developed by Wells and Bunger. (4) It should be mentioned here that the mining costs are highly site-specific. An important conclusion of the study showed that at a small scale, initial mining costs are quite low (e.g., $4-5/bbl). Each site contains examples of rich material near or at the surface. This reduces front-end operating costs and allows the project to develop a more favorable, early cash flow which, in turn, enhances the attractiveness for investment.

A report was prepared analyzing the labor markets and community infrastructure in the Asphalt Ridge and Sunnyside areas. (5) Development of tar sands in either of these areas would be of tremendous economic benefit and should enjoy good community support.

Market: The U.S. market can be divided into paving asphalts, 70%; cutbacks, 4%; emulsions, 10%; roofing asphalts, 13%; and specialty asphalts, 3%. Western states consume about one-third of the nation's annual usage of over 180 million bbl. Utah is currently a net importer of asphalt. Local prices for paving asphalt currently vary between $20 and $25/bbl. Details of the marketing of asphalt have been studied. Results of these studies include logistic details of various modes of transport such as: Rail, Truck and Pipe Line and costs of transportation. Preliminary studies of marketing and distribution costs seem to indicate that these costs, while not prohibitive, have a significant effect on the project economics.

Financial Analysis: Preliminary analysis of costs and revenues, as a function of project scale have been conducted and are shown in Figure 2. The costs include capital cost at 12% interest on debt. Economics of the project include a suite of asphalt specialty products. A 12% ROI for the project is projected. The level of return is considered quite good when compared with other natural resource development projects.The results of the feasibility study have helped define the requirements for research and development in Phase-II.

Technical Discussion of Phase-II Project

Resources: Each resource or deposit has its own, unique mineral and geologic characteristics. Depending upon the nature of deposit i.e. site specific, different operating conditions would be required to extract the bitumen and to produce specification-grade asphalt. Several variables pertaining to mineralogy under study are: (a) the degree of consolidation and (b) the fines content which effect the process design and tailings disposal. Samples from various deposits will be processed through the PDU to obtain performance data on each and to supply samples for further study.

Mining: The model developed by Wells and Bunger has extensive capabilities for conducting the task of mine design. Extensive core hole data is required to perform mine design. To consolidate this effort, core hole data has been obtained from the files of the UGMS. Unfortunately, this data is very limited and sparse, but sufficient enough to draw qualitative conclusions. Most of the data obtained by various companies is still proprietary. Currently, our efforts concententrate on obtaining the data from these companies on restricted access basis. If successful, this data will be used as a data base in the model and to run mine design programs such as krige and secplot to identify the rich ore zone, overburden and mine access points. Otherwise, estimates based on geologic field experience will be made to develop input data for economic evaluation programs.

Extraction: The central part of the extraction technology is the licensed hot-water technology from the University of Utah. The consolidated nature of tar sand and the high viscosity of bitumen requires special treatment. In this process, a small amount of hydrocarbon solvent is added and mechanical shear is used to disengage the bitumen from sand. Hot water is added to reduce viscosity and provide for surface wetting. This mixture is passed through digestion stage before entering the float cells. Size of the tar sand, solvent-to-sand ratio and temperature are some of the variables to be studied in the extraction process to optimize process conditions that are site-specific. Grade, size and consolidation will determine the extraction efficiency and economics.

PDU: The central requirement for the Phase-II research and development effort is the construction and operation of a process development unit (PDU). The process development unit is of a continuous, modular design. The PDU is designed to obtain performance and rate data on key units and to provide process streams for compositional and properties analysis. As shown in Figure 3, the simplified flow sheet of the process is divided into three modules.

- Module 1 consists of the conditioning, predigest, digest and flotation units. The digester configuration is a novel concept developed by JWBA. The primary characteristic of the digester is the short residence time required. The support structure for the PDU has been designed and constructed at JWBA's industrial site. Module 1 has been designed and fabricated, and will be operated to perform some controlled runs in the near future.

- Module 2 consists of the dilution and separation units. Design of module 2 is complete and fabrication is currently underway. The configuration and design of the separator is a novel concept of JWBA and is based on controlled gravity separation. Process variables such as diluent ratio, mixing speed and temperature will be studied for their effect on viscosity and separation of bitumen. This is expected to perform efficiently in separating water, bitumen and sand under the existing process conditions. Even though this module appears to be the simplest of the three, in practice this module will have a large influence on process efficiency and economics because of the critical separation stage.

- Module 3 consists of the distillation and finishing units. Distillation involves a two-stage process to provide greater flexibility in operation and controlling process conditions. The finishing stage is primarily used to alter the properties of the asphalt to meet the specifications. The details of this stage are presently being developed. The distillation module will have both atmospheric and vacuum operating modes. Variables such as temperature, pressure and reflux ratio will be studied. The design of module 3 is completed and fabrication of the distillation column is under way.

The process control of Module 3 is mainly performed by a stand-alone computer. Data acquisition and storage is on-line for all modules. State-of-the-art in data acquisition, instrumentation and control are being employed in this PDU to ensure accurate material and energy balances of the process.

Project Optimization: Figure 4 shows the various operations in the overall project optimization program. The basic concept of this integrated economic and technical optimization program is to study the effect of all possible factors involved in the development of a viable commercial project. A marketing and distribution model is being developed by considering various modes of transportation. Non-linear constrained optimization and linear programming techniques are being used for this model. This program will be written in fortran and C languages with data base and graphics capabilities. This integrated package is expected to be functional in the first quarter of 1990.

Commercial Development Plan

Results of the Phase-II Research and Development program will lead to engineering and financial data expected to verify the attractiveness of the project for commercialization. Considerable interest has been expressed among the private sector in the JWBA project. The current Phase-II work will be completed by December of 1990, at which time the project will move to a large-scale pilot plant facility. The pilot plant facility will be on the order of 125 tons/day. The current business plan calls for only two stages of financing to reach the commercial scale. Current plans call for completion of the financial development details with partners by mid 1990.

References

1. Bunger, J.W., and Oblad, A. G., "Selected Projects Leading to the Commercialization of Oil Shale, Tar Sands and Coal Located in the State of Utah", UEES, 1977.

2. Miller, J.D., et al, "Hot-water extraction process for bitumen extraction from Utah tar sands", U.S. Patent numbers: 4,120,776; 4,410,417; 4,470,899 and 4,486,294.

3. Oblad, A.G., et al, "Tar Sand Research and Development at the University of Utah", Annual Reviews of Energy, 1987

4. Wells, H.M., and Bunger, J.W., "Economic Evaluation of Oil Shale and Tar Sand Resources Located in the State of Utah", Final Report, UEES,1984.

5. Bunger, J.A., "Labor Market Comparisons for the Asphalt Ridge and Sunnyside Resource Development Areas", Human Resources Market Analysis, College of Business, University of Utah, 1988.

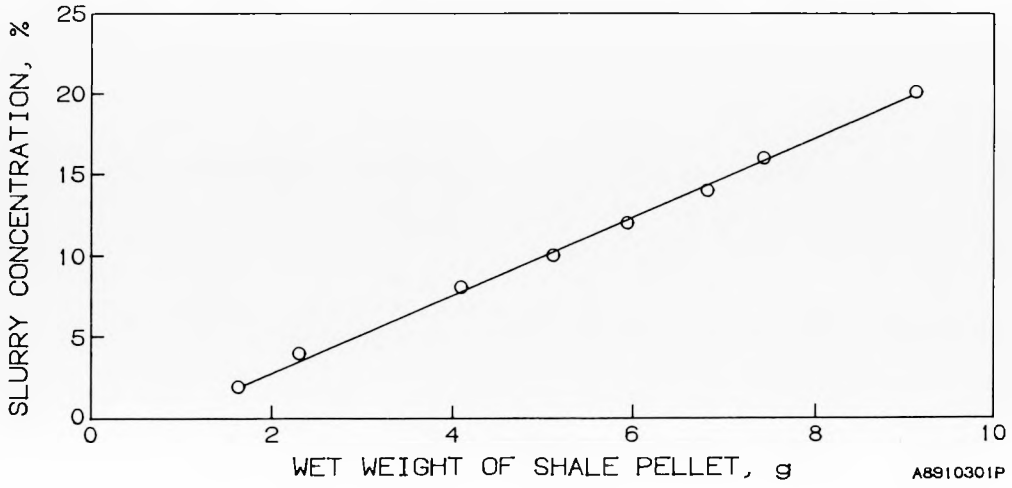

Figure 1. Standard curve: plot of slurry concentration vs. wet weight of shale pellet.

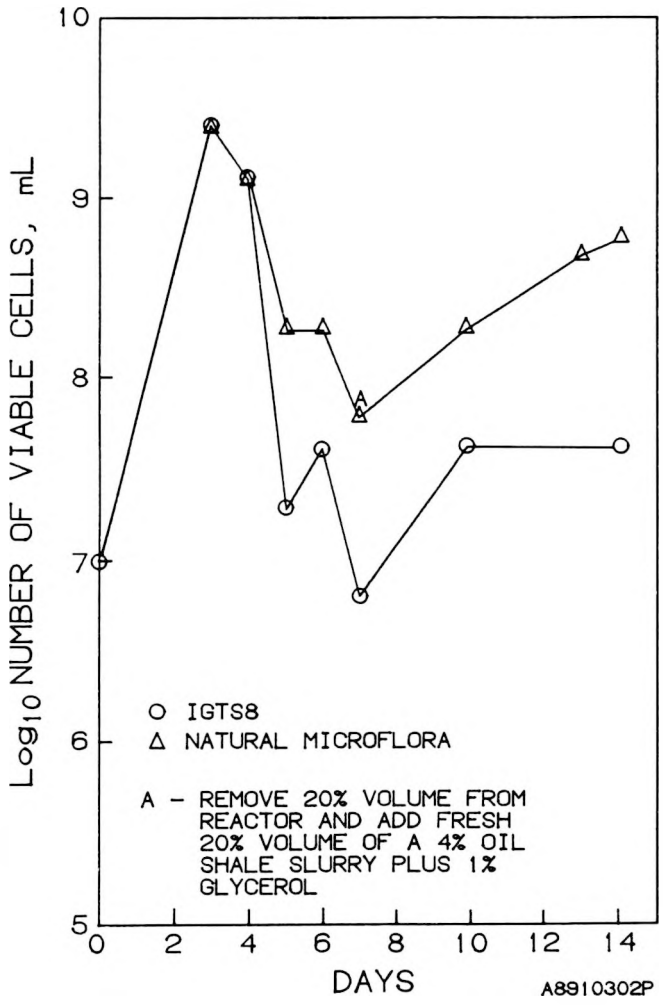

Figure 2. Growth of IGTS8 and the natural microflora in a 4% oil shale slurry.

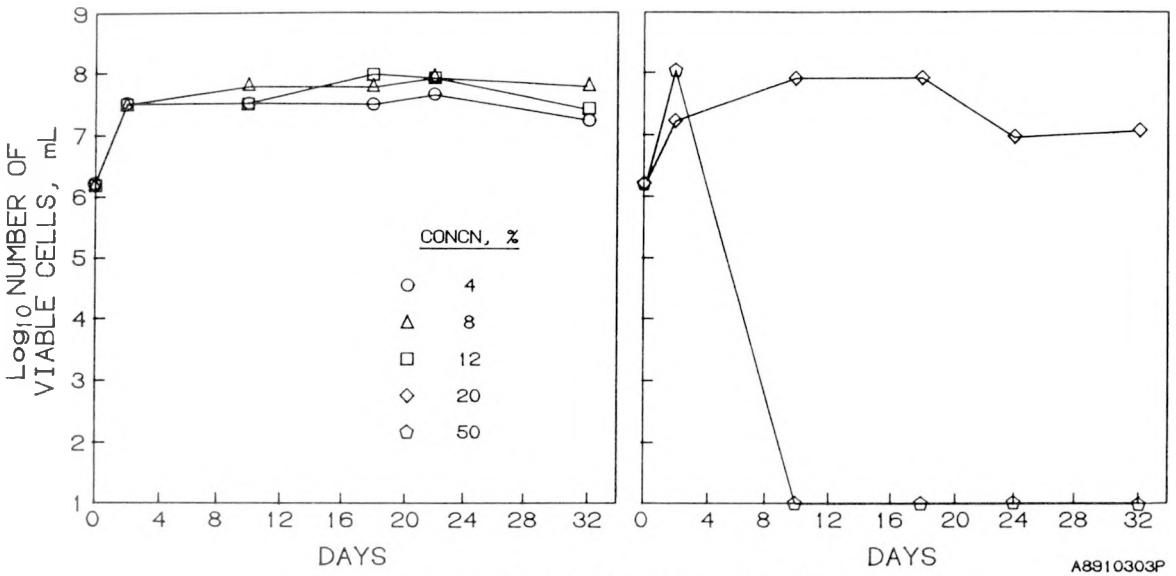

Figure 3. Effect of various oil shale concentrations on cell growth in the presence of glucose.

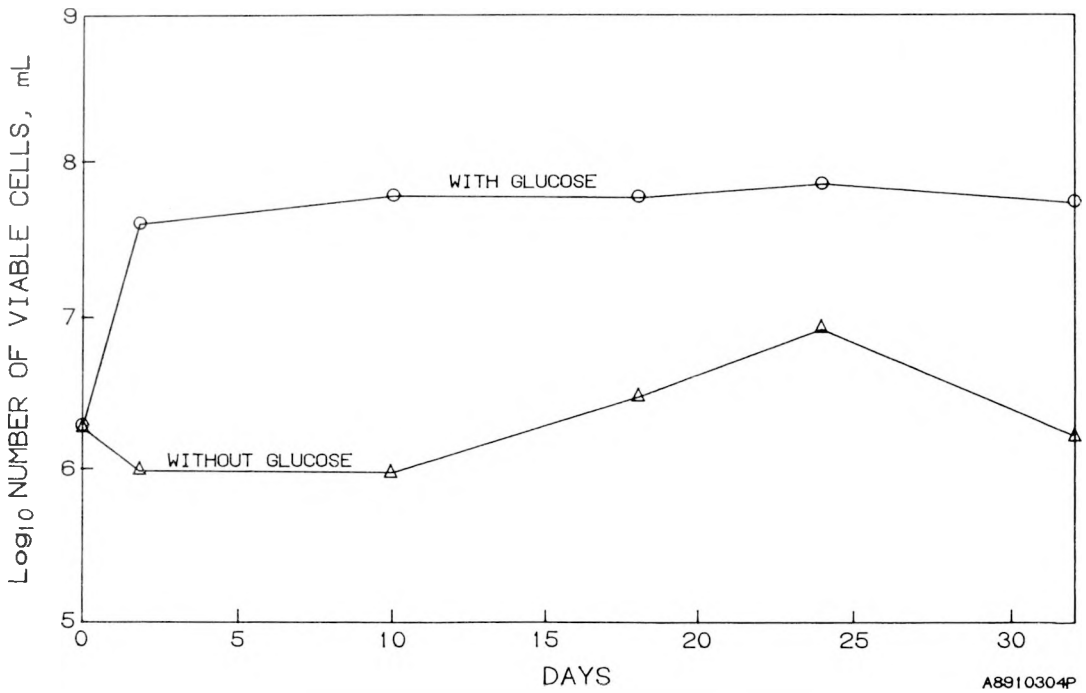

Figure 4. Cell growth in an 8% oil shale slurry with and without glucose.

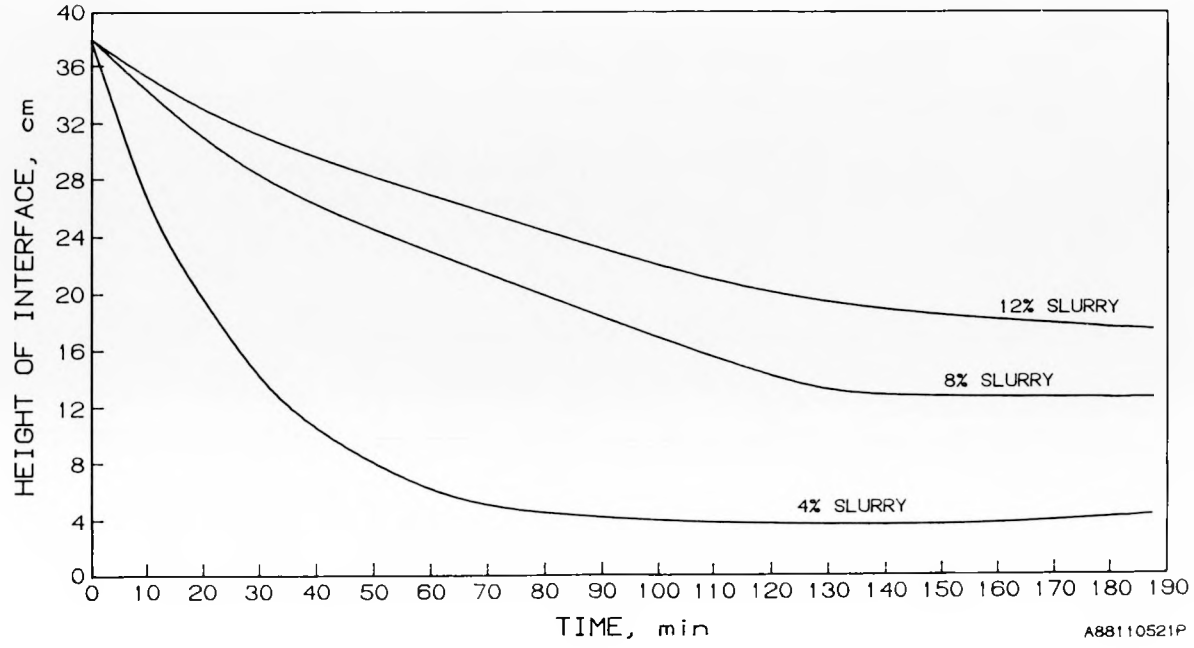

Figure 5. Settling characteristics of oil shale.

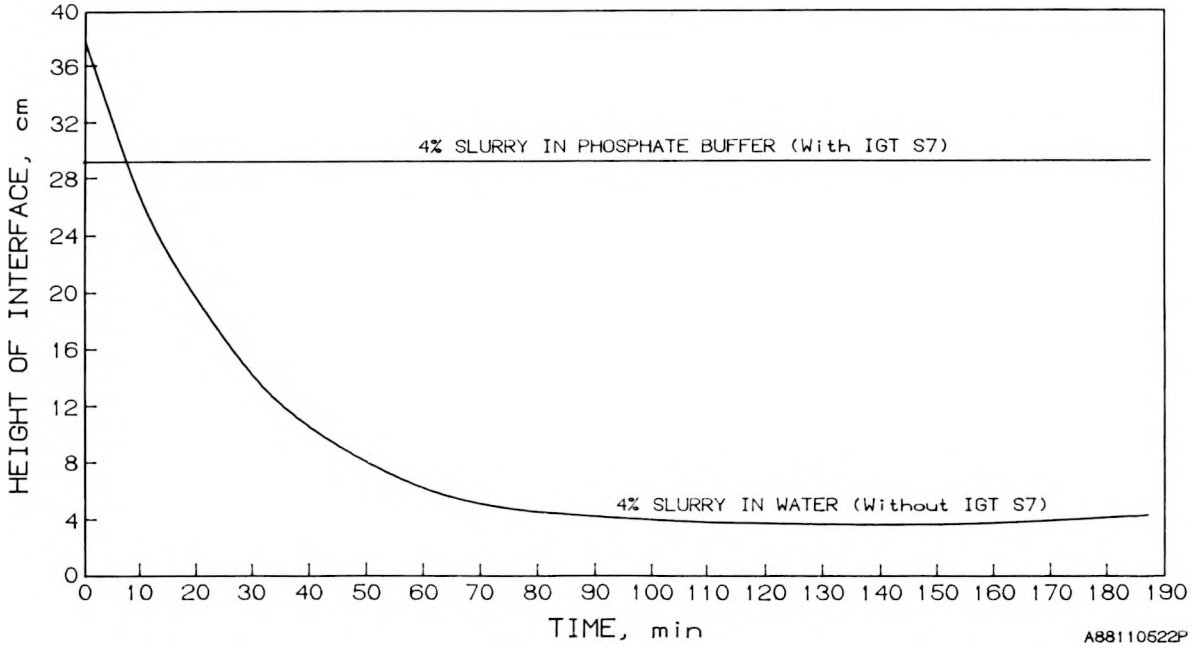

Figure 6. Settling characteristics of oil shale.

Volatile Compound Evolution From Programmed Temperature Pyrolysis of Big Clifty and McKittrick Tar Sands at 10 C/Min Heating Rate

John G. Reynolds

Lawrence Livermore National Laboratory
University of California
Livermore, California 94550

ABSTRACT

Big Clifty (Kentucky) and McKittrick (California) tar sands were pyrolyzed at a 10°C/min heating rate from room temperature to 900°C. The volatile compounds were detected on-line and in real time by tandem mass spectrometry using MS and MS/MS detection.

Evolution of hydrocarbons and heteroatomic-organic species occurs in two regimes: 1) low temperature (T_{max} values of 158 to 197°C), corresponding to entrained organics, and 2) moderate temperature (T_{max} values of 435 to 500°C), corresponding to cracking of hydrocarbons. Methane has slightly higher T_{max} values of 526 and 502°C for Big Clifty and McKittrick tar sands, respectively. In almost all cases for individual hydrocarbons, the T_{max} values for Big Clifty tar sand are several degrees higher than the corresponding T_{max} values for McKittrick tar sand.

H_2 exhibits evolution in three temperature ranges: hydrocarbon cracking, secondary char (550 to 650°C), and high (above 650°C). Both tar sands have similar profile behavior. Except for a very small amount evolving at hydrocarbon cracking temperatures, CO evolution is dominated by high temperature complex gas-equilibrium chemistry for both tar sands. The CO_2 profiles are, however, distinctly different with Big Clifty being dominated by high temperature evolution (probably carbonate decomposition).

H_2S profiles were also distinctly different. The Big Clifty profile exhibited evolution in the hydrocarbon cracking temperature range, and in the range for FeS_2 decomposition. The McKittrick profile was dominated by a large, broad maximum in the low temperature range.

INTRODUCTION

We have been studying several U. S. tar sand deposits by laboratory pyrolysis and bitumen characterization to assist in the ultimate understanding and development of tar sand recovery processes. For pyrolysis in particular, we have studied both the whole tar sands from the Asphalt Ridge,[1] Sunnyside[2,3] and Big Clifty[1,4] deposits as well as the pyrolysis of the asphaltenes derived from the bitumen extracted from the Big Clifty deposit by the Texas Gas and Development pilot plant.[4] In general, the evolution of hydrocarbons starts around 350°C and continues to approximately 550°C, irrespective of the tar sand deposit. However, differences among the tar sands were observed in the temperatures of maximum evolution (T_{max}) of the hydrocarbons, as well as in the evolution profiles of the noncondensible gases, such as H_2, CO, CO_2, and H_2S.

For the bitumen studies we have examined Asphalt Ridge, Sunnyside, Big Clifty, McKittrick, Arroyo Grande, and Athabasca (Canada) tar sands by metal speciation techniques (SEC-ICP-AES and porphyrin/nonporphyrin separations) applied to V, Ni,

and Fe.[5,6,7] In general, the size distribution and speciation of the metals in the bitumens resemble that of heavy crude oils and residua,[8] having bimodal distributions with a small percentage of extractable or distillable petroporphyrins.

Tar sand is defined as any sand or rock which is impregnated with heavy oil or bitumen, excluding coal, oil shale or gilsonite.[9] Of the U.S. deposits, California has the fifth largest amount, accounting for approximately 8% of the total estimated 63 billion barrels of recoverable bitumen.[10] The McKittrick deposit in the San Joaquin Valley of California, is an unusual deposit because its sand matrix is a diatomite formation. This allows for a particularly high saturation of oil (35 wt % bitumen) because of the very high porosity.[5,6] This high oil saturation makes the deposit attractive for both extractive and pyrolysis type recovery methods. As a result, the deposit has attracted commercial interest, in the past.[9] Large scale pilot plants for both solvent extraction and above ground pyrolysis have been constructed and operated near the deposit.[11]

This paper reports the programmed temperature pyrolysis behavior of McKittrick tar sand at a 10°/min heating rate and compares these results to pyrolysis of Big Clifty tar sand under the same conditions.

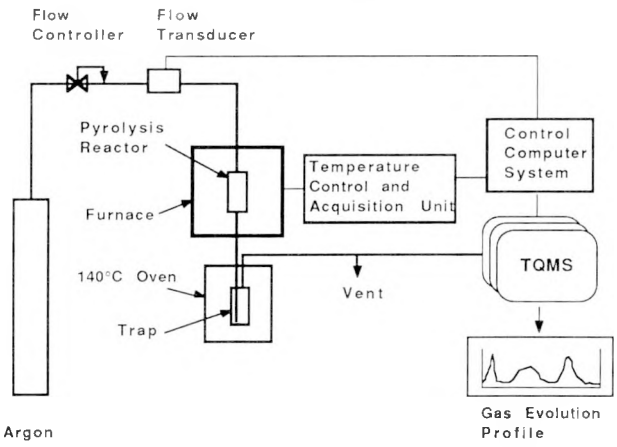

Figure 1. Programmed Temperature Pyrolysis Apparatus.

EXPERIMENTAL

Pyrolysis Apparatus. Figure 1 shows the pyrolysis apparatus used to obtain the results given in this report. Experimental equipment and pyrolysis conditions have been discussed in detail elsewhere.[1-4,12] The pyrolysis was performed using Ar as a carrier gas at 30 cc/min flow rate. For these experiments, 1/4" diameter quartz tubes were used as reactors. This eliminated any temperature gradient across the reactor. In all cases, the heating rate was 10°C/min, contrasting the 4°C/min heating rate used in previous studies.[1-4] The pyrolysis furnace was in-house built, and was regulated by an Applied Test Systems 2010 furnace controller. The reactor effluent flowed into a stainless steel trap held at 140°C in a box oven. (It is important to note the volatile material examined is limited to compounds which have gas-phase volatility of 140°C or lower.) Subsequent lines going to the detection system were kept at 200°C. This is necessary to prevent water adsorption causing holdup during compound evolution.[13]

Mass Spectrometer Detector. The detection and quantitation of compounds were performed by a Triple Quadrupole Mass Spectrometer (TQMS).[14] The apparatus has been discussed elsewhere in detail.[15,16] Briefly, the spectrometer allows for on-line, real-time analysis utilizing computer controlled MS and MS/MS detection. Table 1 lists the species routinely detected and the m/z ions used. Of the 33 species listed, 20 are quantitated with the appropriate calibration standards. In addition to the hydrocarbons, O-, N-, and S-containing compounds detected, Ar and Kr were also monitored both in MS and MS/MS mode to calibrate relative intensities and compensate for spectrometer drift. Thermocouple calibration and residence time are two important parameters in determining the correct temperature values. The thermocouples used are generally within ±1°C at hydrocarbon evolution temperatures. (This value varies depending upon evolution temperature). Residence time of the species in the system has varied from 3 to 5°C depending upon design. The values reported here have been corrected for this.

Table 1. Pyrolysis Products Monitored by TQMS (Species and m/z)

Hydrocarbons		O,N Compounds		S Compounds	
CH_4	16/14, 16	CO	28/84	CH_3SH	48/45
C_2H_4	28/26, 26	CH_3CO	43/16	COS	60/32
C_2H_6	30/27, 30	CO_2	44/16	C_2H_5SH	62/29
C_3H_6	42/39, 42	CH_3COOH	60/45	CH_3SCH_3	62/47
C_3H_8	44/29	C_4H_5N	67/40	SO_2	64/48
C_4H_8	56	C_5H_5N	79/52	CS_2	76/32
C_4H_{10}	58	C_6H_5OH	94/65	C_3H_7SH	76/42
C_5H_{10}	70	H_2O	18	C_4H_4S	84/45
C_5H_{12}	72			$CH_3C_4H_4S$	97/53
C_6H_6	78/52			H_2S	34/32
C_6H_{12}	84/56				
C_6H_{14}	86				
$CH_3C_6H_5$	92/63		H_2	2	
C_7H_{10}	94/79				

Tar Sand Samples. Big Clifty tar sand was prepared by grinding under liquid N_2. The McKittrick tar sand was fragile enough to be ground by using a spatula.

The Big Clifty tar sand comes from the surface mining pit in Logan County, Kentucky, and was supplied by Martin C. Noger of the Kentucky Geological Survey. The McKittrick tar sand comes from the surface mining pit in the Elk Hills Oil Field, San Joaquin Valley, approximately one mile southwest of McKittrick, California, and was made available by Rodger Johnson of Texaco Oil Company.

RESULTS AND DISCUSSIONS

The ultimate aim of this research is to assist in the creation and development of pyrolysis-type recovery processes. An important part of tar sand pyrolysis is the

behavior of hydrocarbons. Eventually, these hydrocarbons will be recovered and probably be refined to transportation fuels on a commercial scale. Because of this emphasis, the pyrolysis behavior of several hydrocarbons have been examined (see Table 1), and will be discussed here in some detail.

Hydrocarbons

Figure 2 shows the $C_4H_9^+$ ion evolution as a function of pyrolysis temperature at the 10°C/min heating rate. All hydrocarbons of C_4H_{10} and larger produce the $C_4H_9^+$ ion in the mass spectrometer because it is a very stable ion. The $C_4H_9^+$ ion is representative of the large hydrocarbons and reflects the evolution behavior of hydrocarbons in general, except for methane (see below).

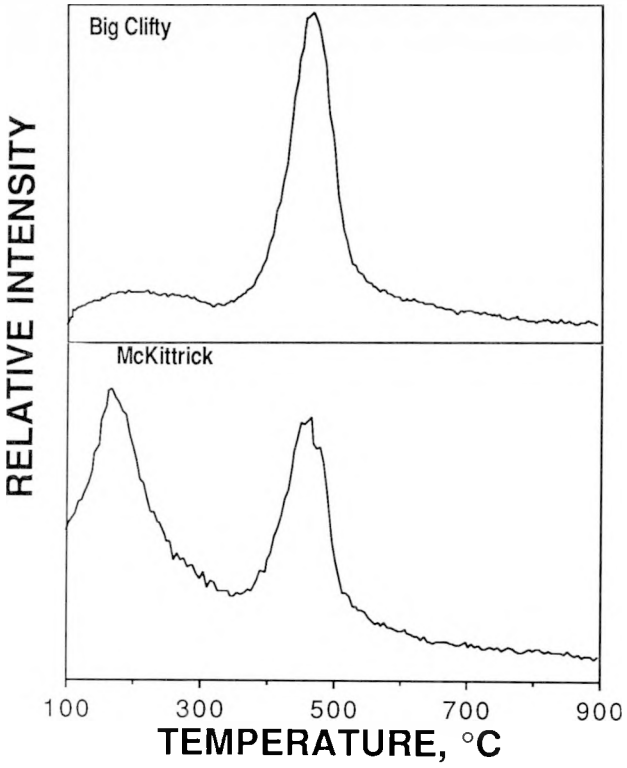

Figure 2. $C_4H_9^+$ Ion Evolution as a Function of Pyrolysis Temperature for Big Clifty (*Top*) and McKittrick (*Bottom*) Tar Sands at the 10°C/min Heating Rate.

The Big Clifty profile in Figure 2 exhibits a prominent maximum at moderate pyrolysis temperatures T_{max} value of 466°C. This accounts for the majority of the $C_4H_9^+$ ion evolving (approximately 80%). This maximum occurs at temperatures for pyrolysis-type hydrocarbon cracking reactions,[17] and has been assigned in previous reported profiles as due to bitumen cracking reactions.[1-4] The Big Clifty profile also exhibits a broad maximum from 150 to 250°C, with a T_{max} value of 197°C, which accounts for the minority of the $C_4H_9^+$ ion evolving (approximately 20%). This maximum has been assigned previously to entrained or trapped hydrocarbons.[1-4] As the tar sand bitumen begins to soften upon heating, hydrocarbons volatilize and are liberated.

Big Clifty tar sand has been examined previously at the 4°C/min heating rate. The results are very similar to the results presented here, except for the following general differences: 1) the T_{max} values for individual hydrocarbons are higher (as expected), and 2) the maximum assigned to entrained materials is either much broader or absent altogether, at the 10°C/min heating rate.

Figure 2 also shows the $C_4H_9^+$ ion evolution behavior of McKittrick tar sand as a function of pyrolysis temperature at the 10°C/min heating rate. The prominent maximum assigned to hydrocarbon cracking has a T_{max} value of 459°C, slightly lower than the T_{max} value for the Big Clifty tar sand. Also evident is the maximum due to entrained materials with a T_{max} value of 165°C, accounting for 55% of the $C_4H_9^+$ ion intensity in the profile. This relatively large amount of entrained material as seen in the $C_4H_9^+$ ion profile distinguishes McKittrick tar sand from the other tar sands studied.[1-4]

Table 2. Temperature of Maximum Evolution of Alkyl Hydrocarbons for Big Clifty and McKittrick Tar Sands at the 10°C/min Heating Rate

Species	Tar Sand	Peak 1 °C (%)	Peak 2 °C (%)
CH_4	BC	-	526 (100)
CH_4	McK	-	502 (100)
C_2H_6	BC	-	480 (100)
C_2H_6	McK	180 (13)	473 (87)
C_3H_8	BC	-	472 (100)
C_3H_8	McK	-	462 (100)
C_4H_{10}	BC	158 (18)	435 (87)
C_4H_{10}	McK	-	450 (100)
C_5H_{12}	BC	-	462 (100)
C_5H_{12}	McK	165 (50)	455 (50)

BC = Big Clifty Tar Sand
McK = McKittrick Tar Sand

Alkanes. Table 2 summarizes the evolution data for alkyl hydrocarbons for both tar sands at the 10°C/min heating rate. Included are the T_{max} values for each of the species and the relative percentages of the total evolution are given in parenthesis. The hydrocarbons evolving due to entrained material (indicated at Peak 1) have T_{max} values from 165 to 180°C. However, this maximum is not evident in many of the cases. This is contrary to previous studies at the 4°C/min heating rate. Big Clifty,[1,4] Sunnyside,[2,3] and Asphalt Ridge[1] tar sands all showed intensity in this range except for methane and a few other cases. The anomalous behavior observed in Table 2 is probably due to the faster heating rate (broader peak) and the generally smaller sample size (noisier profile) used in these other studies.

The T_{max} values for hydrocarbon evolution due to cracking reaction (indicated as Peak 2) vary from 435 to

526°C. Methane has the highest T_{max} values. For a specific tar sand, as the hydrocarbon chain increases in length, the T_{max} values decrease, reaching a minimum at C_4H_{10}. This behavior has been seen before for tar sands[1-4] and oil shales.[15,16,18] The decrease no doubt reflects the decrease in bond energies with increasing substitution on the carbon chain.[19] The origin of the minimum at C_4H_{10} is unknown, but may be due to some partitioning in the reactor effluent trap (see Figure 1).

The C_4H_{10} T_{max} value assigned to hydrocarbon cracking for Big Clifty tar sand is abnormally low for what would be expected from extrapolating from the 4°C/min data.[1,4] This profile had exceptionally bad noise for some undetermined reason, making reading the T_{max} value virtually impossible. Application of a generous smoothing program lead to the listed value.

Comparing the T_{max} values of Big Clifty tar sand to the corresponding values for McKittrick tar sand shows all the McKittrick values are lower. The biggest difference is methane (see below). The only exception to this is C_4H_{10} T_{max} value for Big Clifty tar sand.

The relative distribution of total evolution for a specific hydrocarbon depends upon the tar sand and the hydrocarbon. No evolution for entrained hydrocarbons is seen in Table 2 for methane and C_3H_8. For all tar sand and related samples, entrained C_3H_8 has never been detected. The reason is probably due to using MS/MS detection (reduction in ion current) along with poor ion response for this particular combination. Evolution due to entrained methane also is not seen except for Sunnyside tar sand at a 4°C/min heating rate.[2,3] Because of high volatility, methane should dissipate more rapidly than other hydrocarbons, and should have the lowest probability of detection. (The unusually low API gravity of the bitumen[20] may be reason for being able to detect methane in Sunnyside tar sand).

These previous results suggest entrained hydrocarbons of all chain lengths are probably evolved for all tar sands studied, but the combination of detector response, sample size, bitumen saturation, and hydrocarbon volatility, prevent the detection in some cases.

Alkenes. Table 3 summarizes the evolution behavior for selected alkenes for both tar sands. Except for C_2H_4, all the alkenes show evolution in the low temperature range assigned to entrained materials, and in the moderate temperature range assigned to hydrocarbon cracking reactions.

For the hydrocarbon evolution due to entrained materials, the T_{max} values vary from 165 to 197°C. For Big Clifty, evolution due to entrained materials accounts for a minor amount of the total evolution for a specific alkene. For McKittrick, except for C_2H_4, evolution due to entrained material accounts for roughly one-half the total evolution for a specific alkene.

For the hydrocarbon evolution due to cracking, the

Table 3 Temperature of Maximum Evolution of Alkenyl Hydrocarbons for Big Clifty and McKittrick Tar Sands at the 10°C/min Heating Rate.

Species	Tar Sand	Peak 1 °C (%)	Peak 2 °C (%)
C_2H_4	BC	-	497 (100)
C_2H_4	McK	-	472 (100)
C_4H_8	BC	197 (12)	466 (88)
C_4H_8	McK	165 (46)	459 (54)
C_5H_{10}	BC	172 (20)	466 (80)
C_5H_{10}	McK	165 (59)	455 (41)
C_6H_{12}	BC	197 (22)	473 (78)
C_6H_{12}	McK	172 (60)	468 (40)

BC = Big Clifty Tar Sand
McK = McKittrick Tar Sand

T_{max} values vary from 455°C to 497°C, but unlike the alkanes, these values do not decrease as the hydrocarbon chain increases. Except for methane, C_2H_4 has the highest T_{max} for all the hydrocarbons for Big Clifty tar sand. This is not the case for McKittrick, where the T_{max} for C_2H_4 is second to both methane and ethane. This behavior of Big Clifty has been seen before in several oil shales and tar sands [1-4,15,16]

The biggest differences seen in Table 3 are in the relative distributions of a specific hydrocarbon. The percentage of the total hydrocarbon evolving from entrained material is always higher for McKittrick compared to Big Clifty. Also for McKittrick, entrained material accounts for the majority of the hydrocarbon evolved for C_5H_{10} and C_6H_{12}.

This behavior is contrary to the behavior at the 4°C/min heating rate, where the relative distributions are much more in favor of evolution due to entrained alkenes for Big Clifty. For example, for C_6H_{12} evolution, the distribution is 47% entrained and 53% cracking at the 4°C/min heating rate;[1] and 22% entrained and 78% cracking at the 10°C/min heating rate. It is suspected, if McKittrick was pyrolyzed under identical conditions as the Big Clifty (much larger reactor and sample size, slower heating rate), the relative distribution at 4°C/min would be even more in favor of evolution due to the entrained alkenes.

Aromatics. Figure 3 shows benzene evolution as a function of pyrolysis temperature for the two tar sands at the 10°C/min heating rate. Obvious in both profiles is the maximum due to hydrocarbon cracking. This maximum has a T_{max} value of 469°C and accounts for 100% of the benzene evolved for Big Clifty tar sand. Likewise, this maximum has a T_{max} value of 476°C and accounts for 55% of the benzene evolved for McKittrick tar sand. This is contrary to the behavior seen for both the alkanes and alkenes (see Tables 2 and 3), where Big Clifty T_{max} values are generally much higher than the corresponding T_{max} values for McKittrick.

Only the McKittrick profile exhibits evolution due to entrained benzene, with the maximum having a T_{max}

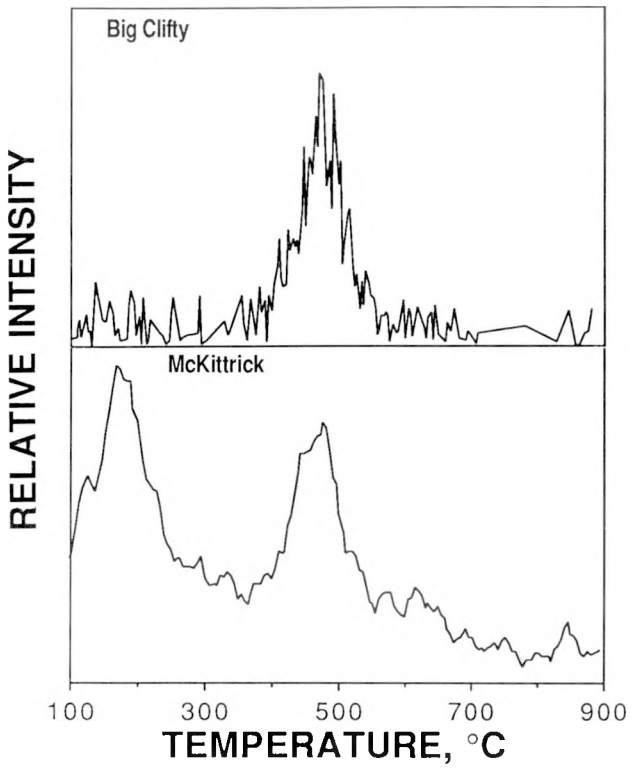

Figure 3. Benzene Evolution as a Function of Pyrolysis Temperature for Big Clifty (*Top*) and McKittrick (*Bottom*) Tar Sands at the 10°C/min Heating Rate.

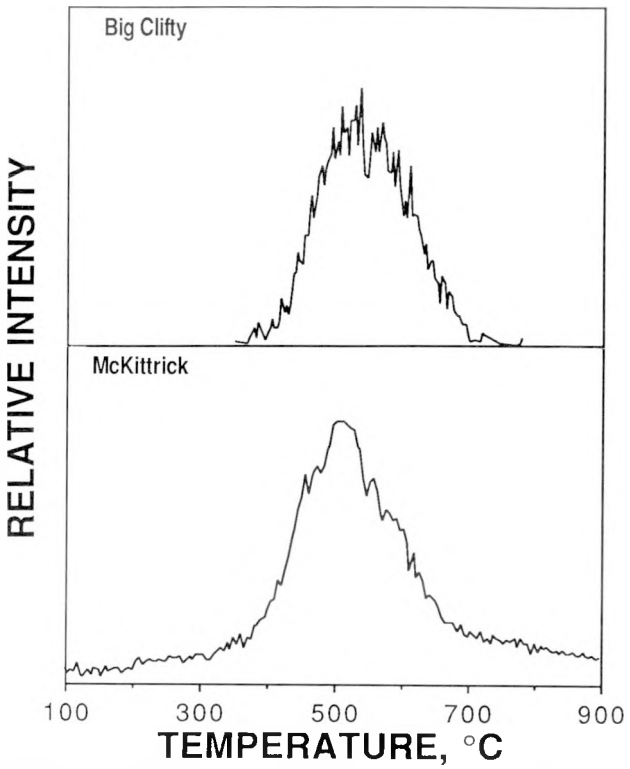

Figure 4. Methane Evolution as a Function of Pyrolysis Temperature for Big Clifty (*Top*) and McKittrick (*Bottom*) Tar Sands at the 10°C/min Heating Rate.

value of 174°C, and accounting for 45% of the benzene evolved. This evolution is not observed in the Big Clifty profile which is contrary to the 4°C/min heating rate profile,[4] where 39% of the benzene is evolved at low temperatures. Comparing Figure 3 to the profile of the 4°C/min heating rate published previously, the poorer signal-to-noise in the 10°C/min profile contributes to the difficulty in detecting evolution in the low temperature range.

Benzene evolution shown in Figure 3 is also typical for toluene evolution. The maximum assigned to cracking reactions has a T_{max} value of 466°C and accounts for 100% of the toluene evolved for the Big Clifty tar sand. Likewise, this maximum has a T_{max} value of 450°C and accounts for 56% of the toluene evolved for McKittrick tar sand. The lower T_{max} values for toluene compared to benzene have been attributed to differences in the type of bond cleavage to produce the species or to possible aromatization reactions to form benzene.[1]

Methane. Figure 4 shows the methane evolution as a function of pyrolysis temperature for both tar sands at the 10°C/min heating rate. The Big Clifty tar sand profile has an obvious broad maximum which has been assigned to hydrocarbon evolution due to cracking reactions, as in the case for the other hydrocarbons. This maximum is at a higher temperature (see Table 2), and is much broader than for the other alkanes. The higher T_{max} value reflects the nature of the methyl-substrate bond breaking in forming methane.[19] This broader distribution has been seen before in other tar sands[1-3] and in oil shale pyrolysis.[15,16,18]

Also evident in the profile is a shoulder on the high temperature side of the prominent maximum. This shoulder has been observed before in tar sand and oil shale pyrolysis and has been attributed to secondary coking and charring reactions. As the nonvolatile organic fragments lay down on the sand matrix and the sides of the reactor during cracking, more methyl groups are cracked off forming methane. This type of chemistry is also seen for hydrogen (see below).

The bottom profile of Figure 4 is methane evolution for McKittrick tar sand. Although there is a slightly distorted maximum, the profile has a similar shape to that of the Big Clifty tar sand -- broad maximum, with an unresolved shoulder on the high temperature side of the maximum. The T_{max} value is lower than that of the Big Clifty tar sand, which is consistent with the behavior of the other evolving hydrocarbons.

Non Hydrocarbons

In addition to the hydrocarbons discussed above, noncondensible gases, water, and some heteroatomic organic species are detected during pyrolysis. These compounds are important commercially because they represent possible environmental problems, energy-balance and consumption concerns, as well as potential new product feed stocks.

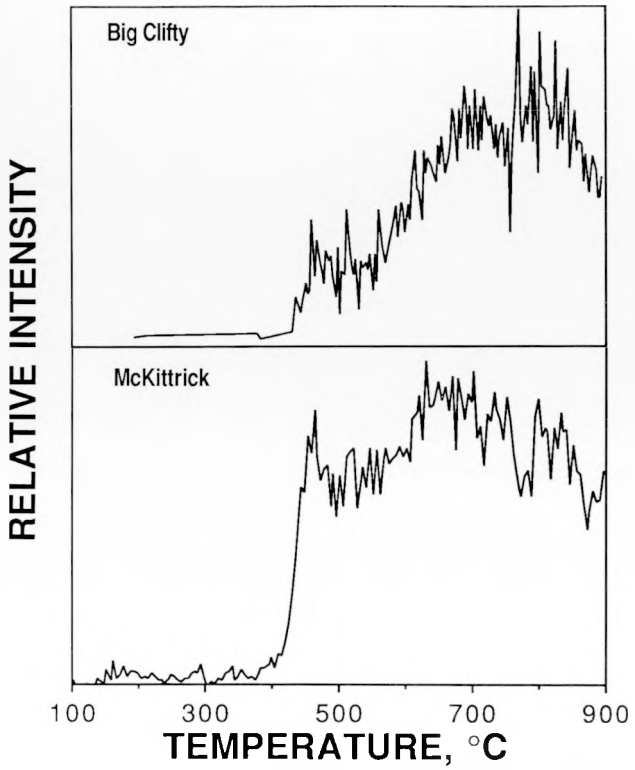

Figure 5. Hydrogen Evolution as a Function of Pyrolysis Temperature for Big Clifty (*Top*) and McKittrick (*Bottom*) Tar Sands at the 10°C/min Heating Rate.

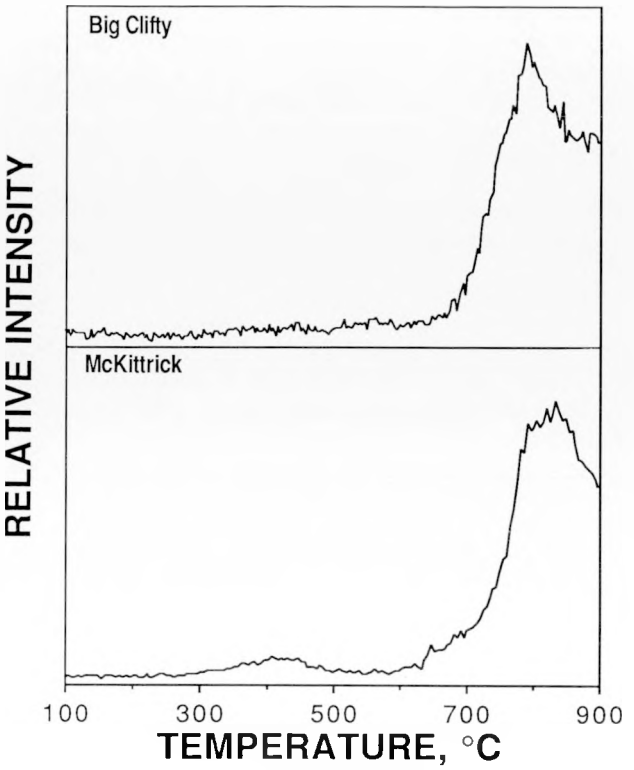

Figure 6. Carbon Monoxide Evolution as a Function of Pyrolysis Temperature for Big Clifty (*Top*) and McKittrick (*Bottom*) Tar Sands at the 10°C/min Heating Rate.

Hydrogen. The top of Figure 5 shows the evolution of hydrogen as a function of pyrolysis temperature for Big Clifty tar sand at the 10°C/min heating rate. This profile has been shown before,[4] and is typical of the hydrogen profiles for tar sands. No evolution is observed below 400°C. Evolution begins above this temperature and can be broken into three categories. The first is hydrogen evolution occurring in the temperature range of cracking reactions. This maximum has a T_{max} value at approximately 466°C and accounts for roughly 6% of the total hydrogen evolved. The next evolution category is in the temperature range of 550 to 650°C. Hydrogen evolution in this range has been assigned to secondary charring and coking reactions as seen in the methane case.

The bulk of the hydrogen evolved is in the high temperature range, above 650°C, and is due to complex equilibrium chemistry. This chemistry has not been completely deconvoluted but is probably fueled, at least in part, by the following chemical reactions: the water-gas shift reaction, equation (1); char gasification, equation (2); and the Boudouard reaction, equation (3).

$$CO + H_2O = CO_2 + H_2 \quad (1)$$

$$CH_x + H_2O \rightarrow H_2 + CO \quad (2)$$

$$CH_x + CO_2 \rightarrow CO + H_2 \quad (3)$$

These reactions have been reviewed extensively in previous discussions about tar sand pyrolysis at high temperature.[1-4]

The bottom profile in Figure 5 is the hydrogen evolution for McKittrick tar sand at the 10°C/min heating rate. The profile is similar to that of the Big Clifty tar sand. The maximum assigned to hydrocarbon cracking reactions has a T_{max} of 459°C, and accounts for approximately 15% of the total evolution. The bulk of the hydrogen is evolved above 550°C and can be accounted for by the same reactions cited above -- secondary char reactions and high temperature complex equilibrium chemistry.

Carbon Monoxide. Figure 6 shows CO evolution as a function of pyrolysis temperature for both tar sands at the 10°C/min heating rate. Examining the Big Clifty profile, no evolution is observed before 300°C. Above this temperature, evolution is barely visible, having a perceptible T_{max} value at approximately 407°C, in the same temperature range as the generation of hydrocarbons. The origin of this maximum is not known for sure, but is tentatively assigned to the decomposition of organic compounds through decarbonylation of carboxylic acids[21] and salts, equation (4), or decomposition of ketones and other O-containing organic compounds.[22]

$$RCH_2CH_2COOH \rightarrow CO + H_2O + RCH{=}CH_2 \quad (4)$$

Most of the CO evolution occurs at temperatures above 600°C and is due to chemistry not directly related to hydrocarbon generation. As discussed above for hydrogen evolution, the chemistry is not well defined and is probably due to complex high temperature chemistry shown in equations (1) to (3).

The bottom profile in Figure 6 shows CO evolution for McKittrick tar sand. Although the profile is similar to that for Big Clifty, the maximum in the temperature range of hydrocarbon evolution is more obvious, having a T_{max} value of 412°C and accounting for 7% of the CO evolving. As in the case for Big Clifty, the bulk of the evolution is above 600°C, and probably has the same origin as discussed above.

Carbon Dioxide. The top of Figure 7 shows CO_2 evolution as a function of pyrolysis temperature at the 10°C/min heating rate for Big Clifty tar sand. Evolution is evident with the onset of heating. This has been seen before as CO_2 desorption from SiO_2 of the sand matrix and/or quartz filler.

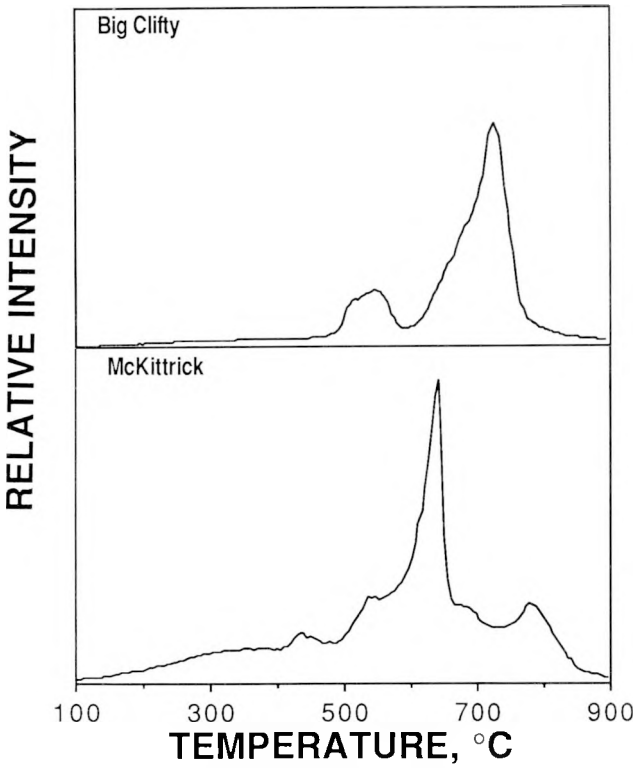

Figure 7. Carbon Dioxide Evolution as a Function of Pyrolysis Temperature for Big Clifty (*Top*) and McKittrick (*Bottom*) Tar Sands at the 10°C/min Heating Rate.

Although difficult to see in the profile, expansion of the data around 400 to 500°C shows a small maximum which roughly coincides with hydrocarbon evolution. The origin of this CO_2 has not been unequivocally assigned, but could be due to the decomposition of O-containing organic compounds such as carboxylic acids and salts[21] by equation (5).

$$RCH_2CH_2COOH \rightarrow CO_2 + RCH_2CH_3 \quad (5)$$

Evolution in this range has been observed for Asphalt Ridge[1] and Sunnyside[2,3] tar sands and very clearly for asphaltenes derived from Big Clifty tar sand bitumen,[4] and has been assigned to organic compound decomposition.

A small, but noticeable maximum is seen in the Big Clifty profile ranging from 500 to 600°C. Evolution in this region could be due to iron-type carbonates decomposing.[23] In addition, these carbonates can react with H_2S to form water and CO_2 by equation (6).[24] The source of H_2S could be decomposing S-containing organics, or some forms of iron-sulfides. Equation (6) has been considered responsible for some CO_2 evolution in Sunnyside tar sand.[2,3]

$$FeCO_3 + H_2S \rightarrow FeS + CO_2 + H_2O \quad (6)$$

The majority of the CO_2 evolution occurs above 600°C, having a prominent maximum at 724°C. This has been assigned previously as due to carbonate decomposition at the 4°C/min heating rate. Approximately 1 wt% of Big Clifty tar sand has been determined to be acid carbonates.[1,2] It must be noted, this high temperature CO_2 evolution could be modified by the high temperature gas-equilibrium chemistry discussed above, particularly because of the water-gas shift reaction, equation (1).

The bottom profile in Figure 7 is CO_2 evolution as a function of pyrolysis temperature for McKittrick tar sand. This profile is much different than the Big Clifty counterpart. More evident is CO_2 evolution with the onset of heating, as well as CO_2 evolution in the temperature range of hydrocarbon evolution. This latter type of CO_2 has a T_{max} value at 435°C, and accounts for approximately 10% of the total CO_2 evolved. A similar CO_2 maximum has been observed for Asphalt Ridge tar sand at the 4°C/min heating rate, having a T_{max} value of 438°C. This maximum has also been assigned primarily to decomposition of O-containing organic compounds. For Big Clifty asphaltenes at the 10°C/min heating rate, where there is no interference with mineral-matter derived CO_2 evolution, the T_{max} value for the same maximum in the hydrocarbon evolution range is 466°C.[25] The slightly higher T_{max} values for asphaltenes suggests either there are other contributions besides organic decomposition to the CO_2 evolution profiles for the tar sands in this temperature range, or the asphaltene precipitation causes an agglomeration effect which raises the activation energy needed for the decomposition reactions. This will be discussed more elsewhere.[25]

The maximum which has a T_{max} value of 546°C in the CO_2 profile of Big Clifty is also evident in the McKittrick profile having a T_{max} value of 538°C. This is probably due to iron-type carbonate decomposition, as in equation (5), or iron-type carbonates reacting with H_2S as in equation (6). This maximum is completely absent in the CO_2 evolution profiles of Big Clifty asphaltenes at 4°C and 10°C/min heating rates.[4,25]

Unlike the Big Clifty case, McKittrick CO_2 evolution

shows a sharp, prominent maximum having a T_{max} value of 636°C. This is in the range for many acid-carbonates to decompose, but the evolution of CO_2 is highly dependent on CO_2 partial pressure.[23,26] X-ray and acid carbonate analyses are in progress to clarify this point. Evolution is also seen at high temperature with a T_{max} value of 736°C. As in the case for Big Clifty, and for H_2, CO, and H_2O, the evolution is governed by complex high temperature chemistry, which has been discussed above.

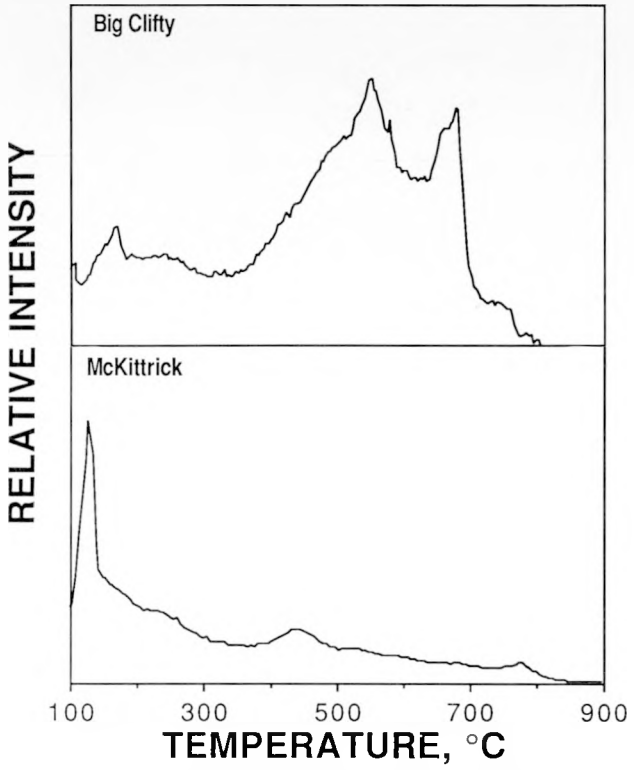

Figure 8. Water Evolution as a Function of Pyrolysis Temperature for Big Clifty (*Top*) and McKittrick (*Bottom*) Tar Sands at the 10°C/min Heating Rate.

Water. Water evolution in tar sands can be broken into roughly six categories based on profiles for both tar sand[1-4] and oil shale pyrolysis:[13] 1) free or surface water (at approximately 100°C) due to absorbed H_2O and decomposition of hydrated clays,[27] 2) entrained water (150 to 200°C) due to H_2O trapped in the bitumen[28] which is liberated upon bitumen softening, 3) quartz and hydrated salt decomposition water (200 to 400°C), 4) hydrocarbon cracking and iron-type carbonate mineral decomposition water (400 to 600°C) due to reactions shown in equations (5) and (6), for example, 5) quartz α to β transition water (approximately 560°C), and 6) mineral decomposition and complex high temperature water (above 600°C) due to mineral decomposition, dehydration and fusing, gasification and water-gas shift reactions.

The top profile in Figure 8 shows H_2O evolution as a function of pyrolysis temperature at the 10°C/min heating rate for Big Clifty tar sand. This profile is similar to, but not exactly the same as the 4°C/min heating rate profile shown previously. All the types of H_2O listed above are evident in the figure. Prominent, however, are maxima with T_{max} values 164°C (entrained H_2O), and 548°C (coincidental with the evolution maximum for iron-carbonate reactions in the CO_2 evolution profile). Also evident at high temperature in the water profile is a maximum with a T_{max} value of 676°C, which is more prominent than seen at the 4°C/min heating rate. Because no CO or CO_2 evolution corresponds to this maximum, the origin is not clear. It could be due to some hydrated mineral decomposing, or could be due to an abrupt change into the high temperature chemistry regime. The water-gas shift reaction appears controlling at temperatures above 550°C under pyrolysis conditions employed here.[29]

The lower profile in Figure 8 shows H_2O evolution as a function of pyrolysis temperature for McKittrick tar sand at the 10°C/min heating rate. Evident is a very sharp maximum having a T_{max} value of 122°C accounting for the majority of the H_2O evolved. As above, this is in the range for free water. This large quantity of free water has also been seen before in water speciation experiments on Diatomite-type tar sand from the San Joaquin valley in California.[30] Water evolution continues throughout the McKittrick profile, decreasing gradually to almost no evolution above 805°C. Small, but noticeable maxima are seen with T_{max} values of 426°C and 775°C. The former maximum occurs in the range of hydrocarbon evolution and has been seen before in the case of Asphalt Ridge tar sand. The high temperature maximum has the same T_{max} value as the small maximum seen in the CO_2 profile (Figure 7), suggesting some carbonate mineral decomposition or related chemistry is occurring. It must be noted that this behavior could easily be modified by complex high temperature chemistry, and may not reflect a simple causality.

Hydrogen Sulfide. The evolution of H_2S in tar sand pyrolysis is generally governed by three phenomena:[24] 1) the decomposition of FeS_2, 2) the decomposition of organo-sulfur compounds, and 3) the capture of H_2S by iron-containing carbonates. The decomposition of pyrite occurs by the two-step equation (7):

$$FeS_2 \rightarrow FeS + 1/2S_2$$
$$H_2 + 1/2S_2 \rightarrow H_2S \qquad (7)$$

The formation of H_2S from this reaction requires hydrogen donors to be present. Pyrolysis of tar sands produces hydrogen from organic compounds in the bitumen, and from secondary charring reactions (see Figure 5). The temperature of H_2S evolution from pyrite is also governed by the particle size.[31] Even though the particle size of the pyrite is really not known well, pyrolysis experiments with extracted tar sands with trace levels of pyrite shows evolution at temperatures above 510°C.[25]

Alternately, equation (8) can describe the pyrolysis of

FeS_2, where the hydrogen comes directly from the organics, producing H_2S and another organo-sulfur compounds.[32]

$$FeS_2 + \text{Organics} \rightarrow FeS + H_2S + \text{R-SH} \quad (8)$$

This suggests several organo-sulfur compounds could be formed during pyrolysis. However, at the 10°C/min heating rate, other than thiophene and methylthiophene (see below), few organo-sulfur compounds are *observed* to evolve. However, this does not rule out the formation of compounds such as those listed in Table 1. Some of these have been reported previously for Big Clifty and Sunnyside tar sands at the 4°C/min heating rate.[2-4] The small reactor volume design, the faster heating rate specific to these experiments here, and poor instrument response are probably responsible for not observing the evolution of these compounds, and that reaction (8) is applicable.

Several types of S-containing organic compounds have been detected in tar sand bitumens.[33-36] Many of these could decompose at elevated temperatures to form H_2S. Thiophene and methylthiophene are detected in the pyrolysis gases for many of the tar sands studied (see below). Although these compounds are very stable in the absence of catalysts, these compounds are known to decompose rapidly at temperatures around 400°C in the presence of hydrodesulfurization catalysts producing H_2S by equation (9):[37]

$$C_4H_4S \rightarrow H_2S + C_4\text{-alkenes} + C_4\text{-alkanes} \quad (9)$$

The effects of pyrolysis have been studied on other S-containing model compounds. S-containing carboxylic acids release primarily H_2S and hydrocarbons when heated to 500°C.[38] Mercaptans are known to react fast under various decomposition conditions like hydrodesulfurization.[22,37] Several of the trace minerals found in tar sands could be potential catalysts to decompose such compounds. (Mineral effects have been documented to dramatically effect sulfur-gas evolution in shales.)[39] Aryl sulfides are more stable and require hydrodesulfurization catalysts to be reactive at lower temperatures.[32] In general, hydrodesulfurization is thermodynamically favorable when S is not associated with an aromatic ring.[32]

The temperature range for the decomposition of these types of compounds has not been unequivocally assigned for tar sand or oil shale. However, experiments with several tar sands, extracted bitumen, and asphaltenes indicate primary H_2S production from organo-sulfur compound decomposition reactions occur in the 400 to 500°C range.[25]

In addition to the producing reactions for H_2S, consumption reactions by iron-containing carbonates, as shown in equation (6) must also be considered. These have been discussed in some detail above. However, because there is currently no way to measure this uptake directly, the amount of H_2S consumed by this type of reaction remains uncertain.

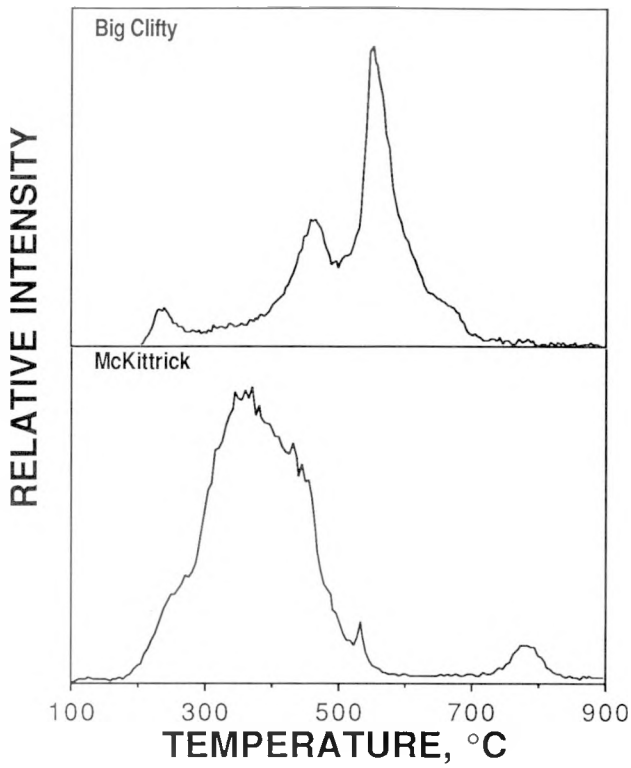

Figure 9. Hydrogen Sulfide Evolution as a Function of Pyrolysis Temperature for Big Clifty (*Top*) and McKittrick (*Bottom*) Tar Sands at the 10°C/min Heating Rate.

The top profile of Figure 9 shows H_2S evolution as a function of pyrolysis temperature for Big Clifty tar sand at the 10°C/min heating rate. The profile is very similar to the 4°C/min profile reported previously. A small maximum with a T_{max} value of 237°C suggests the following: entrained H_2S, elemental S being reduced, or decomposition/reduction of some minerals, for example, iron sulfates. Also seen is a maximum at 456°C, which occurs in the same temperature range as hydrocarbon evolution. This is tentatively assigned to S-containing organic decomposition as discussed above. However, FeS_2 decomposition can not be ruled out in this temperature range.[24]

The prominent maximum in the Big Clifty profile has a T_{max} value of 548°C. This maximum is tentatively assigned as due to pyrite decomposition. Small quantities of pyrite have been detected in Big Clifty tar sands.[40] Not seen due to noise in the H_2S profile for the 4°C/min heating rate is additional low level H_2S evolution extending into higher temperatures. The origin of this H_2S could be due to pyrite of much larger particle sizes. However, pyrolysis of the isooctane insoluble asphaltenes from Big Clifty tar sand bitumen shows a larger, broad maximum around 650°C. This has been tentatively assigned to secondary char type reactions producing H_2S, similar to the reactions discussed above for secondary H_2 and CH_4 production.[4,25] This source can not be ruled out to contributing to the H_2S production in the 400°C+ temperature regime.

The bottom profile of Figure 9 shows H_2S evolution for McKittrick tar sand at the 10°C/min heating rate. The profile exhibits a very large, broad maximum with a T_{max} value of 356°C. The origin of this maximum is not known, but early catalytic cracking literature on California crude oils from the San Joaquin valley shows H_2S evolution even at very low temperatures.[41] This suggests this H_2S is probably from the decomposition of S-containing organic compounds. A variety of S-containing carboxylic acids evolve H_2S at temperatures around 300°C.[42] However, these same studies show pyrite will release H_2S at around 300°C with hydrogen donors present. In the case of McKittrick tar sand, no hydrogen or hydrocarbon is evolving at this low temperature range, making this unlikely. However, the volatilization of organics may not be necessary for them to be hydrogen donors, just the mobilization. Water is also present which could be a potential hydrogen donor.[13]

In the McKittrick tar sand profile, there is a small, sharp maximum with a T_{max} value of 523°C, which is in the temperature range for pyrite decomposition. This is further supported by the small maximum with a T_{max} value of 781°C, which is in the range for FeS decomposition[32] (which could have been formed by equations (7) and /or (8)).

Methylthiophene. The top profile of Figure 10 shows methylthiophene evolution as a function of pyrolysis temperature for Big Clifty tar sand at the 10°C/min heating rate. The noise in this profile makes it difficult to discern a T_{max} value, but comparing this profile to the methylthiophene profile at 4°C/min heating rate shows a maximum in the temperature range of hydrocarbon evolution.

The origin of thiophenes is still a matter of debate. Several studies on bitumens indicate complicated thiophenic structures are abundant in the S-containing fractions.[33-36] Model compound studies reveal thiophenes are stable to pyrolysis up to very high temperatures in the absence of catalysis.[43] However, alkyl thiophenes will loose alkyl groups around 500°C.[44] In addition, thienyl acrylic acid produces thiophene and methylthiophene at 500°C.[38] This could account for how the thiophenes are bound in the bitumen, where thermal release occurs through scission of an alkyl chain. This would also help explain the higher concentration of methylthiophene than thiophene being released,[4] because carbon-carbon bonds at the position α to the ring are generally more reactive than those directly bound to an aromatic ring.

Thiophenes can also be formed by several types of reactions which are amenable with the tar sand pyrolysis conditions employed here: 1) by the reaction of S or H_2S with organic molecules[45,46] (industrial preparation is n-C_4H_{10} + S at 600°C for 1 sec); aluminas and silicas will catalyze these reactions, 2) by the reaction of unsaturated hydrocarbons, like ethylene, with FeS_2 (concentrations of H_2S, FeS_2, and hydrocarbons are all available around 400°C to 600°C in the pyrolysis reactor, as well as several types of naturally occurring alumina and silica minerals that are found in the mineral matrix of the tar sands), and 3) by the decomposition of non-thiophenic organo-sulfur compounds (reactions of glucose and H_2S form a thioglucose which decomposes upon pyrolysis to form thiophene and several substituted thiophenes).[47] Other organo-sulfur compounds could do the same given the thermal stability of thiophenes to pyrolysis-type conditions.[48]

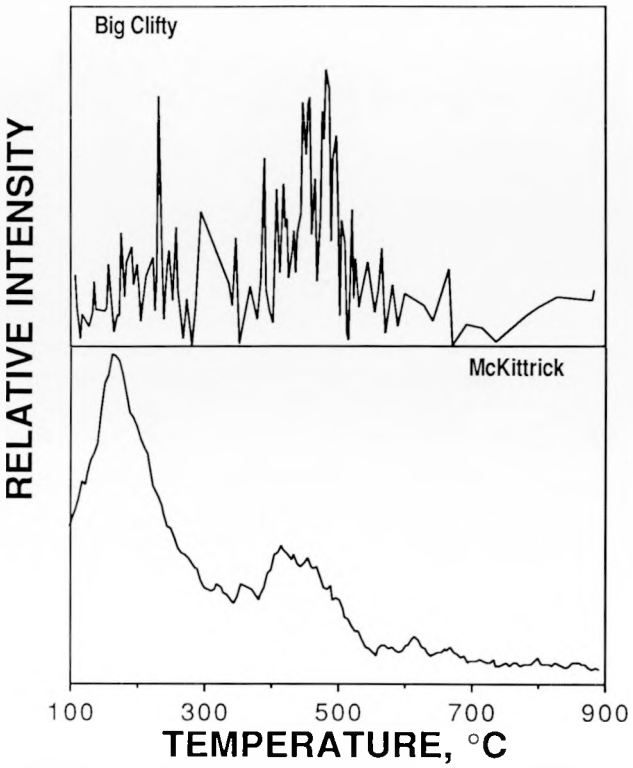

Figure 10. Methylthiophene Evolution as a Function of Pyrolysis Temperature for Big Clifty (*Top*) and McKittrick (*Bottom*) Tar Sands at the 10°C/min Heating Rate.

The bottom profile of Figure 10 shows methylthiophene evolution as a function of pyrolysis temperature for McKittrick tar sand at the 10°C/min heating rate. Unlike the corresponding Big Clifty profile, two maxima are clearly seen. The maximum at low temperature has a T_{max} value of 159°C accounting for 65% of the methylthiophene, and is assigned to evolution due to the release of entrained materials, just as in the case of hydrocarbon evolution (see above). The maximum at moderate temperature has a T_{max} value of 430°C accounting for the balance of the methylthiophene released, and occurs in the temperature range of hydrocarbon evolution. The origin of this methylthiophene is discussed above for the Big Clifty tar sand.

Several other heteroatomic compounds evolved during the pyrolysis of both tar sands. However, because of the small sample size, faster heating rate, and poorer signal-to-noise, the profiles are much noisier than equivalent profiles at the 4°C/min heating rate. Therefore, these species will not be discussed here.

CONCLUSIONS

Several conclusions can be made when comparing the pyrolysis behavior of Big Clifty and McKittrick tar sands:

1) The evolution profiles for Big Clifty and McKittrick tar sands are generally bimodal in shape, having a maximum with T_{max} values around 450 to 500°C, which has been assigned to evolution due to hydrocarbon cracking reactions, and a maximum with T_{max} values around 150 to 200°C, which has been assigned to evolution due to entrained materials in the sand matrix. The exceptions to the bimodal evolution pattern are methane (see below), C_2H_4, and C_3H_8. The evolution of latter two species is thought to be artificially controlled by detection limitations of the equipment, and also have the bimodal evolution pattern. Alternative evolution mechanisms, however, can not be ruled out.

2) Big Clifty tar sand profiles have higher T_{max} values for individual hydrocarbon and heteroatomic compound evolution than the corresponding profiles for McKittrick tar sand.

3) For heavier hydrocarbons (C_5H_{12}, C_6H_6, C_7H_8, C_4H_8, C_5H_{10}, C_6H_{12}), evolution due to entrained materials account for a high percentage (around 50%) of the total hydrocarbons for McKittrick tar sand. This is not the case for Big Clifty tar sand, where evolution due to entrained materials accounts for much less of the total (20% or less).

4) McKittrick tar sand had a much lower T_{max} value for methane evolution than Big Clifty tar sand.

5) A much higher percentage (15%) of the total hydrogen evolves in the hydrocarbon cracking range for McKittrick tar sand than for Big Clifty tar sand (6%). However, hydrogen evolution at higher temperatures exhibited similar profile behavior.

6) A much higher percentage (7%) of the total CO evolves in the hydrocarbon cracking range for McKittrick tar sand than for Big Clifty tar sand. As with hydrogen, however, carbon monoxide evolution at high temperature is similar in both profiles due to the dominance of the complex-equilibrium chemistry.

7) Carbon dioxide evolution is completely different for both tar sands. Big Clifty is dominated by high temperature CO_2 evolution, most likely due to acid-type carbonate decomposition. A smaller amount is detected in the moderate temperature range, most likely due to iron-type carbonates. The McKittrick tar sand exhibited small maxima at hydrocarbon cracking temperatures, and at temperatures which may be due to iron-type carbonate decomposition The prominent maximum (T_{max} value of 636°C) is below the evolution range found for Big Clifty tar sand, but also could be due to acid-type carbonate decomposition.

8) Hydrogen sulfide evolution for Big Clifty exhibits three maxima: at low temperature (probably due to sulfates decomposing or S reduction), at hydrocarbon cracking temperatures, and in the FeS_2 decomposition temperature range. McKittrick tar sand has a completely different H_2S profile having the majority of evolution well below 500°C. Small maxima are also observed at higher temperatures probably due to FeS_2 and FeS decomposition.

ACKNOWLEDGMENTS

I thank Armando Alcaraz and Richard W. Crawford of LLNL for experimental assistance, and Robert W. Taylor of LLNL and Byron G. Spars of Chevron Research Company for useful discussions. This work was performed under the auspices of the U. S. Department of Energy by the Lawrence Livermore National Laboratory under contract number W-7405-ENG-48.

REFERENCES

1. Reynolds, J. G., Crawford, R. W., and Coburn, T. T. 1987 Eastern Oil Shale Symposium Proceedings, KECL 87-175, 101 (1988).
2. Reynolds, J. G., and Crawford, R. W. ACS Div. Petrol. Chem., Preprints, 33(2), 297 (1988).
3. Reynolds, J. G., and Crawford, R. W. Fuel Sci. Tech. Int'l., 7(5-6) 823 (1989).
4. Reynolds, J. G. 1988 Eastern Oil Shale Symposium Proceedings, IMMR88-101, 18 (1989).
5. Reynolds, J. G., Jones, E. L., Bennett, J. A., and Biggs, W. R. ACS Div. Petrol. Chem., Preprints, 33(2), 297 (1988).
6. Reynolds, J. G., Jones, E. L., Bennett, J. A., and Biggs, W. R. Fuel Sci. Tech. Int'l, 7(5-6), 625 (1989).
7. Reynolds, J. G., and Biggs, W. R. Size Exclusion Chromatography-Inductively Coupled Plasma Atomic Emission Spectrographic Study of Fe in Bitumens Derived from Tar Sands. Manuscript in preparation (1990).
8. Reynolds, J. G., and Biggs, W. R. Accounts of Chem. Res., 21, 319 (1988).
9. Westhoff,J. D. 1986 Eastern Oil Shale Symposium Proceedings, KECL86-158, 65 (1987).
10. Kuuskraa, V. A., Hammershaimb, E. C., and Paque, M. Proceedings from the WRI-DOE Tar-Sand Symposium, DOE/METC85/13, DE85 001994, 35 (1985).
11. Marchant, L. C. 1984 Eastern Oil Shale Symposium, Proceedings, IMMR84-124, 125 (1985).
12. Wong, C. M., and Crawford, R. W. Int. J. Mass Spec. and Ion Processes, 60, 107 (1984).
13. Coburn, T. T., Oh, M. S., Crawford, R. W., and Foster, K. G. Energy and Fuels, 3, 216 (1989).
14. Wong, C. M., Crawford, R. W., Barton, V. C., Brand, H. R., Neufeld, K. W.,and Bowman. J. W. Rev. Sci. Instr., 54, 996 (1983).
15. Reynolds, J. G., Crawford, R. W., and Burnham, A. K. Oil Shale Pyrolysis by Triple Quadrupole Mass Spectrometry: Comparisons of Gas Evolution at a 10°C/min Heating Rate. Manuscript in preparation (1990)
16. Reynolds, J. G., Crawford, R. W., and Burnham, A. K. ACS Div. Fuel Chem., Preprints, 34(4), 1106 (1989).

17. Reynolds, J. G., and Beret, S. Fuel Sci. Tech. Int'l., 7(2), 165 (1989).
18. Coburn, T. T. Energy Sources, 7, 121 (1983).
19. Braun, R. L., and Burnham, A. K. Lawrence Livermore National Laboratory Report UCID-21507 (1989).
20. Oblad, A. G., Bunger, J. W., Hanson, F. V., Miller, J. D., Ritzma, H. R., and Seader, J. D. Ann. Rev. Energy, 12, 238 (1987).
21. March. J J. Chem. Ed., 40(4), 212 (1963).
22. Burnham, A. K., and Braun, R. L. ACS Div. Fuel Chem., Preprints, 29(3), 94 (1984).
23. Kracek, F. C. Geological Survey Bulletin 1144-D, US Gov. Print. Off., Washington (1963).
24. Taylor, R. W., Morris, C. J., and Coburn, T. T. 1988 Eastern Oil Shale Symp., Proceedings, IMMR88/101, 147 (1989).
25. Reynolds, J. G., Volatile Compound Behavior in Programmed Temperature Pyrolysis of Tar Sands and Oil Shales: Effects of Asphaltene Separation to Isolate the Organic Compounds from the Influence of the Mineral Matrix. Manuscript in preparation (1990).
26. Campbell, J. H., and Burnham, A. K. 11th Oil Shale Symposium Proceedings, Colorado School of Mines, 242 (1979).
27. Van Olphan, H., and Fripiat, J. J. Eds. Data Handbook for Clay Minerals and other Non-metallic Minerals; (1979), Pergamon Press, Oxford, U.K.
28. Probstein, R. E., and Hicks, R. E. *Synthetic Fuels:* (1982), McGraw Hill-Book Company, New York
29. Coburn, T. T., Crawford, R. W., Gregg, H. R., Oh, M. S. 1986 Eastern Oil Shale Symp., Proceedings, KECL 86-158, 291 (1987).
30. Audeh, C. A. ACS Div. Petrol. Chem., Preprints, 33(3), 466 (1988).
31. Montano, P.A., Vaishnava, P. P., King, J. A., and Eisentrout, E. N. Fuel, 60, 712 (1981).
32. Attar, A. Fuel, 57, 201 (1978).
33. Payzant, J. D., Mojelsky, T. W., and Stausz, O. P. Energy and Fuels, 3, 449 (1989).
34. Bunger, J. W., Thomas, K. P., and Dorrence, S. M. Fuel 58, 183 (1979).
35. Nishioka, M. Energy and Fuels, 2, 214 (1988).
36. Orr, W. L., Sulfur in Heavy Oils, Oil Sands, and Oil Shales, pages 223-243, from *Oil Sand and Oil Shale Chemistry*, Eds. Strausz, O. P. and Lown, E. M. Verlag Chemie, New York 1978.
37. Gates, B. C., Katzer, J. R., and Schuit, G. C. *Chemistry of Catalytic Processes* (1979). McGraw-Hill Book Co., New York.
38. Wong, C. M., Crawford, R. W., and Burnham, A. K. ACS Div. Fuel Chem., Preprints, 29(3), 317 (1984).
39. Wong, C. M., Crawford, R. W., and Burnham, A. K. Anal. Chem., 56, 390 (1984).
40. Noger, M. C. Private communication.
41. Gary, J. H., and Handwerk, G. E. *Petroleum Refining,* (1984) Second Ed., Marcel Dekker, Inc., New York.
42. Fadeff, S. K., Burnham, A. K., and Richardson, J. H. Lawrence Livermore National Laboratory Report UCID-19751 (1983).
43. Attar, A., Corcoran, W. H., and Gibson, G. ACS Div. Fuel Chem., Preprints, 21(7), 106 (1976).
44. Martin, R. L., and Grant, J. A. Anal. Chem., 37, 649 (1965).
45. Hartough, H. D. *Thiophene and its Compounds*, Interscience, New York (1952).
46. Hartough, H. D., and Meisel, S. L. *Compounds with Condensed Thiophenic Rings,* Interscience (1954).
47. Moers, M. E. C., de Leeuw, J. W., Cox, H. C., and Schenck, P. A. Adv. Org. Geochem., 13(4-6), 1087 (1988).
48. Ferm, R. J. Chem. Rev. 57, 621 (1957).

The Chemical Aspects of Alberta Tar Sand Bitumens

by

O.P. Strausz, T.W. Mojelsky, T.M. Ignasiak, Z. Frakman, J.D. Payzant, and E.M. Lown
Department of Chemistry
University of Alberta
Edmonton, Alberta CANADA T6G 2G2

Abstract Comparison of the molecular composition of the bulk material of the distillable portion of Athabasca tar sand maltene with the undistillable, heavier aromatic maltene and asphaltene portions leads to the conclusion that they have originated from different biotic source materials.

Introduction

Our knowledge and understanding of the chemical composition of tar sand bitumens have greatly improved in the last decade or two. Many individual constituent compounds and homologous series of compounds have been detected and structurally identified. Most of these compounds had been known before to be present in crude oils, but nevertheless many of them have been found in bitumens for the first time and were subsequently shown to be present in conventional crude oils as well. Some of the compounds in question were chemically novel, in the sense that they had not been reported before in the literature. The high molecular weight, non-distillable portion of the bitumen, however, still presents a provocative challenge to the efforts of research chemists, yielding only small, tantalizing fragments of structural information even with the use of the most sophisticated analytical techniques. Another, still difficult problem remaining, is the analysis of the composition of the bulk portion of distillates which are largely made up of complex mixtures of known, well-defined stoichiometric compounds of extremely great number and variety. In this connection, field ionization mass spectrometry has been shown to be a highly effective tool to probe into the problem of composition.

In this article we present some results on the field ionization mass spectroscopic studies of bitumens and the degradative oxidation of tar sand asphaltenes.

Results and Discussion

Chromatographic fractions of Athabasca (Canada, Alberta) tar sand maltene were subjected to field ionization mass spectrometric studies at 240°C.[1] In field ionization mass spectrometry, ionization is achieved by the exposure of the sample molecules to a strong electric field (~10^5V/cm) which is capable of removing an electron from any molecule. This kind of ionization produces parent ions only, making it highly useful for the analysis of complex hydrocarbon mixtures like petroleums. The sensitivity within a compound class is nearly independent of the molecular weight and changes little even on going from one compound class to other, not too different compound classes. Therefore, in the following, it is assumed that all hydrocarbon molecules in the samples studied have the same ion yield response.

Figure 1 shows the capillary gc trace of the saturate fraction of the maltene which is distillable at 240°C and 10^{-3} torr pressure (18.2% of the maltene and 90% of the total saturates). The spectrum shows the characteristic features of Alberta oil sand saturates, most of the material eluting in the form of a broad unresolved hump with one or more maximum on which are superimposed sharp peaks owing to the so-called biological marker molecules. The challenge lies in the analysis of the unresolved humps. Figure 2 reproduces the field ionization mass spectrum (FIMS) of the same material. As seen from the Figure, the components lie in the 180–700 dalton mass range, with a concentration distribution featuring two maxima at C_{15}–C_{20} and C_{29}–C_{31} and a minimum around C_{26}. From the insert of the reconstructed spectral distributions of the C_{32} and C_{33} compounds, one can see that the most intense peaks correspond to m/z = 440 and 454 daltons, corresponding to the elemental formulae $C_{32}H_{56}$ and $C_{33}H_{58}$, respectively. They are members of the C_nH_{2n-8} series, representing pentacyclic hydrocarbons (hopanes and their isomers). The next most intense peaks are the tetracyclics followed by the tri- and bicyclics. The monocyclics and hexacyclics are present at these carbon numbers only in trace quantities and heptacyclics as well as acyclic are absent altogether. Now plotting separately the relative abundances for each class of cycloalkanes as a function of carbon number in the molecule, Figures 3 and 4, we find that the concentration maxima (with the exception of the monocyclic series for which no comparative data exist) closely coincide with those of the prominent biomarker molecules in the series for the same oils (bicyclic terpanes C_{16}, tricyclic terpanes C_{20} and C_{23}, steranes C29 and C22 and hopanes C29, C30).[2] These correlations clearly suggest that the bulk of the saturate fraction is made up of a mixture of isomerized, rearranged and degraded varieties of the 1–5 ring biological molecules.

Lending additional support to this proposition is the fact that this correlation can be extended to include the monoaromatic as well as higher aromatic compound classes. This point is illustrated by Figures 5 and 6. From similar plots both the tricyclic diaromatics and tricyclic triaromatic series show a maximum at C_{17} followed by a smooth decline up to at least C_{40}. This maximum is shifted downward by two carbon atoms in carbon numbers as compared to the maximum for the tricyclic saturates, Figure 3. In general, it appears that the higher the aromaticity, the larger is the shift to lower carbon numbers for the maximum concentration, as illustrated for the pentacyclic

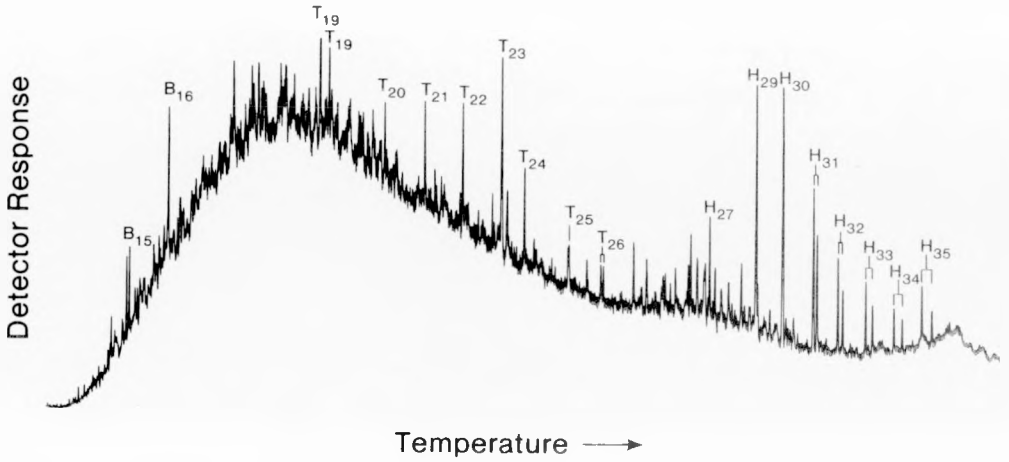

Figure 1. Capillary gas chromatographic trace of the saturate fraction of Athabasca bitumen. B: tricyclic terpane; T: tricyclic terpane; H; hopanes (pentacyclic terpanes). Subscripts signify the carbon number in the series. Reproduced from Reference 1 with permission.

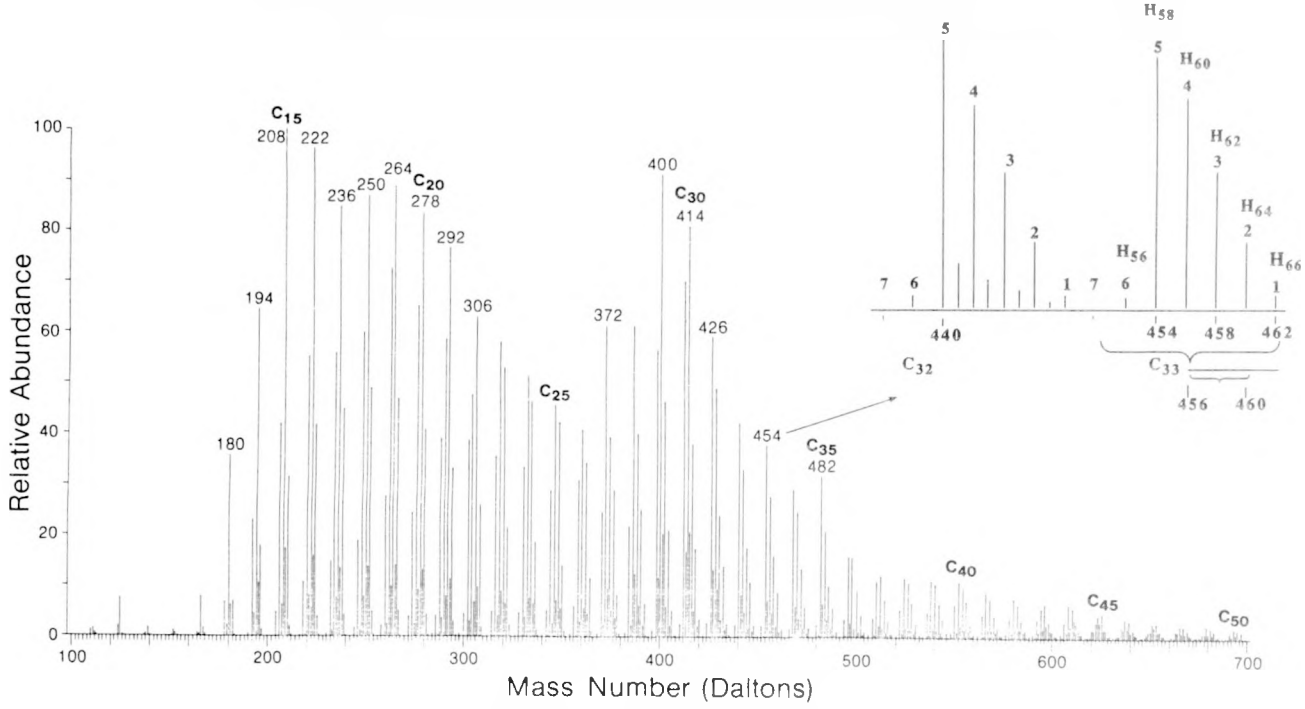

Figure 2. FIMS trace for the saturate fraction of Athabasca bitumen. Numbers above peaks are the mass numbers in daltons. Insert: reconstructed enlargement of the peak clusters for C_{32} and C_{33} compounds. Reproduced from Reference 1 with permission.

series in Figure 7. The manifested trend can be readily explained by invoking increasing cracking with increasing aromaticity in the original saturated pentacyclic precursors.

The main conclusion that can be drawn from these compositional studies of the distillable hydrocarbon fraction of Athabasca and, in general, of Alberta tar sand bitumen, is that the bulk of these hydrocarbons originated from mono- through pentacyclic terpenoid hydrocarbon precursors. The *normal* alkyl complements of these bitumens are missing owing to the extensive microbiological degradation of the original precursor oil, leaving behind the branched terpenoid hydrocarbons.

The above conclusion appears to apply to many of the heterocyclic components of the maltene as well with the exception of the thiophenic, fluorenone, fluorenol and carbazole class compounds. Thus, it has been shown that all Alberta tar sand bitumens contain cyclic terpenoid sulfides and sulfoxides having two through six rings (4–14%),[3] and di-, tri- and pentacyclic terpenoid carboxylic acids[4] as main components of the polar fraction of the maltene. The parent cyclic terpenoid hydrocarbons of these heterocycles have been shown to be present in the saturate fraction of the maltene.

The absence of aliphatic alkanes and especially of *normal* alkanes in the distillable portion of Alberta tar sand maltenes is in sharp contrast with the relative abundance of *normal* alkanoic moieties in the asphaltene and in the heavy, non-distillable portion of the bitumen. These *n*-alkanoic moieties consist of either *n* -alkyl side chains attached to:

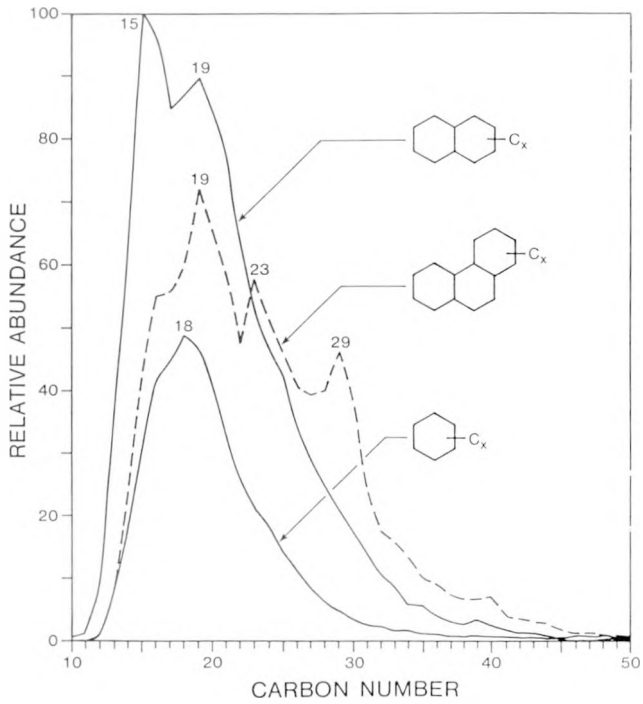

Figure 3. Relative abundance vs. carbon number for the monocyclic, dicyclic and tricyclic hydrocarbons in the saturate fraction of Athabasca bitumen. Reproduced from Reference 1 with permission.

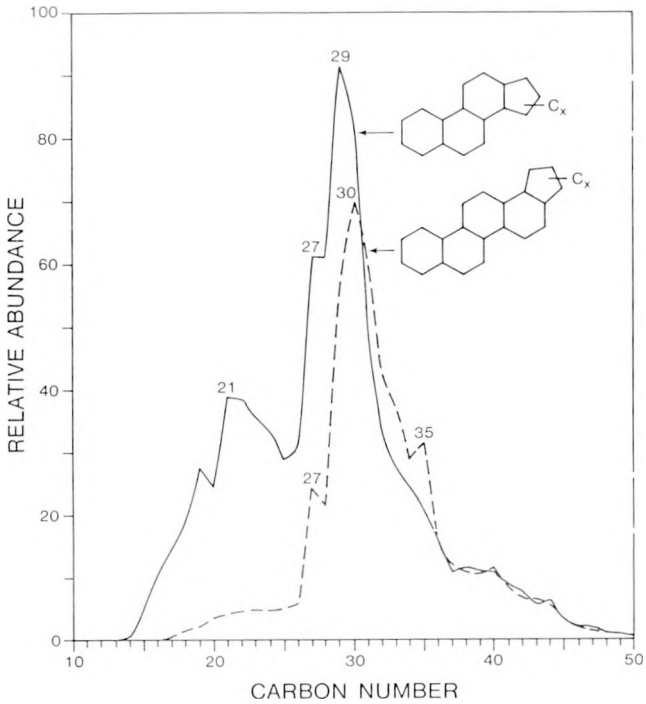

Figure 4. Relative abundance vs. carbon number for the tetracyclic and pentacyclic hydrocarbons in the saturate fraction of Athabasca bitumen. Reproduced from Reference 1 with permission.

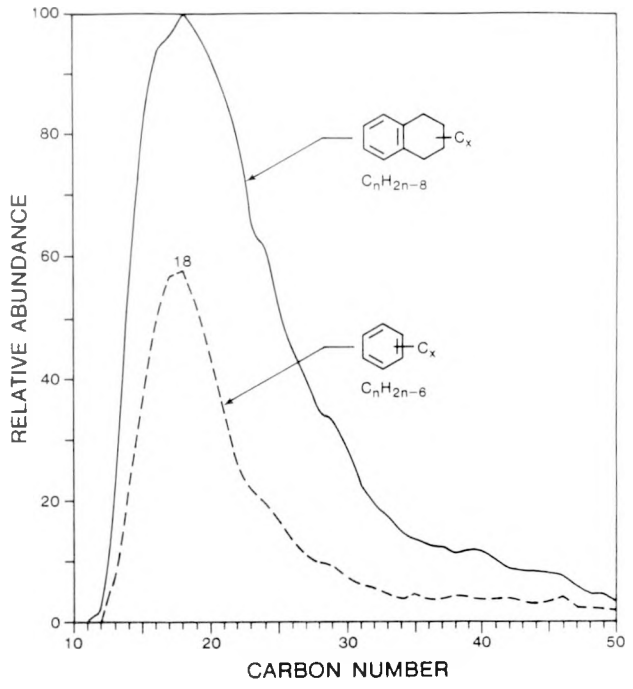

Figure 5. Relative abundance vs. carbon number for the monocyclic and dicyclic hydrocarbons in the monoaromatic fraction of Athabasca bitumen. Reproduced from Reference 1 with permission.

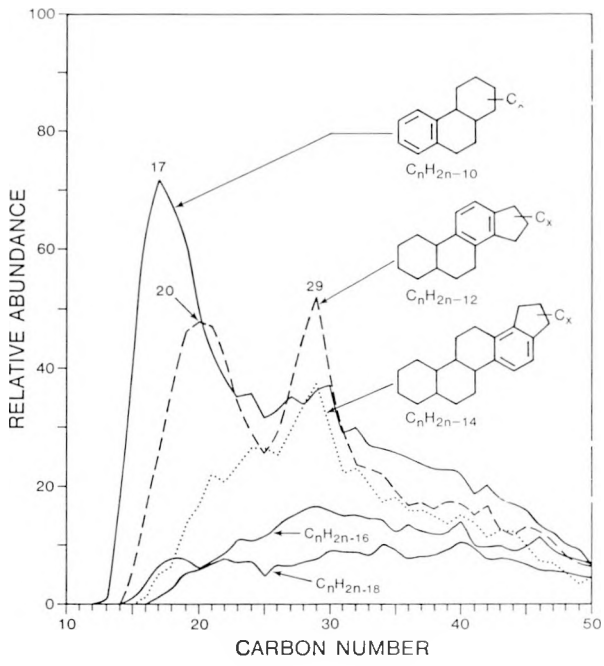

Figure 6. Relative abundance vs. carbon number for the tricyclic, tetracyclic and pentacyclic hydrocarbons in the monoaromatic fraction of Athabasca bitumen. Reproduced from Reference 1 with permission.

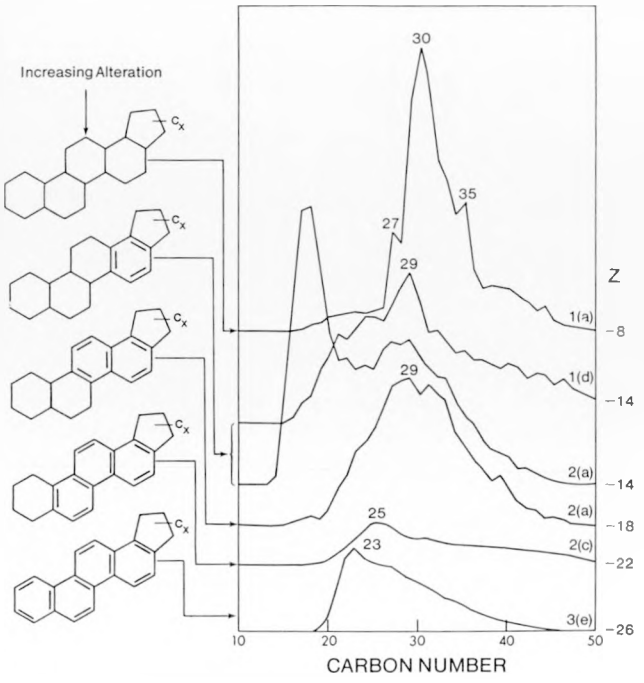

Figure 7. Relative abundance vs. carbon number of hydrocarbons in Athabasca maltene. Comparison of the relative abundances of pentacyclic hydrocarbons with 0–4 aromatic rings. Reproduced from Reference 1 with permission.

i) aromatic rings of hydrocarbons;
ii) thiophenic rings;
iii) thiane or thiolane rings; and
iv) naphthenic rings,

or *n*-alkenyl bridges connecting the types of ring structures mentioned above with one another. The alkyl side chains attached to aromatic carbons can be converted cleanly and nearly quantitatively to alkanoic acids one carbon atom longer than the side chain by Ru(VIII)-catalyzed oxidation using sodium metaperiodate as the oxidant. Alkyl chains attached to

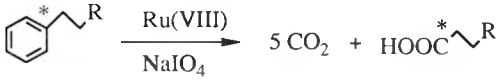

naphthenic carbons are not affected by Ru(VIII)-catalyzed oxidation and therpefore the method permits the selective oxidation of the aromatic-anchored alkyl chains and their quantitative determination as alkanoic acids.[5]

About 66% of the Athabasca maltene is distillable at 240°C and 10^{-3} torr and this is the portion that has been analyzed by FIMS. In an effort to determine whether the residue is *n*-alkyl substituted, as is the asphaltene, or whether it is terpenoid-type like the distillable portion,the residue was separated into five chromatographic fractions and each was subjected to Ru(VIII)-catalyzed oxidation. With the exception of the saturate fraction all fractions, the monoaromatic, polyaromatic and the two resin fractions gave a homologous series of *n*-alkanoic acids with carbon numbers at least up to C_{25}. The maximum concentration of the *n*-alkanoic acids occurred at ~C_{11}, beyond which the concentrations showed a gradual decline. It may be assumed that, as is the case with asphaltene, the low molecular weight end of the acids was lost due to their volatility and the true concentration distribution of the *n*-alkyl side chains on the aromatic rings had its maximum at C_1 with a gradual decline as the carbon number in the side chain increased.

When an alkyl chain is attached at both ends to aromatic rings then oxidation takes place at both ends, resulting in a dicarboxylic acid. If the chain happens to be *n*-alkanoic then the resultant acid will be an α,ω-di-*n*-alkanoic acid. A homologous

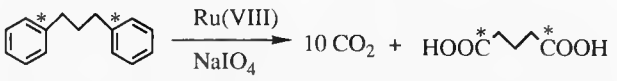

series of α,ω-di-*n*-alkanoic acids was indeed detected in the Ru(VIII)-catalyzed oxidation of all the fractions that produced *n*-alkanoic acids. This finding establishes the existence of *n*-alkanoic– and only *n*-alkanoic–bridges between aromatic units, in addition to the *n*-alkyl– and only *n*-alkyl– side chains on the aromatic rings.

If an alkyl group is attached at one end to an aromatic unit and at the other, to a naphthenic unit, then the Ru(VIII)-catalyzed oxidation converts the aromatic end to a carboxylic group but leaves the other end remaining in the involatile matrix unaltered:

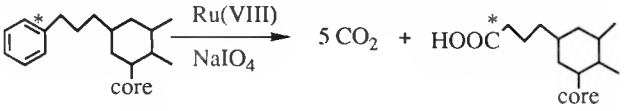

Thermolysis of the oxidized residue may liberate the aliphatic acid and any alkyl side chains that may be attached to the naphthenic ring:

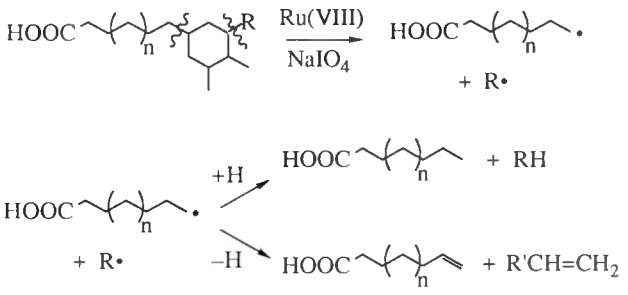

Thus, thermolysis should yield alkyl carboxylic acids, alkenyl carboxylic acids, alkanes and terminal alkenes. This is indeed the case with the oxidized residues from all the four fractions having aromatic contents. Each of these fractions gave, on thermolysis, following Ru(VIII)-catalyzed oxidation, a homologous series of *n*-alkanoic acids, 1-*n*-alkenoic acids, *n*-alkanes and 1-*n*-alkenes. As in the previous cases all the acids and aliphatic hydrocarbons detected had the *normal*, unbranched carbon skeleton.

The appearance of these products proves the existence of *n*-alkyl chains attached to cycloalkanes and *n*-alkenyl bridges connecting aromatic with naphthenic rings in the non-distillable aromatic fractions of the maltene and suggests that the high molecular weight portion of the maltene had a different precursor from the lower molecular weight, distillable portion. Thus, the heavier portion appears to have been derived from alkanoic biotic sources while the lighter portion from terpenoid sources.

Similar studies involving the Ru(VIII)-catalyzed oxidation–thermolysis were also carried out on the asphaltene fraction of the oil. The alkanoic acids arising from the Ru(VIII)-catalyzed oxidation were determined quantitatively and the results are plotted in the form of absolute concentrations of alkyl chain as a function of chain length in Figure 8. The maximum concentration, as seen from the Figure, occurs at C_1 and gradually falls off to and beyond C_{22}. The distribution of alkyl chains would probably be similar to that of all the *n*-alkanoic acids-yielding fractions. Also, as in the case of the aromatic fractions, only the *n*-alkanoic types of monocarboxylic acids

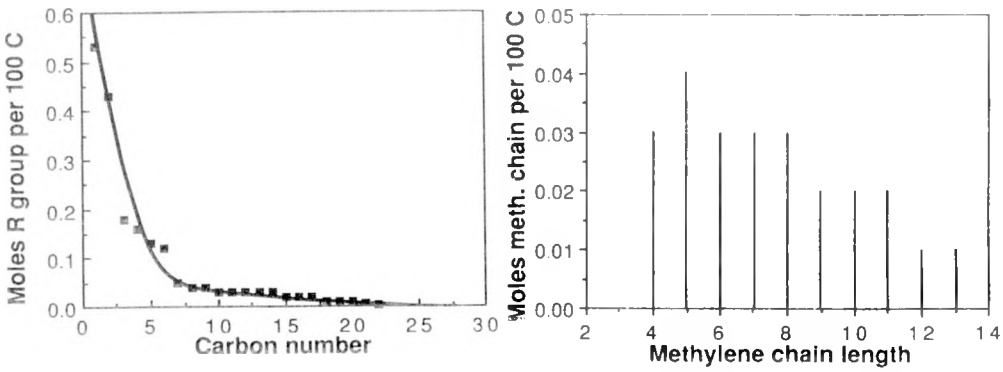

Figure 8. Distribution of the *n*-alkanoic (left) and α,ω-di-*n*-alkanoic (right) acids from the Ru(VIII)-catalyzed oxidation of Athabasca asphaltene.

could be detected in the oxidation products of the asphaltene.

As with the aromatic fractions, oxidation of the asphaltene also yielded a homologous series of α ω -*n*-dicarboxylic acids. Their distribution has been determined quantitatively and the results are presented in Figure 8 as a plot of absolute concentration *vs* carbon chain length in the polymethylene bridge between two aromatic units in the original asphaltene structure. Thermolysis of the oxidized residue yielded homologous series of *n*-alkanoic and 1-*n*-alkenoic acids, along with series of *n*-alkanes and 1-*n*-alkenes.

These results, taken together, show that the asphaltene originated from the same *n*-alkanoic source material as the heavy aromatic fraction of the maltene.

Additional light on the structure of asphaltene and the nature of its biotic source materials comes from studies on the composition of the distillable oil produced on mild pyrolysis of the asphaltene. The pyrolysis oil was found to contain homologous series of *n*-alkyl-substituted five- and six-membered cyclic sulfides, thiophenes, benzothiophenes and dibenzothiophenes.[6] Branched alkyl substituted derivatives of these sulfur compounds, however, were not detected. The carbon number distribution of the sulfides, thiophenes and benzothiophenes can be seen from the gas chromatograms reproduced in Figures 9–11. The structure of the compounds identified:

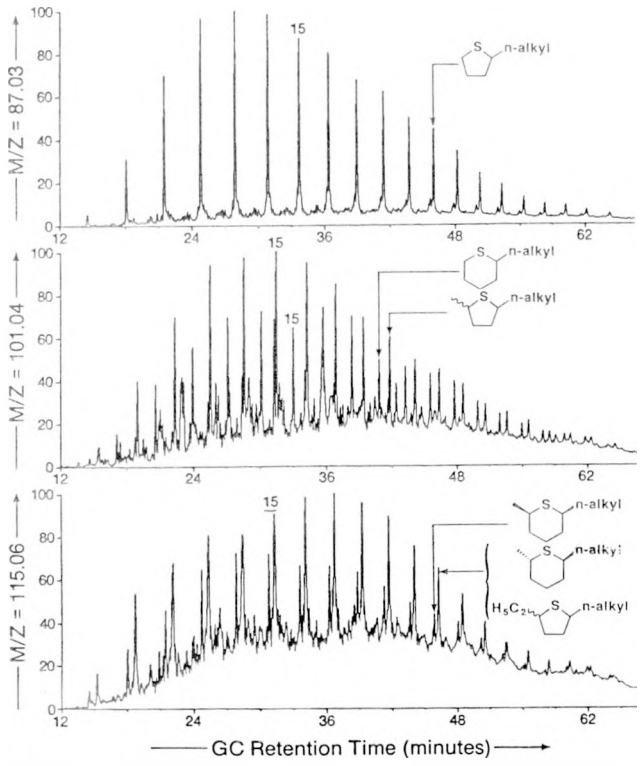

Figure 9. Distribution of the monocyclic sulfides in the pyrolysis oil of Athabasca asphaltene as determined by single ion recording gas chromatograph – mass spectrometric measurements. Reproduced from Reference 6 with permission.

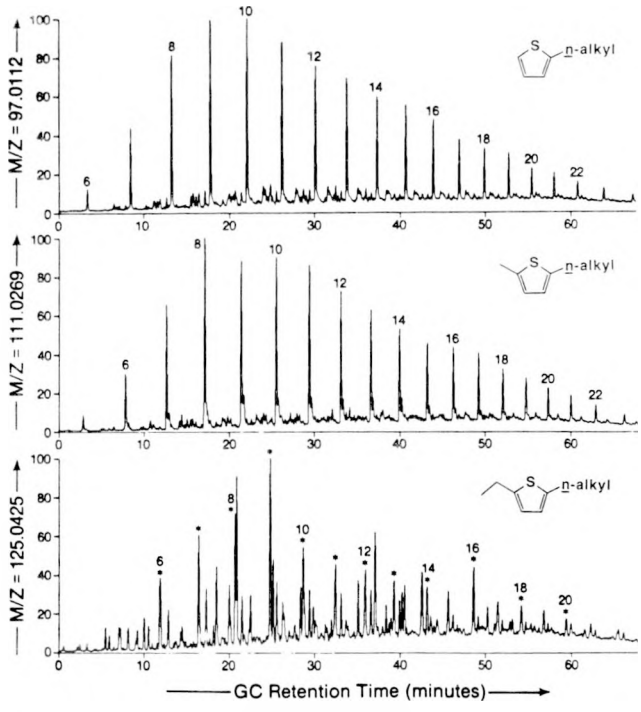

Figure 10. Distribution of the thiophenes in the pyrolysis of Athabasca asphaltene as determined by single ion recording gas chromatograph – mass spectrometric measurements. Reproduced from Reference 6 with permission.

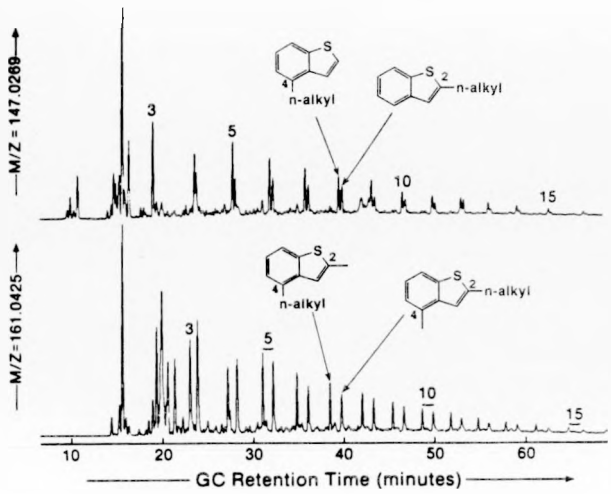

Figure 11. Distribution of the *n*-alkyl benzo[b]thiophenes in the pyrolysis oil of Athabasca asphaltene as determined by single ion recording – mass spectrometric measurements. Reproduced from Reference 6 with permission.

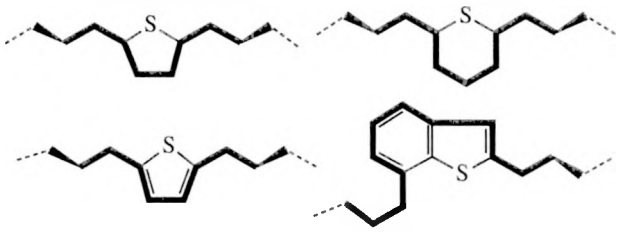

and the absence of other types of branched structures clearly manifest the *n*-alkanoic origin of these materials. The substitution pattern of these compounds can be rationalized in terms of the cyclization of an *n*-alkanoic precursor, as indicated by the heavy lines in the above structural formulae.

Consequently, in view of the vast and clearly-manifested structural differences between asphaltene and heavy aromatics on the one hand and the distillable, lighter fractions of the maltene on the other, one is forced to conclude that they have originated from different biotic source materials.

Acknowledgements

The authors thank the Alberta Oil Sands Technology and Research Authority (AOSTRA) for continuing financial support and Dr. Theodore J. Cyr of AOSTRA for many helpful discussions and valuable advice in the course of these studies.

References

1. J.D. Payzant, A.M. Hogg, D.S. Montgomery and O.P. Strausz, AOSTRA J. Res., 1, 175, 183, 203 (1985).

2. C.F. Hoffmann and O.P. Strausz, Amer. Assoc. Petrol. Geol. Bull., 70, 1113 (1986)

3. J.D. Payzant, D.S. Montgomery and O.P. Strausz, Org. Geochem., 9, 357 (1986).

4. T.D. Cyr and O.P. Strausz, Org. Geochem., 7, 127 (1984).

5. O.P. Strausz, Preprints, Amer. Chem. Soc., Div. Petrol. Chem., 33, 264 (1988); T.W. Mojelsky, D.S. Montgomery and O.P. Strausz, AOSTRA J. Res., 3, 43 (1986); *ibid.* 2, 177 (1986); 2, 131 (1985).

6. J.D. Payzant, D.S. Montgomery and O.P. Strausz, AOSTRA J. Res., 4, 117 (1988).

Use of Biomarkers, Including Aromatic Steroids, to Indicate Relationships Between Oil Sands/Heavy Oils/Bitumens and Conventional Oils, Western Canada Basin

by

P.W. Brooks, M.G. Fowler, and R.W. Macqueen
Institute of Sedimentary and Petroleum Geology
Geological Survey of Canada
Calgary, Alberta CANADA T2L 2A7

Abstract. Results of triaromatic steroid analyses support our previous suggestion of a single family of Lower Cretaceous oil sands/heavy oils, and confirm a genetic link between these and bitumens from Paleozoic "carbonate trend" deposits. Biomarker distributions from both saturated and aromatic fractions indicate that Mesozoic and Paleozoic oil sands/heavy oils/bitumens are closely related to conventional Lower Cretaceous-Mississippian oils of the Western Canada Sedimentary Basin, but are very different from conventional Middle and Upper Devonian oils.

Introduction

With designated reserves of 268 billion cubic metres ($268x10^9m^3$) in Alberta alone, the quantities of oil sands/heavy oils/bitumens in the Western Canada Sedimentary Basin (WCSB) are immense.[1] In comparison, reserves of light and medium gravity conventional oil in place are estimated at about $7.4x10^9m^3$.[2] In a series of earlier papers we have shown: a) that bitumens/heavy oils in all of the major WCSB Lower Cretaceous oil sands/heavy oil deposits, although moderately to strongly biodegraded, share many common features in their saturated hydrocarbon biomarker distributions, suggesting a common source; b) that "carbonate trend" bitumens present in Paleozoic formations, although strongly biodegraded, can be divided into two groups; and c) that at least one of these two groups shows very similar biomarker characteristics to those of the Lower Cretaceous samples, indicating a common or very similar source.[3,4] An obvious next step in increasing our understanding of the Western Canada Basin and its hydrocarbon resources is to compare the geochemistry of the oil sands/heavy oils/bitumens with that of light and medium gravity conventional oils of the Basin, the subject of this paper. Accordingly, we extend our studies here through examination of the distributions of aromatic steroids in oil sands/heavy oils/bitumens previously analyzed, and in a suite of conventional light and medium gravity oils. Because aromatic steroids are moderately to strongly resistant to biodegradation, they offer particular promise in the study of strongly biodegraded material, eg. "carbonate trend" bitumens.

Geological Setting

Oil sands/heavy oils/bitumen deposits of WCSB form three deposit groups: those hosted by Lower Cretaceous sediments including the Athabasca-Wabasca, Peace River and Cold Lake deposits, the largest single group with reserves estimated to be about $198x10^9m^3$; the heavy oils of Alberta and Saskatchewan located in a large number of small reservoirs in the Lloydminster region with reserves in Alberta of about $9x10^9m^3$ in the Lloydminster area alone; and the "carbonate trend" bitumens hosted by Paleozoic carbonate rocks which subcrop beneath the Cretaceous deposits with reserves poorly known but at least about $70x10^9m^3$.[1,5] We have examined more than 80 samples from all of the major deposits noted.[3,4,6]

In-place reserves of conventional light and and medium gravity oil total about $7.4x10^9m^3$, with 39% hosted mainly by Devonian carbonate reefs and platformal sediments in some 1300 pools; 32% in Cretaceous clastic reservoirs in some 1200 pools; 20% located mainly in carbonate sediments of Carboniferous and Permian age and occurring in about 400 pools; and 5% in Jurassic sediments of diverse lithology and 4% in Triassic sediments, predominantly carbonates, with Jurassic and Triassic pools together numbering about 500.[2] To date we have examined about 120 conventional light and medium gravity oils from a wide variety of stratigraphic and geographic locations, to be discussed in detail in a forthcoming paper.[7]

Organic Geochemistry

Steranes

Figure 1 is a ternary diagram of the relative abundance of C_{27}-C_{28}-C_{29} steranes in more than 100 conventional oils from WCSB. As noted on Figure 1, all the conventional oils we have examined, with the exception of the Upper Cretaceous, show similar sterane carbon number distributions to the Paleozoic and Lower Cretaceous oil sands, heavy oils and bitumens.[8]

However, other features of the biomarker distributions in WCSB conventional oils allow eleven families of conventional oils to be distinguished.[8] Of particular concern in this paper are two families of conventional oils, those reservoired in Upper Devonian formations such as the Leduc and Nisku, and those

reservoired in Mississippian and Lower Cretaceous formations. The relationship of these conventional oils to the oil sands/heavy oils/bitumens has been discussed frequently.[9] On Figure 1 these conventional oil families and all of the oil sands/heavy oils/bitumens plot close together. However, the two conventional oil families can be distinguished easily from one another using other biomarker parameters. One of the most significant parameters is the presence of 28,30-bisnorhopanes in the Mississippian/Lower Cretaceous oil family and their absence in the Devonian oils. The 28,30-bisnorhopanes have also been shown to be present in all of the Lower Cretaceous oil sands/heavy oils/bitumens, and in many Paleozoic bitumens.[3,4] The implication of this latter result is that there may be two families of bitumens in the Paleozoic deposits, one of which is genetically related to the Lower Cretaceous bitumens.

Triaromatic Steranes

As an extension of our previous studies we have examined the distribution of triaromatic steranes in conventional oils from WCSB, and in many of the Paleozoic and Mesozoic oil sands/heavy oils/bitumens reported on previously.[3,4] Triaromatic steranes are known to be more resistant to microbial alteration than the common saturated fraction biomarkers, steranes and terpanes.[10] Furthermore, it has been shown that triaromatic sterane carbon number distributions may be used for oil-oil and oil-source rock correlations in a manner similar to that for the saturated steranes.[11]

Figure 2 shows the distribution of triaromatic steranes, as indicated by m/z 231 fragmentograms, in bitumens isolated from Cold Lake (Lower Cretaceous), Athabasca (Lower Cretaceous) and two Grosmont (Devonian) samples for which the gross compositions and saturated fraction biomarker distributions have been previously reported.[3,4] Representative bitumens from these deposits show variable degrees of biodegradation in the order Cold Lake<Athabasca>Grosmont A<<Grosmont B as shown by the presence or absence of regular steranes and 17α(H)-hopanes. The bitumens from Cold Lake, Athabasca and Grosmont A are believed to be genetically related based on many biomarker parameters, among the most significant of which is the presence and relative abundance of 28,30-bisnorhopanes.[3,4] Bitumens from Grosmont B were suggested to possibly belong to a second family because they do not contain bisnorhopanes.[4]

The relative distributions of the triaromatic steranes for the above four bitumen samples are strikingly similar, as shown in Figure 2. This is readily verified from, for example, the ratio of $(20R)C_{27}/(20R)C_{28}$ (peaks D/E) triaromatic steranes, as shown on Figure 2. These data further support our previous conclusions that the Paleozoic and Mesozoic oil sands/heavy oils/bitumens are genetically related. Furthermore, they indicate that bitumens from Grosmont A and Grosmont B families are very similar in agreement with the results obtained from hydrous pyrolysis of asphaltenes.[6] We emphasize that the traces obtained for these four bitumens, as shown in Figure 2, are representative of all of the samples that we have studied.

Figure 3 shows triaromatic sterane distributions for the two Grosmont (Devonian) bitumens shown in Figure 2, and representative triaromatic sterane traces for conventional oils recovered from Mississippian-Lower Cretaceous and Upper Devonian reservoirs. The ratios of $(20R)C_{27}/(20R)C_{28}$ triaromatic steranes (peaks D/E) is given for each sample shown on Figure 3. It is apparent from the relative distributions that the Grosmont bitumens and hence the Lower Cretaceous oil sands/heavy oils (from Figure 2) are extremely similar in triaromatic sterane composition to the conventional oils reservoired in the Mississippian and Lower Cretaceous. Furthermore, it is immediately apparent that the triaromatic sterane composition of the Upper Devonian oils is very different from either the Lower Cretaceous and Devonian oil sands/bitumens and the Mississippian and Lower Cretaceous conventional oils (see, for example, the distributions of peaks A, B and C; and the ratio of peaks D/E).

Figure 4 is a summary ternary diagram for the carbon number distributions of triaromatic steranes from the conventional oils we have studied to date from WCSB.[8] It is apparent from Figure 4 that the Devonian conventional oils (two families of Upper Devonian and one Middle Devonian family) have enriched abundances of C_{28} triaromatic steranes compared to oils from reservoirs of other ages, and thus can be readily distinguished from other families. The Mesozoic and Paleozoic oil sands/heavy oils/bitumens all plot closely with conventional oils from the Mississippian and Lower Cretaceous reservoirs.

Other differences are also apparent between Devonian conventional oils and the oil sands/heavy oils/bitumens such as the presence of C_{30} regular steranes in the latter which are not present in conventional Devonian oils. Indeed, cross plots of biomarker ratios of saturated biomarkers and triaromatic biomarkers appear to be one of the best methods of separating oils into families and for correlation purposes. Figure 5 shows one such cross plot as an example, in which the ratios of C_{28}/C_{29} saturated steranes are compared to the ratios of C_{27}/C_{28} triaromatic steranes for the conventional oils studied to date from the Western Canada Basin. The mean value is plotted for each family together with the spread of data. The oils from Mississippian and Lower Cretaceous reservoirs plot very close together - well away from all Devonian oil families and from those of the Upper Cretaceous. Data from Paleozoic and Mesozoic oils and heavy oils/bitumens plot within the spread of the Mississippian and Lower Cretaceous data for this and many other cross plots.[8]

Conclusions and Implications

- Triaromatic steranes are indeed less susceptible to microbial alteration compared to saturated sterane and terpane biomarkers and are therefore excellent markers for biodegraded oils;
- Triaromatic sterane carbon number distributions are an excellent tool for oil-oil and oil-source correlation purposes;
- Distribution of triaromatic steranes when used together with saturated biomarkers provides an excellent method of oil-oil correlation;
- Using triaromatic sterane distributions we have reinforced our previous conclusions that the Paleozoic and Mesozoic oil sands/heavy oils are genetically linked;
- Triaromatic sterane distributions suggest a close genetic relationship between our two previously distinguished Paleozoic "carbonate trend" bitumen families, supporting the results obtained from hydrous pyrolysis of asphaltenes;[4,6]
- Biomarker distributions (both aromatic and saturated) of Paleozoic and Mesozoic oil sands/heavy oils are strikingly similar to those for conventional oils from Mississippian and Lower Cretaceous reservoirs, but very different from those of the conventional Devonian oils studied to date;
- From this we believe that the source(s) for the Lower Cretaceous and Mississippian conventional oils in the Western Canada Basin is also a primary candidate as the effective source for the Paleozoic

and Lower Cretaceous oil sands/heavy oils, and that the Devonian source system (eg. Duvernay Formation) has had little if any input to the oil sands/heavy oils/bitumens of WCSB.

Acknowledgements

We thank personnel of the Oil Sands Sample Bank, Alberta Research Council, Edmonton, for providing initial samples used in this study; Sneh Achal and Margaret Northcott for excellent technical assistance; and Claudia Thompson for word processing of the manuscript.

References

1. Energy Resources Conservation Board, "Alberta's reserves of crude oil, oil sands, gas, natural gas liquids and sulphur, at December 31, 1986," Report ST-87-18, Energy Resources Conservation Board, Calgary, Alberta, 1987.

2. Podruski, J.A., Barclay, J.E., Hamblin, A.P., Lee, P.J., Osadetz, K.G., Procter, R.M., and Taylor, G.C., "Conventional Oil Resources of Western Canada (Light and Medium), Part I: Resource Endowment," Geological Survey of Canada Paper 87-26, 149 p., 1988.

3. Brooks, P.W., Fowler, M.G., and Macqueen, R.W., "Biological marker and conventional organic geochemistry of oil sands/heavy oils, Western Canada Basin," Organic Geochemistry, vol. 12, pp. 519-538, 1988.

4. Brooks, P.W., Fowler, M.G., and Macqueen, R.W., "Biomarker Geochemistry of Cretaceous Oil Sands, Heavy Oils and Paleozoic Carbonate Trend Bitumens, Western Canada Basin," in Meyer, R.F., and Wiggins, E.J. (eds.), Proceedings, Fourth UNITAR/UNDP International Conference on Heavy Crude and Tar Sands, published by Alberta Oil Sands Technology and Research Authority, Edmonton, Alberta, vol. 2, Geology, Chemistry, pp. 594-606, Discussion, pp. 629-631, 1989a.

5. Kramers, J.W., and Mossop, G.D., "Geology and development of the Athabasca and Cold Lake Oil Sands Deposits", Field Trip No. 8, Geological Association of Canada, Mineralogical Association of Canada Annual Meeting, May 25-27, 48 pp, 1987.

6. Fowler, M.G., and Brooks, P.W., "Organic geochemistry of Western Canada Basin tar sands and heavy oils. 2. Correlation of tar sands using hydrous pyrolysis of asphaltenes", Journal of Energy and Fuels, vol. 1, pp. 459-467, 1987.

7. Brooks, P.W., Fowler, M.G., and Macqueen, R.W., "Identification of conventional oil families using biomarker and conventional organic geochemistry, Western Canada Basin", to be submitted to the Canadian Society of Petroleum Geologists, Calgary, Alberta, 190.

8. Brooks, P.W., Fowler, M.G., and Macqueen, R.W., "Use of biomarker geochemistry to distinguish families of crude oils in Western Canada Sedimentary Basin", Abstract in 14th International Meeting on Organic Geochemistry, Paris, September, 1989b.

9. Deroo, G., Powell, T.G., Tissot, B.P., and McCrossan, R.G., "The Origin and Migration of Petroleum in the Western Canada Sedimentary Basin", Geological Survey of Canada Bulletin 262, 136 p., 1977.

10. Wardroper, A.M.K., Hoffman, C.F., Maxwell, J.R., Barwise, A.J.G., Goodwin, N.S., and Park, P.J.D., "Crude oil biodegradation under simulated and natural conditions - II. Aromatic steroid hydrocarbons", Organic geochemistry, vol. 6, pp. 605-617, 1984.

11. Moldowan, J.M., Seifert, W.K. and Gallegos, E.J., "Relationship between petroleum composition and depositional environment of petroleum source rocks", American Association of Petroleum Geologists Bulletin, 69, pp. 1255-1268, 1985.

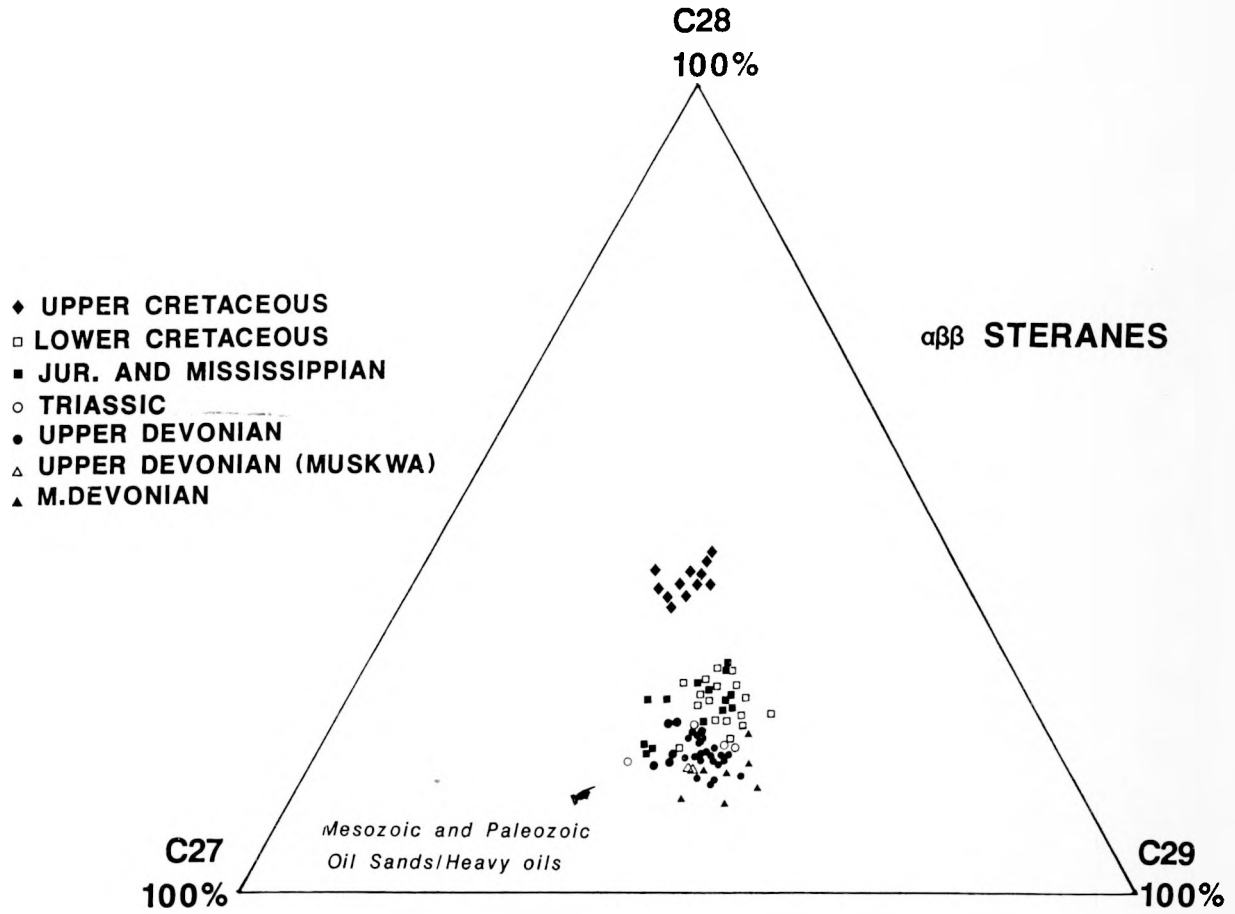

Figure 1. Ternary diagram for the distributions of sterane carbon number (C_{27}:C_{28}:C_{29}) for conventional oils from the WCSB. Also indicated is plot position of Lower Cretaceous and Paleozoic oil sands/heavy oil bitumens.

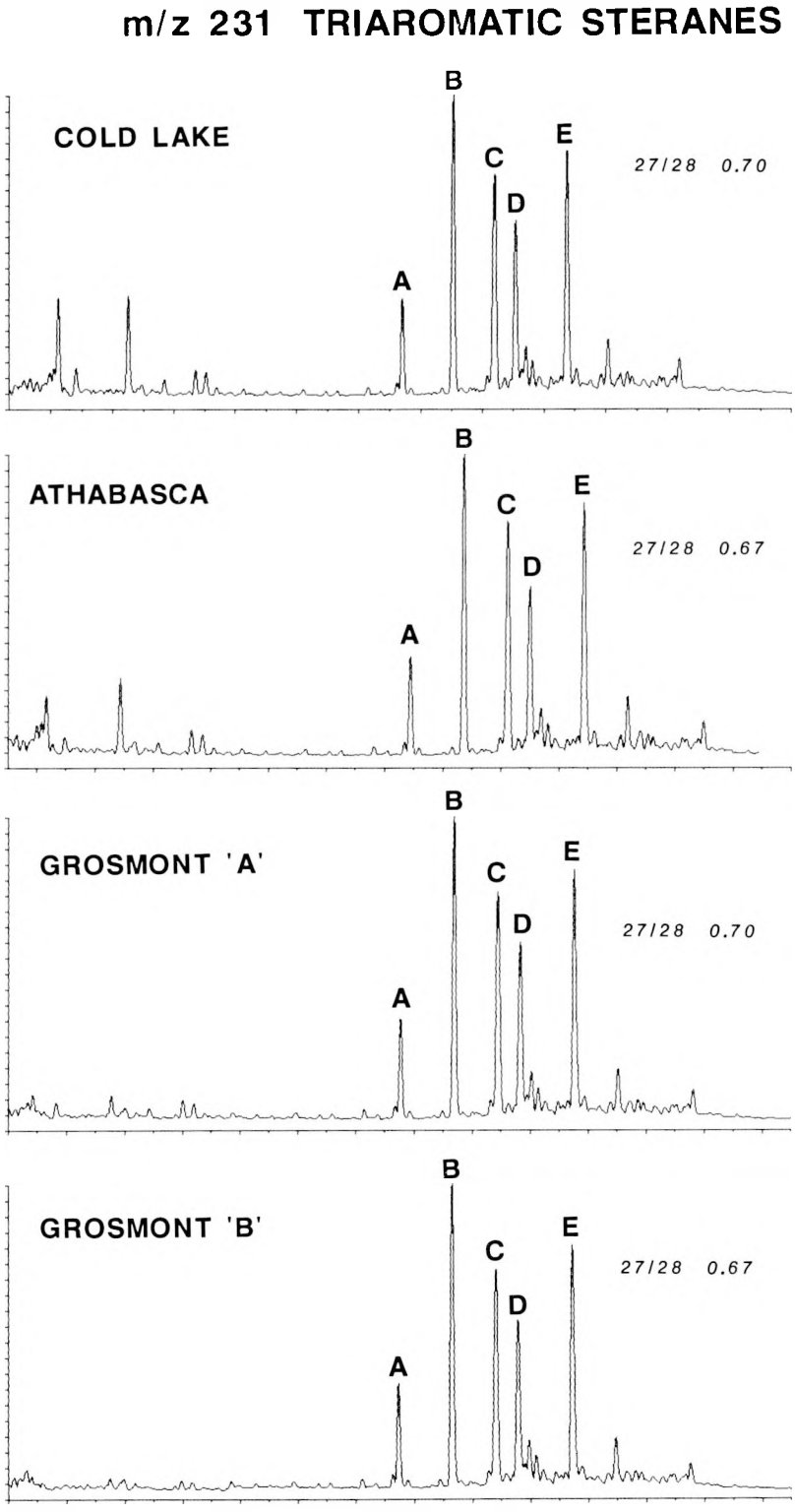

Figure 2. The m/z 231 fragmentograms showing the distributions of triaromatic steranes isolated from Cold Lake, Athabasca and two Grosmont bitumen samples. A=(20S)C_{26}; B=(20R)C_{26}+ (20S)C_{27}; C=(20S)C_{28}; D=(20R)C_{27}; and E=(20R)C_{28}.

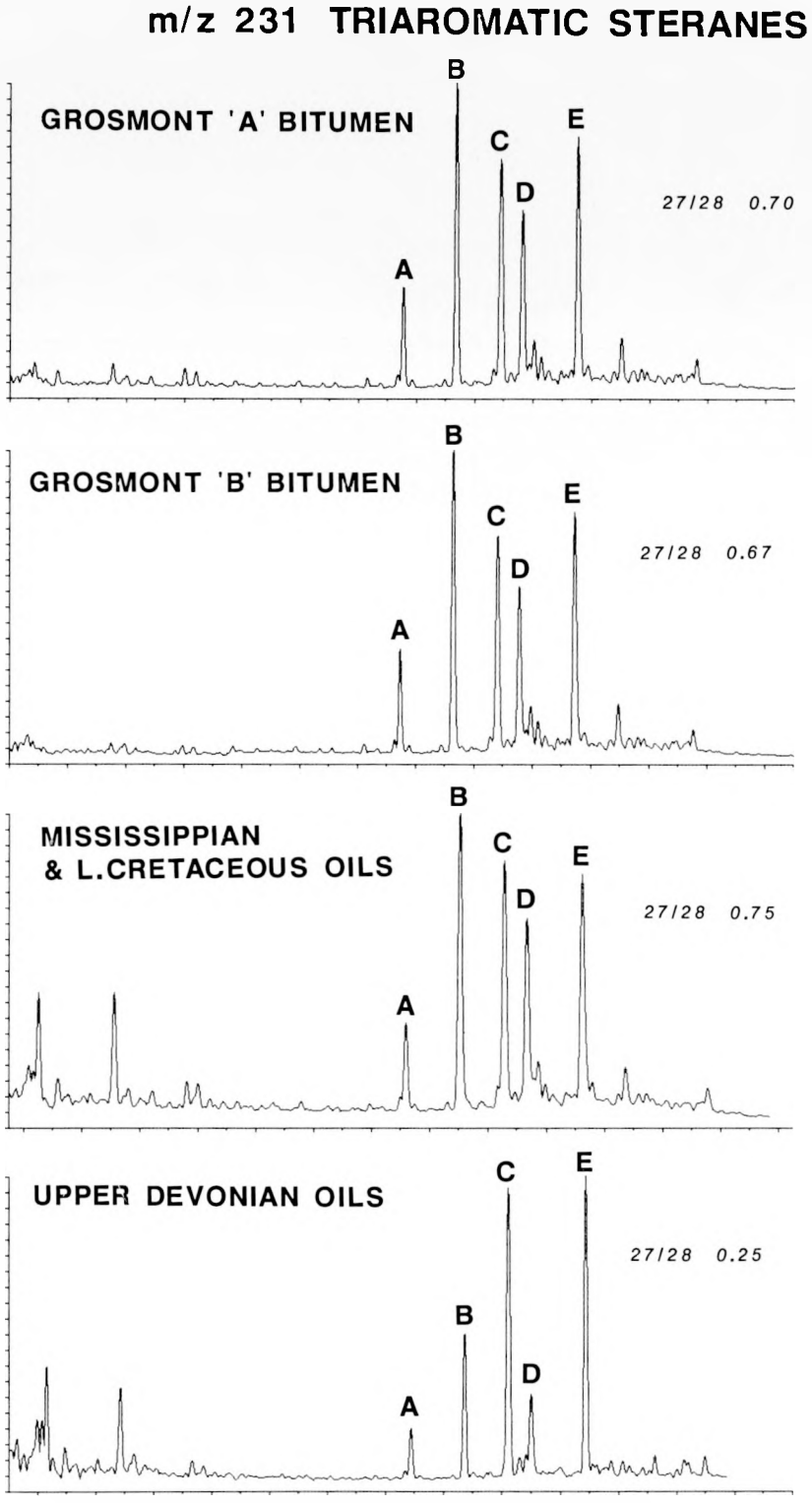

Figure 3. The m/z 231 fragmentograms showing the distributions of triaromatic steranes isolated from two Grosmont bitumens and conventional oils from Mississippian-Lower Cretaceous and Upper Devonian reservoirs. Refer to Figure 2 for peak identifications.

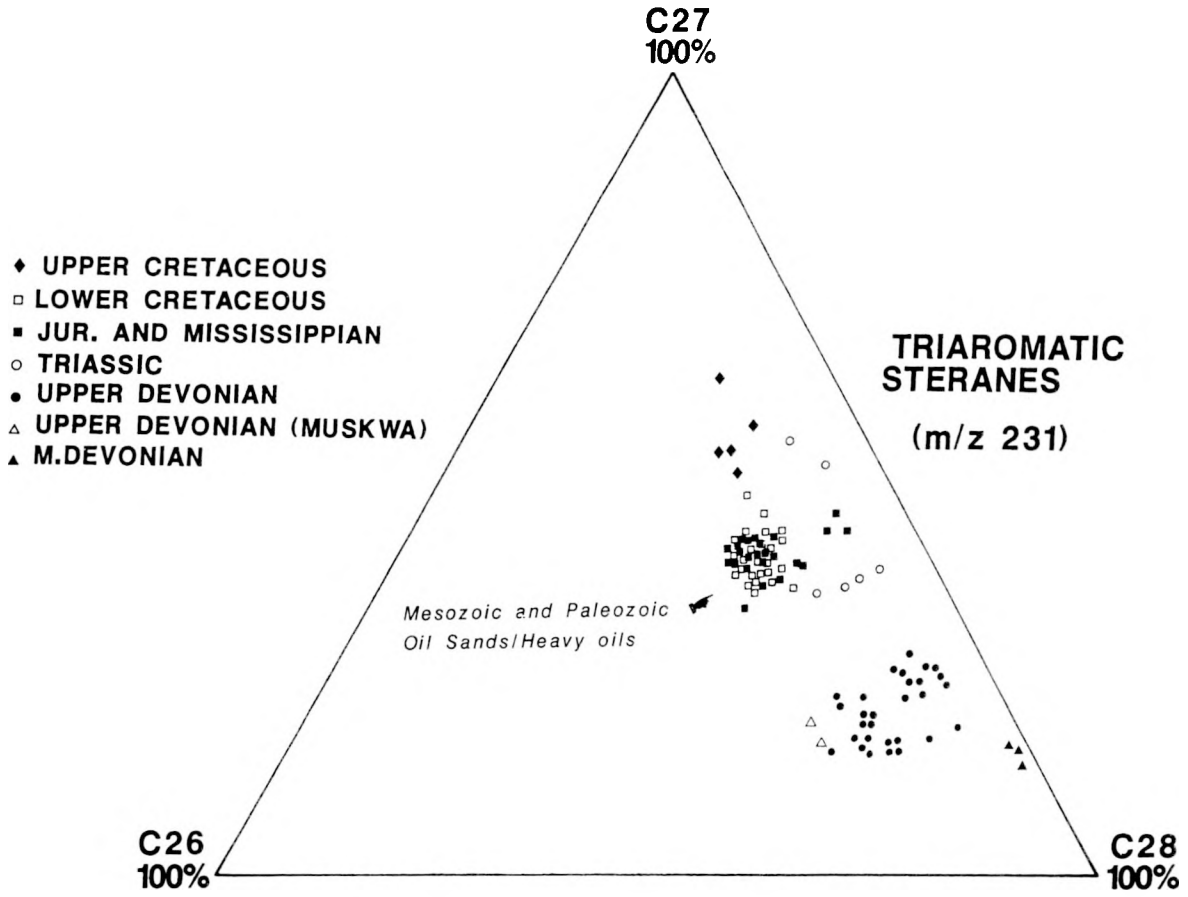

Figure 4. Summary ternary diagram for the carbon number distributions of triaromatic steranes from conventional oils from the WCSB. Also indicated is the plot location of the Lower Cretaceous/Paleozoic oil sands/heavy oils.

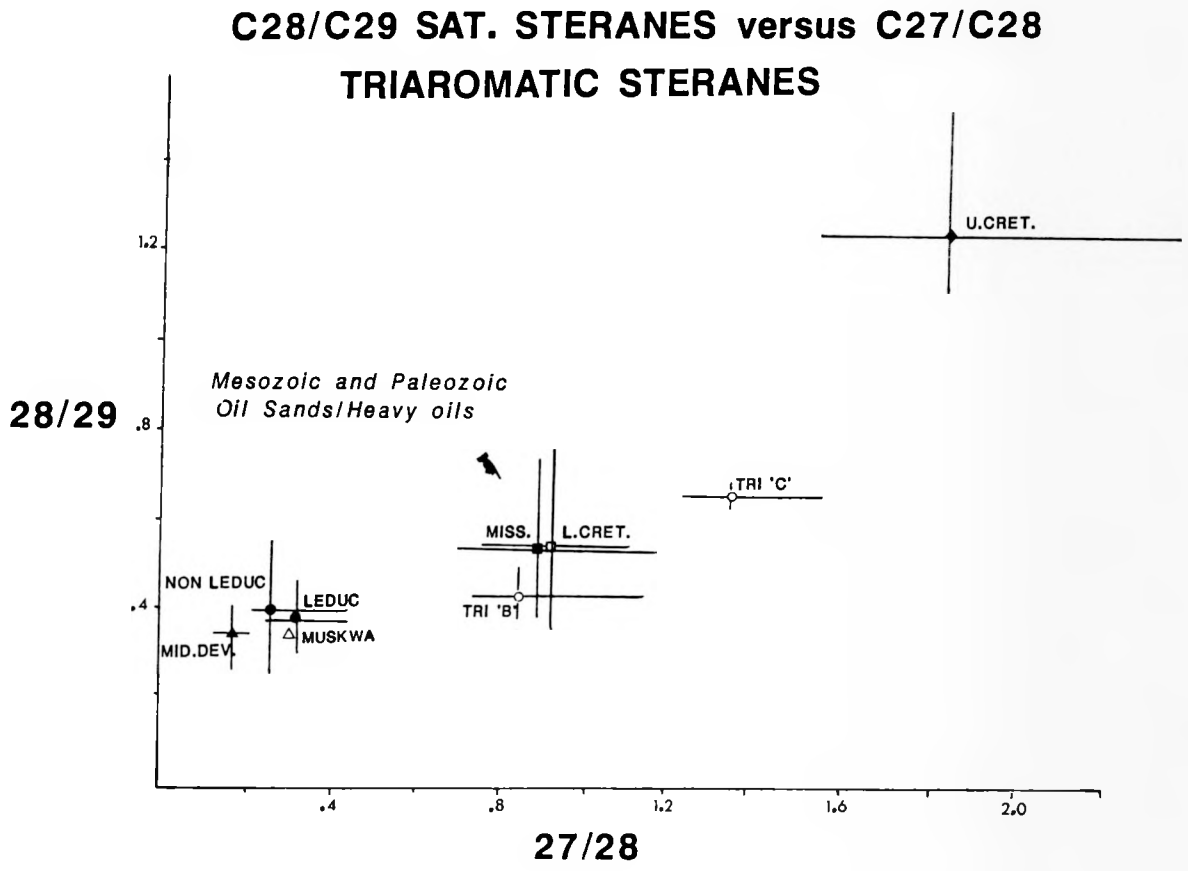

Figure 5. Cross plot of the ratio C_{28}/C_{29} saturated steranes versus C_{27}/C_{28} triaromatic steranes for conventional oils from the WCSB. Shown on each family is the mean value together with the range for each parameter. Also indicated is the plot position of the Mesozoic and Paleozoic oil sands/heavy oils.

Relationship of Chemical Type Composition with Rheological Properties of Asphalts

by

M.A. Poirier
Esso Petroleum Canada
Sarnia, Ontario CANADA N7T 7M1
H. Sawatzky
Energy Research Laboratories, CANMET
Ottawa, Ontario CANADA K1A 0G1

Abstract. This work deals with the study of asphalt and asphalt components derived from Cold Lake bitumen. A major aspect of this study was the separation of Cold Lake asphalt into saturates, naphthene aromatics and propane precipitated asphalt. The latter is high in polar aromatics and asphaltenes. These separated fractions and petroleum wax were blended in significant proportions with another asphalt and Cold Lake asphalt and the effects on the asphalts' rheological properties were determined. The low temperature properties were of special interest. In addition, the chemical type characterization was performed on processed Cold Lake residue, air blown asphalt and appropriate asphalts obtained from various conventional crudes. The Penetration Index (temperature susceptibility), Pen-Vis number, low temperature stiffness, ductility and glass transition temperature were investigated. The Penetration Index was shown to correlate with the asphaltene/wax + polar aromatic ratio. The saturates fraction in the only compound-type that increases the Pen-Vis number when blended into asphalt and this fraction also significantly reduces stiffness at -20°C. Both the low temperature stiffness and ductility are influenced by the Colloidal Instability Index (saturates + asphaltenes/naphthene aromatics + polar aromatics). The glass transition temperature was found to correlate with the polar aromatics content.

Introduction

A major market exists for asphalt derived from Cold Lake bitumen. Therefore asphalt from this bitumen and fractions from it, are the major samples for our study of the effect of composition on asphalt quality.

The influence of the composition of asphalts has been recognized for a long time as an important factor in controlling the performance of such materials. Among the numerous characteristics selected to assess asphalt performance, the rheological properties of pure asphalt or mixes are the most important. The rheological properties of asphalts have always been associated with their composition. However, in order to utilize effectively the compositional data, more definitive correlations between composition and properties are needed. This information will allow the selection of asphalt cement to give desired performance, and would provide pertinent data for crude selection for asphalt manufacture. Both would lead to better pavement durability.

Asphalt is a very complex mixture of compounds which can be separated into four generic fractions: saturates, naphthene -aromatics, polar aromatics and asphaltenes. Depending upon its composition and stress level or shear rate, asphalt could have a Newtonian or non-Newtonian behaviour. Asphalts with Newtonian flow (sol type) are those which have directionally lower asphaltene content, high ductility and are temperature susceptible (low Penetration Index). On the other hand, asphalts with non-Newtonian flow (gel type) are characterized by a more colloidal structure resulting from high asphaltene content, low ductility and low temperature susceptibility (high Penetration Index).

Although gel type asphalts may be preferred to sol types because of their higher Penetration Index, which is associated with better low temperature performance and low rutting susceptibility, current specifications exclude them by requiring a minimum ductility and/or

limiting wax content. These two properties are associated with asphalt heterogeneity.

It is the objective of this study to relate composition of asphalts with their physical and rheological properties. This was done by blending selected fractions (saturates, naphthene-aromatics and propane precipitated asphalt, which was used as an asphaltene concentrate) with various vacuum residues to produce 150/200 penetration grade asphalts, and observing the change in properties with respect to the original asphalt.

The fractions used in this study were obtained from Cold Lake asphalt because it does not contain wax, which would affect the composition and properties of the saturates and naphthene-aromatics fractions. Cold Lake asphalt was first propane deasphalted to produce a deasphalted oil (DAO) and propane precipitated asphalt. The DAO was separated according to the Corbett separation method (ASTM D4124) to produce the saturates and naphthene-aromatics used in this study.

Asphalt blends were prepared from Cold Lake, visbroken Cold Lake and Peace River residues and correlations of the composition with Penetration Index, ductility, glass transition temperature and creep compliance were determined.

Peace River residues were included in this study because they are examples of asphalts having properties that do not meet specifications.

Experimental

Deasphalting Procedure

A sample of Cold Lake 150/200 penetration asphalt was deasphalted to provide approximately 1.5 L of deasphalted oil (DAO) to be further separated into saturates, naphthene-aromatics and polar aromatics.

The deasphalting work was carried out in a continuous pilot plant deasphalting unit using propane as the solvent. A DAO density target of 0.96 kg/L was selected to provide acceptable DAO quality. The feed, DAO and asphalt properties are presented in Table 1. Since the propane precipitated asphalt, (PPA) was used as blending component, the composition has been determined by the ASTM D4123 procedure. The compositional data are presented in Table 1.

The results show that deasphalting does not selectively separate the polar aromatics and asphaltenes from the saturates and naphthene-aromatics as it was originally thought. However, it allows production of a large amount of asphaltene free fraction (DAO) and PPA with low saturation content. The composition of the PPA has been taken into consideration in the interpretation of the results.

Compound-Type Separation

All samples were separated into asphaltenes, saturates, naphthene-aromatics and polar-aromatic compounds according to the ASTM D4124 method. The deasphalted DAO Cold Lake was also separated by a scaled up procedure of the chromatography portion of this method as shown in Fig. 1.

Asphalts and Blended Asphalt Samples

Four different 150/200 penetration asphalts made from Peace River, Cold Lake and visbroken Cold Lake crudes have been used as reference samples. The other samples (total of four) were prepared by blending 10 to 15 wt % of selected compound-type fractions with vacuum residues from the same crude as the reference samples to produce 150/200 penetration grade asphalt. The samples used in this study are described in Table 2. In order to correlate the composition with the rheological properties it was important to use samples of the same penetration grade.

Determination of Rheological Characteristics

These rheological characteristics were determined by measuring the shear compliance J(t) versus loading time at -20°C using a sliding plate rheometer and the apparent viscosity versus shear rate at 60°C using a cone and plate viscometer. The procedure for the cone and plate measurements is described in ASTM D3205. The modifications of the sliding plate rheometer method have been described by Gaw.[1]

The time dependent creep compliance J is determined in the latter from the shear stress (γ) and time dependent strain (γ) according to the equation:

$$J(t) = \frac{\gamma(t)}{T}$$

The stiffness as defined by Van der Poel[2] is related to the compliance by:

$$S(t) = \frac{3}{J(t)}$$

Determination of Glass Transition Temperatures and Wax Contents

The glass transition temperature (T_g) has been determined by Differential Scanning Calorimetry (DSC). This technique is also used to determine the wax content of asphalt[3]. The glass transition temperature of asphalt has been the object of several studies[3-5]. Schmidt et al.[5] were among the first to report on glass transitions.

Determination of Ductility

Ductility is determined by measuring the extent of elongation of asphalt samples under defined conditions of temperature and stretching rates according to ASTM D113.

Results and Discussion

Blending Effects on Asphalt Compositions

Naphthene-Aromatics

Blending naphthene-aromatics with Peace River vacuum residues affects the composition significantly (Table 3). A fairly good agreement is found between the calculated and actual saturates and asphaltenes contents. However, some of the naphthene-aromatics interact with polar aromatics and asphaltenes leading to an increase in the polar aromatics fraction. The sum of the naphthene- aromatics and polar aromatics is similar in both cases. Although the naphthene- aromatic content is lower than expected, it is increased relative to the saturates content, which provides the desirable compositional change.

In the visbroken Cold Lake case, good agreement of the calculated and found overall composition is observed. Visbreaking is known[6] to cleave alkyl side chains and heteroatom bond which could explain the lack of association of the naphthene-aromatics with the polar aromatics.

Saturates

Blending the saturates fraction with Cold Lake vacuum residue also affects the composition significantly (Table 3). The major changes are the increase of the asphaltenes naphthene-aromatics content at the expense of the polar aromatics content.

The saturates act as a paraffinic solvent, causing the polar aromatics to associate and leading to the formation of asphaltenes in the asphalt with some release of naphthene-aromatics. In contrast to the effect of wax[7], liquid saturates do not degrade the viscosity of Cold Lake asphalt (Table 4). They improve the properties of Cold Lake asphalt.

Propane Precipitated Ashphalt

Blending the PPA with Peace River vacuum residue directionally increases the asphaltene content and decreases the polar aromatics content. This increase in asphaltene content should be reflected on the rheological properties of the asphalt. The presence of naphthene aromatics, polar aromatics and asphaltenes in the PPA appears to be responsible for not changing the naphthene-aromatics/polar aromatics ratio of Peace River as did adding naphthene-aromatics. Good agreement is found between the calculated and actual composition data.

Rheological Properties

Numerous papers [8-13] have been published on the relationship between composition and physical properties. However, to our knowledge none of the papers deals with changing composition of asphalt by blending a given compound-type fraction and comparing the change with the original material. We have selected the Corbett separation method (ASTM D4124) because the composition and physical properties of each compound-type fraction are distinctly different from each other, which is a requirement to obtain good correlation between composition and rheological properties of asphalt. The properties and compositions of the eight asphalt samples examined in this study are presented in Table 4. These data are discussed in the following sections.

Temperature Susceptibility

The temperature susceptibility of asphalt cement is one of the most important properties associated with the low temperature performance of asphalt pavement. Asphalt cement with low temperature susceptibility is the most desirable because it has better resistance to low temperature pavement cracking.

The temperature susceptibility of an asphalt is the variation of its consistency (penetration or viscosity) with temperature. It is measured by the Penetration Index (PI). Asphalt with low temperature susceptibility has a high PI.

The PI as defined by Pfeiffer and Van Doormall[14] is calculated from the equation:

$$PI = \frac{20 - 500\,A}{50\,A + 1}$$

where $$A = \frac{\log_{10} Pen_{T_2} - \log_{10} Pen_{T_1}}{T_2 - T_1}$$

The value of A is determined from a plot of log Penetration (100 g, 5 s) versus temperature.

The temperature susceptibility can also be expressed as ratios of penetrations at different temperatures. However, when there are plotted against PI linear relationships are obtained. Thus only the PI will be discussed.

We have shown in another study[7] that increasing the wax content of an asphalt decreases its PI. However, blending liquid saturates into asphalt increases significantly the PI (Tables 3 and 4). We believe this is largely due to the increase of asphaltene content resulting from the addition of the saturates which increase the association of the polar aromatics.

Blending naphthene-aromatics with Peace River residue and visbroken Cold Lake residue (Tables 3 and 4) does not affect significantly the PI. This is contrary to results reported by Corbett[15] which appeared to indicate that this component contributed most to temperature susceptibility. Also in another study[16] an exceptionally high temperature susceptability was reported for a hydroprocessed asphalt which had a high naphthene-aromatic content as shown in Table 5. However, blending the PPA with Peace River residue increases the asphaltene content at the expense of the polar aromatics (Table 3) and increased the PI compared to the reference sample. Air blowing also increases significantly the PI from -1.9 (Peace River) to -0.13 (air blown Peace River) which is attributed to the increase of asphaltene content from 9.6% to 14.2%. The results indicate that asphaltenes have low temperature susceptibility whereas polar aromatics are very temperature susceptible[8]. This is consistent with results reported by

Corbett[8] on temperature susceptibility of the generic fractions.

From these results it has been possible to correlate the composition of asphalts with the PI. A correlation of the PI with the asphaltenes/(wax + polar aromatics) ratio is shown in Fig. 2. If wax is not included as a compound type in this relationship, a poorer correlation is obtained. The graph shows that increasing the asphaltenes content increases the PI. This is consistent with the air blowing data, e.g Peace River where PI increases with asphaltene content. In this ratio the asphaltenes represent the least temperature susceptible compound-type and the wax and polar aromatics represent the most temperature susceptible components.

The visbroken samples do not fit in this correlation, probably because of the differences in the chemical structures resulting from this type of processing.

Rheological Behaviour of Asphalts

Asphalt is a viscoelastic material which behaves like an elastic solid at low temperature or short loading time and a viscous liquid at high temperatures or long loading times. A good performing asphalt must have the proper consistency over the whole range of temperatures to which the asphalt pavement is exposed. This is why an asphalt with low temperature susceptibility (high PI) is the most desirable.

The creep compliance is one of the most important rheological properties of asphalt cement. It has been identified as the property that could give an indication of pavement rutting under traffic loading conditions[17] but at low temperature reduces brittleness and tendency for pavement cracking.

The stiffness of the asphalt at a loading time of 500 at -20°C is (duplicate results) compared (Table 6) to the Penetration Index and the Colloidal Instability Index (I_c). The latter is defined[18] as the ratio of the asphaltenes plus saturates to the sum of the resins (polar aromatics) and aromatics. It is represented as follows:

$$I_c = \frac{\text{saturates + asphaltenes}}{\text{naphthene-aromatics + polar aromatics}}$$

Unfortunately the stiffness results involve considerable scatter in particular for the Peace River samples. However, according to Fig. 3 there appears to be correlation of stiffness results with PI. For the air blown Peace River samples the results are different from the rest. In general these results are consistent with those reported by Robertson[17] on the correlation between low temperature stiffness and PI. The correlation between stiffness and Colloidal Index was not very good.

Blending naphthene-aromatics into Peace River and visbroken Cold Lake asphalt reduces the stiffness slightly at -20°C. However, blending with saturates, or air blowing, reduces the low temperature stiffness significantly compared to the reference samples.

The apparent viscosity versus the shear rate for the asphalt samples examined in this work is presented in Table 7. All the asphalts have near Newtonian behaviour at 60°C (the viscosity does not change with the shear rate)[19].

The cone and plate viscosity results were similar for the Peace River samples. The addition of saturates to the Cold Lake and Naphthene-Aromatics to the Visbroken Cold Lake significantly reduced the viscosity. The differences between the cone and plate and the capillary tube (ASTM D2171) method is due at least partly to differences in refining conditions in the two tests.

Glass Transition Temperature

In this study, the effect of composition on the T_g has been examined. The relations between the composition of asphalt and their T_g values were reported by Noel et al.[3], Connor and Spiro[20] and Huynh et al.[4]. These authors showed that T_g decreases with increasing paraffinic content. Furthermore, Huynh et al. showed that the longer the paraffinic chains in asphalt the lower the T_g. All these studies indicate that the glass transition temperature is a very important property of asphalt cement. It corresponds to the temperature at which asphalt become brittle (glassy state).

Blending naphthene-aromatics with Peace Riverand Visbroken Cold Lake asphalt does not affect the T_g significantly (Table 4). However, air blowing increases the asphaltenes content at the expense of the polar aromatics which results in a lower T_g. A similar result is observed for blending saturates with Cold Lake asphalt. The saturates content is increased and the polar aromatics are significantly decreased as compared to the reference Cold Lake sample, and the T_g is decreased from -27°C to -35°C. The results show that the polar aromatics content has a large effect on the T_g. With increasing polar aromatics content, the T_g increases. A correlation (R^2 = 0.914) was found between the T_g and the polar aromatics as shown in Fig. 4, excluding the Visbroken samples.

Although in many cases it appears that higher PI values correspond to a lower T_g, a poor correlation (R^2 = 0.16) was observed between these properties. However, the difference in penetration between the asphalts contributes largely for this poor correlation. This is clearly illustrated by comparing Cold Lake asphalt with Peace River asphalt (Table 4). Peace River has a PI of -1.92 and a T_g of -36°C. Conversely, Cold Lake which has a better temperature susceptibility (PI - 0.98) has a higher T_g (-27°C).

Ductility

Newtonian behaviour asphalts (sol type) characterized by lower asphaltene contents have higher ductility. The ductility correlates with the colloidal Instability Index (I_c) (Fig. 5). The results in Tables 4 and 6 show that the ductility decreases with increasing I_c. However, it appears that factors other than I_c such as the penetration would also effect the ductility.

Corbett[8] has reported that naphthene-aromatics do not affect the ductility as much as polar aromatics. This is consistent with our results although blending the naphthene-aromatics with Peace River residue increase the ductility from 83 to 120 cm. Air blowing or blending saturates into asphalt decrease the ductility significantly. This is also relected by an increase of the I_c value.

Conclusions

Blending a given compound-type into asphalt affects its overall composition. The temperature susceptibility of asphalt cement measured by the PI correlates with the asphaltenes/(wax + polar aromatics) ratio. Air blowing or blending saturates into asphalt provide a way to reduce th low temperature stiffness. This reduction in stiffness is reflected by an increase of the PI.

The glass transition temperature is one of th most important properties of asphalt cement relating to the low temperature behaviour of asphalts. It is correlated with the polar aromatics for similar penetration asphalts.

The ductility directionally decreases with increasing I_c.

References

1. Gaw, W.J., Proceeding AAPT, 47, 457, 1978
2. Van der Poel, C., "A General System Describing the Viscoelastic Properties of Bitumen and its Relation to Routine Test Data", J Appl Chem, 4, 221, 1954
3. Noel, F. and Corbett, L.W., "A Study of the Crystalline Phases in Asphalts", J Inst Petrol, 56, (551), 261, 1970.
4. Huynh, H.K., Khong, T.D., Malhotra, S.L. and Blanchard, L.P., "Effect of Molecular Weight and Composition on the Glass Transition Temperatures of Asphalts", Anal Chem, 50, (7), 976, 1978.
5. Schmidt, R.J. and Santucci, L.E., Proceedings AAPT, 35, 91, 1966.
6. Favre, A., Boulet, R. and Behar, F., "Etude par simulation en laboratoire de l'operation de viscoreduction", Rev Inst Fr Petrol, 40, 609, 1985.
7. Poirier, M.A., "Effect of Wax Content on the Rheological Properties of Asphalt Cements", Final Report DSS Contract No. 23440-7-9059/01-SQ, CANMET, Ottawa, Canada, Sept, 1988.
8. Corbett, L.W., "Proceedings AAPT, 39, 481, 1970.
9. Rostler, F.S. and Sternberg, H.W., Ind Eng Chem, 41, 598, 1949.
10. Schweyer, H.E. and Bransford, T.L., Proceedings AAPT, 30, 422, 1961.
11. Corbett, L.W., Anal Chem, 36, 1967, 1964.
12. Corbett, L.W. and Swarbrick, R.E., Preprints Am Chem Soc (Petrol Div), March, 1966.
13. Corbett, L.W., Anal Chem, 41, 576, 1969.
14. Pfeiffer, J.P. and Van Doormall, P.M., "The Rheological Properties of Asphaltic Bitumen", J Inst Petro Tech, 22, 414, 1936.
15. Corbett, L.W., Hydrocarbon Processing, 58, 173, 1979.
16. Poirier, M.A., "Quality and Application of Asphalt Derived from Upgraded Heavy Crude", Final Report DSS Contract No. 23440-5-9075, CANMET, Ottawa, Canada, 1986.
17. Robertson, W.D., "Temperature Susceptibility Characterization of Asphalts", CTAA Proceedings - 27th Annual Conference, 27, 127, 1982.
18. Gaestel, C., Smadja, R. and Lamminan, K.A., "Contribution a la connaissance des proprietes des bitumes routiers", Rev Generale des Routes et Aerodromes, 466, 85, 1971.
19. Poirier, M.A., "Effect of Composition on the Rheological Properties of Asphalt Cements", Final Report DSS Contract No. 233440-7-9058, CANMET, Ottawa, Canada, 1988.
20. Connor, H.J. and Spiro, J.G., J Inst Petrol, 54, (533), 137, 1968.
21. Marvillet, J., Verschave, A. and Duval, J., "Bitumen Polymers for Surface Dressing", paper presented at AEMA Symposium, Las Vegas, March, 1982.

TABLE 1

PROPERTIES OF COLD LAKE 150/200 AND DEASPHALTED FRACTIONS

Cold Lake 150/200 Asphalt	
Penetration at 20°C (100/5)	152
Density at 15°C kg/m^3	1032.6
Viscosity at 135°C, cSt	276
Deasphalted Oil (DAO)	
Yield, LV%	39.0
Density at 15°C, kg/m^3	961.4
Refractive Index at 67°C	1.5164
Viscosity at 100°C, cSt	29
Propane Precipitated Asphalt (PPA)	
Yield, LV%	61.0
Density at 15°C, kg/m^3	1078.3
Composition (ASTM D4124)	
Saturates, wt %	3.5
Naphthene-Aromatics, wt %	27.4
Polar Aromatics, wt %	40.2
Asphaltenes, wt %	28.9

TABLE 2

ASPHALT SAMPLES

Samples (1)	Penetration at 25°C (100/5)
1. Air Blown Peace River	161
2. Peace River	189
3. Cold Lake	157
4. Visbroken Cold Lake	150
5. 90 wt % Visbroken Cold Lake (90 Pen) 10 wt % Naphthene-Aromatics	177
6. 88 wt % Peace River (61 Pen) 12 wt % Naphthene-Aromatics	184
7. 90 wt % Peace River (313 Pen) 10 wt % Propane Precipitated Asphalt (PPA)	165
8. 87 wt % Cold Lake (47 Pen) 13 wt % Saturates	185

(1) Except for sample 1 all asphalts are vacuum residues.

TABLE 3

EFFECT OF BLENDING SATURATES, NAPHTHENE-AROMATICS AND PROPANE PRECIPITATED ASPHALT ON THE COMPOUND-TYPE DISTRIBUTION (WT %)

Sample	Saturates	Naphthene-Aromatics	Aromatics	Ashphaltenes
Peace River	22.0	39.4	29.0	9.6
Peace River + 12% NA Found	17.6	42.7	30.2	9.5
Calculated	19.4	46.7	25.5	8.4
Peace River + 10% PPA Found	21.9	39.6	27.3	11.1
Calculated	20.2	38.2	30.1	11.5
Cold Lake	11.5	34.0	39.6	14.9
Cold Lake + 13% SATS Found	21.0	33.9	27.8	17.3
Calculated	23.0	29.6	34.4	13.0
Visbroken Cold Lake	12.5	39.6	24.2	23.7
Visbroken Cold Lake + 10% NA Found	12.1	44.0	23.7	20.2
Calculated	11.3	45.6	21.8	21.3

TABLE 4

PROPERTIES OF 150/200 PENETRATION ASPHALTS

Sample	Peace River	Peace River + NA	Peace River + PPA	Air Blown Peace River	Cold Lake	Cold Lake + Sat	Visbroken Cold Lake	Visbroken Cold Lake + NA
Penetration at 25°C (100/5)	189	184	165	161	157	185	150	177
.4°C (100/5)	13.5	13.5	14.8	22	15.5	22	18.5	22
Penetration Index	-1.92	-1.94	-1.50	-0.13	-0.98	-0.54	-0.61	-0.62
Viscosity at 60°C, Poise	252	319	286	272	845	686	716	524
Ductility at 25°C (5 cm/min), cm	83	120	91	46	>150	124	111	89
Wax, wt % (DSC)	3.3	3.3	3.3	3.3	0	0	0	0
Glass Transition Temperature, °C	-36	-34	-37	-42	-27	-35	-33	-33
Composition (ASTM D4124)								
Saturates, wt %	22.0	17.6	21.9	26.2	11.5	21.0	12.5	12.1
Naphthene-Aromatics, wt %	39.4	42.7	39.6	35.5	34.0	33.9	39.6	44.0
Polar Aromatics, wt %	29.0	30.2	27.3	24.1	39.6	27.8	24.2	23.7
Asphaltenes, wt %	9.6	9.5	11.2	14.2	14.9	17.3	23.7	20.2
I_c	0.46	0.37	0.49	0.68	0.36	0.62	0.57	0.48

TABLE 5

CHEMICAL COMPOSITION OF HYDROPROCESSED COLD LAKE ASPHALT

Residfined 85/100	
Saturates %	10.6
Naphthene-Aromatics %	47.0
Polar Aromatics %	25.3
Asphaltenes %	17.1
PI	+1.22

TABLE 6

CREEP RESISTANCE AND DUCTILITY OF 150/200 PENETRATION ASPHALT VERSUS

COLLOIDAL INSTABILITY INDEX AND PENETRATION INDEX

	Stiffness at 500s -20C, MPa	Ductility 25C, cm	I_c	PI
Peace River	37 and 25	83	0.46	-1.92
Peace River + 12% NA	32 and 23	120	0.37	-1.94
Peace River +10% PPA	32 and 23	91	0.49	-1.50
Peace River Air Blown	19 and 23	46	0.68	-0.13
Cold Lake	16 and 14	150	0.36	-0.98
Cold Lake +13% SATS	7 and 6	124	0.62	-0.54
Visbroken Cold Lake	12 and 12	111	0.57	-0.61
Visbroken Cold Lake +10% NA	9 and 11	89	0.48	-0.62

TABLE 7

VISCOSITY OF ASPHALT AT 60°C

Sample	Cone and Plate at 0.1 s^{-1} Shear Rate, Poise	ASTM D2171, Poise
Peace River	434	252
Peace River + NA	440	319
Peace River + PPA	447	286
Air Blown Peace River	431	272
Cold Lake	1245	845
Cold Lake + Sat	1079	686
Visbroken Cold Lake	1264	716
Visbroken Cold Lake + NA	785	524

Tar Sands and Their Water Content

by

Costi A. Audeh
Central Research Laboratory
Mobil Research and Development Corporation
Princeton, New Jersey 08543-1025

Abstract. Tar sands are a well established hydrocarbon resource base. However, their utility is hindred by the need for separating the bitumen from the sand. Techniques applicable for this separation include hot water flotation, solvent assisted flotation and solvent extraction. Although hot water flotation is commercially practiced, its applicability is restricted to tar sands in which the sand particles are separated from the bitumen by an envelope of water. Such sands are usually described as water wet. We wanted to develop a technique by which we could determine if a tar sand is water wet and is thus amenable to the hot water flotation process.

We have found that only a fraction of the water content of a tar sand can be removed by treating a sample of tar sand with anhydrous methanol and by drying at room temperature under reduced pressure. Further, an additional amount of water is removed when the dried sample is subjected to the usual Dean and Stark entrainment distillation. This procedure identifies two types of water which are best described as extraneous and intrinsic and their sum is equal to the total water content of the tar sand as determined by entrainment distillation. We believe that the extraneous water is located at the exterior surface of the bitumen and the intrinsic is not. Possibly it forms a layer between the sand particles and their bitumen envelope. We believe that the presence of the intrinsic water indicates that the tar sand is water wet and would be amenable to the hot water process. For a series of tar sand samples from Utah, we have found that the amount of extraneous water varies and that of the intrinsic is constant. Further, by heating the clay fines recovered from the bitumen-free sand to about 400°C, water of hydration was also identified.

Introduction

Tar sands are a well-established resource base, however, crude oil remains the main source of liquid hydrocarbon fuels. It is estimated that worldwide there are 4×10^{12} barrels of hydrocarbons in-place in the tar sand resource [1] and about 0.8×10^{12} barrels of proven crude oil reserves [2]. Of the 57×10^{6} barrels/day of crude oil produced worldwide about 0.24×10^{6} is syncrude obtained by coking the bitumen recovered by water flotation from tar sands [2]. The reason for this disparity is the need for separating the bitumen from the sand and upgrading the recovered bitumen to specification products.

Three primary techniques have been used to accomplish separating the bitumen from the sand: (a) flotation, (b) solvent and solvent assisted extraction and (c) direct coking [3]. Of these, hot water flotation followed by some solvent treatment became commercial in Canada in 1973 [3]. In this process the operating mechanism of separation is: (a) heating the bitumen so as to make it less viscous and more mobile by mixing with hot water; (b) separating the sand from the tar as a result of the decrease in viscosity and increase in mobility; (c) formation of globules from the separated tar which eventually form a froth and float to the top of the water [4].

The overall operating mechanism of the solvent-assisted process is the same as that of the hot water process. However, viscosity reduction which brings about mobility increase is enhanced by the solvent. Also, for a tar sand with bitumen that is denser than water, the solvent also reduces the density of the separated bitumen and allows it to float. It has been suggested [4] that the success of such recovery processes is contingent upon the presence of a thin film of water around the sand particles. Although the presence of this film of water is important, its existence has only been inferred [5] and its quantity has not been determined [6].

We wanted to develop a technique by which we could determine if a tar sand contains more than one type of water and possibly differentiate between them.

Experimental

Materials

Several samples of Utah tar sands were used in these experiments. The bulk samples varied in size from 1-2 lb of tar sand in plastic bags, to several hundred pounds in 55 gallon drums. After the bulk samples were handled the remaining unused portions were stored under argon (small samples) and carbon dioxide (drum samples). Bitumen-free sand was recovered and saved after the bitumen was extracted with dichloromethane or toluene.

Preparation of Aliquots for Water Determination

For water determinations in which more than one procedure was used, the amount of tar sand required for all the procedures was calculated and the bulk material appropriately sampled. In the case of the 1-2 lb. samples, the whole material was riffled and appropriately sampled.

Determination of Total Water Content of a Tar Sand, ASTM D95

About 300 ml of toluene was added to about a 100 gm sample of the tar sand placed in a distillation apparatus equipped with a Dean and Stark receiver [7]. The mixture was then refluxed so as to entrain the water in the tar sand sample by the boiling toluene. Heating was continued until all the water was removed from the tar sand and collected in the Dean and Stark receiver. The volume of the collected water was then measured.

Determination of the Extraneous Water Content

Two procedures were used:

- A 100 gm sample was placed in a 500 ml flask and the sample subjected to a vacuum distillation at a pressure of about 0.1 mm at room temperature. The distilled material which was collected in a receiver cooled in liquid nitrogen was examined and identified.

- A 50 gm sample of the tar sand was spread uniformly in a Buchner funnel. 4 x 50 ml of anhydrous methanol were used to "wash" the sample. All the washings were saved. Water in the methanol was identified by gas chromatography. Residual methanol in the washed tar sand was removed at room temperature under reduced pressure.

Determination of the Intrinsic Water Content

Two procedures were used:

- Tar sand samples from which water was removed at room temperature by distillation at reduced pressure or by washing with anhydrous methanol had their water content determined by entrainment distillation, according to the procedure of ASTM D95.

- Tar sand samples from which water was removed by distillation at reduced pressure or by washing with anhydrous methanol were heated to the melting point of the bitumen, ~80°C, and subjected to distillation at reduced pressure. The material condensed in the liquid nitrogen trap was collected and identified.

Determination of the Presence of Water of Hydration

In a typical experiment the bitumen-

free sand was size-separated by sieving. The fraction which passed a 325 mesh sieve, i.e., particles smaller than 44 microns, was heated in flowing dry argon at a rate of 20°C/min in a DuPont 951 thermogravimetric analyzer. Weight loss in the 350-400°C temperature range and identification of water by FTIR confirmed the presence of water of hydration.

Results and Discussion

Sand, bitumen and water are the three components of a tar sand. Each of these components is determined by a standard analytical procedure. The sand and the bitumen are determined by extraction with a polar organic solvent and the water by a Dean and Stark distillation. Physical inspection of a tar sand sample clearly shows the location of the bitumen in relation to the sand. Usually a tar sand sample is uniformly bitumen-colored and does not contain bitumen-free sand. Thus the bitumen surrounds the sand particle and is the organic matrix in which the sand is embedded. In contrast to the clear location of the bitumen in a tar sand sample, the location of the water is unclear.

Total Water

We have found that the total water content of a sample of tar sand may vary. For example, in one set of experiments several water determinations were conducted on 100 gm aliquots taken randomly from two separate 500 lb samples, Samples A and B, of a Utah tar sand sample. Table 1 shows the results of these determinations and demonstrates the variability of the water content of the same sample.

TABLE 1

Total Water Content of a Utah Tar Sand by Entrainment Distillation with Toluene

Sample No.		Water, % Wt.
A	1	7.4
	2	3.2
	3	4.5
	4	5.2
	5	3.2
B	1	4.5
	2	5.0
	3	4.6
C	1	3.2
	2	3.5

Physical inspection of the aliquots did not reveal gross differences in their appearance which could explain the variation in their water content. The water content was in the 3-7% range. A third Utah tar sand sample, Sample C, was a 10 lb sample which was split into two sizes, Sample C-1, material which passed a 1/4" screen and C-2, material held by the same screen. In this case the water content was reasonably consistent and was about 3.4%.

The operating principle of the method used in determining the water content of a tar sand involves total solubility of the bitumen in toluene and thus separation of the bitumen from the sand and concomitant separation of water from wherever it occurs. Since this method also requires the use of refluxing toluene [7], the water is vaporized and entrained. Clearly such a procedure cannot differentiate between water on the surface of the bitumen and water that is not. Any water contained in the bitumen or trapped between the sand particles and the bitumen is entrained by the toluene and is included in this determination.

Extraneous Water

To distinguish between water contained in the bitumen and water on its surface, the procedures to be used should not disturb the sand/bitumen matrix and should only allow the recovery of water only on the surface of the bitumen during the water determination. This we achieved by two procedures which gave consistent results. By using corresponding aliquots of the samples studied in the water determination experiments reported in Table 1, we determined, in the first procedure, the water content by vacuum distillation at room temperature. Since the bitumen is not a liquid at room temperature, only the water on the surface of the bitumen could escape but water entrapped between the sand and the bitumen could not. Similarly, in the second procedure we used cold anhydrous methanol to wash the sand and thus dissolve only the water on the surface of the bitumen. Earlier, we had determined that the solubility of the bitumen in cold anhydrous methanol was less than 0.05% by weight. Table 2 shows the results of these experiments and shows that this procedure removes a fraction of the total water content of tar sand. Clearly, a change in the operating principle gives different values. This we attribute to the difference between the location of the water removed and that of the remaining fraction of the total water which was not removed. To confirm that this procedure is quantitative, known amounts of water were mixed with the tar sand samples which were subjected to room temperature vacuum distillation and dehydration by cold methanol and the vacuum distillation or washing with methanol was repeated. Over 95% of the added water was recovered. Water as determined by this procedure is best described as extraneous.

TABLE 2

Water Content of a Utah Tar Sand
Water on the Surface of Bitumen,
Extraneous Water

Sample No.		Water, % Wt. Distillation*	Methanol
A	1	7.1	7.0
	2	2.9	-
	3	4.1	4.2
B	1	4.1	-
	2	4.6	4.4
	3	4.1	-

**Vacuum distillation at room temperature*

Intrinsic Water

By implication the water which was not removed by the procedures described under extraneous water is entrapped within the bitumen/sand matrix. Here, also, two procedures to determine the water content of the samples were used. Both procedures gave similar results. Aliquots of the samples prepared as a result of the experiments of Table 2 were used for these procedures. In the first procedure a sample was heated to about 80°C, the "melting point" of the bitumen, and the sample subjected to vacuum distillation. The material which collected in the liquid nitrogen trap was a small amount of water, about 0.4%, and trace quantities of hydrocarbons. For the second procedure the standard method, ASTM D95, used for determining the total water content of a tar sand was applied to the remaining aliquots and the water content of each of the aliquots determined. Table 3 shows the results of these experiments and shows that a small amount of water remained in the tar sand after the extraneous water was selectively removed.

TABLE 3

Water Content of a Utah Tar Sand
Intrinsic Water in the Bitumen

Sample No.		Water, % Wt. Distillation	Dean and Stark
A	1	0.3	-
	2	-	0.2
	3	0.5	0.4
B	1	0.4	-
	2	0.4	-
	3	0.5	0.3

This amount of water represents the remaining fraction of the total water which was determined by the standard analytical procedure and which was not accounted for by the selective removal procedure. Also, the total amount of water which could be calculated from the data reported in Tables 2 and 3 corresponds well to the total amount of water reported for the corresponding samples in Table 1. We believe that this type of water is best described as intrinsic. For Utah tar sands studied the amount of intrinsic water determined is about 0.4%. Assuming sand grains 100 microns in diameter this water would be sufficient to form a film about 0.2 microns in thickness around the grains.

Water of Hydration

Bitumen-free, dry sand recovered from the tar sand by solvent extraction was separated by sieving into several mesh size fractions. The fines, defined as the particles that pass a 325 mesh sieve [5], represented, in our samples, about 5% by weight of the dry sand. About 40% of the fines is a mixture of clay minerals. A representative sample of these fines was studied by thermogravimetric analysis. A small loss in weight which was detected in the 350-400°C temperature range confirmed the presence of water of hydration of the clay component of the dry bitumen-free sand. We believe that this type of water differs from intrinsic water in that it could not be removed by entrainment distillation with toluene. However, the amount of water lost from the fines is small and represents less than 0.01% of the weight of the tar sand.

Conclusion

The water content of a tar sand can be differentiated by a procedure that removes extraneous water selectively and leaves the intrinsic water intact. Fines in the bitumen-free sand contain a significant amount of clay which contains a third type of water, water of hydration.

Literature Cited

1. Canada-Venezuela Oil Sands Symposium, Edmonton, Alberta, March, 1977.

2. Worldwide Report, Oil and Gas Journal, 85, No. 52, 33, (1987) and 86, No. 52, 43 (1988), Coal and Synfuels Technology, 10, No. 3, 1 (1989).

3. Shumacher, M. M., Editor, "Heavy Oils and Tar Sand Recovery and Upgrading," Noyes Data Corporation, Park Ridge, NJ, 1982, p. 248.

4. Sanford, E. C., Can. J. Chem. Eng., 61, 554 (1983).

5. Takamura, K., Can. J. Chem. Eng., 60, 538 (1982) and references therein.

6. Hall, A. C., Collins, S-H., and Melrose, J. C., Soc. Pet. Eng. J. 249 (April, 1983).

7. 1985 Annual Book of ASTM Standards, Section 5, Vol. 5.01, ASTM, Philadelphia, PA, D95-83, 60 (1985).

Definition and World Resources of Natural Bitumen

by

Richard R. Meyer
U.S. Department of the Interior
Geological Survey
Reston, Virginia 22092

ABSTRACT

The United Nations Information Centre for Heavy Crude and Tar Sands defines natural bitumen as a petroleum having a viscosity greater than 10,000 cp and defines crude oil as less viscous than 10,000 cp. Heavy crude oil has a density between 10^{o} and 20^{o} gravity API and extra-heavy oil a density below 10^{o} gravity API. These definitions are supported by R.J. Byramjee, Total-CFP, who divides heavy oil into two classes, 10^{o}-14^{o} and 15^{o}-20^{o}. BP Exploration Company, however, has proposed that all hydrocarbons more viscous than 100 cp simply be termed heavy oil. For resource studies, a definition based on density is advantageous because, although viscosity data are rarely published, density data are readily available. Natural bitumen includes the material commonly termed tar sands, oil sands, or natural asphalt. It is here considered only as a source of synthetic fuels and not for limited use as road metal or mastic, its principal application in the past. Excluded are the scientifically interesting but quantitatively insignificant solid hydrocarbons: the pyrobitumens, asphaltites, and mineral waxes.

The demonstrated resource of natural bitumen in place amounts to about 2500 billion barrels, with an additional 865 billion barrels inferred. Present production for synthetic fuels amounts to 345,000 barrels per day, although an indeterminant additional amount is mined for use as road material. Of the demonstrated resource in place, about 68% is found in North America, mostly in Alberta, Canada; 27% in the Soviet Union; 5% in Europe; and small amounts elsewhere. All the inferred resource is in North America, mostly in Canada. In the U.S., the resource in place in the ten largest deposits is estimated to total about 42 billion barrels and, in Canada, about 2,500 billion barrels.

Using an assumed worldwide recovery factor of 15% of bitumen in place, both surface and in situ, for all technologies from all deposits, natural bitumen represents a petroleum recoverable resource of about 500 billion barrels.

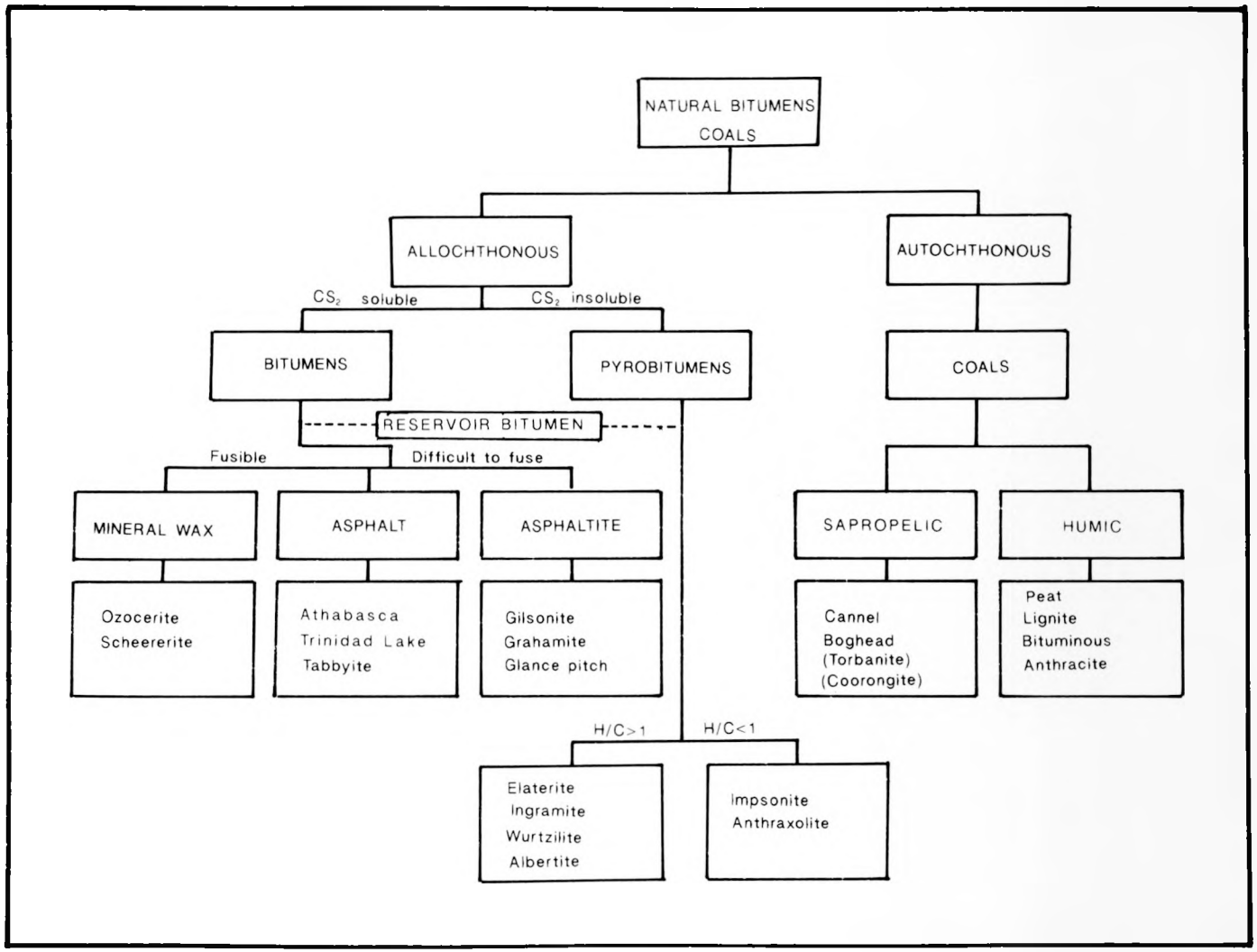

Figure 1. A classification of natural bitumen and coal (modified from Hunt, 1979 and Rogers and others, 1974; H/C hydrogen to carbon ratio).

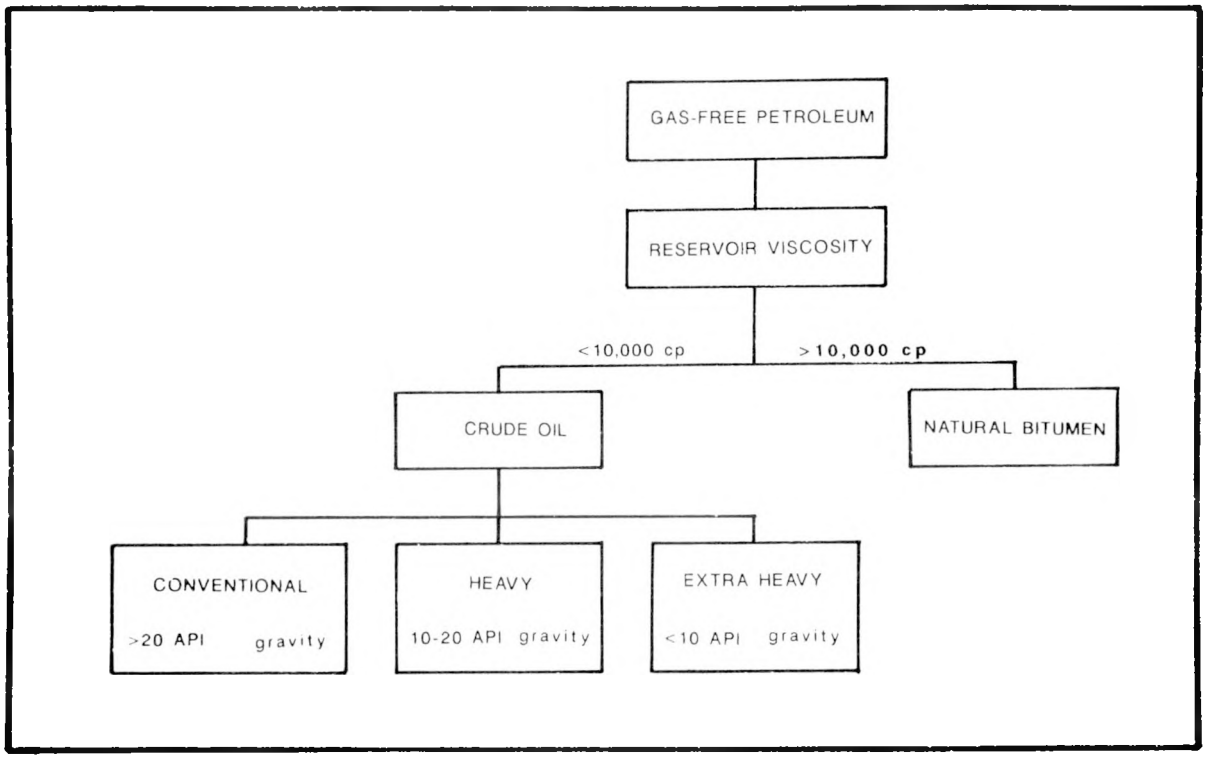

Figure 2. Atomic ratios of coals and natural bitumens (from Hunt, 1979; H/C-hydrogen to carbon ratio; (N+S)/O-nitrogen plus sulfur to oxygen ratio).

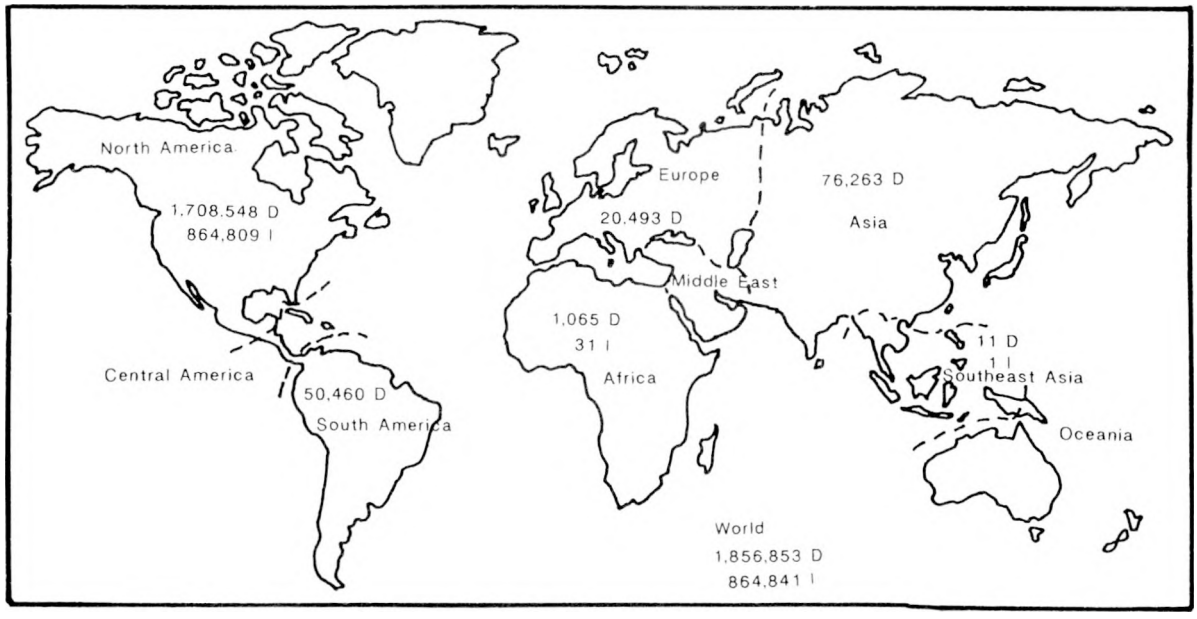

Figure 3. World natural bitumen resources (million barrels; D-demonstrated resources; I-inferred resources).

The Orinoco Delta, A Future Exploratory Province for Heavy and Extra Heavy Oils

by

Lucas G. Zamora, Luis Gonzalez S., and Luz M. Linares
Lagoven, S.A.
Caracas 1010A, Venezuela

Abstract

Along the Orinoco Oil Belt there are four known large Miocene fluviodeltaic depocenters, each one of which is located in front of a present day river basin outlet. These river basins are believed to have been the feeders of the said depocenters. A fifth Middle Miocene fluviodeltaic depocenter is postulated to exist in the Southern Orinoco Delta area, at the Eastern end of the Belt, next to the well known Cerro Negro area.

This depocenter, very similar to the Cerro Negro depocenter, would have been fed by a river basin occupied today by the Yuruari-Cuyuní system. This system has been draining to the Esequibo since the beginning of the Late Miocene, according to this hypothesis. The proto-Yuruari river basin, as it is here named, would have yielded a volume of sediments of the same order of magnitude, and of the same composition as the sediments in Cerro Negro.

Given the geological and petroleum history of the Southern flank of the Eastern Venezuela basin, and provided that the southern Orinoco Delta area shared this condition, any accumulations of hydrocarbons would follow the model of the Orinoco Oil Belt.

On the basis of the above hypothesis, an expectancy of oil in place for the Middle Miocene in the southern Delta has been calculated by probabilistic methods as being from about four billion to about thirty six billion cubic meters.

Introduction

The Orinoco Oil Belt (Figure 1) has been defined, for practical purposes as a series of

> "extensional, non-discrete crude-oil producing areas along the southern third of the Maturín (Eastern Venezuela) basin, north of the Orinoco River and the Precambrian Guayana Shield" (Martínez, 1987)[1].

After an extensive evaluation drilling effort, completed by 1983, the productive area was defined as extending from the Machete area at its western end, to the Tucupita oil field in the Cerro Negro Area. The area beyond this point, into the Orinoco Delta, was left to future evaluation. The attractiveness of this latter area has been considered low. The swampy deltaic terrain as well as the difficult access, added to the large amount of oil reserves already identified in the Belt, gives the area a secondary priority for exploration. The extreme thinning of the Oficina Formation, by wedging against the Tucupita high, a prominence of the unconformity at the top of the Cretaceous section in Los Indios well, has been used as an argument against

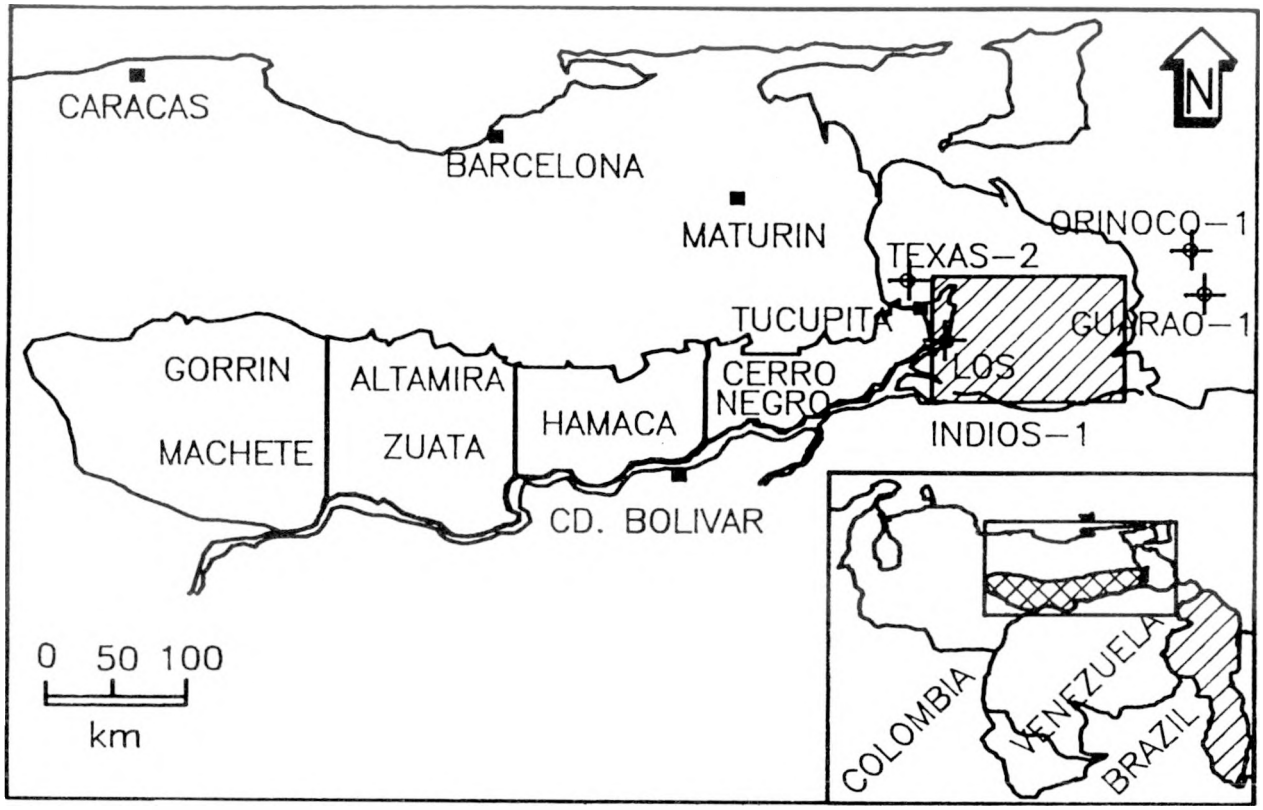

FIGURE 1. LOCATION MAP, SOUTHERN ORINOCO DELTA

the prospectivity of the area east of the said oil field. The Oficina Formation is the reservoir rock for all the oil accumulations in the southern flank of the Eastern Venezuela basin.

Other considerations can be made regarding the atractiveness of the area for hydrocarbon exploration. This considerations are based on the regional geologic and physiographic framework, and on the high probability that the area shares all the geological characteristics, and the hydrocarbon generation and accumulation history, of the southern flank of the Eastern Venezuela basin. On the contrary, if the Southern Orinoco area belonged to the Atlantic province the prospectivity would be low, given the unsuccessful exploratory drilling offshore Guyana and in the Delta Platform (wells Orinoco-1 and Guarao-1).

A preliminary evaluation has been carried on in order to have a sound basis for long term exploration planning. The ideas and the hypothesis here shown follow the thinking of a school of geologists that believe in an eastern extension of the Orinoco Oil Belt beyond the Tucupita high.

The Middle Miocene Depocenters of the Orinoco Oil Belt

The Oligocene through early Middle Miocene transgression covered a preexisting surface, in the Belt region, which consisted of three main physiographic provinces: The first, basinwards, of almost continuous sedimentation since Cretaceous time through the Miocene, corresponds to an area north of the hinge line, with a present day basement dip of 3° to 4° to the north; the next, south of the hinge line, corresponds to a platform area where the Cretaceous sediments are absent and where the basement dips 1° to the north; and the third, the edge of the Tertiary and the younger section, to the south, covers a basement surface with monadnocks and erosional valleys filled with alluvial sediments.

The monadnocks and river valley province was carved out by the rivers that fed the sedimentary prism of the southern flank of the Eastern Venezuela Basin. These rivers drained into the corresponding principal deltaic systems, which constitute the main producing areas of the Orinoco Belt.

Three main regional transgressive episodes have been identified (Latreille et al., 1983)[2] in the Tertiary of the Belt. The first occurred at the beginning of the Miocene, and only reached the northern half of the Machete area.

A second, more extensive, covered the earlier Tertiary sediments and the pre-Cretaceous to Cretaceous rocks cropping out at the northern flank of the Guayana Shield, during the first

half of the Middle Miocene. This cycle, and the lower third of the following transgression are represented by the Oficina Formation, bearer of the reservoir rocks of the Orinoco Oil Belt. The third cycle deposited the Freites Formation, the youngest Miocene unit in the area. The main sand depocenters of the largest fluviodeltaic regional episode, within the Oficina Formation, are shown in the map (Figure 2). They correspond to the main producing areas of the Belt: Machete to the west, followed by Zuata, Hamaca and finally Cerro Negro at the easternmost end.

Each one of the deltaic depocenters is located in front of the outlet of a present day river basin, as depicted in Figure 2. The deltaic lobes of Machete are in front of the Cuchivero River, the lobes of Zuata face the outlet of the Caura River basin, Hamaca corresponds to the Aro River and the Cerro Negro depocenter is in front of the Caroní River basin outlet.

Due to the stability of the Guayana shield these river basins are believed to have maintained its present day general north south attitude at least since the Oligocene, when the first Tertiary transgressive cycle reached the province. This transgression probably was a response to the first orogenic pulse that caused the lifting of the Serranía del Interior, and of the northern flank of the Eastern Venezuela Basin. There is no doubt that since the Oligocene time there have been changes in shape and area of drainage, but the existence of Miocene deltaic lobes to the north proves the permanence of the river basin outlets since then up to present time.

The Middle Miocene Sand Depocenter of the Southern Orinoco Delta Area

The largest present day basin, draining northwards on the northern flank of the Guayana Shield is the Essequibo River basin, whose northern half is constituted by the Cuyuní River

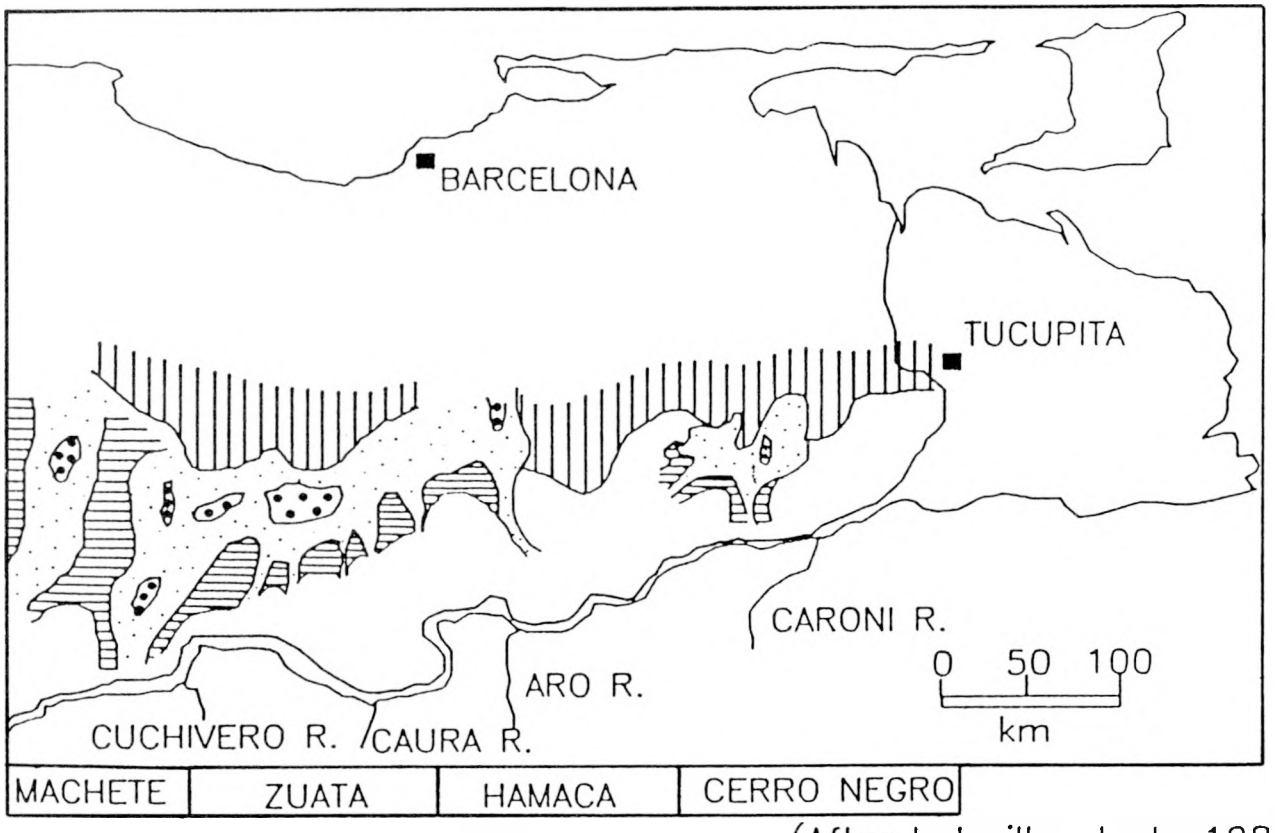

FIGURE 2. MIDDLE MIOCENE DELTA DISTRIBUTION IN THE ORINOCO BELT.

subbasin. There is a strong north-south component in the drainage of the latter, parallel to the prevailing direction of the Cuchivero through Caroní river basins. This north-south component could be the relict of a preexisting river basin draining to the north, and whose area would have been about the size of the Cuyuní River subbasin.

This ancestral river basin, the proto-Yuruari would have drained northwards, into the Orinoco Delta area, via an outlet probably located as shown in Figure 3. The probable proto-Yuruari system of river courses is shown by means of the hachured pattern. The Yuruari and upper Cuyuní rivers, together with the Aponguao would constitute a south to north linear drainage system. Parallel to the latter, and also running to the norht, a second ancestral river, made by de confluence of the Venamo and upper Mazaruni would join the proto-Yuruari near the present day Orinoco Delta.

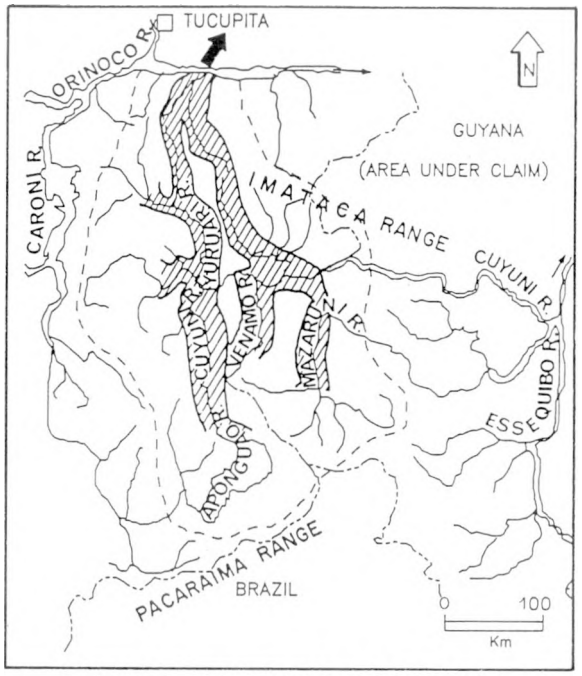

FIGURE 3. PROTO - YURUARI RIVER BASIN

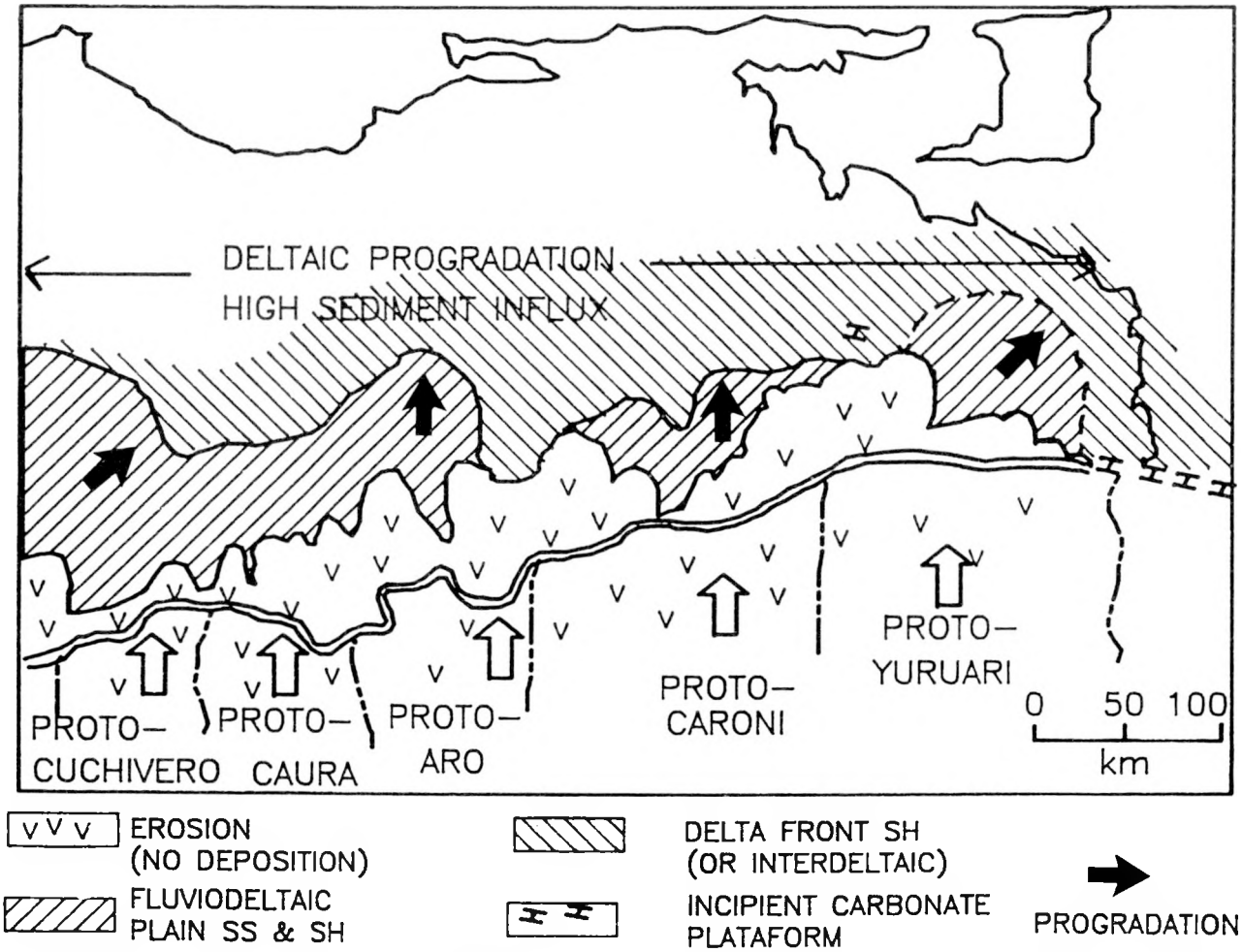

FIGURE 4. EARLY MIDDLE MIOCENE PALEOGEOGRAPHY AND SEDIMENTATION.

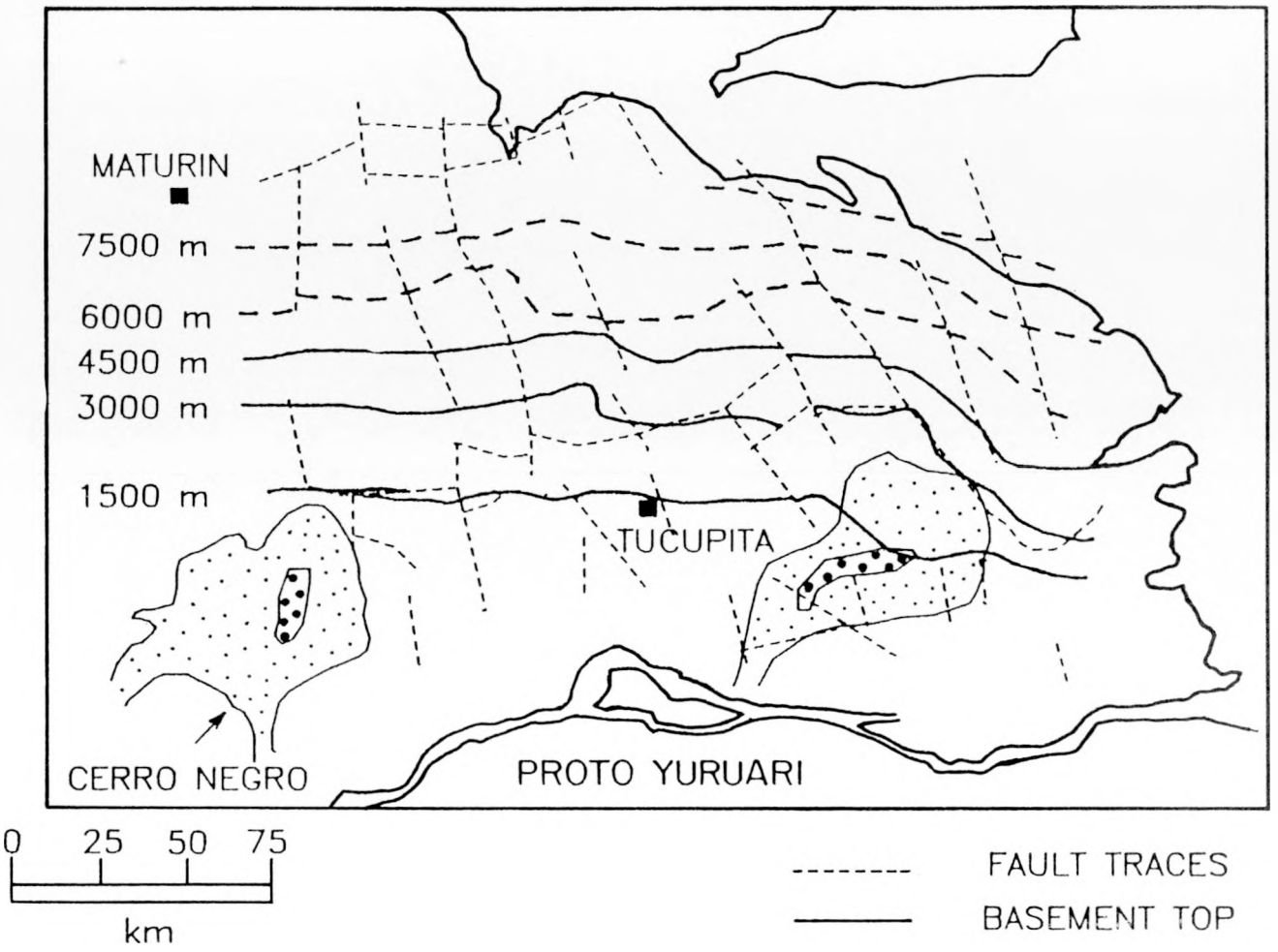

FIGURE 5. POSTULATED MIDDLE MIOCENE DEPOCENTER.

The proto-Yuruari river basin would then be confined, as shown in Figure 3, between the western divide of the Cuyuní and the Yuruari river basins, the Pacaraima Range to the south and an eastern divide that would have run from the Potaro region to the Imataca Range, leaving out to the east the lower Cuyuní and lower Mazaruni river courses.

This ancestral basin, with approximately eighty thousand square kilometers would be second only to the present day Caroní basin. It is easy to imagine an ancestral delta, fed by river system, located to the east of Tucupita, and having a similar size to the Cerro Negro delta (Figure 4). A sand depocenter would then exist north of the proto-Yuruari outlet and to the east of the Tucupita high (Figure 5).

The sedimentary prism built out off the Essequibo River mouth was made up mostly of carbonates from the Paleocene and until the Middle Miocene (Bellizzia, 1983)[3]. This suggests that very clear water, with limited suspended load, reached the area, allowing the carbonate platform growth. Its vertical buildup was due to continuous subsidence, perhaps the effect of an eastward tilting of the Guayana Shield edge. By the end of the Middle Miocene a high clastic sediment discharge reached offshore Guayana and the carbonated growth ended in that area. Subsequently a rapid progradation began until the Quaternary.

It is here interpreted that the sudden influx of large amounts of clastics was the result of the capture of a large river basin, like the proto-Yururari, by the Essequibo system.

This, then, would terminate the postulated prograding deltaic lobes east of Tucupita by the beginning of Late Miocene.

The offshore Delta Platform wells Orinoco-1 and Guarao-1 show an almost completely clastic sequence, from the continental Cretaceous up to the Pleistocene fill and the present day delta front sediments brought in by the Orinoco River. Only a few carbonate beds were developed in the platform during the early Middle Miocene,

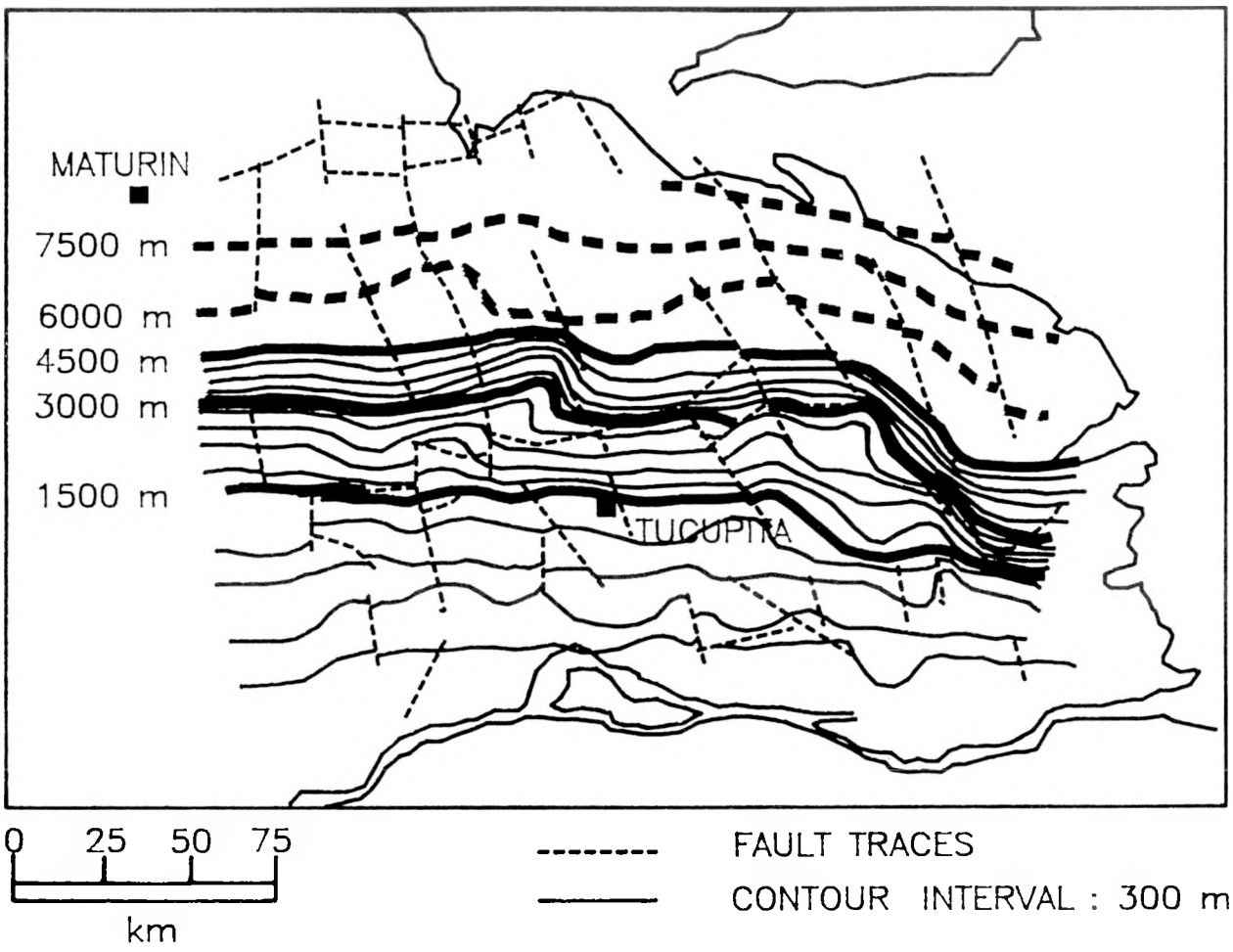

FIGURE 6. STRUCTURE OF THE MAGNECTIC BASEMENT, ORINOCO DELTA

probably due to the absence of an effective fine clastic load in the water by that time. These wells would then be located beyond the edges of the deltaic lobes, herein postulated to exist in the southern Orinoco Delta, by the beginning of the Middle Miocene.

Similarities Between Cerro Negro and the Southern Orinoco Delta Area

The Southern Orinoco Delta and the Cerro Negro areas would share the following geological characteristics, according to the above expressed hypothesis and to the known geological framework of the northern flank of the Guayana Shield:

Known facts:

a) Both areas are located at the northern edge of the Guayana Shield and show a similar basement profile (Figures 5 and 6).

b) Both are transected by basement-involved faults at an angle to the strike of the flank (Figures 5 and 6).

c) Both areas are crossed by the up-to-basin fault system, that parallels the strike of the basement and delineates reservoirs at the northern edge of the Belt, such as in the Pilón, Jobo, Temblador and Uracoa fields.

Hypothetical similarities:

a) Both areas would show a similar stratigraphic framework, with a continental to transitional Cretaceous onlapping the Precambrian basement, and being truncated by a pre-Tertiary unconformity.

b) Both areas would have Middle Miocene transgresive fluviodeltaic lobes of equivalent size, resulting from prograding deltas fed by

large river systems, also of equivalent size, which ran south to north through the northern edge of the Guayana Shield (Figures 4 and 5).

c) Both areas would have, at their northern edge, a system of interfingering delta front sandstones and prodelta shales, cut by up-to-basin basement-involved faults.

d) Both areas would show, then, a regional migration system, constituted by the basal Tertiary transgressive sandstones connected to Cretaceous source beds via vertical faults, and by the collecting sandstone fingers described above. This system would permit long distance hydrocarbon migration into the area.

e) The main regional trapping mechanism would be, for both areas, one of stratigraphic restrictions plus lack of mobility due to high viscosity of the oil.

f) The regional seal could be, for the Southern Orinoco Delta Middle Miocene sands, the same as for Cerro Negro: the shaly facies of the Oficina Formation or its equivalent. The shaly facies of Freites Formation, or its equivalents, would also contribute as a seal.

Hydrocarbon History

The presence of hydrocarbon accumulations in the nearby fields of Tucupita, Uracoa, Isleño, Pilón, Temblador, Morichal and Cerro Negro, western neighbors of the Southern Orinoco Delta area, added to Pedernales, and the southern Trinidad fields, due north of the Delta, gives to the latter a high probability of hydrocarbon existence. So far only to the east, into the offshore Delta Platform area, hydrocarbon accumulations have not been found.

It is sound and reasonable to believe that any hydrocarbon in the Southern Orinoco Delta area would have the same origin as the hydrocarbons of the Orinoco Belt, provided that they share a common geological history.

The studies on geochemistry and petroleum origin of the Maturín subbasin carried on by Audemard et al. (1985)[4] and Talukdar et al. (1986)[5] have demonstrated that the most probable source rocks for the oils of the Orinoco Belt are the marine shales and limestones of the Guayuta Group, in the deepest parts of the subbasin. Thermal immaturity precludes generation either in situ or Tertiary sourced.

The oil would have migrated from the Creataceous marine source beds deep in the basin, and up into the porous sandy facies of the Middle Miocene of the Southern Orinoco Delta.

This would have happened via vertical faults belonging to the two basement-involved tensional fault systems of the region: first, a scissor-like system, at an angle to the strike of the basement, with a long regional extent and a north to northwest strike; and second the up-to-basin system, parallel to the strike of the basement (Figure 6).

Long distance migration then would have occurred along the transecting fault systems, the continuous sandy facies of the delta lobes and the basal sandy fluvial systems, following the model shown in Figure 7. Continuous inspissation and biological action would have degraded the crudes updip, creating high viscosity plugs at the stratigraphic restrictions near the river basin outlets to the south.

Appraisal

An evaluation of the Southern Orinoco Delta was made using the PAQC-84, a computerized appraisal program. The premises for the estimation of volumes and probabilities on the basis of the hypothesis of the existance of a Middle Miocene transgressive deltaic system in the area, were as follows:

- Sandstone bodies of a deltaic sequence, of the same type, continuity and quality of the ones in Cerro Negro, constitute the reservoir rock. They have a volume of the same order of magnitude of the reservoir rock volume in Cerro Negro.

- Oil was generated in sufficient amount down in the basin, to the north, since Miocene times. The source rock would be the Cretaceous marine shales and limestones.

- The oil migrated long distances into the reservoir rocks of the Middle Miocene in the Delta area. Degradation occurred by inspissation and biological action, with the final result that the oil accumulated updip was of the heavy and extraheavy type.

- A regional seal, similar to the one that covers all the Orinoco Oil Belt, is also effective over the Delta area.

- The trapping is of the stratigraphic type, with viscosity plugs retaining the oil.

The most probable volume of oil place, in case of success, is 20.5×10^9 m^3 according to the results of the appraisal. The probability of success, however, is 64.9%. This means that the risked most probable volume of oil in place would be 13.3×10^9 m^3.

The curve on figure 8 shows the probability distribution of the expected volumes of oil in place in the Southern Orinoco Delta. It gives a probability of 52.8% to the low success volume expectancy of 4.4×10^9 m^3, given by the PAQC-84, and a 8.5% probability to the high success volume of 36.5×10^9 m^3.

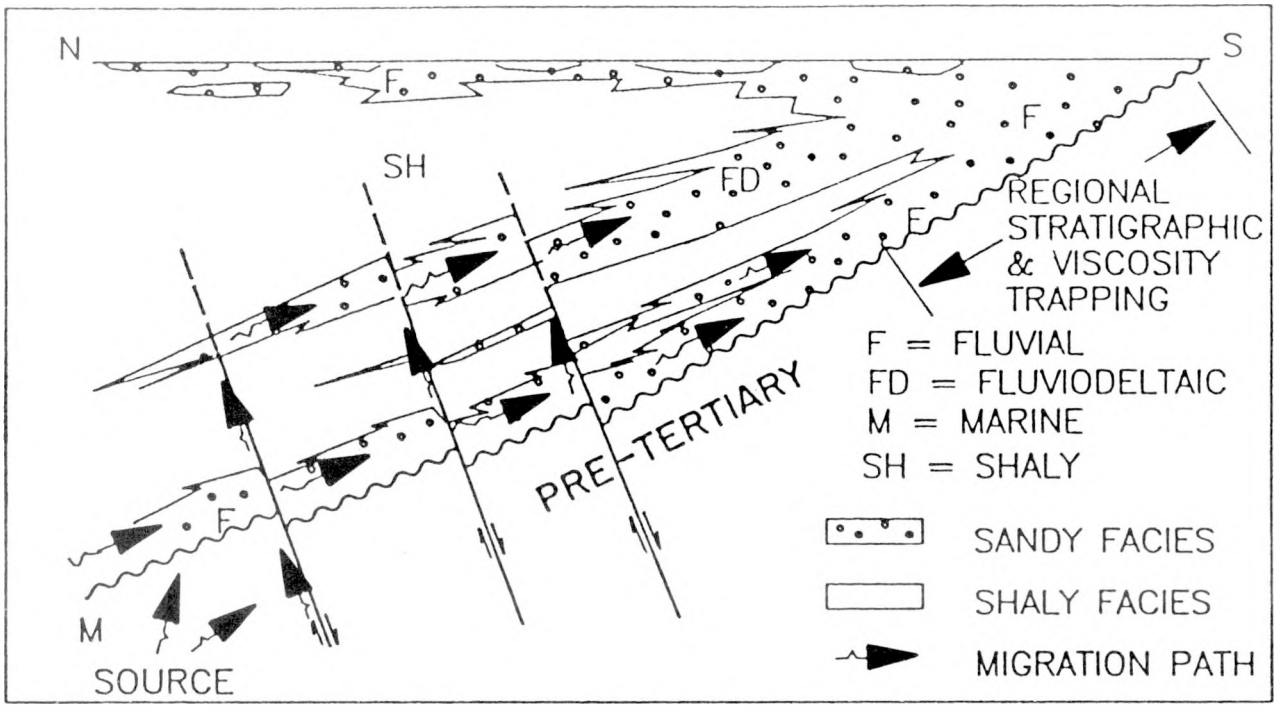

FIGURE 7. MIGRATION MODEL

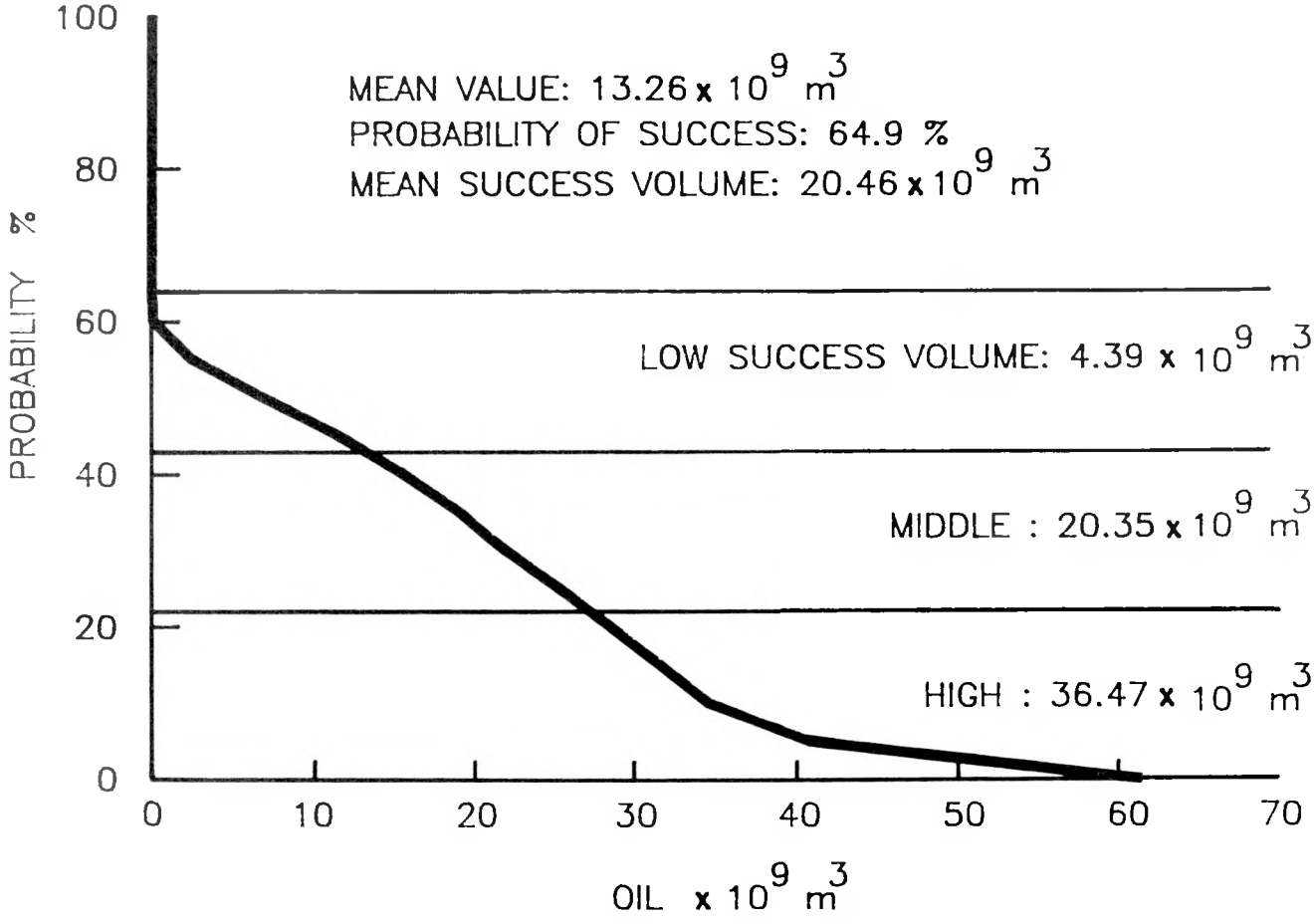

FIGURE 8. EXPECTATION CURVE FOR OIL IN PLACE

Conclusion

The area east of the Tucupita high, so far virtually unexplored, is to be considered as a future objective. It is expected to contain from 4.4 to 36.5 x 10^9 m^3 of heavy and extraheavy oils, provided that it bears a geological and petroleum history similar to the rest of the southern flank of the Eastern Venezuela Basin.

Favorable conditions are believed to exist in the region. Basement magnetic data, subsurface and physiographic data from neighboring areas and its location on the southern flank of the Maturín subbasin, added to the known existance of oil due north and west of it, support its prospectiveness. Future energy demand will prompt the exploration of this difficult region.

References

1. A. R. Martínez, 1987, "The Orinoco Oil Belt, Venezuela", Jour. Petrol. Geol. 10(2), pp. 125-134.

2. M. Latreille, P. Baumann, F. Audemard, N. de Audemard, I. Azpiritxaga. F. Cassani, I. De Mena, A. Isea, and M. Taheri, 1983, "Modelo geológico integrado de la Faja Petrolífera del Orinoco",INTEVEP, S.A. and BEICIP (unpublished report).

3. A. Bellizzia, 1983, "Geología y recursos minerales de la Guayana Esequiba y Guyana y recursos energéticos de las cuencas de Guayana y Tacutu", Lagoven, S.A. (unpublished report).

4. N. de Audemard, F. Cassani, and M. Taheri, 1985, "Origen y correlación de crudos pesados y extrapesados de la Faja Petrolífera del Orinoco", Informe no. INT-00987, 85, INTEVEP, S.A. unpublished report).

5. S. Talukdar, O. Gallango, and A. Ruggiero, 1986, "Estudio geoquímico regional de la Subcuenca de Maturín, integración e interpretation: Informe no. INT-01543,86, INTEVEP, S.A. (unpublished report).

Heavy-Oil Resource Potential of Southwest Missouri

by

Bruce W. Netzler
Missouri Department of Natural Resources
Division of Geology and Land Survey
Rolla, Missouri 65401

Abstract. Southwestern Missouri's heavy oil occurs in sandstones of the Pennsylvanian age Cherokee Group, at very shallow production depths ranging from 100 to 150 feet. The Cherokee contains four potential reservoir horizons: 1) Lower Warner interval, 2) Upper Warner interval, 3) Lower Bluejacket interval, and 4) Upper Bluejacket interval. The Lower Bluejacket and the Upper Warner contain most of the potential heavy oil reserves. The gravity of this oil ranges from 25 to 8 degrees API and is very viscous to nearly solid.

Previous realistic estimates of reserves in place range from 1.4 to 8.3 billion barrels of oil (Wells, 1974; Wells and Heath, 1979). The economic cutoff for production of heavy oil in Missouri is around $20/barrel. Using this amount and a proven recovery rate of up to 50 percent of oil in place using existing methods, this resource is worth from 14 to 85 billion dollars.

There have been 715,000 barrels of oil produced from southwest Missouri (Vernon County) from the onset of production records in late 1966 through 1988. From 1983-1985, over half of Missouri's total oil production came from heavy oil deposits in this area.

Introduction

When one thinks of Missouri, one might think of the St. Louis Cardinal baseball team or excellent canoeing rivers or perhaps the largest lead mining district in the world; but one does not usually think of extensive heavy oil deposits. For a state that is surrounded on three sides by big oil producing areas (Illinois Basin, Arkoma Basin, and Anadarko Basin), Missouri has come up pretty empty when it comes to easily producible hydrocarbons. But the future stardom of Missouri lies with its shallow heavy oil deposits just waiting to be exploited.

Geology

Location

Heavy oil deposits have been reported from several counties in western Missouri. Figure 1 shows a general area extending from Barton County in southwestern Missouri to Caldwell County, northeast of Kansas City. The more concentrated, thicker, and shallower deposits, and therefore the most promising for future development are those in Barton, Vernon, and southern Bates Counties.[1]

1989 Eastern Oil Shale Symposium November 15-17, 1989 Institute for Mining and Minerals Research, University of Kentucky

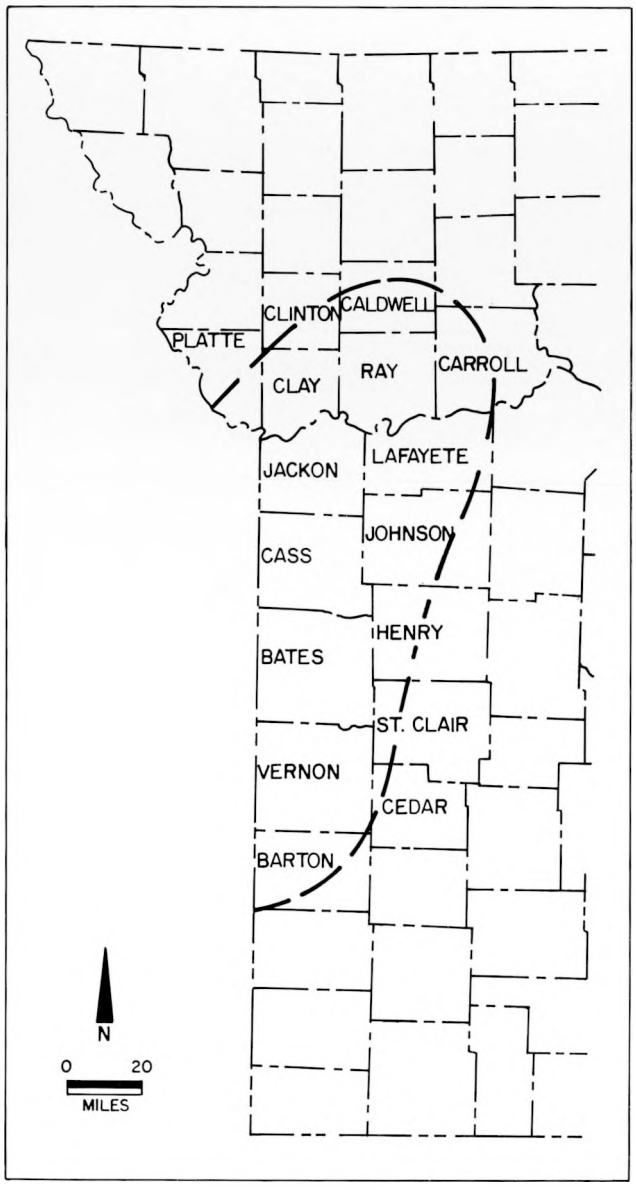

Figure 1 — Map of heavy oil occurrences in Missouri (after Wells, 1979).

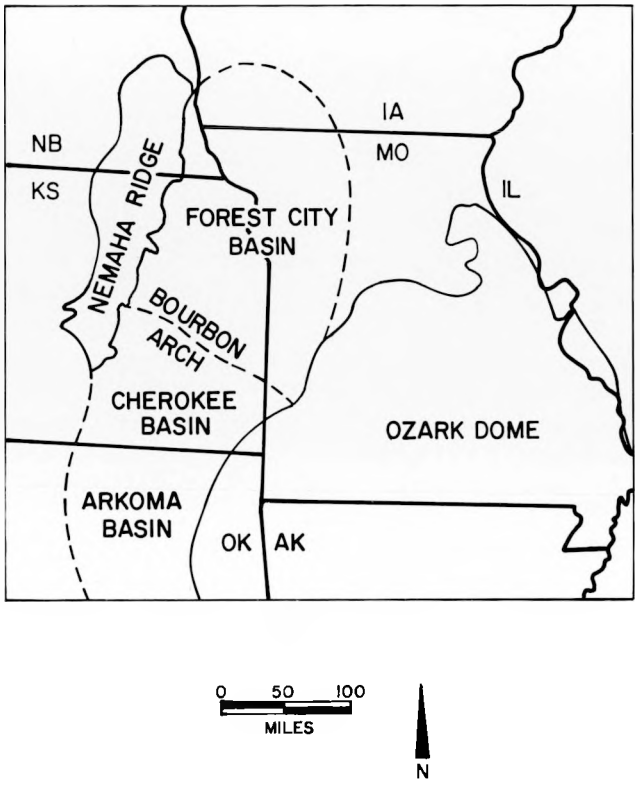

Figure 2 — Structural features of mid-continent (after Tomes, 1986).

Figure 3 shows the thickness of the "Upper Warner" interval in a portion of Vernon County, while figure 4 shows the structural features of the same area. When these two figures are compared, it becomes obvious that the structural complexion of the pre-Pennsylvanian surface had much to do with the thicknesses of the "Upper Warner." As can be seen, the thickest sandstone intervals are on the downthrown sides of the faults and in the synclinal axes. The faulting is confined to the Mississippian and older rocks since no offset is observed in the overlying Pennsylvanian sandstones (McCracken, 1971).[3]

Structural Setting

The most favorable heavy oil areas lie in an area around the Bourbon Arch. Figure 2 shows the structural features of Missouri. According to Ebanks and James (1974), the Bourbon Arch was a low positive feature which separated the Forest City Basin to the north from the Cherokee Basin to the south until submergence in the Middle Pennsylvanian. At the end of the Mississippian Period, regional emergence and subaerial exposure occurred forming a paleo-karst surface. As the Pennsylvanian seas covered the midcontinent area the well known cyclic sedimentation of the Pennsylvanian began. The Lower Cherokee rocks presently have a regional dip of from 3 to 5 degrees to the northwest as a result of the Ozark Uplift.[2]

Major Heavy Oil Bearing Sandstones

The sandstones of the Atokan and Lower Desmoinesian Series have been described as the major reservoirs of heavy oil in western Missouri. These sandstones are formally parts of the Weir, Bluejacket, Warner, and Riverton Formations. Figure 5 shows the relationship of the formational names to the historical names used for these heavy oil bearing sandstones.

The sandstones, shales, siltstones, claystones, and limestones of the lower Pennsylvanian have been described as being deposited in a fluvial-deltaic environment. Distributary channel, crevasse splay, point bar, and possibly braided stream deposits appear

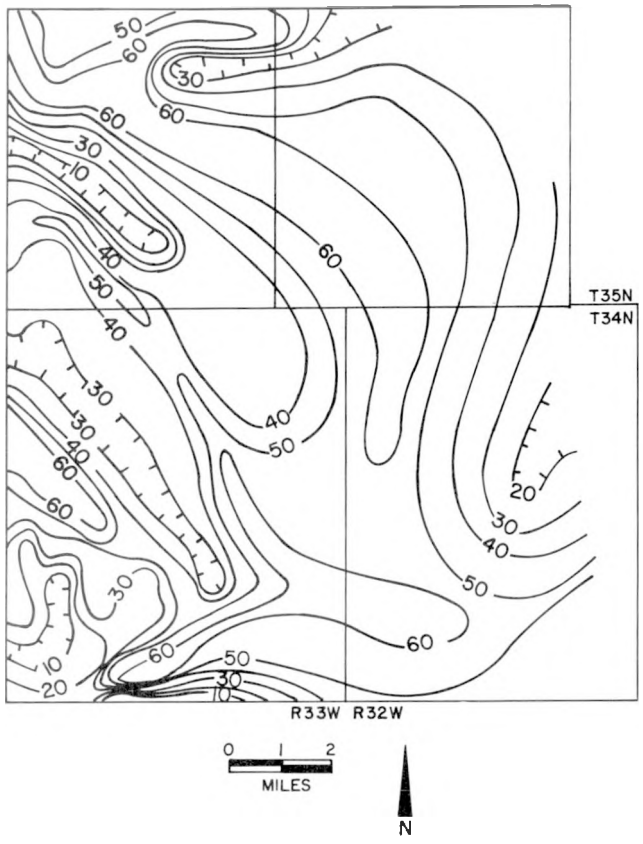

Figure 3 — Isopach/isolith map of the "Upper" Warner Sandstone interval; southwest Vernon County, Missouri (Tomes, 1986). Contour interval — 10 feet.

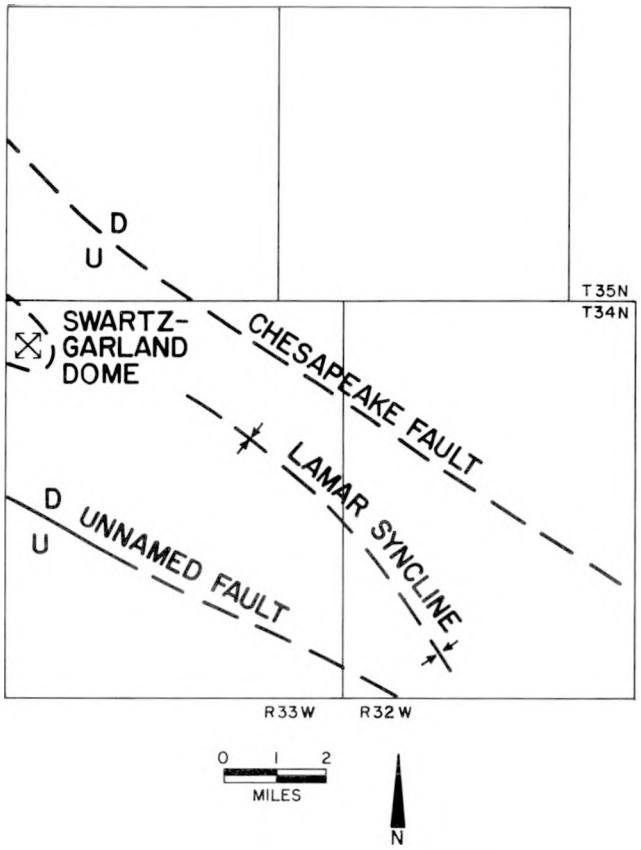

Figure 4 — Structural features of southwest Vernon County, Missouri (Tomes, 1986).

to be represented by the Upper and Lower Bluejacket and the Upper and Lower Warner sandstones.

Tomes (1986) interprets the "Upper" and "Lower" Bluejacket sheet sandstones as proximal crevasse splays infilling interdistributary lakes and bays.[4] As would be expected, these sheet sandstones have a channel facies, which in this case, can be from 35 to 60 feet thick.

Carmel Energy, Inc. has delineated another sandstone which they have tentatively named the "Eastburn," which lies stratigraphically between the "Lower Bluejacket" and the "Upper Warner" sandstones. Discriminating between the "Eastburn" sandstone and the "Lower Bluejacket" sandstone may be problematic. This is the unit from which they have successfully produced since 1978. The success of their operation hinged on their understanding of the detailed stratigraphic information of this sandstone.

> "A complete stratigraphic sequence of the Eastburn sandstone (in ascending order) consists of: (1) a thin basal conglomerate less than 6 cm thick, which contains limestone, siderite, and unidentifiable pebbles replaced by pyrite; (2) a sandstone sequence exhibiting medium-scale sedimentary structures, (horizontal, parallel bedding, massive-bedding, crossbedding, and slumped cross-bedding); which are laterally continuous within each separate point-bar body; and (3) rippled (4-6 cm) and horizontally bedded, sandstones and silts. Overlying the sandstone is a silty shale with small lenses of sandstone (2-4 cm thick) incorporated randomly throughout the zone."[5]

The Eastburn sandstone is thus divided into a more permeable lower facies (with very few shale partings) and a finer grained less permeable upper facies (with large amounts of silt and clay). The thickness variations in this unit are due to variations in the upper unit, with the lower unit maintaining a 12 to 16 foot thickness across the field (Ebanks and Weber, 1982).[6] This facies differentiation is typical of point bar deposits.

In a study by Tomes (1986), he interprets the environment of deposition for the "Upper Warner" (fig. 5) as a distributary channel system on a westward prograding, hi-constructive, delta lobe. The main facies being the distributary point bar

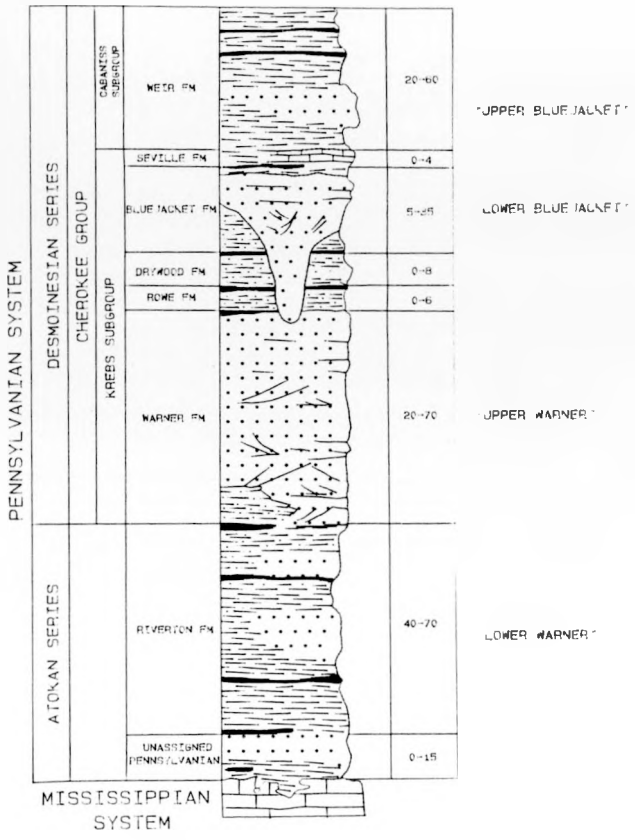

Figure 5 — Generalized stratigraphic column of Lower Pennsylvanian strata.

deposits. These have been interpreted to have been deposited by a meandering distributary system confined to existing valleys developed in the underlying Mississippian terrane. The point bar deposits coalesced, forming elongate multi-storied sandstones. As valley tops were breached, sandstones were coalesced, forming the tabular "Upper Warner" sandstone bodies. Most of the sandstone facies encompassed in the "Upper Warner" fall into the subarkose range of Folk's sandstone classification, which uses quartz-feldspar-rock fragments as end members.[4]

Tomes (1986) delineates five sandstone facies in the "Upper Warner" sandstone described above.

Subfacies H1 is a massive bedded sandstone and commonly occurs at the top of all Cherokee sandstones. It is very fine grained and contains locally abundant zones of early diagenetic siderite and shaly laminae. Heavy oil staining and residual bitumen are not present in this subfacies when it occurs at the top of the "Upper Warner" interval. This subfacies also occurs at the base of the "Upper Warner" just above the shale pebble conglomerate (subfacies H5). Subfacies H1 is not an important oil bearing zone.

Subfacies H2 is a very fine grained, parallel laminated sandstone. The parallel laminae are composed of siderite, altered phyllosilicates, and muscovite. These laminae form a significant barrier to vertical permeability. The massive subfacies H1 usually lies above this subfacies with a gradational contact and subfacies H2 overlies subfacies H3 (described below). The fine grained, parallel laminated sandstone of subfacies H2 is one of the two important oil bearing subfacies of the "Upper Warner" sandstone because of its volume and stratigraphic position.

Subfacies H3 is a very fine grained, ripple trough crossbedded sandstone. This subfacies shows multiple stacked sequences of ripple trough cross laminae with some climbing ripple sequences. Subfacies H3 is the most voluminous subfacies within the "Upper Warner" sandstone. Within this subfacies the transition from heavy oil saturation to bitumen (dead oil) occurs without a change in sedimentary structures or lithology. Subfacies H3 is usually overlain gradationally by the parallel laminated subfacies H2.

Subfacies H4 is a fine to medium grained, planar crossbedded sandstone. Even though this subfacies has the best reservoir characteristics because it falls stratigraphically near the base of the "Upper Warner," it usually only contains dead oil. Also, volumetrically speaking, it is not thick enough to contribute significantly.

As the hydrocarbons migrated up through the subfacies described above, the parallel bedded subfacies H2 served as the capping subfacies. Since the massive bedded subfacies H1 usually occurred above subfacies H2, no hydrocarbon got through into this part of the sandstone. Subfacies H3, the ripple trough crossbedded sandstone usually was just below the capping parallel laminated sandstone of subfacies H2, allowing the ripple trough crossbedded sandstone to serve as a good reservoir for the hydrocarbons.[4]

Diagenesis of the "Upper Warner"

Tomes (1986) describes the diagenetic history of the "Upper Warner" in great detail. Table 1 summarizes the paragenetic sequence of "Upper Warner" sandstones.

After hydrocarbons were emplaced, all further diagenesis stopped until the "Upper Warner" was brought within the meteoric ground-water regime by erosion of overlying strata. According to Ebanks and James (1974), the heavy oil in this strata is a mature hydrocarbon which has been subjected to destruction of lighter paraffins and asphaltenes by anaerobic bacteria and water washing, as opposed to an immature kerogen stage. This statement is supported by the presence of a flushed zone (dead oil or bitumen in pore spaces) underneath the heavy oil saturated

Stage	Diagenetic Features	Paragenetic Evidence
1st	Siderite, pyrite, FeO nodules	Well developed siderite "eyes" displace detrital grains; only common in shaly zones; FeO nodules deform adjacent laminae.
2nd	Quartz overgrowths	Syntaxial quartz overgrowths formed on clay-free grains. Euhedral quartz faces often bounded by sparry calcite. First diagenetic mineralization in cleaner intervals.
3rd	Sparry calcite	Low packing indices of quartz grains associated with calcite indicates early emplacement.
4th	Secondary porosity	Remnant pieces of calcite and calcite replaced grains in enlarged pores.
5th	Kaolinite, rutile	Euhedral kaolinite "books" and acicular rutile present in secondary pores in minor amounts.
6th	Hydrocarbons	Preservation of diagenetic mineralization in oil bearing zones and alteration in water bearing zones (i.e., illite pseudomorphous after kaolinite).
7th	Meteoric flushing	Bitumen in pores and low gravity oil are evidence of loss of lighter end volatiles.

Table 1. Inferred paragenetic sequence of the "Upper Warner" sandstone, Vernon County, Missouri.[4]

zone and the presence of higher gravity oil in the more deeply buried Cherokee rocks to the west in Kansas.[2]

A local source for the heavy oil is suggested by the following statement:

> "The tar/heavy oil in the Warner and Bluejacket probably was generated in the enclosing shales. Evidence for this is the high organic matter content of some shales and the discontinuity of the sandstone reservoir rocks, which precludes migration from more distant sources."[10]

History of Production Methods

Phillips Petroleum Company (1955 to 1958)

Early in 1955, Phillips Petroleum Company began work on testing a counterflow underground combustion process to produce the highly viscous oils of southwest Missouri. At the time Phillips was preparing for this test all available data indicated that a direct drive method, in which the combustion front and the injected air stream moved in the same direction, would not work for highly viscous oils because the heated and thinned oil would be driven ahead of the combustion front by the air pressure into the unheated rock and congealed, forming a gas permeability barrier which smothered the combustion.

Laboratory experiments conducted by Trantham and Marx of Phillips, first demonstrated that this permeability barrier would not develop if the injected air came from the opposite direction that the combustion front was moving. The air would force the heated and thinned oil back through the combustion zone, thus keeping a gas barrier from forming.

> "Here thermal cracking produces relatively light hydrocarbon products which pass through the heated rock behind the fire front (largely in the vapor phase) and are incapable of causing a gas permeability block."

Through core drilling several possible test locations were delineated in western Missouri. The site selected near Bellamy, Missouri, was a 12 foot thick section of tar sandstone which extended from 49 to 61 feet below the surface. The sandstone was underlain and overlain by siltstones and shales which served as a seal. The core analysis showed that the sandstone was divided into an upper less permeable zone and a lower more permeable zone.

Well Patterns

The Phillips field testing program involved a total of seven different well spacing patterns, including five- and seven-spot patterns, a 15 well line drive pattern and a 10 well radial pattern.

The line drive pattern used in the counterflow combustion test consisted of three lines of five wells each, with the middle line being production wells and the outer lines being injection wells. Spacing

between the wells in each line was 5 feet, and spacing between the production and injection well lines was 15 feet. Interspersed in this pattern were 20 observation wells which monitored the temperature and advance of the fire front.

Preliminary Reservoir Conditioning

Before testing began, Phillips had to prepare the reservoir. The sandstones in this area had approximately 50 percent of their pores filled with water and 50 percent filled by immobile tar with a viscosity of greater than 500,000 cp. The water in the sandstones was flushed out by injection of air. When most of the water had been removed, the combustion test could begin.

Test Data

Phillips conducted the line drive counterflow combustion test for 9 days. Following this period of controlled stabilized operation, a sudden air breakthrough led to a termination of the test. Phillips determined later that thermally induced fractures had penetrated some of the injection wells, causing breakthrough. A comparison of the produced oil and the original tar in place shows that the oil produced had been significantly upgraded.

	Typical Composite Field Test Oil	Original Tar in Place
API gravity	26	10
Viscosity (cp at 75°F)	10	500,000

Results

Results from this test and the other well spacing configuration tests showed Phillips that the rate of air injection is a critical factor in fire front propagation. Also, it was shown that air transmissibility through the test sandstone increased about 20 fold as the counterflow combustion zone passed through the sandstone. This phenomenon was attributed to the predictable extensive thermal fracturing that occur on a local scale.

Summary of Test Results

"1. Production of low viscosity oil from essentially immobile hydrocarbon in consolidated bituminous sandstone by counterflow underground combustion is technically feasible under the field conditions prevailing at Bellamy.

2. Production wells can be operated as high temperature condensate wells, with no lifting equipment required.

3. Produced oil can be separated into arbitrary heavy and light fractions at the wellhead through condensation in properly selected heat exchangers.

4. Neither emulsion problems nor corrosion problems appeared to be major difficulties under Bellamy conditions."[7]

Carter Oil Company — Deerfield Steam Drive Test (1955-1959?)

The Deerfield steam drive pilot test was located in Vernon County, Missouri and undertaken by the research (Esso Production Research Company) and production (Humble Oil and Refining Company) departments of Carter Oil Company. When the test began detailed reservoir information was not known. It was not until after testing began, that core results showed that there was not enough oil in place to constitute a commercial oil production operation. Work continued after this point to fully evaluate field performance of steam injection as a recovery method.

Description of Pilot Test

The location of the test was about 10 miles north of Deerfield in the Stotesbury Oil Field (fig. 6), which is west of Nevada, the Vernon County seat, and only a few miles from the Kansas border.

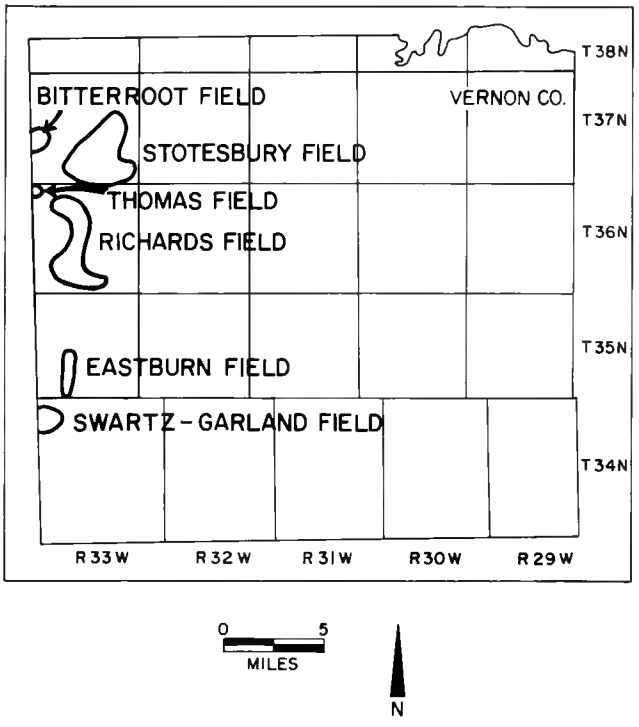

Figure 6 — Vernon County oil field map.

The test was conducted in the Warner Sandstone, Cherokee Group, Pennsylvanian Age. The top of the Warner was about 160 feet below the surface and dipped to the northwest at about 12 to 15 feet per mile. The average thickness was about 45 feet with two types of hydrocarbon saturation present. The lower portion contained a thick tar that would not flow under the influence of a steam drive. The upper 26 feet of the sandstone contained hydrocarbon that responded to the steam drive test. The following information shows formation and reservoir properties of the Deerfield Test:

Average depth, ft	160
Average thickness of net sand, ft	26
Porosity, percent	23.5
Air permeability, md	450
Oil saturation, bbl/acre-ft	535
Initial reservoir pressure, psig	50
Initial reservoir temperature, °F	60
Total test area, acres	5.625
Oil gravity, API	18
Oil viscosity, cp at 60°F	1000
Oil viscosity, cp at 100°F	210
Oil pour point, °F	15
Formation water, total dissolved solids, ppm	14000
Chloride concentration, ppm	5300
pH	7.4

Initial field testing included a two well air injection test and a two well water injection test. No oil was produced by either test. These wells were later used in the steam injection tests. Development of the steam injection test occurred in four stages over a 5-year period, beginning in 1954. Refer to figure 7 for well locations.

Phase 1 consisted of a two well test using the same two wells as the initial water flood test but injecting steam into one well and producing from the other. Wells 1 and 1W were about 117 feet apart.

Phase 2 consisted of drilling three more production wells (3, 7, and 11) completing the first five-spot pattern.

Phase 3 consisted of drilling the remaining center producers (wells 4-6) and the rest of the injection wells (2W-9W).

Phase 4 finished out the 25-well test by drilling the peripheral wells needed to surround the injection wells with production wells.

The pilot project when completed consisted of nine inverted five-spot patterns on five-eighths acre spacing. Nine wells were steam injection wells and 16 were oil production wells. All wells were completed as open-hole with 4½ inch casing cemented to the top of the Warner Sandstone. Pumps were installed in the production wells but as the test matured, many wells flowed.

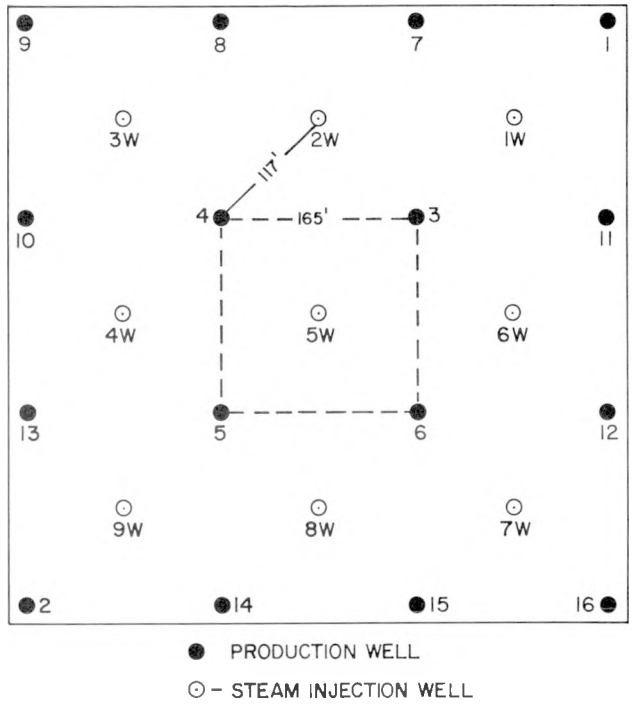

Figure 7 — Well locations, Deerfield Steam Pilot (after Vallory et al., 1967).

Results

Over the life of the test, each injection well received from 45,000 to 73,000 bbls (as condensate) steam. Production from the central portion of the field (fig. 7) amounted to 4,679 bbls of oil, with a water-oil ratio of 41:1. The peripheral production wells produced a total of 2,073 bbls of oil, with a water-oil ratio of 138:1. This resulted in an average water-oil ratio of 70:1 for the Deerfield steam pilot test. The gravity of the oil produced increased about 3 degrees from its pre-test rating of 18 API to 21 API.[8]

Shell Oil Company (1963-1966)

In mid-January 1963, Shell Oil Company purchased 80 acres in sec. 8, T. 36 N., R. 33 W., Vernon County, Missouri. Information concerning this project is very scarce because of Shell's policy of confidentiality, but it is estimated that Shell cored over 600 holes before it began its pilot project.

The information that has been pieced together indicates that Shell operated a steam pilot and a

combustion pilot in Vernon County, Missouri. The horizon tested was the Warner Sandstone of the Cherokee Group, Pennsylvanian Age. The Warner Sandstone was about 250 feet deep and reached a thickness of approximately 45 feet. Both the steam and combustion pilots were developed on 2½ acre inverted five-spot patterns.

Combustion Test

In February 1964, operations began on the combustion pilot with the initiation of Shell's "gentle formation heating" technique. This process begins with steam injection to heat the formation so that when air injection starts, combustion is initiated spontaneously. Air injection began in April 1964, and ended in April 1965, with a total of 434 million cubic feet of air being injected.

Termination of the combustion came in May 1965, with the injection of approximately 30,000 bbls of cold water. Shell's combustion pilot test produced 346 bbls of oil.

Steam Test

The steam pilot operations began in March 1964, and ended in November 1965, with the injection of 50,050 tons of steam and 165,000 bbls of hot water. Approximately 102,000 bbls of cold water were injected in December 1965, and January 1966, to conclude injection operations. Upon the end of production operations in February 1966 a total of 6,600 bbls of oil were produced.

Henry Petroleum Company (1975-1976)

Henry Petroleum Company unsuccessfully tried to produce heavy oil from what is now the Eastburn Field (sec. 33, T. 35 N., R. 33 W.) in Vernon County, Missouri (fig. 6). Although there is very little information on their efforts it is believed that Henry Petroleum operated a liquid nitrogen injection project which was abandoned after very little oil was recovered.

Bar-Co-Roc, Incorporated (1920's to 1960's?)

There have been several references to quarry operations on outcrops of heavy oil sandstone deposits. The most notable was a quarry and plant near Iantha, Barton County, Missouri. This plant produced tar sandstone which was crushed and used for paving material. It was noted that the untreated tar sandstone lacked enough binding asphalt that road failure was seen when it was used to pave streets in the local area, but after mixing with some asphalt the paving results improved greatly. Unfortunately, no one tried to extract oil from these quarried tar sandstone deposits.[9]

Jet Engine Test (?)

At some point in Missouri's past, an unnamed company attempted a thermal recovery test using jet engine exhaust gases directed downhole. No real information is available on the test but it was presumed to be unsuccessful.

Electrical Current Injection Test (?)

It has been reported that an operator had attempted to inject electrical current into the heavy oil sandstones with the hope of heating the oil so that it could be produced. The only result noted was a large electric bill.

Bitterroot Field (secs. 19 and 30, T. 37 N., R. 33 W.)

The first wells were drilled in this Vernon County field near the turn of the century (fig. 6). Oil gravity averaged from 16 to 22 API gravity. Very little information is known about the development of this field over the years.

Americana Oil Company and Mo-Ky Oil Company (1966). These two companies operated adjacent leases in the Bitterroot Field. The only information available indicates that they operated a water drive project that resulted in some success.

Grant Oil Company (1970). Grant Oil operated in the Vernon County-Bitterroot Field area for an undetermined amount of time. Information on this operator is almost nonexistent.

Dotson Oil Company (1966-1980)

Dotson Oil Company operated what appeared to be an air injection project in the Thomas Field (fig. 6) located in sec. 6, T. 36 N., R. 33 W., Vernon County for an undetermined period of time. Thirty-one wells were drilled on this lease and cumulative production totaled 17,953 bbls of oil.

Benyon Energy Company (1979)

Benyon Energy conducted CO_2 and steam injection tests in Barton County (fig. 1). These tests were reported to be in the Bluejacket Formation, Cherokee Group, Pennsylvanian Age. Based on

initial results, average oil production per well is expected to be 10 bbls per day.[10]

Jones-Blair Energy Incorporated (1982-1987)

In 1982 Jones-Blair began steam injection operations in the old Stotesbury Field located in secs. 26, 27, and 35, T. 37 N., R. 33 W., Vernon County, Missouri (fig. 6). To delineate the reservoir, about 80 core holes were drilled. Reservoir parameters are as follows:

Gravity, API	19-23
Viscosity, cp	609?
Reservoir temperature, °F	60
Average permeability, md	375
Average pay thickness, ft	25
Depth to top of pay, ft	185-200
Barrels per acre foot	1100
Oil saturation	70%
Water saturation	30%

This reservoir was previously produced around World War I. Production probably ranged about 5 to 6 bbls/day/well eventually dropping to ¼ to ½ bbl/day/well before abandonment.

Initial tests involved the huff and puff method of steam injection. Jones-Blair designed a carbon dioxide vaporizer to use with the injection of steam and other chemicals in these tests. Reservoir conditioning occurred with the injection of 20 tons of carbon dioxide at a temperature of up to 650 degrees F per well, followed by the gradual increase of steam and carbon dioxide with other chemicals for permeability control. Injection-production cycles averaged 45 days in length with a heat content approaching 500 million BTU per well. Air lift processes were used instead of pump jacks to produce the oil.

Development of this field proceeded with the drilling of wells in alternating rows of injection and production wells. This field was plugged due to declining oil prices and not because of depleted oil reserves. Upon abandonment of this steam project, 133,018 bbls of oil were produced.[11]

Carmel Energy, Inc. (1978-present)

In 1978 Carmel Energy entered into a Department of Energy cost sharing contract to test its Vapor Therm system in Vernon County, Missouri. Carmel Energy began studies on leases in secs. 28 and 33, T. 35 N., R. 33 W. which is now called the Eastburn Field (fig. 6). Some very preliminary work was done in this area by Henry Petroleum, as stated earlier.

Carmel Energy's patented Vapor Therm process involves the generation of a mixture of superheated steam, nitrogen, and carbon dioxide to be injected into the shallow heavy oil bearing Pennsylvanian sandstones. The inert gases repressurize the formation while the heated vapors reduce the viscosity of the oil so that it can be removed much easier. According to Carmel's tests, there is no need to purify the boiler feed water and there are no vented gases which can cause air pollution. This process can be utilized with either the huff and puff or direct drive methods. Average reservoir properties are as follows:

Depth to top of sand, ft	100-110
Net feet of pay	20-23
Structure	Channel, 1° dip
Sand grain size	Fine to very fine
API gravity, degrees	20-23
Porosity, percent	25
Permeability, md	650
Oil saturation, percent	60
Reservoir pressure, psig	54
Oil viscosity	700 cp @ 70°F
	80 cp @ 100°F
	40 cp @ 130°F
	10 cp @ 210°F

Carmel Energy's operation is Missouri's largest commercial heavy oil project. To date, Carmel has produced over 550,000 bbls of heavy oil. When prices dropped drastically in 1986, Carmel began curtailing its thermal injection. At present, Carmel has drastically cut back on its operating costs and is averaging only about 5,500 bbls per year. At its peak, Carmel was averaging 10,000 bbls of oil per month.[12]

Electromagnetic Energy Incorporated

Electromagnetic Energy, Inc. is testing a microwave sourced thermal recovery technique to attempt production of the heavy oil in the Eastburn Field (fig. 6). This test has not been completed and no results are available at this time.

MW Inc. — Town Oil Company (1989)

A secondary water drive injection test was initiated in the old Bitterroot Field (fig. 6) using horizontally drilled wells as injection and production wells. Eleven laterals were drilled to a vertical depth of approximately 150 feet with lateral distances from 150 to 200 feet in length. The change from vertical to horizontal was accomplished in approximately 20 feet of radius. Nine of the laterals were drilled in the direction of permeability and two were drilled perpendicular to the direction of permeability. Initial tests were not successful but additional tests are planned in the near future.

Reserve Estimates

Over the years, estimates on the amount of heavy oil in place have ranged from a few million barrels to a very speculative, 75 billion barrels. In 1974, Wells made an estimate of oil in place of 8.3 billion barrels. This estimate was made on the existing data at that time and did not result in any published material. Between 1974 and 1979, additional studies were undertaken, with partial support from the Department of Energy, which allowed for a revised estimate based on more data. In 1979, Wells and Heath published an estimate of heavy oil in western Missouri at from 1.4 to 1.9 billion barrels. The area that this estimate covered included mainly Vernon, Barton, Jasper, and the western portion of Cedar and Dade Counties (fig. 1).[14]

Recovery rates in the range of 50 to 60 percent are obtained from the recent heavy oil operations in Vernon County. Using these rates and an average price of $20 per barrel, the value of the reserve approaches 40 billion dollars.

Although the area covered by the Wells and Heath study is considered to be the most promising, other areas to the north may prove to be substantial with further study. Also, it is interesting to note that at the time of the Wells and Heath report the stratigraphy of the Eastburn Oil Field was not well known. Even though the "Eastburn" sandstone named by Carmel Energy, Inc. may be only a local development, the possibility of other similar relationships between the established Bluejacket and Warner sandstones definitely exists.

Summary

Missouri is blessed with substantial quantities of very shallow (100-150 feet) heavy oil saturated sandstones in the basal Pennsylvanian rocks in western Missouri. If Missouri is ever to be compared with the likes of its oil rich neighboring states, it will probably be due to the exploitation of its heavy oil deposits. Now is the time to prepare the background studies delineating more heavy oil areas, so that when the price of oil again increases dramatically, we will be ready to use existing resources instead of importing ever increasing amounts of oil.

Recent studies by Bradshaw (1985) and Tomes (1986), are the type of studies which help us to better understand the complex nature of the heavy oil bearing sandstones that exist in Missouri. Of special note is a thesis that is just being defended by Darrell W. Rosiere. His thesis, through the University of Missouri-Rolla, Department of Petroleum Engineering, is entitled, "Relative Permeability Measurements for Thermal Applications to Heavy Oil Reservoirs in Western Missouri." Unfortunately, submittal deadlines do not allow me time to incorporate his results into this paper, but I am sure this thesis will provide information that will be available to future heavy oil exploitation.

References

1. J.S. Wells, "Background Information on Heavy Oil Resources in Missouri," Brochure-7, Missouri Department of Natural Resources, Division of Geology and Land Survey, Rolla, Mo., pp. 11, Aug., 1979.

2. W.J. Ebanks, Jr. and G.W. James, "Heavy Crude Oil Bearing Sandstones of the Cherokee Group (Desmoinesian) in Southeastern Kansas," *in* Hill, L.V., (Ed.), Oil Sands; Fuel of the Future: Canadian Society of Petroleum Geology, Memoir #3 pp. 19-34 1974.

3. M.H. McCracken, "Structural Features of Missouri," Report of Investigation No. 49: Missouri Department of Natural Resources, Division of Geology and Land Survey, Rolla, Mo., pp. 99, 1971.

4. R.J. Tomes, "Environmental and Diagenetic History of the 'Upper' Warner Sandstone: SW Vernon County, Missouri," Thesis, Colorado State University, Fort Collins, CO., pp. 194, 1986.

5. D.T. Bradshaw, "Geologic Variables Influencing Production in the Eastburn Field, Vernon County, Missouri," Thesis, Wichita State University, Wichita, KS., pp. 125, Feb., 1985.

6. W.J. Ebanks, Jr. and J.F. Weber, "Development of a Shallow Heavy Oil Deposit in Missouri," Oil and Gas Journal, pp. 222-234, Sept. 27, 1982.

7. J.C. Trantham and J.W. Marx, "Bellamy Field Tests: Oil from Tar by Counterflow Underground Burning," Journal of Petroleum Technology, pp. 109-115, Jan., 1966.

8. V.V. Valleroy, B.T. Willman, J.B. Campbell, and L.W. Powers, "Deerfield Pilot Test of Recovery by Steam Drive," Journal of Petroleum Technology, pp. 956-964, July, 1967.

9. W.V. Searight, "Asphaltic Rocks in Western Missouri," IC-13, Missouri Department of Natural Resources, Division of Geology and Land Survey, Rolla, Mo., pp. 26, 1957.

10. K. Thompson (Ed.), "Major Tar Sand and Heavy Oil Deposits of the United States,"

Interstate Oil Compact Commission, Chapter 8, Jan. 1984.

11. Excerpts from Dec. 2, 1982, Missouri Oil and Gas Council Meeting Minutes, Jerry Jones, V.P. Jones-Blair Energy, Inc.

12. J.S. Sperry, "Heavy Oil Recovery System Completes Three Field Tests in Mid-Continent Region," Oil and Gas Journal, pp. 225-237, July 27, 1981.

13. L. Town, Town Oil Co., personal communication, Oct., 1989.

14. J.S. Wells and L.J. Heath, "Inventory of Heavy Oil in Western Missouri," BETC-1808-1, Department of Energy, Sept., 1979.

Athabasca South: Resource Characterization of an Active In Situ Pilot Area

by

J.R. MacGillivray, D.A. Wynne, D.A.W. Keith, T. Berezniuk, D.M. Wightman and H. Berhane
Alberta Research Council
Alberta Geological Survey
Edmonton, Alberta CANADA T6H 5X2

Abstract. The Lower Cretaceous McMurray/Wabiskaw Deposit (Athabasca Oil Sands) is the largest bitumen deposit in Alberta, Canada. The objective of this paper is to discuss the distribution of resources (bitumen and gas) in the southern region of this deposit (Townships 67-79, Ranges 1-18W4).

The McMurray Formation sediments (fluvial to estuarine to marginal marine) infilled valley systems that were developed on the sub-Cretaceous unconformity. The fluvial sands (quartz arenites to sub-litharenites) at the base of the McMurray Formation are the best reservoir (little mud, amalgamated channel sands) although they do not have great lateral extent. Two valley systems are present and the northern part of the main (eastern) valley contains the thickest oil sands (more than 45 metres of >6 wt.% bitumen). An abrupt bitumen/water contact occurs in the east along a Paleozoic escarpment created by the dissolution of underlying Devonian salts. The secondary valley consists of thinner oil sands (less than 20 metres of >6 wt.% bitumen) with a gradational bitumen/water contact trending east/west. Both valley systems are locally underlain by bottom water or contain water sands. A gas field is present in the northeast.

The Wabiskaw Member (Clearwater Formation) sands (litharenites) conformably overlie the McMurray Formation and were deposited in a marginal marine setting as the Boreal Sea transgressed from the north. These sands differ mineralogically from the McMurray Formation and have greater lateral continuity. The best Wabiskaw Member sand, from a resource viewpoint, was developed in the east-central area (over 35 metres of >6 wt.% bitumen). This sand dips gradually to the southwest and has a gas cap in its updip end. Structure, facies, and bitumen biodegradation were all major factors in the bitumen trapping.

1989 Eastern Oil Shale Symposium November 15-17, 1989 Institute for Mining and Minerals Research, University of Kentucky

Introduction

The Cretaceous Mannville Group and its equivalents contain the bulk of Alberta's bitumen reserves. The Athabasca Oil Sands Area is the largest of Alberta's three Oil Sands Areas and within it the McMurray/Wabiskaw stratigraphic interval contains most (145 billion m^2 or 909 billion barrels) of the reserves.[1]

The objective of this paper is to describe the geological setting and the distribution of bitumen, gas, and water sands for the southern portion (Fig. 1) of the Athabasca Oil Sands Area (Townships 67 to 79, Ranges 1 to 18W4). The results presented are from the third in a series of resource characterization reports being prepared on the McMurray/Wabiskaw stratigraphic interval by the Alberta Geological Survey, a department of the Alberta Research Council. Flach published on Athabasca North, and Keith et al. and MacGillivray et al. published on Athabasca Central.[2,3,4,5]

Method

Data for all wells in the area were examined and a subset of 697 logged wells were selected for detailed analysis. Using, where available, four wells per township, wells were selected on the basis of geographic distribution, quality of the well logs (gamma ray, resistivity, and porosity), and the presence of core analysis data. Picking of formation tops and marker horizons was done by visual examination of the well logs. Lithology and formation fluid saturation data was calculated using a computerized log analysis package operating on a microcomputer. Cores from 63 wells in the study area were examined to document the facies.

The log analysis system was calibrated from core analysis data. Separate constants were determined for the McMurray Formation and the Wabiskaw Member. Lithology data were derived from a volume of shale calculation based on the gamma ray log curve response. Porosity was calculated using a complex-lithology crossplot algorithm with shale corrected density and neutron logs. Formation fluid data were derived using the Simmandoux water saturation equation.

A relational database was designed and built to manage the data used for mapping. Tables were created for well identification and location data, the core analysis data, the formation and marker horizons data, and all data derived from the log analysis system. All data except the formation and marker horizons were obtained in digital form.

Standard reports using SQL (Standard Query Language) were designed to extract data for the structure and isopach (sand, bitumen, water, and gas) maps. A special report using embedded SQL was designed to extract data for the bottom water maps. Use of the database simplified data verification and maintenance of data consistancy for all maps.

An automated procedure was developed to extract data from the database, contour the data, and produce a finished map. Contouring was performed by using Surface II, a contouring package

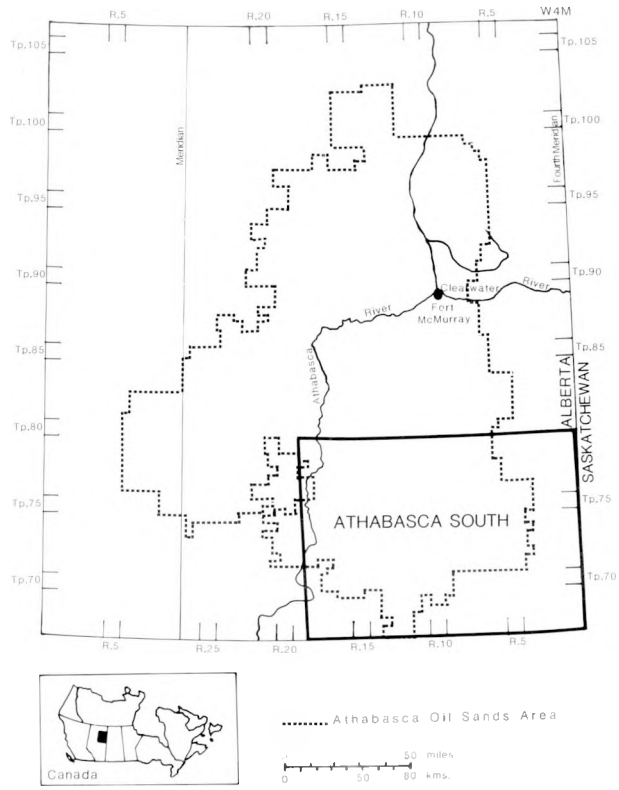

Figure 1. Location of the study area (Athabasca South) an extent of the Athabasca Oil Sands Area.

developed by the Kansas State Geological Survey. The finished products were produced by using software packages developed at the Alberta Geological Survey.

Stratigraphic Setting

Regional Stratigraphy

The regional stratigraphy of the Athabasca Oil Sands Area was discussed by Keith et al.[4] The McMurray Formation, a Lower Cretaceous succession of unconsolidated sands and shales, is the lowermost formation in the Mannville Group and overlies an unconformity developed on Middle Devonian carbonates (Fig. 2). Previous work has shown that deposition of the McMurray Formation was controlled by regional depressions in the sub-Cretaceous erosional surface. The topography is at least partly the result of salt dissolution in the Middle Devonian Elk Point Group and the associated collapse of the overlying Beaverhill Lake Group.[2,6,7,8,9] Within the study area the McMurray Formation ranges in thickness from over 100 m in the east to less than 10 m in the west where it thins against the Wainwright Ridge, a Devonian paleotopographic high.[10,11]

Although there is some debate as to specific depositional environments within the McMurray Formation, it is generally accepted that the formation is a channelized succession with some degree of marine influence.[4] At the end of McMurray Formation time the boreal sea transgressed southward, resulting in the deposition of

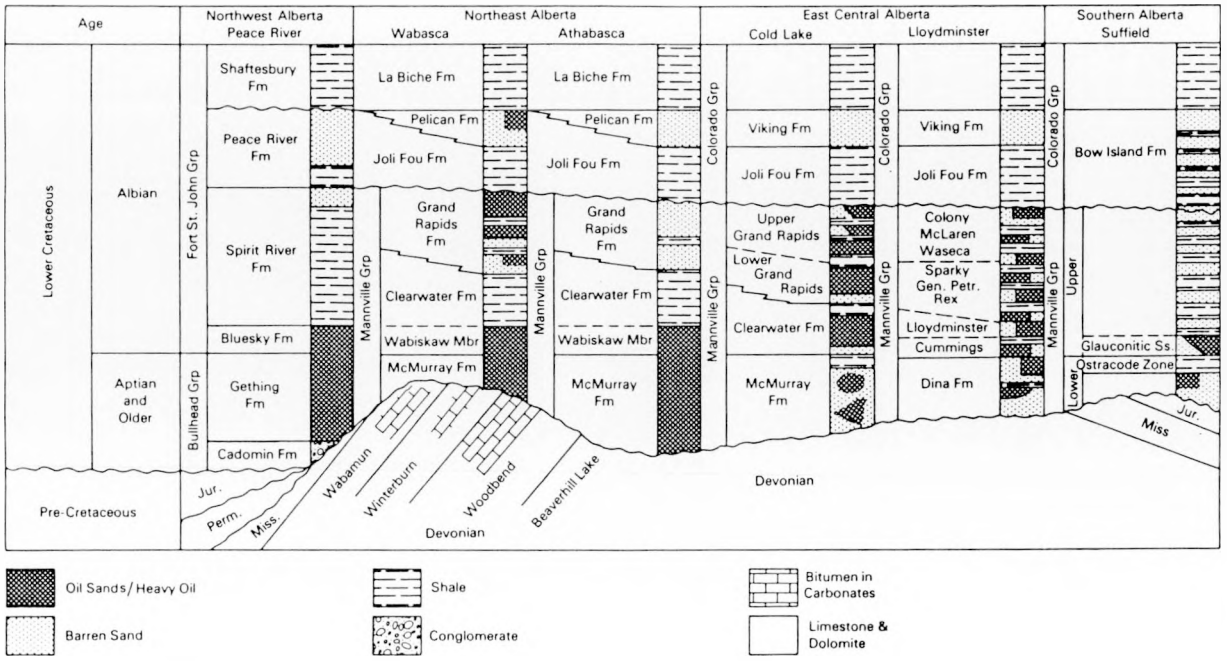

Figure 2. Regional stratigraphy of the Lower Cretaceous in Alberta (Modified from Kramers.[12])

the overlying marine sands and shales of the Clearwater Formation. The Wabiskaw Member, which directly overlies the McMurray Formation, is a glauconitic sand at the base of the Clearwater Formation.

The McMurray Formation is stratigraphically equivalent to the Gething Formation of northwestern Alberta and the Dina Formation of east-central Alberta. The Wabiskaw Member of the Clearwater Formation is probably coeval with the Bluesky Formation of northwestern Alberta, the Cummings Formation of east-central Alberta, and the Glauconitic sandstone of southern Alberta.[1,2]

Local Stratigraphy

The datum used to approximate the top of the McMurray Formation within the study area is the base of the lowermost marine shale occurring above the sub-Cretaceous unconformity. This is the same datum as used by Flach in the northern part of the deposit and Keith et al. in the central area.[2,3,4] This shale was selected as the datum because of its proximity to the top of the McMurray Formation (as verified by core study), its ease of recognition on geophysical well logs, and its regional extent. Within Athabasca South the datum shale is missing (Fig. 3) in the east-central area due to what has been tentatively interpreted as an erosional event at the base of the Clearwater Formation.

The presence and absence of the datum in the study area is represented by two wells, 7-25-77-6W4 (Fig. 4) and 10-2-74-5W4 (Fig. 5).

In well 7-25-77-6W4 (Fig. 4) there is a thick (95 m) McMurray Formation with interbedded shales and coals at the base. This unit is overlain by a series of blocky sands, which are in turn overlain by a unit of coarsening up

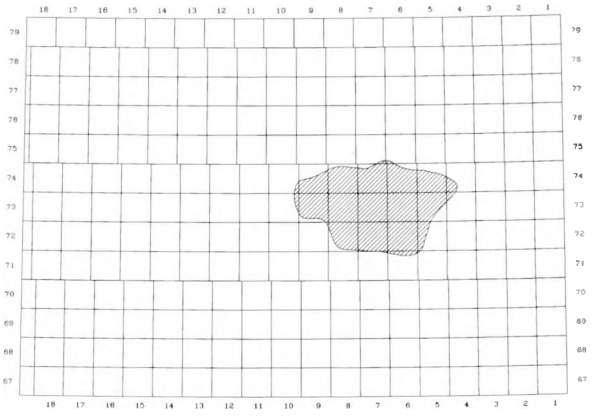

Figure 3. Map of the study area indicating where the datum shale is absent.

sequences, and interbedded sands and shales. The Wabiskaw Member of the Clearwater Formation conformably overlies the McMurray Formation in this well. The Wabiskaw Member is informally divided into "D", "E", and "F" sand/shale units. The datum is present at the base of the first Wabiskaw Member shale above the sub-Cretaceous unconformity.

In well 10-2-74-5W4 (Fig. 5) the McMurray Formation is thinner (50 m) than in the previous well. The McMurray Formation in this well consists of shales and blocky sands overlain by a coarsening up sequence, a fining up sequence, and another coarsening up sequence. Overlying the McMurray Formation is a thick (35 m) Wabiskaw Member sand. This sand is tentatively correlated to the combined "D" and "E" intervals. There is no datum present in the 10-2-74-5W4 well. For

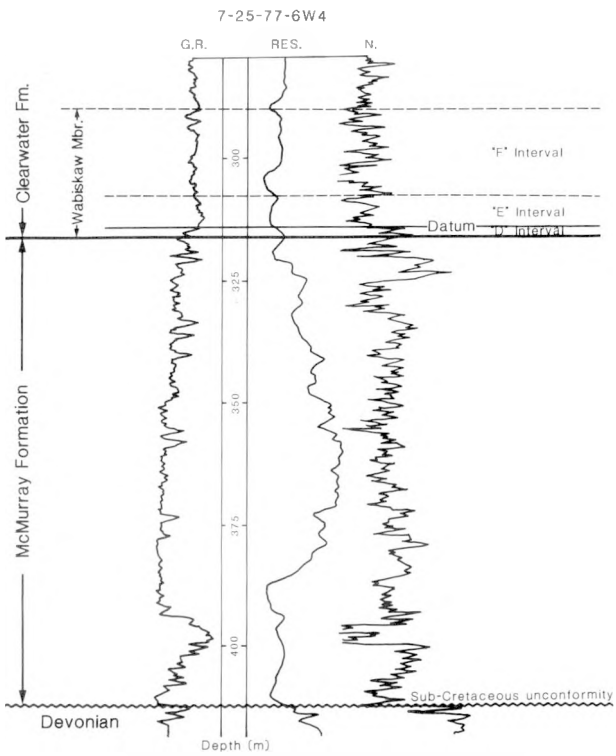

Figure 4. Rrepresentative well for the Athabasca South area (datum present).

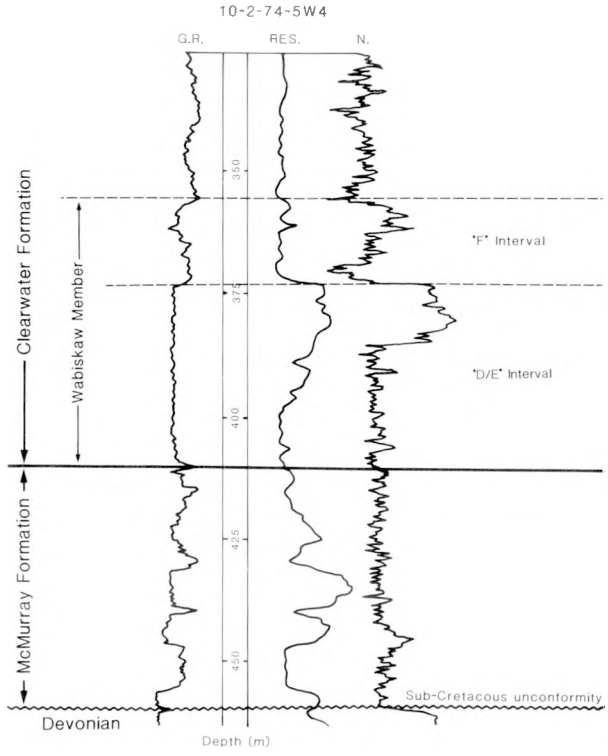

Figure 5. Representative well for the Athabasca South area (datum absent).

mapping purposes in this area the top of the McMurray Formation is the base of the thick Wabiskaw Member sand.

Geological Setting

The McMurray Formation thickness is mainly controlled by the topography on the sub-Cretaceous unconformity. Assuming the top of the McMurray Formation to be relatively flat, and ignoring the effects of differential compaction, an isopach map of the McMurray Formation (Fig. 6) will produce a "mold" of the sub-Cretaceous unconformity surface.[4,10,11]

During McMurray Formation time the sub-Cretaceous unconformity was lowest in the east due to salt dissolution within the underlying Middle Devonian Elk Point Group. Resultant McMurray Formation deposition was in excess of 100 m within these paleotopographic lows. To the west and southwest is a paleotopographic high, identified as the Wainwright Ridge; it was formed by resistant units in the Late Devonian strata.[10,11] This ridge has been traced farther north by Keith et al. into the Athabasca Central area and named the "Grosmont High" after the formation from which it is composed.[3,4] The McMurray Formation thins to less than 10 m over the Wainwright Ridge. A spur of the Wainwright Ridge trends north-south through the moderately thick (30 to 60 m) McMurray Formation of the central part of the study area. Over parts of the spur the McMurray Formation thins to less than 30 m. This overall ridge and valley topography of the study area has been recognized from regional maps of the McMurray Formation.[13]

By the end of McMurray Formation time, the topographic lows had been filled. The transgression of the boreal sea led to the deposition of the Clearwater Formation sands and shales in a marine environment. The relatively even distribution of the Wabiskaw Member sands and shales is readily apparent from the Wabiskaw Member isopach map (Fig. 7). In the east-central region the Wabiskaw Member thickens (exceeding 50 m). This is the area discussed previously where the datum shale is absent. In the southeast region, deltaic sands of the Clearwater Formation are present.[14] The southern Clearwater Formation sands are outside the scope of this study and thus will not be discussed.

Resource Distribution

The blocky channel sands of the McMurray Formation and the thick Wabiskaw Member sand form the main reservoirs within the study area. A location map of all McMurray Formation and Wabiskaw Member pilot sites (Fig. 8) indicates the proximity of the insitu recovery projects to these sands.

McMurray Formation

The McMurray Formation sands are unconsolidated, subangular to subrounded, fine grained, quartzose to subquartzose. McMurray Formation sands are more quartzose (Fig. 9) and cleaner than Wabiskaw Member sands but do contain trace amounts of kaolinite and illite.

Two thick sand trends are evident within the McMurray Formation (Fig. 10). These thick sands

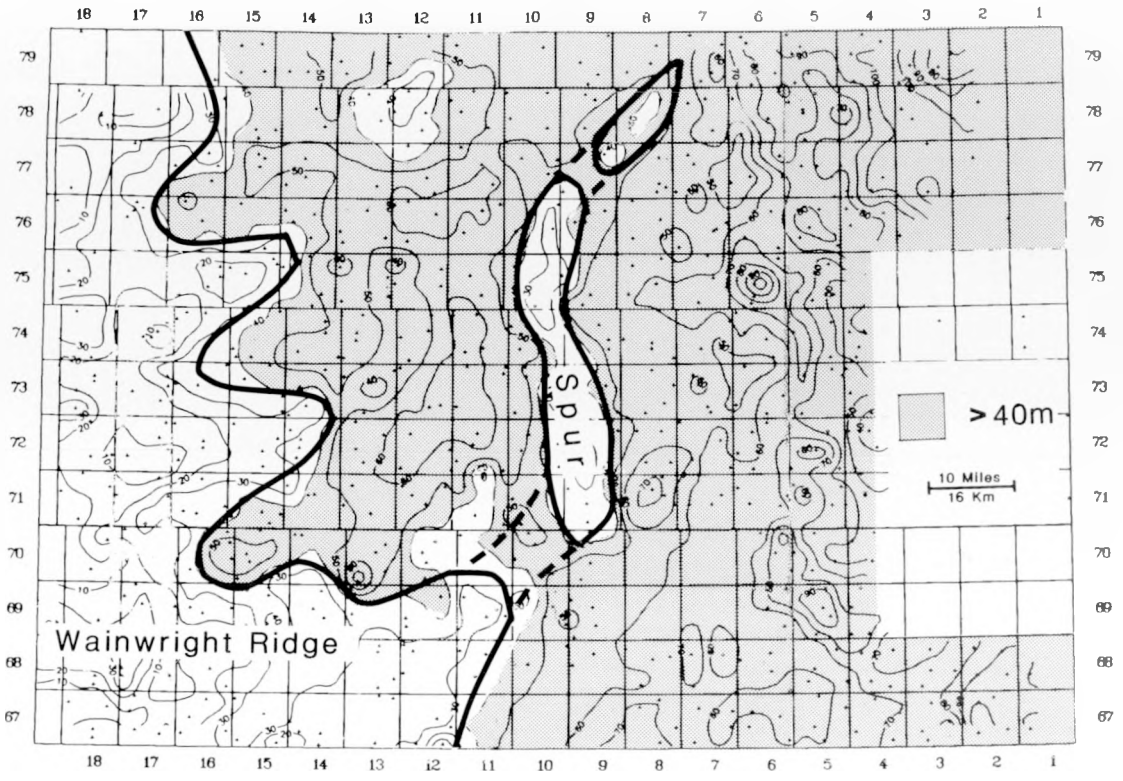

Figure 6. Isopach map in metres from the datum to the sub-Cretaceous unconformity approximating the McMurray Formation isopach map. Contour interval is 10 m and isopach values of greater then 40 m are shaded. McMurray Formation "thins" reflect underlying Paleozoic structural highs; these are labelled Wainwright Ridge and Spur.

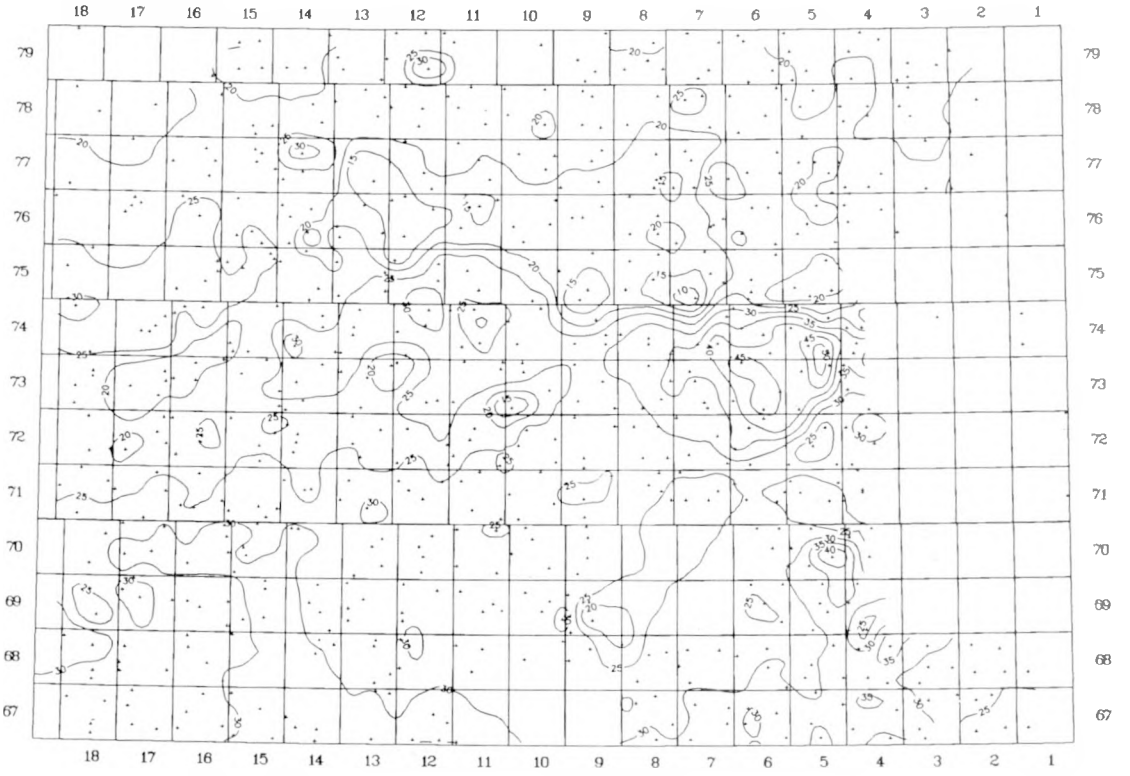

Figure 7. Isopach map of the Wabiskaw Member. Contour interval is 10 m.

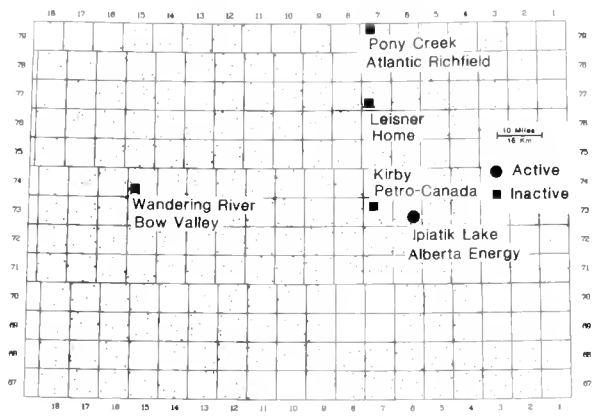

Figure 8. Location of currently active (circles) and inactive (squares) pilot sites.

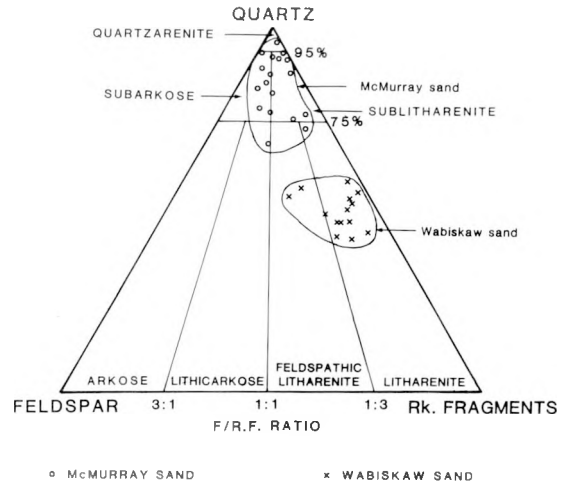

Figure 9. Framework composition of the McMurray Formation and Wabiskaw Member sands.

trend north-south and correspond to the paleotopographic lows indicated on the McMurray Formation isopach (Fig 6). Keith et al. referred to the northern extension of these trends as the main and secondary valley systems.[3,4] The eastern, or main valley system, exceeds thicknesses of 80 m of sand over the area of underlying salt dissolution. These very thick sands are restricted to the northeast and southwest corners of the study area. The rest of the main valley system has between 20 and 50 m of sand. The secondary valley system generally has thicknesses of between 20 to 30 m of sand (Fig. 10). Three sand bodies of between 10 to 20 m thickness trend generally east-west off the Wainwright Ridge and appear to be tributary systems of the secondary valley system.

The thickest oil sands are concentrated in the northern half of the main valley system (Fig. 11). Up to 50 m of oil sands (greater than 6 weight percent bitumen) are present in localized areas. The southern half of the main valley and the northern portion of the secondary valley have between 5 and 15 metres of oil sands. Bitumen distribution is controlled by the availability of clean sand to serve as a reservoir. The location of the best McMurray Formation reservoirs are therefore closely related to the distribution of the channel sands within the valley systems.

Water and bottom water sands were defined as those sands containing less than 3 weight percent bitumen. Bottom water sands are differentiated from water sands by being either in contact with, or within a metre or less of, overlying bitumen sands (greater than 3 weight percent bitumen). The water sands (Fig. 12) are best developed in the northeast corner (greater than 70 m) and the southeast corner (greater than 60 m) within the thick main valley sands overlying the area of salt dissolution. The rest of the water sands are generally restricted to the southern two thirds of the study area and occur within the two valley systems and their tributaries.

The bottom water sands (Fig. 13) are best developed along the bitumen/water contact in the northeast updip corner of the reservoir and in the central part of the main valley system sands. Other smaller occurrences are scattered throughout the valley systems. Bottom water sands can play an important part in recovery strategies.[2,15,16,17]

McMurray Formation gas sands (Fig. 14) are present in the northern part of the main and secondary valley systems. The most extensive gas sands are in the northeast corner where they exceed thicknesses of 10 m. The gas is trapped structurally along the updip end of the reservoir in local highs in the area of salt dissolution. Another gas sand occurs in the northern part of the secondary valley system and is trapped within a local structural high.

Two major bitumen/water contacts are present within the McMurray Formation. An abrupt bitumen/water contact is in the northeast corner of the study area. Here the transition from thick oil sands (Fig. 11) to thick water sands (Fig. 12) occurs within a single township (9.6 km, 6 miles). From the structural cross section through the bitumen/water contact (Fig. 15) it can be seen that, while this contact occurs within the area of underlying salt dissolution, the controls on bitumen entrapment are not structural.

While the discontinuous nature of the McMurray Formation sands is evident from the cross section (Fig. 15), the bitumen did manage to migrate around the thick shales of the 6-20-77-5W4 well and into the upper sands of the 7-22-77-5W4 well. This suggests that communication existed among the sands between these wells and that the facies changes of the thick valley system sands do not account for the bitumen trapping.

The bitumen trapping mechanism appears to be similar to that described by MacGillivray et al.

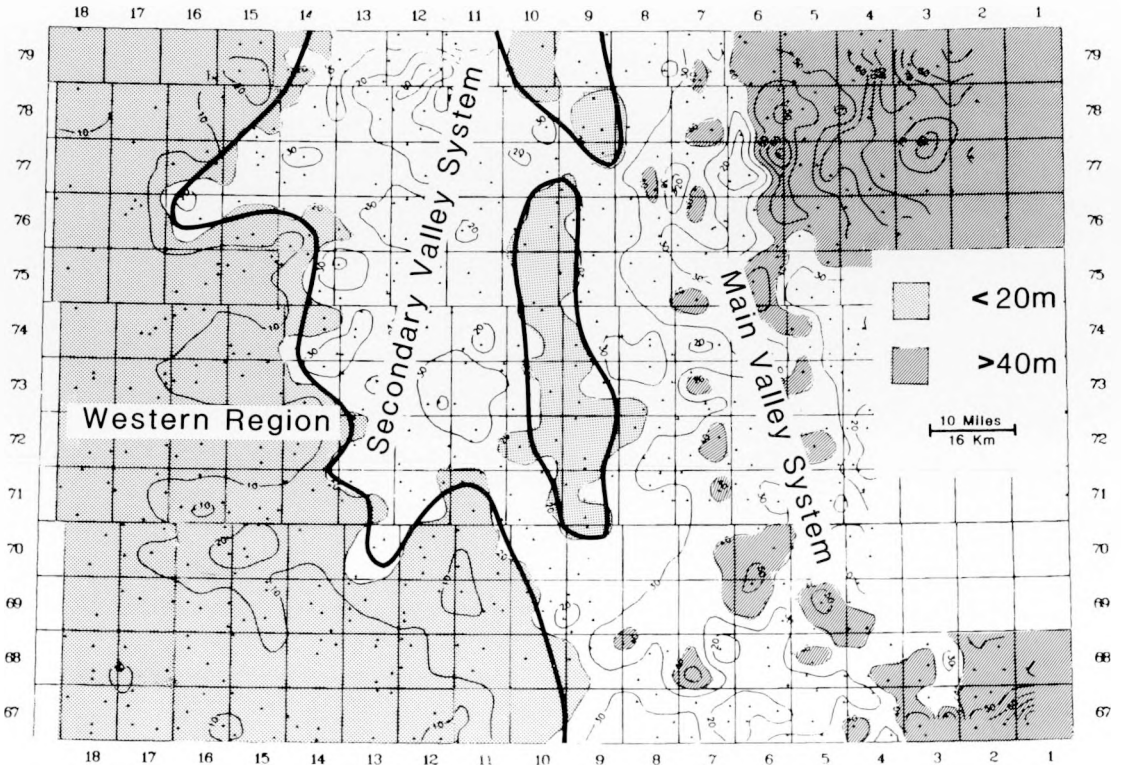

Figure 10. Isopach map of total sands within the McMurray Formation; thin sands in the western region and thicker sands of the main and secondary valley systems in the eastern part of the study area. The contour interval is 10 m. Isopach values less than 20 m are in light shading and those greater than 50 m are in dark shading.

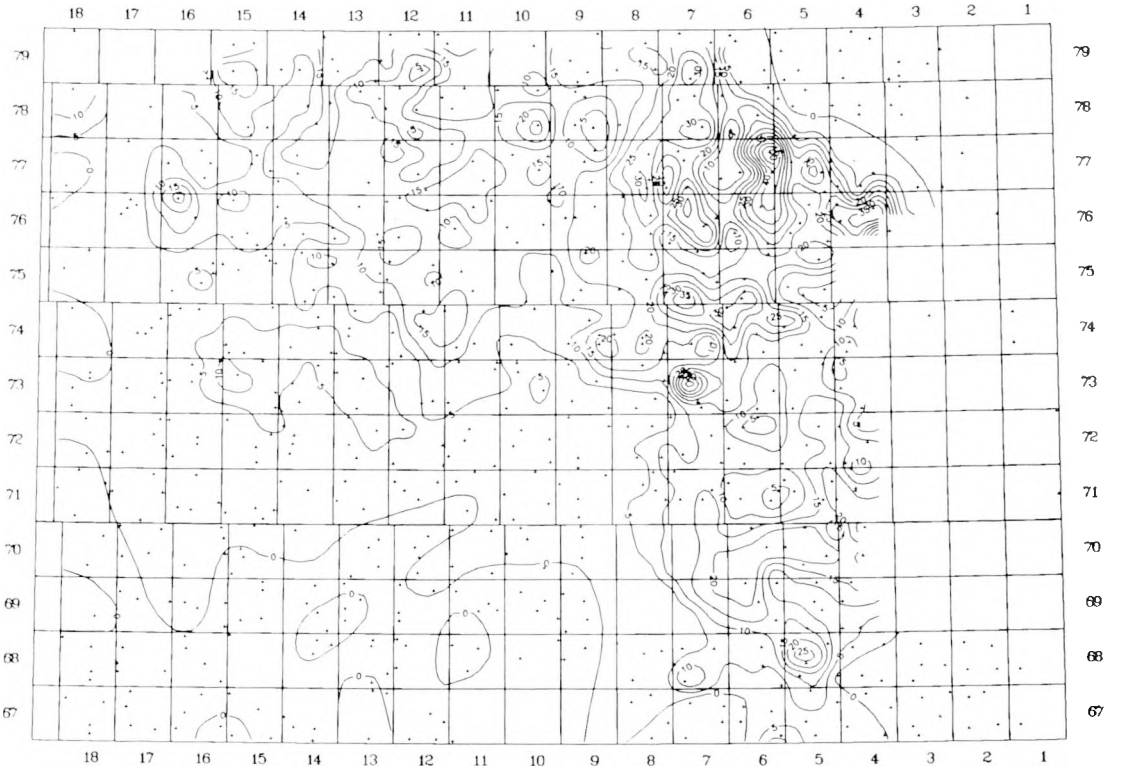

Figure 11. Isopach map of McMurray Formation sands with greater than 6 weight percent bitumen. Contour interval is 5 m.

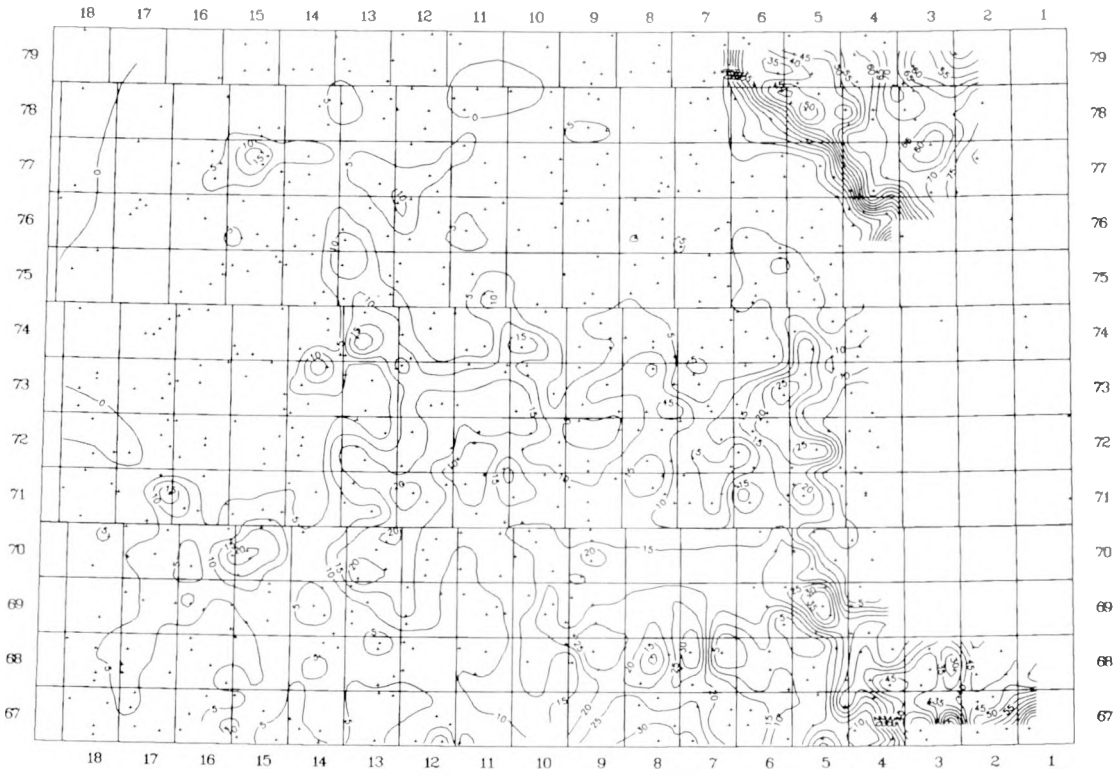

Figure 12. Isopach map of McMurray Formation water sands. Contour interval is 5 m.

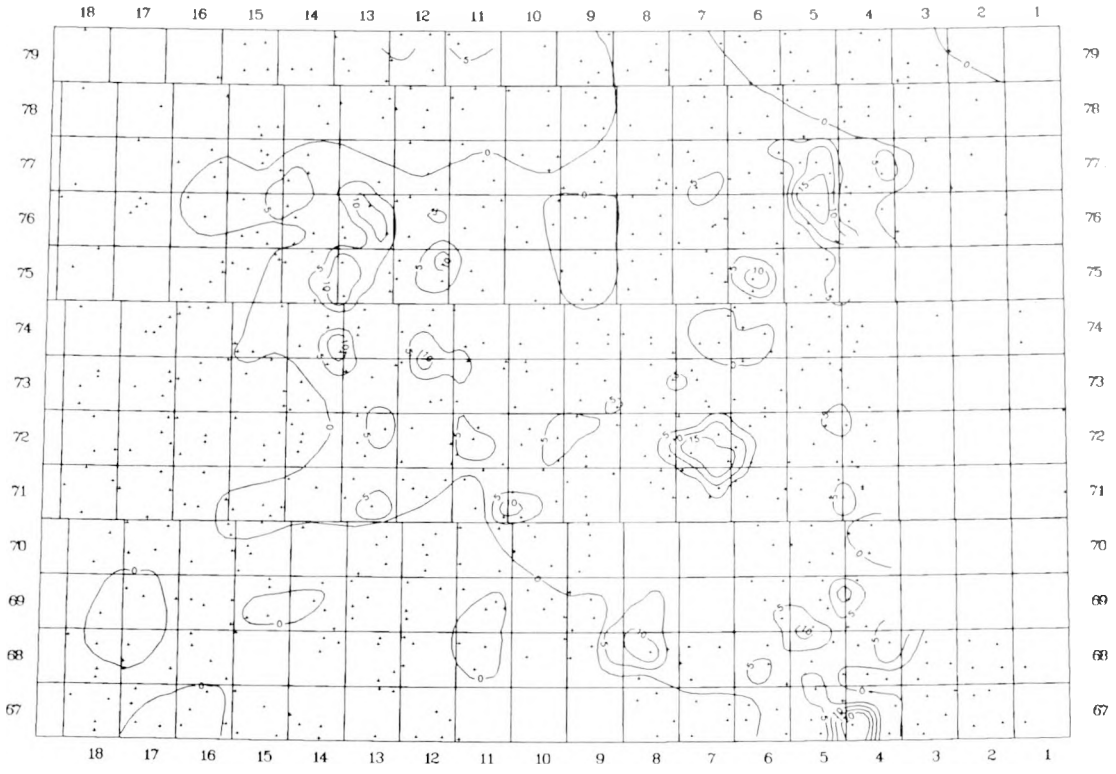

Figure 13. Isopach map of McMurray Formation bottom water sands. Contour interval is 5 m.

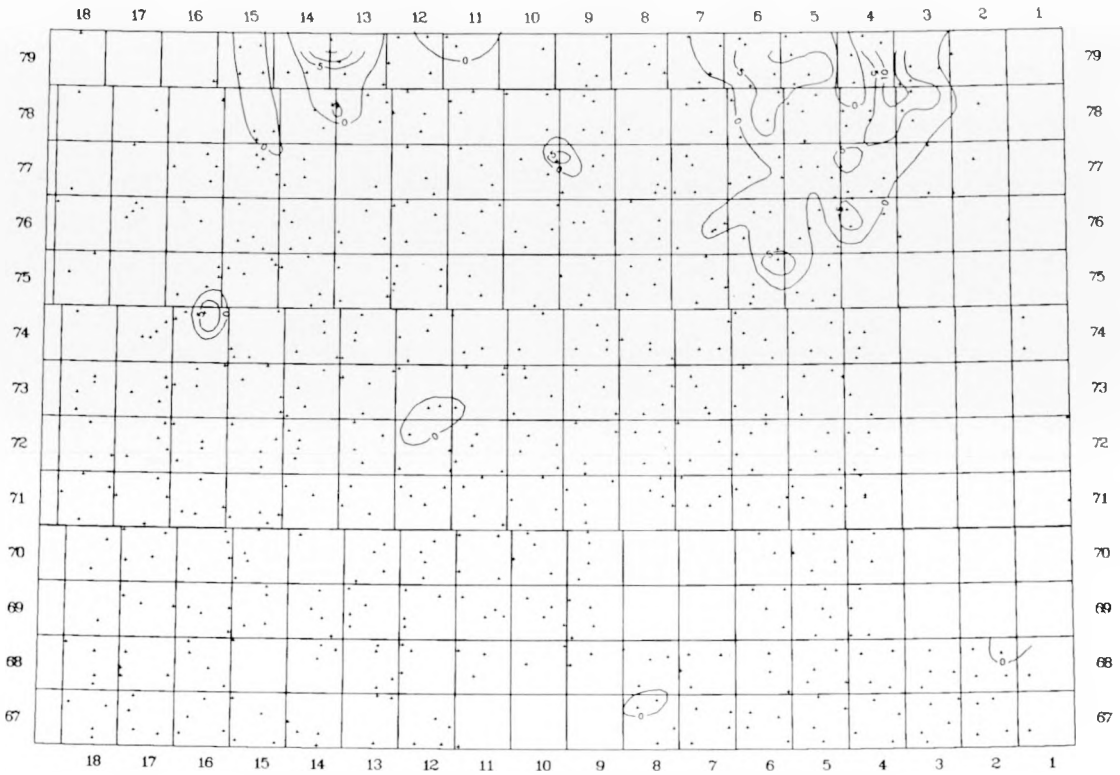

Figure 14. Isopach map of McMurray Formation gas sands. Contour interval is 5 m.

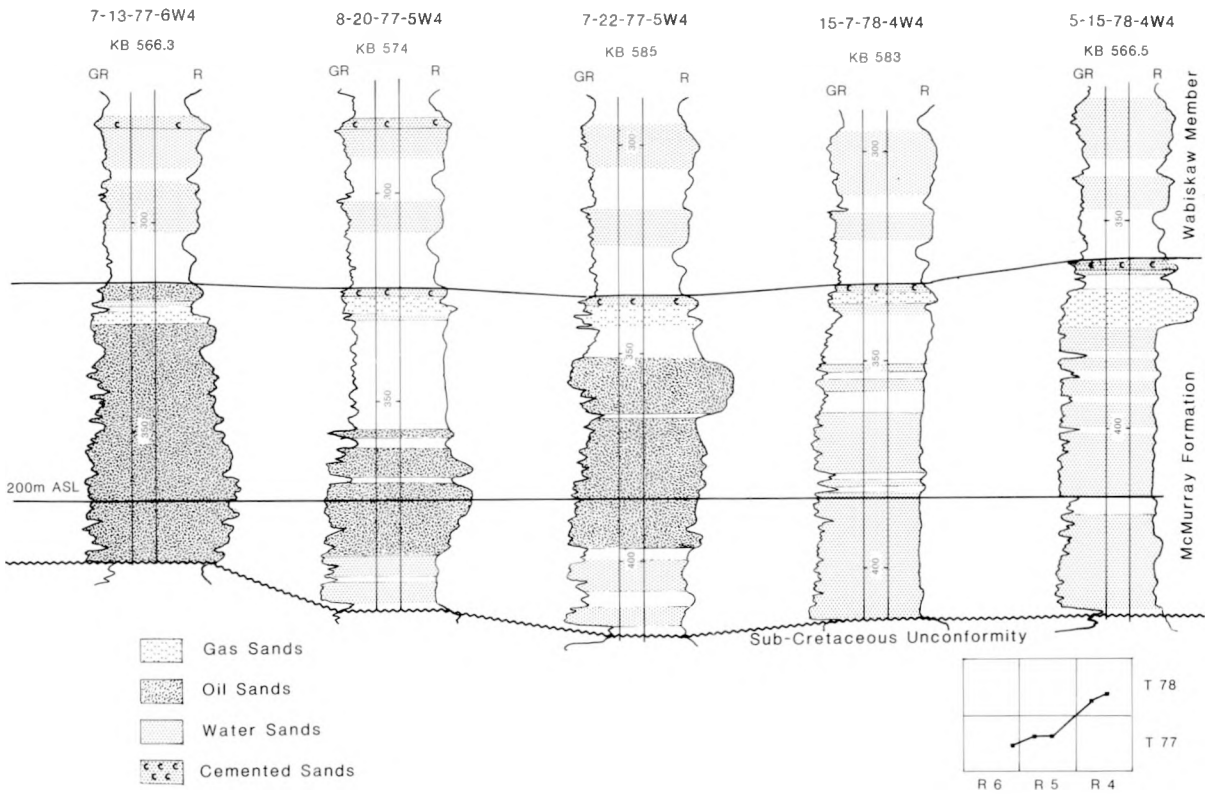

Figure 15. Structural cross section through the bitumen/water contact in the northeast corner of the study area. Gas sands are lightly shaded, water sands have intermediate shading, and oil sands are darkly shaded.

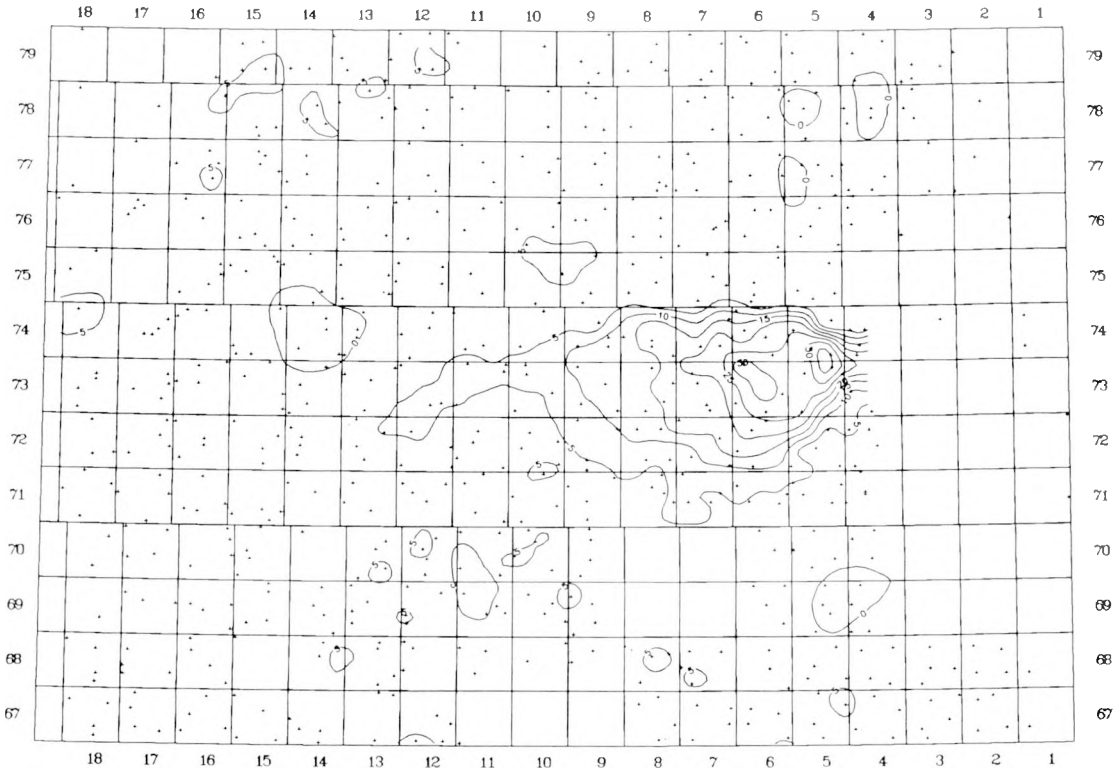

Figure 16. Isopach map of Wabiskaw Member sands. Contour interval is 5 m.

for the Athabasca Central study area.[5] The bitumen is thought to have originated in the deeper parts of the basin to the west and migrated eastward updip.[18,19] The Clearwater Formation shales act as a cap rock for the reservoir and the final termination of bitumen migration appears to have occurred when the bitumen was biodegraded to the point of immobility.[18,20]

The second bitumen/water contact occurs along the southern portion of the secondary valley system. This bitumen/water contact is mainly structural in nature and the water sands represent the downdip portion of the reservoir.

Wabiskaw Member

The Wabiskaw Member sands are unconsolidated, angular to subangular, poorly sorted, muddy sands with varying amounts of glauconite (as high as 16% by volume). They are classified as litharenites and feldspathic litharenites (Fig. 9). Feldspar alteration is common and the main clay mineral constituent is kaolinite. Illite, smectite, and chlorite are also present.[21]

The Wabiskaw Member consists of two intervals that contain sands: the "E" and "F" intervals (Fig. 4). This paper is concerned primarily with the lower of these, the "E" interval. Wabiskaw Member "E" sands (Fig. 16) are generally less than 5 m thick throughout the study area except for the east-central region where they exceed 35 metres thickness. These sands have been interpreted by Decker et al. as marine delta front sands.[21]

Within the "E" interval of the Wabiskaw Member the bitumen is restricted to the thick sand (Fig. 17) where over 25 m of bitumen saturated sand (greater than 6 weight percent bitumen) occurs. Water sands (less than 5 m thick) occur throughout the study area (Fig. 18) and are present along the southwest (5 m thick) and eastern (15 m thick) edges of the thick Wabiskaw Member sand. Bottom water sands (Fig. 19) occur only in the thick Wabiskaw Member sand (less than 10 m thick) and are present at both its updip and downdip ends. Gas sands (Fig. 20) within the Wabiskaw Member occur only along the eastern updip mapped limit of the thick sand.

The relationship of the formation fluids and the continuity of the Wabiskaw Member sands can be observed from the cross section through the thick east-central Wabiskaw Member sand (Fig. 21). While there is a structural flexure in the sand it does not appear to be great enough to provide structural closure of the reservoir in the east. The trapping mechanism for the Wabiskaw Member bitumen appears to be in part facies dependent (as the bitumen is restricted to the sand body), with the overlying Wabiskaw Member shales forming the cap rock, and bitumen biodegradation playing an important role in the final trapping. The occurrence of bottom water in the updip end of the reservoir is due to the bitumen trapping mechanism. The Wabiskaw Member gas is trapped structurally in the updip end of the sand.

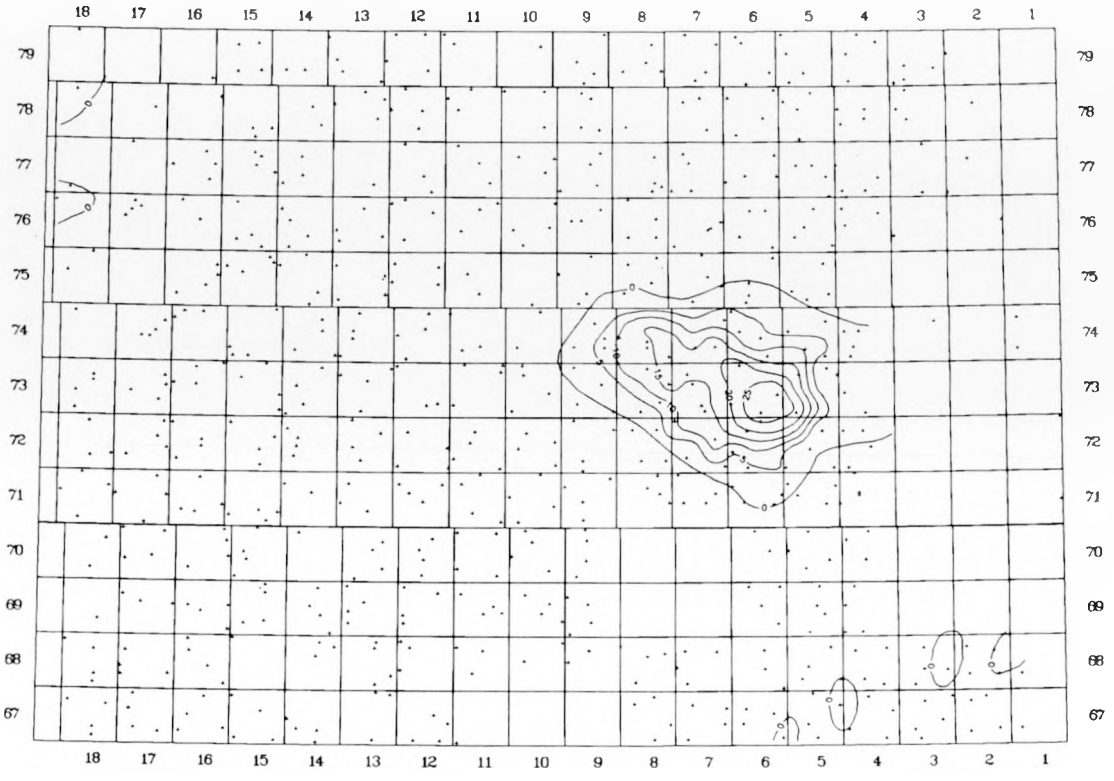

Figure 17. Isopach map of Wabiskaw Member sands with greater than 6 weight percent bitumen. Contour interval is 5 m.

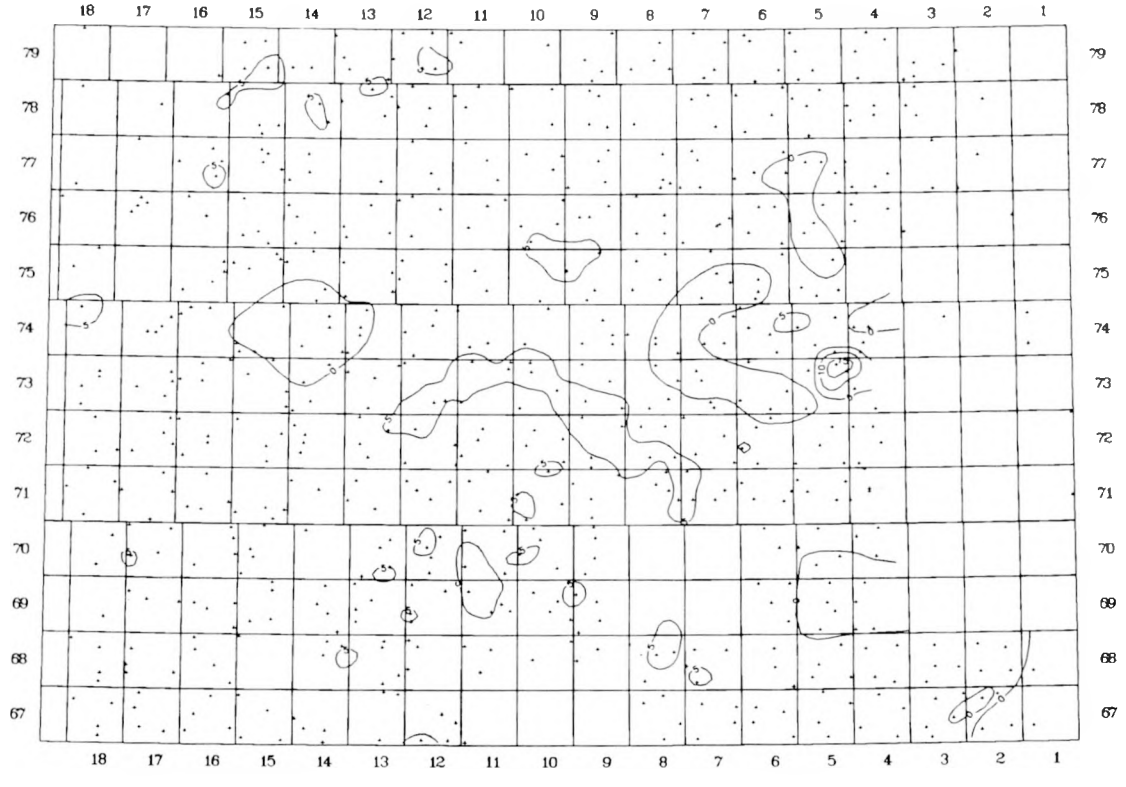

Figure 18. Isopach map of Wabiskaw Member water sands. Contour interval is 5 m.

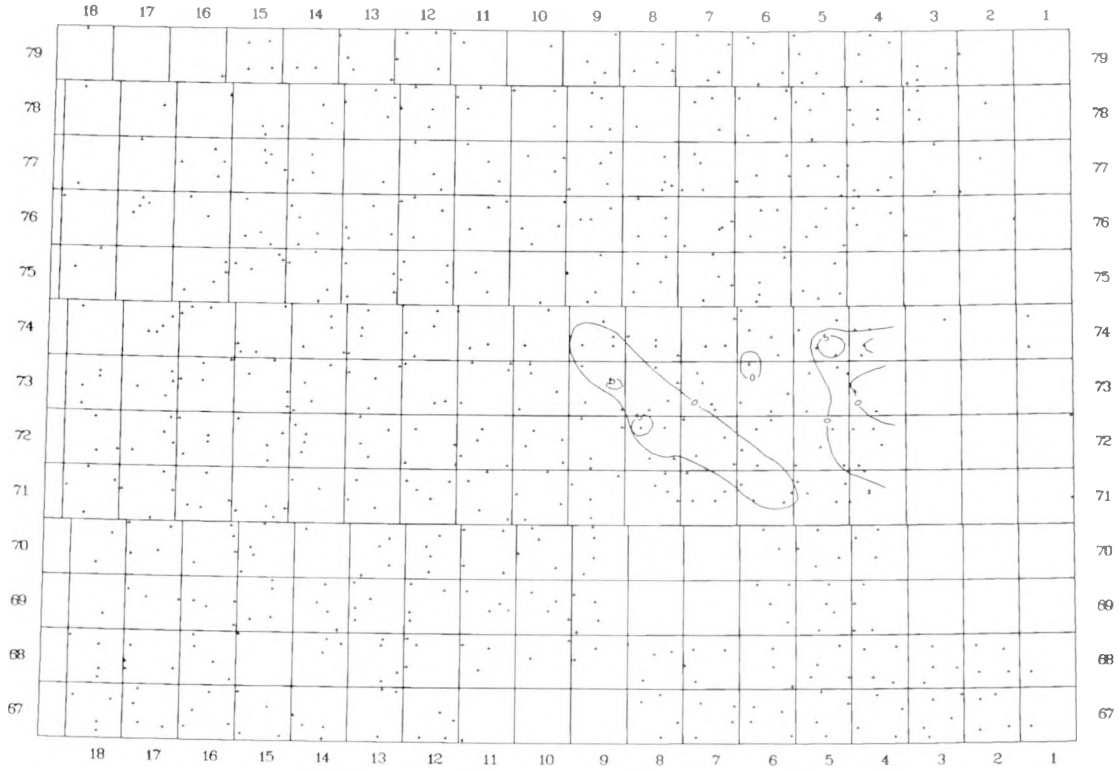

Figure 19. Isopach map of Wabiskaw Member bottom water sands. Contour interval is 5 m.

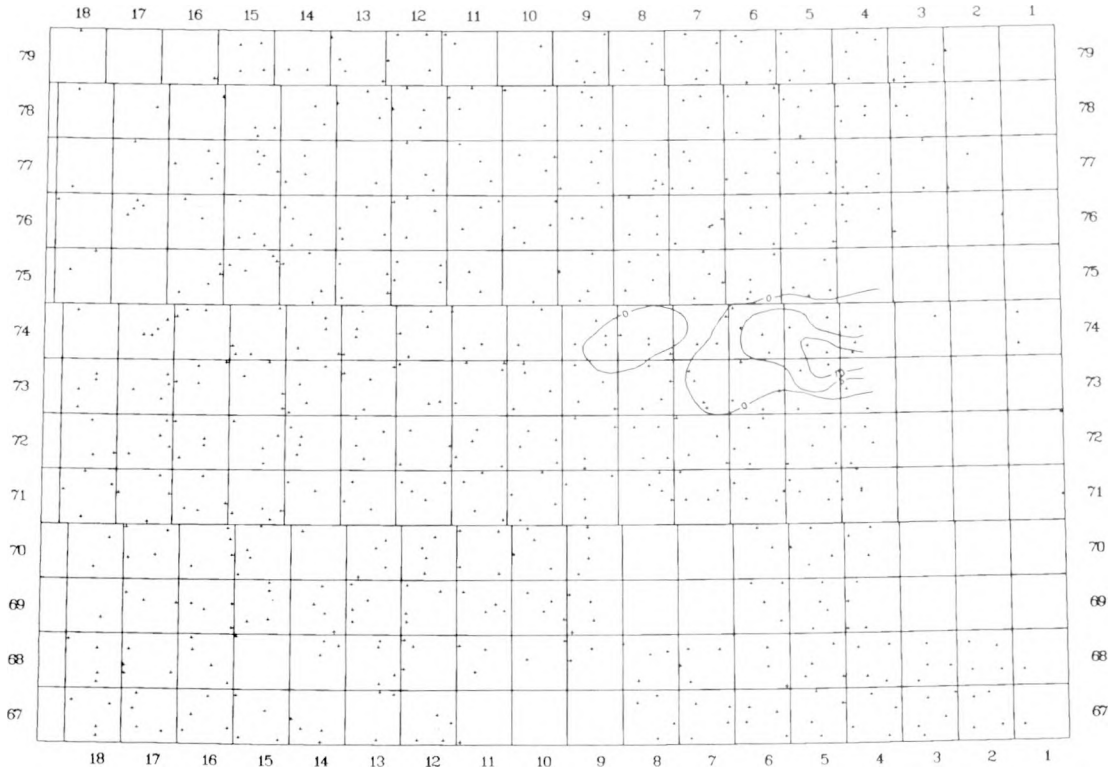

Figure 20. Isopach map of Wabiskaw Member gas sands. Contour interval is 5 m.

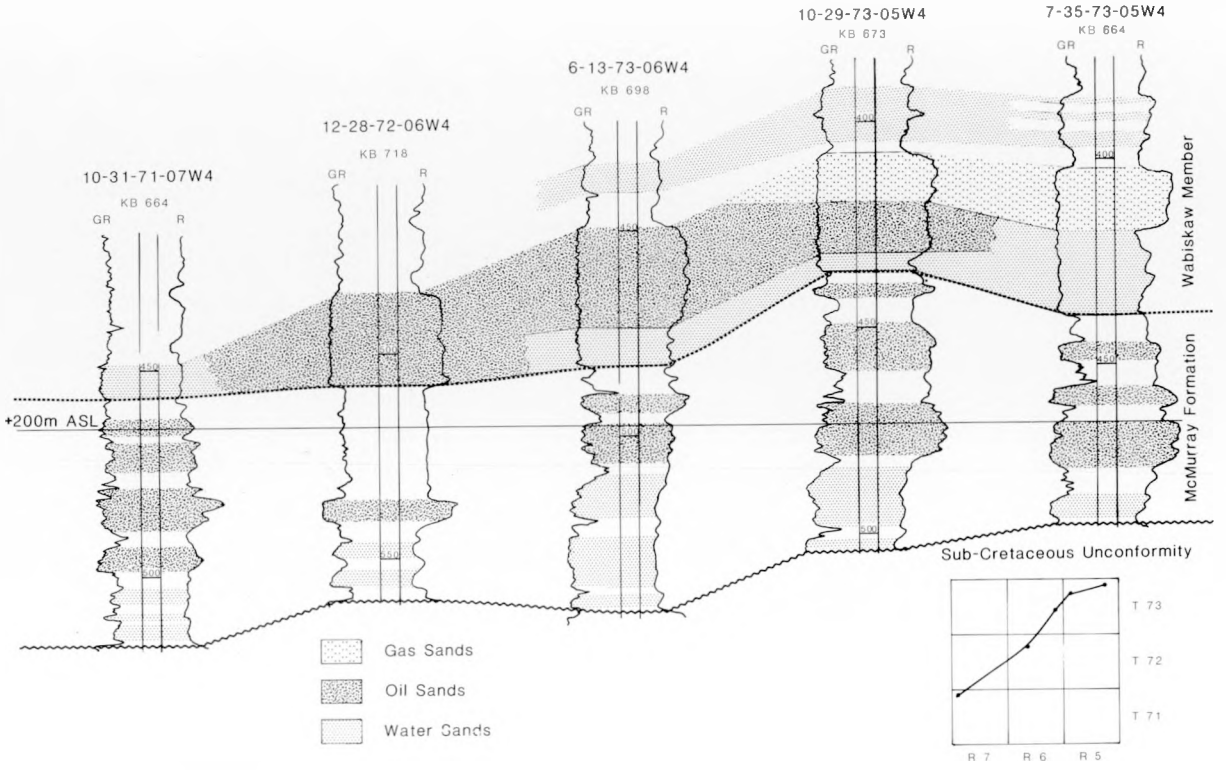

Figure 21. Structural cross section through the east-central Wabiskaw Member sand. Gas sands are lightly shaded, water sands have intermediate shading, and oil sands are darkly shaded.

Summary

The bitumen and gas distribution within the study area is controlled by the availability of clean sands. The McMurray Formation valley system sands and the thick sand of the Wabiskaw Member form the best reservoirs. The sands of the McMurray Formation tend to be thicker but lack the lateral continuity of the Wabiskaw Member sands. The bitumen migrated updip in both reservoirs and its biodegradation played a major role in the trapping mechanism. Bottom water is associated with both reservoirs in their updip end. The gas is trapped structurally in both the McMurray Formation and the Wabiskaw Member.

Conclusions

1. The best McMurray Formation reservoir in the study area is the northern half of the main valley system.
2. The McMurray Formation gas is structurally trapped and occurs in areas of local structural highs.
3. The bitumen trapping mechanism for the McMurray Formation is mainly due to bitumen biodegradation in the east and structure in the southwest.
4. The major Wabiskaw Member reservoir is a thick sand deposited in the east-central region of the study area.
5. Gas trapping within the Wabiskaw Member is controlled by facies and structure.
6. Bitumen trapping within the Wabiskaw Member is a combination of facies and bitumen biodegradation.

Acknowledgments

The authors gratefully acknowledge the funding provided by the Alberta Oil Sands Technology and Research Authority, the Department of Alberta Energy, and the Alberta Research Council for this project. The assistance of Robert Hale in refining the graphics software, and Kelly Roberts and Parminder Sahota for taking special care of the plotter was also most appreciated.

References

1. Alberta Energy Resources Conservation Board, "Atlas of Alberta's Crude Bitumen Reserves," Energy Resources Conservation Board Reserve Report Series 38, 51 p., 1984.

2. Flach, P.D., "Oil Sands Geology - Athabasca Deposit North," Alberta Research Council, Bulletin 46, 31 p., 1984.

3. Keith, D.A.W., D.M. Wightman, S.G. Pemberton, J.R. MacGillivray, T. Berezniuk, and H. Berhane, "Fluvial, Estuarine and Shallow Marine Sedimentation in the Lower Cretaceous McMurray Formation and Wabiskaw Member (Clearwater Formation), Athabasca Oil Sands Area, Alberta," UNITAR Fourth International Conference on Heavy Oil and Tar Sands, Edmonton, Alberta, pp. 53-78, August 1988.

4. Keith, D.A.W., D.M. Wightman, S.G. Pemberton, J.R. MacGillivray, T. Berezniuk and H. Berhane, "Sedimentology of the McMurray Formation and Wabiskaw Member (Clearwater

Formation), Lower Cretaceous, in the Central Region of the Athabasca Oil Sands Area, Northeastern Alberta," in James, D.P. and D.A. Leckie (Ed.), "Sequences, Stratigraphy, Sedimentology: Surface and Subsurface", Canadian Society of Petroleum Geologists Memoir 15, pp. 309-324, 1988.

5. MacGillivray, J.R., D.M. Wightman, D.A.W. Keith, D.D. Bell, H. Berhane and T. Berezniuk, "Resource Characterization of the Central Region of the Lower Cretaceous McMurray/Wabiskaw Deposit, Athabasca Oil Sands Area, Northeastern Alberta," UNITAR Fourth International Conference on Heavy Crude and Tar Sands," Edmonton, Alberta, pp. 109-132, August 1988.

6. Hume, G.S., "Results and Significance of Drilling Operations in the Athabasca Bituminous Sands," Transactions of the Canadian Institute of Mining and Metallurgy, v. 50, pp. 298-333, 1947.

7. Carrigy, M.A., "Geology of the McMurray Formation, Part III, General Geology of the McMurray Area," Alberta Research Council, Memoir 1, 130 p., 1959.

8. Stewart, G.A., "Geological Controls on the Distribution of Athabasca Oil Sands Reserves," in Carrigy M.A. (Ed.), "The K.A. Clark Volume, Papers on the Athabasca Oil Sands," Alberta Research Council, Information Series 45, pp. 15-26, 1963.

9. Martin, R. and F.G.S. Jamin, "Paleogeomorphology of the Buried Devonian Landscape in Northeastern Alberta," in Carrigy, M.A. (Ed.), "The K.A. Clark Volume, Papers on Athabasca Oil Sands," Alberta Research Council, Information Series 45, pp. 31-43, 1963.

10. Williams, G.D., "The Mannville Group (Lower Cretaceous) of Central Alberta," Bulletin of Canadian Petroleum Geology, v. 11, pp. 350-368, 1963.

11. Ranger, M.J. and S.G. Pemberton, "Marine Influence on the McMurray Formation in the Primrose Area, Alberta," in James, D.P. and D.A. Leckie (Ed.), "Sequences, Stratigraphy, Sedimentology: Surface and Subsurface", Canadian Society of Petroleum Geologists Memoir 15, pp. 439-450, 1988.

12. Kramers, J.W., "Geology of the Wabasca A Oil Sand Deposit (Grand Rapids Formation)," in Hills, L.V. (Ed.), "Oil Sands, Fuel of the Future," Canadian Society of Petroleum Geologists, Memoir 3, pp. 68-83, 1974.

13. Ranger, M.J., "The Paleotopography of the pre-Cretaceous Erosional Surface in the Western Canada Basin," (abstract) in Stott, D.F., and D.J. Glass (Ed.), "The Mesozoic of Middle North America," Canadian Society of Petroleum Geologists, Memoir 9, p. 570, 1983.

14. Wightman, D.M., S.G. Pemberton and C. Singh, "Depositional Modeling of the Upper Mannville (Lower Cretaceous), East Central Alberta: Implications for the Recognition of Brackish Water Deposits," in "Reservoir Sedimentology," Society of Economic Paleontologists and Mineralogists Special Publication No. 40, pp. 189-220, 1987.

15. Kasraie, M. and S.M. Farouq Ali, "Steamflooding Bottom Water Reservoirs," Petroleum Society of the CIM, Regina, Saskatchewan, Paper No. 5, October 1987.

16. Kisman, K.E., D.A. Best and J. Huyer, "Water Sands Intervals - An Advantage or Disadvantage?," Alberta Oil Sands Technology and Research Authority Technical Conference, Advances in Petroleum Recovery and Upgrading Technology 1987, Session 1, Paper 3, June 1987.

17. Proctor, M.L., A.E. George and S.M. Farouq Ali, "Steam Injection Strategies for Thin, Bottomwater Reservoirs", Proceedings of the Society of Petroleum Engineers California Regional Meeting, Ventura, California, April 1987.

18. Masters, J.A., "Lower Cretaceous Oil and Gas in Western Canada," in Masters, J.A. (Ed.), "Elmworth - Case Study of a Deep Basin Gas Field," American Association of Petroleum Geologists, Memoir 38, pp. 1-33, 1984.

19. Moshier, S.O. and D.W. Waples, "Quantitative Evaluation of Lower Cretaceous Mannville Group as Source Rock for Alberta's Oil Sands," American Association of Petroleum Geologists Bulletin, v. 69, pp. 161-172, 1985.

20. Mossop, G.D., "Geology of the Athabasca Oil Sands," Science, v. 207, pp. 145-152, 1980.

21. Dekker, F., C. Visser and P. Dankers, "The Primrose-Kirby Area in the Southern Athabasca, Alberta, Canada: A Detailed Geological Investigation," American Association of Petroleum Geologists, Studies in Geology no. 25, pp. 507-520, 1987.

Heavy Crude and Tar Sand Resources in the Soviet Union

by

Gerard S. Medaisko
UNITAR/UNDP Information Centre for Heavy Crude and Tar Sands
United Nations, New York, N.Y. 10017

In the Soviet Union, deposits of Heavy Crude and Tar Sands are widespread. Ultimate resources of heavy oil and natural bitumen are large, possibly larger even than conventional crude resources.

Heavy oil resources in the USSR have been estimated variously at 200 to 900 billion barrel-in-place, five (5) to ten (10) percent of which falls into the "Reserves" category, and natural bitumen-in-place at anywhere between 800 to 1,153 billion barrel. The UNITAR/UNDP (*) Information Centre for Heavy Crude and Tar Sands (INFOCEN) carries several other sets of figures but has strong reservations about considering any of these figures as reliable. The discrepancies can be explained by the fact that accurate data on Russian heavy oil and bitumen is lacking, owing to their limited production which represents but a small percentage of the 4.6 billion barrel of crude and condensate which the Soviets will be producing in 1989, assuming predicted outputs meet targets.

For Soviet Scientists, the definition of heavy oil and bitumen differs to some extent from the definition proposed by INFOCEN at the Caracas 2nd International Conference on Heavy Crude and Tar Sands, in 1982 (Pl. 1). One of the most immediate differences is that Soviet Chemists do not recognize extra heavy crude oil as a separate category; In Russia, all mobile hydrocarbons with viscosities ranging from 30 to several thousand centipoises are regarded as heavy crude whereas bitumen are non mobile or very low mobility hydrocarbons with viscosities up to several million of centipoises (cit. R. Kh. Muslimov). In addition, heavy crude deposits have an oil/water contact whereas in the case of bitumen deposits, the host rock pores themselves often contain free water.

Heavy crude and natural bitumen are encountered practically in every petroleum provinces of the Union, namely: The South Caspian basin (Azerbaijan, Southern Kazakhstan); The Pricaspian basin (Northern

(*) UNITAR is the United Nations Institute for Training and Research. UNDP is the United Nations Development Programme.

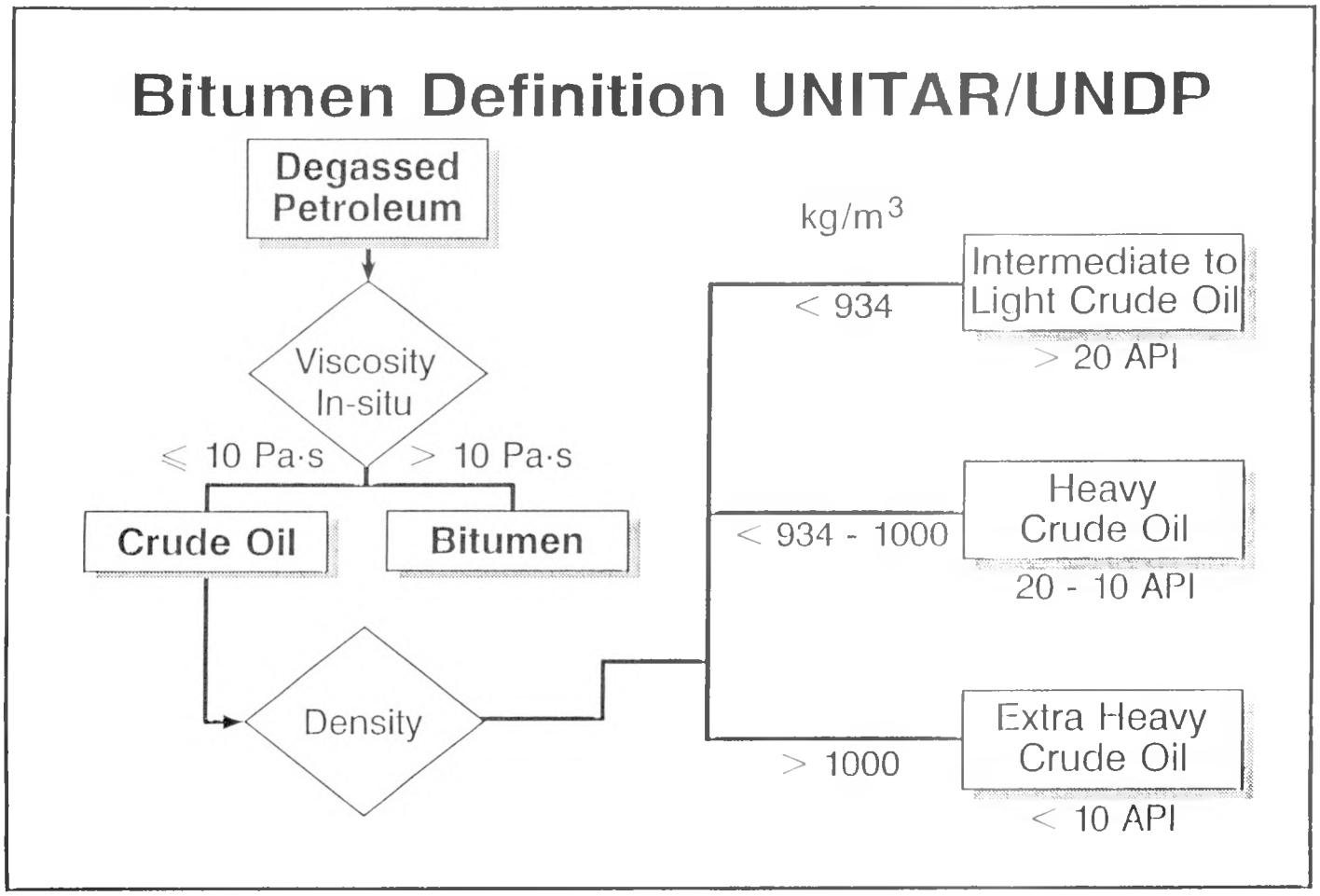
Bitumen Definition UNITAR/UNDP
Degassed Petroleum
Viscosity In-situ
≤ 10 Pa·s
> 10 Pa·s
Crude Oil
Bitumen
Density
kg/m3
< 934
< 934 - 1000
> 1000
Intermediate to Light Crude Oil
> 20 API
Heavy Crude Oil
20 - 10 API
Extra Heavy Crude Oil
< 10 API

Kazakhstan); The Volga-Urals basin (Kuybyshev, Orenburg, Perm, Tataria, Ulyanovsk, Western Bashkiria); The Timan-Pechora basin (Komi); The Pripyat and Dnepr-Donetz basins of Byelorussia; Siberia and the Sakhalin Island. Their stratigraphic range extends from the Vendian (Vendsk)-Cambrian basement of Eastern Siberia to the Quaternary sediments of the South Caspian Region. In 1985, INFOCEN published a catalog of the main deposits in U.S.S.R. which is in the process of being up-dated.

The main deposit areas are shown on Plate 2. Geographically, they lie on both sides of the Urals, in the European part of Russia to the west, as well as in the Asiatic part (Western and Eastern Siberia, and Sakhalin Island) to the east.

For a long time, it was thought that the bulk of heavy oil and tar resources had accumulated west of the Ural Mountains, but a recent reassessment made the pendulum swing toward the Asian part of the country. There are over 1000 known accumulations of heavy oil and natural bitumen in the Soviet Union, some 400 of which are located west of the Urals while the rest are in Siberia or the Russian Far East. However, most activities in relation with the exploration, production, processing and up-grading of heavy crude are concentrated to-day in Western U.S.S.R., in the broad Volga-Urals basin which extends from the Caspian Sea in the south to the Franz Yosef Islands in the north.

From a geological standpoint, there seems to be a more complex habitat than the simple divisions described in the previous chapter. To the west of the Urals, heavy oil and bitumen resources are associated with platform deposits related to the Fino-Baltic basement shield. East of the Urals, they are found within platform deposits which are associated with the Sino-Siberian basement shield, except for the Sakhalin Island fields which are directly related to the Circum Pacific orogenic system. The Euro-Siberian platform area is rather stable, whereas the Circum Pacific belt is an active orogen characterized by a series of interactive horst and graben features. Finally, in the southern part of the country, heavy crude and bitumen are related to the great Alpine orogenic belt which extends in an east-west direction, from China to Spain.

Another feature of Russian heavy oil and bitumen occurences is that more often they are associated with carbonate reservoirs (70%) than with sand and sandstone rocks. This fact is hindering production and necessitates using specialized EOR methods.

In the following chapters, the main occurences of heavy oil and bitumen in the U.S.S.R. will be reviewed briefly.

1. WESTERN U.S.S.R.

West of the Volga-Urals range of mountains, the main heavy crude deposits are found in the South Caspian basin (Azerbaijan ASSR (*) and Southern Kazakhstan SSR (*); the Pricaspian basin (Northern Kazakhstan SSR); the Volga-Urals basin (Tataria ASSR, Kuibyshev region, Orenburg region, Ul'yanovsk region, Western Bashkiria region); the Timan-Pechora or Timano-Pechorsky basin (Komi ASSR); the North Caucasus area and in Byelorussia. As to the main natural bitumen resources, they are encountered in the South Caspian basin, the Volga-Urals basin, the Timan-Pechora basin as well as in Ukraine.

1.1 SOUTH CASPIAN BASIN

The South Caspian basin covers essentially the Azerbaijan and part of the Kazakhstan Republics.

1.1.1 Azerbaijan Republic

Located on the western shore of the Caspian Sea in a North Caucasus platform basin: the Kura basin, the Azerbaijan Republic contains over 25 heavy oil fields in and around the Baku area, on the Apsheron Peninsula, and some 10 high-grade bitumen deposits.

Heavy oil reserves-in-place are estimated at over 210 million barrels and natural bitumen-in-place at 30-50 million barrels. These figures are small and probably well below the potential of the area.

(*) ASSR stands for Autonomous Soviet Socialist Republic. SSR stands for Soviet Socialist Republic.

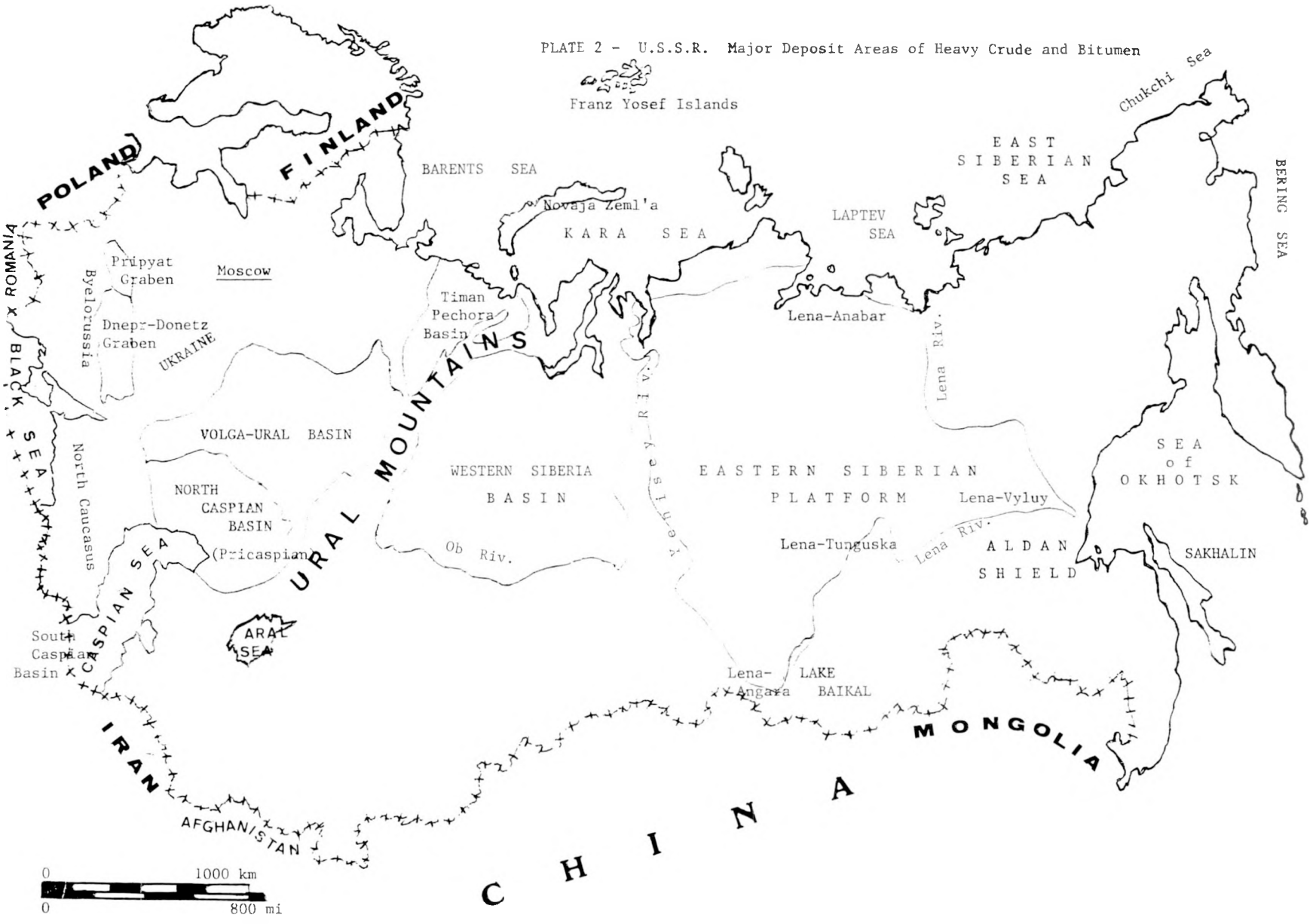
PLATE 2 - U.S.S.R. Major Deposit Areas of Heavy Crude and Bitumen
Franz Yosef Islands
Chukchi Sea
BERING SEA
EAST SIBERIAN SEA
BARENTS SEA
Novaja Zeml'a
KARA SEA
LAPTEV SEA
FINLAND
POLAND
ROMANIA
BLACK SEA
Pripyat Graben
Moscow
Byelorussia
Dnepr-Donetz Graben
UKRAINE
Timan Pechora Basin
URAL MOUNTAINS
Yenisey Riv.
Lena-Anabar
Lena Riv.
VOLGA-URAL BASIN
North Caucasus
NORTH CASPIAN BASIN
(Pricaspian)
CASPIAN SEA
WESTERN SIBERIA BASIN
EASTERN SIBERIAN PLATFORM
Lena-Vyluy
Ob Riv.
Lena-Tunguska
Lena Riv.
ALDAN SHIELD
SEA of OKHOTSK
SAKHALIN
ARAL SEA
South Caspian Basin
Lena-Angara
LAKE BAIKAL
IRAN
AFGHANISTAN
MONGOLIA
CHINA
0 1000 km
0 800 mi

Baku is the oldest petroleum province in the Soviet Union. Commercial production of conventional oil was established there in 1871 and fields like Balakhany, Binagady, Romany, Sabunvich (Sabunchy), etc., have continuously been in production ever since, from a Middle Pliocene sandstone reservoir. Starting around 1910, new fields at Akhtarma-Pashalin, Cheildag, El'daroyuginsk, Lokbatan, Shubany, Tulkitepe and Umbaki, were added to the old ones, many of them producing from a Miocene sandstone. Most of these fields contain heavy oil and natural bitumen as well as lighter oil. Of all the fields in the Kura basin, Tulkitepe is probably the most significant.

Underground oil mining was attempted in Shubany from 1923 to 1935 but it was an economic failure. More recently, EOR efforts were renewed: Steam-soak operations were started in Lokbatan in 1972 and are continuing to this day. Underground thermal mining has been underway in Balakhany field since 1975 and is yielding approximately 4,000 b/d. Soft terranes and abundant natural gas combine to render operations difficult and hazardous. Otherwise, the recovery project is patterned after that at Yarega which will be examined later in this paper, under paragraph 1.4.1. There have been attempts at fire-flooding the Umbaki field reservoirs which yield 13.6 and 16.5° API oil while foam injection and surfactants have been tried in other fields (cit. Richard Meyer and A.A. Meyerhoff).

The largest bitumen deposit in the Kura basin is at Cheildag, 24 km southwest of Baku, on the Caspian shoreline. The bitumen fills the pores of a Miocene sandstone reservoir and reserves have been estimated at 24 million barrels. Like most bitumen deposits in Azerbaijan, Cheildag has been earmarked for open cast mining.

1.1.2 Kazakhstan Republic

Like the Azerbaijan Republic, the southern part of the Kazakhstan Republic, on the eastern edge of the Caspian Sea, occupies one of the several North Caucasus platform basins. The northern part, however, corresponds with the Pricaspian basin (Pricaspiisk).

Heavy oil reserves are estimated at well over 2 billion barrel recoverable, while bitumen resources in excess of 2.1 billion barrel have been identified, according to "Soviet Geography, November 1984 issue".

Among the several locales of interest with respect to heavy oil and natural bitumen are, from north to south: The Buzachi Peninsula fields and the Mangyshlak Peninsula fields.

1.1.2.1 The Buzachi Peninsula fields

The Buzachi Peninsula at the northeastern end of the Caspian Sea is a positive feature associated with a basement arch trending east-southeast, which separates the PriCaspian basin to the north from the South Caspian basin.

Oil reserves in excess of one (1) billion barrels are reported for the whole area (Oil & Gas Journal, July 18, 1983, citing Soviet authors). Richard Meyer of the U.S.G.S. quotes a higher figure of five (5) billion barrels. There are several heavy oilfields along the Buzachi trend, the two largest being the Karazhanbas and Kalamkas fields.

The Karazhanbas field, discovered in 1974, contains more than 500 million barrels of heavy oil according to Schumacher, some 35 million of which could probably be produced by primary recovery. The oil is paraffinic (4%) with a high sulphur content (2.5%). The oil gravity is not known to us.

The Kalamkas field was placed on production in 1978 from several pay zones in the Jurassic and Cretaceous. The oil is sweeter than in Karazhanbas as it contains 1.2 % sulphur but its gravity of 26° API is high. Accordingly, the field does not qualify as a heavy crude field under the INFOCEN definition. Reserve estimates are of the same order of magnitude as in Karazhanbas.

Current production from both fields is reported at 40-50,000 b/d. It is assisted by steam and surfactant flooding.

1.1.2.2 The Mangyshlak Peninsula Fields

The Mangyshlak Peninsula is the surface expression of a basement buried hill which developed in the Turanian Platform that

acts as the foreland of the North Caucasus Alpine ranges.

Trending east-southeast parallel to the main Caucasus axis, the Mangyshlak Peninsula is Kazakhstan's main oil producing region. Conventioanl oil and gas are encountered in sandstone reservoirs within the Triassic, Jurassic and Lower to Middle Cretaceous.

The two largest heavy crude fields known in the area, Tyubedzhik and Uzen, are located on the southern flank of the Mangyshlak horst. Together with the Buzachi Peninsula fields, they produce 84 percent of Kazakhstan's crude oil. The Tyubedzhik field has been compared to a layer cake in which natural bitumen is trapped within over fifty (50) sandstone reservoirs extending from the surface to a depth of 600 metres. These reservoirs are Jurassic and Lower to Middle Cretaceous in age. Production in the Uzen field was put in jeopardy when waterflooding was first attempted using cold water. Following the start of water injection, all wells became plugged and production drastically declined. Upon resuming injection with heated sea water, production was restored to its initial 180,000 b/d.

High grade bitumen deposits are found in the vicinity of the fields above at Karasyaz-Taspas and Beke-Bashkandusskiy. The Karasyaz-Taspas accumulation, the largest of the two, extends over a distance of 100 km along the southern flank of the Mangyshlak Peninsula. According to Mingareyev and Tuchkov, the bitumen is contained within beds of Middle Jurassic and Middle Cretaceous age (Aptian Albian). Reserves have not yet been assessed but are considerable.

Development of the Mangyshlak Peninsula production is one of the priorities of the current Russian Five-year Plan.

1.2 PRICASPIAN BASIN

The Pricaspian basin covers some 500,000 km 2 on the northern shore of the Caspian Sea. It is sometimes referred to as the North Caspian basin and it separates the South Caspian basin on the south from the Volga-Urals basin on the north.

The geological history of the basin is rather complex. Its sedimentary column is very thick and most likely exceeds 20-25,000 meters.

Heavy oil and bitumen are exclusively found in the Emba salt sub-basin, in the eastern half of the Pricaspian basin, east of the Volga River. Total estimated in-place resources of heavy oil and bitumen are three (3) billion barrels.

Oil was discovered there in 1889, associated with salt plugs and salt domes, but production did not start until 1911. Most fields contain heavy oil and/or natural bitumen within a variety of reservoirs ranging in age from Triassic through Lower Cretaceous. The most prolific reservoir is the Emba sand reservoir in which oil saturation is still in the 65-80% range in spite of its 75 years history of production. The oil has a very high viscosity but the sand porosity is also high, ranging from 21 to 36%.

Following several successful waterflood projects which had a good recovery factor, EOR methods are now being used in the Emba salt basin. They involve steam injection and in situ combustion and are closely monitored by the Institute of Mining of Alma-Ata and the Institute for the Chemistry of Oil and Natural Salts in Gur'yev, both of which are located in Kazakhstan.

The most representative heavy oil fields in the Emba area are, from north to south: Shubar-Kuduk, Kenkiyak, Munyayly-Mola, Makat, Tanatar, Dossor, Sagiz, Teren'Uzyuk, Kara-Arna and Prorva.

The Kenkiyak field however does not qualify as a heavy oilfield under INFOCEN definition since oil averages 23.5° API. It is nevertheless produced by steam injection.

The Teren'Uzyuk field, at the confluence of the Emba River with the Caspian Sea, is the site of two EOR projects. In that part of the field where oil averages 19.4° API, in-situ combustion operations have been on going since 1985. Elsewhere, where oil is heavier (18.1° API), steam injection is being employed. In a like manner, at Kara-Arna where oil has a 15° API gravity, both in-situ combustion and steam injection are employed at the same time.

As to the bitumen deposits, over fifty (50) of them are reported by Dvorets et al., and Khalimov et al., also related to salt domes. In several deposits, the bitumen content ranges from 15 to 20% in weight. In the asphalt lake located near the Shubar-Kuduk heavy oilfield, the bitumen content reaches 95%.

1.3 VOLGA-URALS BASIN

The Volga-Urals basin, extending along the western flank of the Urals mountain belt in a foreland position, is a vast and complex area which is some 700,000 km 2 in size. It is bounded on the south by the Pricaspian basin, from which it is separated by the Orenburg arch; on the west by the Eastern European platform; and on the north by the Timan-Pechora basin. The intervening Timan ridge, a sort of basement spur, separates the Volga-Urals basin to the south from the Timan-Pechora or Timano-Pechorsky basinal unit to the north.

Oil was first struck in the Volga-Urals basin in 1929, but the potential of the basin remained unclear until the discovery of Permian oil in Ishimbay, within the Perm region, in 1932. The basin production rose steadily till 1975 when it peaked at 1.5 billion barrels for that year, after which the prominence of the basin as Russia's prime oil area was challenged by the huge discoveries made in Siberia. By 1983, the Volga-Urals basin was producing 1 billion barrels a year only and numerous attempts were made at slowing down the production decline by application of EOR techniques (Steam injection, polymers and surfactants flooding, etc.,).

In 1978, Trenin and Rubtsova (cit. A.A. Meyerhoff and R.F. Meyer) listed 882 oilfields, 166 oil and gasfields, and 118 gas and condensate fields, a total of 1166 fields, in the basin. Few fields have been added since. By the end of 1984, the Volga-Urals complex of basins had produced 37 billion barrels of conventional crude oil and although production is declining, it may well last into the next century. The Upper Devonian (Frasnian) and Lower Carboniferous (Visean) are the main oil reservoirs, whereas the Permian formation produces most of the gas in the basin.

The Volga-Urals region is also well endowed with heavy crude and tar sand accumulations. Some 338 heavy oil fields have been identified in which the oil is in the Upper Devonian and the Lower Carboniferous, at depths ranging from a few metres below the surface to a maximum of 2,000 meters. In a like manner, several hundred bitumen/asphalt deposits have been found at shallow depths, mostly of Permian age, but they have not been developed yet.

In-place reserves of heavy crude and bitumen are estimated at 37-40 billion barrels for the whole Volga-Urals basin.

The four main locales of heavy crude and bitumen in the Volga-Urals basin are: The Melekess depression fronting the Orenburg Arch on its northern flank, the Tatar Arch which occupies a central position in the basin, the Perm Oblast (*) in the north of the basin, and the Bashkiria Republic on the east of the Tatar Arch.

1.3.1 Melekess Depression

The east-west Melekess depression is situated near Dimitrovgrad, formerly Melekess, in the Tataria ASSR, and also covers parts of the near-by oblasts of Kuybyshev, Orenburg and Ulyanovsk.

The Melekess basin contains over 200 heavy crude and bitumen deposits, most of them in Permian rocks. Beskrovnyy cites bitumen reserves of 130 billion barrels (19 billion tons) almost equally divided between Tataria ASSR (50-60 billion bbl or 7-9 billion tons) and the Ulyanovsk oblast (70 billion bbl or 10 billion tons). Nikita Dvorets of the U.S.S.R. State Planning Committee corroborates the figures and claims that bituminous rocks capable of yielding an additional 70-100 billion bbl (10-15 billion tons) of bitumen exist in the Devonian and the Carboniferous rocks. The main heavy oil and bitumen accumulations in the Melekess basin are, from west to east: The Zhigulevsk field, the Malyy-Kinel field, the Borovskoye field and the Buguruslan Sadki field

1.3.2 Tatar Arch

The Tatar Arch is a major domal feature

(*) An Oblast is equivalent to a region.

close to the centre of the Volga-Urals basin. Its extends across most of Tataria ASSR, part of Udmurtia ASSR to the north, and part of the Bashkiria Republic to the east.

Heavy crude and natural bitumen are particularly important on and around the Tatar arch. The Tataria ASSR has a well developed infrastucture and the bitumen is an appropriate feedstock for the several refineries in the area as well as a good material for road paving.

It should be noted that in the U.S.S.R., the bulk of natural bitumen produced is used for construction work and road surfacing.

On the Tatar arch, bitumen impregnations are found in Permian sediments, from the surface all the way down to a depth of 400 meters. Their gravities range from 2.9 to 17.5° API.

Surface mining of bitumen started in 1906 in the Shugurovsky field and continued through the middle of World War II in 1943. Adits were dug into which the bitumen flowed by gravity. Currently, pilot production of bitumen is underway in several fields such as Ashal'Chinsk (Ashal'Chi), Sugushlinsk (Sugushly), and Mordovo-Karmaly (Mordovo-Karmal') but work is held up for lack of suitable equipment. Other fields in the area are, from north to south: Romashkino, Novosuksinskkoye, Tuymazy, and Pioner.

Overall production figures do not reflect the potential of the area on account of the problems encountered during the scaling up of experimental laboratory recovery.

1.3.2.1 Ashal'Chinsk (Ashal'Chi) Field

The Ashal'Chinsk tar sands deposit is quite representative of the various bitumen deposits in the area. The Permian sandstone reservoir contains 14 wt % of bitumen with a specific gravity of 15° API and 4 percent sulphur. The top of the reservoir is at depths of 60-80 meters below the surface and the thickness of the reservoir ranges from 20 to 30 meters.

Several EOR techniques have been tried under the supervision of the Kazan Institute of Technology. In particular, a satisfactory recovery level (80%) was obtained in the laboratory when extracting the bitumen with a water solution containing 1 percent by weight of sodium silicate.

The Podlessk deposit a short distance from Ashal'Chinsk is very similar but it contains lighter oil with a gravity of 17° API.

1.3.2.2 Sugushlinsk (Sugushly) field

In the Sugushly tar sand deposit, the Permian sandstone reservoir is at a depth of 76.5-85 meters and has a thickness of 6-8 meters. The tar sands are 6 wt % bitumen with a viscosity of 9 million centipoise under reservoir conditions.

Several EOR methods have been piloted but none was found satisfactory: Injection of steam, sulphuric acid, solvents, as well as in-situ combustion involving two patterns with different well spacings, reservoir stimulation by hydroabrasive material and high frequency electric currents. Open pit surface mining still provides the most profitable recovery method.

1.3.2.3 Mordovo-Karmaly (Mordovo-Karmal') Field

The Mordovo-Karmaly field (Karmalskoye) is associated with a complex anticlinal structure having two separate tops.

The reservoir is at depths of 65 to 91 meters below the ground level and its thickness ranges from 25 to 30 meters. Reservoir pressure is 49-67 psi. The average organic content of the deposit is 12.64 wt %; The oil has a gravity of 15.7° API with a 4.1 wt % sulphur content. Its viscosity is 2,000-5,000 cp.

The deposit has been under exploitation since 1978. In-situ combustion is conducted on the southern dome and steam recovery implemented on the northern one.

Reserves are substantial but there are no figures for the moment.

1.3.2.4 Romashkino Field

Located north of the Tatar Arch northern dome, this is a very large field with

reserves well over 120 billion bbl (20 billion tons) of recoverable oil in a shallow Devonian sand reservoir. The bulk of the oil has a gravity of 31° API and therefore does not meet the UNITAR INFOCEN definition.

1.3.3 Perm Oblast

The Perm region coincides with the Upper Kama basin and is host to a large variety of crude oils with many different characteristics. In the northern part of the basin, crudes have a lower sulphur content than in the southwest for instance and yield a lesser amount of resinous material as well.

Heavy oil is not only associated with Permian sandstone and limestone deposits at shallow depth, but also with Middle and Upper Devonian reef limestones, and with Lower through Upper Carboniferous limestones and sandstones.

One of the main accumulations is the Sokolova field located some 120 km to the west of the city of Perm. Sokolova crude is 16.2°API with a 0.3% sulphur content, a 0.24% wax content and 12.3% asphaltene content.

1.3.4 Bashkiria ASSR

The Bashkiria Republic is on the east of the Tatar arch. It coincides with the Sernovodsk-Abdullino basin which is an eastern extension of the Melekess Depression.

There are several heavy oil deposits in the Sernovodsk-Abdullino basin with gravities ranging from 15.3 to 22.1° API. The main reservoir is the Upper Devonian sandstone but several accumulations were also found in Lower Carboniferous, Upper Carboniferous and Lower Permian.

The largest deposit is the Arlan field in Upper Devonian sandstone. Oil is viscous and has a high sulphur content of 3.1-3.4 wt %. Chemical flooding was started in 1967 in the Nicolo-Bere sector of the field but results are unknown to us. Elsewhere in Bashkiria, polymer flooding was succesfully tested more recently.

1.4 TIMAN-PECHORA BASIN

The Timan-Pechora (Timano-Pechorsky or Tumano-Peckorsk) basin covers 1,500,000 km 2 to the north of the Volga-Urals basin. It extends both onshore (350,000 km 2) and offshore (1,150,000 Km 2). It covers all of the Komi ASSR and is the northernmost oil province of the Soviet Union.

From a geologic standpoint, the Timan-Pechora basin is an old Ordovician-Triassic foreland area of the Eastern European Platform which developed during the Caledonian orogeny.

There are over 80 conventional oil and gas fields in the Timan-Pechora basin. Reservoirs range in age from Silurian to Lower Permian according to the location of the fields in the basin.

The same remark applies to heavy crude and natural bitumen deposits which are abundant and are found also in Upper Silurian, Devonian, Upper Carboniferous and Lower Permian strata.

Heavy oil reserves in the Timan-Pechora basin are estimated at 15 billion barrels by Soviet Geologists, of which 20% are said to be economically recoverable, and bitumen resources at 4.5-5 billion barrels.

Heavy oil and bitumen deposits are widespread but they appear to follow certain trends.

1.4.1 Ukhta-Yarega Trend

There is a concentration of heavy oil and bitumen deposits in the Ukhta-Yarega area along the Timan arch, on the southwestern edge of the basin, where most bitumen occurs in Devonian reservoirs.

In addition to the Yarega field which was discovered in 1932, but in the vicinity of which surface pits were hand dug in the middle of the 18th century, other fields of importance are: Dzh'yersk, Gausbergrovsk, Iskos'Gora, Khudoiol, Kushkodzh, Nibel, Nizhnaya-Omra, Nyamed, Sediol, Verkhnaya-Omra, Vezhavozh, and Voyvozh. All these fields are producing from Middle Devonian sandstones but some of them have additional pay zones in Upper Devonian Limestones (Dzh'yersk) or in Lower Carboniferous (Khudoiol, Nizhnaya-Omra).

The Yarega oil field is located 1,300 km to the northeast of Moscow. It was first placed on pilot production in 1939 but has only been operating on a commercial basis since 1970. The production method at Yarega is called thermal mining for it combines thermal stimulation by cyclic steam injection and steam drive with drainage mining. Presently, there are three mines in operation. The gravity of the oil ranges from 17.4 to 19.0° API.

The Yarega oilfield went through three phases of development. From 1939 to 1950, mining techniques were used but oil recovery was poor and did not exceed 1.5 percent. After World War II, shafts were dug in and large chambers excavated at a depth of 200 meters below the surface. Tunnels were driven from the chambers, underneath the heavy oil zone and oil was allowed to flow by gravity into the tunnels. In the late 40s, directional drilling from the underground chambers was successfully attempted and raised the production level to 4-4.5 percent. Production peaked out at 7,800 b/d in 1952 and by 1968 had declined to 172 b/d. In the depleted areas, oil recovery had only reached 6 per cent of the initial oil-in place. From 1968 onwards, various methods of reservoir stimulation were tested. In or about 1970, injecting steam from the upper chambers increased the recovery factor to 50 per cent of the oil-in place. Current production is 10,000 b/d and more shafts are being added to bring the production level to 32,000 b/d in the early 1990s.

The Vezhavozh deposit which is located a short distance to the south of Yarega is a Yarega-look-alike type of field.

Based on the success of thermal mining at Yarega, numerous attempts were made at thermal mining in the Soviet Union with varying results. The technology has been licensed through the Resources Science Corp (RSC) of Tulsa, OK, a Williams Brothers Engineering affiliate. In 1976, RSC Technology of Canada conducted a feasibility study in adapting the Yarega thermal mining methods to the Athabasca oil sands of Alberta.

1.4.2 Pechora-Gorod Trend

A second trend parallel to the Ukhta-Yarega trend runs NW-SE in the middle of the basin and contains four major heavy oil and tar sand deposits: Aranets, Mutny-Materik, Pechora-Gorod and Yugid. The first two have a Devonian sandstone reservoir and the last two produce from a Lower Carboniferous (Visean) sandstone.

1.4.3 Usa Field Trend

A third trend parallel to the first two but closer to the central part of the basin is host to the giant Usa field discovered in 1963 and to its numerous northern satellites like Kharyaga and Srednemakharika. In Usa, recoverable reserves from the various reservoirs are estimated at 3 billion barrels but we have no break down between light and heavy oil reserves. The main producing zone is a Lower Devonian shallow water limestone for the light oil, whereas heavy crude is encountered in Uppermost Devonian and Uppermost Carboniferous to Lowermost Permian carbonate reservoirs.

In 1982, the Upper Carboniferous and Lower Permian reservoirs were injected with steam using 5 steam generators. Initial production from ten wells was 1,860 b/d. Elsewhere in the field, a small in-situ combustion pilot plant was installed in 1984 but no production details are available.

The Kharyaga field lies 100 km north of Vozey (Voseiskoye), beyond the Arctic Circle. It contains some highly viscous crudes and production start-up has been held up on account of severe production problems. The Srednemakharika field located some 60 km east of Vozey yields light oil in the Middle Devonian and heavier oils in the Upper Silurian-Lower Devonian (20° API) as well as in the Upper Carboniferous-Lower Permian (12.3° API). Oil in-place in the field Siluro-Devonian reservoir is estimated at 200 million barrels.

1.4.4 Pay Khoy Trend

This is the northernmost trend in the basin and it is also striking north-northwest. It can be followed into the Franz Josef archipelago, in the Barents Sea, where

bitumen deposits are abundant in the Triassic and Jurassic strata.

Arctic offshore drilling began in 1983 in the Pechora Sea and has since moved north-westwards into the Barents Sea.

Several of the heavy oil fields located in the Timan-Pechora basin do not qualify under the UNITAR definition given in Tab.1 since they contain medium light oil with gravities ranging from 25.00 to 36.00° API.

1.5 NORTH CAUCASUS AREA

The Caucasus is but a segment of the great Alpine orogenic belt referred to on page 2 hereinabove. The name "North Caucasus area" as used in this paragraph, is applied to all Caucasus ranges as well as to the North Caucasus foredeep which is sub-divided into several basins (Azov-Kuban, Terek-Kuma, Rioni, and Kura). The Kura basin has already been examined under paragraph 1.1.1 dealing with Azerbaijan.

Heavy oil and bitumen accumulations are found in the Miocene and Eo-Oligocene reservoirs of the Azov-Kuban basin, as well as in the Jurassic limestones of the Caucasus ranges and the Mio-Pliocene sediments of the Rioni basin.

1.5.1 Caucasus Ranges

Some 25 bitumen deposits are scattered through the main Caucasus Range in rocks ranging from Middle Devonian to Cretaceous. The largest one is the Balkar bitumen field which has an areal closure of 170 x 12 km and extends along the crestal zone of the range. The bitumen impregnates three Upper Jurassic dolomite beds with thicknesses ranging from 7 meters for the upper one to 27 meters for the middle one and 20 meters for the lowest. Bitumen saturation is approximately 5 percent in weight. Other deposits have saturation of 25 percent and more.

1.5.2 North Caucasus Foredeep

The North Caucasus foredeep basin is sub-divided into two separate units by the north-south striking Stavropol arch: the Azov-Kuban basin on the west and the Terek-Kuma basin to the east.

There are several small bitumen deposits in the Azov-Kuban basin. Miocene strata are the host reservoir but bitumen impregnations are encountered also in underlying pay levels in the Oligocene, the Eocene and the Paleocene.

Heavy crude with gravities of 14 to 19° API have been found in shallow Pliocene reservoirs at depths of less than 1,000 meters, at several locations in the basin. Deeper oil has been found also in rocks ranging from Paleocene to Miocene, between 1,000 and 2,800 meters. The mains fields are: Nefte-Gory, Asfaltovoy-Gory.

In the Terek-Kuma basin, there are minor bitumen deposits and one heavy oil field (17.4° API) at Praskoveya-Chkalovo, on the Kuma River, in which the reservoir is an Upper Cretaceous carbonate at 2,800 meters. The field is credited with 450 million bbl in-place and is the largest heavy-oil field in the North Caucasus area.

According to the Russian Authors (cit. A.A. Meyerhoff and R.F. Meyer), heavy oil in-place in the North Caucasus area is estimated at over 1 billion barrels and bitumen in-place at 13.5 billion barrels.

1.5.3 Rioni Basin

There are a dozen bitumen accumulations in Miocene and Pliocene sandstone and limestone within the Rioni basin. Some bitumen saturations are very high and of the order of 50 percent in weight but we are lacking reliable data.

1.6 BYELORUSSIA AND UKRAINE SSR

We gather in this paragraph the heavy oil and bitumen occurences which are known in the westernmost part of the Soviet Union, namely in the Prypiat-Dnepr-Donets graben system.

1.6.1 Prypiat Graben

The Prypiat Graben of Byelorussia, on the Polish border, covers an area 20,000 km2 in size. It contains some 24 oilfields spread along the graben axis but only those fields located in the central and southern parts have heavy oils (Gravity ranging from 15.9 to 27.5°API) in a series of Devonian reservoirs.

The largest accumulation was found in the Kopatkevichi (Kopatkevichskoye) field where oil is 11.6°API with a 8 wt % sulphur content and a 25% asphaltene content. For that reason, the field was dubbed non commercial. Other fields of importance are: Dneprovskoye, Ostashkovich. Ozemlino, and Sudovaya, the first one and the last two being considered as noncommercial.

Tentatively, heavy oil and bitumen resources of the Prypiat Graben are estimated at under 1 billion barrels.

1.6.2 Dnepr-Donets Graben

The Dnepr-Donets graben of the Ukraine is an eastern extension of the Prypiat graben but it had a different geological record from the Uppermost Devonian onwards.

The Dnepr-Donets area covers 80,000 km 2 and is a gas prone basin with some 160 gasfields in which the two main pays are the Carboniferous and Permian sands and sandstones. There are also numerous heavy crude fields with oil densities of 10.7 to 18.5°API and high sulphur contents. Heavy oil reservoirs are mostly sands and sandstones ranging in age from Upper Permian through Triassic and Jurassic to Lower Cretaceous.

The main heavy crude fields are: Brigadirov, Khovanovka, Shul'gora and Velikiy-Zagorovskoye. Cumulative reserves are not known to us but are probably much smaller than in the Prypiat graben.

1.7 MISCELLANEOUS

In the rest of European Russia, there are small heavy oil and bitumen deposits in several locales, namely in Estonia, in the Rybinsk depression northeast of Moscow and at Shun'ga in Karelia.

2. EASTERN U.S.S.R.

In the Eastern part of the U.S.S.R., heavy oil and tar sands deposits are found in Siberia and in the Sakhalin Islands.

The Siberian Platform is one of the largest bituminous provinces of the U.S.S.R., as it contains over 60 percent of all known bitumen resources in the country. Most accumulations are concentrated in Eastern Siberia where they are associated with the Aldan and Anabar basement shields. The heavy oil endowment of Western Siberia is very small in comparison. With the exception of the sizeable Russkaya (Russkoye) oil and gas field, located between the Pur and the Tar Rivers, all other deposits found in the Turukhan (Turukhansk) and Chun (Chuna River) regions of Western Siberia are limited in size.

With regards to conventional oil, Siberia is a relative newcomer since gas was discovered in 1953 in the Berezov field, and oil in 1960 near Shaim on the Konda River; 1965 saw the discovery of the super-giant Samotlor oilfield in which the first well was placed on production in 1968. Since that date, Siberia has made giant strides and it accounts to-day for 60% of the Soviet Union's hydrocarbon production.

2.1 WESTERN SIBERIA

Western Siberia is bounded by the Urals on the west and the Yenisey River which flows from south to north into the Kara Sea on the east.

The geology of Western Siberia is dominated by the presence of a Mesozoic basin which has an areal extent in excess of 1.5 million km 2 and a sedimentary column with a maximum thickness of 8,000 meters. The basin is sub-divided into several units which have different production records: gas is abundant in the North-Central and Northeastern gas districts, oil is produced in the Middle Ob district which is host to the huge Samotlor field, and both oil and gas are produced in the Western Ob (Shaim) and Southeastern districts.

Heavy Oil and bitumen deposits are normally found in the folded belts bordering the units above.

2.1.1 North-Central District

There are several bitumen deposits on the flanks of the northwest trending Taz arch which separates that district from the Northeastern gas district to the northeast. In addition to the Russkoye field already mentioned, there are the Ay-Yansk, Van-Yegan, and Taz fields.

The Russkoye field has a surface closure of 300 km 2, north of the Arctic Circle. It was discovered in 1968 and contains 18°API oil in a Cretaceous (Cenomanian) reservoir at a depth of 800 meters, with a very large gas cap. Reserves are estimated at 500 million to 5 billion barrels. Fire flooding was began in mid-1983 but for the time being the field is shut-in for want of pipeline outlets and adequate production facilities.

2.1.2 Middle Ob District

Heavy oil deposits are scarce in the district and the density of the oil is normally too high and does not fit the UNITAR requirements. The largest deposit is the Ay-Yaun field in which the oil is 22°API with a 1.5 wt % sulphur content.

2.1.3 Western Ob District

The district contains several heavy oil accumulations. The most important is the Yeremino deposit, in the Gari-Sverdlovsk oblasts, in which there are several pay zones in the Middle Cretaceous (Aptian, Albian) sandstones. Oil is heavy to extra heavy with gravities ranging from below 10°API to over 20° API.

2.1.4 Turukhan and Chun Districts

The Turukhan (Turukhansk) and Chun (Chuna) bituminous regions are considered as being in Western Siberia when, in fact, they are both located on the right bank of the Yenisey River and should be regarded as being on the western edge of Eastern Siberia, at the periphery of the Lena-Tunguska basin.

In Turukhan, bitumen has been mined since the 1950s for local use. The reservoirs are in Vendian, Middle and Upper Cambrian and Ordovician with a content grading from 1.0 to 2.8 percent in weight. As to the Chun (Chuna-Taseyeva) deposits they are found within Vendian and Cambrian limestone rocks at depths ranging from the surface to 250 meters. More studies are needed to obtain a better idea of the economic potential of these two large areas.

2.2 EASTERN SIBERIA

The Siberian platform covers 2,827,000 km 2 between the Yenisey River on the west and the Circum Pacific Orogenic Belt on the east.

Heavy oil and bitumen accumulations are numerous and equally divided between the various troughs and basins which border the Anabar and Aldan shields, such as the Lena-Anabar, Lena-Tunguska (Tungus) and Lena-Vilyui (Villuisk). Ultimate resources of bitumen are set at 70 billion barrels in the Lena-Anabar basin alone, at over 25 billion barrels in the Lena-Tunguska, and at 600-700 billion barrels in the Lena-Vilyuy (Tereshchenko et al., 1986). The main reservoir rocks are Vendian (Vendsk), Cambrian and Permian, and to a lesser extent Ordovician and Upper Proterozoic.

Both the geological environment and the habitat of the oil are complex and will not be examined in this paper.

2.2.1 Lena-Anabar Basin

The Anabar basement arch is a positive area which is striking east-west on the northern edge of the East Siberian Platform. It is bordered on its northern flank by the Lena-Anabar basin which extends offshore into the Laptev Sea. The Anabar arch is comprised of several uplifts to which are associated as many bitumen deposits, namely: The Upper (East) Anabar, Koti-Maimechen and Rassokha deposits are related to the Anabar arch sensu stricto; the Kuoisk, Central Olenek, Olenek and Sololisk fields are associated with the Olenek basement arch; and the Munsk, Siligir-Markha and Udzhinsk fields are respectively on the Munsk, Aykhal and Udzhinsk arches.

The Anabar basin is a Carboniferous to Cretaceous trough with a rather deep sedimentary column. Early drilling (1912-1914) in the Nordvik area discovered heavy oils with gravities ranging from 11.5°to 23.1°API in Permian and Triassic sandstone reservoirs at a depth averaging 1,500 meters. Salt tectonic seems to be the controlling factor for the oil accumulations in the basin.

2.2.1.1 Anabar Arch (Sensu stricto)

The Anabar arch is the locus of the East Anabar, Koti-Maimechen (Kotuy-Maymecha) and Rassokha bitumen accumulations. Reservoirs
: the Upper Vendian sandstone, the basal
mbrian sandstone, a Lower Cambrian carbonate in the East Anabar deposits; Late Proterozoic, Middle to Upper Cambrian dolomitic limestone and Lower Ordovician dolomite and limestone in Koti-Maimechen; and Permian deltaic sandstone in Rassokha.

The East Anabar or Upper Anabar bitumen field is also known under the name of Kuonama (or Kuonamka) deposit. It is a very small accumulation on the eastern slope of the Anabar Arch.

The Koti-Maimechen bituminous field is found on the Western slope of the Anabar arch.

As to the Rassokha bitumen field, it is located on the northwest slope of the Anabar arch, north of the Rassokha Proterozoic to Cambrian heavy oil area.

2.2.1.2 Olenek Arch

The Olenek (or Udzha-Olenek, or Levoberezhno-Olenek) trend is host inter alia to the Olenek deposit which is possibly the largest bitumen accumulation in the Soviet Union and certainly the largest one in Eastern Siberia. The Olenek deposit lies on the northern flank of the arch by the same name. The bitumen impregnates sandstones of Permian age which were deposited in a paralic environment. The field is not delineated yet and its reserves are still conjectural. Kopylova and Danuskevskaya claims that the impregnated area in Olenek is 120 km long by 50 km wide and contains approximately 900 billion barrels of bitumen of which 90 billion are producible by primary methods. If this is the case, the Olenek bituminous area would probably be of the same order of magnitude as the Athabasca sands in Canada. However, it should be said that the estimates of the ultimate resources at Olenek vary widely between 45 billion barrels and 900 billion barrels.

The Central Olenek bitumen deposit, across the Lena River and up-stream from the larger Olenek bituminous area, is possibly one of the best known fields in the region.

It comprises several accumulations in beds of Proterozoic to Cambrian age, the two best accumulations forming the Sololisk (Solola) and Kuoisk (Kuoyka River) fields. These fields have multiple pays in the Upper Proterozoic and Lower Cambrian, which vary in thickness from a few meters to as much as 70 meters for the Upper Cambrian reservoir.

2.2.1.3 Munsk-Aykhal-Udzhink Arches

These arches are more or less aligned along the same east-west striking trend which runs parallel and to the south of the Anabar arch.

Bitumen deposits are scattered within three large areas fringing the arches above: (i) The Arga-Sala area covers some 10,000 km 2 at the western periphery of the trend but its geology is not yet unraveled; (2) The Aykhal-Siligir Markha area in the central part of the trend is about 6,000 km 2 (Khalimov et al.); (3) The Munsk (Muna River)-Tyung River area on the eastern end of the trend is fringing the northern edge of the Lena-Vilyuy basin.

In the Siligir-Markha deposit, bitumen impregnations are found in Middle and Upper Cambrian as well as in Lower Ordovician. The pay levels vary from less than one meter to as much as 15 meters in thickness and the bitumen content averages 5 wt % with peaks of 15 percent though.

In the Munsk-Tyung (Muna-Tyung) field, bitumen impregnations are associated with Middle and Upper Cambrian carbonates as well as Carboniferous sandstones. However, rather than impregnating the pores of the rocks, the bitumen is found in fissures and in veins.

2.2.2 Lena-Tunguska Basin

The Lena-Tunguska (Tungus) basin is located on the western edge of the East Siberian platform, along the Yenisey River which is considered as the dividing line between West and East Siberia.

It is bordered on the west by the Turukhan (Turukhansk) bitumen province and on the south by the Chun (Chuna-Taseyeva) bitumen area which are both described under paragraph 2.1.4.

In the Lena-Tunguska basin, there are numerous Vendian, Cambrian and Ordovician outcrops containing abundant bitumen as impregnations in the pores of the rocks or agglomerated in small pockets of gilsonite.

The largest deposit is the Chunya River deposit in the southern one-third of the basin, in which bitumen impregnations are found in Lower Ordovician limestone and sandstone reservoir beds.

2.2.3 Lena-Vilyui Basin

The Lena-Vilyui (Lena-Vilyuy or Villuisk) basin is a Vendo-Cambrian shallow basin located on the northern flank of the Aldan shield where it covers some 175,000 km 2. It is filled with terrigenous clastics and carbonates containing major bitumen accumulations.

The four largest bitumen deposits in the basin are: The Tolbin and Sinsk fields to the northwest of the Aldan arch, and the Inglisk and Yunsk fields to the east of the arch.

2.2.3.1 Tolbin Field

The Tolbin (Tuolba or Tolba River) field is essentially a Proterozoic multi payzones field with shut-in production from 9 potential zones in the Middle and Upper Proterozoic. Bitumen saturation reaches 50 percent in weight locally.

2.2.3.2 Sinsk Field

The Sinsk field straddles the northern flank of the Aldan arch, west of the subsidiary Yakutsk ridge, in the Yakutsk ASSR.

There are several pay zones averaging 10 meters in thickness and saturated with bitumen. Details are missing regarding the potential of the field

2.2.3.3 Ingilisk and Yunsk fields

These fields are located in the Aldano-Maiski sub-basin which is comprised between the eastern plunge of the Aldan arch (Aldano-Uchur Range) and the Maya River farther east. The main objective in that area is the Precambrian Rifean which is between 2,000 and 3,000-meter thick. Bitumen saturation varies between 15 and 50 percent per weight.

The resources of the Lena-Vilyuy basin are enormous and temporarily set at 600-700 billion barrels.

2.2.4 Miscellaneous Areas

There are several other heavy oil and bitumen deposits in the intervening area between the Lena-Vilyuy and the Lena-Tunguska basins (= Nepa-Botuoba arch) as well as in the Lake Baikal area to the south of it, and in the Barzugin River basin immediately to the east of the lake.

Solid bitumen dominates along the Nepa-Botuoba arch where, incidentally, the world's first Precambrian giant gasfields were discovered. In Lake Baikal, tar balls comparable to the Lake Tanganyika tar balls and to the Dead Sea asphalt wash ashore during the rainy season, while large bitumen deposits have been reported on the southern and southeastern shores of the lake. Finally, heavy oil with gravities ranging from 12.8 to 18.3° API has been found in shallow wells drilled into the Quaternary alluvium and the underlying Tertiary sand and gravels on the southern shore of the lake.

2.3 Sakhalin Island

There are several heavy crude fields on Sakhalin Island, namely: The Okha, East Ekhabi, Katangli, Uiglekut, and Yuzhno-Nevel fields. There are also a dozen conventional oilfields containing one or more heavy oil zones. Finally, there are numerous bitumen deposits and several asphalt lakes like the Okha Lake and the Nutovo Lake.

Heavy-oil resources in-place are estimated at 1 billion barrels and bitumen at 10 million barrels.

2.3.1 Okha Field

The Okha field is located on the northern tip of the island, in the North Sakhalin basin. The oil has a density of 22.2° API and is found at depths of 30 to 700 meters.

Both steam injection and a steam-water-steam process have been successfully applied.

2.3.2 East Ekhabi Field

The East Ekhabi field was discovered in 1947. Oil gravities range from 17 to 22°

API. The field is located to the east of the Ekhabi light oil field (32° API) discovered in 1936, and immediately to the south of the Okha field.

Oil in-place estimates and other characteristics are missing.

2.3.3 Uiglekut Field

The Uiglekut field is in the southern part of the North Sakhalin basin. Oil has a density of 19.4° API with a sulphur content of .62 wt % and an asphaltene content of 2.43 per cent by weight.

2.3.4 Katangli Field

The Katangli field which is near and to the south of Uiglekut was discovered in 1935. Katangli oil is 19° API and contains 0.56 wt % sulphur and 2.10 wt % asphaltene. Steam injection has been tried with moderate success.

2.3.5 Yuzhno-Nevel Field

The Yuzhno-Nevel field is located in the South Sakhalin basin, along the southwestern coast of the island which borders on the Tatar Strait. The oil has a density ranging from 14.9 to 17.7° API.

In the Sakhalin Island, most oil and bitumen reservoirs are either Miocene or Pliocene. The crude has gravities comprised between 12 and 20° API and a low sulphur content averaging 0.55 wt %.

3. CONCLUSION

I have attempted my best to present a synopsis of the heavy crude and tar sands sector in the Soviet Union. I have tried to be as concise as possible but this is a very large country and it has numerous deposits!

As a matter of conclusion, it can be said that the resource base is abundant, but it is scattered under a variety of climates, environments and habitats that makes mining and production costly, very costly. The Russians have the talents and the manpower required, they also possess the basic technology, but they are probably lacking suitable equipment and facilities and, above all, the capital base to acquire them.

Note: The opinions expressed in this review are those of the author and do not necessarily reflect the views of the United Nations Organization.

Characterization of Heavy Oil Produced from the Wolf Lake In Situ Combustion Project

by

R.F. Alex, B. Fuhr, and C. Reichert
Alberta Research Council
Edmonton, Alberta CANADA T6H 5X2
H. Sawatzky and K. Jha
Energy Mines and Resources, CANMET
Ottawa, Ontario CANADA K1A 0G1
M. Polikar
BP Resources Canada, Ltd.
Edmonton, Alberta

Abstract. Heavy oil produced over a one year period by an in situ oxygen combustion process was compared to oil extracted from a core sample prior to initiation of the fireflood. These samples were fractionated and analyzed to determine the changes occurring in the oil as a result of the recovery process.

The combustion-produced oil exhibited a decrease in viscosity and density relative to the core sample. Analyses by GC-MS indicated that light straight-chain alkanes and small aromatic molecules were formed during the combustion process. Changes in carbon number distribution were consistent with thermal cracking of the oil and subsequent fractionation during movement through the formation.

The properties of the oil produced up to one year after commencement of the in situ combustion process should not cause any special problems during subsequent upgrading and refining.

Introduction

As conventional oil deposits continue to decline worldwide, there has been an increasing emphasis on the use of heavy oil and bitumen. The high viscosity of these materials, however, results in little or no primary production from deposits. The application of heat is usually required to reduce the viscosity of the oil and allow it to flow.

A variety of processes have been developed for this purpose. Most supply heat in the form of steam or in situ combustion to reduce viscosity and mobilize the oil in the formation. The application of heat often produces more than physical changes in the oil. In particular, the relatively high temperatures to which the reservoir oil is subjected during in situ combustion can cause chemical changes as well. A number of studies have shown that under these conditions, thermal cracking, low temperature oxidation, coke formation, and other chemical changes can take place[1-10]. These chemical changes clearly have consequences with respect to production of the oil. In addition, the chemical composition and quality of the produced oil are major determinants in the upgrading and refining processes.

The recovery of heavy oil and bitumen by in situ combustion (or fireflood) has been receiving increasing attention in recent years. The results of detailed analyses on several samples produced by an in situ combustion process in a heavy oil reservoir in Saskatchewan, Canada were compared to those of oil produced from the same field under primary recovery conditions[1,2]. A large increase in the naphtha distillation fraction was observed as was a marked increase in the aromaticity of the lower boiling fractions.

We undertook a similar study involving a field pilot at an oil sands reservoir at Wolf Lake, Alberta[11]. A comprehensive comparison of properties between oil extracted from a core sample and oil subsequently produced by in situ oxygen combustion over a three month period was completed. The main objective of this work was to assess the quality of the in situ combustion-produced oil with respect to the subsequent upgrading and refining processes. The results of this study (hereafter called phase one) revealed significant differences between the oil produced by fireflood and that derived from the core sample. Large reductions in viscosity and density for production samples were accompanied by substantial increases in the percentages of materials boiling in the naphtha and middle distillate ranges. The produced oil exhibited these effects very early in the production cycle. It was concluded that the quality of this oil would cause no special problems in the subsequent upgrading process.

A determination of the oil quality produced during later stages of the in situ oxygen combustion process was of crucial importance in establishing the long term utility of this recovery process. A second phase of this study was undertaken, covering the period from seven to twelve months after initiation of the fireflood. The results from both phases of the study are presented here. These data collectively detail the effects of the in situ combustion process on the properties of the produced oil over a one year period.

Experimental

All production samples were collected from an in fill drilled well in a five spot pattern. These samples were labelled with the dates they were collected (year/month/day e.g. 880327); the fireflood commenced on approximately September 1, 1987. Previous to this, a core sample was obtained from the same reservoir. The core sample was prepared by toluene extraction and may have lost some light ends during subsequent rotary evaporation, despite the 0.5% residual toluene. Each production sample was dewatered by ultracentrifugation prior to analysis.

Analyses were conducted on the whole oil and subsequent distillation cuts. Each sample was distilled into naphtha (115-204°C), middle distillate (204-345°C), gas oil (345-442°C), and residue (>442°C) cuts. The latter three cuts were further fractionated by column chromatographic separation. A flow scheme illustrating the separation procedure and the analyses performed on the various fractions is shown in Figure 1.

Results and Discussion

Whole Oil Analysis

Some analytical data for the whole oils from phase 1 (Samples: Core, 870929, 871023, 871116) and phase 2 are given in Table 1. There is a significant reduction in viscosity between the core sample and the fireflood-produced oils. This observation is consistent with those from previous studies, both in the laboratory and in the field, which involved changes to heavy oils under thermal conditions.[1,3,8,10] It is reasonably clear that this viscosity reduction stems from an increase in the percentages of the naphtha and middle distillate cuts. These distillation data are shown in Table 2. A careful analysis reveals that the viscosity of the produced oil is most closely correlated with the wt% of middle distillate in the sample. The general increase in the wt% of the naphtha and middle distillate cuts for the produced oils versus the core is balanced by a decrease in the weights of the residue cuts.

A consideration of the physical mechanism believed to be operating during the early stages of an in situ combustion process suggests that this visocosity reduction stems from a dilution of the oil with lower boiling material produced and vapourized as a result of thermal cracking near the firefront. It must be appreciated, however, that the recovered oil will consist not only of material formed at the firefront. The steam zone which precedes the combustion region will transfer heat to the virgin or native oil in the formation. The consequent reduction in viscosity will mobilize this oil and lead to simultaneous production of both virgin oil and volatile material formed near the firefront. The compositional details of the produced oil are perhaps even more complex than this consideration suggests. Laboratory studies have shown that there is fractionation of crude oil as it moves through a quartz matrix, resulting in a redistribution of the saturate hydrocarbon fraction in favour of the lower molecular weight n-alkanes[12,13] with increasing migration distance.[12,13] This redistribution was accentuated by the presence of clays in the mineral phase. The results from the Saskatchewan study[1,2] indicate that this type of fractionation is occurring during the in situ oxygen combustion process. Thus, the portion of the produced oil derived from mobilized native material need not be fully representative of the formation oil. Similarly, one might expect the volatile material, formed by thermal cracking at the firefront, to condense and undergo a certain amount of fractionation in the formation. Finally, the fact that the produced oil is from an in fill drilled well leaves open the possibility that oil altered in an earlier fireflood process may be mixed with virgin oil. These considerations must be kept in mind when analyzing the data from the whole oil.

The wt% of both nitrogen and sulfur in the produced oil of phase one decreased slightly relative to the core sample (Table 1). This is likely a reflection of the dilution of the produced oil by low boiling material formed near the firefront. This material would not be expected to contain large amounts of sulfur- or nitrogen-containing components. On the other hand, the wt% of oxygen in the produced oil showed a small increase relative to the core sample. Based on the lower acid numbers for the produced oil (Table 1), the added oxygen in this material appears to be in a non-polar (i.e. nonacidic) form. Similar results have been observed in related studies involving laboratory simulation of in situ combustion.[6] If any polar oxygen-containing compounds (e.g. carboxylic acids) are formed during the combustion process, adsorption onto the formation matrix or preferential distribution into the aqueous phase would account for their low concentration in the produced oil.

It should be noted that the oxygen supplied during the in situ combustion process is not the only potential oxygen source. Laboratory studies produced evidence that water also plays this role during the thermal cracking of oil.[5,6] Whatever the source of oxygen, the decrease in acid number for oil produced during the in situ combustion process suggests that the small increase in oxygen-containing material should not cause serious problems during upgrading at this stage of production.

Given the number of factors affecting the composition of the produced oil, little more can be gained by analyzing the whole oil. An analysis of the distillation cuts and chromatographic fractions follows.

Naphtha

The data for the naphtha distillation cuts are shown in Table 3. The naphtha content in each of the produced oil samples is higher than that of the core sample. In an effort to minimize loss of light ends, some of the toluene used to extract the core sample was left in the naphtha cut. For this reason, a full analysis of this sample was not performed.

The aromatic content of the samples was measured by both supercritical fluid chromatography (SFC) and ASTM D1319 (fluorescent indicator adsorption), the balance by both techniques being the saturates (Table 3). The results of these two methods are in good agreement. Early in the production cycle, there is an increase in amount of olefins present. These are likely formed by thermal cracking near the firefront and produced early in the cycle due to their relatively high volatility. A similar argument may be used to rationalize the increase in aromatics during the early recovery phase. As the production cycle continues, the amounts of both olefins and aromatics decrease in the naphtha fractions. Two plausible explanations for these observations may be advanced. An argument based on the cumulative effects of oil movement and fractionation as the firefront advances is consistent with this data. While the volatile material from the current firefront continues to migrate preferentially, the heat-induced advance (and subsequent fractionation) of the virgin oil is occurring. The composition of the produced oil should eventually reach a steady state with respect to the various compounds produced by thermal cracking and the mobilized native oil. Alternately, the data could be indicating a change in field operating conditions from fireflood to steam flood, thus halting the production of small, volatile compounds by thermal cracking.

A consideration of production dynamics and formation properties suggests that some variation in oil constitution is to be expected as production continues. The irregular advance of the combustion zone, variation in the efficiency of combustion, differences in oil density in the matrix, and channeling effects should lead to fluctuations in the composition of the produced oil. This type of behaviour may be observed in the phase two data with respect to the amounts of olefins and aromatics present.

The amounts of both sulfur and nitrogen in the naphtha cuts of the produced oil show a marked increase relative to the core sample. This is likely due to small, volatile nitrogen- and sulfur-containing molecules formed during the combustion process and produced early in the recovery cycle. The magnitude of the increase in the amount of nitrogen for the 871116 sample is particularly striking. The levels of both sulfur and nitrogen fall off and vary within a limited range in later samples, consistent with the previous arguments based on steady state production dynamics and fractionation.

A GC-MS analysis revealed some changes in the oil as a result of the in situ combustion process. The total ion chromatograms (derived from the GC-MS analysis) for the naphtha cuts of the core and phase one samples are shown in Figure 2. The shift towards peaks of shorter retention times (ie. lower boiling material) as the combustion process proceeds is consistent with the produced oil being diluted with smaller molecules produced near the firefront. The reconstructed ion chromatograms for the straight and branched chain paraffins (or open chain saturates) in the naphtha cuts, shown in Figure 3, reveal further evidence in support of this view. These show that the core sample contains only small amounts of n-paraffins while the phase one samples have increasing amounts of C_6 to C_{12} n-alkanes. These molecules are likely formed from the scission of alkyl-substituted aromatic compounds or the cleavage of naphthenic rings.

The results of a GC-MS compound type analysis are shown in Figure 4. The core sample consists mainly of alkyl benzenes plus 1- and 2-ring saturates (naphthenes). The samples from early in the combustion process show a relative growth with time of alkyl benzenes, benzocycloparaffins, and the single compound naphthalene. In addition, the distributions of 1- and 2-ring saturates are shifted to lower carbon numbers in the early phases of the fireflood recovery. These changes may also be attributed to thermal cracking of larger molecules at the firefront. There is also a small relative increase in the open chain alkanes during the early phase of the combustion process, consistent with the observed appearance of the homologous n-alkanes in the reconstructed ion chromatograms (Figure 3).

The phase two data reveal more complex changes occurring in the naphtha cuts. The earlier trend for the 1- and 2-ring naphthenes is reversed, with these compound classes now growing relative to the alkyl benzenes. The cumulative effects of fractionation in the formation and the advancing firefront are probably responsible for this behaviour.

An alternate presentation of the GC-MS data is illustrated in Figures 5 and 6. These highlight the changes in carbon number distribution for the open chain saturates and alkyl benzenes, respectively, as a function of time. Both compound classes exhibit similar behaviour as the production cycle progresses: there is a small but persistent shift towards lower carbon number. This result is consistent with the preferential migration of lighter material through the formation to the production well. While it is tempting to place interpretations on the relative areas under the bargraphs in Figures 5 and 6, these comparisons are not justified. The bargraphs for the individual samples were not normalized to the same constant.

Two general conclusions may be drawn from the previously analyzed data for the naphtha cut. Changes in the relative distribution of the compound classes which occur early in the production cycle tend to be transitory, as witnessed by the behaviour of the 1- and 2-ring naphthenes. On the other hand, the shifts towards lower carbon number in the individual compound classes as the combustion process evolves tend to be more enduring.

Middle Distillate

The data in Table 4 shows the large relative increase in the wt% of the middle distillate cuts in the phase one fireflood samples compared to the core sample. As discussed previously, the reduction in viscosity of the fireflood whole oil samples is most closely correlated with the wt% of this cut. The amount of nitrogen increases dramatically during phase one but returns to lower levels late in phase two of the recovery process. The amount of sulfur follows a similar but less striking variation to that of nitrogen. These observations are consistent with previous arguments based on the formation of small nitrogen- and sulfur-containing molecules which are produced early in the production cycle.

The aromatic contents of the middle distillate cuts show an increase relative to the core material for the phase one samples but return to core levels later in phase two. Similar behaviour was observed for the wt% of aromatics in the naphtha cuts and a similar explanation may be advanced. The early enrichment of the produced oil by volatile aromatic molecules produced by thermal cracking is later moderated by the increasing production of mobilized and fractionated virgin oil.

The chromatographic yields for the middle distillate cuts are shown in Table 5. The increase in wt% of aromatics early in the combustion cycle (by SFC) is reflected in the increased wt% of fraction 3 for the 871023 and 871116 samples. The variation in wt% aromatics is inversely related to the wt% of saturates, the polar fractions 4 and 5 varying little over the production cycle.

A set of GC-MS compound type analyses were performed on the chromatographic fractions from the middle distillate cuts. While these analyses reveal small variations in some of the fractions, in general there are no dramatic changes in distribution of compound types or carbon numbers. The open chain saturates from fraction 1 and the alkyl benzenes from fraction 2, both as a function of time, are shown in Figures 7 and 8. It may be observed that the distribution of carbon numbers changes little for either group as the in situ combustion process proceeds.

Chromatographic fraction 3, which contains the bulk of the di- and polyaromatics, exhibits some variation in the relative distribution of compound types. As may be observed in Figure 9, the 871023 sample shows dramatic increases in the single compounds naphthalene and phenanthrene/anthracene. While this increase is short-lived for the former, the enhancement of the unsubstituted triaromatics persists into phase two. The large relative value in the wt% of fraction 3 for the 871023 sample (Table 5) can be associated with these increases in napthalene and phenanthrene/anthracene. It may also be noted (Figure 9) that this latter compound type, as a whole, exhibits a slow but steady growth in relative intensity during the time period of the study.

The alkyl benzenes in fraction 3 show some variation in carbon number as the fireflood proceeds. There is a shift towards lower carbon number later in phase one which reverses itself as phase two progresses. The variation in relative intensity for the benzocyclo- and benzodicycloparaffins appears to be complex. While some of the changes taking place in fraction 3 may be related to dilution of the oil with fractionated products formed near the firefront, the details are not clear.

The relative changes between compound classes for fraction 4 are of interest. As the in situ combustion process occurs, there is an increase in the phenanthrene/anthracene content with a concomitant decrease in alkyl benzenes and benzocycloparaffins. These changes could be a result of new compound formation via condensation type reactions, as opposed to thermal cracking. The oxidation of alkyl benzene or benzocycloparaffin side chains (a plausible occurrence during in situ oxygen combustion) could provide the necessary substrates to synthesize phenanthrenes and anthracenes by ring closure.[14]

Fraction 4 contains a high proportion of dibenzothiophenes and a two-ring terpenoid sulfide series. These two classes were measured together as their molecular weights are the same, but both series were observed. Figure 10 shows the changes to this compound class as a function of time. Again, there is a shift to lower carbon number early in the production cycle which is reversed during the later phases. This behaviour was common to almost all of the compound classes in this fraction and is consistent with earlier arguments. Fractionation of the mobilized native oil in the formation would result in a lower carbon number distribution in the produced oil relative to the core sample during early phases of the combustion process. This shift would be reversed as the heavier (i.e. more "retained") components in each compound class were produced later in the cycle. The polar nature of the compound classes in this fraction argues against the presence of any firefront-affected material.

Gas Oil

Some data for the gas oil distillation cuts are shown in Table 6. There is no clear trend to the variations in wt% for this cut. These variations are likely due to factors such as channeling and formation heterogeneities. There is little change in either the nitrogen or sulfur content between the core and produced oil samples. The column chromatographic data for the gas oil cuts are shown in Table 7. There are few obvious trends in the fraction yields. Most of the major changes involve the redistribution of aromatics between fractions 2 and 3.

The GC-MS analyses of the chromatographic fractions from the gas oil distillation cuts reveal little change in distribution between compound classes. Figure 11 shows the compound class diagram (selected samples) for fraction 1. Although there is a small relative increase in the open chain compounds for the 871116 sample, this change is transitory. The GC-MS analyses for the other fractions show little variation in relative compound class. There are some changes with respect to carbon number distribution in some of the fractions. The open chain group from the saturates fraction 1 and the alkyl benzenes

from fraction 2 are shown as a function of time in Figures 12 and 13, respectively. A slow but sustained shift towards lower carbon number is observed for both compound classes over the period of the study, in accord with fractionation of the oil during migration through the formation.

Residue

Some data for the residue cuts of the core and fireflood-produced oils are given in Table 8. The wt% of the residue cuts decrease significantly during phase one. While there is a reversal of this trend for the phase two samples, a return to the core sample levels is not achieved. This "trough" in the wt% of the residue cut correlates with the increased wt% of the middle distillate cut during this period (Table 2). There is no significant change in the wt% of nitrogen or sulfur over the time period of the study. The modest increase in the wt% of oxygen at the end of phase one would not be expected to cause problems during upgrading of the produced oil.

The column chromatographic yields for the residue cuts are shown in Table 9. Of considerable interest is the negligible increase in the asphaltene content of the produced oils relative to that of the core sample. Any low temperature oxidation occurring during the in situ combustion process is clearly not affecting the produced oil. One would again expect no major problems in the subsequent upgrading process. Similarly, no general increase in polar material is observed in the residue cuts. It may be observed that the wt% of fraction 3 (di- and polyaromatics) undergoes a gradual decrease as the in situ combustion process proceeds.

The yields for all of the chromatographic fractions undergo considerable fluctuations during the period of the study. The dynamics of the formation and the in situ process are the likely causes of this behaviour. Changes in the conformance and temperature of the combustion zone coupled with formation heterogeneity would be expected to cause substantial variations in the composition of the produced oil.

The GC-MS analyses of the chromatographic fractions from the residue distillation cuts show little relative change in the compound classes. The only alteration worthy of mention in this regard is illustrated in Figure 14, which shows the compound classes for fraction 1 (selected samples) as a function of time. A small relative increase in the open chain and 1-ring saturate groups is observed, although the 4- and 5-ring naphthenes remain the predominant compound classes. It should be noted that Figure 14 represents only that portion of fraction 1 with sufficient volatility to be observed by the GC-MS technique.

There is significant variation in the distribution of carbon numbers within some of the compound classes as the combustion process proceeds. These variations, however, are not uniform. An example of this is depicted in Figure 15, which shows the change in the open chain saturates from fraction 1 as a function of time. The maximum in the carbon number distribution changes several times over the time period of the study. This may again be attributed to the complex nature of the recovery process.

Summary and Conclusion

Upgrading of the produced oil from the in situ combustion field pilot is reflected in the reduced viscosity and density of the whole oil and increases in the amount of material boiling in the naphtha and middle distillate ranges. A concomitant decrease in the wt% of the residue cut is observed. The absence of an increase in acid number or asphaltene content during the study are auspicious signs for the subsequent upgrading of the produced oil.

The naphtha cut exhibited significant increases in aromatic content early in the production cycle. In addition, there was a sustained shift to lower carbon numbers in the various compound classes. This presence of "new" compounds in the naphtha cut as a result of the combustion process was highlighted by the appearance of C_6 to C_{12} n-paraffins.

The aromatic content of the middle distillate cut also increased early in the production cycle although there was little indication of permanent shifts in compound classes or carbon number distributions. It was the relative growth in the wt% of the middle distillate cut which most affected the quality of the produced oil.

The wt% of the gas oil cuts underwent little change as a result of the fireflood and there appeared to be little relative change with respect to compound classes in the chromatographic fractions. There were, however, shifts to lower carbon number for some of these classes.

The wt% of the residue cuts for the fireflood-produced oils were lower than that of the corresponding cut from the core sample. There was no significant change in the nitrogen or sulfur content of the residue over the time period of the study. In addition, there were negligible increases in the asphaltene and polar components of the residue cuts from the produced oils relative to the core sample.

It is generally concluded that the quality of the oil produced during the one year period of this in situ oxygen combustion process should cause no major problems in the subsequent upgrading of the oil. On the contrary, the properties of the oil suggest that the recovery process itself resulted in a small but significant amount of upgrading.

Acknowledgements

The authors would like to acknowledge BP Resources Canada, Petro-Canada, and the Canada Centre for Mineral and Energy Technology (CANMET) for funding this study under the Energy Conversion Cost-Shared Program 1988/1989 and BP Canada, Petro-Canada, and Alberta Oil Sands Technology and Research Authority for supplying the samples and granting permission to publish. The skilled technical assistance of the Oil Sands Analytical Group and Mr. Marv Rawluk (GC-MS) are gratefully acknowledged.

References

1. C. Reichert; B. Fuhr; H. Sawatsky; R. Lafleur; B. Verkoczy; D. Soveran; K. Jha, "Fireflood Recovery Process Effects Upon Heavy Oil Properties", Fuel Science and Technology International, 7 (1989) 851.

2. K.N. Jha; R. Lafleur; H. Sawatsky; B. Verkoczy; D. Soveran; C. Reichert; B. Fuhr, "The Effect of Recovery Processes on the Characteristics of the Produced Heavy Oil", Fourth UNITAR/UNDP Conference on Heavy Crudes and Tar Sands, preprint Vol. V, August, 1988, paper 41.

3. M.R. Fassihi; K.O. Meyers; K.R. Weisbrod, "Thermal Alteration of Viscous Crude Oils", SPE 14225, Presented at the 60th Annual Technical Meeting of the SPE, Las Vegas, NV (1985).

4. R.G. Moore; J.P. Millour; D.W. Bennion; D.A. Best, "Comparison of Laboratory and Field Performance of In Situ Combustion", Presented at the Fifth Annual Advances in Petroleum Recovery and Upgrading Technology Conference, Calgary, Alberta (1984).

5. J.C. Monin; A. Audibert, "Thermal Cracking of Heavy-Oil/ Mineral Matrix Systems", SPE 16269, Presented at the SPE International Symposium on Oil Field Chemistry, San Antonio, Texas (1987).

6. J.C. Monin; A. Audibert, "Alteration of Heavy Crudes Under High Pressure Steam Conditions", ACS Symposium on the Chemistry of Enhanced Oil Recovery, Division of Petroleum Chemistry, Philadelphia, Penn., Proceedings 29, No. 4 (1984) 1223.

7. A. Audibert; J. Roucache, "Modification in the Composition of Crude Oils During In Situ Combustion", ACS Symposium on Advances in Oil Field Chemistry, Division of Petroleum Chemistry, Toronto, Ontario, Proceedings, (1988) 185.

8. J. Jou; M.R. Gray; J. Thiel, "Structural Changes in Cold Lake Bitumen Due to In Situ Combustion", Alberta Oil Sands Technology and Research Authority Journal of Research, 5 (1989) 75.

9. J.M. Jacobson; M.R. Gray, "Structural Group Analysis of Changes in Peace River Bitumen Caused by Thermal Recovery", Fuel, 66 (1987) 753.

10. M.G. Ursenbach; R.G. Moore; J.D.M. Belgrave; D.W. Bennion, "Variation of Oil Properties During In Situ Combustion", Presented at the Canadian Heavy Oil Association Quarterly Meeting, Calgary, Alberta, Proceedings (1989).

11. C. Reichert; B. Fuhr; G. Williams; M. Polikar, "Alterations to Bitumen Produced by the In Situ Combustion Process at the Oxygen Wolf Lake Project, Alberta", Draft Report.

12. J.V. Bonilla; M.H. Engel, "Chemical and Isotopic Redistribution of Hydrocarbons During Migration: Laboratory Simulation Experiments", Organic Geochemistry, 10 (1985) 181.

13. J.V. Bonilla; M.H. Engel, "Chemical Alteration of Crude Oils During Simulated Migration Through Quartz and Clay Minerals", Organic Geochemistry, 13 (1988) 503.

14. R.T. Morrison; R.N. Boyd, "Organic Chemistry", Allyn and Bacon, Boston, (1976) 992-996.

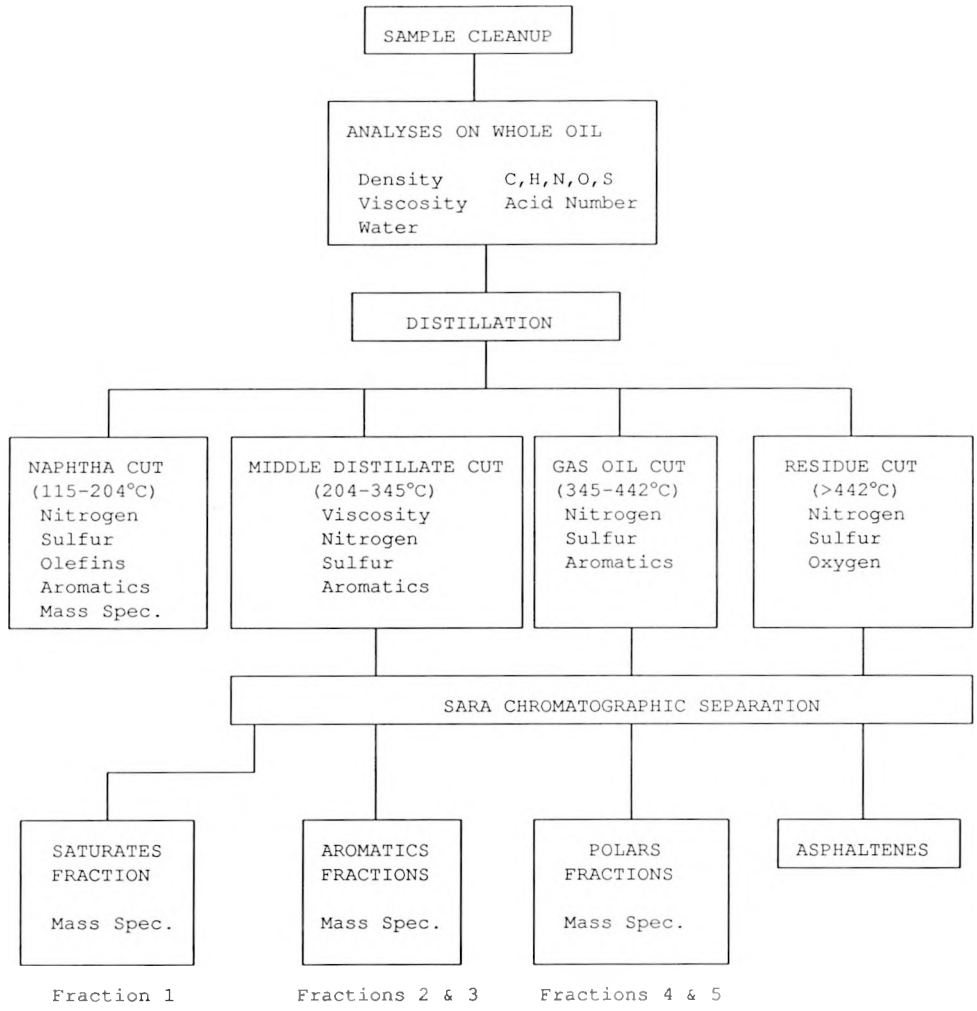

Figure 1: Flow scheme showing sample separation procedure and analytical techniques.

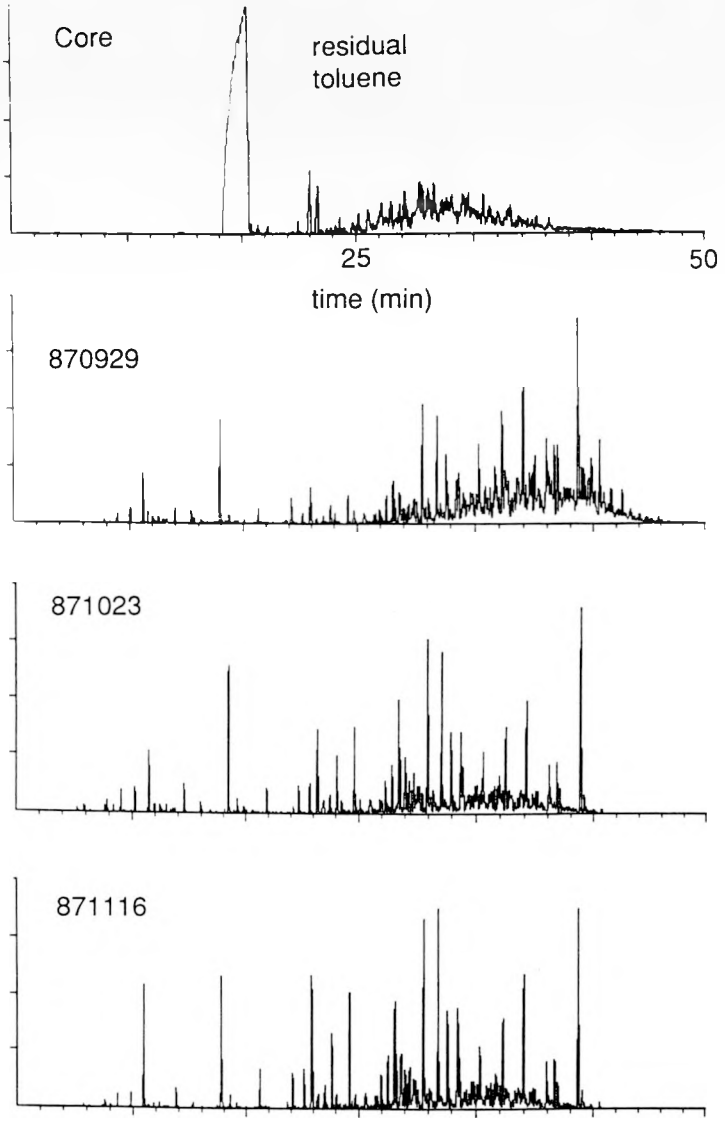

Figure 2. The mass spectrum total ion chromatograms for the naphtha cuts of the core and phase one samples. Ion current in arbitrary units on the y-axis.

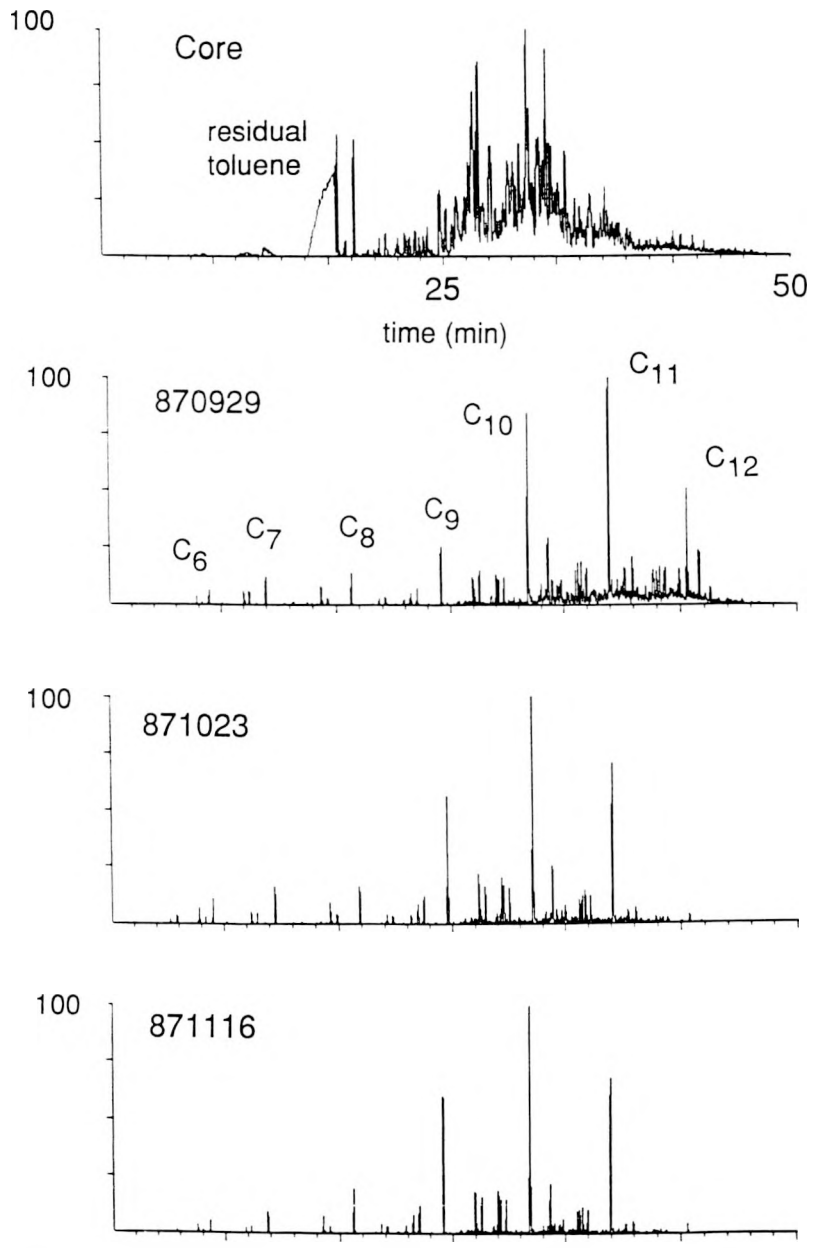

Figure 3. Reconstructed ion chromatograms for the open chain saturates in the naphtha cuts of the core and phase one samples. Relative ion current (%) on the y-axis.

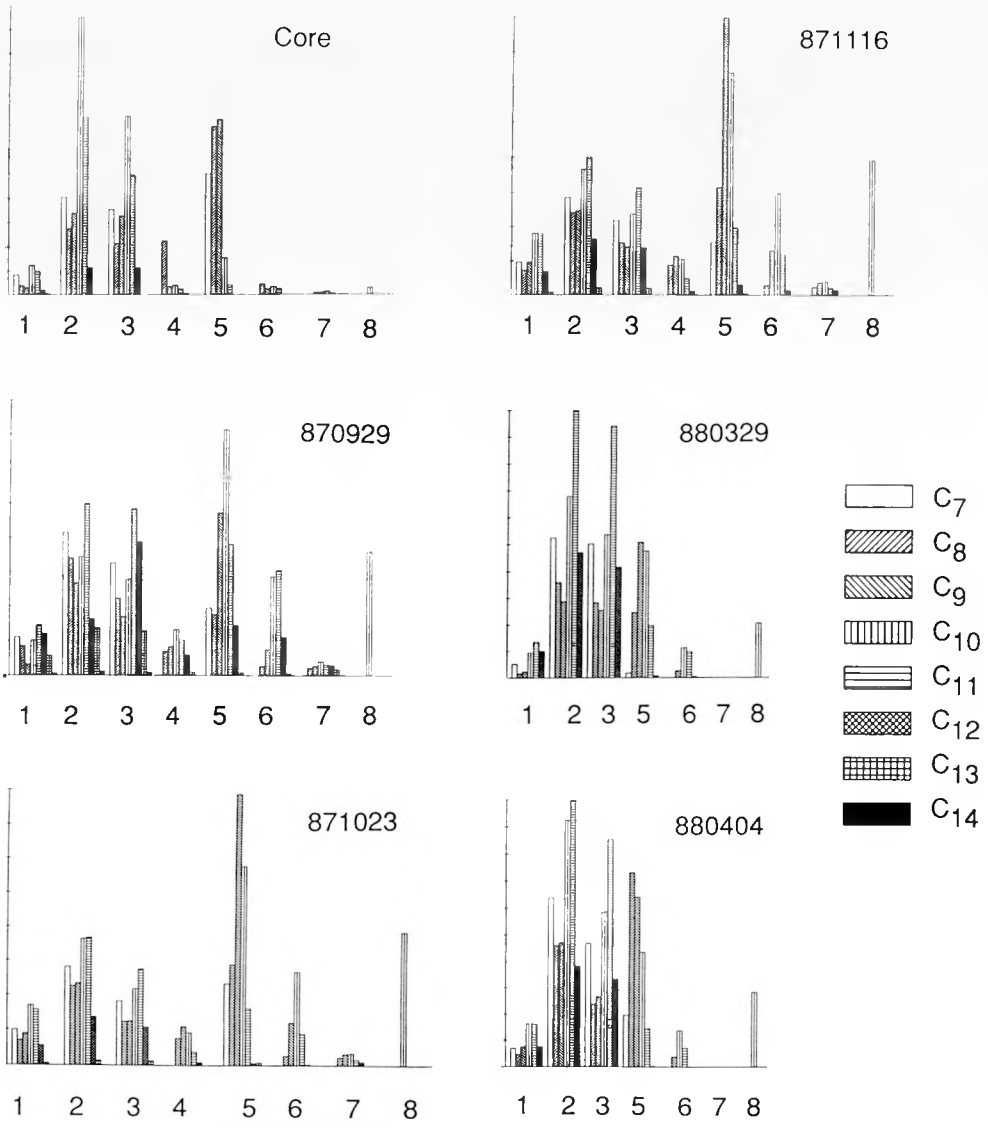

Figure 4. GC-MS analysis of the distribution of compound classes in the naphtha cuts. Intensity (arbitrary units) on y-axis.

1= open chain saturates
2= one-ring saturates
3= two-ring saturates
4= three-ring saturates
5= alkyl benzenes
6= benzocycloparaffins
7= dibenzocycloparaffins
8= naphthalene

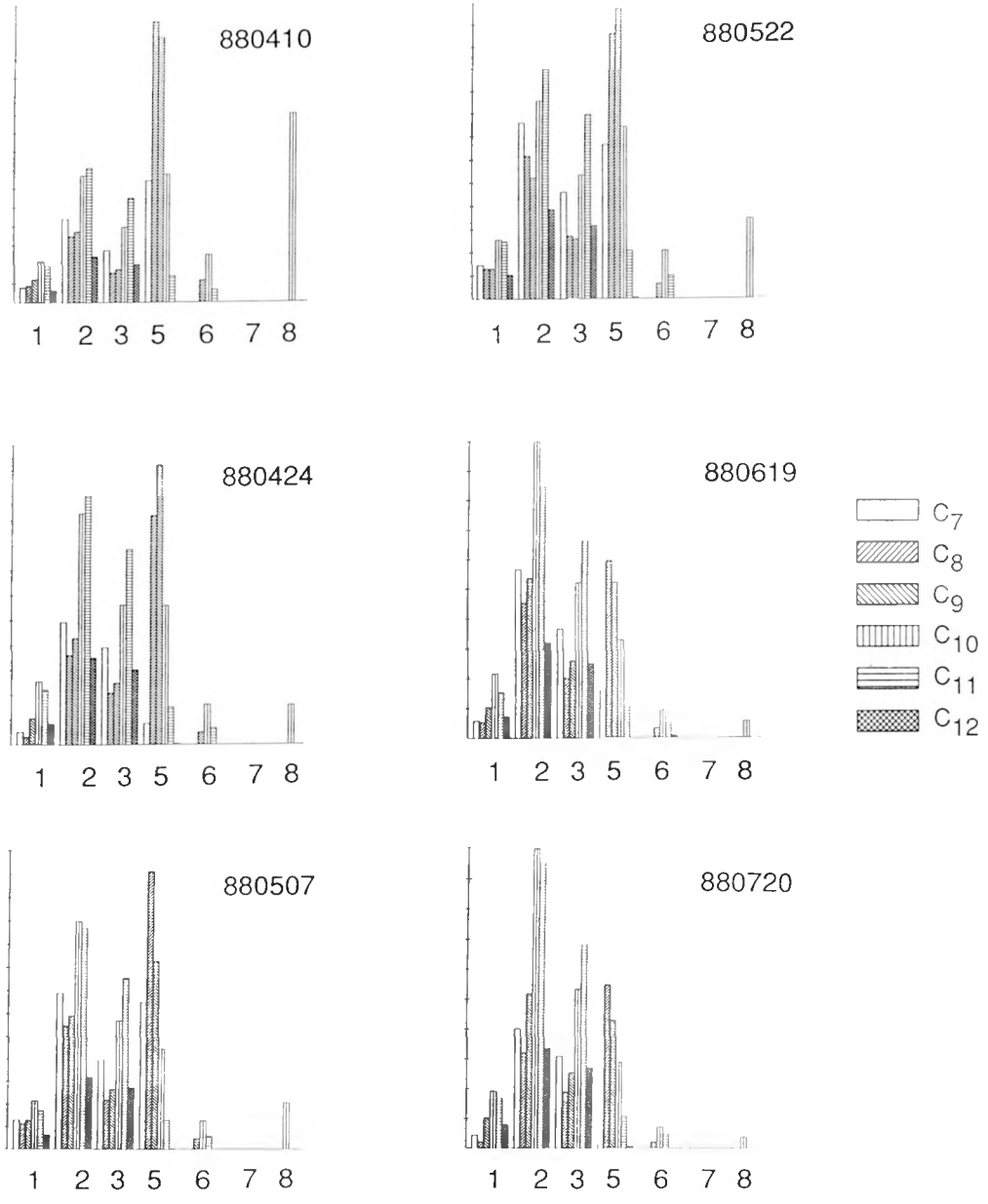

Figure 4. (cont.)

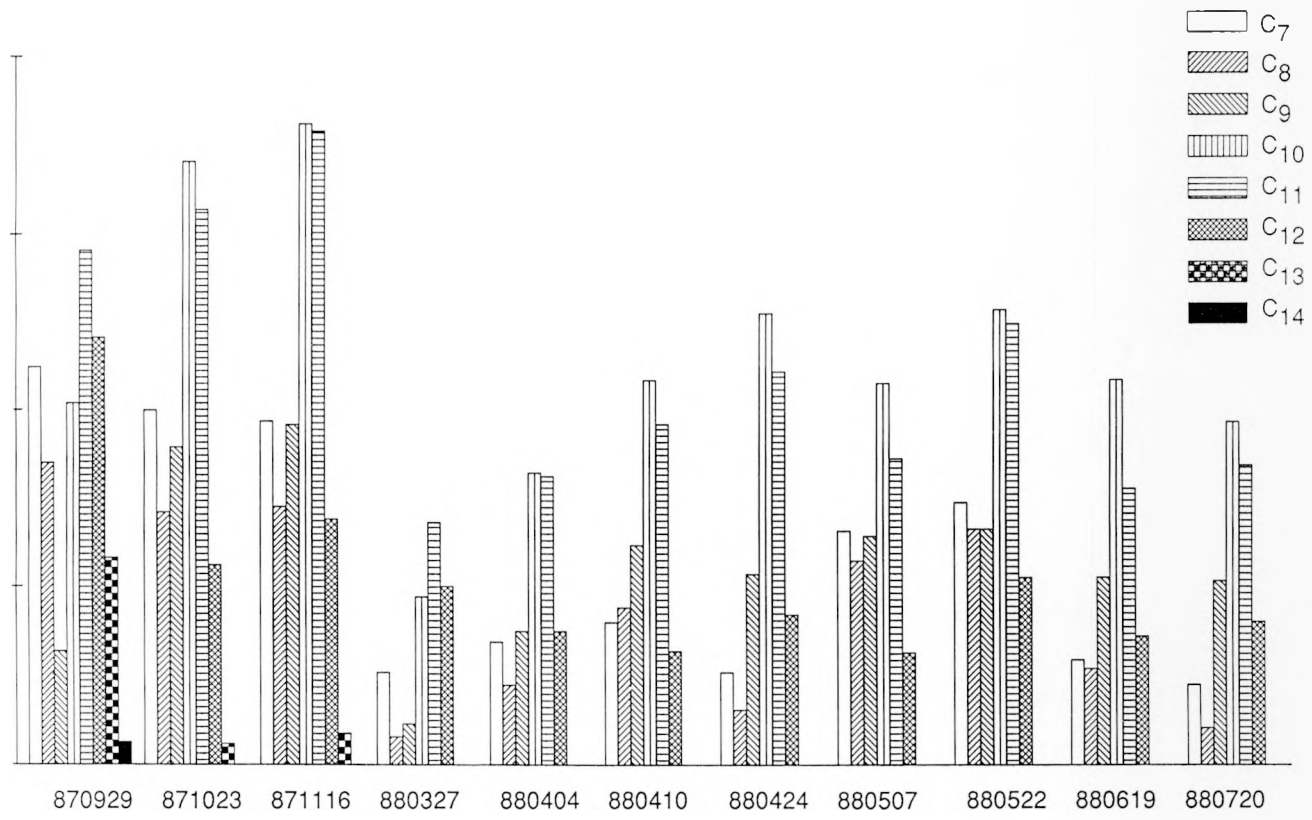

Figure 5. GC-MS analysis of the open chain saturate compound class from the naphtha cuts over the time period of the study.

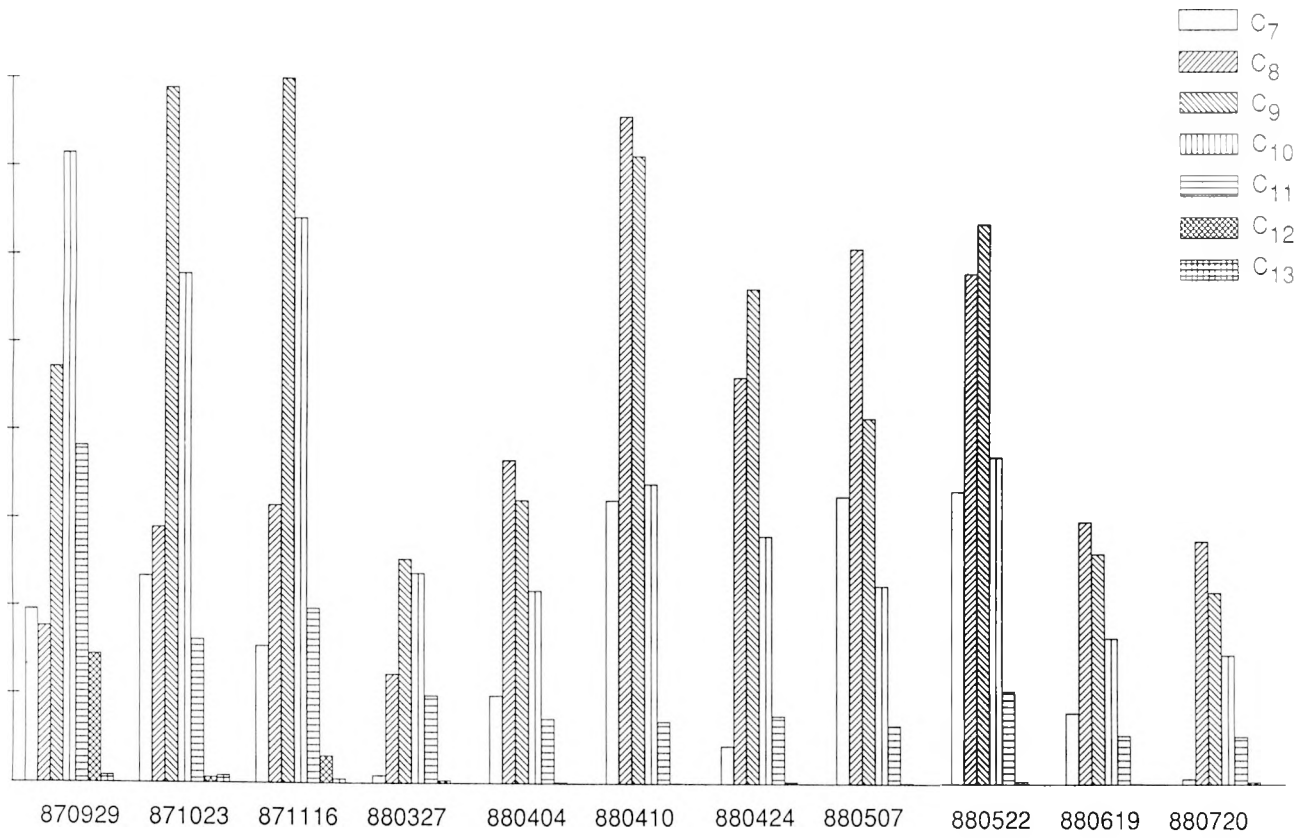

Figure 6. GC-MS analysis of the alkyl benzene compound class from the naphtha cuts over the time period of the study.

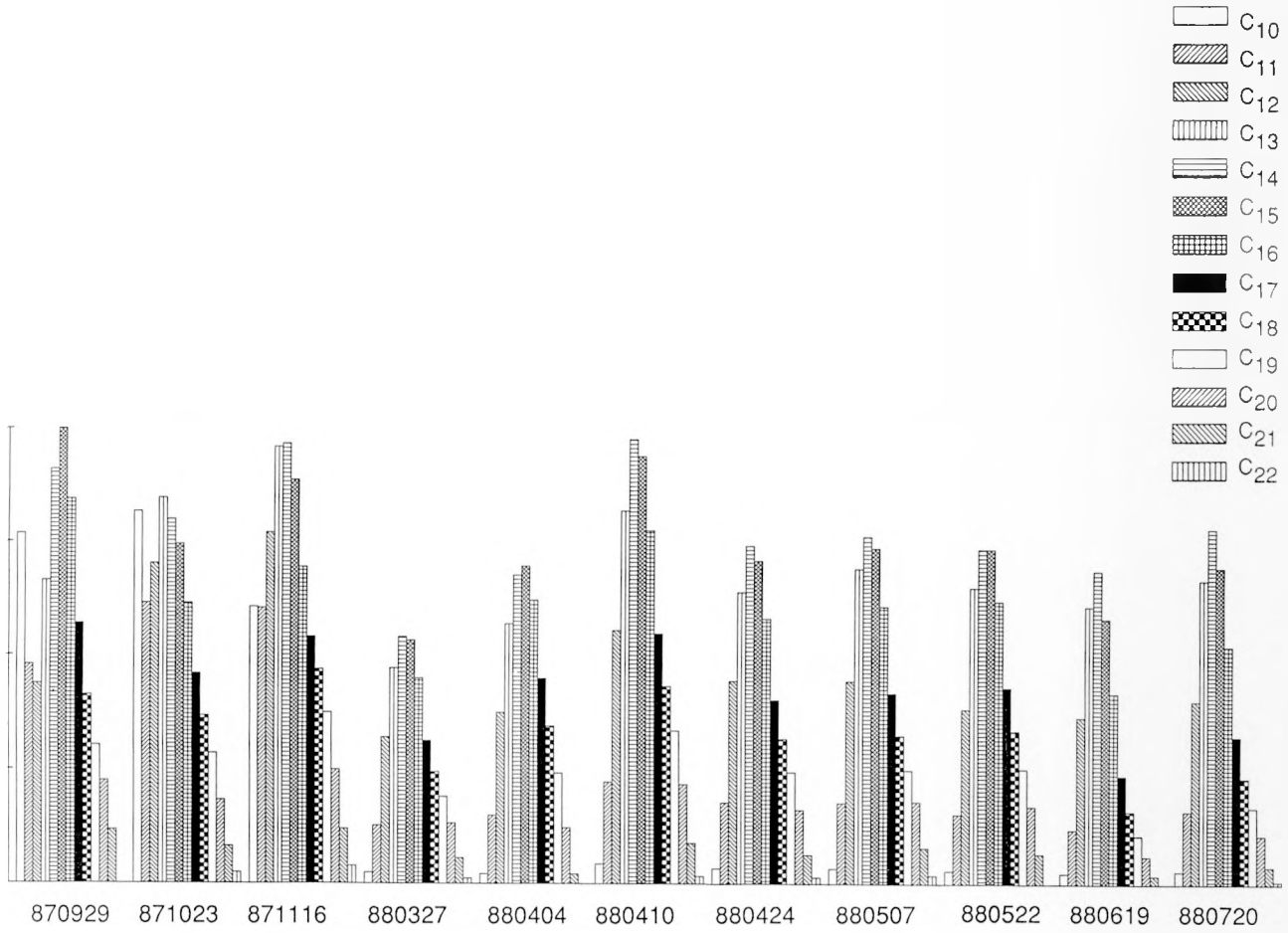

Figure 7. GC-MS analysis of the open chain saturate compound class from fraction 1 of the middle distillate cut as a function of time.

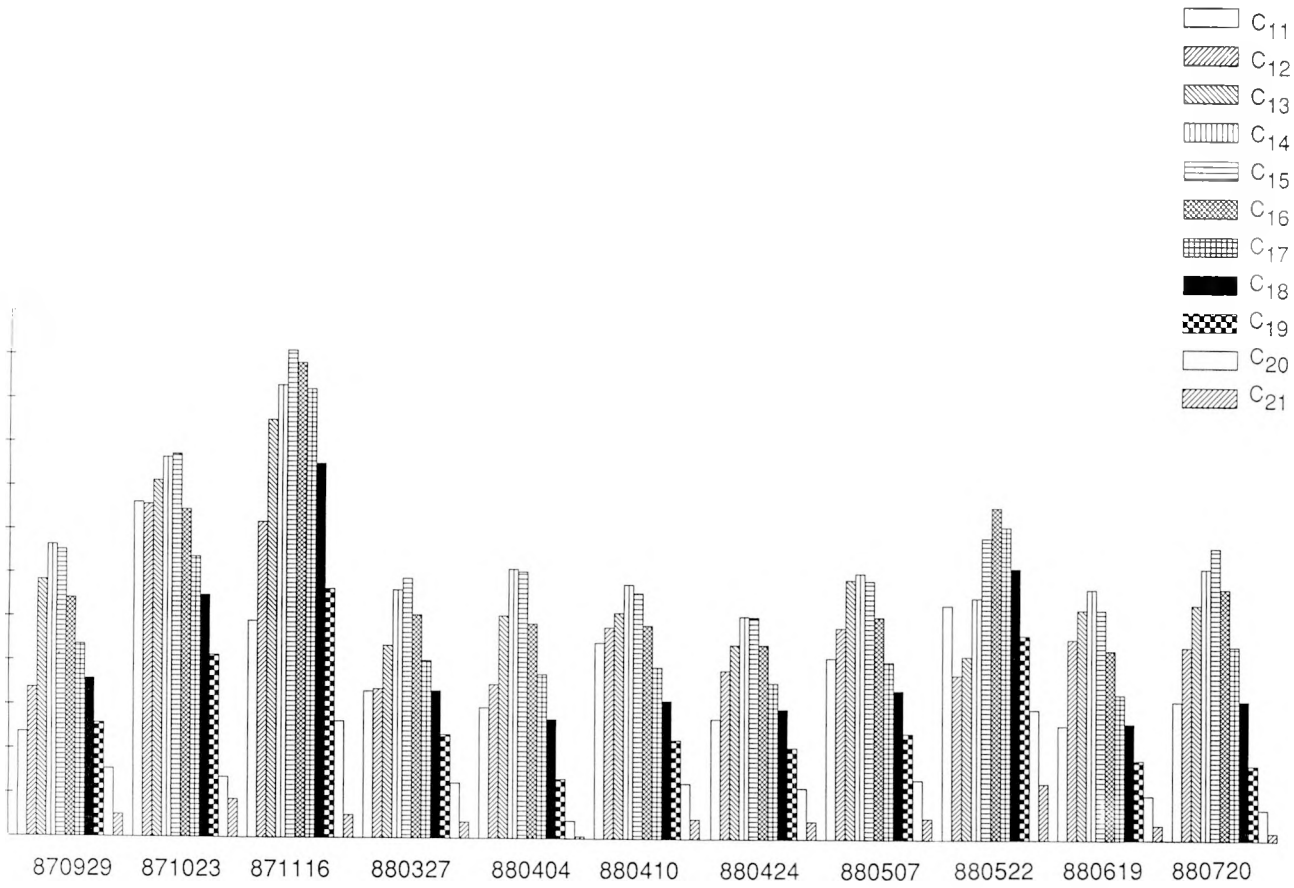

Figure 8. GC-MS analysis of the alkyl benzene compound class from fraction 2 of the middle distillate cut as a function of time.

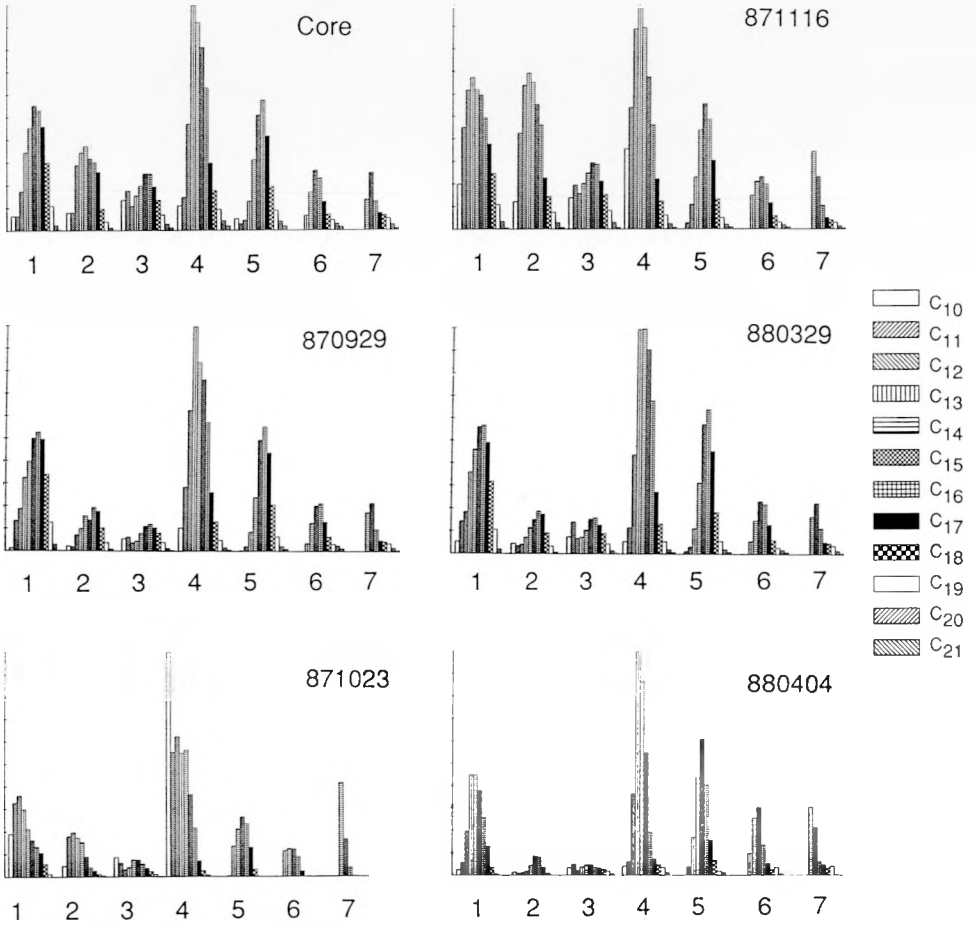

Figure 9. GC-MS analysis of the distribution of compound classes in fraction 3 of the middle distillate cuts.

1= alkyl benzenes
2= benzocycloparaffins
3= benzodicycloparaffins
4= naphthalenes
5= naphthocycloparaffins
6= fluorenes
7= phenanthrenes/anthracenes

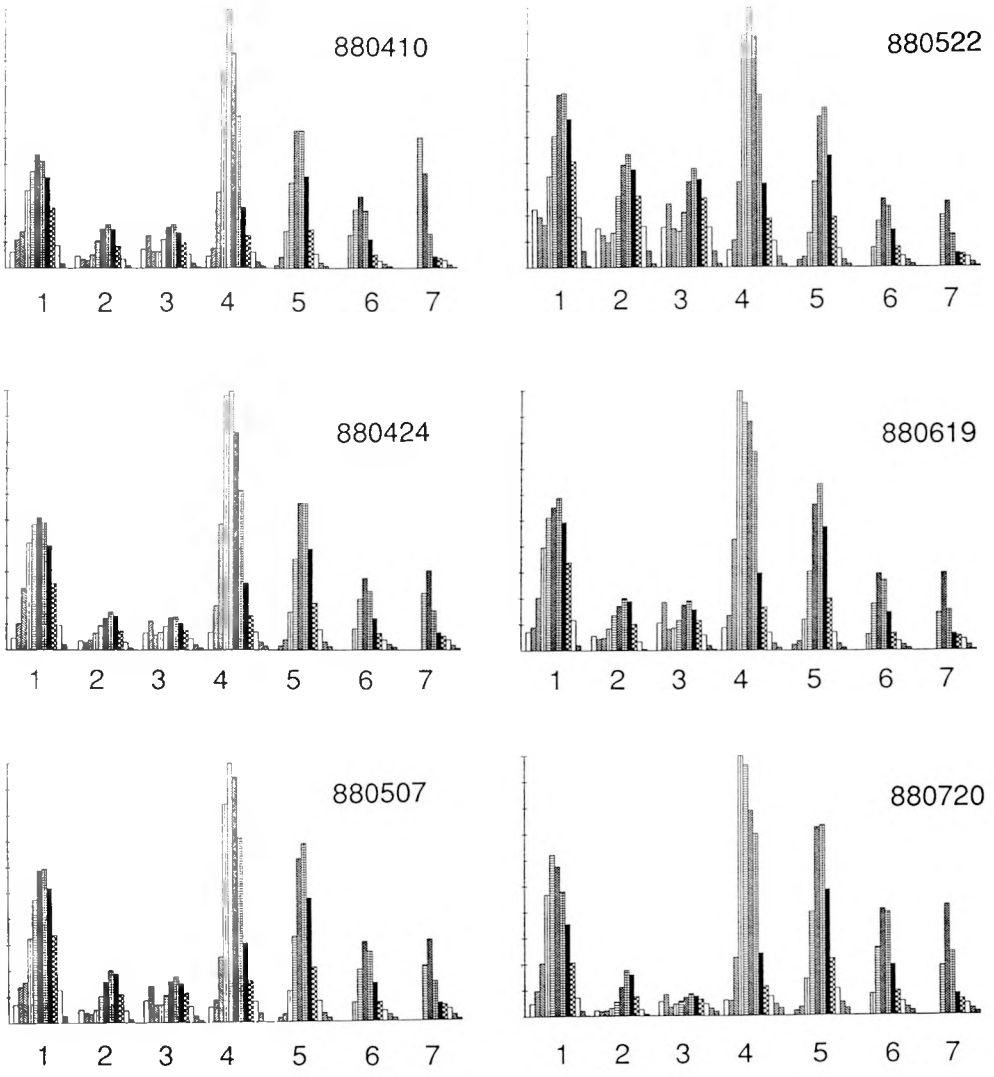

Figure 9. (cont.)

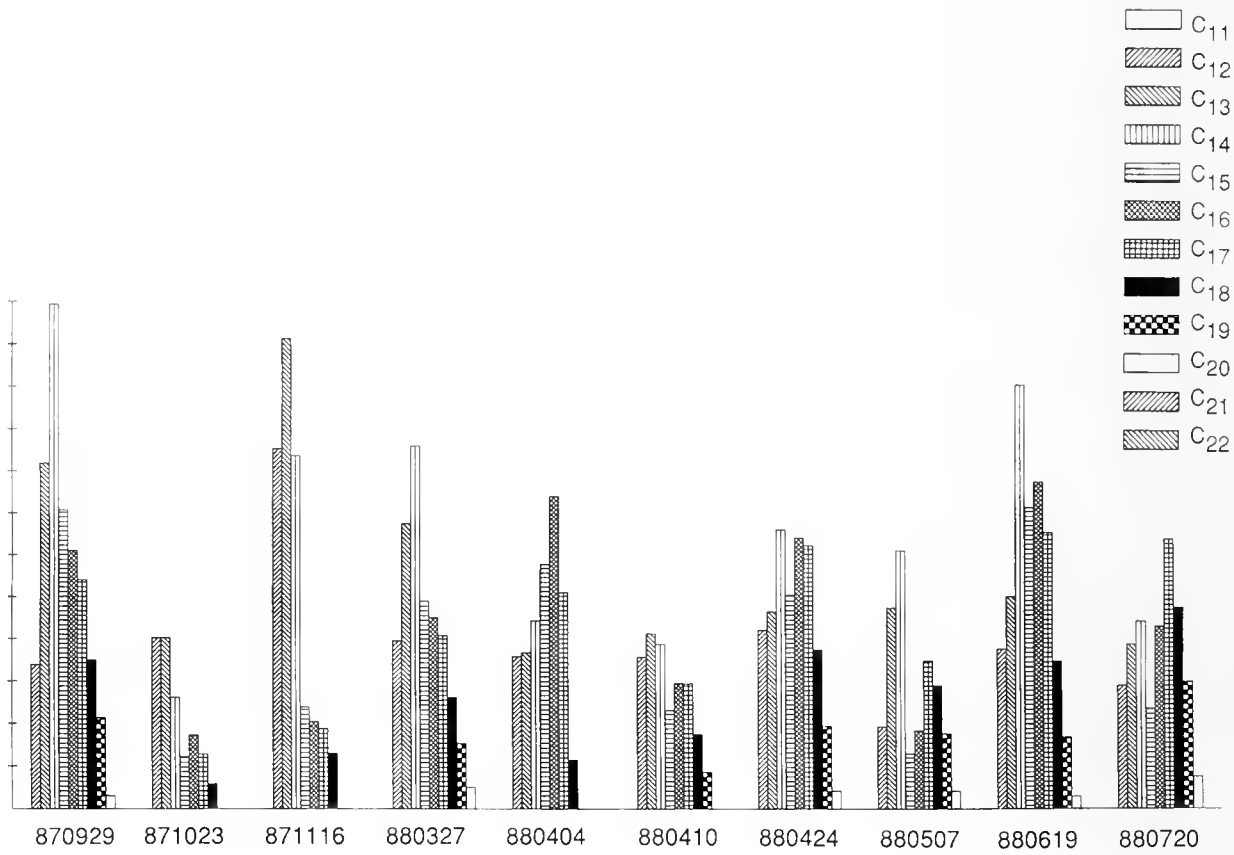

Figure 10. GC-MS analysis of the dibenzothiophene compound class from fraction 4 of the middle distillate cut as a function of time.

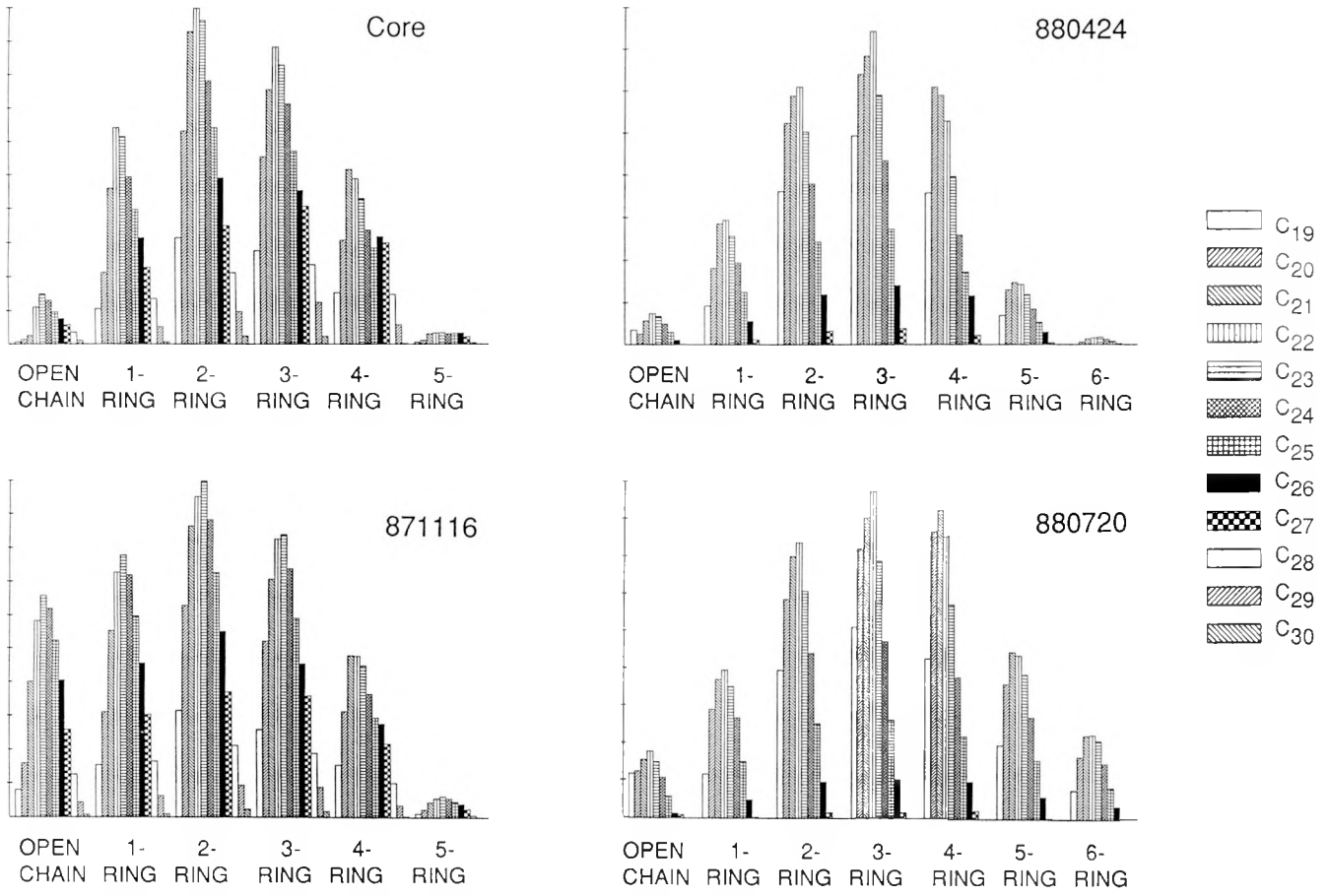

Figure 11. GC-MS analysis of the distribution of compound classes in fraction 1 of the gas oil cuts (selected samples).

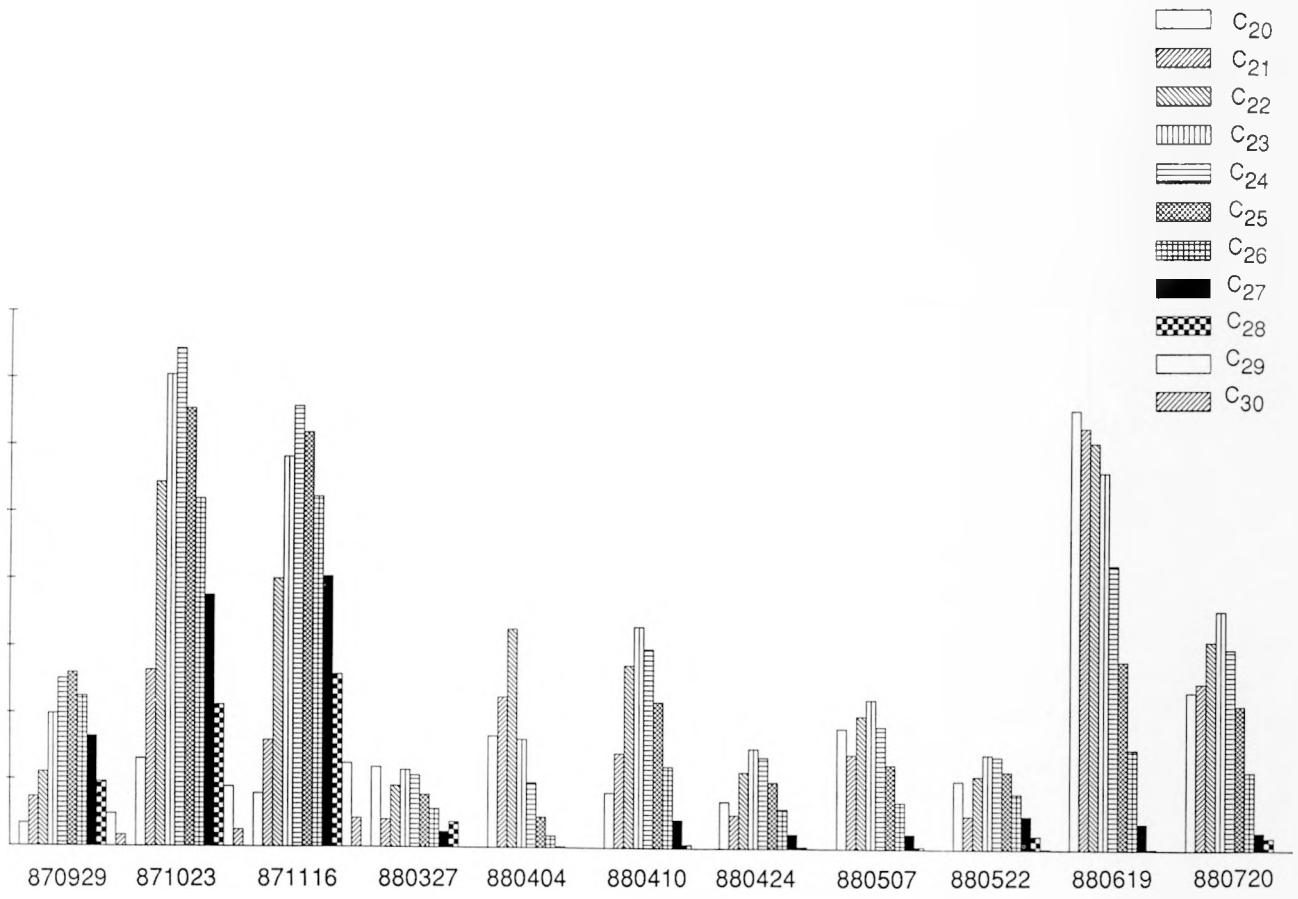

Figure 12. GC-MS analysis of the open chain saturate compound class from fraction 1 of the gas oil cut as a function of time.

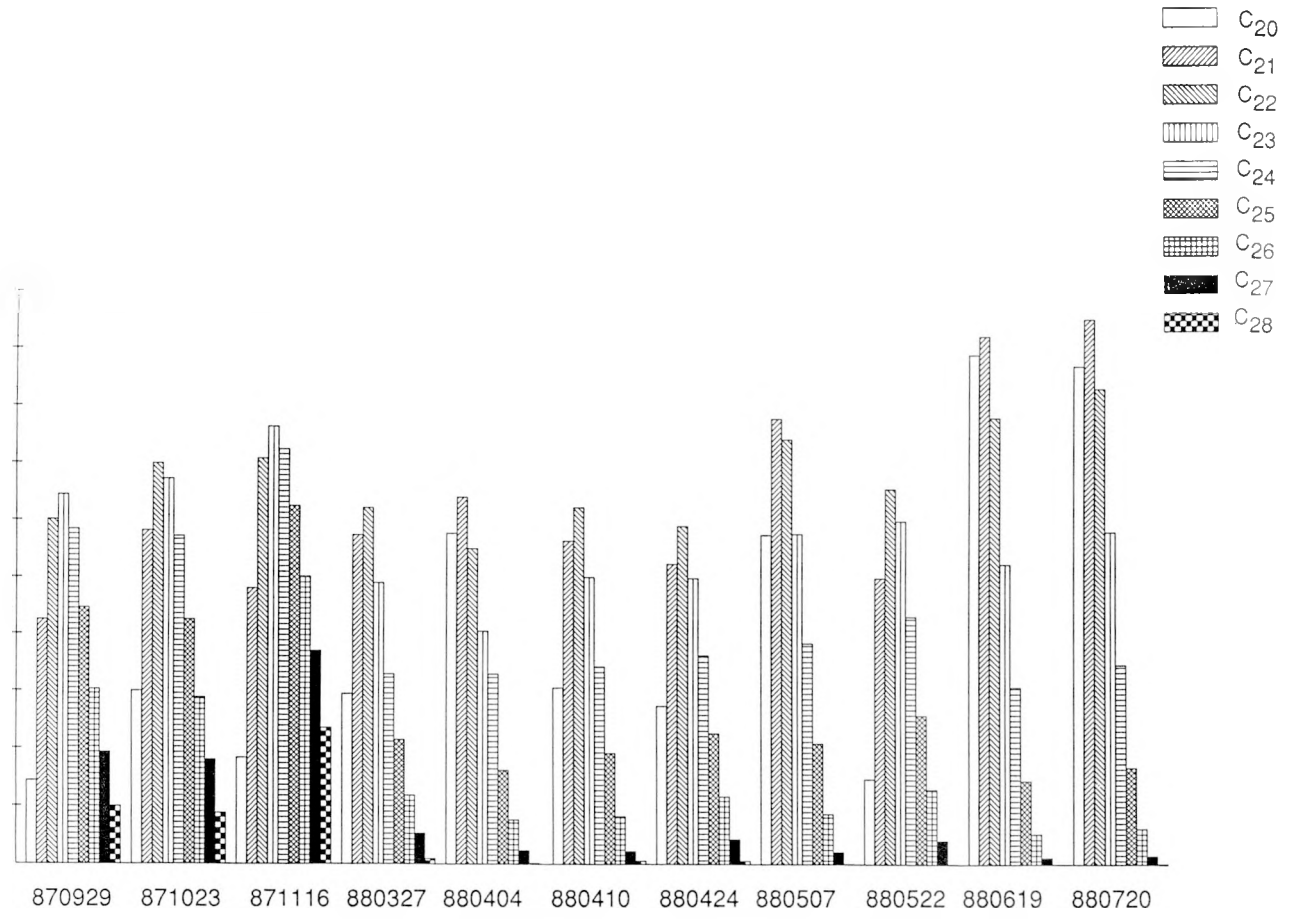

Figure 13. GC-MS analysis of the alkyl benzene compound class from fraction 2 of the gas oil cut as a function of time.

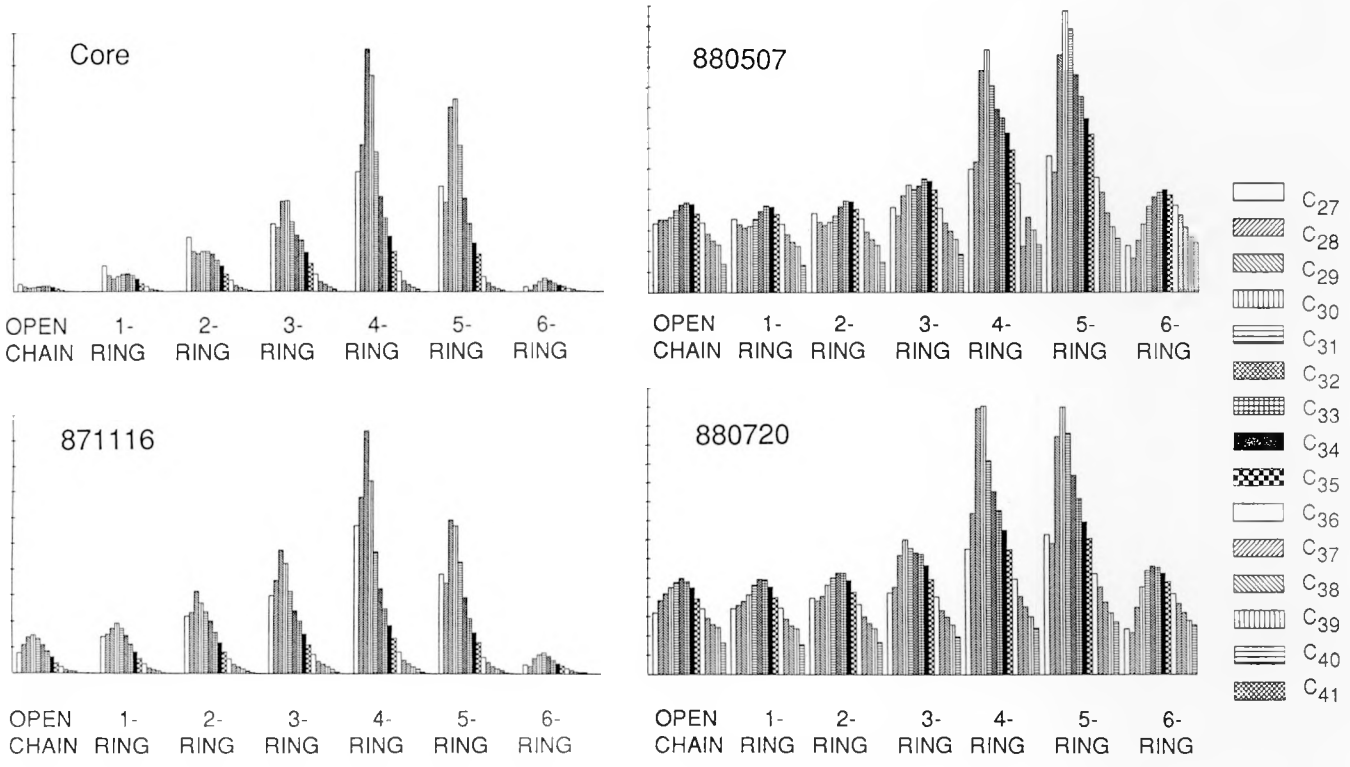

Figure 14. GC-MS analysis of the distribution of compound classes in fraction 1 of the residue cuts (selected samples).

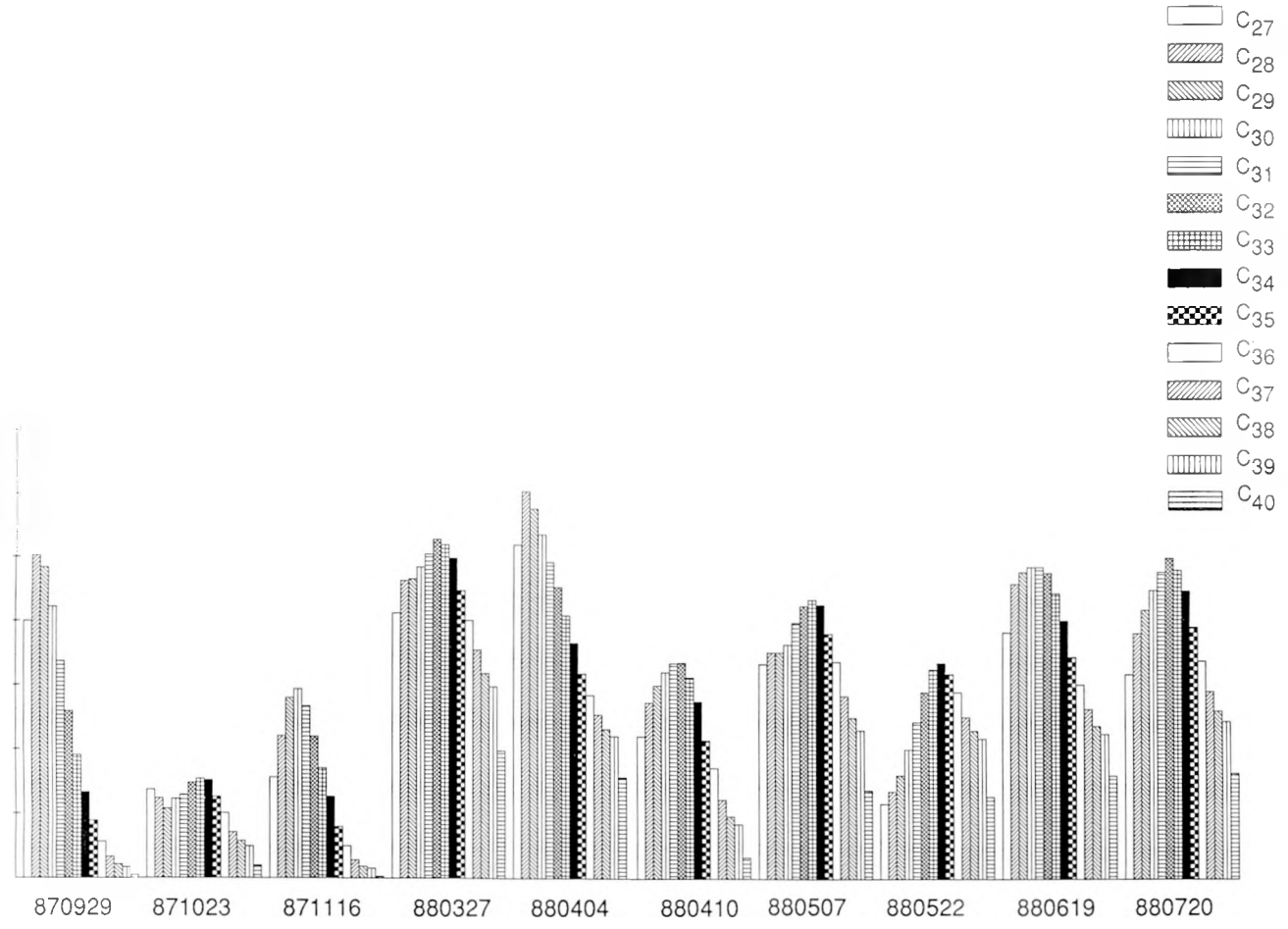

Figure 15. GC-MS analysis of the open chain saturate compound class from fraction 1 of the residue cut as a function of time.

Table 1: **Analytical Data for Whole Oil Samples**

SAMPLE	DENSITY g/ml@25°C	VISCOSITY cps, T(°C)	WATER wt%
Core	.9894	@25°: 49400±600 @60.6°: 1300±37 @80.3°: 372±5	
870929	.9888	@25°: 12700 @60.6°: 557 @80.3°: 175	0.07(Vol%)
871023	.9795	@25°: 1765 @60.6°: 148 @80.3°: 59	0.08(Vol%)
871116	.9688	@25°: 820 @60.6°: 92.7 @80.3°: 39	0.05(Vol%)
880327	.9924	@30°: 9450 @80°: 208	0.17
880404	.9835	@30°: 5630 @80°: 155	0.10
880410	.9810	@30°: 2180 @80°: 88.1	0.08
880424	.9858	@30°: 5140 @80°: 143	0.23
880507	.9879	@30°: 6450 @80°: 170	0.14
880522	.9828	@30°: 4000 @80°: 132	0.13
880619	.9906	@30°: 6720 @80°: 170	0.15
880720	.9898	@30°: 7460 @80°: 179	0.15

SAMPLE	NITROGEN[a] wt%	OXYGEN[a] wt%	SULFUR[b] wt%	ACID NO.[c] mg KOH/g	CARBON[a] wt%	HYDROGEN[a] wt%
Core	0.60	0.47	4.80	1.32	83.9	10.67
870929	0.41	0.72	4.45	1.16±0.01	84.21	10.31
871023	0.34	0.93	4.13	1.05±0.01	84.01	10.22
871116	0.36	0.62	4.27	0.95±0.03	83.84	10.77

a measured by CHN combustion analysis; oxygen by difference
b measured by IP 242
c measured by ASTM D664

Table 2: Distillation Data (Vol%) for Whole Oil Samples

SAMPLE	NAPHTHA (115-204°C)	MIDDLE DISTILLATE (202-345°C)	GAS OIL (345-442°C)	RESIDUE (>442°C)
Core	0.8*	17.7	16.5	65.0
870929	2.59	19.56	17.66	60.19
871023	2.54	24.33	15.58	57.55
871116	3.21	30.27	19.72	46.80
880327	1.52	18.99	21.71	57.78
880404	2.16	17.64	16.66	63.54
880410	3.43	22.06	15.44	59.07
880424	2.60	20.17	18.66	58.57
880507	2.55	18.53	19.69	59.23
880522	4.04	18.85	21.55	55.56
880619	3.06	18.99	13.67	64.28
880720	2.47	18.61	15.99	62.93

*contains residual toluene used in extraction of the oil from the core

Table 3: Analytical Data for Naphtha Cuts

SAMPLE	AROMATICS[a] (wt%)	AROMATICS[b] (vol%)	OLEFIN[b] (vol%)	NITROGEN[c] (mg/L)	SULFUR[d] (wt%)	DISTILLATION (vol%)
Core	-	-	-	<1.0	0.29	0.8*
870929	29.9	32.6	5.6	29.0	1.23	2.59
871023	35.4	34.5	11.4	137.0	1.39	2.54
871116	34.3	32.1	12.5	196.0	1.41	3.21
880327	17.2	15.7	4.1	7	0.77	1.52
880404	19.6	18.5	4.2	12	0.93	2.16
880410	34.2	31.7	6.3	17	1.16	3.43
880424	22.0	24.2	6.2	5	0.95	2.60
880507	21.8	21.9	2.9	15	1.00	2.55
880522	26.7	23.4	3.8	20	0.92	4.04
880619	16.8	15.6	3.3	13	1.03	3.06
880720	16.0	14.4	3.6	13	0.86	2.47

a measured by supercritical fluid chromatography; the balance are saturates
b measured by ASTM D1319
c measured by chemiluminescence
d measured by ASTM D1552

* contains residual toluene

Table 4: Analytical Data for Middle Distillate Cuts

SAMPLE	VISCOSITY (cts)	AROMATICS[a] (wt%)	NITROGEN[b] (wt%)	SULFUR[d] (wt%)	DISTILLATION (vol%)
Core	3.99	37.5	0.0010[c]	1.63	17.7
870929	3.66	39.5	0.0075[c]	2.12	19.56
871023	3.47	48.1	0.024[c]	2.62	24.33
871116	3.69	45.4	0.028[c]	2.27	30.27
880327		36.8	0.04	2.01	18.99
880404		36.3	0.08	1.99	17.64
880410		40.6	0.05	1.73	22.06
880424		37.8	0.02	2.13	20.17
880507		37.8	0.03	1.88	18.53
880522		38.4	0.03	2.01	18.85
880619		35.4	0.05	1.97	18.99
880720		37.4	<0.01	2.01	18.61

a by supercritical fluid chromatography; the balance are saturates
b measured by CHN combustion analysis unless otherwise specified
c measured by chemiluminescence
d measured by ASTM D1552

Table 5: Middle Distillate Cut Chromatographic Yields (Wt%)

SAMPLE	Fraction 1 SATURATES	Fraction 2 AROMATICS	Fraction 3 AROMATICS	Fraction 4 POLARS	Fraction 5 POLARS
Core	57.5	18.3	19.2	1.0	1.5
870929	54.8	19.7	13.5	2.5	4.2
871023	45.9	18.9	30.4	1.6	1.4
871116	52.1	18.1	21.9	1.1	2.5
880327	60.4	18.1	16.3	2.0	2.5
880404	65.1	20.7	10.2	1.1	1.8
880410	52.9	17.7	26.1	1.0	1.0
880424	57.9	18.5	17.8	1.2	1.6
880507	59.5	17.2	16.9	1.9	1.1
880522	57.0	14.5	21.5	1.5	3.0
880619	60.8	17.0	16.3	1.5	1.7
880720	63.6	22.0	8.8	0.7	1.0

Table 6: Analytical Data for Gas Oil Cuts

SAMPLE	NITROGEN[a] (wt%)	SULFUR[c] (wt%)	DISTILLATION (vol%)
Core	0.043[b]	3.29	16.5
870929	0.072[b]	3.36	17.66
871023	0.066[b]	3.28	15.58
871116	0.10[b]	3.24	19.72
880327	0.14	3.41	21.71
880404	0.09	3.01	16.66
880410	0.10	2.86	15.44
880424	0.14	3.15	18.66
880507	0.20	3.59	19.69
880522	0.15	3.41	21.55
880619	0.10	3.46	13.67
880720	0.16	3.25	15.99

a measured by CHN combustion analysis unless otherwise stated
b measured by chemiluminescence
c measured by ASTM D1552

Table 7: Gas Oil Cut Chromatographic Yields (Wt%)

SAMPLE	Fraction 1 SATURATES	Fraction 2 AROMATICS	Fraction 3 AROMATICS	Fraction 4 POLARS	Fraction 5 POLARS
Core	36.8	9.5	40.9	7.3	4.2
870929	31.7	18.9	35.4	7.9	7.9
871023	33.7	17.3	40.4	4.7	3.7
871116	35.7	8.2	37.7	6.9	9.3
880327	31.8	14.7	36.1	5.8	8.7
880404	35.1	22.9	34.8	4.2	3.9
880410	35.4	19.2	33.6	4.3	5.0
880424	34.9	19.6	32.0	4.8	6.2
880507	35.1	22.4	30.5	3.8	4.6
880522	30.6	15.8	37.3	5.9	8.0
880619	43.4	31.0	17.9	5.0	0.6
880720	39.5	25.5	22.8	3.3	5.8

Table 8: Analytical Data for Residue Cuts

SAMPLE	NITROGEN[a] (wt%)	SULFUR[b] (wt%)	OXYGEN (wt%)	DISTILLATION (vol%)
Core	0.58	5.78	1.01	65.0
870929	0.51	5.53	1.03	60.19
871023	0.57	5.28	1.00	57.55
871116	0.37	5.39	1.39	46.80
880327	0.66	5.12		57.78
880404	0.58	5.17		63.54
880410	0.61	5.28		59.01
880424	0.69	5.64		58.57
880507	0.62	5.67		59.23
880522	0.67	5.63		55.56
880619	0.66	5.19		64.28
880720	0.65	5.54		62.93

a measured by CHN combustion analysis
b measured by ASTM D1552

Table 9: Residue Cut Chromatographic Yields (Wt%)

SAMPLE	Fraction 1 SATURATES	Fraction 2 AROMATICS	Fraction 3 AROMATICS	Fraction 4 POLARS	Fraction 5 POLARS	ASPHALTENES
Core	11.2	4.8	19.2	11.5	30.0	23.5
870929	12.1	8.2	18.7	7.9	23.0	28.8
871023	8.8	10.3	19.7	10.2	25.6	24.1
871116	11.5	9.4	19.4	9.1	25.0	25.3
880327	10.3	7.0	17.5	32.3	2.5	25.2
880404	12.8	4.7	14.5	7.9	29.2	22.7
880410	10.2	6.9	11.6	8.5	32.5	23.8
880424	11.1	7.6	13.4	8.1	31.0	24.4
880507	10.8	6.5	12.0	8.0	29.3	24.8
880522	6.7	8.5	14.2	12.8	25.1	25.4
880619	12.2	6.5	12.5	6.6	29.8	25.4
880720	9.9	8.0	13.3	7.6	28.2	24.6

GEOLOGY, GEOCHEMISTRY AND RESOURCE CHARACTERIZATION

Western Oil Shales Attrition and Breakage: Testing and Mineral Characterization

by

Ulrich Grimm and Glenn Swaney
U.S. Department of Energy
Morgantown Energy Technology Center
Morgantown, West Virginia 26505

Abstract. Retorting oil shale weakens the structural strength of the material and causes the formation of fines which are carried out of the reactor and can significantly deteriorate the quality of the products. The goal of this work is to develop, in a systematic manner, a predictive model based on fracture experiments and process properties. Preliminary work using simple drop shatter tests has been conducted with two western oil shales. Their Fischer assay values were 23 and 65 gal/tons. The breakage behavior was investigated on material which had been exposed to temperatures between ambient and 1,000°C. In this range the oil shale materials undergo several chemical and physical changes. These are the pyrolysis of the organic compounds, the calcination of dolomite, and, possibly, the burnout of residual char to generate heat for the retorting process. The onset of sintering of the spent shale material in this range is apparent. Accompanying changes in the mineral composition were studied by X-ray diffraction. The drop shatter tests were designed to acquire fundamental design information for the construction of a more advanced test apparatus which allows single particle breakage testing under process temperatures and atmospheres. The hot impact tester (HIT) will investigate fracture attrition of shales by impacting single, hot shale particles with a high-speed pneumatic piston.

Introduction

Mineral and structural changes in oil shale during retorting cause considerable attrition of the original material. The fines thus produced are potentially detrimental to process equipment, product composition, and the environment. Dust contamination in shale oil liquids is known to cause many problems, such as depositing in pipes and heat exchangers, deactivating catalyst beds during the upgrading and refining process, and generally imposing serious separation and disposal problems. The goal of this work is to develop, in a systematic manner, a predictive model of the formation of fines based on fracture experiments and process properties.[1] This model may be useful in attacking one of the problems involved in retorting oil shales, the contamination of the product liquids by particles of the shale minerals.

Preliminary work to measure the material strength using a simple drop shatter test method has been conducted on two western oil shales, with Fischer assay values of 23 and 65 gal/tons. The breakage behavior was investigated on material which had been exposed to temperatures between ambient and 1,000°C. This range extends well above the process temperatures sufficient for the oil shale pyrolysis in which considerable amounts of char are produced. The residual carbon content could be utilized to supply the heat

* Oak Ridge Associated Universities Postgraduate Research Fellow

required for the pyrolysis of the oil shales by means of a gasification or combustion process.[2] The process temperature for these reactions would be around 1,000°C.[3] The kinetics of mineral transformation and energy conversion reactions in the range above the pyrolysis have been extensively studied.[4,5,6] They can significantly alter the strength of the spent shale material. The onset of sintering could eventually be used in an agglomerating environment to obtain an easily disposable process residue. However, no data are available on the material strength of the spent shales under these conditions. The extent of the mineral reactions has been determined by X-ray diffraction. They were not carried out as a kinetic study but used to characterize a quasi equilibrium condition which could be related to the friability of the material. The X-ray diffraction pattern can be interpreted to reflect the real composition of the shale material at the elevated temperatures since the quenching of the samples was reasonably fast. This cannot be said for the material strength data as will be shown. The problem has been recognized and resulted in the design and construction of a HIT which is not yet operational. This facility is an automated single particle tester and will investigate particle breakage at process temperatures and atmospheres by impacting a high-speed plunger on a falling particle. The studies reported here were carried out to determine the impact forces which have to be included in the performance characteristics of the HIT.[1]

Experimental

Oil Shale Samples

The oil shale materials used in this investigation were obtained through the DOE Project Office in Laramie, Wyoming, and supplied by the courtesy of the Western Research Institute. They originated at the Anvil Points facility near Rifle, Colorado, and were labeled as western oil shale (WOS-65 and WOS-23) according to their Fischer assay values. They arrived at the Morgantown Energy Technology Center (METC) in the form of precut blocks measuring approximately 10 by 10 by 20 cm. Exact measuring and weighing resulted in specific gravities of 2.13 g/cc for WOS-23 and 1.66 g/cc for WOS-65. The results from the chemical analysis of the raw and spent shales materials are presented in Table 1. The elemental composition of the ash material was determined by X-ray fluorescence spectroscopy.

Sample Preparation

The oil shale blocks were inspected for consistency. Only samples with visible parallel bedding layers of uniform thickness were chosen for the drop tests. This was done to avoid further breakage

Table 1. Composition of the Raw and Spent Oil Shales

Composition	WOS-23	WOS-65
Ash	67.44%	57.1%
Volatile Matter	32.01%	42.56%
Total Carbon	16.83%	29.02%
Mineral Carbon	4.78%	3.34%
Hydrogen	1.64%	3.43%
Nitrogen	0.51%	0.92%
Sulfur	0.79%	1.95%
Moisture	0.56%	0.34%
Btu	2,285	5,389
Ash Fusion: ID(°C)	1,212	1,170
ST	1,230	1,193
HD	1,238	1,202
FD	1,252	1,232
Spent Shale Composition		
SiO_2	54.77%	48.8%
CaO	23.93%	17.39%
MgO	8.10%	5.95%
Fe_2O_3	2.66%	4.53%
K_2O	1.68%	1.37%
Al_2O_3	6.46%	9.76%
ZnO	0.05%	0.03%
SrO	0.05%	0.08%
P_2O_5	0.33%	0.46%
TiO_2	0.28%	0.39%
MnO	0.03%	0.04%

by crack propagation along preexisting fault lines. These specimens were then cut on a diamond saw (Di-met Cutter by Buehler) to cubes of about 18 mm edge length for WOS-65. The WOS-23 cubes were cut smaller so that the weight of the pyrolyzed and calcined samples became the same for both grades of oil shale. The samples were then dried and stored in a desiccator for further treatment.

Randomly selected cubes were crushed and sifted to sizes below 150 micrometers for a total of about 1 kilogram. This material was also stored in a desiccator for later use in the mineralogical investigation.

Test Procedures

It was not expected that mineral formations across bedding layers would be identical to those within the layers. The mineralogical studies on the well- mixed powders were therefore restricted to overall reactions which are possible in the specific shale materials under equilibrium conditions. The experimental investigation of the cubed material was carried out to obtain breakage data on the original rock material. Drop testing was used to determine the forces required to break these particles and to present the results on a relative friability scale. Mineralogical analysis of the major specimen were done by X-ray diffraction

spectroscopy on the powdered oil shale samples which were previously exposed to temperatures between ambient and 1,000°C. For this purpose, 1 to 2 gram samples were weighted into alumina crucibles on a precision laboratory balance. The crucibles were loaded into a Lucifer high-temperature melting furnace which is fully programmable and has a maximum operating temperature of 1,650°C. Heat ramps were programmed for 20°C/min (up and down), and the residence time was varied from 24 hours (20° to 400°C), 12 hours (400° to 700°C), to 4 hours (above 700°C). All tests were carried out in air. The temperatures for the heat treatment were spaced into 100°C intervals except where conditions required a 50°C spacing. The weight loss was recorded at the end of each test run and the sample was analyzed for the remaining organic and mineral carbon content. Whenever this form of carbon was present, it was removed by low-temperature ashing as commonly used in coal mineral testing. The actual X-ray diffraction analysis was contracted out.

Drop testing was carried out using the precut cubes described under sample preparation. The precise cutting of these specimen resulted in a very narrow size range for the initial distribution function. Each experiment was conducted using 20 particles. They were individually weighed and placed on a ceramic palette which was inserted into a Lindberg muffle furnace. The heat up rate in this furnace could not be controlled and decreased from 35°C/min in the range from ambient to 400°C down to 10°C at 1,000°C (maximum for this furnace). The residence times were between 36 and 12 hours. The individual particles were weighed again after the heat treatment and stored in a desiccator until the drop tests commenced. As previously reported,[1] a drop height of 12.2 m seemed to yield the best results as far as breakage was concerned. Single particles were dropped from this height on a 50 cm diameter by 5 cm thick stainless steel target. The breakage products were collected in a polyethylene drum liner which was held open with a specially constructed tripod stand. The plastic bag also helped minimize secondary breakage of the fragments resulting from the impact of the particles. Neglecting air resistance, the velocity at impact was calculated to be 15.46 m/sec. The average energy available for breakage was calculated using this velocity and the average mass of the particle for each test. The collected fragments were classified on screens from 9.5 to .125 mm. Generally, the percentage of the mass of the particles with sizes below 9.5 mm was a useful indicator for the friability of the product.

The carbon content of all samples heat treated below 700°C was determined with a UIC/Coulometrics carbon analyzer as total carbon and mineral carbon. The difference was called organic carbon.

Results and Discussion

Drop Testing

The drop tests reported here were carried out on cubes which were heat treated but cooled to ambient condition before the tests. It was not possible to test under real process conditions and the data, therefore, correspond to materials which were quenched at various points in the process. However, the data were useful in the design of the HIT concerning the forces needed to cause breakage. They were also utilized in the modeling effort pertaining to the breakage function.[7]

Upon heating, the western oil shales of this investigation showed two distinguished stages in which weight loss occurs. Figure 1 presents the results of these tests and their dependency on previous heating conditions. The graphs illustrate the carbon loss as well as the weight loss at the respective temperatures. These data for WOS-23 and WOS-65 were taken from tests on the powdered material which were carried out to show the mineral transformation during heat treatment.

The total carbon plots show that the first rise is accompanied by decreasing organic matter content, i.e., the kerogen pyrolyses. The second rise coincides with the disappearance of the carbonate material when the dolomites calcine. This temperature range was found to be 100 to 150°C higher for the WOS-23 which also showed up in the X-ray diffraction pattern.

The weight loss curves of Figure 1 were overlaid in Figure 2 with curves representing the percentage of material passing a 9.5 mm opening sieve. The apparent friability (i.e., percentage of mass of particles smaller than 9.5 mm) curves for WOS-23 and WOS-65 show maxima at different temperatures. This cannot be explained by considering the small difference in the mineral composition of the oil shales which originate from the same mine. It can also not be explained through the error introduced by having a constant drop height but different sample weights as indicated by the weight loss curves. The friability graphs, nevertheless, can be directly compared in the range where weight loss no longer occurs. This was achieved by cutting the WOS-23 slightly smaller than the WOS-65 which resulted in equal weight at temperatures above 700°C. The spent shale cubes at this range had an average weight of 7.2 g and with a final velocity of 15.46 m/sec, the impact energy comes to 0.86 nm (Newton meters).

A possible explanation of the apparent deviation in the amount and the temperature of the maxima in the friability

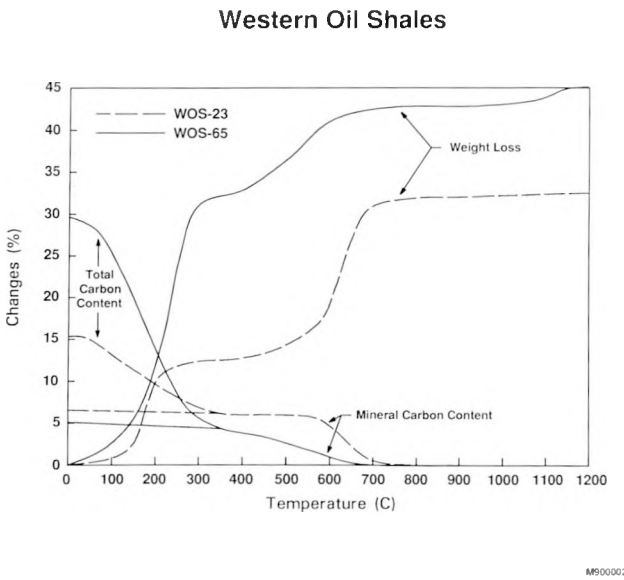

Figure 1. Weight Loss Graphs for WOS-23 and WOS-65 Versus Temperature

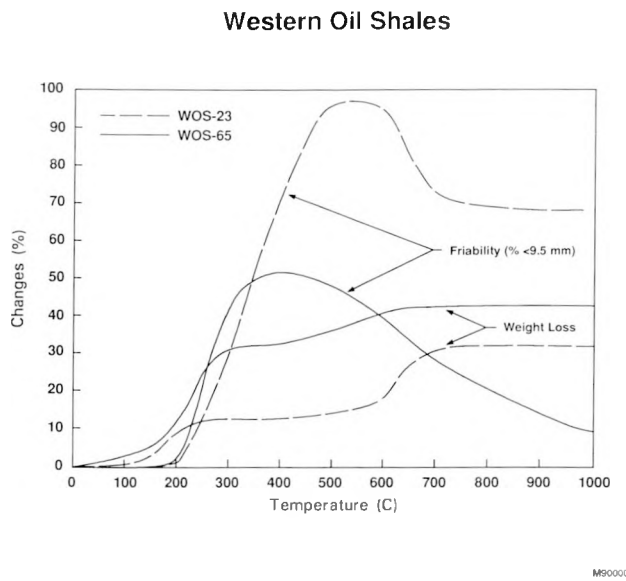

Figure 2. Weight Loss and "Friability" Versus Temperature

graphs can be derived by a visual inspection of the heat-treated oil shale cubes. It has been elucidated that in shales with less than 35 g/t Fischer assay, the kerogen tends to be imbedded in the rock structure while above this value the minerals are imbedded in the kerogen.[8]

Figure 3 shows cubes of both oil shales after the heat treatment at the specified target temperatures. It can be seen that in case of WOS-65 a meltdown occurs at around 400°C. What the graph actually shows is the solidified mineral matter of the shale after it was exposed to 400°C for 24 hours. There was no organic carbon left. Figure 4 shows this particular cube in a close-up and after it was opened with a pen knife. This particle shows that the center was liquid at one time with sufficient mobility for the liquid phase to run out. The outside cubic structure must have been depleted of organic material before melting had set in. All specimens heated to higher temperatures show evidence of this liquid center. The core of these particles had a sponge-like appearance with uniform coloration and no discernible bedding layer structure. This can only be interpreted by assuming that considerable mixing took place. As stated previously, the heat treatment facility for the drop tests samples had no heat rate controls. A high heating rate, however, could pass the cubes fast enough through the critical liquefying range, that the liquid could be contained within the original shape of the particle. The WOS-23 however did not behave in a similar manner and displayed well-defined remanents of the original bedding layers throughout the whole shape.

As a consequence, the products of the shatter tests have their own characteristic shapes. The particles formed from WOS-65 did not show any preferential orientation of the breakage pattern and displayed irregular pattern. The WOS-23 broke preferentially in between bedding layers and the products resembled flakes and plates. It is therefore conceivable that these materials crack under differing mechanisms. The WOS-65 shows the genuine breakage of a homogeneous body, while the basic comminution of WOS-23 occurs along pre-existing cracks parallel to the bedding layers. This could explain the difference in the friability between both spent shale materials.

The difference in the structure of WOS-23 and WOS-65 can furnish an explanation for the shift in the maxima of the friability with temperature. The WOS-23 maximum friability occurs in the range where the carbonates calcine. In this process carbonates tend to shrink by about 40 percent thus weakening the rock structure. The drop test results also show a very high residual friability at higher temperatures. This indicates that almost no cross linkage occurs between bedding layers by mineral reactions. In the case of the WOS-65, the maximum shifts to the range where the kerogen pyrolyzes, confirming that at this high oil content the minerals are imbedded in the kerogen. Since considerable mixing takes place in

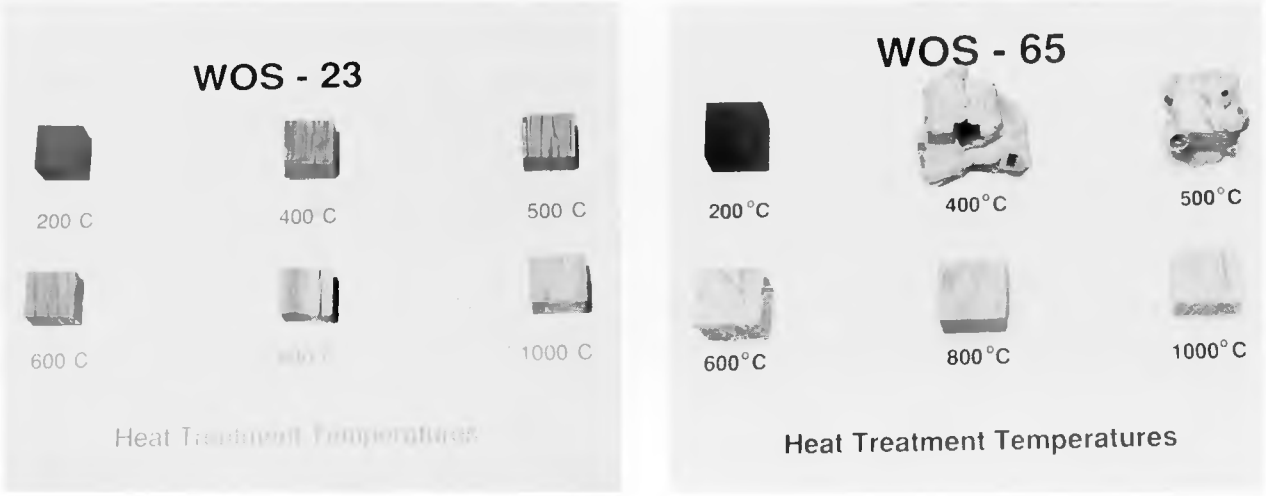

Figure 3. Oil Shale Cubes With Heat Treatment Temperatures

this phase, all mineral reactions studied on the powdered materials can happen. This might be the reason for the increasing stability of the spent shale materials at higher temperatures.

The behavior of the minerals caused by the heat treatment of both oil shales was studied on well-mixed pulverized samples. This was done not to study the kinetics of the reactions but to gain some equilibrium data which could help in the interpretation of material strength behavior. The graphs presenting the total integrated intensities of the major crystalline constituents in the shale and their products are shown in Figures 5 and 6.

Several papers have been published dealing with the mineral reactions during heating of oil shales very similar to WOS-23 and WOS-65.[4,5,6] It was therefore not the intent of this investigation to generate new kinetic data for these systems, but to identify possible mechanisms which could effect the strength of spent shales. The samples were heated beyond the temperatures used in the drop tests to extend the range of the X-ray studies to the onset of sintering which would contribute considerably to the strengthening of the material. No attempt has been made to identify the so-called mystery compounds. Their presence in the mixed WOS-65 residue has probably contributed to the increase in strength as can be seen in the friability curves and would explain the steady slope of the curve which could not be interpreted as sintering. However, the disappearance of their signals was a good indication of the start of the sintering process. Testing the friability at these temperatures could not be done with the equipment presently available and has to wait for the completion of the HIT. The temperature dependence of the mineralogical transformations as they appear by their X-ray intensities can be described as follows:

- Quartz
  - WOS-23. Beginning with about 15 percent, the intensity increases at 550°C to a maximum of 32 percent at 650°C and decreases to 10 percent at 900°C.
  - WOS-65. Starts out with 18 percent, increases in intensity around 400°C to a maximum of 36 percent at 600°C and decays exponentially to 3 percent at 900°C.
- Carbonates
  - WOS-23. Calcite and dolomite decrease at about 550° to 600°C and are gone at 700°C.
  - WOS-65. The carbonates begin to decompose at 400°C with dolomite disappearing at 500°C and calcite at 600°C. This is about 150° to 200°C lower than for WOS-23.

Figure 4. WOS-65 Cube at 400°C

- Albite
  - WOS-23. Albite is originally at 22 percent and begins to increase in intensity at 600°C, reaches 66 percent at 700° to 800°C, and decreases rapidly to 41 percent at 900°C.
  - WOS-65. The albite signals increase from 31 percent beginning at 400° to 500 C to about 80 percent at 800°C and decrease rapidly to 23 percent at 1,000°C.
- Melilite

  The melilite signals appear in both spent shale materials at about 600°C and increase to a maximum between 900° and 1,000°C. In addition a second signal showed up in the spent WOS-23 around 900°C. This mineral has not been identified.

The data presented here were generated by measurements on test specimen at ambient temperatures after a previous heat treatment. All the particles used in the drop tests appeared to be "brittle." However, after the observation of a "liquid" phase in the case of WOS-65, the tested particles must have undergone a plastic phase similar to baking and swelling coals. It cannot be expected

X-Ray Difraction Pattern WOS-65

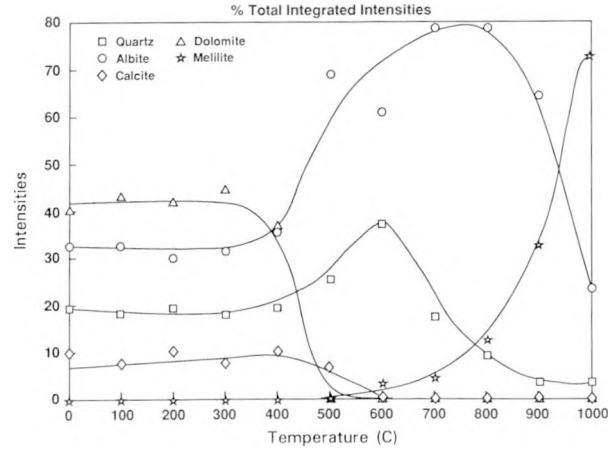

M90000239

Figure 5. Total Integrated X-Ray Intensities of the Major Minerals in WOS-23 Versus Temperature

X-Ray Difraction Pattern WOS-23

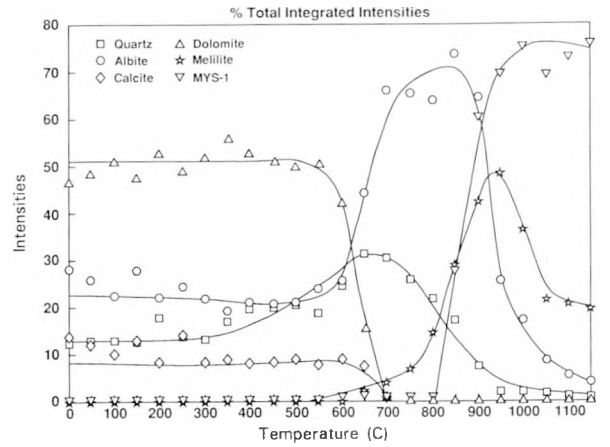

M90000238

Figure 6. Total Integrated X-Ray Intensities of the Major Minerals in WOS-65 Versus Temperature

that oil shales under these conditions behave as they would after cooling. In order to measure the breakage at process temperatures, a HIT has been designed, and its construction is about 80 percent complete. The principle of this single particle shatter apparatus is outlined in Figure 7. A second material test apparatus, the rolling attrition tester (RAT), has been built and tested with eastern oil shale.[7] The results are presented in a second paper at this symposium.

Conclusions

Two oil shales of similar mineralogical but differing kerogen content have been characterized with respect to their behavior upon heating. It was found common to both of them that the steepest increase in friability occurred during the pyrolysis reaction. This increase in friability continued in the lean shale WOS-23 to a maximum in the range where the calcination of the dolomites takes place. In the same region a slight strengthening of the spent material can be observed for the richer shale WOS-65. Similar mineral components in both shales lead to similar reactions in the spent material. The formation of melilite was common to both materials at temperatures above 500°C. This seemingly helped strengthen the particles of WOS-65. Comparable behavior could not be detected for WOS-23. A possible explanation derives from the observation that WOS-65 undergoes a melting process before the pyrolysis which causes a more even distribution of the mineral grains in the product. The WOS-23 tends to break parallel to the bedding layers along preexisting defect lines. The formation of new mineral specimen does not lead to a cross linkage between these layers in the temperature range of this investigation. An evaluation of these results lead to several conclusions. The very rich western shale should not be retorted under low heating rate conditions as in a fixed-bed process. A fluidized bed or other process which prevents agglomeration seems to be more applicable. In case of the leaner shale which tends to break up in flakes, a fluidized bed can easily be defluidized by the emerging shapes. The strengthening of the spent WOS-65 at relative low temperatures seems to favor an agglomerating process for the char utilization and could result in an environmentally safe product for disposal. The high friability of the spent WOS-23 at fairly high temperatures on the other hand suggests using a packed-bed application for the residual carbon combustion.

Acknowledgements

We wish to thank John J. Renton of the West Virginia University Geology Department for providing the X-ray diffraction data and their analysis.

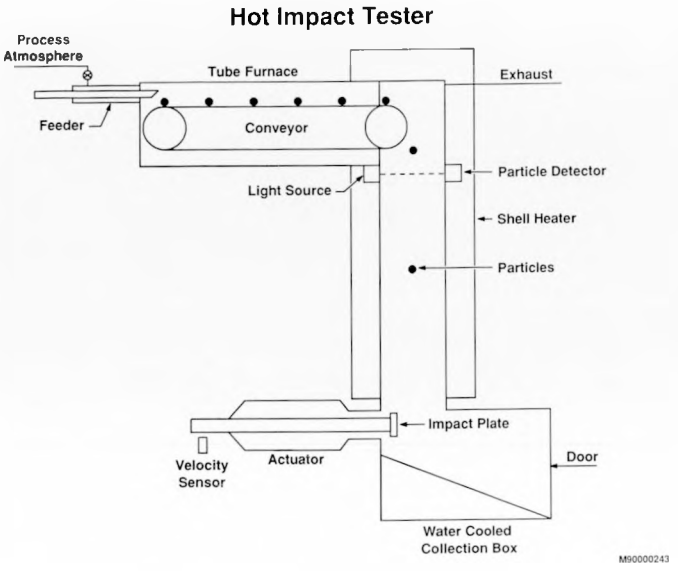

Figure 7. Schematic of the Hot Impact Tester

References

1. U. Grimm and P. H. Kneisel, "Studies on Oil Shale Attrition," Proceedings, 1988 Eastern Oil Shale Symposium, p. 393, Lexington, KY, December 1988.

2. L. Docter, Paper Presented at 68th Annual Meeting of AIChE, Los Angeles, November 20, 1975.

3. W. J. Thomson, M. A. Gerber, M. A. Hatter, and D. G. Oakes, "Kinetics of Oil Shale Char Gasification," ACS Symp. Ser. (United States), v. 163, 1981, pp. 115-127.

4. A. K. Burnham, C. D. Stubblefield, and J. H. Campbell, "Effects of Gas Environment on Mineral Reactions in Colorado Oil Shale," Fuel, 1980, v. 59, pp. 871-878.

5. K. A. Helling and W. J. Thomson, "DXRD Studies of Oil Shale Mineral Reactions," Symposium on Advances in Oil Shale Technology, Denver Meeting, April 5-10, 1987.

6. W. J. Thomson, "Mineral Reactions During High-Temperature Oil Shale Processing," 18th IECEC, Orlando, FL, August 21, 1983, v. 2, pp. 512-517.

7. U. Grimm and G. Swaney, "Eastern Oil Shale Attrition and Breakage: Testing and Modeling," Proceedings of the Eastern Oil Shale Symposium, Nov. 15-17, 1989, Lexington, KY.

8. J. W. Smith, "Theoretical Relationship Between Density and Oil Yield for Oil Shales."

Changes In the Clay Mineralogy of Eastern Oil Shale Induced by Retorting

by

T.L. Robl and A..M. Rubel
Center for Applied Energy Research
University of Kentucky
Lexington, Kentucky 40506
R.I. Barnhisel
Department of Agronomy
University of Kentucky
Lexington, Kentucky 40506

Abstract. The mineralogy of several eastern oil shales have been examined, including; samples from the Cleveland Member of the Ohio Shale, the New Albany Shale, and the Sunbury Shale. Retorted eastern oil shales from pilot tests of the Dravo Traveling Grate Retort, Petrobras' Petrosix Retort, the KENTORT II Retort and a series of spent shales from fixed bed experiments, performed across a range of temperatures, were also examined. The oil shales were composed primarily of clays (70-80%), with lesser quartz (10-25%), and sulfides (2-5%). The clays included illite (61-71%), chlorite (3-11%) and kaolinite (3-7%), with minor amounts of vermiculite and smectite (<4%). The raw and retorted shales were extracted with dilute (6N) H_2SO_4 to measure the effects of mineralogic transformations on the chemical reactivity of the materials.

The principal effects of retorting on the shales was the decrystallization of kaolinite, the partial decrystallization of illite, and the transformation of pyrite to pyrrhotite. Illite decrystallization correlated with processing temperature. The attenuation of the illite 001 peak was directly correlatable to the acid solubility of Al and K. The solubility of Fe was proportional to the degree of pyrite conversion to pyrrhotite. Fe solubility was reduced by the conversion of the iron sulfides to oxides.

Introduction

Oil shale consists primarily of minerals. Organic matter usually constitutes no more than about 10 to 25% of the shale. The nature of the minerals and their chemical and physical transformations upon retorting have a major bearing as to how the shale can be processed, the types and extent of kerogen and shale oil interactions, and the disposal characteristics of the spent shale. The objectives of this paper are to report some of the preliminary findings of on-going research into the nature of the mineralogy of Eastern oil shale; the extent and nature of mineralogic transformations which take place during processing; and the effect these transformations have upon the chemical characteristics of the shale.

Materials.

Four types of materials have been examined, including: 1) a series of unprocessed oil shales; 2) oil shales which have been processed in the Dravo and Petrobras (Petrosix) pilot plants; 3) shales processed in the KENTORT II retort; and, 4) shales which have been systematically pyrolyzed in a fixed bed retort. Oil shales examined include the Sunbury Shale, recovered from a core drilled in Fleming County Kentucky; three samples of the Cleveland Member of the Ohio Shale (simply referred to as Cleveland shale herein), from bulk samples collected in Lewis, Fleming and Montgomery Counties of Kentucky; and the Blocher and Clegg Creek Member of the New

Albany Shale, collected from a core in Marion County, Kentucky. The Cleveland sample from Montgomery County was the feedstock for the Petrobras, KENTORT II, and fixed bed experiments. The feedstock for the Dravo retort test consisted of 1/3 Sunbury and 2/3 Cleveland Shales also mined in Montgomery County, Kentucky.

Methods and Procedures.

Clay Analysis. One of the objectives of the study was to quantitatively determine the clay composition of the shales. A brief description of the procedure used follows, more detailed discussions can be found in Rich and Barnhisel.[1]

The samples were crushed to approximately 6.4 mm with a jaw crusher then pulverized in a ring and puck mill for 5 minutes. The powdered samples were low temperature ashed and/or treated with hydrogen peroxide to remove the organic matter. Unoxidized sample splits were also processed. The samples were then separated into size fractions using an elutriation technique.[2] Each size fraction was vacuum oriented on clay tiles. Five sample size fractions were separated for the materials from the fixed bed retort, and two sizes for the rest of the samples. Size separation is necessary to keep larger particles from masking smaller particles in X-ray diffraction analysis, as the clay minerals typically have smaller particle size distributions and would be the last to settle out. Separate tiles were saturated with either potassium or magnesium. Various heat treatments were then applied (Figure 1). The chemical and physical treatments are necessary to determine the nature and extent of the mixed layered clays.

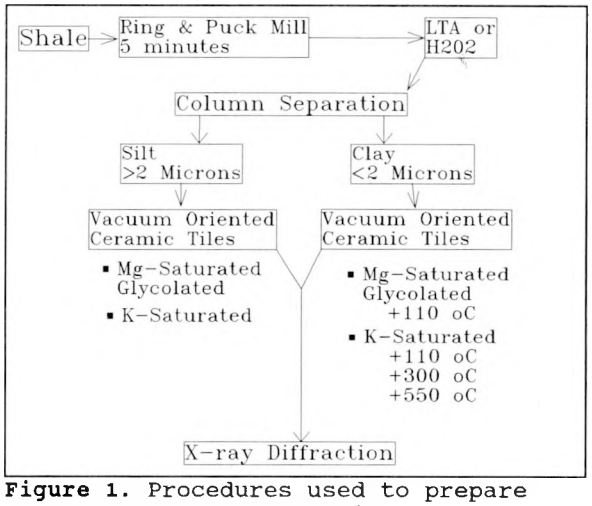

Figure 1. Procedures used to prepare samples for X-ray analysis.

The samples were X-rayed using Cu K-α radiation. The K-saturated samples were scanned following 25, 110, 300 and 550 °C heat treatments and Mg-saturated glycerated fractions were scanned following 25 and 110 °C heat treatments. The proportions of the clay minerals in the feedstock samples were computed from peak height measurements of the basal reflections (001) of the clays and the 4.3 Å quartz peak.[1]

Fixed Bed Pyrolysis. Fractions (140 g) of a sample of Cleveland shale were retorted in a fixed bed apparatus.[3] The shale was heated at a rate of 4 °C/minute to the maximum or "soak" temperature which was held for thirty minutes. A nitrogen sweep, at a rate of 22 cm^3/minute, as measured at room temperature and pressure, was used throughout the runs. Sweep gas flow rates at maximum temperature ranged from 50 to 84 cm^3/min. The soak temperature was incremented for each run by approximately 50 °C, spanning the temperature range from 400 to 850 °C. The soak temperature was briefly exceeded during temperature ramping by up to 14 °C, and the final soak temperature varied from the target, by 2 to 7 °C.

Extractions. Samples of the KENTORT II and fixed bed materials were extracted with H_2SO_4. One gram of sample was mixed with 100 ml of 6N H_2SO_4. The samples were agitated periodically and left to react for approximately 24 hours at room temperature. The extracts were diluted 1:1 with distilled-deionized water and analyzed with an inductively couple plasma spectrometer (ICP).

Results and Discussion

Mineralogy of the Oil Shale Samples.

Eastern oil shale comprises a small component of the Devonian and Mississippian Black Shales, a large and extensive body of sedimentary rocks. A discussion of the regional variation of the mineralogy of these rocks is beyond the scope of this paper. However, a large study of the clay mineralogy of Devonian Shales of the Appalachian Basin was conducted by the U.S. Geologic Survey, with findings similar to this work.[4] The major element chemistry of the shales within the oil shale outcrop belt of Kentucky suggests the mineralogy of the shales to be fairly consistent and homogeneous.[5]

In general, the inorganic component of the oil shales in Kentucky consists of clay minerals, the most abundant being Illite, a 2:1 layer clay (i.e. two layers of tetrahedrally coordinated silica sandwiching a octahedrally coordinated alumina layer), with the interlayers consisting of potassium. In general the illite was found to be comparatively well crystallized (Figure 2) and represented about 2/3 of the minerals (Table I) in the study samples. Second in abundance was chlorite, a 2:1:1 clay, which comprised approximately 10% of the minerals. Kaolinite, a 1:1

clay, was always present, but in generally low abundances, i.e. 5% or less.

Mixed-layer clays were indicated in some of the samples. Vermiculite, a 2:1 clay which has a limited expansion characteristic, appeared to be the major interlayered mineral, with smectite, a 2:1 clay capable of undergoing extensive interlayer expansion, also present. Mixed-layered clays were only a small component of the clay minerals (i.e. <4%).

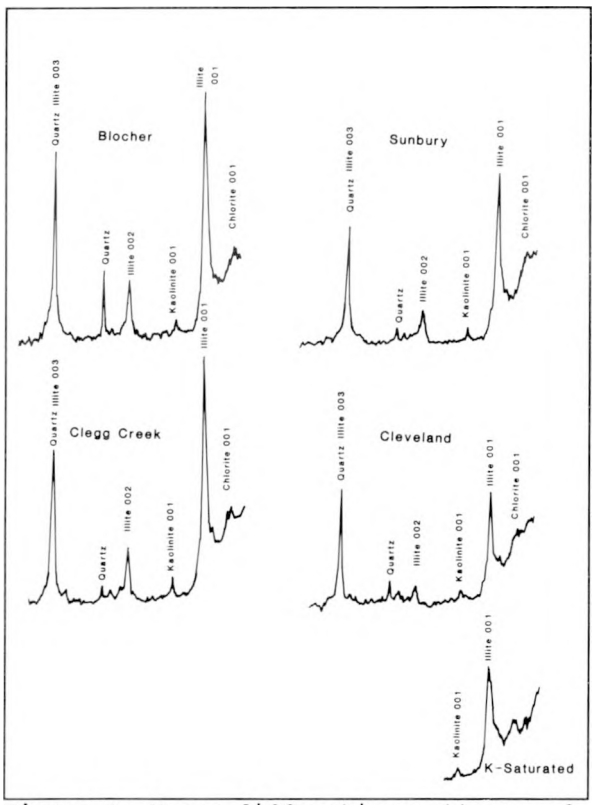

Figure 2. X-ray diffraction patterns of eastern oil shales, for mg-saturated and glycerated silt size fraction (except where noted).

	Il	Chl	Kao	Qtz
Clegg Creek	71	10	7	11
Blocher	68	3	3	26
Sunbury	61	11	6	20
Cleveland	63	10	3	23

Table I. Normalized silicate composition of eastern oil shale samples. Cleveland is a average of three samples. Il = Illite, Chl = Chlorite, Kao = Kaolinite and Qtz = Quartz.

Quartz (SiO_2) was the most abundant non-clay mineral present (about 25%), and pyrite and marcasite (FeS_2) were ubiquitous, present at abundances of 2 to 5 weight %.

Many other minerals have been found in the shale, and are either locally abundant or more generally distributed in low abundance. These constitute a long list and include such minerals as calcite, dolomite, galena, sphalerite, chalcopyrite, apatite, and several types of feldspar.

Changes in Mineralogy Induced by Retorting.

X-ray diffraction patterns from the Cleveland oil shale, and shale processed in the Dravo and Petrobras pilot plants illustrate the nature of mineralogic changes which are induced by retorting (Figure 3). These include the loss of the kaolinite reflection at 7 Å (001) and the attenuation of the 001 and 002 illite reflections at 10 Å and 5 Å, respectively. These attenuations are much more severe in the Dravo sample, to the degree that the second order illite peak was lost. The intensity of 14 Å 001 chlorite peak does not appear to have been changed in these samples, suggesting this mineral to be stable at the retorting temperatures. The Dravo technology is a directly heated retort, using a oxidative front to provide heat to pyrolyze the shale.[6] This sample has probably been heated to a higher temperature than that from the Petrobras retort, which is indirectly heated.[7]

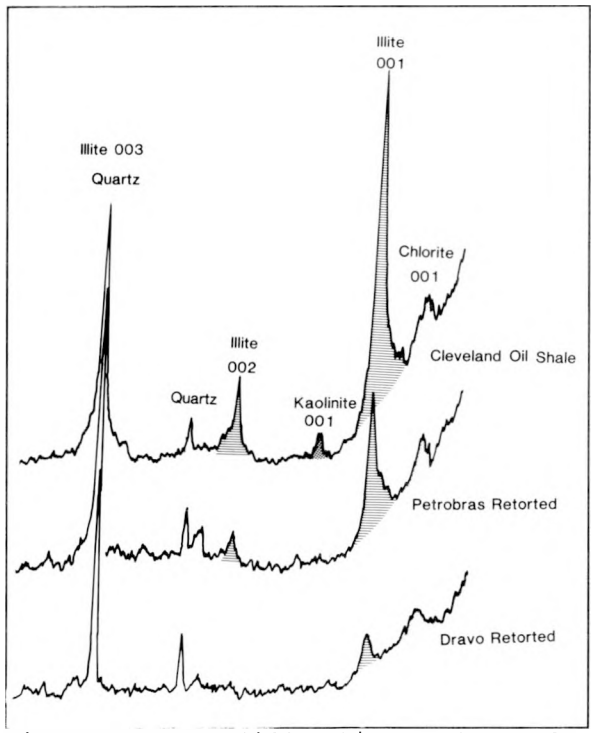

Figure 3. X-ray diffraction patterns for Cleveland shale and oil shales retorted in the Petrosix and Dravo pilot plants.

The KENTORT II technology incorporates a fluidized bed retorting zone integrated with a fluidized bed gasification zone. Shale from the

gasifier is then combusted in a fluidized bed which provides process heat.[8] The pyrolyzer is operated at approximately 525 °C, the gasifier approximately 750 to 800 °C, and the combustor at approximately 850 °C. Thus materials from the various process steps have been incrementally heated, and the latter also oxidized. Because the gasification and retort zone are integrated, a fraction which had only been pyrolyzed could not be collected. A Petrobras sample which used the same shale as the KENTORT II samples and was pyrolyzed at approximately same temperature is used in the comparison.

X-ray diffraction patterns of samples from the KENTORT II technology (Figure 4) indicate illite to exhibit a pattern of decrystallization as a function of processing temperature. Almost complete illite decrystallization is indicated for the combusted sample. Kaolinite is decrystallized early and is essentially absent in the pyrolyzed sample. Chlorite again appears to be relatively stable. X-ray diffraction patterns from the samples which were processed in the fixed bed retort (Figure 5) show similar patterns, although some indication of kaolinite is found in the pyrolyzed sample from the 455 and 496 °C runs.

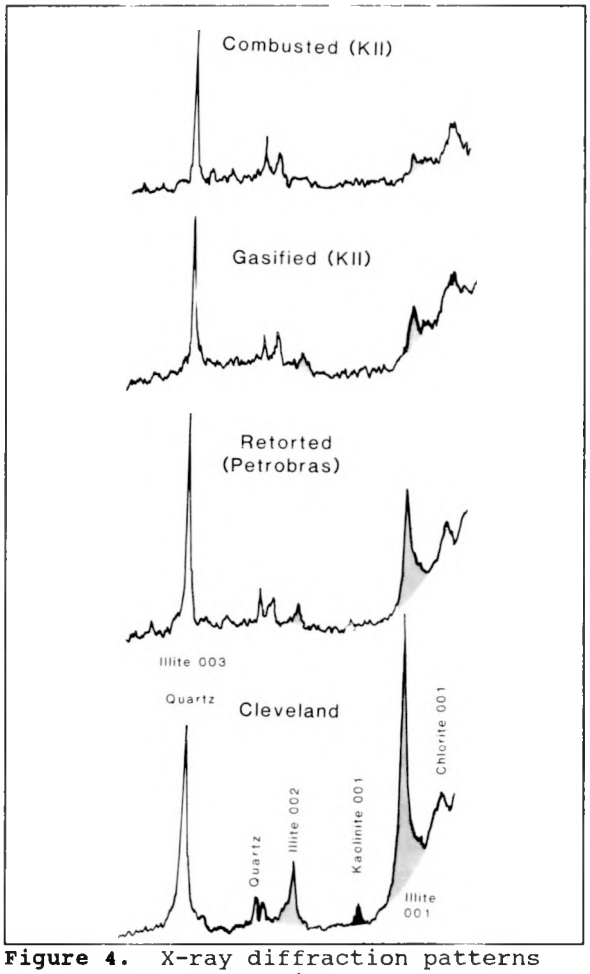

Figure 4. X-ray diffraction patterns for KENTORT II materials.

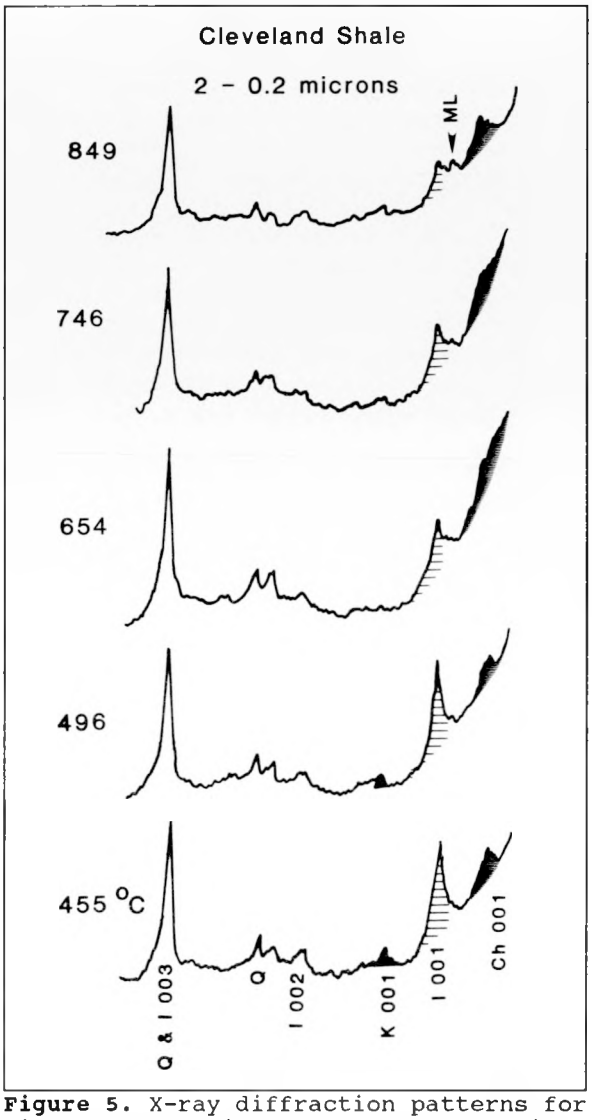

Figure 5. X-ray diffraction patterns for fixed bed materials processed at various temperatures.

The X-ray diffraction patterns did not indicate the development of any new mineral phases such as Richterite or Mullite. Neoformed minerals either are not present; or are present in abundances below that which could be measured by X-ray (about 2-5%); or are not sufficiently crystallized to give reflections discernable above background noise.

The Effect of Mineralogic Changes on the Acid Solubility of the Shales.

The KENTORT II and fixed bed materials were extracted with sulfuric acid to determine if changes in mineralogy could be directly and quantitatively related to changes in the acid solubility of the materials. The silicates originally present in the raw shale are only sparingly soluble in sulfuric acid. The change in their solubility provides some measure of the change in the chemistry of the

minerals induced by retorting. In addition, because sulfuric acid is the most inexpensive of common industrial acids, the composition of the extract may have economic implications for processing of the spent shales after retorting.

Extracts for retorted and gasified KENTORT II materials were higher in Fe, Mg and Zn, (Table II) compared to extracts from the shale after combustion. This is probably due to oxidation of the elements to higher valences which are less soluble. Previous work using, Mössbaur spectroscopy indicated that most of the Fe in the raw and retorted shale to be in the ferrous (Fe^{2+}) state, and was converted to the ferric state (Fe^{3+}) in the combusted shale.[9]

The concentration of Al and K were highest in the combusted shale extracts and appear to be related to the decrystallization of illite. Changes in the crystallinity of the illite was measured by ratioing the height of the illite 001 peak to that of the 100 quartz reflection at 4.3 Å (the much stronger 101 quartz reflection at 3.3 Å coincides with the 003 illite reflection). Quartz is stable at the retorting temperature studied, thus a decrease in this ratio is a reflection of the decrystallization of the illite. A strong correlation between the amount K and Al which could be extracted and the degree of illite decrystallization is found (Figure 6). Thus the solubility of these elements are a function of clay decrystallization, in turn a function of temperature, and do not appear to be sensitive to oxidation. This is reflected in a comparison of the composition of the combusted and retorted extracts (Figure 7).

	Raw	Retorted	Gasified	Combus.
Fe	4.92	26.37	23.31	9.51
Al	5.76	11.10	13.68	20.30
K	2.20	5.67	8.47	8.99
Mg	0.64	2.84	1.66	0.40
Na	0.10	0.67	0.57	0.68
Zn	0.33	0.52	0.48	0.33
V	0.07	0.11	0.22	0.52
Se	0.09	0.14	0.11	0.11
Cu	0.09	0.09	0.11	0.08
Ni	0.09	0.11	0.07	0.08
Mn	0.03	0.20	0.06	0.04

Table II. Elemental composition of H_2SO_4 extracts in g/Kg of shale for KENTORT II materials.

The extracts from the fixed bed materials showed a somewhat different pattern. In this case most of the elements, including K and Al, increased in concentration with temperature up to approximately 750 °C and then decreased (Figures 8 and 9). The exception being Fe which shows a maxima at the highest temperature.

The fixed bed samples were pyrolyzed under reducing conditions and thus the decline in elemental

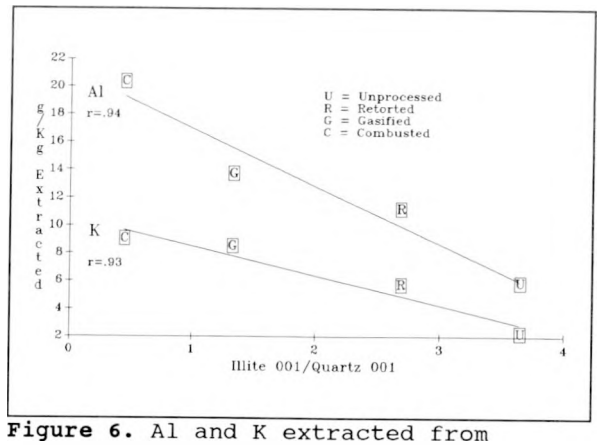

Figure 6. Al and K extracted from KENTORT II samples as a function of degree of decrystallization of Illite.

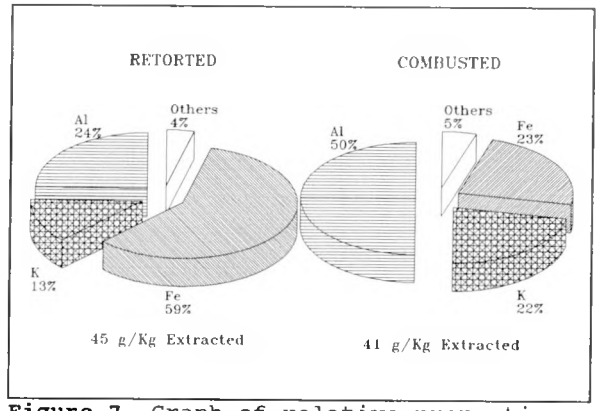

Figure 7. Graph of relative proportions of major elements extracted from the retorted and combusted shale fractions of the KENTORT II materials.

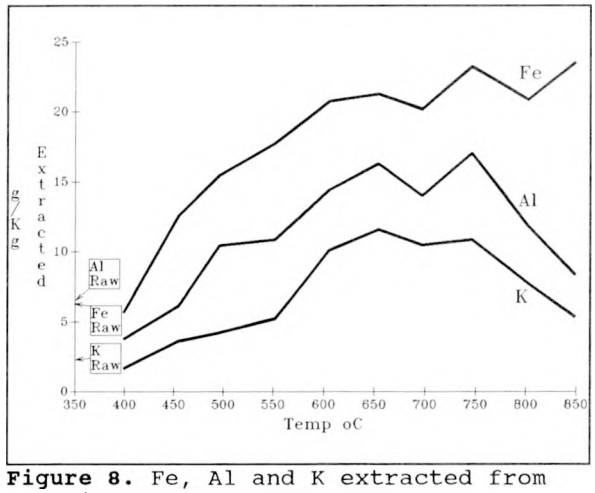

Figure 8. Fe, Al and K extracted from the fixed bed retorted shale as a function of temperature.

solubility at the higher temperatures cannot be explained by oxidation. The explanation may lie in the examination of the particle size distribution. A comparison of the 849 °C sample with those from lower temperatures (Figure 10), indicates a relative

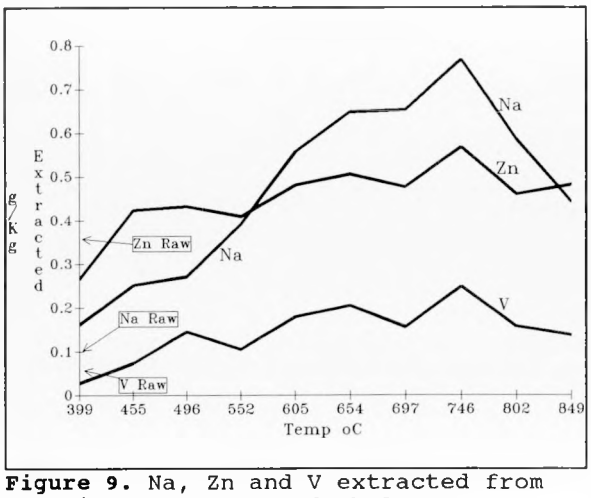

Figure 9. Na, Zn and V extracted from the fixed bed retorted shale as a function of temperature.

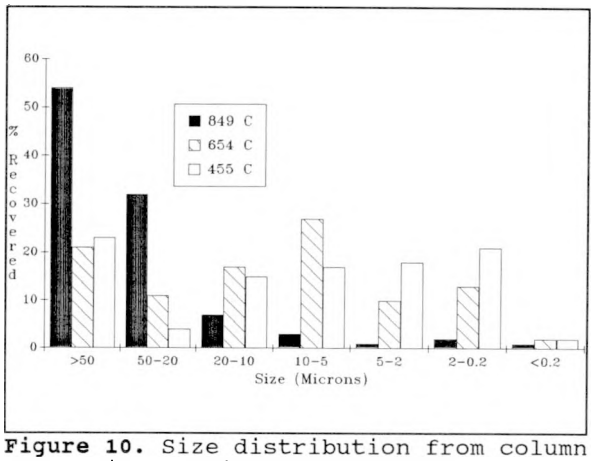

Figure 10. Size distribution from column separation of fixed bed retorted materials for samples processed at various temperatures.

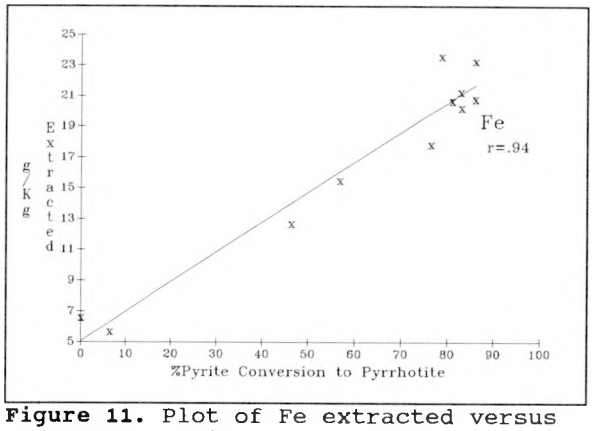

Figure 11. Plot of Fe extracted versus calculated pyrite to pyrrhotite conversion.

high proportion of the shale to be fractionated to the coarsest particle size, which suggests that the high temperature sample may have been partially sintered. Thus the decrease in elemental solubility may be due to the development of a vitreous or even microcrystalline phase.

Fe does not follow this trend. Its solubility is most likely controlled by changes in the sulfide phase. Although the abundance of iron sulfides are too low in the Cleveland shale to be accurately measured by the X-ray technique used, the conversion of FeS_2 to FeS (pyrite to pyrrhotite) could easily be calculated stoichiometrically. The relationship between the acid solubility of Fe and pyrite conversion is excellent (Figure 11).

Summary

The major minerals present in the oil shales of Kentucky include, illite, chlorite, kaolinite, quartz, and iron sulfides. The principal effects of retorting on these minerals was the decrystallization of kaolinite, the partial decrystallization of illite, and the transformation of pyrite to pyrrhotite. The decrystallization of illite appeared to be a function of processing temperature and was directly correlatable to the acid solubility of Al and K. The solubility of Fe was proportional to the degree of pyrite conversion to pyrrhotite. Fe solubility was reduced by the conversion of the iron sulfides to oxides.

Acknowledgements

The authors would like to express there thanks and appreciation to Mr. Gerald Thomas of the staff of the Center for Applied Energy Research for his help in the analysis of the acid extracts.

References

1. Rich, C.I. and R.I. Barnhisel, 1977, Preparation of Clay Samples for X-ray Diffraction Analysis. Chapter 23, in, Minerals and the Soil Environment, J.B. Dixon and R.L. Jones, Eds., Soil Sci. Soc. Am. Madison, Wis., p. 797-808.

2. Beavers, A.H. and R.L. Jones, 1966, Elutriation for Fractionating Silt. Soil Sci. Soc. Amer., Proc., V30, p. 126-128.

3. Rubel, A.M. and T.T. Coburn, 1981, Influence of Retorting Parameters on Oil Yield from Sunbury and Ohio Shales. Proc., 1981 East. Oil Shale Symp., Lexington, KY, p. 21.

4. Hosterman, J.W. and S.I. Whitlow, 1981, Clay Mineralogy of Devonian Shales in the Appalachian Basin. U.S. Geol. Sur., Open File Report No. 81-585, 178 p.

5. Robl, T.L., A.E. Bland, D.W. Koppenaal and L.S. Barron, 1983, Geochemistry of Oil Shales in Eastern

Kentucky. Ch. 9. in, Geochemistry and Chemistry of Oil Shale, Amer. Chem. Soc. Symp. Series 230, p.159.

6. Forbes, F., F. W. Kinsey and L. J. Colaianni, 1983, Dravo Process in the Means Oil Shale Project. Proc, 1983 East. Oil Shale Symp., Lexington, KY, p. 337.

7. Ivo, O.C., J. Rezende and E.M. Piper, 1982, Applicability of the Petrosix Process to Kentucky Oil Shale. Proc., 1982 East. Oil Shale Symp., Lexington, KY, p. 191.

8. Carter, S.D., 1987, The KENTORT II Concept: A Process Description. Proc. 1987 East. Oil Shale Sym., Lexington, KY, p. 271.

9. Rubel, A.M., S.D. Carter, T.L. Robl, 1989, Shale Sulfur and Iron Chemistry in the KENTORT II Process. Preprints, Div. of Pet. Chem., Amer. Chem. Soc., V. 34, No. 1, p. 87.

Morphology of Sulfide Minerals in Eastern Oil Shale

by

Glenn M. Mason
Western Research Institute
University of Wyoming Research Corporation
Laramie, Wyoming 82071

Abstract. X-ray diffraction (XRD) and scanning electron microscopy/energy dispersive X-ray analysis (SEM/EDX) were used to investigate the mineralogy and crystalline morphology of sulfide minerals in Chattanooga Shale. Gravity concentration and digestion procedures were used to isolate the materials from samples of bulk shale. Iron disulfide mineral abundance averaged 7.6 wt %, with a range of 1 to 17 wt % for the entire section. Pyrite (isometric FeS_2) was the most abundant sulfide mineral identified, with all classic crystalline morphologies observed including pyritohedral, octahedral, and cubic, also, framboidal and pyrite replacement of organic matter, as well as nondistinct crystalline masses. Other sulfide minerals identified were marcasite (orthorhombic FeS_2), pyrrhotite (hexagonal $Fe_{1-x}S$), sphalerite (tetrahedral ZnS), and galena (isometric PbS). Sulfur-bearing alteration minerals identified were gypsum (monoclinic $CaSO_4 \cdot 2H_2O$) and copiapite (triclinic $Fe_{14}O_3(SO_4)_{18} \cdot 63H_2O$), which appeared as crystalline masses on the surfaces of sulfide minerals.

Introduction and Background

Devonian seas transgressed central North America leaving organic-rich muds deposited over thousands of square miles. Known as the Chattanooga Shale in Tennessee, and by various names in other regions, these formations represent a major source of hydrocarbons. A primary concern for the development of eastern oil shale is the high concentration of sulfide minerals in the formation. Sulfurous emissions, acid drainage, and the release of deleterious trace elements are some of the environmental problems facing commercial development.

Eastern oil shales, the Chattanooga Shale in Tennessee, and the various other time-equivalent black shales in the central portion of the United States, represent a major source of hydrocarbons. In this study, sulfide minerals from a Chattanooga Shale core from central Tennessee were investigated in order to study their morphology (form).

The Chattanooga Shale was deposited when Devonian seas transgressed and regressed central North America approximately 340 million years ago, leaving a thick deposit of organic-rich muds over hundreds of thousands of square miles. This black mud has became known as the Antrim Shale in Michigan, the Ohio Shale in Ohio and northeastern Kentucky, the New Albany Shale in northwestern Kentucky and Indiana, and the Chattanooga Shale in southern Kentucky, northern Alabama, and throughout Tennessee.[1]

The Chattanooga Shale is overlain by the Fort Payne chert and the Maury Formation, which is phosphatic immediately above the contact, and conformably underlain by the Leipers Limestone. The Chattanooga Shale is subdivided into two members: the upper member called the Gassaway (subdivided into the upper, middle, and lower), and the lower member called the Dowelltown (subdivided into upper and lower).

General mineralogy of the Chattanooga Shale consists of quartz, clay minerals, feldspars, sulfide minerals (primarily pyrite), calcite and others. Additionally, the shale contains 5 to 20 wt % organic matter. A detailed investigation of the bulk and clay mineralogy of this core hole was presented by Mason et al.[2]

Bulk and clay mineralogical analyses of samples from this core hole in central Tennessee, first presented by Mason et al.,[2] served as the starting point for the investigation of the sulfide minerals. Botinelly[3] estimated pyrite abundance in the Chattanooga Shale as approximately 10 wt % for the samples he investigated. Leimer and McGowan[4] reported the Upper Gassaway Member to contain 12 wt %, the Lower Gassaway 9 wt %, and the Upper Dowelltown Member 4 wt % pyrite.

Mason[5] estimated iron disulfide mineral content (pyrite and marcasite) of the entire Chattanooga Shale section at the study locality was 7.6 wt %. The Upper Gassaway Member contained 12.8 wt %, the Middle Gassaway Member 6.7 wt %, the Lower Gassaway Member 9.2 wt %, the Upper Dowelltown Member 3.4 wt %, and the Lower Dowelltown Member 6.0 wt %. Figure 1 is a graphic representation of the distribution of pyrite (including marcasite) by estimated weight percent for the Chattanooga Shale section.

Experimental

Samples for this study were selected from a core hole drilled by the United States Department of Energy in Dekalb County, Tennessee. Figure 2 illustrates the area of Tennessee underlain by the Chattanooga Shale and the location of the core hole from which samples for this study were obtained.

Materials were initially concentrated to facilitate investigation by a gravity concentration technique involving a simple flotation process. Samples were screened to -48 mesh (350 μm), then heavy minerals were concentrated using the established prospecting technique, panning, whereby lighter fractions are washed away leaving heavier materials behind. The technique involved three basic steps: (1) wetting the sample with a detergent-dispersant to reduce surface tension of the water and to reduce any floating tendencies of the minerals, (2) de-sliming (washing away fines with distilled water), and (3) panning to concentrate heavy minerals (in this study sulfide minerals). After panning to a concentrated heavy sulfide mineral fraction, samples were transferred to glass vials, washed again with distilled water, then oven-dried at 85° C (185° F). All samples were characterized by X-ray diffraction (XRD) following the procedures described by Mason.[2,5]

Scanning electron microscopy/energy dispersive X-ray analysis (SEM/EDX) was used to observe detailed morphology and provide rapid, direct chemical verification of minerals. An Amray model 1820, computer enhanced, digital imaging scanning electron microscope equipped with a Tracor Northern model 5500 Series II energy dispersive X-ray analyzer was used for all phases of this study. Samples were viewed uncoated or gold coated using an Edwards S150B sputter coater. Instruments were operated according to the standard procedures outlined by the manufacturers.

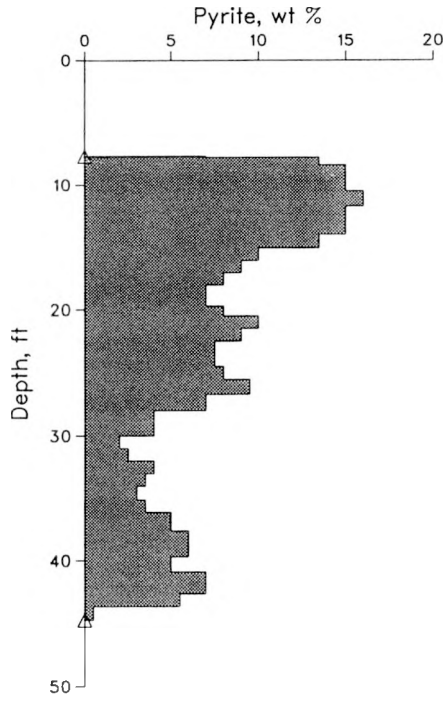

Figure 1. Distribution of disulfide minerals in U. S. DOE core hole TTU/LETC no. 1.

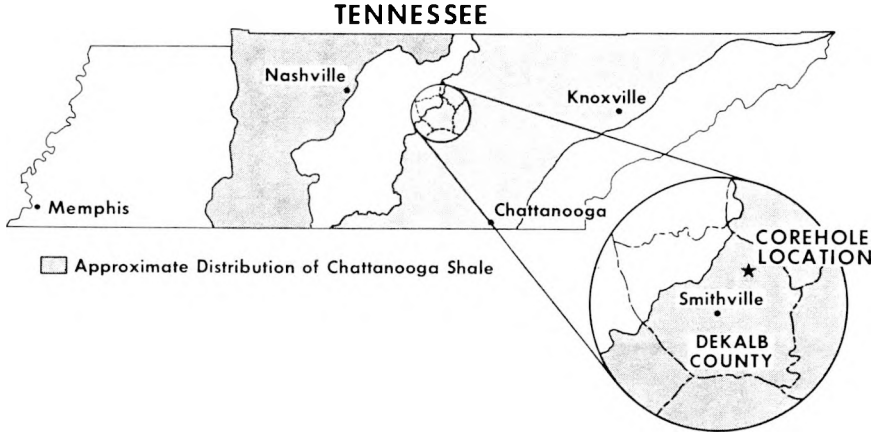

Figure 2. Location of U. S. DOE core hole TTU/LETC no. 1 and distribution of Chattanooga Shale in Tennessee.

Results and Discussion

Sulfide Formation

In sediments containing abundant organic matter, such as the Chattanooga Shale, reactions involving organic matter and the formation of sulfide minerals are closely related. A specialized group of bacteria obtain sulfur needed for biosynthesis from reduction of the inorganic sulfate ion, the sulfate-reducing bacteria Desulfovibrio and Desulfotomaculum, rapidly reduce sulfate producing sulfide. For these organisms, sulfate is the terminal oxidizing agent for their respiration. This process oxidizes metabolizable organic matter to CO_2 and HCO^{3-} with a reduction of sulfate to reduced sulfur species H_2S and HS^{-6}.

Sulfate reduction under anoxic conditions, can be summarized by the following equation.[7]

$$2CH_2O + SO_4^{2-} \Rightarrow S^{2-} + 2CO_2 + 2\,H_2O \qquad (1)$$

If the pH is above 7 during sulfate reduction, HS^- will form rather than H_2S.[8] If H_2S is generated as a consequence of sulfate reduction, the biota can be strongly effected due to the compounds toxicity. The formation of iron compounds can be related to oxidizing conditions which can serve to incorporate available iron as siderite ($FeCO_3$). Because of the anoxic conditions present during the formation of the Devonian black shales, evidenced by the preservation of the organic matter, the formation of disulfide compounds are emphasized. Iron sulfides (primarily pyrite) will form if there are any reactive iron compounds present; equations (2) through (5) summarize the formation of pyrite.[9,10,11]

$$2Fe^{3+} + S^{2-} \Rightarrow 2Fe^{2+} + S^0 \qquad (2)$$

$$S^0 + S^{2-} \Rightarrow S_2^{2-} \qquad (3)$$

$$Fe^{2+} + S_2^{2-} \Rightarrow FeS_2 \qquad (4)$$

or

$$FeS + S^0 \Rightarrow FeS_2 \qquad (5)$$

Pyrite

Pyrite (FeS_2) is the most widespread and most abundant of sulfide minerals, especially in sedimentary sediments. Pyrite in the Chattanooga Shale has a very diverse appearance, representing many crystallographic forms and shapes. Pyrite belongs to the isometric crystal system, the $2/m\,\bar{3}$ crystal class, and is known to occur as cubes, pyritohedrons, and octahedrons or modifications thereof. In the samples of the Chattanooga Shale studied, all crystallographic forms of pyrite were identified including cubic (Figure 3), pyritohedron (Figure 4), and octahedron (Figure 5). Many modifications or combinations of these three basic crystallographic forms for pyrite were observed including the combinations of cube + pyritohedron (Figure 6) and cube + octahedron (Figure 7). All examples of pyrite had the chemical composition verified by EDX. Figure 8 is an example of a typical EDX spectrum obtained from a point examination of pyrite crystals. The distinct crystals observed ranged in size from 10 to 100 μm.

In addition to distinct pyrite crystal forms, much of the pyrite observed existed as nondistinct masses, only positively distinguishable by EDX. Most pyrite appeared in hand specimen as nondistinct masses. However, under carefui examination with the SEM, it could be observed that the pyrite masses displayed either some crystalline form or growth striations.

Other notable morphologies of pyrite occurred in the form of pyrite framboids or microscopic aggregates of crystals. Figure 9 is an SEM photomicrograph of a pyrite framboid illustrating the classic raspberry-like appearance. Pyrite replacement of organic matter is not uncommon in many sedimentary formations, but relatively rare in the Devonian Shales. Figures 10 and 11 are SEM photomicrographs portraying pyrite replacement of organic matter, probably wood. In Figure 11, a higher magnification view of Figure 10, some of the original cell structure can be recognized, although greatly distorted by burial and replacement.

Other Sulfides

During the course of this investigation, distinct sulfide phases other than the predominate phase of pyrite were identified. Pyrrhotite ($Fe_{1-x}S$), marcasite (FeS_2), sphalerite (ZnS), and galena (PbS) were also associated with or found in the Chattanooga Shale. Although less abundant than pyrite, sufficient quantities of these minerals were

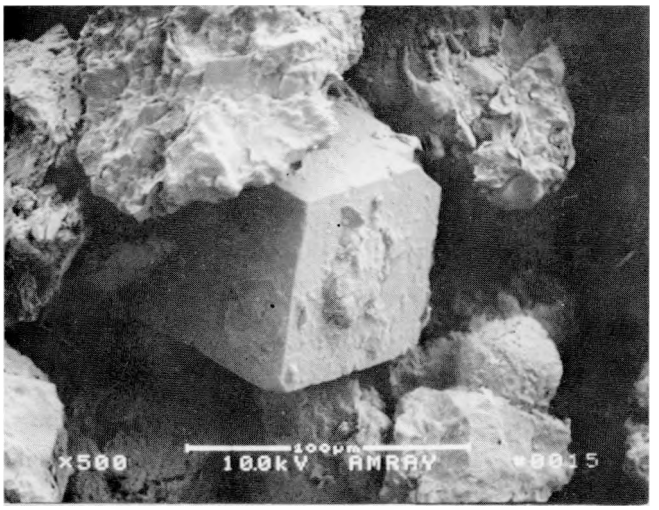

Figure 3. SEM photomicrograph of cubic pyrite (FeS_2). Depth of sample 19.0-19.7 feet.

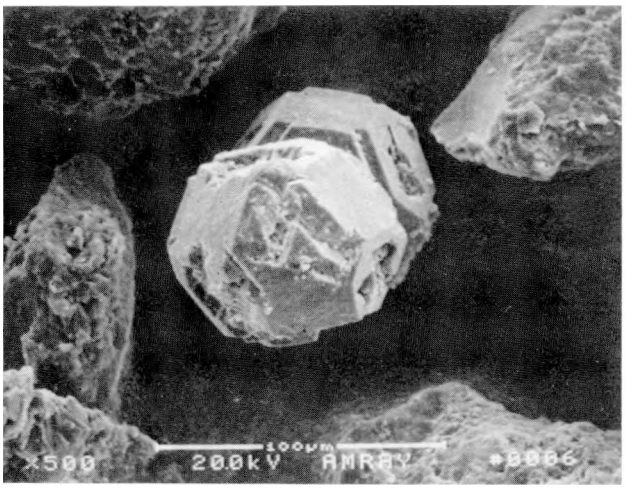

Figure 4. SEM photomicrograph of pyritohedral pyrite (FeS_2). Depth of sample 8.4-10.5 feet.

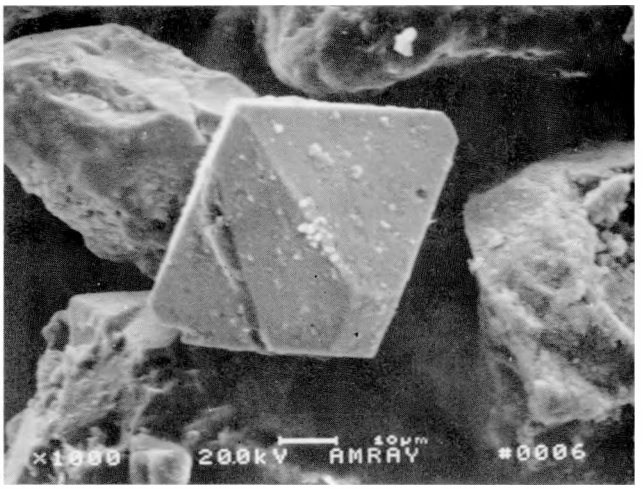

Figure 5. SEM photomicrograph of octahedral pyrite (FeS_2). Depth of sample 8.4-10.5 feet.

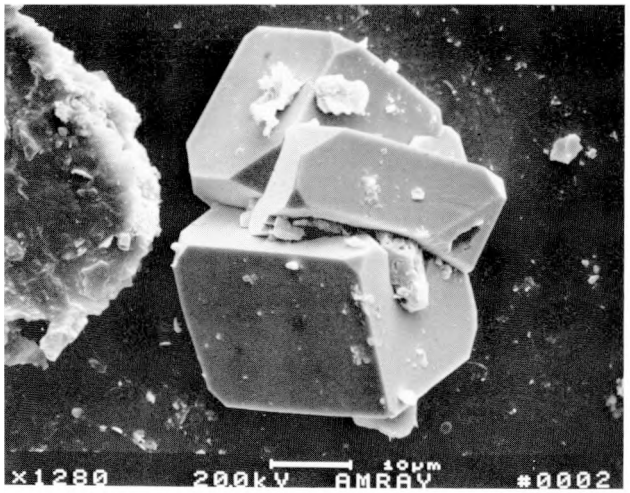

Figure 6. SEM photomicrograph of cubic + pyritohedral pyrite (FeS_2). Depth of sample 8.4-10.5 feet.

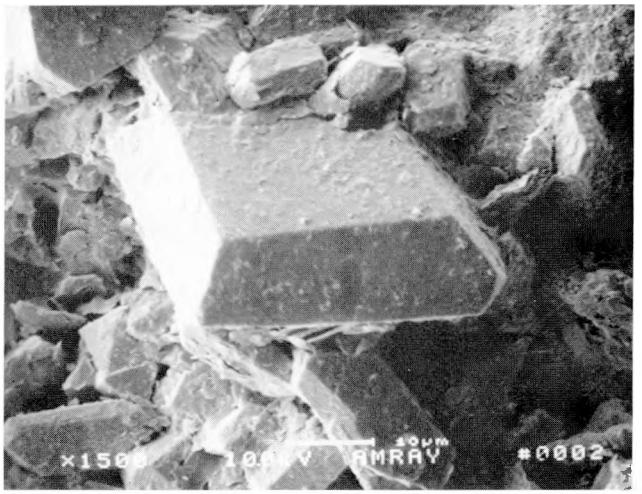

Figure 7. SEM photomicrograph of cubic + octahedral pyrite (FeS_2). Depth of sample 42.6-43.6 feet.

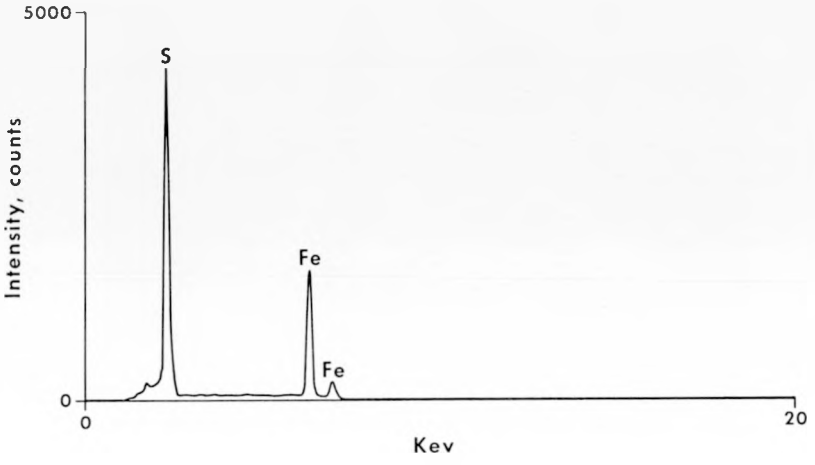

Figure 8. EDX spectrum of pyrite.

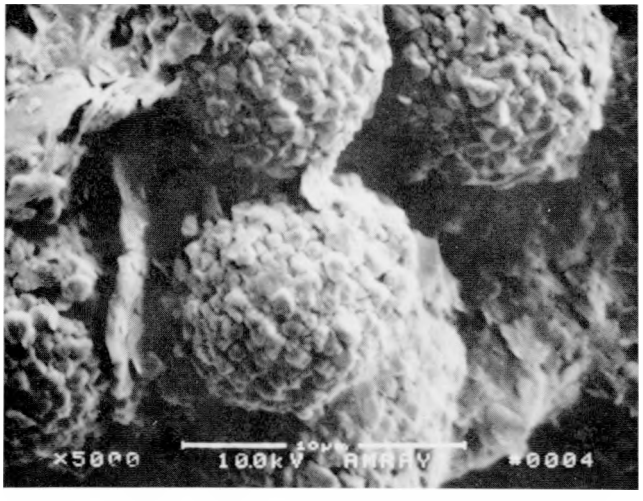

Figure 9. SEM photomicrograph of a pyrite (FeS_2) framboid. Depth of sample 19.0-19.7 feet.

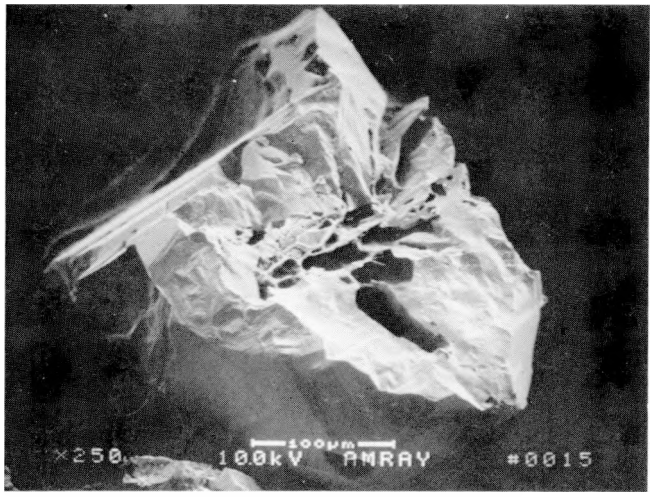

Figure 10. SEM photomicrograph of pyrite (FeS_2) replacement of organic matter. Depth of sample 33.0-34.0 feet.

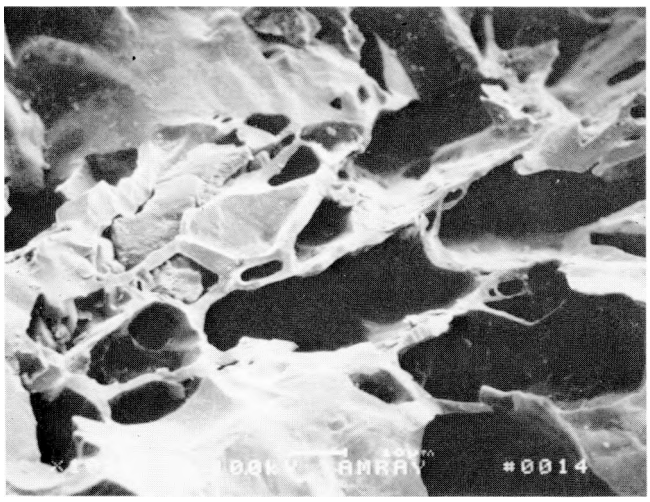

Figure 11. SEM photomicrograph of pyrite (FeS_2) replacement of organic matter with original cell structure visible. Depth of sample 33.0-34.0 feet.

present to be identified by X-ray diffraction. [2,5] Sphalerite and galena were noted to be abundant in distinct zones, especially in the upper Gassaway Member of the Chattanooga at the transitional boundary with the overlying Maury Formation.

Pyrrhotite ($Fe_{1-x}S$), a hexagonal sulfide mineral belonging to the 6/m 2/m 2/m crystal class, is generally not as common in sediments as pyrite. Pyrrhotite forms under conditions that are too deficient in iron to form pyrite or as a heat alteration product of pyrite. Easily distinguishable from pyrite by XRD or when good crystal morphology can be observed, pyrrhotite was very difficult to distinguish from the other iron sulfides by EDX because of the similarity in chemistry and somewhat irregular stoichiometry of pyrrhotite-type minerals. Figure 12 is an SEM photomicrograph illustrating the hexagonal crystal morphology of pyrrhotite.

Marcasite (FeS_2), an orthorhombic di-sulfide of iron, has the same chemistry as pyrite but a different crystal morphology. Belonging to the 2/m 2/m 2/m crystal class, marcasite forms under surface sedimentary conditions, but favors a more acidic environment than pyrite. Marcasite can be distinguished from pyrite by XRD or morphology, it is virtually indistinguishable from pyrite by EDX because of their identical chemistry. Figure 13 is an SEM photomicrograph illustrating the stepped or radiating crystal morphology of marcasite.

Sphalerite (ZnS) the most abundant zinc mineral and galena (PbS) the most abundant lead mineral are generally intimately associated. Sphalerite is a tetrahedral mineral of the $\bar{4}$ 3 m crystal class, was very difficult to identify by morphology alone. Good examples of a tetrahedral crystal morphology were not observed. Identification of sphalerite was accomplished by XRD and elemental analysis by EDX. Figure 14 is an SEM photomicrograph of sphalerite. Figure 15 is an EDX spectrum verifying the chemistry of sphalerite. Galena is an important lead mineral, although not generally found in large abundances in shales. Galena belongs to the isometric crystal system of the 4/m $\bar{3}$ 2/m crystal class. Generally occurring as cubic or cubo-octahedral modifications of the cubic form.

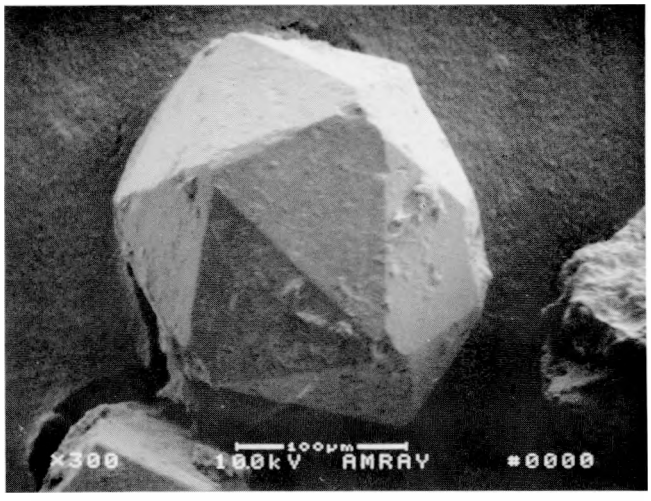

Figure 12. SEM photomicrograph of pyrrhotite ($Fe_{1-x}S$). Depth of sample 42.6-43.6 feet.

Identification of galena in the sediments of the Chattanooga Shale was accomplished by a combination of visual recognition of the cubic form with verification by EDX. It was necessary to verify the chemistry of galena by EDX because of the abundance of cubic pyrite forms also being present in the same samples. Figure 16 is an SEM photomicrograph illustrating the cubic crystal morphology of galena. Figure 17 is an EDX spectrum verifying the chemistry of galena.

Sulfide Alteration Minerals

Sulfur-bearing alteration minerals were very common in the samples of raw and sulfide concentrated samples studied. These alteration minerals were predominately gypsum, but occasionally the iron sulfate hydrate copiapite could be identified.

Gypsum ($CaSO_4 \cdot 2H_2O$), the most common alteration mineral identified in the samples, could be easily identified by its monoclinic crystal habit belonging to the 2/m crystal class. Gypsum samples observed could be easily identified by extensive twinning, prismatic lenticular habit, and occasional rosette-like or flower-like growths (Figure 18). Although the morphology of gypsum in the samples was very distinctive, verification of the crystals could be easily accomplished by EDX (Figure 19).

Another sulfur-bearing alteration product identified in sulfide concentrated samples of Chattanooga Shale was copiapite ($Fe_{14}O_3(SO_4)_{18} \cdot 63H_2O$). Copiapite, a triclinic mineral of the $\bar{1}$ crystal class, occurs as a secondary mineral formed by the oxidation of sulfides, especially pyrite. Generally the mineral is very unstable, with the structure starting to lose water a temperatures as low as 70° C (158° F) with complete dehydration occurring at 300°C (572° F).[12] Identified only by SEM, because quantities of the mineral were insufficient for detection by XRD, copiapite appeared as tabular crystals, sometimes highly modified, usually as aggregations on or filling surface features of pyrite. Figure 20 is an SEM photomicrograph of copiapite on pyrite. Figure 21 is a higher magnification photomicrograph of copiapite with the triclinic crystalline habit clearly visible.

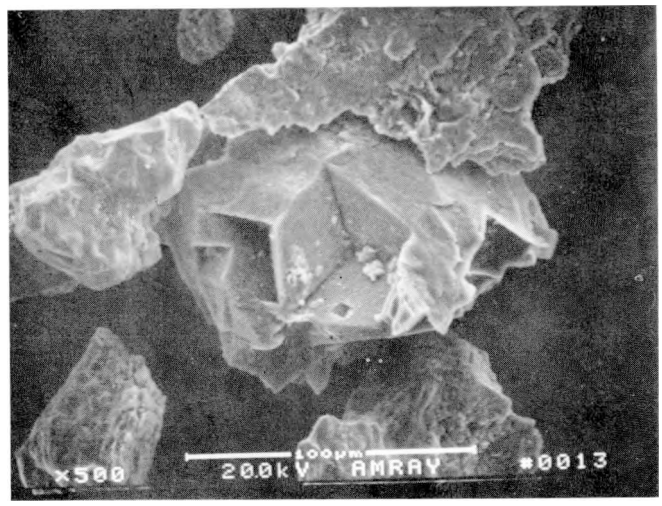

Figure 13. SEM photomicrograph of marcasite (orthorhombic FeS_2). Depth of sample 7.8-8.4 feet.

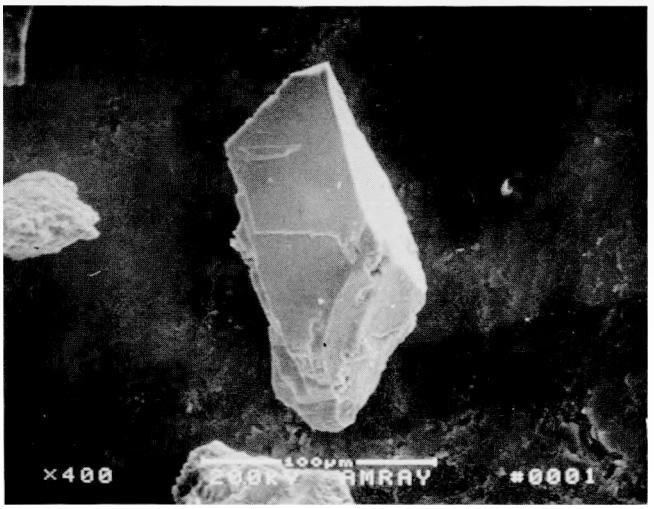

Figure 14. SEM photomicrograph of sphalerite (ZnS). Depth of sample 7.8-8.4 feet.

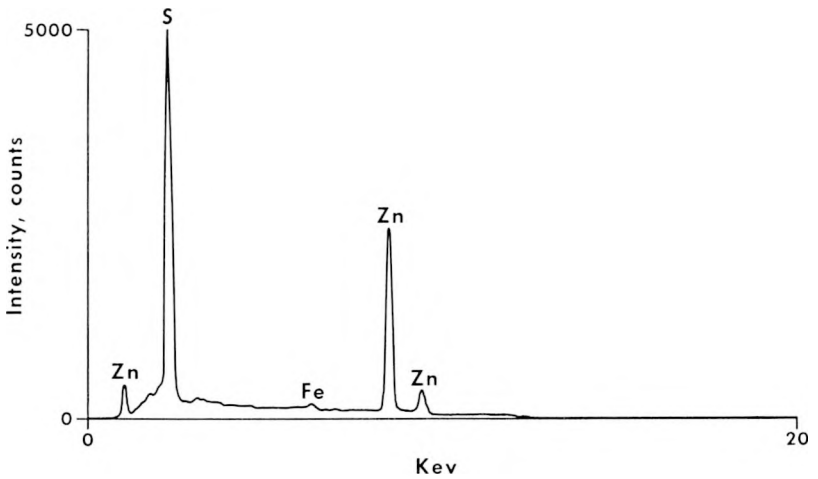

Figure 15. EDX spectrum of sphalerite. Some Fe substitution.

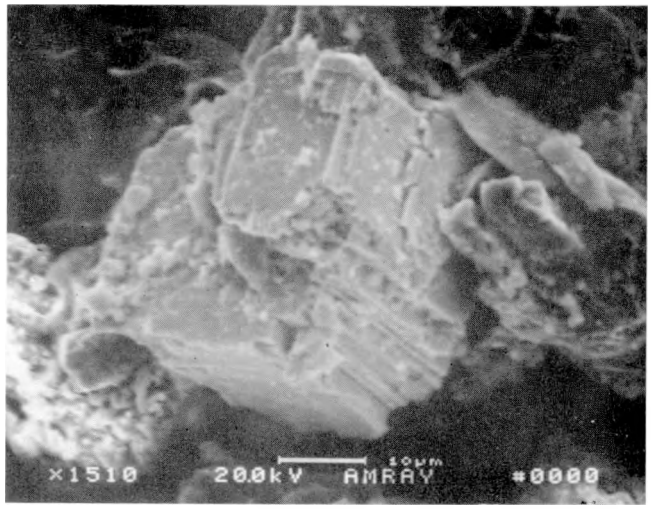

Figure 16. SEM photomicrograph of galena (PbS). Depth of sample 7.8-8.4 feet.

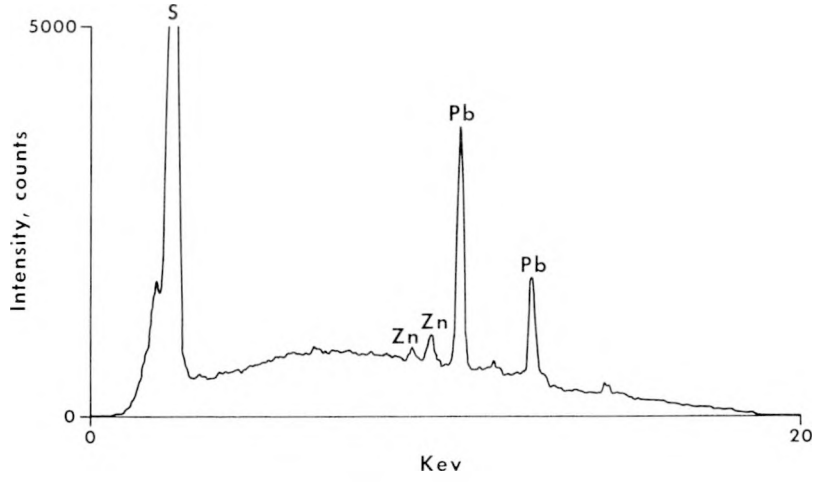

Figure 17. EDX spectrum of galena. Some Zn substitution.

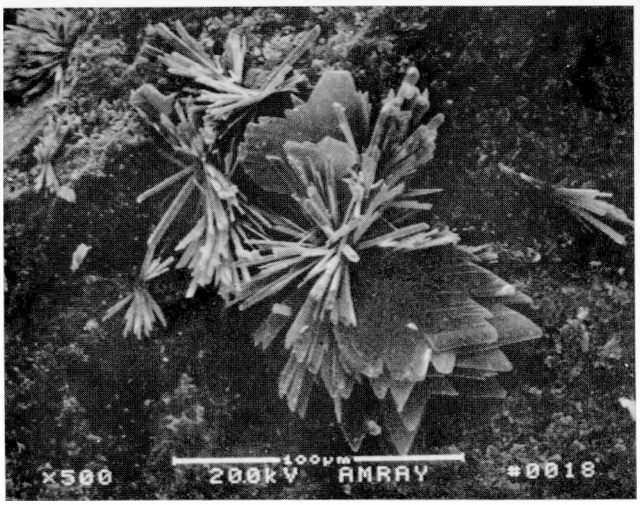

Figure 18. SEM photomicrograph of gypsum ($CaSO_4 \cdot 2H_2O$). Depth of sample 23.5-24.5 feet.

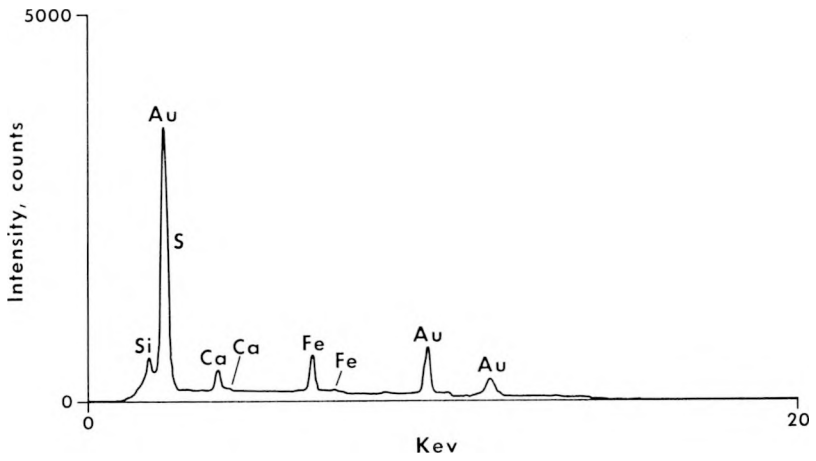

Figure 19. EDX spectrum of gypsum (gold coated). Iron from underlying pyrite. Silica from clay mineral contaminates.

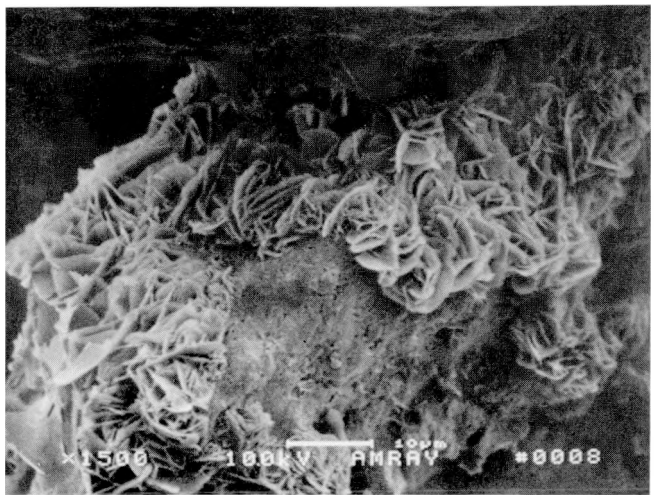

Figure 20. SEM photomicrograph of copiapite ($Fe_{14}O_3(SO_4)_{18}{\cdot}63H_2O$). Depth of sample 19.0-19.7 feet.

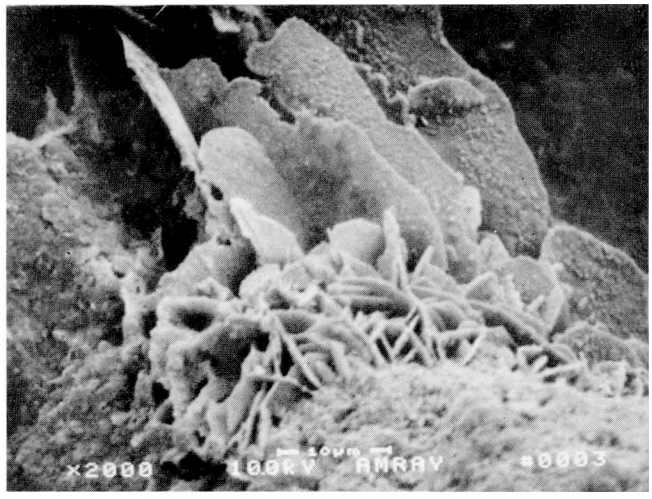

Figure 21. SEM photomicrograph of copiapite ($Fe_{14}O_3(SO_4)_{18}{\cdot}63H_2O$). Depth of sample 19.0-19.7 feet.

Conclusions

- Sulfide minerals identified in the Chattanooga Shale in this study were pyrite (isometric FeS_2) and marcasite (orthorhombic FeS_2), pyrrhotite (hexagonal $Fe_{1-x}S$), sphalerite (tetrahedral ZnS), and galena (isometric PbS).

- Sulfur-bearing alteration minerals were gypsum ($CaSO_4 \cdot 2H_2O$) and copiapite ($Fe_{14}O_3(SO_4)_{18} \cdot 63H_2O$) which appeared as crystalline masses on the surfaces of sulfide minerals.

- Crystal morphologies of pyrite observed were pyritohedral, octahedral, and cubic, also, framboidal and pyrite replacement of organic matter.

- Sulfide morphology displayed no detectable stratigraphic trends.

Acknowledgement

The author expresses thanks and appreciation to the United States Department of Energy for funding this work under Cooperative Agreement DE-FC21-86MC11076.

Disclaimer

Mention of specific brand names or models of equipment is for information only and does not imply endorsement.

References

1. Conant, L. C. and Swanson, V. E., "Chattanooga Shale and Related Rocks of Central Tennessee and Nearby Areas," U. S. Geological Survey Professional Paper 357, 1961.

2. Mason, G. M., Spackman, L. K., and Leimer, H. W., "Mineralogic Characterization of a Chattanooga Shale Core from Central Tennessee," Proceedings, 1984 Eastern Oil Shale Symposium, Lexington, KY, pp. 393-400, 1984.

3. Botinelly, T., "Mineralogy of the Chattanooga Shale," U. S. Geological Survey, Trace Elements Memorandum Report 474, 1952.

4. Leimer, H. W. and McGowan C., "Chattanooga Shale in Tennessee; Resource Evaluation," American Association Petroleum Geologists Bulletin, v. 66(6), 1983.

5. Mason, G. M. "The Association of Trace Elements with Pyrite in Chattanooga Shale," Proceedings, 1988 Eastern Oil Shale Symposium, Lexington, Kentucky, November 1988, p. 197-211, March 1989.

6. Postgate, J. R. and Campbell, L. L., "Classification of Desulfovibrio Species, the Nonsporulating Sulfate-reducing Bacteria," Bacteriological Review, v. 30, p. 732-738, 1966.

7. Berner, R. A., Scott M. R., and Thomlinson C., "Carbonate Alkalinity in the Pore Waters of Anoxic Marine Sediments," Limnology and Oceanography, v. 15, p. 544-549, 1970.

8. Drever, J. I. The Geochemistry of Natural Waters, Printice-Hall Inc., Englewood Cliffs, New Jersey, 388 p., 1982.

9. Rickard, D. T., "The Microbiological Formation of Iron Sulfides," Geology, v. 20, p. 49-66, 1969.

10. Roberts, W. M. B., Walker A. L., and Buchanan A. S., "The Chemistry of Pyrite Formation in Aqueous Solution and its Relation to the Depositional Environment," Minerlogica Deposita, v. 4, p. 18-29, 1970.

11. Deer, W. A., Howie R. A., and Zussman J., Rock-Forming Minerals, Vol. 5: Non-Silicates, Longman Group Limited, London, England, 371 p., 1962.

Organic Geochemistry, Petrography, and Maturation Trends of the Ohio Shale in Eastern Kentucky

by

Susan M. Rimmer and D.J. Cantrell
Department of Geological Sciences
University of Kentucky
Lexington, Kentucky 40506
Patrick J. Gooding
Kentucky Geological Survey
University of Kentucky
Lexington, Kentucky 40506

ABSTRACT

Organic petrographic and geochemical data indicate a southeastwards increase in maturation of the Ohio Shale (Devonian-Mississippian) within Kentucky. Reflectance levels of dispersed organic material in the Cleveland Shale increase from 0.5% in the outcrop belt in central Kentucky, to slightly over 1.0% in Pike County, eastern Kentucky. Similar reflectance trends are observed in other shale units including the Upper and Lower Huron. A decrease in fluorescence intensity of liptinitic components, such as Tasmanites, accompanies this reflectance increase, as does a shift in fluorescence color towards the red. In the highest rank areas of eastern Kentucky, fluorescence is almost absent.

Kerogen in the Cleveland Shale is primarily Type II, as indicated by petrographic observations and Rock-Eval data. TOC contents of this shale decrease from over 12% in the outcrop belt, to less than 2% in Pike County, eastern Kentucky. Tmax values for this unit range from under 430 degrees C in the outcrop belt, to over 450 degrees C in eastern Kentucky, confirming the increase in maturation trends indicated by the reflectance data.

Organic Geochemistry and Organic Petrology of Paleozoic Oil Shales In Canada

by

F. Goodarzi, M.G. Fowler, and W.W. Nassichuk
Institute of Sedimentary and Petroleum Geology
Geological Survey of Canada
Calgary, Alberta CANADA T2L 2A7

Abstract. Several Paleozoic oil shales, ranging in age from Ordovician to Carboniferous, occur in many different parts of Canada. These oil shales are of marine and nonmarine origin and therefore show diverse geochemical and petrological characteristics which will be discussed here.

Oil shales of Ordovician age include the Collingwood oil shale of southern Ontario and various deposits in the eastern Arctic Islands including one in the Boas Formation on Southampton Island. The Collingwood consists of mostly type II amorphous organic matter deposited under marine conditions. Although the Boas also contains type II amorphous organic matter, biomarker evidence suggests that it may have been deposited under hypersaline conditions. The Devonian Marcellus and Kettle Point formations of Ontario contain oil shales of marine origin. Organic matter in the Devonian deposit are often dominated by large *Tasmanales* algae. Carboniferous oil shale deposits are widespread in the Atlantic provinces and include the Alberta Shale of New Brunswick, the Pictou Group of Nova Scotia and the Rocky Brook Formation of Newfoundland. Most of these deposits are associated with lacustrine conditions and *Botyroccocus brauni* is a major contributor to their organic matter. The Carboniferous Emma Fiord Formation on Devon Island in the Canadian Arctic Archipelago is another rich oil shale deposited under lacustrine conditions.

Introduction

Geochemical and geological factors affecting the exploitation of several Canadian oil shales ranging in age from Ordovician to Cretaceous were reviewed by Macauley and coworkers in 1985.[1] Since that time the Geological Survey of Canada has continued to study oil shales for the ultimate possibility of the production of shale oil, for their potential as oil source rocks (an oil shale is essentially a very rich immature oil-source rock) and also for their general scientific interest.

This very brief report summarises some recent work on Canadian Paleozoic oil shales (Figure 1) concentrating on their organic geochemistry and petrology. Of the oil shales listed in Tables 1 and 2, three were not mentioned at all in the 1985 Macauley report.[1] Two of these are the Arctic deposits, the Boas and Emma Fiord formations; the third is the Marcellus Formation deposits in Ontario. Additional organic geochemical and petrological work has been done on all the other deposits, much of which has been published. The economic potential of an oil shale, specifically its ability to generate hydrocarbons, partially depends on the type of organic matter present. There are other factors of course such as the thickness of the unit and the amount of overburden. Organic geochemical investigations in combination with organic petrological studies can provide explanations for the variation in hydrocarbon potential between different deposits or in an individual deposit. As indicated in Table 2 there are considerable variations in these Paleozoic deposits. This is a reflection of their different depositional settings (Table 1) and also the source of the organic matter. The Ordovician and Devonian oil shale intervals were deposited in marine environments whilst those of Carboniferous age were all deposited in lacustrine settings. The evolution of land plants during this period also affected the type of organic matter available.

Ordovician oil shales

Considerable interest exists in Ordovician organic-rich oils and sedimentary deposits because of the occurrence in different parts of the world of deposits with properties quite distinct from deposits of other ages.[2,3,4] The unique character of many of the Ordovician deposits may be due to the presence of the alga *Gloeocapsomorpha prisca* Zalessky 1917.[2,3,4] In many Ordovician organic-rich intervals including for example the Yeoman Formation in the Williston Basin[4,5] in Western Canada or the Guttenberg "oil rock"[6] in U.S.A. this organism constitutes over 90% of the organic matter. Such deposits have been informally termed kukersites.[7,4] Ordovician organic-rich units in Canada have recently

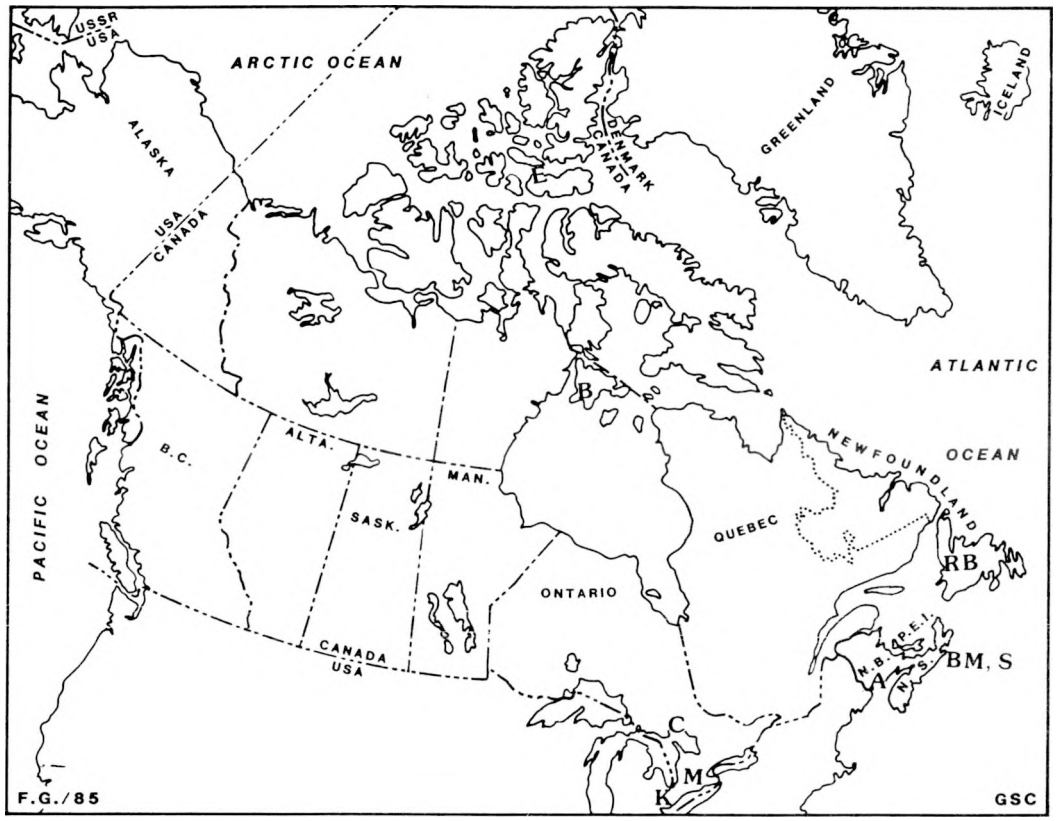

Figure 1. Map of Canada showing the locality of the oil shales. Ordovician, C: Collingwood and B: Boas; Middle Devonian, M: Marcellus; Upper Devonian, K: Kettle Point; Lower Carboniferous, E: Emma Fiord, B.M.: Big Marsh; R: Rocky Brook; A: Albert Shale.

been reviewed[6,4] and, as discussed below, it has been shown that neither the Boas nor the Collingwood is a kukersite-type deposit although some scientists have suggested that *G. prisca* was a major contributor to deposits in the Boas.[3]

The Collingwood oil shale (Edenian to Maysvillian ages in the middle-Upper Ordovician Lindsay Formation is perhaps one of the best known oil shale deposits in Canada and is the only Canadian oil shale that has been exploited commercially. Oil was reported sporadically from the Collingwood between 1859 and 1861 prior to the discovery of nearby conventional oil. Organic matter in the Collingwood consists almost entirely of amorphous material (Plate 1a) rather than the morphologically distinct telaginite which is present in kukersites.[6] Occasional algal bodies can be distinguished. The most abundant of these are acritarchs but leiosphaeridae-like algae and rare *G. prisca* are also present. Other faunas observed include brachiopods, conodonts and chitinozoans.

The organic carbon content of the Collingwood oil shales can exceed 10% but the average is around 5 to 6%.[8] Rock-Eval analysis of the less mature Collingwood samples indicates that they contain type II-I organic matter. Hydrogen indices are commonly in the 500 to 600 range with some samples showing values above 650.

Compared to kukersite type deposits the gas chromatograms of Collingwood samples differ by showing higher concentrations of C_{19+} n-alkanes and acyclic isoprenoids.[9,8,4] The less mature Collingwood samples have a slight odd carbon number preference between nC_{15} and nC_{19} but most samples show a smooth distribution of n-alkanes over this range. Collingwood samples show pristane to phytane ratios of 1.39 to 1.83 suggesting that they were deposited under mixed oxic-anoxic conditions. After n-alkanes and acyclic isoprenoids, the next most abundant class of saturated hydrocarbons in the Collingwoood extracts are n-alkylcyclohexanes.[4] These compounds are characteristically found in high concentrations in kukersite extracts. However, their distribution in the Collingwood is unusual. Immature samples show bimodal distribution with the C_{23} and the C_{25} n-alkylcyclohexanes in highest abundance and an odd carbon number preference. Compared to kukersite extracts the methyl-n-alkylcyclohexanes are in much lower concentration and the polycyclic biomarkers such as steranes and terpanes are present in higher concentrations.

Table 1. Paleozoic oil shales in Canada.

Name	Location	Age	Depositional Setting
Boas	Southampton Island	Upper Ord.	marine, hypersaline
Collingwood	S. Ontario	Upper Ord.	marine
Marcellus	S. Ontario	Middle Dev.	marine
Kettle Point	S. Ontario	Upper Dev.	nearshore marine
Albert Shale	New Brunswick	Lower Carb.	lacustrine
Big Marsh	Nova Scotia	Lower Carb.	lacustrine
Rocky Brook	Newfoundland	Lower Carb.	lacustrine
Emma Fiord Formation	Ellesmere Island	Lower Carb.	lacustrine
Various - associated with coals	Nova Scotia	Upper Carb.	alluvial flood basins

Table 2. Geochemical and petrological data.

Deposit	% TOC	OM Type	HI	OM appearance	Maturity
Boas	10-20	II	550-680	predom. amorph	immature
Collingwood	5-6 (→10+)	II-I	500-650	predom. amorph.	immature-mature
Marcellus	9-12	II	590-650	amorph. + telalginite	low-mod. mature
Kettle Point	5-8 (→10)	II-III	280-430	telalginite + terrestrial	immature
Albert Shale	4-10 (→29)	I	500-1000	lamalginite	immature
Big Marsh	4-5	II-III	220-400	predom. lamalginite	mature - high mature
Rocky Brook	4-15	I	700-900	lamalginite	variable (immature)
Emma Fiord	4-50	II-I	320-800	predom. telalginite	immature
Stellarton	6-7 (→20)	I	600-800	lam. + telalginite	mature

Fowler[4] concluded that samples from the Collingwood showed enough chemical features in common with kukersite samples to suggest that *G. prisca* was a significant contributor to the organic matter of this deposit. The classic kukersite chemistry is diluted in the Collingwood by contributions from other organisms, especially bacteria. This is expected from the amorphous appearance of the organic matter indicating intensive microbial weathering of the primary organic matter during diagenesis.

The Collingwood was probably deposited under normal marine conditions that had relatively high productivity in the surface waters. The bottom waters were probably reducing enough to allow only reworking of the primary organic matter by anaerobic bacteria, thus ensuring the preservation of high amounts of organic matter.

Organic-rich Upper Ordovician strata have been reported over a wide area of the eastern Canadian Arctic including on Akpatok, Baffin and Southampton islands.[8] The most extensively studied is the Boas oil shale on Southampton Island. The Boas is thought to be of Richmondian age[10] and hence is slightly younger than the Collingwood. Two distinct organic-rich units have been recognised within the Boas.[8] The upper unit was described as a brownish-black to dark brown, finely laminated, fissile very organic-rich (10-20% TOC), limestone and the lower unit as a light to medium brown poorly laminated, well indurated organic (TOC 2-6%) limestone. Microscopic examination under ultra-violet light shows that the organic matter in the Boas oil shales is, like the Collingwood, mostly amorphous. Only a few fragments of algal bodies (none recognisable as *G. prisca*) and acritarchs can be distinguished. The organic matter is concentrated in organic-rich laminations parallel with the bedding plane. In reflected light, occasional rounded bodies with an appearance similar to vitrinite can be seen concentrated along some laminations. Framboidal pyrite, sometimes partially oxidised is also present.

Rock-Eval analysis of Boas oil shale samples (Table 2) indicates that they contain immature type II organic matter.[8] Gas chromatography (GC) analysis and gas chromatography-mass spectrometry (GC-MS) analysis indicate that the hydrocarbon composition of the Boas extracts[4,8] is quite different from the "classic" Ordovician biomarker signatures shown by kukersites or their derived oils. This is additional evidence for the lack of a significant contribution from *G. prisca*. These include a higher concentration of C_{19+} n-alkanes, acyclic isoprenoids and polycyclic biomarkers. The Boas samples show a number of features expected for carbonate sediments deposited under highly reducing and probable hypersaline conditions, including a very low ratio of pristane to phytane, a high relative abundance of gammacerane, a high abundance of C_{34} to C_{33} or C_{35} 17α(H)-hopanes and the presence of 1-alkyl-2,3,6-trimethylbenzenes. These latter compounds are thought to be derived from a carotenoid found in the Chlorobiacea family of green sulphur bacteria[11] and thus indicate a contribution from these organisms.

Devonian oil shales

The two Devonian oil shales discussed herein from the Marcellus and Kettle Point formations are both located in southern Ontario. The older of the two the Marcellus is a widely distributed formation of Middle Devonian age. It consists of five distinct lithologic sub-units of which the uppermost and lowermost are organic-rich.[12] The uppermost units, which range in thickness from 0.4 m to 1.15 m are the more organic-rich. They show TOC contents up to and occasionally greater than 12% and contain type II-I organic matter with hydrogen indices (HI) up to 650.[13] Originally they might have had an even greater hydrocarbon potential since the organic matter is early mature to mature. The lowermost interval which is about 2.8 m below the upper sub-unit and ranges from 0.15 m to 0.68 m in thickness, is not as rich showing TOC values usually in the 4 to 5% range and HI values in the 400-500 range.

Most of the organic matter is amorphous although there are significant amounts of tasmanites and other algal bodies present[13]. Chitinozoans, graptolites and scolecodonts are also observed as are non-fluorescing hydrocarbons. No terrestrial derived material could be identified.

There is little difference between the composition of the extracts from the upper and lower Marcellus sub-units.[13] Both show smooth n-alkane distributions with nC_{17} the highest peak which is in agreement with a high algal and/or bacteria contributions. There is a surprisingly high relative abundance of acyclic isoprenoids especially considering the maturity of the samples. The ratio of pristane to phytane shows a narrow range between 1.14 and 1.39 suggesting mixed oxic-anoxic conditions. The sterane carbon number distribution shows about equal amounts of C_{27} and C_{29} with much lower amounts of C_{28} members and is what would be expected for marine derived organic matter of this age.

Diasteranes are relatively abundant compared to regular steranes as is often the case in shale. In summary, the chemistry agrees with the petrology in suggesting that the organic matter of the Marcellus is derived mostly from algal and bacterial sources with no significant terrestrial contribution (Plate 1b).

The Kettle Point Formation is equivalent to the extensive black shale deposits of the eastern United States such as those contained in the Antrim and New Albany formations.[1] The Kettle Point is characteristically a dark grey, brown grey to black, silty argillaceous shale which is essentially noncalcareous.[1] It has been divided into six sub-units which can be correlated with the Antrim shale of Michigan Basin.[14]

The Kettle Point is poorly fossiliferous. Microscopic examination shown abundant alga bodies identified as *Tasmanites* and *Foerstia* (Plate 1c), and scattered leiospheres and conodonts within an amorphous matrix.

TOC contents are generally between 5 to 8% with some samples showing values up to 10%. Oganic material in the Kettle Point Formation is less mature than that in the Marcellus Formation and is not as hydrocarbon rich (Table 2). Hydrogen Indices range up to around 400 and the organic matter can be classified as type II-III.[1]

Extracts of Kettle Point samples show a smooth distribution of n-alkanes with the nC_{15-19} predominating.[9,15] Acyclic isoprenoids are in high relative abundance. The ratio of pristane to phytane is significantly higher for the Kettle Point samples than for those in the Marcellus, sometimes being above 2. This suggests that the Kettle Point Formation was deposited in a more oxic environment than the Marcellus. This is in agreement with the nearshore depositional environment interpreted for the Kettle Point and possibly indicates why the organic matter in the formation indicates a lower hydrocarbon potential. However, this does not satisfactorily explain the presence of the algal bodies and also the higher abundance of steranes relative to hopanes both of which suggest much less bacterial reworking of the primary algal matter than one would expect from such an environment.

Carboniferous oil shales

There are several deposits of Carboniferous-aged oil shales present within the Atlantic provinces of Canada. The Lower Carboniferous oil shales were deposited in Tournaisian to Viséan time in continental lacustrine settings. These include the Albert shale of New Brunswick, the Big Marsh deposit of Nova Scotia and the Rocky Brook Formation of Newfoundland. The characteristics of these deposits have been described in detail in a number of papers by Macauley, Kalkreuth and other workers.[1,16,17,18,19,20]

Recently, a deposit of similar age (Viséan) has been described from the Emma Fiord Formation on Grinnell Peninsula, Devon Island in the Canadian Arctic Archipelago.[21,22] The Emma Fiord oil shale was also deposited in a continental lacustrine environment immediately prior to or synchronous with the initiation of rifting in the Sverdrup Basin.[21,22] An equivalent organic-rich interval occurs in the Emma Fiord Formation on Kleybolte Peninsula on northern Ellesmere Island but in that deposit organic material is overmature, showing Ro values up to 5.0%.

All the Lower Carboniferous deposits show many features in common. One of the most important of these is that the algae *Botryococcus* (Plate d) was a major contributor to their organic matter. This is evident from microscopic examination of the Emma Fiord samples which are dominated by telalginite with the characteristic morphology of *Botryococcus*.[22,23]

The organic matter in Carboniferous deposits in the Atlantic provinces appear to be dominated by lamalginite[17,18,19], that is algae material with no distinct morphology. However, it is evident from the chemistry of the Albert shale extracts that *Botyococcus* was a significant if not the major contributor to organic matter in that unit.[24] This is most evident in sterane distributions which show an unusually large predominance of C_{28} and C_{29} steranes relative to C_{27} steranes.[23] Pristane to phytane ratios of both the Albert shale and Emma Fiord Formation samples are usually much less than 1.0 suggesting very anoxic conditions of deposition[20,24,25]. Interestingly a comparison of the composition of the extracts of the Albert shale and Emma Fiord samples suggest that *Botryococcus* was a more dominant source of the organic matter in the Albert shale than it was in the Emma Fiord; the latter appears to have received a larger contribution from higher land plants. The high algal contribution to these Lower Carboniferous oil shales explains why they tend to by type I kerogens. The Big Marsh deposit shows lower hydrogen indices because of its relatively high maturity not because of greater terrestrial contribution.

Upper Carboniferous oil-shales that are associated with coal deposits are known from several localities in Nova Scotia. The best known is an interval of the Oil-Coal seam of the Pictou group in the vicinity of Stellarton which is often referred to as Stellarite.[1,18,26] The organic matter of the Oil-Coal seam consists almost entirely of telalginite that is *Botryococcus*.[18] Oil-shale intervals have recently been described in other Upper Carboniferous (Pennsylvanian) coal basins in Nova Scotia.[26] These deposits show varying proportions of telalginite, lamalginite and higher land plant derived organic matter, especially liptinitic components and generally have very high organic carbon contents (5-40% TOC).[27] The associated coals show little hydrocarbon potential. The Stellarite material as expeced from microscopic observations is type I organic matter as shown from Rock-Eval analyses.[1,18] The other oil-shale units vary in their hydrocarbon potential depending on the amount of non-liptinitic higher land plant material that is present but most are type II-III.[27] The composition of their extracts are mostly typical of terrestrial derived organic matter with a predominance of C_{23} to C_{33} odd carbon numbered n-alkanes, high pristane to phytane values, a predominance of C_{29} steranes over C_{27} and C_{28} steranes and of terpanes over steranes.[25] There is some variation between samples depending on the input of organic matter. For example, a sample from the Mabou Mines area that has a very high sporinite content shows very high concentrations of C_{25-30} iso-alkanes.[25] Gibling

and Kalkreuth[26] consider these organic-rich units to have been deposited in shallow lakes and/or interdistributary bays with aerobic to anaerobic bottom waters at times of minimal detrital input.

Conclusion

Paleozoic oil shales are widespread in Canada; Ordovician and Devonian deposits were formed mainly under marine conditions, in contrast with the Lower Carboniferous oil shales which were deposited in lacustrine settings. The marine to nonmarine environment of Canadian oil shales is reflected in their petrological and geochemical characteristics.

References

1. G. Macauley, L.R. Snowdon and F.D. Ball, "Geochemistry and geological factors governing exploration of selected Canadian oil shale deposits", Geological Survey of Canada, Paper 85-13, 65 p., 1985.

2. J.D. Reed, H.A. Illich and B. Horsfield, "Biochemical evolutionary significance of Ordovician oils and their sources", Organic Geochemistry, Vol. 10, pp. 347-358, 1986.

3. C.B. Foster, G.W. O'Brien and S.T. Watson, "Hydrocarbon source potential of the Goldwyer Formation, Barbwire Terrace, Canning Basin, Western Australia", Australian Petroleum Exploration Association Journal, Vol. 26, pp. 142-155, 1986.

4. M.G. Fowler, "Organic geochemsitry of oils and organic-rich rocks of Late Ordovician age from Canada, in Schidlowski et al. (eds.), Proceedings of the 9th Alfred Wagener Conference, "Early Organic Evolution Implications for Mineral and Energy Resources, Spring-Verlag, in press.

5. K.G. Osadetz, L.R. Snowdon and L.D. Stasiuk, "Association of enhanced hydrocarbon generation and crustal structure in the Canadian Williston Basin", in Current Research, Part D, Geological Survey of Canada, Paper 89-1D, pp. 35-47, 1989.

6. M.G. Fowler and A.G. Douglas, "Distribution and structure of hydrocarbons in four organic-rich Ordovician rocks, Organic Geochemistry, Vol. 6, pp. 105-114, 1984.

7. A.C. Hutton, "Petrographic classification of oil shale", International Journal of Coal Geology, Vol. 8, pp. 203-221, 1987.

8. G. Macauley, M.G. Fowler, F. Goodarzi, L.R. Snowdon and L.D. Stasiuk, "Ordovician oil shale-source rocks sediments in the central and eastern Canada Mainland and eastern Arctic areas and their significance for frontier exploration", Geological Survey of Canada, Paper 87-91, in press.

9. L.R. Snowdon, "A comparison of Rock Eval pyrolysis and solvent extraction results from the Collingwood and Kettle Point oil shales, Ontario", Bulletin of Canadian Society of Petroleum Geologists, Vol. 32, pp. 327-334, 1984.

10. G. Nowlan, Personal communication, 1989.

11. R.E. Summons and T.G. Powell, Chlorobiaceae in Paleozoic sea revealed by biological markers, isotopes and geology, Nature, Vol. 319, pp. 763-765, 1986.

12. M.D. Johnston, P.G. Telford, G. Macauley and J.F. Barker, "Stratigraphy and oil shale resources of the middle Devonian Marcellus Formation, southwestern Ontario", Ontario Geological Survey, Open File Report, in prep.

13. F. Goodarzi, G. Macauley, J.F. Barker and M.G. Fowler, "Organic petrology and geochemistry of organic-rich beds within the Middle Devonian Marcellus Formation", southwestern Ontario, in prep.

14. D.J. Russell and J.F. Barker, "Stratigraphy and geochemistry of the Kettle Point Formation, Ontario", University of Kentucky, Institute of Mining and Minerals Research, Proceedings, 1983 Eastern Oil Shale Symposium, pp. 169-179, 1983.

15. M.G. Fowler and J.F. Barker, Unpublished results.

16. G. Macauley, F.D. Ball and T.G. Powell, "A review of the Carboniferous Albert Formation oil shales, New Brunswick", Bulletin of Canadian Petroleum Geology, Vol. 32, pp. 27-37, 1984.

17. W. Kalkreuth and G. Macauley, "Organic petrology of selected oil shale samples form the Lower Carboniferous Albert Formation, New Brunswick, Canada", Bulletin of Canadian Petroleum Geology, Vol. 32, p. 38-51, 1984.

18. W. Kalkreuth, G. Macauley, "Organic petrology and geochemical (Rock Eval) studies on oil shales and coals from the Pictou and Antoginish area, Nova Scotia, Canada", Bulletin of Canadian Petroleum Geology, Vol. 35, pp. 263-295, 1987.

19. W. Kalkreuth and G. Macauley, "Organic petrology and Rock Eval studies on oil shales from the Lower Carboniferous Rocky Brook Formation, western Newfoundland", Bulletin of Canadian Petroleum Geology, Vol. 37, pp. 31-42, 1989.

20. A.M. Altebaeumer, "Organic geochemical investigation of selected oil shales of the Albert Formation, New Brunswick", Bulletin of Canadian Petroleum Geology, Vol. 33, pp. 427-445, 1985.

21. G.R. Davies and W.W. Nassichuk, "An Early Carboniferous (Viséan) lacustrine oil shale in Canadian Arctic Archipelago", American Association of Petroleum Geologists, Bulletin, Vol. 72, pp. 8-20, 1988.

22. F. Goodarzi, W.W. Nassichuk, L.R. Snowdon and G.R. Davies, "Organic petrology and Rock-Eval analysis of the Lower Carboniferous Emma Fiord Formation in Sverdrup Basin, Canadian Arctic Archipelago", Marine and Petroleum Geology, Vol. 4, pp. 132-145, 1987.

23. F. Goodarzi, G.R. Davies, W.W. Nassichuk and L.R. Snowdon, "Exsudatinite in Carboniferous oil shale from Arctic Canada", Fuel, pp. 771-773, 1987.

24. A.H. Chowdhury, M.G. Fowler, J.P.A. Noble, P.W. Brooks and L.R. Snowdon, "Petroleum geochemistry of the lacustrine Albert Formation, Moncton Subbasin, New Brunswick, Canada", in GAC/MAC Annual Meeting, Montreal, Program and Abstracts, pp. A132, 1989.

25. M.G. Fowler, Unpublished results.

26. J. Paul, W. Kalkreuth, R. Naylor and W. Smith, "Petrology, Rock-Eval and facies analyses of the McLeod coal seam and associated beds, Pictou Coalfield, Nova Scotia, Canada", Atlantic Geology, Vol. 25, pp. 81-92, 1989.

27. M.R. Gibling and W. Kalkreuth, Petrology of Carbonaceous limestone and shales in Pennsylvanian coal basins of Atlantic Canada, in prep.

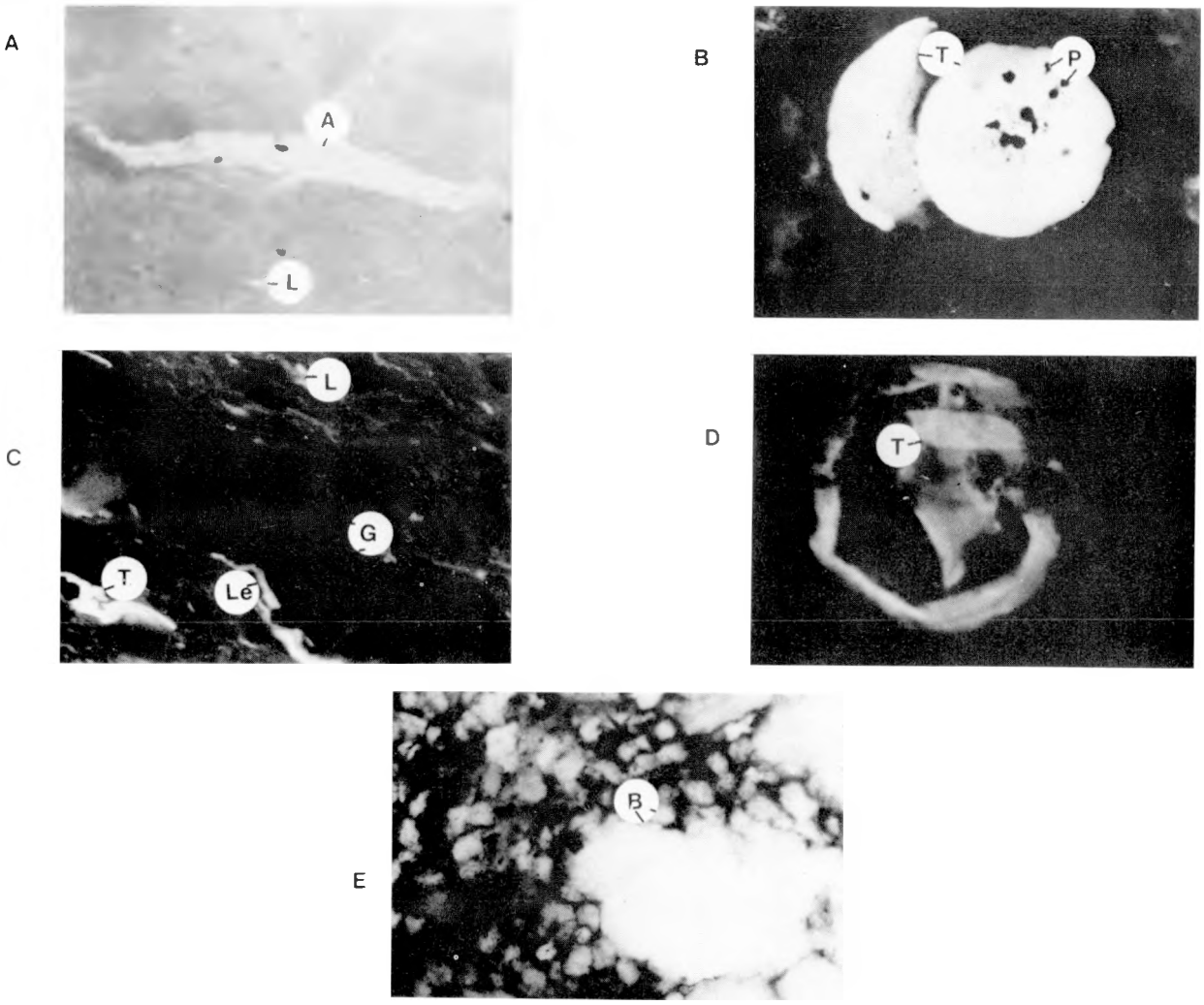

Plate 1

Morphology of organic components of oil shales samples from Paleozoic of Canada. Fluorescent light (blue-violet, exciter filter 450 nm, barrier filter, 520 nm), oil immersion: the long axis of each photograph is 240 microns. For location of oil shales see Figure 1.

a) Amorphous organic materials (A) and liptodetrinite (L) present in Collingwood oil shale, Ordovician, Ontario.

b) Strongly fluorescent *Tasmanales* algae (T) containing pyrite (P) are present in liptodetrinite (L) are present in Marcellus oil shale, Middle Devonian, Ontario.

c) Non-fluorescent Graptolite (G) fluorescent *Tasmanales* algae (T), Thin Leiosphaeridiales (Le) algae and liptodetrinite (L) in Marcellus oil shale, Lower Devonian, Ontario.

d) Large *Tasmanales* algae (T) in Kettle Point oil shale, Upper Devonian, Ontario.

e) *Botryococcus* algae (B) in Emma Fiord oil shale, Lower Carboniferous, Devon Island, Arctic Archipelago.

Directions and Characteristics of Jointing in the New Albany Shale (Devonian-Mississippian) of Southeastern Indiana

by

Curtis H. Ault
Indiana Geological Survey
Bloomington, Indiana 47405

ABSTRACT

More than 1,200 measurements of joint orientations at 27 sites in the New Albany Shale (Devonian-Mississippian) were made in an 850-square-mile study area in southeastern Indiana. The measurements show that primary jointing is east-northeastward and that secondary jointing is mostly north-northwestward. Joints in the thin-bedded New Albany Shale are vertical or nearly vertical, and the most prominent primary joints are commonly spaced 1.5 to 6 feet (0.5 to 2 m) apart but are variable from bed to bed within the New Albany and from site to site. Although the observed lengths of most primary joints are limited by the dimensions of the exposed bedrock, some prominent joints can be traced for more than 1,300 feet (396 m). Secondary joints are much less prominent, much shorter, less linear, and more variable in direction. Many butt against primary joints. Some joints extend vertically into the overlying Rockford Limestone (Mississippian), and some extend into the underlying North vernon Limestone (Devonian). The jointing orientation is controlled mostly by contemporary crustal stress, which is the predominant control of jointing orientation in much of Indiana and adjacent states. A knowledge of fracture directions is needed to help determine directions of fluid and gas transmission in the shale and possible communication with fluids in adjacent rock units; to help predict artificial fracture patterns caused by explosives or hydrofracturing; to help resolve directions of ground-water influx into drill holes and mines; and to help design future surface and underground mines.

INTRODUCTION

The New Albany Shale (Devonian-Mississippian) in southeastern Indiana is at or near the surface in parts of Bartholomew, Jennings, Jefferson, Scott, Clark and Floyd Counties (fig. 1). It strikes northward and its subcrop and outcrop width in the study area ranges from about 20 miles (32 km) near North Vernon in Jennings County to less than 3 miles (5 km) near the Ohio River. Unconsolidated overburden covering the New Albany subcrop is about 100 feet (30 m) at Seymour but is mostly less than 50 feet (15 m) eastward and southward.[1] The full thickness of the New Albany immediately west of its outcrop ranges from about 100 to 140 feet (30 to 43 m).[2] Outcrops where joints in the New Albany can be measured easily are rare because the shale erodes and weathers rapidly and is covered by soil or thin glacial till except where the shale is swept clean in streambeds or where the shale has been exposed in roadcuts, railroad cuts, quarries, and other construction excavations.

The New Albany consists of five

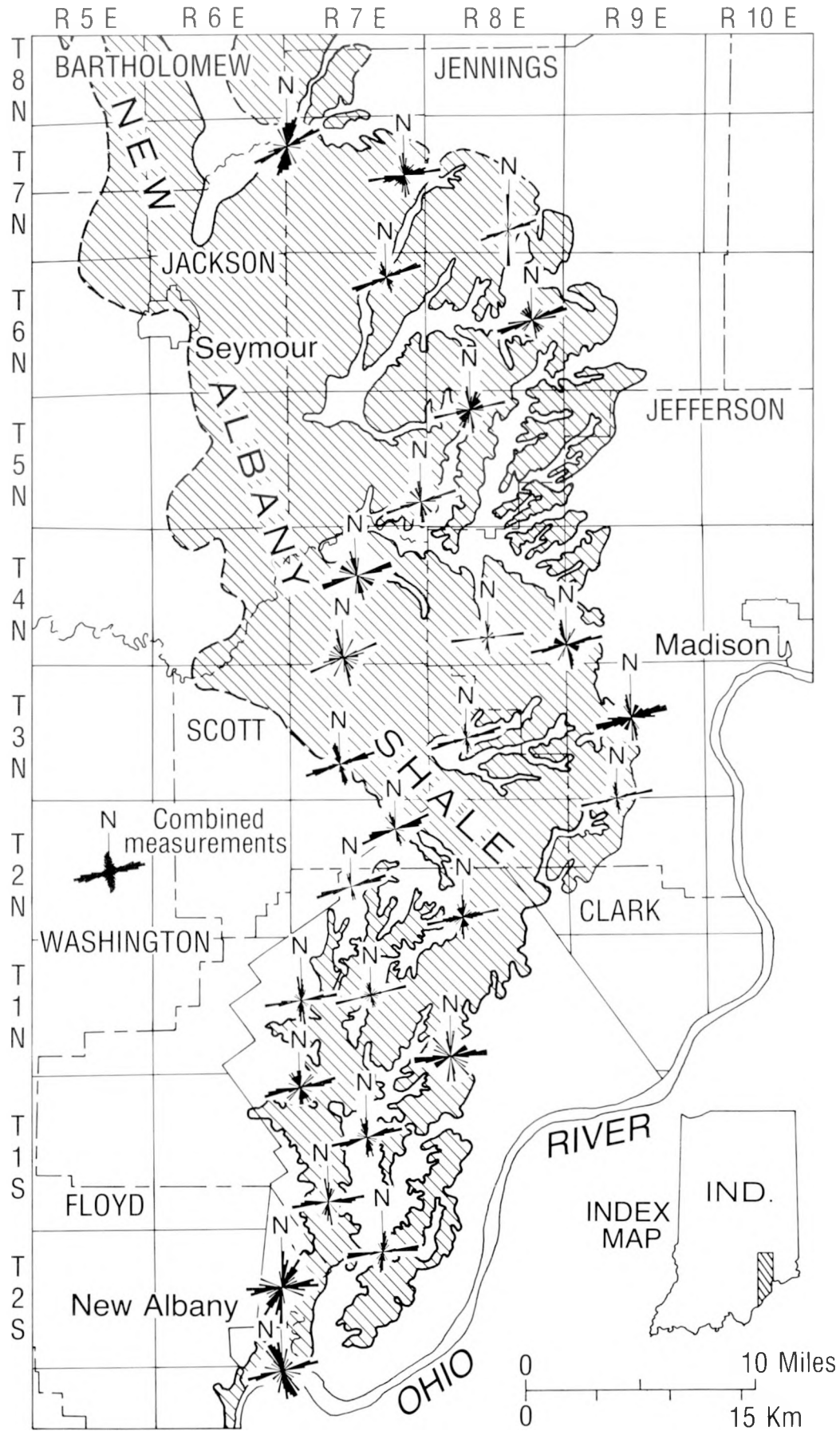
R 5 E
R 6 E
R 7 E
R 8 E
R 9 E
R 10 E
T 8 N
T 7 N
T 6 N
T 5 N
T 4 N
T 3 N
T 2 N
T 1 N
T 1 S
T 2 S
BARTHOLOMEW
JENNINGS
NEW
ALBANY
SHALE
JACKSON
Seymour
JEFFERSON
Madison
SCOTT
Combined measurements
CLARK
WASHINGTON
FLOYD
New Albany
OHIO
RIVER
INDEX MAP
IND.
0
10 Miles
0
15 Km

Figure 1. Map of southeastern Indiana showing directions of jointing in the New Albany Shale and its area of subcrop and outcrop. Joint measurements are in 5° arcs on the equal-area histograms. Outcrop types and statistical data for each location are given in table 1.

members in southeastern Indiana not including the poorly exposed Ellsworth Member, which is present in only part of Bartholomew County. In ascending order the five members are the Blocher, Selmier, Morgan Trail, Camp Run, and Clegg Creek Members, which are recognized primarily by color but also by differences in lithology.[3,4,5] The laminated black shale facies of the New Albany are considered excellent source beds for liquid hydrocarbon and have probably served to a large degree as a source for most of the oil and gas fields in the Illinois Basin.[6]

The shale dips 15 to 20 feet (5 to 6 m) per mile (1.6 km) westward. Because of this dipping, the lower members are exposed mostly in the eastern parts of its outcrop, and the uppermost members, which are richest in organic carbon and trace metals, are exposed in the western parts. The shale is eroded mostly into rounded hills, but the topography is rugged in places, especially where downcutting streams have eroded into the thick limestone and dolomite of the Muscatatuck Group (Devonian) that underlie the New Albany. The erosion of the shale in some areas results in highly variable thicknesses in short distances.

The Rockford Limestone (Mississippian), which overlies the New Albany, is a persistent limestone bed that is a good marker for the top of the New Albany in southeastern Indiana. It is in turn overlain by poorly exposed soft greenish-gray shale of the New Providence Shale (Mississippian).

Reeves (1922) discussed briefly the occurrence of New Albany joints in southeastern Indiana and illustrated the jointing with several photographs.[7] Campbell (1946) made a more detailed study of the joints and related jointing characteristics to individual rock units within the New Albany.[8] Lineback (1970) later discounted Campbell's use of jointing as distinguishing criteria for recognizing rock-unit boundaries.[5]

For this study, joints are defined as fractures or partings in rock with little or no discernible displacement. Much of the New Albany is brittle and well jointed (figs. 2 and 3). Notable exceptions are some soft beds of the Selmier Member (fig. 4) that exhibit few joints and that are poorly exposed except in fresh quarry faces. Any mining or commercial exploitation of the shale for hydrocarbons will be affected by the jointing, which is ubiquitous wherever the shale is exposed. The shale is removed as unwanted overburden at several crushed-stone quarries (fig. 5), and the jointing at these locations causes problems. Test holes, water wells, and other holes drilled into or through the shale may encounter open joints that allow leakage of drilling fluids or considerable influx of ground water in open holes.

Unfractured New Albany Shale is nearly impermeable. I have observed the very slow release of gas from fresh New Albany well cuttings in deeper parts of the Illinois Basin, an indication of the low permeability of the shale. Therefore, artificial fracturing of the New Albany is extremely important for enhancing in situ production of oil and gas from the shale. Hohn has described the transmission and storage of almost all fluids and gases in and through fractures in correlative Devonian shales of West Virginia.[9]

Induced fractures may follow regional joint directions after a short distance from the well bore, although there are no known direct data to substantiate this fact. (See Ault, 1988, for similar phenomena in limestone in quarries in northern Indiana.)[10] Partial support for this rationale is the accepted geophysical thesis that directions of fractures resulting from hydrofracturing in test wells are strong indicators of directions of crustal stress. Therefore, the direct relation of natural jointing in the New Albany to contemporary regional stress discussed below indicates that fractures produced artificially follow the directions determined in this study and that a knowledge of the joint directions is important in placing and spacing oil and gas wells in the New Albany Shale.

REGIONAL JOINTING

The outcrop and subcrop of the New Albany Shale in southeastern Indiana lie on the west flank of the Cincinnati Arch. The regional jointing pattern for near-surface rocks in most of Illinois, Indiana, and western Ohio is similar, notwithstanding the basin and arch configuration in these three states. The most prominent joints (primary joints) trend east-northeastward, and the less prominent orthogonal joints (secondary joints) trend north-northwestward. Primary joints are controlled mostly by lithospheric stress as described regionally by Engelder and in Indiana by Ault and Haumesser.[10,11,12] Secondary joints commonly abut primary joints, which indicates that they formed after the primary joints, a sequence described by Price.[13]

An apparent counterclockwise shift in jointing direction of 50° or more in

Figure 2. Outcrop of well-jointed New Albany Shale along the north shore of the Ohio River at New Albany. The primary joints trending east-northeasterly are about 4 to 12 feet (1.2 to 3.6 m) apart. River silts give the outcrop a light color.

Figure 3. Well-jointed beds of the Morgan Trail Member at the Scott County Stone Co. quarry near Scottsburg, Scott County. The joints are 4 to 5 feet (1.2 to 1.5 m) apart.

Figure 4. Loose quarry block of soft, poorly jointed Selmier Member at the Scott County Stone Co. quarry.

Figure 5. Stripping area for removal of New Albany shale from well-jointed limestone and dolomite of the Muscatatuck Group at Liter's Quarry of Indiana near Jeffersonville, Clark County.

County	Location	Type	Measure-ments	degree ranges	Aver-age	Me-dian	Std. dev.
Clark	S 1/4 CMG 50	qry	51	75-95	83.8	84.0	3.3
Clark	S 1/4 CMG 110	otc-rdct	25	75-95	85.4	84.0	5.0
Clark	E 1/4 CMG 150	qry	51	60-85	74.7	76.0	4.5
Clark	CNWL CMG 156	otc-rdct	24	65-95	83.0	83.0	7.2
Clark	C CMG 201	otc	43	75-90	80.9	81.0	3.8
Clark	CNWL CMG 224	otc-qry	44	70-85	78.0	78.0	2.0
Clark	S 1/4 CMG 247	otc	47	60-90	76.8	76.0	5.3
Clark	CNEL CMG 252	otc	67	75-90	81.9	82.0	2.7
Clark	NE SE 21-2N-7E	otc	36	65-85	73.4	74.0	3.7
Floyd	CSL CMG 28	otc	55	70-85	76.9	77.0	3.2
Floyd	C CMG 63	otc	41	75-100	84.5	85.0	7.2
Jefferson	N SE 16-3N-9E	qry	44	60-90	74.3	74.0	6.6
Jefferson	SW SE 28-4N-8E	otc	41	75-90	81.9	82.0	1.6
Jefferson	NWc 31-4N-9E	otc	34	70-90	77.3	77.0	4.7
Jennings	SW SE 25-5N-7E	qry	19	60-80	73.6	74.0	2.7
Jennings	SEc 5-5N-8E	otc	29	75-80	76.5	76.5	1.8
Jennings	SW SW 2-6N-7E	otc	61	60-80	69.5	70.0	4.3
Jennings	SW SE 14-6N-8E	rdct	28	60-85	70.8	70.0	5.9
Jennings	CW NW 7-7N-7E	otc	46	50-80	61.6	61.0	6.8
Jennings	NW SW 13-7N-7E	otc	53	60-90	78.2	81.0	7.2
Jennings	CS1/2 27-7N-8E	qry	62	60-80	68.1	68.0	3.7
Scott	N 1/4 CMG 295	otc	58	60-85	72.5	72.5	5.5
Scott	NEc 5-2N-9E	otc	64	65-85	75.2	76.0	3.3
Scott	SW NW 28-3N-7E	otc	74	60-85	72.0	72.0	4.5
Scott	NE NW 20-3N-8E	qry	66	60-85	74.0	74.0	3.5
Scott	SE SE 9-4N-7E	qry	21	70-85	76.7	75.0	4.5
Scott	NW SW 33-4N-7E	otc	25	60-90	71.4	67.0	8.5
COMBINED MEASUREMENTS FROM ABOVE							
27 sites			1,209	60-90	75.5	76.0	6.4

Abbreviations: CMG-Clark Military Grant, otc-outcrop, qry-quarry, rdct-roadcut, std. dev.-standard deviation.

Explanation for Table

Selected degree ranges are well-defined clusters of histogram bars that represent prominent directions of jointing in figure 1. Within the degree ranges about two thirds of the measurements can be expected within one standard deviation from the average, and about 95 percent of the measurements can be expected within two standard deviations. This apportionment is only approximate, however, because there is not an exact normal distribution of measurements around the average.

Table 1. Locations and types of outcrops and statistical data on joint orientations of New Albany shales in southeastern Indiana

southernmost south-central and southwestern Indiana is described by Ault and others and is shown on a large scale map of Indiana by Ault.[14,15] The shift in jointing direction may be caused by a shift in regional stress in this area, but no confirming evidence for the change in direction is available for jointing in bordering northwestern Kentucky. Jointing in the New Albany Shale in southeastern Indiana (fig. 1) is apparently not affected by the shift and is consistent with jointing directions in the rest of Indiana. The median jointing direction for primary joints in Indiana exclusive of the shift is 78°, although local deviations from this can be significant.[15] The median direction for primary jointing in the New Albany Shale in southeastern Indiana is 76° (table 1); again, there are local variations even though the overall directions are remarkably consistent.

Most New Albany jointing in southeastern Indiana apparently reflects the fabric of regional stress in Indiana. Jointing in rocks in Indiana may also be affected by steeply dipping flank beds on reefs and by lithology, topography, and stress conditions related to local structure. Of these, only lithology was observed to have a significant effect on New Albany jointing. The effects of topography, particularly on steep slopes, may be disguised by weathering effects; deeply weathered New Albany is so broken and fractured that most original joints cannot be recognized.

METHODOLOGY

All measurements of joint directions shown in figure 1 were taken with a K&E surveying compass (similar to a Brunton compass). The accuracy where measurements could be taken directly on joint surfaces

Figure 6. Prominent joint surface at a small outcrop of New Albany shale in the SW 1/4 SE 1/4 sec. 25, T. 5 N., R. 7 E., Jennings County.

was within 1° and where taken by sighting along joint surfaces was within 2°. Sighting measurements along long joints eliminated deviations caused by small irregularities. Measurements in quarries were made along all faces where the New Albany was exposed to eliminate directional bias, but bias is not much of a problem in most quarries, because joints are so well exposed that a representative sample is not difficult to obtain.

In some areas exposures were small and the number of measurements that could be taken were limited. But even where as few as 19 measurements were taken (fig. 6; table 1, sec. 25-5N-7E, Jennings County), major directions of jointing are apparent. Each joint, regardless of length or prominence, is counted as one measurement on the rose histograms in figure 1. Short, strongly curved fractures, found in some places, are not included in the measurements.

Pentecost and Samuelson determined that the dominant two directions of all joints they measured in east-central Indiana were seen in all three of their length categories for jointing.[16] This indicates that the dominant direction of jointing can be determined without categorizing by length, although short joints tend to have a greater range of direction. Further, in the present study, most prominent primary joints in the New Albany could not be commonly observed in their full length, for they were longer than the exposures where they were measured (fig. 2).

Because presently exposed jointed rocks in some of the outcrops will soon become deeply weathered and most of the current exposures in active quarries will be removed by mining, the exact reproducibility of the measurements shown in figure 1 is unlikely. Some of the original outcrops where measurements were taken 3 years ago are no longer well exposed. Some variability in measurements is also inherent between different investigators because of different recognition and selection of joints to be measured. Major directions of jointing are generally apparent at a site after a sufficient number of measurements, however, even though the proportionate number of joints measured in major directions may not be the same.

All measurements in this study were made on bedrock. Aerial-photo lineaments were not used because the New Albany outcrop and subcrop in southeastern Indiana have been affected by Illinoian and pre-Illinoian glaciation, and the relationship between aerial-photo lineaments on glacial drift and bedrock fractures is not known. Carr found little similarity between photo-lineament directions and jointing directions in southwestern Indiana and did not relate lineaments closely to New Albany gas production from the Corydon, New Middletown, and Laconia Fields.[17] Limited measurements of joint directions in

glacial till at the Meshberger Stone, Inc., quarry near Columbus, Bartholomew County, showed no similarity to directions measured in the underlying carbonate rock of the Muscatatuck Group at the same location.

CHARACTERISTICS OF JOINTING

Primary joints in the New Albany, the prominent joints oriented east-northeastward, range from well-exposed and well-defined linear fractures more than 1,300 feet (396 m) long at the south side of New Albany at the Ohio River (fig. 2) to nearly obscured fractures at small outcrops (fig. 6). Primary joints in the New Albany are commonly spaced 1.5 to 6 feet (0.5 to 2 m) apart (fig. 7), but they are as much as 20 feet (6 m) apart in places. They are vertical to nearly vertical and commonly have smooth faces (fig. 8), some of which are stained by minerals precipitated from ground water. A few rough joint surfaces on loose New Albany quarry blocks had nearly microscopic steplike fracture faces.

Secondary joints are generally perpendicular to the primary joints and are commonly much shorter. They are generally confined between primary joints (fig. 9), but cross joints are numerous in some beds. Secondary joints are more numerous than primary joints in most places. The directions of secondary joints vary more than those of primary joints, and the linearity of secondary joints is not as pronounced. In some exposures the secondary joints are only a few inches apart, but the spacing of these joints varies from bed to bed in the New Albany and from locality to locality. A checkerboard arrangement of joints a few inches apart is exposed in thin beds of the Blocher Member within a few feet of the base of the formation in places (fig. 10). Short, strongly curved shallow fractures are mostly confined to thin shale beds and are apparently related to surface weathering and flaking.

Vertical lengths of the joints in the New Albany range from a few inches in some beds to vertical lengths of more than 10 feet (3 m) through several beds. A few traverse nearly the entire thickness of the formation. (A full thickness of the New Albany is not exposed at any one locality.) Jointing in the New Albany is typically stepwise through individual beds that range from several inches to several feet in thickness (fig. 11). Those beds that are more brittle, particularly in the Blocher, Morgan Trail, and Clegg Creek Members, are more prominently jointed (fig. 3).

In the two outcrops where the Clegg Creek Member and the overlying Rockford Limestone were measured, there is an interconnected network of joints between the two rock units (fig. 12). Many individual joints in both units terminate at the contact between the units. Similarly, in exposures at the base of the formation where the Blocher Member overlies the carbonate rocks of the Muscatatuck Group, the network of New Albany joints is interconnected in part with the joints of the underlying North Vernon Limestone of the Muscatatuck Group. Where observed in the quarries, the Blocher Member is much more profusely jointed than the underlying North Vernon, and there is some slight difference in direction of jointing, but this was not investigated in detail.

The median directions of primary joint groupings in the study area ranges from 61° to 85° and the median direction for all primary joints measured is 76° (fig. 1, table 1). The standard deviation of 6.4° for all measurements grouped about the average of 75.5° shows a very consistent grouping in an east-northeasterly direction.

Predicting the direction of primary jointing at any specific location can be estimated from regional directions but should be based as much as possible on measurements at nearby exposures. Even then, considerable deviation can be expected unless the jointing is measured directly at the site. Generally, at sites where thick New Albany was exposed, little deviation was found in jointing directions from the top of the exposure to the base of the exposure, although no attempt was made to quantify detailed differences in direction in different parts of the New Albany. As discussed above, the frequency and the spacing of the jointing vary significantly with stratigraphic position within the New Albany, but directions are apparently not affected much. The standard deviation of the primary grouping of joints at different locations ranges from 1.6°, an exceptionally tight grouping, to 8.5°, an exceptionally loose grouping (table 1). This indicates that even where the spread of directions of primary groupings is larger than normal, considerable reliance can be placed on initial measurements to forecast other joint measurements at a site.

Fractures were reported by Carr in a core of the New Albany from a test hole in Sullivan County.[17] The core contained fractures, healed in part by mineralization, from a depth of 2,504 feet (763 m) to 2,630 feet (802 m). The maximum depth of jointing of the New Albany in the subsurface in Indiana is not known. Open joints have been observed at depths of several hundred feet in quarries and cores of other formations, and open joints may be expected at similar depths in the New Albany.

Figure 7. Primary joints exposed in a creekbed at the center NE line, Clark Military Grant 252, near Henryville, Clark County. The joints are about 4 feet (1.2 m) apart.

Figure 8. Loose quarry block of New Albany shale showing smooth joint surface at Liter's Quarry of Indiana, Clark County. The block is about 1 foot (0.3 m) thick.

Figure 9.

Secondary joints abutting two primary joints in a creekbed at the center NE line, Clark Military Grant 252, near Henryville, Clark County. The two primary joints are 4.2 feet (1.3 m) apart.

Figure 10. Checkerboard arrangement of small joints in Blocher Member near its contact with the underlying limestone and dolomite of the Muscatatuck Group.

Figure 11.

Stepwise jointing in lower third of the New Albany Shale. The quarry face in this photograph at the North Vernon Quarry, Jennings County, is about 30 feet (9 m) high.

Figure 12. Well-jointed Rockford Limestone overlying the New Albany Shale in a streambed outcrop at the center NE line, Clark Military Grant 252, near Henryville, Clark County. Joints in the Rockford are 2.8 to 3.2 feet (0.9 to 1.0 m) apart.

EFFECTS OF JOINTING

Transmission of fluids and gases

Because of the very low permeability of unfractured New Albany shale, most if not nearly all of the movement of fluids and gases through the shale is through fractures and joints. The strong directional orientation of joints in the New Albany, particularly primary joints, influences the direction of fluid and gas movement through the shale. The preferred flow of fluids will be caused by pressure gradients along a system of open joints (Richard L. Powell, oral communication, 1989). Because open primary joints are commonly the most prominent and have the greatest transmissivity and because shorter open secondary joints commonly feed the primary joints, transmissivity of fluids and gases in many places is greatest along the east-northeasterly direction of the primary joints. If some or most of the primary joints are not open or if interconnection of the secondary with the primary joints is poor, conditions difficult to predict, the direction of greatest transmissivity may be considerably different.

The vertical movement of fluids and gases is much less predictable. The stepwise nature of many of the joints indicates that vertical movement in the shale is greatly hindered not only by joints terminating in individual beds but also by relatively non-jointed beds, such as those in the Selmier Member.

The transmission of fluids from the New Albany into adjacent formations can take place because of interconnected joint systems, but to what extent is unknown. The overlying Rockford Limestone is well jointed in southeastern Indiana but relatively thin, rarely exceeding 2 or 3 feet (0.6 or 0.9 m) in thickness. The Rockford is overlain by soft shales of the New Providence that are poorly jointed. The permeability cap on the New Albany and the Rockford, therefore, is likely good but not perfect.

The underlying limestone of the Muscatatuck Group is well jointed and interconnected to some degree with the New Albany. Many joints from both rock units terminate at the boundary between the two. The joints in the limestone are commonly very prominent (fig. 5), and even a limited access to these joints from the New Albany can allow movements of considerable volumes of fluids and gases between the formations.

The jointing pattern should strongly influence the spacing and positioning of drill holes in the New Albany in southeastern Indiana, whether to produce hydrocarbons or to inject fluids or gas. If a jointing pattern in the area has been determined, holes may be placed to take advantage of any preferential movement of fluids and gases in the direction of the primary jointing. Holes drilled at angles to cross as many open joints as possible, particularly primary joints, should be considered.

Particular patterns of jointing may allow a stronger movement in a direction diagonal to the primary and secondary jointing, a possible explanation for some photo lineations, but no evidence of strong diagonal patterns was observed on outcrop in this study.[17,18]

Induced fracturing of the New Albany to increase in situ production of hydrocarbons from the shale probably produces fractures that are aligned with the natural fracture pattern. As discussed above, the present crustal stress fabric is aligned with the jointing systems of the New Albany as measured in this study. It can be speculated that fractures produced artificially will follow the same stress pattern a short distance from the initial radial fracturing near the test hole. If such speculation is true, the movement of fluids and gases along the artificial fractures can be expected to be most prominent along the primary-joint directions.

I am unaware of any direct measurements of directions of fluid transmission in the New Albany in southeastern Indiana. Until such research is accomplished and made available for publication, the above discussion can be considered only academic.

Open-pit mines

Open-pit mining of the New Albany shale is less difficult and uses less explosive than limestone quarrying, but as in limestone quarrying, jointing dictates some of the blasting practices. Joints allow blasting energy to escape without accomplishing efficient fragmentation of the shale. Blast holes in the shale should not be placed close to prominent primary joints.

Too much explosive will fragment the shale excessively and make it difficult to handle (Steve Tobias, oral communication, 1989); rather, the person doing the blasting should use only enough explosive to "bump" the shale away from the exposure, where it can be handled easily by a front-end loader.

Soft shale, such as that in part of the Selmier Member, absorbs explosive energy. In one quarry operation in southeastern Indiana where the shale is removed from above limestone, crushed stone is loaded into blast holes within the soft sections of the shale to prevent absorption of the explosive energy and to prevent unequal results from the blasting.

There is a danger of loose rock and unstable faces where prominent primary joints are parallel or subparallel to quarry faces. This can be avoided in large part by orienting quarry faces at right angles to prominent joints if there is only one prominent direction or at 45° to prominent orthogonal joints. This not only makes a more stable face but also allows more efficient use of explosives.

Joints in limestone quarries may allow considerable water influx into a quarry because the ground water tends to widen many joints by solution. Water influx through the shale joints is not a problem in quarries in southeastern Indiana where thick New Albany is exposed.

Underground mines

The large outcrop area and numerous potential areas for open-pit mines in the shale, not only in Indiana but also in other states, make it unlikely that the New Albany will be mined underground for hydrocarbon for many years. If the New Albany is eventually mined underground, numerous geologic hazards must be faced.

The well-developed jointing in much of the New Albany makes roof conditions hazardous in underground mining by room-and-pillar methods even though the shale is more brittle and durable than many other shales. Varying humidity in underground mines generally causes flaking and spalling of most shales. Pennsylvanian black shales, which are similar to the New Albany in many respects, make poor roof conditions in some room-and-pillar coal mines in the Illinois Basin. Where present in some mines, thin Pennsylvanian black shales are overlain by limestone, which can be used to anchor roof bolts for additional stability. This is not a perfect solution as evidenced in some mines by roof falls that leave roof bolts surrounded by only a few inches of black shale or hanging with no shale.

The overlying Rockford Limestone in southeastern Indiana may or may not be a candidate for anchoring roof bolts. It can be seen in figure 12 that this bed is strongly jointed itself, at least where observed at the surface. Solution widening of joints in the Rockford is evident at the surface and may be a problem to some depth. There may be areas and depths in southeastern Indiana where the limestone is much less jointed and where it could be used to help stabilize the underlying New Albany, but there is no evidence for that in this study.

The New Albany may be better suited for longwall underground mining, where roof collapse is planned and predictable as mining progresses. Under these conditions, the stability of the roof maybe directly affected by the direction of mining as it relates to the direction of primary jointing. Mining at right angles to the direction of primary jointing will expose rocks fractured parallel to the mine face and may cause premature collapse of the roof. Mining in the direction of primary jointing or at large angles to prominent jointing may be preferable.

CONCLUSIONS

The New Albany Shale of southeastern Indiana is strongly jointed except for the Selmier Member and greenish-gray shales in the Camp Run Member, which are mostly softer than other members of the formation. Primary joints, the most prominent joints, trend east-northeastward, and their overall median direction is 76° in the study area. The standard deviation is 6.4° for the combined measurements grouped about an overall average of 75.5° for the range of 60° to 90°. Secondary joints trend north-northwestward and are shorter and more variable in direction than primary joints. The directions of primary joints are generally predictable from the regional average in the study area, although deviations may be locally significant. Initial measurements may be used to predict other measurements at particular sites. The spacing of primary joints is about 1.5 to 6 feet (0.5 to 1.8 m) in the more strongly jointed parts of the New Albany.

Many secondary joints abut primary joints, and most are confined between primary joints. The vertical extent of jointing ranges from a few inches to nearly the full thickness of the New Albany, but many joints are arranged in a stepwise progression through beds of the New Albany with terminations and beginnings of joints at bedding surfaces within the formation. Joint networks at the top and the base of the formation interconnect in part with joints in the overlying Rockford Limestone and the underlying carbonate rocks of the Muscatatuck Group. Although the amount of communication among the units is unknown, movements of considerable volumes of fluids and gases may be possible.

The jointing pattern of the New Albany in southeastern Indiana is consistent with the regional crustal stress in western Ohio, most of Indiana, and Illinois. Artificial fracturing of the New Albany, following the direction of maximum crustal stress, is postulated to be parallel to the natural jointing. It is also postulated that fluid and gas movement both in natural joints and in induced fractures will preferentially follow directions of primary jointing, mostly east-northeastward in the study area. Fluid and gas movement in the direction of secondary jointing may be much less.

A knowledge of the jointing directions and characteristics helps to determine blasting methods in open-pit quarries and will be important in helping to determine roof-and-pillar conditions in room-and-pillar mines and roof stability in longwall mining.

ACKNOWLEDGMENTS

Jimmy Johnson, systems analyst-programmer for the Indiana Geological Survey, wrote the computer programs for the equal-area histograms in figure 1 and the statistical analyses in table 1. Quarry operators were most helpful in allowing access to their operations. Critical reviews by and discussions with Nancy R. Hasenmueller and Tracy Branam, Indiana Geological Survey, and Richard L. Powell, Geosciences Research Associates, Inc., benefited the report greatly.

REFERENCES

1. H. H. Gray, "Map of Indiana showing thickness of unconsolidated deposits," Indiana Geological Survey Miscellaneous Map 38, 1983.

2. N. R. Hasenmueller and R. K. Leininger, "Oil-shale prospects for the New Albany Shale in Indiana," Indiana Geological Survey Special Report 40, 31 p., 1987.

3. N. R. Hasenmueller, "New Albany Shale," in R. H. Shaver and others, "Compendium of Paleozoic rock-unit stratigraphy in Indiana - a revision," Indiana Geological Survey Bulletin 59, p. 100-102, 1986.

4. J. A. Lineback, "Subdivisions and depositional environments of New Albany Shale (Devonian-Mississippian) in Indiana," American Association of Petroleum Geologists Bulletin, v. 52, p. 1291-1303, 1968.

5. J. A. Lineback, "Stratigraphy of the New Albany Shale in Indiana," Indiana Geological Survey Bulletin 44, 73 p., 1970.

6. M. H. Barrows and R. M. Cluff, "New Albany Shale Group (Devonian-Mississippian) source rocks and hydrocarbon generation in the Illinois Basin" in G. Demaison and R. J. Murris, eds., "Petroleum geochemistry and basin evaluation," American Association of Petroleum Geologists Memoir 35, p. 111-138, 1984.

7. J. R. Reeves, "Preliminary report on the oil shales of Indiana" in "Handbook of Indiana geology," Indiana Department of Conservation Publication 21, pt. 6, p. 1059-1105, 1922.

8. Guy Campbell, "New Albany Shale," Geological Society of America Bulletin, v. 57, p. 829-903, 1946.

9. M. E. Hohn, "The Devonian shale in West Virginia: an important natural gas resource," Mountain State Geology, West Virginia Geological and Economic Survey, p. 31-36, 1989.

10. C. H. Ault, "Cause and effect of jointing in quarries in central and northern Indiana," in G. W. Colton, ed., Proceedings of the 22nd Forum on Geology of Industrial Minerals, Arkansas Geological Commission Miscellaneous Publications MP-21, p. 17-29, 1988.

11. Terry Engelder, "Is there a genetic relationship between selected regional joints and contemporary stress within the lithosphere of North America?," Tectonics, v. 1, p. 161-177, 1982.

12. C. H. Ault and A. F. Haumesser, "A central Indiana model for predicting jointing characteristics in underground mines," Proceedings of the 24th Forum on the Geology of Industrial Minerals, South Carolina Geological Survey, in preparation.

13. N. J. Price, "Fault and joint development in brittle and semi-brittle rock," New York, Pergamon Press, 176 p., 1966.

14. C. H. Ault, Denver Harper, C. R. Smith, and M. A. Wright, "Faulting and jointing in and near surface mines of southwestern Indiana," U.S. Nuclear Regulatory Commission NUREG/CR-4117, 27 p, 1985.

15. C. H. Ault, "Map of Indiana showing directions of bedrock jointing," Indiana Geological Survey Miscellaneous Map 52, 1989.

16. D. C. Pentecost, and A. C. Samuelson, "Fracture study of the Paleozoic bedrock in east central Indiana," Proceedings of the Indiana Academy of Science, v. 88, p. 263-277, 1979.

17. D. D. Carr, "Lineament analysis," in N. R. Hasenmueller and G. S. Woodard, eds., "Studies of the New Albany Shale (Devonian and Mississippian) and equivalent strata in Indiana," Indiana Geological Survey report for U.S. Department of Energy, p. 62-69, 1981.

18. R. L. Powell, "Some geomorphic and hydrologic implications of jointing in carbonate strata of Mississippian age in south-central Indiana," Ph. D. thesis, Purdue University, West Lafayette, Ind., 169 p., 1976.

Pyroclastic Mineral Euhedral Horizons in Eastern United States Devonian Oil Shales

by

James E. Conkin
Department of Geology
University of Louisville
Louisville, Kentucky 40292

Abstract. Literature-entrenched term metabentonite, applied to weathered pyroclastics of original nature of ash falls, should be retained; proposed substitute terms, ash falls and K-bentonites, are less appropriate. To date, metabentonites are not specifically identifiable by x-ray, pyroclastic mineral euhedra, or trace element "fingerprinting." Geographic widespread specific identification and correlation of metabentonites and their enclosing strata can be best accomplished by reference to their stratigraphic-paleontologic context. Internal units of the Late Devonian black shales (New Albany-Chattanooga-Ohio) are recognizable on the bases of essentially chronostratigraphic disconformities of the magnitude of paracontinuities and their associated bone beds, which resulted from rapid physical transgressions, but essentially non-geologic time transgressive, cratonic marine pulsations. Three of these bone beds (14-16), immediately overlying paracontinuities 15-17, respectively, bear pyroclastic mineral euhedral horizons (unnamed one at base of Blocher-lower Dowelltown; Belpre at base of Selmier-upper Dowelltown; and Center Hill at top of upper Dowelltown and/or base of lower Gassaway and its correlatives) which function as a time framework within these Late Devonian black shales. Bone bed 16 at base of Morgan Trail-lower Gassaway represents the position of the Center Hill Metabentonite outside its type locality area of the Eastern Highland Rim of Tennessee. The correlatives of these three pyroclastic horizons are identifiable in southern Indiana, northeastern Kentucky, and Ohio either by their possession of pyroclastic mineral euhedra or by their stratigraphic-paleontologic context. An alternate explanation for the presence of pyroclastic mineral euhedra in bone beds 14 and 15 is that they represent reworking from previously existing pyroclastic horizons; however, the Center Hill Metabentonite (expressed mostly as a weathered biotite tuff in its type area of the Eastern Highland Rim of Tennessee) is represented in the Northern Highland Rim of Tennessee and southern and northwestern Kentucky by the same kinds of pyroclastic mineral euhedra as are present in bone beds 14 and 15, mostly zircon, bipyramidal quartz, apatite, and rarely biotite.

1989 Eastern Oil Shale Symposium November 15-17, 1989 Institute for Mining and Minerals Research, University of Kentucky

Introduction

The present work is a continuation of the author's investigations of weathered wind-fall pyroclastics (metabentonites), their stratigraphic occurrences, and their relationships to essentially chronostratigraphic boundaries formed by paracontinuities and associated bone beds which resulted from rapid, essentially non-geologic time, but physical, transgressions onto the low-lying portions of the craton. The present work is largely prompted by a recent work[1] which did not recognize the stratigraphic uniqueness of five separate paracontinuities and associated bone beds resulting from five rapid, marine pulsations which separate four distinct, interbasinal and correlative internal sedimentary units of the Late Devonian New Albany-Chattanooga-Ohio shales. Three of these pulsations, represented by paracontinuities 14-16, were lumped together as a single diachronous transgression ranging from Early Givetian to late Early Famennian.[1] Further, no reference was made to the three separate and distinct metabentonites which occur with three of the bone beds, which by themselves, testify to the chronostratigraphic natures of these pulsations. Herein, special emphasis is given to the association of the Center Hill Metabentonite with the Bransford Sandstone (at the base of the lower Gassaway and its correlative, bone bed 16, at the base of the Morgan Trail Member of the New Albany) and its implication as to correlation over the studied areas and with the Late Devonian black shales of New York.

Advisability of retention of the term metabentonite for weathered wind-fall pyroclastics is maintained rather than substitution of less applicable terms, K-bentonite[2] and ash bed.[3] Further, it is stressed that at present state of knowledge, the reliable method of ascertaining the identity and correlation of a particular metabentonite is its stratigraphic-paleontologic context.

Present efforts clearly demonstrate that paracontinuities and associated bone beds, framed in a time context of metabentonites, allow essentially chronostratigraphic boundaries to be drawn within the substantive Late Devonian shales (New Albany-Chattanooga-Ohio) and interbasinal correlation of their internal units bounded by these paracontinuities.

The present study covers southern Indiana, Kentucky, Tennessee, and parts of central and southern Ohio as shown in Figure 1. Measured sections showing details of the measured sections are presented in Figures 6-10. Pyroclastic euhedra in the metabentonites are shown in Figure 2.

Weathered Wind-Fall Pyroclastic Terminology

Mesozoic and Cenozoic bentonites differ significantly from Paleozoic metabentonites and this understanding has been implicitely stated by many workers, from the beginning.[4] More recently, clay mineralogists prefer to employ K-bentonites for Paleozoic "bentonites", relying on x-ray diffraction for their identification.[2]

It is significant that metabentonites are associated with (and overlie) wave-marked and/or mud-cracked and bioturbated surfaces which are as a rule merely diastemic, but fortuitously may be paracontinuous or even paraconformable. In fact, many very thin, weathered wind-fall pyroclastic deposits were winnowed on open, shallow sea coasts of much (or most) of their clay-sized fractions and biotite flakes which were moved into deeper, offshore waters where they became disseminated into other sediments; the remaining pyroclastic "lag deposit" then consisted of small, resistant, accessory mineral euhedra such as zircon, bipyramidal quartz, apatite, biotite, and leucoxene and cloudy, weathered fragments of sanidine and sodic plagioclase which testify to the pyroclastic origin of these deposits (Figure 2). Thus, many such weathered and winnowed wind-fall pyroclastics can not be well recognized by clay mineralogy, and it would be inappropriate to call them all K-bentonites. Also, the textural term ash bed[3] is not desirable as a replacement term for metabentonite, or even bentonite or K-bentonite, for although some metabentonites are displayed as weathered tuffs (sand-sized), most are not, but are recognizable either by clay mineralogy and/or by their definitive pyroclastic mineral euhedral suites. Further, some workers[3,5] consider some deposits called bentonites, K-bentonites, and metabentonites to be of various origins, including alteration from non-pyroclastic igneous and/or metamorphic rocks; thus, this is another reason against the term ash as a general replacement term for metabentonite. All Paleozoic metabentonites reported by past or present workers are weathered wind-fall pyroclastics; these past records include the 33 Devonian ones[6] and 43 Ordovician ones[7] in eastern North America.

It has been pointed out[8] that there is no specific term in current use which can be appropriately and universally applied to all kinds of deposits which have been, and are being, called bentonites, K-bentonites, and metabentonites and that the best embracing term for these deposits would be a general term, weathered, wind-fall pyroclastics, prefixed by a descriptive phrase denoting their specific clay mineralogy, general mineralogy, and grain size. If a bentonite or metabentonite be shown to be of non-pyroclastic origin, then it might be described as above, but with deletion of the term pyroclastic. However, this terminology is cumbersome, unnecessary, and complicates the terminology with no advantage gained. Certainly, the prefix meta, as employed in metabentonite, does not imply progressive metamorphism, but merely retrograde metamorphism. For all the above reasons, the term metabentonite should be retained for such Paleozoic deposits.

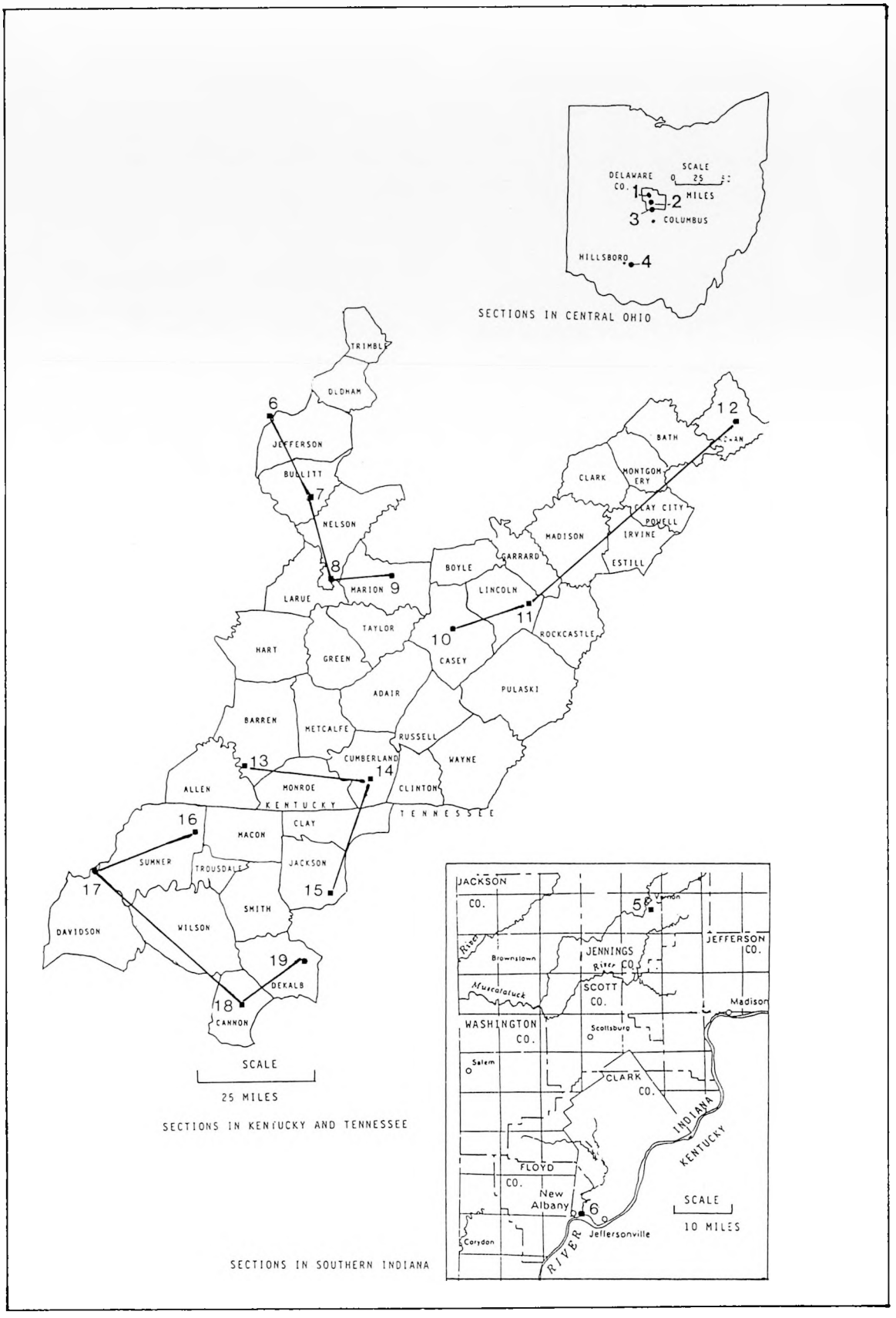

Figure 1. Location on measured sections in studied area.

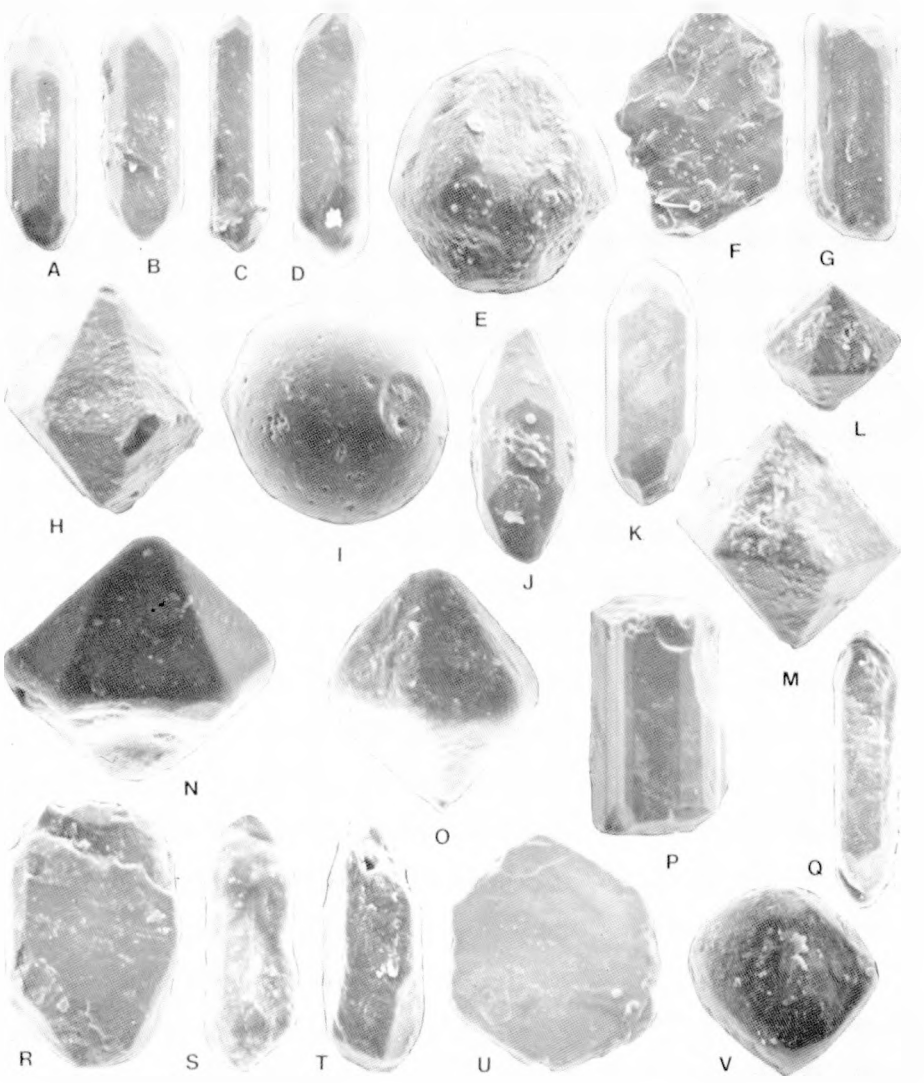

Unnamed Pyroclastic (Bone Bed 14). A-C, zircons: A, Duffin, Hargett, Estill Co., Ky. (X210); B, Blocher, Browns Ford, Allen Co., Ky. (X 252); C, Blocher, Hanover, Jefferson Co., Ind. (X240).

Belpre Metabentonite (Bone Bed 15). D-J, L, M, Selmier: D, Zircon (X288) and E, bipyramidal quartz (X 240), Hanover, Jefferson Co., Ind.; F, biotite (X 129), Montgomery Quarry, Lebanon, Marion Co., Ky.; G, apatite (X 180), Howardstown, Nelson Co., Ky.; H, bipyramidal quartz (X 300), Montgomery Quarry, Lebanon, Marion Co., Ky.; I, rounded sphere of bipyramidal quartz (X 204), Howardstown, Nelson Co., Ky.; J, zircon (X 282), Clay City, Powell Co., Ky.; and L and M, bipyramidal quartz (X 234 and X 372, respectively), Howardstown, Nelson Co., Ky.

Center Hill Metabentonite (Bone Bed 16). K, N-V. K, zircon (X 312), Morgan Trail, Bradfordsville, Marion Co., Ky.; N, bipyramidal quartz (X 336), Morgan Trail, Bradfordsville, Marion Co., Ky.; O, bipyramidal quartz (X 354), lower Gassaway, Chestnut Mound, Smith Co., Tn.; P, apatite, (X 312), lower Gassaway, Center Hill Reservoir, Smith Co., Tn.; Q, zircon (X 300), Morgan Trail, Montgomery Quarry, Lebanon, Marion Co., Ky.; R, zircon (X 390), Morgan Trail, Silver Creek and Ohio River, Floyd Co., Ind.; S and T, zircons (X 390 and X 300, respectively), Bransford Sandstone, Austin Dock, Barren Co., Ky.; U, biotite (X 222), lower Gassaway, Center Hill Reservoir, Smith Co., Tn.; and V, rounded bipyramidal quartz (X 234), Morgan Trail, Bradfordsville, Marion Co., Ky.

Figure 2. Pyroclastic mineral euhedra in bone beds 14-16.

Recognition and Identities of Paleozoic Weathered Wind-Fall Pyroclastics

Metabentonites can be recognized by x-ray diffraction, and, if not by that method, by their possession of definitive pyroclastic mineral euhedra (Figure 2). Unfortunately, to date, neither x-ray diffraction nor pyroclastic mineral euhedra have proven to be definitive for recognition of the identities of specific metabentonites. It is true that certain metabentonites do bear greater or lesser amounts of particular mineral euhedra and/or trace elements, and some do not bear particular mineral euhedra and/or trace elements but there is no known specific euhedral or trace element "fingerprint" for a specific metabentonite.

The closest approach to a specific mineral euhedral "fingerprint" is the abundance of leucoxene euhedra in the Middle Ordovician (late Blackriveran) Pencil Cave Metabentonite of Kentucky and Tennessee, and its correlative, the true Deicke Metabentonite of Missouri; however, leucoxene is present in small amounts in other Blackriveran metabentonites and is abundant in the Middle Ordovician (early Trentonian) "Deicke Metabentonite" of the Upper Mississippi Valley (Minnesota, Wisconsin, and Iowa) and even is present in other Trentonian metabentonites as well. Further, trace element "fingerprinting" has failed in geographic widespread identification and correlation of the Pencil Cave Metabentonite as well, not necessarily because of a flaw in the method itself, but from a lack of attention to the precise stratigraphic positions from which the samples subjected to trace element analysis were taken. The crux of the problem here is that although the Pencil Cave Metabentonite of Kentucky and Tennessee and the Deicke Metabentonite of Missouri are correlatives and do bear leucoxene, the "Deicke Metabentonite" of the Upper Mississippi Valley also bears abundant leucoxer but it is not a correlative of the Pencil Cave and the Deicke for a disconformity cuts out strata which bear the Pencil Cave Metabentonite (Deicke Metabentonite of Missouri). The "Deicke Metabentonite" of the Upper Mississippi Valley (misidentified as the Deicke Metabentonite of Missouri and the Pencil Cave Metabentonite of Kentucky and Tennessee) by trace element workers and by leucoxene "fingerprinting" is actually another and stratigraphically higher metabentonite at the base of the early Trentonian (Carimona Member of the Spechts Ferry Formation and its correlative at the base of the Trentonian Curdsville of Kentucky and the Curdsville Member of the Hermitage Formation of Tennessee).[9] From the above consideration of the problems which can be encountered in attempts at recognizing the identities of particular metabentonites, and their subsequent correlation, it is manifestly obvious that the identity and correlation of a particular metabentonite must be accomplished by reference to its stratigraphic-paleontologic context. The chief tool in ascertaing this context is paracontinuity.

Depositional Site of Occurrences and Its Bearing on Correlation of Metabentonites and Their Enclosing Sequences

Empirically, it is found that Paleozoic metabentonites are preserved along shorelines and overlie diastemic and paracontinuous, or even paraconformable surfaces. Much of the clay minerals are winnowned away into deeper water by wave activity, but many kinds of mineral euhedra included in the ash falls (Figure 2) remain in "lag deposits" along the wave surfaces as evidence of their pyroclastic origin. Clay may also be preserved, if the ash fall were thick and/or fell in less agitated water, or if the shallow sea bottom were topographically irregular and exhibited even moderate relief. If the wave-cut surface directly underlying a metabentonite is paracontinuous, it affords the closest approximation to a chronostratigraphic boundary which can be recognized in the substantive sequence for a paracontinuity is a slight, but significant physical discontinuity and a coincident slight, but significant evolutionary discontinuity which resulted from a rapid, essentially non-geologic time transgressing, marine pulsation widely over the low-lying parts of the craton.

The fact that the magnitudes of time loss along particular paracontinuities are variable as assessed by number of biozones missing does not detract from the value of the paracontinuity in boundary determination and correlation, as within the Late Devonian black shales. The virtue of the paracontinuity is its ability to define in the substantive stratigraphic sequences the positions of the very smallest significant paleontologic-stratigraphic gaps which separate entities of any stratigraphic hierachial magnitude, as with the lower and upper boundaries of the Late Devonian shales and boundaries between internal genetic units of these black shales.

The magnitudes of time losses exhibited by paracontinuities have been estimated by the erection of four orders of paracontinuities;[10] they are: First Order (gap less than a bed, approaching a phylogenetic lineage gap= 66,000 yrs.); Second Order (gaps of a bed or more than a bed, but less than a member= 66,000-130,000 yrs.); Third Order (gaps of members, formations, or groups, less than a stage=130,000-250,000 yrs.); and Fourth Order (gaps of stage or more but less than a series=250,000-16,000,000 yrs.) Thus, time losses along paracontinuities are intermediate between diastems and paraconformities. Neither a diastem nor a paraconformity is of value in chronostratigraphy for the diastem has no discernible significant evolutionary gap while the evolutionary gap on a paraconformity is too great and too variable. It is further seen that a Fourth Order Paracontinuity is of no essential value in chronostratigraphy for it merges into a paraconformity. In fact, it is the Third Order Paracontinuity which is the practical field tool for chronostratigraphy for the absences of members, form-

ations, and groups are generally recognizable in substantive field sections. Even a Second Order Paracontinuity can often be "field recognizable", if the stratigraphic-paleontologic context is precisely known. It is, however, quite difficult to discern the "field position" of a First Order Paracontinuity ("the Holy Grail of stratigraphy") for it defines the ultimate approximation to a formal bed-bed boundary.

It must be stressed that it is the absence of biozones which is the final arbiter of the time-loss magnitude along a surface of paracontinuity, but it is the physcal surface of paracontinuity alone which is field recognizable and marks the precise position in the substantive stratigraphic sequence of the faunal and/or floral gaps assessed by the biozonal and/or phylogenetic lineage gaps themselves. Truly, neither physical stratigraphy alone nor paleontology alone is equal to the tasks of chronostratigraphic boundary determination and correlation. It is not coincidental that significant faunal and/or floral gaps are (when studied in detail) at the positions of disconformities of the nature of paracontinuities. I know of no exception to the coincidence of First, Second, and Third Order paracontinuities with commensurate rank evolutionary gaps which are displayed in the shallow water, marine, cratonic sedimentary sequences.

Paracontinuous Internal Framework within Late Devonian Black Shales

Within the Late Devonian black shales (New Albany-Chattanooga-Ohio), five paracontinuities and five associated bone beds mark the substantive positions of five distinct and separate, stratigraphically superimposed, rapid, and essentially non-geologic time transgressive, marine pulsations separating four distinct internal, sedimentary genetic packages within these Late Devonian black shales; Figure 3 shows numbering of the internal stratigraphic units[10] within the Devonian and Early Mississippian of southern Indiana and northwestern Kentucky and extension of these units into northeastern Kentucky and Ohio. Figure 4 shows the extension of these numbered units from southern Indiana and northwestern Kentucky into the Highland Rim of Tennessee and suggested correlation with the New York section. Figure 5 shows the extension of these internal units of the New Albany Shale into the Late Devonian black shales of Ohio, Michigan, and Ontario. All these five paracontinuities and bone beds are in consistent stratigraphically superimposed relationships to the Protosalvinia zone and conodont zones (Figures 3-5); the correlative positions of the three pyroclastics are recognized either by the presence of definitive pyroclastic mineral euhedra or by the stratigraphic-paleontologic context of the associated paracontinuities and bone beds (Figures 3-5).

It is manifestly obvious that a single and specifically distinct, stratigraphically positioned metabentonite can not occupy more than one stratigraphic position in a single, vertical stratigraphic sequence in a single section, without structural influence. The consistent association of three separate and distinct paracontinuities and associated bone beds with three separate and distinct metabentonites in a consistent superimposed and orderly sequence within the Late Devonian shales (New Albany and Chattanooga) is sufficient proof to establish the essential chronostratigraphic nature of the paracontinuities and associated bone beds within these Late Devonian black shales. The internal units of the Late Devonian black shales can show parvafacies[11] relationships, as illustrated by the Selmier Member of the New Albany Shale. In its type area of central Indiana, it is a gray to olive-gray, clayey shale, but in southern Indiana it is mostly a hard, fissile black shale, with a thin, worm-marked, hard, olive-gray argillaceous zone at its top (as it is in its type area); however, in both parvafacies of the Selmier, its base is delimited by bone bed 15 (overlying directly paracontinuity 16) and delimited at its top by bone bed 16 (directly overlying paracontinuity 17), this regardless of the lithologic variation, thicknesses, or condensation of several biozone. Additionally, it must be noted that, as a general rule, particular superimposed internal units of the Late Devonian black shales (New Albany-Chattanooga-Ohio) display very similar lithologies, verging in many instances, on being essentially identical. Where lithologies of internal units between paracontinuities and associated bone beds and metabentonites vary, this is either due to parvafacies variation or the paracontinuities themselves which cut out particular parts of an internal unit, or even a whole internal unit or more. In many instances, higher on the Cincinnati Arch, paracontinuites, bone beds, and metabentonites are closer together, but do not merge as a single diachronous unit as recently suggested.[1] Certainly, the four separate and distinct bone beds (14-17) and their intimately associated paracontinuities (15-18), three of which bear unique pyroclastic intervals and one (bone bed 17, associated with paracontinuity 18) bears the pelagic Protosalvinia florizone) manifestly do not represent a single condensation lag zone resulting from a single and gradual, physical transgression of the Cincinnati Arch which spanned a geologic time interval from early Givetian through early Famennian as recently suggested.[1]

Certainly, paracontinuities 15 and 16 exhibit some varying amounts of time gaps at different places in reference to conodont zones; even in such instances, the age of any particular sedimentary deposit (including marine physical transgressive ones) is only approximated, and this by the latest biozonal representatives and not by the inferred time spans of the totality of missing biozones. It should be noted also that age determinations should consider evidence from all possible fossil organisms

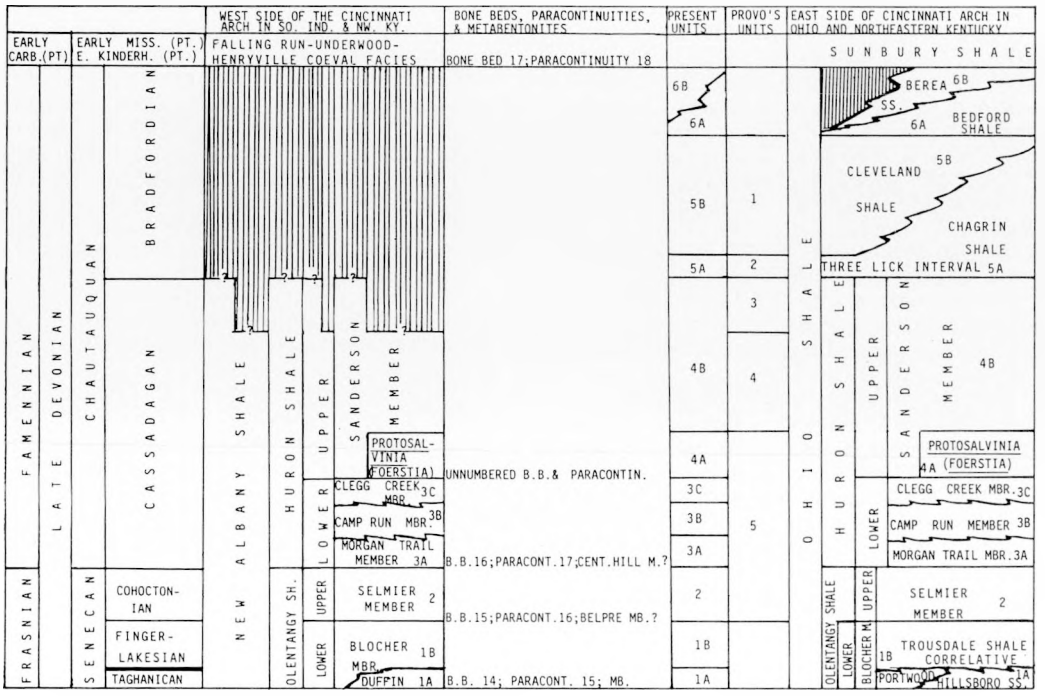

Figure 3. Numbered internal units within Late Devonian black shales of southern Indiana-northwestern Kentucky and Ohio.

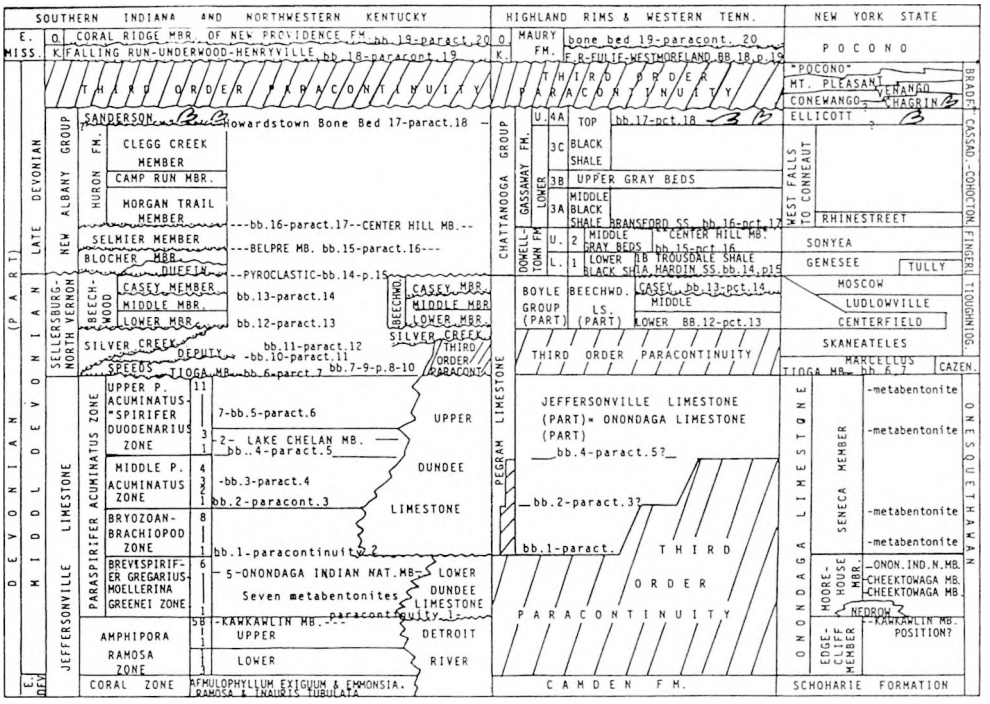

Figure 4. Extension of numbered internal units of the New Albany Shale into Highland Rim of Tennessee and suggested correlation with the New York section.

for evolutionary rates vary within different groups.

Correlation of Late Devonian Black Shales

The New Albany and Chattanooga shales are essentially correlative,[10] neither bearing strata younger than the Sanderson Formation, the base of which is marked by bone bed 17 and associated with Protosalvinia, immediately overlying paracontinuity 18 (Figure 4) while the Ohio Shale bears Bradsfordian beds above the Protosalvinia Zone (Figure 3). Regressive phase ended the Late Devonian of Ohio with deposition of Bedford-Berea. In the areas of New Albany-Chattanooga outcrops, a Third Order Paracontinuity is present so that the basal Early Mississippian (Kinderhookian) marine transgression (represented by paracontinuity 19 and overlying bone bed 18, at the base of the Falling Run-Underwood-Henryville coeval facies of southern Indiana and northwestern Kentucky and the correlative Falling Run-Eulie-Westmoreland of southern Kentucky and Tennessee) mark the Devonian-Mississippian boundary. In Ohio and extreme northeastern Kentucky, the Early Mississippian (Kinderhookian) correlative marine transgression is represented by bone bed 18 and paracontinuity 19, at the base of the Sunbury Shale. These stratigraphic relationships are shown in Figures 3-5.

The disparity between interpretations presented by a recent group of workers[1] and the present author[10,12] regarding the number, nature, and correlation of the internal stratigraphic units within the New Albany, Chattanooga, and Ohio shales and correlation with the New York section may be explicable, in part, by comparison of the degree of stratigraphic detail presented by the two sets of workers.[1,10,12] A result of gross stratigraphy is the failure to recognize the universal presence of the Kinderhookian Falling Run-Underwood-Henryvill coeval facies throughout the surface exposures in southern Indiana and Kentucky, the correlative Falling Run-Eulie-Westmoreland coeval facies of Tennessee and southern Kentucky, and its correlative in Ohio, the Sunbury Shale. The Sunbury is universally accepted as Early Mississippian (Kinderhookian) by all data, including conodont biozone, and, in fact, it is correlated with the Henryville by conodonts. Bone bed 18 at the base of the Sunbury, overlying paracontinuity 19, holds exact stratigraphic relationship not only in Indiana, Kentucky, Tennessee, and Ohio but also in Michigan and southern Ontario (Figure 5).

Further, one metabentonite, the Center Hill, is universally accepted as an in-place, weathered wind-fall, biotite tuffaceous pyroclastic. In the detailing of the internal time framework of the Late Devonian black shales, later in this paper, proof is presented of the interbedding of the Center Hill Metabentonite with bone bed 16 (with the Center Hill present directly below and above paracontinuity 17). This substantiates the author's[12] conclusion that bone bed 16 at the base of the Morgan Trail Member of the New Albany Shale represents the essential position of the Center Hill Metabentonite in Kentucky and southern Indiana. This contradicts the conclusions reached, based on conodont biozonation and radioactive stratigraphy,[1] that the lower Gassaway of Tennessee and southern Kentucky does not correlate with the Morgan Trail of southern Indiana (and indeed, that the Morgan Trail does not occur in Kentucky and Tennessee), that upper Dowelltown (and even lower Dowelltown) of Tennessee and southern Kentucky correlate with the Selmier and even Blocher of southern Indiana and Kentucky, and that lower Gassawy of Tennessee and southern Kentucky correlates with the Clegg Creek (Middle Huron correlative) of southern Indiana and northwestern Kentucky. The net result is miscorrelation not only between black shale internal units of the New Albany and Chattanooga, but olso between the internal black shale unis in Ohio and New York; these miscorrelations are essentially perpetuation of past conclusions based on conodont biozonation and radioactivity.[13,14] It should be clearly understood that biozonation (and even biostratigraphy) has no inherent relationship to chronostratigraphy unless the evolutionary changes can be related to a precise stratigraphic position in the substantive rock sequences. This is not an attempt to deprecate organic evolution as the primary tool for determining the age of strata, but to illustrate that for chronostratigraphic boundary determination and subsequent correlation, physical stratigraphic relationships and biostratigraphy must be employed together. As a tool for chronostratigraphy, the paracontinuity identifies specific field recognizable positions in the substantive stratigraphic sequences of slight, but significant physical gaps and coincident slight, but significant evolutionary gaps.

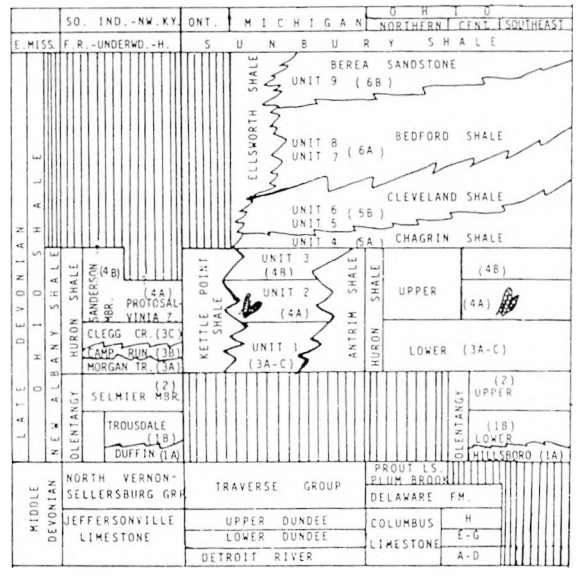

Figure 5. New Albany units extened into Ohio, Michigan, and Ontario.

Details of the Internal Time Framework within Late Devonian Black Shales

Three metabentonites (unnamed one, Belpre, and Center Hill) and five rapid, essentially non-geologic time transgressive, physical marine pulsations, marked by paracontinuities 15-19 and by the overlying bone beds 14-18 (with the Protosalvinia zone's base marked by bone bed 17) are the best field recognizable substantive markers in the Late Devonian New Albany and Chattanooga shales; of these, the metabentonites afford the time framework and they are discussed in some detail herein, with the stratigraphic positions of the metabentonites, bone beds, and paracontinuities shown in Figures 6-10.

The Unnamed Metabentonite at the Base of the New Albany-Chattanooga

Figure 2 presents some of the pyroclastic mineral euhedra which occur in the unnamed metabentonite at the base of the Blocher-lower Dowelltown-lower Olentangy, the basal and stratigraphically oldest internal unit of these Late Devonian black shales in the studied areas. This unnamed metabentonite is intimately associated with bone bed 14 and paracontinuity 15 low on the flanks of the Cincinnati Arch. It must be understood that although the Blocher (and its correlatives, lower Dowelltown of Tennessee and lower Olentangy of Ohio) constitute the stratigraphic basal unit of these Late Devonian black shales, the Blocher (and its correlatives) is not always the local basal unit at any particular locality. In fact, as the crest of the Arch is approached, the lower internal units of these black shales progressively disappear, except where low topography existed on the Arch. The disconformity associated with the Blocher (and its correlatives) changes its time loss magnitude from a paracontinuity low on the Arch until it becomes a paraconformity high on the Arch. This physical transgression is, however, not diachronous which would be the result of a gradual onlap and/or overstep of a single stratigraphic entity significantly transgressing geologic time, but resulted from a rapid onlap and/or overstep of a single stratigraphic entity which did not itself significantly transgress geologic time; this, in spite of the fact that its base is in paraconformable relationship with the underlying strata as the crest of the Arch is approached. This relationship is displayed in Figures 6-10.

The Blocher-lower Dowelltown-lower Olentangy are in the position of the Taghanican Tully Limestone of New York, but the Taghanican is to be considered early Frasnian (late Devonian) rather than late Givetian (Middle Devonian) on the bases of the essentially world-wide chronostratigraphic transgression at the base of the Taghanican; this basal Tully transgression is correlated with paracontinuity 14 of the studied areas (Figure 4). The Duffin Dolomite constitutes a basal facies of the Blocher (Figures 3 and 4).

Belpre Metabentonite

Figure 2 presents some of the pyroclastic mineral euhedra which occur in the Belpre Metabentonite correlative as it is represented in the studued areas. This metabentonite[15] was originally defined in the subsurface of eastern Ohio from an unspecified stratigraphic position within the lower part of the Ohio Shale, varying at different localities from 35 to 257 feet above the top of the Middle Devonian (late Onesquethawan) Columbus Limestone. The stratigraphic position of the Belpre Metabentonite was suggested[16] to be at the position of bone bed 15 (overlying paracontinuity 16), situated at the bases of the Selmier Menber of the New Albany and its correlative, upper Dowelltown of the Chattanooga, for bone bed 15 bears pyroclastic mineral euhedra and it does not merge with bone bed 14 (at the base of the Blocher-lower Dowelltown-lower Olentangy) nor with bone bed 16 (at the base of the lower Morgan Trail-lower Gassaway), as recently suggested.[1] Further, the Selmier does not correlate with the lower part of the Camp Run Member (Huron) of the New Albany Shale of western Kentucky subsurface nor does it straddle the Sonyea and West Falls groups of New York, but its stratigraphic position in the New York section should be basal Sonyea (Figure 4). Thus, the physical transgression (paracontinuity 16, overlain by bone bed 15 and associated with pyroclastic mineral euhedra) is not diachronous, but resulted from a rapid marine onlap and/or overstep of a single stratigraphic entity which did not significantly transgress geologic time.

Center Metabentonite

It has been postulated[10,12] that the Bransford Sandstone (bone bed 16, overlying paracontinuity 17), situated at the base of the lower Gassaway of the Chattanooga Shale of the Northern Highland Rim of Tennessee where the Center Hill Metabentonite is absent as a discrete horizon, represents the stratigraphic position of the Center Hill Metabentonite. In the Eastern Highland Rim of Tennessee, the Center Hill is situated in the upper few tenths of a foot to one foot of the upper Dowellton. The rationale[10,12] for considering the Bransford Sandstone to represent the Center Hill Metabentonite was that paracontinuity 17 (in the Northern Highland Rim of Tennessee) fortuitously cut down into the upper Dowellton eroding the Center Hill Metabentonite as a discrete entity and reworking its resistant pyroclastic mineral euhedra into the immediately overlying bone bed 16.

It was further suggested[10,12] that a like stratigraphic relationship exists on all sides of the Cincinnati Arch between the Selmier Member of the New Albany-upper member of the Dowelltown of the Chattanooga-upper member of the Olentangy of the Ohio and the Morgan Trail-lower Gassaway-lower Huron such that bone bed 16 represents Center Hill outside its type area.

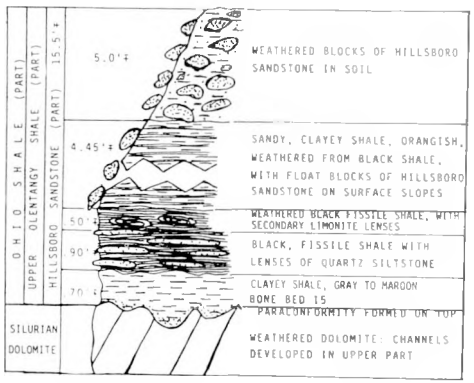

Locality 4. Rhoads Corner, Highland co.

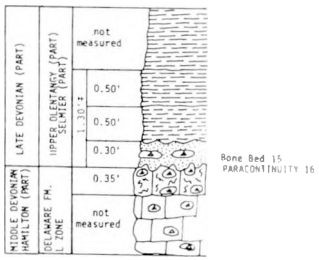

Locality 3. Along Bartholomew Run, Tributary to Olentangy River, Southern Delaware Co.

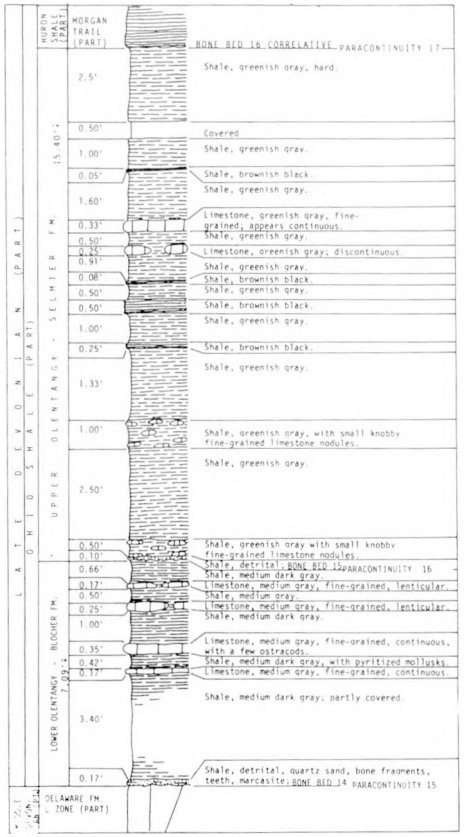

Locality 2. Camp Lazarus Boy Scout Reservation, Delaware Co.

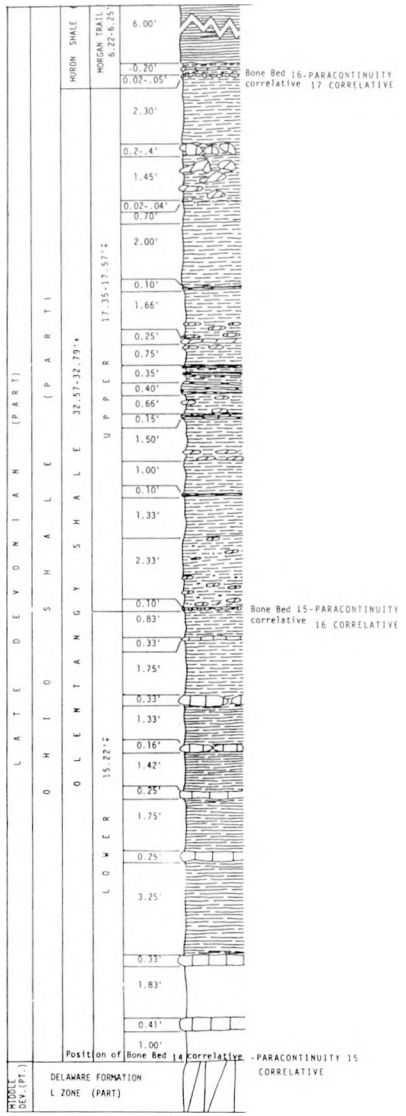

Locality 1. Olentangy Stratotype, Delaware, Delaware Co.

Figure 6. Late Devonian Measured Sections in Central and Southern Ohio.

Sections in Southern Indiana

Sections in Kentucky

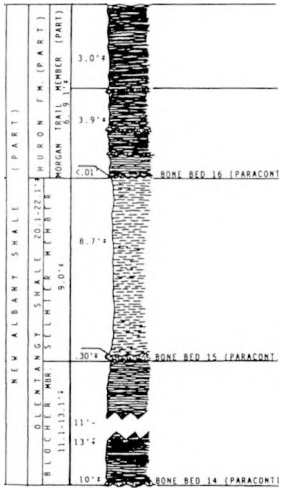

Locality 5. Crosley Lake, Jennings Co., Indiana

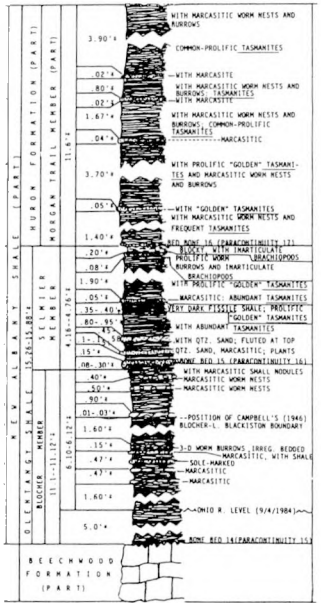

Locality 6. West of Silver Creek, on Ohio River, Floyds Co.

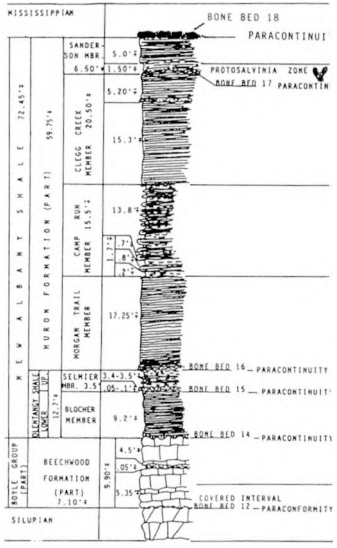

Locality 7. I-65 and Bernheim Forest, Bullitt Co.

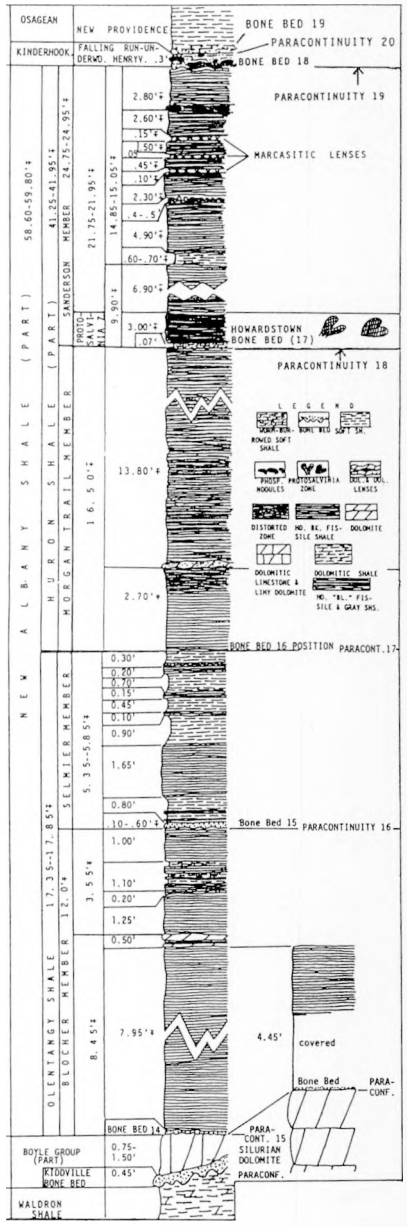

Locality 8. On 84 and Rolling Fork, 3 Miles SE. of Howardstown, Nelson Co.

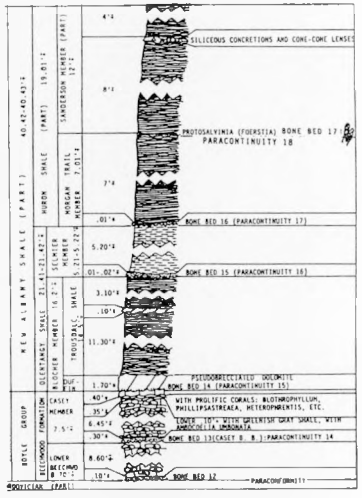

Locality 9. Montgomery Quarry, Lebanon, Marion Co.

Figure 7. Late Devonian and Early Mississippian Measured Sections in Southern Indiana and Northwestern Kentucky.

Sections in Kentucky

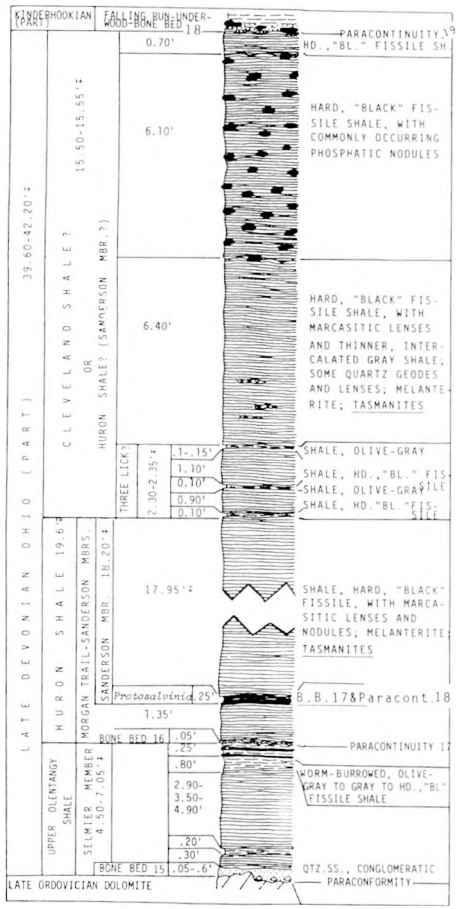

Locality 10. West Side of U. S. 127, 1 Mile North of Liberty, Casey Co.

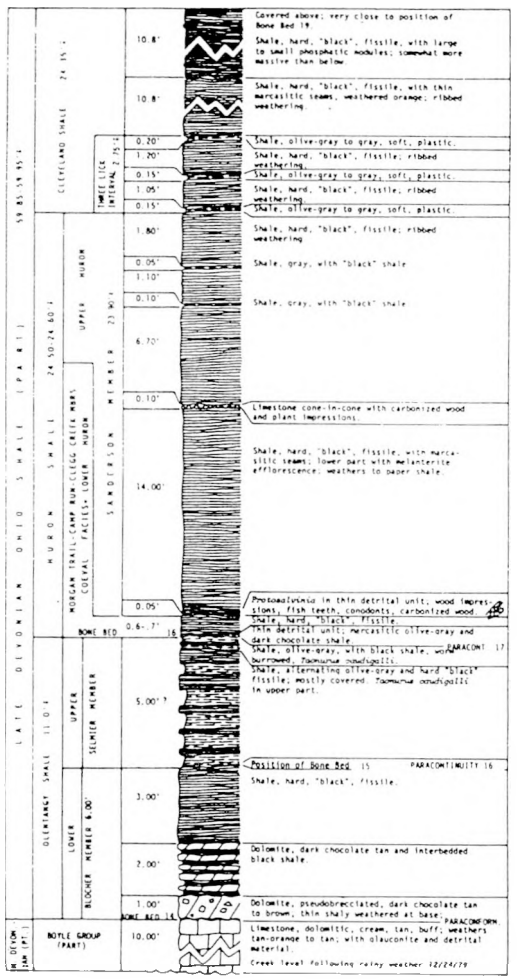

Locality 11. Cedar Creek, Halls Gap Rd., SW. of Crab Orchard, Lincoln Co.

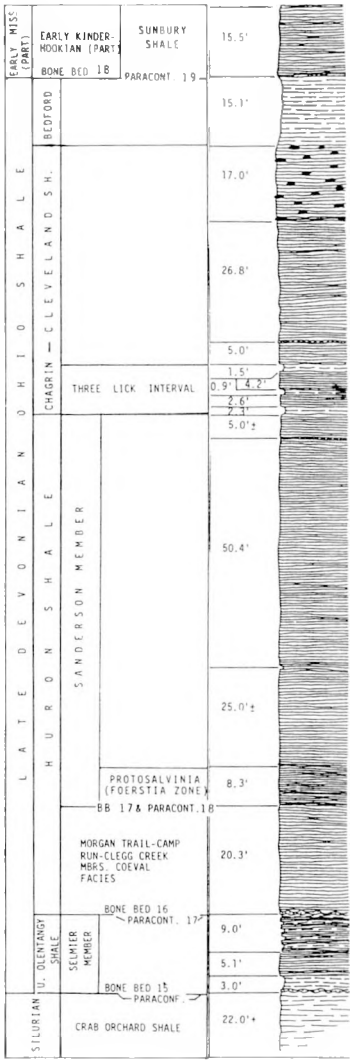

Locality 12. Three Lick Stratotype, on I-64, 1.8 Miles So. of Three LIck Branch, Rowan Co.

Figure 8. Late Devonian and Early Mississippian Measured Sections in Central and Eastern Kentucky.

Sections in Kentucky and Tennessee

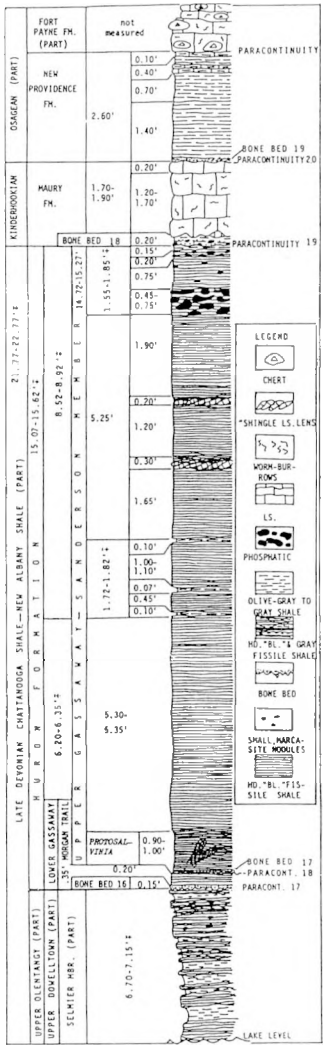

Locality 13. Austin Boat Dock, Barren River Reservoir, Barren Co.

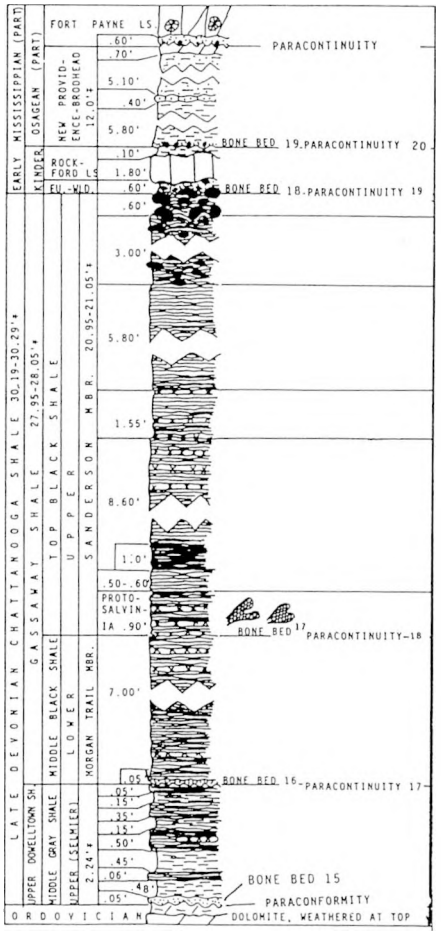

Locality 14. Highway 90, East of Burkesville, Cumberland Co.

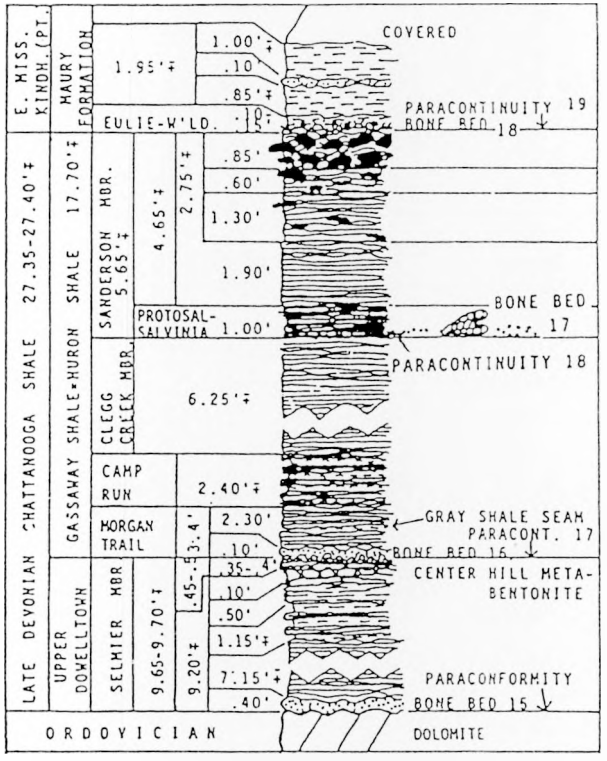

Locality 15. Road to Flynn Creek Structure, 1.2 Miles from Tn. 56, S., SE. of Gainesboro, Jackson Co.

Figure 9. Late Devonian and Early Mississippian Measured Sections in the Cumberland Saddle of Southern Kentucky and Northern Tennessee.

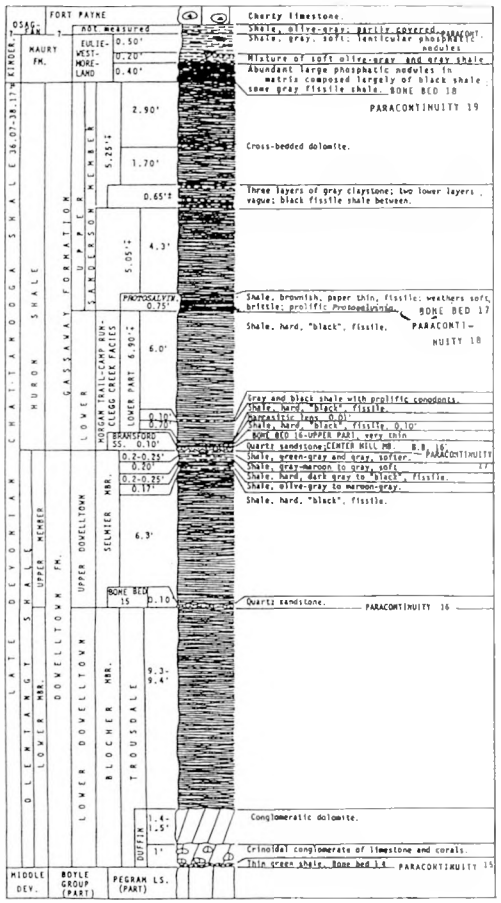

Locality 16. Roadcut on U. S. 31E and Tn 231, One Mile South of Westmoreland, Sumner Co.

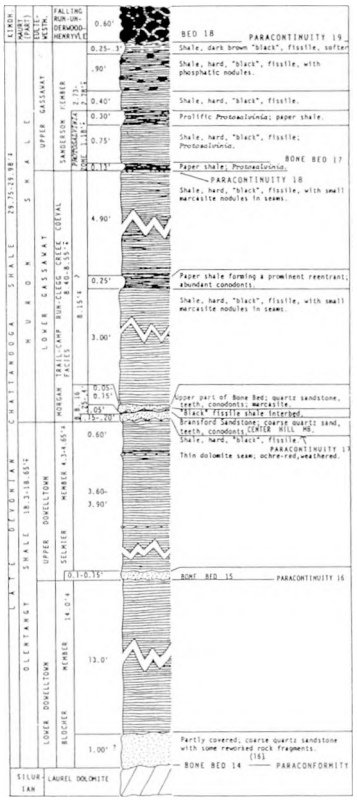

Locality 17. Louisville and Nashville Railroad Cut, at Bakers Station, Davidson Co.

Sections in Northern and Eastern Highland Rims of Tennessee

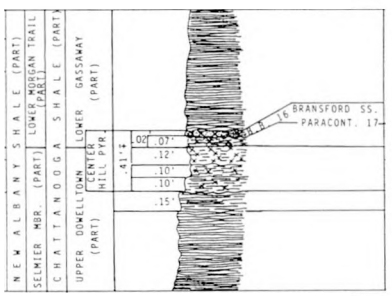

Locality 18. Woodbury, Cannon Co.

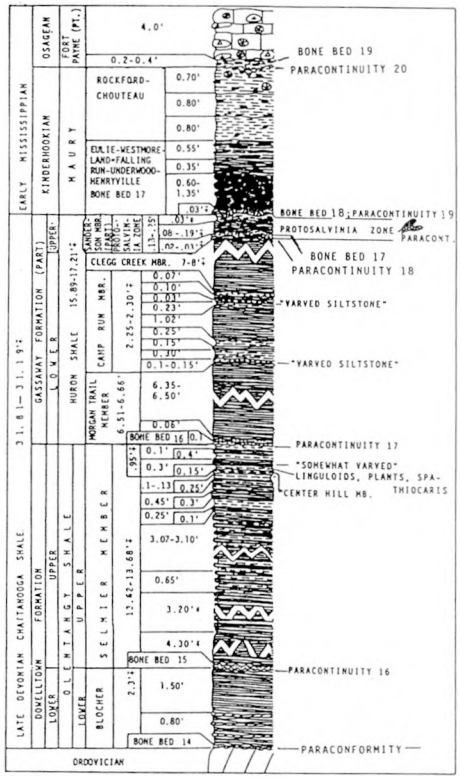

Locality 19. Hurricane Bridge, Dekalk Co.

Figure 10. Late Devonian and Early Mississippian Measured Sections in Tennessee N. and E. Highland Rims.

Figure 11 displays the stratigraphic relationships of the Center Hill Metabentonite and bone bed 16 in the Eastern and Northern Highland rims of Tennessee and the Cumberland Saddle of northern Tennessee and southern Kentucky.

Confirmation of Bone Bed 16 as Position of the Center Hill Metabentonite

Just recently, an outcrop was studied (Figure 1, locality 18) at Woodbury, Cannon County, Tennessee where the Center Hill Metabentonite is present in the upper Dowelltown (just below paracontinuity 17) and also in bone bed 16 (at the base of the lower Gassaway, just above paracontinuity 17) so that the Center Hill Metabentonite and bone bed 16 are both coincident (Figure 11). This not only confirms the postulated[10,12] position of the Center Hill Metabentonite in the Northern Highland Rim, but also that the Morgan Trail Member of the New Albany and the lower Gassaway Member of the Chattanooga are correlatives for each has bone bed 16 at its base and both bear pyroclastic mineral euhedra (Figure 2). Thus, the lower Gassaway and Morgan Trail rapid, physical pulsation is not diachronous, but is separate and distinct from the ones at the base of the Blocher-lower Dowelltown-lower Olentangy and the base of the Selmier-upper Dowelltown-upper Olentangy. The Center Hill Metabentonite in southern Indiana and Ohio is identified either on the presence of pyroclastic mineral euhedra and/or its stratigraphic-paleontologic context.

Alternative Explanation for Presence of Pyroclastic Mineral Euhedral Horizons in Late Devonian Black Shales

An alternative explanation for presence of pyroclastic mineral euhral horizons in Late Devonian black shales, particularly those associated with bone beds 14 and 15, is that they represent reworking from previously existing pyroclastic horizons or from other kinds of igneous and/or metamorphic rocks, and, as such, they do not represent primary wind-fall, pyroclastic horizons. Evidence contrary to this conclusion is that these hypothetical preexisting horizons have not been identified in the stratigraphic record and that the three pyroclastic mineral euhedral horizons recognized in the Late Devonian hold specific and consistent stratigraphic-paleontologic context within these Late Devonian black shales. Further, the "stratigraphically in place" Center Hill Metabentonite of the Eastern Highland Rim of Tennessee (expressed there mostly as a weathered biotite tuff) is represented in the Northern Highland Rim of Tennessee and Kentucky, and even in the Woodbury, Cannon County area (Figure 11), in the Eastern Highland Rim

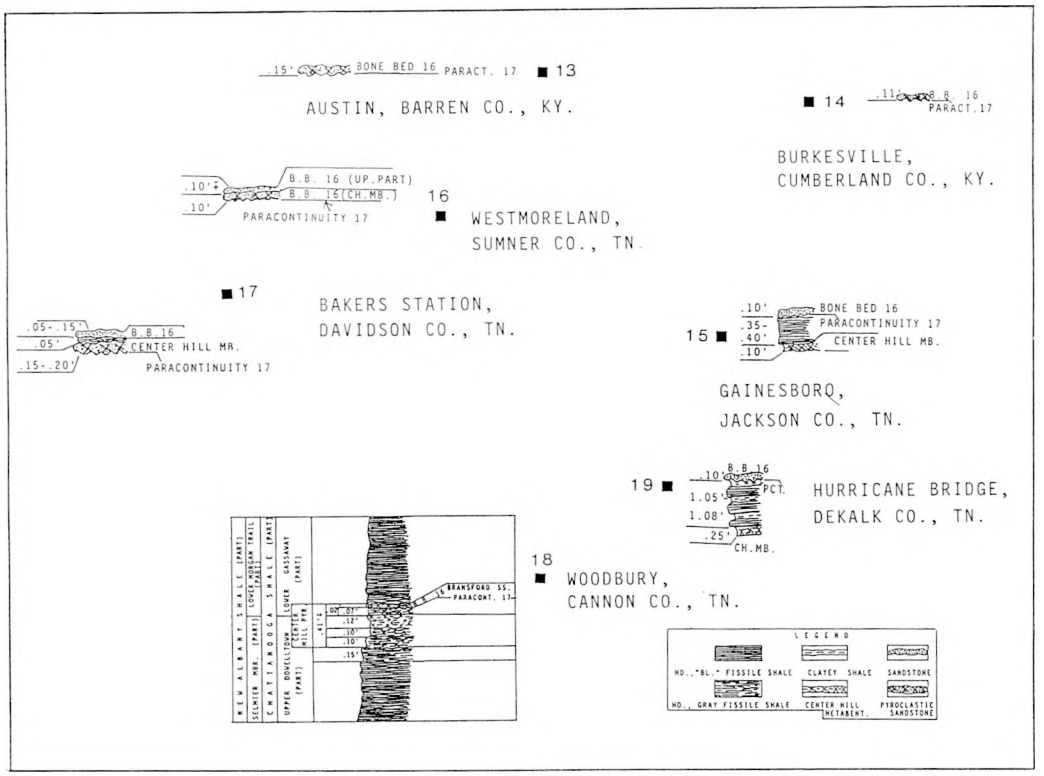

Figure 11. Stratigraphic relationships of Center Hill Metabentonite in Highland Rim of Tennessee and the Cumberland Saddle of northern Tennessee and southern Kentucky.

itself, primarily, by resistant, definitive pyroclastic mineral euhedra (which are also present in the type Center Hill Metabentonite, in subordinate amounts) as in bone beds 14 and 15.

Acknowledgments

Conclusions reported herein concerning the stratigraphic relationships of paracontinuities, bone beds, and metabentonic horizons in the Late Devonian black shales are results of studies pursued under a grant-in-aid from the Petroleun Research Fund (PRF # 13893-82) of the American Chemical Society and from smaller grants from the Arts and Sciences College and the Graduate School of the University of Louisville.

References

1. F. R. Ettensohn, P. T. Goodman, R. D. Norby, and T. H. Shaw, "Stratigraphy and Biostratigraphy of Devonian-Mississippian Black Shales in West-Central Kentucky and Adjacent Parts of Indiana and Tennessee," 1988 Eastern Oil Shale Symposium, Commonwealth of Kentucky, Kentucky Energy Cabinet, Lexington, Ky., 1989.

2. C. E. Weaver, "Mineralogy and Petrology of Some Ordovician K-bentonites and Related Limestones,"Geological Society of America Bulletin, v. 64, pp. 921-944, 1953.

3. J. B. Roen and J. W. Hosterman, "Misuse of the Term 'Bentonite' for Ash Beds of Devonian Age in the Appalachian Basin, " Geological Society of America Bulletin, v. 93, pp. 921-925, 1982.

4. C. S. Ross, "Altered Paleozoic Volcanic Materials and Their Recognition," American Association of Petroleum Geologists Bulletin, v. 12, pp.143-164, 1928.

5. R. E. Grim and N. Güven, "Bentonites, Geology, Mineralogy, Properties and Uses," Elsevier, New York, 256pp., 1978.

6. J. E. Conkin and B. M. Conkin, "Devonian Pyroclastics in Eastern North America, Their Stratigraphic Relationships and Correlations," In J. E. Conkin and B. M. Conkin, eds., Devonian-Mississippian Boundary in Southern Indiana and Northwestern Kentucky, Guidebook of Field Trip No. 7, Ninth International Congress of Carboniferous Stratigraphy and Geology, pp. 74-141, 1979.

7. J. E. Conkin and B. M. Conkin, "Paleozoic Metabentonites of North America: Part 2- Metabentonites in the Middle Ordovician Tyrone Formation at Boonesborough, Clark County, Kentucky," University of Louisville Studies in Paleontology and Stratigraphy No. 17, 47 pp., 1983.

8. J. E. Conkin and B. M. Conkin, "Paleozoic Metabentonites of North America: Part 1-Devonian Metabentonites in the Eastern United States and Southern Ontario: Their Identities, Stratigraphic Positions, and Correlation," University of Louisville Studies in Paleontology and Stratigraphy No. 16, 135 pp., 1984.

9. J. E. Conkin, "Pyroclastics, Paracontinuities, Stratigraphic Boundaries, and Correlation Within Middle Ordovician of Eastern United States and Southern Ontario," Fifth International Symposium on the Ordovician System, Memorial University of Newfoundland, St. John's, Newfoundland, p. 24, 1988.

10. J. E. Conkin, "Late Devonian New Albany -Ohio-Chattanooga Shales and Their Interbasinal Correlation in Indiana, Ohio, Kentucky, and Tennessee," 1985 Eastern Oil Shale Symposium, Commonwealth of Kentucky, Kentucky Energy Cabinet, Lexington, Ky., pp. 217-259, 1986.

11. K. E. Caster, "The Stratigraphy and Paleontology of Northwest Pennsylvania," Bulletin of American Paleontology, v. 21, 185 pp., 1934.

12. J. E. Conkin, "The Center Hill Metabentonite in the Chattanooga-New Albany Shales of Tennessee, Kentucky, and Indiana," 1985 Eastern Oil Shale Symposium, Commonwealth of Kentucky, Kentucky Energy Cabinet, Lexington, Ky., pp. 247-257, 1989.

13. J. B. Roen, "Regional Stratigraphy of the Upper Devonian Black Shales in the Appalachian Basin," In T. E. Roberts, ed., Field Trip Guide for Geological Society of America Ann. Meeting, Cincinnati, Oh., pp. 324-330, 1981.

14. F. R. Ettensohn and L. S. Barron, "Depositional Model for the Devonian-Mississippian Black Shales of North America: a Paleoclimatic-Paleogeographic Approach," in T. E. Roberts, ed., Field Trip Guide for Geological Society of America, Ann. Meeting, Cincinnati, Oh., pp. 344-361, 1981.

15. H. R. Collins, "Devonian Bentonite in Eastern Ohio," American Association of Petroleum Geologists Bulletin, v. 63, pp. 655-660, 1979.

16. J. E. Conkin, B. M. Conkin, and L. Z. Lipchinsky, "Devonian Black Shale in Eastern United States: Part 1- Southern Indiana, Kentucky, Northern and Eastern Highland Rims of Tennessee, and Central Ohio," University of Louisville Studies in Paleontology and Startigraphy No. 12, 63 pp., 1980.

Development of a Coking Indicator for Oil Shales

by

F.P. Miknis
Western Research Institute
University of Wyoming Research Corporation
Laramie, Wyoming 82071

ABSTRACT

The conversion behavior of ten oil shales from seven foreign and three domestic deposits has been studied by combining solid- and liquid-state ^{13}C NMR measurements with material balance Fischer assay conversion data. The extent of aromatization of aliphatic carbons during Fischer assay was measured to determine whether this measurement could be used to define a coking indicator for oil shales. Preliminary results indicate that the greater the carbon aromaticity of the kerogen, the greater the conversion of aliphatic to aromatic carbon. It is suggested that the net increase in aromatic carbon during Fischer assay can be used to develop a quantifiable coking indicator for oil shales. Currently, the tendency to coke during Fischer assay is judged as slight, moderate, or heavy based on visual inspection of the spent shale. The combination of material balance Fischer assay data and NMR measurement represents a second-generation method for evaluating oil shale conversion and coking behavior.

Comparison of Hydroretorting, Fischer Assay and Rock-Eval Analyses of Some World Oil Shales

by

John R. Dyni and Donald E. Anders
U.S. Geological Survey
Denver Federal Center, Colorado 80225
Raymond C. Rex, Jr.
Environmental Technology Transfer, Ltd.
Chicago, Illinois 60616

Abstract. Samples of oil shale of varied origins and ages were collected from 32 deposits in 17 countries. The samples were analyzed by a hydroretorting assay (HRA) method and the results were compared to conventional Fischer assay (FA) and Rock-Eval analyses. Oil-shale types were determined by microscopy in ultra-violet fluorescence mode.

The hydroretorting index, HRI, is defined as (O_{HRA}/O_{FA}) X 100, where O_{HRA} is the quantity of oil determined by HRA and O_{FA} is the quantity of oil determined by FA. For 66 samples that produced 40 or more liters of oil per metric ton of rock by HRA, the HRI ranges from 86 to 460.

The largest improvement in oil yields by HRA was found for thermally immature oil shales of marine origin with organic matter having relatively low hydrogen to carbon ratios. The HRI for 39 such samples (classified as marinites) range from 129 to 460 and average 228. Some of the best examples of this group include Devonian-Mississippian shales of eastern U.S. and Canada, shales of Pennsylvanian age of Indiana, Upper Cretaceous shales of Morocco and Jordan, and the Cambrian Alum Shale of Sweden. The Alum Shale is particularly noteworthy; the HRI for two samples is 302 and 460. On the other hand, the HRI for samples of lacustrine oil shales having relatively high hydrogen to carbon ratios (lamosites) show less improvement; 15 such samples have HRI numbers of 88 to 192 that average 139.

The sum of the S1 and S2 values from the Rock-Eval analyses correlates quite well with oil determinations by FA ($r^2 = 0.88$), but less so with the oil determinations by HRA ($r^2 = 0.67$). The data suggest that the major source of oil from FA analysis appears to be from the fraction of organic matter containing dominant aliphatic carbon, whereas the additional oil generated by HRA analysis may be from that part of the organic matter with dominant aromatic carbon.

Introduction

The HYTORT* process, a method of retorting oil shale in a hydrogen atmosphere at elevated pressure and temperature (hydroretorting), was originally developed by the Institute of Gas Technology (IGT), Chicago, Illinois, as a technique to produce synthetic gas from oil shale of the Green River Formation. Subsequent research demonstrated that oil yields from hydroretorting eastern U.S. Devonian oil shale could be increased by more than 200 percent of Fischer assay yields[1]. Further study, however, demonstrated that oil shales from different deposits did not show the same improved yields, but varied considerably from one deposit to another.

To gain a better understanding of how different oil shales respond to hydroretorting, the U.S. Geological Survey and HYCRUDE* Corporation, a subsidiary of the Institute of Gas Technology, initiated a study to test the behavior of a variety of oil shales collected from deposits that differ in origin and age. Hydroretorting analyses, Fischer assays, and Rock-Eval analyses were made on the samples and the the organic matter was studied by UV microscopy. The results of these analyses are presented in this report.

Oil Shale Samples

More than 100 samples were collected from 32 deposits of oil shale from 17 countries (Table 1). About one-third of the samples are from U.S. deposits, mainly the oil shales of the Green River Formation in western U.S. and the Devonian-Mississippian oil shales of eastern U.S. Because a number of samples were collected for studies other than for this investigation, geologic information about them is incomplete. Therefore, it cannot be assumed that they are truly representative of the deposit from which they were obtained.

The samples were obtained from outcrops, open-pit and underground mines, and drill holes. Most samples appeared to be relatvely fresh, unweathered, material. However, the outcrop samples may have undergone some degradation of organic matter by weathering which may be reflected in the analytical data. When received, the samples were stored in glass bottles sealed with caps lined with aluminum foil to avoid contamination by carton cellulose and bottle-lid waxes. Because no special precautions were made to store the samples in an oxygen-free atmosphere, some low-grade oxidation of organic matter may have occurred prior to analysis.

The sampled deposits of oil shale range from Late Cambrian to Miocene in age. The oil shales were deposited in marine, lacustrine, and terrestrial environments. Some samples, such as those of the Alum Shale from Sweden and Norway, the Heath and Phosphoria Formations from western U.S., and a few samples from the *Posidonia* Shale from West Germany, have been moderately to strongly altered by geothermal heating, but the remaining samples were relatively unaffected by geothermal alteration. The samples of Alum Shale from Norway were too highly altered to yield oil, however, the analytical results for these samples are included in this report for comparative purposes.

*Any use of trade names is for descriptive purposes only and does not imply endorsement by the U.S. Geological Survey.

Methods of Analysis

Shale-oil Analyses

Hydroretorting analyses were made by IGT with a bench-scale hydroretorting assay unit designed and constructed by IGT[2] (Figures 1 and 2). The sample size for the hydroretorting and Fischer assay analyses was 100 gms. The conditions for the hydroretorting tests were standardized at a hydrogen pressure of 1,000 psig (6893 kPa), a maximum retorting temperature of 1,000°F (538°C), and a heating rate of 12-14°F (~7-8°C) per minute with a holding time of 30 minutes at maximum temperature. For samples that produced sufficient quantities of shale oil in the Fischer assay analysis, the specific gravity of the oil, corrected to 60/60°F, is reported.

The data are reported on an "as received" basis. The pyrolytic products reported are oil and water (liters/tonne) and 'gas plus loss' (weight percent). 'Gas plus loss' represents gases (and analytical errors) which are not condensible at ambient temperature and pressure and which may be composed of a variety of light gaseous hydrocarbons, hydrogen, and carbon dioxide. The gases were not analyzed.

Most of the Fischer assays were also made by IGT using the modified Fischer assay method developed

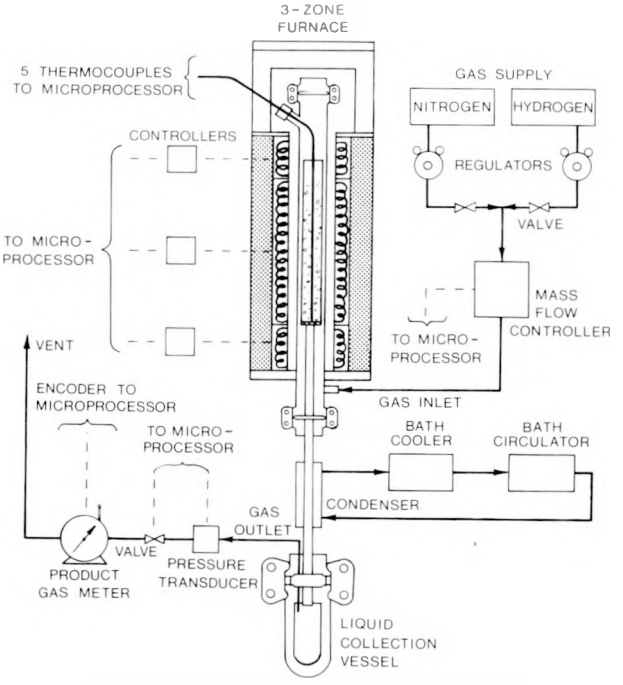

Figure 1. Schematic diagram of the IGT hydroretorting assay unit.

Table 1. Location, Geologic Unit, Age, Class, and Type of Oil-Shale Samples

USGS No.	Country/Locality/Field ID	Geologic Unit	Age[1]	Oil-Shale Class[2]	Type of Sample[3]
	Australia				
	Tasmania				
17	Burnie	Quamby Gp	P	Tasmanite	D
27	China Flat	do	P	do	D
	Queensland				
19	Julia Creek	Toolebuc Fm	K	Marinite	RC
20	Tambo				
	Tambo DH 38	Toolebuc Fm	K	Marinite	DC
	Mount Coolon				
35	QCS1484/36.3-40.64	Suttor Fm	T	Cannel coal	RC
36	QCS1884/42.0-43.0	do	T	do	RC
37	QCS2684/32.7-40.0	do	T	do	RC
	Brazil				
28A	S. Mateus de Sol				
	Ore 133	Irati Fm	P	Marinite	OP
28B	do (benficiated)	do	P	do	OP
	Canada				
11	Manitoba, Waskada				
	Sample 1	Favel Fm	K	Marinite	DC
	Ontario, Clarksburg				
60	CH OGS-83-7, #1	Collingwood Sh	O	Marinite	DC
61	CH OGS-83-7, #2	do	O	do	DC
62	CH OGS-83-7, #3	do	O	do	DC
	Ontario, Sarnia				
63	CH OGS-82-1, LH-1	Kettle Point Fm	D	Marinite	DC
64	CH OGS-82-1, LH-2B	do	D	do	DC
65	CH OGS-82-1, LH-3	do	D	do	DC
66	CH OGS-82-1, LH-4	do	D	do	DC
67	CH OGS-82-1, LH-5	do	D	do	DC
68	CH OGS-82-1, LH-6	do	D	do	DC
12	Saskatch., Man River	Favel Fm	K	do	OC
	China				
26	Fushun, West Pit	?	T	Lamosite-R	OP
34	Maoming, Gintang Mine	?	T	do	OP
47	Huangxian, Beizou Mine	?	T	do	OP
	Czechoslovakia				
24	Kostalov	Kostalov Bed	P	Lamosite?	OC?
25	Kozusice	Menilitic Fm	Oli	Marinite	OC?
	Egypt				
29	Hamrawein, Mine B	Dakhla Fm	K	Marinite?	M
30	do, Main Gallery B	do	K	do	M
31	Quseir, Mine 7				
	Above 2nd phos. bed	Dakhla? Fm	K	Marinite?	M
32	Near Quseir				
	Above 1st phos. bed	Dakhla? Fm	K	Marinite?	OC?
	France				
33	Orbagnoux	Kimmeridgian beds	J	Marinite?	OC?
	Germany, Fed. Rep.				
75	Hessia, Messel	?	Eoc	Lamosite-R	OP?
69	Lower Saxony, Schandelah				
	Borehole 90, 127.8 m	*Posidonia* Sh	J	Marinite	DC
70	Lower Saxony, Schandelah	do	J	do	DC
71	do , Braunschweig	do	J	do	OP
74	do , Marienburg	do	J	do	OC
72	Wurtemberg, Holzmaden	do	J	do	?
73	do , Dotternhausen	do	J	do	OP?

Table 1. Cont. Location, Geologic Unit, Age, Class, and Type of Oil-Shale Samples

USGS No.	Country/Locality/Field ID	Geologic Unit	Age[1]	Oil-Shale Class[2]	Type of Sample[3]
	Great Britain				
7	Scotland, Philps-				
	toun No. 1 mine	Dunnet seam	M	Lamosite-R	M
16	England, Kimmeridge Bay				
	Clavills Hard	Kimmeridge Sh	J	Marinite	OC
	Israel				
22	Yamin				
	CH OS-24, 159-160 m	Ghareb? Fm	K	Marinite	DC
23	Rotem				
	CH BIT-54, 167-168 m	Ghareb Fm	K	Marinite	DC
	Italy				
3	Sicily, Cozzodisi	Tripoli Fm	Mio	Marinite	OP
3A	do	do	Mio	do	OP
	Jordan				
	El Lajjun				
5A	WA-1 (USGS D136322)	?	K	Marinite	OC
5B	WA-2 (USGS D136323)	?	K	do	OC
5C	WA-3 (USGS D136324)	?	K	do	OC
5D	WL-1 (USGS D136325)	?	K	do	OC
5E	IGT48845A	?	K	do	OC
5F	IGT48845B	?	K	do	OC
	Morocco				
13	Timahdit	?	K	Marinite	?
	Norway				
2A	6205	Alum Sh	C	Marinite	?
2B	6274	do	C	do	?
2C	U1143	do	C	do	?
2D	U783	do	C	do	?
2E	7538	do	C	do	?
	South Africa				
4A	Belmont, Corehole DPI,				
	76.68-82.95 m	Whitehill Fm	P	Marinite	DC
4B	Kimberly, Corehole VPI,				
	48.6, 55.6, & 65.6 m	Whitehill Fm	P	Marinite	DC
4C	Transvaal	?	?	Torbanite	?
4D	COMP-1 HI	Whitehill Fm	P	Marinite	?
4E	COMP-2 LO	do	P	do	?
4F	DF-113A/5/2	?	?	?	
4G	DF-130/4L/6	?	?	?	
4H	FN/37/4/C	?	?	?	
	Sweden				
1A	Narke, Hynneberg Pit	Alum Sh	C	Marinite	OP
1B	Billingen, Ranstad Pit	do	C	do	OP
	Thailand				
10A	Mae Sot	Mae Sot Fm	T	Lamosite-G	OC
10B	do	do	T	do	OC
	Turkey				
8A	Beypazari	Hirka Fm	Mio	Lamosite-R?	?
8B	Ulukisla	Ulukisla Fm	Mio	Lamosite-R	?
8C	Goynuk	Sanuyaziyen Gp	Oli	Lamosite-G	?
8D	Seyitomer				
	Shale above lignite	?	Mio	Lamosite-R	?

Table 1. Cont. Location, Geologic Unit, Age, Class, and Type of Oil-Shale Samples

USGS No.	Country/Locality/Field ID	Geologic Unit	Age[1]	Oil-Shale Class[2]	Type of Sample[3]
	U.S.A.				
	Alabama				
46A	Ore 97	Chattanooga Sh	D	Marinite	?
46B	Ore 97B	do	D	do	?
	Colorado				
45	Larimer County				
	Boettcher pit	Niobrara Fm, F bed	K	Marinite	OP
49	Rio Blanco Co. PBD-1	Green River Fm	Eoc	Lamosite-G	DC
50	Rio Blanco Co. PBM-1	do	Eoc	do	DC
21B	Yuma County				
	DH Whomble 1-32	Sharon Springs Mbr	K	Marinite	DC
	Indiana				
14		New Albany Sh	D	Marinite	OC
14F	Standard-benef.	New Albany Sh?	D	do	?
14B	NS-83-715	Shale over coal	Pe	C. marinite?	?
14C	NS-83-760	do	Pe	do	?
14D	NS-84-0	do	Pe	do	?
14E	NS-84-20	do	Pe	do	?
56	MH-10	do	Pe	do	OC
	Kentucky				
52	MH-2	New Albany Sh	D	Marinite	OP
57	MH-11	Sunbury Sh	D	do	OP
	Michigan				
58	MH-12	Antrim Sh	D	Marinite	OP
	Montana				
15		Heath Fm	M	Marinite	OC
15B	MH-7	do	M	do	OC
6	PPR-1	Phosphoria Fm	P	do	T
	Ohio				
54	MH-5	Huron Sh	D	Marinite	OC
55	MH-6	Cleveland Sh	D	do	OC
	Oklahoma				
53	MH-4	Woodford Sh	D	Marinite	OC
	Tennessee				
59		Chattanooga Sh	D	Marinite	OC
	Utah				
51	UBD-1	Green River Fm	Eoc	Lamosite-G	DC
	Wyoming				
41	GB-1-C	Green River Fm	Eoc	Lamosite-G	DC
42	GB-3-C	do	Eoc	do	DC
43	WB-5-C	do	Eoc	do	DC
44	WB-5-C	do	Eoc	do	DC
48	GBW-1	do	Eoc	do	DC
	U.S.S.R.				
76	Estonia, October Pit	'Kukruse Stage'	O	Kukersite	OP
	Yugoslavia				
9A	Aleksinac, Morava Pit	?	Mio	Lamosite-R	OP
9B	do	?	Mio	do	OP

[1] T = Tertiary
Mio = Miocene
Oli = Oligocene
Eoc = Eocene
K = Cretaceous
J = Jurassic
P = Permian
Pe = Pennsylvanian
M = Mississippian
D = Devonian
O = Ordovician
C = Cambrian

[2] C. marinite = Carbonaceous marinite

[3] D = Dump
RC = Rotary cuttings
DC = Drill core
OP = Open pit
M = Mine
OC = Outcrop
T = Trench

by the U.S. Bureau of Mines as described by the American Society for Testing Materials[3]. A few of the Fischer assays were made by Dickinson Laboratories, Inc., El Paso, Texas, using the ASTM procedure. The precision of the hydroretorting and Fischer assay methods are estimated to be ± 2 gallons/ton (~8 liters/tonne).

Rock-Eval Analyses

Rock-Eval analysis is widely used by petroleum explorationists to determine the oil potential, as well as to infer the type of organic matter and degree of thermal maturity, of a petroleum source rock. In recent years, the method has come into use to evaluate oil shales, especially those in Canada by Macauley and coworkers[7-12].

A Rock-Eval analysis includes determinations of "free" hydrocarbons (S1) obtained during heating a 100-mg sample for 3-4 minutes at 300°C, hydrocarbons (S2) obtained by pyrolysis of the remaining organic matter by heating the same sample from 300 to 550°C, T_{max}—the peak temperature at the maximum rate of production of the S2 hydrocarbons, and carbon dioxide (S3) obtained from pyrolysis of the organic matter during heating up to 390°C. The S1 and S2 hydrocarbons and S3 carbon dioxide are reported in mg/g of sample.

Problems in interpetation of the S1, S2, and S3 data may arise when samples containing free hydrocarbons with high boiling points are detected as S2 rather than S1 hydrocarbons and carbonate minerals that thermally decompose at low temperatures (e.g., nahcolite, dawsonite, and ankerite?) whose carbon can be detected and added erroneously to the S3 carbon dioxide obtained from pyrolysis of the organic matter.

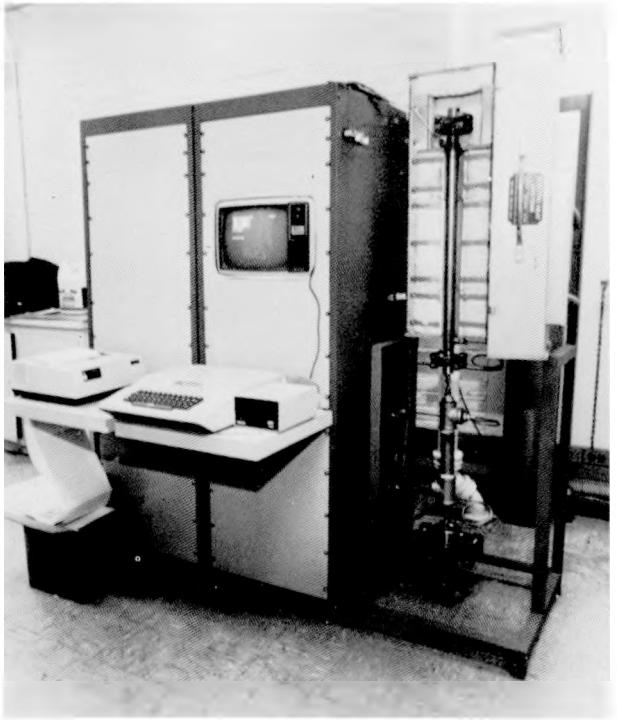

Figure 2. Photograph of the IGT hydroretorting assay equipment.

Several additional quantities are also determined, including total organic carbon (TOC), the hydrogen index (HI), the oxygen index (OI), pyrolyzable carbon (PC), and the petroleum index (PI)[4,5,6]. TOC, in weight percent of the sample, is the sum of organic carbon in the S1 and S2 hydrocarbons plus that determined by oxidizing the residual carbon at 600°C. More refractory forms of organic carbon, if present, may not be measured by Rock-Eval. HI is the amount of hydrocarbons produced by heating and pyrolysis (S1+S2) normalized to TOC (mg HC/g TOC) and OI is the amount of carbon dioxide produced by pyrolysis (S3) normalized to TOC (mg CO_2/ g TOC). Espitalié and others[4] have demonstrated that HI and OI are proportional to atomic H/C and O/C ratios, respectively. Plots of HI versus OI (van Krevelen diagrams) are commonly used to show type and thermal maturity of organic matter in sedimentary rocks. Prolyzable carbon is an estimate of the fraction of organic carbon in the S1 and S2 hydrocarbons relative to the weight of the sample, and it is calculated as (mg S1 + mg S2) X 0.083. The petroleum index is a measure of the amount of free hydrocarbons (S1) relative to the total amount of hydrocarbons (S1+S2) available in the rock: S1/(S1+S2).

In this investigation, the samples were analyzed by Rock-Eval II equipment in the organic geochemistry laboratories of the Geological Survey, Denver, Colorado. The samples were nominally 100 mg, but samples of high-grade oil shale were made smaller so that the quantities of pyrolyzable products were within the linear response limits of the detectors. The Rock-Eval detectors were standardized against a sample prepared from Upper Cretaceous Pierre Shale and the analyses were made by Ted A. Daws. A good summary of the Rock-Eval technique and the precautions necessary in interpreting Rock-Eval data has been published by Peters[6].

Organic Petrography

A.C. Hutton[13,14,15] has developed a scheme for classifying oil shales on the basis of origin and kinds of organic matter recognized in polished sections under the microscope in incident ultraviolet fluorescence (UVF) light and incident white-light modes.

Many of the oil shales used in this study have been classified previously by Hutton[14,15,16]. Some oil shales that were analyzed in this study, but not previously classified by Hutton, were examined by Dyni using Hutton's methodology[17] to determine oil-shale types. Therefore, the oil-shale types assigned to the samples studied in this investigation are partly from Hutton's work supplemented by Dyni's study.

Five types of oil shale as defined by Hutton[15] are recognized in this study:

Lamosite, an oil shale of lacustrine origin whose liptinite component consists of weakly to moderately fluorescing alginite having a lamallar structure in sections perpendicular to bedding. The liptinite is derived from lacustrine green and blue-green algae and associated phytoplankton.

Marinite, an oil shale of marine origin whose organic matter consists commonly of a groundmass of non- to weakly fluorescing bituminite and liptinite consistly chiefly of fluorescing lamellar-

structured alginite derived from marine algae and other phytoplankton.

Tasmanite, a marine oil shale in which the liptinite component is strongly fluorescing tasmanitids.

Kukersite, a marine oil shale in which most of the liptinite component is strongly fluorescing *Gloeocapsomorpha*, a green alga.

Cannel coal, a liptinite-rich coal of terrestrial origin containing abundant, fluorescing sporinite, resinite, and cutinite, as well as typical non-fluorescing vitrinite and other coal mascerals derived from terrestrial vascular plants.

Torbanite, another variety of lacustrine oil shale, in which the liptinite component is derived chiefly from *Botryococcus* and related algae, was not included in this study.

Oil shales can contain a variety of mascerals such as inertinite, bitumen, vitrinite, etc., depending on the depositional environment. It is not uncommon for marine shales, for example, to contain varied amounts of coal mascerals depending on local depositional conditions. Therefore, it cannot be expected that the samples analyzed in this study represent the entire deposit. Variations in the masceralic composition of the organic matter and degree of thermal maturity of an oil shale deposit should change with depth of burial and with paleogeographic location within the depositional basin.

Results and Discussion

Shale-Oil Determinations

The hydroretorting analyses and Fischer assays are summarized in Table 2 and the Rock-Eval analyses are given in Table 3.

The shale oils produced from the lamosites are generally less dense than the oils from the marinites (Figure 3), probably because the lamosites are generally more hydrogen-rich than the marinites.

For most samples, the water yields by HRA and FA correlate closely, but some bias toward higher yields by HRA is indicated (Figure 4). On the other hand, the 'gas plus loss' determinations vary considerably between the two types of analyses and are strongly biased toward higher yields by the HRA method (Figure 5).

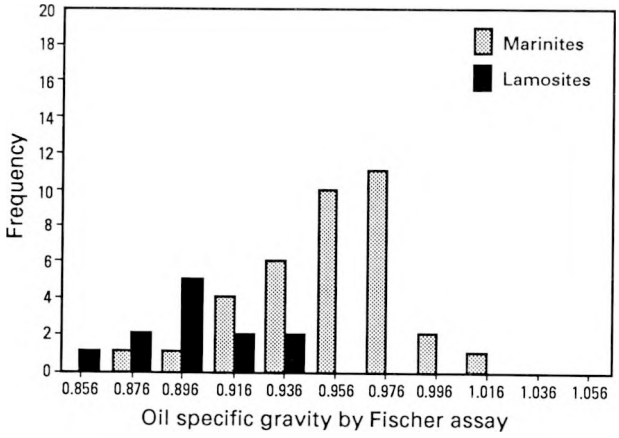

Figure 3. Distributions of the specific gravity of oils produced by Fischer assay analysis for samples grouped into lamosites and marinites. The average specific gravity for the lamosites (12 samples) is 0.889 and for the marinites (36 samples), 0.844.

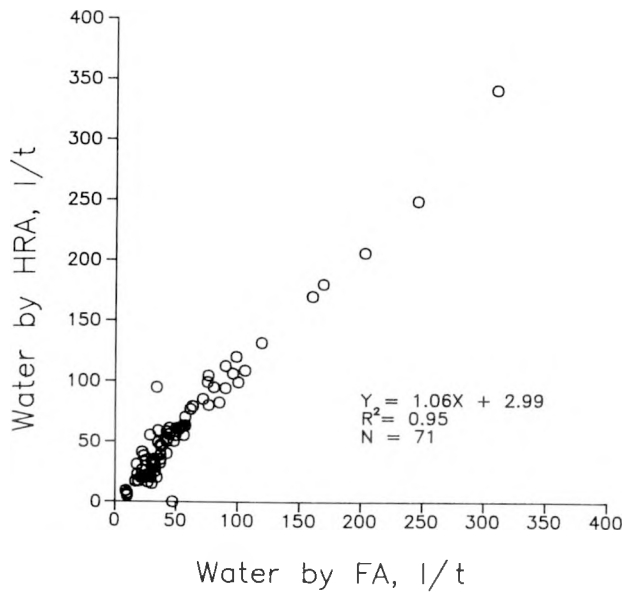

Figure 4. Comparison of water determinations made by Fischer assay and by hydroretorting assay.

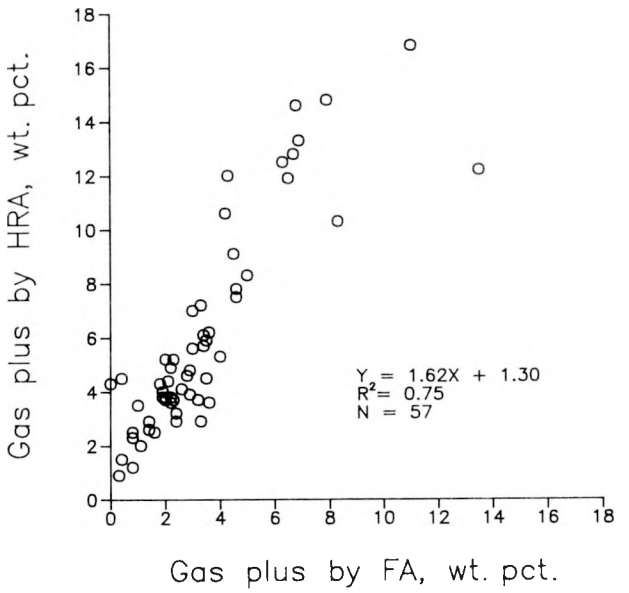

Figure 5. Comparision of 'gas plus loss' determinations made by Fischer assay and hydroretorting assay.

Table 2. Fischer Assay and Hydroretorting Analyses of Oil-Shale Samples

USGS No.	IGT No.	FISCHER ASSAY OIL (l/t)	FISCHER ASSAY WATER (l/t)	FISCHER ASSAY GAS PLUS (wt %)	FISCHER ASSAY Sp. Gr. of oil	HYDRORETORTING ANALYSIS OIL (l/t)	HYDRORETORTING ANALYSIS WATER (l/t)	HYDRORETORTING ANALYSIS GAS PLUS (wt %)	HRI
		AUSTRALIA							
17	---/50304	295.8	47.2	4.6	0.933	255.1	0.0	38.1	86
27	229/50922	240.6	45.4	3.8	0.942	NA	NA	NA	NA
19	227/50009	68.4	118.9	3.0	0.961	116.5	131.5	5.6	170
20	236/51158	3.3	75.9	0.3	NA	20.0	80.0	0.9	606
35	239/51262	104.3	245.8	8.3	0.962	149.1	248.5	10.3	143
36	239/51260	115.1	159.7	6.5	0.949	160.3	169.8	11.9	139
37	239/51261	154.8	309.9	11.0	0.964	174.5	340.3	16.8	113
		BRAZIL							
28	231/50802	77.6	37.1	3.4	0.912	121.1	38.8	5.7	156
28B	---/51386	139.8	31.3	4.6	0.920	222.2	31.7	7.8	159
		CANADA							
11	219/49450	43.0	52.2	2.0	0.964	80.7	60.5	5.2	188
60	---/49299	34.6	10.0	1.4	0.916	66.9	5.0	2.9	193
61	---/49300	35.1	10.0	1.4	0.926	65.3	7.0	2.6	186
62	---/49301	9.6	8.8	0.8	NA	27.0	9.0	1.2	281
63	---/49302	39.2	34.2	2.7	0.947	132.0	20.0	NA	337
64	---/49303	46.3	30.0	2.8	0.956	139.4	14.9	4.6	301
65	---/49304	43.4	29.2	2.6	0.958	120.4	20.1	4.1	277
66	---/49305	30.5	26.3	2.0	0.940	82.8	22.0	3.7	271
67	---/49306	22.5	23.4	1.6	NA	54.9	20.0	2.5	244
68	---/49307	27.1	21.3	2.2	0.948	65.1	20.0	4.9	240
12	219/49451	46.3	52.2	2.3	0.979	95.1	60.1	5.2	205
		CHINA							
26	234/50921	79.1	44.3	4.2	0.880	70.0	61.0	10.6	88
34	235/51065	74.3	61.3	3.4	0.924	125.5	76.7	6.1	169
47	243/950802901	207.5	100.1	6.7	0.894	254.0	98.9	12.8	122
		CZECHOSLOVAKIA							
24	232/50919	117.4	21.1	3.6	0.879	198.6	20.0	3.6	169
25	233/50920	9.2	42.2	0.4	0.937	32.1	58.0	1.5	349
		EGYPT							
29	230/50744	34.2	16.7	1.0	0.974	48.4	16.9	3.5	142
30	230/50743	4.2	89.7	0.4	NA	19.0	94.0	4.5	452
31	230/50745	18.4	98.5	2.2	0.912	34.0	119.9	3.6	185
32	230/50746	80.1	55.9	2.9	0.959	154.1	55.0	4.8	192
		GREAT BRITAIN							
7	215/48958	181.5	28.4	6.9	0.856	172.5	55.0	13.3	95
16	221/49503	244.5	49.2	7.9	1.004	320.2	54.8	14.8	131
		ISRAEL							
22	237/51159	109.2	105.6	5.0	0.977	170.3	108.7	8.3	156
23	237/51160	113.0	95.7	4.5	0.959	146.0	106.1	9.1	129
		ITALY							
3	194/48136	19.6	30.9	0.5	0.906	50.9	259.7	NA	260
		JORDAN							
5C	197/ ?	136.7	NA	NA	NA	237.6	35.1	8.1	174
5D	197/ ?	84.6	NA	NA	NA	141.2	19.6	3.7	167
5E	213/48845A	109.7	37.0	3.3	NA	167.0	32.0	7.2	152
5F	213/48845B	111.4	22.1	3.3	0.964	183.0	41.0	2.9	164
		MOROCCO							
13	222/49563	45.1	31.7	2.0	0.968	94.9	35.0	3.8	210
		SOUTH AFRICA							
4A	198/48549	20.9	42.6	NA	NA	47.0	52.0	NA	225
4B	199/48550	0.8	38.4	0.9	NA	11.0	99.0	NA	1375
4C	190/48038	369.3	55.4	5.0	0.900	391.4	62.7	NA	106
4D	218/49346	91.7	33.8	13.5	0.870	184.4	94.7	12.2	201
4E	218/49347	25.0	32.5	0.0	0.889	50.0	30.0	4.3	200
4F	196/48186	31.2	63.1	3.5	0.944	23.0	79.0	5.9	74
4G	196/48187	16.9	35.0	0.8	0.950	26.0	49.0	2.3	154
4H	196/48188	83.7	75.7	4.3	1.042	94.9	104.3	12.0	113
		SWEDEN							
1A	192/48112	44.6	57.2	3.9	0.974	134.9	63.0	NA	302
1B	191/48111	15.9	26.7	4.0	0.929	73.1	16.0	NA	460
		THAILAND							
10A	195/48147	72.6	48.0	2.5	0.906	83.4	50.0	NA	115
10B	195/48148	53.0	37.1	1.7	0.891	58.1	35.0	NA	110
		TURKEY							
8A	217/49319	101.8	50.1	3.5	0.917	146.8	60.7	4.5	144
8B	217/49320	41.7	168.6	2.9	0.915	80.0	180.0	3.9	192
8C	217/49321	24.6	42.1	0.8	0.859	40.0	50.0	2.5	163
8D	217/49322	277.5	202.8	6.3	0.883	356.6	206.0	12.5	129

Table 2. Cont. Fischer Assay and Hydroretorting Analyses of Oil-Shale Samples

USGS No.	IGT No.	FISCHER ASSAY OIL (l/t)	WATER (l/t)	GAS PLUS (wt %)	Sp. Gr. of oil	HYDRORETORTING ANALYSIS OIL (l/t)	WATER (l/t)	GAS PLUS (wt %)	HRI
		U.S.A.							
46A	---/51387	41.3	32.7	4.0	0.943	116.0	25.0	5.3	281
46B	---/51388	143.0	NA	NA	NA	271.0	38.7	14.9	190
21B	238/51259	23.9	71.4	2.4	0.964	85.0	85.0	3.2	356
45	---	15.0	35.1	NA	NA	31.9	58.7	1.5	213
49	---	104.7	12.3	3.6	0.913	145.9	20.5	7.4	139
50	---	87.4	11.9	2.6	0.913	110.8	19.8	4.9	127
14B	223/50005	20.0	42.1	1.8	0.937	70.6	39.8	4.3	353
14C	223/50006	47.2	53.8	3.0	0.939	138.4	61.7	7.0	293
14D	223/50007	85.1	57.2	4.6	0.966	215.7	70.1	7.5	253
14E	223/50008	51.7	84.7	2.2	0.941	165.5	82.2	3.8	320
14F	---/48672	NA	NA	NA	NA	226.5	34.1	7.2	NA
14F	---/48673	NA	NA	NA	NA	223.6	49.7	8.6	NA
56	---	29.6	44.2	1.9	NA	85.4	55.6	4.0	289
52	---	61.3	19.2	3.2	NA	161.9	17.0	3.7	264
57	---	44.2	25.0	1.9	NA	107.0	34.0	3.8	242
58	---	42.1	32.1	2.4	NA	106.3	31.7	2.9	252
15	193/48117	64.3	89.7	3.6	0.933	140.4	112.3	6.2	218
15B	---	17.5	20.9	0.5	NA	NA	NA	NA	NA
54	---	47.6	15.4	2.7	NA	67.3	19.8	5.7	141
55	---	22.1	30.0	1.1	NA	75.4	33.7	2.0	341
53	---	35.9	37.1	2.3	NA	106.6	46.8	3.7	297
59	860109501	40.5	22.1	2.1	0.934	94.1	26.0	4.4	232
51	---	83.7	7.7	3.2	0.908	109.1	29.6	5.2	130
41	---	63.4	18.3	NA	NA	117.7	22.6	2.7	186
42	---	63.0	23.6	NA	NA	78.7	37.8	5.1	125
43	---	67.6	37.7	NA	NA	111.8	45.6	2.8	165
44	---	65.1	17.9	NA	NA	108.4	30.8	2.0	167
48	---	97.2	13.6	3.1	0.913	137.3	21.7	3.3	141
		YUGOSLAVIA							
9	220/49495	186.8	80.1	6.8	0.861	204.6	94.8	14.6	110
	Maximum	369.3	309.9	13.5	1.042	391.4	340.3	38.1	1375
	Minimum	0.8	7.7	0.0	0.856	11.0	0.0	0.9	74
	Mean	76.6	53.7	3.3	0.932	123.1	62.1	6.2	221
	Count	82	79	73	59	83	83	76	81

NA = not analyzed

Table 3. Rock-Eval Analyses of Oil-Shale Samples

USGS No.	IGT No.	ROCK-EVAL ANALYSES TOC (wt %)	Tmax (°C)	HI (mg/g)	OI (mg/g)	PC (wt %)	S1 (mg/g)	S2 (mg/g)	S3 (mg/g)	S1+S2 (mg/g)	PI S1/(S1+S2)
		AUSTRALIA									
17	---/50304	20.4	440	1089	10	19.0	4.7	223.	2.1	228.	0.02
27	229/50922	20.3	437	974	21	16.7	3.2	198.	4.4	201.	0.02
19	227/50009	13.5	420	410	27	4.7	1.5	55.5	3.7	57.0	0.03
20	236/51158	3.6	424	217	55	0.7	0.0	7.9	2.0	7.9	0.00
35	239/51262	31.0	415	378	83	10.5	9.4	117.	25.9	127.	0.07
36	239/51260	25.8	411	451	69	10.5	10.1	116.	17.9	127.	0.08
37	239/51261	38.5	406	412	73	14.6	17.0	159.	28.1	176.	0.10
		BRAZIL									
28	231/50802	10.8	428	682	6	6.5	4.5	74.0	0.7	78.5	0.06
28B	---/51386	18.8	434	699	36	11.5	6.4	131.	6.8	138.	0.05
		CANADA									
11	219/49450	9.4	411	346	37	2.7	0.3	32.5	3.5	32.8	0.01
60	---/49299	4.5	441	299	95	1.2	0.6	13.5	4.3	14.1	0.04
61	---/49300	4.9	442	257	80	1.1	0.6	12.6	3.9	13.3	0.05
62	---/49301	2.1	436	495	69	0.9	0.4	10.4	1.5	10.9	0.04
63	---/49302	10.4	435	209	46	1.9	0.9	21.8	4.8	22.7	0.04
64	---/49303	11.4	433	341	48	3.3	1.3	38.8	5.5	40.1	0.03
65	---/49304	9.6	435	320	52	2.6	1.1	30.6	5.0	31.7	0.03
66	---/49305	6.8	435	328	78	1.9	1.1	22.2	5.3	23.3	0.05
67	---/49306	4.5	441	287	46	1.2	0.9	13.0	2.1	13.8	0.06
68	---/49307	5.6	431	280	23	1.4	0.9	15.6	1.3	16.5	0.05
12	219/49451	12.1	408	357	54	3.6	0.4	43.4	6.6	43.8	0.01
		CHINA									
26	234/50921	9.5	439	659	18	5.2	0.3	62.5	1.8	62.8	0.00
34	235/51065	10.7	433	482	36	4.3	0.4	51.8	3.9	52.1	0.01
47	243/950802901	30.0	440	425	58	10.6	<0.1	128.	17.6	128.	0.00
		CZECHOSLOVAKIA									
24	232/50919	20.2	441	561	8	9.9	5.5	113.	1.8	119.	0.05
25	233/50920	3.6	424	315	69	0.9	0.1	11.2	2.5	11.3	0.01
		EGYPT									
29	230/50744	5.7	413	415	36	2.0	0.1	23.7	2.1	23.8	0.01
30	230/50743	2.6	402	462	47	1.0	<0.1	12.1	1.2	12.2	0.00
31	230/50745	2.6	424	145	89	0.3	<0.1	3.8	2.4	3.9	0.01
32	230/50746	10.4	414	564	45	5.0	0.6	58.9	4.7	59.5	0.01
		FRANCE									
33	---	5.4	413	784	47	3.6	0.7	42.0	2.6	42.7	0.02

Table 3. Cont. Rock-Eval Analyses of Oil-Shale Samples

USGS No.	IGT No.	ROCK-EVAL ANALYSES TOC (wt %)	Tmax (°C)	HI (mg/g)	OI (mg/g)	PC (wt %)	S1 (mg/g)	S2 (mg/g)	S3 (mg/g)	S1+S2 (mg/g)	PI S1/(S1+S2)
		GERMANY, F.R.									
69	---	9.1	424	530	112	4.1	1.0	48.1	10.2	49.1	0.02
70	---	13.2	413	719	129	8.0	1.2	95.0	17.1	96.2	0.01
71	---	4.1	424	372	176	1.3	0.2	15.2	7.2	15.4	0.02
72	---	12.3	431	659	67	7.0	2.7	81.1	8.2	83.8	0.03
73	---	5.1	435	440	135	1.9	0.7	22.4	6.9	23.1	0.03
74	---	1.8	456	19	105	<0.1	<0.1	0.4	1.9	0.4	0.00
75	---	24.2	433	387	98	8.0	1.7	93.8	23.8	95.5	0.02
		GREAT BRITAIN									
7	215/48958	21.2	455	806	12	14.4	2.0	171.	2.7	173.	0.01
16	221/49503	32.2	416	632	27	17.5	6.2	203.	8.7	210.	0.03
		ISRAEL									
22	237/51159	13.1	402	563	72	6.2	0.4	73.9	9.4	74.3	0.01
23	237/51160	14.0	409	573	82	6.7	0.4	80.3	11.6	80.8	0.01
		ITALY									
3	194/48136	3.8	361	320	41	1.2	2.2	12.0	1.6	14.2	0.15
3A	---	2.3	367	462	65	1.1	2.5	10.6	1.5	13.1	0.19
		JORDAN									
5A	---	22.0	419	720	15	13.6	5.5	158.	3.3	164.	0.03
5B	---	13.2	418	816	30	9.2	3.1	108.	4.0	111.	0.03
5C	197/---	21.6	416	614	19	11.3	3.3	32.8	4.3	36.0	0.02
5D	197/---	14.7	423	524	34	6.5	1.1	77.0	5.0	78.1	0.01
5E	213/48845A	11.1	414	756	36	7.1	2.0	83.8	4.1	85.7	0.02
		MOROCCO									
13	222/49563	7.8	412	497	29	3.3	0.8	39.0	2.3	39.7	0.02
		NORWAY									
2A	---	2.7	510	8	11	<0.1	0.1	0.2	0.3	0.4	0.38
2B	---	3.8	NA	1	20	<0.1	<0.1	0.1	0.8	0.1	0.38
2C	---	4.8	NA	1	47	<0.1	<0.1	0.1	2.3	0.1	0.17
2D	---	6.6	NA	4	13	<0.1	0.2	0.3	0.9	0.5	0.37
2E	---	0.6	445	3	11	<0.1	<0.1	<0.1	0.1	<0.1	0.33
		SOUTH AFRICA									
4A	198/48549	5.5	439	272	23	1.4	1.5	15.1	1.3	16.6	0.09
4B	199/48550	4.6	499	98	23	0.4	0.9	4.5	0.2	5.5	0.17
4C	190/48038	55.9	448	642	21	30.0	0.9	359.	11.9	360.	0.00
		SWEDEN									
1A	192/48112	16.4	422	519	8	7.2	1.0	85.2	1.4	86.3	0.01
1B	191/48111	13.1	433	293	11	3.2	0.6	38.1	1.4	38.7	0.02
		THAILAND									
10A	195/48147	7.8	429	828	80	5.5	0.9	64.8	6.3	65.7	0.01
10B	195/48148	5.2	433	765	97	3.3	0.4	39.4	5.0	39.8	0.01
		TURKEY									
8A	217/49319	6.9	439	1200	135	6.9	0.3	82.8	9.4	83.2	0.00
8B	217/49320	6.4	431	743	110	4.0	0.9	47.7	7.1	48.5	0.02
8C	217/49321	2.1	443	747	135	1.3	0.2	15.9	2.9	16.1	0.01
8D	217/49322	26.8	434	900	68	20.2	1.0	241.	18.4	242.	0.00
		U.S.A.									
46A	---/51387	11.6	436	289	69	3.0	2.1	33.6	8.0	35.7	0.06
46B	---/51388	31.8	434	423	39	11.9	8.0	134.	12.4	142.	0.06
21B	238/51259	7.3	410	287	34	1.8	0.4	20.9	2.5	21.3	0.02
45	---	3.4	435	412	34	1.2	0.8	14.2	1.2	15.0	0.05
49	---	10.8	443	817	99	7.4	0.9	88.4	10.8	89.3	0.01
50	---	7.5	444	798	128	5.1	1.0	60.0	9.7	61.0	0.02
14A	IGT #17	11.4	424	405	18	4.0	2.2	46.2	2.1	48.4	0.05
14B	223/50005	10.7	431	144	32	1.3	0.3	15.4	3.4	15.7	0.02
14C	223/50006	14.8	426	270	39	3.4	0.8	40.0	5.9	40.8	0.02
14D	223/50007	20.0	423	197	41	3.4	0.8	39.6	8.4	40.4	0.02
14E	223/50008	17.4	426	161	34	2.4	0.4	28.2	6.0	28.6	0.01
14F	---/48672	19.8	430	425	79	7.3	3.0	84.3	15.7	87.3	0.03
52	---	10.7	433	418	87	3.9	2.1	44.8	9.3	46.9	0.04
57	---	7.9	431	325	80	2.3	1.5	25.8	6.3	27.3	0.06
58	---	6.4	435	380	75	2.2	1.4	24.5	4.8	25.9	0.05
15	193/48117	22.9	428	269	50	5.2	1.2	61.7	11.6	63.0	0.02
15B	---	3.3	437	196	145	0.6	0.3	6.5	4.8	6.8	0.04
6	---	2.0	458	0	83	<0.1	<0.1	<0.1	1.7	---	0.00
54	---	7.9	434	360	89	2.5	2.0	28.4	7.0	30.4	0.06
55	---	7.6	428	393	40	2.6	1.1	30.0	3.1	31.0	0.03
59	860109501	7.5	441	278	58	1.8	1.3	20.8	4.4	22.1	0.06
51	---	8.3	445	748	111	5.3	1.6	62.0	9.2	63.5	0.02
41	---	6.2	438	791	122	4.2	1.0	49.2	7.6	50.2	0.02
42	---	5.6	443	803	149	3.8	0.8	45.4	8.5	46.1	0.02
43	---	6.7	437	749	141	4.2	0.6	50.0	9.4	50.6	0.01
44	---	6.5	435	829	143	4.6	0.6	54.2	9.4	54.8	0.01
48	---	8.3	444	633	121	4.5	1.5	52.4	10.0	53.8	0.03
		U.S.S.R.									
76	---	35.1	432	962	51	28.2	0.5	337.	18.1	338.	0.00
		YUGOSLAVIA									
9	220/49495	24.0	442	910	25	18.2	0.2	219.	6.1	219.	0.00
9	---	22.6	437	690	18	13.1	0.5	156.	4.1	157.	0.00
	Maximum	55.9	510	1200	176	30.0	17.0	359.	28.1	360.	0.38
	Minimum	0.6	361	0	6	<0.1	<0.1	<0.1	0.1	<0.1	0.00
	Mean	12.1	430	478	61	5.6	1.7	64.4	6.3	66.8	0.05
	Count	95	92	95	95	95	95	95	95	94	95

NA = Not analyzed

To compare the oil determinations by the hydroretorting method to the Fischer assay data, the term, hydroretorting index, is introduced. The hydroretorting index (HRI) is defined as the volume of oil determined by HRA relative to the volume of oil obtained by Fischer assay multiplied by 100:

$$(O_{HRA}/O_{FA}) \times 100.$$

The HRI for all samples ranges from a low of 74 to 1375 (Table 2). The highest value of 1375, reported for sample 4B, may be subject to considerable analytical error because of the small amount of oil found by FA analysis. Because of the uncertainty of the data, sample 4B is omitted from further discussion.

Although most samples showed significant improvement in oil yields by HRA, samples 4F, 7, 17, and 26 inexplicably produced less oil by HRA than by FA. Samples 7 (a lamosite) and 17 (a tasmanite) are high-grade oil shales, whereas samples 4F (of unknown oil-shale type) and 26 (a lamosite) are moderate- and low-grade oil shales, respectively. The HRA or FA analyses, or both, may be in error. The data for sample 17 are also suspect because the 'gas plus loss' and water determinations by FA appear to be inversely, rather than directly, related to 'gas plus loss' and water determininations by HRA as is the case for most samples.

The distributions of the HRI for 49 samples of marinite and 16 samples of lamosite are plotted in Figure 6. The HRI for the lamosites ranges from 88 to 192 and averages 140, whereas the HRI for the marinites ranges from 129 to 606 and averages 250. The marinites respond better to hydroretorting than the lamosites.

Marinites. Most samples of Devonian and Mississippian oil shale (marinites) of eastern United States and Canada respond well to hydroretorting. For example, the HRI for eight samples of oil shale from Alabama, Kentucky, Ohio Michigan, and Tennessee ranges from 141 to 341, and averages 244. Similarly, the HRI for the sample of Woodford Shale from Oklahoma is 297,

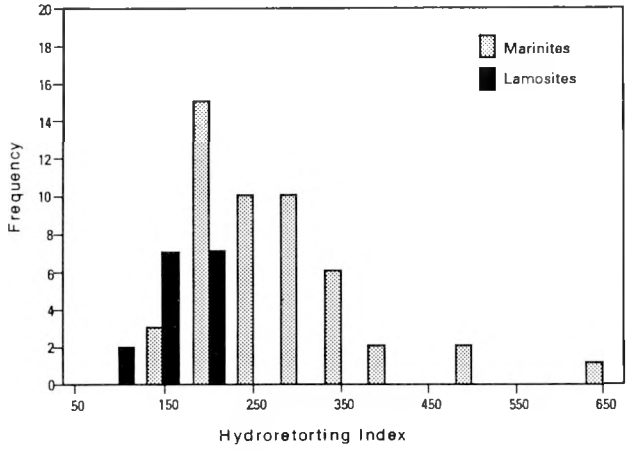

Figure 6. HRI distributions for 49 marinites and 16 lamosites.

and the average HRI for six samples of shale from the Kettle Point Formation from near Sarnia, Canada, is 278.

A set of five samples (14B, 14C, 14D, 14E, and 56) collected from black shales from Indiana that overlie several coal beds of Pennsylvanian age gave HRI values ranging from 253 to 353; oil yields by HRA are as much as 216 l/t of rock. According to Shaffer and others[20], these samples are oil shales of mixed fresh water and marine origin. They are tentatively identified as carbonaceous marinites (Table 2).

Samples of marinites from Cretaceous rocks in western United States and Canada also show relatively high HRI values. For example, sample 21B from the Sharon Springs Member of the Pierre Shale of eastern Colorado has an HRI of 356 and a sample of the F bed from the Niobrara Formation north of Denver has an HRI of 213. Somewhat lower ratios (188 and 205) were found for two samples of marinite from the Favel Formation in Manitoba and Saskatchewan, Canada. Two samples of marinite from the Cretaceous Toolebuc Formation, Queensland, Australia have HRI values of 170 and 606. However, the latter HRI is for sample 20 which did not yield sufficient oil by pyrolysis to be of ecocomic importance.

Samples of marinites from Upper Cretaceous marine rocks of North Africa and the Middle East, such as the Timahdit oil-shale deposit in Morocco, oil shales in the Dakhla Formation in Egypt, the Yamin and Rotem deposits of the Ghareb Formation in Israel, and the El Lajjun deposit in Jordan have HRI values ranging from 129 to 452. Omitting sample 30 because of its low oil yields by pyrolysis, the average of the HRI determinations for these samples is 167. Because some of these deposits are associated with phosphorites, they may have value as an energy source for the production of phosphates[18].

Samples of marinite from the Permian Irati Formation in Brazil show modest increases in shale oil yields by HRA analysis (HRI values of 156 and 159). Samples of the Permian Whitehill Formation in South Africa—the counterpart of the Irati Formation in Brazil—show somewhat higher HRI values of 200, 201, and 225.

One of the most interesting marinites is the Upper Cambrian Alum Shale of Sweden. Two samples (1A and 1B) have HRI numbers of 302 and 460, respectively. Sample 1A from Narke, Sweden, yielded 45 l/t of oil by FA and 135 l/t of oil by HRA. Sample 1B from Billingen shows evidence of moderate thermal alteration of the organic matter when viewed in the field or under the microscope. A higher level of thermal maturity for sample 1B is also suggested by normalizing the HRA oil yield to TOC; the HRA yield is 8.2 l/t for sample 1A and 5.6 l/t for sample 1B, indicating that less organic carbon is available to form oil in sample 1B.

The Swedish Alum Shale, where not altered appreciably by geothermal processes, has excellent potential for production of shale oil and combustible gas by hydroretorting, and for uranium and other

metals[19]. Although samples of Alum Shale from Norway contained as much as 7 weight percent TOC, they were found to be too thermally altered to yield appreciable oil by Rock-Eval, therefore, they were not analyzed by HRA and FA.

A sample of marinite (diatomite) from evaporitive rocks of Miocene age in Sicily shows good improvement in oil yield by HRA over FA (HRI of 278). Two samples of lipitinite-rich tasmanite (4C and 17) show no improvement, or even poorer oil yields, by HRA compared to FA.

Lamosites and Cannel Coals. In contrast to the marinite samples, the degree of improvement in HRA oil yields compared to FA yields for the lamosite samples was generally less (Figure 6). HRI determinations for eight samples of oil shale from the Green River Formation in Colorado, Wyoming, and Utah range from 125 to 186 and average 148. The HRI values for samples of lamosites from China, Czechoslovakia, Scotland, Thailand, Turkey, and Yugoslavia are similar or lower than those for the Green River samples. Three samples of cannel coal from Mt. Coolon, Queensland, Australia, show results similar to the lamosite samples.

Rock-Eval Results

The results of the Rock-Eval analyses are listed in Table 3.

Total Organic Carbon. TOC determinations for 95 samples range from 0.63 to 55.9 weight percent. The average TOC value for all samples is 12.1 weight percent. Samples 2E, 6, and 74 which have low TOC values are among those that were strongly altered by geothermal heating. These and possibly other samples may contain additional organic carbon that is too refractory to be measured by the Rock-Eval equipment.

To evaluate the effectiveness of the conversion of organic carbon to shale oil, the oil yields by FA and HRA were divided by TOC (FA/TOC and HRA/TOC). The frequency distributions for these data for the lamosites are compared with similar data for the marinites in Figures 7 and 8. As expected the conversion of organic carbon to oil by Fischer assay is clearly lower for the marinites than for the lamosites. However, the difference in oil yields between the two types of samples becomes less when the HRA/TOC values are compared. The organic matter of the lamosites has less capacity for conversion to oil by HRA than the organic matter in the marinites.

T_{max} Results. T_{max} for 92 oil-shale samples ranges from 361° to 510°C, and averages 430°C. Seven samples known to be thermally more mature than most of the samples tested have either high T_{max} values or unreliable values because too little S2 pyrolyzate was produced to measure T_{max} accurately. These samples include samples 2A and 2E of Alum Shale, Norway; sample 4B of the Whitehill Formation, South Africa; sample 6 of the Phosphoria Formation, Montana, and sample 74 of the *Posidonia* Shale, Germany. Two unusually low T_{max} values were recorded for samples 3 and 3A of tripolitic oil shale from Sicily (361° and 367°C). The reason for these low values is not clear.

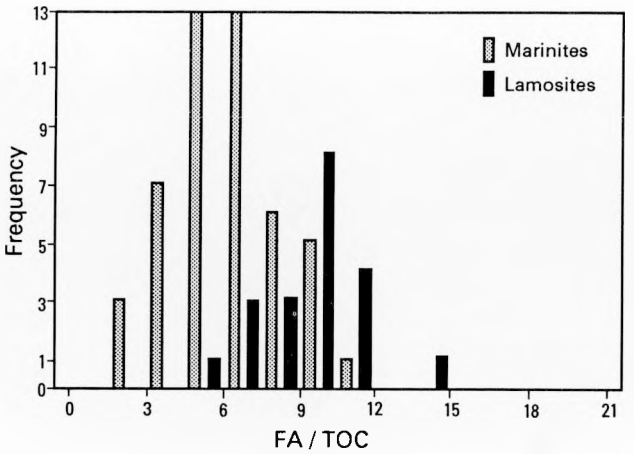

Figure 7. Distributions of oil yield by FA (liters/tonne) divided by TOC (wt. pct.) for 48 marinites and 20 lamosites. The average FA/TOC values are 4.9 for the marinites and 9.6 for the lamosites. Data from Table 3.

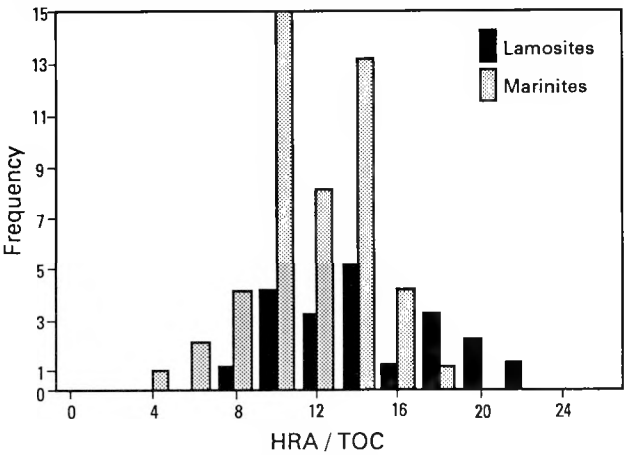

Figure 8. Distributions of oil yield by HRA (liters/tonne) divided by TOC (wt. pct.) for 48 marinite and 20 lamosite samples. The average HRA/TOC values are 10.6 for the marinites and 13.3 for the lamosites.

Figure 9 shows the frequency distribution of T_{max} for 83 samples, excluding values for the anomalous samples above. The average T_{max} for the 85 samples is 429°C.

The frequency distributions of T_{max} for 22 lamosites and for 60 marinites (excluding the seven marinite samples mentioned above) are dissimilar (Figure 10). The average T_{max} value for the lamosite samples is 439°C, or 13° higher than the average T_{max} value of 426°C for the marinite samples. Assuming that the range of thermal maturity for both sets of samples is approximately the same, the data suggest that T_{max} values for lamosites tend to be higher than those for marinites. Tissot and others[22] have also noted this relationship. Peters[6] suggests that the higher T_{max} values for oil shales containing abundant hydrogen-rich type I kerogen (typically, the liptinite-rich oil shales) is due to strong cross-linkage of long aliphatic chains and a lack of thermally less stable heteroatomic bonds.

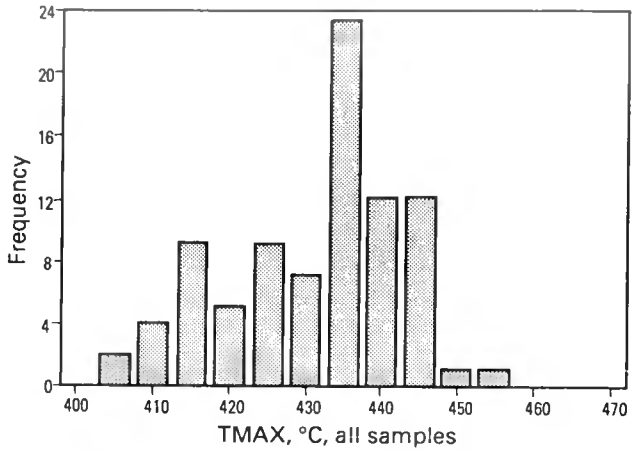

Figure 9. Distribution of T_{max} determinations for 83 samples of oil shale. Values less than 400°C and more than 460°C are not plotted. The average T_{max} value is 429°C.

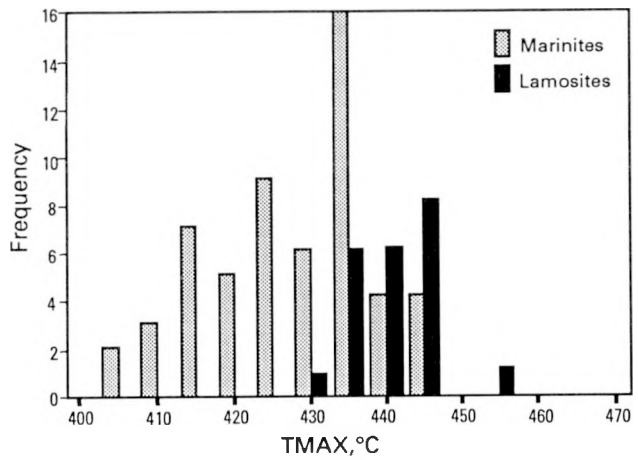

Figure 10. Distributions of T_{max} determinations for 58 marinites and 22 lamosites. The average T_{max} values are 426°C for the marinites and 439°C for the lamosites.

T_{max} temperatures could be useful to the process engineer in retort design and in determining energy requirements for retorting oil shale that contains organic matter of different types and of varied degrees of thermal maturity.

T_{max} plotted against specific gravity of the shale oil from the Fischer assay analysis shows an inverse relationship (Figure 11). As T_{max} decreases, the specific gravity of the shale oil increases. The lighter oils from Fischer assays are associated with the lamosites and tasmanites, whereas the heavier oils tend to be associated with the marinites and cannel coals. Figures 10 and 11 suggest that specific gravity data plotted against depth in bore holes may be a useful tool to study changes in thermal maturity and type of organic matter in an oil-shale deposit. Indeed, such profiles through the Green River oil-shale deposits in Colorado suggest that systematic changes observed in profiles of the specific gravity of shale oil with depth are related to

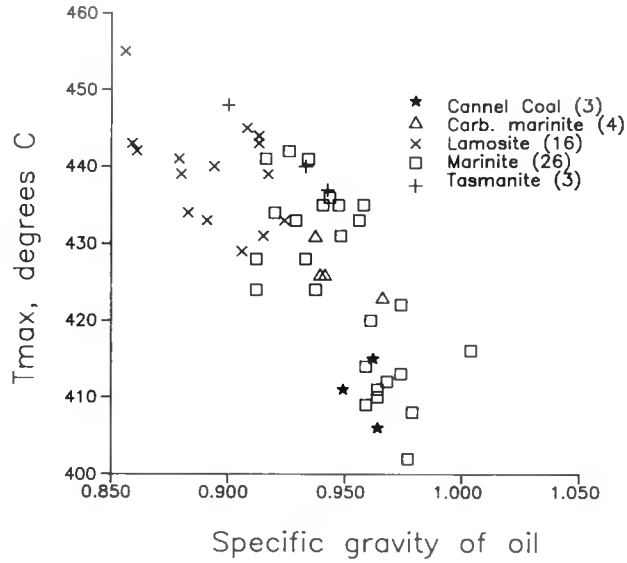

Figure 11. Specific gravity of shale oil obtained by Fischer assay vs. T_{max} for 52 samples.

both thermal maturity and type of organic matter (J.R. Dyni, 1989, unpublished data).

S1, S2, and S3. The S1, S2, and S3 data from Table 3, normalized to 100 percent, are plotted on a ternary diagram in Figure 12. Samples 2A-2E, 6, 15B, 31, 71, and 74 have S3 values greater than 30 mg/g rock and are not included in the diagram for the sake of clarity. Most of these samples are also thermally mature or overmature.

The lamosite samples contain relatively small amounts of S1 hydrocarbons, whereas the range of S1 hydrocarbons for the marinite samples is greater. The range of S3 carbon dioxide relative to S1 and S2 hydrocarbons is about the same for both marinites and lamosites.

Hydrogen and Oxygen Indexes. HI and OI data for 95 samples of oil shale are plotted in Figure 13. Although there is no clear division of the samples into kerogen types I to III as suggested by Tissot[22], the samples of lamosite, tasmanite, and kukersite have HI values greater than about 400 mg/g and varied OI values, whereas the marinite samples have a broad range of HI and OI values.

Some samples having the lowest HI values are thermally mature or overmature. Excluding the most mature samples (2A-2E, 4B, and 74), the averages for HI and OI values for the various types of oil shale are:

Type and no. of samples	HI	OI
Kukersite (1)	962	51
Tasmanite (3)	902	17
Lamosite (22)	740	87
Marinite (58)	416	56
Cannel coal (3)	414	75

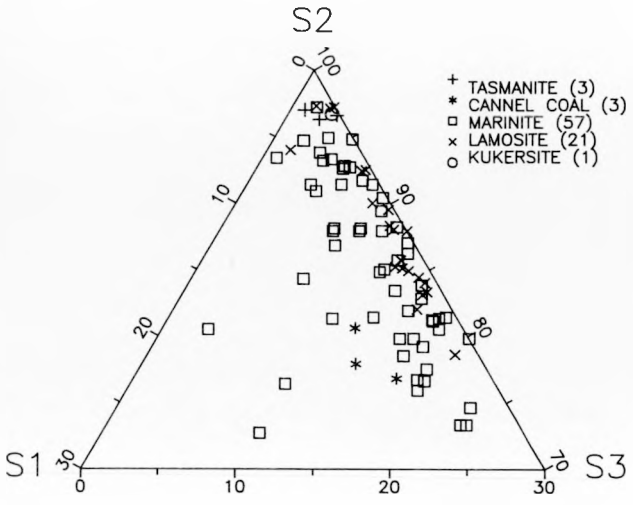

Figure 12. Ternary diagram of S1, S2, and S3 data for 85 samples from Table 3 normalized to 100 percent.

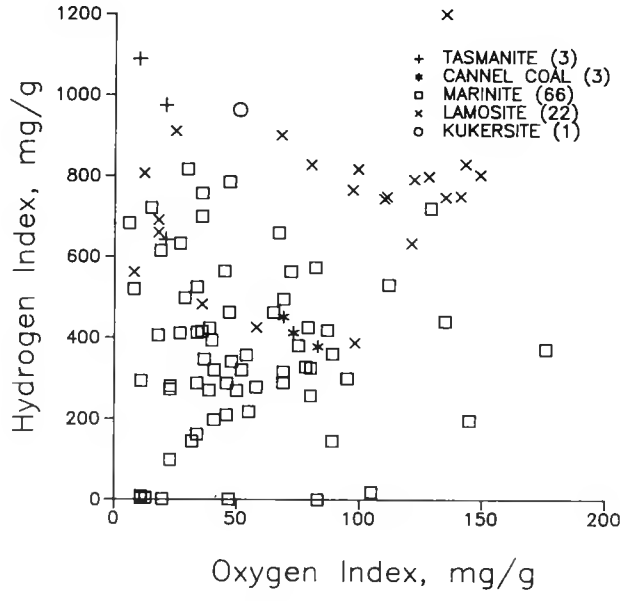

Figure 13. Hydrogen index vs. oxygen index for 95 samples of oil shale.

The oxygen index (OI) ranges from 6 to 176 and averages 61 mg CO_2/g TOC (Table 3). The Green River Formation samples (41-44 and 48-51) have OI values ranging from 99 to 149 which are much higher than those reported by Tissot[23] from the same formation, perhaps because of instrumental differences and because Tissot's samples were from deep wells in the Uinta Basin, Utah, whereas the authors' samples are from shallower depths.

A log-log plot of HI and HRI values (Figure 14) shows a inverse relationship, but a rather low degree of association (r^2 = 0.46). As the hydrogen content decreases, more oil is produced by hydroretorting. As expected, the hydrogen-rich lamosites and tasmanites plot toward higher HI and lower HRI values, whereas the converse is true for the marinites.

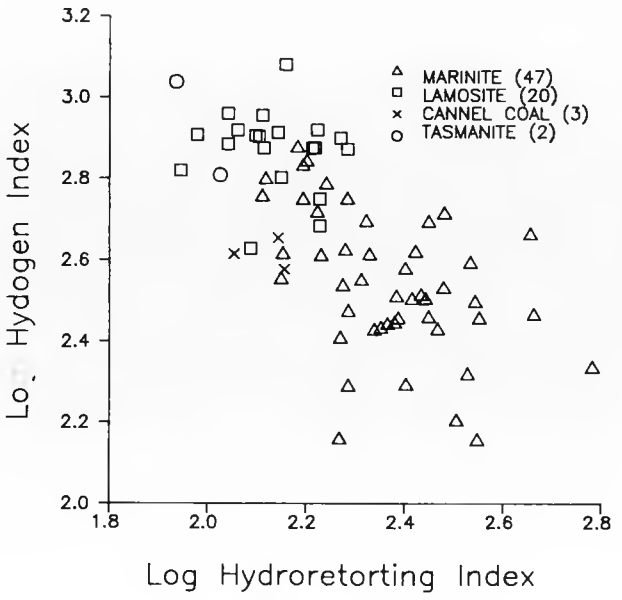

Figure 14. Hydrogen index vs. hydroretorting index for 72 samples of oil shale.

Bienner and Espitalié[24] found that the amount of hydrocarbons produced by Fischer assay correlates well with the amount of hydrocarbons produced by Rock-Eval for a variety of oil shales and that good estimates of oil + gas yields by Fischer assay can be made from the Rock-Eval data. These workers reported that the amount of oil produced is specific to the type of organic matter; type I kerogen (abundant in lamosites) yields proportionately more oil than gas than type II and type II organic matter produces proportionately more oil than gas than type III kerogen. Similar results were found for the samples of this study (Figures 15-17).

The sum of S1 and S2 hydrocarbons is plotted against oil yield by Fischer assay in Figure 15 for 74 samples. A surprisingly good fit was found (r^2 = 0.91), despite the fact that S1 and S2 measures oil and hydrocarbon gases, whereas 'gas plus loss' is measured separately by the Fischer assay.

Bienner and Espitalié[24] also showed that PC correlates well with oil + gas determined by Fischer assay. Similarly, PC shows a strong association (r^2 = 0.93) with the quantity of oil determined by Fischer assay for the samples of this study (Figure 16).

The difference between TOC and PC is the unreacted carbon that remains in the char after pyrolysis by Rock-Eval. Because the amount of unreacted carbon averages about one-third more in the group of marinite samples than in the lamosites, it would be reasonable to assume that some of the unreacted carbon that does not convert to oil by conventional Fischer assay reacts to form oil when it is hydroretorted. To test this idea, the difference between the HRA and FA oil yields was compared to the difference between TOC and PC in Figure 17. The degree of association (r^2 = 0.64) between TOC-PC and OIL_{hra-fa}

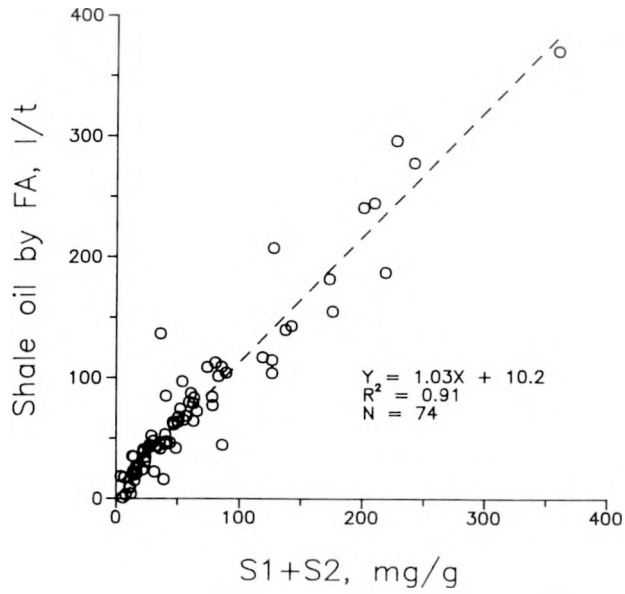

Figure 15. The sum of S1 and S2 hydrocarbons vs. shale oil determined by Fischer assay.

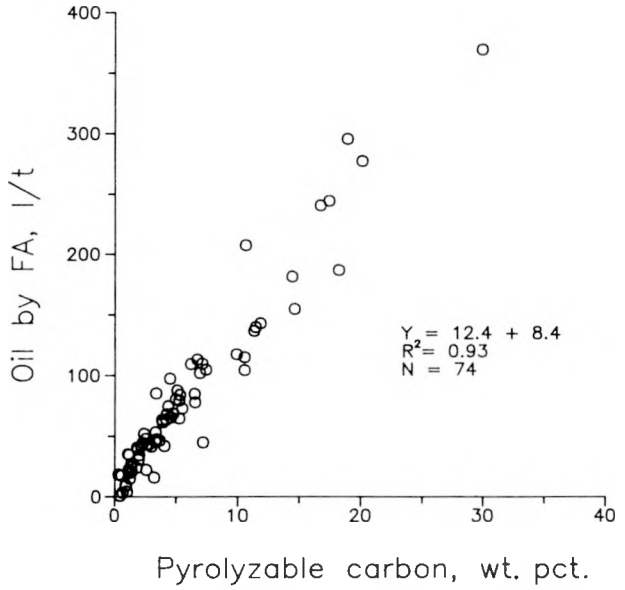

Figure 16. Pyrolyzable carbon vs. oil determined by Fischer assay for 74 samples.

does suggest that some the unreacted carbon from the Fischer assay analysis contributes to the additional oil obtained by hydroretorting.

Relation of Oil Yields to Carbon Types

Miknis and others[25] have shown that organic carbon in oil shale is divisible into aliphatic carbon and aromatic carbon on the basis of ^{13}C NMR studies. From Table 1 of their work[25], it seems that the marinites have higher aliphatic to aromatic carbon ratios than the lamosites. These authors found that the amount of

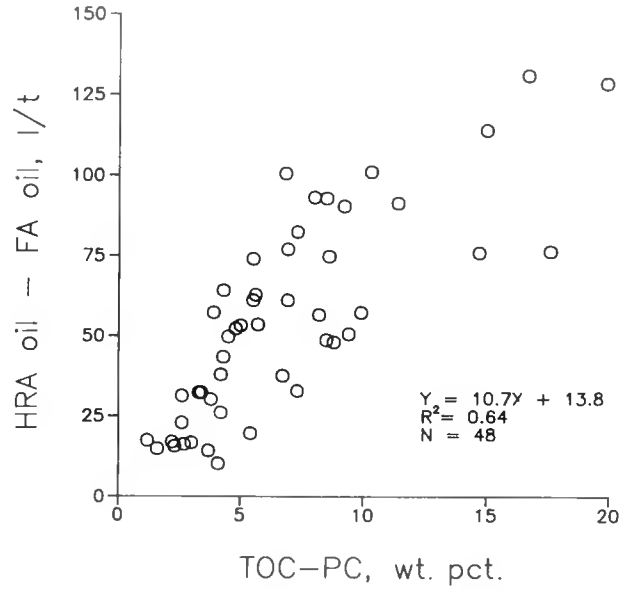

Figure 17. Plot of total organic carbon - pyrolyzable carbon vs. the difference in oil yields by HRA and FA for the marinite group of samples.

shale oil and gas produced by Fischer assay is proportionate to the aliphatic carbon fraction of the rock, whereas the aromatic carbon fraction appears to be largely nonreactive and remains in the carbonaceous residue of the spent shale. If this is true, Figure 17 suggests that some of the aromatic carbon contributes to the additional oil (and gas) formed during hydroretorting of the marinite samples.

With increasing thermal maturity, however, some of the reactive carbon (probably both aromatic and aliphatic types) that can produce oil and gas by FA and HRA is evidently converted to a less reactive form of carbon. For example, the samples of Alum Shale from Norway, which are thermally overmature, have PC/TOC ratios of less than 0.01, yet TOC ranges from about 3 to 7 percent. Similarly, of the two samples of Alum Shale from Sweden, sample 1B, known to be thermally more mature than sample 1A, has a PC/TOC ratio of 0.25, whereas the sample 1A has a ratio of 0.44. Also, the oil yields by FA and HRA relative to TOC for sample 1B are less than for sample 1A.

Some of the reactive carbon that can produce oil and gas is evidently converted by increasing thermal maturation to a nonreactive carbon. The following general model is suggested:

$$C_{al} + C_{ar} + C_{in} = TOC,$$

where C_{al} is aliphatic carbon that can produce oil and gas by conventional Fischer assay, C_{ar} is aromatic carbon that can produce additional oil and gas by hydroretorting, and C_{in} an inert or refractory form of carbon that is not available for production of oil and gas by either pyrolysis method.

The inert carbon could be derived from a primary masceral having little or no potential for oil and

gas (i.e., charcoal) or may form diagenetically from either of the other carbon types as a function of increasing thermal maturity of the rock, oxidation through weathering, or other causes.

Conclusions

Oil shales of varied ages and origins showed a wide range of response to hydroretorting that seems to be dependent upon the type of organic matter and the degree of thermal maturation of the oil shale. Oil shales of marine origin that have relatively low HI/OI ratios (marinites) show the best improvement in oil yields by hydroretorting relative to oil yields by Fischer assay. For those oil shales having relatively high HI/OI ratios, including those of lacustrine origin (lamosites) and liptinite-rich marine oil shales (tasmanite), improvement in oil yields by hydroretorting relative to Fischer assay is less.

This study supports the work by Miknis and others[25] that the oil obtained by Fischer assay is derived chiefly from the aliphatic carbon fraction of the organic matter and that the additional oil obtained by hydroretorting appears to be from largely the aromatic carbon components of the organic matter. Some nonreactive carbon, derived from aromatic carbon components and perhaps from some of the aliphatic carbon constituents of the organic matter, does not form oil or gas on hydroretorting, but converts to char in the spent shale.

The large increases in oil yields of the marinite group of oil shales that result from hydroretorting will require new assessments of the oil potential of these deposits.

References

1. F.C. Schora, J.C. Janka, and P.A. Lynch, "Progress in Commercialization of the Hytort Process," Proceedings 1982 Eastern Oil Shale Symposium, Institute for Mining and Minerals Research, University of Kentucky, Lexington, p. 183-190, 1982.

2. P.A. Lynch, and others, "The Hydroretorting Assay--A New Technique for Oil Shale Assessment," [abstract] Joint Fuel/Petroleum Division Meeting, American Chemical Society, St. Louis, Missouri, April 8-13, 1984, preprint, 13 p., 1984.

3. American Society for Testing Materials, "Standard Test Method for Oil from Oil Shale (Resource Evaluation by the USBM Fischer Assay Procedure), Designation D 3904-80", Annual Book of ASTM Standards, p. 513-525, 1980.

4. J. Espitalie and others, "Source Rock Characterization Method for Petroleum Exploration," 9th Annual Offshore Technology Conference Proc., Vol. 3, pp. 439-444, 1977.

5. D. M. Clementz, G. J. Demaison, and A. R. Daly, "Well Site Geochemistry by Programmed Pyrolysis," 11th Annual Offshore Technology Conference Proc., Vol. 1, pp. 465-470, 1979.

6. K.E. Peters, "Guidelines for Evaluating Petroleum Source Rock Using Programmed Pyrolysis," American Assoc. Petroleum Geologists Bull., Vol. 70, pp. 318-329, 1986.

7. George Macauley, "Cretaceous oil shale potential of the Prairie Provinces, Canada," Geological Survey of Canada Open File Report OF 977, 61 p., 1984.

8. W. Kalkreuth and G. Macauley, "Organic petrology and geochemical(Rock-Eval) studies on oil shales and coals from the Pictou and Antigonish areas, Nova Scotia, Canada," Bull. Canadian Petroleum Geology, vol. 35, p. 263-295, 1987.

9. George Macauley, "Cretaceous oil shale potential in Saskatchewan," Oil and Gas in Saskatchewan, Saskatchewan Geological Society Special Pub. No. 7, p. 255-270, 1984.

10. George Macauley and Wolfgang Kalkreuth, "Organic petology of selected oil shale samples from the lower Carboniferous Albert Formation, New Brunswick, Canada," Bulletin of Canadian Petroleum Geology, vol. 32, p. 38-51, 1984.

11. George Macauley and L.R. Snowdon, "A Rock-Eval appraisal of the Ordovician Collingwood oil shales," Geological Survey of Canada Open File Report OF 1092, 12 p., 1984.

12. George Macauley, L.R. Snowdon, and F.D. Ball, "Geochemistry and geological factors governing exploitation of selected Canadian oil shale deposits", Geological Survey of Canada Paper 85-13, 65 p., 1985.

13. A.C. Cook, A.C. Hutton, and N.R. Sherwood, "Classification of Oil Shales," Bull. Centres de Recherches Explor.-Prod. Elf-Aquitaine, Vol. 5, No. 2, pp. 353-381, 1982.

14. A.C. Hutton, "Classification of Oil Shales—a Petrographic Approach," Nineteenth Oil Shale Symposium Proceedings, Colorado School Mines Press, Golden, p. 27-37, 1986.

15. A.C. Hutton, "Petrographic classification of oil shales," International Journal of Coal Geology, Vol. 8, pp. 203-231, 1987.

16. B.J. Solomon, A.C. Hutton, D.A. Henstridge and J.F. Ivanac, "Stratigraphy and organic petrography of Mississippian and Devonian Oil Shale at the Means Project, East-Central Kentucky," Proceedings 1984 Eastern Oil Shale Symposium: Institute for Mining and Minerals Research, University of Kentucky, Lexington, pp. 365-392, 1984.

17. A.C. Hutton, "Short Course, Organic Petrography of Oil Shales," University of Wollongong and U.S. Geological Survey, 306 p., 1988.

18. T. Minster, and others, "Oil shale-phosphorite prospects in the east Mediterranean," Industrial Minerals, No. 222, pp. 47-60, 1986.

19. Astrid Andersson, and others, "The Scandinavian Alum Shales," Sveriges Geologiska Undersökning, Ser. Ca, NR 56, 50 p. [in English], 1985.

20. N.R. Shaffer and others, "Oil Shale of Pennsylvanian Age in Indiana," Proceedings 1984 Eastern Oil Shale Symposium, Institute for Mining and Minerals Research, Univ. Kentucky, Lexington, pp. 401-412, 1985.

21. P.T. Crisp, and others, "Australian Oil Shales: A Compendium of Geological and Chemical Data," Departments of Geology and Chemistry, Univ. Wollongong, Australia, 109 pp., 1987.

22. B.P. Tissot and D.H. Welte, "Petroleum Formation and Occurrence," Springer-Verlag, New York, 699 p., 1984.

23. B.P. Tissot, G. Deroo, and A. Hood, "Geochemical study of the Uinta basin; formation of petroleum from the Green River Formation," Geochimica and Cosmochimica Acta, Vol. 42, pp. 1469-1486, 1978.

24. F. Bienner and J. Espitalié, "Caracterisation de roches bitimineuses d'origines diverses par essais Fischer et correlations avec les resultats de pyrolyses du type Rock Eval," Institut Français du Petrole, Géolgie No. 23702, Projet D70 77047, 47 p., 1980.

25. F.P. Miknis and others, "^{13}C NMR measurements of the genetic potentials of oil shales," Geochimica and Cosmochimica Acta, Vol. 46, pp. 977-984, 1982.

Microscopic Characterization of Emulsion Interfaces

by

R.J. Mikula, V.A. Munoz, and W.W. Lam
CRL, Fuel Processing Laboratory
Department of Energy, Mines and Resources, CANMET
Devon, Alberta CANADA T0C 1E0

ABSTRACT

Certain process steps, in the extraction of oil from oil sands or during enhanced oil recovery, produce emulsions which must be broken in order to separate the oil. Microscopic characterization of these emulsions is therefore an important step in the prediction of processing characteristics and process yields. The size distribution of the process emulsion can determine how efficiently the oil can be separated from the water and by what means: mechanically or chemically.

Optical and scanning electron microscopy coupled with automated image analysis have been applied to characterization of the size distribution of the dispersed phase in many of these emulsion systems. In addition, it is possible to characterize the nature of the dispersed phase by using fluorescence behaviour in the optical system or via x-ray analysis with the scanning electron microscope. In certain cases it is possible to determine the chemical composition of the interface between the dispersed and continuous phases. Results from our laboratory illustrate the great potential of microscopic techniques, not only for studying the morphology of these economically important emulsions, but also for compositional determinations of the interface itself. Understanding these systems will lead to the development of improved methods of breaking these emulsions to increase production and reduce the cost of many petroleum extraction processes.

Introduction

Scanning electron microscopy (SEM) and optical microscopy (OM) are powerful tools for the characterization of emulsions and mixtures formed during extraction of bitumen or oil from oil sands and oil reservoirs. Enhanced oil recovery (EOR) by fireflood or steam injection often produces difficult to handle emulsions which are also amenable to characterization using SEM and OM techniques.

SEM is useful in the characterization of mineral components in emulsion systems when direct observation of the emulsion can be accomplished. This technique involves conventional freeze fracture methods but without subsequent metal coating or the creation of replicas. This retains the option of characterizing the components by measuring their respective x-ray spectra. This is particularly sensitive to the higher Z components such as minerals and clays. Optical microscopy, on the other hand, with fluorescence techniques can be sensitive to the composition of the organic components.

Several examples of the techniques currently in use at CANMET's Fuel Processing Laboratory will be illustrated in this paper, on samples relating to the extraction of bitumen from oil sands.

Experimental

The scanning electron microscope (SEM) used is a Hitachi X-650 equipped with both energy and wavelength dispersive spectrometers. An EMscope 2000 cryo-stage is used to prepare the frozen hydrated froth samples. The laboratory procedure involves freezing the sample in a liquid nitrogen slush and keeping it frozen and under vacuum in the cryo-stage. The sample is then fractured to reveal the interior of the frozen sample before transferring it to the cold stage in the SEM. The cold stage in the SEM is a Hexland DN302; its temperature is maintained at ~ 90 K by an Oxford ITC4 nitrogen heat exchanger and temperature-controller unit. The energy dispersive x-ray detector used in the cryo-stage work is a 30 mm^3 Si(Li) Tracor Northern detector coupled to the SEM and to the automated image analyzer. Low electron energy (10 to 20 keV) and short acquisition times are used in order to minimize beam damage and local evaporation of the sample while accumulating x-ray spectra in the spot mode.

A Carl Zeiss research microscope with a reflected light system was used for the microscopic study of the middlings obtained from bench scale extractions. The light source is a high pressure mercury lamp, HBO 100 W/2, used in combination with a reflector and a set of filters providing an incident wavelength between 450 and 490 nanometers (blue light). This produces fluorescence of the bitumen components allowing the determination of the droplet size distribution by image analysis. The advantage of fluorescence microscopy is that the clays and other minerals present in the middlings are not visible and therefore their interference is eliminated.

The scanning electron microscopy and optical microscopy methods are described in detail elsewhere[1-6].

The effect of iron on o/w emulsions was investigated using an emulsion made of 12.5 g bitumen, 5 mg iron (III) chloride, 0.1 g Redicote E-64-R cationic asphalt emulsifier (Armak Chemicals) and 250 ml 0.1 % HCl. Iron (III) chloride was added with the HCl solution and the Redicote emulsifier. The bitumen and solution were mixed at 82°C for 3 minutes, at a speed of 600 rpm using an RW 20 DZM (Janke & Kunkel) mixer. After mixing, the o/w emulsion samples were quickly frozen in liquid nitrogen for observation in the electron microscope.

The laboratory extraction of bitumen from the oil sand was accomplished by mixing 200 grams of tar sand with 120 grams of water for 20 minutes. The temperature was kept constant at 82°C by immersing the reaction vessel in a constant teperature bath. The mixing was done with a Brinkmann PT 35/4 homogenizer set at 4,000 rpm. The sodium pyrophosphate was added with the water at various concentrations to examine its effect on the mean oil droplet diameter of the oil-in-water emulsion produced in the middlings layer which is found below the froth layer.

Results and Discussion

Figure 1 shows a comparison between white light and blue light micrographs of oil sands. Under white light, it is very difficult to distinguish the bitumen components from the clays. Under blue light, the bitumen components associated with clays and silicates are clearly distinguishable. In addition, it is possible to measure the fluorescence spectrum of these bitumen components and therefore determine some of their chemical characteristics. The nature of the bitumen association with clays and other mineral particles can then be determined qualitatively using microscopy. These associations are important in determining the processing behaviour of the oil sands feed.

The first step in the extraction of bitumen from oil sands in the Clark hot water process is the separation of the bitumen in the primary flotation vessel. The action of caustic solution (sodium hydroxide) at elevated temperature (about 80°C) separates the bitumen product from the tailings sand. After this initial step, the middlings layer undergoes secondary flotation with the introduction of gas to facilitate separation of the bitumen. The remainder of the extraction process, applied to the combined products of these two steps, is devoted to removal of water and fine clays which were carried over with the bitumen product.

Initially, the bitumen separating from the sand forms what can be thought of as an oil in water (o/w) emulsion. At some point, however, it inverts and at the top of the separation vessel becomes a water in oil (w/o) emulsion. An understanding of the mechanism and the kinetics of this phase inversion will help in applying determining which techniques might be applied to maximize water and mineral drainage from the bitumen phase.

Both optical and electron microscopy are important in characterizing the behaviour of the dispersed phases throughout this process.

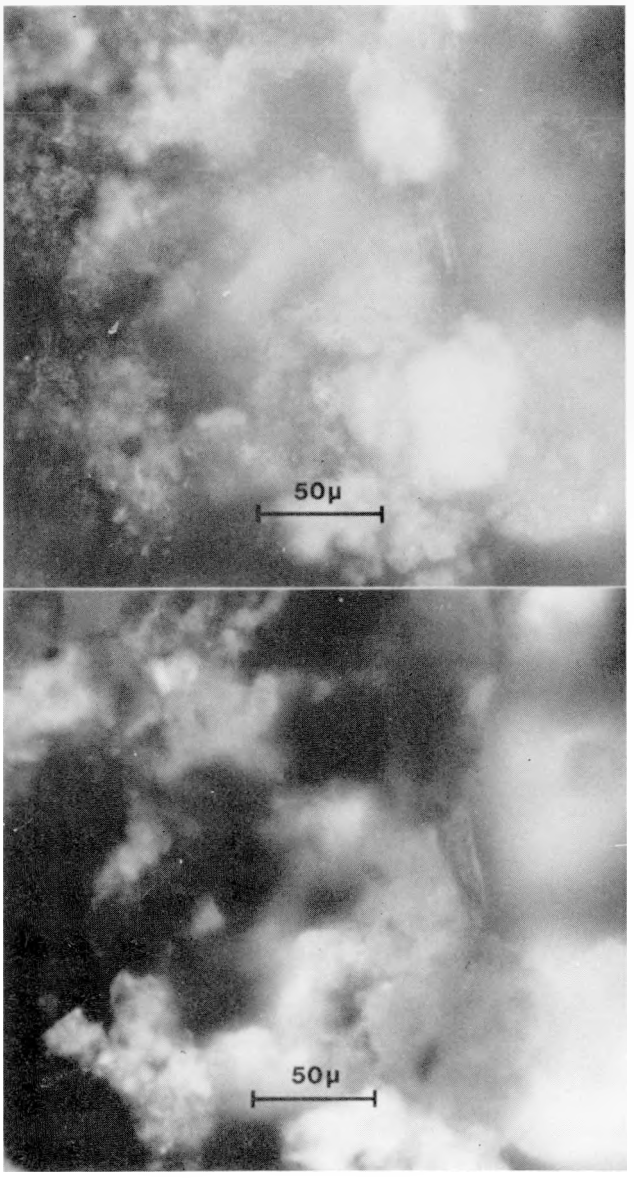

Figure 1: Oil sands sample under white light (TOP) and with the bitumen components fluorescing under blue light (BOTTOM).

Figure 2 shows an SEM micrograph of a primary froth cell sample with a significant number of air bubbles. The air in the primary froth is entrained during the initial mixing of the oil sands with steam and caustic solution. Figure 3 shows a much higher magnification of the interior surface of the air bubble. At the air water interface, the bitumen is present as small bitumen droplets on the order of one micron in size. Since these are frozen hydrated samples observed directly in the electron microscope, it is possible to identify the various phases in this field of view from their x-ray spectra. The oil or bitumen phase is characterized by a significant sulphur x-ray (Figure 4). At higher incident electron energy, the x-ray signal is obtained from deeper in the specimen, and Figure 5 which is an x-ray spectrum taken at 15 KV incident energy clearly shows a significant Al and Si signal which is indicative of clays. This might indicate that clays are playing a role in stabilizing these small bitumen drops at the air water interface. Unfortunately, limitations in resolution with the direct observation technique and the x-ray signal volume prevent one from determining this on such a small scale. However, it is well known that fine clays can adversely effect processability [7] and with these techniques it is possible to determine the role of clays in stabilizing these emulsion systems.

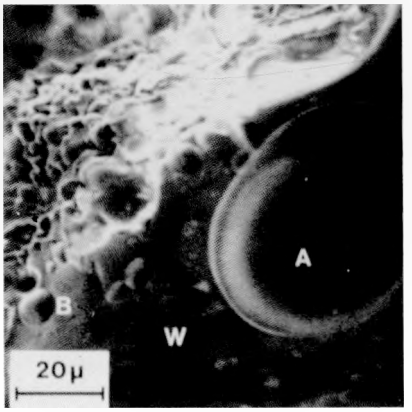

Figure 2: Frozen hydrated froth sample in the SEM. The air (A), bitumen (B) and water (W) phases are labelled.

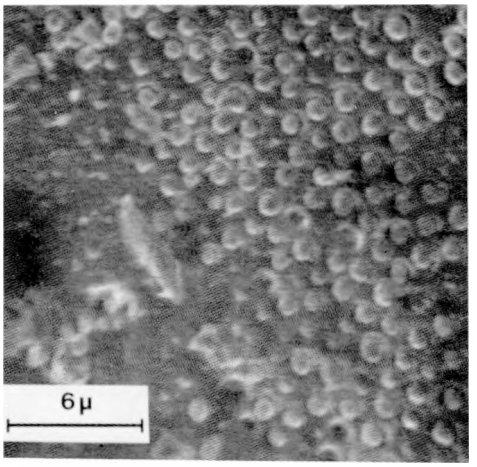

Figure 3: High magnification view of interior of air bubble in Figure 2 showing small bitumen droplets at the air/water interface.

Clearly, a complete understanding of the phase inversion process during bitumen extraction will involve an appreciation of the fundamental structure of the bitumen, air and water interfaces at a microscopic level. Another factor in determining processability is the presence of iron compounds and in particular, iron hydroxides and iron carbonates [1,8,9]. Studies with field samples were supplemented with the study of model emulsions in order to isolate the effect of iron compounds from fine clays and changes in bitumen composition. In these model emulsions it was possible to identify chemical differences at the interface [1,6]. Figures 6, 7 and 8 illustrate this when iron (III) is added to a model emulsion system. It is possible to directly observe the iron concentrated at the emulsion interface. Similar studies applied to

emulsions formed during oil sands extraction will allow one to evaluate the relative importance of clays or other minerals in determining oil sands processability.

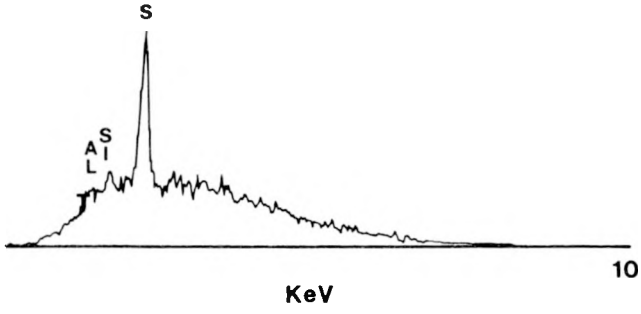

Figure 4: X-ray spectra of the dispersed bitumen phase with 10 KV incident electron energy. The sulphur peak is typical of bitumen and heavy oils.

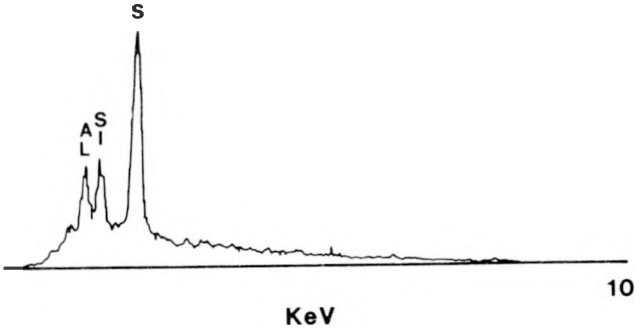

Figure 5: X-ray spectra of the dispersed bitumen phase in Figure 3 at 15 KV incident electron energy. With a higher incident electron energy, the x-ray signal is excited from deeper in the sample and in this case shows that there are significant clays in the water phase or at the bitumen/water interface.

The size distribution of the dispersed phase is important in determining many processing efficiencies. For instance, the final separation of water from the bitumen is often accomplished using centrifugation. If the droplet size is less than about one micron, the density difference between the bitumen and water and the residence time in the centrifuge is not sufficient to separate the phases. In the secondary flotation process, where gas is introduced to facilitate the separation of bitumen from the water and clays, the optimum efficiency is obtained when the bitumen droplets are smallest. The size of the middlings droplets are a function of the reagent added in the primary flotation step and often maximizing yield of the primary bitumen product does not correspond to the optimum droplet size for further processing of the middlings. A trade off might be necessary in order to optimize total bitumen yield. Optical microscopy coupled with automated image analysis can be used to quantify the bitumen size distributions produced with different reagents at different concentrations. Figure 9 shows a typical field of view for a middlings sample when no reagents are used to enhance the bitumen recovery. At various reagent concentrations, the size distribution of the bitumen phase in the middlings can be quantified by observation of many fields of view.

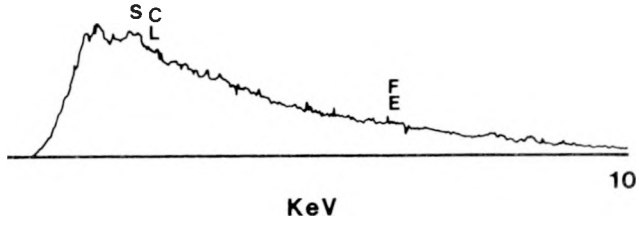

Figure 6: X-ray spectra of the continuous water phase in the model emulsion prepared with iron chloride. The spectra is quite featureless except for the brehmstrahlung background.

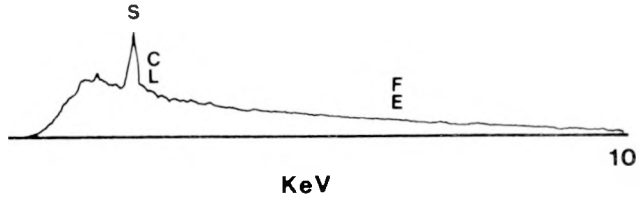

Figure 7: X-ray spectra of the dispersed oil phase in the model emulsion. The sulphur peak typical of these bitumens is clearly evident.

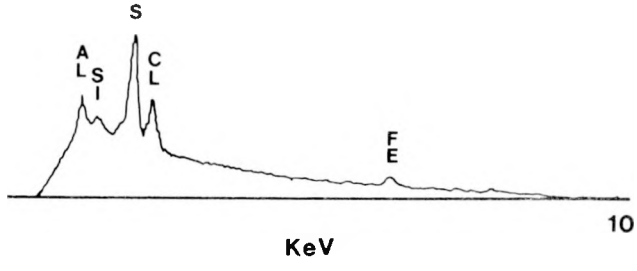

Figure 8: X-ray spectra of the interface between the oil and water phases of the model emulsion. Iron is evident at this interface but not in either of the two phases. The chlorine is in the emulsifier and also appears at the interface but not in the bitumen or water phases.

In the middlings produced from oil sands in which the bitumen was extracted from the oil sand with water only (82°C), a mean diameter of 2.2 microns was determined for the middlings bitumen (Figure 9). The addition of sodium pyrophosphate instead of sodium hydroxide can enhance bitumen recovery because of the different mechanism for bitumen removal. In simple terms, the sodium pyrophosphate can be

thought of as a complexing agent for the multivalent metal ions which can bridge the oil and mineral phases. Sodium hydroxide, on the other hand, acts by forming surfactants with some of the organic components[10,11,12,13]. At a sodium pyrophosphate concentration of 0.024 mg/g oil sand, the mean droplet diameter in the middlings did not change compared to the control trial. A subsequent experiment with a reagent concentration of 0.24 mg/g oil sand produced a dramatic increase in the mean droplet diameter to 6.2 µm. Further increase in the reagent concentration to 2.4 mg/g oil sand produced oil droplets of 2.1 microns which again is not significantly different compared to the control experiment. The peak in the middlings droplet size distribution is likely due to a competition between the complexing action of the sodium pyrophosphate and changes in pH which influence surfactant formation and double layer interactions.

This behaviour indicates that careful attention should be paid to the relationship between primary froth yield and secondary froth yield in order to maximize total bitumen extraction efficiency.

The complex interactions between the bitumen, water, clay and other mineral components (in particular iron carbonates and hydroxides) not only lead to carry over of water with the bitumen product, but just as importantly, to loss of bitumen with the tailings streams. A particularly difficult component of the oil sands processing tailings stream is the sludge. Sludge is a very stable, very difficult to dewater, combination of water, clays, and bitumen (roughly 70/28/2). High iron content in the sludge minerals relative to the oil sands feed indicates that iron compounds are bridging the organic and mineral and water components. A popular theory of sludge structure is the so-called card house where the three dimensional structure helps to trap water and prevent consolidation of the sludge minerals. The direct observation techniques which have been used in the study of oil sands processing streams can also be applied to the sludge component of the tailings stream.

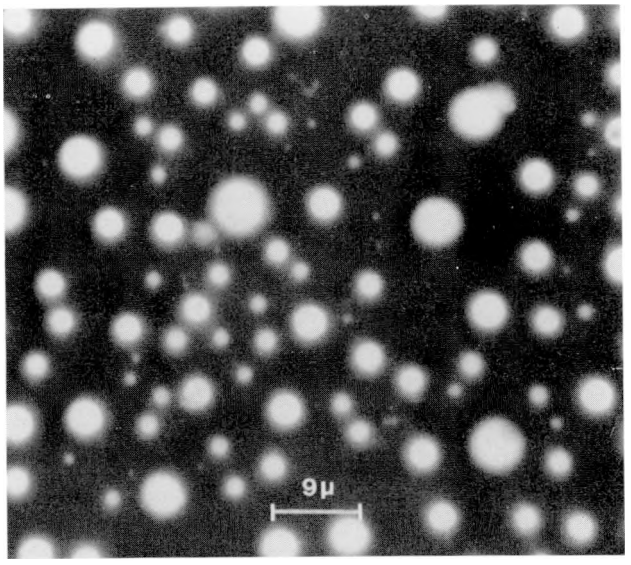

Figure 9: Photomicrograph under blue light of bitumen dispersed in the middlings. This is the control run with no reagent added, mean droplet diameter = 2.2µm.

It is possible to slowly sublime the ice component from the sample without disturbing the underlying clay/bitumen morphology. Figure 10 shows a sludge sample which, after sublimation, reveals the highly structured relationship between the clays and bitumen components.

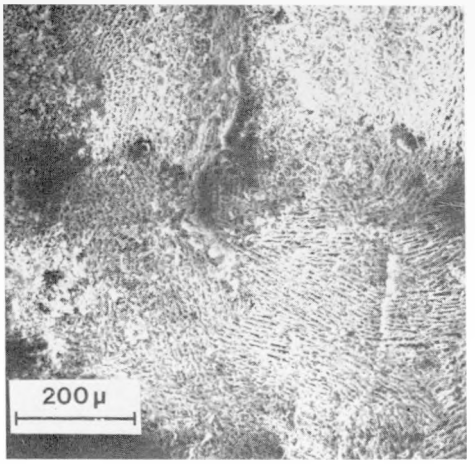

Figure 10: The card house structure of oil sands tailings sludge revealed after sublimation of a frozen fractured sample.

An economic means of dewatering and consolidating this oil sands sludge is vital to the future development of the oil sands resource. Tailings ponds currently occupy over 23 square kilometers and it is the stability of the sludge which is preventing reclamation of these ponds. An understanding of the chemical and physical nature of the sludge is vital to the ultimate solution to the sludge build up in the tailings ponds.

Summary

SEM and OM techniques are complimentary, both in the size regime which they can easily resolve and in the nature of the compositional information. The SEM is useful in characterizing the mineral components when working with frozen hydrated samples and direct observation, whereas the optical microscope can characterize the organic components when using blue incident light and observing the fluorescence of the organic phase.

Optimizing extraction processes involves an understanding of the complex interactions between the bitumen, minerals and water phases. Improvements in primary flotation yield may hinder efficient separation in the secondary flotation circuit or increase sludge volumes. An understanding of the interactions and definition of the system on a fundamental level is the only way to efficiently improve the total extraction process.

Microscopy has applications in characterization of samples from feed to refined product in oil sands processing streams. The simple size distribution of the

dispersed phase in these emulsion systems reveals important clues as to the ultimate processing behaviour of a given oil sands feed.

This information coupled with the ability to characterize mineral components, and in particular those which are active at the emulsion interface, will allow one to predict and ultimately improve oil sands processability.

Acknowledgment

The authors are grateful to K.C. McAuley and M.A. Hewlett for their contribution in preparing the photomicrographs.

References

1. R. J. Mikula, V. A. Munoz and W. W. Lam, "Microscopic Characterization of Oil Sands Processing Emulsions", Fuel Science & Techn. Int., 7 (5-6), 727-749, 1989.
2. W. B. Bald, "The Relative Efficiency of Cryogenic Fluids Used in the Rapid Quench Cooling of Biological Samples", J. Microscopy, 134, 261-270, 1984.
3. W. B. Bald and A. W. Robards, "Supercritical Nitrogen - The Optimum Coolant for Cryofixation", Proc. 11th Int. Congr. on Electron Microscopy, Kyoto, 1986.
4. A. W. Robards and Sleytr, U.B., "Low Temperature Methods in Biological Electron Microscopy", in Practical Methods in Electron Microscopy, A. M. Glauert, ed., Vol. 10, Elsevier 1985.
5. R. J. Mikula, "Application of X-ray Microanalysis to Tar Sands Emulsions", Colloids Surf., 23, 267-271, 1987.
6. R. J. Mikula, "Chemical Characterization of an Oil/Water Emulsion Interface via Electron Microscope Observation of a Frozen Hydrated Sample", J. Colloid Interface Sci., 121(1), 273-277, 1988.
7. Sanford, E. C., "Processability of Athabasca oil sand: Interrelationship between oil sand fine solids, process aids, mechanical energy and oil sand age after mining", Can J. Chem Eng., 61:554-565, 1983.
8. Kotlyar, L. S., Sparks, B. D., and Kodama. H., "Some chemical and mineralogical properties of fine solids derived from oil sands", AOSTRA J. Res., 1(2):99-106, 1984.
9. Yong, R. N. and Sehti, A. J., "Mineral particle interaction control of tar sand sludge stability", J. Can. Pet. Tech., Oct.-Dec., 76-82, 1978.
10. Greenland, D. J., "Interactions between humic and fulvic acids and clays", Soil Sciences, 3:34-41, 1971.
11. Pickering, W. F. "Selective chemical extractions of soil components and bound chemical species", CRC Critical Reviews in Analytical Chemistry, 12:233-266, 1981.
12. Kotlyar, L. S., Sparks, B. D., and Kodama, H., "Effect of sodium pyrophosphate treatment on the separation of organic compounds from agglomerated oil sands solids", Fuel, 65:1221-1225, 1986.
13. Kotlyar, L. S., Sparks, B. D., Kodama, H., and Grattan-Bellew, P. E., "Isolation and characterization ogf organic-rich solids present in Utah oil sand", Energy and Fuels, 2:589-593, 1988.

Examination of Wet- and Dry-Sieved Eastern Oil Shale and Microbial Reduction in Its Sulfur Content

by

E.J. Krieger, R.M. Pfister, and J.R. Ridge
Department of Microbiology
The Ohio State University
Columbus, Ohio 43210-1292

Abstract. Eastern oil shale represents a large source of potential energy. However, the relatively high amount of sulfur and nitrogen it contains renders widespread oil production from this source economically and environmentally unfeasible. Therefore, it would be useful to develop biological methods to reduce the amount of these elements in the shale prior to processing. A variety of microorganisms have been enriched from crushed Indiana New Albany oil shale in defined media limited with respect to available sulfur and/or nitrogen. Analyses of freshly ground shale in an electron microscope have indicated the presence of a relatively high number of microorganisms and particles of various sizes. Greater than 70% of the fractions of freshly ground and beneficiated shale collected by common dry-sieve sizing are larger than 325 mesh, whereas when wet-sieved, > 70% of the fractions are smaller than 325 mesh. The samples of -325 mesh shale particles have a significantly higher concentration of sulfur than larger particles as determined using an energy dispersive x-ray fluorescence spectrometer. Treatment of ground shale with 5.0 M HNO_3 results in 50-80% reduction of sulfur present correlated to particle size. Exposure of pretreated shale to a mixed culture inoculum results in approximately 5-12% further reduction in sulfur depending on particle size and medium composition.

Introduction

The large deposits of Devonian oil shale in the Eastern United States represent a substantial source of potential energy. Surface-mine accessible deposits are present in Alabama, Indiana, Kentucky, Michigan, Ohio, and Tennessee.[14] It has been proposed that the most efficient method of converting the organic material, kerogen, to a final synthetic liquid fuel product is pressurized fluidized-bed hydroretorting (PFH). This technique differs from other retorting methods in that it operates at an elevated pressure and hydrogen is consumed in the process.[14] Therefore the economic feasibility of utilizing Eastern oil shale as an energy source can be enhanced by minimizing the amount of hydrogen consumed and by reducing the amount of process steps which must be accomplished under high pressure.

By lowering the amount of sulfur and nitrogen present in the feed shale the amount of hydrogen consumed in the production of hydrogen sulfide and ammonia is reduced. Removal of these elements prior to retorting also reduces the requirement for pressurized removal systems associated with the PFH process. These systems would be necessary to protect the environment from release of such gases. A significant amount of the pyritic sulfur can be removed by beneficiating the raw shale. The separation and recovery of the organic portion from the inorganic material in this process requires very small particles be suspended in water as a slurry (Pressurized Fluidized-Bed Hydroretorting of Eastern Oil Shales, a technical proposal presented by the Institute of Gas Technology, Chicago, IL to the U.S. Department of Energy). This feedstock would be in a form amenable to microbial processing to reduce the residual organic sulfur and nitrogen content prior to PFH. Studies have shown that a variety of microorganisms are capable of degrading several different sulfur containing compounds which have been chosen as representative of the organic sulfur moieties found in coal.[1,5-12,15] Also it has been demonstrated that microbial communities exist inside hard substrata such as sandstone, quartz and limestone.[2,3,4] Therefore, this research has been directed at isolating organisms from an Indiana New Albany oil shale and developing techniques to gain physical and chemical information about that substrate before and after various experimental treatments.

Materials and Methods

The enrichment medium used to isolate microorganisms from handground Indiana New Albany oil shale consisted of (g/l): glucose, 5.0; $NaC_2H_3O_2$, 5.0; $NaNO_3$, 2.0; $NaSO_4$, 2.0; tryptophan, 1.0; lysine, 1.0; CaCl, 0.25; $FeCl_3$, 0.25; MgCl, 0.25; $MnCl_2$, 0.25; $NaMoO_4 \cdot 2H_2O$, 0.025, and ZnCl, 0.25. The buffer system used to prepare this medium at pH 5, 6, 7, or 8 was comprised of 0.125M KH_2PO_4 and 0.187 M Na_2HPO_4 in appropriate ratios. Sulfur-free (S-free) and nitrogen-free (N-free) media were prepared by excluding the $NaSO_4$ or the $NaNO_3$, tryptophan and lysine. The plating medium was either a formulation of the above with 16.7 g agar (Difco) added per

liter or Nutrient Agar (Difco, Detroit, MI). Organisms were Gram-stained and examined using standard microbiological techniques.

The National Institute of Occupational Safety and Health (NIOSH) method of asbestos fiber analyses by transmission electron microscopy (TEM) was modified to observe and measure the size of shale particles and microorganisms associated with shale and coal.[13] The particles were prepared for observation by suspending 1.5 mg shale samples in double distilled water and filtering them through a Millipore type DA membrane filter (0.65 μm pore size, 25 mm diameter) in a glass Millipore vacuum filtration apparatus. Circular portions of the filters were cut out using a #4 cork borer and these were affixed to glass microscope slides with ringbinder adhesive rings. The slides were placed on acetone-soaked Jaffee wicks in glass petri dishes for approximately 10 minutes or until the filters became clear. The samples were then coated with pure carbon in an Edwards E306A high vacuum evaporator. A portion (1/4) of the carbon coated filter was placed upside down onto 200 mesh copper EM grids which had previously been overlayered with collodion support film and coated with carbon. The grids were placed into an acetone distillation column bath for 2 hrs to dissolve and wash away the cellulose filter. The grids were observed by TEM in a Zeiss 10 equipped with an ORTEC energy dispersive X-ray fluorescence spectrometer (EDXS). The modified NIOSH method allows for microorganisms associated with the particles to be quantitated by direct count in the TEM, which is the accepted method for enumerating asbestos fibers in a sample. The number of cells per 10 openings in each grid were counted. The dimensions of approximately 100 randomly selected particles visible on the EM grid were measured using a Zeiss videoplan computer attached directly to the Zeiss EM 10 which calculated the particles' average length, width, and area.

Particle surfaces and associated microorganisms were observed by scanning electron microscopy (Hitachi S500 SEM). Sections of microscope slides were affixed to SEM stubs with colloidal silver paint. The shale particles were suspended in double distilled water, a drop of which was placed onto the glass slide and allowed to air dry. These were then sputter coated with gold in a Technics Hummer III coating device.

The Indiana New Albany Shale in all experiments was either handground with a mortar and pestle or crushed in a Spex stainless steel ball mill for approximately 2 minutes. The beneficiated Indiana New Albany oil shale was obtained from the Mineral Resource Institute at the University of Alabama through the Institute of Gas Technology, Chicago, Illinois. The Meigs Creek #9 coal samples were handground in a mortar and pestle. The particles were separated with respect to size by passing them through a stack of standard sieves either dry with physical agitation or rinsed with double distilled water. The sieves were 100, 200 and 325 mesh with pore openings of 149 μm, 75 μm, and 45 μm, respectively. The fractions collected were designated as +200 (-100/+200), -200 (-200/+325) and -325 mesh.

The elemental composition of bulk shale samples was determined using a Tracor Spectrace 4050 energy dispersive X-ray fluorescence spectrometer (EDXS). The dry shale samples for these analyses were approximately 1.0 g and ground to uniform texture. The spectra were collected with the following low or high energy parameters (low/high): 12/45 KV tube voltage, 0.15/0.20 mA tube current, none/#5 filter, 10/20 KEV maximum energy, and 100/100 seconds live time. The percentage of sulfur present in these bulk samples was also quantitated using the EDXS. This technique required sulfur standards composed of, or contained within, a matrix similar to shale. Therefore, since the percentage of sulfur for the MH-6 shale sample obtained from the Mineral Resource Institute (University of Alabama, Tuscaloosa, AL) had already been determined by accepted analytical techniques, that quantity was used as the base value to which flowers of sulfur was added to develop standards containing 0.8 to 10.0% sulfur. The parameters for the standards and quantitative sulfur analyses were as follows: 12 KV tube voltage, 0.20 mA tube current, no filter, 10 KEV maximum energy and 50 seconds live time. Each sample was analyzed three times and the % S values reported represent an average of the three results.

Pretreatment experiments were conducted by collecting counts corresponding to the K(α) line energies of various elements with the EDXS at low and high energy levels for representative samples of the bulk shale before treatment. The ground shale (+200 and -200 mesh dry sieved) was placed into and shaken with 5.0, 1.0 and 0.5 M HNO_3 or NaOH; 100 mM on 100 μm EDTA; or double distilled water at a ratio of 1.0 g shale to 100 ml solvent for 1, 24 and 60 hours. The shale was recovered by centrifugation after each time period (10 minutes at 4,500 rpm's), rinsed twice and dried overnight at 80°C. The samples were then stirred and/or gently crushed to restore the mixture to its original form, weighed and transferred to sample holders for the EDXS. The shale samples were all analyzed under conditions identical to those employed prior to incubation.

Various inocula were applied to pretreated ground shale samples. In all experiments, the shale was pretreated with 5.0 M HNO_3 for 4 hours and the harvested shale was rinsed until the final supernatant was at pH 3.5-4.0. The percentage of sulfur was established using the EDXS for each sample before and after pretreatment. In the first set of experiments the inoculum was prepared by placing colonies of the Indiana New Albany oil shale isolates into 20 ml sterile physiological saline, centrifuging the suspension and resuspending the resulting pellet in 15 ml sterile saline. The CFUs/ml were determined by standard dilution and spread plating techniques using plate count agar (PCA, Difco). Two flasks containing 100 ml S-free medium at each temperature and pH combination (pH 6 at 35°C; pH 7 and 8 at 25°C and 35°C) had the pretreated -100/+200 or -200/+325 mesh (dry-sieved) shale samples added. One each of these flasks had 1.0 ml of the inoculum added and the other was an uninoculated control. After 7 days incubation, the CFUs/ml for each flask were determined, the shale harvested by centrifugation, dried and analyzed with the EDXS. The inoculum for the next set of experiments was 1.0 ml of the supernatant from the previous experiment which contained a +200 mesh shale sample, had an inoculum added and was incubated at pH 7 and 25°C. Two test flasks and 2 control flasks for each size shale (-100/+200 and -200/+325 mesh dry-sieved) containing 100 ml S-free medium at pH 7 were prepared. The test and control flasks each contained a shale sample and 1.0 ml of the inoculum was added to the test flasks. All flasks were incubated for 18 days at 25°C on a rotary shaker. The shale was recovered by filtration (Whatman #4), dried overnight at 80°C and analyzed with the EDXS. In the next experiments, the S-free medium without sodium acetate was amended with either glucose or glycerol (0.5% w/v) or had no carbon source added. Two test flasks and two control flasks containing 1.5 g pretreated -325 mesh (wet-sieved) shale and 100 ml nutritionally amended S-free media (pH 7.0) were prepared. The inoculum added to the test flasks was from the same source and prepared in the same manner as that described for the previous experiment. The flasks were incubated at 25°C for 18 days on a rotary shaker. The shale was recovered by filtration

(Whatman, 0.45 μm pore opening, cellulose nitrate), dried overnight at 80°C and analyzed in the EDXS. For the next experiment, a second mixed starter culture was developed as previously described for the initial inoculum. A 1.0 ml aliquot of the inoculum was added to each of 5 flasks containing 100 ml sterile S-free medium (ph 7.0) amended with glycerol. Each of two of these flasks had a 1.0 g wet-sieved +200 or -325 mesh shale sample added to it. The fifth inoculated flask had a 1.0 g sample of -200 mesh pretreated wet-sieved shale. Three flasks, each containing the same medium as the test flasks and either a 1.0 g sample of +200, -200, or -325 mesh pretreated wet-sieved shale were not inoculated. After 20 days incubation at 25°C on a rotary shaker, plate counts were done and the shale was recovered by filtration as describe above, dried overnight at 70°C and analyzed in the EDXS under the same parameters as when run prior to pretreatment and incubation.

Results

A list of the Gram reactions and morphologies of microorganisms isolated from Indiana New Albany oil shale is given in Table 1. The most prevalent types of microorganisms were Gram-positive cocci. The average percentage weight recovered of +200, -200 and -325 mesh fractions collected after dry- and wet-sieving handground or wet-sieving beneficiated Indiana New Albany oil shale is presented in Table 2. More than 70% of the handground shale was retained by the 200 and 325 mesh sieves when dry. However, more than 70% of the handground and approximately 90% of the beneficiated was washed through the -325 mesh sieve with water. Figure 1 contains scanning electron micrographs of the three different sized fractions collected by wet-sieving. Figure 2 contains electron micrographs (TEM) of shale and coal particles with the microorganisms associated with those materials visible. The numbers of microorganisms in samples of wet-sieved shale and coal particles, determined by direct count in the TEM, are presented in Table 3. The Indiana New Albany oil shale and the Peabody coal samples were determined to contain 4.0×10^{10} cells per gram, respectively. This was calculated as follows:

$$\#\text{ of cells/g particles} = \frac{\text{ave \# cells}}{\text{1 grid opening}} \times \frac{\text{1 grid opening}}{\text{area of grid opening}} \times \frac{\text{area of filter}}{\text{1 filter}} \times \frac{\text{3 filters}}{\text{total grams particles}}$$

where the area of 1 grid opening was 0.005 mm^2, the area of 1 filter was 201 mm^2 and the total grams of particles applied to the filters were 0.0015 g. Listed in Table 4 are the average length, width, and area of particles in wet-sieved fractions of ground Indiana New Albany oil shale determined using TEM. The average area of a particle in wet-sieved samples determined to be +200, -200, or -325 mesh was 1.38, 0.532, or 0.265 mm^2, respectively. The average percentage of sulfur in dry- and wet-sieved handground or wet-sieved beneficiated Indiana New Albany oil shale is presented in Table 5. The fraction of handground shale which would not pass through the 200 mesh sieve when dry contained 3.642% sulfur whereas the fraction which was retained by this sieve when washed through contained only 3.299% sulfur. The smallest sized particles collected by dry- and wet-sieving handground shale contained very similar amounts of sulfur, 3.821% and 3.872%, respectively. The +200 mesh wet-sieved beneficiated samples contained 2.993% sulfur and the -325 mesh beneficiated samples contained 3.355% sulfur.

Listed in Table 6 is the percent decrease of several elements in ground (dry-sieved) Indiana New Albany oil shale after various chemical pretreatments for 60 hours. The percentage of decrease in sulfur content was calculated as follows:

$$\%\text{ decrease} = \frac{(\text{ave. \% S or ave. \# counts})_{initial} - (\text{ave. \% S or ave. \# counts})_{final}}{(\text{ave. \% S or ave. \# counts})_{initial}}$$

The 5.0 M HNO_3 treatment for 60 hours removed 70-75% sulfur and iron and 80-84% calcium. Whereas the 5.0 N NaOH treatment for the same length of time removed 58-66% sulfur but apparently no iron and only 16-27% calcium. The double distilled water and EDTA treatments resulted in removing much lower amounts of these elements. After 1 hour treatment with 5.0 M HNO_3 (data not shown), 67-72% sulfur, 70-73% iron and 81-84% calcium were removed. However, after 1 hour treatment with 5.0 N NaOH (data not shown), only 15-20% sulfur, negligible amounts of iron and 16-20% calcium were removed. Figure 3 represents spectra collected with the EDXS from a sample of dry-sieved -200 mesh shale before and after the 60 hour treatment with 5.0 M HNO_3. In addition to the elements listed in Table 6 and labelled in Figure 3 (Si, S, K, Ca, Mn, Fe, Zn, As), the following elements have been demonstrated by these analyses to be present: Ti, V, Ni, Cu, Sr, Y and Mo. The results from the experiments in which a mixed inoculum of shale isolates was incubated with 5.0 M HNO_3 pretreated shale (+200 and -200 dry-sieved) are presented in Table 7. The pretreatment resulted in a 56.4% and 57.3% decrease in the sulfur content of the +200 and -200 mesh shale samples, respectively. The largest further reduction in sulfur was 9.5% which occurred in the +200 mesh sample in the pH 7.0 inoculated flask incubated at 25°C. Reductions of 7.4% and 7.9% sulfur were observed in the -200 mesh samples incubated after inoculum was added at 25°C in pH 7.0 and 8.0, respectively. The results from the experiment in which an inoculum derived from the initial mixed cultures experiment are presented in Table 8. The +200 and -200 mesh dry-sieved samples were pretreated in 5.0 M HNO_3 resulting in 55.2% and 56.7% reduction in sulfur content. The average percent decrease for the +200 mesh controls and test samples was 4.46 (± 1.55) and 7.06% (± 0.156), respectively. The -200 mesh controls showed a 5.44% (± 1.15) average decrease and the test samples a 12.6% (± 2.26) average decrease. The results from the nutrient amendment experiments are listed in Table 9. The pretreatment of the -325 mesh wet-sieved shale with 5.0 M HNO_3 resulted in a 54.9% reduction in sulfur content. After 18 days incubation, the reduction in the percent sulfur in the shale from the test flasks amended with glucose or glycerol was decreased by 8.51% and 6.71% or 9.10% and 5.11%, respectively. However, the decrease in the percent sulfur of the shale from the control flasks was only 3.33% and 1.21% or 1.99% and 1.92%, respectively. There appeared to be no significant decrease in the average sulfur content of the shale from the test flasks without an added carbon source as compared to the shale from those control flasks. The results of the experiment in which mixed culture inoculum developed from the original Indiana New Albany oil shale isolates are listed in Table 10. The percent decrease in sulfur content of the +200, -200 and -325 mesh wet-sieved samples as a result of pretreatment were 50.4, 50.5, and 56.3%, respectively.

The shale from the inoculated flasks after 20 days incubation showed the following percentages of decrease with respect to sulfur: +200, 5.96 and 2.80%; -200, 8.73%; -325, 6.50 and 6.00%. The uninoculated controls for the three size fractions showed less than 1% reduction in sulfur. The electron micrograph (SEM) in Figure 4 shows shale particles coated with microorganisms following incubation with a mixed culture inoculum.

Discussion

A large number and variety of microorganisms are present in the Indiana New Albany oil shale and Peabody coal samples examined. Although a significant number have been isolated from the shale and coal (data not shown) in our enrichment protocols, it is likely that there are organisms present which may not be viable or are viable but not culturable by our methods. The TEM technique developed to enumerate microorganisms by direct count has provided data to support these ideas. The shale and coal samples were determined to have approximately 10^{10} cells/g present, however, when aliquots of the sterile water used to wet-sieve the samples were spread plated, only 10^6 cells/g were observed.

Approximately 40% of the shale particles which were unable to pass through the -325 mesh screen when dry were able to be washed through with water. This suggests that smaller particles remain associated with one another or with larger particles when handled dry, but become dissociated when suspended in water. The beneficiated material which was prepared by a process involving suspension in water appeared to be comprised mainly of particles smaller than -325 mesh. The TEM technique for particle analysis also provided information concerning the actual size of the particles in the wet-sieved samples. The areas of the +200, -200, and -325 mesh particles were calculated to be 1.38, 0.532, and 0.265 mm^2, respectively. The large standard deviations associated with these figures are due to the fact that in randomly selecting the more than 100 particles to measure, a few uncharacteristically small and/or large particles were included. If only the size ranges which included the majority (0.85%) of the particles, thereby excluding some of the infrequently measured sizes the area of the particles in each of the fractions were 0.012 to 3.05, 0.000 to 1.67, or 0.01 to 0.40 mm^2 (data not shown). In each case, a portion of the remaining 15% was an entire order of magnitude larger and their exclusion would greatly decrease the standard deviations associated with the size ranges reported.

Energy dispensive fluorescence spectroscopy is a very effective method to quantitate the percentage of total sulfur present in bulk shale samples as well as to identify and evaluate changes in a wide range of other elements which may also be of interest. It appears that the samples comprised of the smallest particles consistently contain the highest percentage of sulfur and that fraction of the beneficiated shale contains approximately 10-15% less sulfur than the handground shale.

Pretreatment of shale with 5.0 M HNO_3 resulted in greater than 50% reduction in sulfur content within the first hour. Treatment with 5.0 N NaOH required 60 hours of contact to remove approximately the same amount of sulfur. Since the iron content was also decreased by approximately the same amount as the sulfur when treated with 5.0 M HNO_3, we propose that this treatment is removing the pyrite present and the sulfur which remains is likely to be of an organic nature. We are currently developing iron standards for the EDXS which will enable us to determine if a decrease in iron is associated with the decrease in sulfur content which occurs after incubation with the mixed culture inoculum. If no further decrease in iron is seen, this would indicate that the microorganisms are removing organic sulfur and not pyritic sulfur.

The mixed culture experiments indicate that the consortium derived from Indiana New Albany oil shale can further reduce the amount of sulfur present in pretreated handground shale. Under our growth conditions, it appears that the highest reductions in sulfur occur at pH 7.0 and 25°C. The results also indicate that reduction in sulfur by this inoculum requires that the medium be supplemented with a carbon source and that no significant difference in sulfur removal is seen when either glucose or glycerol is added. As seen by SEM, microorganisms after inoculation and incubation coat the particle surfaces. Scanning electron microscopy has also been used to demonstrate that cells are present on the surfaces of freshly ground particles (micrographs not shown). Also, since uninoculated pretreated controls in these experiments result in 10^5 to 10^7 CFUs/ml and uninoculated pretreated controls with essentially no nutrients supplied supported 10^4 to 10^5 CFUs/ml, it appears that native shale contains, protects and supplies the necessary nutrients for a community of microorganisms.

There is a complex indigenous population of microorganisms present in oil shale and coal. Gaining further insight into its ecology and the physiology of the community's members will hopefully allow us to enhance the reductions in sulfur we've demonstrated. This type of information and the techniques we are developing can also be used in investigating other similar substrates.

References

1. Fedorak, P.M. and D.W.S. Westlake. 1983. Microbial degradation of organic sulfur compounds in Prudhoe Bay crude oil. Can. J. Microbiol. 29:291-296.
2. Fliermans, C.B. and D.L. Balkwill. 1989. Microbial life in deep terrestrial subsurfaces. Bioscience 36:370-377.
3. Friedman, E.I. 1982. Endolithic microorganisms in the Antarctic cold desert. Science 215:1045-1053.
4. Golubic, S., I. Friedman and J. Schneider. 1981. The lithobiontic ecological niche, with special reference to microorganisms. J. Sed. Petrol. 51:475-478.
5. Kargi, F. 1987. Biological oxidation of thianthrene, thioxanthene and dibenzothiophene by the thermophilic organism *Sulfolobus* acidocaldarius. Biotechnol. Lett. 9:478-482.
6. Kodama, K. 1977. Induction of dibenzothiophene oxidation by *Pseudomonas jianii*. Agric. Biol. Chem. 41:1193-1196.
7. Kodama, K., K. Umehara, K. Shimizu, S. Nakatani, Y. Minoda and K. Yamada. 1973. Identification of microbial products from dibenzothiophene and its proposed oxidation pathway. Agric. Biol. Chem. 37:45-50.
8. Kodama, K., S. Nakatani, K. Umehara, K. Shimizu, Y. Minoda and K. Yamada. 1970. Microbial conversion of petro-sulfur compounds. Part III. Isolation and identification of products from dibenzothiophene. Agric. Biol. Chem. 34:1320-1324.
9. Laborde, A.L. and D.T. Gibson. 1977. Metabolism of dibenzothiophene by a *Beijerinckia* species. Appl. Environ. Microbiol. 34:783-790.
10. Monticello, D.J., D. Bakker and W.R. Finnerty. 1985. Plasmid-mediated degradation of dibenzothiophene by *Pseudomonas* species. Appl. Environ. Microbiol. 49:756-760.
11. Mormile, M.R. and R.M. Atlas. 1988. Mineralization of the dibenzothiophene biodegradation products 3-hydroxyl-2-formyl benzothiophene and dibenzothiophene sulfone.

Appl. Environ. Microbiol. 54:3183-3184.

12. Nakatani, S., T. Akasaki, K. Kodama, Y. Minoda and K. Yamada. 1968. Microbial conversion of petro-sulfur compounds. Part II. Culture conditions of dibenzothiophene-utilizing bacteria. Agric. Biol. Chem. 32:1205-1211.

13. NIOSH. 1979. "Physical and chemical analysis method 239," Natl. Inst. Occup. Safety and Health, USPH/NIOSH "Membrane filter method for evaluating airborne asbestos fibers," U.S. Dept. Health, Education, and Welfare.

14. Rajaram, V. 1985. Commercialization of eastern United States oil shales - a review. Mining Eng. 37:1381-1385.

15. Yamada, K., Y. Minoda, K. Kodama, S. Nakatani and T. Akasaki. 1968. Microbial conversion of petro-sulfur compounds. Part I. Isolation and identification of dibenzothiophene-utilizing bacteria. Agric. Biol. Chem. 32:840-845.

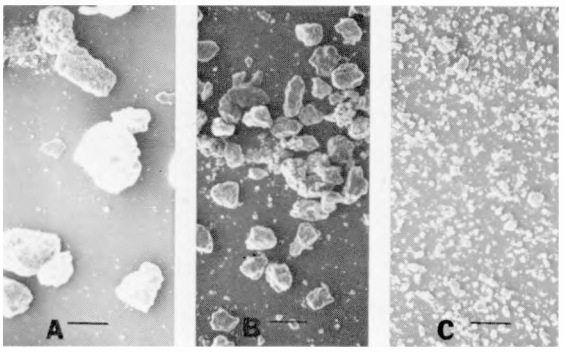

Figure 1. Scanning electron micrographs of shale particles which were determined by wet-sieving to be: (A) -100/+200; (B) -200/+325; and (C) -325 mesh (x 65, size bar = 100 μm).

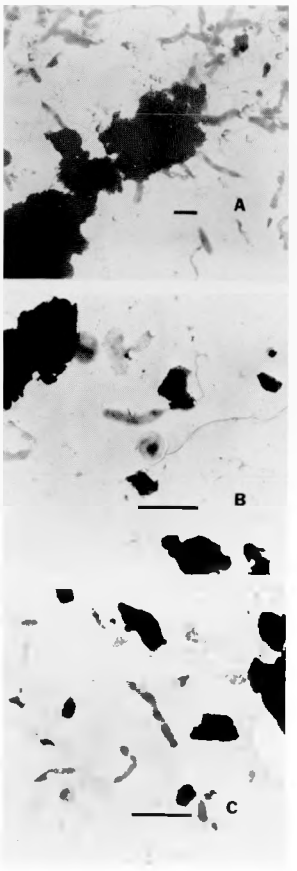

Figure 2. Transmission electron micrographs showing various microorganisms associated with freshly ground Indiana New Albany Oil shale (A: x 3150, size bar = 2 μm) and Peabody coal (B and C: x 8000, size bar = 2 μm).

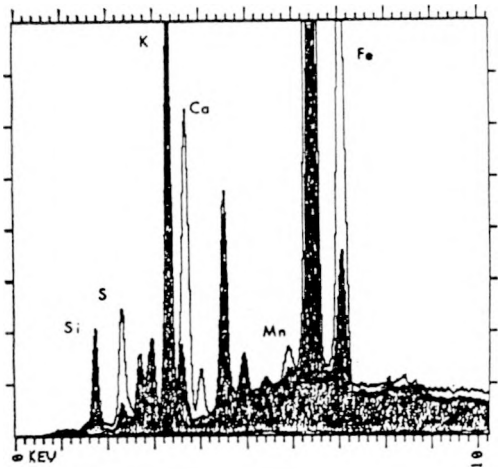

Figure 3. Two spectra obtained using an energy dispersive x-ray fluorescence spectrometer to analyze a sample of -200 mesh, dry-sieved Indiana New Albany oil shale before (unshaded spectrum) and after (shaded spectrum) pretreatment for 60 hours with 5.0 M HNO_3.

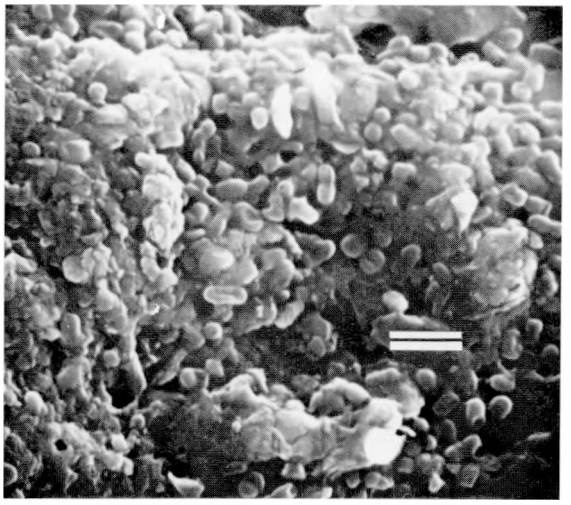

Figure 4. Scanning electron micrograph of pretreated shale particles coated with microorganisms following incubation with a mixed culture inoculum (x 6000, size bar = 2 μm).

Table 1. The Gram stain reaction and morphologies for 16 microorganisms isolated from Indiana New Albany oil shale.

Isolate	Gram Reaction	Morphology
1	+	cocci in clusters
2	+	tiny cocci, pairs, short chains, clusters
3	-	small coccobacilli, pairs, short chains, clusters
4	-	rods, chains
5	-	rods, long chains with sheaths
6	+	tiny cocci, pairs, chains, clusters
7	+	cocci, pairs, short chains
8	+	cocci/oval, pairs, short chains
9	-	coccobacilli, short chains
10	+	cocci, short chains (flattened at junctions)
11	+	rods with spores
12	+	cocci, pairs, tetrads
13	+	coccobacilli, pairs, tetrads, clusters
14	-	rods (curved)
15	-	short rods, pairs
16	+	coccoid, "coryneform"-like

Table 2. Average percentage of +200, -200, and -325 mesh fractions collected after dry- and wet-sieving handground or wet-sieving beneficiated Indiana New Albany oil shale.

Oil Shale	Average Percent Recovered		
	+200	-200	-325
HANDGROUND			
Dry-sieved	40.0	31.4	26.1
Wet-sieved	19.3	7.7	73.0
BENEFICIATED			
Wet-sieved	9.9	2.5	87.2

Table 3. Enumeration of microorganisms found in wet-sieved Indiana New Albany oil shale and Peabody coal by direct count in a transmission electron microscope.

Control	Average Cells/Grid Opening	Std. Dev.	# Cells/g
1	0.9	0.99	
2	1.5	1.43	
	$Average_{20}$ = 1.2	1.24	
SHALE			
+200	513.9	61.0	
-200	519.3	103.1	
-325	469.1	90.9	
	Average $_{30}$ = 500.8	86.8	4.0×10^{10}
COAL			
+200	119.7	21.0	
-200	121.6	32.2	
-325	166.0	22.6	
	$Average_{30}$ = 135.8	26.2	1.09×10^{10}

Table 4. The average length, width, and area of particles in wet-sieved fractions of ground Indiana New Albany oil shale determined using transmission electron microscopy.

Mesh Size	Average Length (μm)	Average Width (μm)	Average Area (mm^2)
+200 (101)[a]	21.1 (15.2)[b]	22.5 (14.0)	1.38 (2.30)
-200 (115)	11.9 (10.4)	12.3 (10.2)	0.532 (1.64)
-325 (106)	9.0 (7.6)	9.0 (7.4)	0.265 (0.566)

[a] Number of particles sized [b] Standard deviation

Table 5. Average percentage of sulfur in the +200, -200, and -325 mesh fractions collected after dry- and wet-sieving handground or wet-sieving beneficiated Indiana New Albany oil shale.

	Average % S	Standard Deviation
HANDGROUND		
Dry-sieved		
+200	3.642	0.0515
-200	3.821	0.1473
Wet-sieved		
+200	3.299	0.0654
-200	3.152	0.0980
-325	3.872	0.0705
BENEFICIATED		
Wet-sieved		
+200	2.993	0.0254
-325	3.355	0.0193

Table 6. The percent decrease of several elements in dry-sieved handground Indiana New Albany oil shale after various chemical pretreatments for 60 hours.

		% Decrease							
Treatment	Mesh Size	Si	S	K	Ca	Mn	Fe	Zn	As
5.0 M HNO_3	+200	9.3	73.8	1.9	83.8	29.5	75.0	87.0	67.6
	-200	5.5	69.9	---	80.6	23.1	73.0	78.7	63.4
5.0 N NaOH	+200	16.6	66.0	5.8	9.0	---	---	35.8	65.4
	-200	26.9	58.1	9.0	---	---	---	*	*
dd H_2O	+200	18.6	18.9	8.2	25.5	---	---	14.9	---
	-200	10.0	13.9	6.5	27.7	---	---	10.8	---
100 mM EDTA	+200	13.0	8.3	8.8	82.6	18.9	8.4	21.3	29.8

--- No apparent decrease * Data not available

Table 7. The percent change in the sulfur content of +200 and -200 (dry-sieved) Indiana New Albany oil shale before and after incubations with a mixed culture inoculum.

	Sample		% Change in Sulfur Content	
	pH	Temp	+200 Mesh	-200 Mesh
Test	6	35	-3.71*	+3.84*
	7	25	-9.45	-7.35
	7	35	+1.41	-2.88
	8	25	-2.41	-7.94
	8	35	-5.90	-2.44
Control	6	35	+0.57	-3.17
	7	25	-2.96	-6.07
	7	35	-0.56	+0.51
	8	25	+0.88	-5.42
	8	35	-0.19	-4.21

*"-" indicates an apparent decrease in sulfur

"+" indicates an apparent increase in sulfur

Table 8. The average % sulfur concentration of +200 and -200 mesh (dry-sieved) Indiana New Albany oil shale samples determined in an EDXS before and after incubation with a mixed culture inoculum. The S-free medium was pH 7 and the incubation temperature was 25°C.

	Initial		Final			
Test	Ave. % S	Std. Dev.	Ave. % S	Std. Dev.	CFU/ml	% Decrease
+200	1.598	0.029	1.487	0.032	1.9×10^{11}	6.95
	1.631	0.012	1.514	0.062	2.1×10^{10}	7.17
-200	1.679	0.043	1.495	0.075	1.2×10^{11}	11.0
	1.713	0.013	1.469	0.035	3.5×10^{11}	14.2
Control						
+200	1.623	0.019	1.533	0.057	$<10^5$	5.55
	1.635	0.027	1.580	0.040	7.7×10^9	3.36
-200	1.696	0.047	1.590	0.078	2.7×10^6	6.25
	1.687	0.037	1.609	0.072	4.2×10^7	4.62

Table 9. The percent sulfur in -325 mesh (wet-sieved) pretreated Indiana New Albany oil shale samples before and after 18 day incubation with a mixed culture inoculum in S-free medium (pH 7) altered with respect to carbon source.

		Before		After			
	Amendment	Ave. % S	Std. Dev.	Ave. % S	Std. Dev.	CFU/ml	% Decrease
Test	Glucose	1.574	0.0227	1.440	0.0159	2.6×10^{11}	8.51
		1.580	0.0242	1.474	0.0159	2.1×10^{10}	6.71
	Glycerol	1.573	0.0278	1.430	0.0337	1.2×10^{10}	9.10
		1.566	0.0228	1.486	0.0155	3.4×10^{11}	5.11
	None	1.569	0.0254	1.476	0.0261	3.8×10^{8}	5.93
		1.555	0.0155	1.491	0.0275	3.6×10^{8}	4.12
Control	Glucose	1.590	0.0268	1.537	0.0270	2.0×10^{3}	3.33
		1.564	0.0110	1.545	0.0292	1.0×10^{3}	1.21
	Glycerol	1.556	0.0280	1.525	0.0040	$<10^{3}$	1.99
		1.565	0.0175	1.535	0.0191	$<10^{3}$	1.92
	None	1.556	0.0165	1.520	0.0160	1.1×10^{4}	2.31
		1.592	0.0155	1.518	0.0327	2.6×10^{5}	4.65

Table 10. The average percent sulfur concentration of pretreated wet-sieved Indiana New Albany oil shale samples determined in an EDXS before and after incubation with a mixed culture inoculum. The S-free medium amended with glycerol was at pH 7.0 and the incubation temperature was 25°C.

	Initial		Final			
	Ave. % S	Std. Dev.	Ave. % S	Std. Dev.	CFU/ml	% Decrease
TESTS						
+200	1.661	0.0365	1.562	0.0095	1.4×10^{11}	5.96
	1.643	0.0352	1.597	0.0165	3.6×10^{10}	2.80
-200	1.616	0.0450	1.475	0.0232	4.0×10^{9}	8.73
-325	1.692	0.0459	1.582	0.0051	5.0×10^{10}	6.50
	1.650	0.0142	1.551	0.0116	3.7×10^{10}	6.00
CONTROLS						
+200	1.637	0.0261	1.623	0.0355	5.0×10^{5}	0.86
-200	1.620	0.0235	1.608	0.0080	$<10^{5}$	0.74
-325	1.671	0.0243	1.687	0.0295	6.7×10^{6}	$^{+}0.96$

Water-Jet Assisted Mechanized Oil Shale Mining Factory Tests

by

Wilhelm J. Kogelmann
Alpine Equipment Corporation
State College, Pennsyvania 16801
Edward D. Thimons
U.S. Bureau of Mines
Pittsburgh, Pennsylvania 15236
Joseph E. Virgona
U.S. Department of Energy
Grand Junction, Colorado 81502
L. Alan Weakly
Exxon Company, USA
Grand Junction, Colorado 81502

Abstract. The U.S. Department of Energy's Grand Junction Projects Office is participating in a $1.5 million Cooperative Agreement with Alpine Equipment Corporation/Astro International Corporation ("Alpine") of State College, Pennsylvania to evaluate the water-jet-assisted (WJA) mechanical cutting of oil shale under actual mining conditions. The cost of the 24-month, three-phase Technology Development Project, started in February 1988, is shared equally between Alpine and the Department of Energy. Alpine has designed and manufactured a standard-sized roadheader (boom-type continuous miner) for water-jet-assisted (WJA) factory cutting tests. This WJA rock miner is being used for testing of novel PDC "diamond" cutting tools and of high-pressure-water (HPW) components to be incorporated in a heavy-duty, high-production WJA mechanized mining machine. Field testing of the machine will be conducted in an underground oil shale mine located in the Piceane Basin of western Colorado. Additional support will be provided by the U.S. Bureau of Mines Pittsburgh Research Center and oil shale companies, through the Colorado Mining Association.

The novel PDC "diamond" bits (picks), especially the rotating "point-attack" bits with semi-round "domed" PDC inserts, showed excellent impact resistance and outstanding wear characteristics when compared to standard tungsten-carbide ("carbide") tools.

Water-jetting considerably reduced dust levels and increased tool life. However, the water-jets could not penetrate oil shale, a dense dolomitic limestone with kerogen, even at high water pressure and at low traversing speed (i.e. a slow cutter head rotation). No significant reduction of cutting forces through water-jet-assist was observed. In order to control dust and cool the cutter bits for increased tool life, a water pressure of up to 207 bar (3,000 psi) seems to be adequate. In order to further reduce pressure and thus water flow, the use of "through-flush" cutter bits is being investigated.

Introduction

When Alpine Equipment Corporation ("Alpine") commenced the design of a WJA oil shale mining machine laced with carbide bits (picks) and with novel polycrystalline diamond composite (also called "compound"), commonly abbreviated PDC, tools it was found that very little information was available in this field.

WJA Carbide Cutter Bits (Picks)

Available information on cutting with WJA carbide drag bits was derived from laboratory tests with extremely low cutting speeds, less than 0.5 m/s (100 fpm)[1]. Rock cutting machines such as roadheaders (boom-type continuous miners) have cutting speeds (peripheral bit tip speeds) in the range of 1.0 to 4.0 m/s (200 to 800 fpm). The cutting speeds of typical coal mining machines such as drum-type continuous miners (CMs) and shearers are between 2.0 and 4.0 m/s (400 to 800 fpm). Some cutting machines for the construction industry such as trenching and road-milling machines have bit tip speeds as high as 7.0 m/s (1400 fpm).

A limited amount of data was available for WJA cutting tests with a standard roadheader conducted by British Coal in a limestone mine in England[2].

These tests were conducted with a standard roadheader equipped with an in-line ("milling" auger) cutter head having only one cutting speed. Furthermore, this roadheader had no sumping (telescoping) cutter boom.

The available data were insufficient to provide the design parameters for a mining machine which was to investigate the potential of WJA cutting of oil shale.

PDC Cutter Bits Without WJA

Although rotary PDC drill bits are being widely and successfully employed, mainly in the petroleum industry, there was very little information published on cutting applications. Cutting tests with a shearer in coal, sandstone and shale at the Secunda Collieries in South Africa with radial PDC bits (14,000 bits; 2 million tons coal mined) were conducted. These tests showed that PDC "diamond" bits lasted nine times longer than carbide-tipped bits[3].

In laboratory cutting tests by the U.S. Bureau of Mines in hard and abrasive sandstone, radial PDC bits showed potential for 10 to 20 times longer lifetime than with standard conical carbide tools[4].

Water-Cooled PDC Rotary Drill Bits

At Unocal's Energy Mining Division Long Ridge Mine near Parachute, Colorado, a 89 mm (3.5 in.) diameter PDC bit drilled 27,614 m (90,600 ft.) and is still in use[5]. In comparison a conventional carbide bit of the same diameter has an average life of less than 150 m (500 ft.) before regrinding or reconditioning[6]. The average drill footage for PDC bits is 12,000 m (40,000 ft.). Thus, a PDC bit lasts some 80 times longer than a carbide tool. A PDC bit costs approximately 10 times more than a carbide bit. The PDC "diamond" cutters (blanks) constitute about 75% of the bit's costs.

Unocal reconditions their valuable PDC drill bits in-house. A PDC drill bit reconditioning process encompasses: the rotation of a PDC cutter to expose a new cutting edge, the replacement of a PDC cutter, or the rebuilding of a backing and replacement of a PDC cutter[6].

The PDC cutters of the drill bits at Unocal utilize air mist flushing. The excellent performance of PDC drill bits in oil shale inspired Alpine to introduce PDC "diamond" drag bits for rock cutting.

Information From Existing WJA Mining Machines

In order to provide for water-jet-assist, cooling of the bit tip, and for dust suppression (wetting of the crushing zone) the water-jet has to impinge exactly 1 to 2 mm (0.04 to 0.08 in.) ahead of the bit tip. A misaligned jet might even reduce the cutting efficiency of a bit. At cutting tests in England with 1,400 bar (20,000 psi) water-jets aimed ahead of the bit tip the cutting force increased when compared to cutting at lower water pressure. This seems to be caused by the jet's "hold-down" effect[7].

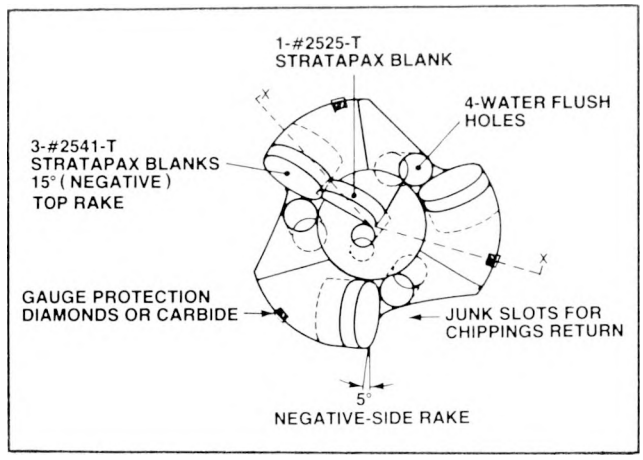

Figure 1. Excellent Performance of Rotary PDC PDC Drill Bits in Oil Shale Inspired Alpine to Introduce PDC "Diamond" Cutter Bits (Picks) for Rock Cutting.

Before Alpine commenced design of the WJA cutting system of its oil shale miner, existing WJA coal and rock mining machines were investigated. None of the machines had water-jets which could be adjusted (1) for manufacturing errors and wrong tolerances and (2) for wear of the carbide-tipped cutter bits.

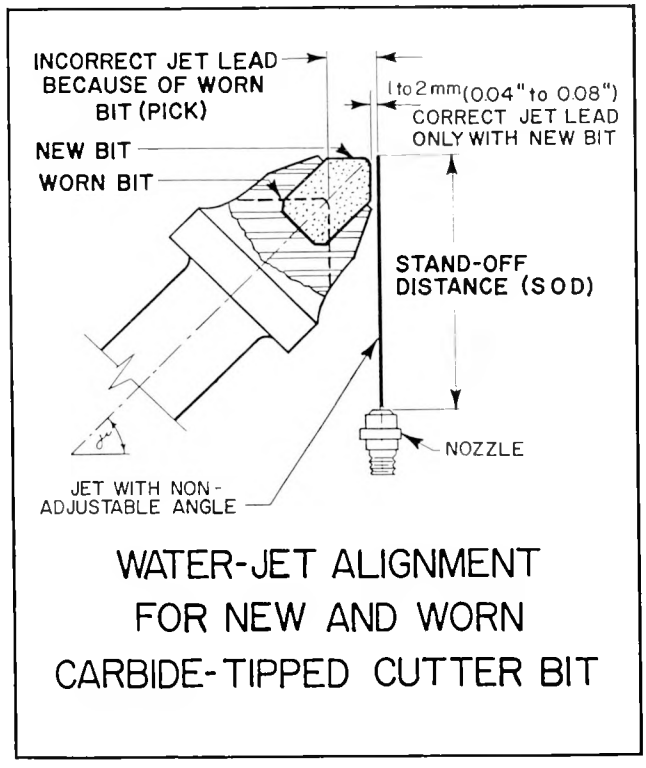

Figure 2. An Improperly Aligned Water-Jet Is Ineffective.

Figure 3. WJA Coal Shearer Eickhoff EW-200/170-L In a Longwall Installation Of The Auguste Victoria Colliery, Marl, Germany[7]. WJA Is Ineffective Because Misaligned Water-Jets Either Hit Bits (Picks) or Miss Proper Impingment Point at Face.

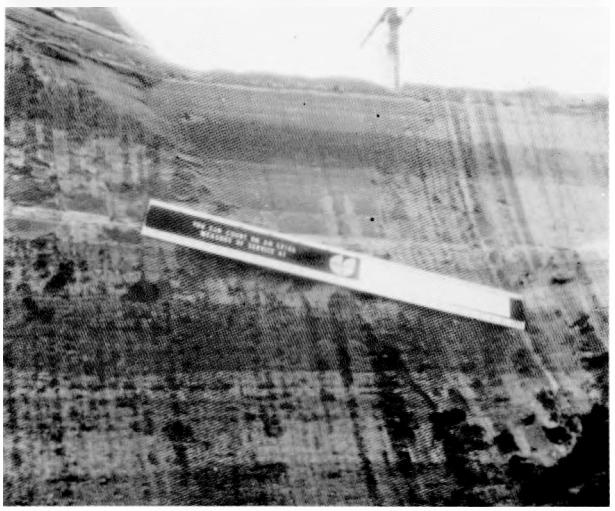

Figure 4. Artificial Face for Factory Cutting Tests Consisting of Oil Shale Boulders Cast into Lean Concrete.

Test Stand And Artificial Face

Eighteen metric tons (20 short tons) of oil shale boulders were shipped from Exxon's Colony mine in Colorado to Alpine's plant in Pennsylvania. These boulders were cast into lean concrete. The boulders were carefully placed so that their lamination planes were level thus matching the actual conditions in the mine.

Table 1: Specifications Of Oil Shale For Test Stand At Alpine's Factory

Item	Specifications
Source Of Mineral:	Colony Oil Shale Project Exxon Company, U.S.A. near Parachute, Colorado
Mineral:	Dolomitic limestone containing varying amounts of kerogen comparable to the Mahogany Zone of the Green River Formation.
Grade:	120 to 158 l/metric ton (30 to 38 gallons/short ton)
Density (in situ):	2.03 to 2.15 g/cm^3 (127 to 134 lb/ft^3)
Uniaxial (unconfined) compressive strength:	85.52 to 109.66 MPa (12,400 to 15,900 psi) Average 89.66 MPa (13,000 psi)
Tensile Strength:	Average 11.03 MPa (1,600 psi)

Instrumentation And Data Acquisition System

The WJA oil shale miner's functions are measured by 17 transducers and sensors which are monitored directly at (1) the operator's instrument panel and (2) a micro-computer based data storage and analysis system.

The data acquisition system is depicted in Figure 5.

WJA Roadheader For Factory Cutting Tests

Alpine modified a standard roadheader (boom-type continuous miner) for WJA cutting. The machine was equipped with custom-made components such as a sumping (telescoping) cutter boom with two types of transverse ("ripper") cutter heads and a novel, angle-adjustable water-jetting system.

Water-Jet Alignment

In order to provide for water-jet-assist, cooling of the tool, and for efficient dust suppression (wetting of the crushing zone) the water-jet has to impinge exactly 1 to 2 mm (0.04 to 0.08 in.) ahead of the bit tip. Alpine designed and manufactured two cutter heads with unique water-jet alignment systems.

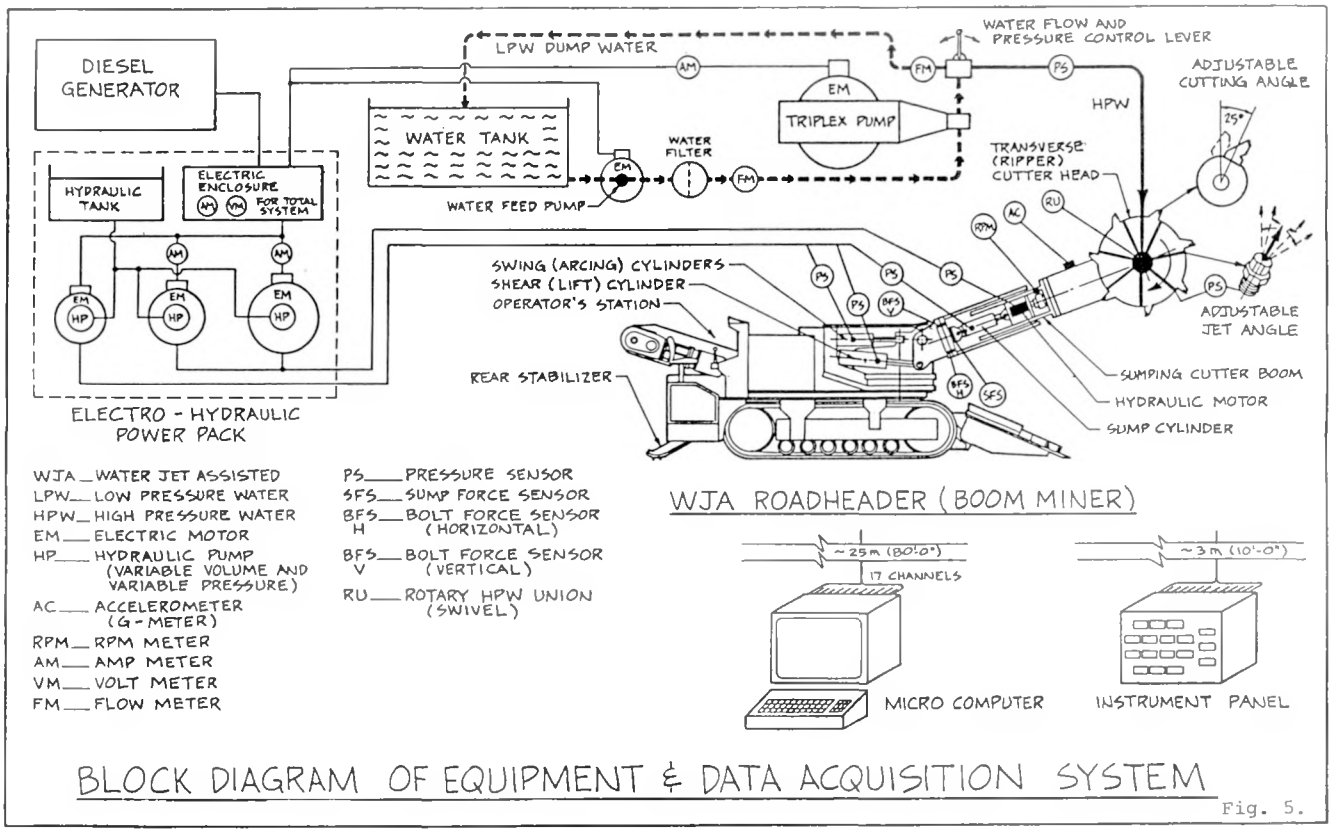

BLOCK DIAGRAM OF EQUIPMENT & DATA ACQUISITION SYSTEM

Fig. 5.

The HPW feed tubes of the cutter head are of straight design exceeding considerably the minimum required length of 102 mm (4 in.) for low-turbulence, high-efficiency flow of the high-pressure-water to the jet's nozzle.

Nozzles with 0.6 mm (0.024 in.) and 0.8 mm (0.032 in.) diameters were used. Jet stand-off-distances (S.O.D.) were 63.5 mm (2.5 in.) and 68.6 mm (2.7 in.).

Transverse "Ripper" Cutter Heads

Two transverse "ripper" heads were designed and manufactured because this type of head permits best control and measuring of cutting parameters.

Adjustable Bit (Pick) Angles

In order to find the most effective rake angle of the PDC "diamond" bits, one cutter head was equipped with unique angle-adjustable blocks (tool holders) which were designed and manufactured by Alpine.

Sumping (Telescoping) Cutter Boom

The cutter boom is equipped with a hydraulic sumping ("plunging") device in order to measure exactly the sumping (normal) forces exerted to the cutter head.

Electro-Hydraulic Power Pack

In order to obtain good and useful test data, a hydraulic cutter head drive system was selected over a conventional electric drive.

With an electric cutter motor speed and torque are not fully variable and adjustable as with a hydraulic drive. With an electrically powered cutter head, bit (pick) forces and speeds cannot be held constant because of peaks created by the kinetic energy of the rotor which acts like a flywheel. Furthermore, the hydraulic system is best suited for installation of sensors for microprocessor control and monitoring of test parameters.

The power pack utilizes variable-volume, pressure adjustable axial piston pumps. This system which drives the cutting assembly has a total installed electric power of 78 kW (105 hp).

Figure 6. WJA Roadheader with HPW Pump and Instrument Panel at Test Face.

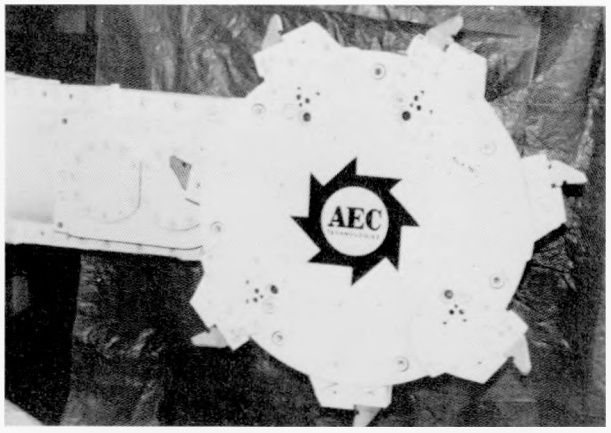

Figure 7. Alpine's WJA Transverse "Ripper" Cutter Head with Angle Adjustment for Bits (Picks).

High-Pressure-Water (HPW) System

The HPW system consists of a 3,785 l (1,000 gallon) tank, a 170 l/min (45 GPM), low-pressure feed (charge) pump and a triplex plunger pump, powered by a 149 kW (200 hp) electric motor. Both pressure and flow rate of the HPW pump are adjustable. The maximum pressure the pump was operated during the WJA cutting tests was 552 bar (8,000 psi).

Adjustable Jet Angle Of Alpine's WJA System

The nozzle assemblies of the WJA cutter head of the Alpine oil shale miner can be adjusted along two axes. Thus, the water-jet can be aimed exactly ahead of the bit tip in its plane of rotation.

HPW Tubing To Nozzle Assembly

Tests conducted by the U.S. Bureau of Mines showed that the major pressure loss which occured between the nozzle and the rock face, is directly affected by the amount of fluid turbulence that develops just upstream from the nozzle. When installing a straight tubing with a minimum length of 102 mm (4 in.) the jet's average stagnation pressure, for all stand-off-distances, was 35% greater than with bent and curved tubing[8].

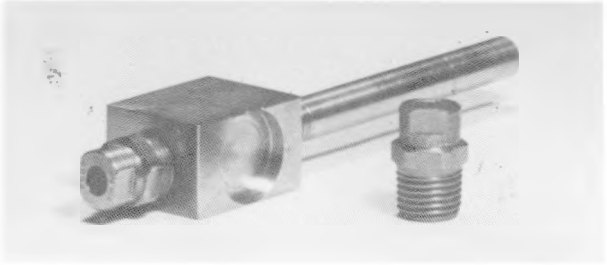

Figure 8. Angle-Adjustable Nozzle Assembly with Straight HPW Tubing.

The two styles of WJA cutter heads of the Alpine roadheader have straight HPW tubing which exceed the length recommended by the U.S. Bureau of Mines.

Table 2: Condensed Specifications Of WJA Roadheader And HPW System

Item	Specifications
TOTAL TEST SYSTEM	
Overall Weight, approx.	35 metric tons (39.5 short tons)
Total Installed Power	260 kW (348 hp)
WJA ROADHEADER	
Cutting Principle	Transverse ("ripper") head
Sump Stroke	406 mm (16 in.)
Cutter Bits, Number	7
Spacing	12.7 mm (0.5 in.)
Cutter Head, Number	2
Diameter	902 mm (35.5 in.) and 889 mm (35 in.) over bit tips
Rotation	0 to 194 $min.^{-1}$ (RPM)
Adjustable Bit Angles	
Cutter Head No. 2	Adjustable (0^{o} to -25^{o})
Cutter Head No. 1	Not adjustable
ELECTRO-HYDRAULIC POWER PACK	
Hydraulic Pumps, Number	3
Type	Axial piston, variable volume and variable pressure
HPW SYSTEM	
Water Tank, Volume	3,785 l (1,000 U.S. Gallons)
Feed (Charge) Pump, Flow	170 l/min. (45 GPM)
Pressure	21 bar (300 psi
HPW Pump, Type	Triplex plunger
Flow	Variable, max. 170 l/min. (45 GPM)
Pressure	Variable, max. 552 bar (8,000 psi)
ELECTRICAL SYSTEM	
Motors, Type	AC, 3-phase, 4-pole
Number	8
Power	460 volts, 60 Hz (c/s)
Crawler Drive Motors	2 x 7.5 kW (2 x 10 hp)
Chain Conveyor Motors	2 x 7.5 kW (2 x 10 hp)
Hydraulic Pump Drives	56 kW (75 hp) 15 kW (20 hp) 7.5 kW (10 hp)
HPW Pump Drive	149 kW (200 hp)
Feed Pump Drive	2.2 kW (3 hp)
WATER-JETTING SYSTEM	
Nozzle, Number	1 per bit
Location	In front of bit
Design	Leach & Walker
Material	Tungsten-carbide
Diameter	0.6 mm (0.024 in.) and 0.8 mm (0.032 in.)
Stand-Off-Distance (S.O.D.) Of Jet	63.5 mm (2.5 in.) and 68.6 mm (2.7 in.)

Cutter Bits (Picks)

Both conventional tungsten-carbide ("carbide") and PDC "diamond" tools were used in the factory cutting tests.

Carbide Tools Used At Factory Cutting Tests

Tungsten-carbide ("carbide") tools have been available for more than 50 years. Performance and wear characteristics for carbide tools both in coal and rock are well understood and documented.

Rotating, conical carbide-tipped "point-attack" tools are by far the preferred choice for drum-type continuous miners for production of coal, rock salt, trona, and potash. In the United States coal mining industry most longwall shearers are tooled with these type of tools.

Practically all modern roadheaders for rock cutting utilize rotating, conical carbide "point-attack" tools.

It was, therefore, decided to use a commercially available, rotating carbide-tipped "point-attack" bit (pick) as a "yardstick" (baseline data) for evaluating the performance of both WJA carbide and PDC "diamond" tools at the factory cutting tests. This bit had a 45^{o} attack angle, a gauge of 63.5 mm (2.5 in.), and a 19.07 mm (0.75 in.) diameter carbide insert with a 75^{o} cone angle.

Historical Development Of Rotating Carbide And PDC "Diamond" Rock Bits

This tool development is shortly described because Alpine used in 1989 a similar approach to the development of rotating PDC "diamond" "point-attack" bits as it did in 1970 to the development of rotating carbide bits (picks).

In 1970, Alpine Equipment Corporation ("Alpine") developed, in cooperation with a major American tool manufacturer, rotating, conical "point-attack" carbide bits[9]. An Alpine roadheader, equipped with a transverse "ripper" cutter head, working at uranium Mine No. 35 of Kerr-McGee Corporation near Grants, New Mexico was tooled with these novel carbide bits in 1970. The next application for these novel rotating carbide tools was cutting of hard standstone floor ("dinting") in a main entry at Greenwich Collieries near Ebensburg, Pennsylvania. The rotating carbide bits outperformed non-rotating "flat" carbide bits in these difficult applications. Alpine Equipment exported numerous cutter heads to Europe and Australia, mainly to VOEST-Alpine AG of Austria for use on Alpine Miners. Meanwhile, all manufacturers have equipped their roadheaders with rotating carbide tools for excavation of difficult-to-cut rock.

At the D.O.E. oil shale mining project, Alpine utilized again the same design approach: install novel PDC "carbide" inserts into rotating, conical "point-attack" bits (picks). This novel PDC "diamond" tool performed exceptionally well.

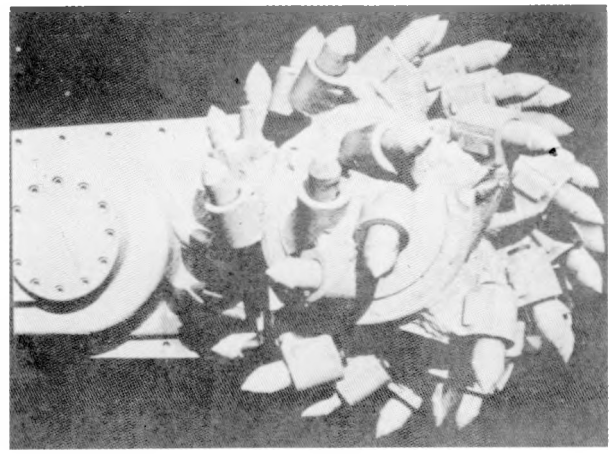

Figure 9. World's First Rock Cutter Head for Roadheaders (Boom-Type Continuous Miners) for Rotating Carbide "Point-Attack" Bits was Introduced by Alpine Equipment Corporation in 1970.

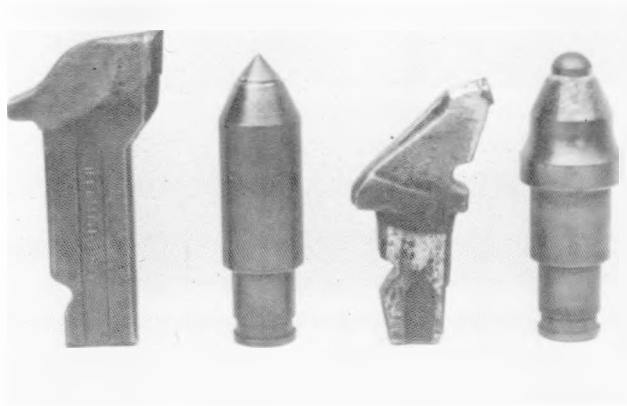

Figure 10. Evolution of Rotating, Conical "Point-Attack" Bits (Picks) with Carbide and PDC "Diamond" Inserts.

From Left to Right:
- Radial Carbide Bit
- Rotating Carbide "Point-Attack" Bit (Introduced 1970)
- Radial PDC "Diamond" Bit
- Rotating PDC "Diamond" "Point-Attack" Bit (Introduced 1989).

PDC "Diamond" Cutting Tools

At this project, for the first time, PDC "diamond" drag bits were tested on a standard-size WJA rock mining machine.

Technical Information On PDC

Polycrystalline diamond composites (also called "compounds" and "compacts") were invented by General Electric Company ("GE") in 1976[10]. GE's disc-shaped PDC cutters are being marketed under the tradename "Stratapax". PDC is about 300 times as wear resistant as carbide making it an ideal cutting tool. The PDC button or blank consist of a thin layer of polycrystalline diamond integrally sintered at ultra-high pressure and high temperature to a cemented tungsten-carbide backing (substrate).

PDC cutters are available in various shapes and sizes. In this project, disc-shaped and semi-round "domed" PDC cutting inserts were tested.

Thermal Stability. The thin PDC "diamond" layer which is only 0.3 to 1 mm (0.01 to 0.04 in.) thick is very sensitive to high temperatures[11]. At high temperatures, the presence of cobalt in the PDC layer catalyzes the transformation of diamond to graphite.

PDC cutters must not be exposed to temperatures in excess of 700° C (1,300° F) for a sustained period of time[12]. Furthermore, there is a large difference between the thermal expansion coefficients of diamond and cobalt, leading to increasing internal stresses as the temperature is raised. This problem is compounded by the difference in the thermal expansion coefficients of the PDC layer and its tungsten-carbide substrate. The high thermal sensitivity of the PDC blanks might be one of the main reasons why PDC bits have mainly been used in rotary drilling where the tools are always submerged and cooled in water or in bentonite slurry. The cutting tests conducted by Alpine showed that WJA, even with a low water pressure of 69 bar (1,000 psi), reliably cooled the PDC inserts and prevented thermal degradation of the valuable PDC insert.

Impact Resistance Of PDC Cutters. At the beginning of the development of PDC tools, uncertainty about the impact resistance of the PDC, i.e. the diamond cutter's ability to withstand high impact loading in hard rock cutting, was a matter of great concern to Alpine. An extensive literature survey and interviews with PDC manufacturers revealed that good data and design parameters were only available for rotary drilling applications, which generally do not experience high impact loads, perhaps with the exception of the collaring cycle of a drilling operation.

Fortunately, the concerns about limitations of impact resistance of PDC cutters was unfounded. Reports about shattering on impact were for PDC cutters of early design which had no chamfer on the PDC "cutting edge".

Cutter bits with chamfered PDC blanks proved extremely impact resistant. The chamfer increases the area of diamond contacting the rock and distributes the forces at the cutting edge over a larger area thus reducing stress and loads on the thin PDC layer.

A great advance in cutting technology was the introduction of rotating "point-attack" bits with "round nosed" PDC inserts. These bits showed outstanding impact resistance with WJA and "dry" cutting albeit at far higher cutting forces than with disc-shaped PDC blanks.

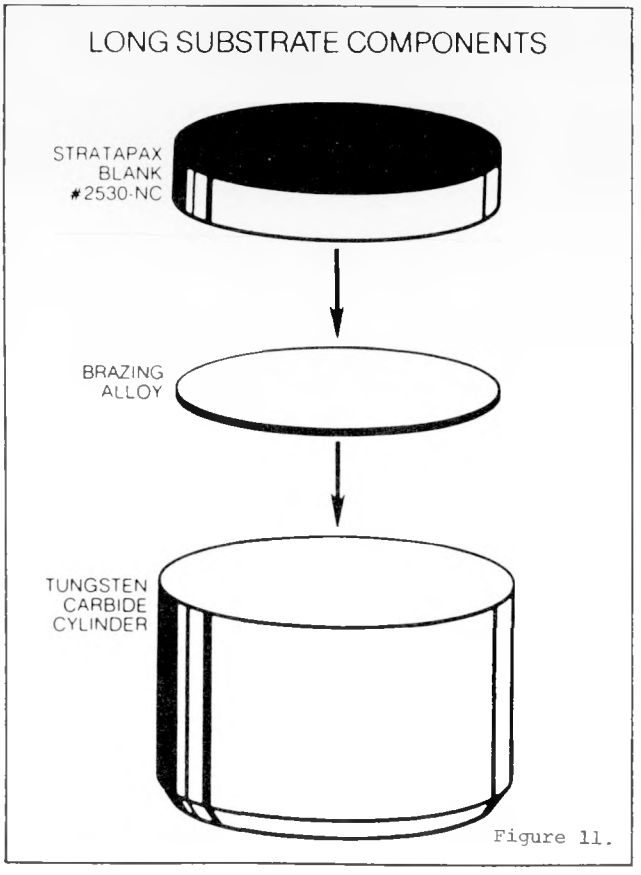

Figure 11.

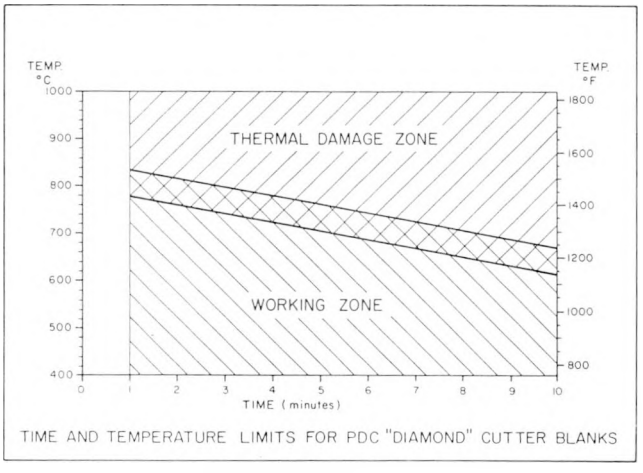

Figure 12. The Temperature of the PDC "Diamond" Insert Should be Limited to 700° C (1,300° F) Regardless of the Cutting (Surface) Speed.

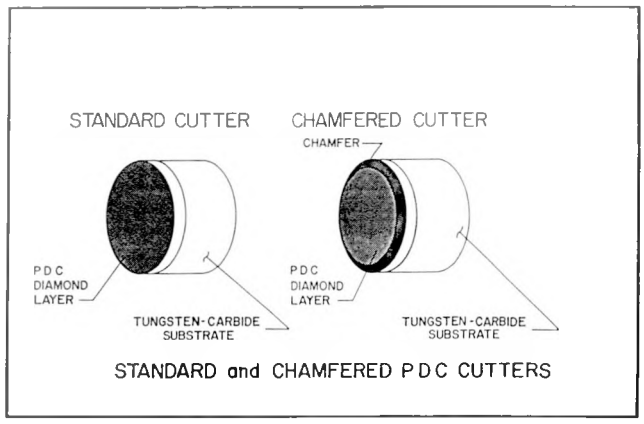

Figure 13. Chamfered PDC Cutters are Far More Impact Resistant than Standard Non-Chamfered PDC Cutters.

Semi-round "domed" and chamfered PDC "diamond" inserts showed exceptionally good impact resistance. Not a single PDC insert was destroyed at high (9 m/s; 1,800 fpm) cutting speeds, normal sumping forces per bit of up to 71.2 kN (16,000 lbf) and a maximum mechanical power of up to 71 kW (95 hp) per bit.

Rake Angle Of Disc-Shaped PDC Blank. A negative rake angle of -15^{o} to -20^{o} was found to be the most advantageous for cutting with radial bits (picks).

Cutting Forces. Practically no significant force reduction was provided by water-jet-assist (WJA). The variation of resultant bit forces with WJA was in the 5% to 10% range.

The following typical resultant bit (pick) forces were measured:

Rotating "point-attack" bit with semi-round PDC insert:	600 daN (1,350 lbf)
Rotating "point-attack" bit with carbide insert:	530 daN (1,190 lbf)
Radial bit with chamfered PDC blank at -20^{o} rake angle:	450 daN (1,015 lbf)
Radial bit with standard, non-chamfered PDC blank at -20^{o} rake angle:	340 daN (765 lbf)

PDC "Diamond" Cutting Tools Used In WJA Cutting Tests

Four types of custom-engineered PDC tools were designed, manufactured and tested.

(1) A rotating "point-attack" bit with a semi-round "domed" PDC insert with a diameter of 19.07 mm (0.075 in.)

(2) A non-rotating "forward-attack" bit with a 13.3 mm (0.52 in.) diameter standard, non-chamfered PDC blank (cutter).

(3) Two types of radial bits (picks) with 13.3 mm (0.52 in.) diameter chamfered PDC blanks (cutters).

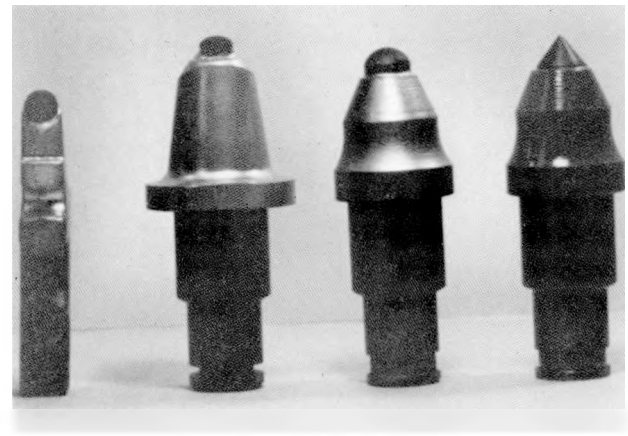

Figure 14. Cutter Bits (Picks) Tested by Alpine.

From Left to Right:
- Radial Bit with Disc-Shaped PDC "Diamond" Blank
- Non-Rotating "Forward-Attack" Bit with Disc-Shaped PDC "Diamond" Blank
- Rotating "Point-Attack" Bit with Semi-Round "Domed" PDC "Diamond" Insert
- Rotating "Point-Attack" Bit with Cone-Shaped Tungsten-Carbide Insert.

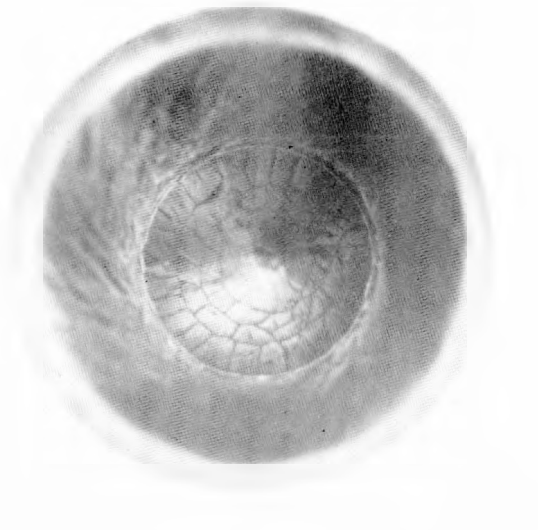

Figure 15. Thermal Damage to Carbide Insert of "Point-Attack" Bit Caused by Dry Cutting Causes Rapid Tool Wear.

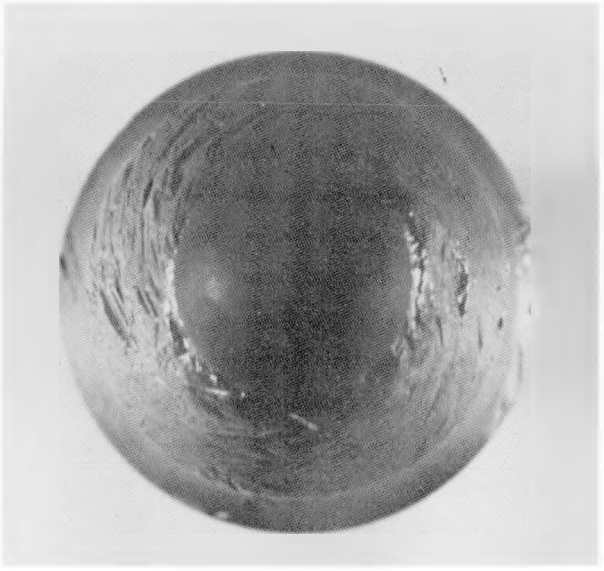

Figure 16. Impact Resistant Semi-Round "Domed" PDC "Diamond" Insert Shows No Wear after Hard WJA Cutting. Notice Wear on Steel Shank Caused by Hard Oil Shale.

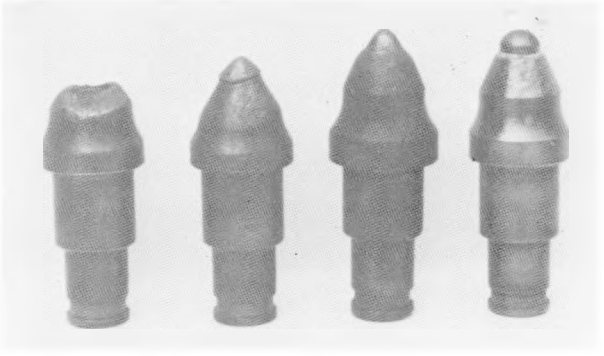

Figure 17. Comparison of Wear Resistance of Rotating "Point-Attack" Bits (Picks).

From Left to Right:

- Completely Worn Carbide Bit (Carbide Insert Missing)
- Carbide Bit in Advanced Wear State (Note Reduced Length of Bit)
- Carbide Bit After a Few Minutes of Cutting (Sharp Conical Tip was Rounded)
- PDC "Diamond" Insert Shows No Wear after Cutting Same Period of Time as Carbide Bits.

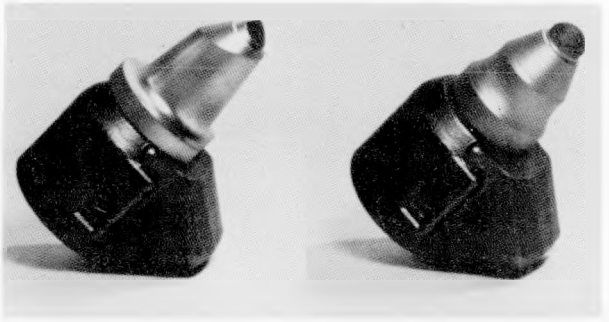

Figure 18. PDC "Diamond" Bits and Blocks (Tool Holders).

Left: Non-Rotating "Forward-Attack" Bit with Disc-Shaped PDC Blank.
Right: Rotating "Point-Attack" Bit with Semi-Round "Domed" PDC Insert.

Advantages And Potential Of PDC "Diamond" Tools

PDC "diamond" tools, properly cooled by water-jets at modest pressure, offer the following advantages over carbide-tipped tools, an over fifty-year-old cutting technology:

Increased Tool Life. The use of chamfered and semi-round "domed" PDC cutters did away with the chipping and flaking problems encountered with early non-chamfered PDC designs[14]. This design improvement resulted in up to 80 times longer tool life in oil shale when compared to conventional rotary carbide drill bits. At the factory cutting tests in oil shale, no wear of the PDC layers on the "diamond" bits (picks) was detected. Based on these cutting tests Alpine expects the PDC bits to last up to 50 times longer than carbide tools.

Rock Of High Strength Can Be Cut. The oil shale from Exxon's Colony Mine has an uniaxial (unconfined) compressive strength of 85.5 to 109.7 MPa (12,400 to 15,900 psi). This hard and competent rock was readily cut by PDC bits. Alpine is confident that PDC tools can cut most sedimentary rocks as claimed by diamond manufacturers. They reported that rock as hard as 193 MPa (28,000 psi) was economically cut by PDC bits[13].

Optimization Of Size Of Cuttings. Through selection of PDC blanks, which are available in numerous shapes and sizes, and by matching them with optimum cutting parameters (speeds and forces) rock sizes can be optimized for retorting purposes.

Lighter And Less Costly Mining Machines. Disc-shaped PDC cutters require less thrust and cutting force than carbide tools which dull rapidly. Thus, a mining machine designed for PDC tools can be built lighter and less powerful than a machine for carbide bits resulting in lower capital cost.

Lower Tool Consumption. Cutter bit consumption contributes the largest portion of the cost of excavation ($ per ton) of ore and rock. The long-lasting PDC tools have the potential to lower these costs considerably.

Replacement Of Roller Disc Cutters. PDC tools have captured a large share of the market of the petroleum industry which was formerly held by roller bits[14]. PDC "diamond" bits (picks) offer the same potential for mining and tunneling. Expensive roller disc cutters, costing several thousand dollars per bit, could be replaced by energy-efficient PDC "diamond" drag bits costing a fraction of it at comparable excavation capacity. Roller disc cutters initially attack the rock by crushing it i.e. the disc has to overcome the uniaxial compressive strength of the oil shale which is eight times higher than its tensile strength. A drag-type cutter bit (pick) attacks the rock's low tensile strength for energy-efficient cutting.

This provides the potential for a relatively light-weight machine such as a roadheader to cut hard rock which previously only could be encountered with a heavy and thus expensive tunnel boring machine (TBM) tooled with roller disc cutters.

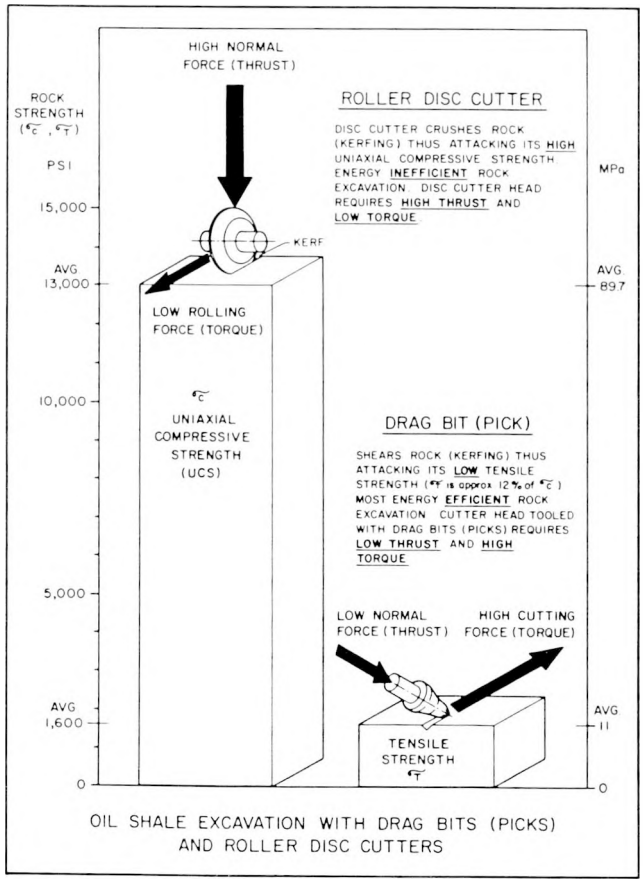

Figure 19. A Roller Disc Cutter Attacks the Rock's High Compressive Strength. A Drag Bit Attacks its Low Tensile Strength.

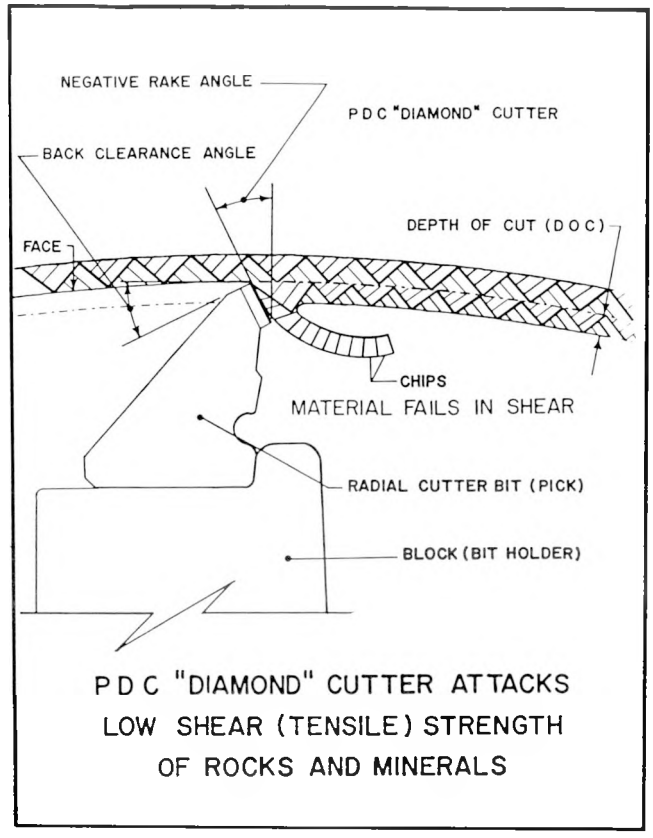

Figure 20. The Sharp PDC "Diamond" Blank Attacks the Low Tensile Strength of the Rock for Energy-Efficient Cutting.

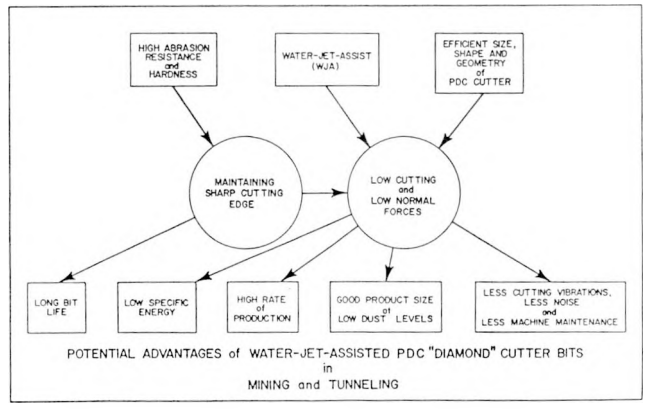

Figure 21.

WJA Factory Cutting Tests

Alpine investigated in its factory tests the impact of water-jet-assist (WJA) on (1) the oil shale, (2) the cutting forces, (3) the cutting tools (bits) and (4) on safety matters.

Rock Structure vs. Effectiveness Of Water-Jet

The rock's structure and consistency has the greatest influence on the effectiveness of a water-jet. For example, sandstone, which is easy-to-cut with water-jets, has hard particles (quartz grains) which are imbedded in a relatively soft matrix. The water-jet attacks the soft matrix and washes out the hard quartz grains. This can be compared to washing out the soft mortar of a brick wall with a water hose, causing the hard bricks to fall out.

Oil shale, which is a dolomitic limestone, is consistent and dense. It does not have a soft matrix which could be effectively attacked by the water-jet. The water-jets could not penetrate the oil shale even when the cutter head was run at low speeds of 10 $min.^{-1}$ (RPM) and at a water pressure of 552 bar (8,000 psi). Similar results were reported by British researchers where 1,400 bar (20,300 psi) water-jets on a roadheader could not penetrate limestone[15].

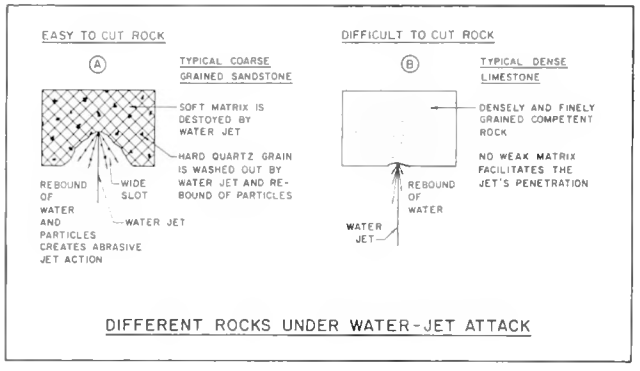

DIFFERENT ROCKS UNDER WATER-JET ATTACK

Figure 22. Water-Jets Could Not Penetrate the Oil Shale, a Dense Dolomitic Limestone.

No Cutting Force Reduction Through WJA

The tests in this project have shown that water-jet-assist does not significantly reduce cutting forces. Similar findings were reported for WJA cutting tests with longwall coal shearers[7] and roadheaders[15]. With water pressures from 69 to 552 bar (1,000 to 8,000 psi) the cutting forces varied only between 5 and 10 percent.

Reduction Of Dust

The adjustable, well aimed water-jets eliminated dust make even at a low water pressure of 69 bar (1,000 psi). Even with non-adjustable water-jets, good dust reduction was reported for coal shearers at 207 bar (3,000 psi) water pressure[7]. No sparking was observed during WJA cutting tests.

Hydraulic (Fluid) Power Requirements

Although WJA provided practically no reduction in cutting forces, it takes a high amount of energy to power a HPW jet. For example it takes 43 kW (58 hp) to power a 1,400 bar (20,300 psi) water-jet from a 0.8 mm (0.0315 in.) diameter nozzle. At 207 bar (3,000 psi), which is considered by many experts, the practical pressure limit for WJA, the hydraulic (fluid) power requirement is still 2.3 kW (3.10 hp) per 0.8 mm (0.0315 in.) nozzle diameter. Although, this fluid power requirement is relatively high, it is acceptable because of the very important benefits of WJA: significantly lower dust levels, considerable longer tool life, and no frictional ignition of methane.

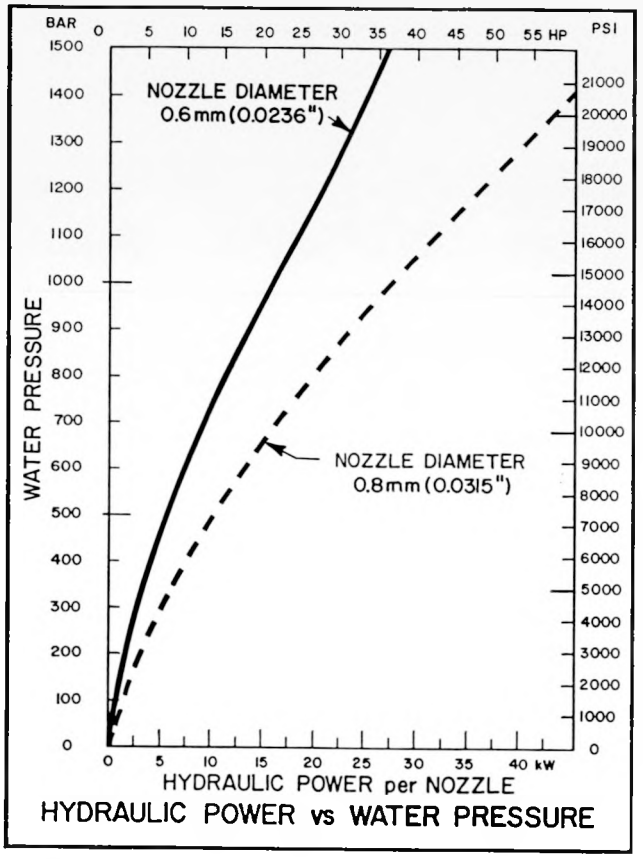

Figure 23.

Water Pressure vs. Flow Volume

High pressure creates high water flow volumes which might not be acceptable in most mining and tunneling operations. A nozzle of 0.8 mm (0.0315 in.) diameter has a flow rate of 5.7 l/min. (1.5 GPM) at 200 bar (2,900 psi) which increases to 15 l/min. (4 GPM) at 1,400 bar (20,300 psi).

Objectives And Tool Development Plans

Factory cutting tests conducted by Alpine have shown the great benefits of WJA for dust suppression and increase of tool life, especially with the novel PDC "diamond" cutter bits. However, the high cost and energy-inefficiency of high-pressure-water jetting was also demonstrated.

It is, therefore, Alpine's objective to maintain the aforementioned benefits of WJA by minimizing water flow and pressure. The best and, most likely, only way to achieve this is to minimize the jet's stand-off-distance (S.O.D.). The best technical solution for this objective is utilization of the "through-flush" design, especially with wear resistant PDC "diamond" bits (picks).

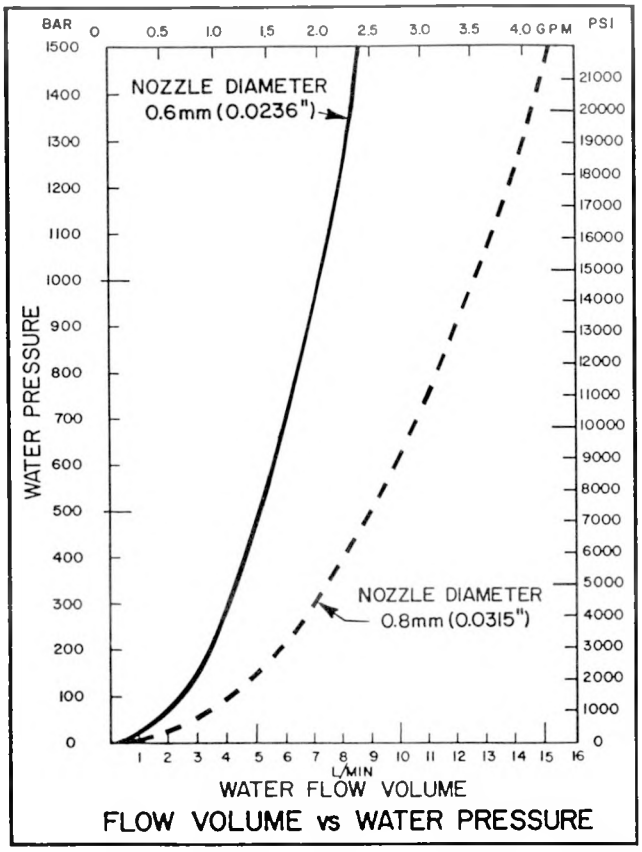

Figure 24.

The following illustration shows a "through-flush" bit design based upon a patent by W.W. Roepke of the U.S. Bureau of Mines[16]. Alpine plans to manufacture and test a similar "through-flush" bit design.

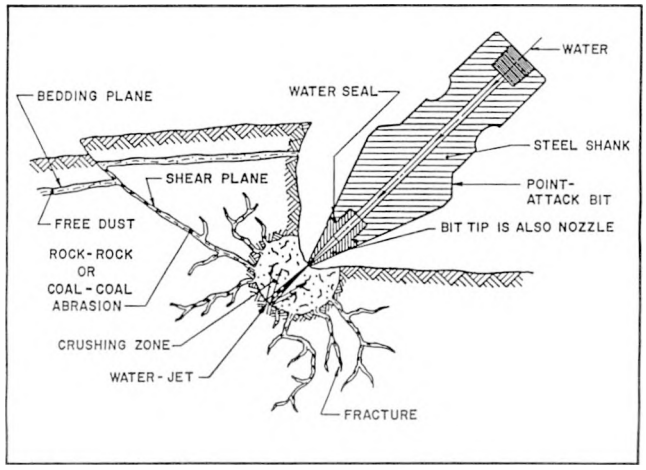

Figure 25. Ideal "Through-Flush" Bit: Cutting Insert is Integral Part of the Bit Tip.

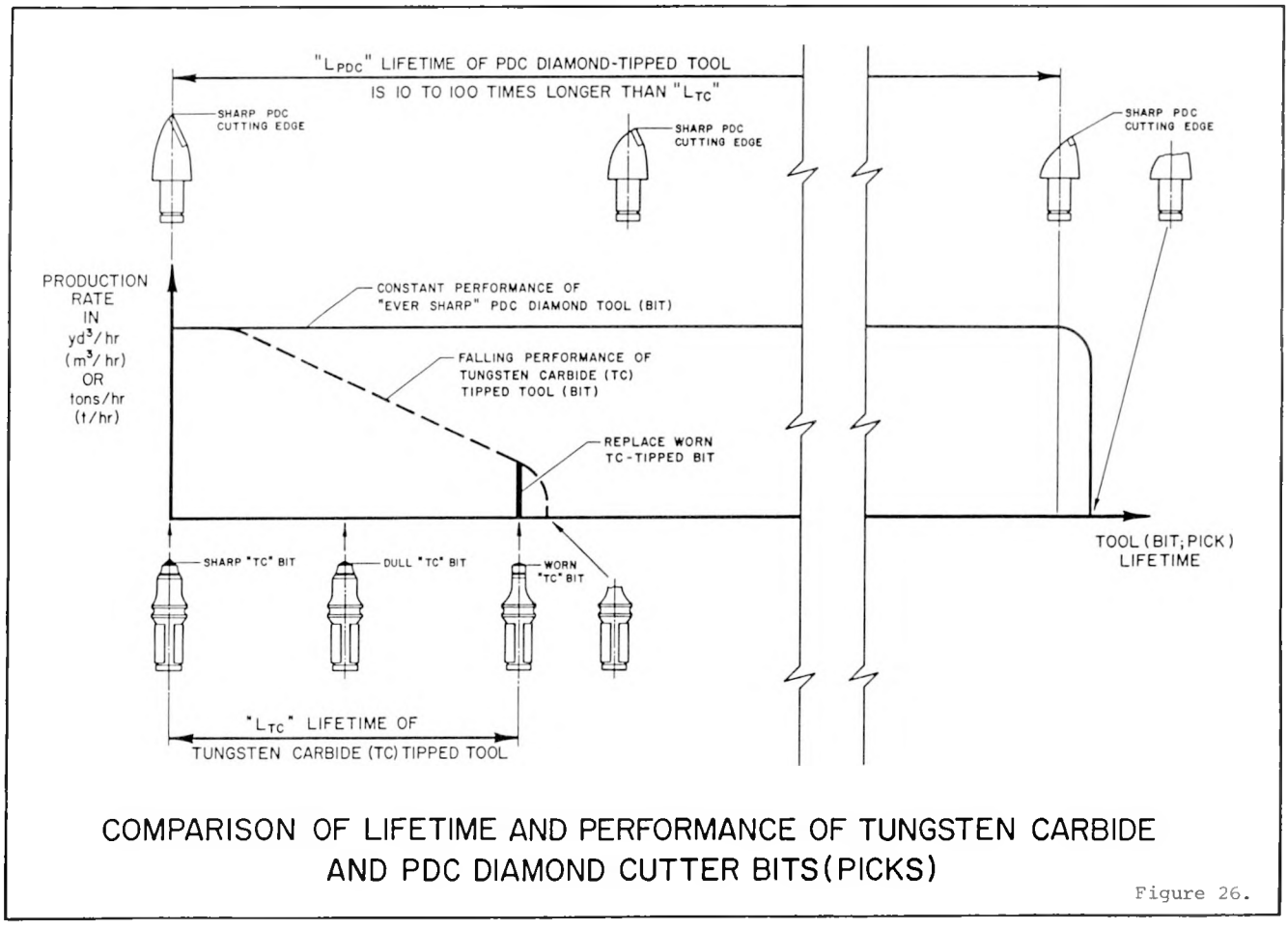

COMPARISON OF LIFETIME AND PERFORMANCE OF TUNGSTEN CARBIDE AND PDC DIAMOND CUTTER BITS(PICKS)

Figure 26.

References

1. Hood, M., "Water-Jet-Assisted Rock Cutting -- The Present State Of The Art", Paper On Water-Jet-Assisted Cutting, *Proceedings*: Bureau Of Mines Open Industry Meeting, Comp. by C.D. Taylor and R.J. Evans, BuMines IC 9045, pp. 3-20, Pittsburgh, PA, June 21, 1984.

2. Morris, A.H. and Tomlin, M.G., "Experience With Boom-Type Roadheader Equipped With High-Pressure-Water-Jet Systems For Roadway Drivage In U.K. Coal Mines", *Proceedings* Of Bureau Of Mines Industry Meeting On Water-Jet-Assisted Cutting, Pittsburgh, Pennsylvania, June 21, 1984.

3. Collin, W.D. and Kornecki, J.A., "The Development And Use Of Diamond Picks For Longwall Shearers At Secunda Collieries", *Proceedings* Of The Mining '85 Conference, p. 7, Johannesburg, South Africa, 1985.

4. Plis, M.N., Wingquist, C.F., and Roepke, W.W., "Preliminary Evaluation Of The Relationship Of Bit Wear To Cutting Distance, Forces, And Dust Using Selected Commercial And Experimental Coal- And Rock-Cutting Tools, U.S. Bureau Of Mines, *Report* Of Investigation No. RI 9193, 1988.

5. "Record Drill Bit Footage In Colorado Oil Shales", *Engineering & Mining Journal (E&MJ)*, p. 77, March 1989.

6. Baloo, G.L., "Development Of Production Drill Bits And Blast Rounds", *Proceedings* Of 22nd Annual Oil Shale Symposium, Colorado School Of Mines, pp. 85-95, April 19-20, 1989.

7. Taylor, C.D., Thimons, E.D., and Kovscek, P.D., "Evaluation Of Water-Jet-Assisting Capability On Longwall Shearers", U.S. Bureau Of Mines, *Report* Of Investigation No. RI 9270, 1988.

8. Kovscek, P.D., Taylor, C.D., and Thimons, E.D., "Techniques To Increase Water Pressure For Improved Water-Jet-Assisted Cutting", U.S. Bureau Of Mines *Report* Of Investigation No. RI 9201, 1988.

9. Leibee, D.L., "State Of The Art Of Cutting Tools For Continuous Miners, Roadheaders And Tunneling Machines", *Proceedings* Of German-American Symposium On Mining Technology, Mexico City, April 18, 1979, Vol. 2, Paper No. 5.

10. Nassau, K. and Nassau J., "The History And Present Status Of Synthetic Diamond", *Lapidary Journal*, Vol. 32, No. 1, April 1978, pp. 76-96 and Vol. 32, No. 2, pp. 490-508, May 1978.

11. Clark, I.D., "PCD Drill Bits And Their Applications In The Mining Industry", *Indiaqua*, No. 51/3, pp. 123-128, 1988.

12. Prakash, V. and Appl, F.C., "Temperature Distribution In Synthetic Diamond Cutters During Orthogonal Rock Cutting", *SPE Drilling Engineering*, pp. 137-143, June 1989.

13. Atkins, B.C., "Development Of Stratapax Blank Tools For Chain Sawing Of Natural Stone", *Project Report* by General Electric Co., Worthington, Ohio, pp. 3-7, March 1980.

14. Dennis, M. and Clark, D.A., "Major PDC Bit Improvements In Mid 1980s", *Oil & Gas Journal*, pp. 62-68, September 28, 1987.

15. Fowell, R.J., Waggot, A., and Anderson, I., "Full Scale Boom Tunnelling Machine Water-Jet Trials At Pressures Up To 140 MPa", *Proceedings* Of The 9th International Symposium On Jet Cutting Technology, pp. 323-339, Sendai, Japan, October 4-6, 1988.

16. Roepke, W.W., "Dust Controlling Method Using A Coal Cutter Bit", *U.S. Patent* No. 4,251,109, February 17, 1981.

Eastern Oil Shale Attrition and Breakage: Testing and Modeling

by

Ulrich Grimm and Glenn Swaney
U.S. Department of Energy
Morgantown Energy Technology Center
Morgantown, West Virginia 26507-0880

Abstract

While some work has been done on the attrition of oil shales at room temperature or in a specific process, no generalized study has been conducted at the high temperatures typically encountered in a retorting process. To facilitate these studies, a rolling attrition tester (RAT) has been designed and constructed. It consists of a 10-inch diameter drum suspended and rotating in an electric furnace at temperatures up to 1,000°C. Tests have been run on raw and pyrolized eastern oil shale obtained from the Cleveland Seam in Bullitt County, Kentucky. Similar to the results of earlier drop tests, the attrition is most prevalent near the normal retorting temperature of 400-600°C.

The matrix method of Broadbent and Callcott for coal grinding and breakage has been adapted to model the hot attrition results. Since the RAT performs multi-particle tests, the resulting breakage matrix also contains information on probability and selection for breakage. A general attrition prediction method is proposed which is based on the breakage matrix of the material and the intensity and frequency of the collisions in the process.

Background and Scope

The attrition and breakage of particulate material constitute two large areas of research whose industrial importance cannot be overemphasized. In every process involving the handling of solids, the breakdown of material has an important effect, be it desired (as in comminution) or unwanted (as in attrition). Unfortunately, the relative attention these areas have received is ill-portioned to their importance, with research efforts on attrition being fairly neglected in comparison to comminution and grinding. Although this paper deals specifically with attrition, the processes involved are similar, and considerable use is made of literature on comminution.

The original impetus for the present work came from the problem of dedusting shale oil, where even low concentrations of particulates in the range 0.2-300 μm represent yet another stumbling block to the commercialization of this energy resource. In addition, increasingly stringent environmental regulations have made gas phase entrainment of fines during retorting a subject of considerable importance.[1,2,3] More recent interest has focused on the use of oil shale in fluidized-bed combustors, where the problem of fines generation and entrainment is clear.[4,5,6] In general, attrition can be expected to be a problem in cyclone separators, electrostatic precipitators, filters, scrubbers, fluidized beds, screw feeders, lift pipes, and pneumatic conveying systems of all kinds. One recent discussion of energy processing technology points out the need for more solids transport research, where

"Particular attention must be given to plugging, attrition, and erosion."[7]

Fundamentally, there are two ways to approach the subject of attrition, which can be loosely termed practical and theoretical. Work in the former category involves the development of testing methods and standards for evaluating materials and processes, fitting of attrition or grinding data to empirical distributions, and the development of empirical relations between process and material parameters and output. If the process and conditions of interest are sufficiently close to those of the data on which an equation is based, then its prediction is usually very good. For some time to come, it is probably safe to say that most of the practically useful information on attrition will result from this type of work. Unfortunately, this means that the state of the art in this area consists of a fragmented collection of relationships, each of which has rather limited applicability.

A more theoretical approach to attrition seeks how material properties and structure affect the physics of the breakage process. This type of understanding will eventually lead to development of a more unified approach to the subject, but this area of science is insufficiently evolved at this point to yield useful results, or good agreement with data. What follows is hopefully a combination, rather than a compromise, of practical and theoretical approaches.

The ultimate goal of this research is to characterize the breakage and attrition of oil shale, and to show how this can be related to various material properties and process parameters to develop a predictive model. Since most of the forces causing attrition in practice are collisional in nature, we use both single- and multi-particle impact tests, rather than long time scale compression/crushing tests. The work presented here was done using the rolling attrition tester (RAT), a high-temperature, multi-particle testing drum. Multi-particle tests have the advantage of quickly providing enough data to be statistically significant. However, without the use of a tracer,[8,9] it is impossible to distinguish between the probability or selection for breakage and the breakage function itself. Single-particle tests are generally very time-consuming, but they can provide this information. We currently are constructing an apparatus to perform this type of testing.

Apparatus

The RAT is a high-temperature tumbler for measuring the attrition and breakage of solids caused by low velocity impacts, and is illustrated schematically in Figure 1. The drum is made of 0.312 cm (1/8-in) thick, 316 stainless steel, and is 25.4 cm (10 in) in diameter by 20.32 cm (8 in) wide. The drum door opening is 15.24 cm (6 in) wide, and spans 90° of the drum's circumference. The door is 0.159 cm (1/16-in) thick, and overlaps the opening by at least 2.54 cm (1 in) on all sides. It is fastened using six 3/8 UNC studs and nuts, and is sealed with a ceramic felt gasket to prevent fines from escaping. To preserve the shape of the cylindrical interior where attrition takes place, the door is fitted with an insert made of the same material as the drum. One shelf, 3.81 cm (1.5 in) high by 0.312 cm (1/8-in) thick, is mounted inside the drum and is removable.

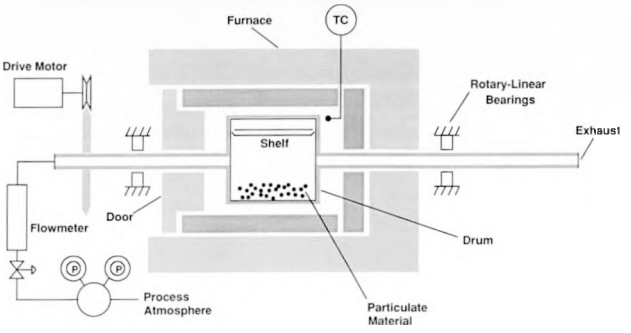

Figure 1. Rolling Attrition Tester (RAT) Schematic

Two 3.18 cm (1.25 in) diameter shafts extend 91.4 cm (36 in) from the ends of the drum, and are hollow to allow the drum to be purged with process gases. Six triangular supports are positioned radially around each shaft and are welded to the drum ends to reinforce the structure. The transmission consists of 29.2 cm (11.5 in) and 6.35 cm (2.5 in) diameter, mating V-groove wheels mounted to the shafts of the drum and motor, respectively. The drum is suspended by its shafts inside a 5,600 watt Lindberg furnace by linear-rotary bearings mounted exterior thereto. These bearings allow the drum to be removed from the furnace for easy loading/unloading, without requiring the experimenter to lift the (substantial) weight of the rotating assembly.

The furnace is equipped with a Lindberg Model 847 temperature controller, which supplies a typical maximum heating rate of about 45°C/min and accuracy within 1 percent. The RAT is driven by a Cole-Parmer Master Servodyne DC motor/generator and controller system which features adjustable, constant-speed, reversible output up to 300 rpm and 0.735 N-m (6.5 in-lb) torque, continuous torque monitoring, and variable limiting-torque protection circuitry. This translates to RAT speeds of 0-70 rpm. The motor controller is powered through a

timer, allowing the tumbling cycle to be programmed so that the apparatus requires no attention after starting. The shaft ends are capped by fittings which allow the tubing to remain stationary as the shaft rotates. Purge gas flow rates are monitored using a Brooks rotameter whose maximum capacity is 4.6 lit/min. The table containing the entire apparatus is situated under a fume hood to remove any fugitive gases.

Experimental

The oil shale sample studied was obtained from the Clegg Creek member of the New Albany shale (Upper Devonian) in Bullitt County, Kentucky. Its Fischer Assay is 15 gallons/ton, and it has an apparent density of 2.2 g/cm^3. This material was ground and sized into five sieve fractions: + 12.5 - 16.0 mm, + 6.3 - 9.5 mm, + 3.35 - 6.3 mm, + 1.00 - 3.35 mm, and + 0.500 - 1.00 mm. A representative sample of particles from these fractions (except the smallest) were weighed individually to determine the quality of the mass distributions.

The effects of three primary parameters (temperature, feed size, and tumbling time) were studied. In addition, several runs were conducted using air instead of nitrogen as the process gas for purposes of comparison. The shelf was left installed in the drum for all work presented here. Experiments were run with 50-300 g of feed material; larger amounts yielded the same results as smaller, although the level of noise was generally lower. These amounts actually used were limited by availability of material. After loading the drum with weighed material, a gasket was cut and the door sealed. Runs at higher temperatures required using anti-seizing compound on the studs. The furnace door insulation was installed after sliding the drum inside. The purge line was connected to a tank of dry nitrogen and the flow rate set to 1.2 lit/min. The furnace was started and ran at full power up to the desired set point; samples were heat treated at maximum temperature for at least 2 hours, then tumbled at temperature for a desired number of revolutions. Heating power was turned off and, after cooling below 50°C, the purge gas was also shut off.

In designing the experimental procedure, the RAT was considered as a scaled-down version of the coke testing tumbler, ASTM D 3402, which is 91 cm (36 in) in diameter by 45.5 cm (18 in) wide and rotates at 24 rpm. The limiting usable speed for a rotating drum (at which particles barely drop) is given by

$$f = (1/2\pi)\sqrt{2g/D} \qquad (1)$$

where g is gravity, D is the drum diameter, and f is the frequency. By this relation, the D 3402 tumbler operates at 54% of critical speed; this translates to a RAT rate of about 40 rpm, which was used for all experiments. Incidentally, scaling the recommended charge of 10 kg down according to the RAT volume results in feed loads of somewhat more than 300 g, but sufficient material was not available.

For analysis, samples were sieved into eleven fractions (maximum size shown): 16.0 mm, 12.5 mm, 9.5 mm, 8.0 mm, 6.3 mm, 2.36 mm, 1.18 mm, 0.600 mm, 0.250 mm, and 0.150 mm. The smallest fraction was analyzed by Coulter counter and separated into sixteen fractions (typical maximum size shown): 3.17 µm, 3.99 µm, 5.03 µm, 6.34 µm, 7.99 µm, 10.06 µm, 12.68 µm, 15.98 µm, 20.13 µm, 25.36 µm, 31.95 µm, 40.26 µm, 50.72 µm, 63.9 µm, 80.51 µm, and 101.44 µm.

Results

Mass distributions for the various feed fractions are shown in Figure 2, where the masses of 40-70 particles from each fraction are plotted. Linearity of these plots indicates that the distributions are approximately log-normal. Closer scrutiny of frequency plots of these data reveals a hint of a bimodal shape or more complex shape, which is probably due to the possible orientations of the non-spherical particles when interacting with the sieve. Particles from the smallest fraction (not shown) were not individually weighed because the balance had insufficient resolution and because they are extremely difficult to handle.

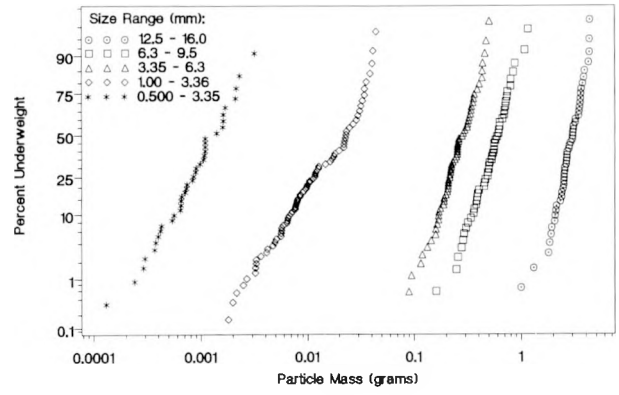

Figure 2. Particle Mass Distribution for Various Sieve Fraction of Eastern Oil Shale (EOS-15)

One interesting result which is not readily apparent from Figure 2 concerns the shape of the particles. In the largest sizes, the maximum and minimum diameters are roughly comparable. However, particles in the range of 1-2 mm exhibit a noticeable preference for an oblong shape, with diameter ratios of 6 not

uncommon. This is best explained by noting that the long dimension is always parallel to the bedding plane. As the particle size becomes comparable to the varve thickness, the difference in inter- and intra-layer bonding strengths becomes significant in determining the breakage properties of the material (apparently intra > inter).

To study the effect of temperature, experiments were run at 20, 150, 300, 400, 500, 600, 700, 800, and 900°C using 150 g of 1.6 cm feed material and tumbled for 10 minutes (400 revolutions). The results of this study are shown in Figure 3, where we define breakage to be the quantity of material reduced to less than 50% of its original size and attrition to be material smaller than 150 µm. Similar to the findings of previous research,[10] particle strength passes through a minimum. This is indicated by a maximum in the breakage and attrition curves at about 500°C and a minimum in the average fines particle size. Destruction of the kerogen occurs primarily in the range 300-400°C, while mineral fusion and consequent particle strengthening occur from 600 to 900°C. This average fines particle size is in the range 13-30 µm, which is comparable to the typical size of various mineral inclusions found in prior research on oil shale.[11]

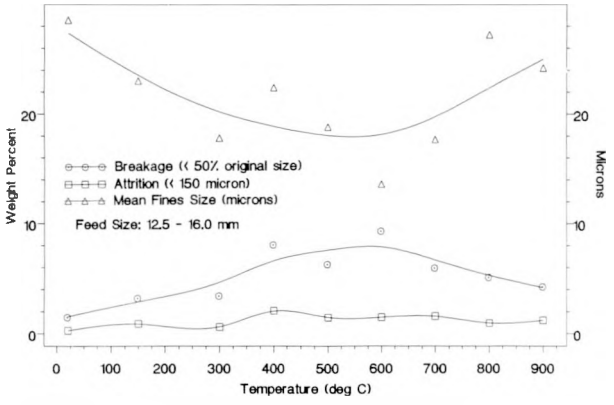

Figure 3. Effect of Temperature on Breakage and Attrition of EOS-15 Under N_2 After 400 Revolutions

To study the effect of feed particle size, experiments were run at 500°C and 800 revolutions for each of the feed sizes indicated. These data are shown in Figures 4 and 5, which also include the results of two analogous experiments conducted under air for comparison. Since the RAT is 25.4 cm in diameter, it can only generate low energy collisions; consequently, the breakage observed is rather low, especially if considered on a number (rather than weight) basis, even when using spent oil shale in its weakest state. Another problem with breakage arises because its definition requires interpolation of the sieve data in some instances. Apart from the resultant noise in the breakage data, we observe a maximum in breakage and a minimum in attrition for a particle size of about 3 mm.

Speculating on these data, it seems that the primary cause of attrition for the larger particles is impact with the drum wall. The impact energy delivered to an asperity decreases with decreasing particle mass, hence, the observed reduction in attrition. For smaller particles,

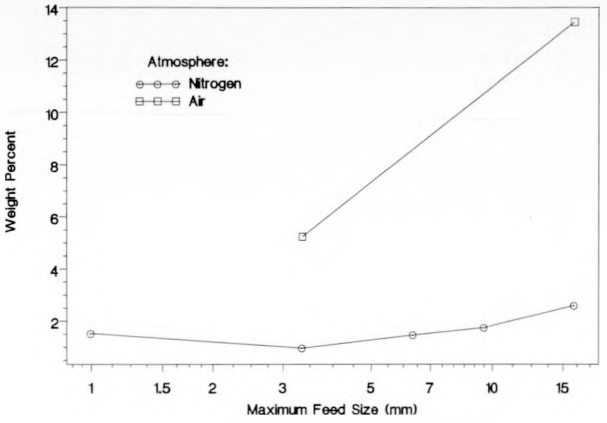

Figure 4. Comparison of Attrition (< 150 µm) Under N_2 and Air After 800 Revolutions for Various Feed Sizes

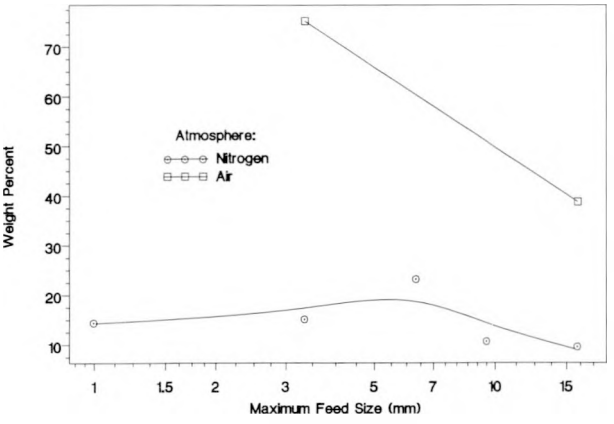

Figure 5. Comparison of Breakage (< 50% original size) Under and Air After 800 Revolutions for Various Feed Sizes

the major cause of attrition is abrasion with other particles and the drum wall. Note that the number of particles and the probability of particle-particle contact are much greater for smaller particles, hence, the increase in attrition of finer material. The reduction in breakage for these fines occurs because the very low energy collisions and abrasive forces are incapable of fracturing the particles. The increase in breakage of large particles with decreasing particle

size is more difficult to account for. One possibility is that the characteristic size of existing microcracks becomes comparable to the particle size, making the particles more susceptible to fracture.

The data for air are consistent with these trends and clearly demonstrate the need for a controlled atmosphere, since both the attrition and breakage rates are about five times greater than for those done under nitrogen. After heat treatment under nitrogen, the samples appeared black and coated with char, while samples heated in air were a light orange-brown. The presence of oxygen is apparently effective in removing the last traces of more highly polymerized kerogen which gives the particles substantial residual strength. The observed change in breakage and attrition rates hardly seems surprising in light of the apparent chemical changes.

To focus more closely on the attrition and breakage in the retorting temperature range of 400-600°C, additional experiments were conducted at 400, 500, and 600°C under air and nitrogen and tumbled for 800 revolutions. These data are presented in Figures 6 and 7. Again the breakage data for the tests in nitrogen are problematic, in this case showing no clear trend. The attrition results show a very slight decrease in attrition with increasing temperature which indicates that the particles attrite most at 400°C. A close inspection of the attrition data in Figure 3 shows that they are consistent with these findings over this temperature range.

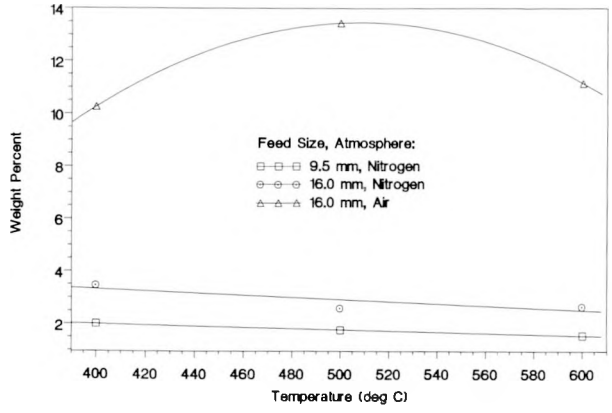

Figure 6. Effect of Temperature on Attrition (< 150 μm) of EOS-15 After 800 Revolutions

In contrast, the corresponding data for air show a maximum at 500°C for both attrition and breakage, indicating that the chemical processes involved (as implied by the temperature dependence) are markedly different. Clearly, the ambient gas has a much stronger effect than the ambient temperature.

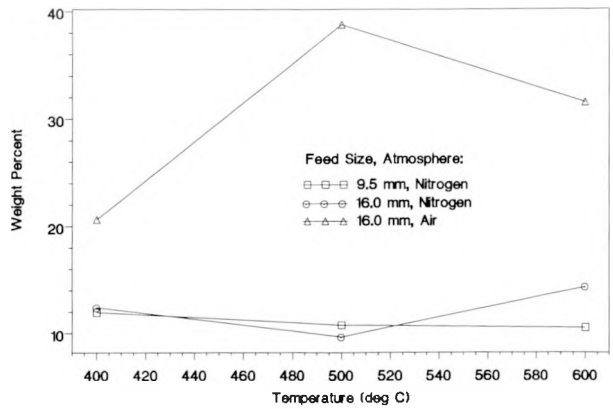

Figure 7. Effect of Temperature on Breakage (< 50% original size) of EOS-15 After 800 Revolutions

The effect of tumbling time at 500°C under nitrogen was studied by tumbling 16.0 mm feed material for 400, 800, 1,200, and 2,000 revolutions. These data are presented in Figures 8-10. Figure 8 is a plot of the complete product and feed distributions for 2,000 revolutions, and serves mainly to indicate that even the maximum attrition/breakage observed was fairly small. In this plot, equal areas represent equal masses of material; the extreme width of the distribution effectively obscures the attrition data.

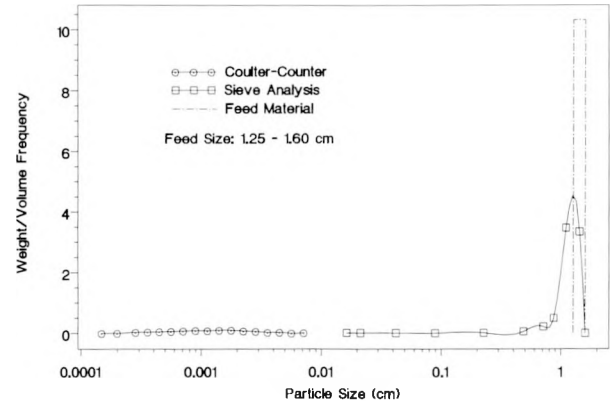

Figure 8. Complete Particle Size Distribution for EOS-15 at 500°C After 2,000 Revolutions Under N_2

Figure 9 is a Rosin-Rammler plot of the fines distributions. Approximate linearity here indicates a fairly log-normal distribution, but there is a very consistent and noticeable upward non-linear deviation for the larger fines particles. This is consistent with the results of several other researchers for data on coal breakage but, to our

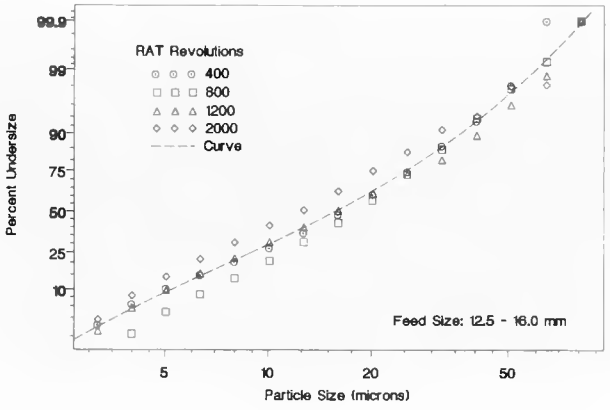

Figure 9. Distribution of Fines for EOS-15 at 500°C Under N_2

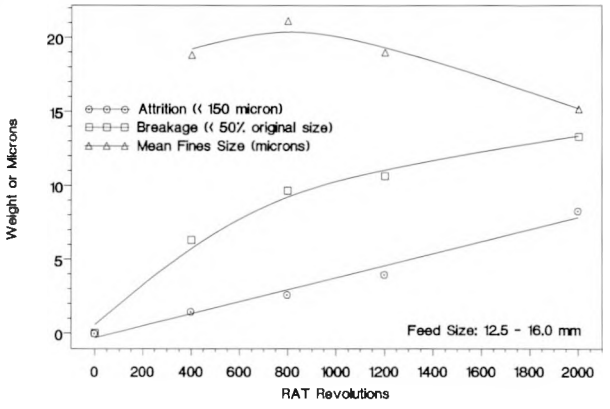

Figure 10. Effect of Tumbling Time for EOS-15 at 500°C Under N_2

knowledge, no explanation for this has been put forth.[12]

Figure 10 shows breakage, attrition, and mean fines size as a function of tumbling time. The breakage and attrition rates are nearly linear functions of tumbling, as would be expected for such initial rate data. No leveling of these rates is indicated. The mean fines size decreases with increasing tumbling also, as expected; but, linearity of this trend is unclear.

Modeling

Although work on grinding and breakage in recent years has relied more heavily on population/kinetic models,[13] we have chosen to adapt the older matrix method of Broadbent and Callcott[14] for this work. This decision was based on the inherent simplicity of the method, and the admission by other researchers that population models have been largely reduced to curve fitting.[12] Furthermore, population models create an unrealistic picture of the attrition process, in the sense that particles must be "broken out" of their original size fraction in order to attrite.

Since the RAT performs multi-particle tests, it is not possible to take data to simultaneously determine the breakage and selection functions, i.e., to answer the questions "Did the particle break?" and "What did it form, if it broke?" Broadbent and Callcott demonstrate a method of determining the selection function from experimental data, but this is based on an assumed breakage function. Therefore, we simplify their method by combining selection and breakage into one size reduction matrix, B. Its dimensions are N x N, where N is the number of size fractions used for analysis. One cycle of breakage can then be calculated using the relation

$$\vec{p} = B\vec{f} \qquad (2)$$

where $\vec{p}$ and $\vec{f}$ are the product and feed weight frequency distribution vectors, respectively. For ease of orientation, we adopt the convention that increasing subscripts refer to larger particle size fractions, i.e., $\vec{f}_1$, represents the finest particles in the feed, and B_{1N} is the fraction of the largest particles which, upon breaking, form daughter particles in the finest fraction. B is then an upper triangular matrix and the sum of each of its columns is unity. Physically, a column j of B is the product distribution which would result after one cycle if the feed contained only size fraction j. B is related to the true breakage and selection function matrices, B' and S, according to

$$B = B' S + I - S \qquad (3)$$

Considering one cycle as a single revolution of the RAT, the product obtained after k revolutions should in theory be given by $B^k\vec{f}$. The only significant utility of this model lies in the ease with which repeated applications of a breakage process can be predicted. For example, N experiments can be run using N monodisperse feed fractions tumbling 400 revolutions. The resultant product distributions would then form the columns of B^{400}. It is then trivial to predict the results after 800, 1,200, 1,600, etc., revolutions.

What is more interesting is that, given B^k, it is also possible to calculate $B^{k/2}$, i.e., to extract the square root of B^k. Broadbent and Callcott mention the ease with which products of B can be calculated due to its upper triangular form, with computational requirements increasing as N^2 instead of N^3 for full matrices. Here the difference is even more dramatic, since taking the square root of a full matrix involves

simultaneous solution of a system of N^2 quadratic equations in N^2 unknowns. The square root of an upper triangular matrix can be obtained using a straightforward back-substitution algorithm. The method is similar to the back-substitution which normally follows Gaussian elimination in the solution of linear systems. Here, however, instead of proceeding from the corner to the top row, we start on the main diagonal and move along progressive super-diagonals toward the opposite corner.

Elements on the main diagonal are simply the square roots of the corresponding elements in the original matrix:

$$B^{1/2}_{ii} = \sqrt{B_{ii}} \qquad (4)$$

If we use the subscript ranges $k = 2 \ldots N$ and $j = k \ldots N$, and the definition $i = j - k + 1$ to scan the super-diagonals of $B^{1/2}$, the remaining elements can be calculated from the formula

$$B^{1/2}_{ij} = \frac{B_{ij} - \sum_{m=i+1}^{j-1} B^{1/2}_{im} B^{1/2}_{mj}}{B^{1/2}_{ii} + B^{1/2}_{jj}} \qquad (5)$$

The notation $B^{1/2}_{xy}$ refers to an element of the desired matrix, not the square root of an element of the given matrix. Note that for the first super-diagonal, the summation term is zero since $i+1 > j-1$.

For large particles and short tumbling times, most of the breakage and attrition results from particle-wall collisions. If interparticle collisions can be neglected, this means that given B^{512}, for example, it is possible to take repeated square roots of this matrix to determine B. Since B corresponds to one revolution, this method provides a way of correlating RAT data with that derived for single particle (albeit low velocity) impacts.

As a preliminary test of this method, runs were performed on all the larger feed sizes through 1.0 mm. Since the fines were very small, it was not practical to separate them in large enough quantities to use as feed materials, and it was decided to assume that the fines do not attrite. This means that the off-diagonal elements in the first x columns of B were taken to be zero, where x is the number of fines fractions. To reduce the size of the matrix for this preliminary work, adjacent fines fractions were combined giving a total of 13 fractions (8 coulter-counter + 5 sieve). Data for 800 revolutions of tumbling were used to create B^{800}. Taking the square root of this matrix generated B^{400}, B^{100}, and $B^{12.5}$, among others. Ignoring the half-revolution error, these were then combined to form B^{512}, from which B can be calculated as described above. In addition, B^{1200} and B^{2000} were calculated.

A comparison of some of these calculations with the experimental fines distribution data is shown in Figure 11. Data from B^{800} was used to predict distributions at 1,200, 2,000 and 400 revolutions, and this figure indicates that the overall quantity of fines produced is reasonably estimated for all cases except perhaps 2,000 revolutions. However, qualitative changes in the distribution at longer tumbling times (i.e., a shift toward smaller particles) are clearly not reflected in the model. This is to be expected since we assumed that the fines did not attrite. Physically, this assumption is apparently wrong because, although the fines experience no significant impact velocity with the drum wall, they are subjected to continual abrasion and grinding forces as well as being periodically smashed by larger falling particles. Obviously, some form of breakage/selection function must be assumed for the fines; this constitutes a promising area for future work.

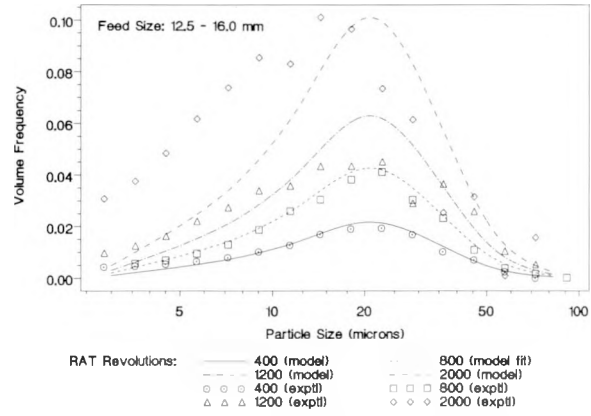

Figure 11. Matrix Model Extrapolation Around 800 Revolutions of EOS-15 Fines Distributions at 500°C Under N_2

Collisions, whether macroscopic (breakage) or microscopic (attrition), form a natural basis by which differing processes can be characterized, compared, and studied. This means that the complete task can be divided into two major efforts. First, processing operations (pneumatic transport, fluidized bed, etc.) must be studied to determine the frequency and intensity of collisions involved. Second, the reaction of the particles to controlled collisions must be understood and related to its material properties, for which considerable data are available.[15,16]

Conclusions

The RAT is a unique facility for high-temperature particle attrition testing under controlled process gases. Experiments done on a 15 gallon/ton eastern oil shale indicate several interesting trends which are in general agreement with previous findings, where applicable:

1. Attrition and breakage under nitrogen are most prevalent in the temperature range 400-600°C, which also corresponds to a minimum in the mean size of resultant fines.

2. The feed and fines distributions are approximately log-normal, and the fines distributions are very similar to those for coal breakage.

3. Breakage exhibits a maximum as a function of feed size, while attrition passes through a minimum. This is caused by fundamental differences in the physical mechanism (impact versus abrasion) by which large and small particles attrite and break.

4. Attrition and breakage rates after heat treatment in air are some 5 times higher than in nitrogen, demonstrating the importance of ambient gases.

5. Preliminary work with the matrix method shows some promise in predicting attrition versus time, but more work is needed to select an appropriate fines breakage/selection function.

Acknowledgement

The authors would like to thank Philip Kneisl for his design and conception of the apparatus.

References

1. J. F. Carley, "Attrition of Spent Oil Shales During Pneumatic Conveying and Cyclone Separating," 14th Oil Shale Symposium Proceedings, Colorado School of Mines, 207, 1981.

2. B. G. Place, R. Hobbs, T. F. Turner, and D. Katz, "Shale Oil Aerosol Removal Using a Venturi Scrubber: Environmental Research on WRI's 10-Ton Oil Shale Retort," 18th Symposium Series, Colorado School of Mines, 1985.

3. G. M. Rinaldi, R. C. Thurnau, and J. T. Lotwala, "Wet Scrubbing for Control of Particulate Emissions from Oil Shale Retorting," 12th Oil Shale Symposium Proceedings, Colorado School of Mines, 321, 1981.

4. N. V. Dung, G. C. Wall, and G. Kastl, "Continuous fluidized bed retorting of Condor and Stuart oil shales in a 150 mm diameter reactor," Fuel, 66, No. 3, 1987.

5. A. M. Rubel, E. Davis, and L. Tungate, "The Effect of Bed Temperature and Fluidization Velocity on the Chemistry of Bench Scale Fluid Bed Retorting of Kentucky Oil Shale," Fuel Proc. Tech., 16, 163-172, 1987.

6. S. D. Carter and D. N. Taulbee, "Fluidized Bed Steam Retorting of Kentucky Oil Shale," Fuel Proc. Tech., 11, 251-272, 1985.

7. Anon, "Amundson Report: Energy Processing," Chemical Engineering Progress, 84, No. 3, 17-19, 1988.

8. H. Rumpf, Ed. Symposion Zerkleinern, Vortrage und Diskussionen des 1. Europaischen Symposions, Dechema, Frankfurt, a.M., April 10-13, 1962.

9. R. P. Gardner and L.G. Austin, "A Chemical Engineering Treatment of Batch Grinding," in Rumpf, 217-248, 1962.

10. U. Grimm and P. Kneisl, "Studies on Oil Shale Attrition," 1988 Eastern Oil Shale Symposium, Lexington, Kentucky, 1988.

11. U. Grimm and L. Shadle, "Size, Mineral, and Organics Distribution in Crushed Oil Shales," Chem. Sep., Dev. Sel. Pap. Int. Conf. Sep. Sci. Technol., 1, 2, 199-218, 1986.

12. Peters Rit, A.W.P.G., M. Hagg, and J. van Brakel, "Characterization of Mechanical Strength of Coal Particles," I. Chem. E. Symposium Series No. 69, Powtech 83, Pergamon, 1983.

13. S. R. Broadbent and T. G. Callcott, "A Matrix Analysis of Processes Involving Particle Assemblies," Phil. Trans. Roy. Soc., 249, 99-123, 1956.

14. J. A. Herbst and D.W. Furstenau, "Scale-up Procedure for Continuous Grinding Mill Design Using Population Balance Models," Intl. J. Miner. Proc., 7, 1-31, 1980.

15. Blanton, Dischler, and Patti, "Mechanical Properties of Devonian Shales from the Appalachian Basin," DOE Report DOE/MC/08216-1332, 1981.

16. F. E. W. Duvall, H. Y. Sohn, and C. H. Pitt, "Physical Behavior of Oil Shale at Various Temperatures and Compressive Loads," Fuel, 64, No. 2, 184-188, 1985.

ENVIRONMENTAL AND RECLAMATION RESEARCH

Chemical Equilibria Model Analysis of Hope Creek Eastern Oil Shale Lysimeter Leachate Data

by

Michael E. Essington
Western Research Institute
University of Wyoming Research Corporation
Laramie, Wyoming 82071

Abstract. Leachates from field lysimeters containing an eastern oil shale, a retorted eastern oil shale, and an oil shale fines/retorted oil shale mixture were subjected to chemical equilibria model analysis by the GEOCHEM model. Results of the chemical equilibria model analysis provided a more detailed characterization of the chemistry of oil shale materials. The aqueous chemistry of the lysimeter leachates is dominated by free ionic metal species and metal sulfate ion pairs. Activity diagrams show that free metal ion activities (with the exception of Ca^{2+}) are directly related to SO_4^{2-} activities. This suggests that the aqueous activities of the metals examined are not supported by metal sulfate solid phases. However, an examination of metal sulfate ion activity products (IAPs) as a function of time show that the IAPs approach constant values after approximately 800 days of the field study. For the great majority of the metals examined, the IAP values suggest leachate undersaturation with respect to even the most stable metal sulfate phases. Leachates from all three materials are predicted by GEOCHEM to approach equilibrium with respect to gypsum ($CaSO_4 \cdot 2H_2O$) and goethite (FeOOH). In addition, leachates from the oil shale lysimeter are predicted by GEOCHEM to approach equilibrium with respect to melanterite ($FeSO_4 \cdot 7H_2O$), Fe-jurbanite ($FeSO_4OH$), and franklinite ($ZnFe_2O_4$). Aluminum activities in all three lysimeter leachates fall within the stability region of several basic aluminum sulfates. However, Al^{3+} activities in the lysimeter leachates are not supported by sulfate phases.

Introduction

The analysis of solid waste leachate data often includes the application of computer-based ion association models. These models, also termed chemical equilibria models, are based upon thermodynamic principles and use ion association constants, solubility product constants, and analytical concentration data to predict the distribution of an element between free anionic or cationic species, ion pairs and complexes, and solid phases. Although the ion association model has a firm theoretical basis, the computer codes used to perform the model calculations have a number of inherent shortcomings.

The more significant of these problems includes (1) an incomplete data set on solids controlling solution chemistry, their stoichiometry, crystallinity, and thermodynamic properties; (2) discrepancies in reported values for solubility and ion pair formation constants; (3) inability to thermodynamically describe various classes of reactions that influence leachate concentrations such as adsorption/desorption and ion exchange; (4) lack of thermodynamic data to characterize ion pair and complex ion formation reactions involving metal ions and organic ligands; (5) lack of accurate thermodynamic data for reduction-oxidation (redox) reactions; (6) variations in the thermodynamic data sets, both in the number of species considered and the associated data, used by the different chemical equilibria model computer codes; and (7) thermodynamic data are generally only available for standard conditions (298 K and 0.101 MPa). Such shortcomings cast doubt on the validity of model predictions, particularly when the models are applied to complex multicomponent systems such as spent oil shale. However, model predictions do provide a first approximation for understanding the complex chemistry of multicomponent systems.

Despite the shortcomings associated with chemical equilibria models, they have been extensively applied to provide useful insights into the chemistry of spent oil shale leachates. Saether and Runnells[1] and Stollenwerk and Runnells[2] used the thermodynamic models WATEQFC[3] and WATEQ2[4] to examine the solution chemistry of fluorine, molybdenum, and boron in spent oil shale leachates. They further used the model predictions to suggest the presence of fluorite (CaF_2) and powellite ($CaMoO_4$) in spent oil shale samples. Esmaili et al.[5] used WATEQFC to characterize retorted oil shale aqueous

extracts and to examine solubility relationships. Reddy and Lindsay[6] examined the solubility relationships of calcium and magnesium minerals in spent oil shales using an ion association model. Simularly, Reddy et al.[7] examined calcium and magnesium mineral solubility relationships and mineral transformations associated with spent oil shale recarbonation. Essington and Spackman[8] used the PHREEQE[9,10] chemical equilibria model to elucidate the chemical status of spent oil shale leachates as a function of solid-solution contact time, temperature, solid:solution ratio, and carbon dioxide partial pressure. Essington et al.[11] and Essington and Spackman[12] used the GEOCHEM[13] chemical equilibria model to provide insights into the solution and solid-phase chemistry of combusted eastern and western reference oil shale and recarbonated combusted western reference oil shale. Reddy et al.[14] used leachate data from weathering eastern (combusted and raw) oil shales and the WATEQFC model to elucidate the solubility relationships for zinc.

In additon to the generation of descriptive information on ion speciation and solubility relationships in spent oil shale leachates, chemical equilibria models have been used to predict element concentrations in spent oil shale leachates, generate thermodynamic data, identify attenuation mechanisms, and develop mineral weathering sequences. Essington and Spackman[8] and Essington et al.[11] observed that fluoride concentrations in spent oil shale leachates are controlled by the solubility of fluorite. Based on this information, Essington[15] used the GEOCHEM code to predict the range of fluoride concentrations expected in retorted and combusted oil shale leachates. In general, the predicted range encompassed the measured values. Data generated from the application of the chemical equilibria models PHREEQE and GEOCHEM, using spent oil shale leachate data, have been used to generate the solubility product constant for powellite and the ion pair formation constants for $CaMoO_4^0$, $KMoO_4^-$, and $NaMoO_4^-$.[16] Spackman et al.[17,18] used the GEOCHEM model to examine arsenate and selenite chemistry in retorted oil shales and distinguish between the attenuation mechanisms of adsorption and precipitation. Sullivan et al.[19,20] applied the WATEQFC model using leachate data from weathering eastern and combusted eastern oil shales. From the model predictions, they developed a weathering scheme that identified the secondary mineral forms of aluminum and iron and the chemical mechanisms for the production of acidity.

A great majority of studies that have used chemical equilibria models to characterize spent oil shale aqueous chemistry have been conducted under well-defined laboratory conditions. These studies include the characterization of equilibrium column leachates,[1,2] the characterization of equilibrium aqueous extracts as a function of several experimental variables such as temperature, solid-to-solution ratio, carbon dioxide partial pressure, and reaction time,[6-8,11,12,21] and the characterization of aqueous extracts from equilibrium and nonequilibrium laboratory simulated weathering studies.[14,19,20] Yet, the chemical equilibria model evaluation of leachates from field spent oil shale disposal sites has not been conducted.

Recently, a five-year field lysimeter study designed to evaluate the leaching characteristics of eastern oil shale and retorted eastern oil shale was completed.[22] Over 3800 leachate samples were collected and subjected to chemical analysis over the course of the study. Data evaluation included an analysis of element concentration and leachate pH changes with time as influenced by waste type. Limited chemical equilibria model analyses were also performed and the results used to suggest mechanisms controlling leachate chemical composition and acid generation. However, these evaluations were not detailed in scope. The objective of the present study is to provide a more detailed characterization of the chemistry of leachates from eastern oil shale materials by subjecting the leachate concentration data from the lysimeter study to chemical equilibria model analysis.

Methodology

The Hope Creek eastern oil shale field lysimeter study was initiated in 1983 and completed in 1988. The study was designed to evaluate the environmental and reclamation characteristics of eastern oil shale and retorted eastern oil shale. The overall study objectives, lysimeter construction, raw and retorted eastern oil shale and associated materials (overburden and soil), emplacement configuration, sampling depths and frequency, and leaching results are reported elsewhere.[22-27] The oil shale used in the study was mined from the Sunbury Shale and the Cleveland Member of the Ohio Shale and processed using the Dravo traveling grate retort. Overburden material was mined from the Nancy Member of the Borden Formation. The soil used in the study was from the Gilpin soil series.

Although eight lysimeters were constructed to simulate eight solid waste emplacement configurations, only three lysimeters were chosen for treatment by a chemical equilibria model. The emplacement designs for these three lysimeters were similar, the only significant difference being the type of waste material examined. Thus, the leachate chemistry of one waste type could be directly compared to that of another waste type. Lysimeter L3 contained a six-foot depth of a retorted oil shale/oil shale fines mixture overlaid with two feet of overburden material and a surface two feet of soil. Lysimeter L6 contained a six-foot depth of retorted oil shale with a surface cover identical to that of L3. Lysimeter L7 contained a six-foot depth of oil shale fines overlaid with three feet of overburden material and a surface foot of soil.

Leachates for model analysis were collected from sampling ports located at a depth of 10 feet (bottom of the lysimeter). Leachates examined in the present study are designated L310, L610, and L710 to identify lysimeter and leachate sampling depth. Each lysimeter contained three sampling ports at the 10-foot depth: left, center, and right ports. Model analysis was conducted on 20 samples (for which complete chemical analysis data were available) from each port for a total of 60 analyses per lysimeter. Leachate samples chosen for model analysis, as well as the chemical composition of the leachates, are reported by Essington.[28]

The chemical analyses of lysimeter leachates were treated with the chemical equilibria model GEOCHEM. The model calculates the free ionic and ion pair species distribution of the leachate components by numerically solving a set of coupled nonlinear algebraic equations by successive iterations. Each mass-balance equation relates total soluble element concentration to free ionic and ion pair species concentrations using appropriate stability constants and stoichiometry. The equations are iterated numerically until a constant effective ionic strength for the solution is obtained. Conversion of GEOCHEM's thermodynamic data for use in the mass-balance equations and conversion of species concentrations to activities requires activity coefficients. Single-ion activity coefficients for charged species are calculated using the Davies equation. Single-ion activity coefficients for neutral species are calculated using the Setchenow-Harner-Owen equation with k_m equal to

0.1.

Lysimeter leachate chemical components considered in the chemical modeling are: pH, pe, Ca, Mg, K, Na, Fe(II), Fe(III), Mn, Cu, Cd, Zn, Ni, Pb, Al, SO_4, $B(OH)_4$, and MoO_4. Chemical analyses were also performed to determine total organic carbon (TOC), Cr, As, Se, NH_4, NO_3, Cl, and PO_4 concentrations in leachates. However, these were not considered in the model analysis because there was insufficient characterization for modeling purposes, insufficient modeling capabilities, or the concentrations were consistently below detectable concentrations. Species considered by the model are shown in Table 1. Stability constants describing the formation of these species are tabulated by Essington.[28] The model predictions that are of greatest interest are the predicted free ionic activities. For the components listed above, excluding pe, these are H^+, Ca^{2+}, Mg^{2+}, K^+, Na^+, Fe^{2+}, Fe^{3+}, Mn^{2+}, Cu^{2+}, Cd^{2+}, Zn^{2+}, Ni^{2+}, Pb^{2+}, Al^{3+}, SO_4^{2-}, $B(OH)_4^-$, and MoO_4^{2-}. The free ionic activities will be used in the construction of activity diagrams to examine solubility relationships. Model predictions of secondary interest are the aqueous distributions of the components between free and ion pair species.

A number of assumptions are made in the application of GEOCHEM to the lysimeter leachate data. Calculation of the distribution of total Fe between Fe(II) and Fe(III) in each solution requires a value for the redox potential (pe). Because this parameter was not measured, estimation of pe for each solution is required. For the model evaluations, a moderately reducing pH + pe value of 9.0 was chosen. Thus, pe for each solution was calculated by subracting solution pH from 9.0. Results of a sensitivity analysis of the predicted Fe^{2+}/Fe^{3+} distribution to pe are listed in Table 2. Solution data for this evaluation were taken from lysimeter L610. These results show that Fe^{2+} dominates the Fe^{2+}/Fe^{3+} couple. Further, Fe^{2+} activity is invarient over a wide range of pe values, and predicted Fe^{3+} activities are directly correlated to assumed pe values. Thus, conclusions based on the predicted activities of Fe^{3+} must be interpreted cautiously.

Total organic carbon data were also compiled over the duration of the lysimeter studies. However, this information was not used in the model evaluations because GEOCHEM requires input for specific components. Because this is not available, the next option is to model the functional group composition of the organic carbon using several simple organic compounds.[29] However, this requires knowledge of the types and relative proportions of organic functional groups present.

Table 1. Aqueous Phase Species Considered in the GEOCHEM Evaluations

Metal	Aqueous Species
Ca^{2+}	$CaSO_4^0$, $CaB(OH)_4^+$, $CaMoO_4^0$, $CaOH^+$
Mg^{2+}	$MgSO_4^0$, $MgB(OH)_4^+$, $MgMoO_4^0$, $MgOH^+$, $Mg_4(OH)_4^{4+}$
K^+	KSO_4^-, $KHSO_4^0$, $K_2SO_4^0$, $KMoO_4^-$, $KB(OH)_4^0$, KOH^0
Na^+	$NaSO_4^-$, $NaHSO_4^0$, $Na_2SO_4^0$, $NaMoO_4^-$, $NaB(OH)_4^0$, $NaOH^0$
Fe^{3+}	$FeSO_4^+$, $Fe(SO_4)_2^-$, $Fe(SO_4)_3^{3-}$, $FeHSO_4^{2+}$, $FeB(OH)_4^{2+}$, $Fe[B(OH)_4]_2^+$, $FeOH^{2+}$, $Fe(OH)_2^+$, $Fe(OH)_3^0$, $Fe(OH)_4^-$, $Fe_2(OH)_2^{4+}$, $Fe_3(OH)_4^{5+}$
Fe^{2+}	$FeSO_4^0$, $Fe(SO_4)_2^{2-}$, $Fe(SO_4)_3^{4-}$, $FeHSO_4^+$, $FeB(OH)_4^+$, $FeOH^+$, $Fe(OH)_2^0$, $Fe(OH)_3^-$, $Fe(OH)_4^{2-}$
Mn^{2+}	$MnSO_4^0$, $Mn(SO_4)_2^{2-}$, $Mn(SO_4)_3^{4-}$, $MnHSO_4^+$, $MnB(OH)_4^+$, $MnOH^+$, $Mn(OH)_2^0$, $Mn(OH)_3^-$, $Mn(OH)_4^{2-}$, $Mn_2(OH)_3^+$
Cu^{2+}	$CuSO_4^0$, $Cu(SO_4)_2^{2-}$, $Cu(SO_4)_3^{4-}$, $CuHSO_4^+$,$CuB(OH)_4^+$, $Cu[B(OH)_4]_2^0$, $CuOH^+$, $Cu(OH)_2^0$, $Cu(OH)_3^-$, $Cu(OH)_4^{2-}$, $Cu_2(OH)_2^{2+}$
Cd^{2+}	$CdSO_4^0$, $Cd(SO_4)_2^{2-}$, $Cd(SO_4)_3^{4-}$, $CdHSO_4^+$, $CdB(OH)_4^+$, $Cd[B(OH)_4]_4^{2-}$, $CdOH^+$, $Cd(OH)_2^0$, $Cd(OH)_3^-$, $Cd(OH)_4^{2-}$, $Cd_4(OH)_4^{4+}$
Zn^{2+}	$ZnSO_4^0$, $Zn(SO_4)_2^{2-}$, $Zn(SO_4)_3^{4-}$, $ZnHSO_4^+$, $ZnB(OH)_4^+$, $Zn[B(OH)_4]_4^{2-}$, $ZnOH^+$, $Zn(OH)_2^0$, $Zn(OH)_3^-$, $Zn(OH)_4^{2-}$, $Zn_2(OH)_6^{2-}$
Ni^{2+}	$NiSO_4^0$, $Ni(SO_4)_2^{2-}$, $Ni(SO_4)_3^{4-}$, $NiHSO_4^+$, $NiB(OH)_4^+$, $Ni[B(OH)_4]_3^-$, $NiOH^+$, $Ni(OH)_2^0$, $Ni(OH)_3^-$, $Ni(OH)_4^{2-}$, $Ni_4(OH)_4^{4+}$
Pb^{2+}	$PbSO_4^0$, $Pb(SO_4)_2^{2-}$, $Pb(SO_4)_3^{4-}$, $PbHSO_4^+$, $PbB(OH)_4^+$, $Pb[B(OH)_4]_2^0$, $Pb[B(OH)_4]_3^-$, $PbOH^+$, $Pb(OH)_2^0$, $Pb(OH)_3^-$, $Pb(OH)_4^{2-}$, $Pb_4(OH)_4^{4+}$
Al^{3+}	$AlSO_4^+$, $Al(SO_4)_2^-$, $Al(SO_4)_3^{3-}$, $AlB(OH)_4^{2+}$, $Al[B(OH)_4]_2^+$, $Al[B(OH)_4]_3^0$, $Al[B(OH)_4]_6^{3-}$, $AlOH^{2+}$, $Al(OH)_2^+$, $Al(OH)_3^0$, $Al(OH)_4^-$, $Al_2(OH)_2^{4+}$, $Al_3(OH)_4^{5+}$
H^+	HSO_4^-, $H_2SO_4^0$, $B(OH)_3^0$, $HMoO_4^-$, $H_2MoO_4^0$, $MoO_2(OH)^+$, MoO_2^{2+}

Table 2. The Influence of pe on the $(Fe^{2+})/(Fe^{3+})$ Distribution

pe	$-\log(Fe^{2+})$	$-\log(Fe^{3+})$
nc[a]	3.02	--
4.0	3.02	11.83
5.0	3.02	10.83
6.0	3.02	9.83
7.0	3.02	8.83

[a] Not considered. Fe_T is assumed to exist only in the Fe(II) oxidation state (the redox reaction $Fe^{2+} = Fe^{3+} + e^-$ is not considered).

Because such information is not available for the lysimeter leachates, inorganic-organic interactions were not considered by GEOCHEM. It is well known that soluble organics can significantly influence solution chemistry, specifically, the distribution of trace metal cations between free ionic and complexed species. Because organic ligands were not considered in the model evaluations the model predictions must be interpreted cautiously.

Finally, GEOCHEM calculations assume that the modeled systems are at 298 K. Clearly, this condition is not met in field studies. However, the absence of this condition does not diminish the value of the model results, particularly if they are used as a first approximation of the complex chemistry of leachates from processed oil shale solid wastes.

Results and Discussion

Solution Speciation

The predicted aqueous speciation of elements in a leachate will be a function of the chemical composition of the leachate, the number of aqueous species considered in the model computations, and the magnitude of the stability constants that describe ion pair or complex ion formation. Because the anion chemistry of the lysimeter leachates is dominated by sulfate, cationic constituents are predicted to distribute between free ionic species and sulfate ion pairs. The sulfate ion pairs that dominate are of the form MSO_4^{m-2}, where M is the metal cation with m+ valence. Additionally, higher order sulfate ion pairs such as $M(SO_4)_2^{m-4}$ and $M(SO_4)_3^{m-6}$ are significant when M is Cd or Pb.

Figure 1 illustrates the percentage of total metal cation occurring as the free ionic species for Fe(II), Cd, and Al predicted by GEOCHEM. The Fe(II)/Fe(III) couple is dominated by Fe(II) (as illustrated in Table 2). Thus, only the distribution of Fe(II) is illustrated. The free ionic species distributions for Ca, Mg, Mn, Cu, Zn, and Ni are similar to those depicted by Fe(II). The percentages of these elements occurring as the free ionic species are bracketed by those predicted Fe(II) and Cd distributions. The free ionic species distributions of Na and K in the lysimeter leachates were generally greater that 90%.

In general, the percentage of any given metal occurring as the free cation is not highly variable as a function of time in lysimeter L310 and L610 leachates. Similarly, metals in L710 leachates, collected after approximately 600 days of study, show similar free-cation distributions to those predicted for L310 and L610 leachates. For the L710 leachates collected in the first 600 days of the study, the percentage of free metal increases with time from an initial minimum. Initially low free-metal percentages (high percentages of metal-sulfate ion pairs) that increase with time in lysimeter L710 leachates are a result of initially high sulfate concentrations that decrease with time.

The predicted aqueous distribution of molybdenum in L310 leachates was dominated by $HMoO_4^-$, $H_2MoO_4^0$, and $MgMoO_4^0$ with greater than 80% of the total soluble molybdenum occurring in these species. Molybdate distributions in L610 and L710 leachates were dominated by $HMoO_4^-$ and $H_2MoO_4^0$ with less than 30% of the total soluble molybdenum occurring in the $MgMoO_4^0$, MoO_4^{2-}, $CaMoO_4^0$, and $NaMoO_4^-$ species. Boron is predicted to exist as $B(OH)_3^0$ in all leachates examined. Boron speciation into $M_a[B(OH)_3]_b^{am+}$ ion pairs was not predicted due to the limitations in the GEOCHEM thermodynamic data.

Solubility Relationships

The GEOCHEM calculated metal and ligand activities are used to construct solubility diagrams. These diagrams are used to define the chemical status (saturated, undersaturated, supersaturated) of the lysimeter leachates with respect to solids that may potentially occur in the oil shale materials. The dissolution of the solid $M_aL_b(s)$ in contact with an aqueous solution can be described by the reaction:

$$M_aL_b(s) = aM^{m+}(aq) + bL^{l-}(aq) \qquad (1)$$

where M is a metal ion with charge m+, L is a ligand ion with charge l-, and a and b are stoichiometric coefficients subject to the electroneutrality condition am = bl. For the reaction in equation 1 at equilibrium, the equilibrium solubility product constant, K_{sp}, is defined as:

$$K_{sp} = (M^{m+})^a(L^{l-})^b \qquad (2)$$

where parentheses signify the thermodynamic activity of the species enclosed.

A log transformation of equation 2 and rearrangement yields:

$$pK_{sp}/b - (a/b)pM^{m+} = pL^{l-} \qquad (3)$$

where p designates -log. Thus, the stability line for solid $M_aL_b(s)$ plotted on a pM^{m+} versus pL^{l-} graph will have a -a/b slope and a pK_{sp}/b intercept. The predicted metal and ligand activities, when plotted on such a diagram, shows the chemical status of a solution with respect to solid $M_aL_b(s)$. Data points that plot on the stability line suggest that the solution is saturated with respect to $M_aL_b(s)$. This is generally indirect evidence that the solid may be present and may be controlling the concentrations of M or L, assuming that equilibrium conditions prevail. If the predicted activity data do not plot on the stability line, then one of two conditions may exist: solution undersaturation or supersaturation with respect to $M_aL_b(s)$. Both conditions suggest that solution chemistry is not controlled by the particular solid or that equilibrium has not been achieved. An undersaturated condition suggests that there is a potential for $M_aL_b(s)$ to dissolve, if it is present or added to

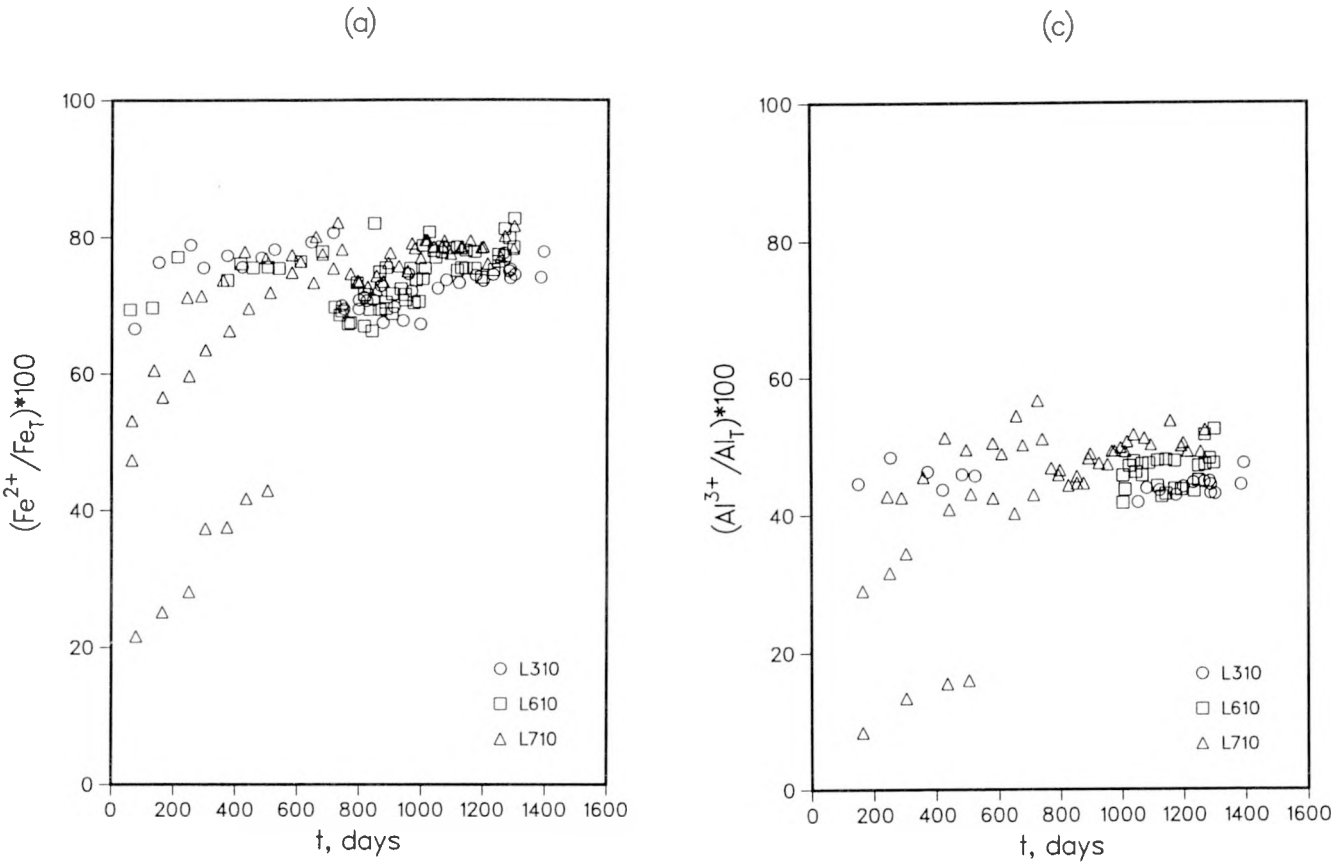

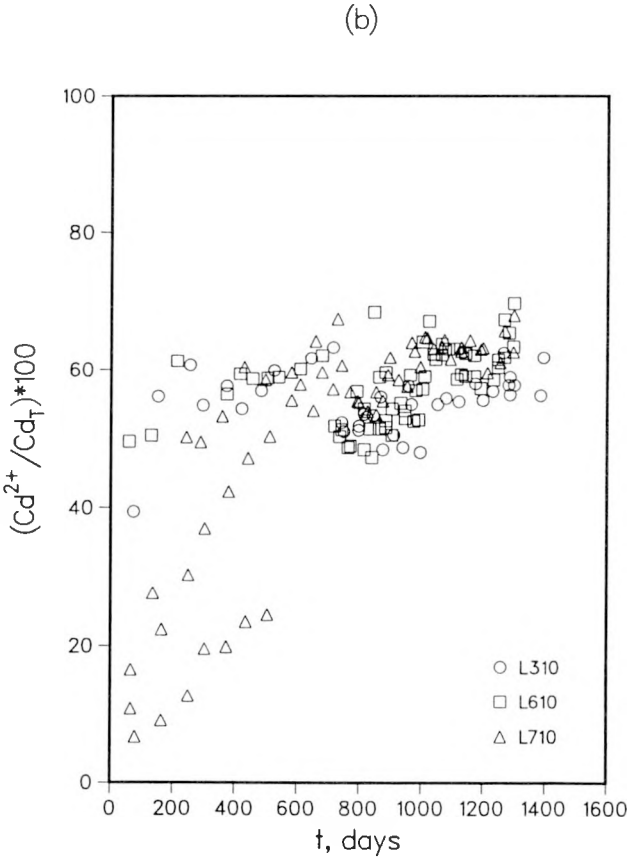

Figure 1. Percentage of Total Fe(II), Cd, and Al Occurring as the Free Ionic Species

the system. Further, a supersaturated condition merely suggests that there is a potential for $M_aL_b(s)$ to precipitate.

The GEOCHEM predicted activity data can also be used to examine solubility equilibria as a function of time by plotting the ion activity product (IAP) as a function of sampling time. Ion activity product values are a property of the solution and are calculated for specific mineral phases using the predicted ion activities. For example, the IAP for solid $M_aL_b(s)$ has the form:

$$IAP = (M^{m+})^a(L^{l-})^b \qquad (4)$$

If the calculated IAP is numerically equal to K_{sp}, then GEOCHEM predicts that the solution is controlled by the solid $M_aL_b(s)$. Ion activity product values greater than K_{sp} suggest solution supersaturation and IAP values less than K_{sp} suggest undersaturation. Solubility relationships used in this study are listed in Table 3.

The dominant anionic component of the lysimeter leachates is SO_4^{2-}. Thus, a great majority of the constructed solubility diagrams relate free-metal ion activity to SO_4^{2-} activity and, correspondingly, allow metal sulfate solubility equilibria to be evaluated. Figure 2 illustrates the calcium sulfate equilibria for the lysimeter leachates. The activities of Ca^{2+} are inversely related to those of SO_4^{2-}. During the early stages of the study, all leachates are predicted to be supersaturated with respect to gypsum. However, after approximately 800 days of study, gypsum IAP values stabilize at a value slightly greater than the

Table 3. Solubility Relationships Used in this Study

Reaction	pK_{sp}
$CaSO_4 \cdot 2H_2O$ [gypsum] = $Ca^{2+} + SO_4^{2-} + 2H_2O$	4.64[21]
$MgSO_4 \cdot 7H_2O$ [epsomite] = $Mg^{2+} + SO_4^{2-} + 7H_2O$	2.14[33]
$FeSO_4 \cdot 7H_2O$ [melanterite] = $Fe^{2+} + SO_4^{2-} + 7H_2O$	4.66[3]
$FeOOH$ [goethite] + $3H^+$ = $Fe^{3+} + 2H_2O$	0.02[34]
$KFe_3(SO_4)_2(OH)_6$ [K-jarosite] + $6H^+$ = $K^+ + 3Fe^{3+} + 2SO_4^{2-} + 6H_2O$	14.8[33]
$NaFe_3(SO_4)_2(OH)_6$ [Na-jarosite] + $6H^+$ = $Na^+ + Fe^{3+} + 2SO_4^{2-} + 6H_2O$	11.2[33]
$FeSO_4OH$ [Fe-jurbanite] + H^+ = $Fe^{3+} + SO_4^{2-} + H_2O$	10.06[20]
$MnSO_4 \cdot H_2O$(c) = $Mn^{2+} + SO_4^{2-} + H_2O$	-0.47[34]
$CuSO_4 \cdot H_2O$(c) = $Cu^{2+} + SO_4^{2-} + H_2O$	2.61[34]
$CdSO_4 \cdot {}^8/_3H_2O$(c) = $Cd^{2+} + SO_4^{2-} + {}^8/_3H_2O$	1.87[33]
$ZnSO_4 \cdot 7H_2O$ [goslarite] = $Zn^{2+} + SO_4^{2-} + 7H_2O$	1.96[33]
$ZnFe_2O_4$ [franklinite] + $8H^+$ = $Zn^{2+} + 2Fe^{3+} + 4H_2O$	-6.87[14]
$NiSO_4 \cdot 7H_2O$ [morenosite] = $Ni^{2+} + SO_4^{2-} + 7H_2O$	2.36[33]
$NiFe_2O_4$ [trevorite] + $8H^+$ = $Ni^{2+} + Fe^{3+} + 4H_2O$	-10.63[35]
$Al(OH)_3$ [gibbsite] + $3H^+$ = $Al^{3+} + 3H_2O$	-8.77[33]
$AlSO_4OH$ [jurbanite] + H^+ = $Al^{3+} + SO_4^{2-} + H_2O$	3.8[30]
$Al_4SO_4(OH)_{10}$ [basaluminite] + $10H^+$ = $4Al^{3+} + SO_4^{2-} + 10H_2O$	-22.4[36]
$KAl_3(SO_4)_2(OH)_6$ [alunite] + $6H^+$ = $K^+ + 3Al^{3+} + 2SO_4^{2-} + 6H_2O$	1.4[36]

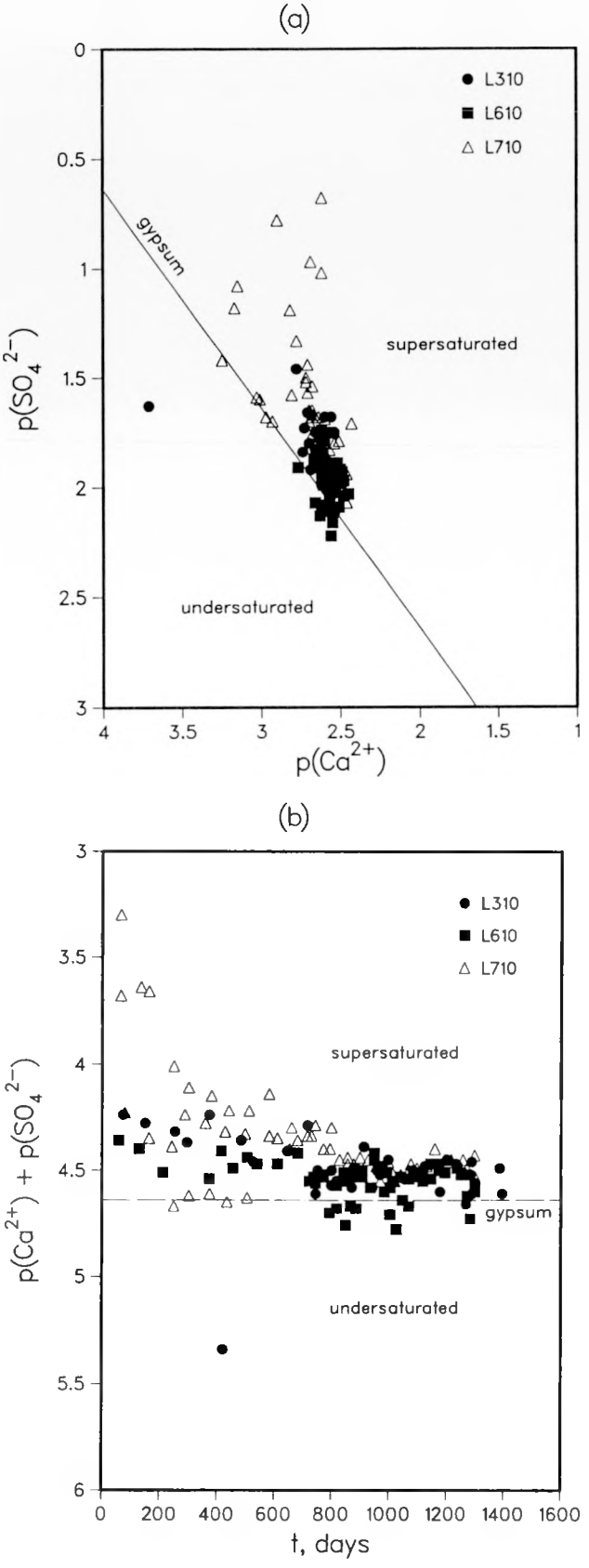

Figure 2. Calcium Sulfate Equilibria in Lysimeter Leachates

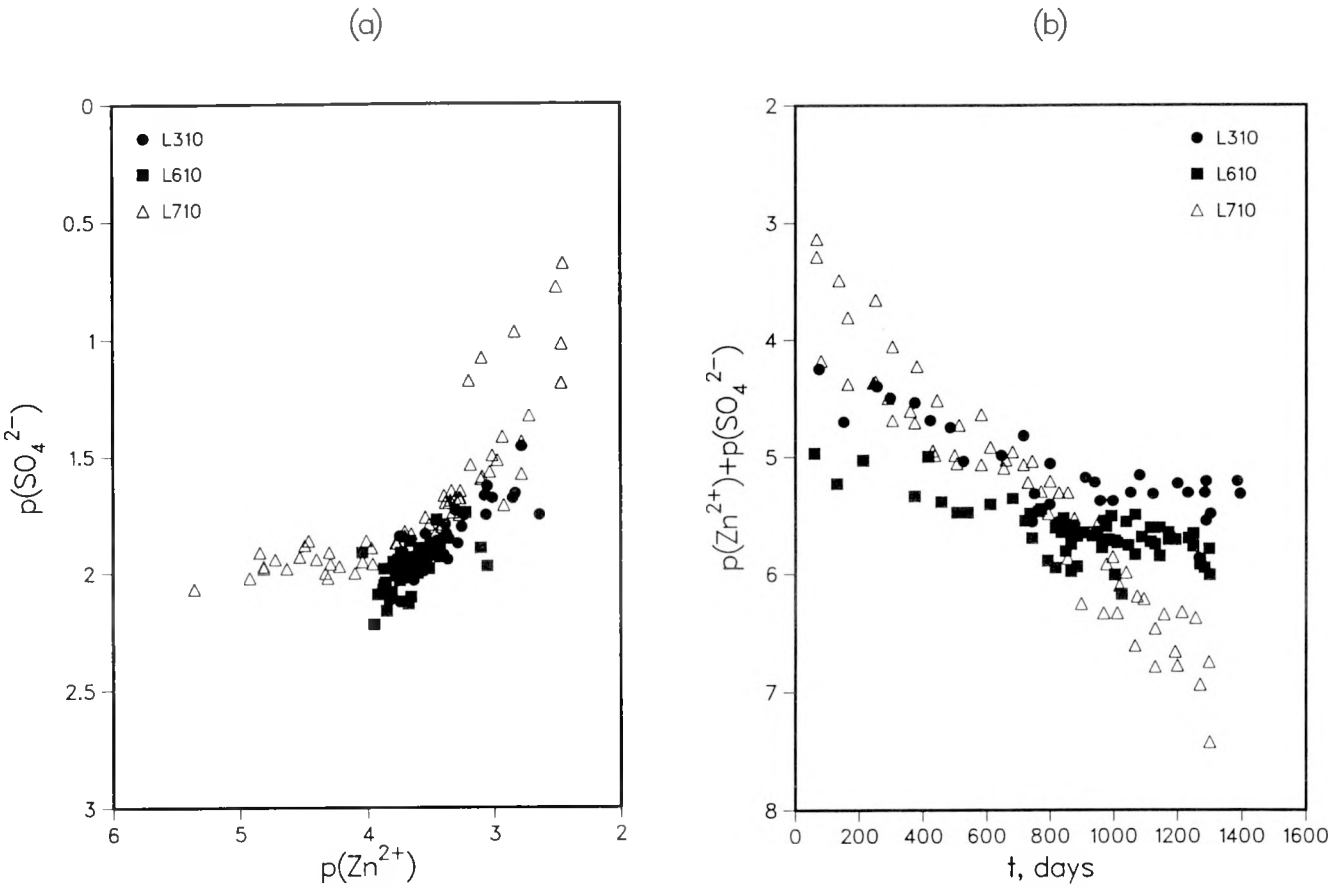

Figure 3. Zinc Sulfate Equilibria in Lysimeter Leachates

K_{sp}, suggesting supersaturated conditions. However, due to the assumptions used in the model analysis and the inherent uncertainties in the thermodynamic data, a calculated pIAP within ±0.5 of pK_{sp} is not an unreasonable definition of saturation. Thus, the lysimeter leachates are predicted by GEOCHEM to approach saturation with respect to gypsum. A similar conclusion was reached by Robl using the WATEQ code.[22]

Metal sulfate equilibria relationships for Mg, Mn, Cu, Cd, Zn, and Ni were similar. This relationship is illustrated with Zn in Figure 3. In general, metal ion and SO_4^{2-} activities in L710 leachates are directly related. Metal ion and SO_4^{2-} activities in L310 and L610 leachates are directly related or unrelated. Metal sulfate IAP values for L710 leachates continuously decrease with time. Metal sulfate IAP values for the L310 and L610 leachates also decrease with time, although not to the same extent as L710 leachates, and the calculated IAP values appear to stabilize after approximately 800 days of study. Irrespective of the predicted variances in calculated IAP values, all leachates are highly undersaturated with respect to even the most stable metal sulfates (Table 3).

Sullivan et al.[20] examined the equilibrium weathering of New Albany and Chattanooga Shales using the WATEQFC model. They found that oil shale extracts under moderately reducing and acidic conditions were saturated with respect to melanterite ($FeSO_4 \cdot 7H_2O$). Although SO_4^{2-} activities are directly related to those of Fe^{2+}, the L710 leachates approach saturation with respect to melanterite from supersaturation (Figure 4). Leachates from the lysimeters containing retorted oil shales (L310 and L610) are, in general, undersaturated with respect to the ferrous sulfate and the calculated IAP values are highly variable with time.

As previously noted, predicted Fe^{3+} activities are directly related and highly sensitive to the redox status of the leachates. Because leachate redox values for model input were estimated and not measured values, conclusions based on GEOCHEM predicted Fe^{3+} activities must be interpreted cautiously. The ferric iron sulfate equilibria illustrates that SO_4^{2-} and Fe^{3+} activities are directly related (Figure 5). Lysimeter leachate equilibria with respect to some ferric sulfate minerals commonly associated with acid sulfate weathering are also illustrated in Figure 5. In general, the calculated IAP values for Na- and K-jarosite are highly scattered and suggest that the lysimeter leachates are undersaturated with respect to these minerals.

The lysimeter leachates were also evaluated with respect to a basic iron sulfate solid phase (Fe-jurbanite, $FeSO_4OH$), whose stoichiometry and stability were suggested by Sullivan et al.[20] from eastern oil shale equilibrium leachates. Lysimeter L710 leachates were supersaturated with respect to Fe-jurbanite and calculated IAP values approached a constant value after approximately 800 days of study. Given the assumptions used to predict Fe^{3+} activities, it is plausable to conclude that the L710 leachates approach saturation with respect to Fe-jurbanite. Further, differences in the L710 IAP values and the Fe-jurbanite K_{sp} may also result from errors associated with the noncritical determination of K_{sp}. Lysimeter L310 and L610 leachates were also supersaturated with respect to Fe-jurbanite.

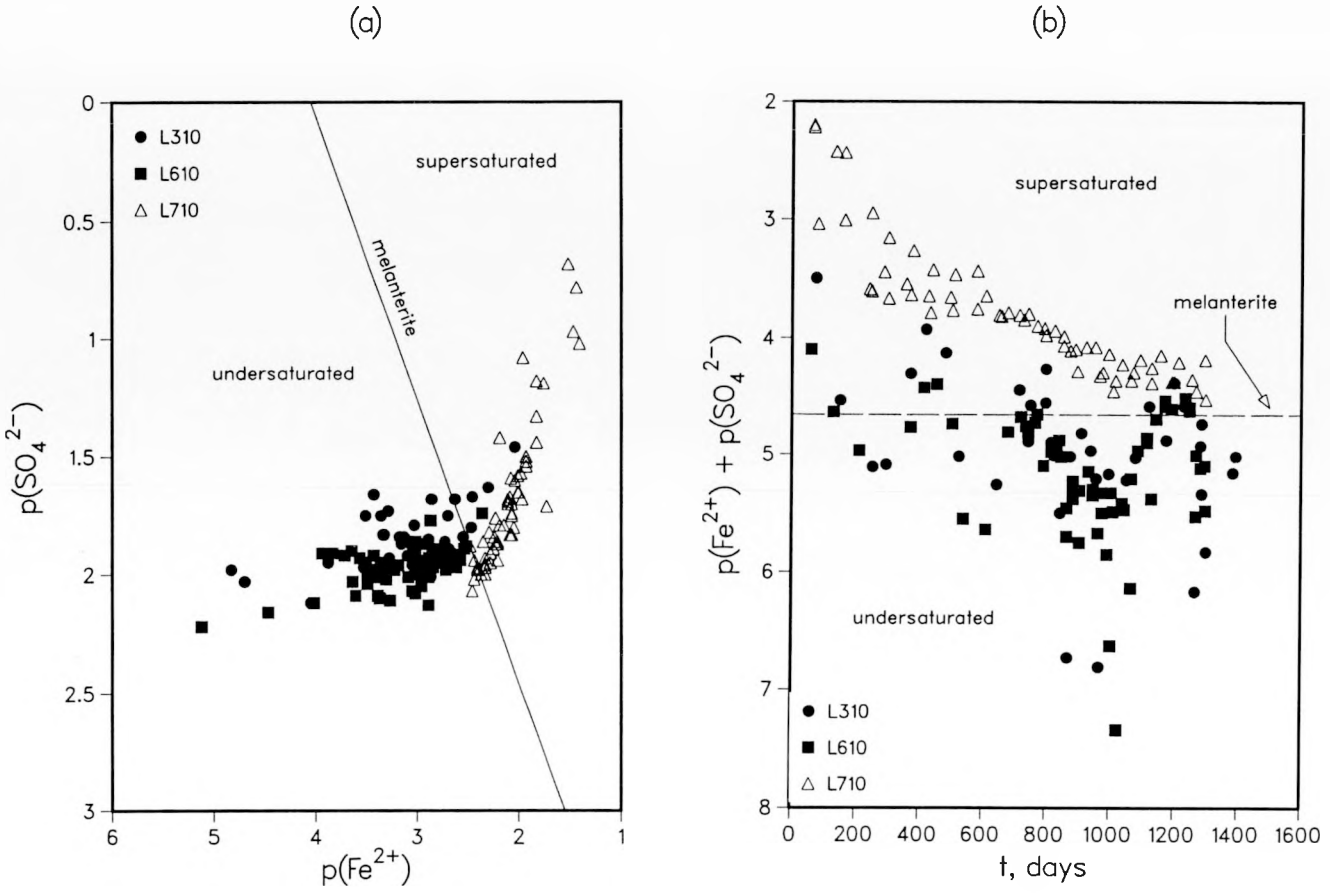

Figure 4. Ferrous Sulfate Equilibria in Lysimeter Leachates

However, the IAP values for these leachates were variable with time. Finally, The Fe^{3+} equilibria data suggest that the lysimeter leachates may be saturated with respect to goethite (Figure 6), again supporting the observations of Robl.[22]

Reddy et al.[14] examined the solubility relationships of zinc associated with New Albany and Chattanooga Shale leachates. Zinc activities in leachates with pH values greater than 7.0 were supported by Zn_2SiO_4 (willemite), whereas zinc activities in leachates with pH values less than 5.0 were supported by $ZnFe_2O_4$ (franklinite). The status of the lysimeter leachates with respect to franklinite and $NiFe_2O_4$ (trevorite) is illustrated in Figure 7. The diagrams show that the leachates are undersaturated with respect to the ferrite phases. The leachates were also undersaturated with respect to the Cu-ferrite solid phase (not shown). Because there are potential errors associated with the predicted Fe^{3+} activity values lysimeter leachate saturation with respect to the metal ferrites, especially franklinite, cannot be ruled out. Evaluation of the stability of the metal silicate phases was not possible because silicon concentrations in the lysimeter leachates were not determined.[22]

Aluminum chemistry was evaluated with respect to a number of solids predicted to occur in weathering acid sulfate materials.[19,20,30-32] The status of the lysimeter leachates with respect to aluminosilicates such as kaolinite could not be determined because soluble silica concentrations were not determined.[22] The pH versus $p(Al^{3+})$ activity diagram (Figure 8) suggests that Al^{3+} in L710 leachates may be controlled by alunite $[KAl_3(SO_4)_2(OH)_6]$ or jurbanite $(AlSO_4OH)$. Lysimeter L310 and L610 leachates are undersaturated with respect to basaluminite $[Al_4SO_4(OH)_{10}]$ and supersaturated with respect to alunite. All leachates are undersaturated with respect to gibbsite $[Al(OH)_3]$.

Plots of mineral IAP values versus study duration (Figure 7) show that soluble Al in the lysimeter leachates is not supported by the basic aluminum sulfates. In general, L310 and L610 leachates are supersaturated with respect to alunite and jurbanite and undersaturated with respect to basaluminite. Leachate from L710 are undersaturated with respect to alunite and basaluminite and become undersaturated with respect to jurbanite with study duration. This latter condition is inconsistent with the findings of Sullivan et al.[19,20] They report that acidic New Albany and Chattanooga Shale leachates are saturated with respect to jurbanite.

Conclusions

Results of the chemical equilibria model analysis of leachates from field lysimeters provided a more detailed characterization of the chemistry of oil shale materials. The aqueous chemistry of an eastern oil shale, retorted eastern oil shale, and an oil shale fines/retorted oil shale mixture is dominated by free ionic metal species and metal sulfate ion pairs. Activity diagrams show that free metal ion activities (with the exception of Ca^{2+}) are directly related to SO_4^{2-} activities. This suggests that the aqueous activities of the metals examined are not supported by metal sulfate solid phases. However, an

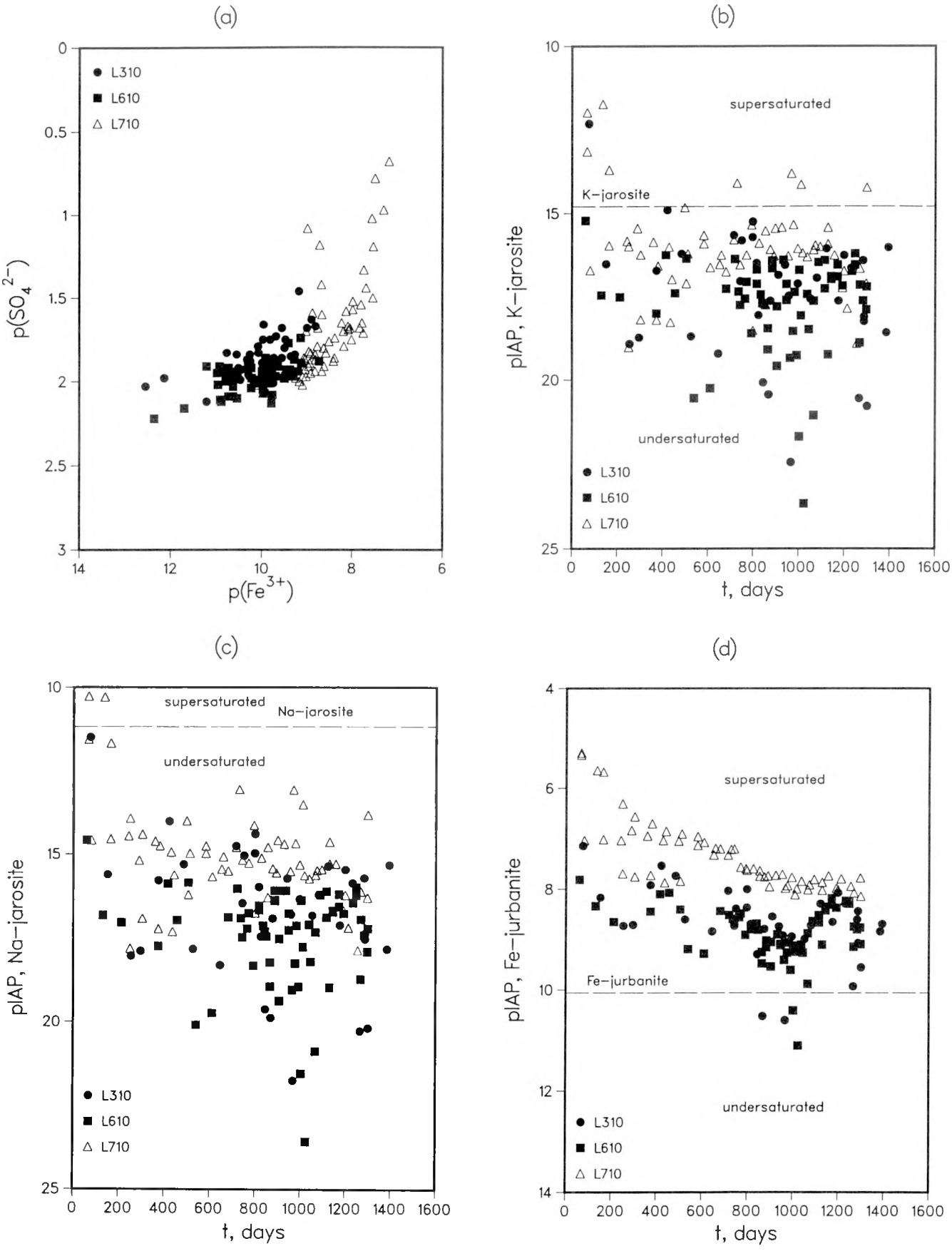

Figure 5. Ferric Sulfate Equilibria in Lysimeter Leachates

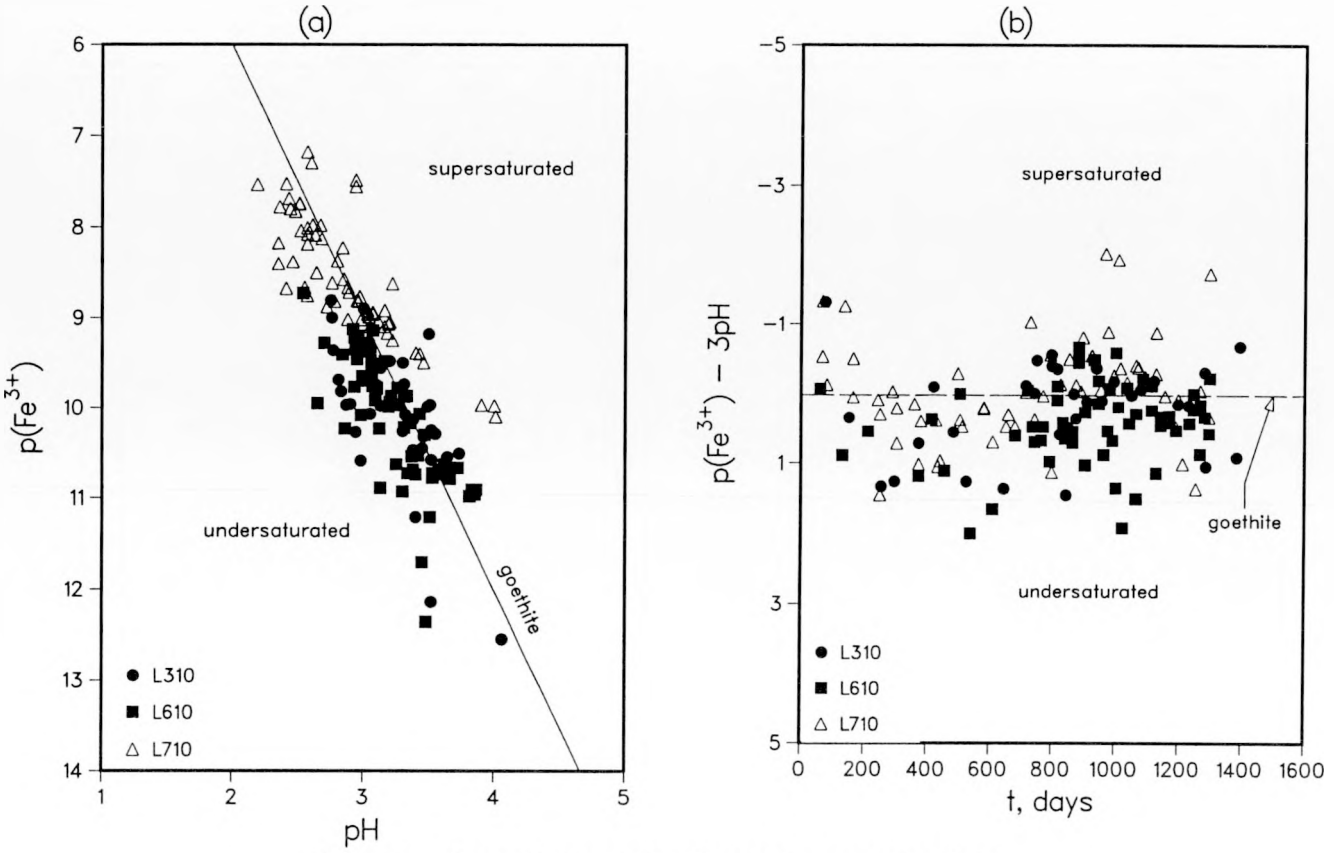

Figure 6. Ferric Hydroxide Equilibria in Lysimeter Leachates

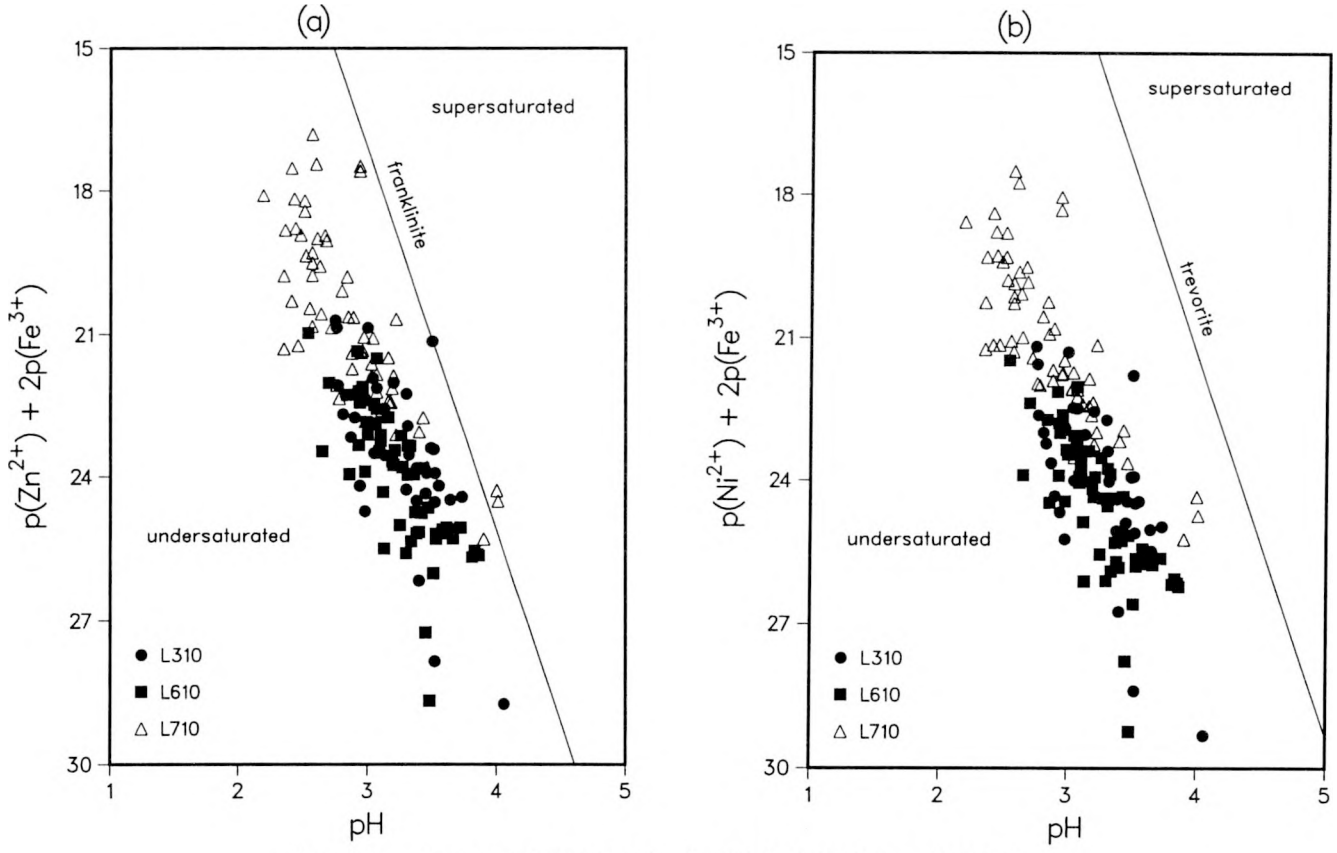

Figure 7. Zinc and Nickel Ferrite Equilibria in Lysimeter Leachates

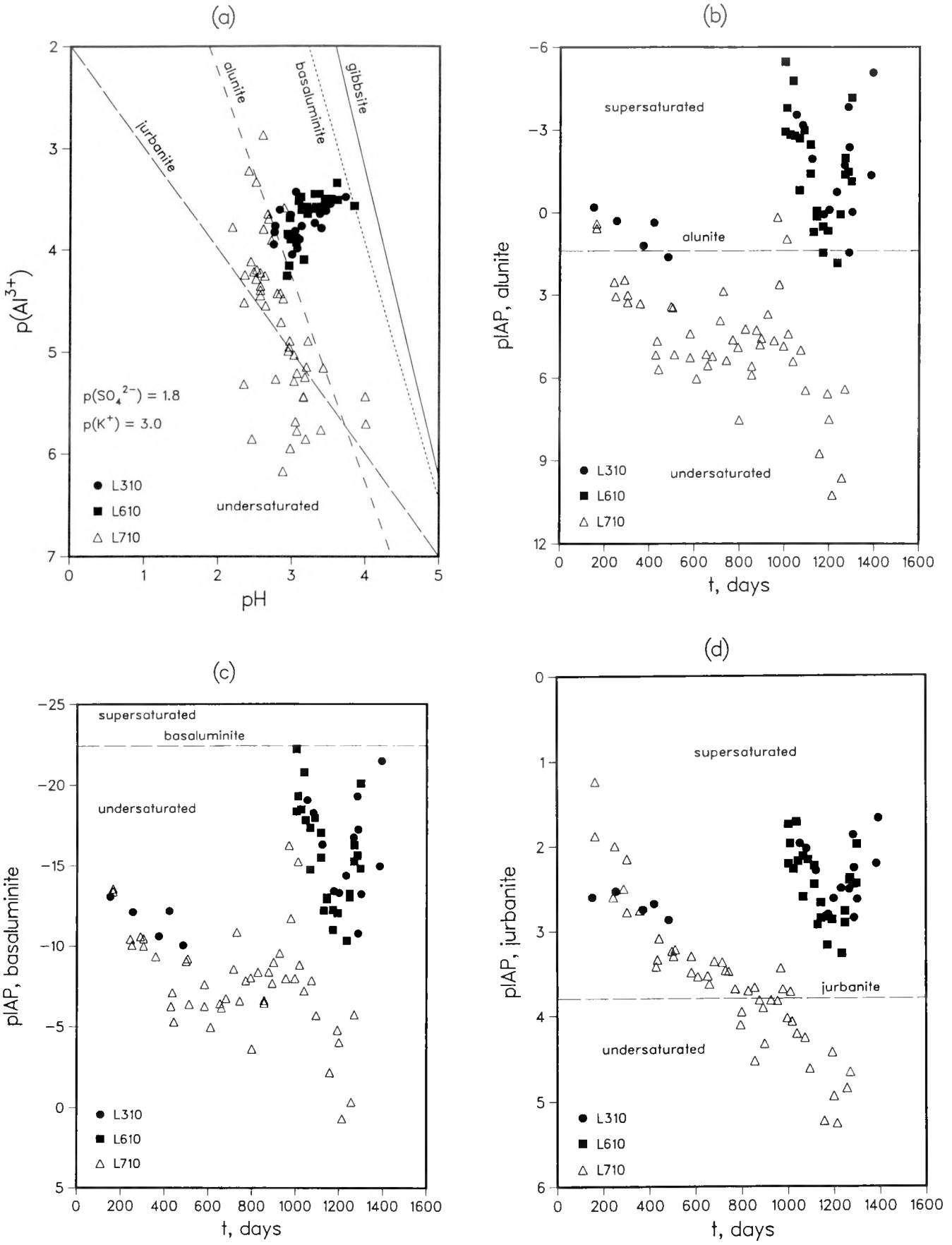

Figure 8. Aluminum Sulfate Equilibria in Lysimeter Leachates

examination of metal sulfate ion activity products as a function of time show that the IAPs approach constant values after approximately 800 days of the field study. For the great majority of the metals examined, the IAP values suggest leachate undersaturation with respect to even the most stable metal sulfate phases. Leachates from all three materials are predicted by GEOCHEM to approach equilibrium with respect to gypsum and goethite. In addition, leachates from the oil shale lysimeter are predicted by GEOCHEM to approach equilibrium with respect to melanterite, Fe-jurbanite, and franklinite. Aluminum activities in all three lysimeter leachates fall within the stability region of several basic aluminum sulfates. However, Al^{3+} activities in the lysimeter leachates are not supported by sulfate phases.

Acknowledgements

I wish to thank Dr. Thomas Robl for providing the leachate concentration data for model analysis and the United States Department of Energy for funding this work under Cooperative Agreement Number DE-FC21-86MC11076.

References

1. Saether, O.M., and D.D. Runnells, 1980, Geochemistry of Fluorine in Oil Shale Leachates. 13th Oil Shale Symposium Proceedings, Golden, CO, 362-368.

2. Stollenwerk, K.G., and D.D. Runnells, 1981, Composition of Leachate from Surface-Retorted and Unretorted Colorado Oil Shale. Environ. Sci. Technol., 15: 1340-46.

3. Runnells, D.D., and R.D. Lundberg, 1981, Hydrogeochemical exploration for Uranium Deposits: Use of the Computer Model WATEQFC. J. Geochem. Explor., 15: 37-50.

4. Truesdell, A.H., and B.F. Jones, 1974, WATEQ - A Computer Program for Calculating Chemical Equilibria in Natural Water. J. Res. U. S. Geol. Surv., 2: 233-248.

5. Esmaili, E., R.B. Carroll, and L.P. Jackson, 1985, Assessing Potential Trace Metal Leachability of Retorted Oil Shale by Complexometric Agents. 18th Oil Shale Symposium Proceedings, Golden, CO, 326-337.

6. Reddy, K.J., and W.L. Lindsay, 1986, The Solubility Relationships of Calcium and Magnesium Minerals in Processed Oil Shale. J. Environ. Qual., 15: 1-4.

7. Reddy, K.J., W.L. Lindsay, F.W. Boyle, and E.F. Redente, 1986, Solubility Relationships and Mineral Transformations Associated with Recarbonation of Retorted Shales. J. Environ. Qual., 15: 129-133.

8. Essington, M.E., and L.K. Spackman, 1986, Recarbonation of Retorted Oil Shale: The Influence on Mineralogy and Leachate Chemistry. Laramie, WY, DOE Report DOE/FE/60177-2433.

9. Parkhurst, D.L., D.C. Thorstenson, and L.N. Plummer, 1980, PHREEQE - A Computer Program for Geochemical Calculations. U.S. Geological Survey, Water Resources Investigations, 80-96.

10. Felmy, A.R., D.Girvin, and E.A. Jenne, 1984, MINTEQ: A Computer Program for Calculating Aqueous Geochemical Equilibria. Athens, GA, Environmental Protection Agency.

11. Essington, M.E., L.K. Spackman, J.D. Harbour, and K.D. Hartman, 1987, Physical and Chemical Characteristics of Retorted and Combusted Western Reference Oil Shale. Laramie, WY, DOE Report DOE/MC/11076-2453.

12. Essington, M.E., and L.K. Spackman, 1988, Inorganic Geochemical Investigations of Spent Oil Shales. Laramie, WY, DOE Report DOE/MC/11076-2701.

13. Sposito, G., and S.V. Mattigod, 1980, GEOCHEM: A Computer Program for the Calculation of Chemical Equilibria in Soil Solutions and Other Natural Water Systems. University of California, Riverside, CA.

14. Reddy, K.J., P.J. Sullivan, and J.L. Yelton, 1988, Solubility Relationships of Zinc Associated with Acid Mine Drainage. J. Environ. Qual., 17: 712-714.

15. Essington, M.E., 1987, Modeling Fluoride Chemistry in Hydrated and Recarbonated Spent Western Oil Shales. 1987 Eastern Oil Shale Symposium Proceedings, Lexington, KY, 21-33.

16. Essington, M.E., Calcium Molybdate Solubility in Spent Oil Shale and a Preliminary Evaluation of the Association Constants for the Formation of $CaMoO_4^0$(aq), $KMoO_4^-$(aq), and $NaMoO_4^-$(aq). Environ. Sci. Technol., in press.

17. Spackman, L.K., K.D. Hartman, J.D. Harbour, and M.E. Essington, Adsorption of Oxyanions by Spent Western Oil Shale: I. Arsenate. Environ. Geol. Water Sci., in press.

18. Spackman, L.K., K.D. Hartman, J.D. Harbour, and M.E. Essington, Adsorption of Oxyanions by Spent Western Oil Shale: II. Selenite. Environ. Geol. Water Sci., in press.

19. Sullivan, P.J., J.L. Yelton, and K.J. Reddy, 1988, Solubility Relationships of Aluminum and Iron Minerals Associated with Acid Mine Drainage. Environ. Geol. Water Sci., 11: 283-287.

20. Sullivan, P.J., J.L. Yelton, and K.J. Reddy, 1988, Iron Sulfide Oxidation and the Chemistry of Acid Generation. Environ. Geol. Water Sci., 11: 289-295.

21. Reddy, K.J., J.I. Drever, and V.R. Hasfurther, 1988, Application of Geochemical Models to Oil Shale Solid Waste. Laramie, WY, DOE report in press.

22. Robl, T.L., 1989, Field and Laboratory Leaching Studies of Retorted Kentucky Oil Shale. Lexington, KY, DOE report in press.

23. Koppenaal, D.W., R.R Kruspe, T.L. Robl, K. Cisler, and D.L. Allen, 1984, The Examination of Eastern Oil Shale Disposal Problems - The Hope Creek Field Study. 1984 Eastern Oil Shale Symposium Proceedings, Lexington, KY, 199-206.

24. Robl, T.L., G. Thomas, K. Cisler, and D. Koppenaal, 1985, Leaching Characteristics of Eastern Oil Shale: First Year Data Summary of the Hope Creek Study. 1985 Eastern Oil Shale Symposium Proceedings, Lexington, KY, 117-129.

25. Robl, T.L., J. Obley, G. Thomas, W. Jones, and M. Shirav, 1986, Elemental Release Characteristics of Eastern Oil Shales: Comparison of Field and Laboratory Results. 1986 Eastern Oil Shale Symposium Proceedings, Lexington, KY, 231-243.

26. Robl, T., J. Obley, B. Schram, G. Thomas, and J. Kung, 1987, Leachate Composition and Elemental Release Pattern for Eastern Oil Shale Materials from the Hope Creek Field Study. 1987 Eastern Oil Shale Symposium Proceedings, Lexington, KY, 59-66.

27. Robl, T.L., L.S. Barron, W. Schram, and G. Thomas, 1988, Final Summary of Data from the Hope Creek Field Lysimeter Study. 1988 Eastern Oil Shale Symposium Proceedings, Lexington, KY, 115-121.

28. Essington, M.E., Chemical Equilibria Model Analysis of Hope Creek Eastern Oil Shale Lysimeter Leachate Data. Laramie, WY, DOE report in press.

29. Mattigod, S.V., and G. Sposito, 1979, Chemical Modeling of Trace Metal Equilibria in Contaminated Soil Solutions Using the Computer Program GEOCHEM, in Jenne, E.A., ed., Chemical Modeling in Aqueous Systems, ACS Symposium Series No. 93, American Chemical Society, Washington, DC, 837-856.

30. Nordstrom, D.K., 1982, The Effect of Sulfate on Aluminum Concentrations in Natural Waters: Some Stability Relations in the System Al_2O_3-SO_3-H_2O at 298 K. Geochim. Cosmochim. Acta, 46: 681-692.

31. Karathanasis, A.D., V.P. Evangelou, and Y.L. Thompson, 1988, Aluminum and Iron Equilibria in Soil Solutions and Surface Waters of Acid Mine Watersheds. J. Environ. Qual., 17: 534-543.

32. von Freiesleben, N.E., 1988, Sulfate Mobility in an Acid Danish Forest Soil. J. Environ. Qual., 17: 278-284.

33. Ball, J.W., D K. Nordstrom, and E.A. Jenne, 1980, Additional and Revised Thermodynamical Data and Computer Code for WATEQ2 - A Computerized Chemical Model for Trace and Major Element Speciation and Mineral Equilibria of Natural Waters. U.S. Geological Survey, Water Resources Investigations 78-116.

34. Lindsay, W.L., 1979, Chemical Equilibria in Soils. John Wiley and Sons, New York, NY, 449 p.

35. Naumov, G.B., B.N. Ryzhenko, and I.L. Khodakovsky, 1974, Handbook of Thermodynamic Data. U. S. Geological Survey, PB226722.

36. Adams,F., and Z. Rawajfih, 1977, Basaluminite and Alunite: A Possible Cause of Sulfate Retention by Acid Soils. Soil Sci. Soc. Am. J., 41: 686-692.

The Use of Activated Carbon in the Treatment of a Synthetic Oil Shale Processing Wastewater

by

Ronald W. Ballard, William P. Bonner, Rafael Bustamante, Sachin V. Prabhu
Department of Civil Engineering
Tennessee Technological University
Cookeville, Tennessee 38505

Abstract. Results from batch carbon adsorption experiments are reported that determined removal of four selected contaminants from a synthetic wastewater for a pressurized, fluidized-bed hydroretorting oil shale process. Acetone and thiocyanate exhibited very low affinities for activated carbon, while larger quantities of pyrrole and propionitrile were removed. All four compounds, however, demonstrated low adsorbances relative to other organic species that are successfully removed from solution by activated carbon. The presence of other compounds in multiple solute experiments had little effect on the adsorption of acetone due to its low affinity for activated carbon. The adsorption of pyrrole in multiple solute experiments was consistently less than that in single solute experiments due to competition for active sites in multiple solute experiments. Propionitrile and thiocyanate, on the other hand, demonstrated a decrease in adsorption in the presence of multiple solutes except at very low concentrations. All data were reasonably fitted with the Freundlich isotherm.

Introduction

As society becomes more and more advanced in technology, its demand for energy continues to increase. As conventional sources of energy diminish, alternative sources must be developed. One alternative source of energy that is currently being investigated is that from Eastern oil shale. In a three-year Department of Energy sponsored project, the Institute of Gas Technology (IGT) is developing the pressurized, fluidized-bed hydroretorting (PFH) process for the production of oil from Eastern oil shales. Conventional oil shale retorting technologies are not as efficient for Eastern oil shales as the PFH process. Organic carbon conversions up to 28-40% have been reported for conventional thermal retorting while increased organic carbon conversions have been obtained in mini-bench scale tests for hydroretorting.[1]

As with the development of any new technology, the environmental impact associated with its use must be investigated. As the PFH process is being developed, environmental data are being generated. As a subtask of the IGT project, Tennessee Technological University (TTU) is investigating the treatability of selected organics determined to be present in the retort wastewater.

During the PFH process, water vapor generated from shale moisture and high-temperature water is in intimate contact with the oil and solid matrix at high temperature and pressure, resulting in the presence of various organic and inorganic constituents in the wastewater stream.[2] Treatment of this stream is imperative prior to its recycle or discharge. Some of the compounds found in the wastewater stream are known to be treatable by conventional methods; therefore, TTU and IGT selected

four representative organic species from those for which treatment was less certain. Those four organic compounds are acetone, propionitrile, pyrrole, and thiocyanate. This paper addresses the treatability of these four compounds by adsorption onto activated carbon.

Theoretical Principles

Adsorption is the accumulation of material at the interface between phases. For applications to water treatment, adsorption from solution occurs when impurities in the liquid accumulate at a solid-liquid interface. Several adsorbents are used in industry; however, activated carbon is the most widely used because it is both an inexpensive and a nonpolar adsorber.[3] Activated carbon is produced by a two-step process: (1) An organic material (coal, bone, hardwood, nut shells, etc.) is pyrolized and (2) the resulting residue of carbon and hydrocarbons is oxidized to produce a highly porous material with an activated surface.[3] Activated carbon is marketed in powdered and granular forms. Powdered activated carbon (PAC) is pulverized so that 95-100% will pass a 100-mesh sieve and 50-95% will pass a 325-mesh sieve.[4] Granular activated carbon (GAC) is designated by two numbers such as 20/40. This means that the GAC is composed of particles passing a 20-mesh sieve and retained on a 40-mesh sieve.[4]

The adsorption process occurs in four steps:

(1) the transport of the solute from the bulk solution phase to the boundary layer or surface film surrounding the adsorbent particle,

(2) the transport of the solute across the boundary layer to the exterior surface of the adsorbent particle,

(3) the diffusion of solute into the active pores of the adsorbent particle, and

(4) the physical or chemical binding of adsorbate to the internal surface of adsorbent.[5]

In general, the above process is utilized in one of two systems. One is the batch system which generally uses PAC, and the second is the continuous flow system which utilizes GAC.

Results from carbon adsorption studies are reported in the form of isotherms. The Freundlich isotherm is the most commonly used isotherm[3] and has been used in this study. The isotherm developed by Freundlich is an empirical equation (as are other isotherms) that describes the adsorption process. The equation for this relationship is

$$X/M = KC^{1/n} \qquad (1)$$

where X is the amount of solute adsorbed in mg, M is the weight of the adsorbent in grams, C is the concentration of solute remaining in solution after adsorption, and K and n are constants that must be developed for each solute.

The Freundlich equation can be put in a useful form by taking the logarithm of both sides:

$$\log (X/M) = \log K + 1/n(\log C) \qquad (2)$$

A plot of log (X/M) versus log C will yield a straight line if the data follow the Freundlich isotherm.[4]

Even though several compounds have been studied for treatability by activated carbon adsorption, the data available is very limited in comparison to the vast array of synthetic chemicals that exist and are continually being produced.[6] Furthermore, total adsorption of mixtures of compounds cannot be determined from adsorption data available for the individual components of such mixtures.[4] Therefore, experimentation is necessary to determine the adsorption of acetone, propionitrile, pyrrole, and thiocyanate. Consequently, a series of batch experiments were conducted for both single and multiple solute solutions. The data were plotted to determine whether they fit the Freundlich isotherm and to determine the effect that the presence of the other compounds had on the adsorption of individual compounds.

Methods and Materials

Materials

The activated carbon used for experimentation was Filtrasorb 300 (F-300, Calgon Corporation), specifically, a 20/40 GAC. For batch experiments, PAC was prepared from the 20/40 GAC by grinding in a ball mill and then sieving. The fraction passing a 200-mesh sieve but remaining on a 400-mesh sieve was collected. The sieved carbon was dried to constant weight at 105 degrees Celsius and stored in a dessicator. Water used to prepare synthetic waste solutions was organic-free distilled water. All chemicals used were reagent grade. All glassware was cleaned by soaking in chromic acid overnight, rinsing a minimum of five times, and oven-drying at 105 degrees Celsius.

Batch Experiments

Using distilled water, stock solutions of the selected compounds were prepared in the initial concentration range and subsequent concentrations made by dilution. Light resistant ground glass stoppered reagent bottles with

volumes slightly greater than one liter were used as reactors. One liter volumes of synthetic waste solutions were added to the reactors in varying concentrations, stirred for four hours with a magnetic stirrer, and then sampled to determine initial solute concentration. A fixed weight of activated carbon was thoroughly wetted, added to the bottle, and this solution stirred for four hours. Samples were then taken and filtered through 0.2 micron filter paper, and the final solute concentration determined. These data were tabulated and used to develop Freundlich isotherms.

Analyses

Concentrations of acetone, propionitrile, and pyrrole were determined by a Hewlett-Packard Model 5890A Gas Chromatograph (GC), and thiocyanate concentrations were determined by a colorimetric procedure for cyanides amenable to chlorination.[7] Absorbances for these colorimetric analyses were measured using a Perkin-Elmer Lambda 3 UV-Visible Spectrophotometer.

Results and Discussion

Batch carbon adsorption experiments were conducted to determine the adsorption of acetone, propionitrile, pyrrole, and thiocyanate by activated carbon in single solute solutions. Experiments with multiple solute solutions (solutions containing the four compounds in approximately equal concentrations) were conducted to determine the effect of multiple solutes on the adsorption of single solutes. The results from these experiments with acetone are shown in Figures 1 through 3. Figure 1 shows the Freundlich isotherm for the single solute experiment, Figure 2 shows the Freundlich isotherm for the adsorption of acetone from solutions containing multiple solutes, and Figure 3 shows the results from both of these experiments. The low affinity of acetone for activated carbon is evidenced by the maximum value of 46 mg of acetone removed per gram of carbon at a final concentration of 1162 mg/l. Very little difference is seen in the data for single and multiple solute experiments, probably because of the low affinity for activated carbon. With so little acetone being adsorbed, all of the active sites were certainly not filled, thus the presence of other compounds had little effect on the amount of acetone adsorbed. The scatter of data is also attributed to the low adsorption of acetone. When such small differences exist in initial and final concentrations, small errors in analysis are magnified in the values of X and thus the values of X/M. To ensure the sufficiency of the four-hour contact time between activated carbon and acetone, experiments were conducted to determine acetone concentration as a function of time after carbon was added. The data shown in Figure 4 illustrates that for a solution with an initial concentration of approximately 9 mg/l, the four-hour contact time was more than adequate for equilibrium to be reached. Similar results were obtained for solutions with higher concentrations.

Figures 5 through 7 show results from the experiments conducted with propionitrile. Figure 5 shows the Freundlich isotherm for the single solute experiment with propionitrile, Figure 6 shows the Freundlich isotherm for the adsorption of propionitrile from solutions containing multiple solutes, and Figure 7 shows the results from both of these experiments. The adsorption of propionitrile in single solute experiments ranged from 0.5 to 223 mg per gram of carbon with a final concentration range of 3 to 1200 mg/l. The adsorption of propionitrile in multiple solute experiments ranged from 1 to 28 mg per gram of carbon with a final concentration range of 3 to 700 mg/l. The results from single solute experiments fit the Freundlich isotherm very well as shown in Figure 5, although some scatter of data was observed in Figure 6 in the results of multiple solute experiments when fitted to the Freundlich isotherm. The differences in the adsorption of propionitrile onto carbon in the single and multiple solute experiments are illustrated in Figure 7. At final concentrations below 10 mg/l, the presence of multiple solutes appears to enhance the adsorption of propionitrile; however, at higher concentrations, the reverse effect is observed. Others have suggested a possible explanation of this phenomenon as being different mechanisms of adsorptions in different concentration ranges.[8] Above final concentrations of approximately 10 mg/l, classical interference is observed, i.e., the competition for active sites increases and less propionitrile is adsorbed. This trend would be expected to continue with increasing concentrations and numbers of solutes. Figure 8 shows the results from equilibrium experiments performed with a propionitrile solution containing an initial concentration of approximately 9 mg/l. The four-hour contact was more than sufficient for equilibrium to be reached between propionitrile and activated carbon.

Results from pyrrole experiments are shown in Figures 9 through 11. The results from single solute experiments are shown in Figure 9, the results from multiple solute experiments are shown in Figure 10, and the results from both are shown in Figure 11 for comparison. As with the results for propionitrile, results from single solute experiments with pyrrole fit the Freundlich isotherm.

Although some scatter of data is present in the multiple solute experiments, these data also fit the Freundlich isotherm very well. Figure 11 demonstrates that the adsorption of pyrrole in multiple solute experiments was consistently less than in single solute experiments. This is reasonable due to the competition for active sites in multiple solute experiments. Figure 12 demonstrates that a four-hour contact period for pyrrole with activated carbon was more than sufficient to reach equilibrium.

Figures 13 through 15 show the results of thiocyanate experiments in the form of Freundlich isotherms. Figure 13 shows the results for single solute experiments, Figure 14 shows the results for multiple solute experiments, and results from both experiments are shown in Figure 15. A very low affinity for activated carbon is evidenced by a maximum value of 24 mg of thiocyanate removed per gram of carbon at a final concentration of 655 mg/l. At final concentrations below 20 mg/l, the presence of multiple solutes appears to enhance the adsorption of thiocyanate; however, at higher concentrations the reverse effect is observed. This response is similar to that of propionitrile. It is probably due to different mechanisms of adsorption in different concentration ranges. Classical interference is observed for final concentrations greater than 20 mg/l. As the competition for active sites increases, less thiocyanate is adsorbed. As with the results for acetone, the low adsorbances of thiocyanate contribute to the scatter of data that is present even in single solute experiments. All compounds show some scatter in multiple solute experiments, due to competition for active sites. The results of tests with thiocyanate, however, show scatter in single solute experiments as well (as did acetone). This may be due to the sensitivity of the analyses when small differences in initial and final concentrations exist, as previously discussed for acetone. Figure 16 illustrates that a contact time of four hours was allowed for equilibrium to be reached between thiocyanate and activated carbon, although it appears that about three hours would have been sufficient.

In addition to comparing results for adsorption from single and multiple solute solutions for each compound, it is also beneficial to consider the relative quantities of solutes adsorbed in the multiple solute solutions. This can be accomplished by determining the average mole fraction adsorbed of each compound in the multiple solute experiments.[9] The following relationship is used:

$$Z_i = \frac{q_i}{q_t} \qquad (3)$$

where Z_i = the mole fraction of compound i adsorbed onto carbon, q_i = the moles of i adsorbed, and q_t = the total moles of all compounds adsorbed in a given experiment, thus the value of q_t is the mass loading of the adsorbent in moles. The parameter $\bar{Z}_i$, the average mole fraction of compound i adsorbed, can be calculated from data for multiple solute experiments to determine if there are preferences of some compounds over others. The values of $\bar{Z}_i$ obtained for acetone, propionitrile, pyrrole, and thiocyanate were 0.17, 0.17, 0.44, and 0.22, respectively. This indicates that the adsorption of pyrrole was most preferred. The values of Z_i were considerably less for the other three compounds.

Conclusions and Plans for Future Study

By conducting a series of batch carbon adsorption experiments, the adsorption isotherms for acetone, propionitrile, pyrrole, and thiocyanate were determined. The data are well represented by Freundlich isotherms. Adsorption of all compounds is low relative to other compounds in which removals of several thousand milligrams per gram of carbon can be obtained.

The presence of other compounds in multiple solute experiments had little effect on the adsorption of acetone due to its very low affinity for activated carbon. The adsorption of pyrrole in multiple solute experiments was consistently less than that in single solute experiments due to competition for active sites in multiple solute experiments. Propionitrile and thiocyanate, on the other hand, demonstrated a decrease in adsorption in the presence of multiple solutes except at very low concentrations. When adsorbed from a multiple solute solution, propionitrile showed enhanced adsorption at final concentrations below 10 mg/l and reduced adsorption for higher concentrations. Similarly, thiocyanate, when adsorbed from a multiple solute solution, demonstrated enhanced adsorption at final concentrations below 20 mg/l and reduced adsorption at higher concentrations.

After determining the average mole fraction of each compound adsorbed in the multiple solute experiments, the compounds were ranked in order of preference for adsorption. Pyrrole was the most preferred, with $\bar{Z}_i$ = 0.44. The other three compounds, thiocyanate, acetone, and propionitrile, were less preferred with $\bar{Z}_i$ values of 0.22, 0.17, and 0.17, respectively.

Based on the very low affinities of acetone and thiocyanate for activated

carbon, as well as the small adsorbances of all compounds relative to other compounds that are successfully removed from solution by activated carbon, the use of activated carbon as a primary treatment method for these compounds may not be practical. Other experiments underway at TTU indicate that the four compounds of this study are treatable biologically. The effluent from a biological reactor will contain small residuals of the four compounds as well as metabolic by-products, which will each impose a chemical and possibly a biochemical oxygen demand. Carbon adsorption may be desirable as a polishing process to follow biological treatment. Future tests will include exposure of effluent from a small scale continuous flow biological reactor to activated carbon.

References

1. Punwani, D. V., Lau, F. S., and Roberts, M. J., "Pressurized Fluidized-Bed Hydroretorting of Eastern Oil Shale," Proceedings, 1988 Eastern Oil Shale Symposium, Lexington, Ky., pp. 359-370, 1988.

2. Mensinger, M. C., Roberts, M. J., Rue, D. M. and Lau, F. S., "Environmental Data from Moving-Bed Hydroretorting of Three Eastern Oil Shales," Proceedings, 1988 Eastern Oil Shale Symposium, Lexington, Ky., pp. 133-146, 1988.

3. Tchobanoglous, George, and Schroeder, Edward D., Water Quality, Reading, Mass.: Addison-Wesley Publishing Company, 1987.

4. Benefield, Larry D., Judkins, Jr., Joseph F., and Weand, Barron L., Process Chemistry for Water and Wastewater Treatment, Englewood Cliffs, N.J.: Prentice-Hall, Inc., 1982.

5. James M. Montgomery Consulting Engineers, Inc., Water Treatment Principles and Design, New York: John Wiley & Sons, 1985.

6. Dobbs, Richard A., and Cohen, Jesse M., "Carbon Adsorption Isotherms for Toxic Organics," EPA-600/8-80-023, 1980.

7. Standard Methods for the Examination of Water and Wastewater, 16th Edition, American Public Health Association, American Water Works Association, and Water Pollution Federation, Washington, D.C., 1985.

8. Wilczak, Andrzej, and Keinath, Thomas M., "Single- and Bi-Solute Sorption of Heavy Metal Cations on Activated Carbon," Presented at the Symposium of Activated Carbon Technology for the 20th Annual Meeting of the Fine Particle Society, Boston, Mass., August 22-26, 1989.

9. Godrej, Adil N., Boardman, Gregory D., and Gallagher, Daniel L., "Analysis of Multicomponent Sorption by Means of Sorption Ratios," Presented at the 20th Annual Meeting of the Fine Particle Society, Boston, Mass., August 22-26, 1989.

Acknowledgments

This research is being conducted by Tennessee Technological University under a subcontract with the Institute of Gas Technology which is a prime contractor to the U. S. Department of Energy. The support, assistance, and cooperation of Michael C. Mensinger, Francis S. Lau, Dharam V. Punwani, and Michael J. Roberts with the Institute of Gas Technology is gratefully acknowledged.

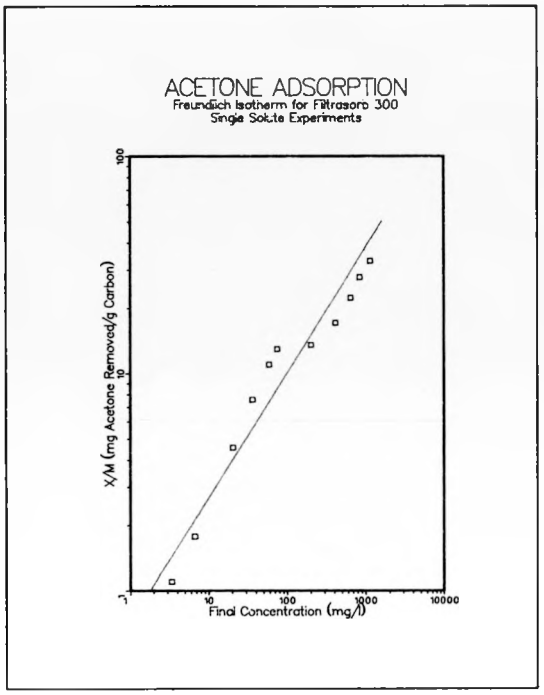

Figure 1

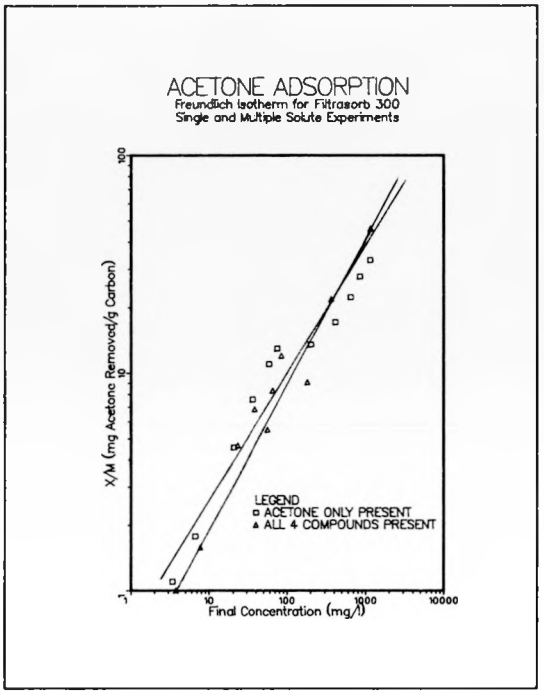

Figure 3

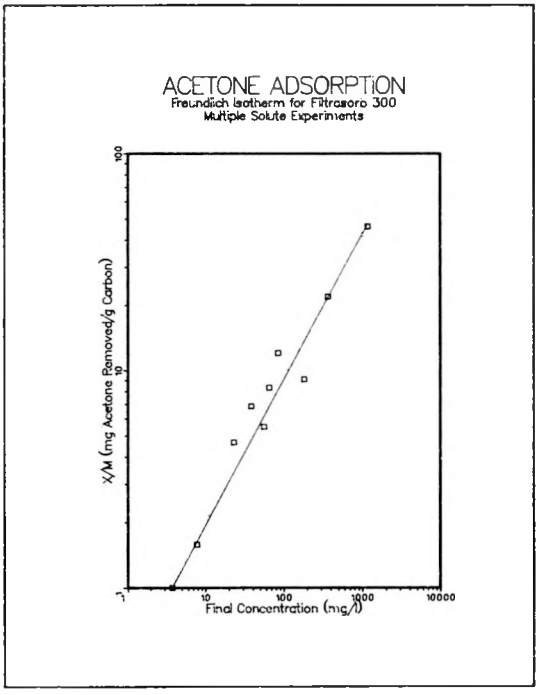

Figure 2

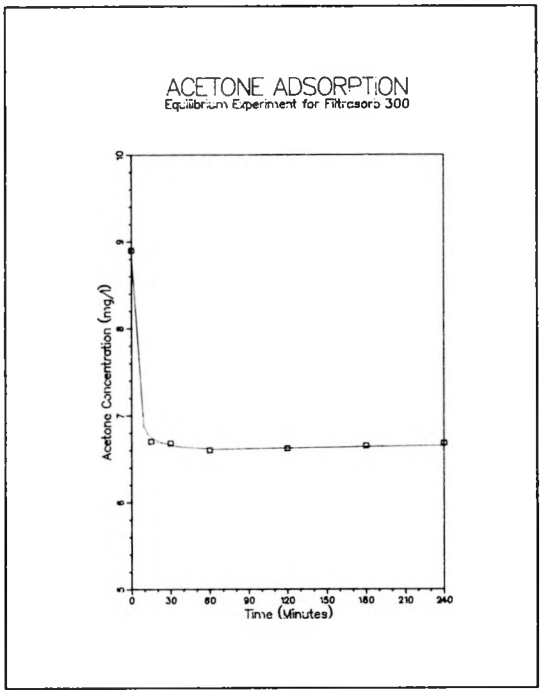

Figure 4

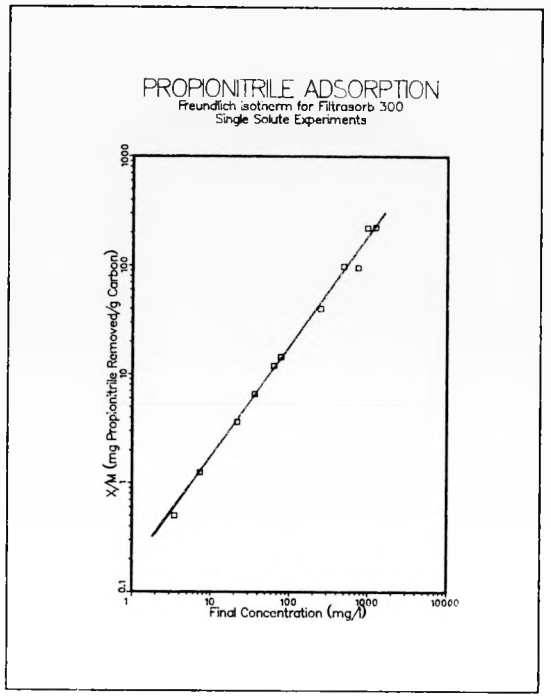

Figure 5

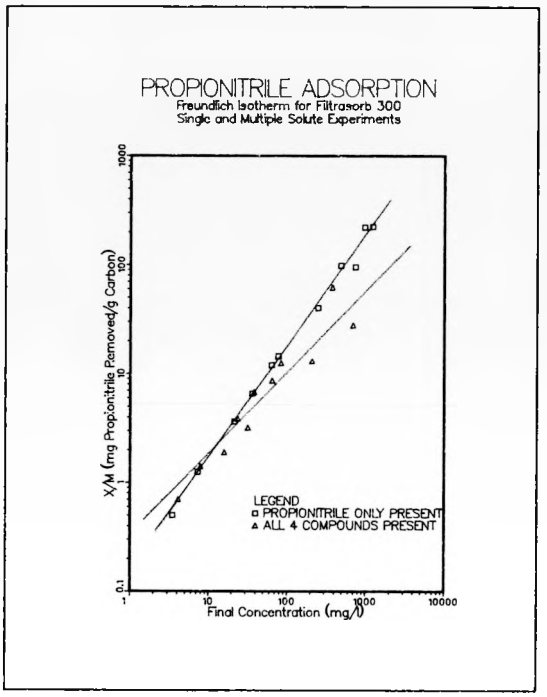

Figure 7

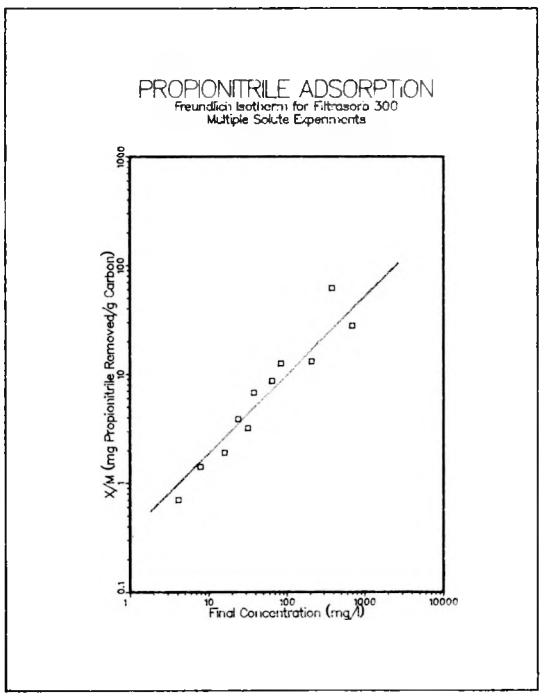

Figure 6

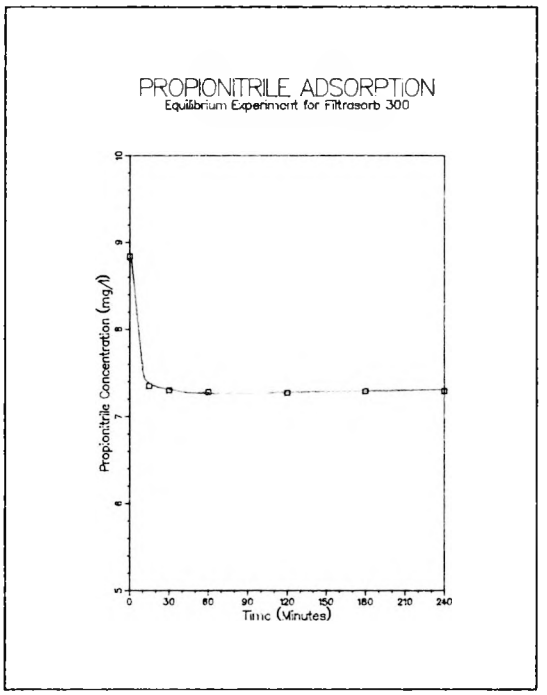

Figure 8

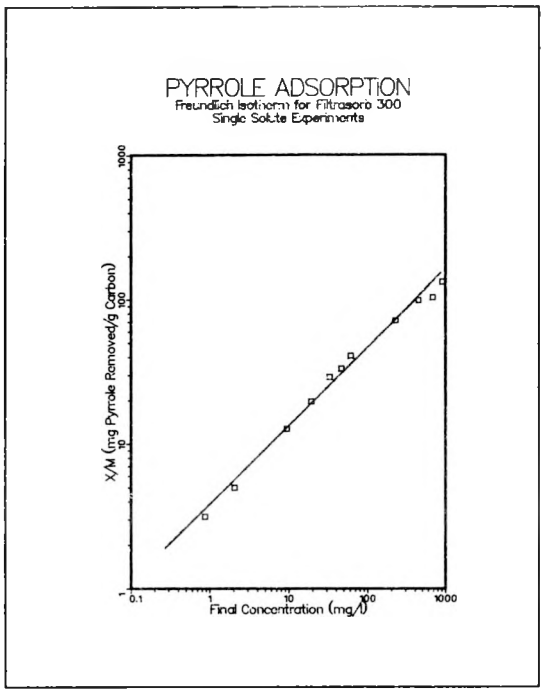

Figure 9

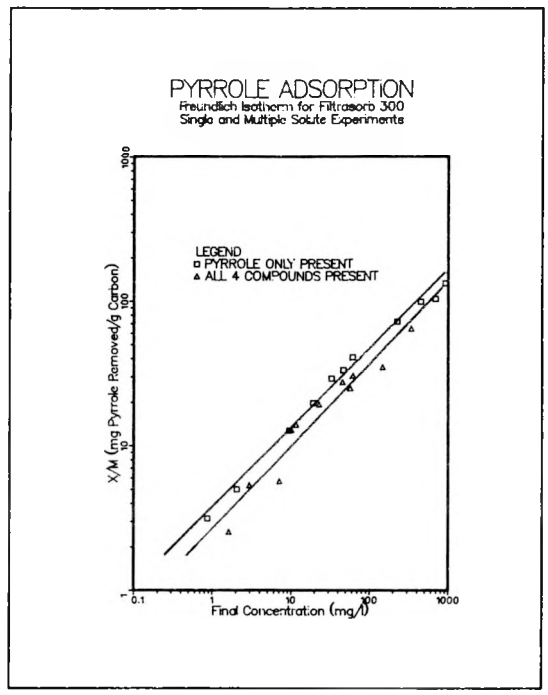

Figure 11

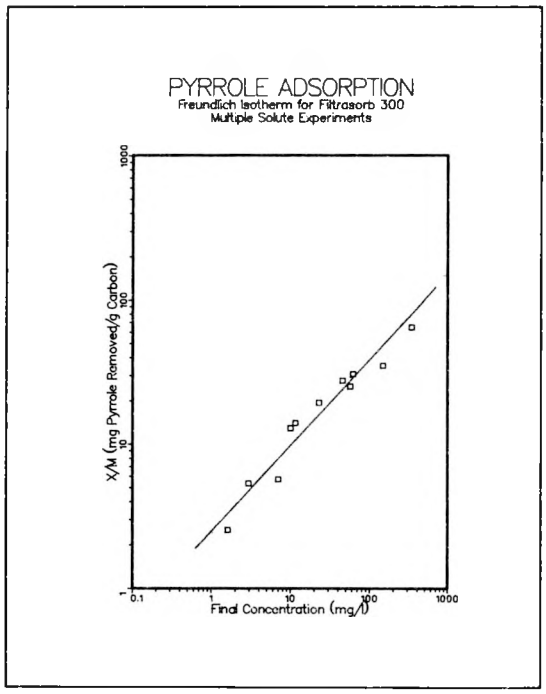

Figure 10

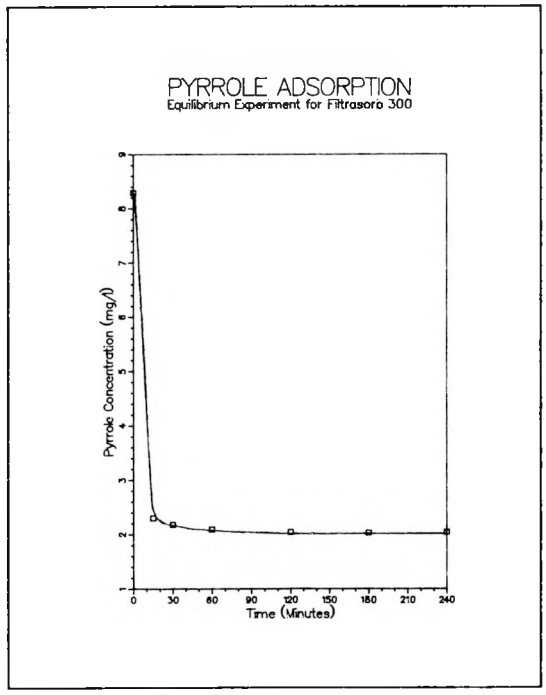

Figure 12

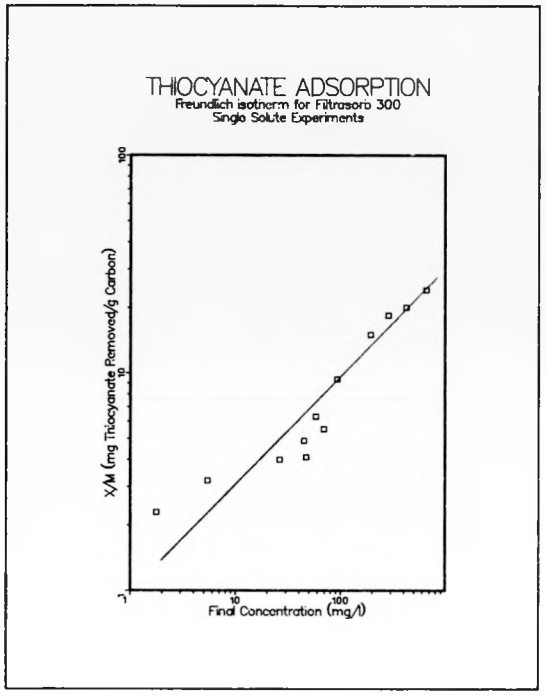

Figure 13

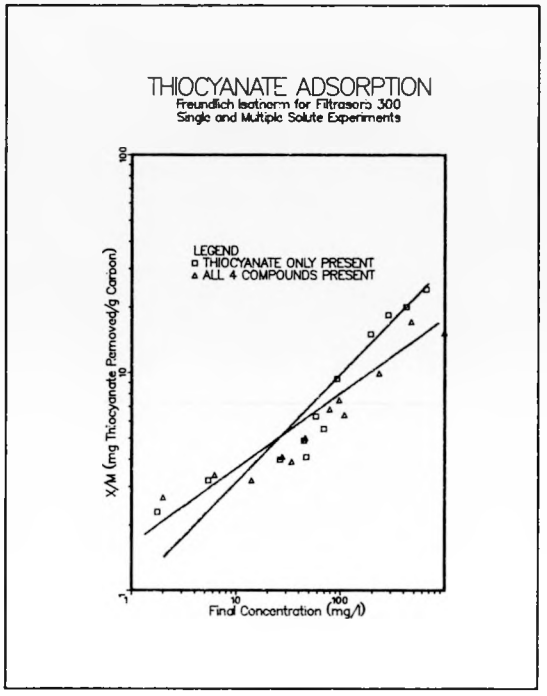

Figure 15

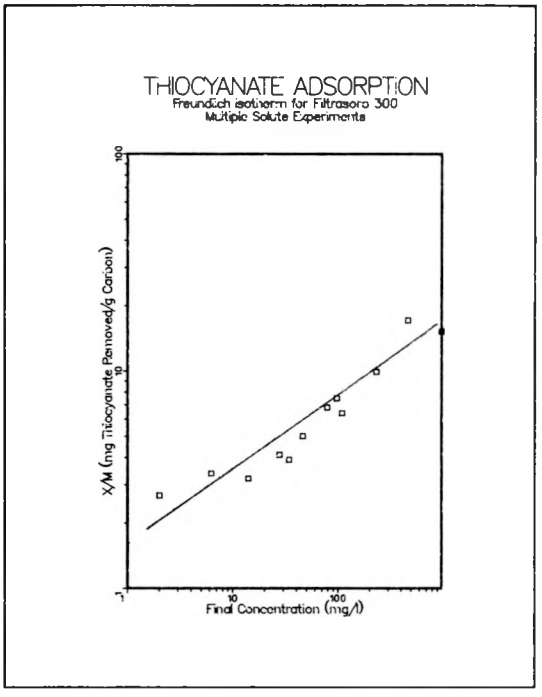

Figure 14

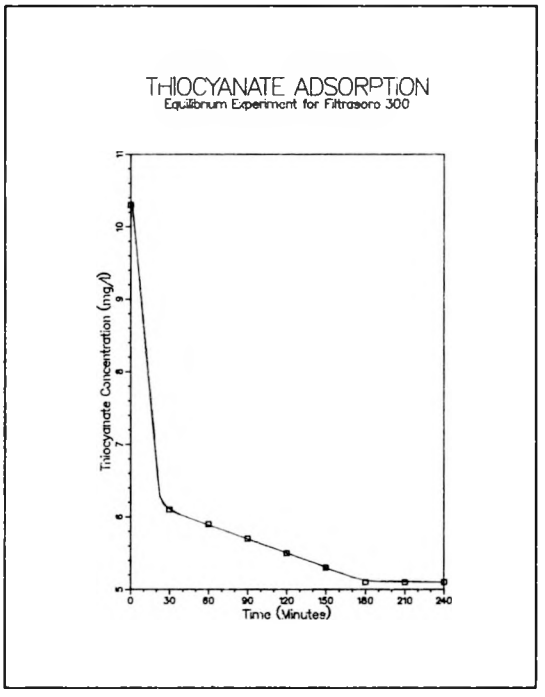

Figure 16

Biological Treatability of Selected Organic Components of an Oil Shale Processing Wastewater

by

Sandra Miles, Rafael Bustamante, William P. Bonner
Department of Civil Engineering
Tennessee Technological University
Cookeville, Tennessee 38505

Abstract. Biological treatability experiments are reported for the synthetic waste of a pressurized, fluidized-bed hydroretorting oil shale process. Batch activated sludge experiments indicate that acetone, propionitrile, pyrrole, and thiocyanate are biodegradable. Chemical oxygen demand (COD) values were reduced to minimum values of 20 to 40 mg/L in batch tests, and specific substrate concentrations were reduced to nondetectable levels in multiple substrate experiments. In double substrate combinations involving acetone, propionitrile, and pyrrole, contaminants were metabolized simultaneously. Lag phases were present in all experiments involving the thiocyanate species, but it appears that the lag phase may be eliminated in continuous flow studies, which have been initiated and will involve all four substrates.

Introduction

Although research into alternative sources of energy is not as popular as it was in the 1970's, it is no less important than it was during those energy-crisis years. Supplies are currently adequate, but conventional fuels continue to be depleted at increasing rates. To avoid a major, nation-crippling energy crisis in the future, alternative fuel technologies should be developed now.

A new fuel technology which appears very promising is the pressurized, fluidized-bed hydroretorting (PFH) process being developed by the Institute of Gas Technology (IGT; Chicago, IL) for use with Eastern oil shales. Mini-bench scale laboratory tests in the three-year, Department of Energy-sponsored project indicate that up to 87 percent organic carbon conversion and 250 percent oil yield (based on Fischer Assay) are possible with PFH.[1] When these results are considered with other factors such as water availability, an industry based on PFH processing of Eastern shales can be economically competitive with conventional retorting of Western shales.[1]

In recent laboratory studies, shale oil has been found to increase the life of paving materials by as much as 50 percent.[2] A pavement which contains 10 to 20 percent shale oil is not as vulnerable to "moisture and embrittlement damage" as conventional asphalts. Additional testing may prove this to be a beneficial use of shale oil even though, as a fuel, it may not be economically competitive with imported oil.[2]

Environmental considerations are imperative in the development of a new technology. As IGT investigates the PFH processing of Eastern oil shales, it is also addressing environmental impacts of a hydroretorting facility. As a subtask of the PFH project, Tennessee Technological University (TTU) is performing laboratory tests to determine the treatability of selected organic constitutents of the expected sour water. This paper is concerned solely with the biological treatability studies of the TTU subtask.

Although relatively little wastewater is produced in the PFH process

(50 mL per kg of dry, raw shale, based on calculations using HYTORT data from reference 3), the number and strengths of contaminants in the water necessitate treatment of the effluent before recycle or discharge. Testing of a mini-bench-scale moving-bed hydroretorting unit yielded the wastewater composition shown in Table 1 (excluding metallic compounds, the treatment of which is being considered in other subtasks of the PFH project).[3] Over 90 percent by weight of the wastewater contaminants are in the forms of ammonia and hydrogen sulfide. Using standard unit operations, these compounds can be removed to concentrations that meet environmental discharge regulations. Four contaminants for which treatment was less certain were selected and each of these contaminants is similar in structure to several of the other wastewater components identified in the mini-bench-scale wastewater analysis. The biological treatability of acetone, propionitrile, pyrrole, and thiocyanate, as contaminants of the PFH wastewater, is being determined in connection with this research.

The general biological wastewater treatment method explored for treating the PFH waste is activated sludge. This method was chosen over others (e.g., anaerobic fluidized-bed reactors) because it is relatively quick, low in cost, simple, and reliable. Although continuous flow studies will be conducted before making a recommendation for design requirements of a treatment process, batch studies are necessary to determine treatability of the individual contaminants and compatibility of the substrates in a multi-component system.

The removal of substrate (or growth of microorganisms) may be monitored in batch biological studies by gross parameters such as chemical oxygen demand (COD) or dry cell weight.[4] A typical pattern for microbial growth in a batch reactor is shown in Figure 1. The numbered growth phases are: (1) lag phase, in which cells are acclimating to the carbon source, (2) log phase, in which growth is a first order reaction, (3) decreasing growth phase, in which declining substrate availability limits growth, (4) stationary phase, in which substrate is exhausted, and (5) endogenous phase, in which cells lyse and are used as substrate by other microorganisms.[4, 5]

The logarithmic phase of growth is of primary interest in batch studies because it yields the specific growth rate μ, as defined by the relationship

$$dX/dt = (\mu)X \quad (1)$$

where X = concentration of microbial mass and dX/dt = change of microbial mass concentration with time. The integrated form of the equation is

$$\ln X \ln X_0 = (\mu)t \quad (2)$$

where X_0 = initial concentration of microbial mass in the batch reactor. A plot of the natural log of biomass concentration with time, then, is a straight line with slope μ (4). The dependence of the specific growth rate on substrate concentration is defined by Monod, or saturation, kinetics:

$$\mu = (\mu_{max})\,[S]/(Ks + [S]) \quad (3)$$

where μ_{max} = the maximum specific growth rate attainable using the given microbial concentration, X = substrate concentration and Ks = substrate concentration at half the maximum growth rate (half-saturation constant). This results in a growth expression of

$$dX/dt = (\mu_{max})[S](X)/(Ks + [S]) \quad (4)$$

The growth rate in the log phase, thus, depends on both substrate and biomass concentrations.[4, 5]

Another important parameter is the cell yield coefficient, γ, or the amount of cell mass produced per unit mass of substrate utilized. Using this parameter, the rate of substrate utilization may be related to the rate of microbial growth and defined as

$$dS/dt = -\mu(max)[S](X)/(Y(Ks + [S]) \quad (5)$$

Using these simple relationships, therefore, batch studies may be performed to determine cell yield coefficients and the relationships between substrate concentration and specific growth rates and substrate utilization rates.[4, 5] Although the batch parameters may not be identical to those observed in a continuous flow operation, they do provide approximate guides for beginning the continuous flow studies.

Experimental Methods and Materials

Acclimation of Microorganisms

Seed for the reported set of experiments was obtained from a municipal wastewater treatment facility. Samples of the heterogeneous culture were acclimated to sole carbon sources of acetone, propionitrile, pyrrole, and thiocyanate in 250 mL shaker flasks. In addition to the carbon source and microbial seed, each flask contained inorganic salts which provided essential nutrients and minerals. A list of the inorganic salts and essential nutrients is given in Table 2. Flasks were prepared containing sole carbon sources of approximately 100, 300, and 600 mg/L substrate, respectively. Three serial transfers of the microbial seed to new growth media confirmed acclimation, as evidenced by heavy bacterial growth on nutrient agar. Every three days the mixtures were allowed to settle, and the supernatant was discarded. Carbon sources were replenished, and cultures were restored to volume with prepared synthetic waste solution. Sodium thiocyanate was used as the source of the thiocyanate species throughout the reported set of studies.

When healthy, visible microbial seed was present in the shaker flasks, samples were removed to begin growing larger microbial populations in 1.5-L batch reactors. Compressed air was supplied to the cultures through diffuser stones. The reactors contained 600 and 1200 mg/L sole carbon sources, respectively, and the synthetic waste solution. Twice weekly, one third of the contents of each reactor was discarded, the mixtures were allowed to settle, and a second third was discarded as supernatant. The reactors were restored to volume using sole carbon sources and synthetic waste components. These reactors were maintained continuously throughout the course of the study.

Following several weeks of culture acclimation, batch reactors were initiated containing multiple substrates. Double substrate reactors contained either 300 or 600 mg/L each of all two-substrate combinations. Reactors were also prepared which contained 150 and 300 mg/L each, respectively, of all four substrates. Seed from the multiple substrate reactors was obtained from the appropriate single substrate batch reactors.

Batch Experiments

Batch experiments were performed to determine the biological removal patterns of each of the substrates and substrate combinations with time. COD was used as a gross parameter to monitor the substrate concentrations. Single substrate experiments were performed in 2-L batch reactors using a total volume of 1.5 L or 2 L, depending on the number of samples which were expected to be taken. Reactor start-up involved placing the desired amount of substrates and synthetic waste components in the reactor, aerating to mix thoroughly, and adding acclimated inoculum one minute before removing the "time zero" sample. COD tests were performed on filtered (0.45 µm) samples taken every 3 to 24 hours, depending on the duration of the experiment. The closed reflux, colorimetric COD test, as described in reference 6, was employed.

In order to monitor cell growth within the batch reactors, optical density and dry cell weight measurements were taken. However, flocculation of cells within the reactors prevented the recovery of samples which yielded consistent weight measurements. COD, therefore, was the only experimental parameter which provided reliable results. This prevented determination of accurate cell yield coefficients, but substrate removal rates could be determined.

Multiple substrate experiments were performed in 6-L reactors, and additional samples were taken for specific substrate analyses. The acetone and propionitrile experiment samples were analyzed using a Hewlett-Packard 5987A gas chromatograph/mass spectrometer to determine the presence of microbial intermediates or end products. Other multiple substrate experiment samples were analyzed using a Hewlett-Packard 5890A gas chromatograph. To analyze for thiocyanate, the colorimetric test for cyanides amenable to chlorination, as described in reference 6, was used.

Discussion of Results

Single Substrate Experiments

Single substrate batch experiments were performed using initial concentrations of approximately 100, 300, and 600 mg/L, respectively, of acetone, propionitrile, and pyrrole. Batch experiments involving thiocyanate were performed using initial concentrations of 300, 100, and 50 mg/L because thiocyanate is considered a difficult species to degrade.[7] Lower concentrations of thiocyanate were also used because little sludge had accumulated in the acclimation reactors containing 600 mg/L or more thiocyanate, and it was possible that these higher concentrations were inhibitory to microbial metabolism.

The biological removal of single substrates is illustrated in Figures 2 through 5. A summary of the data is provided in Table 3. Minimum COD concentrations for reactors containing approximately 600, 300, and 100 mg/L acetone, respectively, were reached in 44, 29, and 31 hours of biological treatment. For the propionitrile reactors, 49, 47, and 31 hours, respectively, were required to reduce the COD to minimal levels. The removal of pyrrole with initial concentrations of 600, 300, and 100 mg/L was accomplished in 80, 61, and 54 hours, respectively. For the treatment of thiocyanate, reaction times of 207, 240, and 288 hours were required to reach minimum COD values in reactors initially containing 300, 100, and 50 mg/L thiocyanate, respectively. Extended lag phases were evident in each of the single substrate thiocyanate batch studies. Although poor acclimation was assumed to be the reason for the lag periods, additional time in the acclimation reactors failed to eliminate the lag phases in repeat batch experiments.

It should be noted that COD was not reduced to a level of zero in any of the experiments, as might be expected when using a specific parameter for substrate removal. Because the COD test is sensitive to any compound which is oxidizable by potassium dichromate, substances such as minor intermediates, end products, and oxidizable inorganic

nutrients prevent the COD from reaching zero. The minimum COD values illustrated in Figures 2 through 5 represent biological treatment which may make the effluent suitable for recycle or discharge.

The removal rates, reported in Table 3, were determined using linear regression analyses of semi-log plots of the batch treatment experiments, as given in Figures 6 through 9. These figures are the logarithmic plots of the single substrate experiments, the log phases of which are evident as linear regions. The steepest linear portions of the plots were used to compute first order rates of removal. The biological treatment of acetone resulted in removal rates of 0.030, 0.063, and 0.023 hr^{-1} for initial concentrations of 600, 300, and 100 mg/L acetone, respectively. The removal rates obtained during the batch biological treatment of propionitrile were 0.029, 0.034, and 0.034 hr^{-1} for initial substrate concentrations of approximately 600, 300, and 100 mg/L, respectively. The similarity of the removal rates would appear to indicate that propionitrile was being removed at the maximum rate (i.e., microorganisms were growing near the maximum specific growth rate of μ_{max}).

Biological removal rates for batch pyrrole experiments were 0.012, 0.015, and 0.015 hr^{-1} for initial pyrrole concentrations of approximately 600, 300, and 100 mg/L, respectively. Based on these findings alone, it again appeared that microorganisms were able to grow at approximately the maximum growth rate at all three initial substrate concentrations. Initial thiocyanate concentrations of 300, 100, and 50 mg/L resulted in removal rates of 0.0086, 0.010, and 0.0046 hr^{-1}, respectively. The apparent inconsistency of the removal rates may be due to insufficient numbers of data points during the logarithmic growth phases in those experiments. Because of the lag phases, it was difficult to predict exactly when the most rapid substrate removal would occur, and the highest frequency of sampling was not always at the most appropriate time.

Double Substrate Experiments

Combinations of two of the four substrates were used to determine the biological treatment compatibility of acetone, propionitrile, pyrrole, and thiocyanate in batch reactors. It was desired to determine whether the various substrates interfered with the removal of other substrates and whether substrates were being metabolized simultaneously or sequentially. For these reasons, specific analyses were performed on samples from some of the double substrate experiments using GC and GC/MS techniques. The results of the studies are summarized in Table 4.

Figure 10 illustrates the removal of 300 mg/L each for acetone and propionitrile in a single batch reactor. The COD reached a minimum of 12 mg/L following 38 hours of biological treatment. Acetone was not detectable by GC/MS analysis after 48 hours of treatment, at which time propionitrile was present at a concentration of 0.27 mg/L according to GC/MS purge and trap analysis. Acetone and propionitrile were metabolized simultaneously at almost exactly the same rates. The removal rate for the double substrate experiment was 0.059 hr^{-1} (based on COD), as illustrated by Figure 11. The biological treatment of acetone and propionitrile together did not require longer treatment than for each of the substrates individually. Figure 10 also illustrates the residual COD which may remain when initial substrate has been exhausted. GC/MS analyses, however, revealed no intermediates or end products other than carbon dioxide.

The biological removal of acetone and pyrrole in the same reactor system is shown in Figure 12. The COD reached a minimum following 84 hours of treatment, at which time both acetone and pyrrole were not detectable by GC analysis. The removal rate based on COD was 0.017 hr^{-1}, slightly greater than the removal rate for pyrrole alone but significantly lower than the removal rate for acetone alone. Semi-log plots illustrating log phase removal are shown in Figure 13. Concentrations of the two compounds, as indicated by GC analyses, revealed that acetone and pyrrole were being metabolized simultaneously but at different rates. The removal of the two substrates together did not require longer than the removal of pyrrole, the more slowly metabolized substrate.

Figure 14 illustrates the biological treatment of propionitrile and pyrrole together in a batch reactor. Again, the substrates were removed simultaneously, with propionitrile being metabolized more rapidly than pyrrole, as determined by GC analyses. The composite, COD-based removal rate was 0.0084^{-1}, which was less than the rates for either of the two substrates individually. Log-phase metabolism is shown in linear portions of Figure 15. The removal of propionitrile in the double substrate experiment did not require longer than the removal of propionitrile alone, but the removal of pyrrole did require longer than its removal as a single substrate.

Figures 16 through 21 illustrate double substrate experiments involving the thiocyanate species. It should be noted that lag phases were present in the single substrate thiocyanate

experiments. Double substrate batch studies with thiocyanate were very similar. From the figures, two distinct growth phases were evident. Acetone, propionitrile, and pyrrole, respectively, were removed before thiocyanate was metabolized. These trends cannot be appropriately termed sequential or preferential metabolism, in which one substrate suppresses the metabolism of another, since substrate pairs exhibited similar removal patterns as the various substrates individually. In each case, two removal rates were computed, as shown in Table 4, corresponding to the two log phases of the experiment.

Four Substrate Experiment

Figures 22 and 23 illustrate the removal of acetone, propionitrile, pyrrole, and thiocyanate simultaneously. Concentrations of 150 mg/L of each of the substrates were initially present. In addition to COD, GC analyses and colorimetric thiocyanate analyses were performed. In this experiment, the lag phase for thiocyanate metabolilsm was significantly shortened. At the time this experiment was performed, preliminary studies were being conducted with a continuous flow unit, from which seed for the experiment was taken. The reduced lag phase is promising, as it indicates that a continuous flow unit will facilitate acclimation of microorganisms to the thiocyanate species and eventually eliminate the lag phase. All other substrates were metabolized in the four substrate experiment in times similar to those observed in single and double substrate studies. Removal rates observed in the four substrate experiment were: acetone, 0.038, propionitrile, 0.048, pyrrole, 0.018, thiocyanate, 0.017, and COD, 0.014 hr^{-1}. (It should be noted that the fact that the COD removal rate is not the average of the other removal rates is not a discrepancy. Specific removal rates of the individual compounds are based on substrate concentrations, not the COD of the substrates. These values cannot be meaningfully compared with the COD removal rate.) Within 98 hours of biological treatment in the four substrate experiment, all contaminants had been reduced to nondetectable levels (i.e., less than 1 mg/L).

Conclusions

Synthetic wastewater solutions containing acetone, propionitrile, pyrrole, and thiocyanate were shown to be treatable in batch biological reactors, both individually and in combinations of two and four substrates. The COD values of the various solutions were reduced to low levels of 20 to 40 mg/L, indicating that the substrates were being completely metabolized. GC and thiocyanate analyses of multiple substrate experiments confirmed this hypothesis. In all experiments for which specific substrate concentrations were determined, contaminants were removed to nondetectable levels.

In double substrate experiments involving acetone, propionitrile, and pyrrole, simultaneous removal of substrates was achieved. This result was promising since simultaneous metabolism of contaminants is highly preferred in an actual treatment facility. Sequential removal would necessitate acclimation periods between the successive removal mechanisms, potentially increasing hydraulic residence times and, therefore, costs. The lag phase which was observed during the metabolism of thiocyanate in single and double substrate experiments was shortened in the four substrate experiment, the seed of which was taken from a newly installed continuous flow reactor. This result shows promise that the lag phase may eventually be eliminated through seeding with properly acclimated cultures.

Future Studies

Tests have been initiated in a continuous flow reactor which will be used for several experiments involving waste solutions containing mixtures of acetone, propionitrile, pyrrole, and thiocyanate. The hydraulic residence time within the unit which is now being operated is five days. The flow rate to to the unit will be gradually increased while sampling influent and effluent of the reactor. The goal of the studies will be to achieve a high quality effluent in the least possible hydraulic residence time.

Acknowledgments

This research is being conducted by Tennessee Technological University under a subcontract with the Institute of Gas Technology, which is a prime contractor to the Department of Energy. The support, assistance, and cooperation of M. C. Mensinger, F. S. Lau, M. J. Roberts, and D. V. Punwani with the Institute of Gas Technology is gratefully acknowledged.

Table 1
Analysis of Sour Water Generated by the Hydroretorting of Tennessee Shale[3]

Contaminant	mg/Liter of Sour Water
Thiocyanate	7,350
Sulfide Sulfur	58,500
Miscellaneous Sulfate Sulfur	7,150
Acetone	200
MEK	50
Pentanone	15
Phenol	40
Methyl Phenol	30
Acetonitrile	360
Propionitrile	40
Aniline	500
Methyl Anilines	180
C_2-Pyrrole	15
Methyl Pyridines	30
C_2-Pyridines	5
Cyanide	45
Unidentified	180
Fluorine	19

Table 2
Components of Synthetic Waste Solution

$(NH_4)_2SO_4$	500 mg/L
$MgSO_4 \cdot 7H_2O$	100 mg/L
$MnSO_4 \cdot H_2O$	10 mg/L
$FeCl_3 \cdot 6H_2$	0.5 mg/L
$CaCl_2$	7.5 mg/L
KH_2PO_4	526 mg/L
K_2HPO_4	1070 mg/L
Tap water	100 mL/L
Distilled water	to volume

Table 3
Data Summary for Single Substrate Experiments

Substrate	Approximate Concentration (mg/L)	Initial COD (mg/L)	Final COD (mg/L)	Reaction Time (hr)	Removal Rate (hr)
Acetone	600	873	27	44	0.030
	300	594	20	29	0.063
	100	199	31	31	0.023
Propionitrile	600	884	24	49	0.029
	300	527	29	47	0.034
	100	202	26	31	0.034
Pyrrole	600	1155	35	80	0.012
	300	580	59	61	0.015
	100	246	20	54	0.012
Thiocyanate	300	415	44	207	0.0086
	100	173	36	240	0.010
	50	101	39	288	0.0046

Table 4
Data Summary for Double Substrate Experiments

Substrates (300 mg/L each)	Initial COD (mg/L)	Final COD (mg/L)	Reaction Time (hr)	Removal Rate (hr^{-1})
Acetone, Propionitrile	1042	12	38	0.063, 0.062
Acetone, Pyrrole	1047	20	34	0.026, 0.026
Propionitrile, Pyrrole	901	54	118	0.043, 0.016
Acetone, Thiocyanate	1011	41	231	0.0074, 0.0084
Propionitrile, Thiocyanate	951	46	213	0.010, 0.013
Pyrrole, Thiocyanate	1012	36	243	0.0055, 0.013

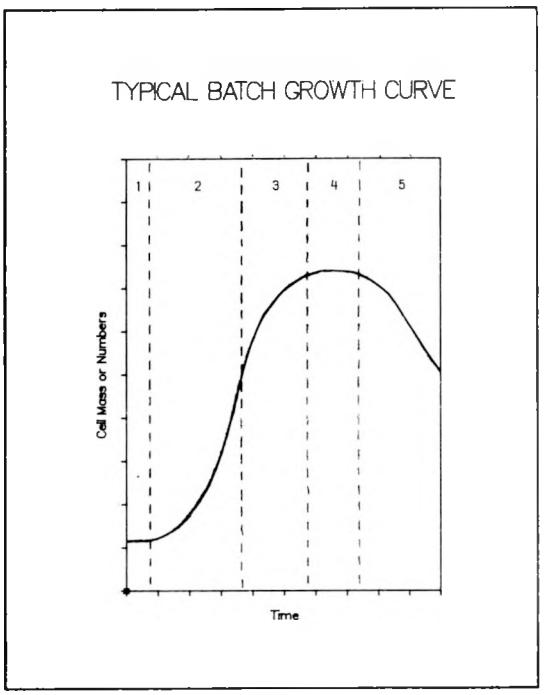

Figure 1

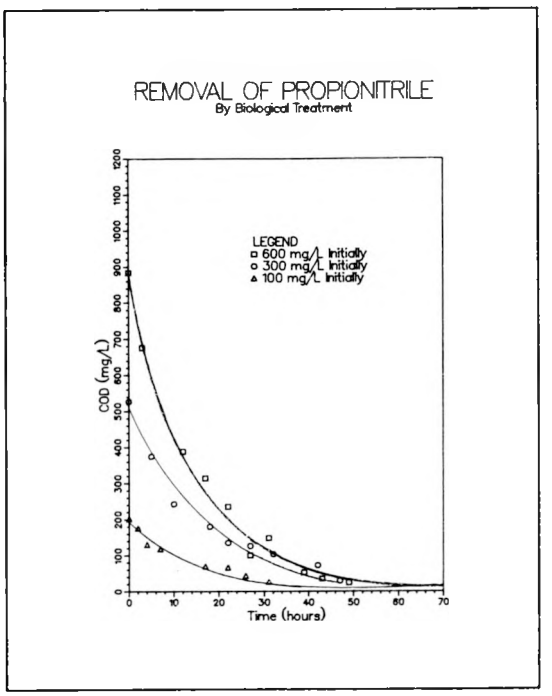

Figure 3

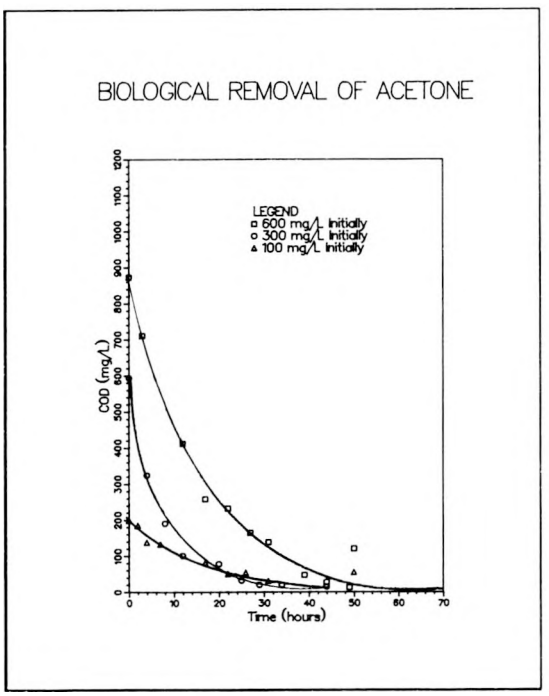

Figure 2

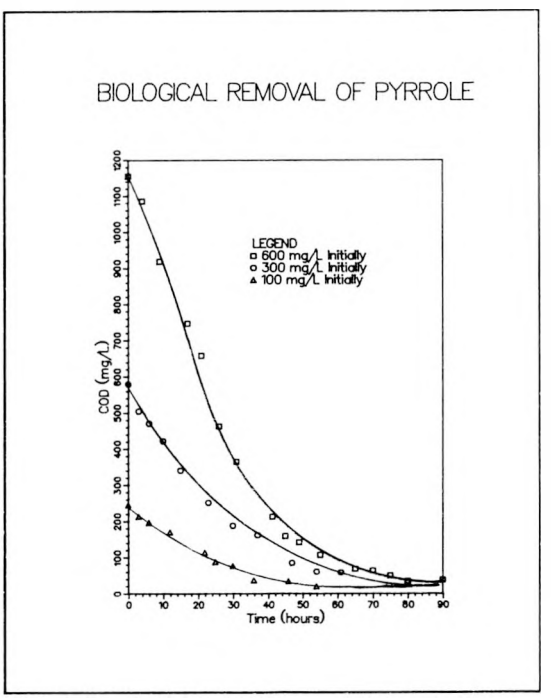

Figure 4

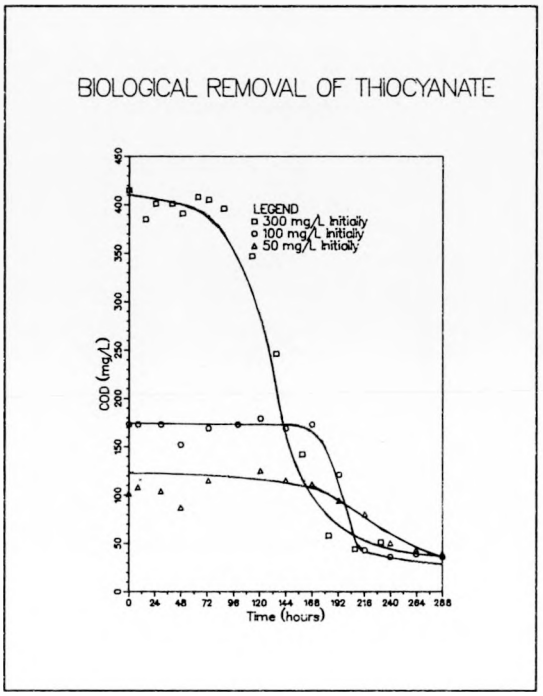

Figure 5

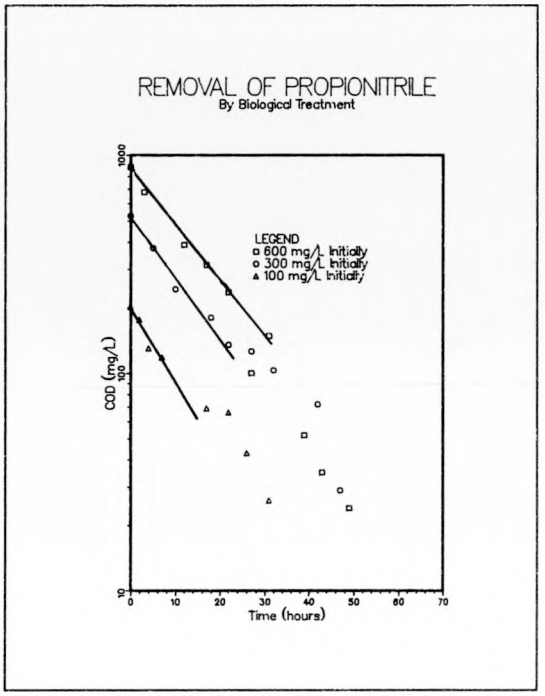

Figure 7

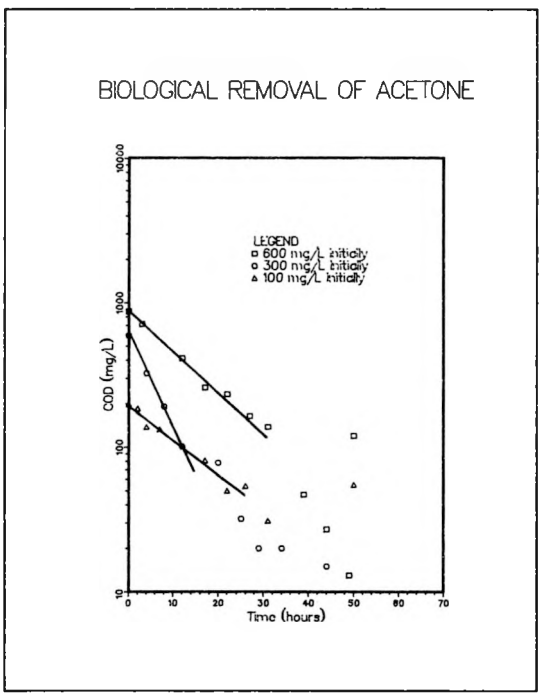

Figure 6

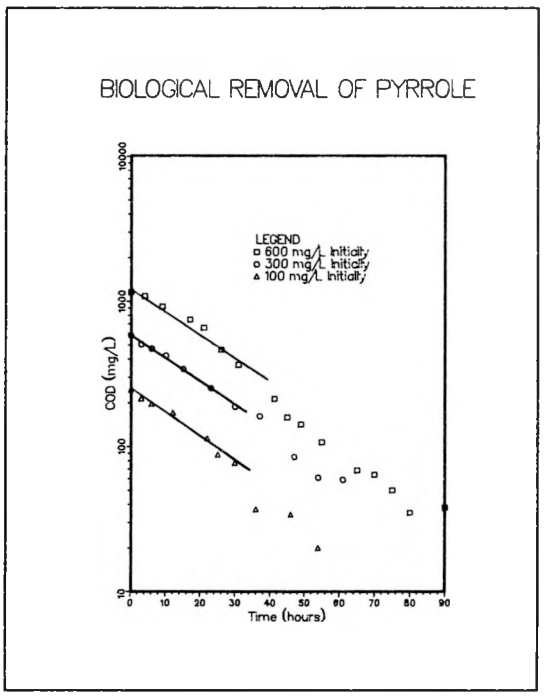

Figure 8

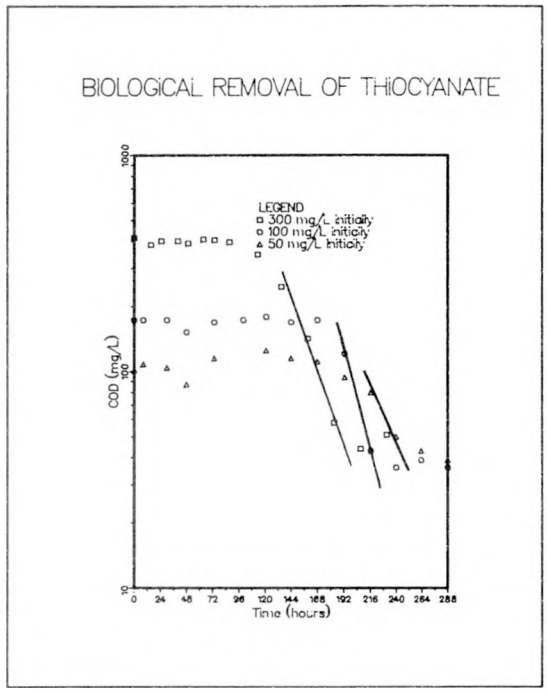

Figure 9

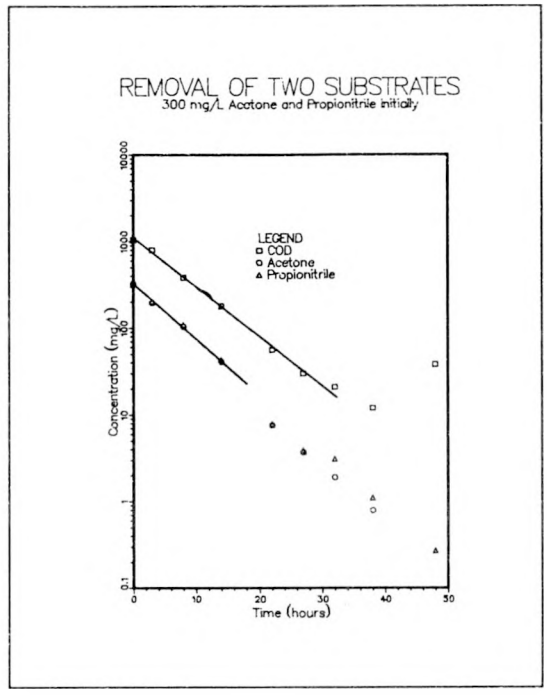

Figure 11

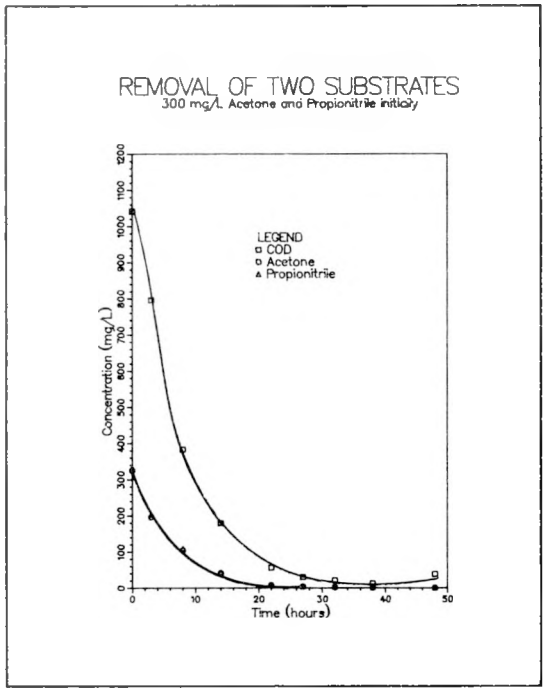

Figure 10

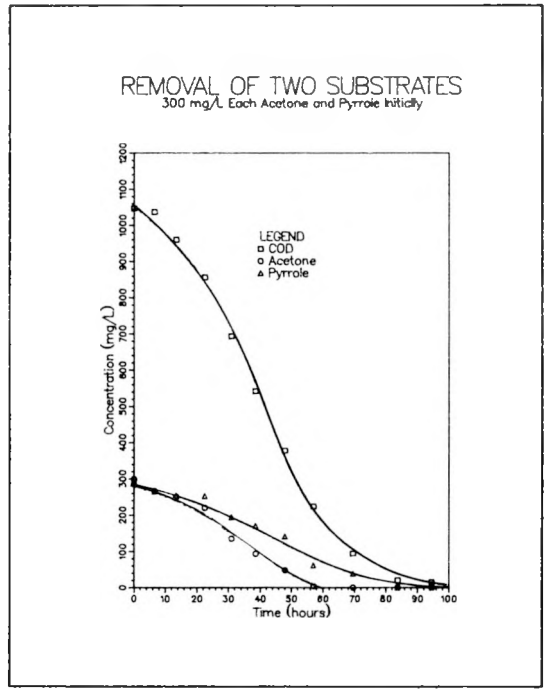

Figure 12

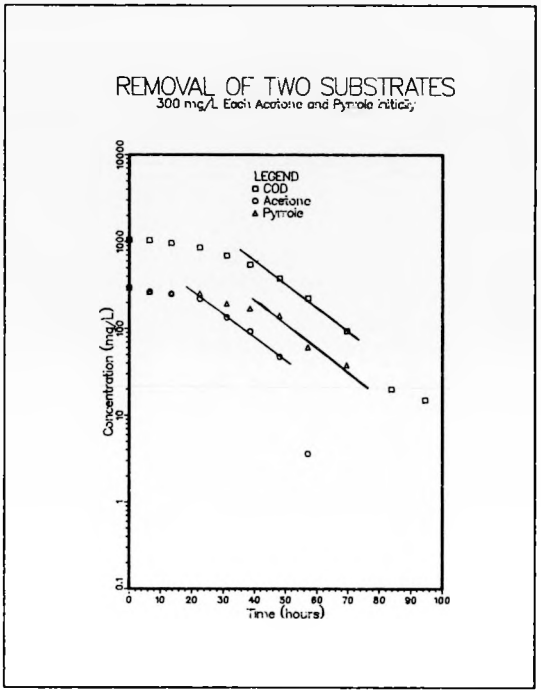

Figure 13

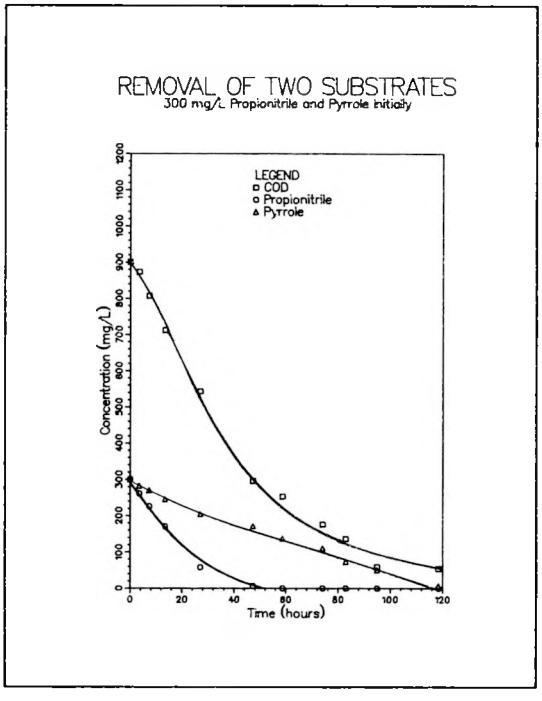

Figure 14

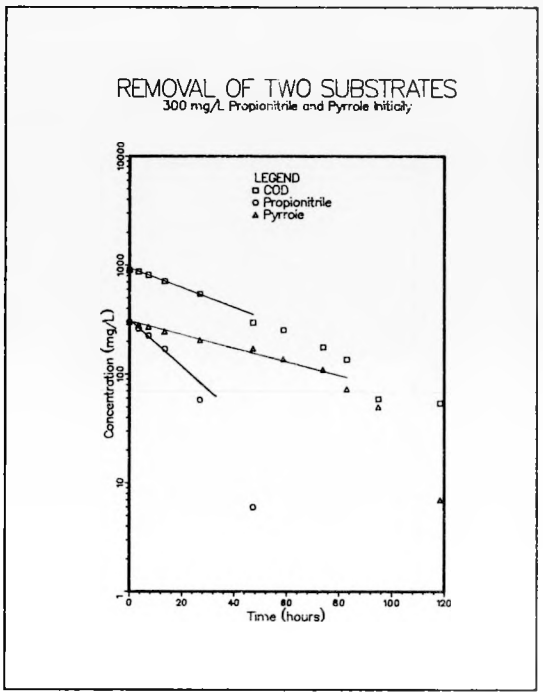

Figure 15

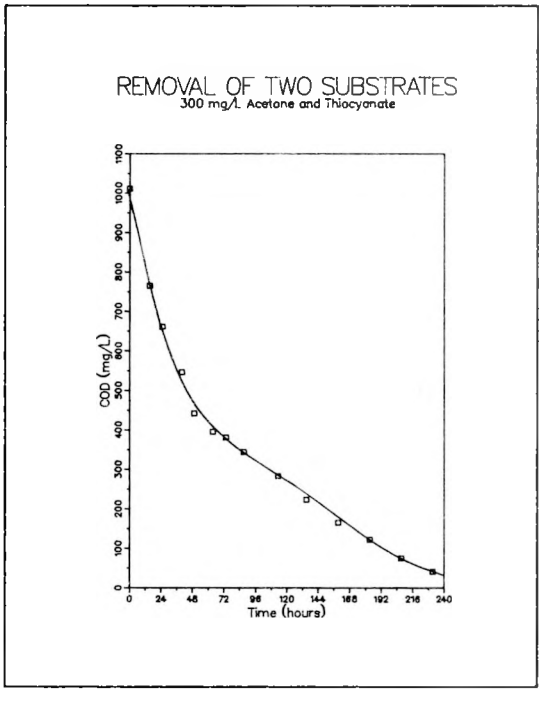

Figure 16

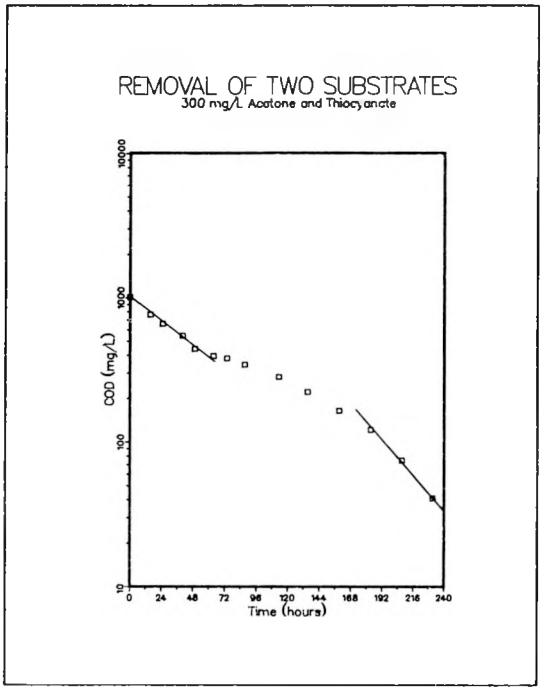

Figure 17

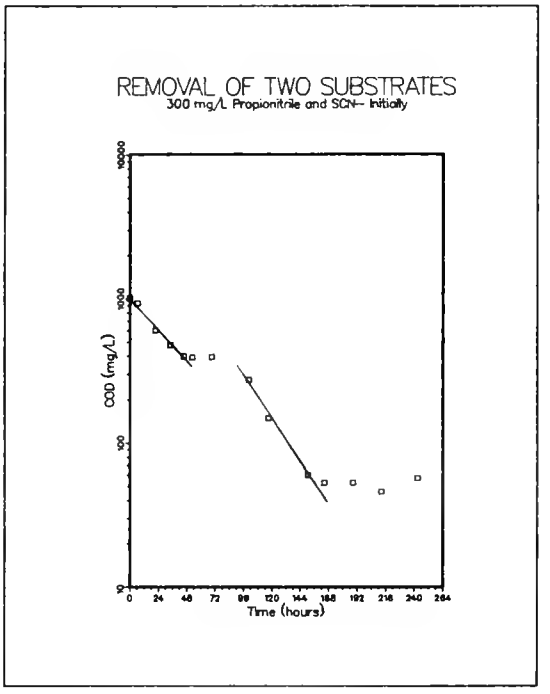

Figure 19

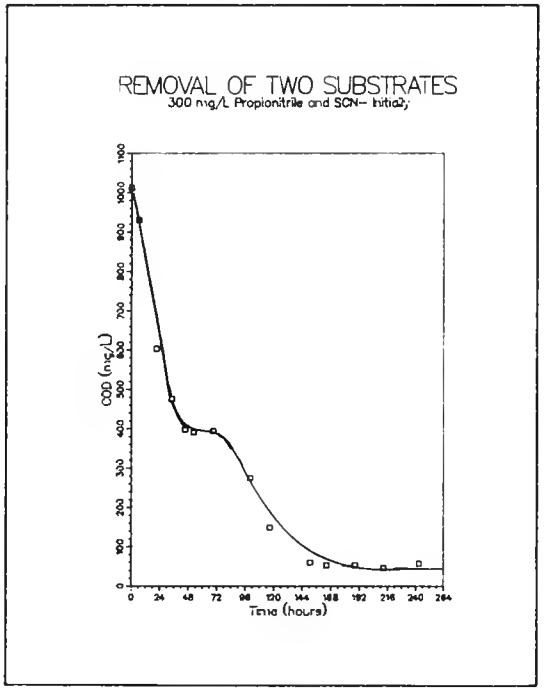

Figure 18

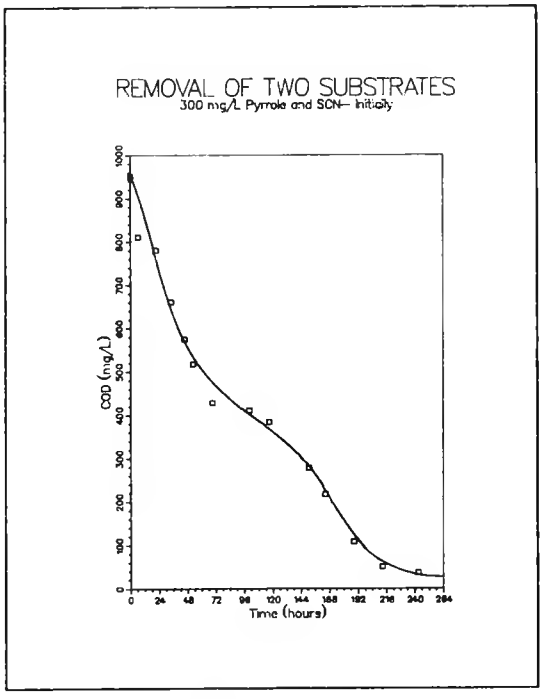

Figure 20

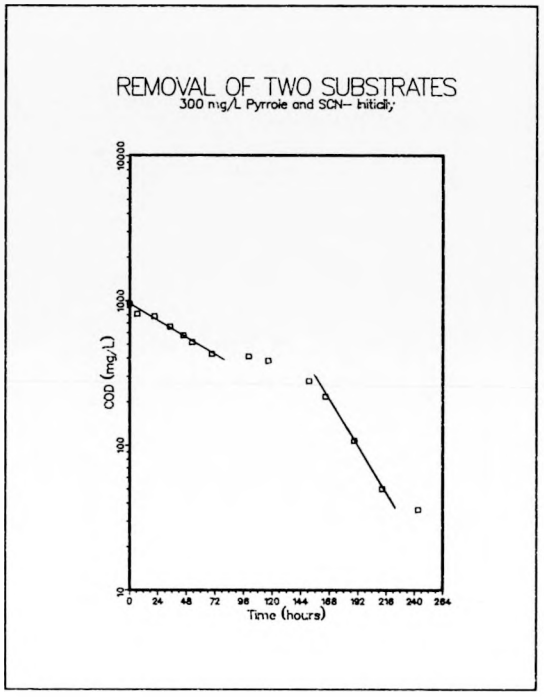

Figure 21

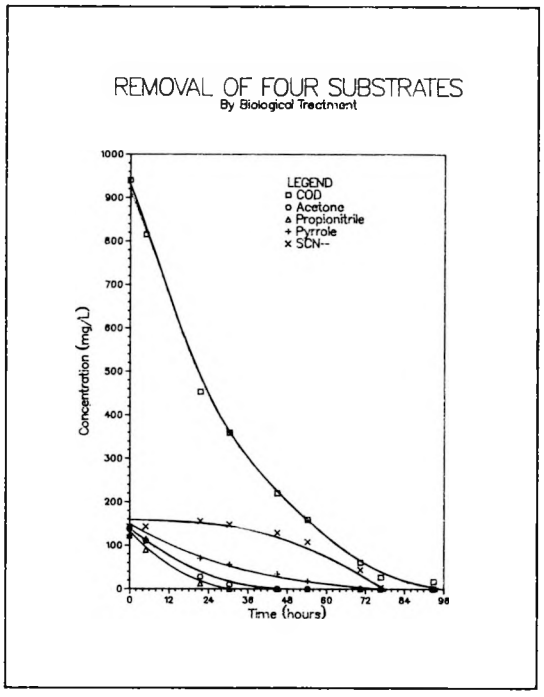

Figure 22

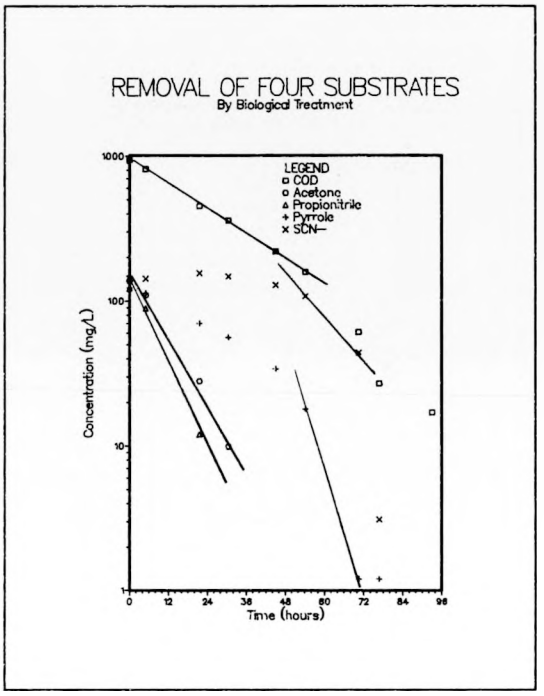

Figure 23

References

1. Punwani, D. V., Lau, F. S., and Roberts, M. J., "Pressurized Fluidized-Bed Hydroretorting of Eastern Oil Shales," Proceedings, 1988 Eastern Oil Shale Symposium, Lexington, KY, pp. 359-370.

2. "West Tests Long-Life Asphalt," Engineering News Record, September 14, 1989.

3. Mensinger, M. C., Roberts, M. J., Rue, D. M., and Lau, F. S., "Environmental Data From Moving-Bed Hydroretorting of Three Eastern Oil Shales," Proceedings, 1988 Eastern Oil Shale Symposium, Lexington, KY, pp. 133-146.

4. Gaudy, A. F., Jr., and Gaudy, E. T., Elements of Bioenvironmental Engineering. San Jose: Engineering Press, 1988.

5. Metcalf and Eddy, Inc., Wastewater Engineering: Treatment, Disposal, Reuse. New York: McGraw-Hill Book Co., 1979.

6. Standard Methods for the Examination of Water and Wastewater, 16th Edition, American Public Health Association, American Water Works Association, and Water Pollution Control Federation, Washington, D. C., 1985.

7. Mudder, T. I., Whitlock, J. L., "Biological Treatment of Cyanidation Wastewaters," Proceedings of the 38th Industrial Waste Conference, Purdue University, May 10-12, 1983.

Kinetics of Selected Heavy Metal Dissolution from Shale

by

Eric A. Robertson III, H. Scott Fogler, and John J. Gyenese
Department of Chemical Engineering
The University of Michigan
Ann Arbor, Michigan 48109

Abstract. In order to efficiently reduce the level of heavy metals in oil shale by dissolution, knowledge of the dissolution rates is essential. Reducing the levels of these metals reduces the environmental impact of the disposal. In our studies, we have examined the rates of the dissolution of barium, cadmium and iron from retorted Indiana New Albany shale using hydrochloric and nitric acids as solvents. The kinetics of these reactions is complicated by parallel reactions where the heavy metal ion is present as several different salts, each with its own dissolution kinetics. The most effective first approach to describing the shale system is to use a power law model of the dissolution of the metal species from all possible sources, in effect an average dissolution rate. Some of the kinetic parameters of this system are examined and possible ways of taking advantage of this situation are discussed. Furthermore, it has been observed that the addition of sodium chloride to aqueous hydrochloric acid enhances the dissolution of barium from retorted shale by a factor of roughly 8 over the rate in aqueous hydrochloric acid.

Introduction

Eastern oil shales are a promising source of fuel. With further development, the oil shale can produce fuels to supplement current sources such as oil and gas and help alleviate shortages that develop in these sources. The retorting process extracts the oil from the shale, leaving behind the spent shale which must be disposed of safely. Although the spent shale currently meets Environmental Protection Agency (EPA) regulations regarding its disposal, these regulations change from time to time. It is the purpose of this research to prepare for these changes, particularly in the event that the spent shale from the retorting process should not meet more stringent EPA regulations regarding the leaching of heavy metals from the shale. In such cases, the spent shale must be pretreated in some fashion to reduce the extent of heavy metal leaching. We study the kinetics of heavy metal dissolution in order to select a treatment process that effectively reduces the levels of these heavy metals in the spent shale.

The first phase of the analysis is to determine the dissolution rates in simple systems. The second phase is to develop methods of enhancing the dissolution rates. The results from the first phase are used as a reference in judging the effectiveness of the enhancement procedure.

Kinetic Rate Expression

The study of the dissolution kinetics of heavy metals from shale is complicated by several of the properties of shale. First, the composition and physical properties of the raw shale vary from one type of shale to the next. For these studies, Indiana New Albany Shale has been selected as the subject for all experiments. Second, the shale is composed of many different chemical species. A particular heavy metal species can be represented in the shale in a variety of different

forms, i.e. oxides, sulfates, etc. The study of the dissolution of each of these compounds for each metal in shale is not practical in the scope of this IGT subtask. Therefore, we have decided to study the dissolution kinetics of a few of the heavy metals in two different aqueous acid solvents. This paper presents the results of the dissolution studies for iron, cadmium, and barium in hydrochloric acid and nitric acid. Cadmium and barium were chosen because of their toxicity and iron was chosen because of its relative abundance in Indiana New Albany shale. An abbreviated list of the trace element analysis of Indiana New Albany Shale is presented in Table 1.

Table 1: Trace Elemental Analysis*
Indiana New Albany Shale

Element		Raw Shale	Retorted Shale
Ba	Barium	280	340
Cd	Cadmium	3.4	3.8
Cr	Chromium	62	70
Fe	Iron	4.5%	5.1%
Pb	Lead	35	41

*ppm except where noted

For our initial attempts at describing quantitatively the dissolution rates, we have selected the power law form of the kinetic rate expression as our model. This model presumes the dissolution rate is proportional to the reactant concentration to some power.

$$-r' = k\,[\,\text{acid}\,]^{\beta} \qquad (1)$$

The reactant in this case is the particular acid being considered (hydrochloric acid or nitric acid). The kinetic rate constant ,k, and reaction order ,β, are parameters to be determined experimentally using the method of initial rates. If the initial rate of reaction can be determined and the initial acid concentration is known, then a simple log-log plot of rate versus acid concentration will produce a straight line with slope β and intercept log (k), assuming the power law model adequately describes the kinetics of the system.

Apparatus and Procedure

The experimental procedure for determining the initial rate of reaction given a specific initial acid concentration is to expose a quantity of shale to the acid and monitor the rate of accumulation of the metal species in the solvent phase. The reaction vessel consists of a magnetically stirred 500 ml Erlenmeyer flask. The magnetic stirrer keeps the shale particles uniformly suspended and the solution "well mixed", allowing the system to be sampled without changing the shale to solvent ratio and thereby simplifying the computations required to determine the initial reaction rate.

The shale is ground using a ball mill to eliminate any mass transfer limitations, guaranteeing the system to be in a kinetically limited regime. Two grams of ground shale are placed in the flask followed by 100 ml of solvent. Samples are taken periodically over a span of 15 to 20 minutes and immediately filtered through a 0.45 μm filter to quench the reaction by separating the shale from the acid. The filtrate is then analyzed for the metal species by atomic absorption (GBC 903 Atomic Absorption Spectrophotometer).

Acidic Dissolution Results

The results obtained for iron, barium and cadmium dissolution from retorted Indiana New Albany shale are presented in Figures 1, 2, and 3. Over the concentration range studied, the logarithm of the initial rate is linearly related to the logarithm of the initial acid concentration. This implies that the choice of a power law kinetic rate expression is adequate for this initial phase of the research. The results for the iron dissolution study (Figure 1) show that the dissolution rates observed for hydrochloric acid and nitric acid are approximately the same at the same concentrations. This indicates that hydrochloric acid and nitric acid are equally effective at dissolving iron from retorted shale.

The results for barium dissolution in hydrochloric acid and nitric acid are presented in Figure 2. Over the range 0.1 M to 2.4 M, the specific reaction rate observed for the dissolution in hydrochloric acid is three times the specific reaction rate observed for the dissolution in nitric acid, indicated by the vertical offset of the hydrochloric acid data from the nitric acid data. Furthermore, one observes that the lines are parallel, indicating that the dissolution in hydrochloric acid and the dissolution in nitric acid follow the same kinetic expression with respect to reaction order. Based on the dissolution rates of barium observed for these systems, hydrochloric acid would be a better choice of solvent than nitric acid. The final choice obviously involves other considerations such as availability and cost of the solvent, which are not in the scope of this work.

The results obtained for the dissolution of cadmium from retorted Indiana New Albany Shale using hydrochloric acid as the solvent are presented in Figure 3. A meaningful rate for nitric acid could not be determined because the cadmium concentration in the samples were below the limit of detection for the atomic absorption unit. The nitric acid experiments were performed at 0.01 M, 0.1 M and 1.0 M acid. The hydrochloric acid experiments were performed over the same range of concentrations. Rates could be determined for the dissolution of cadmium from hydrochloric acid at these concentrations. This indicates that the hydrochloric acid brought about a more rapid dissolution of cadmium than did the nitric acid over the range of acid concentrations studied. However, because rates could not be determined for the nitric acid system, quantitative information is not available.

A comparison of these results is presented in Figure 4, where only the power law correlation is

shown for clarity. Table 2 lists the kinetic parameters used in constructing Figure 4. These parameters were obtained from a least squares analysis of the data. The reaction orders range from 0.3 for cadmium in hydrochloric acid to 0.6 for iron and barium. This similarity of reaction orders indicates that there is in general little difference in the dependence on the acid concentration for the systems studied. Furthermore, it implies that varying the acid concentration is not an effective means of selectively removing one heavy metal in preference to another. The relative rate of dissolution is simply the ratio of the dissolution rates observed for the system. For example, the selectivity of the relative dissolution rate of barium to iron (over the range 0.01 M to 1.0 M) would be given by [2].

$$S_{Ba/Fe} = \frac{r_{Ba}}{r_{Fe}} = \frac{k_{Ba}\,[HCl]^{0.6}}{k_{Ba}\,[HCl]^{0.6}} \qquad (2)$$

This ratio is clearly independent of hydrochloric acid concentration so varying the concentration has no significant effect on the relative dissolution rate of barium to iron.

Table 2: Comparison of Kinetic Parameters

Element	Acid	k	β
Fe	HCl	1.2×10^{-6}	0.6
	HNO3	9.0×10^{-7}	0.4
Ba	HCl	1.6×10^{-9}	0.6
	HNO3	6.9×10^{-10}	0.6
Cd	HCl	4.0×10^{-10}	0.3

Also note that the rate constant for iron dissolution is three orders of magnitude greater than the rate constants for cadmium and barium. This difference may be of some use should it ever be desirable to preferentially remove iron over barium or cadmium from the retorted shale.

Enhancement by Acid - Salt Systems

The studies of Kline and Fogler have shown that the dissolution of silicate materials by hydrofluoric acid can be catalyzed by the presence of salts in the solvent. It was shown that even though the salt had no dissolution capacity whatsoever, the dissolution could be enhanced by as much as a factor of 10 by simply adding salt to the mixture. Furthermore, LeBlanc and Fogler showed that the dissolution of manganese dioxide could be enhanced by as much as 5 orders of magnitude by altering the solution potential and taking advantage of the semiconductor properties of manganese dioxide. Though this does not apply to the dissolution of heavy metals from oil shale in general, it does indicate that the dissolution rate of naturally occurring semiconductor compounds can be enhanced (or retarded) by a judicious choice of solvent.

This previous work in the area of salt catalysis suggested that the addition of salts to acid systems might improve the dissolution rates of heavy metals from retorted shales. The first attempts at enhanced rates were with barium dissolution in hydrochloric acid – sodium chloride systems. The results are presented in Figures 5 and 6 and in Table 3. The dissolution rates obtained using 0.01 and 0.1 M aqueous sodium chloride were one–half and one–third the rate observed for barium dissolution in 0.1 M aqueous hydrochloric acid. This indicates that the brine solutions have some intrinsic capacity to dissolve barium. The rate obtained for 0.01 M aqueous sodium chloride in 0.1 M aqueous hydrochloric acid indicates no significant enhancement. However, the rate observed for 0.1 M aqueous sodium chloride shows a significant enhancement, almost a factor of 8, over the rate for 0.1 M hydrochloric acid alone. This enhancement is not due solely to the dissolution capacity of the salt. This can be seen by considering the rate of dissolution in the acid versus the rate of dissolution in the brine. If there were no interaction of the salt with the acid, the dissolution rate expected for the acid – salt combination would be about 5×10^{-10} gmol Ba / gm shale / min. The rate observed for the 0.1 M acid – 0.1 M salt was 28×10^{-10}, nearly six times the rate expected assuming there were no interaction. This indicates that the salt is participating in some synergistic fashion in the dissolution mechanism. This synergistic combination of hydrochloric acid and sodium chloride is a promising development in our studies of enhanced dissolution of heavy metal from retorted shale.

Table 3: Enhancement in HCl – NaCl System

[HCl] gmol/l	[NaCl] gmol/l	dissolution rate*	Enhancement of Barium Dissolution
0.0	0.01	0.92	0.2
0.0	0.10	1.1	0.3
0.1	0.00	3.7	1.0
0.1	0.01	3.4	0.9
0.1	0.10	28.0	7.6

* rate in units of 1×10^{-10} gmol Ba / gm shale / min

Conclusions and Future Work

The data for the dissolution in hydrochloric acid and nitric acid indicates that the kinetics generally follows a reaction of order 0.6, suggesting that varying acid concentration is not an effective means of selectively removing heavy metals for the species studied. Additionally, iron dissolution rates are roughly three orders of magnitude greater than those observed for cadmium and barium in the same acids and concentration ranges. This may be of use should it ever become desirable to remove iron from the spent shale. Finally,

sodium chloride appears to participate synergistically in the dissolution of barium from retorted shale in aqueous hydrochloric acid solvents.

Future work involves the inclusion of chromium in the list of heavy metal species to be studied because of its toxicity and because a broader base of information is desirable for further work in the salt enhancement area. The results observed for barium dissolution in acid - salt systems suggest this is a promising means of enhancing dissolution rates. Therefore, work will obviously continue in the salt enhancement area.

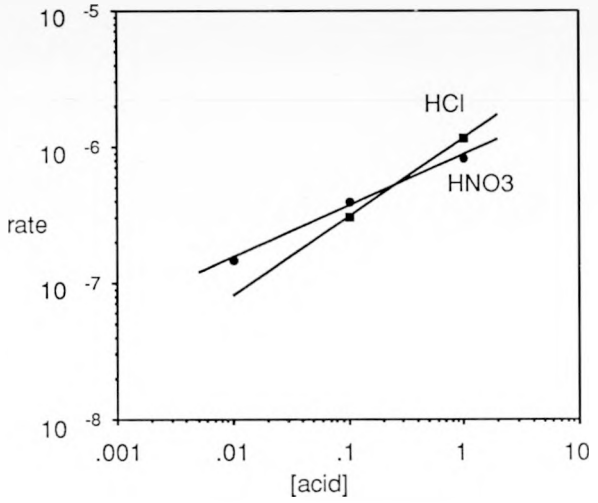

Figure 1. Kinetics of iron dissolution from retorted shale in hydrochloric and nitric acid solvents. Rates in units of gmol metal / gram shale / min; concentration in units of gmol / l.

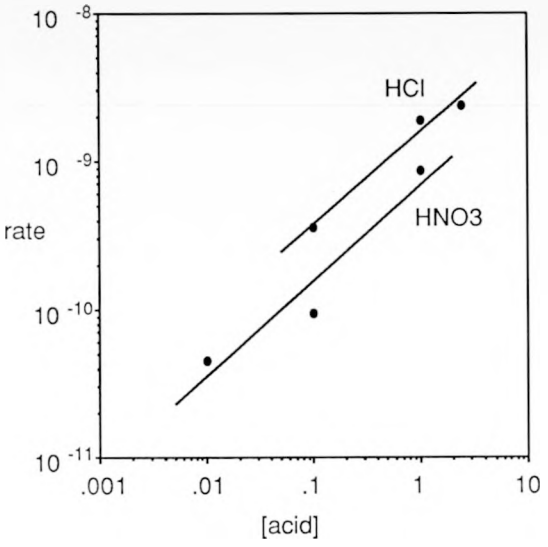

Figure 2. Kinetics of barium dissolution from retorted shale in hydrochloric acid and nitric acid solvents.

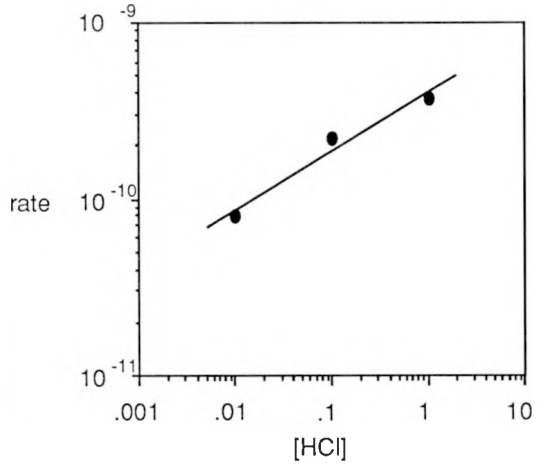

Figure 3. Kinetics of cadmium dissolution from retorted shale in an aqueous hydrochloric acid solvent

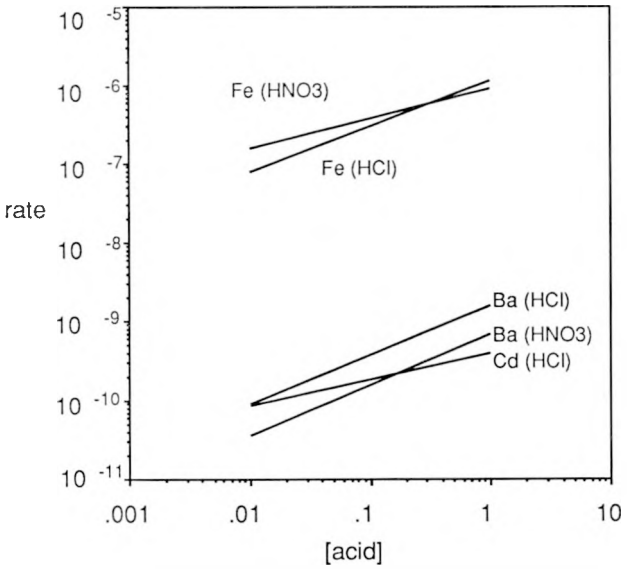

Figure 4. Comparison of dissolution rates of selected heavy metals from retorted shale.

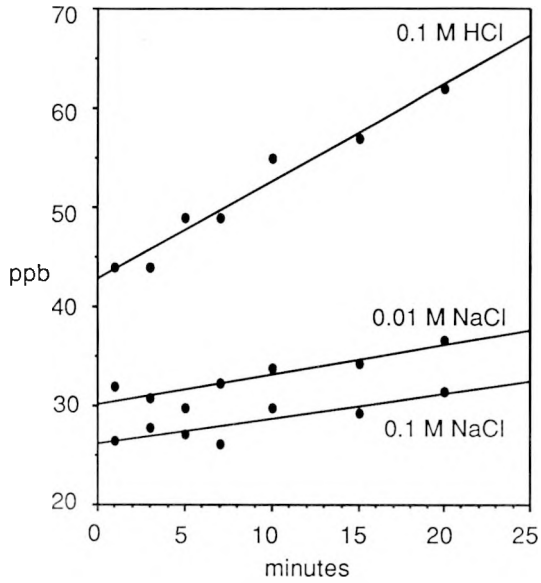

Figure 5. Barium dissolution from retorted shale using a brine solvent.

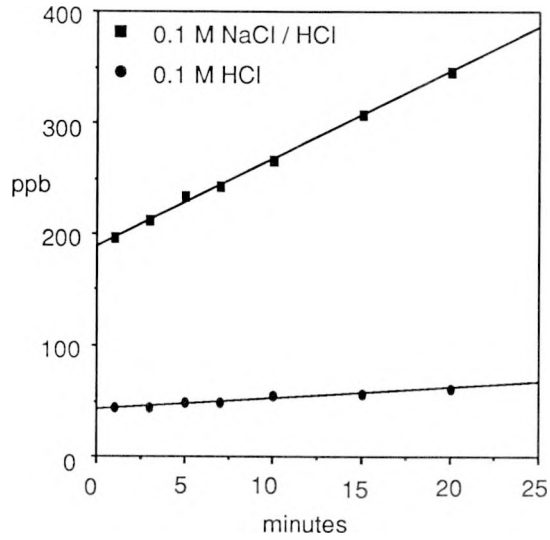

Figure 6. Barium dissolution from retorted shale using an aqueous HCl – NaCl solvent

Evaluation of Oil Shale Solid Waste for Soil Stabilization

by

John P. Turner
Department of Civil Engineering
University of Wyoming
Laramie, Wyoming 82071
Kunal J. Suryavanshi
Ground Engineering Consultants
Denver, Colorado 80225

Abstract. Cementitious oil shale solid wastes are evaluated for potential use as soil stabilizers. A testing program is described which consisted of index tests, compaction properties, and unconfined compressive strength of several mixtures of spent shale and soil. Two types of soil are evaluated for possible spent shale stabilization, a sand with nonplastic fines and a highly plastic clay. Three types of eastern spent shale and one western spent shale are evaluated for stabilizing potential. The results of the testing program are presented and show that, based on unconfined compressive strength, soil stabilization using spent oil shale is technically feasible and may be a cost-effective method for improving the engineering properties of highway pavement subgrades.

Introduction

Some oil shale solid wastes contain pozzolanic silica and alumina that react in the presence of water to form hydrous cements. Apparently, these pozzolanic materials begin to form at temperatures above about 1100 degrees F. Above 1700 degrees F, the cementitous components are diminished, apparently through sintering of the pozzolanic silica and alumina.[1] The development of strength by hydrated western spent shale has been attributed to the formation of tobermorite gel, low sulfate-sulfoaluminate, and ettringite.[1] Based on the chemical reactions that occur when spent shale is mixed with water, oil shale solid waste can be categorized as an "active" soil stabilizer. By mixing spent shale with water and soil, it may be possible to produce new materials with improved engineering properties. The use of oil shale solid waste for soil stabilization could improve the economics of shale oil production while mitigating one of the environmental liabilities (disposal of solid wastes). To the best of our knowledge, oil shale solid waste has never been used as a soil stabilizer.

The objective of this work is to assess the technical feasibility of using oil shale solid waste as a soil stabilizer. To achieve this objective, a study was conducted to determine whether compacted mixtures of oil shale solid waste, water, and soil could be produced with sufficient compressive strength for use as stabilized highway subgrades. Additional details can be found in Suryavanshi (1989).[2]

Laboratory Testing Program

Materials

Soils. Two types of soil were tested, including one coarse-grained (Soil A) and one fine-grained (Soil B). Soil A is classified as A-2-4 in the AASHTO Soil Classification System and Soil B is classified as A-7-6. Each soil was characterized and classified by the following tests: particle size analysis, specific gravity of soil solids, liquid limit, plastic limit, plasticity index, moisture-density relationships, and unconfined compressive strength (cohesive soil only). The results of particle size analysis and the Atterberg limits are summarized in Table 1.

Oil Shale Solid Wastes. Four different oil shale solid wastes were evaluated for stabilizing potential. Shale A (western) was produced by the combustion of oil shale from the Green River Formation in the Piceance Basin of Colorado and was retorted by the Lurgi-

Table 1. Soil Index Properties[1]

Particle Diameter (mm)	Percentage Passing, by weight Soil A	Soil B
4.75	95	100
2.00	84	84
0.85	72	65
0.425	56	61
0.150	40	53
0.075	25	47
Plastic Limit (%)	not measurable	25
Liquid Limit (%)	26.3	50
Plasticity Index	non plastic	25

1. The following test procedures were used:
Particle size analysis of soils, AASHTO T88
Liquid limit, AASHTO T89
Plastic limit & plasticity index, AASHTO T90

Ruhrgas process. Shales B, C, and D all were produced by the combustion of eastern oil shales. Shale B was derived from the fluidized-bed combustion of Chatanooga Shale. Limestone was added during the combustion to capture sulfur emissions. Shale C also was produced by fluidized-bed combustion of Chatanooga Shale, but without the addition of limestone as a scrubber. Shale D was produced by fluidized-bed combustion of New Albany Shale and limestone was added during combustion. The combustion process conditions for Shales B and D are described in detail by Sullivan, et al. (1987)[3]. Table 2 summarizes the types of spent shale used in this study.

Methods

Sample preparation for strength tests. Samples of soil and soil/spent shale were prepared by mixing the desired proportions of soil, spent shale, and water and then compacting the mixture using the Harvard Miniature apparatus. Mixing was achieved in two ways. In method 1, the soil and spent shale were mixed dry and then water was added to the dry mix. In method 2, the soil was mixed at its optimum water content, the spent shale was mixed at its optimum water content, and then the two were mixed together. These two methods were used to evaluate whether the mixing sequence affects the engineering properties. Each sample was compacted in 5 lifts using 25 blows per lift. Each sample was extracted from the mold and allowed to cure seven days before being tested in unconfined compression.

Two curing techniques were used with Soil B. In the first method, samples were cured while wrapped in plastic in a moist room for seven days. It was found

Table 2. Spent Shale Types and Sources

Spent Shale	Source	Process[1]
A	Green River Fm.	Lurgi-Ruhrgas
B	Chatanooga Shale	FBC, w/limestone
C	Chatanooga Shale	FBC, no limestone
D	New Albany Shale	FBC, w/limestone

1. FBC = Fluidized-Bed Combustion

that the moisture content following the seven day curing period was nearly the same as the molding water content. This curing method yields the lowest stength and probably represents a lower bound on the potential strength increases using spent shale. In the second method, samples were cured wrapped in plastic for three days, and then cured unwrapped for an additional four days. This technique was used in an attempt to maximize the strength increase by making sure that sufficient moisture was present for hydration of the spent shale, followed by drying of the specimen to reduce the moisture content and increase the strength. These different methods provide a means to evaluate the effects of curing method on the strength of Soil B stabilized with Shale A.

Moisture-Density Relationships (Compaction Test). The purpose of the moisture-density test, commonly called the compaction test, is to determine the moisture content at which the maximum dry density of the soil can be achieved. Increasing the density of a stabilized soil is desirable for engineering purposes for increased shear strength, decreased compressibility, and decreased permeability. The moisture content corresponding to the maximum dry density of a soil is called the "optimum" moisture content. Specifications for field compaction of highway subgrades usually are based upon the contractor obtaining 90 to 95 percent of the maximum dry density. All tests were conducted in accordance with ASTM D 558-82, "Test Methods for Moisture-Density Relations of Soil-Cement Mixtures".

For this study, moisture-density relationships were determined by compacting soil and soil/spent shale mixtures at different moisture contents and then plotting moisture content versus dry density. Figure 1 shows a typical moisture-density curve, in this case for Soil A mixed with 10 percent by weight of Shale A. The soil and spent shale were first mixed dry, and then water was added to the dry mix (mixing method 1).

Unconfined Compression. The unconfined compressive strength (q_u) following a 7-day curing period was used to evaluate the potential increase in strength for soils treated with spent shale, compared to untreated samples. The unconfined compression test also was used to determine the percentage of spent shale required to yield the greatest strength increase, and as a means of comparing the stabilizing potentials

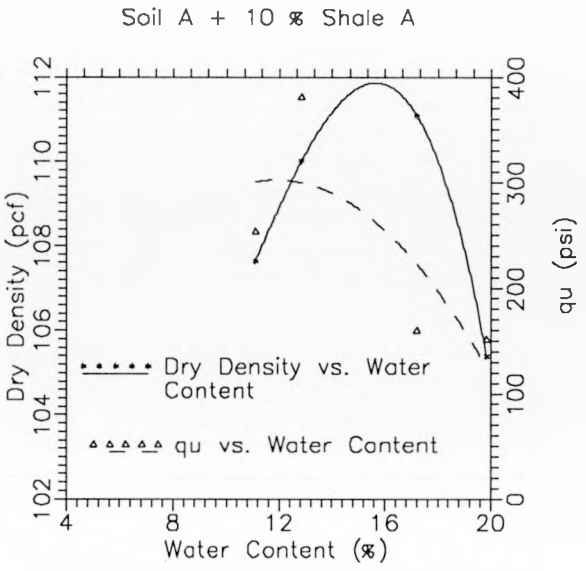

Figure 1. Compaction curve and unconfined compressive strength of Soil A.

of the four types of spent shale. Figure 1 also illustrates how unconfined compressive strength varies with moisture content for Soil A with 10 percent of Shale A.

The testing procedure consists of compressing a cylindrical sample of soil at a loading rate corresponding to 0.5 to 2 percent strain per minute. The rate of strain is such that it causes the sample to fail in about five minutes. The sample deformation and load are monitored at specified time intervals. Loading is continued until a visible failure plane is observed or until a maximum of 20 percent strain is reached. All tests were conducted in accordance with ASTM D-2166, "Standard Test Method for Unconfined Compressive Strength of Cohesive Soils".

Testing Schedule

Unconfined compressive strength (q_u) tests were conducted to evaluate the strength criterion. Soil A was mixed with all four types of spent shale at 0, 10, 15, 20, and 25 percent by weight. Moisture-density relationships were conducted using Harvard Miniature samples. Each sample was cured for 7 days and then tested in unconfined compression. A total of 133 samples were tested. Soil B was mixed and tested with Shale A only, at 0, 3, 10, 15, 20, and 25 percent by weight, and at moisture contents ranging from 17.0 percent to 27.0 percent. Soil B was evaluated with Shale A only, because these materials are under consideration for use in an FHWA demonstration project involving the stabilization of a highway subgrade consisting predominantly of Soil B with Spent Shale A.

Results and Discussion

Table 3 summarizes the results of compaction and unconfined compression tests for Soil A. The maximum strengths and maximum dry densities are reported for each type of spent shale. Table 4 summarizes the results of compaction and unconfined compression tests conducted on Soil B.

Strength

The unconfined compressive strengths presented in Table 3 show that spent shales A, B, and D significantly increased the strength of Soil A, while spent shale C resulted in a strength decrease. The maximum unconfined compressive strength of Soil A without spent shale is 75 psi. The two eastern shales combusted with limestone (Shales B and D) yielded the highest strengths, exceeding 600 psi. The western spent shale (Shale A) yielded unconfined compressive strengths of over 400 psi. Shale C, which was produced by the combustion of eastern oil shale without the addition of limestone, actually caused the strength of Soil A to decrease compared to the strength of Soil A with no spent shale. The maximum unconfined compressive strength of Shale C by itself is only 23 psi, indicating further that eastern oil shale solid waste may not be suitable for soil

Table 3. Maximum Dry Densities and Compressive Strengths for Soil A[1]

Spent Shale	% Spent Shale	$q_{u,max}$[2] (psi)	Max Dry Density (pcf) w_q[3]		w_γ[4]
none	0	75	12.0 %	118.4	13.0
A	10	303	11.8	111.8	15.6
	15	273	14.0	115.5	14.8
	20	284	15.6	116.1	14.1
	20	477[5]	15.2	115.1	15.2
	25	200	14.7	110.8	15.3
B	10	507	14.6	119.3	14.2
	15	422	11.7	119.2	11.7
	20	418	12.2	118.9	14.0
	20	644[5]	15.1	119.8	15.1
	25	335	12.8	117.3	12.7
C	10	41	11.6	114.8	12.6
D	10	287	9.7	115.5	9.8
	15	264	15.3	116.3	15.4
	20	282	14.8	117.5	15.7
	20	657[5]	16.8	119.1	16.8
	25	225	15.4	114.3	14.5

(1) Soil A is fine sand with nonplastic fines.
(2) $q_{u,max}$ = maximum unconfined compressive strength.
(3) w_q = moisture content corresponding to $q_{u,max}$.
(4) w_γ = moisture content corresponding to maximum dry density.
(5) Mixing method 2.

Table 4. Maximum Dry Densities and Compressive Strengths for Soil B[1]

Spent Shale	% Spent Shale	$q_{u,max}$[2] (psi)	w_q[3]	Max Dry Density (pcf)	w_γ[4]
none	0	437[5]	21.0	107.3	21.1
	0	57[6]	17.7	107.3	21.1
A	3	36[6]	19.6	103.0	22.7
	10	46[6]	21.3	102.4	20.6
	10	380[5]	22.5	105.5	22.8
	15	326[5]	24.6	102.7	22.6
	20	400[5]	26.2	101.8	23.8
	25	325[5]	25.7	102.2	23.1

(1) Soil B is a highly compressible clay.
(2) $q_{u,max}$ = maximum unconfined compressive strength.
(3) w_q = moisture content corresponding to $q_{u,max}$.
(4) w_γ = moisture content corresponding to maximum dry density
(5) Sample cured wrapped in plastic at room temperature for three days, then cured unwrapped for four days.
(6) Sample cured wrapped in plastic in the moist room for 7 days.

stabilization, unless limestone is added during combustion. The mineralogy of most eastern oil shales, consisting predominantly of quartz, would not be expected to yield pozzolanic materials without the addition of limestone, which adds calcium in the form of quick lime to the combusted waste material. Western oil shale from the Green Formation has a mineralogy that apparently does produce cementitious materials upon combustion. The inorganic mineral matrix of Green River Formation oil shale consists essentially of dolomite, calcite, illite, and quartz. Although not understood fully at this time, combustion of these materials at the proper temperatures produces pozzolanic silica and alumina that give western spent shale its cementing properties when mixed with water.

It was observed that the highest unconfined compressive strengths are obtained when Soil A and the spent shales are mixed independently at their respective optimum moisture contents and then combined (mixing method 2), compared to mixing method 1 at the same moisture content. Mixing method 1 entails mixing the shale with soil in a dry condition and then adding water to the mixture. One possible reason for the higher strengths obtained using method 2 is that the better miscibility of water with spent shale produces more pozzolan-forming hydrates compared to method 1. In method 1, the surface of the spent shale shale particles may not be exposed thoroughly to the available water, resulting in less cementation. Mixing method 1 yielded the highest strengths in the range of 10 to 15 percent by weight of spent shale, while mixing method 2 yielded the highest strengths in the 15 to 20 percent range. In general, the water content that corresponds to the maximum strength is not the same as the moisture content that yields the maximum dry density ("optimum moisture content"). This behavior is typical for cemented soils, and can be important in developing field construction specifications. For example, it may be advantageous to develop construction specifications for compacted densities that optimize the strength and durability of the subgrade, rather than obtaining 90-95 percent of the maximum dry density.

Unconfined compression tests on Soil B, a highly plastic clay, using Shale A (Lurgi) as the stabilizer, show that the curing method has a significant influence on the strength. This effect appears to be controlled primarily by the moisture content that results from the curing method. The maximum unconfined compressive strength of Soil B with no spent shale is 57 psi when tested immediately after mixing, and occurs at a moisture content of 17.7%. If Soil B is allowed to cure for three days in a moist room and then allowed to cure at room temperature and humidity for four days, the unconfined compressive strength is 437 psi. This occurs at a mixing moisture content of 21.0%, but the moisture content after the curing period is 4.0 percent. The strength of Soil B, like most clays with high plasticity, is highly dependent upon its moisture content. This behavior also is predominant when Soil B is stabilized with spent shale. When cured in a moist room for seven days, the moisture content is approximately the same as the mixing moisture content, and the unconfined compressive strength decreases slightly compared to the strength with no spent shale. When cured for three days in the moist room and four days at room temperature and humidity, the unconfined compressive strength increases dramatically, although it is still slightly less than the strength of Soil B with no shale cured under the same conditions. These results indicate that the addition of spent shale to Soil B does not increase the unconfined compressive strength and, therefore, may not be an appropriate method for soil stabilization. However, independent tests conducted by the Federal Highway Administration using Soil B mixed with 10 percent Shale A yielded an R-value of 34 compared to an R-value of 7 for Soil B with no spent shale. R-value, or resistance value, is a relative measure of subgrade support used for highway pavement thickness design and indicates the ability of a subgrqde soil to resist lateral deformation under traffic loading. In addition, by adding 10 percent of Shale A to Soil B, the plasticity index decreased from 25 (highly plastic) to 13 (moderately plastic), thus improving the suitability of Soil B as a subgrade material. It is concluded that spent shale A may have the potential to improve the engineering behavior of Soil B, although these improvements are not apparent with respect to unconfined compressive strength.

Summary and Conclusions

Oil shale solid waste has the potential to be used as a low-cost construction material. This potential is a result of the cementing properties of spent shale when it comes in contact with water to form hydrous cements. This paper evaluates the technical feasibility of using oil shale solid waste for soil stabilization, based primarily upon increases in the unconfined compressive strength of spent shale-stabilized soils. The important findings of this study are as follows:

1) Soil stabilization using spent shale appears to be technically feasible. This is based on:

a) Increases in the unconfined compressive strength of Soil A (fine sand) when mixed with three different spent shale types. These include a combusted western shale and two eastern shales combusted in the presence of limestone. The unconfined compressive strength observed for Soil A without any spent shale added was 75 psi. With spent shale, the unconfined compressive strength ranged from 150 psi to 660 psi.

b) An increase in the R-value and a reduction in the plasticity index of Soil B (highly plastic clay) when mixed with Shale A (combusted western shale). Unpublished results from the FHWA, Central Direct Federal Division indicate an increase in the R-value from 7 to 34 for same-day strength and an R-value of 41 for 8-day strength. The plasticity index of Soil B decreased from 25 to 13 upon the addition of 10 percent Shale A.

2) Solid waste from eastern oil shale does not appear to have good potential as a soil stabilizer unless limestone is added during combustion. Limestone added as a sulfur-absorbing agent (scrubber) increased the cementing properties of Chatanooga oil shale solid waste dramatically, compared to the solid waste produced without the addition of limestone. Adding limestone during combustion apparently results in the formation of quick lime in the solid waste, which increases the pozzolanic properties of the hydrated spent shale.

3) The method of mixing the soil, spent shale, and water significantly affects the strength of the stabilized soils. When the soil and spent shale are mixed independently at their optimum moisture contents and then combined (mixing method 2), higher strengths were obtained, compared to mixing the soil and spent shale dry and then adding water to the dry mix (mixing method 1).

Recommendations for further research and development of spent shale utilization include the following:

1) The durability of soils stabilized with spent shale should be evaluated in detail. This should include resistance to freeze-thaw and wet-dry conditions.

2) The long-term performance of spent shale-stabilized subgrade soils should be evaluated, preferably by construction and monitoring of highway pavement test sections.

3) Further research is necessary to identify and evaluate the chemical characteristics of spent shale that control spent shale cementation. Other factors, such as raw oil shale source, process conditions such as time-temperature history, and physical properties of the spent shale such as specific surface and grain size distribution should be evaluated.

4) Additional uses of spent shale which take advantage of its cementing characteristics, such as an additive in portland cement, as a highway subgrade by itself, or as a component of grouts, should be explored.

Acknowledgments

The work described in this paper was supported in part by the Western Research Institute and the U.S. Department of Energy, Laramie Projects Office. Dr. Michael Essington is the technical officer for WRI and Mr. Richard McQuisten is the DOE Project Manager. Their support is greatly appreciated.

References

1. Culbertson, W.J., Jr., Nevens, T.D., & Hollingshead, R.D., "Disposal of Oil Shale Ash", Quarterly of the Colorado School of Mines, Vol. 65, No. 4, pp. 89-132, Oct. 1970.

2. Suryavanshi, K.J., "Pavement Subgrade Stabilization Using Oil Shale Solid Wastes", unpublished M.S. thesis, Department of Civil Engineering, University of Wyoming, Laramie, 156 p., Aug. 1989.

3. Sullivan, P.J., Yelton, J.L., and Reddy, K.J., "Acid Mine Drainage Potential of Raw, Retorted, and Combusted Eastern Oil Shale", Final Report under Contract DE-AC20-85LC11062 by Western Research Institute for the U.S. Dept. of Energy, Laramie, WY, 126 p., Sept. 1987.

Environmental and Health Surveillance Monitoring Results at Parachute Creek Shale Oil Project, 1988 and 1989

by

Janie B. Benton
Office of Synthetic Fuels Projects
U.S. Department of Treasury
Washington, D.C. 20220

Abstract. The Parachute Creek Shale Oil Project is one of four synthetic fuels facilities awarded financial assistance under the Energy Security Act of 1980. The Project agreed to develop and implement an Environmental Monitoring Plan (EMP) that incorporates both permit-mandated monitoring and supplemental monitoring in the areas of water, air, solid waste and health surveillance.

During 1988, the Project completed the first tier of supplemental sampling and the second year of health surveillance. The concomitant completion of sample analysis, data management and reporting, and quality assurance/quality control efforts met all the EMP implementation requirements.

The data presented in the Annual Health Surveillance Report and the Tier I Supplemental Monitoring Report are discussed, along with modifications for future sampling and analysis.

Introduction

In 1986, as part of the contractual agreement with the U.S. Synthetic Fuels Corporation, Union Oil Company of California (Unocal) developed an Environmental Monitoring Plan (EMP) for the purpose of monitoring compliance (regulated) and supplemental (unregulated) environmental and health-related emissions from its 10,000-barrel-per-day (BPD) oil shale facility in Parachute, Colorado.

The trip of supplemental sampling for air, water, solids and particulates began in September 1988 and was completed in March 1989. Eighteen of 21 supplemental sampling points were monitored, including seven particulate, 12 gas, one liquid and five solid samples. Analyses produced nearly 800 data points.

Health-related emissions collected during the third and fourth quarters of 1988 and the first two quarters of 1989 included area and personal monitoring, as well as medical surveillance of all job categories.

Highlights of the trial trip, health monitoring, data acquired and lessons learned to date are discussed herein.

Project Description

The Project is located in western Colorado near the town of Parachute in Garfield County. In 1983, Unocal constructed a retort on a five-acre bench carved from Long Ridge. The facility uses shale deposits of the Green River Formation, which are estimated to contain 1.8 trillion barrels of oil, with approximately 85 percent of this resource within the Piceance Basin in western Colorado. The targeted mining interval for the Long Ridge property is the 60-foot zone lying beneath a bed known as the Mahogany Marker.

The underground mine is worked using a room and pillar method. About 14,000 tons per day of raw shale are mined, crushed and stored within the underground facilities. The ore is conveyed to the retort feed bin and pumped through a cone in the vertical retort where it is heated and the hydrocarbons are vaporized and leave the

shale. The retorted shale is removed from the top of the cone and enters discharge chutes for transport by gravity flow into the shale cooling system. It then goes to the surge pile from which it is trucked to the laydown area.

The Shale Disposal Area is located in the East Fork canyon, below Long Ridge. It extends westward and currently involves 582 acres. Of this total, 131 have been permanently reclaimed and 54 have been temporarily reseeded and vegetated for soil stability. Additional acreage up valley will be used for disposal operations as the retorted shale pile continues to expand.

The hydrocarbons from the Retort are condensed by cooling and then are pumped through deashing, fractionation and sulfur recovery units prior to entering the underground pipeline to the Upgrade Facility, ten miles south in Parachute Creek Valley.

The raw shale oil is upgraded by removing shale fines, sulfur, nitrogen and trace metals and by adjusting the pour point of the syncrude. The syncrude can be shipped from the facility by rail or truck. Details of the process can be found in the EMP (Unocal, 1986).

Since plant start-up in mid-1986, unexpected problems inhibited early performance. These problems were not related to the technology but to the shale resource itself. Laboratory data and vendor testing were ineffective in predicting the wear characteristics of raw and retorted shale, and the shale sulfur content proved higher than anticipated. The two major operative problems--design of the retort scraper and the finer-than-expected retorted shale causing problems in the shaft cooling system--have been modified over the past two years. During 1987, production was 17 percent of the design capacity of 10,400 barrels per stream day. In 1988, it was 32 percent, and during 1989, short-term runs have achieved 50 to 60 percent of design with several runs exceeding 60 percent. The syncrude produced has been refined and sold at a nearby facility for a number of standard uses. The commercial applicability of the Project's shale-oil/derived syncrude as a quality refining feedstock is discussed in a paper by Duir, et al.(1989).

Environmental Monitoring Results

The environmental monitoring program is a substantial commitment of manpower and resources to evaluate the three components of the facility: the Mine/Retort, the Upgrade and the Retorted Shale Disposal Area. Pollution control devices include the baghouse on the mine crushing and screening facilities; the low NO_x burners on the boilers and the sulfur recovery unit on the plant fuel gas at the Retort Facility; the runoff collection system and pond at the Spent Shale Disposal Area; the sulfur recovery unit for plant fuel gas; the steam stripper to treat process waters; and the storm water collection system and basin at the Upgrade Facility. Groundwater monitoring is used to detect contamination around the Shale Disposal Area and the Upgrade Facility.

Prior to the approval of the EMP in 1986, the Project had been performing compliance air, water/groundwater and health surveillance monitoring. In 1986, supplemental monitoring was initiated although results focused on health surveillance, pending modification and steady operation of the facilities. Previous publications have outlined the approach taken by Unocal's EMP and the implementation of sampling and analytical techniques designed to achieve the EMP goals (Benton, 1987 and 1988).

Parachute Creek's EMP supplemental sampling uses a tiered approach for environmental monitoring. The Tier I Program emphasizes screening-level analyses of supplemental parameters to identify substances of concern (Unocal, 1986). Currently, twenty-two supplemental points are designated in the EMP (14 gaseous streams, five solids and three aqueous), 12 at the Mine/Retort and 10 at the Upgrade Facility (see Attachment 1). A summary of all the quarterly monitoring performed and health monitoring results are discussed below.

Health Surveillance

Health surveillance data from July 1, 1988 through June 30, 1989, were collected using area and personal monitors. The majority of the data were below established OSHA Permissible Exposure Limits (PEL) and Mined Land Reclamation Board Threshold Limit Values (TLVs). The elevated samples are summarized in Attachment 2 and are discussed below.

For the third quarter of 1988, 64 area samples and 640 personal samples were obtained. The data reported showed five noise samples exceeded the OSHA PEL. Personnel in those areas routinely wear hearing protection. Three syncrude vapor samples and twelve solvent solubles were above detection limits but were less than one percent of the corporate established trigger level of 50 parts per million (ppm). (No OSHA standard has been established for these parameters.)

Fourth quarter 1988 results, based on 53 area and 318 personal samples, found three elevated trace metal samples for the welding area in the mine. Workers in this area wear respiratory equipment, such that worker exposure is reduced; also, improvements were made in the local exhaust system to further reduce exposure potential. Fourteen of the quarterly

samples contained parameters detected at minimal levels. These included solvent solubles (five samples), syncrude vapors (three samples), and polynuclear aromatic hydrocarbons (pyrene and chrysene).

Fifty-four area and 244 personal samples were collected in the first quarter of 1989. Two of these contained benzene above the PEL as a result of sampling during upset conditions. Sampling has been increased to detect any future elevated levels, and employees have been instructed to wear appropriate protective equipment.

Two elevated solvent solubles samples also were collected during upset conditions, when a fire occurred in a belt in the Retort area. Elevated values indicated combustion products were the source.

Second quarter 1989 monitoring included 138 area and 526 personal samples. Five of the compliance samples exceeded established exposure levels; four elevated benzene values were obtained during operational changes in the Retort Utilities area, and one elevated carbon monoxide sample was collected in a mine haulage way that receives minimal pedestrian traffic. Workers were instructed to wear appropriate protective equipment during unusual work conditions.

Supplemental monitoring obtained six syncrude vapor samples with concentrations above the detection level. The results were well below the 50 ppm level of concern, however.

Water/Groundwater

To date, ten EMP quarterly reports have been submitted to Treasury, including compliance monitoring for the Upgrade Clean Water Basin and the Basin Underdrain under an NPDES permit, as well as monitoring of eight groundwater wells around the domestic wastewater treatment basin. Data have been within expected ranges at seven of the monitoring wells. The eighth well yielded continued atypical data and evidence of silting in and was eliminated from the permit.

The Upgrade was designed as a zero discharge facility, and to date, no discharges have occurred from the Basin or the Underdrain.

Supplemental water monitoring included two sampling points; the Retorted Shale Pile Runoff and the Shale Pile Leachate. Neither of these sources have been sampled, because the Project believes a representative sample will not be generated before stabilization of vegetative growth. However, the Project realizes stabilized ground cover may not occur for ten years or more, and plans to establish temporary plots for monitoring during 1990. Leachate and runoff will be sampled, if they are generated, in 1990 and 1991.

Air Quality/Fugitive Emissions

Details of the permit-mandated monitoring are given in the EMP (Unocal 1986). Compliance air monitoring included in the quarterly EMP monthly reports entails source emissions during operations, fugitive dust, continuous ambient air quality and meteorological monitoring and performance testing of continuous emissions monitoring systems (ibid). During 1989, ambient air monitoring data continued within expected ranges, as did fugitive dust emissions/control.

Although the retort and sulfur plants achieved 99-plus percent reduction in pollutants of concern during steady-state operations, exceedances were observed during start-ups and shutdowns. As summarized in Attachment 3, the majority were related to the sulfur plant at the Retort. This system was modified during the August 1989 maintenance turnaround to minimize such emissions.

Supplemental gases and particulates sites and parameters tested are in Attachment 4. Parametric data were compared to environmental levels of significance (LOS) to identify potential issues that required further study. Levels of significance normally were established as 50 percent of the lowest value reported in research findings or based on best professional judgment for each parameter.

All gaseous and particulates samples were obtained as planned. Although the field crews attempted to obtain samples during steady-state operations, at 60 percent of capacity, that goal was not possible in three instances:

- The single Unisulf Tail Gas sample was collected during a period when the catalyst in the Hydrogenation Reactor immediately upstream of the Unisulf Absorber was partially deactivated.
- The Retort Utility Boiler sample from October 1, 1988 was collected during a period of incomplete combustion caused by low combustion air flow.
- All Wetter samples were collected when both the Wetter and upstream process equipment were not operating at design conditions, resulting in above-design temperatures at the Wetter Scrubber Vent and elevated organic levels in the Wetter Stream Water.

Excluding data from these samples, conclusions to be drawn from supplemental gas and particulate analyses are:

- o No supplemental parameters were routinely released in environmentally significant concentrations.
- o Concentrations of trace elements and organic indicators in all stack particulates were below levels of significance.
- o Concentrations of all gas parameters were less than levels of significance in all stacks except the Wetter Scrubber Vent and Unisulf Tailgas Stack.
- o Concentrations of select trace elements and organics were elevated in Wetter Stream Water.
- o Retort and Upgrade sulfur plants achieved 99-plus percent reduction in hydrogen sulfide, ammonia, hydrogen cyanide and most organics.
- o Arsenic and select other trace elements in all sampled solids were elevated relative to average crustal material abundance.

The trial trip was designed to validate sampling and analytical techniques and to derive baseline information. Initial data found no areas of routine permit exceedances or releases of parameters of concern at levels of environmental or health significance. In addition to acquiring baseline data, lessons learned included modifications to supplemental sampling and analytical techniques. Two additional sampling trips are planned.

Lessons Learned

The problems immediately addressed, based on knowledge gained from the trial trip are shown in Attachment 5. These included alteration of two analytical procedures. One was for alternative handling of samples with higher-than-expected hydrocarbons (for elemental analysis) and the other required research for stable organometallic standards to analyze gaseous metals (cadmium and chromium). Validation and testing for these two elements has not been successful, and the Project proposed waiving these two elements from test requirements.

The second category of lessons learned involved the sampling itself. Although every effort was made to monitor during steady-state operations at 60 percent capacity, non-typical conditions occurred at three sites and major equipment failure (a crane) precluded sampling at a fourth site. The Project had redundant equipment in every instance except for the crane that raises the sampling equipment to the ports on stacks. This broke down before the last sampling point. However, overall, the trial trip was very successful in achieving the goals of sampling and analytical validation.

Based on results of the Trial Trip, the Project requested a series of changes to the EMP (Attachment 6). These included elimination of one sampling site because it duplicated another stream already sampled; elimination of two industrial hygiene job categories because the positions were eliminated by operations; modification of four sampling and nine analytical methods for more accurate sampling or more appropriate testing; and two additions to the EMP. One of the additions includes detection limits for elements in particulates. The other addition involves two more sampling trips in an extended timeframe to accommodate the large volume of samples to be obtained. On this basis, sampling in Tier I will occur every six months and extend through 1991.

These changes were discussed and approved at the annual Monitoring Review Committee (MRC) meeting in August, 1989. The MRC is composed of representatives from the Project, the U.S. Department of Energy, the U.S. Environmental Protection Agency and the Colorado Department of Natural Resources. The MRC reviews environmental and health monitoring information to determine if there are trends or patterns in pollutant releases or environmental impacts.

These changes were incorporated in the second sampling trip that was completed in October, 1989. The second supplemental report incorporating these data should be available mid 1990.

Conclusions

Although sulfur emissions during periods of start-up and shutdown continue to exceed operating permit values, the emissions during steady-state plant performance have been within the ranges expected for Compliance parameters. The Project is optimistic that sulfur plant improvements completed in 1989, and longer operating runs will minimize the excess sulfur emissions.

Supplemental monitoring has detected a few parameters at very low levels. To date, no emissions of significant environmental or health concern have been routinely emitted at the Project during on-line operations. Future monitoring should continue to define emissions from this process, and to clarify the environmental acceptability of the oil shale technology

for future operations similar to those at Parachute Creek.

References

Benton, Janie B., 1987. Overview of Environmental Monitoring Data Developed at Four Synthetic Fuels Facilities. In Proceedings, 1987 Eastern Oil Shale Symposium, November 18-20, 1987.

Benton, Janie B., 1988. Preliminary Environmental Monitoring Results: Parachute Creek Shale Oil Project and Forest Hill Heavy Oil Project. In Proceedings, 1988 Eastern Oil Shale Symposium, November 30-December 2, 1988.

Duir, John; Randle, Allen; Reeg, Cloyd, 1989. Report on Unocal's Parachute Creek Oil Shale Project, presented to National Research Council, June 1989.

Unocal Corporation, 1986. Environmental Monitoring Plan for Parachute Creek Phase I Plant. NTIS #PB89-147284/AS.

Unocal Corporation, 1989a. Environmental Monitoring Plan Report, Fourth Quarter 1988. NTIS #PB89-226484/AS.

Unocal Corporation, 1989b. Environmental Monitoring Plan Report, First Quarter 1989. NTIS #PB89-226492/AS.

Unocal Corporation, 1989c. Environmental Monitoring Plan Report, Second Quarter 1989. SFC/PC-01/SH-03/E-4118.

Unocal Corporation, 1989d. Environmental Monitoring Plan, Annual Report, October 1, 1987-September 30, 1988. NTIS #PB89-191043/AS.

Unocal Corporation, 1989e. Environmental Monitoring Plan, Supplemental Environmental Data Report, Trial Trip Results, July 31, 1989. NTIS #PB89-226500/AS.

Attachment 1. **TIER I SUPPLEMENTAL SOURCE MONITORING POINTS**

Identifier*	Point Description for Tier I Supplemental Monitoring	Sampled During Trial Trip**
MINE/RETORT FACILITY		
R1-3E	Finish Screening Dust Collector	X
R2-4E	Retorted Shale	X
R2-5E	Wetter Scrubber Vent	X
R2-6E	Recycle Gas Heater Stack	X
R2-9E	Retorted Shale Pile Runoff	N/A
R2-10E	Retorted Shale Pile Leachate	N/A
R2-13I	Wetter Stream	X
R3-2I	Retort Make Gas (Inlet to Retort Sulfur Recovery Unit)	X
R3-3I	Treated Retort Make Gas (Outlet from Retort Sulfur Recovery Unit)	X
R3-4I	Retort Fuel Gas (Confidential)	X
R4-2E	Retort Utility Boilers Stack	X
R4-7E	Retort Gravity Separator Fugitive Emissions	X
UPGRADE FACILITY		
U1-4E	Unicracker/DW Charge Heater Stack	X
U1-11E	Guard Bed Inerts (Spent)	X
U1-13E	Dearseniter Reactor Catalyst (Spent)	X
U2-3I	Upgrade Fuel Gas (Confidential)	X
U3-1E	Unisulf Tailgas (Outlet from Upgrade Sulfur Recovery Unit)	X
U3-7I	Acid Gas (Inlet to Upgrade Sulfur Recovery/Unisulf Unit)	X
U5-4E	Active Basin Fugitive Emissions	X
U5-10E	Active Basin Sludge	N/A
U5-15E	Upgrade API Separator Sludge	X

* The identifier uniquely locates the monitoring point on the simplified flow diagrams in Appendix A of the EMP. The first two characters are the diagram number (R = Mine/Retort facility, U = Upgrade facility). The next two characters locate the point on the diagram (E = emission point; I = internal stream).

** X = Samples taken as planned; N/A = Not available for sampling.

Attachment 2. **HEALTH SURVEILLANCE MONITORING SAMPLES ABOVE THE PERMISSIBLE**
Page 1 of 2 **EXPOSURE LEVEL OR ABOVE DETECTION LIMITS AT PARACHUTE CREEK, JULY 1, 1988 - JUNE 30, 1989**

Type of Sample (Area/Personal)	Location	Parameter (No. of Samples)	Concentration
THIRD QUARTER 1988			
P	Mine Bolter Operator	Noise (1)	96.2 dBa
P	Loader Operator	Noise (1)	89.7 dBa
P	Pneumatic Hammer Operator	Noise (1)	90.6 dBa
P	Bulk Operator	Noise (1)	90.4 dBa
P	Unisoar/Unicracker Operator	Noise (1)	91.4 dBa
A	Utilities Area B	Syncrude Vapor* (1)	0.15 ppm
A	Unisoar/Unicracker	Syncrude Vapor* (1)	0.05 ppm
P	Unisoar/Unicracker	Syncrude Vapor* (1)	0.12 ppm
P	Mine Operators	Solvent Solubles** (8)	0.04-0.19 mg/m^3
P	Retort Operators	Solvent Solubles** (4)	0.02-0.15 mg/m^3
FOURTH QUARTER 1988			
P	Retort Sulfur Recovery Unit Operator	Solvent Solubles** (1)	0.51 mg/m^3
P	Maintenance	Chromium (2) Iron (1)	3.4 mg/m^3 12 mg/m^3
A	Upgrade	Syncrude Vapor* (2)	0.09-0.50 mg/m^3
P	Retort	Pyrene** (1)	0.005 mg/m^3
P	Upgrade	Syncrude Vapor* (1)	0.26 ppm
A	Retort Belt 15	Solvent Solubles (1)	0.25 mg/m^3
P	Retort	Solvent Solubles (3)	0.34-0.43 mg/m^3

Attachment 2. **HEALTH SURVEILLANCE MONITORING SAMPLES ABOVE THE PERMISSIBLE**
Page 2 of 2 **EXPOSURE LEVEL OR ABOVE DETECTION LIMITS AT PARACHUTE CREEK, JULY 1, 1988 - JUNE 30, 1989**

Type of Sample (Area/Personal)	Location	Parameter (No. of Samples)	Concentration
FOURTH QUARTER 1988 (cont.)			
A	Retort	Pyrene** (1) Chrysene** (1)	0.0002 mg/m^3 0.0003 mg/m^3
P	Retort	Chrysene** (2)	0.0002-0.0003 mg/m^3
P	Retort	Pyrene** (1)	0.0002 mg/m^3
FIRST QUARTER 1989			
A	Mine	Benzene (1)	1.0 ppm
A	Retort	Solvent Solubles** (2)	0.015-0.85 mg/m^3
P	Upgrade	Benzene (1)	1.9 ppm
SECOND QUARTER 1989			
A	Mine	Carbon Monoxide (1)	50 ppm
A	Retort	Benzene (3)	12 ppm
P	Retort	Benzene (1)	0.07 ppm
A	Upgrade	Syncrude Vapor* (1)	0.15 ppm
P	Upgrade	Syncrude Vapor* (1)	0.12 ppm
P	Upgrade	Syncrude Vapor* (1)	0.02 ppm
P	Upgrade/Loading	Syncrude Vapor* (3)	0.48 ppm

* Permissible Exposure Limits or Threshold Limit Values have not been established for this parameter. A corporate exposure limit has been established at 50 ppm.

** These parameters occurred above detection limits, but were found far below levels of environmental or health significance.

Attachment 3: **TOTAL EXCESS EMISSIONS IN 1989 DURING STARTUP AND SHUTDOWN OPERATIONS**

Month	Location	No. of Exceedances	Total Emissions
January	Retort Sulfur Plant Flare	4	45,200 lbs SO_2
February	Retort Sulfur Plant Flare	2	156,560 lbs SO_2
March	Upgrade Heater	5	204,645 lbs SO_2
	Upgrade Boilers	1	270 lbs SO_2
April	Retort Sulfur Plant Flare	7	433,350 lbs SO_2
	Upgrade Sulfur Recovery	1	7,200 lbs Sulfur
May	Retort Sulfur Plant Flare	2	3,785 lbs SO_2
June	Retort Sulfur Plant Flare	7	333,400 lbs SO_2
July	-	-	-
August	Upgrade Flare	2	6,844 lbs Sulfur
September	Retort Sulfur Plant Flare	2	6,300 lbs SO_2

Attachment 4. **SUPPLEMENTAL GAS AND PARTICULATE SITES SAMPLED AND PARAMETERS**
Page 1 of 3 **ANALYZED**

Sites Sampled	Parameters Analyzed* Inorganic	Organic
GAS		
Wetter Scrubber Vent (R2-5E)	Arsenic	Benzene
Recycle Gas Heater Stack (R2-6E)	Cadmium	Benzo (a) pyrene
Retort Make Gas (R3-2I)	Chlorine	Phenol
Treated Retort Make Gas (R3-3I)	Chromium	Naphthalene
Retort Fuel Gas (R3-4I)	Mercury	2-Butanone
Retort Utility Boilers Stack (R4-2E)	Hydrogen Sulfide	Aniline
Unicracker/DW Charge Heater Stack (U1-4E)	Carbonyl Sulfide	Pyrrole
	Carbonyl Sulfide	Pyridine
Upgrade Fuel Gas (U2-3I)	Ammonia	Nitrobenzene
Unisulf Tailgas (U3-7I)	Hydrogen Cyanide	Quinoline
Acid Gas (U3-7I)		2-Amino-naphthalene
		Acetonitrile
		Ethanethiol
		Thiophene
		2-Pyrrolidone
Active Basin Fugitive Emissions (U5-4E)**	Hydrogen Sulfide	Ethanethiol
	Carbon Disulfide	Acetonitrile
Retort Gravity Separator Fugitive Emissions (R4-7E)**	Carbonyl Sulfide	2-Butanone
		Benzene
		Thiophene
		Pyrrole
		Pyridine
		Phenol
		Aniline
		Nitrobenzene
		Naphthalene
		Quinoline

* The parameters analyzed for all samples shown are in accordance with the Environmental Monitoring Plan, Table 5.2-9, unless noted otherwise.

** Fugitive emissions parameters are measured from equilibrated headspace of water samples from these sites. Cyanide and ammonia were not analyzed because no acceptable analytical methods were available at the time of sampling.

Sites Sampled	Parameters Analyzed* Inorganic	Organic
PARTICULATE		
Finish Screening Dust Collector (R1-3E)	Antimony	Benzene
	Arsenic	Benzo (a) pyrene
Wetter Scrubber Vent (R2-5E)	Boron	Phenol
Recycle Gas Heater Stack (R2-6E)	Cadmium	Naphthalene
Retort Utility Boilers Stack (R4-2E)	Carbon	2-Butanone
Unicracker/DW Charge Heater Stack (U1-4E)	Chlorine	Aniline
	Fluorine	Pyrrole
	Lead	Pyridine
	Mercury	Nitrobenzene
	Molybdenum	Quinoline
	Nitrogen	2-Amino-naphthalene
	Selenium	Acetonitrile
	Silver	Ethanethiol
	Sulfur	Thiophene
	Inorganic Carbon	2-Pyrrolidone
	Organic Carbon	Aliphatics
	Total Sulfides	
	Total Cyanides	
SOLID		
Retorted Shale (R2-4E)	Antimony	Benzene
Wetter Stream (R2-12I)	Arsenic	Benzo (a) pyrene
	Boron	Phenol
	Cadmium	Naphthalene
	Carbon	2-Butanone
	Chlorine	Aniline
	Fluorine	Pyrrole
	Lead	Pyridine
	Mercury	Nitrobenzene
	Molybdenum	Quinoline
	Nitrogen	2-amino-aphthalene
	Selenium	Acetonitrile
	Silver	Ethanethiol
	Sulfur	Thiophene
	Inorganic Carbon	2-Pyrrolidone
	Organic Carbon	Aliphatics
	Total Sulfides	
	Total Cyanides	

* The parameters analyzed for all samples shown are in accordance with the EMP, Table 5.2-9, unless noted otherwise.

Attachment 4. **SUPPLEMENTAL GAS AND PARTICULATE SITES SAMPLED AND PARAMETERS ANALYZED**
Page 3 of 3

Sites Sampled	Parameters Analyzed* Inorganic	Organic
LIQUID		
Wetter Stream (R2-13I)**	Electrical Cond.	Benzene
	Total Susp. Solids	Benzo (a) Pyrene
	pH	Phenol
	Antimony	Naphthalene
	Arsenic	2-Butanone
	Barium	Aniline
	Beryllium	Pyrrole
	Boron	Pyridine
	Cadmium	Nitrobenzene
	Carbon	Quinoline
	Chlorine	2-Amino-naphthalene
	Copper	Acetonitrile
	Chromium	Ethanethiol
	Iron	Thiophene
	Fluorine	2-Pyrrolidone
	Lead	Aliphatics
	Manganese	
	Mercury	
	Molybdenum	
	Nickel	
	Nitrogen	
	Selenium	
	Silver	
	Sulfur	
	Vanadium	
	Zinc	
	Inorganic Carbon	
	Organic Carbon	
	Polar Organic Carbon	
	Nonpolar Organic Carbon	
	Total Sulfides	
	Total Cyanides	
	Dissolved Sulfur Species	
	Dissolved Nitrogen Species	

* The parameters analyzed for all samples shown are in accordance with the EMP, Table 5.2-9, unless noted otherwise.

** Hydrogen sulfide and hydrogen cyanide were not analyzed because no laboratory has been contracted which is capable of performing these analyses.

Attachment 5: **LESSONS LEARNED DURING TRIAL SAMPLING TRIP, EMP SUPPLEMENTAL MONITORING AT PARACHUTE CREEK**

Type of Problem	Description	Remedial Alternative(s)
ANALYTICAL		
Gaseous Metals	Cadmium and chromium standards not available for quantitative analyses of gases.	Literature search and laboratory tests failed to develop organometallic standards. Further effort would require research outside the scope of the EMP, and these tests were proposed for deletion from monitoring.
Elemental Analysis of Solids by XRF	Neutron activation analysis of sludges and solids was hindered by higher-than-anticipated hydrocarbons in the sample, precluding pelletization and posing potential flammability problems.	Use Nitric Acid-Microwave Digestion and Analysis by ICP-MS Sampling.
SAMPLING		
Unsteady Operative Conditions and Sampling Equipment Malfunctions	Upset conditions during sampling at Retort Utility Boilers, Upgrade Unisulf Plant and Wetter Scrubber produced off-spec samples. Mechanical failure of the crane precluded sampling Recycled Gas Heater Stack.	Daily planning meetings to address non-routine problems and maximize deployment of field equipment and crews. (Equipment redundancy is used in all cases except industrial crane.) Supplemental monitoring trips expanded from three to five to provide more accurate and effective monitoring program.

Attachment 6. **RECOMMENDED CHANGES TO THE EMP**
Page 1 of 3

Item #	Parameter or Method	Current EMP Method	Proposed Changes
ANALYTICAL METHODS			
1.	Sulfides, Total (Solids)	Methylene Blue Colorimetry EPA Method 376.2	Ion Chromatography EPA Method 300, Amperometric Detection
2.	Chlorine (Solids)	XRF of a Pelletized Sample	Digestion by ASA[a] 26-3.3 and Analysis by Ion Chromatography EPA Method 300
3.	Nitrogen Gases	None	Eliminate from Head Space Analysis for Active Basin Only
4.	Nitrogen	Chemiluminescent Detection of NO	Kjeldahl EPA Method 351.2
5.	Fluoride	Ion Selective Electrode, Standard Methods 1438	Ion Chromatography EPA Method 300
6.	Inorganic Carbon, Organic Carbon, and Polar Organic Carbon	IR and Colorimetric Detection of CO_2	Flame Ionization Detection of CH_4
7.	Ammonia	Acidimetric Titration Standard Methods 417D	Colorimetric Nesslerization Standard Methods 417B
8.	Elements, Gaseous (As, Cr, Cd, Hg, Cl)	Acid/Base Impingers, ICP/ Analysis	Charcoal Cartridge[b] NAA/Analyses
9.	Sulfur (Solids)	XRF of a Pelletized Sample	Nitric Acid-Microwave Digestion and Detection by LECO Analyzer
SAMPLING METHODS			
10.	Elements (Solids)	XRF of a Pelletized Sample	Nitric Acid-Microwave Digestion and Analysis by ICP-AES[a]

Item #	Parameter or Method	Current EMP Method	Proposed Changes
11.	Boron (Solids)	KOH Fusion/Acid Digestion and Analysis	Nitric Acid-Microwave Digestion and Analysis by OCP-AES[a]
12.	Retort Gravity Separator Fugitive Emissions (R4-7E) by Liquid Headspace Analysis	N/A	Retort Gravity Separator Fugitive Emissions (R4-7E) by Collection of Associated Vent Gas[c]
13.	All Sites (Ammonia, Hydrogen Cyanide)	4-Impinger Sampling Train	2-Impinger Sampling Train
14.	Retort Utility Boilers	N/A	Eliminate[d]
INDUSTRIAL HYGIENE			
15.	Compactor Job Category	N/A	Delete[e]
16.	Unisoar Area Job Category	N/A	Delete[e]
EMP ADDITIONS			
17.	Number of Stack Sampling Trips	N/A	Increase from three to five[g]
			mg/m^3
18.	EMP Detection Limits for Particulates[h]	None	Antimony 0.25 Barium 0.25 Boron 0.001 Cobalt 0.05 Copper 0.1 Iron 0.4 Fluorine 1.0 Lead 0.05 Manganese 0.05 Molybdenum 2.5 Nickel 0.05 Selenium 0.1 Silver 0.05 Vanadium 0.015 Zinc 0.25

a) ASA = American Soil Association

b) Gaseous arsenic, cadmium, chromium, mercury and chlorine will be collected on charcoal cartridges and analyzed by a neutron activation analysis (NAA). During the May 24-25, 1988 MRC meeting, EMP change No.2 replaced sample collection on charcoal with collection in an acid/base impinger. This change also substituted Inductively Coupled Plasma (ICP) for NAA. Attempts to validate the acid impinger collection of mercury resulted in unacceptable spike recoveries. Thus, collection of trace elements on charcoal was investigated. Transmission and collection efficiencies for mercury using charcoal cartridges and NAA are acceptable. The remaining elements are being validated.

c) During plant operation, gaseous emissions from the Retort Gravity Separator liquid are continuously swept from the separator through a vent line using a downstream blower. Because this vented gas contains effectively all of the separator gaseous emissions, analysis of this vent would provide a more representative measurement of emission from this site than the headspace analysis of separator liquid. Accordingly, in place of the headspace protocol, Unocal proposes to sample this site for fugitive emissions parameters from the vent pipe using standard stack gas sampling methods.

d) Emission from the three combustion sources (Retort Utility Boilers, Unicracker/DW Charge Heater, Recycle Gas Heater Stack) are nearly identical (Tables 5-1, 5-3 of Unocal's EMP). Deletion of this site will still provide for one fuel gas combustion source at each location (Retort and Upgrade).

e) In 1986, Unocal began laying down retorted shale using end-dump trucks rather than belly-dumps. Subsequent testing showed that compaction sufficient for pile stability was achieved solely through the dumping of the retorted shale in this manner. As since that time no compactor has been used on the retorted shale pile, Unocal recommends that the Compactor job category be dropped from the Industrial Hygiene supplemental monitoring list.

f) One process operator is assigned to both the Unicracker/DW and Unisoar areas of the Upgrade Facility, and samples obtained for the Unicracker/DW operator are therefore representative of the Unisoar area.

g) The remaining two stack sampling trips were to have involved the collection of two sets of samples each. Due to the large volume of samples and extended sampling timeframe involved with the collection of two samples, Unocal recommends that only one set of samples be collected per trip, and that four rather than two additional sampling trips be conducted at a frequency of two per year.

h) EMP detection limits for these elements were derived following the same procedure used for the parameters listed in Table 5.2-11 (page 5.2-69) of Unocal's EMP. These EMP detection limits were calculated by taking one-half of the lowest TLV values listed in the Threshold Limit Values and Biological Exposure Indices (AGGIH) manual.

Simulated Climate and Shale Pile Response Within a Large Scale Environmental Chamber Developed in Wyoming

by

Quentin D. Skinner
Range Management Department
University of Wyoming
Laramie, Wyoming 82071
Tim L. Reeves, John R. Turner, and Victor Hasfurther
Department of Civil Engineering
University of Wyoming
Laramie, Wyoming 82071

Abstract: The University of Wyoming, College of Agriculture, and Department of Energy have developed an environmental chamber covering two lysimeters 10 feet wide, 10 feet deep, and 24 feet wide. This facility was designed to simulate temperatures from -20 to 120 degrees Fahrenheit, 10 to 100 percent relative humidity, rain from 0 to 5 inches per hour, and light of up to 4800 candles at the surface of filled lysimeters. This facility is now being used to quantify amount of water entering combusted shale embankments, how it moves within this shale material, and finally how embankment strength is altered, Tracking water movement into and within shale material is being accomplished by simulating the climate over exposed lysimeters filled with like shale materials in western Colorado. The purpose of this paper will be to: 1) describe the Wyoming facility and why it was constructed, and 2) report how accurately this environmental structure simulates actual field temperature and relative humidity collected a year earlier in Colorado.

Introduction

Economic development in the semi-arid western United States has been and will continue to be strongly dependent on the extraction of energy resources. Many factors will determine the ability of the energy industry to operate cost-effectively in a global market. One factor, which has become increasingly important in the last 20 years, is the effect of energy development on the environment. New energy resources, such as oil shale, must be developed in ways that minimize the adverse environmental effects caused by the disposal of solid wastes.

Large scale development of energy resources by industry must insure that waste disposal embankments are designed to: 1.] be physically stable structures, 2.] prevent or minimize the release of unacceptable compounds, and 3.] provide economically acceptable post land development. The costs of meeting these environmental criteria will be taken into account by the energy industry before engaging in new, large-scale energy development projects. At this time, major questions exist on how to meet these criteria in acceptable and cost-effective ways. New energy technologies, such as oil shale, will produce enormous quantities of solid wastes. For example, the principal solid waste products of oil shale extraction may be as much as 130 percent of the undisturbed oil shale volume (Reeves et al. 1986) 1. It is estimated that a mature oil shale industry would generate over 10 billion cubic feet of solid waste per year. This could cover an area 75 miles to a depth of 150 feet after 30 years of operation.

Disposal of these waste products would constitute an environmental problem because processed oil shale contains potentially toxic trace elements, inorganic salts, and potentially toxic residual organic constituents (Pacific Northwest Laboratory 1982) 2. These factors are primarily a function of the raw shale mineralogy, the retorting process, and the specific process variables used in retorting. Consequently, the licensing of a commercial oil shale operation to dispose of processed oil shale

in a surface embankment will require accurate estimates of the physical stability of the proposed embankment, including the potential risk of failure (safety factors), estimates of the potential release of pollutants to the environment, including surface and ground water systems, the rate of release of such pollutants, and changes in these processes or environmental impacts with time (Reeves et al. 1986) 3.

Water is the key factor controlling the stability of solid waste embankments and a solvent, as well as, the transport mechanism for release of unacceptable compounds to the surrounding environ-ment. The University of Wyoming, Industry, and Department of Energy, therefore, initiated the research project " Modeling of Hydrologic Conditions and Solute Movement in Processed Oil Shale Solid Waste Under Simulated Climatic Conditions," during 1987. The purpose of this paper is to present an overview of this project in support T.L. Reeves following paper, "Rainfall Simulation And Hydrologic Monitoring of a Combusted Western Oil Shale in Large Lysimeters".

Objectives

The main purpose of the project "Modeling of Hydrologic Conditions and Solute Movement in Processed Oil Shale Solid Waste Under Simulated Climatic Conditions," is to physically model and observe three interacting factors which would affect the disposal and behavior of processed oil shale embankments and to compare these observed physical data to computer generated data in an evaluation of model performance. These three factors are: 1) hydrology, 2) geotechnical stability, and 3) geochemistry. An associate purpose of this research is to conduct these investigations at a scale that is sufficient to help describe commercial scale embankment behavior by hopefully creating boundary free conditions. There are five major objectives:

1. Assess the unsaturated movement and redistribution of water and the development of potential saturated zones in disposed processed oil shale waste.

2. Assess the unsaturated movement of solubles and major chemical constituents in disposed processed oil shale.

3. Assess the physical and constitutive properties (index properties, shear strength, stress-strain properties, and compressibility of processed oil shale and determine potential changes in these properties caused by disposal and weathering.

4. Assess the use of previously developed computer model(s) to describe the infiltration, unsaturated movement, redistribution, and drainage of water in disposed processed oil shale.

5. Evaluate the stability of theoretical, commercial scale, processed oil shale waste embankments using computer models.

Approach

The basic design to accomplish the purpose and objectives of this research project is as follows:

1. Bench scale, large pile embankment, and modeling research were proposed as a way to a) confirm existing research published at bench scale, b) explore any difference between results of bench research and data obtained from embank-ments where boundary free conditions may exist, c) utilize bench scale research results to explain large embankment pile behavior, and d) use data collected from bench and embankment research to evaluate and modify existing models for predicting solid waste pile behavior.

2. Large embankments would be contained in lysimeters to facilitate a) experi-ment control, b) obtaining data relevant to disposal site climate, c) replication of experiments, and d) applying climate stress to containerized solid waste embankments.

3. Replication of climate and climate stress of containerized solid waste embankments would be accomplished by a) developing an environmental chamber over large scale lysimeters on the University of Wyoming Campus, b) constructing large scale lysimeters, open to the atmo-sphere, on a field site where disposal of solid wastes may occur, c) placing the same waste material and instrumen-tation in both lysimeter sites in the same way, d) installing a meteorological station next to the field site and then monitor, store, and transfer climate data there to the laboratory lysimeters at the University of Wyoming, and e) simulate the field site climate in the environmental chamber/lysimeters for a period of time and then apply climate stress to bracket low and high climate extremes around actual atmospheric data collected.

4. Characterize the waste material using bench scale research techniques: a) before placing it in lysimeters, b) after being exposed to the field site and simulated climates, and c) after climate stress.

5. Choose a solid waste material a) recognized as a possible by-product produced by industry, b) representative of a viable process to be used by industry, and c) place it in lysimeters in a way representative of how industry would in a commercial scale disposal scenario.

6. Insure that university, government agency, and industry share equal interest, participation, and financial responsibility for conducting this research program.

7. Use decarbonized shale as a first waste material to be studied.

Project Description

Introduction: This program is being conducted in cooperation with Rio Blanco Oil Shale Co., Inc., a subsidiary of Amoco Corp., Exxon Co. USA, (Colony Shale Oil Project), the University of Wyoming, and the Department of Energy. Separate cooperative agreements have been established between the University of Wyoming and each of these parties. Approximately 500 tons of processed oil shale waste (Lurgi - decarbonized) has been provided by Rio Blanco Oil Shale, Co., Inc. to carry out this study. The processed oil shale, however, is fractioned into two parts. Approximately 90% by weight of the material is solid surge bin material and approximately 10% of the waste is from flue gas dust. A 90/10 ratio of surge bin wastes and flue gas dust are used for all parts of the field site study. A 95/5 ratio are used for the laboratory study. Waste material left after placing shale in field lysimeters was the reason we used less flue gas dust.

The research program combines a bench top research and testing program with the operation of three large scale field lysimeters (7.3 x 3.0 x 3.0 m deep), and the operation of two large scale laboratory lysimeters (7.3 x 3.0 x 3.0 m deep) enclosed by a large scale environmental chamber and climatic control system. The following discussions provide a brief outline of the methods being utilized for this study.

Bench top research and testing program

The bench top testing program has been designed to characterize the processed waste for initial hydrologic properties, initial soluble chemistry, initial soil mechanical properties with geochemical interactions, and to evaluate on going or potential changes in these properties which may be caused by disposal or weathering in the lysimeters. All tests, therefore, will be conducted on samples of the initial material, from samples obtained during the operation of the lysimeters in a limited coring program, and from samples excavated from the lysimeters after completion of operations.

Saturated as well as unsaturated hydraulic properties are being determined. Saturated hydraulic conductivity of the material will be determined using a relatively new technique developed by Olsen et. al. (1985). Unsaturated hydraulic properties will consist of developing a water characteristic for the material which relates pore pressures to volumetric water contents. Water characteristics will be developed for a range of densities to include the density at which processed shale was emplaced in the lysimeters. Water characteristics between 0 and -15 bars (-217.5 psi) will be developed for the draining condition, and between 0 and -2 bars (-29 psi) for the filling condition, accounting for hysteresis. Unsaturated hydraulic conductivity values will be empirically developed from the water characteristic relationships.

Leachate chemistry will be analyzed by utilizing the same flow pump apparatus used for saturated hydraulic conductivity tests. The chemical concentration and characterization of leachates will be described by developing breakthrough curves for all major chemical constituents. Breakthrough curves relate the concentration of a given chemical constituent to the number of pore volumes leached. Leachate will be primarily analyzed for SO4, thiosulfate, fluoride, chloride, pH, total organic carbon, (TOC), total inorganic carbon (TIC), electrical conductivity, total dissolved solids (TDS), alkalinity, and the following metals: Al, B, Ca, Cu, Fe, K, Mg, Mn, Na, P, Lb, and Se. In addition, a limited program will be set up to analyze leachates for volatile and semi-volatile organic species (EPA 624, 625).

Soil mechanical properties or index properties will be determined for the waste material in order to classify it using the Unified Soil Classification System. In this manner, the soil mechanical properties of the processed oil shale waste can then be classified and compared to other soil materials. These index properties also indicate how the material will behave in a waste embankment. The index properties which will be tested for are: specific gravity of solids, grain size distribution, Atterberg limits, moisture-density relationships, shear strength, stress-strain properties, and consolidation (compressibility).

Field lysimeters

Three lysimeter cells, each 7.3 x 3.0 x 3.0 m deep, were filled with processed oil shale waste (September 1987) at Rio Blanco Oil Shale Co.,Inc., Tract C-a in the Piceance Basin of Colorado. Each cell represented a different disposal scenario or treatment. Cell #1 was filled with straight processed oil shale; Cell #2 was filled with a processed oil shale overburden mixture with a 46 cm soil surface cap; and Cell # 3 was filled with 0.6 m of straight processed oil shale, 1.8 m of overburden to act as a hydraulic barrier, and a 46 cm top soil surface cap. The processed oil shale in all three lysimeters was filled as 1 foot lifts 30.5 cm (1 foot) compacted to approximately 1400 kg/m3. A moisture content of 15% was used.

In situ instrumentation was installed at various depths in each cell to monitor soil moisture, temperature, and total horizontal and vertical stress. In addition, soil-water access tubes (suction cup lysimeters) were installed in each cell to hopefully monitor in situ soil water chemistry. A detailed description of the specific instrumentation utilized and the monitoring schedule will be discussed in the section titled "Lysimeter Instrumentation and Monitoring" below.

A self logging meteorologic station was also installed at the field site. This data logging station can be monitored and accessed via micro computer from the University of Wyoming. Meteorologic variables being monitored are wind speed at two heights, wind direction, solar radiant flux, ambient temperature, relative humidity, and rainfall depth, duration, and intensity.

The University of Wyoming "Watershed Climate and Hydrology Simulation Laboratory" [WCHSL]

The [WCHSL] laboratory is an indoor facility which is composed of two lysimeter cells, each 7.3 x 3.0 x 3.0 m deep, enclosed by a climatically controlled environmental chamber. The environmental chamber has the following control ranges: ambient temperature -26 to 40.5.degrees C (-15 - 105 degrees F), relative humidity 10% - 80% at extremes in temperature, solar radiation 0 - 4,500 ft-candles intensity (metal halide), and rainfall 0 - 127 mm/hr (0 - 5 in/hr) produced by the Lafayette rainfall simulation system. The entire system is controlled through a computer system in which climatic simulation programs can be programed and modeled in the environmental chamber.

The two lysimeter cells were filled with shale during October 1989. One was filled with a 95/5 ratio of surge bin/flue gas dust mixture at 15% water content. The second was filled with 60% 95/5 ratio of surge bin/flue gas dust and 40% raw shale overburden at 15% moisture. These will serve as replicates of the first two lysimeter cells at the field site. Although the WCHSL laboratory will be capable of growing vegetation on the plots, the second cell was not filled with a top soil surface cap as at the field site. Climate simulation within the environmental chamber will follow that recorded at the field site at Tract C-a.

In situ instrumentation, closely matching that at the Rio Blanco field lysimeters were installed during placement of the processed oil shale into the UW lysimeters.

Lysimeter instrumentation and monitoring

In situ volumetric water contents are being monitored in each lysimeter cell (field and UW laboratory) using two methods: Time Domain Reflectometry (TDR), and Neutron Attenuation. The primary method for obtaining these measurements will be by TDR, a relatively new technique for monitoring soil water that is accurate, and can provide measurements with an extremely high degree of vertical resolution. The data obtained by neutron attenuation will be primarily used as backup data.

TDR data for each cell is obtained at eight depths: 15, 30, 45, 60, 75, 168, 259, and 289 cm. at Tract C-a and at two additional depths at UW [5&10 cm.]. Thermocouples for measuring in situ temperature are placed at 15, 30, 45, 60, 168, and 259 cm. Stress gages for measuring total stress are placed at 75, 168, and 259 cm. Instrumentation at each depth was placed in duplicate at the Tract C-a field lysimeters and triplicate at UW. TDR and Neutron probe readings for water content measurements are measured at the Tract C-a on a monthly basis. Neutron probe readings for backup data are taken at the same depths as TDR probes. Thermocouples are automatically scanned and recorded by depth at 6 am and 6 pm daily using the automatic data logging equipment. TDR readings for water content measurements are taken in the UW Lysimeter-Laboratory before and after storm events applied to the embankments. Neutron probe measurements are taken periodically. Thermocouples scanned by data logging equipment at 6 am and 6 pm daily. Stress cells are monitored quarterly.

Computer modeling

Literature reviews are being conducted to determine several geotechnical stability models and several hydrologic unsaturated flow models capable of simulating the conditions in an oil shale waste embankment. Based on these reviews, a determined number of hydrologic and geotechnical model(s) will be chosen for evaluation. A history matching procedure will then be followed. In this procedure, boundary conditions for the imposed climatic conditions, the shale emplacement, etc. will be input to the models. Each model will be evaluated based on its flexibility, efficiency, and accuracy in predicting the physical data produced from the lysimeters.

Chamber Atmosphere Results

Background

The Colorado embankments were constructed in October of 1987 and covered to keep water out using tarp material. This was carried out to assure that we could start simulation experiments:

1. with a known amount of water representing a logical part of a yearly climate cycle (winter).

2. with a rainfall event that would represent precipitation falling as snow and entering Colorado shale embankments from freeze/thaw events of the snowpack and embankment surfaces.

3. complete building the W.C.H.S. Laboratory, construct the shale embankments within the environmental chamber, and test all components of this new facility before simulating the Colorado climate over the field site starting with a date tarp material was removed.

Construction of the W.C.H.S. Laboratory was completed in September and shale embankments finished by November of 1988. These were covered with insulation and tarp material to:

1. Complete testing the climate control system of the environmental chamber.

2. Program computer systems to run and control all climate components of the environmental chamber.

3. Model data sets collected from and for the Colorado field site to simulate temperature, solar radiation, relative humidity, and design rain storms within the W.C.H.S. Laboratory environmental chamber.

4. Test modeled data sets using the computer programs developed in 2 above.

The tarp material was removed from the Colorado field site lysimeters on December 18,1987. Atmospheric data starting on the 18th was modeled and started controling the W.C.H.S. Laboratory on April 18,1988 after tarp material and insulation was removed from the shale embankments within the environmental chamber. The first simulated rainfall event representing the winter 1987/88 snow pack melt on the field site lysimeters was applied within the chamber on September 11, 1988. This event represented water movement into the field lysimeters from December 18, 1987 to April 14, 1988.

The details of water movement in shale embankments are covered in the next paper. Results dicussed here represent examples of how the environmental chamber controls modeled or recorded data for the Colorado field site. Figure 1 illustrates a 10 day data recording of set points modeled for the field site verses atmospheric conditions within the chamber. This rainy to dry period follows the application rain simulating snow melt on September 11. DS8500 is the smart end driver for the climate control system. Temperature and relative humidity are measured within the return air duct leaving the environmental chamber and are compared to the set points telling the DS8500 what is wanted as an atmospheric condition. Temperature and relative humidity are monitored every 30 seconds by the DS8500 and then averaged and recorded every hour for a permanent data point within a data aquisition system. New set points for the modeled Colorado field site atmosphere conditions are sent to the DS8500 every hour.

Generally, the set and atmosphere temperature recorded by the DS8500 follow each other with modeled conditions. The difference in the set and recorded atmosphere relative humidity reflect surface drying through evaporation. There is approximately 30 percent difference between the lower end of the actual relative humidity and the set value just after snowmelt and during the frequent

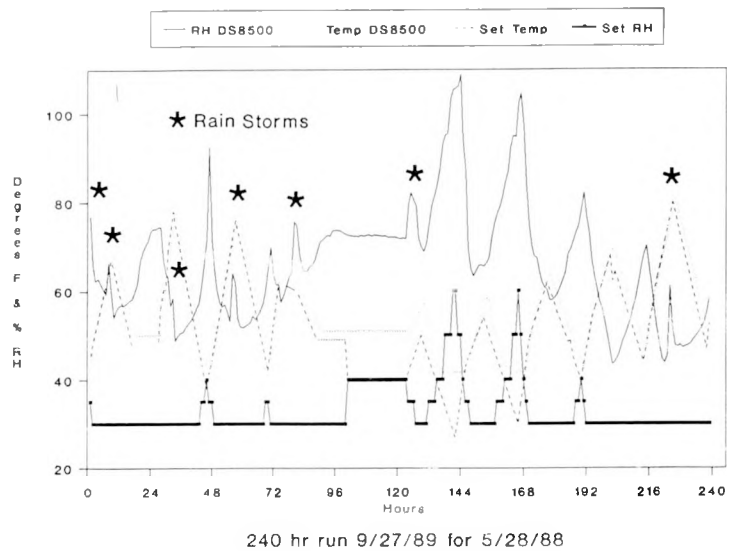

Figure 1: The W.C.H.S. Laboratory's environmental chamber's actual and set temperature and relative humidity just after snowmelt and during frequent rain storm events.

rains. This difference is reduced to approximately 15 percent by the end of this 10 day data set. The drop in set temperature just after 96 hours is caused by down time for the computer driving the environmental chamber. The time it takes to bring the actual and set relative humidity values togehter is related to how long it takes to dry the surface of the shale embankments out to a point where evaporation of embankment water does not take place.

Figure 2, a 96 hour section of data from the 10 day data set of Figure 1, shows that diurnal change in modeled conditions can be recorded and that the change in relative humidity caused during a specific rainstorm is recorded by actual measurements. As temperature decreases and rain falls relative humidity increases.

Figure 3 represents the data set following Figure 1. Only one storm event occurs in this 10 day period and consequently the modeled and actual relative humidity are following each other during the warm periods of days. Diurnal fluctuation causes the major difference between modeled and actual recorded conditions.

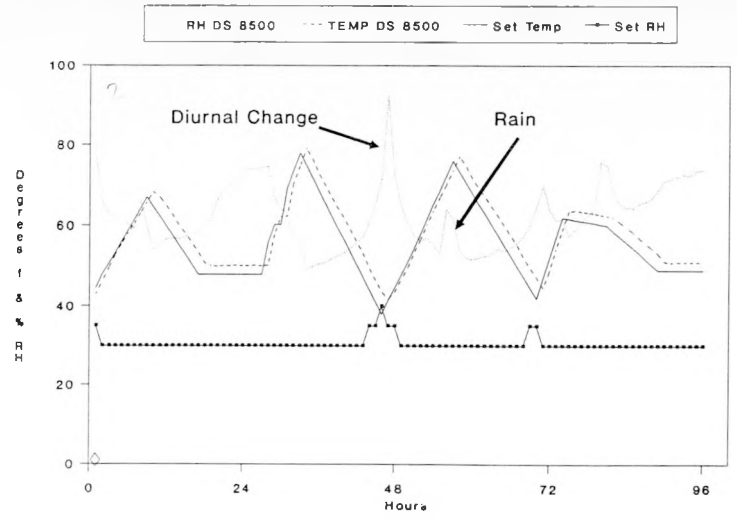

96 HR run 9/27/89 for 6/2/88

Figure 2: The W.C.H.S. Laboratory's environmental chamber's actual and set temperature and relative humidity showing diurnal and storm event response.

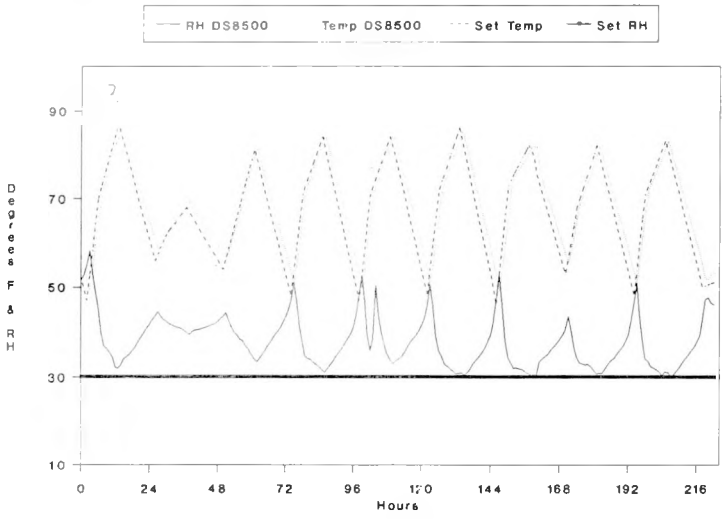

223 hr run 10/5/89 for 6/5/88

Figure 3: The W.C.H.S. Laboratory's environmental chamber's actual and set temperature and relative humidity while shale embankments are in the process of finally drying out through the process of evaporation and little rain.

Figures 4 and 5 illustrate the environmental chamber's ability to model atmospheric conditions for about 20 days during dry conditions in Colorado. Storm events at hours 169 and 195 raise the actual relative humidity about 15 percent for approximately 4 days. After these days the surface of the pile must dry out and model and actual relative humidity track each other.

Summary

The construction of the Wyoming Watershed Climate and Hydrology Simulation Laboratory is a major attempt to bridge bench and field scale research needs. It was built to help solve environmental science issues and upgrade academic excellence. This large scale facility may be sufficient in size to alleviate boundary condition constraints observed by conducting bench scale research. Boundary conditions observed at bench scale may modify modeling effort results used to predict what actually happens in applied field situations. This laboratory may also supplement field research by being able to simulate climate under present time. Eventually the facility can then be used to

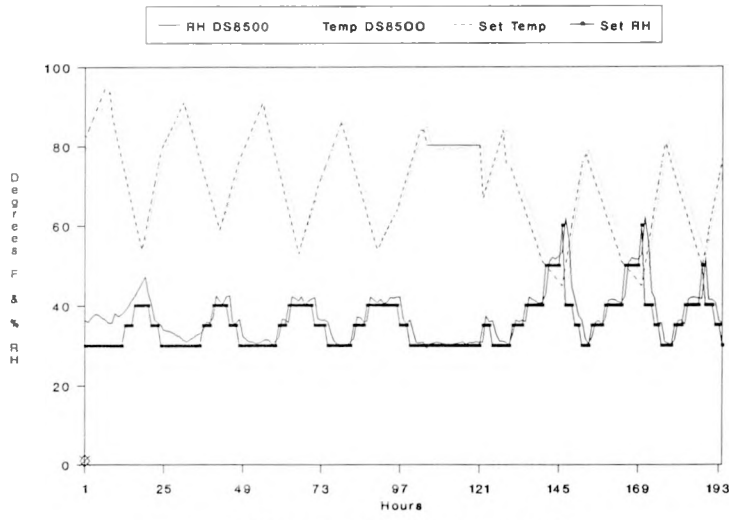

240 hr run 10/24/89 for 6/22/88

Figure 4: The W.C.H.S. Laboratory's environmental chamber's actual and set temperature and relative humidity while shale embankments are subjected to a dry climate regime.

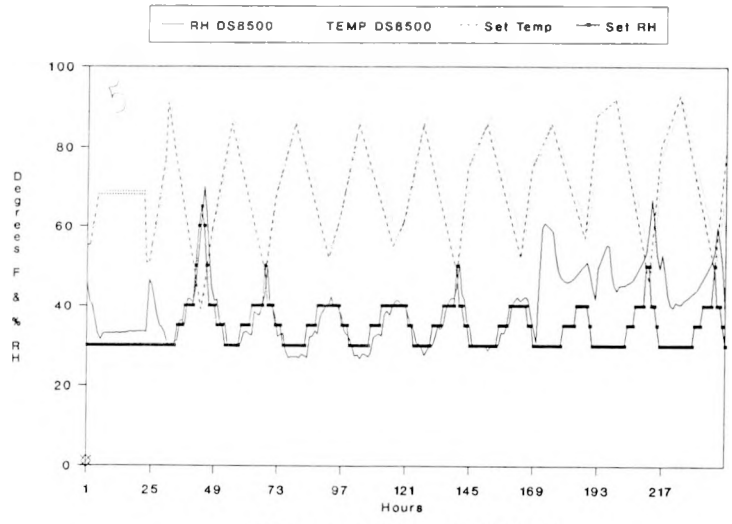

240 hr run 10/14/89 for 6/12/88

Figure 5: The W.C.H.S. Laboratory's environmental chamber's actual and set temperature and relative humidity while shale embankments are subjected to a dry climate regime.

accelerate controlled testing of climates for past or future records or predictions. Finally data recorded from this laboratory can be used to test, validate, or construct models concerned with explaining or predicting physical, chemical, and biological phenomenon.

Preliminary results collected show how the modeled and actual temperatures and relative humidity compare during wet and dry periods. Modeled and actual data correspond well during dry periods. Actual simulated atmosphere relative humidity is raised compared to the modeled condition as the surface of the combusted shale material becomes wet during and after designed rain storm events. This separation of modeled verses actual relative humidity slowly decreases as water is evaporated from the surface of the shale material and removed from the environmental chamber's closed air circulating system. Proof of the value for this facility, as used for the project described, rests with how well it simulates water movement dynamics within shale embankments constructed at Tract C-a Colorado. Preliminary results of water movement are presented in the following paper, "Rainfall Simulation And Hydrologic Monitoring of a Combusted Western Oil Shale in Large Scale Lysimeters".

REFERENCES

1. Reeves, T.L., P.J. Sullivan, P.A. Gilbert, M.E. Essington, Q.D. Skinner, and G.P. Hale. 1986. Research Needs for the Surface disposal of Processed Oil Shale Solid Waste: Physical, Hydrological, and Geochemical Parameters. U.S. Department of Energy, Office of Fossil Energy, DOE/METC-86/6071, 87 p.

2. Pacific Northwest Laboratories. 1982. Western Oil Shale Development: A Technology Assessment. Volume 4: Solid Waste from Mining and Surface Retorts. Pacific Northwest Laboratory, Richland, WA. PNL-3830 Vol. 4 UC-11, 61 p.

3. Olsen, H.W., R.W. Nichols, and T.L. Rice. 1985. Low-Gradient Permeability Measurements in a Triaxial System. Geotechnique 35(2):145-157.

Rainfall Simulation and Hydrologic Monitoring of a Combusted Western Oil Shale in Large Scale Lysimeters

by

Tim L. Reeves
Department of Civil Engineering
University of Wyoming
Laramie, Wyoming 82071

Abstract. A research program has been developed at the University of Wyoming to physically model (produce) climatic and hydrologic processes and study hydrologic, geotechnical, and geochemical factors affecting the behavior of large scale oil shale waste embankments. Physical data produced will be used to evaluate computer generated data in an evaluation of model performances. To accomplish these tasks, large scale lysimeters filled with processed oil shale have been established at a field site in the Piceance Basin, Colorado, and within a large scale environmental laboratory at the University of Wyoming. The operation and climatic control of this laboratory, called the Watershed, Climate, and Hydrology Simulation Laboratory (WCHS), is briefly described.

The purpose of this paper is to specifically describe the rainfall simulation system used within the WCHS Lab and to show preliminary results of resultant moisture flux in the disposed processed oil shale.

Introduction

A detailed knowledge of soil water behavior within processed oil shale is of primary importance to the design of a physically and chemically stable waste embankment. The Geotechnical design and knowledge of the movement of potentially toxic salts and other solubles is primarily dependent on the accurate measurement of water infiltration, flux, direction, and velocity in both saturated and unsaturated zones.

Many hydrological, geotechnical, chemical, and environmental processes associated with a processed oil shale waste embankment will be estimated by computer models. Estimates produced by these models will be used to modify or create embankment designs to meet regulatory performance criteria, or to analyze existing embankments for performance specifications. Unfortunately, the licensing of a commercial-scale embankment may have to be strongly based on estimates made from computer models regarding embankment performance. This would be especially true for the performance evaluation of time dependant variables. It is necessary, therefore, that developed computer models that are used to estimate the hydrologic, geochemical, or geotechnical properties of engineered embankments be verified and tested by field and laboratory research, physical models, embankment prototypes, etc. [1]

Project Background

A research program was developed at the University of Wyoming to physically model (produce) climatic and hydrologic processes and observe three interacting factors which would affect the disposal and behavior of processed oil shale embankments and to compare these observed physical data to computer generated data in an evaluation of model performance. These three factors are: 1) hydrology, 2) geotechnical stability, and 3) geochemistry. This research program has five major objectives:

- Assess the unsaturated movement and redistribution of water and the development of potential saturated zones in disposed processed oil shale waste.
- Assess the unsaturated movement of solubles and major chemical constituents in disposed processed oil shale.
- Assess the physical and constitutive properties (index properties, shear strength, stress-strain properties, and compressibility of processed oil shale and determine potential changes in these properties caused by disposal and weathering.

- Assess the use of previously developed computer model(s) to describe the infiltration, unsaturated movement, redistribution, and drainage of water in disposed processed oil shale.

- Evaluate the stability of theoretical, commercial scale, processed oil shale waste embankments using computer models.

The unique approach of this research is to conduct these investigations at a scale sufficient to describe commercial scale embankment behavior. This approach has been accomplished by establishing five large scale lysimeters, each 7.3 x 3.0 x 3.0 m deep, filled with processed oil shale. Approximately 400 tons of processed oil shale waste (Lurgi - combusted) was provided by Rio Blanco Oil Shale Co., Inc. (RBOSC) to carry out this study. The processed oil shale is made up of two parts. Approximately 90% by weight of the material is solid surge bin material and approximately 10% of the waste is from flue gas dust. A 90/10 ratio of surge bin wastes to flue gas dust are used for all parts of this study.

Three of the lysimeters were established at the RBOSC, Tract C-a in the Piceance Basin of Colorado. Two lysimeters were established in the Watershed, Climate and Hydrology Simulation Laboratory (WCHS) located at the University of Wyoming. The processed oil shale in all three lysimeters was placed as 30 cm (1 foot) lifts compacted to approximately 1400 kg/m^3. A moisture content of 15% was used.

Purpose

The Watershed, Climate and Hydrology Simulation Laboratory (WCHS) is an indoor facility which is composed of two lysimeter cells, each 7.3 x 3.0 x 3.0 m deep, enclosed by a climatically controlled environmental chamber. This facility was specifically designed and built so that a large range of climatic conditions could be physically applied to the processed oil shale which was filled in the lysimeter cells. The environmental chamber has the following control ranges: ambient temperature -26° C - 40.5° C (-15° F - 105° F), relative humidity 20%-80% at extremes in temperature, solar radiation 0-4,500 ft-candles intensity (metal halide lamps), and rainfall 0-127 mm/hr (0-5 in/hr) produced by the Lafayette rainfall simulation system. The environmental system is controlled by a microcomputer system in which climatic simulation programs can be programed and modeled in the environmental chamber. The climate data currently programed for simulation in the laboratory was recorded from the RBOSC field site at Tract C-a.

The purpose of this paper is to specifically describe the rainfall simulation system used within the WCHS laboratory and to show preliminary results of the resultant moisture flux in the processed oil shale. This is considered to be the critical system in producing and physically modeling the hydrologic processes in the processed oil shale.

Rainfall Simulation

Rainfall simulators have been used in the United States for approximately 50 years in the study of runoff, erosion, and infiltration. Many devices have been designed, studied, and modified to artificially apply water to plots with properties of true rainfall. Most rainfall simulators fall into two basic categories, drop forming simulators, and spray nozzle type simulators, each having advantages and disadvantages in simulating actual rainfall. [2] The specific desired properties of a particular rainfall simulator are dependant on the specific objectives of the research. Raindrop size, size distribution, drop velocity, rainfall intensity, intensity variation during a storm, and the direction of drop impact are some of the important properties to rainfall simulation and which have been considered in rainfall simulator design. [2] Historically, nozzle type simulators could produce a wider range of drop sizes, however, the drop size distribution would change as pressure was adjusted to simulate different intensities. Drop size distribution could be controlled with drip type systems by varying the size of the tip on which a rain drop would form, however, because drops essentially start at zero velocity, great heights were required to obtain terminal velocity of the drops. Furthermore, drop formers such as hypodermic needles, lengths of yarn, or plastic tubing, would need to be spaced within a few centimeters of each other to obtain satisfactory intensity distributions. [2]

There are three basic components to producing rain and modeling storms in the WCHS Lab at the University of Wyoming, 1) the rainfall simulators, 2) the creation of design storms, and 3) the microcomputer controlled driver. Rainfall simulation over the 45 m^2 area (480 ft^2) of processed oil shale within the laboratory is accomplished using five rainfall simulators which are controlled by microcomputer.

Rainfall Simulators

The rainfall simulators used in the WCHS Lab are a prototype which was developed by researchers at the United States Department of Agriculture, Science and Education Administration (USDA-SEA) Erosion Research Unit at Lafayette, Indiana for use in soil erosion studies. The simulators were constructed by personnel at Lafayette and shipped to the University of Wyoming in the fall of 1988. These are a nozzle simulator which have many of the advantages of both drop forming and nozzle type simulators. Research conducted by the developers has shown that these simulators produce a distribution of raindrop sizes that is similar to that of runoff producing storms in the midwest. Raindrop size distribution does not change with different rainfall intensities, and the energy associated with produced drops is a minimum of 80% of terminal velocity. With the computer controlled driver and electronic systems which were added at the University of Wyoming, the simulators can be continuously controlled between 0 and 127 mm/hour (0 - 5 in/hr). Control of these factors is important to the infiltration and runoff of precipitation, and therefore, important to the simulation of climate and hydrologic processes in the WCHS Lab. Preliminary testing, conducted at the University of Wyoming, has shown that the Lafayette rainfall simulators are extremely accurate in producing the desired depth of rainfall, the desired rainfall intensity, and an even distribution of rainfall occurs over the plot area in the WCHS Lab.

Design Storms

Design hyetographs or design storms are theoretical storms created using an average or theoretical time distribution which has been based on actual storm events. The purpose of creating design storms is to study or predict theoretical storm runoff for the design of structures, drainage, or containment systems. It has been found that the time distribution of rainfall intensity occurring within a storm greatly affects the quantity and time distribution of runoff. The infiltration of rain into the ground, therefore, is also greatly affected by the time distribution of rainfall intensity. Infiltration is probably the single most important factor to the successful physical modeling of soil moisture flux into the processed oil shale.

Many procedures have been developed to create design hyetographs. Two methods were considered to design rainstorms for application in the WCHS lab. One method was developed by the U.S. Soil Conservation Service and is considered to be universally applicable in most of the United States. [3] The other method was developed at the University of Wyoming and is considered to be applicable for Wyoming and the semi-arid western United States. [4] The major difference in these methods is that the design methodology developed at the University of Wyoming produces larger intensity peaks for short duration storms than the SCS method, and smaller intensity peaks for storms of longer durations. This has been observed to be a common characteristic of rain storms. [5]

The method developed at the University of Wyoming[(4)] is currently being used to create design storms for application by the rainfall simulators onto the processed oil shale. Using this method, two dimensionless intensity distributions have been created for storms to be produced by the rainfall simulators. One intensity distribution is used for short duration (convective) storms which are subjectively defined as being less than 4 hours [4]. The other intensity distribution is used for general type storms, defined as being greater than 4 hours. Both distributions are considered to be second quartile storms. This means that the peak intensity of the storm will occur in the second quarter of the storms duration. Figure 1 graphically shows the dimensionless intensity distribution hyetograph which was designed for storms less than 4 hours duration. Figure 2 shows the dimensionless intensity distribution hyetograph which was designed for storms of greater than 4 hours duration. Note that the peak intensity of these distributions occurs at 30% of a storms duration making it a second quartile storm. Design storms are created by combining actual storm depth-duration information, taken from the RBOSC field site at Tract C-a, with the appropriate intensity distribution shown by Figures 1 and 2. Table 1 shows the calculations of a design storm which was applied to the processed oil shale on September 30 1989. This storm was 0.5 cm in depth (0.21 in) and lasted 1.75 hours. The intensity distribution represented by Figure 1 was used to create this storm because its duration was less than 4 hours. Figure 3 graphically shows the hyetograph of the applied design storm.

Computer Control

The computer controlled driver was written to create the design storm information, such as that in Table 1, and provide continuous control to the rainfall simulators. The computer controlled driver is a program being operated on a microcomputer and is a part of the larger computer driving system for the WCHS Lab. The computer is equipped with a digital-to-analog data acquisition and control system (d/a system). The combined system operates as follows:

1) The program requires two data inputs from the data base acquired at the RBOSC field site Tract C-a, the depth of rainfall desired, and the duration over which this rainfall is to occur.

2) The program creates or "models" a design storm using one of the two design intensity distributions. The modeled storm now has a digital format, similar to that of Table 1, which describes specific rainfall rates to be applied over specific time periods.

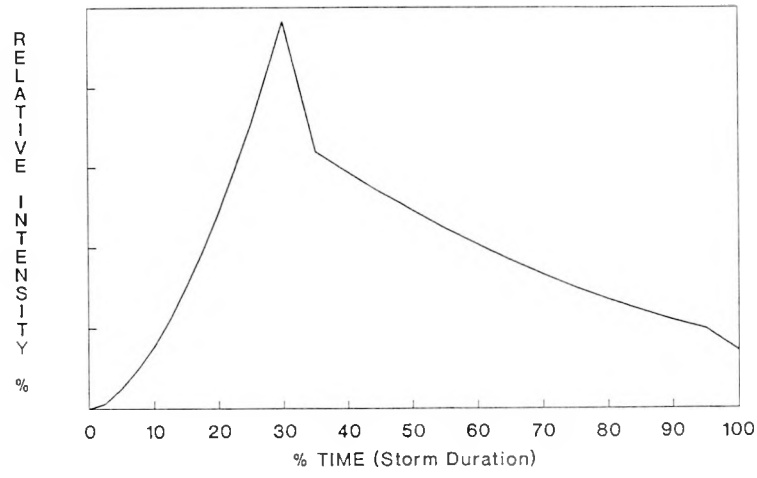

Figure 1. Dimensionless intensity distribution used for creating design storms less than 4 hours in the WCHS Laboratory.

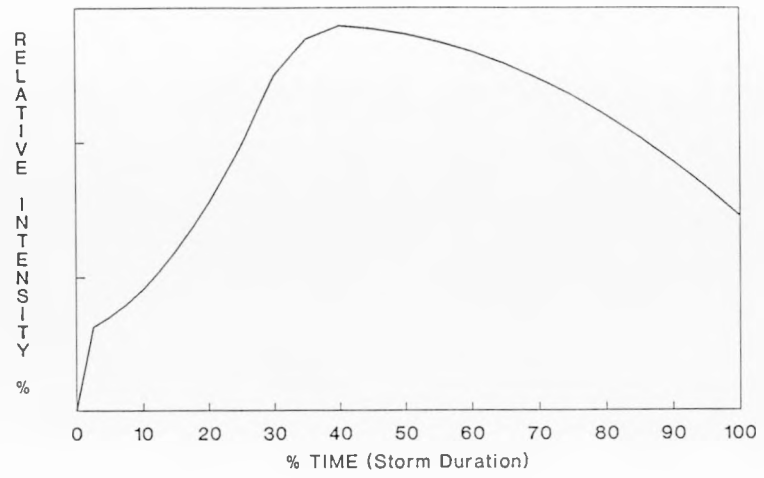

Figure 2. Dimensionless intensity distribution used for creating design storms greater than 4 hours in the WCHS Laboratory.

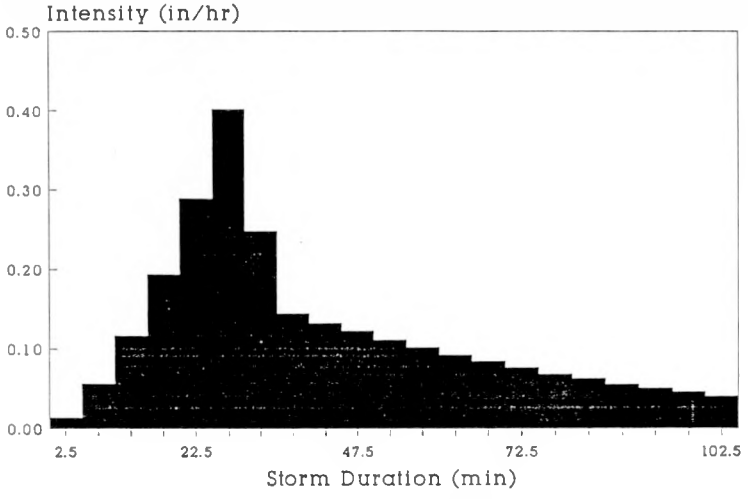

Figure 3. Hyetograph of a design storm applied in the WCHS Lab on September 30, 1989. The storm was 0.53 cm in depth and the duration was 1.75 hours. Rainfall intensity was modified in five minute intervals.

3) The program driver converts the digital information to analog signals via the d/a system. These analog signals are interpreted by specially built control circuitry which in turn drives the motor and pump systems on the five rainfall simulators.

In this manner, rain storms, such as that graphically illustrated in Figure 3, are applied to the processed oil shale.

Moisture Flux

Rainfall simulations within the WCHS lab began the week of September 11, 1989. The date, and duration of rainfall within the lab as well as settings for temperature, humidity, and radiant flux are determined by climatic data obtained at Rio Blanco Oil Shale Co., Inc. Tract C-a (RBOSC), recorded near the field lysimeters. Climate simulations within the laboratory is continuous, however, it lags the recorded climate at RBOSC by 17 months. The simulated climate in the WCHS lab in September 1988, therefore, is that measured for late April and early May 1988 at RBOSC.

The first rainfall simulation in the WCHS Lab was not based entirely on climatic data. Rather, the first rainfall simulation was used to input a slug of water into the lysimeters that represented the flux of water input by spring snow melt at the RBOSC field lysimeters during April 1988. This volume of water was measured by evaluating the surface moisture profiles within the field lysimeters.

The infiltration of water into a partially frozen soil as snow pack ablation occurs is an extremely complicated and dynamic process. The practice of inputing a slug of moisture in the spring to simulate snow melt is the same as that used for computer models simulating unsaturated groundwater flow, water balance, and solute transport. This practice is based on two assumptions: 1) the amount of water infiltrated into the surface during the winter months is negligible because of frozen soil conditions. Frozen or

Table 1. Design Storm which was applied in the WCHS Laboratory on September 30, 1989. The storm depth was 0.5 cm applied over 1.75 hours.

Time Interval (min)	% Time	% Rain	Cumm. Depth (cm)	Cumm. Depth (in)	Incr. Depth (cm)	Incr. Depth (in)	Inten. (cm/hr)	Inten. (in/hr)
0 - 5	4.8	0.6	0.003	0.001	0.003	0.001	0.038	0.015
5 - 10	9.5	2.9	0.015	0.006	0.013	0.005	0.145	0.057
10 - 15	14.3	7.5	0.041	0.016	0.025	0.010	0.297	0.117
15 - 20	19.1	15.2	0.081	0.032	0.041	0.016	0.493	0.194
20 - 25	23.8	26.7	0.142	0.056	0.061	0.024	0.734	0.289
25 - 30	28.6	42.6	0.226	0.089	0.084	0.033	1.021	0.402
30 - 35	33.3	52.4	0.279	0.110	0.053	0.021	0.630	0.248
35 - 40	38.1	58.2	0.310	0.122	0.030	0.012	0.368	0.145
40 - 45	42.9	63.5	0.338	0.133	0.028	0.011	0.338	0.133
45 - 50	47.6	68.3	0.363	0.143	0.025	0.010	0.312	0.123
50 - 55	52.4	72.8	0.389	0.153	0.023	0.009	0.284	0.112
55 - 60	57.1	76.8	0.409	0.161	0.023	0.009	0.259	0.102
60 - 65	61.9	80.5	0.429	0.169	0.020	0.008	0.236	0.093
65 - 70	66.7	83.9	0.447	0.176	0.018	0.007	0.216	0.085
70 - 75	71.4	86.9	0.465	0.183	0.015	0.006	0.196	0.077
75 - 80	76.2	89.7	0.478	0.188	0.015	0.006	0.175	0.069
80 - 85	81.0	92.2	0.493	0.194	0.013	0.005	0.160	0.063
85 - 90	85.7	94.4	0.503	0.198	0.013	0.005	0.142	0.056
90 - 95	90.5	96.4	0.513	0.202	0.010	0.004	0.130	0.051
95 - 100	95.2	98.2	0.523	0.206	0.010	0.004	0.117	0.046
100 - 105	100.0	99.9	0.533	0.210	0.008	0.003	0.104	0.041

partially frozen conditions greatly reduces both the hydraulic conductivity and the soil water potential, limiting infiltration. 2) the WCHS lab, like a computer model, can not simulate snow of the same depth, density, and water content as that occurring in the field, and furthermore, the amount of snow lost by sublimation cannot be measured.

In situ volumetric water content is monitored in the both the field lysimeters at RBOSC Tract C-a and in the WCHS Lab using two methods: Time Domain Reflectometry (TDR), and Neutron Moderation. The primary method for obtaining these measurements is by TDR. In general, TDR measures water content through a correlation between the measured apparent dielectric constant of the three phase (soil-water-air) media, an electrical property, and the volumetric water content (θ_v).Preliminary bench-top research has shown that TDR can be used to measure volumetric water content in the combusted oil shale to ± 2% of gravimetric determinations [6]. In the WCHS Lab, instrumentation to measure θ_v by TDR has been placed at 10, 15, 20, 30, 46, 76, 152, 213 cm in the processed oil shale. Instrumentation was also placed at similar depths in the processed oil shale at the field lysimeters at RBOSC Tract C-a.

Figure 4 shows the soil moisture profile from a lysimeter at the RBOSC field site at the time the processed oil shale was placed in the lysimeters in October 1987, and after spring snow melt in April 1988. The large flux of water which infiltrated from spring snow melt is readily observed at the 45 cm depth. The change in the volumetric water content within a unit volume of soil over a unit time period is the volumetric flow rate, or flux (J). The equation of continuity, expressed in terms of flux is:

$$J = - \int_0^z \frac{\partial \theta_v}{\partial t} \, dz \qquad (1)$$

where:

J = darcian flux
θ_v = volumetric water content
t = time
z = depth

The difference in the areas of two moisture profiles plotted together, one at time t_0 and the other at t_1, represent the change in volume of water with respect to the time period t_1 - t_0. This area essentially represents the right hand side of equation (1). An analysis of this type was applied to these data.

The shaded area of Figure 5 represents the change in volume of water in the processed oil shale between the October and April sampling dates with an interest in the 15 to 160 cm depth. Using planimetry, the area between these curves was found to represent 4.8 cm^3 of water per cm^2 of cross sectional area (1.9 in). These measurements indicate that the flux of water from spring snow melt into the processed oil shale at RBOSC Tract C-a was 4.8 cm.

Based on these measurements from the field lysimeters, 4.8 cm of water was input by the rainfall simulators in the WCHS lab over a period of 4 days to simulate snow melt. Figure 6 shows the hyetograph for this input slug of moisture over a 48 hour period. The design storm modeling by the driving program used the intensity distribution for a general (> 4 hour) storm, applying 4.8 cm of water to the processed oil shale in 48 hours.

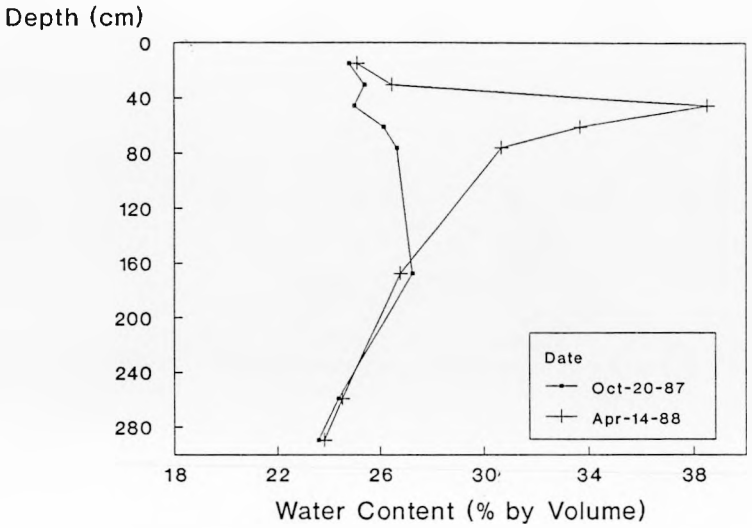

Figure 4. Soil moisture profiles at RBOSC field lysimeter at the time of installation (October 1987) and after spring snow melt (April 1988).

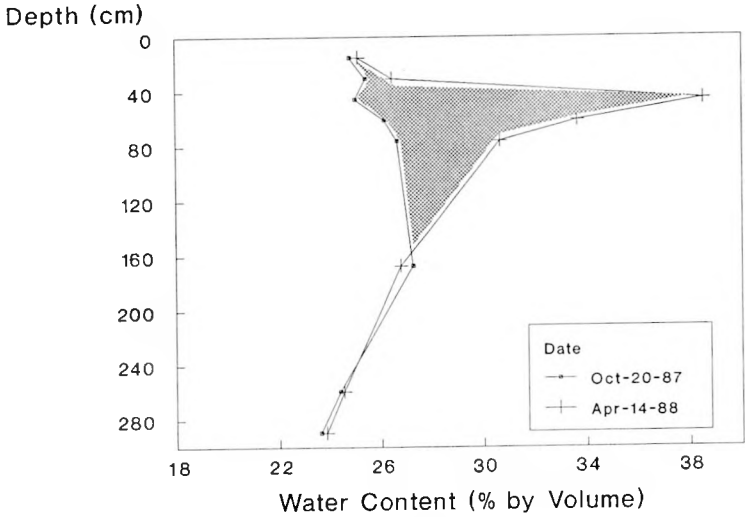

Figure 5. Shaded area representing the change in volumetric water content between 15 and 160 cm at the RBOSC field lysimeter.

Volumetric water content was measured in the processed oil shale by TDR on September 10, 1989 prior to the snow melt simulation, and on September 18, 1989 after the snow melt simulation. Figure 7 shows the soil moisture profiles in the processed oil shale for these two sampling dates. Comparing Figure 4 and Figure 7 shows similar shapes to the soil moisture profiles at RBOSC and at the WCHS Lab. The water which infiltrated to a depth of 40 cm can be easily noted in Figure 7. These data were then analyzed to determine the change in volumetric water content by planimetry. Figure 8 shows the shaded area representing the change in volumetric water content between 0 and 60 cm. The average flux for the 0 to 60 cm depth was found to be 3.8 cm. This measurement is reasonably close to the 4.8 cm which was measured for the RBOSC lysimeter.

Conclusions

A description of the rainfall simulation system which has been built for the Watershed, Climate, and Hydrology Simulation Laboratory at the University of Wyoming has been presented. This paper presented preliminary data showing the simulation of rainfall in the WCHS Lab and the hydrologic monitoring and analysis which is being conducted as part of this research program. These data to determine the redistribution, flux, velocity, and direction of water within processed oil shale will be combined with geotechnical and geochemical data also being analyzed in this research program. These data will be used to compare, evaluate, and develop computer models to evaluate embankment behavior.

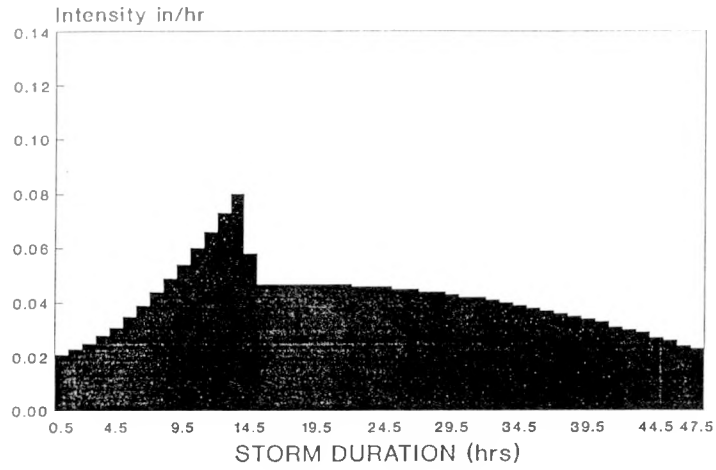

Figure 6. Hyetograph of the design storm applied to input a slug of moisture simulating spring snow melt. The storm depth was 4.8 cm and the duration was 48 hours. Rainfall intensity was modified in 1 hour intervals.

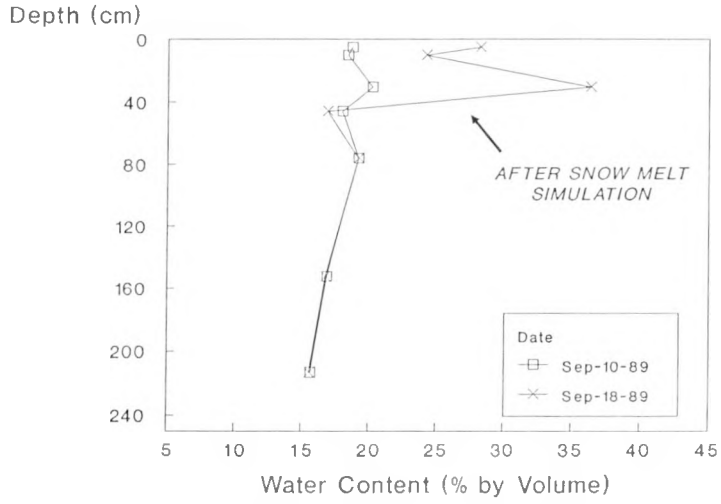

Figure 7. Soil moisture profiles at the WCHS Lab lysimeter before and after input of a moisture slug to simulate snow melt September 11 - 14, 1989.

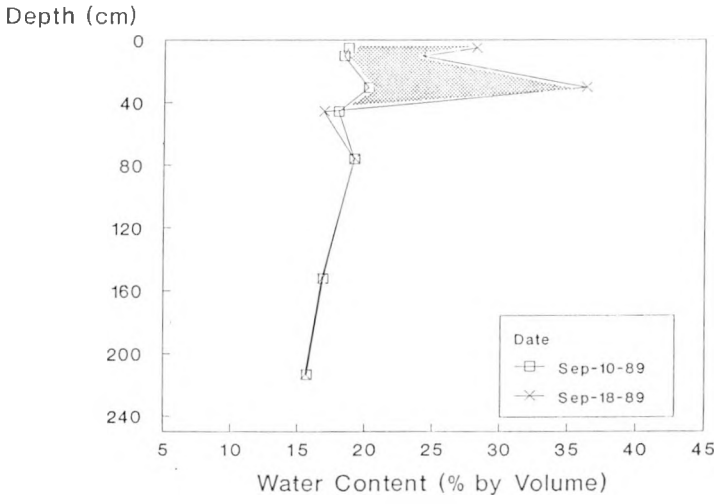

Figure 8. Shaded area representing the change in volumetric water content between 0 and 60 cm at the WCHS Lab.

Data presented in this paper indicate that the hydrologic processes can be adequately reproduced in the WCHS Lab. Precipitation produced by the rainfall simulation system was used to simulate the spring snow melt observed at the field lysimeters at RBOSC Tract C-a. The flux which was measured with this input slug of precipitation was close to that measured at the RBOSC field lysimeters.

References

1. Reeves, T.L., P.J. Sullivan, P.A. Gilbert, M.E. Essington, R. McQuisten, Q.D. Skinner, and G.P. Hale, "Research Needs for the Surface Disposal of Processed Oil Shale Solid Waste: Physical, Hydrological, and Geochemical Parameters", U.S. Department of Energy, Office of Fossil Energy, DOE/-METC-86/6071, 87 p., 1986.

2. Meyer, L.D., "Methods for Attaining Desired Rainfall Characteristics in Rainfall Simulators", *IN*: Proceedings of the Rainfall Simulator Workshop, Tucson, Arizona, U.S. Department of Agriculture Science and Education Administration, Agricultural Reviews and Manuals, ARM-W-10, p 35-44, July 1979.

3. U.S. Soil Conservation Service, "A Method for Estimating Volume and Rate of Runoff in Small Watersheds", SCS-TP-149. U.S. Department of Agriculture, 1973.

4. Tyrrell, P.T, "Development of Design Rainfall Distributions for the State of Wyoming", M.S. Thesis, Civil Engineering Department, University of Wyoming, 71 p., 1982.

5. Rankl, J.G. and D.S. Barker, "Rainfall and Runoff Data from Small Basins in Wyoming", Wyoming Water Planning Program Report No. 17, 195 p., 1977.

6. Reeves, T.L., S.M. Elgezawi, and T.G. Kaser, "An Evaluation of Hydrologic, Geotechnical, and Chemical Behavior of Processed Oil Shale II: The use of Time Domain Reflectometry (TDR) for monitoring *in situ* Volumetric Water Content in Processed Oil Shale", *IN*: Proceedings 22nd Annual Oil Shale Symposium, Colorado School of Mines, p 218-226, 1989.

PROJECTS AND PROCESS TECHNOLOGY

Prediction of Particle Size Distribution for Eastern Oil Shales Using the Self Similarity Approach

by

R.K. Mehta and C.W. Schultz, G.D. Irvin and J.B. Bates
Mineral Resources Institute
University of Alabama
Tuscaloosa, Alabama 35487

Abstract. The physical beneficiation of oil shale requires grinding the shales to an extremely fine particle size range to ensure effective liberation of the kerogen. This paper offers a simple scheme based on the self similarity approach for predicting the complete size distribution of the ground product. It is shown that the self-similar characteristic curve is unique to the combination of feed oil shale and mill type but independent of the mill operating conditions. The characteristic particle size (d_{50}) used in constructing the characteristic curve (nondimensionalized particle size distribution curve i.e. F_3 (d) v/s d/d_{50}) can be predicted by a modified Charles energy-size reduction relation ($\bar{E}$ v/s d_{50}). Therefore, using the characteristic curve, the complete particle size distribution of the ground oil shale for a given specific energy input to the size reduction device can be made.

INTRODUCTION

The objective of comminution is to predict the particle size distribution of a comminuted product as a function of the operating conditions of the size reduction device used (such as mill speed, size and degree of media filling, grind time or feed rate, etc.) and the energy expended in grinding. During the last 20 years, mathematical modeling of comminution has been done using matrix differential equations expressed in terms of the rate of breakage of particles in different size classes and the distribution of the broken particles into finer size classes. This approach, known as population balance[1,2] has been extensively used to obtain the predicted particle size distributions of the comminuted product which compared reasonably with those obtained experimentally.

The underlying assumption in this approach is the first order particle breakage kinetics. Dry-ball mill grinding is the most common operation characteristic of such phenomena. However, wet grinding in stirred ball mills, which are increasingly used for fine grinding, is characterized by non-first-order breakage kinetics. This non-linearity will therefore require these equations to be linearized over a narrow range, eventually leading to complex computations for solving numerically the linearized matrix differential equations. Secondly, in the fine particle regime, the description of ultrafine grinding must consider the distribution of particle strength together with a dependence of the grinding kinetic parameters (mostly those associated with selected function values) on the consistency of the pulp in the mill while grinding[3]. This is due to large changes in "slurry viscosity" as the material is being ground during which an increasing amount of ultrafine particles is produced.

In view of the complex breakage situation encountered in fine grinding, a simpler procedure is needed in order to reduce the complexity of computations. This paper offers a simple scheme to predict the particle size distribution of ground oil shale based upon a modified Charles relationship and self similarity approach.

PROCEDURE

Stirred Ball Milling. Continuous grinding tests were carried out using -100 mesh Alabama and Indiana shales. The feed stock (-100 mesh) to a Netzsch mill was prepared in a rod mill (11" length x 8.25" dia.) using 27 stainless steel rods (8.75" length x 0.6" dia.) each weighing 402 gms. The amount of shale used was 1000 gms. The grinding was carried out at 40% solids for 30 minutes. Grinding under these conditions gave a product which was approximately -100 mesh. Figure 1 shows the stirred ball mill grinding flowsheet. The

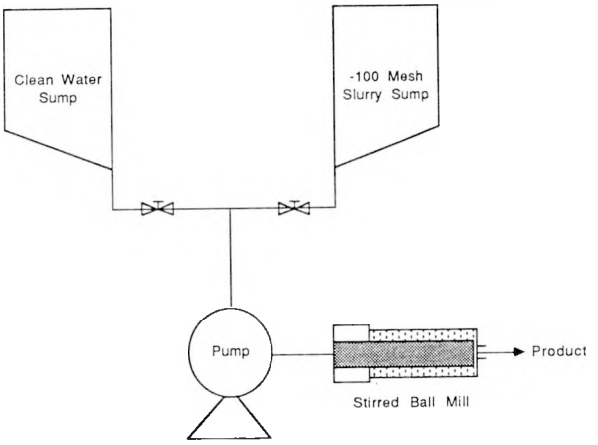

Figure 1. Schematic diagram of the Netzsch LME-4 Stirred ball mill setup for continuous wet grinding.

grinding was carried out using stainless steel media of 2mm diameter. The degree of media loading filling the mill varied between 80%-90%. The rotor speed was varied between 1200-1600 rpm and the slurry feed rate was varied between 100-400 cc/min. Slurry % solids were varied between 33-42%. The base power recorded during these tests was 1300 watts. Tables 1 and 2 list continuous grinding data collected for Indiana and Alabama shales at different operating conditions.

RESULTS AND DISCUSSION

Energy Size Reduction Relationships in the Context of an Empirical Approach. The Charles equation[4] is an empirical relation which is often used to correlate energy input with some characteristic size of the particle distribution obtained by coarse grinding. If the representative size is taken to be the 50% passing size, the Charles equation is of the form referred to as a modified Charles equation:

$$\bar{E} = A \left(d_{50,P}^{-\alpha} - d_{50,F}^{-\alpha} \right) \qquad (1)$$

Where $\bar{E}$ = Energy input to the mill (kwh/t)
A, α = Constants
$d_{50,P}$ = 50% passing size or median size of the product (microns)
$d_{50,F}$ = 50% passing size or median size of the feed (microns)

Because these shales had different feed size and, product size was not much finer than feed size, therefore, for the purpose of comparing the energy utilization among different oil shale, the approximation made to equation (1), where

$$d_{50,F}^{-\alpha} << d_{50,P}^{-\alpha}$$

is no longer valid. Hence, equation (1) was used as such in the original form. A logarithmic transformation of equation yields:

$$\log \bar{E} = \log A + \log \left(d_{50,P}^{-\alpha} - d_{50,F}^{-\alpha} \right) \qquad (2)$$

If this form of the Charles equation is appropriate for a material-grinding device combination then a plot of log $\bar{E}$ against log

$$d_{50,P}^{-\alpha} - d_{50,F}^{-\alpha}$$

should result in a straight line of slope one. A major disadvantage of this technique is that it requires the determination of on a trial and error basis until the slope of line obtained becomes unity. However, for comparison purposes, an approximate estimate of α was obtained by plotting $\bar{E}$ v/s $d_{80,P}$ on a log-log scale. The estimates of α for Alabama and Indiana shales were found to be 2.4 and 3.57 respectively. Using values of α thus obtained, the data of $\bar{E}$ v/s

$$d_{50,P}^{-\alpha} - d_{50,F}^{-\alpha}$$

on log-log scale was plotted. This plot is shown in Figure 2. It was interesting

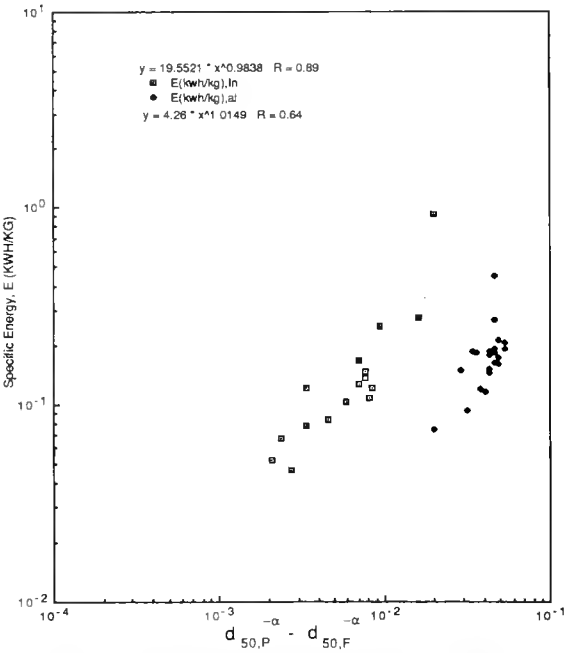

Figure 2. Energy-size reduction relationship (Charles plot) for the stirred ball grinding of Alabama and Indiana shales under various operating conditions using the John option of LME-4 Netzsch mill

to note that the slope of these plots turned out to be close to 1.0 as they should, if the empirical Charles relationship holds true for this material-grinding device combination.

Table 1. Continuous Grinding Data for Indiana Shale at Different Operating Conditions.

Sample	Feed Size *	Media Filling	% Solids	Feed Rate (cc/min)	Net Power (Watts)	Specific Energy (Kwh / kg)	Product (Microns) d_{50}	d_{90}
Product 1	1	80	33	430	1700	0.536	5.7	16.2
Product 2	1	80	33	322	1700	0.715	4.9	14.8
Product 3	1	80	33	184	1700	.1252	4.7	13.7
A1	2	80	46.13	---	1296	---	6.3	18.9
A2	2	80	46.13	540	2050	0.462	5.2	14.8
A3	2	80	46.13	720	3100	0.524	5.6	15.8
B1	2	80	43	150	1440	.1203	4.9	13.9
B2	2	80	43	150	1990	.1662	4.0	11.1
B3	2	80	43	150	2980	.2489	3.7	10.5
B4	2	80	43	150	3285	.2744	3.2	8.1
C1	2	80	43	275	1440	.0664	5.4	15.4
C2	2	80	43	275	1800	.0830	4.5	12.9
C3	2	80	43	275	2750	.1268	4.0	11.5
C4	2	80	43	275	3160	.1457	3.9	11 4
D1	2	85	45	250	1580	.0777	4.9	13 9
D2	2	85	45	250	2080	.1023	4.2	11.7
D3	2	85	45	300	2950	.1202	3.8	10.9
D4	2	85	45	300	3300	.1354	3.9	10.8

Feed Size 1 Corresponds to - 100 mesh d_{50}= 14.2 and d_{90} = 51.0 microns
Feed Size 2 Corresponds to - 100 mesh , d_{50} =15.3 and d_{90} = 50.5 microns.

Table 2. Continuous Grinding Data for Alabama Shale at Different Operating Conditions % Solids (45) , Feed (-100 Mesh) d_{50}= 23.9 and d_{90}= 84.0 Microns

Sample	Media Filling (%)	Rotor Speed (rpm)	Feed Rate (cc/min)	Net Power (Watt)	Specific Energy (kwh/kg)	Products (Microns) d_{50}	d_{90}
Al1	85*	1350	240	2915	.1492	4.4	11.8
Al2	85	1400	275	3200	.1430	3.7	10.3
Al3	85	1450	275	3550	.1586	3.5	9.9
Al4	85	1500	275	3860	.1725	3.5	9.8
Al5	85	1550	275	4250	.1899	3.4	9.4
Al6	85	1600	275	4570	.2042	3.4	9.2
Al7	83**	1350	150	2250	.1843	4.1	11.6
Al8	83	1400	170	2500	.1807	4.0	11.1
Al9	83	1450	200	2880	.1770	3.7	10.6
Al10	83	1500	205	3100	.1858	3.7	10.5
Al11	83	1550	215	3340	.1909	3.6	10.4
Al12	83	1600	215	3710	.2120	3.5	10.1
Al13	87***	1200	300	1820	.0745	5.1	13.8
Al14	87	1300	300	2245	.0919	4.2	11.3
Al15	87	1400	300	2900	.1188	3.9	10.8
Al16	87	1500	300	3650	.1495	3.7	10.2
Al17	87	1550	300	3950	.1618	3.6	10.1
Al18	87	1600	300	4430	.1815	3.6	10.0
Al19	87	1600	200	4360	.2679	3.6	9.8
Al20	87	1600	450	4250	.1160	3.8	11.2
Al21	87	1600	120	4350	.4450	3.6	9.6

* Void Volume = 1265 cc
** Void Volume = 1245 cc
*** Void Volume = 1180 cc

Another interesting feature of this plot is the relative grindability of the shales in the particle size ranges finer than 150 microns. The curve on the far left side of the plot is characteristic of a material which is harder to grind and the plot on the right is for material that is easier to grind. Therefore, resistance to grinding of the shales based on the modified Charles approach in the fine grinding regime was higher for the Indiana shale than the Alabama shale. The size reduction to energy input correlation is much better for the Indiana shale than the Alabama shale as shown by the correlation coefficients in Figure 2. This indicates that the breakage pattern of Alabama shale particles is relatively complex.

Self-Similar and Self-Preserving Size Distribution. The size distributions of the comminuted products obtained at different operating conditions were analyzed and d_{50} particle size limitations were determined. Using these d_{50} values, the size distribution of the ground products were plotted in the modified dimensionless size axis (d/d_{50}) in Figures 3 and 4 to

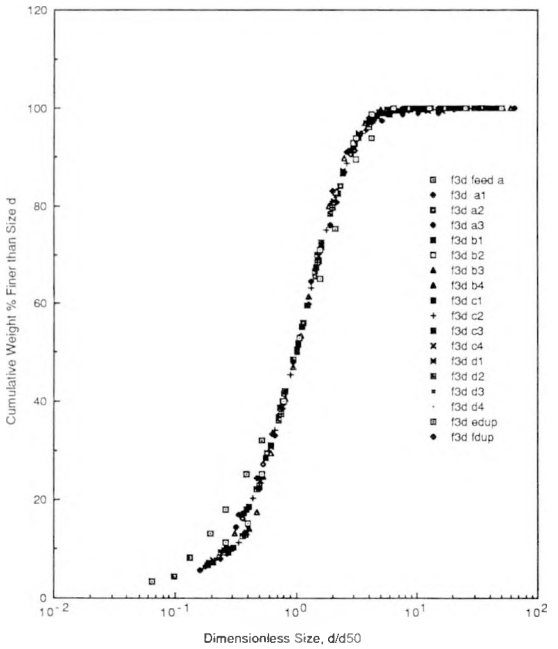

Figure 3 . Self-preserving similarity size spectra of the Indiana shale particles ground in a LME-4 Netzsch stirred mill

obtain the "characteristic curves" for Indiana and Alabama shales. The size distribution points obtained with different experimental conditions fall onto the same curve indicating that the characteristic curve remains constant with changes in the levels of the operating variables. This is in agreement with observations reported by others[5].

The self-preserving nature of the characteristic curve implies that the size distribution of a comminuted rock or product can be predicted if the following are known.

(i) The shape of the characteristic curve;
(ii) The d_{50} value of the ground shale for any set of conditions of the experiment.

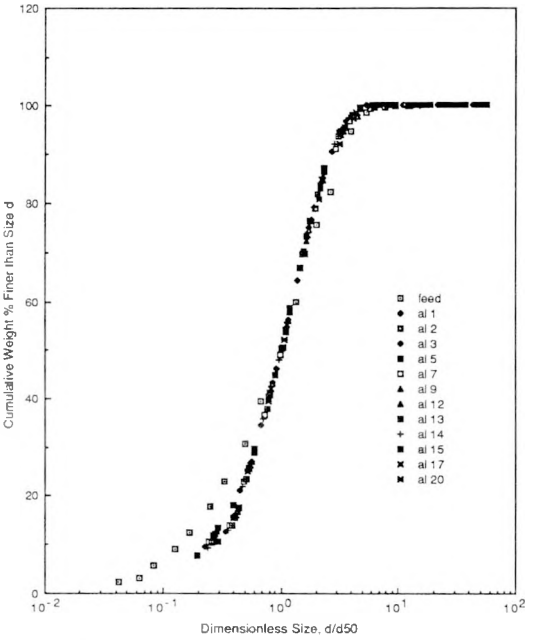

Figure 4 . Self-preserving similarity size spectra of the Alabama shale particles ground in a LME-4 Netzsch stirred mill

Quantification of the Characteristic Curve. The characteristic curve was quantified using the equations proposed for the reduced efficiency curves encountered in hydrocyclone classification. The most suitable equation for defining these curves are ones proposed by Lynch and Rao[6] and Plitt[7].

The Lynch and Rao equation is given as

$$F_3(d) = \frac{e^{\gamma x}-1}{e^{\gamma x}+e^{\gamma}-2} \qquad (3)$$

and the Plitt equation is given by

$$F_3(d) = 1-\exp\left(-.693\left(d/d_{50}\right)^m\right) \qquad (4)$$

When equations 3 and 4 are used to represent the characteristics curve, $F_3(d)$ represents the cumulative weight fraction of ground material passing size d. γ , m is a constant and x represents dimensionless size (d/d_{50}). In equation 3 an iterative procedure is used to evaluate the constant γ whereas in equation 4, the constant m can be evaluated directly as a logarithmic function using the method of least squares. Hence, equation 4 has been adapted in the present analysis for representing the characteristic curve.

The equation for the characteristic curve plotted in Figure 3 after evaluation of the constant m is:

$$F_3(d) = 1-\exp\left(-.693\left(d/d_{50}\right)^{1.0883}\right) \qquad (5)$$

Predicting the Particle Size Distribution of Comminuted Products. The self similar particle size curve as represented by

equation 4 and shown in Figures 3 and 4 in conjunction with the energy-size reduction relation (Figure 2) is useful for predicting the entire size distribution of a ground product for a given expenditure of energy as follows:

(i) Corresponding to the level of the specific energy input to the mill, obtain the median size of the comminuted product using the plot such as that in Figure 2.

(ii) Substitute the value of d_{50} obtained in equation 4 to yield entire particle size distribution.

In order to validate the approach a grinding test was carried out with Indiana shale. Minus 100 mesh slurry feed at 31% solids was ground at 1400 rpm using a feed rate of 225 cc/min. The media loading was kept at 87%. The level of specific energy input was determined as 128 kwh/t.

Using the correlation shown in Figure 2, d_{50} was calculated as 4.183 microns as compared to an experimentally determined value of 4.2 microns. The predicted size distribution based on the values of (d_{50} = 4.183) is plotted in Figure 5 along with the experimentally determined size distribution. It is apparent that the experimental and predicted d_{50} agree well and are in excellent agreement with regard to the coarser size distributions. However, the agreement is not as good for the finer sizes. This may be due to the complex transport behavior of the particles in the 1-3 micron range. In this context, it is worth mentioning that in the absence of a phenomenological model in ultrafine grinding regime, this simple modeling scheme is of potential use for scale up and circuit simulation purposes.

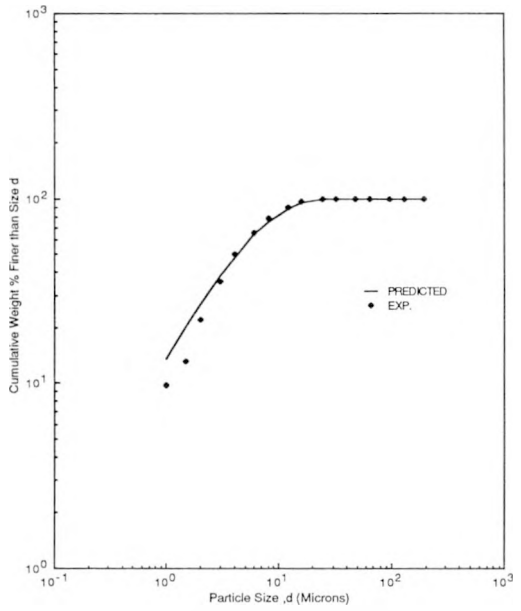

Figure 5. The predicted particle size distribution based upon the Charles plot and similarity size spectra along with the experimental size distribution for the Indiana shale in the Netzsch mill

CONCLUSIONS

1. In tests of the Alabama and Indiana oil shales fine grinding data collected in the Netzsch mill under various operating conditions was described by the modified Charles relationship yielding a slope of unity. Therefore, the approach can be useful for scale up purposes. Also, it was found that the Alabama shale is easier to grind to the finer particle sizes than the Indiana shale.

2. The similarity feature of the particle size distribution profiles of comminuted shales enabled us to reduce the particle size distributions of the different products to a single self-similar and self-preserving size spectra. This was achieved by non-dimensionalizing the particle size of a given distribution with reference to the median size of the distribution.

3. The characteristics of the self-preserving particle size distributions was specific to the material-grinding device combination, but was found to be independent of the size and most of the operating conditions of the comminution device.

4. The self-preserving size spectra of Indiana shale was successfully described by an equation such as that proposed by Plitt for reduced efficiency curves obtained in hydrocyclone classification.

5. Using the observations in (1) and (4), we were able to predict the complete size distribution of the ground shale (Indiana) for a given specific energy (kwh/kg) expenditure on the size reduction device.

6. The comminution phenomenon is very specific to the combination of feed material (such as its origin, grain structure, etc.) and type of comminution device used (John, Molinex or low speed attritor). Therefore, this is simply a note of caution to be careful in comparing specific energy values among different research studies.

7. The results of this study suggest that the use of a modified Charles relationship and self similarity approach in the fine particle regime has potential use for scale up and circuit simulation purposes.

ACKNOWLEDGEMENTS

This paper is the result of a research subcontract on "oil shale beneficiation research" performed under IGT Subcontract S1-14063 for the Institute of Gas Technology. The financial and technical support are gratefully acknowledged. We acknowledge the expert typing by Toni Jones and Mary Robinson, and critical review by Mr. Carl Rampacek, Acting Director of the Mineral Resources Institute.

LIST OF SYMBOLS

A	Coefficient of Charles Equation
d	Particle size, microns
$d_{50,F}$	Median size or 50% passing size of the feed, microns
$d_{50,P}$	Median size or 50% passing size of the product, microns
$\bar{E}$	Specific energy input, kwh/t or kwh/kg
$F_3(d)$	Cumulative weight % or fraction finer than size d
m	Adjustable parameter
x	Dimensionless size, d/d_{50}
α	Exponent of Charles Equation
γ	Adjustable parameter

REFERENCES

1. J.A. Herbst, G.A. Grandy and D.W. Fuerstenau, "Population Balance Models for the Design of Continuous Grinding Mills," Paper 19, X International Mineral Processing Congress, London, 1973.

2. J.A. Herbst and D.W. Fuerstenau, "Mathematical Simulation of Dry Ball Milling Using Specific Power Information," Trans. AIME, Vol. 254, p. 343, 1973.

3. Sepulveda, J.E., "A Detailed Study on Stirred Ball Mill Grinding," Ph.D Dissertation, Dept. of Metallurgy and Metallurgical Eng., University of Utah, Salt Lake City, UT, 1981.

4. Charles, R.J., "Energy-Size Reduction Relationship in Comminution," Trans. AIME, Vol 208, pp. 80-88, 1957.

5. P.C. Kapur, "Self-Preserving Size Spectra of Comminuted Particles," Chemical Engineering Science, vol. 27, pp. 425-431, 1972.

6. Lynch, A.J. and Rao, T.C., "Modeling and Scale-up of Hydrocyclone Classifiers," Proceedings 9th International Mineral Processing Congress, Cagliary, Italy, April, 1975.

7. L.R. Plitt, "A Mathematical Model of the Hydrocyclone Classifier," CIM Bulletin, Volume 69, pp. 114, 1976.

Pressure Cycle Comminution of Eastern Oil Shale

by

M. Misra and M. Paoli
Department of Chemical Engineering
University of Nevada-Reno
Reno, Nevada 89557
M. Rao
Department of Electrical Engineering/Computer Science
University of Nevada-Reno
Reno, Nevada 89557

ABSTRACT

Separation of kerogen from eastern oil shale can be accomplished by fine grinding followed by froth flotation. Fine grinding is energy intensive. It is estimated that 40-45 kWh/ton of energy is required for grinding oil shale to minus 10 micron size by high speed ball mill whereas the energy demand is in the range of 90-100 kWh/ton for conventional ball mill grinding. In this study, an energy efficient pressure cycle comminution technique is used for grinding oil shale. In pressure cycle grinding, the energy required to break the particle is applied directly into the particle. As a result, particle breakage can be achieved at a substantially lower energy input as compared to high speed and conventional ball mill. The effect of various parameters such as permeability, porosity, saturation time and applied pressure on the process performance has been discussed. The synergistic effect of surface energy modifiers for the comminution of oil shale has been experimented. The results of these experiments are tabulated and conclusions are drawn.

INTRODUCTION

The power requirement for the comminution of ores is on the order of 32 billion kWh per annum in USA. This corresponds to 2% of the total electrical energy [1-2]. Mineral processing industries rely on the conventional tumbling mills for the size reduction. Although tumbling mills are the most important comminution devices, nevertheless, they are energy intensive and inefficient. In a tumbling mill operation it is calculated that only 0.6% of the energy is used for grinding and the rest is being wasted. Table 1 shows the distribution of energy for a typical comminution operation [3-4].

Bolt Friction	4.3 %
Gear Losses	8.0 %
Heat Losses from Drum	6.4 %
Heat Absorbed by Air Circulation	31.0 %
Heat Absorbed by Product & Steel	47.6 %
Unaccounted Energy	2.1 %
Product Reduction	*0.6 %*
TOTAL	**100.0**

Table. 1: Ball Mill Energy Consumption.

In recent years significant amount of research has been directed to reduce the energy demand for comminution by increasing the efficiency and/or by utilizing process control strategies. Progress has been substantial in the areas of process control and simulation, liberation analysis and the study of the large ball mills [4-17]. However it can be emphasized that research in the area of new grinding process development are limited, as a matter of fact, non-existent. One of the promising concept is the pressure cycle comminution [18]. This approach involves hydraulically developing and propagating micro cracks along the grain boundaries where the applied energy can initiate the fracture with minimum waste.

Oil Shale Grinding:

Recent studies have shown that oil shale can be ground to an extremely fine size at a moderate energy input if stirred ball mill grinding techniques are used. Previous work on oil shale grinding are given in Table 2. Conventional ball mill grinding of oil shale to 80% finer than 20 microns requires a specific energy input in the range of 46-72 kWh/ton depending on the types of shale used. Grinding shale to minus 10 microns in a conventional ball mill may require in excess of 100 kWh/ton. In contrast, the energy for grinding oil shale to 80% passing 20 microns in a stirred ball mill is about 26 kWh/ton. These studies indicate that grinding in a stirred ball mill can reduce the energy demand by at least 50% as compared to conventional ball mill grinding. Nevertheless, the energy requirement for ultra-fine grinding is still astronomically high. The objective of the current research program is to utilize a novel pressure cycle comminution technique to fracture oil shale at a lower energy input as compared to existing processes [19].

PROCESS DESCRIPTION:

In this paper a novel pressure cycle comminution technique will be used for the size reduction of oil shales. The pressure cycle techniques have been used for the comminution of fossil fuel minerals. This process uses instantaneous pressure fluctuation and rapid depressurization to shatter the ore. The process involves three major steps:

1. Loading a liquid filled vessel with oil shale
2. Pressurizing the fluid slowly according to a predetermined wave form (depending on the properties of the ore),
3. Releasing the confining fluid pressure suddenly.

Oil Shale	Mill Type	Energy Input (kWh/ton)
Colorado (Mahogany Zone)	Rod Ball Mill	25-45
Michigan (Antrim Shale)	Ball Mill	46
Colorado (Anvil Point)	Ball Mill	72
Kentucky (Ohio Shale)	Ball Mill	46
Kentucky (Ohio Shale)	High Speed Stirred Ball Mill	26

Table 2. Energy-Size Relationship For Different Oil Shales
(Product Size 80% passing 20 Microns)

The basic pressure cycle comminution process involves pieces of ore saturated with air at one atmosphere. These pieces, when immersed in the fluid reservoir, are invaded by the fluid as it is pressurized. The fluid forced into the micro-cavities of the ore pieces, also creates additional fractures and micro-cracks depending on the local stresses. In this way the internal pressure is increased until it reaches the external pressure. The sudden release of the confining pressure results in very high stress gradients in all regimes of the specimens (i.e., the stress differential between the inside and outside), thus causing the material to fracture into small particles. For effective fracturing, it is important that the specimen be saturated with the fluid and that the de-pressurization should be very rapid so that the differential stress will cause the micro-cracks to burst. Also, since the external stress leads to differential strain between mineral grains and the surrounding matrix, due to differences in relative stiffness, breakage is expected to occur around the grains. This should reduce the incidence of "over grinding" and, hence, improve subsequent flotation and recovery processes.

THEORETICAL CONSIDERATIONS:

The flow of fluid inside an ore specimen can be approximated by the general equation of heat flow in a solid sphere as follows [20]:

$$\left\{\frac{(d^2T)}{dx^2}+\frac{(d^2T)}{dy^2}+\frac{(d^2T)}{dz^2}+\frac{1}{k}\frac{(d^3q)}{dt^3}\right\}=\left\{\frac{1}{\alpha}\frac{dT}{dt}\right\} \quad (1)$$

Where

t, the time
T, the temperature
q , the heat generated per unit volume,
α , the thermal diffusivity (thermal conductivity, the specific heat, the material density),

Assuming an uniform sphere with a constant (α), and that the pressure is analogues to the temperature, the above heat conduction equation can be approximated to,

$$\left\{\frac{1}{(\alpha_0)}\frac{dP}{dt}\right\}=\left\{\frac{(d^2P)}{dr^2}+2\frac{dP}{(r\,dr)}\right\} \quad (2)$$

Where,

P, the pressure
r, the radius of the specimen from the center
α_0, is the fluid diffusivity and is given by,

$$\left\{\frac{1}{\alpha_0}\right\} = \left\{\frac{\mu}{k}(\beta_e - \beta_s + \eta(\beta_f - \beta_s))\right\} \quad (3)$$

Where,

μ, the water viscosity,
k, the material permeability,
η, the material porosity,
β_e, the effective ore compressibility,
β_s, the solid compressibility of the ore,
β_f, the water compressibility.

The normalized solution would be,

$$\frac{P}{P_0} = 1 + 2\frac{r_0}{(\pi r)}\sum_{n=1}^{\infty}\frac{((-1)^{(n+1)})}{(n)}\sin\frac{(n\pi r)}{(r_0)}e^{(-\beta t n^2)} \quad (4)$$

Where, $\beta = \frac{(\pi^2)}{(r_0\alpha_0)}$, the normalized time constant.

P_0, the applied pressure
P, the required pressure at radius r at time t.

From these equations, for a given average ore size with known porosity, permeability and compressibility it is possible to predict the pressure and the hold time necessary for a successful comminution.

EXPERIMENTAL SETUP:

The prototype of the laboratory setup is shown in Fig. 1. It is comprised of a pressure vessel (which can withstand pressure up to 5000psi), an IBM - AT controlled positive displacement fluid reservoir, and transducers and sensors along with a very fast acting dump valve. A small motor/adapter combination controlled by the AT is used to open and close the valve automatically on command. The setup includes a wattmeter which with the A/D converter can automatically record the total power consumed in each test, including the losses in the electric motors and the pump [18]. The pressure vessel is a cylindrical stainless steel chamber which has a 140 mm diameter and is 150 mm in height. The dumping valve is installed on one corner of the reactor. The opening and closing of the valve is controlled by the computer. The dumping valve is manufactured by NordBerg company.

RESULTS AND DISCUSSIONS:

The pressure cycle comminution is an emerging energy efficient concept in grinding. Several of interrelated variables control the operation and comminution steps. The variables can be divided into two groups:

1. Process Variables:

   Saturation pressure
   Pressure rise time
   Hold time
   Pressure release time
   Energy requirements

2. Ore Characteristics

   Size (nominal diameter)
   Permeability
   Porosity

Process Control:

The manipulation of the process variables need a computer controlled operation [21]. A typical computer controlled pressure rise time, hold time and release time are given in Fig. 2. Pressure in the reactor can be increased to 5000 psi (maximum) in several minutes and it can be released in 20 milliseconds. The release time is limited by the modified dump valve used in the system. However, calculation showed that such a rapid release time is sufficiently fast enough to develop fluid expansion inside the rock (at 5000 psi external pressure) and thus to shatter the particles.

The pressure rise time (required to force the liquid into the particles) can be controlled based on three different waveforms. These waveforms are linear, exponential and parabolic as shown in Fig. 3. The energy required to achieve the maximum pressure depends on the types of pressure rise curve used. Preliminary experiments showed that the exponential and parabolic pressure rise techniques are more appropriate than the linear pressure rise technique.

The saturation time required for oil shale can be varied over a wide range. This is controlled by a simple command given by the computer. An example of the computer control sequence is given in Fig. 4.

Experiments With Oil Shale:

A series of experiments were conducted with Indiana oil shale. Monosize oil shale samples were prepared by dry and wet screening technique. Experiments were conducted as a function of particle size, saturation pressure, hold time and pressure rise time. In order to accomplish the penetration of fluid into the oil shale, a minimum saturation pressure of 3700 psi is required. Due to the inherent nature of eastern oil shale (laminated rock with low permeability), longer pressure hold time and multiple cycles are required. Pressure treatment caused a surfacial (or layered) breakage of oil shale. To quantify the effect of pressure cycle on the surfacial breakage, standard grinding tests with pressurized oil shale were conducted. The fine material produced during the pressure treatment was removed by wet screening on 400 mesh screen. The coarse (+400 mesh) materials were ground in a standard ball mill. The size analysis of the crushed products were conducted using conventional screening technique. The effect of pressure cycle on the breakage of Indiana oil shale is given in Table 3.

As can be seen, after 5 multiple pressure cycle, the amount of minus 1.7 mm materials produced was 14.21% as compared to 5.73% without pressure treatment. Similarly the fines produced in multiple cycles increased from 0 to 4.3%.

Effect Of Surface Energy Modifiers:

In the early thirties it was suggested by Rehbinder that certain chemicals can reduce the cohesive force which holds the discrete particles together [22]. This phenomena is referred to as the Rehbinder effect. The Rehbinder effect is supposed to reduce the surface binding energy due to the adsorption of surface active agents at the cracks and in the flaws [23-25]. There are two kinds of Rehbinder effects, "the external effect" and the other one is "the internal effect". As far as grinding is concerned the "external effect" is insignificant. The "internal effect" which arises due to the penetration and the adsorption of additives at the cracks are responsible for the decrease in surface energy and the cohesive force. Some of the

chemicals which were used as ore softeners are chlorides of sodium and aluminium [26]. Plant tests showed that these reagents have some effect on the breakage, however, the effect was not significant. This is not surprising because the mill dynamics, fluctuations and the solution chemistry in the grinding mill can mask the effect of these reagents. On the other hand if these additives are allowed to penetrate the ore through the cracks and micro-cavities then it can be effective in decreasing the surface binding energy. In that regard a series of tests were conducted with selected surface energy modifiers. The effect of surface energy reducers during the pressure cycle comminution is given in Fig. 5. Oil shale samples were pretreated with sodium chloride solution for 24 hrs. After 24 hrs oil shale particles were removed from the solution and was transferred into the pressure reactor. The reactor pressure was increased in an exponential form and was kept for 5 minutes at 4333psi. The pressure cycle was repeated three times. Notice that pressure treatment and surface energy modifiers enhanced the breakage.

Feed size : -30 X 16 mm
Pressure : 5000 psi
Rise time : 500 secs (exponential)
Hold time : 600 secs (each cycle)

Product Size, mm	Cumulative Percent Passing				
	No Pressure	Pressurized			
		Cycle 1	Cycle 2	Cycle 3	Cycle 5
-30.00	100.00	100.00	100.00	100.00	100.00
-16.00	72.83	77.81	83.69	88.23	92.23
-8.00	16.8	18.23	23.50	30.21	36.41
-3.36	6.97	8.30	11.12	14.21	18.50
-1.70	5.73	6.43	9.46	11.23	14.21
Fines (-38 microns removed before grinding)	0	<1	<1	2.30	4.30
Grinding conditions:	200mmX200mm ball mill, 30% ball charge, 200 grams oil shale; 3 mins grinding.				

Table 3. Effect of Pressure Cycle on the Breakage of Indiana Oil Shale.

CONCLUDING REMARKS:

The pressure cycle comminution technique has demonstrated an excellent potential for the comminution of oil shale. The synergistic effect of surface energy modifiers and pressure treatment is a novel concept for the comminution of oil shale and other minerals. Research and development work are in progress in this direction. The objective of this paper is to report some of the research findings. This paper can be construed as a progress report rather than a technical paper.

ACKNOWLEDGEMENTS:

Financial support from the Institute of Gas Technology is gratefully acknowledged. Authors wish to thank Dr. Schultz of the University of Alabama and Mr. Lau and Mr. Punwai of IGT and Mr. Green of Terra Tek for their helpful suggestions. Thanks to Mr. Green, President of Terra Tek, for giving us the high pressure reactor to be used in this project.

REFERENCES:

1. Herbst, J.A., et al., "Comminution and Energy Consumption", Publication No. NMAB-364, *National Academy Press*, Washington, D.C., 1981.
2. Stairmand, C.J., "The Energy Efficiency of Milling Processes", *Italian Congress,* Chemistry Days 1963, Milan, 1963.
3. Department of Energy, Energy Data Report, "Power Production, Consumption and Capacity", *U.S. Department of Energy*, December 1978.
4. Lawrison, G.C., "*Crushing and Grinding*", CRC Press, Cleveland, Ohio, 1974.
5. Austin, L. G., et al., "Process Engineering of Size Reduction: Ball Milling", *AIME*, 1984.
6. Herbst, J. A., Editor, "*Control 84*", AIME, 1984
7. Arbiter, N and Harris, C. C., "Scale - Up Problem with Large Ball Mills", *Mineral and Metallurgical Processing,* Vol. 1, May 1984.
8. Burns, S and Erskini, J. G., "Experience with Large Diameter Ball Mills", *Minerals and Metallurgical Processing,* Vol. 1., No. 1, 1984.
9. Herbst, J. A., Lo, Y. C and Rajamani, K., "Population Balance Method Prediction of the performance of Large Diameter Mills", *Minerals and Metallurgical Processing,* May 1985.
10. Herbst, J. A., et al., "Population Balance Approach to Ball Mill Scale-up", *SME/AIME Trans.* Vol. 272, 1982.
11. Rowland, C. A. Jr, and Erickson, M. T. "Large Ball Mills Scale-up Factors to be Studied Relative Grinding Efficiency", *Minerals and Metallurgical Processing*, 1984.
12. Herbst, J. A., Grandy, G.N. and Fuerstenau, D.W., "Population Balance Method for the Design of Continuous Grinding Mills", *Proc. Int. Min. Proc. Congress,* IMM, London 1974.
13. Narayana, S. S, "Modelling the Performing of Industrial Ball Mills using Single Particle Breakage Data", *Int. Journal of Min. Proc.,* Vol. 20, 1987.
14. Herbst, J. A., et al., "*Estimill - A Program for Grinding Simulation and Parameter Estimation with Linear Models*", University of Utah.
15. Miller, J.D. and Lin., C.L., "Methodology For Detailed Liberation Analysis in Mineral Processing", *Acta Sterologica*, 1986.
16. Miller, J.D. and Lin., C.L., "Effect of Grain Size Distribution and Grain Type on Linear and Areal Grade Distribution", *Process Mineralogy,* TMS, 1981.
17. Herbst, J. A., et al., "Development of Multicomponent - Multi Size Mineral Liberation Model", *AIME Annual Meeting,* 1988.
18. "Energy - efficient concept for fine size reduction of rocks & ores", report submitted by Terra Tek to NSF, TR 89-40, Dec. 1988.
19. Misra, M. Hilleke, F. " Power Requirements For Ultrafine Grinding of Eastern Oil Shale," *Proceedings of the 1987 Eastern Oil Shale Symposium,* 1987.
20. Carslaw, H. S., "*Conduction of Heat in Solids*", 1947, Oxford University Press.
21. M. Rao, M. Paoli, M. Misra, "Control and Implementation of Ore Reduction by Hydraulic Pressure Cycle", accepted for presentation at 1990 ISMM Conference, March 5-7, 1990, New Orleans, LA.
22. Rehbinder, P. and Kalinkosvskay, N., *Journal of Technology and Physics*, Vol. 2, USSR, p. 276.

23. Somasundaran. P. and Lin. J., "Effect of the Nature of Environment on Comminution Process" *Industrial and Engineering Chemistry,* Process Design and Development, Vol. 11, p. 321.
24. Westbrook, A. "*Environment Sensitive Mechanical Behavior*", Gordon and Breach Publishing, New York, p. 247.
25. Westwood, A., "Tewksbury Lecture: Control and Application of Environment Sensitive Fracture Process", *Journal of Materials Science,* Vol. 9, p. 1871-1891.
26. Hartley, et al., "Chemical Additives for Ore Grinding; How Effective Are They?", *Eng. Min. Jour.,* Vol. 179.

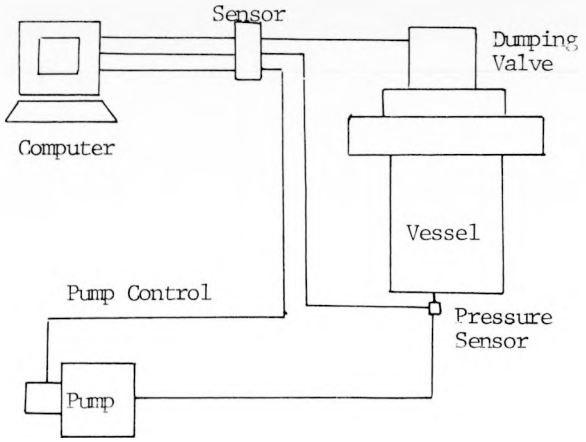

Fig. 1. Prototype of the Laboratory Setup.

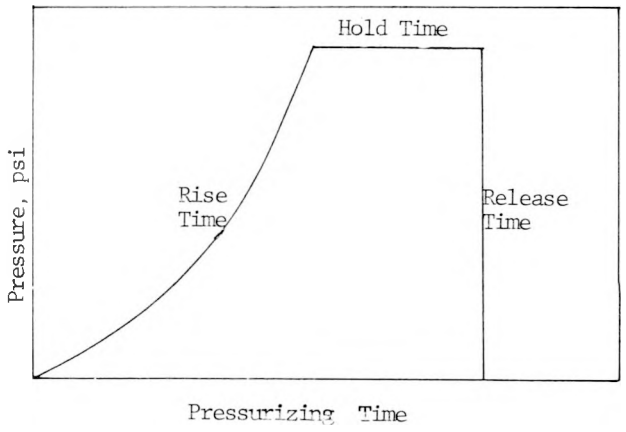

Fig. 2. Three Steps of Pressurization

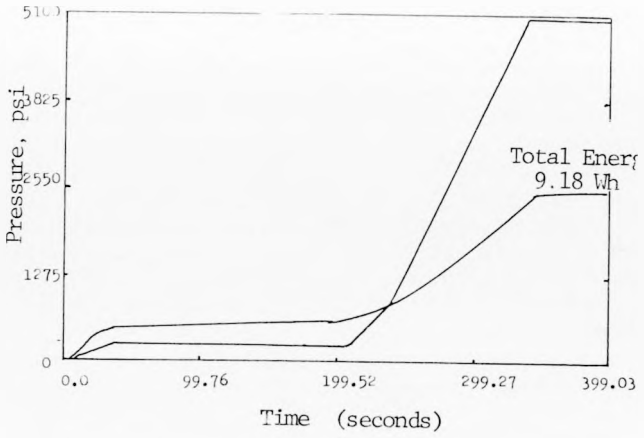

Fig. 3a. Exponent Pressure Rise Curve

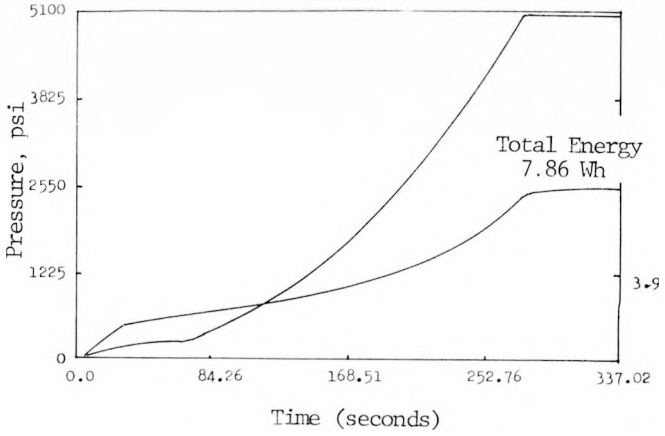

Fig. 3b. Parabolic Pressure Rise Curve

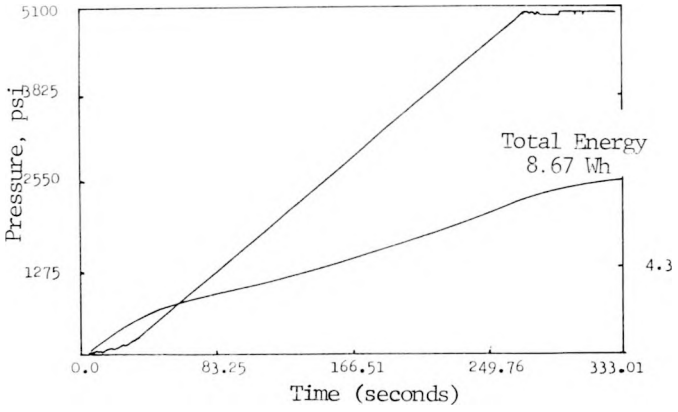

Fig. 3c. Linear Pressure Rise Curve

```
ARE YOU GOING TO RUN SYSTEM OR JUST PLOTTING A PREVIOUS RUN?
TYPE Y TO RUN SYSTEM  Y

*****************************************************************
*      BEFORE PROCEDING                                         *
*                                                               *
*      1 CLOSE REACTOR TO SEAT COVER THEN BACK OFF 1/2 TURN     *
*      2 CONNECT COMPUTER TO SYSTEM                             *
*      3 TURN CONTROL BOX ON AND SET TO COMPUTER CONTROL        *
*      4 TURN WATER ON                                          *
*      5 TURN ON AND CONNECT AIR                                *
*      6 CLOSE REACTOR DRAIN VALVE                              *
*      7 HAVE RISE TIME WAVEFORM INFORMATION OR USERS FUNCTION  *
*        IN LINE No.9076                                        *
*****************************************************************

ARE YOU READY TO CONTINUE? Y/N  Y

FILENAME?  TEST
TITLE FOR PLOTS?  TEST1
PEAK PRESSURE 200-5000 PSI?  5000
INPUT THE HOLD TIME AT PEAK IN SECONDS? 600
CHOOSE WAVEFORM FOR PRESSURE RISE:
1  RAMP P(T)=A*T
2  PARABOLIC  P(T)=A*T^2
3  EXPONENTIAL  P(T)=A*EXP(BT)
4  USERS PLACE DEF FNPT(T) STATMENT IN LINE No.9076

INPUT THE RAMP CONSTANT 'A'(PSI/SEC)? 20

INPUT THE NUMBER OF PRESSURE CYCLES YOU WISH TO PERFORM? 5

THE PRESSURE RISE TIME FUNCTION IS TO BE
RAMP   P(T)= 20*T
PEAK PRESSURE IS TO BE 5000 PSI
HOLD TIME AT 5000 PSI IS 600 SEC
FOR A TOTAL OF 5 CYCLES

IS THESE DATA CORRECT? Y/N Y
```

Fig. 4. The Format of Computer Input

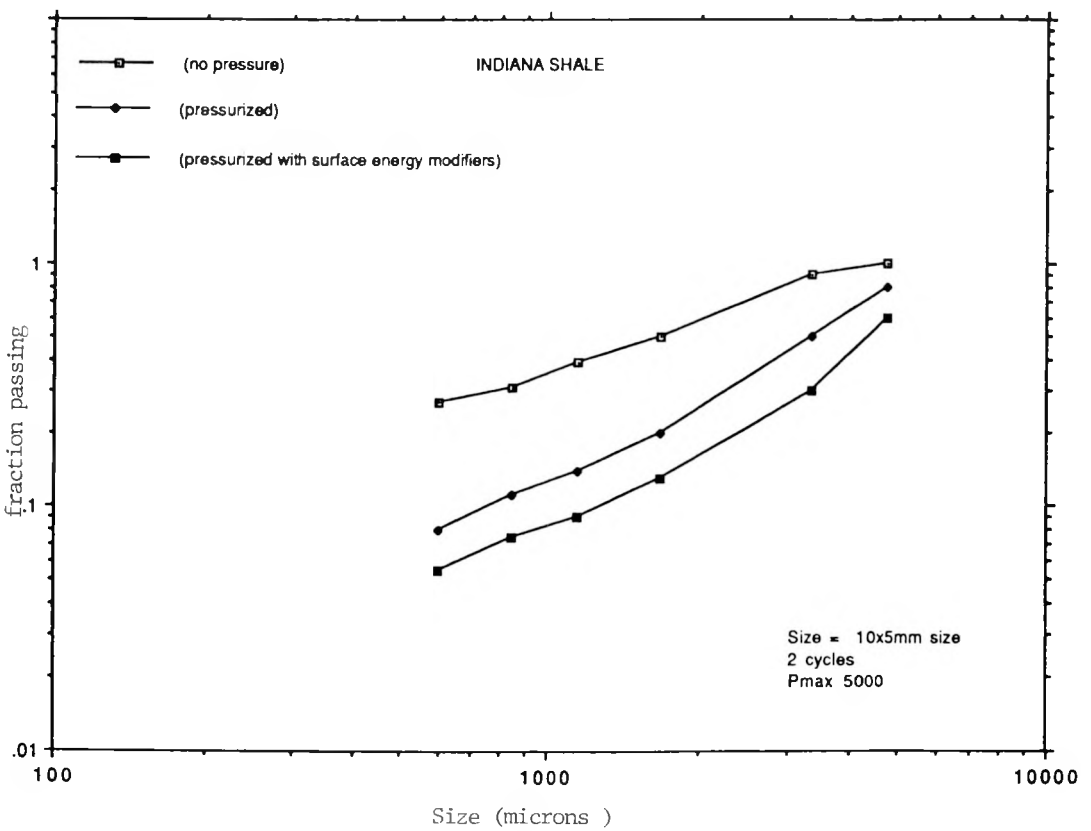

Fig. 5. Effect of Surface Energy Modifiers

Application of Licado Process to Eastern Oil Shale

by

R. Venkatadri, B.I. Morsi, and S.H. Chiang
Department of Chemical and Petroleum Engineering
University of Pittsburgh
Pittsburgh, Pennsylvania 15261

Abstract. The LICADO process is a novel beneficiation process developed at the University of Pittsburgh. It is a surface-property driven process in which the liquid CO_2-water interface is used for the differentiation and separation between the kerogen-rich shale and mineral matter. The process is carried out at room temperature and a pressure of about 850 psig.

Prior to carrying out beneficiation tests, contact angle measurements were conducted at atmospheric pressure as well as at elevated pressures. These experiments revealed that the surface of oil shale was rendered hydrophobic by liquid CO_2. A 2-inch Batch Research Unit was utilized to study the influence of various operating parameters on the product quality as well as oil recovery of Indiana and Alabama shales. The effect of various dispersants was examined. Additional experiments were conducted in a modified Batch Research Unit where the upgraded product was captured on a screen. Tests were also performed in a semi-continuous mode.

Introduction

In recent years, there has been a great deal of interest in beneficiation of fossil fuels such as coal and oil shale.[1,2] The LICADO process was originally developed at the University of Pittsburgh as a novel and alternate way to produce premium quality coal by physical beneficiation. The process has been recently applied to beneficiation of selected eastern oil shales.

The LICADO process uses liquid CO_2 at about 850 psig and room temperature to separate mineral matter from the upgraded kerogen in oil shale. The operation is carried out by contacting an oil shale-water slurry with liquid CO_2. Because of the inherent difference in surface properties, the hydrophobic kerogen-laden particles are preferentially attached to the liquid CO_2-water interface and then transferred to the liquid CO_2 phase. The hydrophilic mineral-rich particles remain in the aqueous phase. In this manner, it is possible to achieve the desired upgrading of the raw oil shale.

The main advantages of the LICADO process are that liquid CO_2 is a low cost material and is easily available. The dewatering requirements for the upgraded product are reduced since the product is reasonably dry. Liquid CO_2 has some unique properties such as low viscosity and surface tension which will permit its separation easily from the upgraded product with low operational costs. Liquid CO_2 is also non-toxic and non-flammable. The drawback of the process is that it is carried out under high pressure, which indicates a high capital cost.[3] The initial results reported in this paper indicate that the LICADO process is a promising new technique for beneficiating oil shale.

Experimental

A majority of the experiments were carried out with a sample of Indiana oil shale supplied by Mineral Resources Institute, Alabama (MRI). The average particle size by weight of this sample was 7 microns with a Fischer Assay of about 12 gal/ton and it contained 78% ash. In addition, parametric studies were conducted with a sample of Alabama oil shale also furnished by MRI. This was fine ground in a rod mill to 10 microns. The raw shale had an ash content of 80%.

The effect of dispersants on process performance was investigated by employing a conventional dispersant, Sodium Hexametaphosphate (SHMP) and also two alcohols, 1-Octanol and 2-Octanol. Dosages of up to 1000 ppm in solution were used to facilitate beneficiation. The solubilities of 1-Octanol and 2-Octanol in water at room temperature are 400 ppm and 790 ppm, respectively. The reagent was introduced at the desired dosage in a 2-5% slurry of the Indiana oil shale in water. The solution was preconditioned by vigorous

agitation for at least 1 hour prior to performing the agglomeration experiments. The density of the Indiana oil shale was measured with a Quantasorb Helium Pycnometer. The density of the raw oil shale was measured to be 2.30 gm/cc. Correlations for Fischer Assay and carbon yield as a function of material density were developed by MRI. These were utilized to calculate the Fischer Assay of the upgraded product. The oil recovery for the product was subsequently computed from the following relationship:

$$\text{Oil Recovery (\%)} = (\text{Product Yield,\%}) * \frac{(\text{Product Oil Content})}{(\text{Feed Oil Content})} \quad (1)$$

Equipment and Operating Procedure

Four different types of experiments were carried out with oil shale samples:

1. Batch experiments in the 2-inch Batch Research Unit (BRU).
2. Screen-type agglomeration experiments in the modified BRU.
3. Semi-continuous experiments in the 4-inch Research Development Unit (RDU).
4. Contact angle measurements in air and under high pressure in a specially designed apparatus.

The details of the equipment and operating procedures are given below.

The batch experiments were performed in the 2-inch Batch Research Unit (BRU). The unit is shown in Figure 1. It consists of two high pressure cells of 2-inch I.D. connected by a ball valve. The system is provided with two variable speed mixers operating up to an impeller speed of 1700 rpm for agitation of both the aqueous and liquid CO_2 phases. A 900 ml oil shale-water slurry was fed to the lower section of the BRU in each test. Liquid CO_2 was injected from the bottom of the column to produce the upgraded product-refuse separation. At the end of the contact period with liquid CO_2, the upper and lower sections of the BRU were separated by closing the 2-inch ball valve. The contents of the upper cell contained the upgraded product while the refuse fraction was collected in the bottom cell.

Figure 2 shows the 2-inch BRU modified to perform screen-type agglomeration tests. A -80 mesh screen was incorporated in the ball valve separating the upper and lower cells. The screen was inserted to retain the agglomerates of the upgraded kerogen-rich material when the mixture of oil shale-water-liquid CO_2 was drained to the bottom cell. Five hundred ml of slurry was introduced into the top cell after initially closing the ball valve. The system was then pressurized with liquid CO_2 until a small amount (100 ml) was observed to collect as a clear layer above the slurry. The ratio of liquid CO_2 to slurry was maintained at about 0.2 in all the experiments conducted at a slurry concentration of 2% by weight. The liquid CO_2 was vigorously agitated with the oil shale for 3 min at 2500 rpm. The slurry containing the agglomerated product was immediately drained through the screen. The upgraded product agglomerates were captured on the screen and collected after depressurizing the system.

A 4-inch high pressure unit denoted as the Research Development Unit (RDU) was utilized to perform experiments in a semi-continuous mode. The unit is depicted in Figure 3. This apparatus was designed not only for beneficiation experiments but also to study the hydrodynamic characteristics of the oil shale-water-liquid CO_2 system in a stirred column. Prior to performing the experiment, the slurry was premixed with liquid CO_2 for 7 min at 2000 rpm. During the experiment, liquid CO_2 was introduced from the bottom of the separation column through a disperser at a constant flowrate for a specified contact time. The upgraded product was carried up to a collecting cup at the top of the separation column and into a product sampler where the liquid CO_2 left the system through a back pressure valve. Refuse samples remained in the separation column and were withdrawn from the bottom of the cell to a sampler at the termination of the experiment. The pressure, temperature and flowrate were monitored from an instrument panel adjacent to the apparatus.

Surface property measurements were carried out by measuring the contact angle on oil shale pellets in a specially designed high pressure apparatus shown in Figure 4. An overhead mixing cell was used to equilibrate the immiscible liquid CO_2 and water phases and to feed either of these two liquids to the measurement cell by gravity. The measurement cell, equipped with 2-inch windows on opposite sides, was mounted on a rotary table capable of a 180 degree rotation. A sessile drop of water was deposited in a CO_2 environment on a 1 x 1/4 inch thick polished pellet of an eastern oil shale which was contained in a speciment holder. The contact angle of water was measured with an angular protractor inside the eyepiece of the microscope at various liquid CO_2 pressures ranging from zero to saturation pressure at room temperature (about 850 psia). In addition, the contact angle of water was measured at room temperature and pressure with a conventional goniometer.

Results and Discussions

Figure 5 illustrates the variation of the equilibrium contact angle of water on polished samples of an eastern oil shale at various CO_2 pressures up to the saturation pressure of CO_2 at 22°C. At room temperature, the average contact angle was about 44°, but it increased in the presence of liquid CO_2 and reached 115° at the saturation pressure (870 psi). This indicates that the surface of oil shale was being rendered hydrophobic in the presence of CO_2. The conclusion from these results was that it was possible to effect a significant upgrading of the oil shale by the LICADO process.

Batch Experiment Results

Numerous experiments were performed in the 2-inch BRU with the Indiana and Alabama oil shale samples. Table 1 lists the operating variables and conditions utilized in these tests.

Table 1. Process Operating Conditions for BRU

Temperature, ^{o}F	70 - 80
Slurry Concentration, Weight % Solids	2 - 20
Particle Size, microns	7 - 20
Pressure, psig	800 - 960
Contact Time, min	2.5 - 10
Liquid CO_2 Flowrate, ml/min	100 - 350
Agitation Speed, rpm	300 - 2500

The effect of increasing the slurry concentration from 2.5 - 20% revealed that increases in yield were accompanied by an increase in the product ash content. Hence, the slurry concentration was maintained at 5% in subsequent tests. The effect of increasing the flowrate was similar as higher flowrates resulted in increased yields and lower product quality. The yields decreased as the contact time for liquid CO_2 was altered from 2.5 -15 min. Particle sedimentation at the higher contact time was responsible for this phenomenon and it was decided to minimize sedimentation by performing experiments with a contact time of 2.5 -15 min. The settling time at the termination of the batch experiment was also eliminated for the same reason.

An agitation speed of 800 rpm generated higher yields and improved product quality compared to agitation speeds in the range of 1200 - 1600 rpm. This is evident from results in Table 2 for the Indiana oil shale. During these tests, the contact time was maintained at 5 min for a liquid CO_2 flowrate of 200 ml/min. Based on this, subsequent batch experiments were conducted at the lower impeller speed of 800 rpm.

Table 2. Effect of Impeller Speed for Indiana Oil Shale

Agitation Speed (rpm)	Yield (%)	Product Ash (%)
800	27.8	71.6
1200	23.9	74.4
1400	24.5	74.9
1600	25.3	74.3

Figure 6 summarizes the results of batch experiments with the Indiana and Alabama oil shale samples for various operating conditions. It can be observed from Figure 6 that the product yield increases correspondingly with ash in the product. Experiments carried out in the absence of chemical reagents have thus suggested that improved yields can be achieved only at the expense of poorer product quality.

The effect of a conventional dispersant on yield and product quality was investigated by pretreatment of Indiana oil shale with Sodium Hexametaphosphate (SHMP). The dispersant dosage was varied from 100 -700 ppm in solution. Two different contact times were chosen; 2.5 min and 5 min as well as two agitation speeds, 1200 rpm and 800 rpm. The results were not very encouraging as a slight decrease in the yield was registered with larger dosages of the dispersant. However, there was a minor improvement in the product quality as evidenced by lower ash content in the product. The dosage of the dispersant did not substantially influence the results within the range explored.

A marked improvement in process performance was achieved by preconditioning the Indiana oil shale with 1-Octanol. Table 3 shows the experimental results obtained with an agitation speed of 800 rpm in the BRU. The contact time was fixed at 2.5 min and the liquid CO_2 flowrate was maintained at 800 rpm. The dosage of 1-Octanol was varied in the range of 0 - 1000 ppm.

Table 3. Results from Batch Tests on Indiana Oil Shale

Dosage (ppm)	Yield (%)	Fischer Assay (gal/ton)	Oil Recovery (Weight, %)
0	16.8	18.0	25.6
100	24.4	21.3	44.0
300	27.5	22.3	52.0
500	29.8	27.7	70.0
1000	32.9	25.7	71.6

The Fischer Assay and oil recovery were very low in the absence of 1-Octanol. As can be observed from Table 3, a steady increase in the experimental yield was registered as the dosage of the reagent was increased to 1000 ppm. This lends support to the argument that 1-Octanol could behave as a co-agglomerating agent in the process. The product quality also improved and the highest value of Fischer Assay was reached at a dosage of 500 ppm. Oil recoveries in excess of 70% were achieved by using the appropriate dosage of 1-Octanol.

Screen-Type Agglomeration Results

A number of screen-type agglomeration experiments were conducted with Indiana oil shale after preconditioning with 1-Octanol and 2-Octanol. The upgraded product was recovered on a -80 mesh screen installed inside the ball valve of the BRU. The results for the oil recovery and Fischer Assay of the upgraded product in the presence of these reagents are depicted in Figures 7 and 8. The scatter in the data indicates that additional experiments are necessary in order to calculate the standard deviation at each dosage. However, it is clear that a significant improvement in both the recovery and the product quality was brought about using the reagents at dosages exceeding 300 ppm. The Fischer Assay was improved to values exceeding 30 gal/ton with 500 ppm of 1-Octanol and with an oil recovery of nearly 70%. The differences in the behavior of the two alcohols might be related to their different solubilities in water as well as their structure. These reagents not only behave as co-agglomerating agents but also enhance the dispersion of mineral matter in the oil shale. It may be speculated that these alcohols facilitate the bridging of the kerogen-rich particles by the liquid CO_2 by rendering them hydrophobic.

Semi-Continuous Experimental Results

Preliminary experiments were performed using the 4-inch RDU for a premixing time of 7 min, a liquid CO_2 flowrate of 500 ml/min and a contact

period of 15 min. The speed of agitation subsequent to the premixing operation was altered from 1000 rpm to 2050 rpm. A minimum speed of 1700 rpm was necessary to achieve proper dispersion of the liquid CO_2 droplets to improve contact with the kerogen-rich material. Tests were also conducted in the presence of 1-Octanol. The results demonstrated the importance of agitation speed as a process parameter. Higher speeds resulted in increased oil recoveries at the expense of a decrease in the Fischer Assay, suggesting that mineral matter was being entrapped in the agglomerates of the upgraded product.

The RDU is being currently modified to incorporate multi-stage cleaning and extensive tests will be conducted shortly. Results from the batch and semi-continuous tests will be used as a basis to design the experiments to be conducted in the Continuous Research Unit.

Major Conclusions

The LICADO process was found to be an effective way of upgrading eastern oil shale samples. Three different types of experiments were conducted principally with Indiana oil shale. These included batch and screen agglomeration experiments in the 2-inch BRU and semi-continuous experiments in the 4-inch RDU. The influence of various process parameters such as contact time, flowrate, settling time, slurry concentration and agitation speed was examined using the BRU. Significant improvements in beneficiation were obtained by preconditioning the oil shale slurry with two alcohols, 1-Octanol and 2-Octanol.

References

1. D.V. Keller and W. Burry, "An Investigation of a Separation Process Involving Liquid-Water-Coal Systems," Colloids and Surfaces, 22 (1987) pp. 37-50.

2. R.H. Yoon, "Cleaning of Ultrafine Coal by Microbubble Flotation," presented at the First Annual Pittsburgh Coal Conference, September 1984.

3. G. Araujo, D.X. He, S.M. Chi, B.I. Morsi, G.E. Klinzing and S.H. Chiang, "Use of Liquid CO_2 for Fine Coal Cleaning," Energy Progress, 7 (1987) pp. 72-76.

Acknowledgements

The financial support of the U.S. Department of Energy for this work under DOE Prime No. DE-AC21-87MC11089 is gratefully acknowledged.

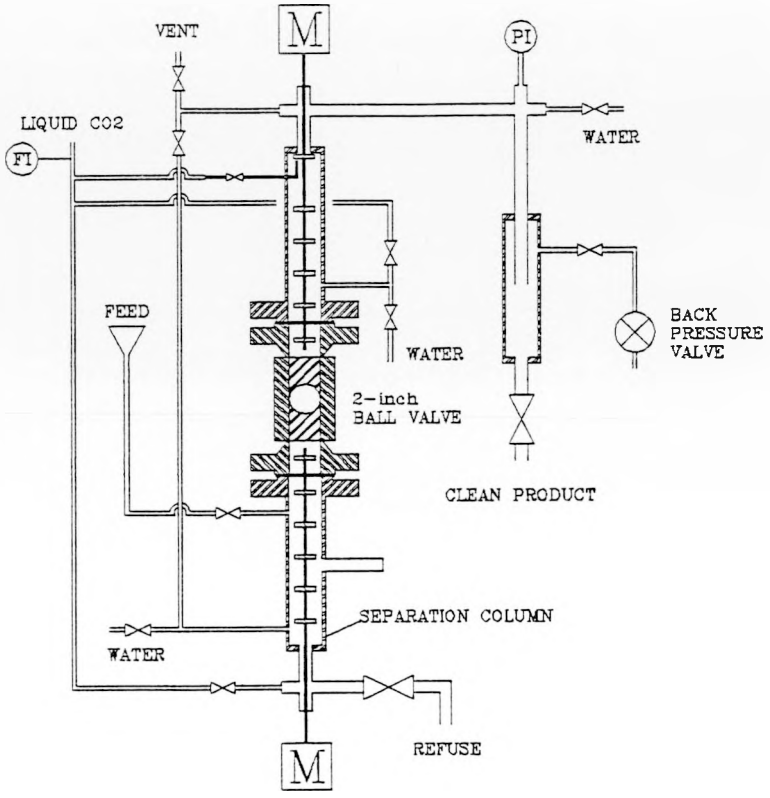

Figure 1. Batch Research Unit

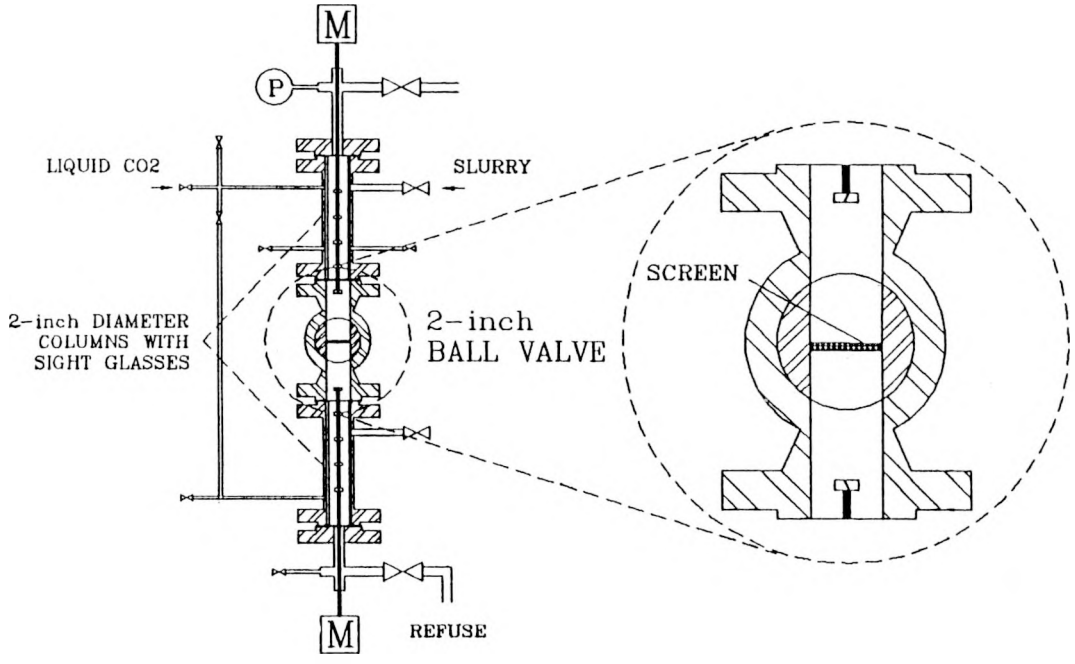

Figure 2. Modified Batch Unit for screen-agglomeration tests.

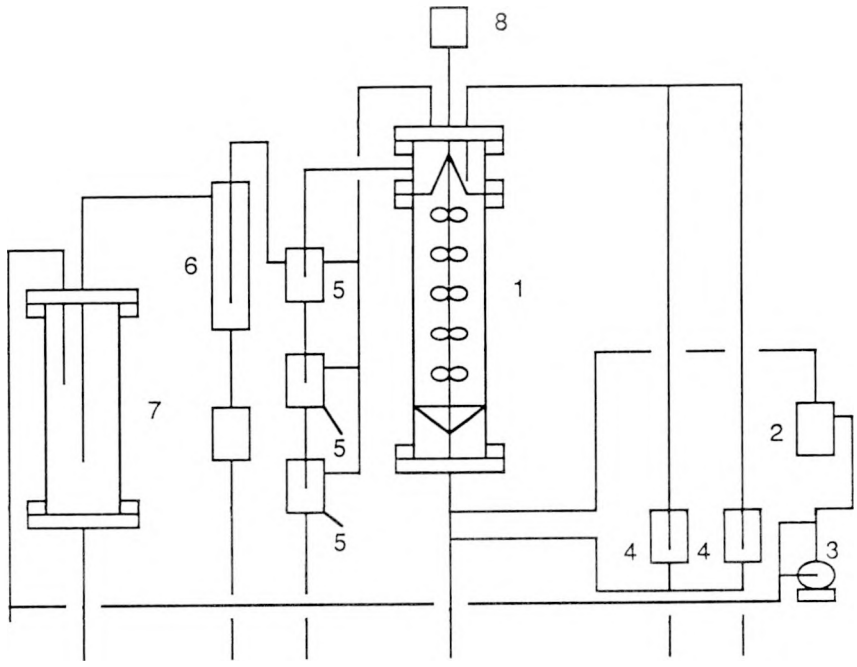

1. Column
2. Flowmeter
3. CO_2 Pump
4. Refuse Collector
5. Product Collector
6. Settling Tank
7. CO_2 Tank
8. Motor

Figure 3. Research Development Unit.

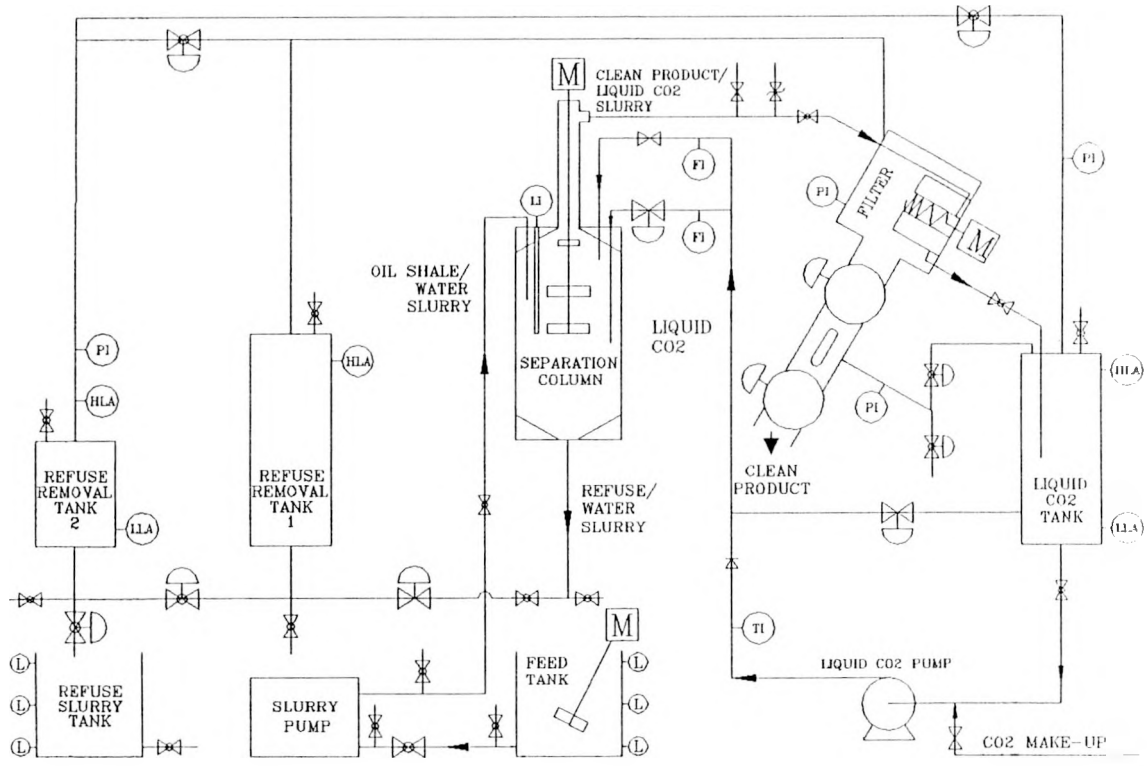

Figure 4. Continuous Research Unit.

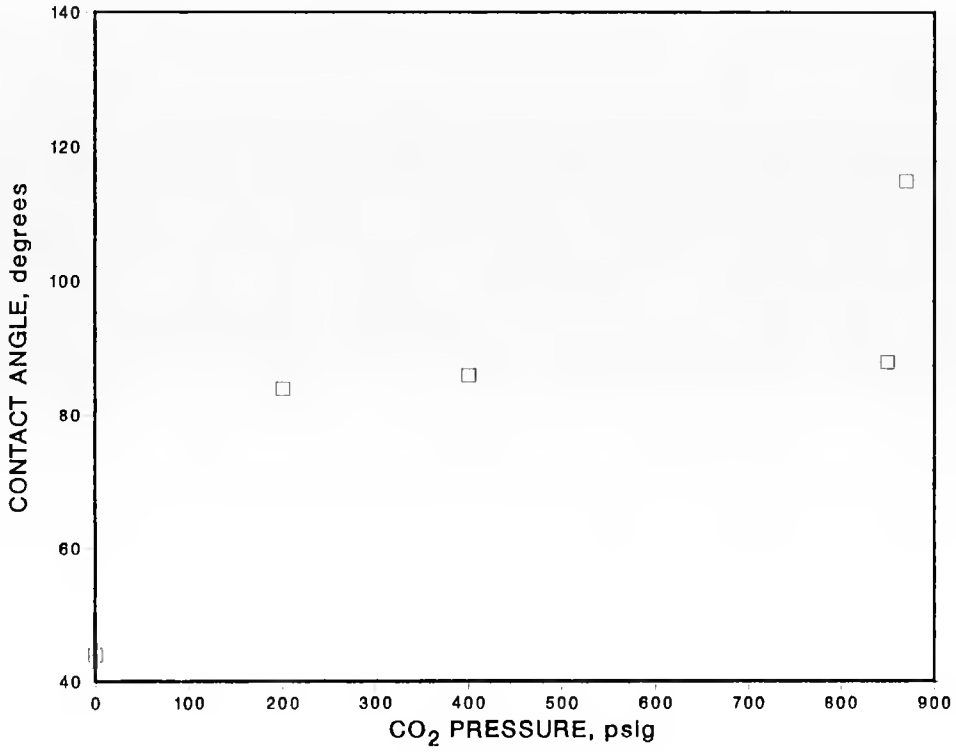

Figure 5. Contact angle versus CO_2 pressure.

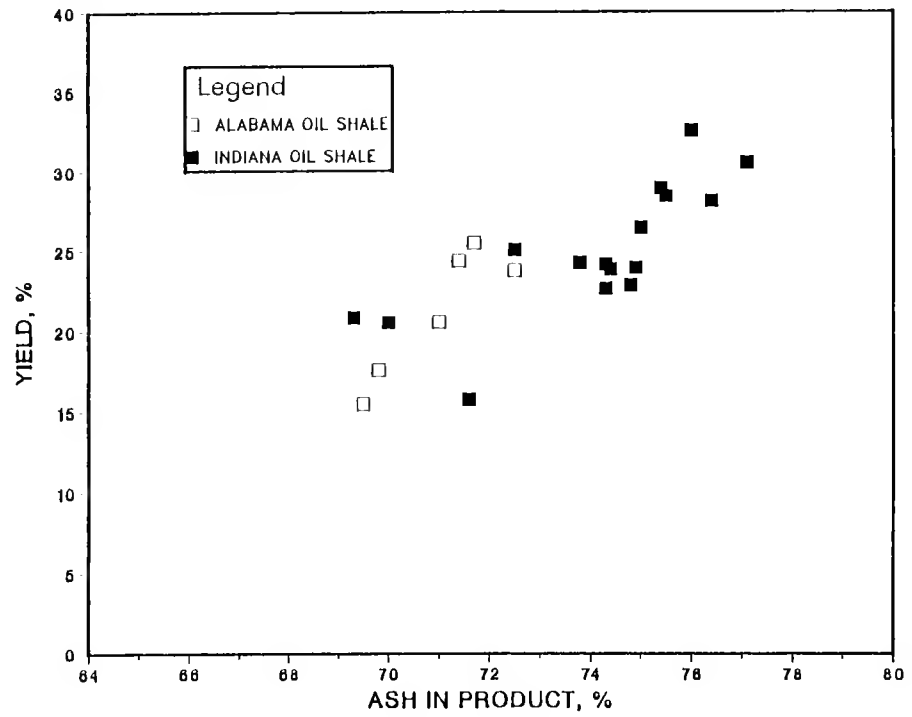

Figure 6. Results of batch tests without dispersants.

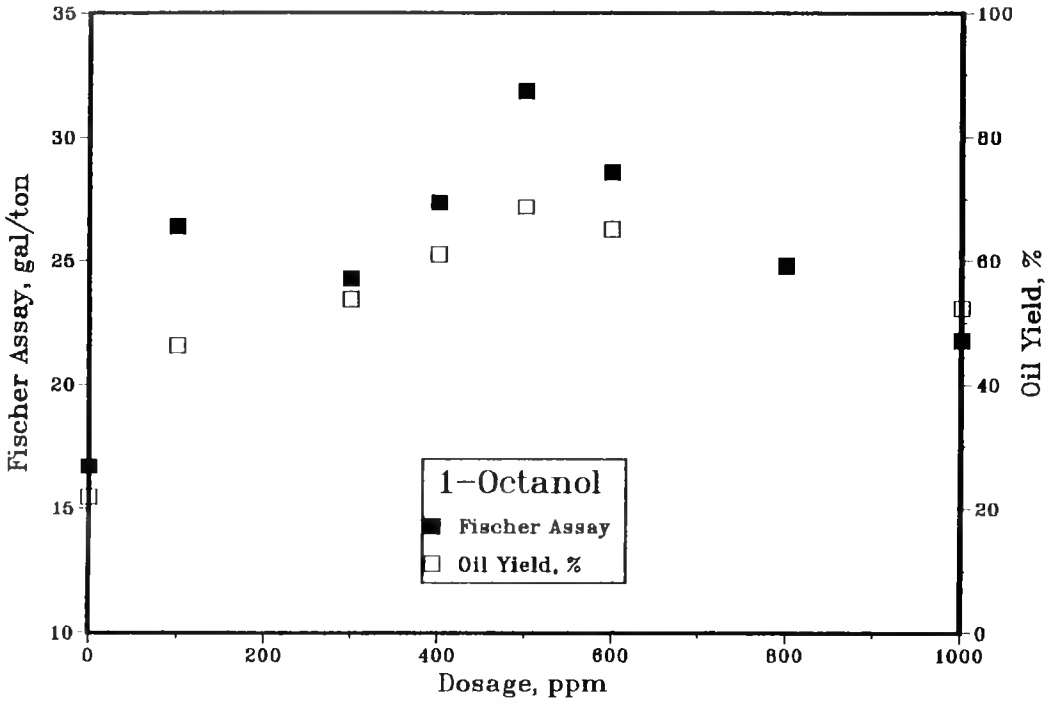

Figure 7. Effect of 1-Octanol in batch tests.

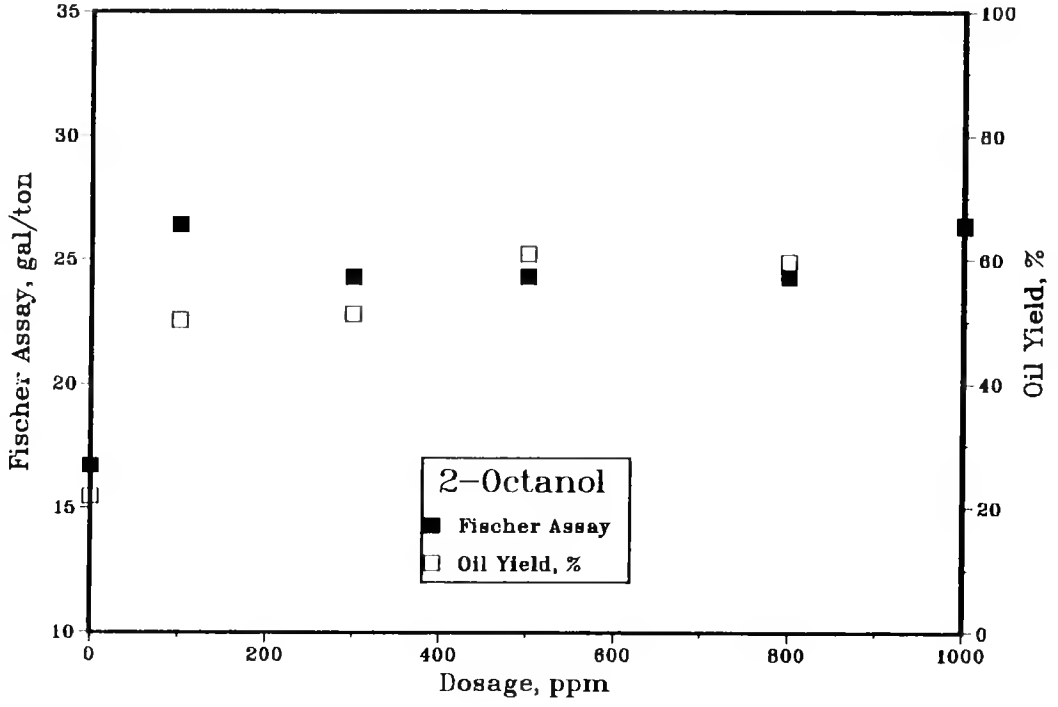

Figure 8. Effect of 2-Octanol in batch tests.

Column Flotation of Eastern Oil Shales

by

C.W. Schultz, J.B. Bates, and W.E. Lamont
Mineral Resources Institute
University of Alabama
Tuscaloosa, Alabama 35487-0204

Abstract: Column flotation tests were performed on Devonian shale samples from Alabama, Indiana, Kentucky, Ohio, Michigan, and Tennessee. All samples tested required ultrafine grinding to yield acceptable products. They did, however, show distinctive differences in their behavior in flotation.

A comparison of the results achievable in laboratory column cells and mechanical flotation cells is made. The data show that in most cases, single stage column flotation is equal to multiple stages of conventional flotation.

The effect of certain column operating and design parameters was investigated in some detail. Parameters investigated included point of feed addition, froth height, column height, air rate, bubble size, and wash water rate. The results indicated that the column height may be a dominant design parameter and that more collection may occur in the froth phase than is commonly believed.

Introduction

The Mineral Resources Institute (MRI) of The University of Alabama is engaged in a research program whose overall objective is to develop a system for the beneficiation of eastern oil shales. Within that broad objective, specific objectives are to determine the potential of column flotation relative to conventional flotation, and to identity the critical design and operating parameters in column flotation.

The current research program which began in 1987 is a continuation of efforts which began at MRI in 1981 and have continued uninterrupted from that date[1,2,3]. This program is the first of that series to focus on newly emerging technologies such as column flotation.

Previous papers from MRI have described the effects of various operating and design parameters on column cell performance. This paper advances our understanding of column cell operation and compares the behavior of various shales in column flotation and in conventional flotation.

Experimental Equipment and Procedure

The arrangement of the column cell and auxiliary equipment for continuous flow testing is shown schematically in figure 1. The feed sump[1] is filled with a sufficient volume of prepared sample to permit a large number of tests to be performed (typically 12). Past experience has shown this is necessary due to high sample variability and variability in the size distribution resulting from ultra fine grinding.

The feed slurry is maintained at about 20% solids and is constantly recirculated and stirred. The sample is metered from the circulating pipe by a peristaltic pump[2]. The feed slurry is diluted with reagentized water[3] by a second peristaltic pump[4]. Wash water[5], also reagentized is supplied through a third peristaltic pump[6]. While this feed system may seem unduly complex it does permit us to independently vary either the wash water

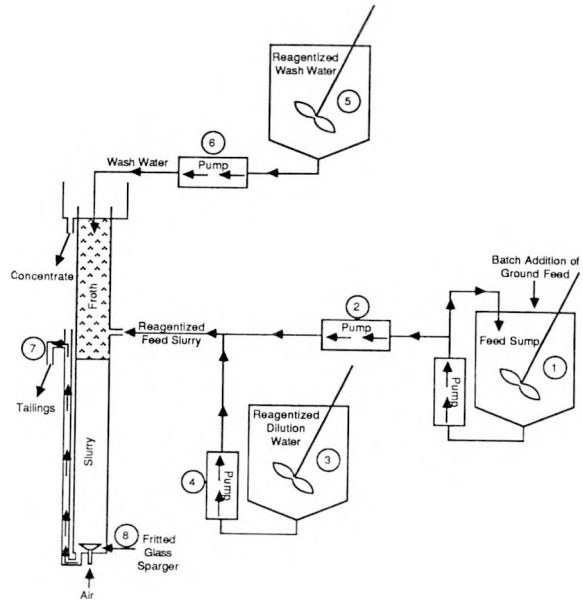

Figure 1. Schematic of Continuous Column Cell Flotation Circuit

rate or the net solids content of the cell. In the tests reported here the feed rate and net percent solids were constant at 12.5 gms/min and 3.3 percent, respectively.

Diluted feed enters the column through 1/4 inch diameter copper tubing and is discharged upwardly at the center of the column. Tailings are discharged through flexible tubing which can be adjusted so as to control the position of the pulp-froth interface.

The column is 7.62 cm internal diameter and 109 cm high. It is made from lucite tubing and is fitted with a 5.1 cm diameter fritted glass air sparger.

In performing a series of tests both the concentrate and tailing are allowed to discharge continuously. The system is allowed to equilibrate for a period of 30 minutes after the pulp and froth reach operating levels. Concentrate and tailing samples are taken simultaneously for timed intervals (five to fifteen minutes, depending on the volume of sample desired). After sampling, a change in operating conditions is made and the system is again allowed to equilibrate. Operating in this fashion a series of six texts can be performed in a day.

Samples are analyzed by measuring their specific gravity with a helium pycnometer. Specific gravity is converted to Fischer Assay oil yield using a previously established relationship. All the data reported here are calculated from specific gravity measurements.

Data from column flotation tests are presented here in the form of grade vs recovery curves. Individual points on the curve represent different air flow rates while all other operating conditions are fixed.

Conventional (mechanical cell) flotation tests were performed in a Denver laboratory flotation cell equipped with motor driven froth paddles. Typically, the tests were performed with an initial solids concentration of 10 percent. Flotation time in the rougher-scavenger stage was fifteen minutes with a total reagent addition of 1.0 lbs/ton of Dowfroth 250.

Grade recovery curves for conventional flotation represent the froth product from the rougher stages and successive stages of froth cleaning.

Development of Basic Operating Conditions for Column Flotation

The primary reason for operating the column cell in a continuous mode is that it permits independent evaluation of such operating parameters as pulp height, percent solids and wash water rate.

In a series of early tests an attempt was made to improve column performance by providing increased residence time. Residence time was increased by increasing the height of the pulp-froth interface, and hence, working volume at a constant feed rate. The pulp-froth interface was raised from 35.5 cm to 71 cm by raising the tailing overflow level. In making this adjustment the pulp level at the higher point was above the feed inlet level (63.6 cm). The result of this adjustment is shown in figure 2. Note that while the oil recovery did increase (at any given air flow rate) there was a more significant decrease in the oil content of the

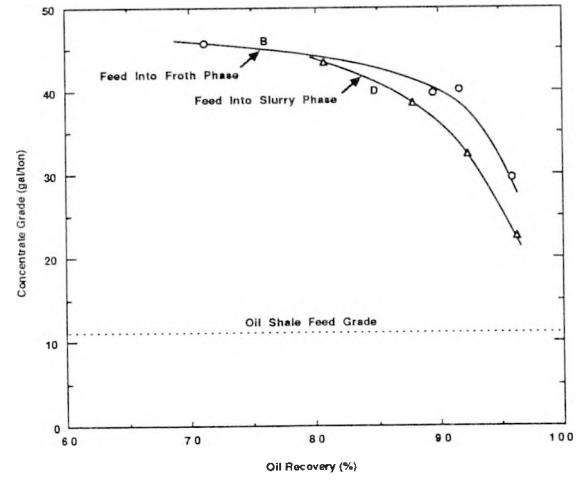

Figure 2. Fischer Assay Oil Grade Versus Recovery Using Column Flotation for Alabama Oil Shale, Effect of Entrance Location of Feed Slurry

concentrate. The net result is an overall more favorable grade-recovery relationship with the pulp-froth interface at the lower level. These observations were made on a sample of Alabama shale ground to a d_{90} of 9.4 microns.

The effect of wash water rate at constant solids content is shown in figure 3. This test performed on the same sample shows that increased wash water rates, as expected, produced a higher concentrate grade but at considerable sacrifice in oil recovery.

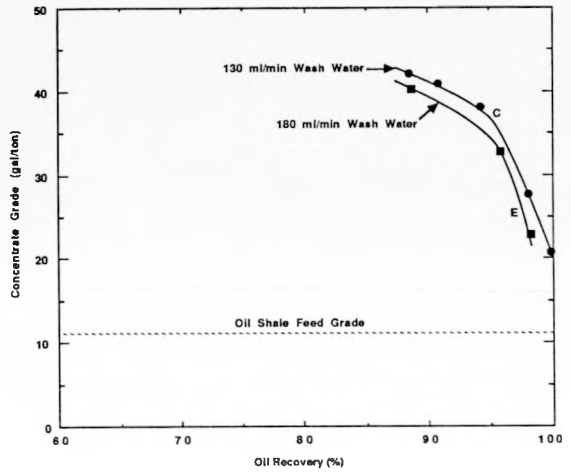

Figure 3. Fischer Assay Oil Grade Versus Recovery Using Column Flotation for Alabama Oil Shale, Effect of Wash Water Addition

The solids content of the pulp has been arbitrarily fixed in this program at 3.3% solids. Earlier work in a batch test mode had shown that any increase in solids is deleterious to both grade and recovery. Feed rate in all tests presented here is fixed at 12.5 gms/minute of dry solids.

The baseline test conditions used in the investigation are summarized in table 1.

Table 1
Baseline Test Conditions

Feed Rate	12.5 gms/min.
Percent Solids	3.3
Pulp Level	35.6 cm
Feed Inlet	63.5 cm
Wash Water Rate	130 cm^3/min

These conditions represent our point of departure in optimizing for a specific case.

Comparison of Eastern Shales in Column and Conventional Flotation

Samples of oil shales from Kentucky, Michigan, Ohio and Tennessee were individually ground, batchwise, for 30 minutes in a laboratory rod mill and for 60 minutes in a laboratory stirred ball mill. Approximately 5 kg of each shale was prepared in this fashion. The ninety percent passing size (d_{90}) and the fifty percent passing size (d_{50}) of each sample are presented in table 2.

Table 2
Comparison of Sizes of Batch Ground Eastern Oil Shales

Shale	d_{90}	d_{50}
Kentucky	12.1	4.8
Michigan	11.3	4.2
Ohio	10.6	4.1
Tennessee	11.2	4.3

A 500 gm portion of each shale sample was removed for conventional flotation tests. The balance of each sample was retained for column flotation tests.

Conventional flotation tests were performed as described earlier. In each case four to five stages of cleaner flotation were employed following a rougher-scavenger stage.

Column flotation tests were performed at baseline conditions and with frother concentrations of 30 and 45 ppm of Dowfroth 250 (1.8 and 2.6 lbs/ton).

The results of the column flotation tests are shown together with the results of mechanical cell flotation tests in figures 4, 5, 6, and 7. Figure 4 shows

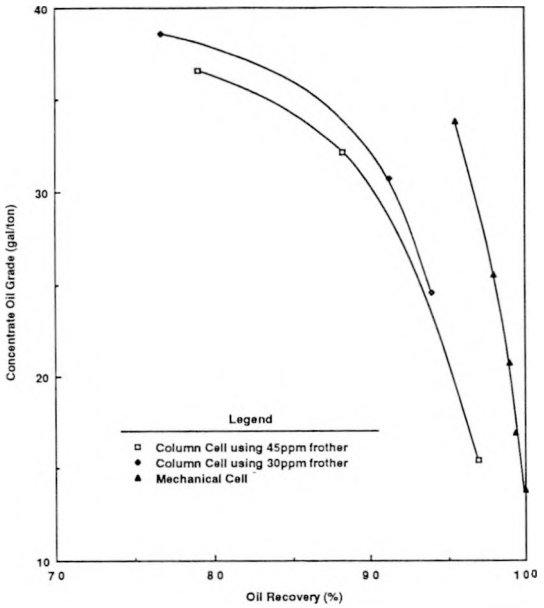

Figure 4. Comparison of Grade Recovery Curves for Column Cell and Mechanical Cell Flotation of Kentucky Oil Shale

that in the case of the Kentucky shale the mechanical cells yield results superior to those attained with the column cell operating at baseline conditions. In all other cases the data show that a single stage of column flotation is at least equal to four or more stages of conventional flotation.

The grade-recovery curves for the four oil shales are shown together in figure 8. Included with these data are

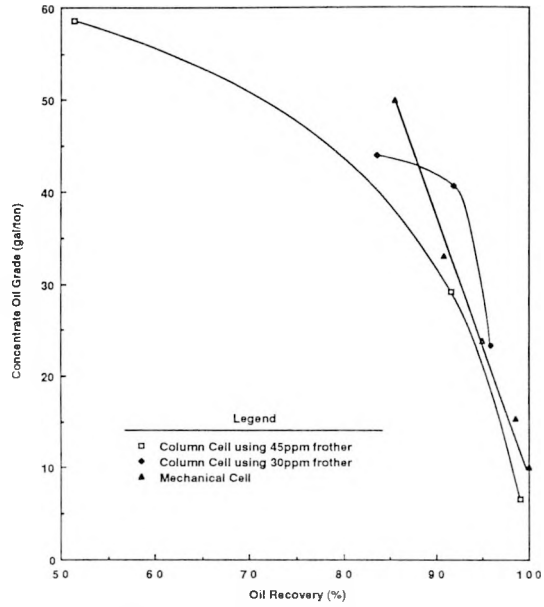

Figure 5. Comparison of Grade Recovery Curves for Column Cell and Mechanical Cell Flotation of Michigan Oil Shale

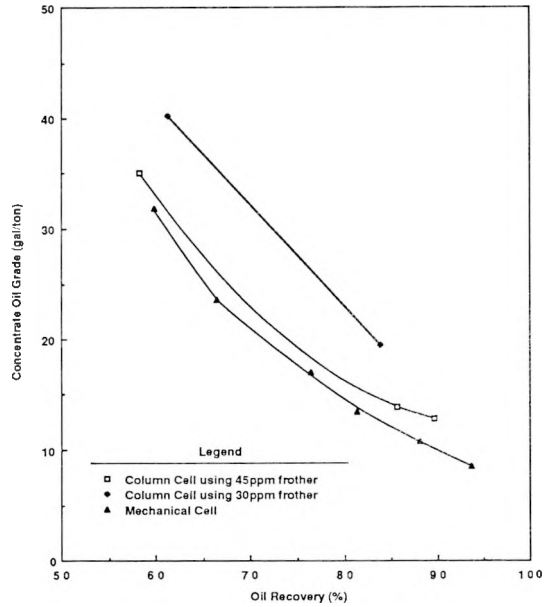

Figure 6. Comparison of Grade Recovery Curves for Column Cell and Mechanical Cell Flotation of Ohio Oil Shale

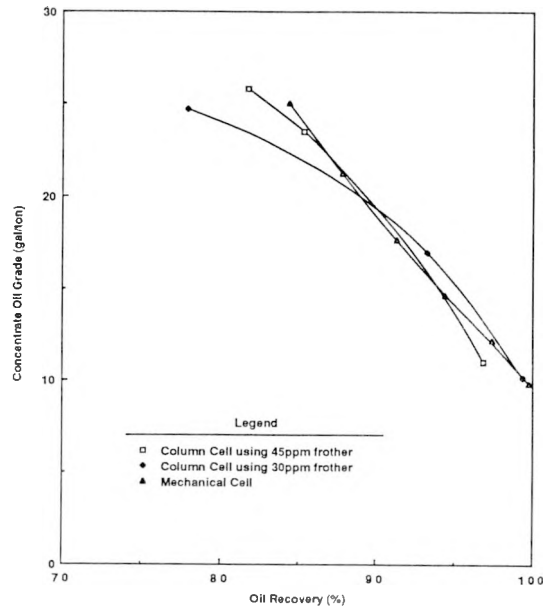

Figure 7. Comparison of Grade Recovery Curves for Column Cell and Mechanical Cell Flotation of Tennessee Oil Shale

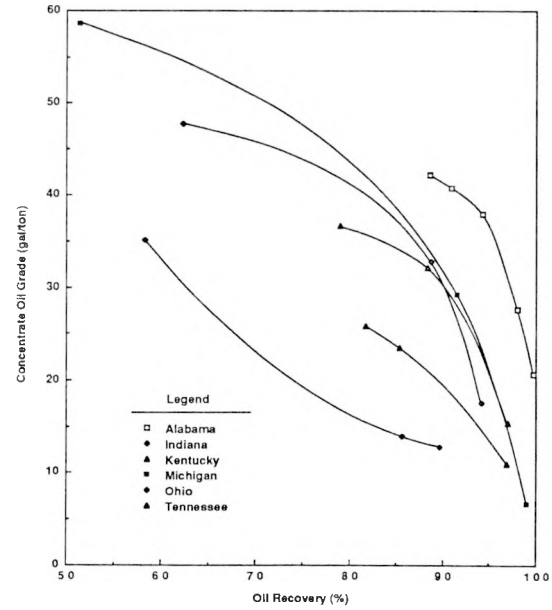

Figure 8. Comparison of Grade Recovery Curves for the Six Eastern Oil Shales Studied

grade and recovery curves for the Alabama and Indiana shales as well. This figure clearly illustrates the difference in behavior of the various shales in flotation. The Alabama shale shows the most favorable response to flotation and the Ohio shale the least favorable. In part, at least, the performance of the Alabama shale may be the result of a slightly finer size distribution than the others (d_{90} = 9.4 microns) and the investigators greater experience with this material. Data published elsewhere (4) have shown that significantly improved recovery can be achieved by reducing the feed rate.

Optimization Tests

Recently a new column cell was built in the MRI laboratories. The new column differed from the one described earlier in that it is built in sections to permit variations in height and in feed inlet position. The variable height configuration also allows us to investigate pulp height and froth depth independently.

A series of tests was performed with the variable height column to gain insight into the effect of feed position and to assess the effect of increased column height. The first pair of grade-recovery curves are shown in figure 9. The lower grade-recovery curve was obtained at baseline conditions, i.e. column height-109 cm, pulp-froth interface 35.6 cm and feed inlet at 63.5 cm. The upper curve in figure 9 resulted from raising the feed inlet to 89 cm while all other conditions were held constant. The effect is similar to that noted in figure 2. The increased height of the feed position resulted in increased recovery in the froth phase with slight decrease in concentrate grade. There is however distinct improvement in the overall grade-recovery relationship.

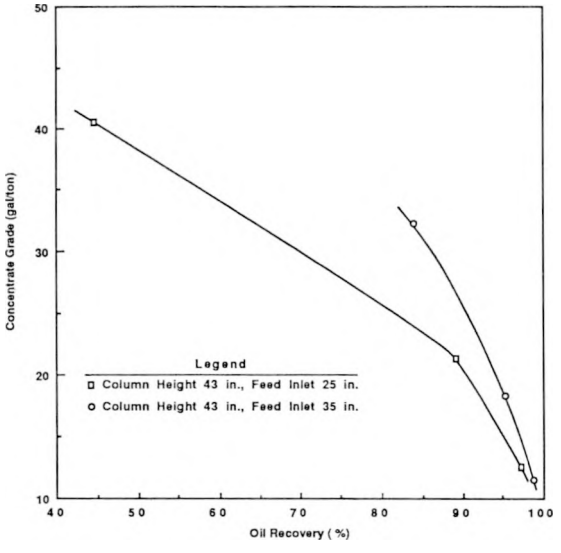

Figure 9. The Effect of Column Height and Feed Inlet Position on Grade - Recovery Relationships

Figure 10 compares the base case with observations made with the column height at 135 cm. Note that both grade and recovery are markedly improved by the increased column height while the effect of raising the feed position is obscured.

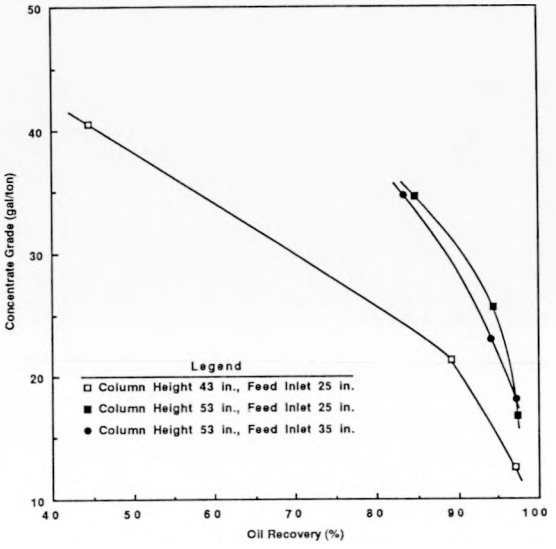

Figure 10. The Effect of Column Height and Feed Inlet Position on Grade - Recovery Relationships

The effect of air sparger pore size at two column heights is shown in figure 11. At the 109 cm column height the finer sparger pore size yields a significantly improved grade-recovery curve. At a column height of 135 cm however the effect of sparger pore size is negligible. While the data are shown as two curves it is difficult to say that the individual points are not all a part of the same grade-recovery curve. All tests shown in figure 11 were conducted with the feed inlet at 63.5 cm and the pulp-froth interface at 35.6 cm.

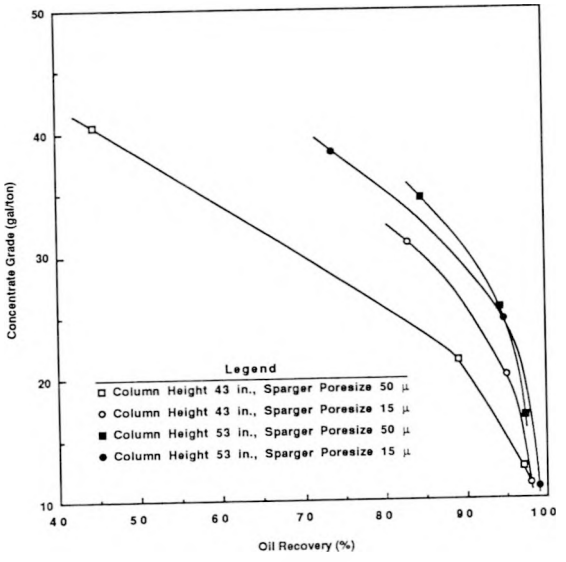

Figure 11. Effect of Column Height and Air Sparger Poresize on Grade and Recovery of Alabama Oil Shale

Conclusions

The data presented here must be regarded as a progress report rather than a finished work. Considerable effort must yet be expended both to improve our understanding of column flotation and to optimize the results achieved on the eastern oil shales.

The results achieved indicate that there is a benefit in operating at lower than normal pulp levels and in introducing feed into the froth phase. Figures 10 and 11 indicated that column height may be a dominant design factor. It should be noted that in those cases the increased column height was devoted entirely to an increase in the froth column.

It is also shown that, in most cases, a single stage of column flotation is at least equal to multiple stages of conventional flotation. We infer from limited optimization tests that the apparent advantage of column flotation over conventional flotation can be further enhanced.

A distinct difference is shown in the flotation behavior of the six shales. This may be attributable to a difference in the liberation characteristics of the various shales. Another possibility is that in certain instances we may have a flocculated condition in which the kerogen rich particles are slime coated by clay minerals. This would result in a decrease in concentrate grade and kerogen recovery.

The results do indicate a need for more focus on flotation chemistry and flocculation-dispersion effects in future investigations.

Acknowledgements

The authors gratefully acknowledge the support of the Department of Energy in funding this project and the Institute of Gas Technology through whom that support was received.

References

1. Hanna, H.S. and Carl Rampacek; "Eastern Oil Shale Investigations at The University of Alabama," Proc. 1981 Eastern Oil Shale Symposium, Lexington, Kentucky, November 15-17, 1981.

2. Lamont, W.E. and H.S. Hanna; "Beneficiation of the Kerogen Content of Eastern Devonian Oil Shales by Flotation," Paper No. 83-621, presented at the SME/AIME Annual Meeting, Atlanta, Georgia, March 6-10, 1983

3. Lamont, W.E., K. Theodorou, and R.C. Rex, Jr.; "Beneficiation-Hydroretort Processing of U.S. Oil Shales," Proc. 1986 Eastern Oil Shale Symposium, Lexington, Kentucky, November 19-21, 1986, pp. 125-131.

4. Schultz, C.W. and John B. Bates; "Operating Parameters in the Column Flotation of Alabama Oil Shale," International Symposium on Advances in Fine Particle Processing, Annual Meeting of the Fine Particle Society, Boston, Massachusetts, August 21-25, 1989.

Beginning of an Oil Shale Industry in Australia

by

Bruce C. Wright
Southern Pacific Petroleum N.L. & Central Pacific Minerals N.L.Sydney, Australia

Summary. The Tertiary oil shale deposits of Queensland Australia contain some 27 billion barrels of insitu shale oil. The Stuart Oil Shale Deposit located near Gladstone (500 km north of Brisbane) contains rich, readily accessible oil shale. The Kerosene Creek Member of the deposit presents an opportunity for selective mining of high grade oil shale (170 litres/tonne). Southern Pacific Petroleum and Central Pacific Minerals (The Companies) have completed preliminary engineering design using Canadian based retorting technology and conventional refining technology to recover the shale oil in a semi-commercial plant to be built 15 km north of Gladstone. The existence of infrastructure including power, water, port facilities and labour creates the most economically attractive oil shale resource in the world.

The objective of the initial plant is to provide the basis for a full scale oil shale industry in Australia and thus support the aim of the Australian Government to maximise energy self sufficiency and minimise balance of payments debts as we enter the 21st century.

Introduction

Preparations are being made for the construction and operation of a semi-commercial plant to process Australian oil shale. This plant is primarily designed to demonstrate the technical feasibility of processing these shales at low cost. Nevertheless it is expected to generate modest profits even at this demonstration level.

This will be the first step in a three staged development of one of the major Australian oil shale deposits which may ultimately provide nearly 10% of Australia's anticipated oil requirements by the end of the century. In turn this development should provide the basis for a full scale oil shale industry in Australia based upon the advantageously disposed oil shale deposits there. New sources of oil are becoming critical since Australian production is declining rapidly while consumption is accelerating.

Oil Supply and Demand

Australia's self sufficiency in transportation fuels has started to decline and not even the most vigorous exploration program is likely to reverse that trend. Figure 1, Australian Oil Supply and Demand, is a compilation of Federal Government and APEA published data and forecasts Australian consumption to rise to 800,000 barrels/day by the year 2000. If we accept their projections of production from known reserves and from new discoveries, Australia will then be facing a shortfall in oil production of nearly 400,000 barrels/day.

At an average price of $US20/barrel, a deficit of 400,000 barrels/day presupposes an import bill in excess of $A3½ billion per year. Australia does not have an industrial base to pay for such imports nor does it have an internal market of a sufficient size to foster such a base.

Furthermore as present low cost Bass straight production declines, oil production costs are likely to soar; in the 15 year period ending in 1984, exploration costs alone to find oil outside Bass straight have averaged over $US13/barrel. With development expenditures added on, such oil can cost over $US20/barrel.

Oil Shale Resources

Eight deposits of Tertiary oil shale have been identified within the coastal region of the state of Queensland, Australia (Figure 2). As shown in Table 1 they contain some 27 billion barrels of insitu shale oil of which our Companies own a net interest in some 20 billion barrels.

The location of these Queensland deposits provides advantages not found elsewhere in the world. They are close to infrastructure including power, plenty of water, port facilities, and labour, and are suitable for cost effective open pit mining. The weather and altitude are similar to the Gulf coast of the U.S. The shale oils derived from these deposits are also relatively low in sulfur, nitrogen and metal impurities. The combination of these factors creates the most economically attractive oil shale resources in the world. They would seem to provide a natural stepping stone of experience for the development of the much larger, but more difficult, shale reserves to be found in the U.S.

Condor deposit has been the subject of a joint study with a Japanese consortium, but although results were promising, the Japanese seem to have lost interest in further shale development. The Rundle deposit is still under joint study for development between our Companies and Exxon as the operator. Shell has just purchased a 42% interest in Yaamba with Peabody Coal retaining an equal interest and the Companies maintaining a minority interest. Nevertheless the Stuart deposit, wholly owned by our Companies, is arguably the most attractive deposit as a starting place for development.

The Stuart Deposit

The Stuart oil shale deposit is situated in the southern half of the Narrows Graben immediately northwest of the industrial city of Gladstone (Figure 2). Gladstone is a deep-water port with an established labour force, power, water and support facilities. Resources total 3.05 billion barrels of oil insitu with a 50 litre/tonne cut-off grade with an average grade over the whole deposit of 94 litres/dry tonne (LTOM). Average overburden to ore ratio is less than 1:1 and both overburden and shale are soft easily dug material which is ideally suited to open pit mining - no blasting is required.

Of great advantage, the deposit contains a relatively rich zone (Kerosene Creek Member) close to the surface (Figure 3). This zone contains the equivalent of 155 million barrels averaging 128 LTOM including 110 million barrels averaging 167 litre per dry tonne and enhances the economics of the demonstration stage and second stage of the planned development.

Canadian Tar Sands

The Canadian experience with Athabasca tar sands is instructive for Queensland shale industry development. The two synthetic crude plants presently processing Athabasca oil sands at Fort McMurray, Alberta have a combined production of nearly 200,000 barrels/day, 20% of total Canadian oil production. The overall processing scheme is remarkably similar to that required for oil shale. As shown in the comparison Table 2 the oil sands operation includes open pit mining, feed preparation, release of the bitumen by a hot water extraction process, followed by coking, and then hydrotreatment. In oil shale processing bitumen extraction and coking processes are combined in the retorting step (as will be the case with Taciuk processed oil sands).

Oil Shale Processing System

Accordingly our Companies began working closely with the Alberta Oils Sands Technology and Research Authority (AOSTRA) and UMATAC Industrial Processors After substantial previous testwork with Queensland shales through six other available technologies, the Companies found that the Taciuk processor offered an optimum combination of effective operation, simplicity, and low capital and operating costs. Developed originally by a Canadian mining engineer of the same name in cooperation with UMATAC as a second generation process for oil sands, the process has been supported by AOSTRA. With only minor modifications, the process is ideally suited to oil shale.
The AOSTRA Taciuk Processor consists of a horizontal rotating vessel containing 4 compartments which house the following process steps:

1. Preheat of the Dried Shale
2. Retort Zone - Oil Shale Pyrolysis
3. Combustion - Spent Shale Combustion
4. Cooling - Heat Recovery from Combusted Shale

Figure 3. schematically shows the arrangements and process flows.

The Processor operates at atmospheric pressure and is in heat balance. Sensible and reaction heat is provided by combustion of a portion of the coke on the spent shale from the retort. The Processor rotates at 4.5 rpm and is driven by a multiple tyre drive system.

In the preheat zone, shale drying is completed. It then enters the retort zone at 250° C through a seal and it's temperature is raised to approximately 500° C by mixing with hot combusted shale ash. The pyrolysis of the kerogen takes place rapidly and super-heated oil and fuel gas is generated. The vapours and gases are withdrawn via a central vapour tube and pass to the oil recovery section.

The spent shale from the retort flows through seals to the combustion zone where a portion of the residual carbon on the shale is burnt with preheated air to provide the heat for the retort. The shale ash at approximately 750° C recycles to the retort via seals. The combustion zone flue gases and the product shale ash flow countercurrent in the shell outside the preheat zone to indirectly preheat the incoming raw shale. The cooled shale ash discharges from the Processor into a moisturizer for dust control before disposal with the mine waste. The Processor flue gases and the dryer flue gases flow to a common wet scrubber before discharge through a stack. AOSTRA carried out bench scale tests for the Companies in 1985 followed by batch tests in 1986. After encouraging results, 2,000 tonnes of Stuart shale were sent to Calgary for bulk testing in the 80 tonnes/day pilot plant there. After a very satisfactory five months testing program, the decision to use the Taciuk systems for the projected development of the Stuart deposit was confirmed.

DEPOSIT	INSITU RESOURCES	SPP/CPM INTEREST
CONDOR	9.65 billion barrels	100.00%
DUARINGA	3.72 billion barrels	100.00%
LOWMEAD	0.74 billion barrels	50.00%
NAGOORIN	2.65 billion barrels	50.00%
NAGOORIN SOUTH	0.47 billion barrels	100.00%
RUNDLE	2.65 billion barrels	50.00%
STUART	3.05 billion barrels	100.00%
YAAMBA	4.14 billion barrels	16.67%
TOTAL	27.07 billion barrels	20.60 billion barrels

Table 1: Table of Deposits

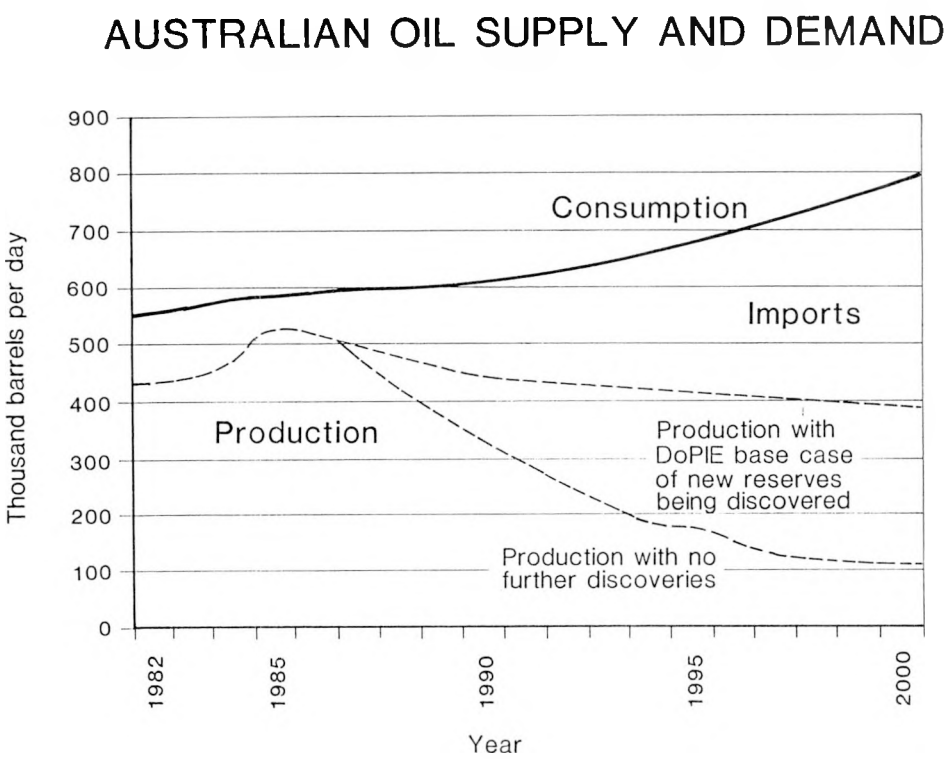

Figure 1

TABLE 2

SYNCRUDE COMPARISON

Alberta OIL SANDS	Stuart OIL SHALE
1. On average, the yield from one tonne of oil sands ore is half a barrel of syncrude (API gravity 35)	1. On average, one tonne of Stuart oil shale also yields half a barrel of syncrude (API gravity 41)
2. The bitumen in oil sands has a hydogen:carbon atomic ratio of 1.50:1	2. Kerogen, the productive ingredient in oil shale, also has a hydrogen:carbon atomic ratio of 1.50:1
3. Produces Syncrude	3. Produces Syncrude
4. Cash operating costs are slightly higher for oil sands, mainly in mining	4. Cash operating costs for Stuart shale oil reflect cheaper mining
5. Oil sands mining: .Technique — Open pit .Rock Hardness — Very soft in summer, Very hard in winter .Disposal Method — Tailings dams .Typical Waste:Ore Better than 1:1	5. Oil shale mining: .Technique — Open pit .Rock Hardness — Medium soft all year .Disposal Method — Inpit and expit dumps .Typical Waste:Ore Better than 1:1
6. Location and infrastructure: .1200 miles to Vancouver, the nearest shipping port. .Fort McMurray weather is sub-zero 5 months of the year. .All infrastructure was imported specifically for oil sands development.	6. Location and infrastructure: .Stuart is just 6 miles from Gladstone Port .Gladstone's climate is similar to US Gulf Coast .Gladstone already has a substantial industrial infrastructure.

At present price levels, both tar sands plants are profitable

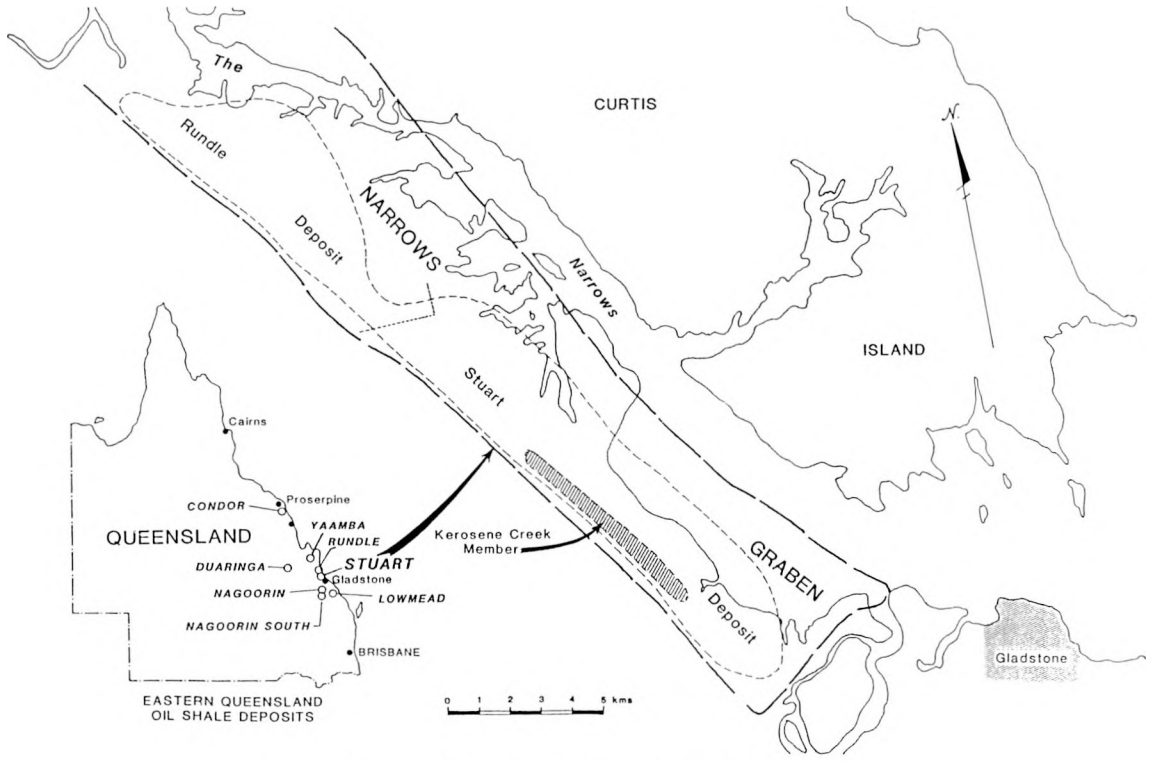

Figure 2: Location of The Narrows Graben

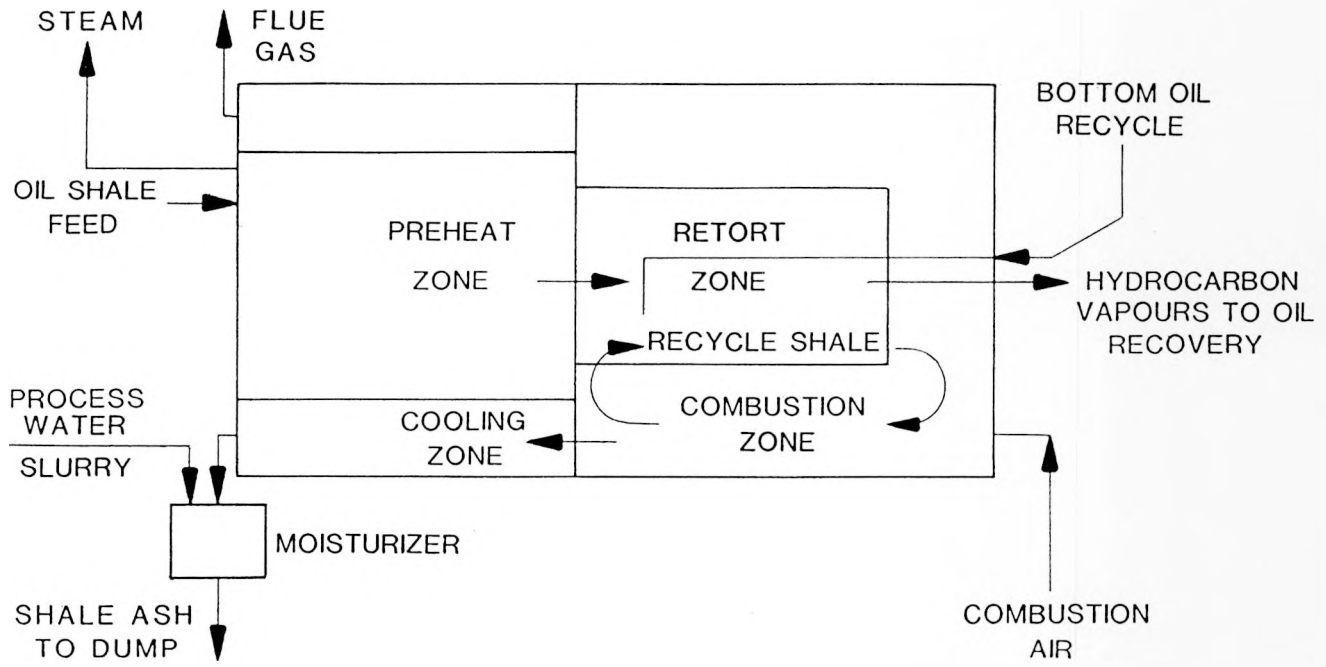

Figure 3: AOSTRA-Taciuk Processor

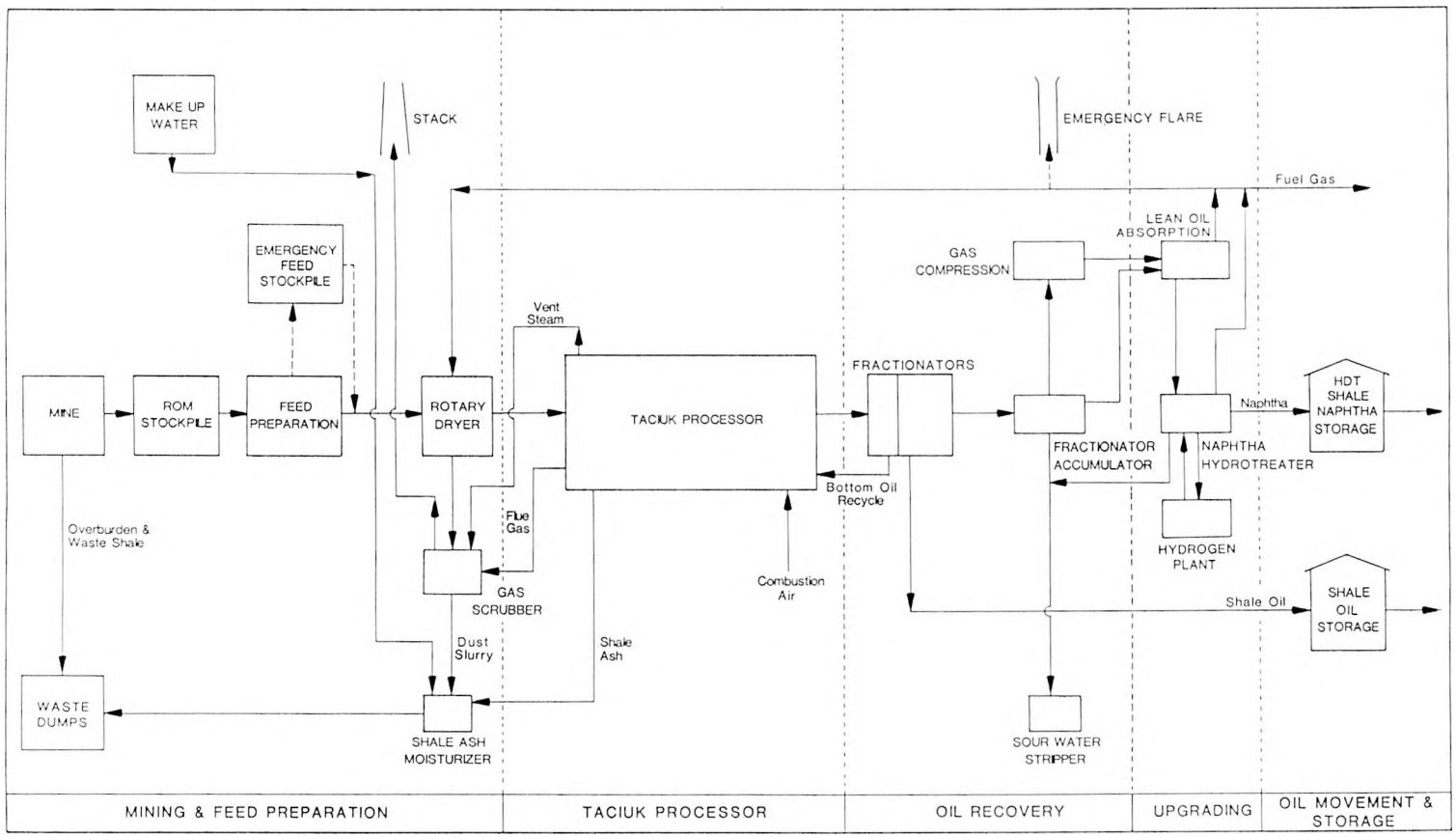

Figure 4: Stuart Initial Commercial Plant Block Flow Diagram

An agreement with AOSTRA grants the Companies exclusive Taciuk process rights for Australia and license free rights in the rest of the world.

Commercial Demonstration

Based upon successful completion of the pilot plant tests, screening study engineering was undertaken to firm up the project definition for a semi commercial plant. The current conceptual design is for a plant processing 6,000 tonnes per stream day of as mined feed shale at an average grade of 170 LTOM and producing, after achieving design capacity operation, approximately 1650 barrels per stream day (BPSD) of upgraded naphtha, and 2600 BPSD of fuel oil. The upgraded naphtha will be suitable as refinery feedstock for gasoline production and the fuel oil can be sold in various fuel oil markets within and without Australia.

The underlying principles upon which plant design has been based are:

1 - Capital, operating costs, and time of construction are kept as low as are consistent with demonstration of the processing technology.

2 - Size of the plant is sufficient to ensure scale up to full commercial size with little technical risk.

3 - The upgraded product can benefit from the excise exemption granted in Australia upon all gasoline products derived from shale oil and the non upgraded products can easily be sold in fuel oil markets.

4 - The income derived from product sales will cover all the plant capital, operating, and financial charges.

Demonstration Plant

A block flow diagram of the plant is shown in Figure 4. which comprises the following components:

1 - A conventional open pit mine capable of furnishing 6,000 tonnes/stream day of selectively mined ore with an average grade of 170 LTOM to the plant. Contract mining will be utilized for this purpose.

2 - Feed preparation to crush the shale to a top size of approximately 6 mm using impact type crushers. It is then dried to approximately 4% free moisture in a conventional rotary dryer.

3 - A Taciuk Processor system as described previously.

4 - Mine waste and shale ash will be trucked to a waste dump adjacent to the mine. As soon as the mine pit has progressed sufficiently, the mine waste and shale ash will be back filled into the pit. The dumps will be covered with a growth layer of top soil and rehabilitated. The dump design and rehabilitation will follow recommendations derived from previously completed environmental acceptability testing programs.

5 - The oil recovery section employs conventional oil refinery technology. The super-heated hydrocarbon vapours produced in the reaction zone pass through cyclones to remove trace shale particles prior to entering the primary fractionator. In the fractionator condensed oil heavy ends and shale fines are concentrated prior to recycling to the reaction zone for pyrolysis to light useable oil product.

The 510°C minus boiling point oil vapour plus gases then pass into a secondary fractionator where condensation of the remaining oil vapour occurs to produce a shale oil, shale naphtha, condensed water and uncondensed hydrocarbon gases. The shale oil is run down, after cooling, to storage tanks and the water is pumped to a sour water stripper for treatment. The naphtha is directed to the naphtha hydrogenation section.

The uncondensed vapours pass from the top of the secondary fractionator to a gas compressor which provides condensate to recover entrained oil vapours for enhanced oil liquid recovery. The gas compressor, via a control loop, also provides the pressure control element to the reaction zone of the Processor. Further recovery of entrained oil vapour is by a lean oil absorption system which uses a cooled stream of shale oil to absorb residual oil vapour and return it to the fractionator. The produced stripped off gas which contains uncondensed LPG and light hydrocarbon gases is used as fuel in the dryer and is available for other fuel gas applications.

6 - The liquid stream from the lean oil absorption system, containing butenes and shale naphtha, is fed to a naphtha hydrotreater where olefins are saturated and sulphur, nitrogen and oxygen are removed by reaction with hydrogen over a catalyst.

The hydrotreater product is fractionated into a butane stream and a hydrotreated naphtha stream with a Reid Vapour Pressure not exceeding 70 kPa. The hydroheated naphtha is of suitable quality for processing in the catalytic reformers of existing Australian oil refineries and is run down to storage.

The butane stream is treated to remove sulphur and used as the feedstock to a hydrogen plant.

Sour water from the hydrotreater is pumped to the sour water stripper for treatment.

7 - Raw water is supplied by nearby Boat Creek Reservoir. Power is supplied from the Capricornia Electricity Board Sub Station at Boat Creek. Telephone service is provided from existing service.

8 - Product transport is by pipeline from storage tanks at the plant site to ship loading facilities at an existing wharf 3 kilometers to the south east.

Stuart Development Plan

The Stuart development plan is shown schematically in Figure 5. Two further stages of development are planned after successful operation of the demonstration plant has removed any technological risk associated with production.

Stage 2 a full size commercial module, probably of 25,000 tonnes per stream day capacity (Taciuk processor about 40 ft in diameter and 160 ft in length).

Stage 1	Stage 2	Stage 3
	Scale Up / Replicate	
Commercial Demonstration	Commercial Module	Full Commercial Plant
Oil Shale Feed		
6,000 tpsd high grade	25,000 tpsd intermediate grade	125,000 tpsd average grade
Products		
4,250 bpsd Hydrotreated Naphtha and Fuel Oil	14,000 bpsd Syncrude	60,000 bpsd Syncrude

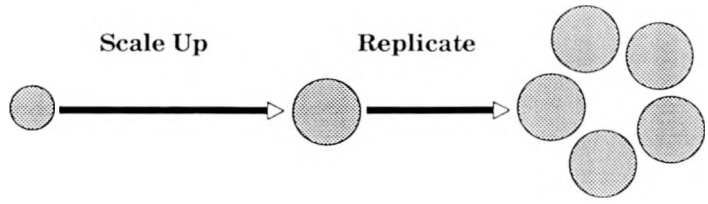

Figure 5: Stuart Development Plan

Stage 3 replication of Stage 2 in modular form for a capacity now planned at 125,000 tpsd.

The Stage 2 plant will utilize the remaining ore to be found in Kerosene Creek with average grade of 140 LTOM while Stage 3 plant will then start using the main body of the deposit averaging 94 LTOM.

Capital Costs as presently estimated in mid-1989 U.S. Dollars would be as follows:

	in million $US (1989) Capital Cost
Stage 1	90
Stage 2	280
Stage 3	1220

The total cost of the Stuart development, including the Stage 1 Demonstration plant, would therefore be approximately $US1,590 million for a production of 66,500 barrels per calendar day.

With the technology risk removed, the Stage 2 and Stage 3 plant can be financed under customary project finance terms. With 70% debt and current interest costs, this complete installation can return an adequate profit without any excise gasoline tax exemption with product prices equivalent to a Dubai oil price of about $US17/barrel. The approximate time table for such development:

Construction and one year operation of Stage 1	=	3 years
Construction of Stage 2	=	3 years
Construction of Stage 3	=	4 years
Total		10 years

Following this timetable the Stuart Development could be replacing over 15% of Australia's projected crude imports by the year 2000.

Niche Market Assessment for Eastern Oil Shale

by

Jerry E. Sinor
J.E. Sinor Consultants Inc.
Niwot, Colorado 80544

Abstract. In an era of low oil prices, synthetic fuel projects cannot be economically justified. However, it is extremely desirable that research and development of synthetic fuels continue, so that improved technology will be available at the time synthetic fuels become necessary. Financing of such research and development is difficult. This paper examines the question of whether nonfuel products from oil shale could be profitable enough that a small-scale oil shale facility could stand on its own. This would make it possible to maintain an ongoing oil shale development effort at a large enough scale to make significant technical progress.

A major problem in considering nonfuel markets for oil shale products is finding a market large enough to accept all of the output from even a small-sized oil shale facility. Price-volume relationships for chemical products were examined. It was concluded that the target market slate should be no more than two or three products. Products which might fall in the desired price-volume range are discussed.

Introduction

The production of conventional refined fuels, such as gasoline, jet fuel and diesel fuel, from oil shale would not be economically feasible under current market conditions. Previous work has shown that the present use of heavy fuel oil in the eastern oil shale region is too small to market unrefined crude shale oil[1]. Therefore, the approach used in this study was to focus on nonconventional products, having perhaps a small potential market size but providing an opportunity to sell oil shale products at considerably more than crude oil equivalent price. To find such potential market niches, it is necessary to emphasize and preserve the differences between shale oil and petroleum, rather than try to make shale oil simply a substitute for petroleum.

The probability of increasing profits by emphasizing nonfuel products under current market conditions is recognized by synthetic fuels projects worldwide. The best example is perhaps Sasol in South Africa. For 1988, Sasol was able to achieve a 34.8 percent increase in earnings per share, despite a reduction of 16 percent in operating income from synfuels. This results from their emphasis on coproduction of chemicals. They now market over 80 different products other than motor fuels. Petrobras in Brazil is putting down shale oil asphalt test strips and modifying retort operation to increase byproduct gas. Oil shale industries in China and the Soviet Union depend heavily on the production of nonfuel products. They claim to produce over 50 products.

Historical Niche Markets for Oil Shale

A historical review of world oil shale industries reveals that nonfuel products or byproducts have been essential features of the most important oil shale industries which existed in the past. Byproducts accounted for up to 60 percent of total income (Sweden). Major byproducts which have been produced include bricks from spent shale, ammonia, sulfur, ammonium sulfate, waxes, lubricants, wood preservatives, liquefied petroleum gases, coke, solvents, medicinal products, cement, asphalt, cresylic acids, and other tar acids.

A historical example of a niche market, or specialty market, was the early development of the oil shale industry in New South Wales, Australia. In about 1865, torbanite from New South Wales was studied and it was discovered that only a five percent addition of this unusually rich shale (180 gallons per ton) to coal would increase the luminosity of producer gas by a factor of six. Producer gas was being widely used for illumination at that time.

As a result, an industry developed in New South Wales, mining and selling the richest shale (80 to 200 gallons per ton), called "export shale," to the United States and Europe. The lower quality shales (less than 80 gallons per ton) were retorted locally for production of liquid fuels and related products. The torbanites of Australia became known as kerosene shales. Eventually the invention of the incandescent mantle, in 1911, ended the export market for raw oil shale.

A niche market, by definition, is a small market requiring product specifications or characteristics which can be met only by a particular producer or product. That product can then command a premium price.

Synthetic Fuels Versus Chemicals

If we wait until declining availability has again raised the price of oil, many years will be required to develop the technology needed for large-scale conversion to synthetic fuels. It is clear that an intermediate stage would be highly desirable--a period when oil shale technology could be developed on a self-supporting basis without relying on fuel prices.

Such a phase might be possible by initially making products for nonfuel markets. In contrast to the markets for fuels, where prospects for increased demand are highly uncertain, the chemical sector in general is expected to continue to out-perform the industrial average. The International Trade Administration's 1988 U.S. Industrial Outlook predicts that organic chemicals production will grow at an annual rate of 2.5 to 3.0 percent through 1993.

There are several other advantages to making products for the chemicals market rather than the fuels market. First, the prices are generally higher. Second, the prices of some products are partially insulated from the effect of fluctuations in crude oil prices, although there is a well-documented long-term correlation between the two (Figure 1). Third, production is often arranged on a contract basis, giving more stability to operations and making it easier to finance new ventures.

A wide variety of chemical compounds are found in the liquids produced by retorting oil shale. In attempting to turn these liquids into marketable chemical products, it may be necessary to transform some of the components into chemical compounds with more desirable properties. Several approaches are possible:

1. Find a use for the entire stream
2. Separate the stream into two or more broad mixtures for sale
3. Separate out and sell the individual components
4. Transform the entire stream
5. Transform the broad mixtures
6. Transform the individual components

The results of many studies suggest that, in general, it is not possible to find a premium market through either Route 1 or Route 4 above. Because of the small concentrations of individual compounds in shale oil, it will be demonstrated that Routes 3 and 6 are of little economic importance. This will lead to the conclusion that attention should be concentrated on broad-cut fractions, which, because of their inherent characteristics, can either be sold for a premium or transformed into products which can be sold for a premium.

Composition of Shale Oil

Shale oil is an extremely complex material. A typical raw shale oil probably contains 1,000 to 3,000 identifiable carbon number homologs and many more positional

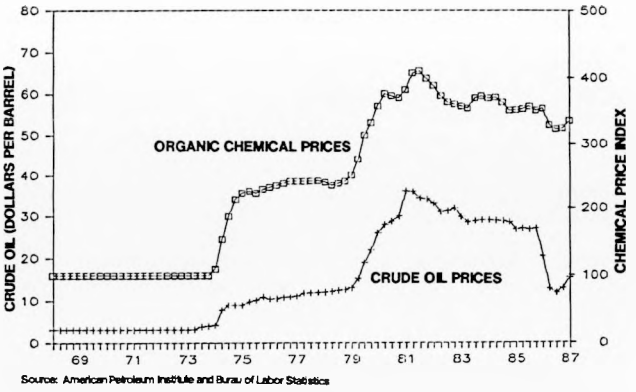

Figure 1. Crude oil and organic chemical prices.

isomers. Because many of these materials are commercially synthesized and sold as specialty products or fine chemicals at prices of up to several dollars per pound, it is intriguing to consider the possibility of extracting them directly from shale oil.

Little information on the realistic concentrations of individual species in shale oil can be found in the literature. A single sample of oil shale can be made to yield oil with widely different portions of saturates, olefins and aromatics, simply by altering the pyrolysis temperature. A detailed analysis for individual chemicals has meaning only if it can be related to commercial operating conditions for a particular process.

The problem posed by shale oil is that all concentrations of individual compounds are very low. Most of those present at more than trace levels are low molecular weight paraffins, which are obtainable from petroleum in large quantities at relatively low prices. The great majority of individual compounds are present at levels of much less than 0.5 percent on the whole shale oil.

Individual compounds that have been identified and for which commercial uses and prices have been established include: all the normal paraffins, several cycloparaffins, alpha olefins, benzene, phenol, cresol, xylenol, and alkylated versions of all the preceding; aniline, quinoline; pyridine, lutidine and collidine; thiophene; indene, naphthalene, pyrene; formic, acetic, heptanoic and benzoic acids; acetonitrile, butyronitrile; and many others.

Market Limits on Individual Chemicals

It is tempting to take the list of chemicals identified above, multiply the concentration of each times current market prices, and conclude that the result is the value of specialty chemicals that could be derived from each barrel of shale oil. If this exercise is carried out, about 20 pounds of saleable chemicals per barrel of shale oil can be identified in western shale oil[2]. On the basis of GC/MS distribution patterns, it is assumed that a similar result could be obtained with eastern shale oil. Even 20 pounds per barrel, if sold at research chemical prices of up to $10 per pound, or even more, would amount to $200 per barrel of shale oil. However, there are two serious flaws with this estimating procedure.

The first flaw is that separation and purification costs are not considered. The fact is that most of the cost of these chemicals, if obtained from complex sources, in the quantities and purities normally furnished, is due to separation and purification costs. Very little of the final selling price could be assigned to the value of the crude

feedstock. This flaw might be glossed over with a statement that, regardless of initial feedstock value, a specialties business could be profitable enough overall to subsidize the production of shale oil. However, there is a second, more serious, fundamental flaw.

Even a small yield, such as 20 pounds per barrel, when multiplied by the production from any reasonably sized oil shale facility, will result in the production of individual chemicals at rates greater than the market could absorb. Compared to fine chemical operations, an oil shale retorting facility is a mammoth, capital intensive operation, and large volumes of product must be sold to carry the capital charges. At 20 pounds per barrel, a 3,000 barrel per day plant would manufacture over 20 million pounds of individual specialty chemicals per year. This is a large amount with respect to current consumption of the highest priced species. When large volumes of a product (with respect to existing consumption) are brought to market, the natural result is a drop in prices.

Decreasing costs (and therefore decreasing prices in a competitive field) as a function of increasing scale of production are a well-recognized phenomenon. However, what has not been recognized is the way this behavior can be used to estimate revenues as a function of project size in the chemical industry. In Figure 2, sales volumes and average sales prices are plotted for all individual synthetic organic chemical compounds for which data were reported to the United States International Trade Commission in 1987. The strength of the correlation is surprising, and a number of useful generalities can be derived from it. For instance, no chemical produced in quantities greater than 100 million pounds per year sells for over $1.00 per pound. With only a single exception (a dye) no chemical produced in quantities greater than one million pounds per year sells for over $3.50 per pound.

Below about one million pounds per year, the curve flattens out, and a wide range of prices is seen. This may be interpreted as evidence of the existence of noncompetitive market niches. Above one million pounds per year, all chemicals become commodities, and competition keeps prices in a narrow range determined by the economies of scale at any given production level.

At production levels below 100,000 pounds per year, all synthetic organic chemicals sell for at least $1.20 per pound. Since these chemicals are derived from a wide variety of different types of feedstocks, it is concluded that the economics of production and marketing at this level require prices of over $1.00 per pound regardless of feedstock cost. In other words, the minimum costs of extraction, purification and marketing are on the order of $1.00 per pound.

The question of what price could likely be obtained for selected chemicals produced in a shale oil facility is difficult to answer. However, based on the amount of individual chemicals that can be extracted from shale oil and the use of the curves developed in Figure 2, it is possible to derive the maximum revenues that probably could be achieved from sales of individual chemicals.

It becomes evident from Figure 2 that it is not practical to produce only the more highly priced chemicals, because those chemicals are in low demand. To illustrate, the following analysis has been made for a 3,000 barrel per day operation, which would produce 350 million pounds of shale oil per year.

Detailed chemical analyses of shale oil suggest that no more than about five percent of total shale oil could be easily extracted and separated into individual compounds. Therefore, if 10 individual chemicals are to be produced, we know that their average concentrations will be less than 0.5 percent, and 1.75 million pounds of each chemical would be produced annually. If each of these chemicals is to be introduced into existing markets without depressing prices, each should account for no more than, say, 10 percent of total production of the particular chemical. Thus,

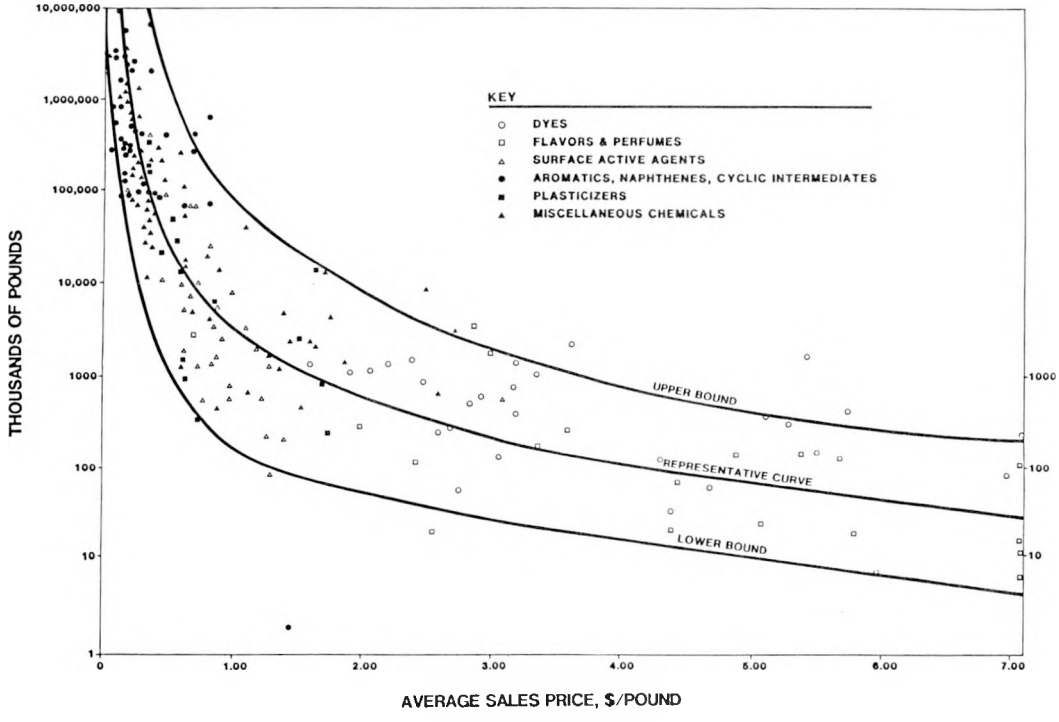

Figure 2. Price-volume relationship for synthetic organic chemicals.

17.5 million pounds per year represents the market level on which prices can be based. The dashed line of Figure 2 represents this production level. At this level, according to the figure, we can predict with reasonable confidence that the average selling price for these materials will be about 60 cents per pound. For the 10 chemicals at 0.5 percent concentration and 60 cents per pound we then calculate that an income of $9.60 per barrel could be obtained. Obviously the facility could not be profitable on the basis of these chemicals alone.

Considering larger numbers of products improves the gross income but not greatly. When more chemicals are considered, the average concentration in the shale oil will be lower. If 20 chemicals are recovered at an average concentration of 0.25 percent, then the production of each will be 876,000 pounds per year. With a minimum market of 8.76 million pounds per year, the average sales price will be 75 cents per pound, and the total income $12.00 per barrel. Thus, income per barrel has increased only slightly, even though extraction and purification costs will have increased greatly due to handling twice as many compounds.

A summary of results appears in Figure 3. Three lines are shown for three different assumptions on the total fraction of shale oil that would be separated into individual chemical species -- 5.0 percent, 7.5 percent and 10 percent. The dashed line represents the concept of incremental additions to the product line, starting with 10 products and 5 percent recovery, adding 10 more products and achieving 7.5 percent recovery, and then adding 20 more products (for a total of 40) to boost total recovery to 10 percent. Even at a yield of 10 percent on total shale oil, which is not considered to be achievable, gross income only reaches about $23 per barrel.

The conclusion reached is that individual chemicals, present in trace amounts, cannot drive the economics of even a small-scale shale oil plant. Rather, a marketing scheme must be developed that makes it possible to sell essentially all the shale oil into large-size markets as a limited number of products which all sell for a premium over crude oil prices.

Broad-Cut Specialty Products

Identification of Potential Niches

The previous section has shown that it is not practical to consider a shale oil operation designed to produce only specific, individual chemicals that could be extracted from raw shale oil. The economics of shale oil production are such that large (relative to the chemical specialties business) cash flows are required, even for what would be considered a relatively small operation. The small concentrations of individual chemicals in shale oil, combined with the volume-price relationship for synthetic organic chemicals and the minimum feasible size for an oil shale facility, result in an economic situation unfavorable for the production of individual compounds.

The other extreme of production possibilities is simply to sell the whole shale syncrude as a conventional refinery feedstock--a straight replacement for petroleum. It is clear, from many studies that have been carried out, and from Unocal's experience with their Parachute Creek project, that this is not practical at any scale, much less for a small-scale (less than 10,000 barrels per day) project at today's crude petroleum prices.

We are left, then, with a set of possibilities to explore in the range between selling whole shale oil as a refinery feedstock and selling individual chemicals ex-

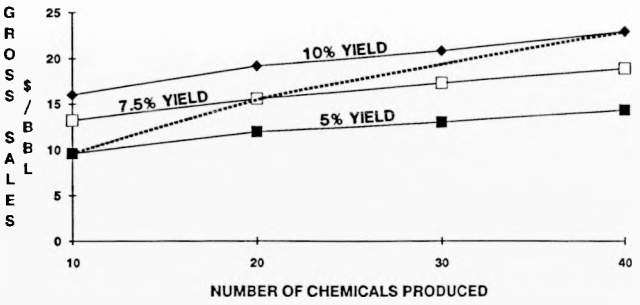

Figure 3. Maximum gross revenues for sales of individual chemicals.

tracted from the oil. For simplicity, this study refers to all such possibilities as specialty products, even though some of them are large-volume commodities on a par with petroleum refining products. The key distinction is that, to be considered, each possibility must exploit some unique characteristic of shale oil such that it could command a higher price than an equivalent volume of petroleum crude oil. Because all such potential products will contain a broad range of chemical constituents, they are termed broad-cut specialty products.

There are several search techniques through which one might hope to discover product possibilities. These include:

- Examining chemical classes present
- Modification of chemical composition
- Analogy with petroleum crude fractions
- Analogy with coal tars
- Analogy with natural products
- Observation of chemical and physical properties
- Observation of market needs
- Consideration of foreign experience

Examining Chemical Classes Present

The compounds in shale oil can be sorted into the same classes as those in petroleum crude. It is then useful to see whether differences in relative proportions of the different classes, or in the make-up of individual chemicals in a class, can suggest a premium value for shale oil.

A classification into paraffins, olefins, naphthenes and aromatics reveals some possibilities. The presence of high molecular weight paraffins suggests that waxes might be produced. Higher concentrations of olefins than would be expected in crude oil suggests that it might be a good feedstock for olefins production in the petrochemical industry. The presence of naphthenes suggests the possibility of making a high density jet fuel.

If the nonhydrocarbon classes of chemicals are examined, large numbers of phenols, cresols and xylenols are seen, suggesting that cresylic acids might be produced. The presence of many types of pyridines suggests that specialty solvents based on the high solvent powers of pyridines would be possible, for example.

Modification of Chemical Composition

If the types and concentrations of chemicals in raw shale oil are not suitable for extraction and purification, then one might consider methods of treating the whole oil to alter these types and concentrations. It may be possible to produce saleable products for niche markets by different types of treatment than are used in petroleum refineries to produce petroleum-based commodities. As

an example, rather than hydrotreating to remove oxygen, it may be desirable to preserve and enhance the phenolic structures to recover a cresylic acid or mixed phenols product.

The distribution of chemical types in shale oil changes radically as retorting temperature and contact time with hot spent shale are increased. Saturates and olefins disappear at higher temperatures, while the oil becomes heavily aromatic. At the same time, the more complex members of homologous series are reduced to the simpler members. Ultimately the most prevalent compounds in the liquid become benzene and naphthalene. Because of the high value and easy marketability of benzene and naphthalene, high temperature shale oil would appear to be of interest. However, there is also a substantial penalty in overall liquid yield which results.

The net effect of increasing retorting temperature appears to be largely the dealkylation of monocyclic and polycyclic aromatic hydrocarbons. This is true for the alkyl phenols as well. If the same type of dealkylation could be achieved without the loss of total liquid yield, a more favorable economic situation should arise. Such a result could perhaps be achieved by sending raw shale oil through a hydrodealkylation process. A number of commercial processes are available for the hydrodealkylation of alkyl benzenes to benzene.

Analogy With Petroleum Crude Fractions

By examining the ways in which petroleum fractions are used and comparing the properties of those fractions with similar fractions from shale oil, methods to improve performance or value may be discovered. Thus, petroleum resids are used to produce bitumen for asphaltic concrete. Comparing the same fraction produced from raw shale oil, a much higher concentration of nitrogenous compounds is found, which contributes to improved moisture resistance in asphalt pavement.

Analogy With Coal Tars

Producing chemicals from shale oil is similar in principle to producing chemicals from coal tar. In both cases the crude feedstock is produced by pyrolysis of a solid fossil fuel. Thus, it is instructive to examine the U.S. coal tar refining industry.

Shale oil, like coal tar, is a complex mixture of many different chemical species, none present in a large concentration. If we may draw an analogy from the coal tar refining industry, then the key to a profitable operation is likely not the low-concentration, high-value chemicals, but rather the disposition of the bulk of the crude shale oil. In current operations in the steel industry, individual chemicals are not recovered. Everything in the light oil fraction is simply put into creosote, with the remainder going into electrode pitch or else being burned for fuel.

By examining ways in which coal tar fractions are used, similar markets may be identified for shale oil. For instance, the major use for creosote is in wood preservation, particularly the preservation of railroad ties. Shale-derived creosote should have the same preservative effect.

Analogy With Natural Products

Large volumes of oils, fats and other chemicals are produced from natural products. In many applications they must compete against petroleum products, but in other applications, their unique properties have allowed them to maintain distinctive market niches. Examples include the many uses of fatty acids. Although native kerogen contains extensive fatty acid structures, most of these are destroyed during retorting. However, it is possible to generate new fatty acids by oxidation of the raw shale oil. This has been done with air, nitric acid, potassium permanganate, etc.

Observation of Chemical And Physical Properties

Specialty product development is based on careful investigation of the chemical and physical properties of the feedstock material. Although such basic parameters as density, boiling range, heat of combustion, melting point, etc., have been carefully measured for a variety of shale oils from different retorts, the properties of most interest for specialty products are seldom studied. These would include such things as biological activity, surface tension, wetting contact angle, adhesion, solubility, solvent power, etc. Patent applications are developed from observations of this sort.

Observation of Market Needs

It is possible to use a reverse approach, by first categorizing chemical specialty products, and then attempting to find ways in which shale oil might be refined or modified to meet those needs.

A breakdown of the United States chemical specialties market was examined for potential shale oil applications. First, based on criteria for minimum acceptable size of a target market, those with total sales less than about $200 million were eliminated. Next, those known to be based mostly on inorganic rather than organic materials were eliminated. Finally, those specialties concerned with food, cosmetic and direct consumer contact were eliminated because of the immense difficulty and expense of registering new products in those areas. The remaining possibilities are shown in Table 1.

TABLE 1

POTENTIAL MARKET TARGETS IN SPECIALTY CHEMICALS ($ Million in Sales in 1988)

Adhesives	$1,300
Agricultural Chemicals	5,600
Antioxidants	300
Biocides	815
Coal and Fuel Additives	160
Construction Chemicals	1,000
Corrosion Inhibitors	240
Defoamers	310
Elastomers	1,410
Gasoline Additives	500
Industrial and Institutional Cleaners	4,400
Industrial Coatings	5,030
Laboratory Chemicals	580
Lubricant and Functional Fluid Additives	950
Lubricants and Functional Fluids (Synthetic)	600
Metal Plating and Finishing Chemicals	700
Oil-Field Chemicals	640
Paint Additives	335
Paper Additives	535
Plasticizers	500
Plastics Additives	2,800
Refinery and Pipeline Chemicals	280
Rubber Processing Chemicals	390
Sealants	645
Specialty Polymers	2,700
Specialty Surfactants	960
Textile Specialties	680
Thickeners	725

Various shale oil fractions could find application to one or more of the categories in Table 1. These are discussed in the following paragraphs.

Tar Acid Fraction. Undoubtedly the tar acid or phenolic fraction of shale oil has the greatest number of potential applications in Table 1. Phenols can be used to make phenol formaldehyde resins, which find applications in adhesives, construction chemicals and industrial coatings. Phenols from shale oil have been used in China for flotation agents in beneficiating a variety of ores and as raw materials for pesticides and insecticides.

Tar Base Fraction. A large number of pyridine compounds have been identified in the tar base fraction of shale oil. Pyridines could find uses as solvents, denaturants and inhibitors in several of the categories in Table 1. Pyridines can dissolve some organic matter not readily soluble in common solvents. They make good steel corrosion inhibitors.

High Boiling Fraction. The high boiling fraction of shale oil does not appear to have a large number of applications in Table 1. Possible applications could be found in sealants and oil field chemicals.

Aromatic Fraction. Extraction of an aromatic fraction from shale oil could produce materials having functions as gasoline additives, plasticizers and rubber processing chemicals.

Nitrogenous Fraction. Nitrogen-containing compounds are distributed throughout the boiling range of shale oil.

Amide groups are destroyed in hydrotreating, but carboxamides, of the form $C_6H_6CONH_2$, are interesting for specialty chemicals because they are amphoteric. Compounds with amphoteric properties (attracted to both water and hydrocarbons) can be used as defoamers, industrial and institutional cleaners, and specialty surfactants.

Pyrrole groups have several commercially important derivatives, used as solvents, plasticizers, industrial coatings and specialty polymers.

Quinoline and its derivatives have a wide variety of applications. They have been used in antioxidants, corrosion inhibitors, and biocides. Derivatives have also been used as catalysts in making rigid foam, as analytical reagents to gravimetrically determine metals, and as the base for quinoline-derived medicines and dyes.

Consideration of Foreign Experience

Specialty products were produced from oil shale and shale oil in many countries in the past. At present, only Russia makes extensive use of such products.

The Soviet experience is instructive in several ways. It shows, as would be expected, that shale oil can be the source of a wide array of chemical products, equivalent to that which can be derived from either petroleum or coal liquids. It also shows that, in spite of the cornucopia of potential products, it is difficult to find competitive niches for these products at a shale oil production level of 10,000 barrels per day. The Soviet shale tar industry has, to a certain extent, followed the path of the United States coal tar industry, developing heavy dependence on just two major products (creosote for wood preservation and pitch for making carbon anodes).

Asphalt Blend

In working through the evaluation procedures outlined above, the product showing the greatest potential promise was found to be an asphalt blending agent.

Early work on western shale oil by the Bureau of Mines byproducts group showed that vacuum distillation of crude shale oil would produce a residue meeting most asphalt specifications. Experiments with air blowing of crude shale oil showed that asphalt could also be produced in this way. An asphalt roadway laid down at the Anvil Points experiment station was still in good shape 30 years later.

More recent work at different institutions in the United States has shown that various western shale oil fractions are highly effective in producing an asphalt that is resistant to moisture damage during freeze-thaw cycles. One of the major causes of asphalt pavement failure is moisture-induced damage. Moisture and repeated freeze-thaw cycles tend to break apart asphalt pavement. The superior resistance to moisture damage exhibited by shale oil asphalts appears to be related to the nitrogen-containing compounds, but to date it has not been possible to identify a specific fraction. While confirming experiments have not yet been carried out with eastern shale oil, the similar nitrogen level suggests that it would be effective also. The United States Department of Energy and the State of Indiana have allocated funds to carry out the necessary laboratory work.

Market Size

Asphalt consumption in the three states of Indiana, Kentucky and Ohio is on the order of 3.7 million tons per year, equivalent to an average of over 50,000 barrels per day. About 75 percent of this total is used to make asphaltic concrete paving. Not all of this material can be considered to be sensitive to a life cycle cost analysis. However, it is estimated that about 50 percent of the total is used on high-traffic streets and highways where a longer-life paving could command a premium. Thus the 3-state area could represent a market of 19,000 barrels per day of premium asphalt. If this is achieved by blending in 20 percent shale asphalt, the result is a demand for about 3,700 barrels per day of shale-derived asphalt.

Laboratory distillations of eastern shale oil suggest that perhaps 50 percent of the total crude oil could be converted to asphalt range material. This is indicated by distillation curves where, at 800 ^{O}F, less than 50 percent of the raw shale oil is distilled.[4] Thus, 3,700 barrels per day of asphalt blend material indicates a total raw shale oil output of 7,400 barrels per day to satisfy the 3-state region.

Prices and Shale Oil Value

If shale oil asphalt were simply sold as a direct substitute for petroleum asphalt (bitumen), the potential sales revenue would not be attractive. Asphalt is essentially a waste product of petroleum refining, being that part of the crude oil barrel that is not easily converted into refined products. Therefore, its price tends to be set by the alternate uses for the residual fraction, which are residual fuel oil and coker feedstock.

The key to developing a niche market for shale-derived asphalt is to be able to demonstrate a longer paving life with such material and to have the asphalt purchased through a life cycle cost analysis. Only in recent years has the concept of life cycle costing become accept-

able for asphaltic concrete pavement. Previously materials would have been purchased strictly on a low-bid basis.

Asphaltic concrete used in highway construction consists of about 4 to 6 percent bitumen and 94 to 96 percent aggregate. Recent values of laid-down costs were $21 per ton for hot-mix asphaltic concrete and $150 per ton for bitumen. Thus, the bitumen accounts for about 36 percent of the total laid-down cost.

Therefore, if an improved bitumen blend results in a 10 percent longer pavement life, then the value of the bitumen is increased by 28 percent. If the improved blend was achieved by blending 20 percent shale-derived bitumen with 80 percent conventional bitumen, then the value assigned to the shale-derived material could be three times that of the petroleum-derived material. The results of a series of such calculations are presented in Figure 4. It shows that shale asphalt values of over $70 per barrel can be achieved for a 7.5 percent pavement life increase with a 10 percent blend.

The value assigned to shale oil in Figure 4 is actually very conservative because it considers only the material cost of the asphaltic concrete. Other large benefits will arise from longer pavement life. They include less frequent interruption of traffic for pavement resurfacing and less wear and tear on vehicles due to pavement being in good condition for a larger fraction of its total lifetime. The cost to the public of traffic delays for resurfacing has been calculated to be equal to or greater than the material cost of the paving itself in many cases. This means that the true value to society of a shale oil blend could be even much higher than the $70 per barrel quoted earlier.

Summary

The most promising product possibility is to make a premium asphalt blending material from shale oil. This meets all the requirements for an exploitable market niche. There is a demand for improved road life in asphalt paving materials, and laboratory tests suggest that asphalt derived from shale oil could meet this demand. This is a need which cannot be satisfied by petroleum, and no immediate competitors from other sources are known either.

The relationship between the cost of bitumen and the total laid-down cost of asphaltic concrete makes it possible to realize a large premium for a bitumen blending material which increases paving life.

Other broad-cut products analyzed include waxes, creosote, tar acids, tar bases, oil-based drilling mud, rubber processing oils, and carbon black feedstock. The last was discarded as having no prospect for premium product values.

Tar acids and tar bases offer good possibilities for product prices well above that for crude oil, but each represents only a small fraction of the whole shale oil. Total value for the tar bases would probably be on the order of $1.00 per barrel of whole shale oil.

Drilling mud and rubber processing oil are two potential markets for a large fraction of the whole shale oil. However, the ability to sell shale oil for these uses is entirely speculative at this time, and extensive market development efforts would be required.

The first two items on the above list, waxes and creosote, have a large potential market volume and the reasonable probability of technical success. Waxes from shale oil have been marketed many times in the past, and

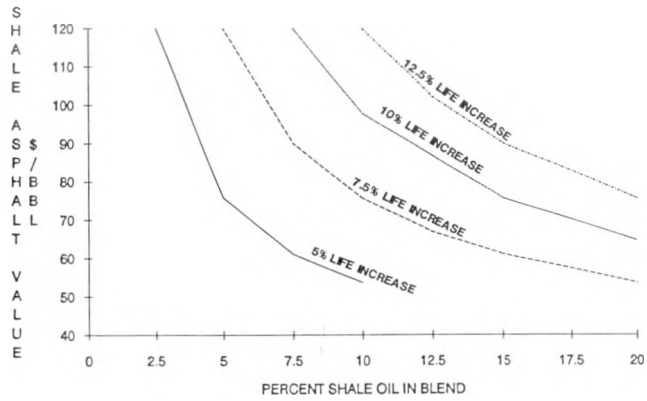

Figure 4. Potential shale oil values in asphalt blends.

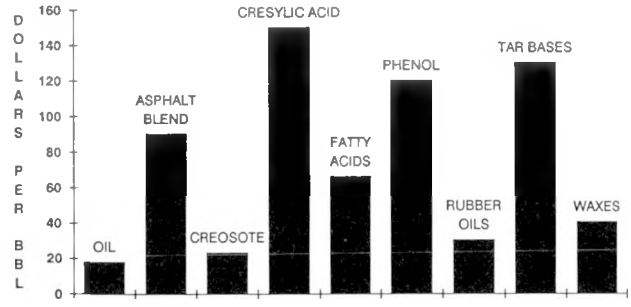

Figure 5. Product prices.

creosote from shale oil has been extensively used in the USSR. The netback prices which could be obtained for these materials, however, would be much lower than appears possible for asphalt (Figure 5).

If improved paving life can be achieved with the use of shale asphalt, then demand in the 3-state region of Kentucky, Indiana and Ohio could support crude shale oil production of approximately 2,000 to 4,000 barrels per day, depending on the blending ratio required. The market value for the asphalt fraction of this material could be on the order of $70 to $100 per barrel, depending on the amount by which paving life can be increased.

References

1. Sinor, J.E., "Marketing Considerations for an Eastern Oil Shale Demonstration Plant," Proceedings, 20th Oil Shale Symposium, Golden, Colorado, April 1987.

2. Sinor, J.E., "Niche Market Assessment for a Small-scale Western Oil Shale Project," Proceedings, 22nd Oil Shale Symposium, Golden, Colorado, April 1989.

3. Carter, S.D., and D.N. Taulbee, "Fluidized Bed Retorting of Eastern U.S. Oil Shale: An Evaluation of Steam as a Fluidizing Medium," Proceedings, 1984 Eastern Oil Shale Symposium, Lexington, Kentucky, November 1984.

PETROBRAS Boosts Oil Shale Fines Processing

by

Antonio Carlso Lisboa and Rubens E. Novicki
Petroleo Brasileiro, S.A.
83900 Sao Mateus do Sul, Brazil
Edwin M. Piper
Stone & Webster Engineering Corporation
Englewood, Colorado 80111

ABSTRACT. The Petrobras oil shale retorting process, PETROSIX, utilizes the particle range of +1/4 inch - 3 1/2 inches. The UPI plant in Sao Mateus do Sul as of September 30, 1989 has 110,000 hours of operation, has processed over 6,400,000 metric tons of shale, has produced 2,800,000 barrels of shale oil and 98,000 metric tons of high Btu gas. However, the nature of the raw oil shale is such that the amount of shale less than 1/4 inch that is mined and crushed and returned to the mine site is about 20 percent, thereby, increasing the cost of oil produced by a substantial number. Petrobras has investigated several systems to process the fines that are not handled by the 65 MTPH UPI plant and the 260 MTPH commercial plant.

The first is the PLASOL entrained bed process to extract oil and fuel gas. A 500 kgh pilot plant was built in the early 80's and has been success- fully operating since then. This low residence time, high heating rate process, depletes oil shale completely of its original potential oil and gas. Both steam and recycle gas have been used for processing gas. The set of data gathered under several operating conditions led to the process optimization. At present, the design of a demonstration plant is underway.

The second is the spouted bed retorting process. A 250 kgh pilot plant has been used to retort the particles employing air as the spouting fluid. Under this mode of operation, the retorting heat can be wholly provided by partial combustion of the organic matter inside the bed, thus eliminating any external heating. The major feature of this technology is to handle the oil shale fines as they are discharged at the PETROSIX solid preparation plant, without any further drying or crushing. Another feature of this system is the ability to process oil shale sludge to recover Btu values.

The third is the circulating fluidized bed (CFB) boiler. A 1 tph (1,000 kgh) steam pilot plant is now in the startup phase. The burning of oil shale fines is a convenient source of heat and steam to meet plant requirements.

This paper provides an updated status of each of these processes in regard to the tests performed, potential contributions to an integrated use of the oil shale mine, and future considerations.

INTRODUCTION

The Oil Shale Industrialization Superintendency is a Department established by PETROBRAS, the Brazilian oil company, to promote the use of the huge national oil shale deposits. Studies were initiated in the middle 50s, and further developed in the 60s from which the PETROSIX process was the result. In 1972, the 65mtph PETROSIX prototype plant started operation at Sao Mateus do Sul, near reserves of 650 million barrels of shale oil. Until 1982, the plant underwent an R&D program designed to evaluate several operating conditions and to make improvements in ancillary equipment; during this period, the plant also generated data for the design of the 260mtph industrial module plant. Startup is scheduled for 1990. Since 1982, the prototype plant has been operated as a full scale plant producing 850 bpd of shale oil, which is sent to a nearby petroleum refinery.

The PETROSIX process consists of a surface moving bed retort in which coarse oil shale particles move downward counter current to hot gases. The solid particles are fed to and withdrawn from the retort by PETROBRAS patented mechanisms that provide a homogenous distribution of particles on the top of the bed. The upward moving hot recycle gases supply the necessary heat of retorting. After retorting, the hot retorted shale exchanges heat with cold recycle gases in a lower zone. Thus, the moving bed provides a convenient way to recover heat from both hot gases and hot particles that leave the high temperature retorting region. A description of the PETROSIX process is referenced (1, 2).

As mentioned previously, a homogenous bed is required for the various particle sizes. This is mandatory to avoid chaneling and subsequent poor heat transfer and overheating. The PETROSIX retort allows smooth operation within the particle size range of 1/4" to 3 1/2". The retort can process some fines, under carefully controlled conditions. However, the introduction of many particles below 1/4 inch increases pressure drop, beyond allowable limits.

The PETROSIX shale preparation plant results in a quantity of raw oil shale particles below 1/4 inch. A more suitable solid-gas contact system is required to cope with this material. The PETROBRAS Oil Shale Industrialization Superintendency selected the entrained bed, the spouted bed and the circulating fluidized bed process systems. A fines process system could enhance the energy balance of the plant, see Figures 1A and 1B.

Figure 1A illustrates the current system in which 25 percent of the whole energy in the PETROSIX feedstock returns to the mine as oil shale fines. This loss accounts for almost 1/3 of the total losses that comprise energy losses to the atmosphere, in the coarse retorted shale and in the sludge, besides that in the fines. Figure 1B shows the improvement in the energy balance that could result from the oil shale fines processing. Figure 1B considers the retorting and burning of oil shale fines. Figure 1B also shows the heat savings that would occur cutting thermal losses and burning coarse retorted shale and sludge. Figures 1A and 1B reflect a situation pertinent to Irati oil shale. The balance is strongly affected by the kind of oil shale; for instance, the processing of Colorado oil shale in the PETROSIX retort gave better results due to the higher carbon conversion that naturally occurs with that kind of shale.

The technologies to process oil shale fines have been developed by PETROBRAS and are presented in the following sections.

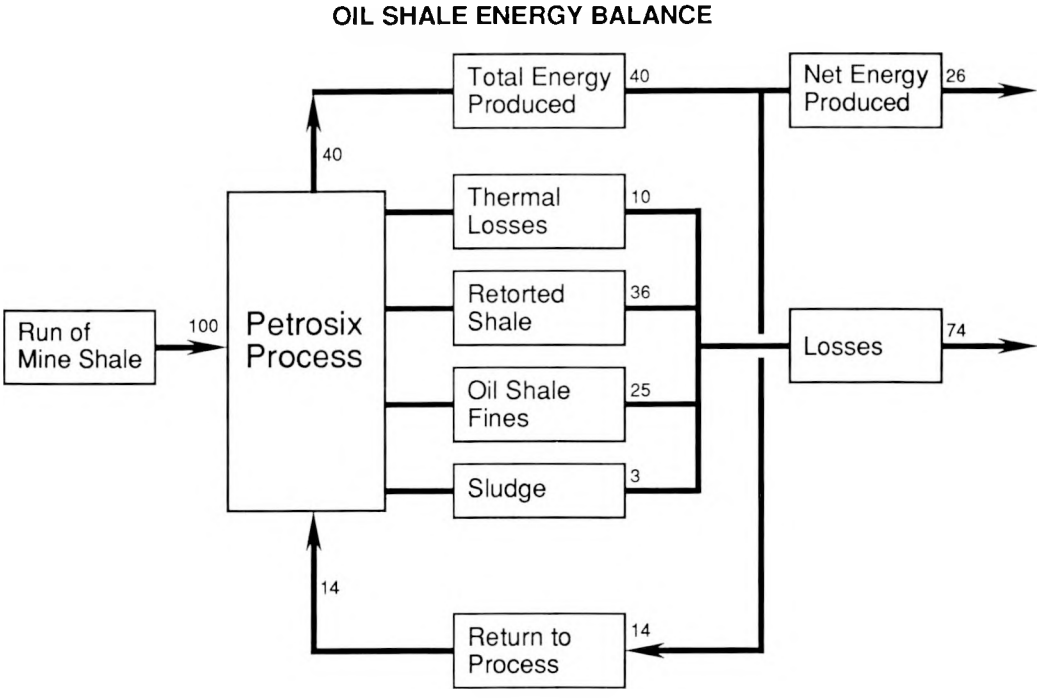

Figure 1A. Current System

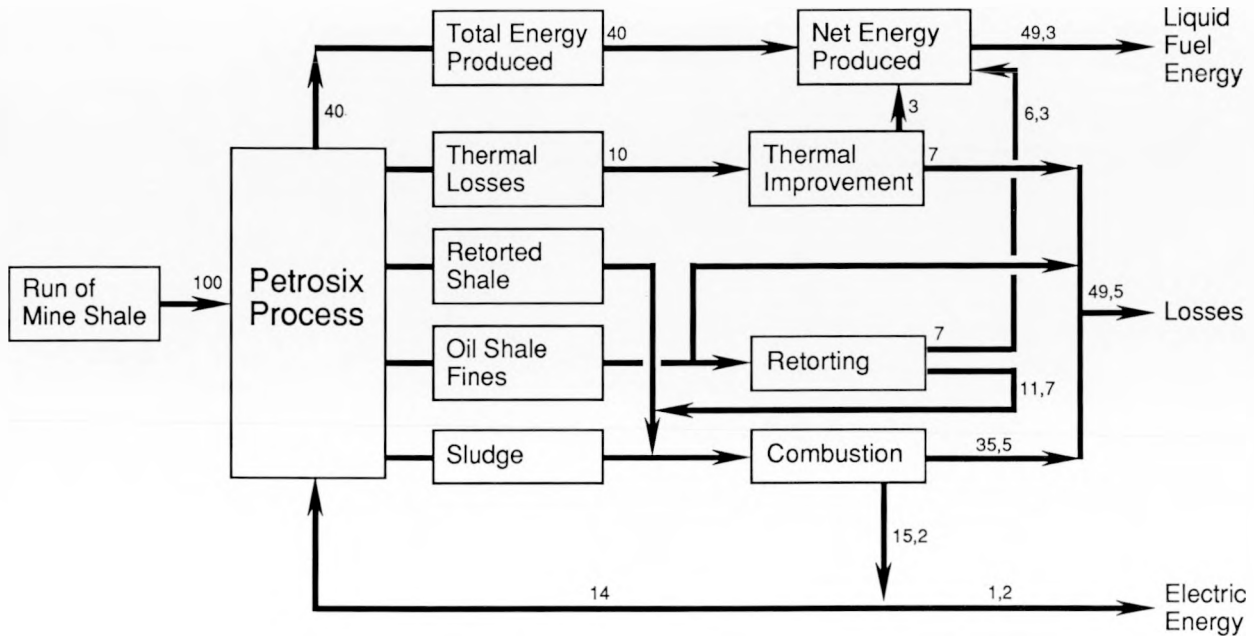

Figure 1B. Ultimate System

The Entrained Bed Process (PLASOL)

The entrained bed process has been studied by PETROBRAS to pyrolyze oil shale fines since the late 70s (3). Initially, a cold flow transparent model pilot plant was fabricated to supply hydrodynamic information. The oil shale to gas mass ratio was highly interesting. The conception and operation of the reactor was simple as long as enough air was supplied to convey the solid particles. Based on the cold model data and some published information (4), a pilot plant was constructed and operated.

As initially expected, the reactor part proved to be trouble free. Eventually, the plant was able to perform long test runs. A wide range of operating conditions has been investigated. Figure 2 depicts the first pilot plant.

An interesting improvement to the PLASOL process consists of preheating the oil shale fines feedstock by a different means utilizing the combustion gases coming from the reactor heating section. Figure 3 depicts the apparatus employed for this purpose. Initially, the particles coming from the feed hopper are heated by a mixture of combustion gases and air in a fluidized bed. The heated particles are then contacted with the recycle gas in a fliudized bed which also promotes the distribution of particles to several reactors. The system also employs a cyclone coupled with a fluidized bed valve to return entrained particles from the heat exchanger to the distributor.

The distributor has been tested separately discharging to several outlets. Within the pilot plant, it was tested feeding only one PLASOL reactor. The entire system has been successfully tested in the PLASOL pilot plant.

The Pilot Plant

The reactor is a 15m high, 4" diameter stainless steel pipe which is inside a furnace which supplies most of the heat requirements. The furnace heater burns diesel oil. The flue gas is introduced at the base of the furnace and moves to the top where it is withdrawn; some other concepts were investigated such as introducing the flue gas into both ends of the furnace, top and bottom, and withdrawing it out at the center. The remaining sensible heat of the flue gas is then used to preheat the oil shale particles feedstock in a fluidized bed; this equipment has been analyzed separately and will soon be integrated in the plant.

The solid feeding system consists of a stock pile, a pneumatic transport line, two feed hoppers, a screw feeder and a venturi type mixer. The pneumatic transport line conveys the particles from the stock pile to the first feed hopper. The particles then flow into the second hopper which discharges into a screw feeder to control the oil shale fines flow. The outlet of the screw feeder is linked to a venture type mixer at the base of the reactor.

The reactor off gas flows through two cyclones where the entrained retorted shale is captured. Due to the high temperature, no oil is collected. The gases containing oil vapor enter two tube and shell heat exchangers where the oil is condensed. The cooling fluid may be either air or water, depending on the cooling rate required. Finally, the gas passes through a venturi scrubber.

The PETROBRAS Oil Shale Superintendency contains a pilot plant system able to clean the oil produced at all of its retorting plants. The

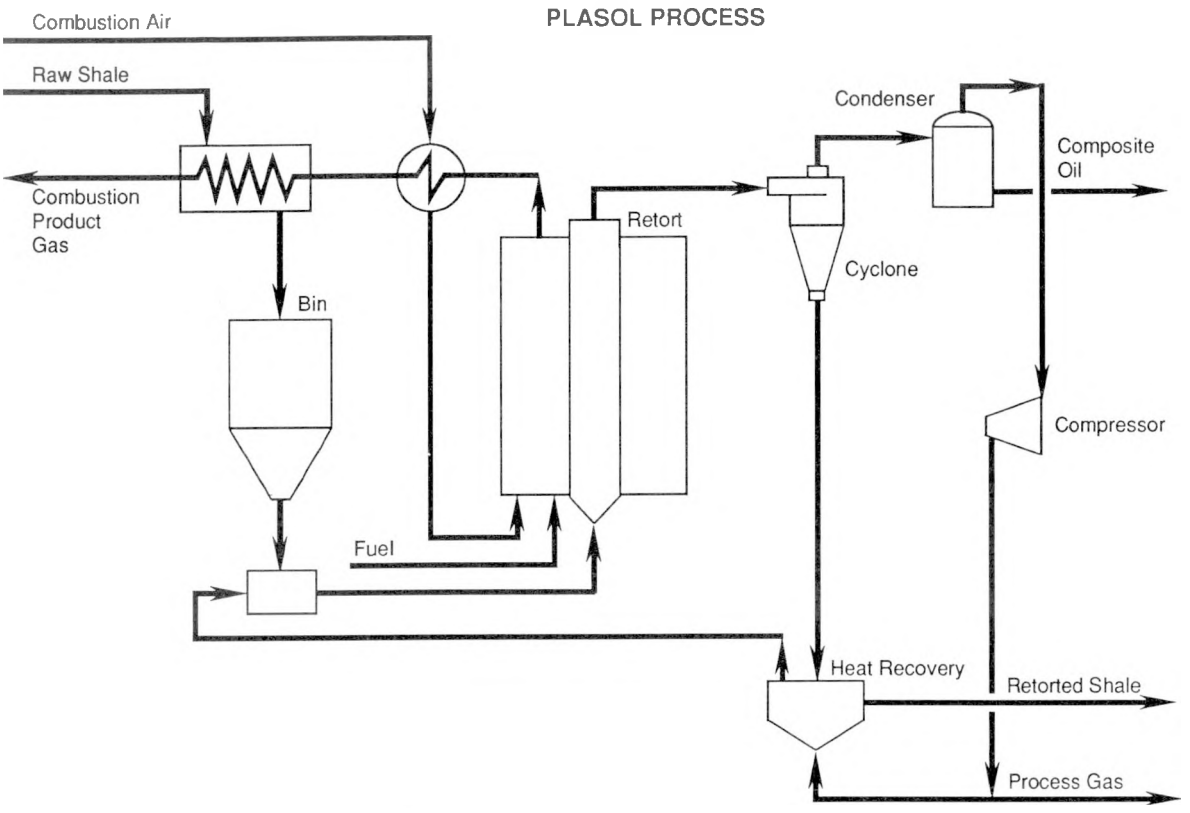

Figure 2. The Entrained Bed Pilot Plant Flow Diagram

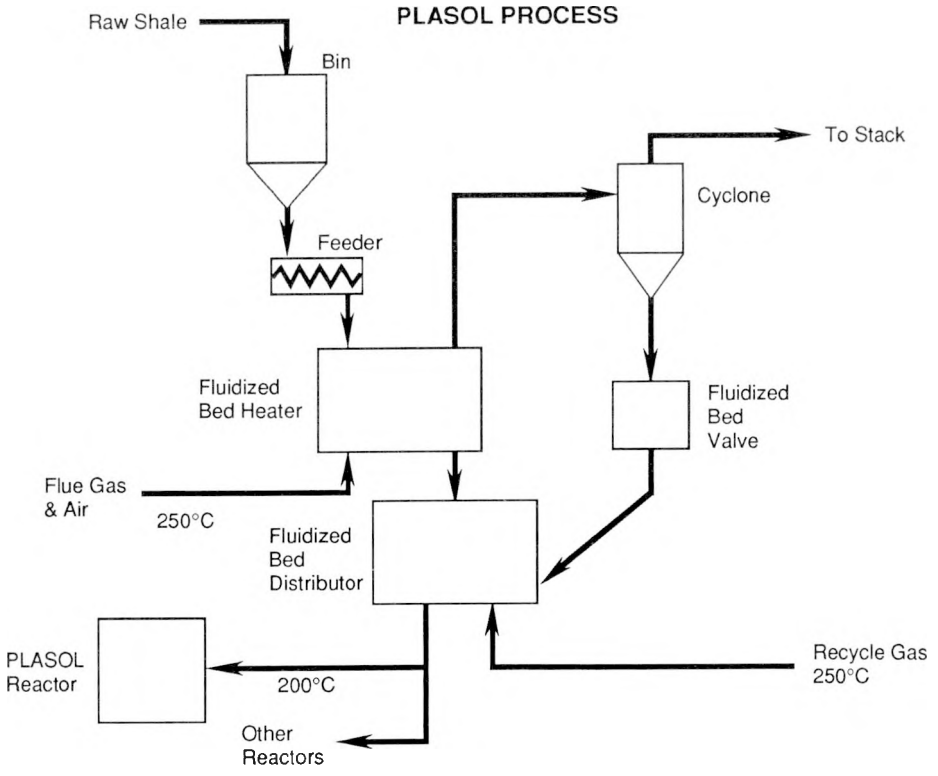

Figure 3. Entrained Bed Pilot Plant with Preheating Variation

cleaning plant contains a decanter, a centrifuge and a filter press. The bulk oil produced at the PLASOL plant is sent to this plant after each test. The ease of cleaning is then analyzed. Most of the oil produced has been cleaned only in the filter press, where pressure drop versus time has been monitored. The solids free water-oil mixture is then put aside to settle in a tank. Some experience has been gained with the use of demulsifiers to break water-oil emulsions.

After cleaning, the oil is analyzed in the laboratory. Table 1 shows some properties of the oil produced by the PLASOL pilot plant. It should be noted that the oil characteristics are strongly affected by test conditions, such as temperature and heating rate.

TABLE 1

OIL AND GAS CHARACTERISTICS OF PLASOL PLANT

Oil	
Density	1.0008
Viscosity	
100°F	93.4 cst
130°F	38.0 cst
Pour Point (°C)	-18
Flash Point (°C)	23
Carbon (% weight)	84.65
Hydrogen (% weight)	10.83
Nitrogen (% weight)	1.28
Sulphur (% weight)	1.08
Carbon Residue (% weight)	10.86
Ash (% weight)	0.05
H.H.V. (kcal/kg)	9841
Gas	
SO_2	0.0
H_2S	11.75
O_2	0.19
N_2	3.75
CO	1.73
CO_2	2.78
H_2	8.51
METHANE	31.59
ETHANE	10.63
ETHENE	10.65
PROPANE	3.85
PROPENE	9.10
C_4	4.85
C_5+	1.02

Operating Conditions

A wide range of operating conditions have been applied in the PLASOL pilot plant. Table 2 shows the range of the main process parameters. The process inherently imposes a high heating rate and low residence time to the particles. Therefore, the solid feedstock characteristics, like moisture content and particle size distribution, must be strictly controlled to result in the most efficient use of the heat supplied by the furnace.

Heat radiated from the reactor wall plays an important role and accounts for a large fraction of the total heat transmitted to the particles. Some analyses were done to know the emissivity of the particles, before and after retorting, and of the inner reactor wall, clean and dirty. These data were fed to a mathematical model that simulates the process. Because of the radiation heat transfer, the gas to solids mass ratio can be kept as low as 0.3. Heat is also transferred to the particles by convection through the gas. A great amount of expertise was obtained in analyzing the heat transfer mechanisms and hydrodynamic parameters associated with oil yield and oil characteristics.

This information has been increased recently with the introduction of an electric heated furnace that replaced the diesel fired furnace. The new furnace, with six independently controlled heated sections, allows one to vary and control the reactor wall temperature better than the diesel fired furnace. Although the electric heated furnace concept will not be used in a large scale plant, it has been useful to master important parts of the process.

Both steam and recycle gas have been employed as retorting gas. When using recyle gas, a blower pumps back the product gas to the inlet gas line. The system for larger plants is to use recycle gas, because it avoids steam production and condensation and absorbs less radiant heat inside the reactor.

Some successful attempts have been made in the development of a mathematical model that describes the momentum, heat and mass transfer inside the reactor, furnace and adjoining equipment (5, 6, 7). The models, besides replacing costly experimental runs, are being used in the design of a demonstration plant.

TABLE 2

PLASOL PROCESS OPERATING CONDITIONS

	Range
Particle	
Size (mesh)	<10
Density	1.9 - 2.3
Moisture (% weight)	3 - 6
Fisher Assay (% weight)	
Oil	7 - 9.5
Gas	2 - 4
Water	1 - 3
Residue	85 - 90
Temperature (°C)	
Retorting	500 - 600
Recycle Gas	450 - 500
Pressure (mmH20)	
Maximum in Bed	500 - 1200
Δ P in Bed	100 - 400
Mass Flow (kg/hr)	
Gas	55 - 70
Shale	100 - 550
Yield Based on Fischer Assay (% weight)	
Oil	80 - 115
Gas	40 - 70
Particle Residence Time (sec)	2 - 5

Although the process may be ready for scale-up, some complementary studies are being made to move to a full scale plant. The first was the preheating of raw oil shale particles in a fluidized bed. The same type of equipment can be used to recover heat from the hot retorted shale particles. As the full scale plant should be modular, requiring a number of similar reactors, an improved way to distribute the particles homogeneously into each reactor has been developed.

The Spouted Bed Process

The spouted bed gas solid technique was first introduced by Mathur and Gishler (8) as a solution for the poor fluidization of coarse solid particles. In their early trials, the materials being considered were only grains and it was a drying process. Later, the technology proved useful for other materials and many experiments have been reported using carbonaceous materials like coal and oil shale, as well as high temperature processes like combustion, pyrolysis and gasification (9, 10, 11).

PETROBRAS began its development on the spouted bed technology in the late 70s. Initially, small cold models were used (12), where features of the technique may be examined. Basic information like minimum spouting velocity and a pressure drop versus flow rate curve were obtained under several conditions of bed height and particle size. The spouted bed was selected to handle the oil shale fines because the fines size distribution is strongly concentrated in the range 1-9 mm, and this range is very appropriate for the technique.

A bench scale plant was designed and built (13). The principal piece of equipment was an 8 cm diameter stainless steel reactor to process 5-10 kg/hr of oil shale. Due to its flexibility, a number of different spouting gases were used, namely steam, nitrogen and air. When employing air, the electric heater that surrounded the reactor could be turned off and the process worked almost autothermically. When employing nitrogen or steam, the electric heat was provided through the reactor wall.

The results provided from the bench scale plant encouraged the design of a pilot plant. While its planning was under way, some tests were performed in a semi-industrial plant (14). The semi-industrial plant was originally used to dry 2mtph of soybean. It contained two 80 cm diameter spouted beds as well as the equipment necessary to transport the particles to and from the vessels. Hot gases were generated in a fluidized bed burning coal. The tests were conducted under a research agreement with the owner of the plant, a local university. The principal purpose of the tests was to assess behavior of the spouted bed with oil shale particles in larger vessels. Successful operation was achieved which encouraged further studies on the process.

PETROSIX processing operations results in a by-product comprising of a mixture of oil, retorted shale and water. This sludge is produced in the oil cleaning facilities of PETROSIX. Most of the time, this sludge is discarded from the filter press, although it can be withdrawn from the centrifuge and decanted. This material will be processed to recover its energy content, and also to comply with growing environmental constraints. Table 3 shows the main characteristics of the available filter cake.

TABLE 3

SLUDGE CHARACTERISTICS

Fischer Assay (% Weight)		
	Oil	30.31
	Gas	1.82
	Water	4.91
	Residue	62.96
Carbon	(% Weight)	40.53
Hydrogen	(% Weight)	3.59
Sulfur	(% Weight)	1.53
H.H.V.	(Cal/g)	4618
Particle Size (inch)		< 1/8

One way to efficiently recover the energy value of the sludge is to provide a means to separate oil from the solids and water. In order to accomplish this task, some tests were conducted in the spouted bed pilot plant. The plant cyclone, close to the reactor gas outlet, operates at temperatures above 450°C, sufficiently high to avoid oil condensing and subsequent sludge formation. This fact alone promotes the necessary condition to separate the oil from the dust.

Table 4 shows the characteristics of both oil shale fines, column 1 and oil shale fines plus sludge, column 2, employed as feedstocks in the present work. The material described in column 2 was produced from raw oil shale (94% weight) and filter cake (6% weight) intimately mixed in a rotary drum. Previously, the filter cake was broken into particles smaller than 1/8". The low sludge percentage in the mixture matches the amounts of oil shale fines and filter cake that will be available when the PETROSIX industrial module goes on stream in 1990.

TABLE 4

SPOUTED BED FEEDSTOCKS PROPERTIES

Fischer Assay (% Weight)	Oil Shale Fines	Oil Shale Fines + Sludge
Oil	8.15	9.52
Gas	2.61	2.78
Water	1.83	7.35
Residue	87.41	80.35
Particle Size		
1/4"	0.75	0.36
6 Mesh	16.94	16.21
14 Mesh	35.38	39.59
20 Mesh	12.96	11.48
Pan	33.93	32.23

Table 5 shows operating conditions and results from two tests, with the feedstocks shown in Table 4. In Test 1, 1500kg of oil shale fines were processed, while in Test 2, 1500Kg of oil shale fines and 100kg of filter cake were processed. No change was made in the equipment

to handle the new feedstock. No operating differences were observed between the two tests. The two feedstocks were very similar, although the filter cake grains could be easily distinguishable. No problems occurred in the screw conveyor that feeds the reactors; some kind of clogging was feared due to the filter cake particles.

TABLE 5

SPOUNTED BED OPERATING CONDITIONS AND RESULTS

	Test 1 (Without Sludge)	Test 2 (With Sludge)
Oil Shale Processed (kg)	1500	1500
Sludge Processed (kg)	0	100
Retorting Temperature (°C)	471	471
Solids Flow (kg/h)	130	133
Air Flow (kg/h)	72	71
Spouting Air Temperature (°C)	27	24
Coarse Retorted Shale Amount (kg)	1014.8	1019.5
Fischer Assay (% Weight)		
Oil	0.25	0.33
Gas	0.44	0.14
Water	0.84	0.47
Residue	98.47	99.06
Carbon (% Weight)	8.62	8.45
Hydrogen (% Weight)	0.64	0.95
H.H.V. (cal/g)	919	972
Fine Retorted Shale (kg)	164.9	209.7
Fischer, Assay (% Weight)		
Oil	1.05	0.75
Gas	0.64	1.18
Water	1.95	1.02
Residue	96.36	97.05
Carbon (% Weight)	9.05	10.73
Hydrogen (% Weight)	0.77	0.90
H.H.V. (cal/g)	861	1197
Oil Produced (kg)	50.6	61.1

It can be observed in Table 5 that a good separation occurred between the constituents of the filter cake. The solids originally present in the cake were trapped in the cyclone while the oil was condensed free of dust downstream. The amount of solids collected in the cyclones increased as well as the amount of oil produced. The results may not be as good as shown, because some dust passed through the cyclone, restoring the sludge in the condensed oil vessels. However, directionally the net results were positive.

Another test was conducted using a mixture with a 12% weight filter cake, with similar results. Some tests with other sludges from PETROBRAS refineries are being planned.

The Pilot Plant

The pilot plant began operation in December 1987. It was designed to use air as the spouting fluid. Figure 4 is a process flow diagram.

The reactor is a 2 m high, 12 inch diameter stainless steel pipe. The spouted bed height is defined by the position of the discharge pipe which allows withdrawal of the particles from the bed. Two pipes are provided at 65.4 cm and 96.8 cm from the cone vertice. Raw shale is fed to the top of the bed.

The solids feeding system consists of a bin and a screw conveyor. The screw conveyor discharges directly into the reactor. The processed shale discharges easily through the overflow pipe and is collected in a bin for the entire test.

Spouting air enters the reactor through one of three inlet pipes, the unique difference being the pipe diameters; 1/2, 1 and 2 inch. Inlet pipes can be changed easily. The diameter of the inlet pipe effects substantially the shape and properties of the spouted bed above. Prior to entering the reactor, the air can be preheated in a furnace. The air temperature from the furnace has a wide range.

The gases and oil vapors exit the reactor and pass through a cyclone dust collector that operates at a high temperature. The cyclone removes the entrained particles from the gas after which the mixture passes through two heat exchangers where oil and water condense. After this step, the light oil is collected in a venturi scrubber. The gas product is sampled and sent to a cromatograph for analysis.

The composite oil flows to the cleaning plant to remove solids and water in a filter press and settling tank.

Operating Conditions

After a short startup period, the pilot plant enters a test program designed to evaluate both thermal and hydrodynamic conditions. The main variables investigated are height, column diameter to gas inlet pipe diameter ratio, retorting temperature and air inlet temperature. Table 6 shows the range of these parameters. Table 6 also lists the values of some dependent variables. These are air to shale mass ratio, bed pressure drop and oil and gas yields. Another very important dependent parameter is the general operational stability of the process which to date has not reflected any uncontrolled departure from the defined test conditions.

The three inlet pipe diameters can be used without restriction and are used to vary the spouting gas flow. A change does not modify the bed pressure drop (including the air) because as the inlet pipe size increases, the pressure drop decreases, more air is admitted to the bed, resulting in constant pressure drop.

The air to shale mass ratio has been a little higher than the theoretical value, perhaps due to heat losses from the reactor. It is believed that this loss accounts for the lower oil yield obtained in the tests than expected.

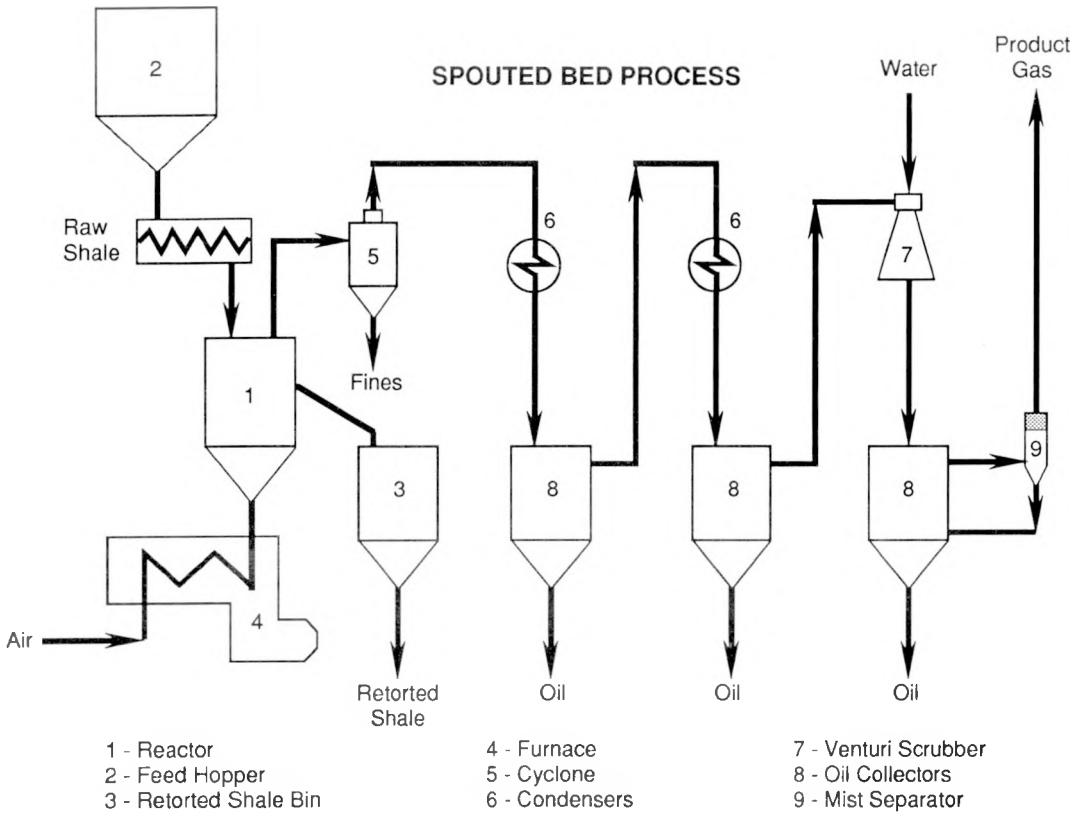

Figure 4. The Spouted Bed Pilot Plant Flow Diagram

TABLE 6

SPOUTED BED GENERAL PROCESS OPERATING CONDITIONS

	Range
Particle	
Size (inch)	< 1/4
Density	1.9 - 2.3
Moisture (% weight)	3 - 6
Fisher Assay (% weight)	
Oil	7 - 9.5
Gas	2 - 4
Water	1 - 3
Residue	85 - 90
Temperature (°C)	
Retorting	420 - 600
Recycle gas	20 - 550
Pressure (mmH20)	
Maximum in Bed	800 - 1500
Δ P in Bed	250 - 500
Mass Flow (kg/hr)	
Gas	45 - 105
Shale	70 - 250
Yield Based on Fischer Assay (% weight)	
Oil	40 - 60
Gas	70 - 100
Particle Residence Time (min)	12 - 30

The bed temperature ranges from 420°C to 600°C. Both extremes result in the lowest oil yields. The 420°C retorting temperature is too low to accomplish the retorting thoroughly in the residence time available and the 600°C retorting temperature promoted more combustion than necessary. The better oil yields were achieved with temperatures in the range of 450°C to 550°C.

An interesting mode of operation occurred with no preheating and the spouting gas entering the reactor at room temperature. Under this mode, the process operated autothermically. In a full scale plant, heat would be exchanged with the inlet air via any hot stream coming out from the reactor. The autothermal reactor proved the versatility of the process.

Table 7 shows the general properties of the oil and gas produced in the process. Oil and gas properties did not differ markedly under the different operating conditions. The high nitrogen content in the product gas because of the air results in poor gas quality which is the main drawback of pyrolysis with partial combustion.

Circulating Fluidized Bed Combustion Process

Industry has recently given significant attention to high velocity fluidization. Indeed, the very well-known fluid catalytic cracking process had its origin in a reactor operating under the high velocity fluidization mode in the early 40s. Later, the bubbling bed mode replaced its processor and dominated the market for a long period. It is not clear why that change took

place, some groups feeling that a bubbling bed physical model was easier to build and study. However in the last decade, a number of processes have appeared utilizing one or the other of the patterns of high velocity fluidization.

TABLE 7

OIL AND GAS CHARACTERISTICS OF SPOUTED BED PLANT

	Spouted Bed
Oil	
Density	0.9309
Viscosity	
100°F	93.8 SSU
130°F	60.5 SSU
Pour Point (°C)	-15
Flash Point (°C)	71
Carbon (% weight)	82.20
Hydrogen (% weight)	11.28
Nitrogen (% weight)	0.57
Sulphur (% weight)	1.22
Carbon Residue (% weight)	2.32
Ash (% weight)	0.01
H.H.V. (kcal/kg)	10120
Gas	
SO_2	1.7
H_2S	0.68
O_2	0.77
N_2	80.56
CO	7.02
CO_2	7.72
H_2	0.38
METHANE	0.49
ETHANE	0.16
ETHENE	0.08
PROPANE	0.08
PROPENE	0.10
C_4	0.13
C_{5+}	0.13

The high velocity fluidization is characterized, as its name suggests, by a very high flow of gas within a bed of particles. Several patterns can be progressively attained when the flow of gases is increased from a bubbling bed (15). Initially, a turbulent bed is observed. The bubbles disappear in the bed and the phenomenon resembles homogeneous fluidization. Most particles remain in the bed but a few are entrained by the gas. It is not easy to determine the exact velocity at which time the pattern changes from a bubbling bed mode and enters the turbulent bed mode. It is usually defined as a range of transition velocities based mainly on pressure fluctuations. If the flow of gas is increased, the fast fluidization occurs. In this mode of operation, the particles are transported upwards, in spite of substantial backmixing; and if more particles are not introduced into the bed, the bed will soon empty. One way to maintain the bed is to provide a constant solid flow into it. An easy way to accomplish this is by recycling the particles entrained from the bed. The recycle gives the particles the opportunity to pass into the reactor again, and a higher residence time can be obtained. The solid recycle can also be used to control the bed temperature. Therefore, the circulating fluidized bed is particularly applicable to combustion processing and substantial efforts have been exerted in this direction.

PETROBRAS' circulating fluidized bed boiler has a capacity to generate 1000 kgh of superheated steam at 350°C and 32 bar. Fresh oil shale particles and entrained retorted shale particles are continuously fed into the bottom of the reactor. The heat produced is transferred to water through tubes inside the reactor. Limestone is also introduced at the bottom of the reactor to absorb SO_2.

The combustion air is introduced as primary air through the distribution grid located at the bottom of the reactor and as secondary air through several taps in the middle section of the reactor.

Combustion temperatures are controlled by varying the solid circulation rate which determines the suspension density, and consequently, the heat transfer rate to the water wall installed inside the reactor.

The heat generated by the combustion reactions is entirely used to produce superheated steam.

The design of the steam generating equipment is very similar to pulverized coal boilers, and consists of a superheater, boiler bank, economizer and tubular air preheater. Table 8 provides the design parameters.

The Pilot Plant

The core of the plant contains the equipment necessary to circulate the solids, i.e., the

TABLE 8

THE CIRCULATING BED PROCESS DESIGN CONDITIONS

Particle	
Size (inch)	< 1/4
Density	2.3
Moisture (% weight)	5.3
Sulphur (% weight)	4.1
Carbon (% weight)	10.0
Hydrogen (% weight)	1.6
H.H.V. (kcal/kg)	1170
Temperature (°C)	
Dense Phase Bed	850
Dilute Phase Bed	850
Recycle Particles	850
Combustion Air	250
Pressure (atm)	
Top of Dense Bed	1
Mass Flow (kg/hr)	
Shale	640
Limestone	600
Recycle Shale	150000
Primary Air	125
Secondary Air	1880
Boiler	
Steam Production (kg/hr)	1000
Steam Temperature (°C)	352
Steam Pressure (bar)	32

reactor, cyclone and the valve in the cyclone leg. The reactor is a 17.6 m high 43 cm x 66 cm rectangular column, refractory lined. The cyclone discharges the collected particles through a valve which allows the particles to return to the bottom of the reactor. The valve contains a bubbling fluidized bed that prevents an upward flow of reactor gases into the cyclone through the cyclone leg. Figure 5 is the flow diagram of the plant.

The reactor section just above the air distribution grid is characterized by a high concentration of solid particles; this is the dense bed. Fresh shale, limestone and recycle particles are fed at this level. Fresh oil shale and limestone enter the vessel through a chute connected from feed hoppers. Above the dense bed is the dilute phase, although no apparent line separates the two regions. The dilute phase region is characterized by a net upward flow of solids and gases, with intense backmixing. The turbulence promotes intense solid gas contact, as well as excellent heat transfer to the water walls within the reactor. Excellent rates of SO_2 absorption are also achieved.

Primary fluidization air enters the reactor through the grid above a wind box. Secondary air enters at three levels above the dense bed region. The secondary air provides the necessary flow to carry over the particles.

Solid ash is discharged from the bottom of the reactor through a pipe connected to a screw conveyor. The screw conveyor action is controlled by the pressure drop in the dense bed region. The hot ash particles are used to preheat the water to the boiler, as well as secondary air in a fluidized bed heat exchanger.

The pilot plant building was completed for startup in October 1988. Initially, all of the solid streams were operated at room temperature and each of the various prices of equipment were proven.

After cold startup, the equipment was prepared for hot startup. Feedstocks of oil shale particles below 10 mesh and below 1/4 inch have been processed successfully. The operation of the solid circulation valve has proved to be reliable.

The fluidizing air stream has been split into a primary air flow and a secondary air flow. The first keeps the dense bed in a turbulent state while the latter carries the particles upward.

Steam has been produced in the pipe lined reactor wall. Thus far only this part of the boiler is in operation the superheater has not been alined to the reactor.

Although the plant has not completed its startup program, no major problems have been experienced that would hamper the smooth operation of the pilot plant equipment.

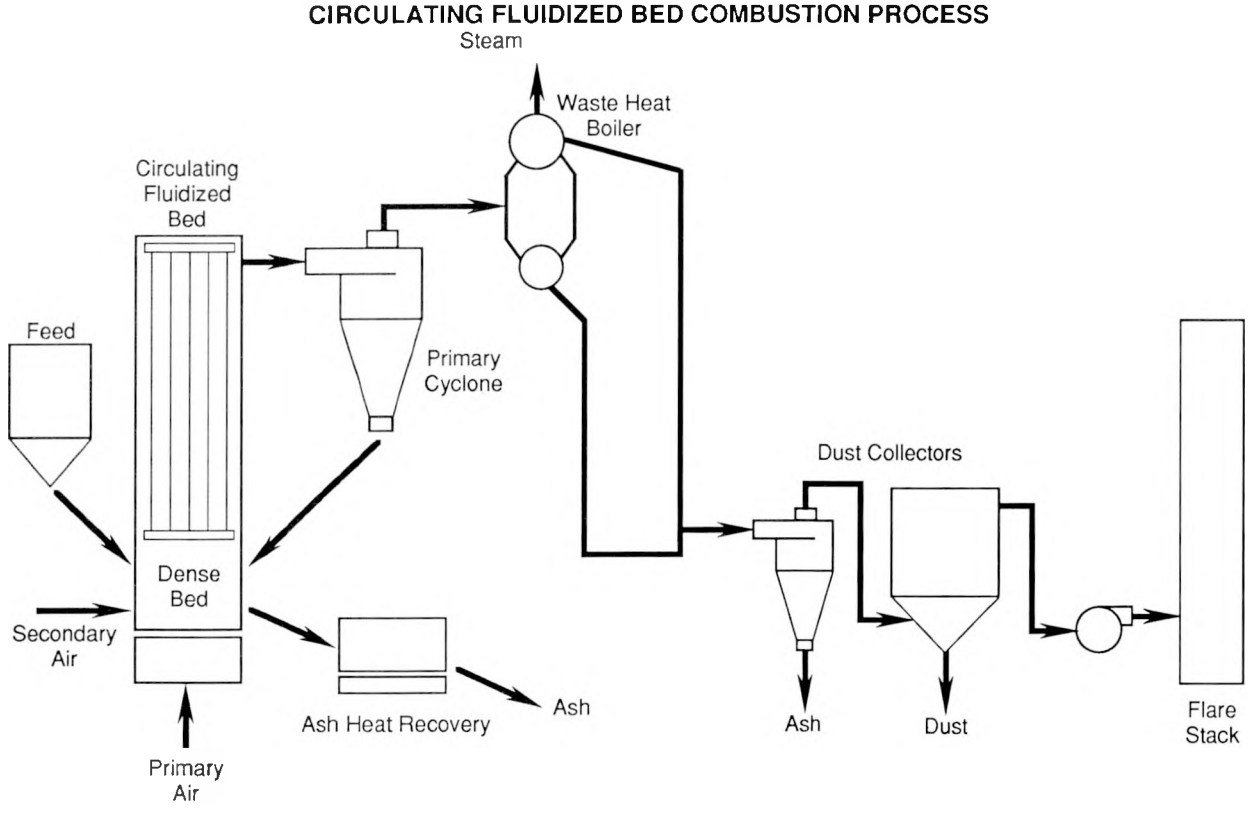

Figure 5. The Circulating Fluidized Bed Boiler Flow Diagram

Conclusions

Many efforts, both theoretical and experimental, have been executed by the PETROBRAS Oil Shale Industrialization Superintendency to promote a satisfactory use of oil shale fines, the particles with dimensions below 1/4 inch, which are discarded from PETROSIX process solid preparation unit.

The current stage of the studies adopts experimental investigations in pilot plants of the entrained bed process (PLASOL), the spouted bed process and the circulating fluidized bed process. The first two accomplish retorting (oil production) of the fines while the last accomplishes the combustion (heat production). The PLASOL unit also processes oil shale sludge to recover its energy content and convert it to a more desirable form for return to the mine fill.

The three processes under development are expected to make a significant heat balance improvement in any oil shale plant that processes only coarse particles, like PETROSIX. Also, the knowledge that is being assembled will add to flexibility when considering future designs of oil shale processing complexes.

The Oil Shale Industrialization Superintendency plans to scale up the processes as soon as the pilot plant test programs are completed satisfactorily.

Literature Cited

1 - NOVICKI, R. E. M., The PETROSIX Process Reaches Commercial Stage, 50th Midyear Refining Meeting, Kansas City, 1985.

2 - TERABE, K., BAPTISTA, A. R. D., Oil Shale Industrialization in Brazil, Beijing, International Conference on Oil Shale and Shale Oil, 1988.

3 - SILVA, J. C., MARTIGNONI, W. P., CASAVECHIA, L. C., GAIZO, U., Desenvolvimento de uma Tecnologia de Retortagem para os Finos de Britagem - o Processo PLASOL, Congresso Brasileiro de Petroleo, 3, 1986.

4 - SOHONs, H. W., et alii, Entrained Solids Retorting of Colorado Oil Shale, Industrial and Engineering Chemistry, 47(3): 461-464, 1955.

5 - MARTIGNOI, W. P., Simulacao do Processo PLASOL - Relatorio No. 3, Sao Mateus do Sul, PETROBRAS/SIX, 1988.

6 - LISBOA, A. C. L., Transferencia de Calor em Leito de Arrasto, Rio de Janeiro, 1987. 153p. Tese, M. S. Universidade Federal do Rio de Janeiro.

7 - BERTOLI, S. L. Transferencia de Calor Radiante em Leito de Arrasto. Rio de Janeiro, 1989. Tese, M. S. Universidade Federal do Rio de Janeiro. (to be published)

8 - MATHUR, K. B., GISHLER, P. E., A Technique for contacting Gases with Coarse Solid Particles, A.I.Ch.E. Journal, 1(2): 157-164, 1955.

9 - ZHAO, J., Coal Combustion in Spouted and Spout-Fluid Beds, Vancouver, 1986. Thesis, M. S., The University of British Columbia.

10 - RAY, T. B., Pyrolysis of Coal in Spouted Bed, Bombay, 1974. 113p. Thesis, Ph.D., Indian Institute of Technology.

11 - Watkinson, A.P., FOONG, G. S. K., CHENG, G., spouted Bed Gasification of Western Canadian Coals, the Canadian Journal of Chemical Engineering, 59: 625-629, 1981.

12 - LEITE, A. C. B., Gaseificacao de Finos de xisto em Reactor de Leito de Jorro - Estudos Hidrodinamicos, Rio de Janeiro, PETROBRAS/CENPES, 1989.

13 - LEITE, A. C. B., WODTKE, R. M. P., LISBOA, A. C. L., RESTINI, F., Pirolise de Finos de Xisto em Reactor de Leito de Jorro, Campinas, Congresso Brasileiro de Eng. Quimica, 6, 1984.

14 - LISBOA, A. C. L., MARTIGNONI, W. P., Leito em Jorro com Finos Menores que Meia Polegada - Ensajos Preliminares, Rio de Janeiro, PETROBRAS/CENPES, 1986.

15 - YERUSHALMI, J., High Velocity fluidization. In: Fluidization, 2nd Ed., 1985. Academic Press, p. 225-291.

Application of Loc-Cat (R) Chelated Iron Scrubbers to Retort Gases

by

Donald Chapman
ARI Technologies, Inc.
Palantine, Illinois 60067

Abstract. The production of oil shale presents some challenging technical problems. Once such requirement involved with production of oil from Eastern or Western Shale is that of removing the sulfur-containing gases from the retort effluent with the minimum of cost and by-product pollutant production.

The LO-CAT Hydrogen Sulfide Oxidation Process is an ideal approach to the desulfurization of the gases from both large scale in-situ retorts and batch or continuous retorting process. This process has been demonstrated on a commercial Western Oil Shale in-situ retorting operation. It has also been licensed for use in sixty other process applications, and over thirty LO-CAT units are in current operation.

The process removes hydrogen sulfide selectively from gas streams and converts it directly to elemental sulfur by use of chemically solubilized iron.

This paper reviews the basic chemistry and configuration of LO-CAT units, and describes the past and future applications of the process to several shale oil production scenarios.

Introduction

The recovery of usable fuel values from oil shale requires separation of the organic components from the shale. This is usually done by retorting.

Retorting can be done either in above ground calciners or in subterranean retorts formed by fracturing the structure in which the shale is deposited and by burning a portion of the oil to provide fuel for the retorting operation.

Above ground retorting can employ direct contacting of the hot combustion products or indirect contacting, in which case the heat for vaporization of the organic components is transferred from the hot combustion products through heat exchange surfaces. The hydrocarbon products are not diluted in this case, and a product of higher quality and greater heating value is obtained. The yield of liquid hydrocarbons is likely to be higher also, because the air used for combustion is not contacted with the shale oil liquids condensing at the retort outlet.

In-situ retorts involve direct contact of the hot combustion gases with the shale being processed. One example of below ground retorting is the LOFRECO process.

The principle of operation of LOFRECO is very simple. A layer of oil shale is fractured and rendered permeable to gas flow by injection wells. Oil is vaporized from the fractured shale and some of the oil is burned to maintain a high temperature in the combustion zone which moves slowly through the bed.

Oil is vaporized and driven out of the hot shale only to cool and condense as the hot gases pass through cooler shale downstream of the fire zone. This liquid oil collects at the bottom of the fracture zone and is pumped to the surface.

The hot, oxygen-depleted gases with the burden of vaporized shale oil are collected by means of downstream wells and the entrained oil is removed. The gases are treated for sulfur removal and burned for power recovery and heat production.

The gaseous products of in-situ and direct retort operations are likely to be quite different in quantity and composition for a given rate of shale oil production.

However, in either of these cases, sulfur compounds will have to be removed from the retort gases before they are acceptable as fuels. The LO-CAT Hydrogen Sulfide Oxidation Process is an ideal approach to the desulfurization of the gases for the in-situ retorting process when it is carried out on a large scale, but it is also a very good candidate for the treatment of gases from batch or continuous retorting by indirect methods.

In both cases, the objective is to desulfurize the gaseous products to produce acceptable fuels for combustion on site or as a sales gas with minimal expenditures of capital and operating costs. It is also necessary that the desulfurization be accomplished without the coproduction of any environmentally unacceptable by-products.

The LO-CAT process removes hydrogen sulfide selectively from gas streams and converts it directly to elemental sulfur which can be used for agricultural or chemical manufacturing purposes. The process uses a water solution of chemically solubilized iron which serves as a solvent for the hydrogen sulfide and also as a regenerable reagent for the chemical oxidation of H_2S to elemental sulfur. The process is ideally suited to the treatment of retort gases because it provides a low cost means of treatment that is very efficient and because it is environmentally the best approach which as been suggested for retorting.

History of the LO-CAT Process

The LO-CAT Hydrogen Sulfide Oxidation Process was developed in the early 1970's and first applied commercially in 1978. The initial applications were in oil refining, natural gas and miscellaneous chemical processing plants.

LO-CAT has been successfully applied to gas streams with hydrogen sulfide concentrations ranging from less than 10 ppm to as much as 100% hydrogen sulfide. Pressures range from vacuum to about 400 psi in commercial service and about 2000 psi in the laboratory. Feed gas composition has little effect on applicability of the process and commercial units treat air, hydrocarbons (fuel or natural gas), pure carbon dioxide, acid gas, hydrogen, and ammonia gas streams. Due to this high degree of versatility and selectivity, LO-CAT is used for H_2S removal in the following commercial applications:

1. amine acid gas
2. natural gas from wells
3. associated gas
4. refinery fuel gas
5. sour water stripper off-gas
6. biogas
7. wastewater treatment plants (odor control)
8. viscose or rayon plants (odor control)
9. carbon dioxide enhanced oil recovery
10. food grade carbon dioxide production
11. pentasulfide production ventilation air
12. coal gasification off-gas
13. shale oil retorting off-gas
14. crude oil storage and loading facilities (odor control)
15. sulfur storage (odor control)
16. geothermal power production vent gas
17. phosphate production off-gas
18. Claus unit tail gas

The main features of the LO-CAT process which set it apart from other hydrogen sulfide removal processes include:

- non-toxicity of the catalyst solution
- extremely high catalytic activity
- great flexibility of application
- high turndown capacity - either sulfur loading or gas flow
- simplicity of the flow scheme

In 1984, the LO-CAT process was demonstrated on a commercial Western Oil Shale in-situ retorting operation at the Seep Ridge, Utah in-situ project.

Geokinetics, Inc. developed and put into practice the LOFRECO in-situ oil shale retorting process in 1983. The flow scheme, shown in Figure 1, involved the liberation of shale oil by heating the oil-bearing shale in fractured underground retorts by burning a portion of the oil in-situ. This process was operated by Geokinetics in Seep Ridge, Utah under a contract with the U.S. Department of Energy (DOE).

The operation in Southeastern Utah involved two 300x300 ft. areas, each containing a 30 foot thickness of oil shale at a depth of 100 feet. Oil production was approximately 400 BBL/Day. The by-product gas produced by the retorting process was burned in an incineration unit. The gas composition varied during the burn period which lasted as long as one year.

In order to meet the State of Utah requirements limiting sulfur dioxide emissions, Geokinetics elected to install a LO-CAT Hydrogen Sulfide Oxidation process licensed by ARI Technologies, Inc. The

LO-CAT process successfully met the State requirements and had demonstrated substantial advantages over the Stretford process tested on a limited scale at the Geokinetics site.

The unit removed 99.8% of the hydrogen sulfide. The inlet gas composition is listed in Table 1.

The suitability of the LO-CAT process for cleaning the gas and for production of elemental sulfur was adequately demonstrated. During the first two months of operation, H_2S loading at the inlet averaged 1600 ppm, and was reduced to about 2 ppm by the LO-CAT unit, with gas flows at approximately the 15,000 SCFM "normal" rate. Catalyst solution circulation rate was maintained at approximately 1500 GPM and catalyst solution strength was 1000 to 2000 ppm iron content.

Chemistry of the LO-CAT Process

LO-CAT is a liquid phase oxidation process which uses a dilute aqueous solution of iron, held in solution by organic chelating agents. The iron oxidizes the hydrogen sulfide ions by removing electrons which reduces the iron. The iron is then circulated to an oxidizer where it is regenerated by contact with air for reuse. LO-CAT does not remove CO_2, COS, CS_2 but mercaptans are oxidized to less odiferous disulfides; however, it does remove H_2S to any level required, converting it elemental sulfur which can be sold or discarded safely.

The basic reactions of the LO-CAT process can be divided into Absorption and Regeneration as follows:

Absorption:

$$H_2S(Gas) + H_2O(Aqueous) \rightarrow H_2S(Aqueous) + H_2O(Aqueous) \quad (1)$$

First Ionization:

$$H_2S(Aqueous) \rightarrow H^+ + HS^- \quad (2)$$

Second Ionization:

$$HS^- \rightarrow H^+ + S^= \quad (3)$$

Oxidation by Metal Ions (Fe^{+++})

$$S^= + 2Fe^{+++} \rightarrow S^o\ (Solid) + 2Fe^{++} \quad (4)$$

Overall Reaction:

$$H_2S(Gas) + 2Fe^{+++} \rightarrow 2H^+ + S^o + 2Fe^{++} \quad (5)$$

Regeneration:

Absorption:

$$O_2(Gas) + 2H_2 \rightarrow O_2(Aqueous) + 2H_2O \quad (6)$$

Regeneration of Metal Ions:

$$1/2\ O_2 + H_2O + 2Fe^{++} \rightarrow 2(OH)^- + 2Fe^{+++} \quad (7)$$

Overall Reaction:

$$1/2\ O_2(Gas) + H_2O + 2Fe^{++} \rightarrow 2(OH^-) + 2Fe^{+++} \quad (8)$$

Adding equations (5) and (8) yields the modified Claus reation:

$$H_2S + 1/2\ O_2 \rightarrow H_2O + S^o \quad (9)$$

In the overall reaction, the metal ions serve to transport electrons from the reaction to the regeneration side, and it is necessary to supply at least two ferric ions per atom of sulfur produced. In this sense, the ferric ions are a reagent. However, they are not consumed in the overall reaction and serve as a catalyst for the reaction of H_2S and oxygen.

In addition to the sulfur forming reaction, thiosulfate ions are also formed whenever sulfide ions and oxygen are in contact with each other. This can occur in liquid oxidation processes whenever sulfide ions are transferred from the absorber to the oxidizer or when dissolved oxygen is transferred from the oxidizer to the absorber.

These by-product reactions are minimized in the LO-CAT process. Due to the high reaction rates which occur in the LO-CAT absorber, sulfide ions are not persistent. In addition, the LO-CAT process can operate at low dissolved oxygen concentrations.

Neither ferrous or ferric ions are stable in aqueous solutions containing sulfide ions and ordinarily will precipitate as either ferric hydroxide or ferrous sulfide as follows:

$$Fe^{+++} + 3OH^- \rightarrow Fe(OH)_3\downarrow \quad (10)$$

or

$$2Fe^{+++} + S^= \rightarrow 2Fe^{2+} + S \quad (11)$$

and

$$Fe^{++} + S^= \rightarrow FeS\downarrow \quad (12)$$

In order to prevent these adverse precipitation reactions from occurring, ARI has developed a system of chelating agents which hold the iron in solution.

Sulfur is formed as a granular solid within the aqueous solution and must be removed by a luquid-solid separation technique such as settling. In general, the sulfur will be formed in the absorber and will be wetted with scrubbing solution. Because sulfur has nearly twice the density of water, it settles fairly rapidly.

Water is created by the chemical reactions which form sulfur, but ordinarily, water must be added to the system to replace losses by evaporation into the oxidizing air and process gas stream. This is true even if the incoming has streams are saturated. The reaction is exothermic and generates about 3500 BTU per pound of sulfur produced (enough to evaporate three pounds of water), while the amount of water produced by the reaction is only a little more than 1/2 lb. per lb. of sulfur.

LO-CAT Flow Schemes for Retorts

The LO-CAT process is usually configured with an absorber column through which the retort gas passes, and a separate oxidizer in which the catalyst solution is aerated with atmospheric air. In the simplest plants both the absorber and the oxidizer are liquid-filled vessels, essentially without internals except for a gas distributor, as shown in Figure 2. This is the configuration most likely to be chosen for an indirect fired retort, which produces a relatively low volume of gas per ton of shale processed.

Large volumes of gas are produced in direct fired retorts, whether they are operated as in-situ systems or above ground. For these systems, a packed column or venturi-packed column combination is more likely to be used. The basic flow scheme remains the same, except that when packed columns are used it is necessary to provide for cleaning accumulated sulfur out of the packing. This is done by equipping the system with a standby column which can be operated while the regular column is being washed.

Figure 3 shows a typical flow scheme for a direct fired system.

In addition to the absorber/oxidizer train shown in these figures, it is necessary to provide for the removal of sulfur from the system. For all but the smallest applications, the sulfur must be treated to produce a molten product suitable for sale to sulfuric acid or other chemical manufacturers. A simple sulfur melting system has been developed to carry out this operation. The design is shown in Figure 4. This figure also shows a sulfur storage system, which must be properly designed to guard against contamination of the molten sulfur by unmeltable solid impurities. Fortunately, there are a number of such systems in operation, and the many potential operating problems have pretty well been worked out by application of these systems to LO-CAT plants used in other industries.

In addition, it is necessary to add chemicals to the process on a continuous basis in order to assure the proper operation of the process. Some of these are:

KOH solution is added to maintain the pH in the 8.0 to 8.5 range for most operations. This is usually the additive used in greatest quantity. It is added at a rate about 2% of that which would be added for removal of the H_2S by chemical conversion to potassium thiosulfate.

ARI-310M makeup solution is added to replace the chelating agents lost by auto-oxidation. This addition is proportional to the amount of sulfur being produced in the plant, although the addition rate is adjusted infrequently and usually set to match the average sulfur production rate.

ARI-310 catalyst solution is added to compensate for the catalyst solution physically withdrawn from the system as samples, losses or blowdown withdrawn to keep the concentration of salts in the operating solution down to manageable levels - usually between 25 and 30 wt%.

A biostat is added at the rate of a few parts per million daily based on the amount of solution in the plant.

A wetting agent is added to help assure that the sulfur particles formed in the process will be wetted by the solution so that it will settle properly and can be separated from the solution without difficulty.

In some processes, surface active materials are carried into the process from cleaning or other operations performed in upstream processes. These may cause periodic foaming, which can be handled by the addition of antifoam agents. This is true of natural gas processing operations, where down-hole corrosion inhibitors and cleaning compounds are occasionally carried over into the gas treating processes. The experience so far in oil shale processing has not shown any significant foaming problem, but the experience is quite limited.

The LO-CAT process is an ideal choice for the removal of hydrogen sulfide from retort effluent gases with minimum cost and by-product pollutant production. Considerable process refinement, catalyst developement work continues to be carried out so the technology will have a minimum of adaptation to undergo when shale oil processing becomes an economic imperative.

Figure 1

Sketch of
LOFRECO Process with
LO-CAT(R) Scrubber

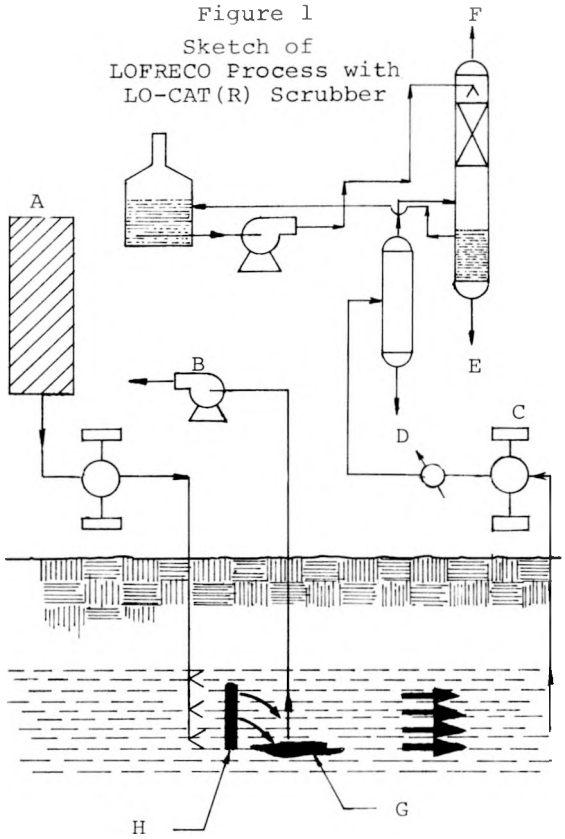

A. Air compressors
B. Oil collection
C. Vacuum pump
D. Secondary oil recovery
E. Sulfur
F. Gas to incinerator
G. Oil collected
H. Fire front

Figure 2

Conventional LO-CAT(R)
Flow Scheme

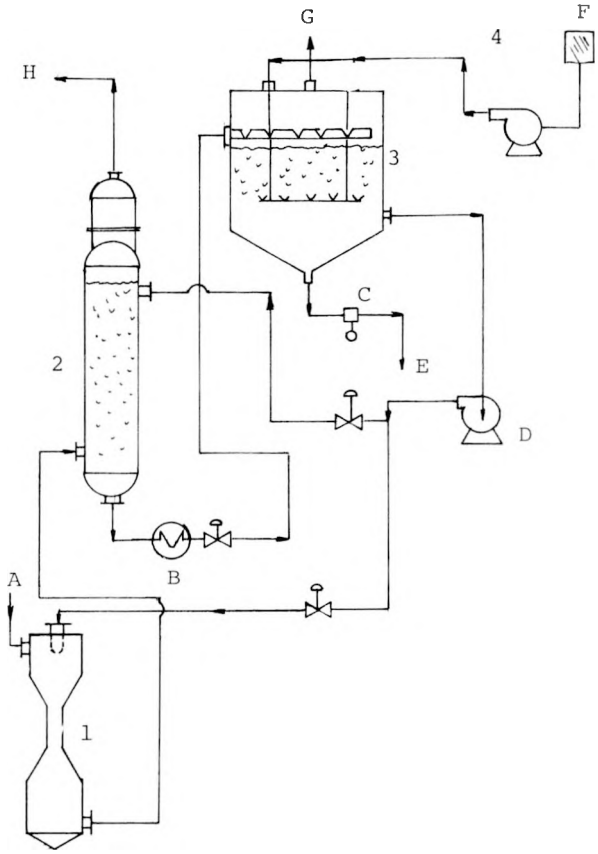

A. Sour gas in
B. Solution cooler
C. Position displacement pump
D. Solution circulating pump
E. To sulfur disposal
F. Silencer
G. To atmosphere
H. Sweet gas out

1. Venturi pre-contactor
2. Liquid filled absorber
3. Oxidizer
4. Air compressor

Figure 3

Flow Scheme
for Conventional
LO-CAT(R) Unit

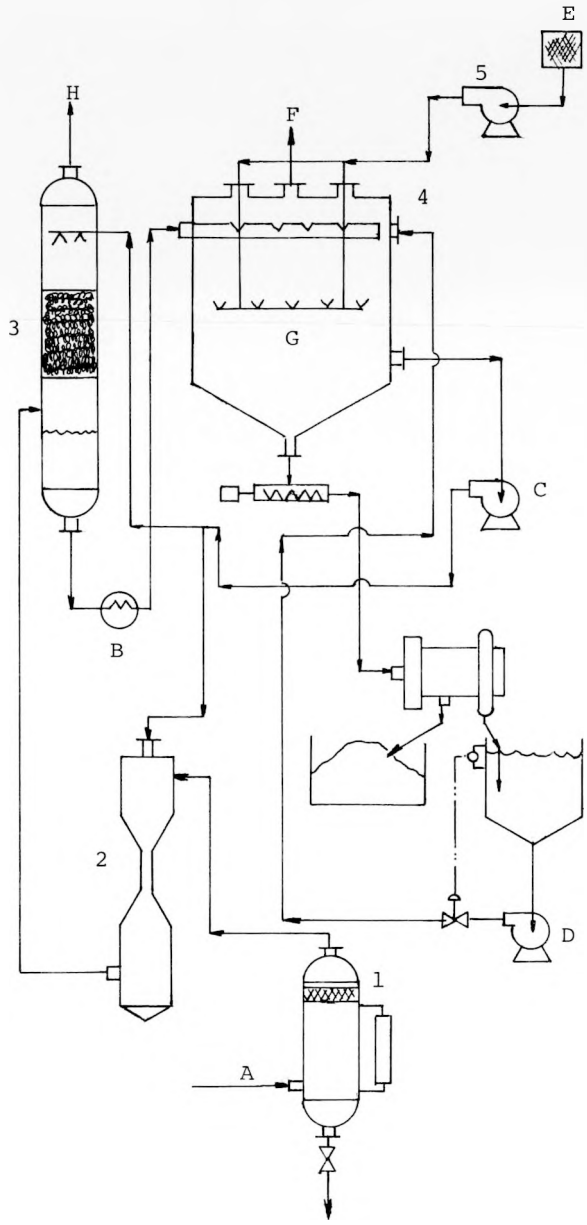

A. Sour gas in
B. Solution cooler
C. Solution circulation pump
D. Clarified solution return pump
E. Silencer
F. To atmosphere
G. Air sparger
H. Sweet gas out

1. Sour gas scrubber
2. Venturi pre-contactor
3. Packed absorber
4. Oxidizer
5. Air compressor
6. Centrifuge
7. Sulfur cake receptacle
8. Clarified solution return tank

Note: Chemical addition equipment not shown.

Figure 4

LO-CAT Sulfur
Melter System

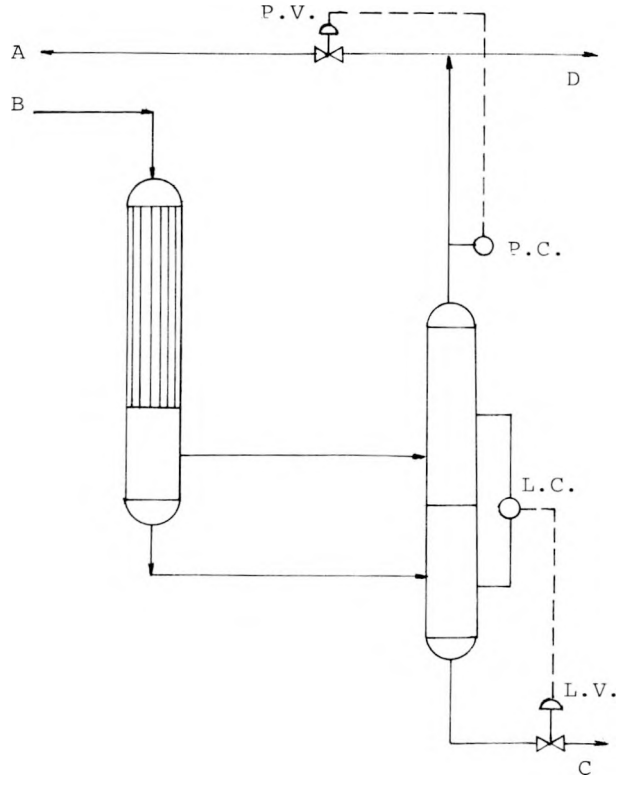

A. Return to LO-CAT
B. Sulfur slurry in
C. To product handling
D. Blowdown

Table 1

Design Conditions for
Geokinetics LO-CAT Unit

Flow	22,000 SCFM
Pressure	0.75 psi
Mositure	10 to 12 vol %
Temperature	100 ^{o}F (maximum)
Gas Composition	(Dry Basis)
H_2S	0.200 (0.2000 maximum)
CO_2	22.17
O_2	1.97
CO	5.31
N_2	58.76
H_2	9.25
COS	0.008
CS_2	---
C_1	1.44
C_2	0.41
C_3	0.29
C_4	0.10
C_5	0.04
C_6^+	0.05
	100.00

Removal of Hydrogen Sulfide by Combusted Rundle Oil Shale: Sulfidation of Iron Oxides

by

John S. Killingley, D. Glenn Callaghan and Stuart J. Day
CSIRO Division of Fuel Technology
Menai, 2234 Australia

Abstract

Oil shale from the Rundle deposit of Queensland, Australia, after retorting and combustion in air, contains hematite and magnetite. Studies of the reactions of hydrogen sulfide with this combusted shale, and with the individual iron oxides, showed the sulfidation kinetics to be first order with respect to hydrogen sulfide with activation energies of 35±1, 59±3, 66±2 kJ mol^{-1} respectively for hematite, magnetite and combusted shale. Under dry conditions the shale trapped 36 mg of hydrogen sulfide per gram of combusted shale. With steam present, the iron oxides did not trap hydrogen sulfide and the combusted shale was also ineffective because, apart from negligible sulfidation of its iron oxide minerals, another sulfur-trapping mineral, calcium oxide, had effectively been removed by silication during combustion. The potential to control hydrogen sulfide (produced during steam retorting of shale) by recycled combusted Rundle shale is therefore poor, but a characteristic of this shale during pyrolysis is that most hydrogen sulfide is released above 500°C, so that by minimising retort temperatures, consistent with appropriate oil recovery, substantial control of hydrogen sulfide should be possible.
(Keywords: Sulfidation; oil shale; iron oxides; hydrogen sulfide).

Introduction

The Rundle oil shale deposit near Gladstone, Queensland, is part of a lacustrine sequence of Eocene age[1]. It has a low carbonate, high clay, mineralogy with montmorillonite, quartz and kerogen present in major amounts. Minor minerals (1-10%) are calcite, siderite, kaolinite, cristobalite, pyrite, illite, feldspar and dolomite.

From the standpoint of pollution control, the disposition of sulfur will be important in the retorting and combustion processes for Rundle oil shale. Combusted Rundle shale contains hematite and magnetite, produced primarily from the oxidation of iron sulfides (pyrite and pyrrhotite) and the decomposition of siderite. Because iron oxides can remove hydrogen sulfide from a gas stream we consider here some aspects of the sulfidation reactions involved when hot combusted shale is recycled directly into the retort to provide heat for kerogen pyrolysis.

Experimental

Experiments were carried out using a small reactor coupled to a high resolution mass spectrometer. In this apparatus, which has been described elsewhere in detail[2], a small bed of sample is heated in a vertical quartz tube through which gas flows at a constant rate. The gas exiting the bed is immediately sampled by a fine quartz capillary which leads directly to the mass spectrometer source.

Initial experiments were conducted using samples of hematite and magnetite to determine the stoichiometry of their reactions with H_2S. Approximately 20 mg of the individual oxides were heated in a stream of standard gas, containing 334 ppm H_2S in nitrogen. Temporal changes in the level of H_2S exiting the sample bed were measured, by monitoring the intensity of the m/z 34 ion (H_2S^+), to estimate the H_2S removed. The hematite used in all experiments was analytical grade Fe_2O_3 (Merck No. 3924) with a grain size of the order of 1 μm or less. For initial experiments we used magnetite that had been prepared by oxidation of pyrite in steam which electron micrographs showed had a very fine open structure, with a grain size equivalent to that of the hematite. For subsequent experiments, samples of mineral magnetite were used which had been crushed to produce particles of less than 150 μm.

Isothermal kinetic measurements were made by step-heating samples of iron oxides or combusted shale in the flowing H_2S standard gas and recording the corresponding decreases in H_2S exiting the sample bed. For each set of experiments, a sufficiently large sample (up to 200 mg) was used to ensure a large stoichiometric excess of the solid reactant. An overall temperature range of about 200 to 570°C was used for the rate measurements, although, for better accuracy, rates for the more reactive samples (hematite and combusted shale) were determined over the lower half of this range.

In a further series of experiments, we investigated the relative amounts of H_2S produced, and the trapping efficiency of combusted shale, under dry and steam conditions. These experiments were made by using consecutive beds of material which were ramp-heated, at 10°C min^{-1}, in either dry N_2 or a 50:50 N_2/steam mixture. Raw Rundle shale, as a practical source of H_2S with associated volatiles, was placed in the first bed and the pyrolysis products passed downwards into a second bed which contained either silica sand, combusted shale, or combusted shale with an additional 5% of CaO. About 200 mg of raw shale was used for experiments in the first bed, and a similar amount of material was used in the second bed. This arrangement simulated aproximately a 1:1 recycle ratio of combusted shale to raw shale. The combusted shale had been prepared by thorough oxidation in air at 800°C.

Results

Sulfur Trapping Capacity

The amount of H_2S removed from the H_2S/N_2 gas stream by the iron oxides was estimated as 2.94 moles per mole of Fe_2O_3 at 500°C and 4.02 moles per mole of Fe_3O_4 at 700°C (the higher temperature was used for magnetite because ramp-heating studies had indicated magnetite to be less reactive than hematite with H_2S). Coincidental with H_2S removal in these experiments was a corresponding release of H_2O. The above data imply the following stoichiometric relationships for the respective oxides:

$$Fe_2O_3 + 3H_2S = Fe_2S_3 + 3H_2O \quad (1)$$
$$Fe_3O_4 + 4H_2S = Fe_3S_4 + 4H_2O \quad (2)$$

The actual reactions probably produced stable sulfide products (FeS_2 + FeS) from the hematite reaction and (3FeS + 1/2 S_2) from the magnetite (pyrite decomposes to pyrrohotite and sulfur at about 600° C), but the stoichiometric ratios allow estimates to be made of the trapping potential of combusted shale containing known amounts of these oxides. Under retorting conditions, in the presence of about 10% hydrogen, the sulfidation reactions are not expected to yield pyrite as a stable phase[3,4]. For the Rundle shale used in this study, we found the total capacity to be 36 mg of H_2S per gram of combusted shale. This corresponds to about 5% iron oxide and compares with a value of approximately 8% determined by X-ray diffraction techniques.

Trapping rate

Data from the trapping experiments for hematite, magnetite and combusted shale were plotted as -ln(1-x) values versus residence time (where x is the fraction of H_2S removed from the gas stream, and the residence time is defined as the volume of the solid in the bed divided by the flow rate). The results showed that the reactions were first order with respect to H_2S. For a range of temperatures, rate constants (k) were obtained from the respective slopes of these lines and are shown as Arrhenius relationships in Figure (1). An additional set of data points is also shown for hematite, obtained from a separate ramp-heated run at 10°C min^{-1} at a specific flow rate; these data are in good agreement with those from the isothermal runs. For the Arrhenius relationship $k = A.e^{-(E_a/RT)}$, values of the activation energy (E_a) and the pre-exponential factor (A) were calculated and are listed in Table (1).

TABLE 1.

Kinetic parameters for H_2S reaction with iron oxides and combusted shale

	A, s^{-1}	E_a, kJ mol^{-1}
Hematite	1.5×10^6	35±1
Magnetite	5.3×10^5	59±3
Combusted shale	5.4×10^7	66±2

The activation energy of the hematite may be compared with a value of approximately 39 kJ mol^{-1} which can be calculated from a plot of Lewis et al.[5] and a value of about 54 kJ mol^{-1} reported by Taylor et al.[6]. From our results, specific values for the rate constant at 500°C can be calculated as 6240, 48, and 1700 s^{-1} for hematite, magnetite, and combusted shale, respectively. In the temperature range of interest for retorting, it is clear that magnetite reacts much more slowly than hematite but these rates are dependent on several variables. For example, the pre-exponential factor, which is related to encounter frequency and geometry, is thought to be affected by particle size of the reacting solid. This was supported by runs on magnetite crushed to finer size (<45 μm) which produced a rate constant greater by a factor of about five, although the activation energy remained about the same. This is consistent with a reduction of particle diameter by about five in the context of gas reacting on the surface of dense solid particles, which have a large stoichiometric excess; for a given volume of material, the total surface area available for reaction will be inversely related to particle diameter. If the intrinsic grain size of the iron oxide in the combusted shale is similar to that of the hematite, then the rate constant of combusted shale relative to that of hematite is reasonable, because the iron oxide content of the combusted shale is about five to ten per cent. It is surprising however that the value of the activation energy for combusted shale is closer to that of magnetite than of hematite, but the combusted shale may contain other oxides which will react with H_2S and the measured value for E_a represents some unknown combination of values for individual minerals in the matrix. Calcium oxide is a potential trapping mineral for H_2S, but the amount available will depend on the calcite component of the shale and the degree to which it has been silicated by reaction with clay minerals in the shale during combustion.[7]

Trapping in the Presence of Steam

Because H_2S is released during shale pyrolysis, largely as a result of the reduction of shale pyrite by hydrogen and water vapour, the addition of steam is likely to affect adversely H_2S trapping by iron oxides in combusted shale. We found that in the presence of steam there was very little absorption of H_2S from the standard gas by the shale, although combusted shale with five per cent added CaO was reasonably effective, and there was a sharp improvement in the rate of H_2S removal when a bed of pure CaO was used. The results from consecutive bed experiments provided a semi-quantitative comparison of gas evolution from raw shale and gas trapping by combusted shale with and without steam. Typical mass spectrometer outputs are shown in Figure (2) for heating in dry nitrogen flow and in Figure (3) corresponding outputs are shown for heating under 50:50 steam/N_2. Data were taken for each run between 200 and 700°C, and areas were measured from ion-intensity/time profiles to obtain estimates of gases evolved between 200 and 500 or 600°C. These estimates, for molecular species of interest, are shown as bar graphs in Figure (4). Because of uncertainties in conversion factors, we have not converted the values to

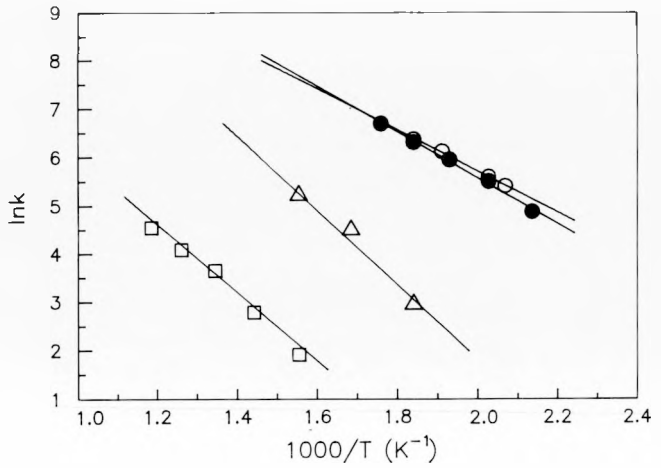

Figure 1. Arrhenius plots of effective rate constants for H_2S reactions with : hematite, isothermal data (o); hematite, ramp data (•); magnetite (□); combusted shale (Δ).

Figure 2. Mass pyrograms for consecutive-bed experiments (dry conditions) showing profiles of selected gases. The second bed contained (a) sand; (b) combusted shale; (c) combusted shale with 5% CaO. Amplification factors for each component to normalise to same height are shown.

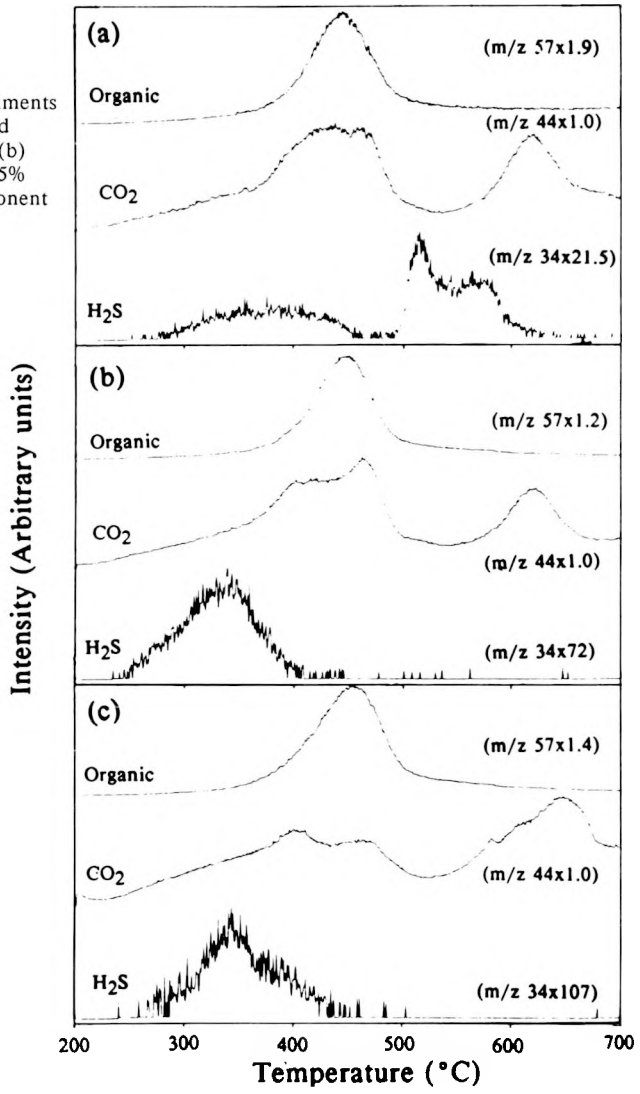

corresponding percentages for the parent molecules. Therefore, the relative amounts for the ions in each cluster represent only approximately the relative amounts of corresponding gases. However, because we have normalised the intensity values to a given mass (m/z 57 - a major organic fragment assumed to be reasonably constant and with mass pyrograms representative of released organics), comparisons of individual species between clusters provide valid estimates of changes in the corresponding gases between different experiments. In general, the respective release profiles for different gases show a shift to lower temperatures when steam is present in the sweep gas. This shift of peak maxima can be as little as 20°C for the organics or as much as 80°C for CO_2 released from siderite decomposition.[8] For gases evolved between 200 and 600°C, an analysis of the results depicted in Figure (4) leads to the following observations:

(i) Under dry conditions, the presence of combusted shale instead of sand in the second bed, caused an approximate five-fold reduction in H_2S. This reflects the effectiveness of the reaction of iron oxides in the shale with H_2S under dry conditions. Emission of H_2S from raw shale (with only sand in the second bed) occurred in two distinct modes - as a long, shallow, peak below 500°C and a characteristic 'sphinx shaped' peak from 500 to 600°C. When the second bed contained combusted shale there was no detectable H_2S release above 450°C, presumably because the kinetics of reactions with iron oxides were fast enough to clean up H_2S in the gas stream. When comparisons are made between corresponding steam and dry conditions, it is apparent that there was a large increase in the H_2S released in steam; an approximate ten-fold increase over sand and a 60-fold increase over combusted shale (the latter reflecting the respective decrease in H_2S level over shale in dry conditions). There was virtually no removal of H_2S by combusted shale under steam conditions, although an approximate 50% reduction was achieved in the case of combusted shale with 5% added lime.

(ii) The m/z 44 (CO_2) level was more than doubled under steam conditions; this was partly because of a 20-30°C shift to lower temperatures for calcite decomposition in steam. Other contributions are probably related to char gasification reactions in steam to produce CO_2 and CO. The lower levels of CO_2 escaping the combusted shale beds, for both wet and dry conditions, probably reflect absorption due to partial re-carbonation of CaO in the shale.

(iii) Amounts of gases released between 200 and 500°C under dry conditions, (Figure (4)), were generally similar to amounts evolved between 200 and 600°C, but the amount of H_2S released under steam conditions is less than half that estimated for the wider range, and there was about one third less CO_2 released than between 200 and 600°C. These differences are due (1) to the bulk of the H_2S being released above 500°C and (2) to siderite decomposing (to release CO_2) below 500°C but decomposition of calcite not commencing until above 500°C.

Of other gases monitored during the trapping experiments, we noted that small amounts of nitric oxide (NO) were released under dry pyrolysis conditions between 400 and 550°C, but none was observed under steam conditions.

Discussion

Rundle shale, under dry retorting conditions, would produce gases with ratios of H_2O/H_2 and CO_2/CO which, correspond thermodynamically, to the equilibrium stable iron oxide phase being magnetite[9]. The presence of steam could lead to the stable phase being hematite, but only in the unlikely event that the H_2O/H_2 ratio was above about 10^5. Research on the desulfurisation of hot producer gas[10] has shown that the kinetics involve the reduction of hematite to elemental iron by CO/H_2, which is then sulfided in a slower, rate determining, step. At 500°C, conditions for reduction to iron include a CO_2/CO mole ratio of less than one and a H_2O/H_2 ratio of less than about 0.5, which are not expected in oil shale retorting. The iron sulfidation reactions are therefore concerned with H_2S reactions of the oxides only, and the amounts of the oxides in the retort will depend on the kinetics of their production there, and on the amounts contained in recycled combusted shale. In the time scale of retorting, it is unlikely that the thermodynamically ordained stable state will be approached, so both hematite and magnetite will be present.

Apart from iron compounds the only other compound in Rundle shale, with significant potential to remove H_2S, is calcium oxide and, as we have demonstrated, CaO mixed with combusted shale will remove some H_2S even with steam present. A problem with Rundle shale, however, is that there may be little free CaO present after combustion because of the silication reaction. The extent of the silication reaction will depend on the combustion temperature as well as the decomposition temperature of calcite, and the latter is related to the partial pressure of CO_2. For example, at a CO_2 partial pressure of 0.1 atmos., the $CaO:CaCO_3$ phase diagram shows CaO to be the stable phase above about 750°C. Because these conditions are generally close to expected combustion conditions, the potential of H_2S trapping by calcium may change substantially with a small change in combustor operations. The preservation of $CaCO_3$ to be recycled into the retort may not, however, be an advantage in the light of findings of Abel and Fischer[11] who reported $CaCO_3$ to be kinetically inert to H_2S although they found that CaO reacted rapidly to form CaS.

In a study on hot fuel gas desulfurisation by calcium-based sorbents, Schrodt and Hahn[12] observed that a CaS layer formed on the exterior of the sorbent and prohibited further reaction with H_2S. We found a similar restriction in the reaction of SO_2 with $CaO/CaCO_3$ in combusted shale[2]. Other authors have stated[9] that "thermodynamically, calcium based sorbants should be effective for H_2S removal, however, kinetically, calcium does not seem to be promising."

In general then, we can say that combusted Rundle shale can effectively remove H_2S from pyrolysis gases under dry retorting conditions by virtue of its iron oxide content, particularly because of the comparatively rapid reaction of hematite. However, additional scrubbing by CaO is likely to be minimal because of the low calcite content and high clay content of the shale which limit the amount of available CaO by silication during combustion. Under steam conditions, the large increase in H_2S produced, coupled with the inability of iron oxides to remove it, means that, unless large quantities of calcium oxide are added, the pyrolysis gas will contain a considerable amount of H_2S.

An important aspect of the release of H_2S from Rundle shale is that the bulk of the organic release occurs at temperatures lower than the release temperatures of the H_2S. This is in contrast to the H_2S release from Colorado oil shale where the bulk of the H_2S is released at lower temperatures and overlaps the release of the organics[13]. For Rundle shale

Figure 3. Mass pyrograms for consecutive-bed experiments (steam conditions) showing profiles of selected gases. The second bed contained (a) sand; (b) combusted shale; (c) combusted shale with 5% CaO. Amplification factors for each component to normalise to same height are shown.

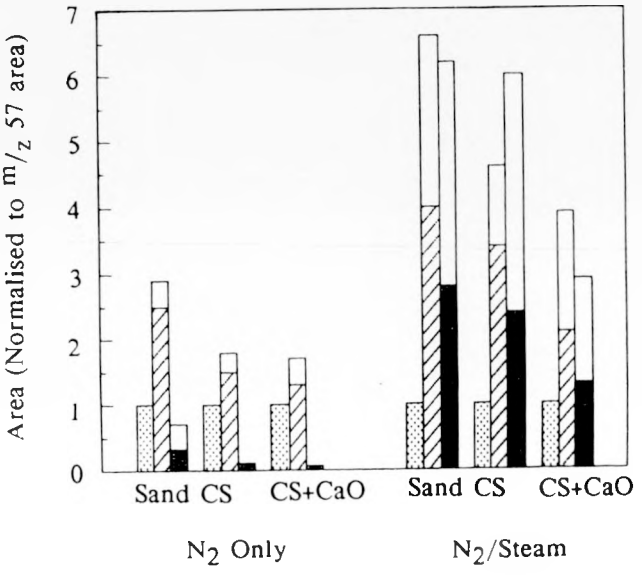

Figure 4. Rundle oil shale pyrolysed at 10°C min^{-1} in consecutive-bed experiments under dry or steam conditions. Graph shows relative changes in gases exiting the second bed, with second bed composition of sand, combusted shale (CS), or combusted shale with 5% CaO. ▨ m/z 57 (organics); ▨ m/z 44 x 0.1 (CO_2); ■ m/z 34 (H_2S. Unshaded portions indicate increase in amounts of corresponding gases for a maximum temperature of 600 instead of 500°C.

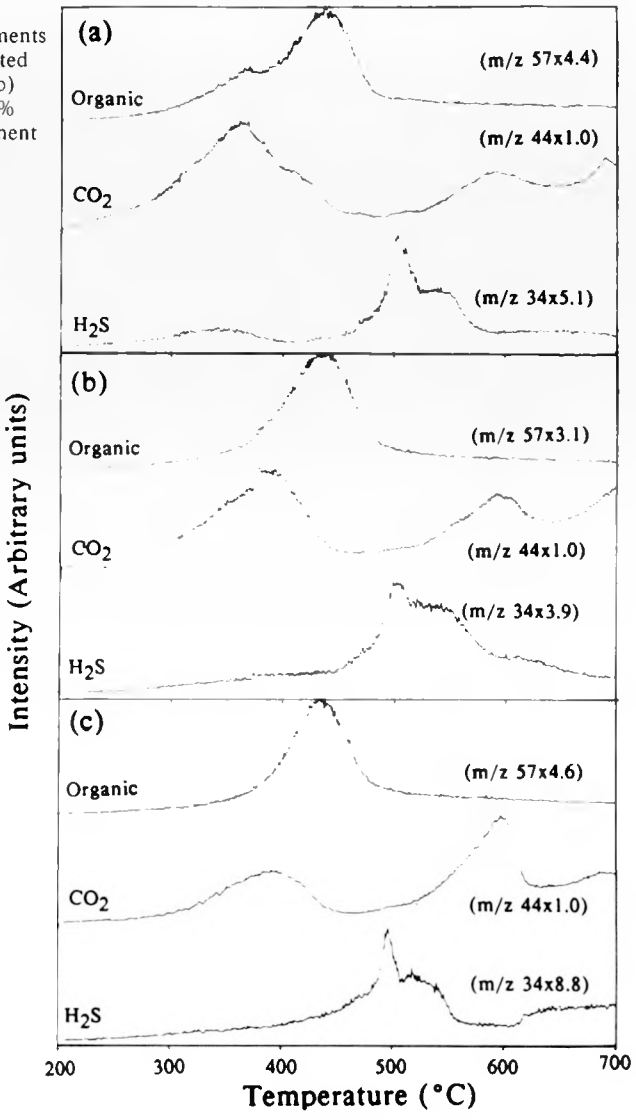

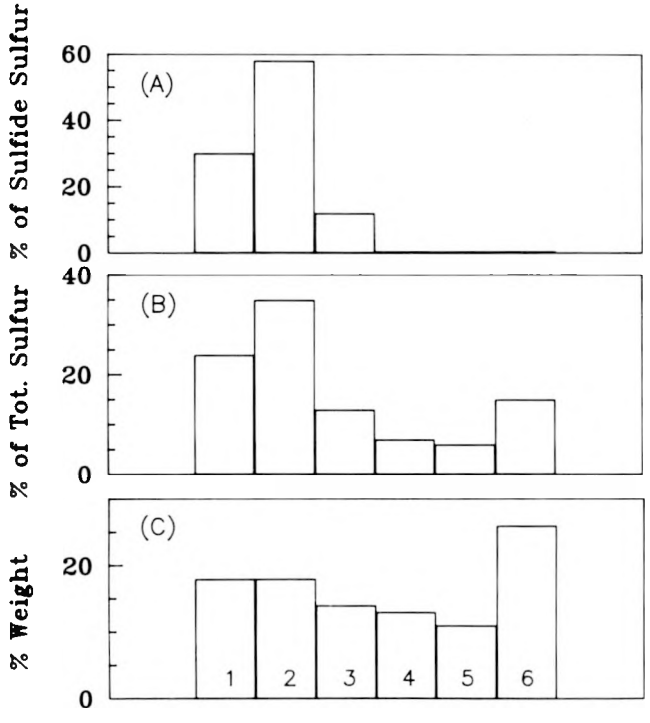

Figure 5. Distribution of sulfide-sulfur (A) and total sulfur (B), as a function of grain size, compared with the weight distribution (C) in Rundle combusted shale. [1, 0-20 μm; 2, 20-90 μm; 3, 90-500 μm; 4, 500-1000 μm; 5, 1000-1400 μm; 6, >1400 μm].

then, in the context of minimising H_2S release, the pyrolysis temperature should be as low as possible and consistent with appropriate product recovery.

A further important consideration is the sulfide content of combusted shale recycled from an actual integrated plant. In the experiments described above we used shale which had been thoroughly oxidised at 800°C and contained no residual sulfide, but in solids from an actual combustor there is likely to be some material which escapes complete oxidation and contains residual sulfide. Combusted Rundle shale from an experimental integrated pyrolysis/combustion rig was analysed for sulfur as a function of grain size, and the residual sulfide sulfur was found to be largely distributed in the finer material (Figure 5). This skewed distribution was a result of relatively short residence times for the smaller particles in the combustor and resulted in almost 90% of the sulfide of the combusted shale residing in material of less than 90 μm size, this fraction representing about one third of the combusted shale by weight. The effect of removing the <90 μm fraction before recycling the combusted shale would have a pronounced effect on the total sulfide sulfur in the retort. In a 1:1 recycle system, for example, there would be about 25% less sulfide present than after recycle of whole shale. For shales of the Rundle type it may be necessary to consider some type of grain-size selection of combusted shale or improved oxidation techniques to minimise the recycling of unoxidised sulfide into the retort. However, advantages of reduced sulfide input to the retort and decreased H_2S in the retort off-gas could be outweighed by larger quantities of SO_2 in the combustor flue gas and higher levels of sulfide in solid wastes (with the potential for more acidic leachates). Therefore each strategy has to be considered with respect to the overall disposition of sulfur and appropriate control measures.

Acknowledgements

This work was partly funded through a collaborative research agreement with Esso Australia Limited. We are grateful for the help of I. Liepa with the mass spectrometer.

References

(1) Henstridge, D.A. and Missen, D.D. Bull. Amer. Assoc. Petrol. Geol., 66, 719-731, 1982.

(2) Killingley, J.S. and Callaghan, D.G. Combustion Studies on Rundle Oil Shale : Inorganic Gases. Fuel, 67, 1349-1352. 1988.

(3) Schrodt, J.T., Yamanis, J., Ota, K., Sodesawa, T. Reaction of Sulfides in Fuel Gases with Iron Oxide in Coal Ashes. Fixed-Bed Experiments and Simulations. Ind-Eng. Chem. Process Des. Dev., 21, 382-390. 1982.

(4) Mikolajska, U., and Stanek, P. Analysis of Equilibrium of the Reactions of H_2S with Fe_2O_3, Fe_3O_4, FeO, Fe, and FeS. Kols. Smola. Gaz. 26(11-12), 247-250. 1981.

(5) Lewis, A.E., Coburn, T.T., Cena, R.J. and Camp, D.W. LLNL Oil Shale Project Review. METC Second Annual Oil Shale Contractors Meeting, Lawrence Livermore National Laboratory, Livermore, Ca. Report UCRL-95140. 1986.

(6) Taylor, R.W., Morris, C.J. and Coburn, T.T. Rates of Chemical Reactions that fix the distribution of sulfur in processing Eastern Oil Shale. Proceedings of the 1988 Eastern Oil Shale Symposium, Lexington, KY.

(7) Campbell, J.H. and Burnham, A.K. Oil Shale Retorting : Kinetics of the Decomposition of Carbonate Minerals and Subsequent Reactions of CO_2 with Char. Lawrence Livermore National Laboratory, Livermore, Ca. Report UCRL 80545. 1978.

(8) Levy, J. and Hurst, H. (in preparation).

(9) Case, G.D. et al. "Chemistry of Hot-gas Cleanup in Coal Gasification and Combustion", Publication. MERC/SP-78/2 Morgantown Energy Research Center, U.S. ERDA, Morgantown, WV, USA. 1978.

(10) Tamhanka, S.S., Hasatani, M. and Wen, C.Y. Kinetic Studies on the Reactions Involved in the Hot Gas Desulfurization using a Regenerable Iron Oxide Sorbent - I. Chem. Eng. Science, 36, 1181-1191. 1981.

(11) Abel, W.T. and Fisher, E.P. "Limestone to remove Hydrogen Sulfide from Hot Producer Gas". Publication MERC/RI-75/3, Morgantown Energy Technology Center, U.S. ERDA, Morgantown, WV, USA, 1976.

(12) Schrodt, J.T. and Hahn, O.J. "Hot Fuel Desulfurization". Publication IMMR 15-PD11-76, Instit. for Mining and Minerals Research, Univ. of Kentucky, Lexington, KY, USA. 1976.

(13) Huss, E.B. and Burnham, A.K. Gas Evolution During Pyrolysis of Various Colorado Oil Studies. Fuel 61, 1188-1196, 1982.

Microbial Desulfurization of Eastern Oil Shale: Bioreactor Studies

by

A. Maka, C. Akin, F. Lau, V. Srivastava, and D.V. Punwani
Institute of Gas Technology
Chicago, Illinois 60616

Abstract. The removal of sulfur from Eastern oil shale (40 microns particle size) slurries in bioreactors by mixed microbial cultures was examined. A mixed culture that is able to remove the organic sulfur from model sulfur compounds present in coal as well as a mixed culture isolated from oil shale enrichments were evaluated. The cultures were grown in aerobic fed-batch bioreactors where the oil shale served as the source of all nutrients except organic carbon. Glucose was added as an auxiliary carbon source. In this study, microbial growth was monitored by plate counts, the pH was checked periodically, and oil shale samples were analyzed for sulfur content. Results show a 24% reduction in the sulfur content of the oil shale after 14 days.

For the efficient microbial removal of sulfur from oil shale, the shale particles and microbes should remain suspended in the bioreactor. The settling characteristics of the oil shale in the bioreactors were examined in the presence of the microbes. Also, the mixing characteristics of the oil shale in the bioreactors were examined. Generally, a mixing rate of 300 rpm resulted in a uniform shale particle concentration at different levels in the bioreactor and an increased microbial growth.

Introduction

The Devonian oil shales of the Eastern United States constitute a significant energy resource for the production of synthetic liquid fuels. It is estimated that over 400 billion barrels of oil may be recovered from these oil resource deposits located in Alabama, Indiana, Kentucky, Michigan, Ohio, and Tennessee. These deposits are located in close proximity to oil refineries, distribution facilities and markets, and water supplies which allows them to be more easily processed.[1]

Oil shale contains organic material primarily kerogen and a small amount of bitumen. The kerogen is a polymer of high molecular weight containing on average several saturated rings with hydrocarbon chains having an occasional isolated carbon-carbon double bond and also containing oxygen and small amounts of nitrogen and sulfur. The sulfur in oil shale is in both organic and inorganic form. The inorganic sulfur is present as pyrite. The organic sulfur occurs in C-S-C bonding in which the carbon atoms may be either unsaturated or saturated. This three-atom grouping may be part of either acyclic or cyclic systems. Some of the sulfur groups in oil shale are thiols, disulfides, and thiophenes.[2,3]

Under a program funded by the U.S. Department of Energy, the Institute of Gas Technology (IGT) is conducting a research program to develop a pressurized fluidized-bed hydroretorting (PFH) process for the production of oil from Eastern oil shales. In this process, high-pressure hydrogen and high temperatures are used to produce higher oil yields than that obtained by other retorting processes. During this retorting process, a significant portion of the hydrogen reacts with the sulfur in oil shale to form hydrogen sulfide. It is economically desirable to reduce the

consumption of hydrogen. One of the ways this can be achieved is by removal of the sulfur compounds from the shale before it is retorted.

Because of the promising results obtained in the microbial desulfurization of coal, that is, >90% removal of inorganic and organic sulfur, microbial desulfurization of oil shale may be feasible.[5-7] As part of the PFH program at IGT researchers at Ohio State University (OSU) have isolated microorganisms from oil shale enrichments.[8]

This paper examines the abilities of a mixed culture isolated from oil shale enrichments by OSU, and pure (IGTS8) and mixed (IGTS7) cultures isolated by IGT from coal bioreactors, under a separate DOE funded program, to remove sulfur from Eastern oil shale. Several oil shale concentrations were examined. Both shake flask and bioreactor experiments were performed. For the efficient removal of sulfur from shale, the shale particles and microbes should remain suspended in the bioreactor. Therefore, the settling and mixing characteristics of the oil shale and microbes in the bioreactor were examined.

Materials and Methods

Cultures

IGTS7 and IGTS8 were provided by Dr. J. Kilbane, Institute of Gas Technology, Chicago, Illinois. These cultures were isolated from coal bioreactors. IGTS7 was a mixed culture and IGTS8 was a pure culture of *Rhodococcus rhodochrous* isolated from IGTS7. These cultures were maintained in a nutrient broth (Difco, Inc., Detroit, MI) or on nutrient agar plates (Difco, Inc., Detroit, MI) at 30°C.

Sixteen pure cultures isolated from oil shale enrichments were obtained from Dr. R. Pfister, Ohio State University, Columbus, Ohio. These were maintained on nutrient agar slants (Difco, Inc., Detroit, MI) at 30°C.

IGTS7M was isolated from a 4% oil shale bioreactor at the Institute of Gas Technology and maintained on nutrient agar plates (Difco, Inc., Detroit, MI) at 25°C.

Oil Shales

Two different beneficiated oil shales (particle size 40 micron) were used in this study. These were Alabama Chattanooga Oil Shale used in the bioreactor experiments and Indiana New Albany Oil Shale used in the shake flask experiments. Both were obtained from the Mineral Resources Institute of the University of Alabama. Ultimate analyses of the samples are given in Tables 1 and 2.

Table 1. Ultimate Analyses of Raw and Beneficiated Alabama Chattanooga Oil Shale.

	Raw	Beneficiated
Ultimate, % dry		
Carbon	16.46	34.29
Hydrogen	1.69	3.18
Nitrogen	0.51	1.55
Sulfur	8.93	8.36
Silicon	--	11.6

Table 2. Ultimate Analyses of Raw and Beneficiated Indiana New Albany Oil Shale.

	Raw	Beneficiated
Ultimate, % dry		
Carbon	13.98	27.42
Hydrogen	1.60	2.79
Nitrogen	0.59	0.97
Sulfur	3.43	2.65
Silicon	--	19.3

Bioreactor Experiments

One-liter round bottom reactors (Cole-Parmer, Chicago, Illinois) with 4-bladed flat disc turbines were used. These reactors were equipped with a stirred motor/controller that allowed stable stirring speeds. The speed was set at 250 rpm, and at this speed there was no settling of the oil shale slurries. Rotameters (Matheson, Joliet, Illinois Tube No. 602) were used to control air flow rates. The air flow rate was maintained at about 80 mL/min which is the maximum flow rate the system can handle.

In the bioreactor experiments, 900 mL of 4% oil shale slurries were added to the bioreactor. The 4% slurries were prepared by adding 4g of oil shale per 100 mL of phosphate buffer (0.125M KH_2PO_4 and 0.187M Na_2HPO_4 in appropriate ratios, final pH 6.8). Oil shale served as the source of all nutrients except carbon. Glucose (15 mM for IGTS7 and IGTS7M) or glycerol (1% for IGTS8) was added to the reactors as a carbon source twice a week.

For examining the ability of IGTS7, IGTS7M, and IGTS8 to remove the sulfur from oil shale, the cultures were pre-grown for several days to late log phase. They were grown at 30°C on a rotary shaker (140 rpm). The cells were grown in basal salts medium (composition 4g K_2HPO_4; 4g Na_2HPO_4; 1.4g Na_2SO_4; 2g NH_4Cl; 0.2g $MgCl_2$; 0.001g $CaCl_2$ and 0.001g $FeCl_3$ per liter), pH 6.8, containing glucose (15 mM) as the carbon source for IGTS7 and IGTS7M and glycerol (1%) as the carbon source for IGTS8 (500 mL in 1 liter flasks). The cells were harvested, washed several times to remove residual sulfur, concentrated and added to the bioreactor at a final concentration of 10^6 cells/mL.

Control bioreactors were operated with the sample bioreactors. In control bioreactors, for the studies with IGTS7 and IGTS7M, though neither culture nor carbon source were added, the natural microflora present in the oil shale grew. Because of this growth, for the bioreactor studies with IGTS8, mercuric chloride (0.1%) was added as an antimicrobial agent to the control bioreactors. The mercuric chloride inhibited the growth of the natural microflora.

The pH was monitored in the reactors and remained at 6.8. Also, microbial growth was monitored by viable plate counts on nutrient agar (Difco, Inc., Detroit, MI).

For sulfur chemical analysis from oil shale, 1 gram portions were removed from the control and sample bioreactors. To facilitate the separation by centrifugation of the cells from the oil shale, the cells were killed by heating. After separation, the oil shale samples were dried in an oven at 103°F. For the determination of sulfur removal, the S:Si ratios were compared with time.

Shake Flask Experiments

For examining the ability of a mixed culture composed of IGTS7, IGTS7M, IGTS8, and the sixteen pure cultures from Ohio State University to remove the sulfur from oil shale, the culture was pregrown as described in the Bioreactor Experiments for Sulfur Removal section. After harvesting and washing the cells, they were concentrated and added to 4% oil shale slurries (50 mL in 250 mL flasks) with and without glucose (15 mM) as the carbon source at a final concentration of 10^8 cells/mL. Cells were periodically added to maintain the concentration in the flask at 10^8 cells/mL. Triplicate oil shale samples and controls were analyzed for sulfur removal as described in the Bioreactor Experiments for Sulfur Removal section at Day 0, Day 7, and Day 14. The controls conditions were: $HgCl_2$ (0.1%) + oil shale + glucose + culture, $HgCl_2$ (0.1%) + oil shale + no glucose + culture, $HgCl_2$ (0.1%) + oil shale + no glucose + no cells, and $HgCl_2$ (0.1%) + oil shale + glucose + no cells. Similar to the bioreactor studies, the pH and microbial growth were monitored.

Stimulation/Inhibition Shake Flask Experiments

For examining the stimulation or inhibition of various oil shale concentrations on the growth of IGTS7. The culture was pregrown, and the cells harvested and washed as described in the Bioreactor Experiments for Sulfur Removal section. After washing, the cells were concentrated (final concentration in flasks 10^6 cells/mL) and added to 4, 8, 12, 20 and 50% oil shale slurries (50 mL in 250 mL flasks) with and without glucose as the carbon source. Glucose (15 mM) was added weekly to the samples. Control flasks contained the oil shale with glucose and no culture. Microbial growth and pH were monitored weekly.

Settling and Mixing Characteristics Experiments

For determining the settling characteristics of oil shale slurries, batch setting tests without agitation were performed and analyzed based on a method by Kynch as described by Badger and Banchero (1955).[9] The change in height of the interface which is the solid-liquid interface between the oil shale and clear liquid, with time was monitored. The settling characteristics of 4% oil shale slurries prepared in a deionized H_2O and phosphate buffer, and 8% and 12% oil shale slurries prepared in deionized H_2O and 4% oil shale slurries with cells were determined.

Agitation Studies

One-liter reactors (Bellco Glass, Vineland, New Jersey) with 8 cm magnetic spinners were used. These reactors were placed on magnetic stirrers (Bellco Glass, Vineland, New Jersey), and different rates of agitation were obtained by adjusting the speed control. The different speeds were determined with a tachometer. For an accurate speed, an average of ten readings with the tachometer were taken.

For examining the effect of different rates of agitation, the uniformity of shale particle concentration at different levels in the bioreactor was determined. The reactors were 12.5 cm high, and samples were taken at 0 cm, 6.25 cm, and 12.5 cm levels. Oil shale samples were removed at these different levels and the wet weight of the shale pellet determined and compared to a standard curve to determine the slurry concentration at the different levels. A standard curve of slurry concentration vs. the wet weight of the shale pellet was constructed (Figure 1). Wet pellet weights for different slurry concentrations ranging from 2% to 20% were obtained in triplicate by centrifuging 25 mL samples at 14,000 rpm for 10 min.

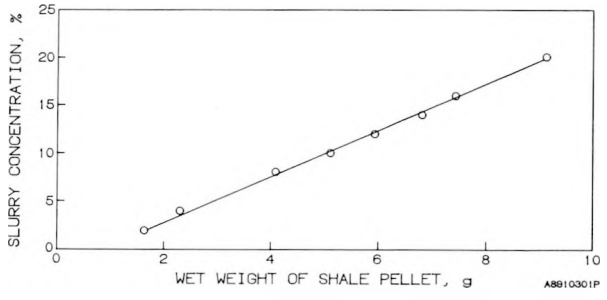

Figure 1. Standard curve: plot of slurry concentration vs. wet weight of shale pellet.

Sulfur Bioassay

The bioassay was performed as described by Kilbane et al. (1989).[7]

Results

Bioreactor Experiments

The mixed culture (IGTS7) and pure culture Rhodococcus rhodochrous (IGTS8) were examined for their abilities to remove sulfur from Eastern oil shale. These cultures were able to use the organic sulfur present in several model sulfur compounds (Table 3). The organic compounds listed in Table 3 are often used as model compounds for the organic forms found in coal and oil shale. In addition, IGTS7 removed about 90% of the organic sulfur from Illinois No. 6 coal.[7]

IGTS7 was initially a mixed culture consisting of seven bacterial types/species based upon colony morphology and bacterial identification.[10] This culture was added to the 4% oil shale bioreactor at a final concentration of 3×10^6 cells/mL. The oil shale served as the source of nitrogen, sulfur, and carbon for growth of the organisms in the batch bioreactor. After 1 month (27 days) incubation, the population increased about threefold to 1×10^7 cells/mL. Chemical analyses of the sulfur content in the oil shale at Day 0 and Day 27 indicated 1% of the sulfur had been removed. The sulfur:silicon ratio at Day 0 was 0.72 and at Day 27 was 0.71. During the 27 day incubation in the batch, oil shale bioreactor, the population of the IGTS7 culture changed. Present, at this time, were 4 bacterial types and 1 yeast based upon colony morphology and microscopic examination. The four bacterial types appeared to be similar in colony morphology to those observed in IGTS7.

The culture (IGTS7M) that evolved in the oil shale bioreactor was examined for its ability to remove sulfur from shale. In this study, to ensure the availability of all nutrients and increased microbial growth, glucose was added as an auxiliary carbon source and the bioreactor was operated on a fed-batch basis. The oil shale served as the source of sulfur. Twenty percent of the oil shale was removed weekly and a fresh 20% slurry volume added. The population increased tenfold from an initial 2×10^6 cells/mL to a final 2×10^7 cells/mL. Chemical analyses of the sulfur content in the oil shale at Day 0 and Day 113 indicated that 16% of the sulfur had been removed. The sulfur: silicon ratio at Day 0 was 0.72 and at Day 113 was 0.61. Oil shale samples taken earlier at Days 27 and 39 did not indicate any sulfur removal. It was inconclusive as to whether this removal was the result of biotic or abiotic action because 11% sulfur reduction was obtained in the control bioreactor after 113 days. Though the control bioreactor was not inoculated with IGTS7 and no glucose was added, microbial growth was observed. At 113 days, the control bioreactor had a cell count of 4×10^6 cells/mL. Several of the colony types present on the nutrient agar plates from the control were similar in appearance to those observed in the IGTS7M culture.

In addition to evaluating IGTS7M's ability to remove sulfur from Eastern oil shale, its ability to utilize the organic sulfur present in the model compounds for growth was examined. The culture used 61% of the sulfur in DBT, 11% of the sulfur in DBT sulfoxide, 53% of the sulfur in DBT sulfone, 25% of the sulfur in trithiane but was unable to use the sulfur present in thianthrene (Table 3).

Rhodococcus rhodochrous (IGTS8) was unable to utilize the sulfur from oil shale for growth. There was no sulfur removal from oil shale by Rhodococcus at 14 and 48 days incubation in the fed-batch reactor. IGTS8 was added (final concentration in the reactor was 10^6 cells/mL) to a 4% oil shale bioreactor in which the oil

Table 3. Sulfur Bioavailability Assay.

Conditions	IGTS8 Kletts/Optical Density* Day 0	Day 4	Difference of Day 4-Day 0	% S Utilization	IGTS7 Kletts/Optical Density* Day 0	Day 4	Difference of Day 4-Day 0	% S Utilization	IGTS7M Kletts/Optical Density* Day 0	Day 4	Difference of Day 4-Day 0	% S Utilization
BSM + Carbon Source**	18	30	12	--	2	109	107	--	11	70	59	--
BSM + Carbon Source + Na_2SO_4 (10 mM)	13	408	395	--	2	800	798	--	15	245	230	--
BSM + Carbon Source + DBT	15	413	398	100	6	390	384	40	14	178	164	61
BSM + Carbon Source + DBT Sulfoxide	13	355	342	86	4	191	187	12	31	108	77	11
BSM + Carbon Source + DBT Sulfone	15	413	398	100	4	335	331	32	11	160	149	53
BSM + Carbon Source + Trithiane	18	30	12	0	6	370	364	37	14	115	101	25
BSM + Carbon Source + Thianthrene	15	66	51	10	5	390	385	40	15	65	50	0

* Average of duplicate samples.

** Basal salts medium + carbon source which was glucose for IGTS7 and IGTS7M and glycerol for IGTS8.

2WP/biostu/PAP

shale was the only available source of sulfur. Glycerol was added as an auxiliary carbon source. The organism initially grew and was the predominant organism present but could not compete effectively with the natural microflora and by the 17th day, IGTS8 colony types were not observed on the nutrient agar plates at dilutions of 10^{-5} suggesting less than 100,000 cells/mL of IGTS8 (Figure 2).

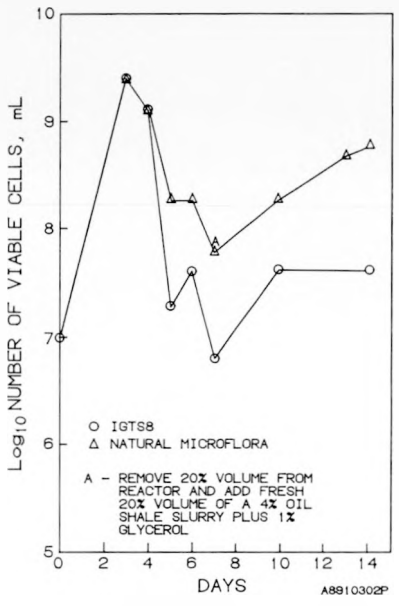

Figure 2. Growth of IGTS8 and the natural microflora in a 4% oil shale slurry.

Shake Flask Experiment for Sulfur Removal

A mixed culture consisting of IGTS7M, IGTS7, the pure culture IGTS8 and the 16 pure cultures, isolated from oil shale environments was examined for its ability to remove sulfur from Eastern oil shale. The culture was added to a 4% oil shale slurry (50 mL in 250 mL flasks) with and without glucose at a final concentration of 10^8 cells/mL. This cell concentration was maintained by periodically adding the culture to the shale. Chemical analyses of the sulfur content of the oil shale after 14 days incubation indicated a 24% reduction of the sulfur content in the presence of glucose, and a 19% reduction of the sulfur content in the absence of glucose (Table 4). No sulfur reductions in the abiotic controls suggest that the reduction observed is the result of biological action.

Observations of the colony morphologies of the mixed culture showed 5 predominant type colonies that were similar to IGTS7 colony types. The IGTS8 colony type was not observed.

Stimulation/Inhibition Shake Flask Experiment

The stimulation or inhibition of various oil shale concentrations on microbial growth was examined. The growth of IGTS7 in 4% to 50% oil shale concentrations with and without glucose was monitored by plate counts on nutrient agar. IGTS7 was capable of growing in oil shale concentrations of 4% to 50% and using oil shale as

Table 4. Ultimate Chemical Analysis on Indiana New Albany Oil Shale Samples for Nitrogen and Sulfur Removal.

	Day 0[a]		Day 7		Day 14		Reduction at 14 Days
	S:Si[b]	S.D.[c]	S:Si	S.D.	S:Si	S.D.	%S
Samples							
4% Oil Shale, 0.27% Glucose, Cells	0.17	0.005	0.15	0.01	0.13	0.001	24
4% Oil Shale, No Glucose, Cells	0.16	0.007	0.15	0.007	0.13	0.004	19
Controls[d]							
0.1% $HgCl_2$, 4% Oil Shale, Cells, 0.27% Glucose	0.17	0.007	0.17	0.001	0.17	0.008	0
0.1% $HgCl_2$, 4% Oil Shale, No Cells, No Glucose	0.17	0.003	0.16	0.002	0.17	0.0	0
0.1% $HgCl_2$, 4% Oil Shale, Cells, No Glucose	0.17	0.003	0.17	0.01	0.17	0.01	0
0.1% $HgCl_2$, 4% Oil Shale, No Cells, 0.27% Glucose	0.17	0.003	0.16	0.001	0.17	0.01	0

[a] Day 0 sample taken after addition to the medium.

[b] S:Si is Sulfur:Silicon.

[c] Standard Deviation of Triplicate Samples.

[d] Abiotic control. The controls defined as abiotic because of no microbial growth on nutrient agar plates. Mercuric chloride (HgCl 0.1%) added as antimicrobial agent.

2WP/biostu/PAP

the sole source of sulfur (Figure 3). The cell growth increase in 4% to 20% oil shale concentrations was 10-fold. By Day 18, in a 4% slurry, cell growth increased from an initial 2 X 10^6 to 4 X 10^7 cells/mL. By Day 18, in an 8% slurry, cell growth increased from an initial 2 X 10^6 to 6 X 10^7 cells/mL. By Day 18 in a 12% and 20% slurry, cell growth increased from an initial 2 X 10^6 to 8 X 10^7 cells/mL. Faster growth was initially observed at the 50% oil shale concentration compared to the 4% to 20%, however, growth decreased more rapidly at the 50% than at the other concentrations. Growth began to decrease at about Day 20 in the 20% slurry whereas in the 4% to 20% slurries growth began to decrease after 24 days (Figure 3).

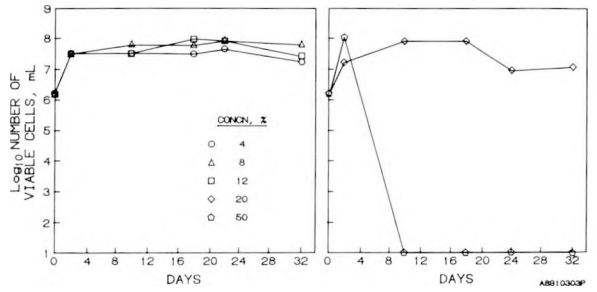

Figure 3. Effect of various oil shale concentrations on cell growth in the presence of glucose.

The addition of glucose to the oil shale slurry stimulated microbial growth. Without glucose, the organisms were not growing but just maintaining themselves. The cell growth increased from 2 X 10^6 cells/mL to 8 X 10^6 cells/mL by Day 24 without glucose whereas with glucose the cell growth increased from an initial 2 X 10^6 cells/mL to 8 X 10^7 cells/mL by 24 days (Figure 4).

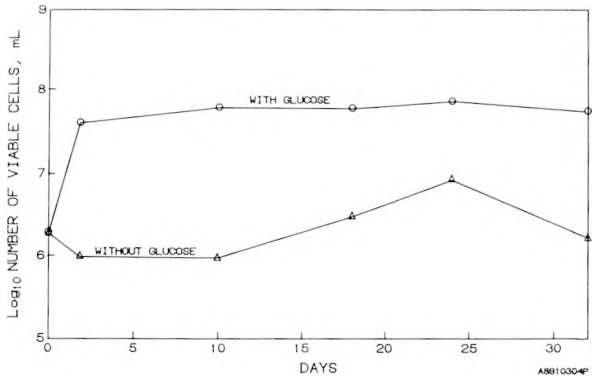

Figure 4. Cell growth in an 8% oil shale slurry with and without glucose.

Settling and Mixing Characteristic Studies

For the efficient operation of the bioreactor the shale particles and microbes should remain suspended in the bioreactor. After the slurry leaves the bioreactor, however, it is desirable to have rapid settling of the shale particles to facilitate the separation of microbial cells. Settling characteristics can be influenced by several parameters that include the concentration and particle size distribution of the oil shale, modification of the particle surface by the adhesion of the microbial cells, and growth medium components.

Batch settling tests without agitation were performed on oil shale samples to determine the effect of oil shale concentration, microbial adhesion to the oil shale, and growth medium components on the settling characteristics. The test was performed by measuring the change in height of the interface which is the solid-liquid interface between the oil shale and clear liquid with time.

The settling of 4%, 8% and 12% oil shale slurries prepared in deionized H_2O was compared to determine the effect of concentration on settling. Concentration changes the settling characteristics of the oil shale. Increasing the oil shale concentration resulted in slower settling of the slurry (Figure 5).

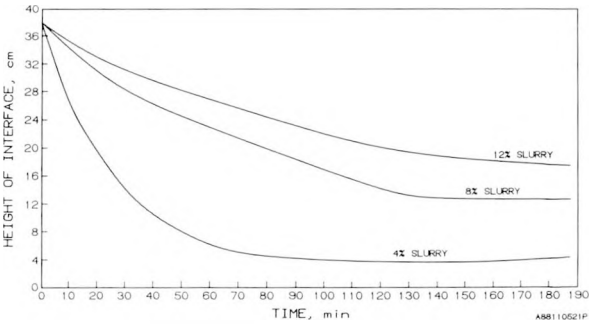

Figure 5. Settling characteristics of oil shale.

To determine the effect of microbial adhesion to the oil shale on the settling, a 4% oil shale slurry from the bioreactor that was incubated with IGTS7 for 49 days and a 4% slurry from the bioreactor that had not been inoculated with IGTS7 were compared. There was no interface observed in the presence of the microbial culture, whereas in the absence of the culture, an interface was observed (Figure 6). The absence of an interface in the 4% slurry from the bioreactor suggests there was minimal to no settling of the oil shale in the bioreactor. This is desirable for the efficient microbial desulfurization of oil shale. A stable suspension, however, is undesirable for the post bioreactor separation operation. A batch settling test without agitation was performed on an effluent from the bioreactor containing a 4% oil shale slurry inoculated with IGTS7 and on an effluent from the bioreactor containing no culture. A distinct interface was observed in the effluent from the bioreactor containing no culture whereas it

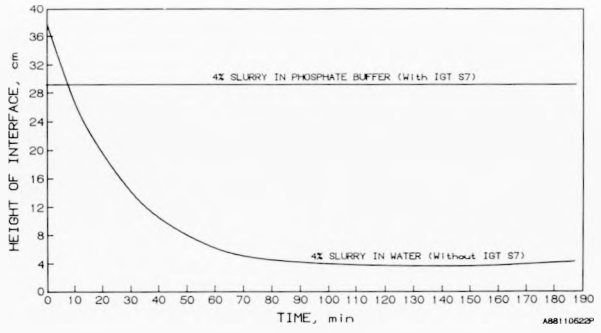

Figure 6. Settling characteristics of oil shale.

was not observed in the effluent from the oil shale bioreactor containing the culture. The effluent from the bioreactor containing the culture was brownish in appearance throughout the solution. This color was attributed to the very fine particles of shale in suspension. The shale remained suspended probably because of microbial association and reduced particle size resulting from the agitation in the bioreactor. Microscopic observations revealed that the cells were adhering to the fine particles.

The settling of a 4% oil shale slurry prepared in a deionized H_2O and phosphate buffer were compared to determine the effect of growth medium components on settling. Settling did take place in a 4% slurry prepared in a deionized H_2O and phosphate buffer. A distinct interface was observed in the slurry prepared in deionized H_2O; however, for the slurry prepared in a phosphate buffer no interface was observed. Rather coalescence did take place which is attributed to settling. These observations suggest that growth medium components affect the settling.

Agitation Studies

The effect of different rates of agitation (62, 170, 240, 300 and 350 rpm) on the uniformity of the shale particle concentration at different levels in the bioreactor and on cell growth was examined. To determine, if settling was occurring in the bioreactor, wet pellet weights of oil shale samples from three different levels in the bioreactor were obtained and compared to a standard curve to determine slurry concentrations at the different levels (Figure 1).

There was no settling of oil shale at the various agitation rates; however, the agitation rates affected cell growth. At a lower rate of agitation, 62 and 170 rpm, the increase in cell growth after 4 days was less than that obtained at higher rates of agitation (240, 300 and 350 rpm). At an agitation rate of 62 rpm, cell growth increased about 50-fold (from 1.36×10^5 to 7.0×10^6) and at an agitation rate of 170 rpm cell growth increased about 100-fold (from 1.36×10^5 to 1.0×10^7). At the higher rates of agitation, cell growth increased 1000-fold (from 10^5 to 10^8) (Table 5).

Discussion

Microbial removal of sulfur from beneficiated Indiana New Albany oil shale has been demonstrated. A mixed culture was developed capable of growing in oil shale concentrations, of 4% to 50%, and using oil shale as the sole source of sulfur (Figure 3). Under aerobic conditions, there was up to a 24% reduction of the sulfur from a 4% oil shale slurry in 14 days. In an abiotic control, no sulfur removal was observed (Table 4).

In the presence of the culture, there was minimal to no settling of the oil shale in the bioreactor. There was no settling of oil shale particles and microbial cells in the bioreactor at agitation rates from 60 rpm to 350 rpm; however, the growth of the culture was affected by the different rates of agitation. At lower rates of agitation 62 to 170 rpm, the population increased 50-fold (1.36×10^5 to 7×10^6 cells/mL) whereas at higher rates of agitation 240 to 350 rpm, cell growth increased about 1000-fold (10^5 to 10^8) (Table 5).

This mixed culture demonstrating sulfur removal consisted of organisms from the natural microflora present in oil shale and several organisms from IGTS7 originally developed to remove organic sulfur from coal based on similarities and differences in colony morphology with IGTS7. It is possible that the organisms capable of removing sulfur from oil shale are naturally occurring in the shale and through selective pressures have evolved. IGTS7 consists of 7 bacterial types. Two of these bacteria were able to grow and utilize the organic sulfur present in model sulfur compounds. These were identified as *Rhodococcus rhodochrous* and *Bacillus sphaericus*.[10] *Rhodococcus* was examined in this study and showed no ability to remove the sulfur from shale. *Bacillus* was not evaluated because of the inability to grow this organism as a pure culture in a non-enriched medium. Therefore, it may be that the organisms in IGTS7 were unable to remove the sulfur from shale. Also, the *Rhodococcus* and *Bacillus* colony types were not observed as colony types present in the mixed culture demonstrating sulfur removal suggesting a native organism(s) in the oil shale was selected.

This mixed culture may be removing the sulfur from shale by an enzyme system rather than removal for growth needs. The cells were not growing in the shake flask experiments where 24% removal of the sulfur was observed (Table 4). The cells were added at high concentrations (final concentrations in the flasks of 10^8 cells/mL) and maintained at this concentration. An increase in microbial growth was not observed.

Table 5. Effect of Different Rates of Agitation on Settling and Growth in the Bioreactor.

Rates of Agitation, rpm	Settling[a] Level in Bioreactor, cm	Sample[b] Slurry Concentration, %[d]	Control[c] Slurry Concentration, %[d]	Increase in Cell Growth, cells/mL After 4 Days in Sample Bioreactor
62	Top (0)	5.0	5.0	
	Middle (6.25)	5.1	4.1	1.36×10^5 to 7×10^6
	Bottom (12.5)	4.6	4.0	
170	Top (0)	4.1	4.0	
	Middle (6.25)	4.0	3.9	1.36×10^5 to 1×10^7
	Bottom (12.5)	4.6	4.0	
240	Top (0)	4.1	5.4	
	Middle (6.25)	4.1	4.8	1×10^5 to 1×10^8
	Bottom (12.5)	3.5	5.0	
300	Top (0)	4.1	5.4	
	Middle (6.25)	3.8	5.4	1×10^5 to 3×10^8
	Bottom (12.5)	4.0	5.4	
350	Top (0)	5.0	5.0	
	Middle (6.25)	5.1	4.1	1×10^5 to 3×10^8
	Bottom (12.5)	4.6	4.0	

[a] For determining if settling was occurring, wet pellet weights from three different levels in the bioreactor were determined and compared to a standard curve to determine slurry concentration.

[b] Slurry and organisms.

[c] Slurry without organisms.

[d] The oil shale slurry in the reactors was a 4% concentration; 36 grams dry oil shale added to 900 mL.

For the efficient operation of the bioreactor, the shale particles and microbial cells should remain suspended in the bioreactor; however, after the slurry leaves the bioreactor, it is desirable to have rapid settling of the shale particles to facilitate the separation of the microbial cells, medium and oil shale. Settling characteristics can be influenced by several parameters that include the modification of the particle surface by the adhesion of the microbial cells, bioproducts, media components, ionic strength of the media and the concentration and particle size distribution of the oil shale. There was a change in the settling characteristics of the oil shale. The more concentrated the oil shale slurry the slower the settling of the shale. When the microbes were present in the oil shale slurry there was minimal to no settling of the shale. This is desired for efficient microbial removal of sulfur and nitrogen from shale. When the shale was present in H_2O, a distinct interface was observed whereas in phosphate buffer, a distinct interface was not observed rather coalescence did take place which was attributed to settling. From these data, it can be suggested that in a microbial process concentrated oil shale slurries can be prepared in an ionic medium where the microbes and oil shale remain suspended for efficient removal of sulfur.

In a solid particle bioreactor, the rate of agitation has to be balanced to ensure that the microbes and the solid particles remain suspended, that adequate oxygen and nutrient transfer is achieved and that no excessive shear forces are generated to avoid abrasive destruction of the microbial cells or further reduction of the shale particle size. In this study, though agitation rates from 60 to 350 rpm resulted in no settling of the oil shale particles and microbes, the lower rates of agitation may not allow adequate oxygen and nutrient transfer because microbial growth did not increase at the lower rates compared to higher rates of agitation (Table 5). In conclusion, these results suggest that a microbial system can be developed in oil shale for the removal of sulfur.

References

1. Janka, J. C. and Dennison, J. M., "Devonian Oil Shale, A Major American Energy Resource." Paper presented at the 1979 Synthetic Fuels From Oil Shale Symposium; Atlanta, Georgia, December 3-6, 1979.

2. Orr, W. L., "Sulfur in Heavy Oils, Oil Sands and Oil Shales," In Oil Sand and Oil Shale Chemistry, ed. by Strausz, O. P. and Lown, E. L., p. 223-243, Verlag Chemie, New York, 1978.

3. Burnham, A. K., "Chemistry of Shale Oil Cracking," In Oil Shale, Tar Sands and Related Materials, ed. by Stauffer, H. C., p. 39-60, American Chemical Society, Washington, D.C., 1981.

4. Punwani, D. H., Lau, F. S. and Roberts, M., "Pressurized Fluidized-Bed Hydroretorting of Eastern Oil Shales," Paper presented at the 1988 Eastern Oil Shale Symposium," Lexington, Kent., p. 359-363, 1988.

5. Kargi, F. and Robinson, J. M., "Removal of Sulfur Compounds from Coal by the Thermophilic Organism Sulfolobus acidocaldarius," Appl. Environ. Microbiol. 44:878-883, 1982.

6. Hoffmann, M. R., Faust, B. C., Panda, F. A., Koo, H. H. and Tsuchiya, H. M., "Kinetics of the Removal of Iron Pyrite From Coal by Microbial Catalyses," Appl. Environ. Microbiol. 42:249-271, 1981.

7. Kilbane, J. and Maka, A., "Microbial Removal of Organic Sulfur From Coal," Final Report (Oct. 1985-1988) DOE Contract No. DE-AC22-85PC81201.

8. Pfister, R. and Krieger, E., "Microbial Desulfurization and Denitrification of Eastern Oil Shale," Monthly Reports (1988-89) DOE Contract No. DE-AC22-85PC81201.

9. Badger, W. L. and Banchero, J. T., "In Introduction to Chemical Engineering," McGraw-Hill Book Co., New York, p. 650-657, 1955.

10. Bulaga, B. and Kilbane, J., "Molecular Biological Enhancement of Coal Biodesulfurization," First, Second and Third Quarterly Reports (Oct. 19889-July 1989) DOE Contract No. DE-AC22-88PC8891.

Nitrogen Chemistry During Oil Shale Pyrolysis

by

Myongsook S. Oh, Kenneth G. Foster,
Armando Alcaraz, and Richard W. Crawford
Lawrence Livermore National Laboratory
University of California
Livermore, California 94550

Abstract

Real time evolution of ammonia(NH_3) and hydrogen cyanide (HCN), two major nitrogen-containing volatiles evolved during oil shale pyrolysis, was measured by means of a mass spectrometer using chemical ionization and by infrared spectroscopy. While the on-line monitoring of NH_3 in oil shale pyrolysis gases was possible by both techniques, HCN measurements were only possible by IR. We studied one Green River Formation oil shale and one New Albany oil shale. The ammonia from the Green River oil shale showed two distinct peaks, while the New Albany shale showed one broad NH_3 peak maximizing at a high temperature. For both oil shales, most NH_3 evolves at temperatures above oil-evolving temperature. The important factors governing ammonia evolution were the presence of inorganic ammonium salts such as Buddingtonite in Green River oil shales, the distribution of nitrogen functional groups in kerogen, and the retorting conditions. The gas phase reactions, such as NH_3 decomposition and HCN conversion reactions, also play an important role in the distribution of nitrogen volatiles, especially at high temperatures. Although pyrolysis studies of model compounds suggests the primary nitrogen product from kerogen pyrolysis to be HCN at high temperatures, we found only a trace amount of HCN at oil-evolving temperatures and none at high temperatures (T > 600 °C).

Introduction

The study of nitrogen (N) species released during oil shale processing is an important research area because both oil shale and shale oil are rich in N. Combustion of N-bearing fuels can produce nitrogen oxides (NO_x), and the emissions of NO_x are limited by law due to environmental concerns. Ammonia is a major N by-product in oil shale processing. Ammonia accounts for most of the N in the retort water and pyrolysis gas streams, and a trace amount of HCN was also observed in those product streams.[1] Both ammonia and HCN are important intermediates in the formation of NO_x during combustion.

We studied NH_3 evolution by pyrolyzing oil shale under a given time-temperature history and measuring the total yield of NH_3 by an ammonia electrode.[2] We learned that: the NH_3 yield increased rapidly as the final pyrolysis temperature increased above 500 °C; NH_3 evolved at oil-generating temperatures came from organic N, while the high temperature NH_3 was from both organic and inorganic sources; the yield at T >500°C was affected by the NH_3 decomposition reaction; and steam worked as an inhibitor for NH_3 decomposition. The ammonia electrode was simple to operate and gave accurate measurements of total ammonia yield for a given pyrolysis condition. However, the electrode method is rather a cumbersome way

*Current Address: Texaco Inc. Research and Environmental Affairs Department, P.O. Box 509, Beacon, NY 12508

to study ammonia evolution kinetics. Earlier, we reported an on-line technique for measuring real-time evolution of NH_3 by means of a mass spectrometer using isobutane chemical ionization.[2-4] In this paper, we summarize the on-line NH_3 evolution rates for one Green River Formation oil shale and one Eastern oil shale as they were pyrolyzed with inert gas (argon) sweep and under autogenous conditions. We also report the evolution of HCN, measured by an infrared spectrometer (IR). We discuss organic/inorganic sources of N and the contribution of the different nitrogen functional groups in kerogen to the NH_3 yield at different pyrolysis temperatures. We also discuss the gas-phase secondary reactions of N volatiles during oil shale pyrolysis.

EXPERIMENTAL

We employed one Green River Formation (western) oil shale and one Eastern U. S. Devonian oil shale in this study. The Green River oil shale was from the Mahogany zone, obtained from Anvil Points mine, CO and has the grade of 22 gal/ton (AP24). The Devonian oil shale was from the New Albany Shale high-grade zone, obtained from Bullitt County, KY, and has the grade of 13 gal/ton (NA13). The chemical compositions of the two oil shales are summarized in Table 1.

About 1 g of oil shale was loaded into a 3/8" o.d. x 21" long quartz tube. We used quartz reactors to minimize reactions with the retort material. We varied the reactor design and the sample size with heating rate to insure the uniform sample temperature during heat-up. The reactor was then placed in a 0.75" i.d. tube furnace. The furnace was heated linearly from 25°C to 900°C. The control thermocouple for the furnace was placed in the inside wall of the furnace. The sample temperature followed the furnace temperature with a roughly constant time lag, unless either endothermic or exothermic reactions occur in the sample bed. In this report, we included the data from pyrolysis at 10 °C/min only. The sweep gas of argon flowed at 40 cm^3/min at 25°C. In the case of autogenous retorting, 40 cm^3/min of argon was introduced down stream of the retort, just above the oil trap. In all cases, the sweep gas plus volatiles flowed through a glass wool trap placed in a 130°C oven to condense heavy components (oil) and then fed to a triple-quadrupole mass spectrometer (TQMS) via an 1/8" stainless steel transport line, heated at 140°C. For ammonia measurements, it is necessary to heat all lines from the reactor to the detector to minimize NH_3 adsorption and desorption as well as ammonia dissolution into condensed water.

Table 1. Chemical Compositions of AP24 and NA13, wt %.

	NA13	AP24
Total C	11.9	16.0
Acid CO_2	1.30	17.8
Org. C	11.5	11.1
Total H	1.48	1.71
Total N	0.43	0.59

The NH_3 concentration in the product gas stream was measured by the TQMS using isobutane chemical ionization (CI).[4] In the electron impact (EI) mode which is a more common ionization technique, the fragment of H_2O (OH) and some methane ($^{13}CH_4$) interfere with NH_3 at m/z 17. The interference by H_2O is very troublesome for NA13, which is a wet shale and evolves much more H_2O than NH_3. In the CI mode using isobutane as a CI reagent, NH_3 could be determined in the presence of water as ammonium ion (NH_4+) at mass 18, because the ionization of water was very inefficient, and almost all the water ions appeared as the protonated species at mass 19. We monitored a few fragments of isobutane and used their profiles to correct the NH_3 evolution profile for long- and short-term TQMS instrumental instabilities. Ammonia evolution profiles were also corrected for the variation of the total flow, and then the calibration factor, which was determined using an 1.08 % or 144 ppm NH_3 standard in argon, was applied.

We tried to introduce a constant flow of trimethylamine or steam at the exit of the oil trap, to monitor the variation of total flow due to volatiles formation. However, neither trimethylamine nor the steam worked well as a flow monitor. The trimethylamine was difficult to handle because of its strong odor and tendency to polymerize and plug the transport line. With steam, it was difficult to establish and maintain a constant flow at a low flow rate (< 100 cm^3/min). So we have decided that the best way of getting the total flow information is to run duplicate experiment in EI mode, in which the total flow rate, sweep gas plus total volatiles flow, can be obtained from the profile of the sweep gas.[5]

We determined the calibration factor before and after each retorting experiment. Because ammonia adsorbs on all surfaces it encounters, we had to allow the calibration gas to flow for a long time (30 mins for 1% NH_3 in argon) before it reaches a constant ammonia concentration. During retorting, the calibration gas was kept flowing through an exit vent at a constant rate. This keeps all surfaces saturated for the final NH_3 calibration.

RESULTS

We have run three identical experiments to determine the reproducibility of our on-line technique. We used AP24 and a 10 °C/min heating rate. Figure 1 shows the ammonia evolution profiles as a function of time from the three runs along with a time-temperature history. The profiles are not corrected for the variations in the total flow. As can be seen, the ammonia profiles by the TQMS are very reproducible. The standard deviation of the areas under three profiles was 2.4 %. The sample temperature increases linearly

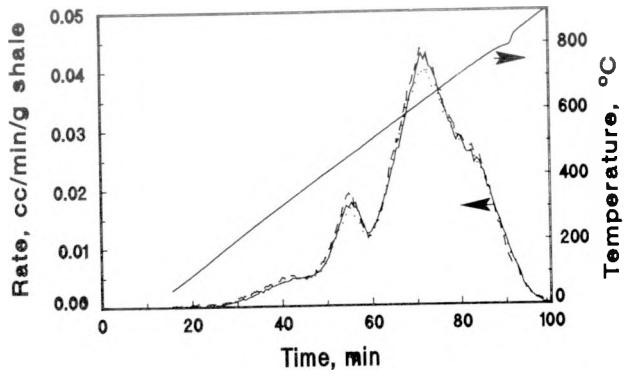

Figure 1. Triplicate measurements of ammonia evolution from AP24 at the 10 °C/min heating rate with time-temperature history.

Table 2. Comparison of ammonia yields (μg NH_3/g shale), measured by a TQMS and by an ammonia electrode.

	NA13	AP24
	By TQMS	
With Sweep Integrated to		
550°C	291	224
900°C	772	841
Autogenous		
550°C	171	193
900°C	954	996
	by Electrode	
Peak Temperature (with Sweep)		
~ 530°C	272	380
~ 737°C	914	853

until it reaches T ~ 780°C. This deviation from linear heat-up results from the endothermic carbonate decomposition reaction and causes the profile to have an artificial shoulder when it was plotted as a function of temperature as will be shown in Figure 2b.

Figure 2 shows NH_3 evolution profiles from the two oil shales at a heating rate of 10 °C/min. The ammonia evolution profile from AP24 has a shoulder at around 350°C, a peak at around the oil-generating temperatures, and a broad high temperature peak considerably larger than the first peak. The high temperature shoulder at 780°C is caused by the nonlinearity of the temperature as mentioned before. The shoulder at 700°C was caused by the noise in the sweep gas profile which was used for the flow correction. By contrast, NA13 has one major peak, although there seems to be a shoulder at around 450°C. The ammonia peak from NA13 is broader and the temperature at the maximum rate of evolution (T_{max}) is higher for NA13 than the T_{max} of the high temperature peak of AP24. At these high temperatures, ammonia decomposes to form N_2 and H_2.[2] Therefore, the different T_{max} may reflect different catalytic potentials of the different oil shale surfaces for the decomposition reaction rather than the difference in the sources and formation mechanisms of NH_3.

It is useful to compare the ammonia yield by the TQMS with total yields measured by using an NH_3 electrode. Table 2 summarizes the yields of NH_3 integrated up to 550°C and up to 900°C and compares them with those from the electrode method. We chose a slightly higher temperature for the intermediate integration point to compensate for the holding time in PT experiments. As shown, for the experiments under argon, the TQMS gives reproducible yields that compare well with the yields determined by the NH_3 electrode. Table 2 also includes the ammonia yields from autogenous experiments.

Figure 3 compares the rate of NH_3 evolution from sweep gas retorting with that from autogenous retorting for the two oil shales.

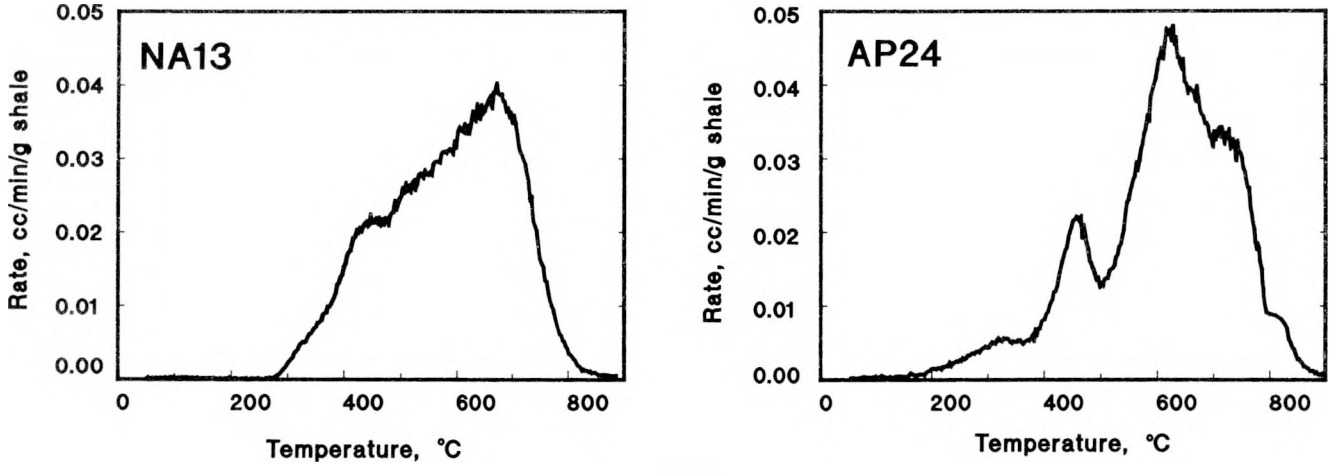

Figure 2. Ammonia evolution from NA13 and AP24.

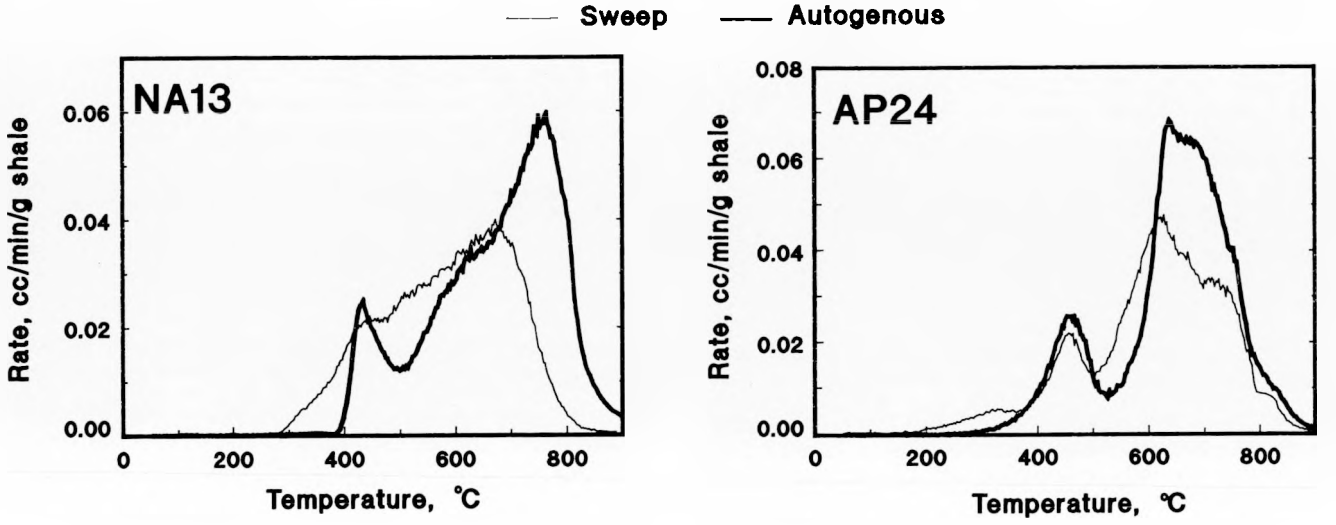

Figure 3. Ammonia evolution from NA13 and AP24 with and without sweep gas.

The AP24 no longer shows the low temperature shoulder under autogenous conditions, and there was much more ammonia evolved at high temperatures. The autogenous retorting of NA13 shows a prominent low temperature ammonia peak and again much higher ammonia yield at high temperatures. For both shales, autogenous retorting gives an ammonia peak with a higher T_{max}.

The on-line measurement of HCN by a TQMS was impossible because m/z 27 is a common fragment of hydrocarbons present in oil shale pyrolysis gas. In addition, the concentration of HCN was low. The other on-line possibility was an IR. We have connected our heated gas transport line to the Digilab FTS-40 FTIR for semi-quantitative measurements of gas evolution. The FTIR was fitted with a special heated light pipe-detector system, normally used for detecting effluent from a gas chromatograph. Even though our FTIR system is not as optimized for on-line data acquisition as the TQMS, we were able to complete a scan every 6.5°C at T < 550°C and 32°C at T > 550°C at 10 °C/min heating rate and plot evolutions of ammonia and HCN as a function of temperature. It was encouraging to see that the ammonia profile duplicates that monitored by the TQMS. Only a trace amount of HCN was observed at low temperatures for AP24 as shown in Figure 4, and no detectable amount of HCN was seen in the case of NA13.

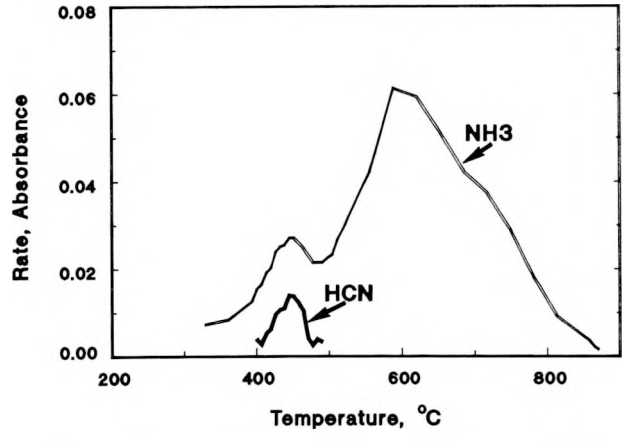

Figure 4. Evolution of NH_3 and HCN from AP24 measured by an FTIR.

Discussion

In order to understand the chemistry involved in NH_3 evolution, we need to look into the distribution of organic/inorganic N sources in oil shales, N functional groups in kerogen, and the extent of NH_3 decomposition reaction over retorting oil shale surfaces under pyrolysis gas environment.

AP24 contains an inorganic N source, Buddingtonite which is an ammonium-containing feldspar.[6] Buddingtonite starts to decompose at around 400°C at the 10 °C/min heating rate, and it is a source of at least half of the NH_3 evolved at high temperatures.[2,3,7] The NH_3 evolution profile from NA13, in which no detectable amount of Buddingtonite was found, suggests that a large amount of NH_3 can evolve from the char matrix at high temperatures. In addition, NA13 is a char-prone oil shale; Fischer assays of this oil shale produce char which contains 55 % of the original organic carbon compared to 20 % from Green River oil shales. Therefore, we expect that NA13 would generate a larger amount of NH_3 from char than Green River oil shales.

While all hydrocarbon gases from oil shale pyrolysis, except CH_4, evolve at around oil-evolving temperatures (between 400 and 600°C at the 10 °C/min heating rate), the higher evolution temperature for most NH_3 from organic N seems to be related to the N-functional types in kerogen and their pyrolysis chemistry. The principal N-

containing species in oil shale kerogen are pyrrole and pyridine types, and there are also some aliphatic N, such as nitriles and amides.[8-10] Pyrolysis of model compounds of pyrroles and pyridines at low temperatures (roughly T < 750 °C) produced mostly rearrangement products and some hydrocarbon gases, but no N-containing species as a gaseous product.[11,14] At higher temperatures, the rupture of the C-N bond in a ring structure produces HCN, NH_3, and N_2.[15-19] The rate of pyrolysis of model compounds reported by Axworthy et al.[17] predicts a T_{max} at a heating rate of 4 °C/min, which is similar to the T_{max} of NH_3 from oil shales under steam.[3]

In contrast, the N in alkyl chains decomposes at lower temperatures even though the literature data were scarce. Polyacrylonitrile decomposes between 250 and 350°C and gives off NH_3 and HCN as the main volatile products. The decomposition of Nylon-66, which breaks the -NH-CO- link, has a much lower activation energy (15 - 42 Kcal/mol) than ring compounds.[20] So it is probable that while the low temperature NH_3 comes from N in alkyl chains, the high temperature NH_3 can come from the pyrolysis of heterocyclic ring compounds, and that the distribution of alkyl and aromatic N can also cause the bimodal evolution profile. The high pyrolysis temperature of pyrroles and pyridines also cause the char produced at 500°C to have a higher organic N/organic C ratio than that in raw shale.[3,21,22]

The model compound pyrolysis also suggests that the primary pyrolysis product from N in oil shale char should be HCN, not NH_3 as we observed in Figure 4. For example, Patterson et al.[15] reported that the pyrolysis of pyrrole produced HCN in 49 % yield, and Axworthy et al.[17] observed that the pyrolysis of pyridine yielded 40 % of the N as HCN with an upper limit of 5 % as NH_3 at 960°C. However, the composition of N volatiles from fuel pyrolysis seems to depend on pyrolysis conditions. For example, industrial coking of coal yields N mainly as NH_3 and N_2 due to NH_3 decomposition.[21] A high degree of conversion of coal-N to HCN gas was observed under very high heating rate conditions, while most gasifier N exist as NH_3.[22] In our fluidized-bed recycle retort system with AP24, the pyrolysis gas contained eight times more NH_3 than HCN at 500°C,[22] and the combustor gas at 625°C contained only a trace amount of HCN, while there was twice as much NH_3 as NO_x.[24] Therefore, it is clear that the secondary reactions of N volatiles in gas phase play an important role in N product distribution.

The NH_3 formation mechanism from kerogen can be summarized as follows:[22]

$T \leq 500°C$, R-NH → R + NH

$T \geq 500°C$, Organic N $\xrightarrow{\text{pyrolysis}}$ HCN

$HCN + H \leftrightarrow CN + H_2$

$CN + OH \rightarrow OCN + H$

$OCN + H \rightarrow NH + CO$

$NH_3 \leftrightarrow NH_2 \leftrightarrow NH \rightarrow N_2$.

The mechanism of converting HCN to NH by H and OH implies the possibility of hydrolysis reaction with HCN. We tested the above mechanism by flowing argon with 1% HCN through a retort filled with quartz sand at a rate of 40 cm^3/min. The TQMS monitored HCN concentration as well as product gases. The same experiment was repeated with argon with 0.5% HCN and 1.18% H_2O. Figure 5a plots the HCN concentration in the exit stream with and without water vapor, and Figure 5b plots NH_3 produced from HCN. Only 10% of the HCN was decomposed at 900°C without H_2O, while almost 40% of the HCN is converted in the case with H_2O. No significant amount of ammonia is observed when there is no steam present and, with steam, roughly 60% of the HCN loss is seen as NH_3. This observation supports the above mechanism, and further emphasizes the importance of gas phase secondary reactions in N-volatile product distribution. In addition, it is quite probable to have a 100% conversion of HCN under our retorting conditions, in which the ratio of N volatiles to H_2O is roughly 1 to 20.

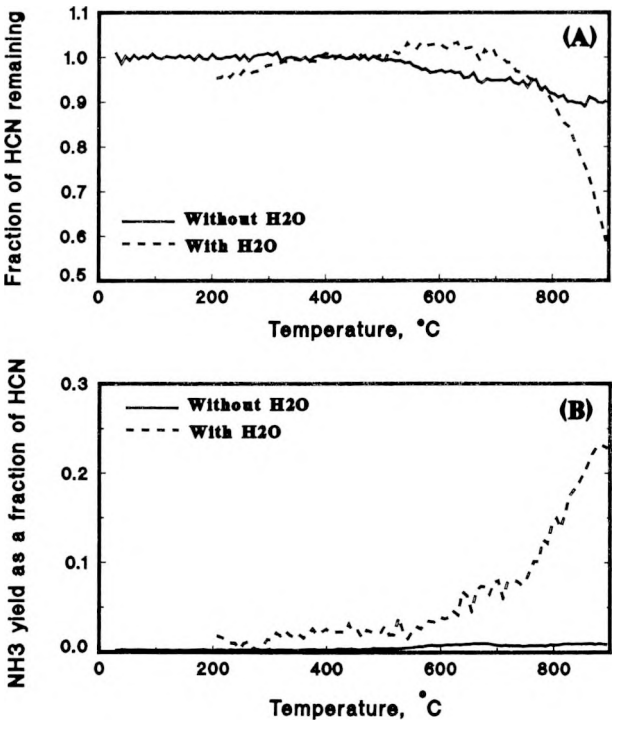

Figure 5. HCN hydrolysis reactions. (A) HCN decomposition; (B) NH_3 from HCN.

Comparison of NH_3 evolution profiles with and without sweep gas shows the effect of both gas-solid and gas phase secondary reactions. Under autogenous conditions, the residence time of volatiles increases as well as the partial pressure of volatiles. As a result, both gas-solid and gas phase secondary reactions are enhanced. The longer residence time of volatiles may have caused the

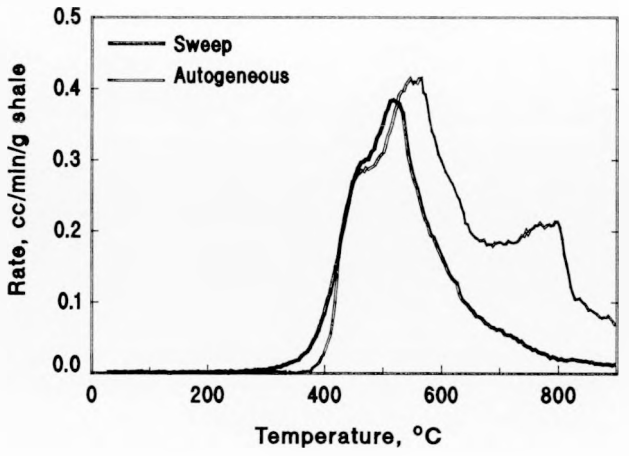

Figure 6. Methane evolution from NA13 and AP24 with and without sweep gas.

disappearance of the low temperature shoulder for AP24 and the sharper ammonia peak at around oil-evolving temperature. The effect of oil cracking does not seem to be important. The ammonia yields up to T = 550°C were about the same in both sweep and autogenous experiments. At high temperatures, higher partial pressure of H_2O and CO_2 and longer residence time enhance char gasification reactions which releases more C as well as N from char. We have observed that much more methane is produced from char gasification at autogenous conditions as shown in Figure 6. The higher partial pressures of H_2O and H_2 also suppress NH_3 decomposition reactions and promote HCN conversion to NH_3.

Conclusions

We measured the real-time evolution of NH_3 and HCN from one Green River formation oil shale and one Eastern U.S. Devonian oil shale. The NH_3 from the Green River Formation oil shale has two distinct peaks, while the New Albany oil shale has one broad peak maximizing at a high temperature. The high temperature peak is due to NH_3 from the decomposition of hetero-cyclic organic N-compounds and, for AP24, the contribution of inorganic N, Buddingtonite, is also significant. We found only a trace amount of HCN at oil-evolving temperatures and none at high temperatures. The gas phase reactions, such as NH_3 decomposition and HCN hydrolysis, play an important role in N-volatile product distribution at high temperatures for both oil shales.

References

1. Sklarew, D. S., and Hayes, D. J., "Trace Nitrogen-Containing species in the Off Gas from Two Oil Shale Retorting Processes," Env. Sci. Tech., 18(8), 600-603 (1984).

2. Oh, M. S., Taylor, R. W., Coburn, T. T., and Crawford, R. W., "Ammonia Evolution during Oil Shale Pyrolysis," Energy Fuel, 2(1), 100-105 (1988).

3. Oh, M. S., Crawford, R. W., Foster, K. G., and Alcaraz, A., "Ammonia Evolution from Western and Eastern Oil Shales," Prepr. Pap. -Am. Chem. Soc., Div. Pet. Chem. 34(1), 94-102 (1988).

4. Crawford, R. W., Coburn, T. T., Miller, P. E., and Oh, M. S., "On-line, Mass Spectrometric Determination of Ammonia from Oil Shale Pyrolysis using Isobutane Chemical Ionization," Amer. Soc. for Testing and Materials, STP1019, 133-143 (1989).

5. Oh, M. S., Coburn, T. T., Crawford, R. W., and Burnham, A. K., "Study of Gas Evolution during Oil Shale Pyrolysis by TQMS," In Proc. Intl. Conf. on Oil Shale and Shale Oil; Zhu Yajie, Ed.; Chemical Industry Press, Beijing, 1988, 295-302.

6. Taylor, R. W., Burnham, A. K., Smith, G. S., Sanborn, R. H., and Gregory, L. S., "Inorganic Nitrogen in Green River Formation Oil Shale," Prepr. Pap.-Am. Chem. Soc., Div. Fuel Chem. 30(3), 338-348 (1985).

7. Oh, M. S., Foster, K. G., Crawford, R. W., Taylor, R. W., Coburn, T. T., Thermal Decomposition of Buddingtonite, Lawrence Livermore National Laboratory UCRL-102156 (1989).

8. Poulsen, R. E., "Nitrogen and Sulfur in Raw and Refined Shale Oils," Prepr. Pap.-Am. Chem. Soc., Div. Fuel Chem., 20(2), 183-197 (1975).

9. Mckay, J. F. and Blanche, M. S., "Analysis of Organic Material Difficult to Recover From Oil Shale," Liq. Fuels Tech., 3(4), 489-521 (1985).

10. Scouten, C. G., Siskin, M., Rose, K. D., Aczel, T., Colgrove, S. G., and Pabst, Jr. R. E., "Detailed Structural Characterization of the Organic Material in Rundle Ramsay Crossing oil Shale," Proc. 4th Australian Workshop on Oil Shale, Brisbane, Dec. 3-4, 1987, 94-100.

11. Patterson, J. M. and Drenchko, P., "Pyrolysis of N-Methylpyrrole and 2-Methylpyrrole," J. Org. Chem., 25(5), 1950-2 (1962).

12. Jacobson, Jr., I. A. and Jensen, H. B. Thermal Reactions of Shale-Oil Components: Methylpyrroles, Buthypyrroles, and Isopropylpyrroles, [Washington] U. S. Dept. of the Interior, Bureau of Mines, 1966.

13. Patterson, J. M. and Soedigdo, S., "Pyrolysis Products of Cycloalkane[a]pyrroles," J. Org. Chem., 32(10), 2969-71 (1967).

14. Patterson, J. M. and Soedigdo, S., "The Thermal Isomerization of Some Trisubstituted Pyrroles," J. Org. Chem.,

33(5), 2057-61 (1968).

15. Patterson, J. M., Tsamasfyros, A. and Smith, Jr. W. T., "Pyrolysis of Pyrrolle," J. Heterocyclic Chem., 5(5), 727-9(1968).

16. Cullis, C. F. and Norris, A. C., "The Pyrolysis of Organic Compounds under Conditions of Carbon Formation," Carbon, 10, 525-37 (1972).

17. Axworthy, A. E., Dayan, V. H., and Martin, G. B., "Reactions of Fuel-Nitrogen Compounds under Conditions of Inert Pyrolysis," Fuel, 57, 29-35 (1978).

18. Houser, T. J., McCarville, M. E., and Biftu T., "Kinetics of Thermal Decomposition of Pyridine in a Flow System," Int. J. Chem. Kinetics, 12, 555-568 (1980).

19. Leidreiter, H. I. and Wagner, H. G., "Investigation about the Thermal Decomposition of Pyridine between 1700 and 2000 K," Z. Phys. Chem. (Munich), 153(1-2), 99-108 (1987).

20. Bamford C. H. and Tipper, C. F. H., Chemical Kinetics, Elsevier Scientific Pub. Co., New York, New York, 1975.

21. Campbell, J. H., Gallegos, G., and Gregg, M., "Gas Evolution during Oil Shale Pyrolysis. 2. Kinetic and Stoichiometric Analysis," Fuel, 59, 727 (1980).

22. Huss, E. G. and Burnham, A. K., "Gas Evolution during Pyrolysis of Various Colorado Oil shales," Fuel, 61, 1188-1196 (1981).

21. Hill, W. H., "Recovery of Ammonia, Cyanogen, Pyridine, and Other Nitrogenous Compounds from Industrial Gases," Chemistry of Coal Utilization, H. H. Lowry Ed., John Wiley & Sons, New York, 1948.

22. Malte, P. C., and Rees, D. P., "Mechanisms and Kinetics of Pollutant Formation during Reaction of Pulverized Coal," Pulverized-Coal Combustion and Gasification, Edited by L. D. Smoot and D. T. Pratt, Plenum Press, New York, 1979.

23. Taylor, R. W. and Morris, C., Internal Memo, LLNL, April 10, 1984.

24. Taylor, R. W. and Morris, C., Internal Memo, LLNL, May 10, 1984.

Acknowledgements

This work was performed under the auspices of the U.S. Department of Energy by the Lawrence Livermore National Laboratory under Contract No. W-7405-Eng-48. Authors also acknowledge Texaco, Inc for the support of M. S. Oh for the preparation of this document.

Pressurized Fluidized-Bed Hydroretorting of Indiana New Albany Shale in Batch and Continuous Reactors

by

Michael J. Roberts, David M. Rue, and Francis S. Lau
Institute of Gas Technology
Chicago, Illinois 60616
Carl Roosmagi
U.S. Department of Energy
Laramie, Wyoming 82070

Abstract. Work is being conducted at the Institute of Gas Technology (IGT) with U.S. Department of Energy (DOE) support to develop a pressurized fluidized-bed hydroretorting (PFH) process for the production of oil from Eastern oil shales. The PFH process, using smaller particle sizes than the moving-bed hydroretorting process, offers higher oil yields and greater reactor mass fluxes through higher selectivity of organic carbon to oil and shorter residence times, respectively.

Batch PFH tests have been conducted to study the effects of shale preheat time (15 to 30 min) and temperature (25° to 320°C), retorting temperature (450° to 710°C), hydrogen pressure (2.8 to 7.0 MPa), particle size (65 to 330 microns), and residence time (5 to 30 min) on the product yields from Indiana New Albany shale. Oil yield has been found to increase with increasing hydrogen pressure. The oil yield was observed to have a maximum at 480°C and to decrease slightly with increasing temperature. At 7.0 MPa hydrogen, the highest oil yield obtained was 130 L/ton (31 gal per ton or 215% of Fischer Assay). Hydrocarbon gas production was found to increase with increasing temperature, but was unaffected by pressure. Decreasing residence time from 30 to 5 minutes had no effect on oil yield but decreased gas yield. Continuous PFH reactor tests produced oil yields and carbon distributions similar to those from the batch tests.

Introduction

The hydroretorting of Indiana New Albany shale in the counter-current, moving-bed HYTORT process has shown to produce oil yields of over 200% of Fischer Assay.[1] An economic study has found that HYTORT is the most economical process presently available for producing oil from Eastern oil shales.[2] Recent work has shown the economics of moving-bed hydroretorting can be further improved by beneficiating the shale prior to hydroretorting.[3] In an effort to lower the cost of Eastern shale oil production still further, work has begun at IGT on a DOE funded program for the development of an advanced hydroretorting process.[4] A block diagram of the major integrated components of the pressurized fluidized-bed hydroretorting (PFH) process is shown in Figure 1.

The shale resource can be completely utilized in the PFH process, however, the commercial size consist (0.3 to 2.5 cm) in a moving-bed reactor requires that the fines from mining and crushing (about 20% of the resource) be discarded, thereby significantly reducing potential oil yield.[5] On a commercial scale, the shale size consist (up to 0.3 cm) used in the PFH process will produce essentially the same oil yield as the results presented here show, if processed at comparable conditions. The larger shale size consist (0.3 to 2.5 cm) used commercially for the HYTORT process will result in a reduction in oil yield (compared with test results utilizing

small particles) due to the effects of hydroretorting large particle sizes.[6] The decrease in hydroretorting oil yield for large shale particles (greater than 0.3 cm) and the potential oil yields for the PFH and moving-bed hydroretorting processes are illustrated in Figures 2 and 3.

There are several advantages of the PFH process compared with the moving-bed hydroretorting process. The fluidized-bed process provides the opportunity for higher oil yields, shorter shale residence times, and thus higher shale throughput. Compared with the moving-bed hydroretorting process, the PFH process requires a much shorter shale residence time because the use of a smaller particle size increases both heat- and mass-transfer rates within the fluidized bed. Studies of the fluidized-bed retorting of New Albany shale in nitrogen, argon, and steam environments have also found short residence times to be effective.[7,8] A shorter shale residence time means that PFH reactors can be smaller, thus less expensive, than moving-bed hydroretorting reactors. The smaller particle sizes used in the PFH process improve the selectivity to oil. The improved selectivity to oil will decrease the hydrogen consumption because, per mole of carbon, oil contains less than half the amount of hydrogen as the product hydrocarbon gas.

PFH process studies have been conducted using Indiana New Albany shale in batch and continuous laboratory-scale reactors. Tests have been conducted to study the effects of preheat conditions, retort temperature, hydrogen partial pressure, residence time, and shale particle size on the carbon conversion to oil and hydrocarbon gases.

Experimental

All batch and continuous PFH tests were conducted with samples from the same batch of crushed and riffled Indiana New Albany shale. Prior to testing, samples were stored in sealed drums blanketed with an inert gas atmosphere. An analysis of the feed shale is provided in Table 1. Schematic diagrams of the two units are presented in Figures 4 and 5. Both units are constructed of 316 stainless steel throughout. The reactors each have inside diameters of 5 cm, and are designed for operation at temperatures and pressures up to 650°C and 7.0 MPa. To reduce costs associated with making many tests in the continuous unit, scoping tests were first conducted in the batch unit to determine the effects of several variables prior to conducting tests in the continuous unit. Operation in a continuous test unit also generates larger quantities of effluent for characterization than are obtained in batch tests. Because both batch and continuous tests were conducted during the same time, it was necessary to have two individual units to conduct tests. Some instrumentation and the data acquisition and control system are shared to minimize equipment duplication. Summaries of test operations are provided below. A detailed description of the batch PFH test operation has been previously reported.[5]

Table 1. Indiana New Albany Shale Composition for Batch and Continuous PFH Tests.

Moisture, wt %	1.79
Ultimate, wt % dry	
Ash	78.19
Total Carbon	14.76
Organic Carbon	14.71
CO_2	0.20
Hydrogen	1.63
Sulfur	3.07
Nitrogen	0.60
Oxygen (from HTW)	3.63

Batch PFH Reactor

The batch PFH unit includes a feed hopper (capable of preheating the shale it contains), reactor, liquid collection receiver, recycle compressor, split-tube furnaces, mass-flow controllers, and a computer control and data acquisition system. In a typical test, 200 g of sized shale is charged to the feed hopper and 200 ml of the same size silica sand is charged to the reactor. The system is pressurized with hydrogen, the reactor is heated to the desired temperature, and the sand is fluidized by circulating gas with the recycle compressor. A small flow of make-up hydrogen is also established. Shale is preheated under the desired conditions of temperature and pressure in the feed hopper and then dropped into the top (top feed) of the preheated reactor. Reactor conditions of temperature, pressure, and gas flow are maintained for the desired time, and then the furnaces are shut off and opened. All product liquids and gases are carefully collected and analyzed.

Continuous PFH Reactor

The continuous PFH unit, shown schematically in Figure 5, includes a feed hopper, reactor, unsteady-state and steady-state solids and liquids receivers, feed and discharge screws, a recycle gas compressor, split-tube furnaces, mass-flow controllers for the recycle gas and make-up hydrogen, and a computer control and data acquisition system. The feed hopper can hold 4000 g of feed shale allowing up to 5 hours of continuous operation at a feed rate of 700 g/h.

Feed shale is charged to the feed hopper, and the unit is sealed and pressure tested. The system is pressurized with hydrogen, the feed hopper is initially heated to 100° to 150°C, and the reactor is heated to the desired test temperature. The recycle compressor is started to initiate a low gas flow, and the calibrated feed screw is then set at the planned shale feed rate. Bed level is monitored by differential pressure and controlled by the

discharge screw rate. After a bed is established, the discharge screw is started at a low rate and the recycle gas rate is increased to fluidize the bed. Make-up hydrogen, at approximately 1.5 L/min, is continuously fed to the system. When the desired bed height is reached, the discharge screw rate is increased to maintain the bed (and the average shale residence time) at a constant level.

Steady-state operation is started after at least three bed turnovers at steady-state conditions have elapsed. Steady-state product liquids and residue shale are collected in separate receivers. Gas samples are taken at the beginning, middle, and end of steady-state operation, and a composite gas sample is taken at the end of the test. All weights are recorded and temperature, pressure, and gas flow data are recorded by computer throughout the test. Analyses are performed on the feed and steady-state residue shale, the product liquid (water and oil), and the product gas. Carbon balance, oil yield, and sulfur-balance calculations are conducted for each continuous PFH test.

Results and Discussion

Tests have been conducted in the batch and continuous PFH units to determine the effects of independent operating variables on the products from pressurized fluidized-bed hydroretorting of Indiana New Albany shale. The independent variables studied include preheat conditions, temperature, hydrogen pressure, residence time, and shale particle size. The ranges of operation for the batch and continuous units are shown in Tables 2 and 3, respectively.

In the commercial application of the PFH concept, economics and energy conservation require that the shale be preheated before being introduced to the hydroretorting reactor. Two series of tests were conducted in the batch PFH reactor to determine if shale preheat temperature or preheat time have any effect on the oil or gas yield. Previous work on moving-bed hydroretorting has shown the oil yield from New Albany shale to be related to the shale heat-up rate.[9] Shale was sized to -60+100 mesh for the tests and a hydroretorting residence time of 30 minutes was used to ensure preheat results would not be masked by an insufficient retorting residence time. Various preheat temperatures and times were tested for the two retorting conditions of 485°C at 4.2 MPa and 565°C at 7.0 MPa. Results of these tests are presented in Figures 6 and 7.

Preheat temperature was varied from 25°C (no preheat) to 320°C and two preheat times of 15 and 30 minutes were tested. Figure 6 shows the effects of preheat conditions on the oil yield. At both retorting conditions, no discernable effects of preheat conditions on oil yield were observed. In Figure 7, the carbon conversions to both oil and gas are shown for various preheat conditions for

Table 2. Batch PFH Tests (Ranges of Operation)

	Ranges
Shale Preheater	
Temperature, °C	25 to 310
Residence Time, min	10 to 30
Retort	
Temperature, °C	450 to 700
Pressure, MPa	2.8 to 7.0
Residence Time, min	5 to 30
Particle Size, mesh (microns)	-200+270 to 160+100 (65 to 200)

Table 3. Continuous PFH Tests (Ranges of Operation)

	Ranges
Shale Preheater	
Temperature, °C	150
Residence Time, min	>30
Retort	
Temperature, °C	482 to 538
Pressure, MPa	2.8 to 4.2
Residence Time, min	20 to 30
Particle Size, mesh (microns)	-60+100 (200)

retorting conditions of 565°C and 7.0 MPa. The batch test results show the oil and hydrocarbon gas yields are unaffected by the preheat conditions.

Since the preheat conditions did not affect the carbon conversion to oil and gas, preheat conditions were arbitrarily set at a temperature of 225°C and a preheat time of 10 minutes for the remaining tests. All subsequent batch and continuous PFH tests were made with similar preheat temperatures and residence times.

Previous work with moving-bed hydroretorting has confirmed a strong correlation between carbon conversion and average particle size.[6] The PFH process utilizes shale particle sizes of 0.3 cm and below. Tests were conducted in the batch PFH reactor to determine the effects of particle size on oil yield and carbon conversion. A series of tests was conducted at retorting conditions of 565°C at 7.0 MPa to determine the effects of particle size on product yields for the PFH process. The shale residence time for all tests was 20 minutes to allow sufficient time for maximum carbon conversion at these conditions. The particle size ranges tested were -200+270, -100+140, and -60+100 mesh, corresponding to average particle sizes of 65, 125, and 200 microns, respectively. The effect of particle size on carbon conversions are presented in Figure 8. The results show that, within the experimental accuracy of the tests, over the size range studied, there was no significant effect of particle size on

carbon conversion to oil or gas. Further PFH tests with larger shale particle sizes will be conducted to determine the particle size above which the carbon conversion to oil starts to decrease.

The high oil yields achieved during hydroretorting of Eastern oil shales are a result of the hydrogen present during retorting. Some of the feed hydrogen present is consumed in the generation of the product oil and gas.[1,10] Tests were conducted in the batch and continuous PFH units to determine the relationship between hydrogen pressure and the carbon conversion to oil and gas. Batch and continuous PFH tests were conducted with -60+100 mesh shale and residence times of at least 20 minutes. Batch tests were conducted over a hydrogen pressure range of 2.8 to 7.0 MPa at two retorting temperatures of 485° and 565°C. Continuous PFH tests were conducted at conditions of 480°C at 2.8 MPa, 480°C at 4.2 MPa, and 538°C at 4.2 MPa. The relationship between hydrogen pressure and carbon conversion to oil and gas is shown in Figures 9 and 10.

Batch tests at 485° and 565°C show carbon conversion to oil and gas both increase linearly with increasing hydrogen pressure. At 485°C, carbon conversions to oil and gas increase from 54% and 10% at 2.8 MPa to 72% and 14% at 7.0 MPa. At 565°C, carbon conversions to oil and gas increase from 54% and 18% at 2.8 MPa to 69% and 21% at 7.0 MPa.

Continuous PFH tests had similar to higher oil yields and lower carbon conversions to gas than batch tests at the same conditions. The two continuous PFH tests conducted at 4.2 MPa had oil yields similar to those of batch PFH tests also conducted at 4.2 MPa, and lower conversions of carbon to gas. The continuous test conducted at 2.8 MPa had a higher oil yield and a lower carbon conversion to gas compared with batch PFH tests conducted at the same pressure.

The relationship between oil yield and hydrogen pressure is illustrated in Figure 11. A comparison of the oil yields from Fischer Assay (500°C in nitrogen) and PFH (480°C in hydrogen) tests shows that the relationship between oil yield and hydrogen pressure may be considered linear over a wide pressure range. However, the oil yield is actually nonlinear with pressure. The oil yield for the PFH tests was found to increase linearly with pressure from 159% of the Fischer Assay oil yield at 2.8 MPa to 210% of Fischer Assay at 7.0 MPa. The maximum possible oil yield for Indiana New Albany shale could be obtained only at a hydrogen pressure well above the 7.0 MPa studied in the PFH tests.

A fluidized-bed reactor provides good heat transfer through intimate solid-solid contact. Short residence times and high shale turnover are therefore possible in the PFH process. Batch and continuous PFH tests have been conducted to study the effects of residence time and temperature on the oil yields and carbon conversions. Series of tests were conducted at 4.2 and 7.0 MPa hydrogen pressure using residence times from 5 to 30 minutes and temperatures from 450° to 705°C. Carbon conversions at the two pressures are presented in Figures 12 and 13.

At both pressures, carbon conversion to oil was highest at 480°C and decreased with increasing temperature. Carbon conversion to gas increased with increasing temperature. Tests conducted at 4.2 MPa show oil yield decreases from a high of 60% of the feed carbon at 480°C to 57.5% at 585°C. Both carbon conversion to gas and total carbon conversion increase with increasing temperature. The continuous tests and the batch test with a 5-minute residence time had the same oil yield, but lower carbon conversions to gas than the batch tests with residence times of more than 20 minutes.

Similar results, but with higher conversions, were obtained at 7.0 MPa. Carbon conversion to oil was found to have a maximum of 72% of the feed carbon at 480°C and to decrease to 68% at 705°C. Carbon conversion to gas and total carbon conversion increased with increasing temperature. Reductions in residence time to as little as 5 minutes did not decrease the oil yield, but did decrease the carbon conversion to gas.

A comparison of the oil yields of the batch and continuous PFH tests at 4.2 and 7.0 MPa with the Fischer Assay oil yield is presented in Figure 14. The PFH process produces oil yields well above the Fischer Assay value for Indiana New Albany shale. At 4.2 MPa hydrogen pressure, the oil yield was found to be 175% of Fischer Assay at 480°C and to decrease to 168% of Fischer Assay at 585°C. PFH processing at 7.0 MPa resulted in even higher oil yields of 209% of Fischer Assay at 480°C decreasing to 196% at 705°C.

Conclusions

Laboratory-scale testing of the PFH process has been been shown to produce the same high oil yields as the moving-bed hydroretorting of Indiana New Albany shale while taking advantage of rapid solid-solid heat transfer. Batch PFH tests have shown that shale preheat time and temperature, and shale particle size from -60+100 mesh to -200+270 mesh do not significantly affect the carbon conversion to oil and gas.

Indiana New Albany carbon conversion to oil and gas in the PFH process increases with increasing hydrogen pressure. Over the pressure range studied (2.8 to 7.0 MPa), carbon conversion to oil and gas can be described as linear with hydrogen pressure.

The PFH oil yield with Indiana New Albany shale was found to have a maximum at

480°C and to decrease with higher reactor temperatures. Carbon conversion to gas increases with increasing PFH temperature. Oil yield was the same for tests with residence times between 5 and 30 minutes, whereas gas yield was lower for tests with short residence times. These results indicate that both the production of oil and the carbon selectivity to oil from Indiana New Albany shale in the PFH process would be most favorable at a temperature of 480°C and a residence time of 5 minutes or less.

Tests conducted in the continuous PFH unit produced the same, or higher, oil yields as those conducted in the batch PFH unit at the same conditions. The gas yield in the top-feed, continuous PFH unit was somewhat lower than in the batch unit. These results are encouraging and suggest that the use of continuous PFH reactors will not result in reductions of PFH oil yield.

References

1. Roberts, M. J., Punwani, D. V., Hu, W.C.S. and Rex, R. C., "Effects of Temperature and Pressure on the Hydroretorting Yields of Three Eastern Oil Shales," AIChE National Meeting, Miami, FL, 1986.

2. Parkinson, W. J., Phillips, T. T. and Barnes, J. W., "An Economic Comparison of Five Process Concepts for Using Eastern Oil Shale," ACS, St. Louis, MO, 1984.

3. Hu, W.C.S. and Rex, R. C., "Economics of Combined Beneficiation/HYTORT Processing of Eastern Oil Shales," Eastern Oil Shale Symposium, Lexington, KY, November 30-December 2, 1988.

4. Punwani, D. V., Lau, F. S. and Roberts, M. J., "Pressurized Fluidized-Bed Hydroretorting of Eastern Oil Shales," Eastern Oil Shale Symposium, Lexington, KY, November 30-December 2, 1988.

5. Findlay, J. G., Knowlton, T. M., Punwani, D. V. and Lau, F. S., "The Effect of Fines Concentration on Gas-Velocity and Particle-Size Distributions in Moving-Packed Beds of Oil Shale," Eastern Oil Shale Symposium, Lexington, KY, November 30-December 2, 1988.

6. "Synthetic Fuels From U.S. Oil Shales. A Technical and Economic Verification of the HYTORT Process," DOE/ET/14102-4, 1983.

7. Coburn, T. T., Taylor, R. W. and Morris, C., "Laboratory Studies of New Albany Shale Flash Pyrolysis Under Solid-Recycle Conditions: Chemistry and Kinetics", Eastern Oil Shale Symposium, Lexington, KY, November 30-December 2, 1988.

8. Carter, S. D., "Fluidized Bed Pyrolysis Kinetics of New Albany Oil Shale," Eastern Oil Shale Symposium, Lexington, KY, 1986.

9. Weil, S. A. and Rue, D. M., "Laboratory Studies on Hydroretorting Eastern Shales," Symposium on Synthetic Fuels From Oil Shales II, Nashville, TN, 1981.

10. Rue, D. M., Lau, F. S. and Punwani, D. V., "Hydrogen Consumption During Moving-Bed Hydroretorting of Raw and Beneficiated Eastern Oil Shales," Eastern Oil Shale Symposium, Lexington, KY, November 30-December 2, 1988.

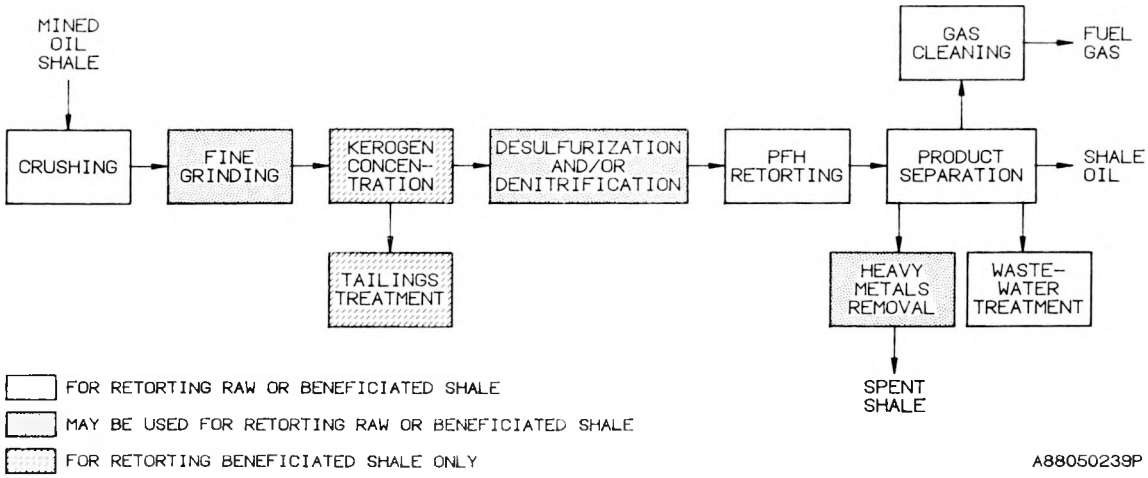

Figure 1. Major components of the integrated PFH process.

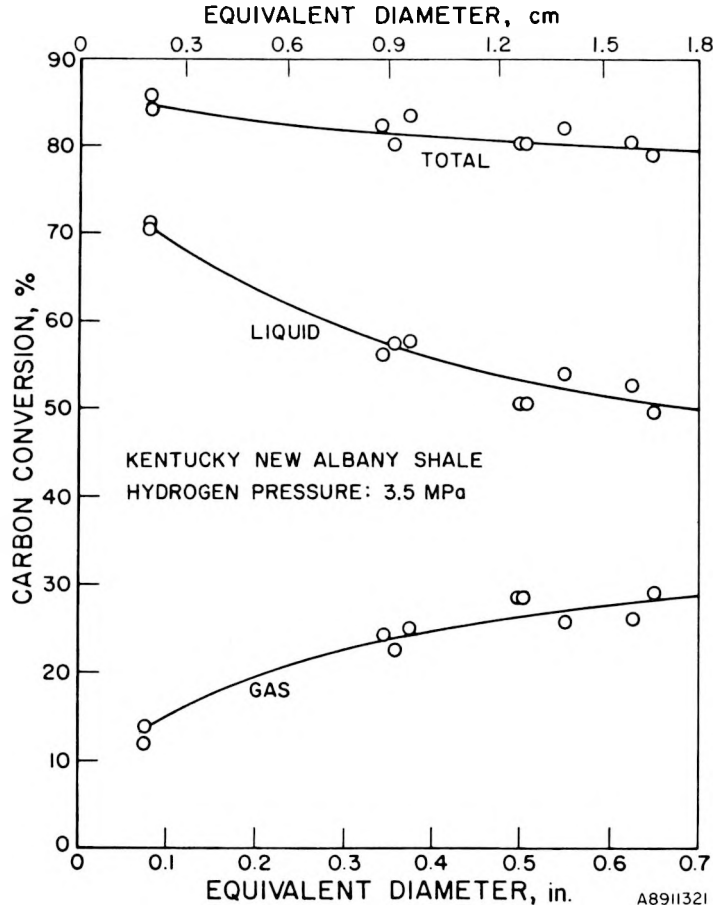

Figure 2. Variation of oil and gas yield with particle size.

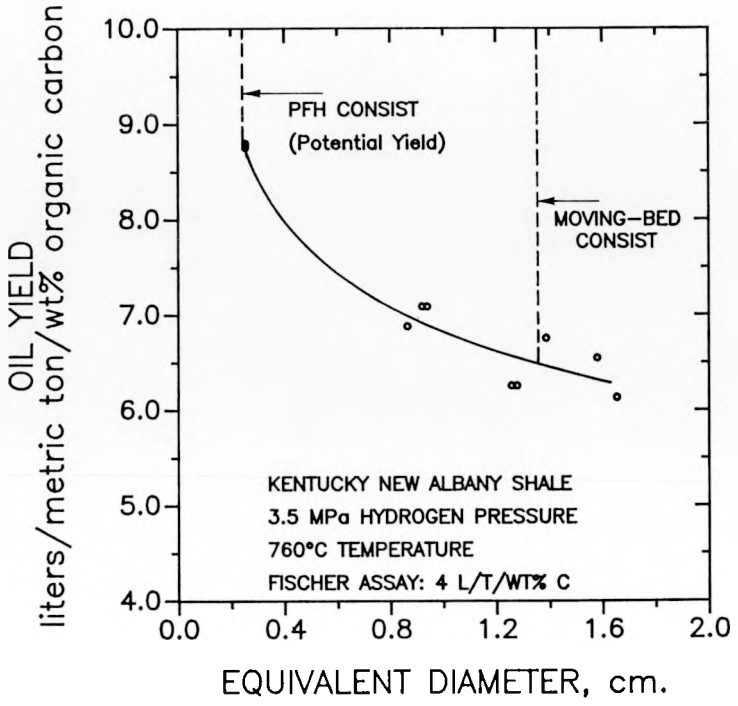

Figure 3. The effect of shale equivalent diameter on normalized oil yield.

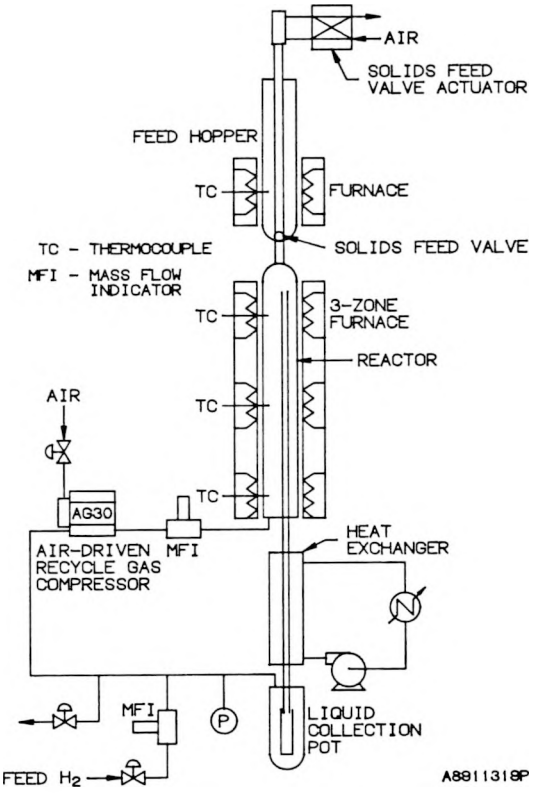

Figure 4. Schematic diagram of batch laboratory-scale PFH unit.

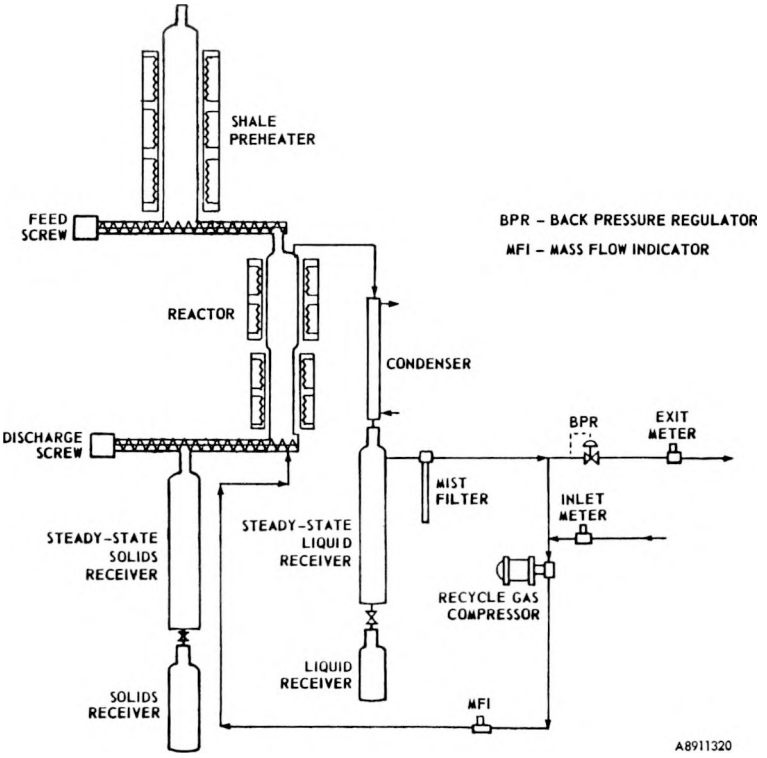

Figure 5. Schematic diagram of laboratory-scale continuous PFH unit.

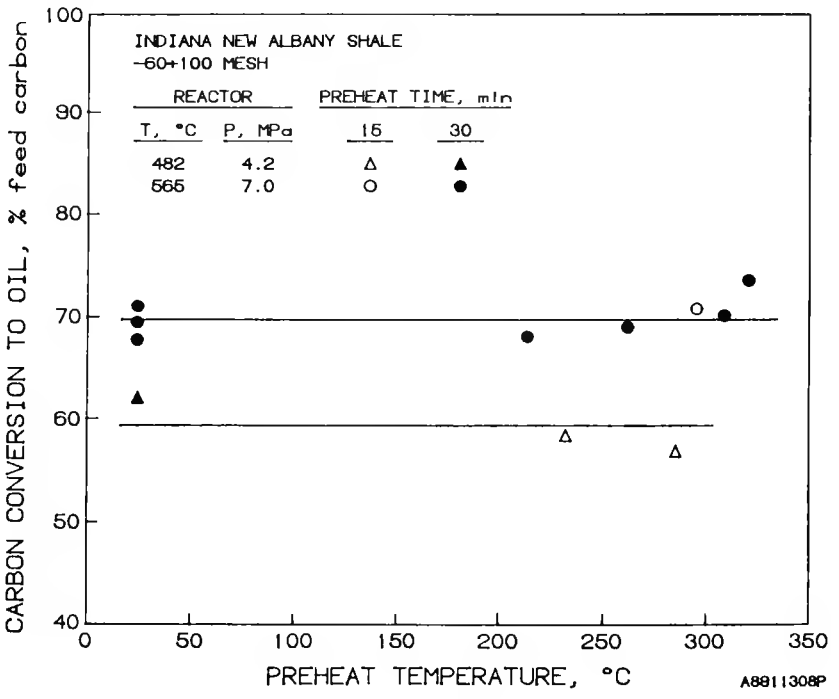

Figure 6. The effect of preheat temperature on feed carbon conversion to oil.

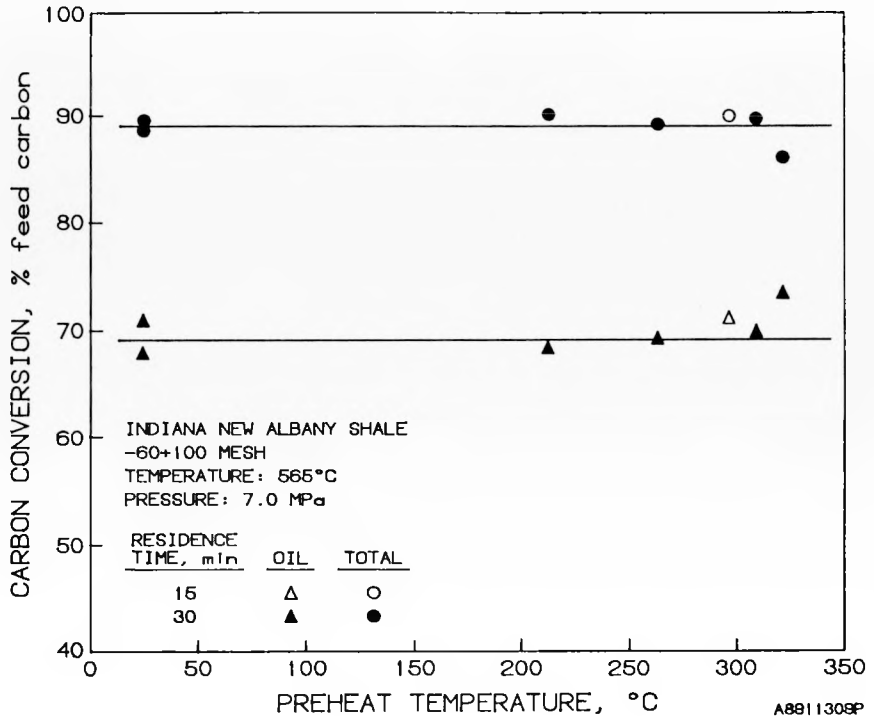

Figure 7. The effect of preheat temperature on feed carbon conversion.

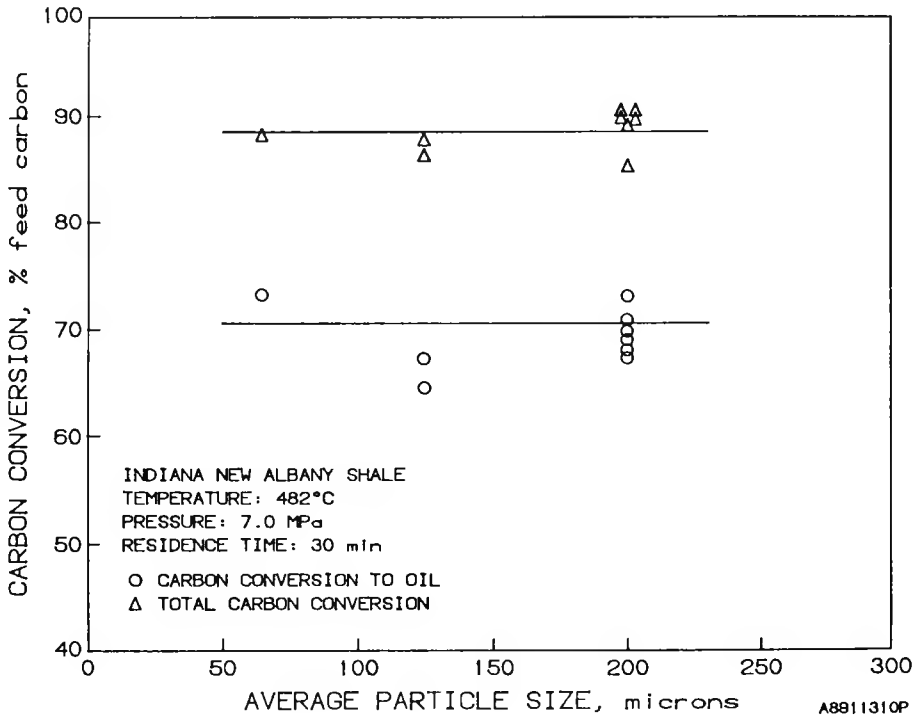

Figure 8. The effect of particle size on feed carbon conversion.

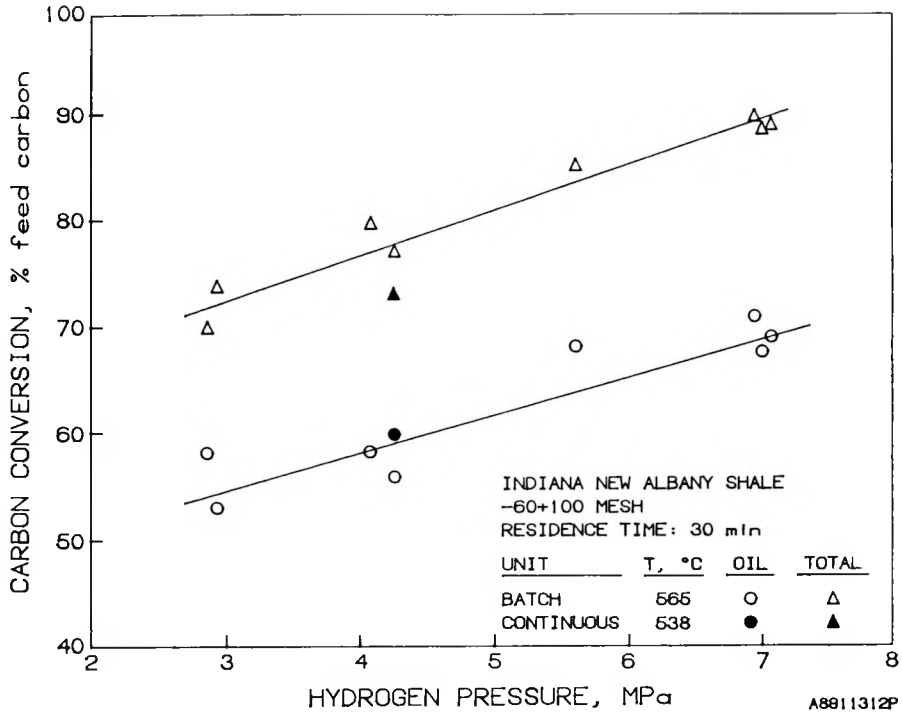

Figure 9. The effect of hydrogen pressure on feed carbon conversion at 550°C.

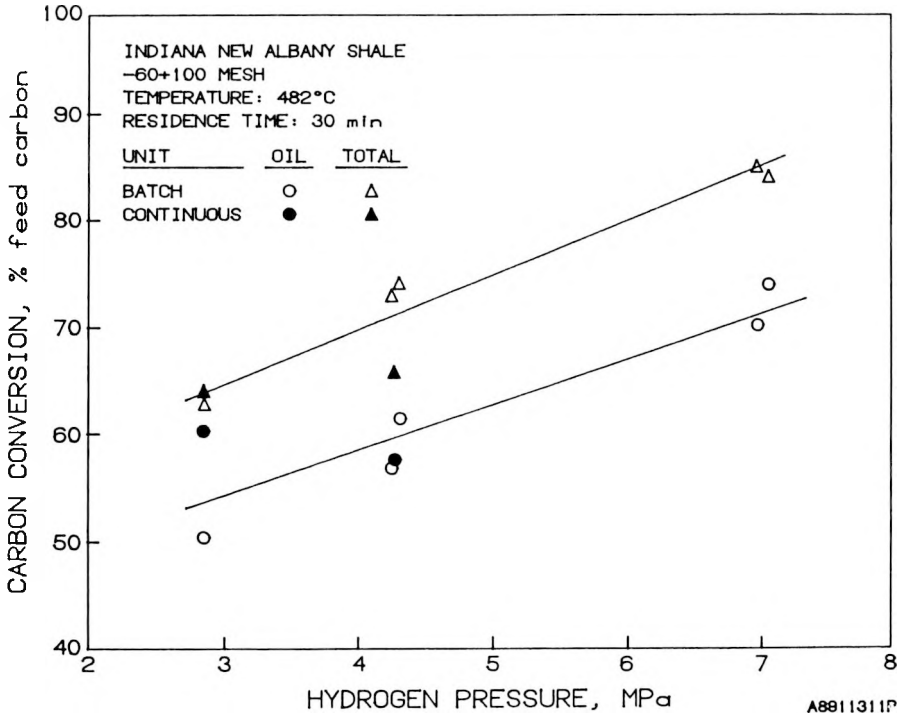

Figure 10. The effect of hydrogen pressure on feed carbon conversion at 482°C.

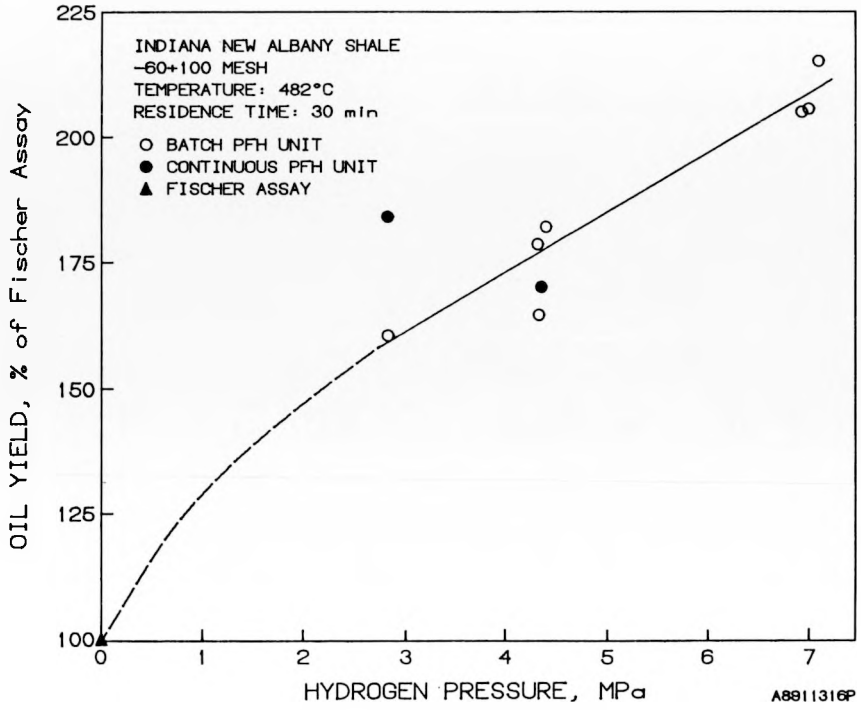

Figure 11. The effect of hydrogen pressure on oil yield.

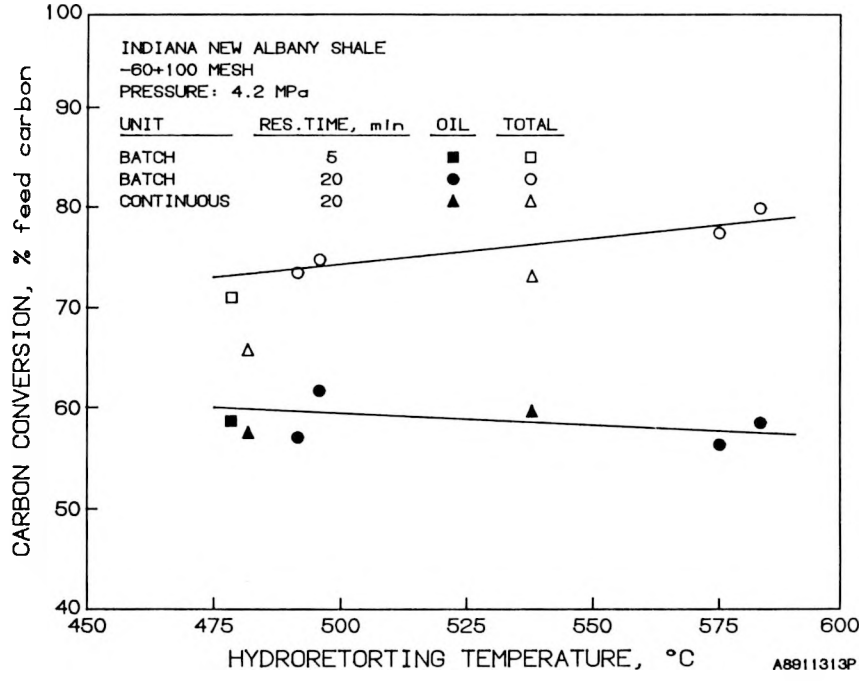

Figure 12. The effect of hydroretorting temperature on feed carbon conversion at 4.2 MPa hydrogen pressure.

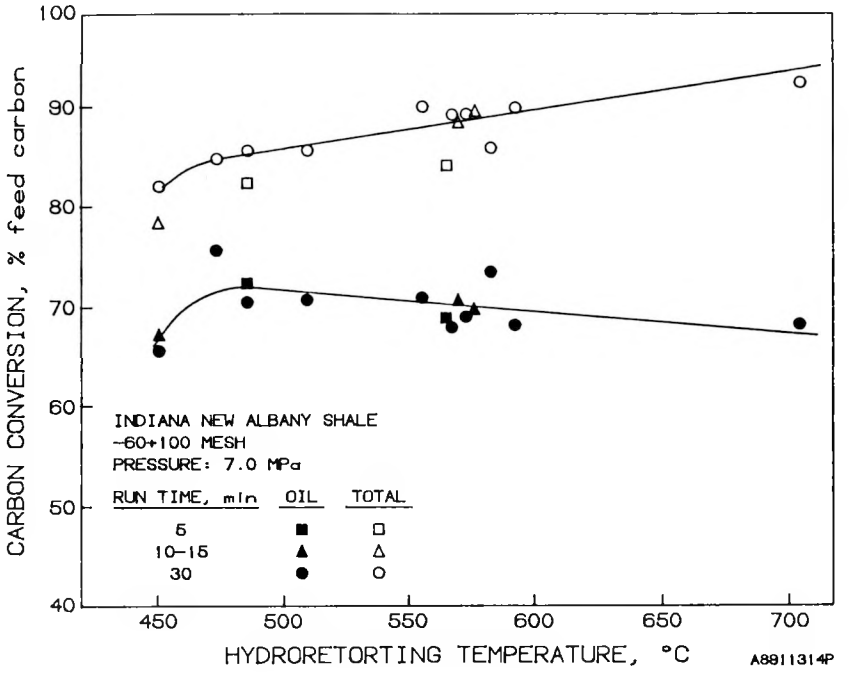

Figure 13. The effect of hydroretorting temperature on feed carbon conversion at 7.0 MPa hydrogen pressure.

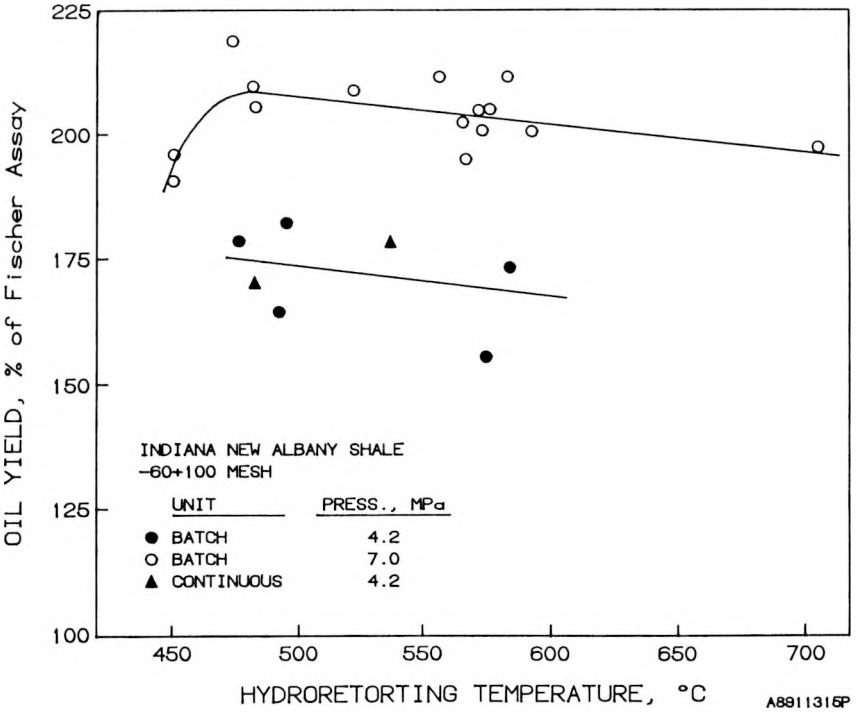

Figure 14. The effect of hydroretorting temperature on carbon conversion to oil.

Fluidized-Bed Retorting of Eastern Oil Shale

by

R.J. Gaire and G. Mazzella
Foster Wheeler USA Corporation
Clinton, New Jersey 08809-4000
T.J. Hand
U.S. Department of Energy
Morgantown Energy Technology Center
Morgantown, West Virginia 26507

Abstract. Under contract to the U.S. Department of Energy, Foster Wheeler developed the conceptual design and economics for an integrated plant to produce 50,000 BPD of syncrude from eastern New Albany oil shale. Objectives of this work were to provide detailed technical and cost information which would serve as a reference data base for DOE and to identify areas where future development is required to realize any potential economic benefits.

The processing scheme was based on fluidized-bed retorting of eastern oil shale at atmospheric pressure with recycle of hot shale solids to supply the heat required for pyrolysis. Essentially complete utilization of the shale energy content was accomplished via combustion of the retorted shale in fluidized-bed boilers. In addition to a high quality syncrude, the integrated plant produces substantial amounts of electric power and sulfuric acid as co-products.

Designs for the retorting and downstream processing systems were based on non-confidential published information with supplementary input from process licensors. The integrated plant design is described in terms of the component process units and support systems and the estimated plant investment is detailed by the individual plant sections. Annual operating costs and the corresponding production costs for syncrude product are highly dependent on the assigned values for co-products. Accordingly, the syncrude production cost could be in the range of $35 per barrel. The syncrude economics are compared with those developed by Foster Wheeler for processing Colorado oil shale, as well as with published estimates for hydro-retorting of eastern shale.

Introduction

In view of the variety of retorting processes and shale feedstocks which may have potential for commercial application, the U. S. Department of Energy initiated a program to develop systems models for oil shale processing. The intent was to employ these models in analyzing various process alternatives and identifying specific areas where future developmental effort could provide substantial economic benefits. In support of this effort, Foster Wheeler USA Corporation developed preliminary designs and cost estimates for commercial scale oil shale processing plants. The resulting technical and cost information were intended to provide a data base for DOE's systems models.

The overall scope of Foster Wheeler's effort included four design cases for producing syncrude oil from run-of-mine oil shale; these were based on:

- Fluidized bed retorting, with lift-pipe combustion, of Colorado oil shale.[1]
- Fluidized bed retorting, with fluidized bed combustion, of Colorado oil shale. [2]
- Directly heated moving-bed retorting of Colorado oil shale. [3]
- Fluidized bed retorting of eastern New Albany oil shale.[4]

This paper summarizes the plant design and economics which were developed for the case study on fluid bed retorting of eastern shale.

Overall Plant Description

The oil shale plant design was developed as a grassroots facility, capable of processing run-of-mine oil shale into a synthetic crude oil product having a maximum nitrogen content of 1000 ppmw and a pour point less than 30°F. The conceptual design was intended to represent mature commercial technology, rather than a first of a kind processing plant. An eastern Kentucky site, adjacent to an oil shale surface mining operation, was assumed as the plant location, and run-of-mine shale, raw water, natural gas, and electric power were assumed to be available at the plant battery limits in sufficient quantities to supply the operating requirements. In addition to the processing units, the grassroots plant was fully integrated to include all the utilities and support systems required for continuous operation.

The integrated processing scheme employed for the conceptual design is shown in Figure 1. Run-of-mine shale ore, delivered to the plant by conveyor, is crushed in three stages to minus 1/4 inch size which is suitable as feed to the retorting process. Provisions are included for stock piling primary crushed ore and for storing 60 hours inventory of retort feed. Crushed shale is pyrolyzed at 975°F and essentially atmospheric pressure in a fluidized-bed retorting system which uses recycle product gas for fluidization and solids transport. The energy value of residual char in the retorted shale is recovered via steam generation in a fluid bed combustor and hot solids from the combustor are recycled to provide the heat required for retorting. The WSA-SNOX Process is used to remove sulfur dioxide from the combustion flue gas before venting the gas to atmosphere. This process employs catalytic oxidation to recover 96% of the contained sulfur dioxide as by-product sulfuric acid. The combusted spent shale is subsequently moisturized to 10% and conveyed to a disposal pile at the mine site.

Raw shale oil is recovered from the retort overhead gas by quenching and subsequent sponge oil absorption of the C_4+ components. Hot centrifugation and electrostatic de-ashing are used to reduce the solids level to 100 ppmw in the raw oil. The ash-free oil is hydrotreated in a fixed bed catalyst system, at elevated temperature and pressure, to reduce the nitrogen content from 1.0% to less than 1000 ppm. Simultaneous reduction of the sulfur level from 1.8% to 25 ppm is accomplished at a hydrogen consumption of 1750 SCF/BBL. Hydrotreated oil is stabilized via fractionation and sent to storage.

Makeup hydrogen for raw oil hydrotreating is produced by steam reforming of the treated retorting make gas. After oil removal, the retort gas is catalytically hydrogenated to saturate the olefinic components and to convert essentially all the sulfur species to H_2S. The LO-CAT Process is used to remove sulfur from the make gas stream. In this process, a liquid phase redox reaction converts the contained H_2S into elemental sulfur which is recovered as a by-product.

Aqueous condensates, containing dissolved CO_2, H_2S, and ammonia, are steam stripped and the stripped water is recycled both for process use and as make-up for spent shale moisturizing. The Phosam-W Process is employed to recover anhydrous ammonia as a by-product from the stripped acid gas stream.

Operation of the processing units is supported by the plant utility systems and general facilities. Steam production, in excess of the plant operating requirements, is used to generate electric power for both in-plant use and for export.

Retorting Design

The retorting system was designed to process 120,000 tons per day of shale feed (dry basis). Based on practical design limitations for vessel sizes, the capacity of a single retorting module was set at 20,000 TPD. Accordingly, six parallel operating modules were required for a nominal syncrude capacity of 50,000 BPD. Characteristics of the New Albany oil shale feedstock were as follows:

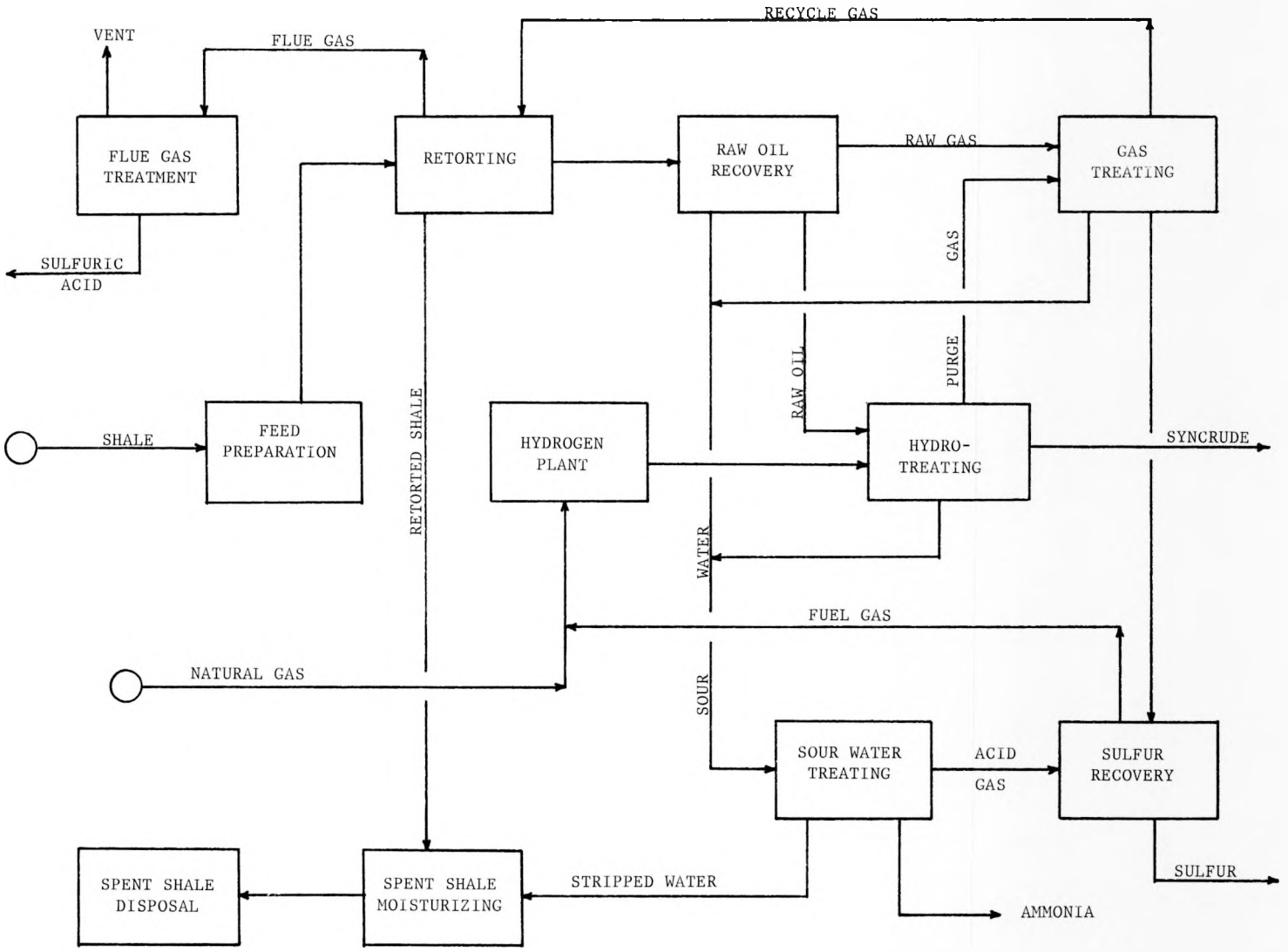

FIGURE 1. BLOCK FLOW DIAGRAM

Fischer Assay, gal/ton	15.0
Organic Matter, wt % (dry)	18.1
Inorganic Matter, wt % (dry)	81.9
Mineral Carbonate, wt % Inorganics	3.0
Pyrite, wt % Inorganics	4.0
Ultimate Analysis, wt % Organics	
Carbon	82.0
Hydrogen	7.4
Nitrogen	2.3
Sulfur	2.0
Oxygen	6.3
Total	100.0
Surface Moisture, wt %	1.0
Water of Hydration, wt %	3.0
Higher Heating Value, Btu/lb (dry)	2,887

The conceptual design for the retorting module was based on fluidized-bed pyrolysis with recycle of hot shale solids. Fluidized-bed combustion of the retorted shale is used to recover the energy content of the residual char. A portion of the retort make gas is recycled to provide the fluidizing medium for the retort, as well as the carrier gas for pneumatic transport of hot solids from the combustor to the retort. Design parameters for the retorting system, as shown in Table 1, were based primarily on published information for the rapid pyrolysis of New Albany shale[5] and for the Chevron STB retorting process.[6]

In accordance with the design basis established for this study, the fluid bed retorting yield was based on achieving 120% of the Fischer Assay yield. The corresponding yield structure, as a percentage of organic matter in the fresh shale feed, was 11.8% gas, 39.3% C_5+ oils, and 48.9% char in the retorted solids. Inspections of the de-ashed shale oil, prior to upgrading via hydrotreating, are shown below:

Gravity, °API	17.2
Pour Point, °F	35
Ash, ppmw	100
Arsenic, ppmw	110
Ultimate Analysis, wt %	
Carbon	83.6
Hydrogen	10.0
Oxygen	3.6
Sulfur	1.8
Nitrogen	1.0

The design retorting yield of 120% of Fischer Assay represents a major process uncertainty. While oil yields up to 125% of Fischer Assay have been reported in small scale fluid bed retorting of eastern oil shale,[7] the use of circulating hot solids as the retorting heat source could promote cracking and coking reactions with a corresponding reduction in oil yield. A significant decrease in yield value would have a major impact on the plant economics.

Furthermore, the high pyrite content in eastern shale increases the importance of the related sulfur chemistry during the retorting and combustion processes. Literature data[5] indicate that extensive decomposition of iron pyrite to form FeS and hydrogen sulfide occurs under retorting conditions. However, only small amounts of hydrogen sulfide were found in the retort product gas apparently due to capture of hydrogen sulfide by the iron oxide which is contained in the recycle combusted shale. While the conceptual design was based on this assumed reaction path, the corresponding gas and solids compositions were not consistent with the reported experimental analyses. A more complete understanding of the pyrite chemistry is therefore needed to support the overall concept for sulfur management and emission control.

Solids attrition presents another area of concern in the design of fluid bed retorting systems. Attrition of oil shale particles will likely occur in fluid bed retorting as a result of the chemical reactions which take place, as well as the physical effects of particle impact and abrasion. Eastern oil shale appears to be less susceptible to attrition caused by retorting reactions than western shale since the decomposition of both kerogen and mineral carbonate is less. However, essentially complete conversion of the char and iron sulfides is achieved during combustion. These chemical changes could result in weakening of the particle structure in combusted shale and thereby increase the rate of attrition. As long as the fines carryover does not exceed the amount of net combusted shale produced, attrition in the fluid bed combustor is not critical. Beyond that limit, insufficient hot solids would be available for recycle to the retort and, consequently, the process would be inoperable.

Plant Performance

The integrated processing plant was designed to convert 123,600 TPD of oil shale into 51,300 BPD of syncrude oil and reject the spent shale solids. Electric power, sulfuric acid, liquid anhydrous ammonia, and molten elemental sulfur are produced as by-products. The overall operating requirements and production rates are summarized in Table 2. From this product slate, it is obvious that the integrated oil shale plant is actually a co-production facility wherein syncrude, electric power, and sulfuric acid are the major end products. From an energy viewpoint, the syncrude product accounts for about 43% of the raw shale energy input while the net electric power generation and heat rejection to the plant cooling system represent 10% and 38%, respectively.

Table 1. Design Parameters

Fluid Bed Retorting

Shale Particle Top Size, in.	0.25
Retorting Yield Structure, % F.A.	120
Retorting Temperature, °F	975
Retorting Pressure, psig	21
Shale Throughput, lb/hr-ft^2	4000
Solids Residence Time, min.	5
Recycle Shale Ratio, lb/lb feed	3.2
Recycle Shale Temperature, °F	1300
Mineral Carbonate Decomposition, %	0
Decomposition of FeS_2 to FeS, %	35

Fluid Bed Combustion

Temperature, °F	1575
Char Combustion, %	97
Mineral Carbonate Decomposition, %	100
Sulfur Retention in Combusted Shale, %	50
Heat Release, 1000 BTU/hr-ft^3	250

Table 2. Plant Operating Summary

R.O.M. Shale Feed (15 gpt), TPD	123,625
Syncrude Product (29° API), BPD	51,300
By-Products:	
Elemental Sulfur, TPD	172
Anhydrous Ammonia, TPD	98
Sulfuric Acid (95%), TPD	3,600
Electric Power, MW	825
Moisturized Spent Shale, TPD	104,875
Operating Consumables:	
Natural Gas, MMSCFD	15
Diesel Oil, BPD	67
Raw Water, GPM	20,875
Catalyst & Chemicals, $/Day	57,310

The normal electric power usage of 160 MW is more than offset by the in-plant production of 985 MW. Consequently, the processing plant is a large base load generator of electric power. Natural gas consumption represents only about 18% of the overall plant fuel consumption while retorting make gas and purge gas from the raw oil hydrotreater provide the major portion of the needed fuel. All aqueous effluent streams are treated and re-used within the plant so that no waste water is discharged from the plant. The two primary areas for water consumption are spent shale moisturizing and cooling tower losses, with the latter accounting for 90% of the total raw water makeup to the plant.

Sulfur Management

In contrast to Colorado oil shale, eastern shale has a low mineral carbonate content and a high pyrite content. In New Albany shale, pyrite accounts for about 71% of the total sulfur, with the balance being about equally split between mineral sulfates and organic sulfur. During combustion of retorted shale, pyrites are roasted to iron oxide and sulfur dioxide; the extent of conversion depending on combustion temperature. At a temperature of around 1600°F, experimental data[8] indicate that about 50% of the pyrite sulfur appears as SO_2 in the flue gas. Consequently, the distribution of the sulfur in the shale feed around the fluid bed retorting/combustion system was as follows:

	% Shale Sulfur
Retort Make Gas	0.8
Raw Shale Oil	5.1
Feed Shale Fines	1.0
Combustor Flue Gas	39.4
Combusted Shale Solids	53.7
	100.0

In the present study, two approaches were considered for controlling the emission of sulfur dioxide from the combustion process; limestone injection and sulfuric acid recovery. The combustion temperature of 1575°F is suitable for sulfur capture by limestone which may be added to the fluid bed combustor. This approach would accomplish control of SO_2 emissions without additional processing equipment, other than for limestone handling. However, additional operating expense is incurred since about 3 pounds of limestone is required for each pound of SO_2 captured.

Alternatively, the offgas from retorted shale combustion may be treated via a proven flue gas desulfurization system, the WSA-SNOX Process, to recover sulfuric acid. The advantages of this route are that a salable by-product is produced and the uncertainty of limestone supply is avoided. As illustrated below, the economics of these alternate methods for managing sulfur emissions clearly favor the recovery of sulfuric acid, even when the capital charges and operating costs for limestone addition are assumed to be zero.

	WSA-SNOX	LIME-STONE
SO_2 Removal, %	96	90
SO_2 Emission, lb/MMBTU	0.5	1.2
Limestone Required, TPD	-	6,540
By-Product Acid, TPD	3,600	-
Capital Cost, MM$	265	-
Syncrude Cost, $/BBL		
Limestone @ $15/ton	-	1.91
Operating Cost	2.22	-
Capital Charge @ 16%	2.50	-
Acid Credit @ $70/ton	(4.91)	-
	(0.19)	1.91

Economic Analysis

Capital costs for the conceptual oil shale plant were estimated on a mid-1987 basis for a location in eastern Kentucky. The installed plant costs were factored from the major process equipment specifications which were developed for individual plant sections. The retorting section represents the major cost element in the physical plant, accounting for over one-third of the installed cost. Costs associated with electric power generation, via combustion of retorted shale with flue gas desulfurization, make up about 38% of the plant cost.

As summarized in Table 3, the total plant investment cost was estimated to be $3.43 billion. By scaling down these costs, the capital investment for a half-size plant, which produces 25,650 BPD of syncrude, was estimated to be $1.89 billion. In addition to the installed plant cost, the capital investment includes allowances for project contingency, initial inventory of catalyst and chemicals, spare parts, start-up costs, and working capital. The project contingency, at 15% of the installed plant cost, provides for omissions and uncertainties in the technical definition of the plant due to the non-specific plant site and the lack of detailed engineering.

The calculated syncrude production cost, based on a plant operating factor of 90% and an annual capital charge rate of 16%, is detailed in Table 4. The capital recovery factor corresponds to a 15% return on investment over a period of 20 years. Under the assumed unit costs, the

Table 3. Estimated Capital Cost*

Basis: Mid-1987, Kentucky

	No. Trains	Cost, $MM
Process Facilities		
Retorting	6	950.8
Raw Oil Recovery	6	147.4
Raw Oil De-Ashing	2	11.4
Gas Treating	2	64.7
Raw Oil Hydrotreating	2	91.8
Oil Fractionation	2	20.6
Hydrogen Plant	2	146.7
Sour Water Treating	2	18.1
Sulfur Recovery	2	34.9
Spent Shale Moisturizing	6	52.7
Feed Preparation	2	270.3
Spent Shale Disposal	-	103.5
Flue Gas Treatment	6	223.2
Total Process Facilities		2,136.1
Support Systems		657.6
Project Contingency @ 15%		419.1
Total Installed Plant Cost		3,212.8
Initial Catalyst Inventory		24.0
Spare Parts		26.5
Start-up Cost		99.1
Working Capital		66.1
Total Plant Investment		3,428.5

* 51,300 BPD Syncrude Capacity

Table 4. Syncrude Production Cost

Basis: 330 Days/Year, 51,300 BPD Syncrude

	Unit Cost	$/BBL Syncrude
Raw Oil Shale	4.00 $/Ton	9.64
Consumables		
Fuel	3.50 $/MMBTU	1.05
Water	1.00 $/1000 Gallon	0.58
Chemicals		1.12
Mobile Equipment		0.21
Operating Labor	20 $/Hr	1.82
Maintenance M & L	4.45%*	7.35
Insurance & Taxes	1.0%*	1.65
Total Operating Cost		23.42
By-Product Credit		
Sulfur	70 $/Ton	0.23
Ammonia	150 $/Ton	0.29
Sulfuric Acid	70 $/Ton	4.90
Electricity	0.04 $/KWH	15.44
Net Operating Cost		2.56
Capital Charge	16%*	32.40
Total Production Cost		34.96

* Annual charge factor on plant investment cost

gross operating expense is almost entirely offset by the by-product credits so that the net operating cost is only $2.56 per barrel of syncrude product. With the capital charges added in, the total cost of producing a barrel of syncrude is about $35. In addition to being capital intensive, the economics in this case are highly dependent on the by-product credits, particularly for the excess electric power which represents 75% of this credit.

Sensitivity of the production cost to by-product values, as well as other major cost elements such as capital charges, plant capacity, and retort oil yield, is illustrated in Table 5. As indicated, by-product values would have to fall below $25/ton for sulfuric acid or 3¢/KWH for electricity in order for the syncrude cost to exceed $40 per barrel. This production cost level would still be attainable even with a 20% decrease in retorting yield, as well as for a processing plant designed for half the capacity. The annual capital charge rate, however, has a more pronounced affect in that a change of one percentage point represents a production cost increment of $2.00 per barrel.

The economics of producing syncrude from eastern New Albany oil shale via fluid bed retorting are compared to those for processing Colorado shale as well as for hydroretorting eastern shale in Table 6. While the Colorado shale cases were based on previous Foster Wheeler studies,[2,3] the costs for hydroretorting of New Albany shale were extracted from an evaluation study by Hycrude.[9] In all cases, the costs were adjusted to reflect the same unit costs for shale and utilities as employed in the present study, thereby assuring a common basis for comparison.

This comparison indicates that co-production of syncrude and electric power from fluid bed retorting of eastern shale can be competitive with processing high grade western shale. The economics further suggest that the co-production concept for eastern shale offers a significant advantage over the hydro-processing route wherein syncrude costs in the range of $53 per barrel are projected. Even in conjunction with beneficiation, hydroretorting of eastern shale does not approach the economic potential of the co-production scheme.

The apparent economic benefits of producing syncrude from eastern oil shale, via the processing scheme considered in this study, are obviously dependent on the market value for the co-products. At a 50,000 BPD capacity, the ability to market 800 MW of base load electric power along with 3600 TPD of sulfuric acid is critical in siting such a plant. The sulfuric acid output from this plant would represent about 3% of the current U.S. demand.

Conclusions

Integration of fluidized-bed retorting of eastern shale with electric power generation via combustion of retorted shale could be an attractive option relative to other shale processing routes for syncrude production. In view of the large amount of electric power produced, the integrated plant more closely resembles a power generating station having oil as a by-product. Therefore, the economics of this processing scheme are extremely site specific. Such a facility needs to be located adjacent to a suitable shale deposit and in an area where a large base load generation of electric power, as well as the sulfuric acid by-product, can be marketed.

Regarding the design of a fluidized-bed retorting and combustion system, a number of uncertainties exist which could significantly impact oil yield, overall efficiency, plant operability, and process scaleup. Accordingly, further development in the following areas is needed to support a practical design.

- Effects of hot solids recycle on retorting yield.
- Combustion of retorted shale in dense phase fluid beds.
- Attrition of shale solids during retorting and combustion.
- Pyrite conversion chemistry and release of sulfur compounds under processing conditions.

Acknowledgements

This study was supported by the U.S. Department of Energy, Morgantown Energy Technology Center, under Contract No. DE-AC21-86MC22134.

References

1. Albulescu, P. and Mazzella, G., "Conceptual Design of Commercial Oil Shale Plants; Topical Report - Fluidized Bed Retorting of Colorado Oil Shale," DOE/MC/22134-1, Foster Wheeler USA Corporation (June 1987).

2. Albulescu, P. and Mazzella, G., "Conceptual Design of Commercial Oil Shale Plants; Topical Report - Fluidized Bed Retorting of Colorado Oil Shale - Alternate Design

Table 5. Syncrude Cost Sensitivity

Sensitivity	Value	Syncrude Cost, $/BBL
Base Case	-	34.96
Sulfuric Acid Value, $/Ton	70*	34.96
	50	36.36
	25	38.12
Electricity Value, ¢/KWH	5	31.10
	4*	34.96
	3	38.82
Capital Charge, % P.A.	16*	34.96
	20	43.06
	25	53.19
Plant Capacity, BPD Syncrude	51,300*	34.96
	25,650	39.48
Retort Yield, % F.A.	120*	34.96
	100	40.22

* Base Case Value

Table 6. Comparative Oil Shale Economics*

Shale	Colorado		New Albany		
F. A. Grade, gpt	30	30	15	13.3	50.2**
Retort Process	Fluid Bed	Moving Bed	Fluid Bed	Hytort	Hytort
Retort Yield, % F.A.	105	100	120	167	169
Syncrude, BPD	54,560	51,590	51,300	55,900	56,940
ROM Shale, TPD	74,200	87,600	123,620	117,590	24,740
Retort Feed, % ROM	98	89	98	81	100
ROM Shale Cost, $/Ton	6.00	6.00	4.00	4.00	42.00**
Capital Cost, $/BPD					
Process Plant	31,610	23,370	47,880	40,440	19,140
Total	43,300	36,330	66,830	59,790	30,310
Syncrude Cost, $/BBL					
Shale Feed	8.16	10.19	9.64	8.41	19.62
O & M	12.18	9.76	13.78	19.65	10.02
Capital Charge***	20.99	17.61	32.40	28.99	14.70
By-Product Credit	(0.67)	(0.73)	(20.86)	(4.17)	(0.97)
Net	40.66	36.83	34.96	52.88	43.37

* Based on 1987 costs and 330 operating days per year.

** Beneficiated shale.

*** Capital charge factor @ 16% per year.

Study," DOE/MC/22134-2, Foster Wheeler USA Corporation (November 1987).

3. Gaire, R. J. and Mazzella, G., "Conceptual Design of Commercial Oil Shale Plants; Topical Report - Moving Vertical Bed Retorting of Colorado Oil Shale," DOE/MC/22134-3, Foster Wheeler USA Corporation (May 1988).

4. Gaire, R. J. and Mazzella, G., "Conceptual Design of Commercial Oil Shale Plants; Topical Report - Fluidized Bed Retorting of Eastern Oil Shale," DOE/MC/22134-4, Foster Wheeler USA Corporation (March 1989).

5. Cena, R. J., and Taylor, L., "Results of Rapid Pyrolysis Experiments Using Eastern U. S. Oil Shale in the Livermore Solid-Recycle Retort," Lawrence Livermore National Laboratory, 1986 Eastern Oil Shale Symposium (November 19-21, 1986).

6. Tamm, P. W., "The Chevron STB Oil Shale Retort", API 46th Midyear Refining Meeting, Session on Synthetic Fuels Processing-Part 1, Chicago, Il (May 13, 1981).

7. Carter, S. D. and Taulbee, D. N., "Fluidized Bed Retorting of Eastern U.S. Oil Shale: An Evaluation of Steam as a Fluidizing Medium," 1984 Eastern Oil Shale Symposium, Lexington, Kentucky (November 26-28, 1984).

8. Doyle, J. B., "Oil Shale Byproduct Combustor," Energy Progress 2, No. 4 (December 1982).

9. "Beneficiation - Hydroretort Processing of U. S. Oil Shales", Final Technical Report Under DOE Grant DE-FG21-85LC11066, Hycrude Corporation (January 1989).

Operation of the 5-lb/hr KENTORT II Reactor in the Solid Recirculation Mode

by

S.D. Carter and D.N. Taulbee
Center for Applied Energy Research
University of Kentucky
Lexington, Kentucky 40506

Abstract. Of great importance to the development of the KENTORT II process is the abatement of oil yield losses caused by direct, solid-solid heat transfer in the pyrolyzer. It is not practical to transfer heat to the pyrolysis zone of the KENTORT II process exclusively with hot gases at the commercial scale. This is due to the relatively low heat capacity of gases and the cross sectional area and superficial gas velocity limitations of fluidized beds. Recirculating hot shale is the most straightforward method of transferring heat to the pyrolysis zone, but it has the potential to significantly reduce oil yields due to coking. Therefore, the primary objectives of this study were to: 1) evaluate the effects of recycle solid temperature, recirculation ratio, and solid type on oil yield and composition in the 5-lb/hr integrated reactor, and 2) investigate methods of reducing oil yield losses.

Solids from the integral gasification section were recirculated to the pyrolysis zone to provide a portion of the heat required for pyrolysis. The recirculating shale from the gasifier had been subjected to either pyrolysis/gasification or pyrolysis/gasification and combustion. Preliminary results indicate that oil yield losses using the pyrolysis/gasification material are reduced if a low temperature recycle stream with a relatively high solid recycle rate is used for a given pyrolysis heat demand. Oil yields remained 15% above the Fischer assay oil yield under the highest pyrolysis heat load conditions when utilizing the low temperature/high recycle ratio combination. The influence of combusted shale is currently under investigation.

Background

It has been shown [1,2,3,4,5] that fluidized bed pyrolysis of eastern U.S. oil shale can enhance oil yields up to 50% above Fischer assay. In addition, fluidized bed technology has the advantages of rapid pyrolysis kinetics (short solid residence time), total use of mined shale, thermal efficiency, and production of a spent shale which has good compaction characteristics. The CAER has investigated fluidized bed pyrolysis of eastern U.S. oil shales for the past several years, and emphasis has recently been broadened to include the development of a commercial retorting concept based on fluidized bed pyrolysis.

While fluidized bed pyrolysis significantly increases carbon conversion to liquid products, approximately 40% of the original carbon remains in the spent shale. This material is ideal for on-site combustion since it has been heated to at least 500°C and is of no value once removed from the process. Additionally, it is a good material for use as a heat carrier because of its small size, relatively low rates of decrepitation, and high heat capacity. Therefore, char combustion and the use of char as a heat transfer medium are integral features of the KENTORT II process.

Since only a portion of the carbon in the char from pyrolysis is required by the combustor to heat the pyrolyzer, an intermediate gasification stage was included in the KENTORT II design to utilize this excess carbon. In addition to the production of synthesis gas, a gasification stage desulfurizes the shale. The removal of sulfur from the shale as H_2S prior to combustion creates a relatively concentrated stream of H_2S which is easier to clean-up than a dilute stream of SO_2 from a combustor. The additional

H_2S also serves as feedstock for elemental sulfur production. Environmentally, the gasification process removes up to 90% of the original sulfur which greatly reduces the potential for acid drainage conditions in the disposal area.[6,7]

Introduction

The low volumetric heat capacity of gases at atmospheric pressure limits the amount of heat that can be transferred by gases in a commercial retorting process. This is particularly true in processes such as KENTORT II where rapid pyrolysis is utilized and where the raw shale is not preheated. In these types of systems, the use of a solid heat carrier is essential, and spent solids from the retorting process have been looked upon as a convenient heat carrier. Hot, retorted solids offer advantages in terms of process efficiency because they are readily available, have a high heat capacity by volume, and can be easily recycled in a fluidized bed system. Moreover, the use of spent shale is advantageous over 'inert' solids because no particle segregation is required once the solid heat carrier exits the pyrolysis zone.

While solid recycle retorting has many advantages, it also has the potential for increased oil coking and cracking in the pyrolysis zone. Several workers have reported substantial oil yield losses when combusted shale is contacted with raw shale in fluidized bed pyrolyzers.[8,9,10] However, these results are not directly comparable to the KENTORT II process, because in the latter case, solids are recycled from a gasification zone rather than an oxidizing zone. This is an issue which has not been sufficiently studied. The coking activities of shales that have been subjected to different types and degrees of post-pyrolysis processing need to be evaluated. Identifying the most active coking sites and formulating practical methods of neutralizing the sites are key areas in making solid-recycle retorting practical.

Another aspect of oil yield loss abatement lies in the relationships between oil yield and solid-recycle process parameters. By understanding these relationships it may be possible to identify an optimal recycle ratio/temperature combination where oil coking is minimized.

The major objective of this study is to offer a precursory examination of oil yield losses during operation of the KENTORT II reactor in the solid recirculation mode. Oil yield as a function of recycle ratio/temperature combinations is evaluated in this study. Also, a comparison between gasified and partially combusted shales, as heat carriers, is presented.

Methodology

Apparatus

The integrated reactor system was operated in two configurations for this study (see Figure 1). The first configuration involved integral operation of the pyrolysis and gasification zones (3-inch ID). Net process heat for this configuration was provided by superheated steam and a furnace external to the gasification section. Heat was transferred to the pyrolysis zone by a combination of hot gases and recirculating hot char from the gasification section. The rate of shale recycle was controlled automatically by an electronic controller that adjusted the flowrate of aeration gas to the J-valve according to the temperature setpoint of the pyrolyzer.

The second mode of operation included an integral fluidized bed combustion zone which furnished heat to the system by combustion of residual carbon in the processed shale. The furnaces external to the reactor system provided heat for start-up and compensated for heat losses from the system. The temperature in the combustor was controlled by blending N_2 with the fluidizing air. Shale was recirculated between the gasifier and combustor to transfer heat, and the pressures were balanced to minimize gas mixing between the reducing and oxidizing zones.

The liquid collection system (see Figure 1) was developed from similar systems used in the past for pyrolysis studies.[6] The main features of the system included: 1) an electrostatic precipitator which trapped the majority of the oil from its aerosol suspension, 2) condensers and filters which collected water and light oil, and 3) on-line gas analysis capable of quantitating vapor phase C_5+ materials.

Flue gas from the combustor passed through a cyclone for fines removal prior to venting, and a sample was pulled from the main gas stream for on-line gas analysis. The sample was cooled, filtered, compressed, and dried before analysis in a series of industrial gas monitors for CO_2, CO, SO_2, NO_x, and O_2.

Oil Shale Sample

Oil shale from the Cleveland Member of the Ohio Shale was used for this study based upon the judgment that it represents one of the shale types in the eastern U.S. that has the highest probability for initial commercial development. Detailed description of the characterization and acquisition of this master sample has been reported previously.[11] The shale was crushed, ground, and screened to a size distribution of 20x60 mesh, yielding five 55-gallon drums of material. The drums were purged with argon and sealed to prevent unnecessary oxidation. The average analysis of the sample is shown in Table 1.

Table 1. *KENTORT II Master Sample Characteristics.*

Ultimate Analysis		Mod. F.A.*	
Component	(wt%)	Component	(wt%)
Carbon	16.7	Oil	7.0
Hydrogen	2.0	(17.7 gal/ton)	
Nitrogen	0.7	Water	4.2
Sulfur	1.7	Gas+Loss	2.6
Ash	74.5		

* Modified Fischer Assay developed at CAER for Eastern shale.

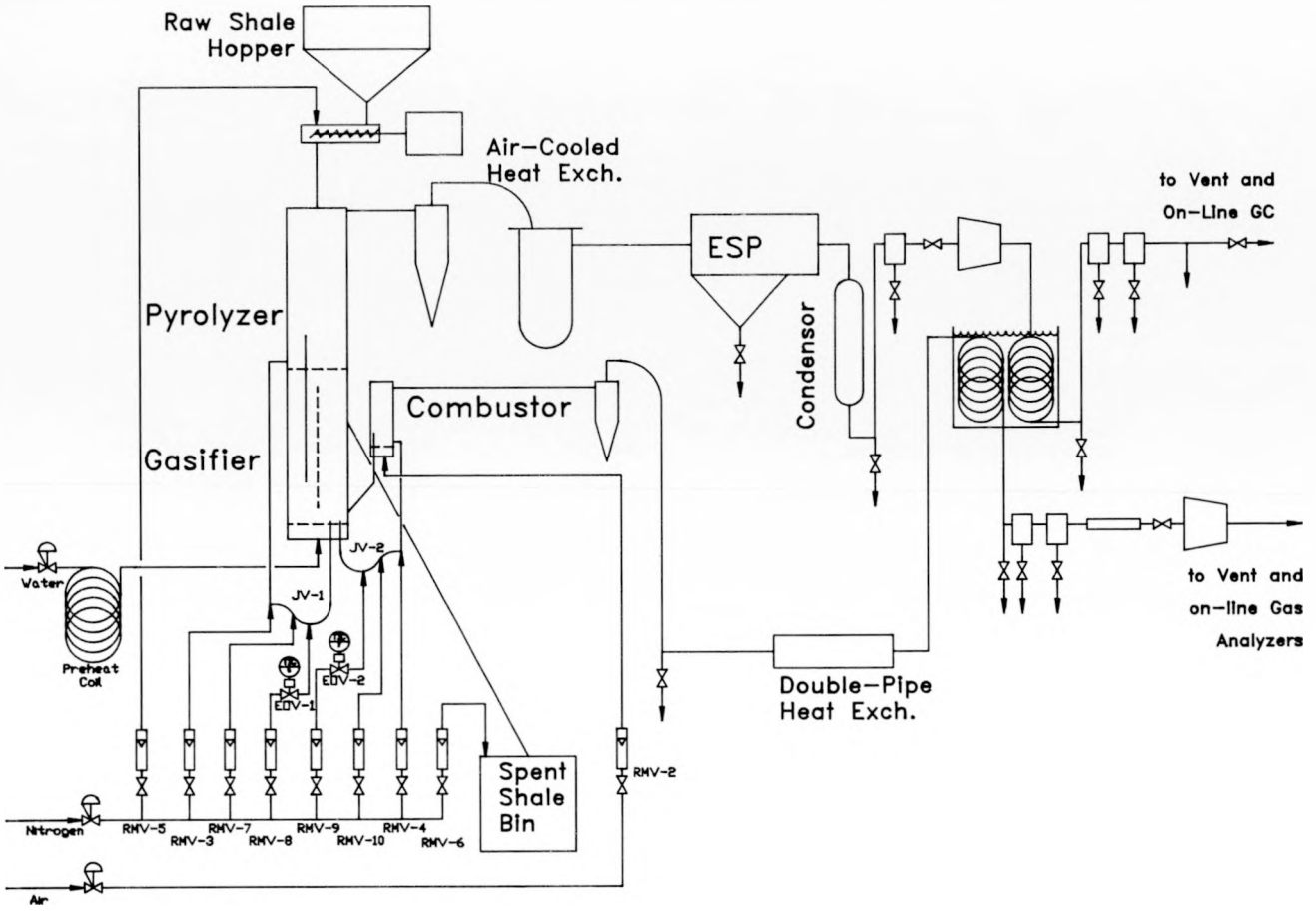

Figure 1. *Simplified flow diagram of the integrated, 5-lb/hr KENTORT II system.*

Procedure

The reactor system was brought to operating temperature with the furnaces while nitrogen flowed through the system to distribute heat. Following the preheating period, the nitrogen flow was replaced with steam, and the system temperatures and pressures were allowed to stabilize. The run was initiated by starting the raw shale screwfeeder, and conditions steadied within 15 to 30 minutes. During the run, light oil and steam condensation were periodically drained from the system. On-line gas samples were taken every 35 minutes for gas chromatography. Otherwise, conditions were maintained as constant as practicable and recorded by a computerized data acquisition system for the duration of the run, typically 2 to 5 hours.

Following the termination of shale feed, the steam flow was continued for 10 minutes which was followed by an overnight cooling period with a small amount of nitrogen purge. Liquids were drained from the various traps in the system when the flow of steam was halted. The collection of solid samples and the quantitation of liquid hold-up in the system was performed on the following day when cool. Oil held up in the system was rinsed from the internals with CH_2Cl_2 and recovered by distillation. The washings were filtered to remove entrained shale fines. Solids recovered in the spent shale bin and cyclone were weighed, and sampled for ultimate analyses. The recovered oil fractions were analyzed both separately and as a whole according to production ratios.

Test Matrices

Two major variables were studied in the pyrolysis-gasification configuration: gasifier temperature and raw shale throughput (Table 2). The gasifier temperature influenced the necessary recirculation ratio to the pyrolyzer, so only gasifier temperature is considered the truly independent parameter of the two. Raw shale throughput was increased from 29 to 52 g/min during the test series to alter the heat load on the pyrolyzer. Pyrolysis temperature and the mass flow of steam were constants in the study.

In the integrated combustor configuration, the gasifier temperature was varied, which dictated the range of recycle ratios in Table 3. The temperature of the combustor was held at approximately 860°C and the raw shale throughput was constant at 40 g/min for these runs.

Table 2. *Average Run Conditions for the 5-lb/hr Integrated Pyrolysis-Gasification Reactor.*

Run #	Mean Bed* Temp., °C		Shale Feed Rate, g/min.	Solid Recycle Temp., °C		Heat Provided by Steam for Pyrolysis %	Solid Recirc Ratio
	Pyrol	Gasif		Meas.	Avg.		
KEN16	524	735	32.14	689	712	54.6	1.58
KEN18	526	756	31.42	706	731	50.3	1.57
KEN20	518	747	29.46	689	718	62.3	1.15
KEN23	528	747	29.42	675	711	55.8	1.61
KEN24	529	812	30.30	734	773	60.5	1.00
KEN25	526	780	38.61	709	745	60.7	1.21
KEN27	533	771	39.88	673	722	52.9	1.91
KEN28	544	783	51.71	689	736	40.2	2.44
KEN29	546	796	46.73	701	749	43.9	2.24
KEN30	536	754	48.54	678	716	41.2	2.52
KEN31	537	827	48.30	727	777	49.7	1.50
KEN32	527	787	48.28	705	746	42.6	1.83
KEN33	530	760	47.25	687	723	38.8	2.22
KEN34	530	763	47.49	687	725	39.7	2.21
KEN35	536	839	47.28	745	792	46.7	1.48
KEN36	532	795	46.18	710	753	45.0	1.76

* Reactor operated at 0 psig ± 5 inches water column.

Table 3. *Average Run Conditions for the 5-lb/hr Integrated Pyrolysis-Gasification-Combustion Reactor System.*

Run #	Mean Bed* Temp., °C		Shale Feed Rate, g/min.	Solid Recycle Temp., °C		Shale Recirc Ratio	Combustor Temp,C
	Pyrol	Gasif		Meas.	Avg.		
KEN46	537	774	39.80	647	711	2.39	861
KEN47	541	788	40.86	658	723	2.50	851
KEN48	537	754	40.00	699	727	2.14	849
KEN49	537	761	41.14	698	730	1.96	853
KEN50	538	773	41.76	691	732	1.90	855
KEN52	536	806	39.64	708	757	1.42	866
KEN53	531	823	38.21	711	767	1.21	868

* Reactor operated at 0 psig ± 5 inches water column.

The shale recycle ratios were determined by performing a heat balance around the pyrolyzer. The enthalpy relations for eastern U.S. oil shale, as derived by Camp, were applied to the specific characteristics of the oil shale sample used in this study.[12] The measured solid recycle temperature was consistently lower than the gasification bed temperature (see Table 2). The measured solid recycle temperature is somewhat low because of heat loss through the sheath and tube fitting securing the thermocouple. However, some temperature drop in the recycle shale temperature is due to heat loss from the lift pipe feeder which was located outside the furnace (see Figure 1). Therefore, the true solid temperature should lie between the measured gasifier temperature and the measured solid recycle temperature. The average of these readings will be used for the later discussions.

Results and Discussion

Carbon Distribution

The portion of carbon remaining in the shale following integral pyrolysis-gasification declined with increasing gasifier temperature which is attributable to the steam-carbon reaction (Figure 2). The steam-carbon reaction is considered the most prevalent gasification reaction because of the high partial pressure of steam in the gasification zone. The increased production of carbon oxides was closely correlated to the decrease in carbon content of the processed solids. It is possible to observe this relationship because the variation in the carbon content of the shale from pyrolysis is small compared to the amount of carbon removed by gasification. Carbon gasification does not appear to be affected by solid recirculation, as the production of carbon oxides from non-recycle and solid-recycle runs are similar when the solid residence time is considered.

Hydrocarbon gas production (C_1-C_4) remained essentially constant throughout the test series. Most of these hydrocarbons were produced in the pyrolyzer, but it appears from comparison to a previous steam retorting study[6] that additional methane was produced in the gasifier. This is attributed to further charring reactions which occur at the significantly higher gasification temperatures. Since the products of pyrolysis and gasification are combined, it is difficult to distinguish between the reactions occurring in each zone. This especially hampers our study of solid-recycle pyrolysis since coking and cracking indicators such as methane and hydrogen are also produced in appreciable amounts in the gasifier.

Nearly 2% of the total carbon was measured in the condensed steam, and this value was essentially constant. The balance of the raw shale carbon was measured as C_5+ components.

Operation with the combustor on-line did not significantly change the carbon distribution with the exception of reducing the carbon content of the processed shale (changes in oil yield will be discussed in a following section). Carbon oxides measured in the combustion gas stream accounted for the reduction of carbon in the solids. Only 10% of the original carbon was combusted during these runs because the recycle capabilities of the system were not sufficient for the small temperature differential between the gasifier and combustor.

Overall carbon balances averaged 90% which were lower than previously obtained in similar equipment configurations. While vapor phase components were measured during steady-state portions of each run, gases and vapors generated during heat-up or shutdown periods were not routinely monitored and were not included in the carbon balance calculations. To determine the amount of gasification that can occur during non-steady periods, the reactor was charged with spent shale and cycled through a typical heat-up and cool-down sequence. From this experiment it was estimated that at least 2% of the overall carbon balance can be attributed to non-steady state gasification. Additionally, evaporation of oil held up in the system and post-run gasification and de-gassing of materials in the spent shale bin during the cooldown period contribute to the carbon balance discrepancy.

Sulfur was removed from the shale primarily in the form of H_2S accounting for 45 to 55% of the total balance (Figure 3). Smaller amounts were distributed to the aqueous phase (6-10%) and into the oil (6-7%). The sulfur content of the spent shale decreased slightly with increasing gasifier temperature. These relationships are consistent with previous gasification studies, so it does not appear that solid recirculation affects sulfur removal.

Operation with the integrated combustor configuration simply produced SO_2 from the residual S in the shale without otherwise affecting the sulfur distribution. The amount of SO_2 produced was small, ranging from 3.3% to 7.6% of the total sulfur for these runs.

Oil Yield

The mean carbon conversion to oil for 8 non-recycle runs was 45.9%, representing a 29% increase above the Fischer assay carbon conversion to oil. The heat for pyrolysis for these runs was provided by a combination of hot gases from the gasification section and external heat through the walls of the reactor. Under these conditions coking losses were relatively small, but were not completely absent since oil vapors must pass through the bed of pyrolyzing shale with the potential to react with shale surfaces and crack to form gases and coke. A situation in which all oil vapor/solid contact is eliminated could be defined as the level of zero coking, but this is not practical.

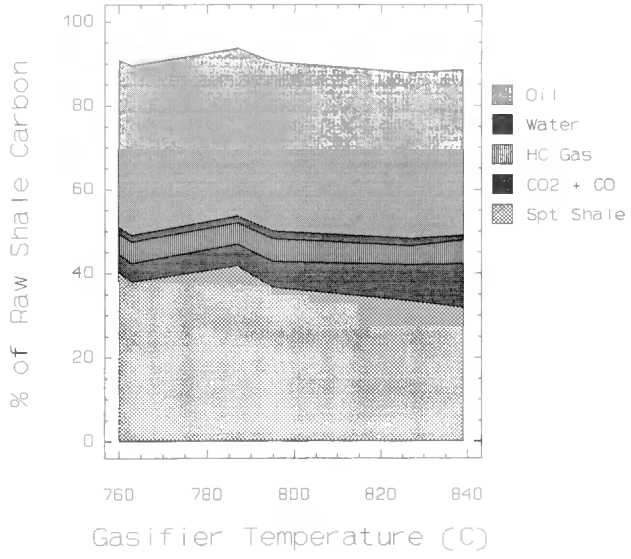

Figure 2. *Distribution of carbon in the products of pyrolysis and gasification.*

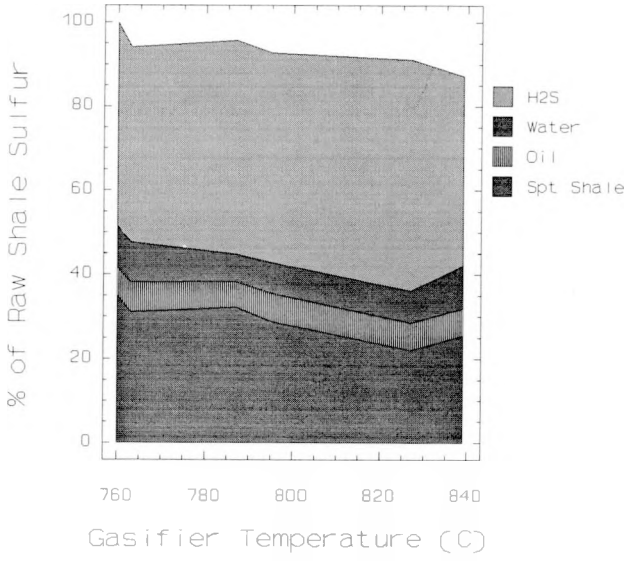

Figure 3. *Distribution of sulfur in the products of pyrolysis and gasification.*

The gas-heating mode of operation provides the lowest realistic level of oil coking in a fluidized bed pyrolyzer, so we define it as the baseline carbon conversion to oil, F_{A0}. The fractional oil loss, X_A, due to vapor phase coking is defined as:

$$X_A = (F_{A0} - F_A)/F_{A0}$$

where F_A is carbon conversion to oil in the solid-recycle mode.

If the usual mass-action laws are applied to oil coking, the rate of oil loss is proportional to the product of the oil vapor concentration and the concentration of active surface sites. Therefore, at a given oil vapor concentration and solid temperature the amount of coking should increase as the number of active surface sites increases. The number of surface sites per unit of oil vapor is proportional to the solid-recycle ratio (gasifier shale/raw shale, w/w). In Figure 4, fractional oil loss, X_A, is shown to increase as the solid-recycle ratio is increased for a given temperature range. Generally, the amount of oil loss also increased at higher solid temperatures for a given solid recycle range.

Under the least severe solid-recycle conditions (low temperature/low recycle ratio), oil yields similar to those from non-recycle operation were obtained. However, only 40% of the pyrolyzer heat was provided by solid recycle for these runs, and this does not represent a realistic scenario on the commercial-scale. A better simulation of large-scale conditions was achieved by increasing the shale feedrate to the operating limits of the reactor, which resulted in 60% heat transfer by solids. Under these conditions, approximately 15% oil loss was observed.

In the KENTORT reactor, a wide range of recycle ratio and recycle-solid temperature combinations may be utilized to transport the same quantity of energy. If oil loss is related to this combination, then the recycle-ratio and recycle-solid temperature could be adjusted to reduce oil losses, providing a simple engineering solution to oil yield reduction. Knowledge of these relationships is essential for the eventual scale-up and design of a solid-recycle system like KENTORT.

By focusing on runs with similar throughputs (KEN#31-36), the examination of recycle-ratio and recycle-solid temperature combinations is facilitated. The inverse relationship between recycle-solid temperature and recycle-ratio, and the direct proportionality between gasifier temperature and recycle-solid temperature are shown in Figure 5. Since these parameters are interrelated, it is sufficient to characterize the conditions for these runs with one parameter. The average recycle-solid temperature was chosen as the classifying condition for the discussions to follow.

Oil loss appeared to increase slightly at increased recycle-shale temperature (i.e., lower recycle ratio) for the gasified material, but this trend occurs within a relatively narrow range of oil yield losses (11-14%) making it difficult to derive more than qualitative conclusions (Figure 6). However, there was evidence noted in several of the product parameters to confirm this apparent relation including higher alkene/alkane ratios, slightly more C_1-C_4 gas, lower viscosity, and lower average molecular weight for the higher recycle temperature runs.[13] The observed trend is not unreasonable since a linear increase in coking rate is expected with recycle ratio while an exponential increase in coking rate is expected with a rise in temperature, making temperature the dominant parameter. The temperature range of this study needs to be extended somewhat to substantiate these results, but there are practical limitations for the combinations of temperature and recycle rate that can be used. For example, it appears that operation at a low recycle temperature is least detrimental to oil yield, but it may not be feasible to operate the gasifier below 700°C without staging. Similarly, an extremely low recycle rate would require a high recycle temperature, forcing the combustor temperature to be excessive.

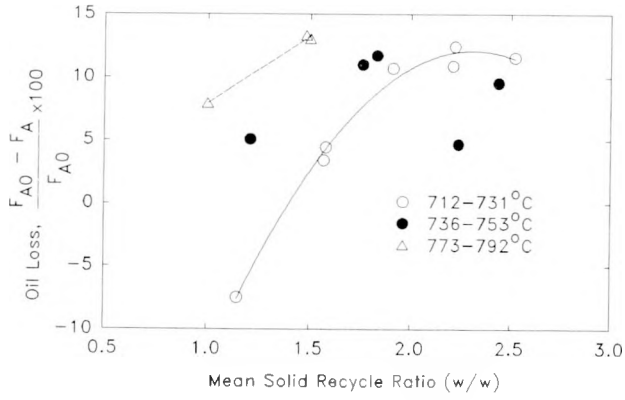

Figure 4. *Effect of solid-recycle ratio and temperature on oil yield loss in the pyrolysis zone.*

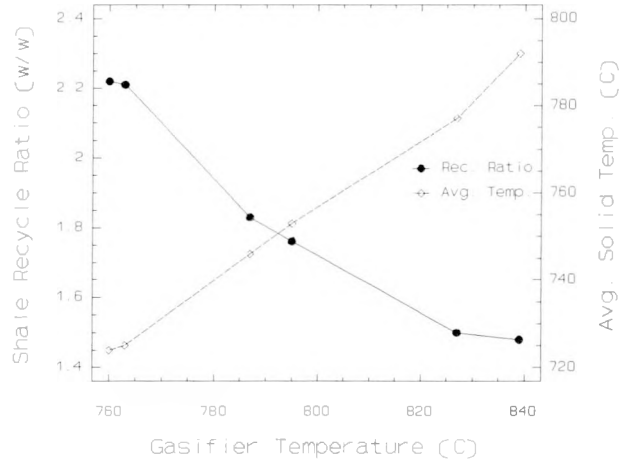

Figure 5. *Relationship of gasifier temperature to the average solid recycle temperature and recycle ratio.*

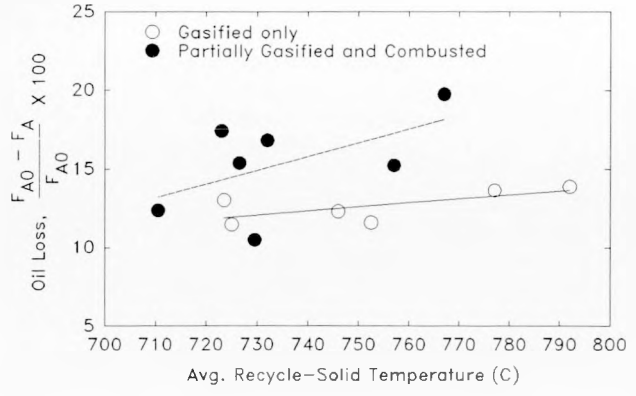

Figure 6. *Oil loss utilizing gasified only and partially combusted shales for heat transfer.*

The previous discussions have focused on the recycle of shale materials that have been gasified only. Preliminary oil loss results utilizing gasified and partially oxidized shale are compared to the non-combusted data in Figure 6. The slight temperature effect observed for the non-combusted shale seems to be accentuated for the partially oxidized materials. Moreover, the use of partially combusted materials, at the highest recycle-solid temperatures, appears to increase oil loss compared to non-combusted materials. Unfortunately, it is presently unclear what effect, if any, that the gasification zone provides. Comparison of data from the present study to recent literature values[8,9,10] suggests that direct transfer of oxidized materials to the pyrolysis zone results in more oil loss compared to recirculation of shale that passes through a gasification interstage. Coburn et al.[8] reported "inconclusive" results that steam pyrolysis in a fluidized bed containing combusted New Albany shale raised oil yields relative to similar experiments using argon for fluidization. As stated previously, this topic deserves much more attention.

It should be noted, however, that although 20% oil yield reduction has been observed in the present study under the most severe conditions, oil yields still remained above Fischer assay. Greater understanding of these oil loss mechanisms only figures to increase the oil yields that can be achieved. Therefore, it is judged that heat transfer by solid recirculation remains a viable technique, and that it certainly merits further investigation.

Conclusions

The recycle of hot, gasified shale to transfer heat to the pyrolysis zone resulted in no significant differences in carbon gasification. Oil yield reduction in the solid-recycle mode of operation is related to the solid-recycle ratio and temperature, and for the conditions studied, the temperature effect appeared to dominate oil yield losses. Oil losses were insignificant under the least severe solid-recycle conditions, but became notable when the percentage of solid-recycle heat was increased to 60%. It appears that it may be possible to reduce oil yield losses by adjusting the combination of solid recycle ratio and temperature. At the highest recycle temperatures, the recirculation of partially combusted shales increased oil losses compared to non-oxidized shales. However, the mechanisms regarding oxidized surfaces and the possible effects of steam in relation to vapor phase cracking and coking in the pyrolysis zone are poorly understood.

Acknowledgments

The work described herein was performed at the University of Kentucky Center for Applied Energy Research under Cooperative Agreement DE-FC21-86LC11086 with the Laramie Project Office of the Morgantown Energy Technology Center (METC), U.S. Department of Energy.

The authors gratefully acknowledge Jerry Hosman, Gary Simpson, and Tim Strehl for operating the unit, and G. Thomas, M. Moore, and A. Howard for product analyses.

References

1. Rubel, A.M., M.J. Margolis, J.K. Haley, and B.H. Davis, 'Proc. 1983 Eastern Oil Shale Symp.,' IMMR83/089, Lexington, KY, 1983.

2. Margolis, M.J., 'Proc. 1981 Eastern Oil Shale Symp.,' IMMR82/066, Lexington, KY, 1981.

3. Richardson, J.H., E.B. Huss, L.L. Ott, J.E. Clarkson, M.O. Bishop, L.J. Gregory, and C.J. Morris, Lawrence Livermore National Laboratory, UCID-19548, 1982.

4. Ahmed, M.M., D.W. Parker, and D.H. Archer, 'Proc. 1982 Eastern Oil Shale Symp.,' IMMR82/075, Lexington, KY, 1982.

5. Rubel, A.M. and S.D. Carter, Preprints Div. Pet. Chem., ACS, 29, 202-208 (1), 1984.

6. Carter, S.D. and D.N. Taulbee, Fuel Processing Technology, 251, 11, 1985.

7. Robl, T.L, K. Cisler, G. Thomas, and D.W. Koppenaal, 'Proc. 1985 Eastern Oil Shale Symp.,' KCERL/85-147, Lexington, Ky, 1985.

8. Coburn, T.T., Taylor, R.W., and Morris, C., 'Proc. 1988 Eastern Oil Shale Symp.,' Lexington, KY, 1988.

9. Dung, N.V., Wall, G.C., Kastl, G., Fuel, 372, 66, 1987.

10. Wall, G.C. and Udaja, P., Fuel, 1340, 67, 1988.

11. Carter, S.D., T.L. Robl, L.S. Barron, and A.M. Rubel, The Development of the KENTORT II Process for Eastern U.S. Oil Shale, Progress Report: Oct. 1- Dec. 31, 1987, under Cooperative Agreement No.: DE-FC21-86LC11086, KECL/88-178, 1988.

12. Camp, D.W., 'Proc. 1987 Eastern Oil Shale Symp.,' KECL87-175, Lexington, Ky, 1987.

13. Taulbee, D.N. and Carter S.D., 'Proc. 1989 Eastern Oil Shale Symp., Lexington, KY, 1989, in press.

Characterization of Liquid and Gaseous Products from the KENTORT II Fluidized Bed Retort/Gasifier

by

D.N. Taulbee and S.D. Carter
Center for Applied Energy Research
University of Kentucky
Lexington, Kentucky 40506

Abstract. Analytical data for the liquid and gaseous products evolved during operation of the KENTORT II in the integrated retort/gasifier mode are presented. The reactor was operated in both a non-recycle mode, in which heat for pyrolysis was provided by the fluidizing media and an external coaxial furnace, and in a solids recycle mode where a portion of the pyrolysis heat was provided by hot gasified shale. Operation of this unit in the solids recycle versus non-recycle mode resulted in moderate declines in oil yield. This decline is explained as enhanced coking and cracking of product on the surface of the hot recycle solids as evidenced by preferential removal of aromatic liquid components and higher alkene/alkane ratios in the product gas. Further, it is shown that inverse variation of the temperature and rate of solids recycle to provide a constant proportion of heat for pyrolysis results in greater oil cracking losses when higher recycle temperatures are used relative to higher recycle rates. In general, the liquid product properties obtained from operation in the solids recycle mode were very similar to those from non-recycle mode operation with the exception of minor improvements in viscosity, average molecular weight, and H/C molar ratios.

Introduction

Fluid bed retorting has been a principal area of research of the oil shale section at the CAER since about 1981. The work reported here pertains to the operation of a 5-lb/hr pyrolysis reactor which combines both retorting and gasification stages into one integrated unit. This represents the latest step in a focused effort to provide proof of concept for KENTORT II. The KENTORT II concept, based on fluidized bed technology, is designed to maximize production of oil and gaseous byproducts and to fully utilize the carbon contained in Eastern Oil Shales without resorting to exotic or high pressure environments.[1] It is also designed to do so in an environmentally acceptable manner.

Inherent in our continuing evaluation and design modifications directed at improving process efficiency for KENTORT II is the requirement that we develop a fundamental understanding of the process chemistry. This includes both organic and inorganic reactions and interactions which transpire within the three stages of this unit, with primary emphasis placed on understanding those reactions which impact on oil yield.

The analytical scheme selected for this study had three objectives. The first was to provide routine ultimate and proximate analyses required for the determination of carbon partitioning, material balances, and confirmation of oil and gas yields. An equally important objective was utilization of the analytical data as a diagnostic tool for better understanding the reaction chemistry within the integrated system. Specifically in this study, what are the detrimental interactions that lead to yield reductions when hot gasified shale is introduced to the retort. Only in more accurately describing these interactions can one reasonably hope to avoid or suppress them via design considerations. The third objective of the analytics include assessment of product quality; i.e, value, and identification of potential environmental problems.

The work reported here is intended as an accompaniment to reports on the operation of the KENTORT II fluidized bed reactor in an integrated pyrolysis/gasification configuration as described in more detail at the 1987-89 Eastern Oil Shale Symposiums.[1-3] The data presented relate directly to the operation of this unit as described in 1988 and 1989[2,3], with the exception that no analytical data are presented from operation following addition of a combustor as most recently reported.[3]

Experimental

Sampling:

A schematic of the KENTORT II integrated retort/gasifier is shown in Figure 1. More detailed descriptions of the operation of this unit can be found elsewhere.[2,3]

Oil streams were collected or measured in one of five locations. These include the air-cooled heat exchanger, the electrostatic precipitator (ESP), a water cooled heat exchanger, by a pair of filter mist coalescers, and by an on-line gas chromatograph used to measure C_5^+ hydrocarbon vapors. The weight of oil collected in the air cooled heat exchanger was determined by dissolution in CH_2C_{12} thus rendering this oil unsuitable for subsequent analyses. Likewise, additional analyses of the C_5^+ vapor phase hydrocarbons were not feasiblesince these materials were measured with an FID detector and not physically collected. Two of the remaining three oil streams, i.e, the water cooled heat exchanger and the filter coalescers, were composited into one fraction termed the light oil. The ESP and light oil fractions were then combined into a single composite, subsequently referred to as the composite oil, according to the weight production of oil in the air condenser plus ESP, using the ESP oil, and the light oil plus C_5^+ vapors, using the light oil fraction.

Though not all oil fractions are collected and combined into the composite, this sample is presumed to be representative of the total product since the two streams that are omitted, the air cooled heat exchanger oil and the C_5^+ vapors, are produced in similar quantities and their respective properties should have offsetting effects on the

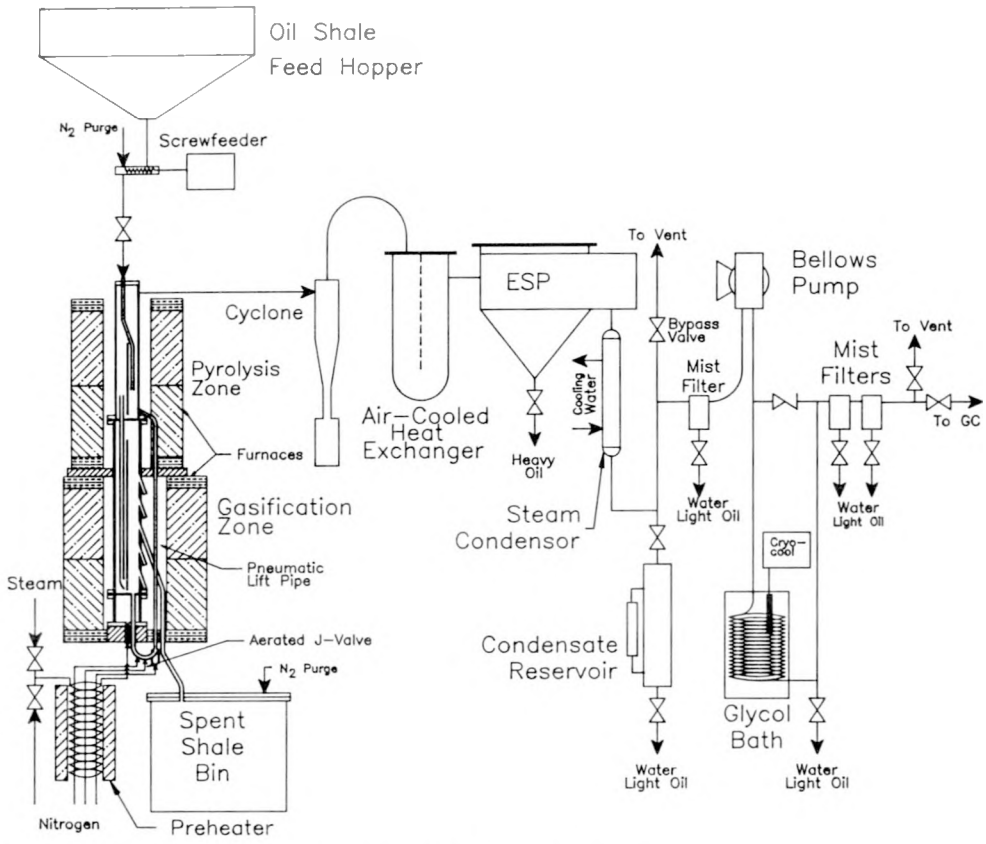

Figure 1. Schematic of KENTORT II in an integrated Retort/gasifier mode.

composite properties. That is, the omitted streams represent the extremes in properties such as H/C ratio, average molecular weight, density, etc. Thus, the effect of omitting both from the composite oil is presumed to be reasonably minor.

Water analyses were conducted on waters collected in the water cooled heat exchanger where the bulk of the fluidizing steam was condensed (>95%). Gas analyses were conducted on a split of the non-condensed gas stream that passed through the sampling loops of a Carle refinery gas analyzer which cycled at 35 minute intervals.

Run conditions and the 'Constant Heat Load' Runs:

Tables 1 and 2 present the significant run parameters and partitioning of the raw shale carbon for those runs, respectively. Additional processing information is given elsewhere.[3] Feed rate is defined as the rate of raw shale to the pyrolyzer (Table 1); solids recycle temperature is an average of gasifier temperature and the measured temperature of the lift pipe through which gasified particles were recycled to the pyrolyzer (an average was used since the value measured in the lift pipe was thought to be erroneously low due to conductive heat loss from the thermocouple well); the solids recycle ratio is the weight of gasified particles returning to the pyrolyzer divided by the feed rate; and solids recycle rate is the product of feed rate and solids recycle ratio. Carbon partitioning in Table 2 is expressed as a percentage of the raw shale carbon.

Note that the first 8 rows of Table 1 (run #'s 4-11) show information for the non-recycle runs, that is for those runs in which gasified was not recycled to the retort requiring that the heat for pyrolysis be provided by the fluidizing media and pyrolyzer furnace. The average values for these runs are shown in one of the bottom rows labeled 'non-recycle ave' both in Table 1 and 2 (as well as in Tables 3-6 to be discussed later). Run #'s 16-36 display data for those runs in which hot gasified shale particles were recycled to the retort. The average values for these runs are shown by the row near the bottom labeled 'recycle ave (all)'. Finally, runs 31-36 represent the 'constant heat load' runs. For these runs, the raw shale feed rate and the portion of heat provided to the retort by the recycle solids (as opposed to the fluidizing media or pyrolysis furnace) was held constant. For these latter runs, the temperature and rate of the recycle solids were inversely varied to meet the constant heat demand thereby allowing the effect of recycle temperature and recycle rate to be studied somewhat independently.

Analytical Procedures:

For the liquid samples, ultimate, heating value, and physical testing were conducted according to ASTM procedures, proximate analyses were obtained by TGA, average Molecular weight was determined by vapor phase osmometry at three concentrations, and oil aromaticity was determined by ^{13}C-NMR on a Varian XL-200 using routine techniques. Details of these analytical procedures have been described in a previous document[4] and will not be discussed here because of the large array of analyses conducted.

Retort off-gases were analyzed on a Carle Series Sx-AGC gas analyzer equipped with both FID and TC detectors using Carle Application #397. A split of the non-condensed gas stream was automatically sampled at 35 minute intervals during steady state portions of a given run. All gas analyses were averaged at the conclusion of the run. Primary standards from Matheson, Inc. were used for calibration.

Results and Discussion

Analyses:

For the sake of clarity, cracking reactions are defined in this report as those reactions in which the weight of volatile products equals the weight of the reactants and in the context of this paper are considered to primarily involve vapor phase reactants. Coking reactions are defined as the those reactions in which a portion of a vapor phase reactant is deposited as non-volatile material onto a solid surface. Charring reactions are defined as those reactions which result in the formation of a carbonaceous coke-like residue from non-volatile reactants.

Table 1.
Selected Processing Conditions.

Run #	Pyrolyzer Temp (C)	Gasifier Temp (C)	Feed Rate (g/min)	Recycle Temp (C)	Recycle Solids Ratio (gasif/feed)	Recycle Rate (g/min)
KEN 4	525.5	802.0	19.72			
KEN 5	542.5	840.0	20.64			
KEN 6	525.5	839.0	15.92			
KEN 7	533.0	802.0	17.82			
KEN 8	532.0	803.0	34.84			
KEN 9	535.0	831.0	33.38			
KEN 10	541.0	832.0	30.50			
KEN 11	539.0	805.0	30.00			
KEN 16	523.5	735.0	32.14	712.0	1.58	50.64
KEN 18	525.5	756.0	31.42	731.0	1.57	49.48
KEN 20	517.5	747.0	29.46	718.0	1.15	33.87
KEN 23	527.5	747.0	29.42	711.0	1.62	47.52
KEN 24	528.5	812.0	30.30	773.0	1.00	30.37
KEN 25	525.5	780.0	38.61	744.5	1.21	46.81
KEN 27	532.5	771.0	39.88	722.0	1.91	76.35
KEN 28	543.5	783.0	51.71	736.0	2.44	126.18
KEN 29	546.0	796.0	46.73	748.5	2.24	104.49
KEN 30	536.0	754.0	48.54	716.0	2.52	122.51
KEN 31	536.5	827.0	48.30	777.0	1.50	72.58
KEN 32	527.0	787.0	48.28	746.0	1.83	88.39
KEN 33	529.5	760.0	47.25	723.5	2.22	104.98
KEN 34	530.0	763.0	47.49	725.0	2.21	105.17
KEN 35	536.0	839.0	47.28	792.0	1.48	69.83
KEN 36	532.0	795.0	46.18	752.5	1.76	81.47
Non-recycle avg.	534.2	819.3	25.40			
Recycle avg. (all)	531.1	778.3	41.40	739.3	1.77	75.67
Recycle avg. (31-36)	531.8	795.2	47.50	752.7	1.83	87.07

The *"non-recycle average"* pertains to run 4 thru 11; *"recycle average (all)"* is for run 16 thru 36; and *"Recycle average (31-36)"* is for run 31 thru 36.

Tables 3-7 present analytical data for the light oils, ESP oils, composite oils, non-condensed gases, and process waters, respectively. In addition, average values are shown in each table for the non-solids recycle runs (runs 4-11), all solids recycle runs (runs 16-36), and the six constant heat load runs (runs 31-36).

The analytical and production data for the light oils are relatively constant for all runs exhibiting only minimal differences in the averages for the non-recycle and solids recycle runs (Table 3). The scatter that is present is attributed more to run-to-run differences in the ESP trapping efficiency, resulting in a variable portion of the total oil partitioning to the light oil fraction, than to differences in the oil produced. This is supported by a general correlation between light oil production and light oil density. For the solids recycle runs, however, there appears to be an inverse correlation between light oil density and recycle solids temperature suggesting that higher temperature surfaces yield lower density oils.

Analogous analytical data for the ESP oils (Table 4) generally show little or no correlation with the processing variables of gasifier, pyrolysis, or solids recycle temperature, solids recycle ratio, or feed rate. This lack of correlation is attributed to several factors including the previously mentioned run-to-run variation of oils partitioning between the ESP and light oil condenser; the difficulty in obtaining representative samples for analyses due to the viscous nature and high water content of the ESP oils; the fact that the single most important variable in terms of oil properties, pyrolysis temperature, was varied over a relatively narrow range for these runs; and the complex interaction of the processing variables in this system which often have opposing effects on a given oil parameter and thus tend to mask correlations.

Even so, there is a positive correlation between recycle solids temperature and the ESP H/C molar ratios. This relation was not apparent for the non-recycle oils when the H/C ratio was plotted against gasifier temperature (there were no recycle solids for direct comparison requiring gasifier temperature be used). The data are highly scattered but since H/C and density typically show an inverse relation, the direct correlation is consistent with the decline in density observed for the light oils. This can be explained as a lowering of the aromaticity of the ESP oils via coking reactions in agreement with composite oil data to be shown later.

A second point concerning the ESP oils is the lack of correlation between the ash content (corrected for water) and processing conditions. That is, there does not appear to be a significant increase in fines carryover for the runs in which either higher gasifier

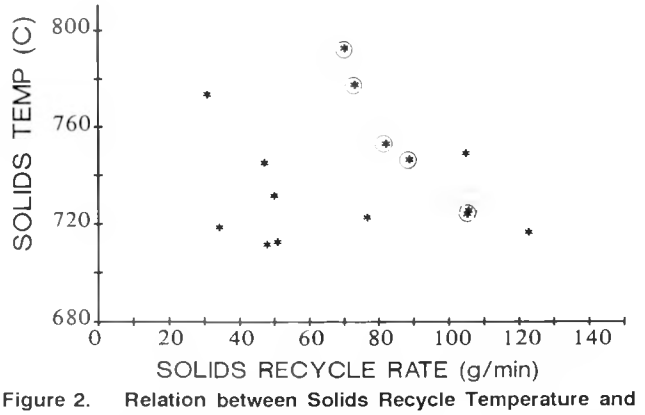

Figure 2. Relation between Solids Recycle Temperature and Solids Recycle Rate. Constant load runs shown encircled.

Table 2.
Carbon Partitioning (Expressed as Percent of Raw Shale Carbon).

Run #	Spent Shale	Oils (Total)	Air Cooled Condensor	ESP Oil	Light Oil	C_5+ Vapor Oils	Off-Gas (Total)	Off-Gas Hydrocarbons	Off-Gas $CO + CO_2$	Process Waters
KEN 4	28.28	53.48	8.56	29.48	8.64	6.79	13.41	4.46	8.95	2.95
KEN 5	28.71	43.78	8.55	19.29	11.70	4.24	18.36	4.08	14.29	2.85
KEN 6	23.82	46.46	10.99	20.95	8.43	6.09	22.59	4.85	17.74	3.46
KEN 7	29.71	49.12	10.45	23.05	10.07	5.55	14.77	4.48	10.29	3.65
KEN 8	35.33	41.96	7.02	21.26	8.41	5.27	12.40	4.21	8.19	1.81
KEN 9	30.06	42.82	7.74	22.50	7.75	4.83	15.58	4.77	10.81	2.04
KEN 10	28.97	46.70	10.80	23.48	7.92	4.50	15.45	4.64	10.81	1.86
KEN 11	31.50	42.23	5.19	24.08	8.73	4.23	14.73	4.82	9.91	2.04
KEN 16	42.87	43.55	6.53	23.43	8.55	5.04	8.52	4.70	3.82	2.02
KEN 18	38.97	44.01	9.94	22.92	6.46	4.68	8.82	4.17	4.66	1.31
KEN 20	39.20	48.97	11.60	22.93	8.99	5.45	8.64	4.98	3.66	1.82
KEN 23	39.18	32.21	4.65	22.14	0.00	5.41	9.36	5.43	3.92	1.62
KEN 24	36.57	41.95	6.55	21.82	8.22	5.36	13.96	5.26	8.69	1.66
KEN 25	39.43	43.26	4.74	24.28	9.32	4.91	9.63	4.37	5.26	2.00
KEN 27	39.28	40.69	4.95	23.27	8.46	4.01	9.00	4.20	4.80	1.76
KEN 28	36.79	41.21	4.46	24.08	8.89	3.80	9.03	4.56	4.47	1.94
KEN 29	35.62	43.43	4.87	24.01	10.57	3.98	11.36	5.00	6.36	1.76
KEN 30	40.70	40.30	4.87	21.32	9.84	4.27	8.74	4.94	3.80	1.97
KEN 31	33.44	39.61	5.80	20.74	8.96	4.11	13.07	4.52	8.55	1.74
KEN 32	41.78	40.23	4.65	22.51	8.85	4.21	10.20	5.01	5.19	1.61
KEN 33	40.40	39.89	5.16	22.56	8.04	4.14	9.06	4.89	4.16	1.54
KEN 34	37.99	40.60	5.27	21.92	9.17	4.24	9.43	5.03	4.40	1.59
KEN 35	31.95	39.50	5.12	21.53	8.25	4.60	15.88	5.59	10.30	1.22
KEN 36	36.76	40.55	5.16	23.40	7.52	4.47	11.45	5.40	6.05	1.81
Non-recycle avg.	29.55	45.82	8.66	23.01	8.96	5.19	15.91	4.54	11.37	2.58
Recycle avg. (all)	38.18	41.25	5.89	22.68	8.13	4.54	10.38	4.88	5.50	1.71
Recycle avg. (31-36)	37.05	40.06	5.19	22.11	8.46	4.30	11.51	5.07	6.44	1.58

Run numbers 4 thru 11 are non-recycle; numbers 16 thru 36 are solids recycle; and numbers 31 thru 36 are the final six *"constant load"* runs.

Table 3.
Light Oils Analyses.

Run #	Density (g/mL)	LO+C_5+ Prod. (% of Total)	% C	% H	% N	% S	% H_2O	H/C (dry)	N/C	S/C
KEN 4	0.896	26.89	83.51	11.38	0.45	1.88	0.50	1.63	0.0046	0.0084
KEN 5	0.894	32.92	85.03	11.80	0.57	2.02	0.20	1.66	0.0057	0.0089
KEN 6	0.894	26.62	83.67	11.56	0.45	2.05	0.34	1.65	0.0046	0.0092
KEN 7	0.900	27.58	84.26	11.36	0.47	2.07	0.40	1.61	0.0048	0.0092
KEN 8	0.885	28.09	85.06	11.48	0.64	2.06	0.13	1.62	0.0065	0.0091
KEN 9	0.884	25.41	84.96	11.63	0.46	2.31	0.24	1.64	0.0046	0.0102
KEN 10	0.887	23.48	84.66	11.22	0.46	1.99	0.14	1.58	0.0047	0.0088
KEN 11	0.889	26.75	84.20	11.09	0.53	2.19	0.18	1.58	0.0054	0.0097
KEN 16	0.889	25.39	85.54	11.16	0.59	2.29	0.38	1.56	0.0059	0.0100
KEN 18	0.870	22.30	85.40	11.50	0.52	2.12	0.22	1.61	0.0052	0.0093
KEN 20	0.881	26.19	85.23	11.35	0.61	2.00	0.22	1.60	0.0061	0.0088
KEN 23	0.888	30.78	85.29	11.84	0.56	1.93	0.22	1.66	0.0056	0.0085
KEN 24	0.882	28.34	86.30	11.84	0.64	1.79	0.18	1.65	0.0064	0.0078
KEN 25	0.886	30.03	85.28	12.01	0.55	1.95	0.27	1.69	0.0055	0.0086
KEN 27	0.883	27.80	85.19	12.28	0.61	2.14	0.17	1.73	0.0061	0.0094
KEN 29	0.883	31.02	85.08	12.00	0.57	2.04	0.21	1.69	0.0057	0.0090
KEN 30	0.896	33.17	83.43	11.62	0.50	2.42	0.24	1.67	0.0051	0.0109
KEN 31	0.884	30.82	83.62	11.45	0.44	2.06	0.19	1.64	0.0045	0.0092
KEN 32	0.882	30.54	83.70	11.52	0.49	1.95	0.17	1.65	0.0050	0.0087
KEN 33	0.873	28.15	85.36	11.62	0.42	1.97	0.13	1.63	0.0042	0.0086
KEN 34	0.887	31.30	83.98	11.32	0.47	2.05	0.32	1.61	0.0048	0.0091
KEN 35	0.881	27.84	84.57	11.70	0.48	1.82	0.19	1.66	0.0049	0.0081
KEN 36	0.875	27.08	84.01	11.99	0.42	2.14	0.17	1.71	0.0043	0.0095
Non-recycle avg.	0.891	27.20	84.42	11.44	0.50	2.07	0.27	1.62	0.0051	0.0092
Recycle avg. (all)	0.883	28.70	84.79	11.68	0.52	2.05	0.22	1.65	0.0053	0.0090
Recycle avg. (31-36)	0.880	29.29	84.21	11.60	0.45	2.00	0.20	1.65	0.0046	0.0089

Run numbers 4 thru 11 are non-recycle; numbers 16 thru 36 are solids recycle; and numbers 31 thru 36 are the final six *"constant load"* runs.

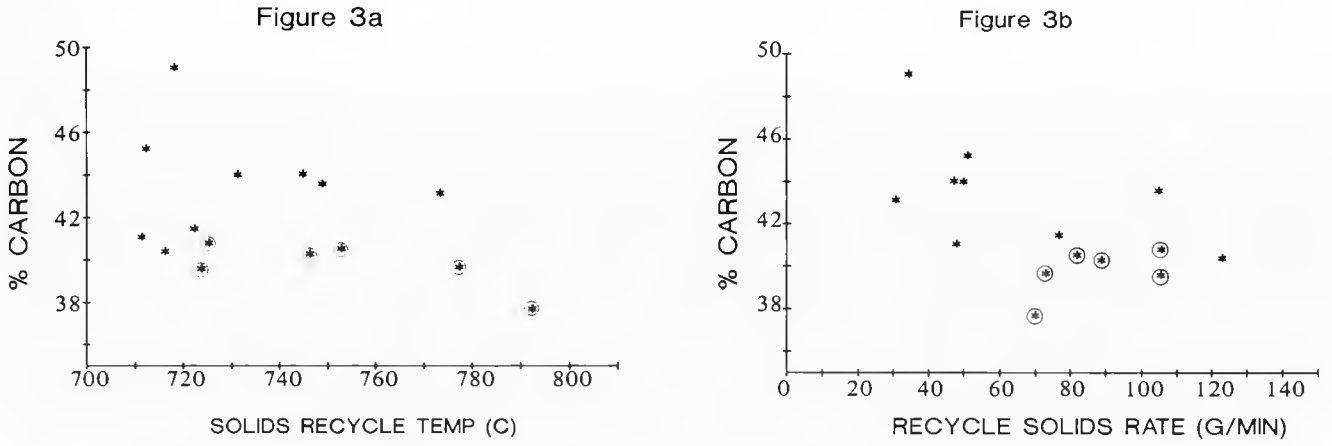

Figure 3. **Partitioning of Raw Shale Carbon to Oil phase as a Function of Recycle Solids Temperature (3a) and Recycle Rate (3b). Constant load runs encircled.**

temperatures or solids recycle rates were used. Thus, particle attrition under more severe gasifier conditions should not be a problem.

In addition to the individual oil parameters given in Tables 3-4, the last three rows give averaged properties for the non-recycle, all of the recycle runs, and the last six recycle runs, respectively. The last six recycle runs, which represent the constant heat load runs, also represent the highest feed rates. Since higher feed rates require that greater amounts of hot gasified shale be recycled to the retort, then, the effect of solids recycle on product oil should be most apparent for these runs.

Note the slightly higher average density of the light oils from the non-recycle runs in Table 3. This is in spite of the fact that on average, more of the oil partitioned to the light oil fraction for the recycle runs which, all else being equal, might be expected to result in an increase in light oil density. This measurement along with the slightly higher H/C ratios for the recycle runs can be explained as selective coking of aromatic components on the surface of the hot gasifier solids.

Scrutiny of analogous ESP data in Table 4 reveals no significant differences in the recycle and non-recycle ESP oil properties when differences in water content are taken into account. Due to the difficulty encountered in obtaining representative samples of this fraction, the data was considered to be less reliable than that for the Light oil or Composite oil and will not be discussed further.

Table 4.
ESP Oils Analyses.

Run #	ESP + AC Prod. (% of total oil)	% H_2O	% C	% H	% N	% S	H/C (dry)	N/C	S/C	% FC (tga)	% Ash (tga)
KEN 4	73.11	1.24	78.35	8.55	1.31	1.65	1.29	0.014	0.0079	9.0	10.5
KEN 5	67.08	17.22	70.95	10.07	1.27	1.54	1.38	0.015	0.0081		
KEN 6	73.38	26.75	63.81	9.50	0.82	1.32	1.23	0.011	0.0077	8.3	1.0
KEN 7	72.42	21.15	66.41	9.52	0.81	1.26	1.30	0.010	0.0071	6.7	2.7
KEN 8	71.91	17.11	67.92	9.18	1.09	1.93	1.29	0.014	0.0106	7.4	2.8
KEN 9	74.59	16.06	68.63	9.22	0.84	1.21	1.30	0.010	0.0066	7.0	3.5
KEN 10	76.52	14.25	70.38	9.64	0.94	1.54	1.37	0.011	0.0082	6.5	2.3
KEN 11	73.25	15.59	69.73	9.50	1.12	1.50	1.34	0.014	0.0081	7.9	2.5
KEN 16	74.61	22.55	62.75	9.20	1.17	1.56	1.28	0.016	0.0093	5.3	5.0
KEN 18	77.80	16.35	69.16	8.33	1.18	1.43	1.13	0.015	0.0077	5.6	3.0
KEN 20	73.79	11.55	70.55	8.54	1.12	1.59	1.23	0.014	0.0084	7.7	3.9
KEN 23	69.22	11.11	72.05	8.78	1.01	1.64	1.26	0.012	0.0085	8.7	3.1
KEN 24	71.66	12.15	71.07	9.32	1.30	1.40	1.35	0.016	0.0074	6.9	3.8
KEN 25	69.97	9.13	75.77	8.68	1.28	1.61	1.21	0.014	0.0080	11.1	4.6
KEN 27	72.20	8.14	75.10	8.91	1.38	1.69	1.28	0.016	0.0084	8.5	3.8
KEN 28	72.15	7.39	75.92	8.81	1.13	1.59	1.26	0.013	0.0078	9.5	4.5
KEN 29	68.98	8.97	76.61	8.64	1.50	1.70	1.20	0.017	0.0083	8.4	3.5
KEN 30	66.83	2.01	78.59	8.68	1.10	1.63	1.29	0.012	0.0078	10.3	3.8
KEN 31	69.18	2.94	76.76	8.75	1.17	1.70	1.32	0.013	0.0083	10.5	4.1
KEN 32	69.46	3.72	78.37	9.00	1.25	1.73	1.31	0.014	0.0083	8.6	3.3
KEN 33	71.85	4.43	77.44	9.09	1.24	1.76	1.33	0.014	0.0085	7.9	3.3
KEN 34	68.70	1.13	79.32	8.94	1.30	1.93	1.33	0.014	0.0091	8.3	3.8
KEN 35	72.16	2.41	78.49	8.99	1.28	1.89	1.33	0.014	0.0090	8.4	3.6
KEN 36	72.92	4.67	76.18	9.15	1.23	1.73	1.36	0.014	0.0085	8.4	4.0
Non-recycle avg.	72.78	16.17	69.52	9.40	1.03	1.49	1.31	0.012	0.0080	7.5	3.6
Recycle avg. (all)	71.34	8.04	74.63	8.86	1.23	1.66	1.28	0.014	0.0083	8.4	3.8
Recycle avg. (31-36)	70.71	3.22	77.76	8.99	1.25	1.79	1.33	0.014	0.0086	8.7	3.7

Run numbers 4 thru 11 are non-recycle; numbers 16 thru 36 are solids recycle; and numbers 31 thru 36 are the final six *"constant load"* recycle runs.

Table 5.
Composite Oils Analyses

Run #	Density (g/mL)	% C	% H	% N	% S	H/C (dry)	N/C	S/C	% H_2O	% Ash (tga)	BTU/lb (dry)	As (ppm)	Ni (ppm)	Fe (ppm)	V (ppm)	Pour Pt. (F)
KEN 4		77.31	9.40	0.84	1.75	1.42	0.0093	0.0085	1.04	6.83	15950					
KEN 5	1.005	73.88	10.15	0.77	1.72	1.41	0.0089	0.0087	11.62	1.14	14570					10
KEN 6	1.000	70.70	10.47	0.55	1.39	1.39	0.0067	0.0074	19.72	0.50	17100					20
KEN 7	1.006	73.40	9.95	0.56	1.30	1.30	0.0065	0.0066	15.43	0.00	16900					30
KEN 8	1.006	75.82	9.17	0.76	1.80	1.27	0.0086	0.0089	12.34	1.30	17050					20
KEN 9	1.003	75.27	9.94	0.73	1.70	1.36	0.0083	0.0085	12.04	0.25	16530					10
KEN 10	1.018	77.74	9.87	0.90	1.53	1.32	0.0099	0.0074	10.94	0.30	16660					10
KEN 11	1.014	73.69	9.89	0.88	1.57	1.36	0.0102	0.0080	11.47	0.20	16720					5
KEN 16	1.029	69.47	9.43	0.83	1.46	1.30	0.0102	0.0079	16.92	3.00	16610					0
KEN 18	1.000	74.70	9.54	0.78	1.57	1.27	0.0090	0.0079	12.77	1.10						0
KEN 20	1.014	75.88	9.71	0.74	1.82	1.40	0.0084	0.0090	8.58	1.00						0
KEN 23	1.010	79.84	9.79	0.80	1.67	1.33	0.0086	0.0078	7.76	1.00	15730					-10
KEN 24	1.012	76.48	10.01	0.83	1.55	1.40	0.0093	0.0076	8.76	3.00	14910					-10
KEN 25	1.007	79.29	9.88	0.91	1.66	1.38	0.0098	0.0078	6.47	4.40	16550					-10
KEN 27	0.999	79.12	9.83	0.90	1.70	1.38	0.0098	0.0080	5.92	4.80	17120					-5
KEN 29	1.005	77.45	9.98	0.93	1.65	1.43	0.0103	0.0080	6.25	3.10	17090	25.3	76.8	383	42.5	-10
KEN 30	1.005	81.47	10.01	0.81	1.80	1.46	0.0085	0.0083	1.42	4.90	17070					0
KEN 31	1.010	80.74	9.82	0.89	1.90	1.40	0.0095	0.0088	2.02	5.00	16810	26.1	71.7	388	36.5	0
KEN 32	1.008	83.69	9.91	0.79	1.85	1.41	0.0081	0.0083	2.64	2.00	17690					5
KEN 33	0.998	82.33	9.88	0.77	1.88	1.37	0.0080	0.0086	3.22	1.50	17340	15.0	69.8	328	33.4	-5
KEN 34	1.017	83.55	10.28	0.78	1.98	1.45	0.0080	0.0089	0.86	2.25	17140					5
KEN 35	1.022	83.32	10.26	0.74	1.78	1.46	0.0076	0.0080	1.79	1.00	17140	21.9	74.1	390	36.6	0
KEN 36	1.022	81.16	9.96	0.76	1.74	1.40	0.0080	0.0080	3.45	3.00	16960	15.6	80.3	392	38.2	0
Non-rec. avg.	1.008	74.73	9.86	0.75	1.60	1.35	0.0086	0.0080	11.80	1.30	16420					15
Rec. avg. (all)	1.011	79.23	9.89	0.82	1.73	1.39	0.0089	0.0082	5.90	2.70	16920	20.8	74.5	376	37.4	0
Rec. avg. (31-36)	1.013	82.47	10.02	0.79	1.86	1.42	0.0082	0.0084	2.30	2.50	17180					0

Run #	Viscosity 40 C (cps)	Conradsen Carbon (%)	Avg. Mol. Weight	% Arom. Carbon	% Naptha (IBP-400 F)	% Mid. Dist. (400-650 F)	% Hvy. Dist. (650-1000 F)	% Resid (>1000 F)
KEN 4	597	25.2	383					
KEN 5	164	13.6	323	39.1				
KEN 6	303	10.7	377	40.7				
KEN 7	359	14.7	340	38.9				
KEN 8	191	14.7	362	39.1				
KEN 9	277	15.0	373	40.4				
KEN 10	381	18.1	372	43.3				
KEN 11	528	22.6	342	41.0				
KEN 16	304	17.3	533	42.9	5.0	24.0	27.0	44.0
KEN 18	236	17.4	459	41.6	9.0	25.0	33.0	33.0
KEN 20	304	18.4		42.8	5.0	57.0	0.0	38.0
KEN 23	160	16.6	421	41.1	5.0	30.0	38.0	27.0
KEN 24	168	16.1	369	40.2	5.0	30.0	32.0	33.0
KEN 25	220	16.9	372	41.2	5.0	25.0	36.0	34.0
KEN 27	256	16.2	382	40.1	5.0	25.0	37.0	33.0
KEN 29	148	17.9	360	40.2	5.0	30.0	30.0	35.0
KEN 30	172	17.8	309	39.6	5.0	25.0	32.0	38.0
KEN 31	180	17.3	294	40.0	4.0	31.0	44.0	21.0
KEN 32	144	17.2	332	40.2	5.0	26.0	39.0	30.0
KEN 33	116	16.4	306	39.4	5.0	25.0	32.0	38.0
KEN 34	144	17.3	291	39.7	5.0	26.0	37.0	32.0
KEN 35	122	17.4		40.6	5.0	31.0	43.0	21.0
KEN 36	140	17.4	305	38.3	5.0	30.0	40.0	25.0
Non-recycle ave.	350	16.8	360	40.4				
Recycle ave. (all)	188	17.2	364	40.5	5.2	29.3	33.3	32.1
Recycle ave. (31-36)	141	17.2	306	39.7	4.8	28.2	39.2	27.8

Effect Of Solids Recycle On Product Composition:

Relating processing conditions to product chemistry is important in order to better understand detrimental reactions and ultimately to improve the process design. Coking and cracking oil losses are important considerations in any solid-solid heat transfer retort.[3]

Figure 2 shows the relation between recycle solids temperature and rate. As can be seen, these parameters were for the most part, varied independently. This implies of course that the proportion of heat supplied to the pyrolyzer by the recycle solids and the fluidizing steam also varied. The exception to this independent variation were the final six runs (circled points in Figure 2) where the raw shale feed rate and heat input from recycle solids was held constant resulting in the strong correlation observed between recycle temperature and rate.

Figure 3 shows oil yields as a function of both recycle temperature and recycle rate. This plot demonstrates that for those runs in which recycle temperature and rate were independently varied, both higher temperatures and higher rates resulted in lower oil yields, presumably from product coking. However, for the six constant load runs shown encircled, it appears that supplying a constant amount of heat energy to the pyrolyzer by inverse variation of these parameters results in higher oil yields when higher recycle rates are used as opposed to higher recycle temperatures. In other words, oil losses are more extensive when fewer higher temperature particles are used to supply the same amount of heat as would be contributed by fewer relatively cooler particles.[3]

Though the intent was to maintain a constant pyrolysis temperature for this set of runs, some variation was unavoidable. When pyrolysis temperature was plotted against the composite oil aromaticity (Figure 4), an inverse relation was found. This was initially puzzling since it is contrary to what had been observed for pyrolysis experiments conducted in the absence of solids heat transfer.[5] So why the inverse relation in this study? The explanation appears to be that pyrolysis temperature roughly correlated with both recycle solids temperature and rate (Table 1) with the exception of the six constant load runs shown encircled in Figure 4. Thus, what is actually depicted in Figure 4 is the effect of recycle solids on oil aromaticity, with the effect of pyrolysis temperature in this range being relatively insignificant.

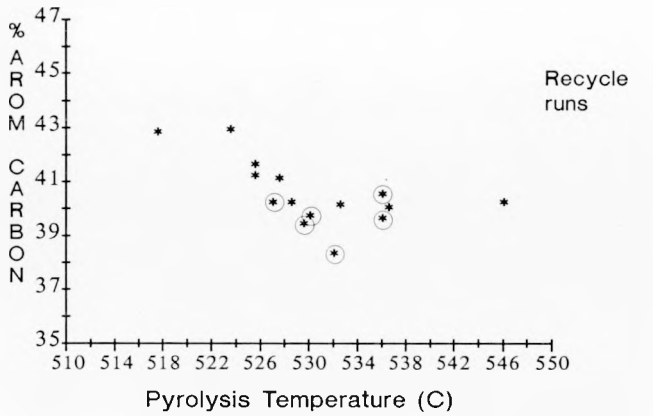

Figure 4. **Aromatic Carbon Content of the Composite Oil as a Function of Pyrolysis Temperature. Constant load runs shown encircled.**

When oil aromaticity is plotted against recycle temperature and rate as in Figures 5a and 5b, an inverse relation is observed for both plots. Though the data are scattered, this inverse relation is significant, particularly when one considers that recycle rate and temperature were generally inversely related, strongly so for the constant load runs. Thus, their impact on oil properties tend to be offsetting, thereby accounting for a portion of the scatter. The trends in Figure 5 are interpreted as evidence that recirculation of hot solids to the retort results in selective removal of aromatics at a faster rate than aliphatics. This removal is presumably via coking reactions since aromatics are known to be more prone to coke deposition in the presence of hot solid surfaces than are aliphatics.

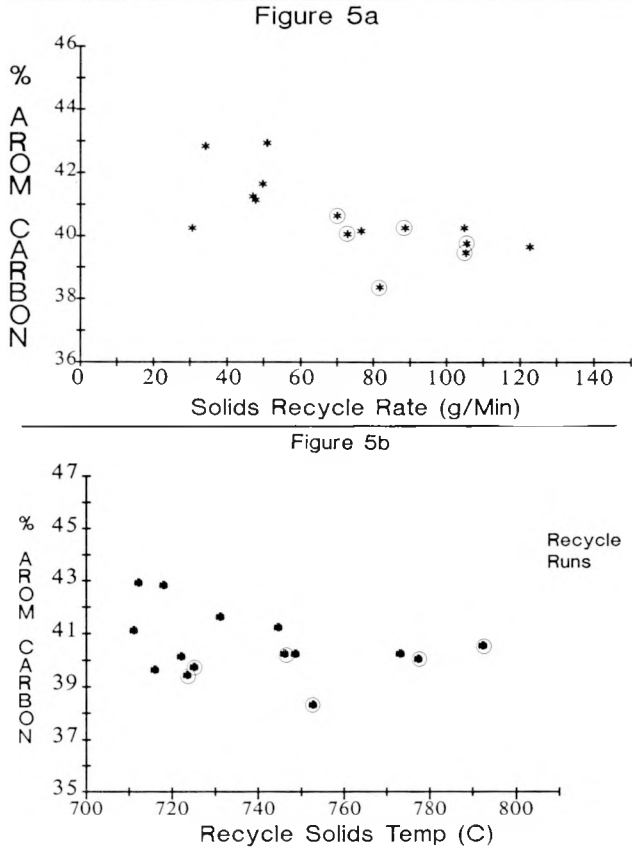

Figure 5. **Aromatic Carbon Content of Composite Oil as a Function of Recycle Solids Rate (top) and Temperature (bottom). Constant load runs encircled.**

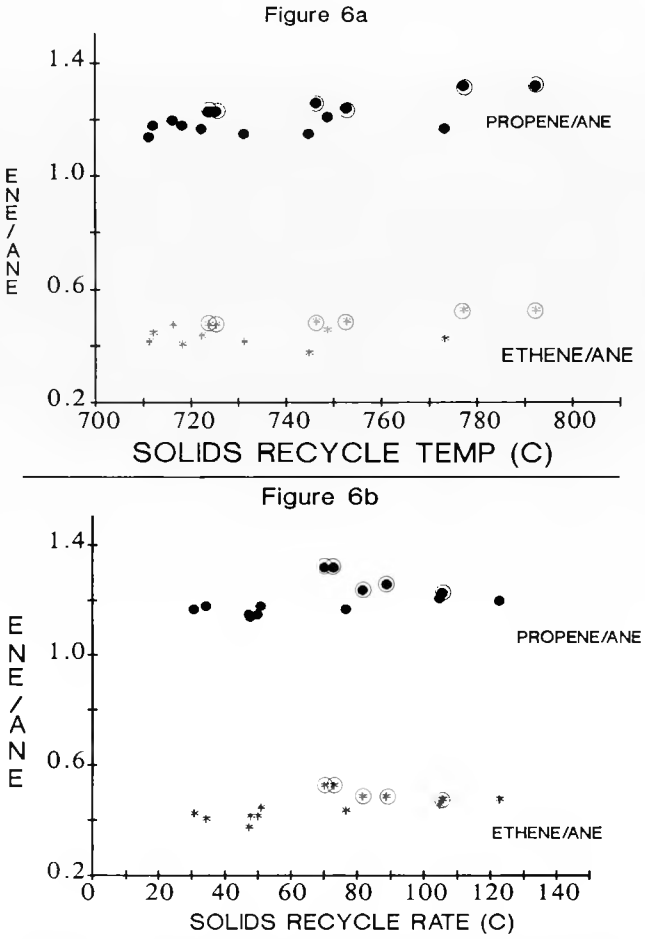

Figure 6. **Alkene/alkane ratios as a Function of Solids recycle temperature (a) and recycle rate (b). Constant load runs are shown encircled.**

This conjecture is supported by the absence of correlation between the aromaticity of the non-recycle oils and pyrolysis or gasifier temperature. Figure 5a shows that this inverse relation between aromaticity and recycle rate holds even for the constant load runs. This is not the case however in Figure 5b where oil aromaticity increases with increasing recycle solids temperature for the constant load runs. The overall data of Figure 5b suggests that hotter particles induce coking at a faster rate as one would expect, but the constant load runs imply that higher recycle rates result in more extensive removal of aromatics than an equivalent amount of heat input by higher temperatures particles.

This brings up an interesting question, namely, if higher recycle rates result in more extensive coking and removal of aromatics for a given heat demand, why do higher recycle temperatures result in somewhat lower oil conversions? A possible explanation may be found in Figure 6a which shows the alkene/alkane ratios for C_2 and C_3 hydrocarbons as a function of recycle solids temperature. Previous work has shown that higher 1-alkene/n-alkane ratios can be used as an indication of enhanced product cracking.[6] So, based on that premise, it would appear that higher recycle temperatures resulted in higher rates of cracking in this study, as one would expect. An analogous plot of alkene/alkane ratios as a function of recycle rate in Figure 6b indicates a similar trend. Together, these plots suggest that either higher recycle temperatures or higher recycle rates induce additional product cracking, again, as to be expected.

Since the alkene/alkane ratio cannot directly correlate with both recycle temperature and rate for the six constant load runs, scrutiny of these runs should reveal which of these parameters is the more dominant in terms of product cracking. This is shown clearly in Figure 7 where the C_2 and C_3 alkene/alkane ratios are plotted

Table 6.
Off-Gas Analyses.

Run #	C1-C4HC Gases (% rs C)	CH4 (% rs C)	C2's (% rs C)	C3's (% rs C)	C4's (% rs C)	CH4 (ft^3/ton)	C2's (ft^3/ton)	C3's (ft^3/ton)	C4's (ft^3/ton)
KEN 4	4.46	1.61	1.06	0.91	0.873	148.8	49.4	28.0	20.1
KEN 5	4.08	1.55	0.99	0.84	0.700	140.4	45.6	25.3	15.9
KEN 6	4.85	1.94	1.14	0.98	0.798	177.0	53.0	29.8	18.2
KEN 7	4.48	1.65	1.07	0.94	0.823	151.7	49.8	28.8	19.0
KEN 8	4.21	1.44	1.01	0.91	0.841	132.7	47.3	28.1	19.4
KEN 9	4.77	1.76	1.13	0.96	0.921	161.9	52.5	29.6	21.2
KEN 10	4.64	1.72	1.09	0.93	0.901	156.9	50.0	28.1	20.5
KEN 11	4.82	1.79	1.16	0.97	0.903	162.2	53.2	29.5	20.5
KEN 16	4.70	1.67	1.16	0.98	0.903	151.3	53.1	29.5	20.5
KEN 18	4.17	1.48	0.99	0.86	0.836	132.6	44.9	25.6	18.7
KEN 20	4.98	1.72	1.24	1.04	0.980	154.8	56.5	31.1	22.1
KEN 23	5.43	1.92	1.36	1.12	1.039	172.0	61.7	33.4	23.3
KEN 24	5.26	1.90	1.29	1.08	0.993	168.8	57.7	32.0	22.0
KEN 25	4.37	1.58	1.06	0.93	0.800	141.8	48.1	27.7	17.9
KEN 27	4.20	1.50	1.01	0.86	0.837	136.7	46.6	26.0	19.1
KEN 29	5.00	1.73	1.25	1.05	0.981	155.3	56.8	31.3	22.1
KEN 30	4.94	1.81	1.19	0.99	0.958	160.3	53.5	29.2	21.3
KEN 31	4.52	1.66	1.12	0.92	0.817	146.8	50.0	27.1	18.0
KEN 32	5.01	1.83	1.25	1.02	0.920	163.9	56.4	30.4	20.6
KEN 33	4.89	1.73	1.22	1.00	0.940	154.3	55.0	29.8	21.0
KEN 34	5.03	1.81	1.23	1.02	0.971	161.4	55.5	30.4	21.7
KEN 35	5.59	2.12	1.34	1.11	1.024	188.7	60.4	32.9	22.8
KEN 36	5.40	1.89	1.25	1.03	1.237	166.3	55.6	30.3	27.3
Non-recycle avg.	4.54	1.68	1.08	0.93	0.845	154.0	50.1	28.4	19.4
Recycle avg. (all)	4.90	1.76	1.20	1.00	0.949	157.0	54.1	29.8	21.2
Recycle avg. (31-36)	5.07	1.84	1.23	1.02	0.985	163.5	55.5	30.1	21.9

Run #	C1-C4's Total (ft^3/ton)	CO_2 (ft^3/ton)	CO (ft^3/ton)	H_2 (ft^3/ton)	H_2S (ft^3/ton)	Ethene/ Ethane	Propene/ Propane	1-Butene/ n-Butane
KEN 4	246	413	412	1004	207		1.21	1.31
KEN 5	227	565	731	1595	249		1.26	1.33
KEN 6	278	731	889	1864	263		1.23	1.31
KEN 7	249	460	487	947	233		1.21	1.32
KEN 8	227	396	359	964	201	0.51	1.25	1.20
KEN 9	265	474	520	1390	268	0.36	1.22	1.23
KEN 10	255	467	516	1575	239	0.49	1.21	1.31
KEN 11	265	399	500	1219	260	0.37	1.22	1.31
KEN 16	254	212	134	880	232	0.44	1.18	1.26
KEN 18	222	240	176	961	238	0.41	1.15	1.17
KEN 20	265	195	134	799	250	0.40	1.18	1.26
KEN 23	290	203	149	834	239	0.41	1.14	1.30
KEN 24	280	424	346	1568	231	0.42	1.17	1.31
KEN 25	236	267	205	1032	219	0.37	1.15	1.19
KEN 27	228	249	188	979	235	0.43	1.17	1.30
KEN 29	266	323	248	1273	255	0.45	1.21	1.30
KEN 30	264	197	140	775	239	0.47	1.20	1.28
KEN 31	242	430	324	1574	230	0.52	1.32	1.45
KEN 32	271	288	176	1080	223	0.48	1.26	1.27
KEN 33	260	224	147	861	198	0.47	1.23	1.29
KEN 34	269	231	161	928	194	0.47	1.23	1.36
KEN 35	305	506	411	1734	187	0.52	1.32	1.43
KEN 36	279	326	207	1246	206	0.48	1.24	1.24
Non-recycle avg.	252	488	552	1319	240	0.43	1.23	1.29
Recycle avg. (all)	262	288	210	1102	225	0.45	1.21	1.29
Recycle avg. (31-36)	271	334	238	1237	206	0.49	1.27	1.34

% rs C in columns 1 thru 5 refers to the percent of raw shale carbon.

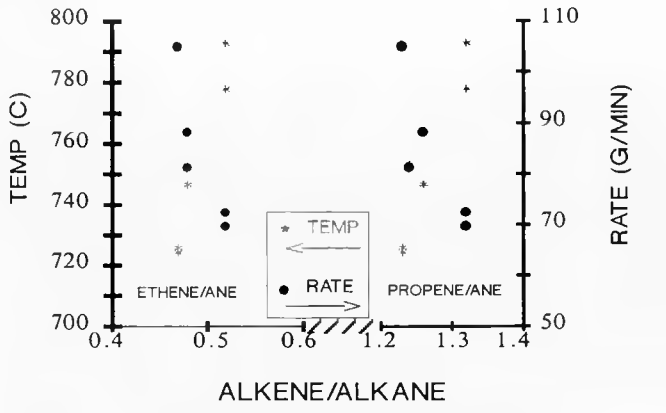

Figure 7. Alkene/alkane ratios for Constant load runs.

against both temperature and rate for the constant load runs only. Both ene/ane ratios increase with higher recycle temperatures indicating that for a given heat demand, the use of higher recycle solids temperature induces more extensive product cracking relative to a higher recycle rate. This conclusion is supported somewhat by a weak correlation between the amount raw shale carbon which partitions to gaseous hydrocarbons when higher recycle temperatures are used relative to higher rates (Table 1). However, this additional gas production is insufficient to account for the incremental oil loss measured with higher recycle temperatures relative to higher rates.

What then accounts for the lower oil yield and higher oil aromaticity observed for the constant load runs when higher recycle temperatures were used? What may be the critical factor in explaining these parameters is the fact that a significant portion of the product distribution from cracking of aliphatics are one ring aromatics.[7,8] Thus, if higher recycle temperatures do in fact enhance cracking relative to higher recycle rates as Figure 7 suggests, then a portion of the increased oil aromaticity for the higher temperature runs may simply reflect additional formation of these components in the gas phase. In other words, higher recycle temperatures may actually coke just as many or more of the aromatic components than higher recycle rates but this is masked because they also induce more rapid formation of these components by rearrangement of the aliphatics following cracking. Admittedly, this is a lot of conjecture from six data points, but this interpretation is congruent with the higher aromaticity, higher alkene/alkane ratios, and lower oil yields observed when higher solids temperatures were used to meet a constant heat demand.

Assuming the presence of hot recycle solids is responsible for an increase in product coking, one would also expect measurable cracking of aliphatics to be reflected by an overall reduction in average molecular weight and viscosity. This was in fact observed as shown in Figures 8 and 9 where the average molecular weight and viscosity are shown to be inversely related to recycle solids temperature and recycle rate and directly related to aromaticity. Again, these relationships were not observed in the non-recycle oils as a function of gasifier temperature (i.e., related to recycle solids temperature) indicating that it is the presence of the hot recycle solids and not variations in the gasifier products passing through the retort which account for these changes.

Though not shown, it was noted that higher feed rates correlated with lower values for both viscosity and aromaticity in the composite oil. These parameters did not correlate with gasifier temperature in the non-recycle oils. This is consistent with Figures 8 and 9 since, on an absolute basis, higher feed rates require that more particles be recycled from the gasifier to meet the additional heat demand. Thus, there were more hot, reactive particles recycled to the retort for the higher feed rate runs which is thought to account for the observed lowering of both viscosity and average molecular weight of the composite oil.

Composite oil density and H/C molar ratios are shown plotted as a function of recycle rate in Figure 10. Though the data is scattered, there appears to be a trend toward lower density and a correspondingly higher H/C ratio with increasing recycle rate. This is also

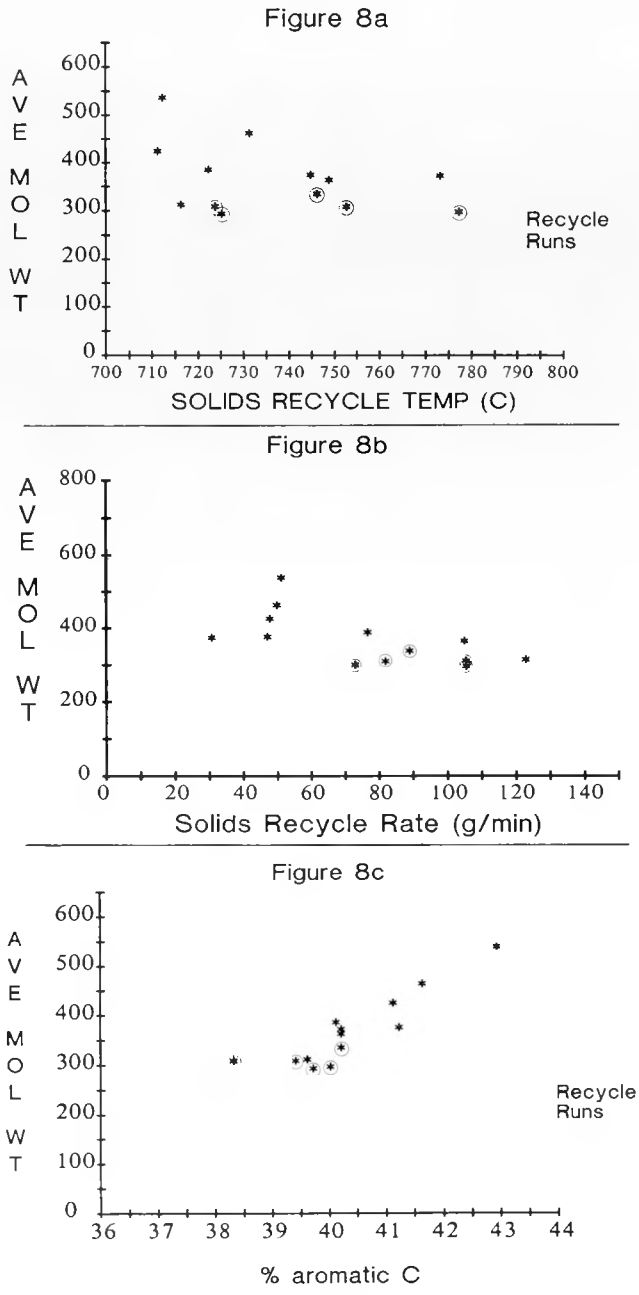

Figure 8. Average Molecular weight of composite Oils shown as a function of solids recycle temperature (top), solids recycle rate (center), and oil aromaticity (bottom). Constant load runs are shown encircled.

consistent with the proposed mechanism of preferential removal of aromatic carbon (higher H/C) accompanied by cracking of aliphatics (lower density) when hot solids are recycled to the retort and is supported by the slightly lower average density found for the light oils from solids recycle (Table 3). The light oil density was lower in spite of the fact that on average, a larger portion of the total product partitioned to the light oil fraction for the recycle runs which, all else being equal, should result in an increase in the light oil density.

A final plot of the partitioning of oil product between the ESP and light oil fractions is shown in Figure 11. Though a variety of factors influenced this partitioning, there is still a perceptible correlation between these fractions and solids recycle rate showing an increase in the production of lighter product with increasing severity. Though not shown, a plot of oil partitioning versus recycle temperature displayed similar trends.

Table 7.
Process Waters Analyses.

Run #	Ph	% Suspended Solids (x100)	Dissolved Solids (%)	% C Total	S Total (ppm)	S as H_2S (ppm)	Cr (ppm)	Mo (ppm)	As (ppm)	Cd (ppm)	Pb (ppm)	Se (ppm)	Ni (ppm)
KEN 4	8.67	0.09	0.067	0.22			<.1	<.2	<.3	0.03	<.3	1.6	<.1
KEN 5	8.63	0.03	0.110	0.27	1520	1430	<.1	<.2	<.3	0.03	<.3	1.5	<.1
KEN 6	8.59	0.10	0.079	0.26	1780	1690	<.1	<.2	<.3	0.03	<.3	1.4	<.1
KEN 7	8.73	0.09	0.107	0.28			<.1	<.2	<.3	<.01	<.3	1.0	<.1
KEN 8	6.53	0.19	0.410	0.28	3040	3030	<.1	<.2	<.3	<.01	<.3	0.9	<.1
KEN 9	8.57	0.21	0.123	0.23	2810	2790	<.1	<.2	<.3	<.01	<.3	0.9	<.1
KEN 10	8.78	0.13	0.113	0.25	2940	1880	<.1	<.2	<.3	<.01	<.3	2.8	<.1
KEN 11	8.81	0.16	0.111	0.26			<.1	<.2	<.3	<.01	<.3	2.4	<.1
KEN 16	8.73	0.21	0.144	0.29			<.1	<.2	<.3	<.01	0.7	<.3	0.23
KEN 18	8.66	0.12	0.163	0.22	1700	1500	<.1	<.2	<.3	<.01	<.4	0.9	<.1
KEN 20	7.95	0.18	0.070	0.27	1200	1000	<.1	<.2	<.3	<.01	0.5	0.5	<.1
KEN 23	8.23	0.15	0.160	0.24	1200		<.1	0.5	<.4	0.05	<.4	0.5	0.14
KEN 24	9.08	0.08	0.069	0.27	1600	1400	<.1	0.5	<.4	0.05	<.4	1.7	0.15
KEN 25	8.82	0.05	0.193	0.31	1200	1100	<.1	0.5	<.4	<.01	<.4	1.2	<.1
KEN 27	9.51	0.05	0.219	0.31	1400	1300	<.1	0.4	<.4	<.01	<.4	0.8	<.1
KEN 28	9.39	0.09	0.183	0.30	1400	1100	<.1	0.5	<.4	0.03	<.4	0.7	<.1
KEN 29	8.70	0.12	0.177	0.30	1200	1000	<.1	<.3	<.4	0.02	<.4	1.6	<.1
KEN 30	9.11	0.22	0.330	0.40	1400	1330	<.1	<.2	<.4	<.01	<.4	<.3	<.1
KEN 31	8.60	0.08	0.401	0.34	1900	1840	<.1	<.2	<.4	<.01	<.4	2.8	<.1
KEN 32	8.76	0.20	0.342	0.41	2180	2080	<.1	<.2	<.4	<.01	<.4	2.9	<.1
KEN 33	8.70	0.16	0.448	0.37	2860	2780	<.1	<.2	<.4	<.01	<.4	<.3	<.1
KEN 34	8.66	0.12	0.476	0.38	2890	2150	<.1	<.2	<.4	<.01	<.4	2.4	<.1
KEN 35	8.64	0.13	0.303	0.31	3200	1550	<.1	<.2	<.4	<.01	<.4	2.7	<.1
KEN 36	8.67	0.20	0.190	0.42	2140	1100	<.1	<.2	<.4	<.01	<.4	2.0	<.1

Run #	Fe (ppm)	Mn (ppm)	Cu (ppm)	Mg (ppm)	Na (ppm)	Ca (ppm)	V (ppm)	Zn (ppm)	Al (ppm)	K (ppm)
KEN 4	0.37	<.01	<.01				<.01	0.03	0.50	
KEN 5	0.25	<.01	<.01				<.01	0.05	0.35	
KEN 6	0.15	0.02	<.01				<.01	<.03	0.50	
KEN 7	0.14	<.01	<.01				<.01	0.02	0.31	
KEN 8	1.00	<.01	<.01				<.01	0.05	0.40	
KEN 9	0.24	0.05	<.01				<.01	0.04	0.44	
KEN 10	0.09	0.01	<.01				<.01	<.03	0.20	
KEN 11	0.12	<.01	<.01				<.01	<.05	0.06	
KEN 16	0.75	<.01	<.01	0.22	1.01	0.25	0.04	<.1	1.33	1.30
KEN 18	0.23	0.10	<.01	0.06	0.31	0.18	<.01	<.1	0.34	0.50
KEN 20	0.26	<.01	<.01	0.05	0.27	0.18	<.01	<.1	0.26	0.17
KEN 23	0.19	0.04	<.01		0.52	0.59	<.01	<.1	0.29	0.26
KEN 24	0.15	0.04	0.01		0.22	0.16	<.01	<.1	0.13	0.13
KEN 25	0.27	0.03	0.01		0.92	0.24	<.01	0.14	0.53	0.35
KEN 27	0.21	0.02	<.01		.034	0.10	<.01	<.1	0.32	0.13
KEN 28	0.34	0.02	<.01		0.54	0.25	<.01	<.1	0.24	0.10
KEN 29	0.21	<.01	0.01		0.27	0.17	<.01	<.1	0.17	0.32
KEN 30	0.14	<.01	<.01	0.07	0.88	0.31	<.1	0.27	<.01	
KEN 31	0.18	<.01	0.02	0.04	0.30	0.14	<.01	<.1	0.19	<.01
KEN 32	0.14	<.01	0.01	0.04	0.23	0.15	<.01	<.1	0.19	<.01
KEN 33	0.27	<.01	<.01	0.05	0.35	0.16	<.01	<.1	0.33	<.01
KEN 34	0.20	<.01	<.01	0.04	0.26	0.16	<.01	<.1	0.23	<.01
KEN 35	0.25	<.01	0.01	0.04	0.24	0.16	<.01	<.1	0.20	<.01
KEN 36	0.26	<.01	0.02	0.05	0.48	0.32	<.01	<.1	0.24	<.01

The data shown in Figures 8-11 have implications for optimal operation of the integrated unit in that not only does one obtain slightly higher yields when using faster recycle rates to meet a given heat demand, but at least for the properties discussed, it appears a somewhat improved product is produced as well.

Finally, it should be emphasized that the product changes being measured in this study were generally small. Comparison of the average elemental composition for the composite oils shown in Table 5 indicate the oils from recycle versus non-recycle runs to be very similar. Based on these data, it can be stated that the recirculation of gasifier solids to the retort does not have a severe impact on composite oil quality. In fact, the small changes that are observed, such as lower viscosity or higher H/C ratios, are generally an improvement which may help compensate for the small decreases in oil yield.

CONCLUSIONS

In summary, recirculation of hot gasifier solids to the retort results in an increase in both cracking and coking reactions.

Figure 9a

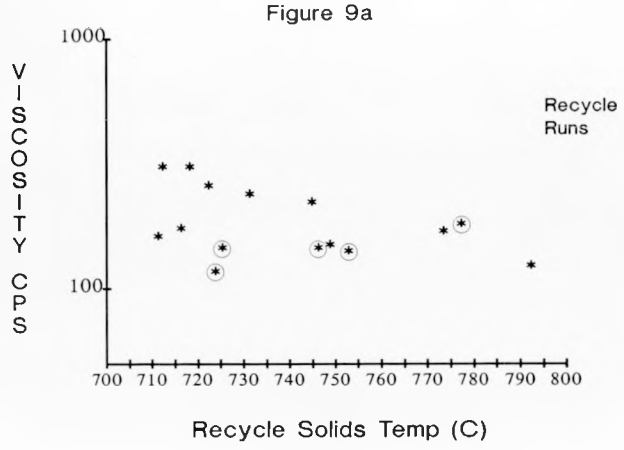

Figure 9b

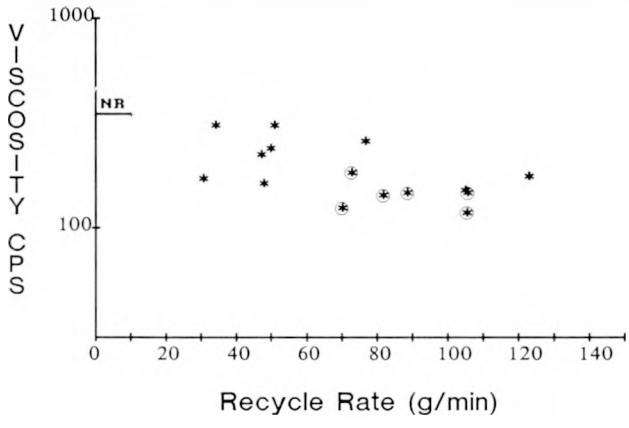

Figure 9c

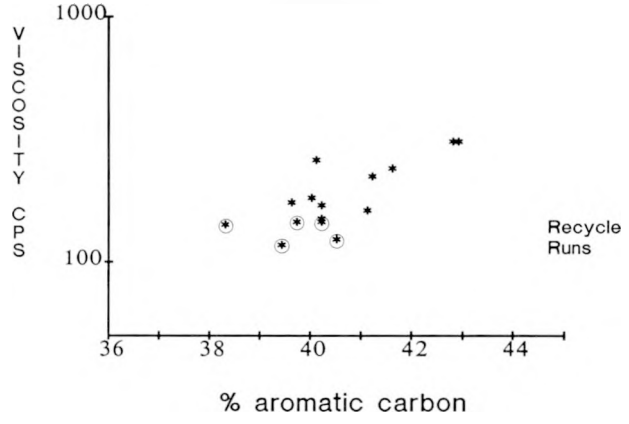

Figure 9. Composite Oil Viscosity plotted as a function of Solids Recycle Temperature (top), Recycle rate (center), and composite oil aromaticity (bottom). Constant load runs are shown encircled.

Aromatics are selectively destroyed by the recycle solids via coking reactions. When solids recycle temperature and recycle rate are inversely varied to provide a constant amount of heat to the pyrolyzer, it appears that higher recycle solids temperatures induce more extensive product cracking leading to enhanced production of aromatics which results in greater oil coking losses. Finally, though oil yields decrease under the more severe recycle conditions, product quality does show some improvement as reflected by lower viscosity and average molecular weight, and higher H/C molar ratios.

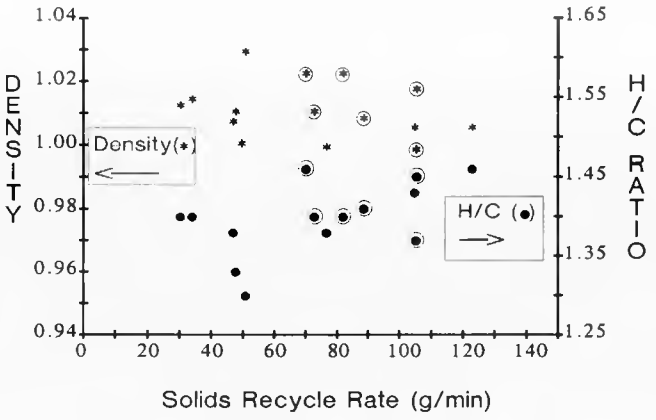

Figure 10. Composite oil density (*) and H/C ratio (o) as a function of solids recycle rate. Constant load runs are shown encircled.

ACKNOWLEDGEMENT

The authors would like to acknowledge the analytical support of a number of individuals including G. Thomas, M. Moore, R. Keogh, J. Hosman, T. Strehl, G. Simpson, C. Dungan, V. Triantafylakkis, and A. Carter. This work was conducted at the Center for Applied Energy Research with funding provided by the Univ. of Ky. and USDoE under Cooperative Agreement No. DE-FC21-86LC11086.

BIBLIOGRAPHY

1. "The KENTORT II Concept: A Process Description", S.D. Carter, *Proceedings: 1987 Eastern Oil Shale Symposium*, Lexington, Ky., Nov. 18-20, 1987, Published by Ky. Ener. Cab. Lab., KECL87-175, Mar., 1988, 271-76.

2. Carter, S.D., D.N.Taulbee, A.M. Rubel, R.T. Abner, "Operation of the KENTORT II Process as an Integrated Pyrolyzer/-Gasifier", *Proceedings: 1988 Eastern Oil Shale Symposium*, Lexington, Ky., Nov. 30-Dec. 2, 1987, Published by Inst. Mining and Min. Res.,IMMR88/101, May, 1989, 27333-340.

3. Carter, S. D., and D. N. Taulbee, "Operation if the 5-lb/hr KENTORT II Reactor in the Solid Recirculation Mode", presented at the 1989 Eastern Oil Shale Symposium, Marriott Griffin Gate Resort, Lexington, Ky., Nov. 15-17, 1989, awaiting publication.

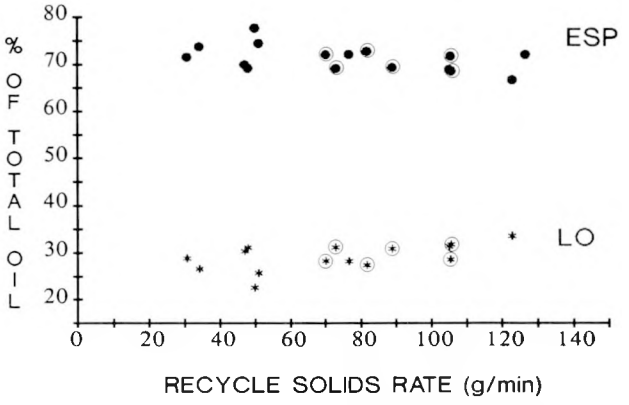

Figure 11. Relative production of light oil (*) and ESP oil (o) as a function of solids recycle rate. Constant load runs are shown encircled.

4. *Research to Improve Process Efficiency, Process Economics, and / or Resolve Environmental Problems Involved in the Utilization of Oil Shale as an Energy Source. Volume I: Technical Proposal.* proposal submitted in Response to PRDA DE-RA20-86LC11070, awarded under Cooperative Agreement no: DE-FC21-86LC11086 to Univ of Louisville, March 17, 1986.

5. Taulbee, D. N. and D. Kahn, "Analyses of Products from the Flash Hydropyrolysis of a Kentucky Oil Shale" *Proceedings: 1984 Eastern Oil Shale Symposium*, Lexington, Ky., Nov. 26-28, 1984, Published by Univ. of Ky. Inst. for Mining & Miner. Res., IMMR84/124, Feb. 1985, 99-116.

6. Burnham, A.K., and J.E. Clarkson, "Determination of Process Yield for Oil Shale Retorting Using Oil Analyses by Capillary Column Chromatography" *Proc. 13th Oil Shale Symp.* J.H. Gary, Ed., Col. Sch. of Mines Press, Golden, Co, 1980, 269.

7. Cypres, R., "Aromatic Hydrocarbons Formation During Coal Pyrolysis" *Fuel Proc. Tech.*, 15, 1987, p 1-15.

8. Greensfelder, B.S., H.H. Voge, G.M. Good, "Catalytic and Thermal Cracking of Pure Hydrocarbons" *Ind. Eng. Chem.*, 41, #41, 1949, p 2573-83.

POSTER SESSION

Specific Gravity-Fisher Assay Relationships Among Eastern Oil Shales

by

C.W. Schultz and J.B. Bates
Mineral Resources Institute
University of Alabama
Tuscaloosa, Alabama 35487-0204

Abstract: The specific gravities of raw oil shales and their beneficiation products were measured with a helium pycnometer. Measured specific gravities show a very high degree of correlation with the oil yield as measured by Fischer Assay and with the carbon content as determined with a LECO CHN analyzer.

The correlations were sufficiently strong to permit the use of specific gravity measurements in the control of pilot plant operations and in the evaluation of laboratory tests.

Specific gravity-oil yield relationships were developed for samples from Alabama, Indiana, Kentucky, Ohio, Michigan, and Tennessee.

Introduction

The Fischer retort was originally developed to measure the liquids generated in the low temperature carbonization of coal (1). It was subsequently adapted by the U.S. Bureau of Mines to the analysis of oil shales (2). Since that time the Fischer assay has become the standard method by which oil shale resources are evaluated.

Unfortunately the Fischer assay, while accurate and reproducible, is time consuming and labor intensive to perform. The generation of large quantity of oil shale samples places a burden on any analytical laboratory. To reduce this burden, the Mineral Resources Institute investigated the relationship between the density of oil shales and the Fischer assay. The objective of the investigation was to establish a rapid, low cost means of evaluating oil shales and oil shale products.

Sample Materials

Six oil shales were included in this investigation. The samples were from the states of Alabama, Indiana, Kentucky, Michigan, Ohio and Tennessee.

The Alabama and Tennessee samples were from the Chattanooga shale formation. Both samples were collected from field sites by MRI personnel. The Alabama sample was taken from a site on Hester Creek in Sec. 18 T 15 R2E of Madison County, Alabama. The Tennessee sample was taken from a site west of Nashville on Interstate 40 at mile marker 192.

The Michigan, Ohio, and Kentucky samples were procured from quarry operators in the respective states. The Michigan sample was from the Antrim formation and was supplied by the Paxton Quarry located at Sec. 30 T31N R7E, Alpena County, Michigan.

The Ohio shale, from the Cleveland formation, was supplied by the GID-CO Quarry located at Galena, Ohio in Delaware County. Skaggs Quarry supplied the Kentucky, New Albany formation shale from its site in Bullit County, Kentucky.

The Indiana sample, from the New Albany formation, was obtained from Terra Tek, Inc. The source of the sample was Lot 257, Clark Military Grant R1N T7E, Clark County, Indiana.

TABLE 1. STATISTICAL ANALYSIS OF DENSITY - FISCHER ASSAY OIL YIELD FOR ALABAMA OIL SHALE

GENERAL LINEAR MODELS PROCEDURE

DEPENDENT VARIABLE: OIL "FISCHER ASSAY OIL YIELD"

SOURCE	DF	SUM OF SQUARES	MEAN SQUARE
MODEL	2	4075.85948640	2037.92974320
ERROR	22	31.96211360	1.45282335
CORRECTED TOTAL	24	4107.82160000	

MODEL F = 1402.74 PR > F = 0.0001

R-SQUARE	C.V.	ROOT MSE	OIL MEAN
0.992219	9.4491	1.20533122	12.75600000

SOURCE	DF	TYPE I SS	F VALUE	PR > F
DEN	1	3844.01286958	2645.89	0.0001
DEN*DEN	1	231.84661682	159.58	0.0001

SOURCE	DF	TYPE III SS	F VALUE	PR > F
DEN	1	365.81992138	251.80	0.0001
DEN*DEN	1	231.84661682	159.58	0.0001

PARAMETER	ESTIMATE	T FOR H0: PARAMETER=0	PR > |T|	STD ERROR OF ESTIMATE
INTERCEPT	211.76433432	20.56	0.0001	10.29787654
DEN	-146.04307892	-15.87	0.0001	9.20351468
DEN*DEN	25.25753376	12.63	0.0001	1.99938747

All of the foregoing samples were used in research efforts to develop a beneficiation system for eastern oil shales. In the course of beneficiation tests enriched products, (concentrates) and depleted products (tailings) were formed. These beneficiation test products along with the crude shales provided the range of oil shale compositions on which the correlations between specific gravity and oil yield are based.

Experimental Procedures

Each beneficiation test product, (e.g. from column flotation tests) was filtered, dried and mixed thoroughly. A sample was taken from the product and its density measured with a Micromeritics Helium Pycnometer. Five replicate measurements were made on each sample.

After measurement of the specific gravity the sample was remixed with the beneficiation product and sent to the analytical laboratory for Fischer assay and for carbon analysis.

Fischer assays were performed by the standard ASTM procedure. Carbon analyses were performed with a LECO, CHN 600 Analyzer.

Statistical Analysis

A statistical analysis was performed on the data generated from each oil shale. The analysis was performed using the "General Linear Models" procedure of the Statistical Analysis System (SAS) software package. The analyses consists of an analysis of variance, an "F" test and a "T" test. The model tested in all cases was of the general form

$$Y = A + BX + CX^2 \qquad \text{Eq } 1$$

or

$$Z = A' + B'X + C'X^2 \qquad \text{Eq } 2$$

where

Y = Fischer assay oil yield (gal/ton)
Z = Carbon content (percent)
X = Density (gms/cc)

A typical statistical analysis, in standard notation, is presented in table 1. Note in this case (Alabama) the value of R square is 0.992219. R square is the ratio of the model sum of squares to the total sum of squares. Thus in this instance 99.22 percent of the total variance is accounted for by the model equation. Values of R square for each of the models are presented in table 2.

Table 2

Shale	R Square	
	Fischer Assay	Carbon
Alabama	0.992219	0.997486
Indiana	0.995151	0.997619
Kentucky	0.991842	0.999626
Michigan	0.995938	0.998816
Ohio	0.995911	0.995365
Tennessee	0.995306	0.983120
All Samples	0.973582	0.989102

Results

The model equations resulting from the statistical analyses of experimental measurement of density, Fischer assay oil yield and carbon content are presented in table 3. The same data for the Alabama shale are presented graphically in figures 1 and 2. Similar relationships for the other oil shales are presented in figures 3 through 14.

Table 3

Predictive Equations for the Fischer Assay Oil Yield and Carbon Content of Eastern Oil Shales

Shale	Model Equations
Alabama	Oil (gal/ton) = 211.764 - 146.043d + 25.258d^2 Carbon (%) = 191.730 - 119.315d + 18.653d^2
Indiana	Oil (gal/ton) = 255.909 - 174.181d + 29.912d^2 Carbon (%) = 187.251 - 118.769d + 18.841d^2
Kentucky	Oil (gal/ton) = 231.371 - 154.479d + 25.761d^2 Carbon (%) = 192.341 - 123.811d + 20.089d^2
Michigan	Oil (gal/ton) = 254.833 - 167.185d + 27.246d^2 Carbon (%) = 182.078 - 113.264d + 17.517d^2
Ohio	Oil (gal/ton) = 319.562 - 231.060d + 41.893d^2 Carbon (%) = 215.564 - 144.220d + 24.374 d^2
Tennessee	Oil (gal/ton) = 205.632 - 135.460d + 22.211d^2 Carbon (%) = 161.308 - 92.207d + 12.736d^2
All Samples	Oil (gal/ton) = 250.307 - 172.991d + 29.941d^2 Carbon (%) = 191.764 - 121.613d + 19.349d^2

Conclusions

Density measurements provide a rapid and accurate method of estimating the Fischer assay oil yield and carbon content of eastern oil shales. Since developing the first models it has been the practice of the Mineral Resources Institute to analyze all beneficiation test products by density measurements. Analysis of test products and material balances presented elsewhere in the symposium are based on density measurements.

Unlike the work of Smith (3) the data presented here are purely empirical and can be said to represent only the specific sample sites. The combined data shows, as might be expected, a higher error than does the data for any individual shale. The data does however indicate an apparently high degree of uniformity in the mineral matter and the kerogen among the various shale formations.

Prospective users of the relationships presented here are further cautioned that the data apply only to raw shales and physically beneficiated products of those shales. It is not expected that the data would apply to thermally or chemically treated materials.

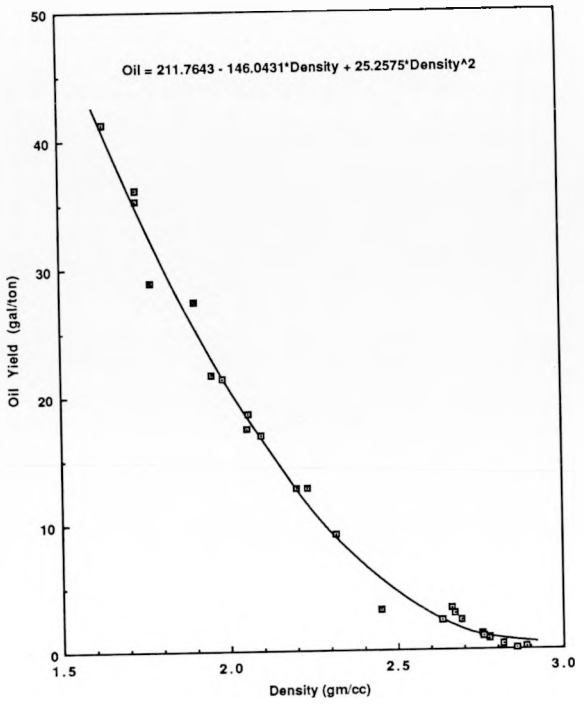

Figure 1. Relationship Between Density and Fischer Assay Oil Yield Alabama (Chattanooga) Shale

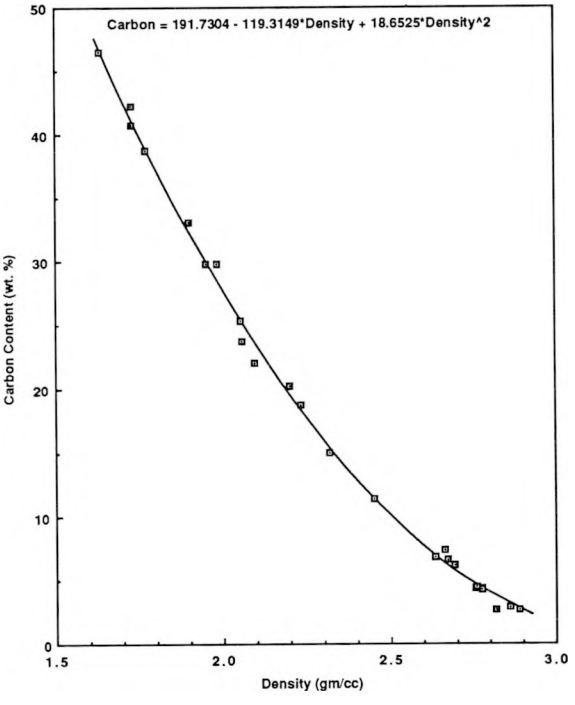

Figure 2. Relationship Between Density and Carbon Content Alabama (Chattanooga) Shale

References

(1) Fischer, Franz and Schrader, Hans, Urteerbestimingen mit einem Alumin schwelapparat: Ztschr. angew Chem. vol 33, 1920 pp 172 - 175

(2) Stanfield, K.E., and I.C. Frost, Method of Assaying Oil Shale by a Modified Fischer Retort. U. S. Bureau of Mines Report of Investigations 4477, 1949

(3) Smith, John Ward, Relationship Between Rock Density and Volume of Organic Matter in Oil Shales. LERC Report of Investigation 76/6 Sept. 1976. Technical Information Center, Energy Research and Development Administration.

Acknowledgements

The authors are indebted to the Institute of Gas Technology and the Department of Energy for their financial support of this project.

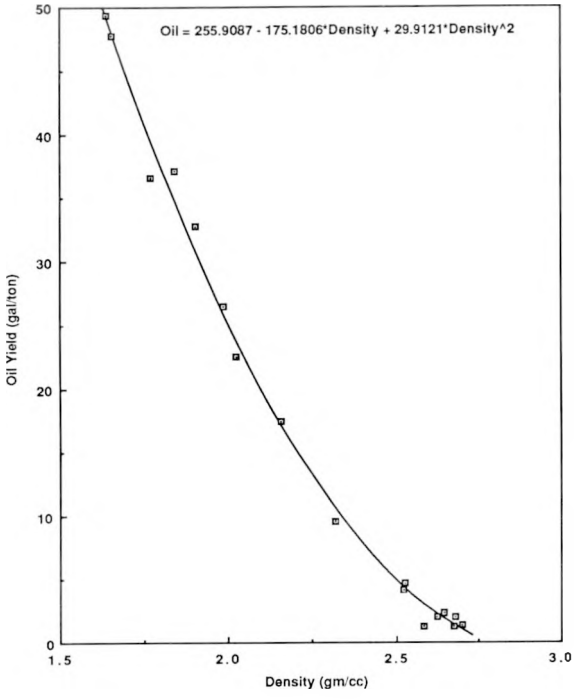

Figure 3. Relationship Between Density and Fischer Assay Oil Yield Indiana (New Albany) Shale

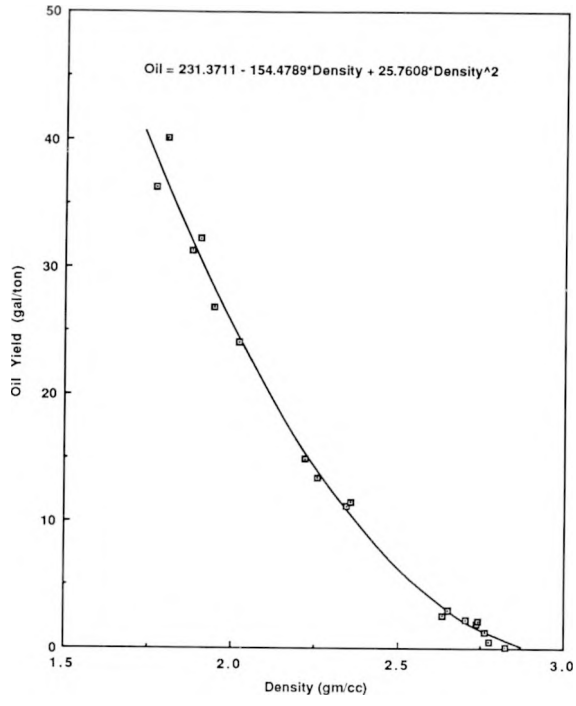

Figure 5. Relationship Between Density and Fischer Assay Oil Yield Kentucky (New Albany) Shale

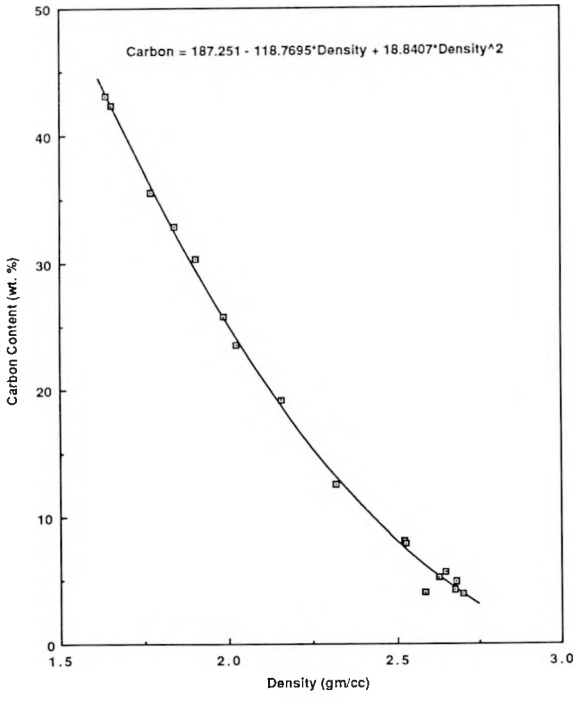

Figure 4. Relationship Between Density and Carbon Content Indiana (New Albany) Shale

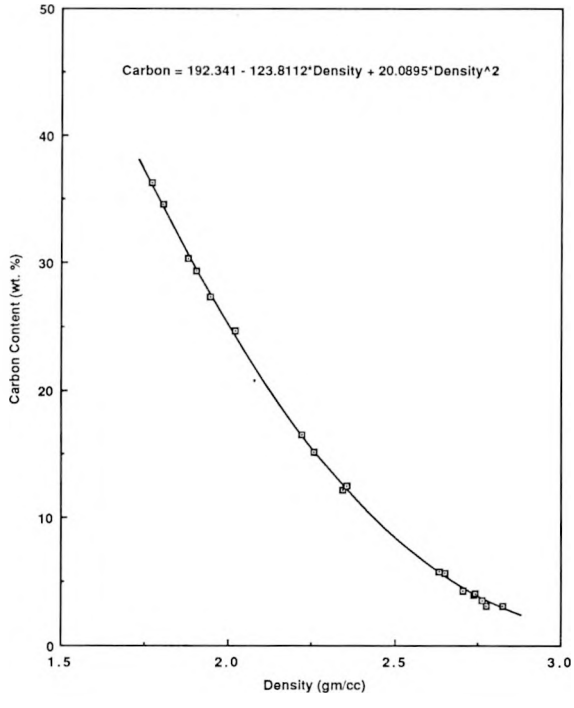

Figure 6. Relationship Between Density and Carbon Content Kentucky (New Albany) Shale

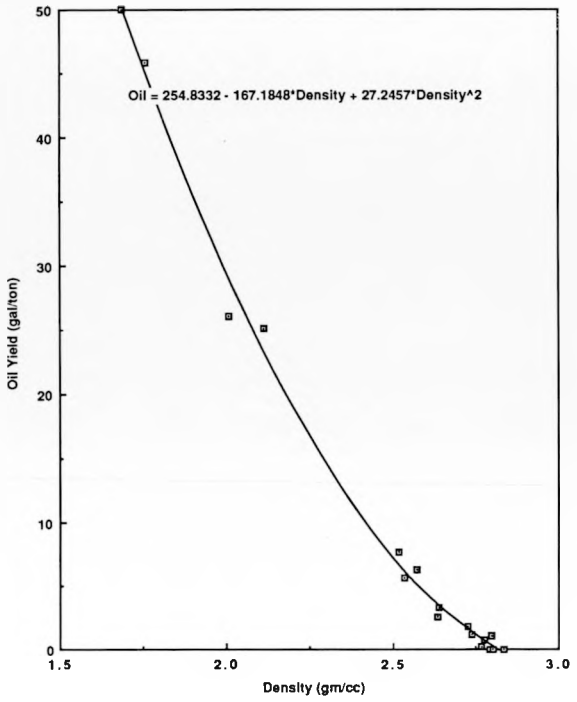

Figure 7. Relationship Between Density and Fischer Assay Oil Yield Michigan (Antrim) Shale

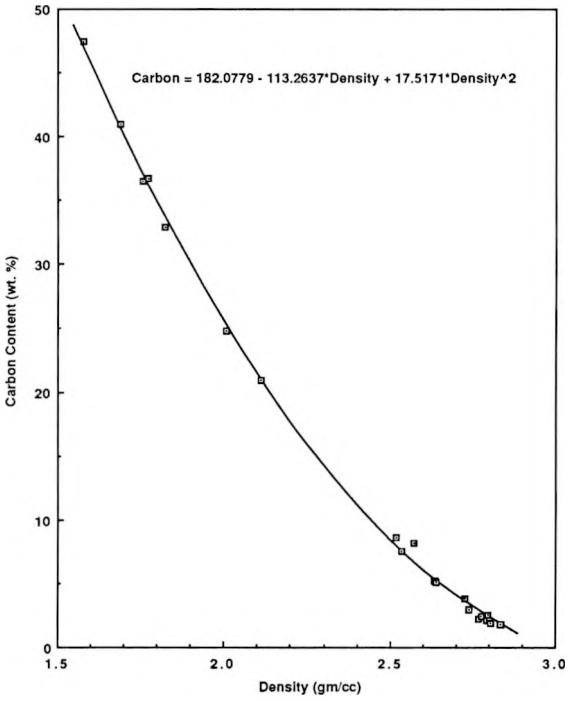

Figure 8. Relationship Between Density and Carbon Content Michigan (Antrim) Shale

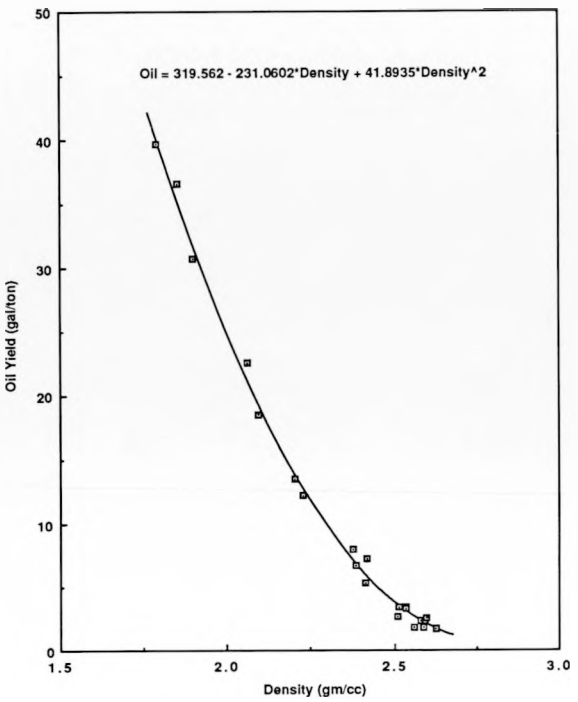

Figure 9. Relationship Between Density and Fischer Assay Oil Yield Ohio (Cleveland) Shale

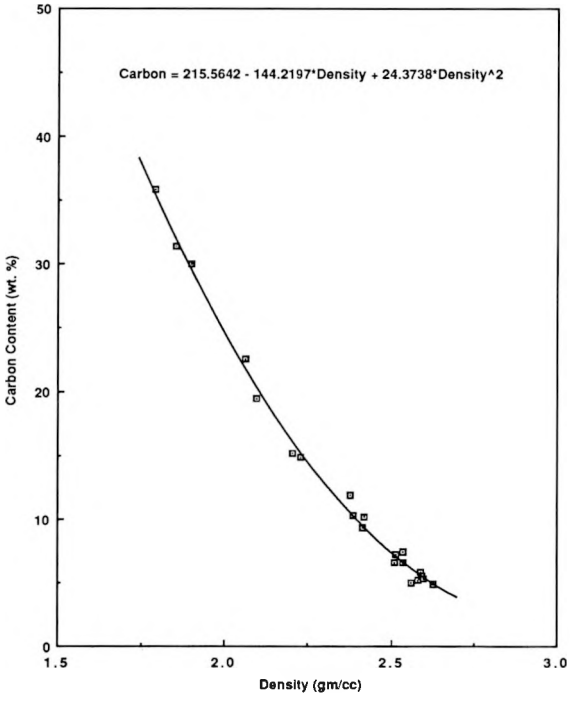

Figure 10. Relationship Between Density and Carbon Content Ohio (Cleveland) Shale

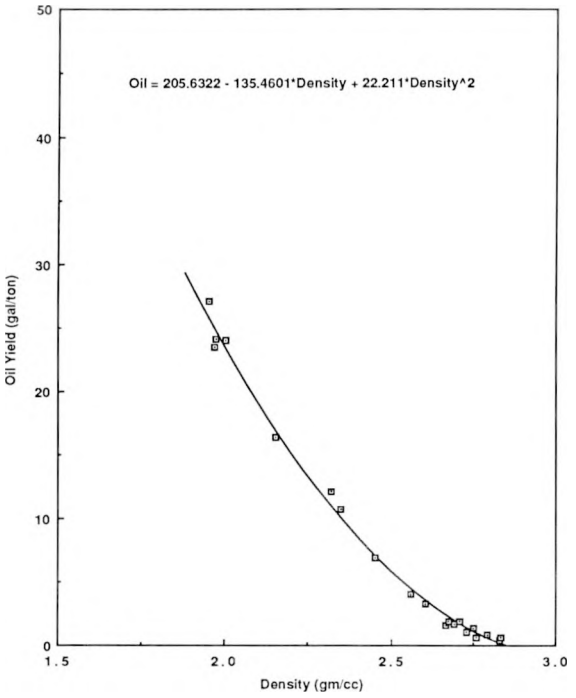

Figure 11. Relationship Between Density and Fischer Assay Oil Yield Tennessee (Chattanooga) Shale

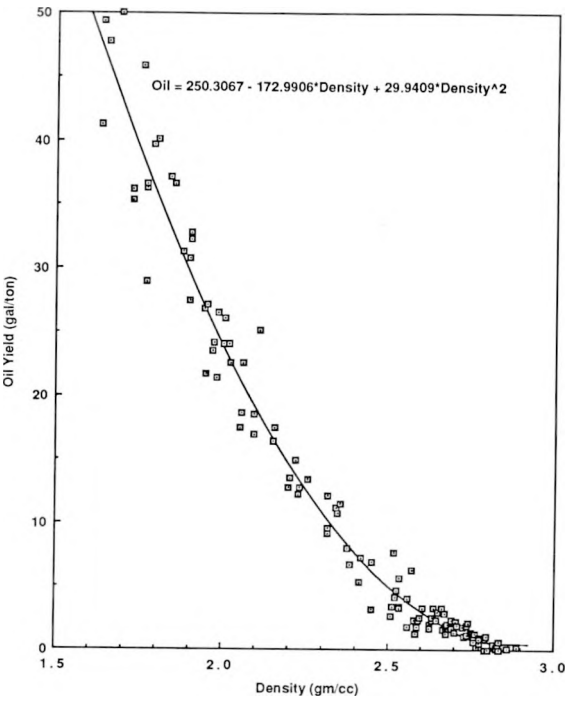

Figure 13. Relationship Between Density and Fischer Assay Oil Yield Eastern Oil Shales (All Samples)

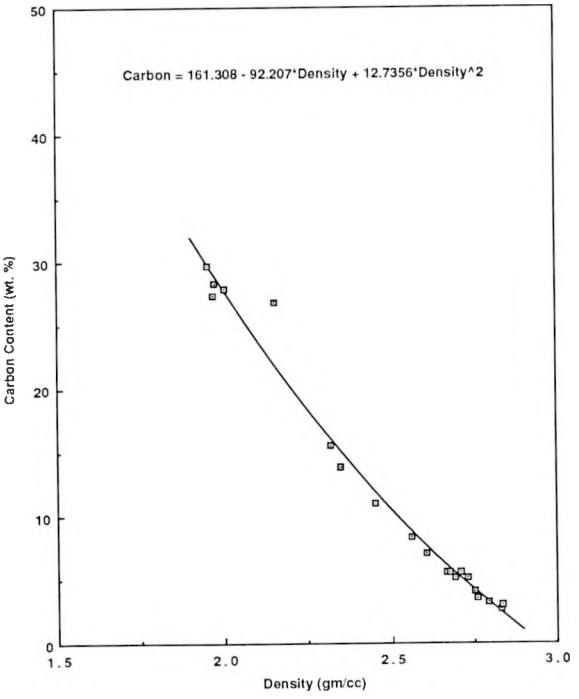

Figure 12. Relationship Between Density and Carbon Content Tennessee (Chattanooga) Shale

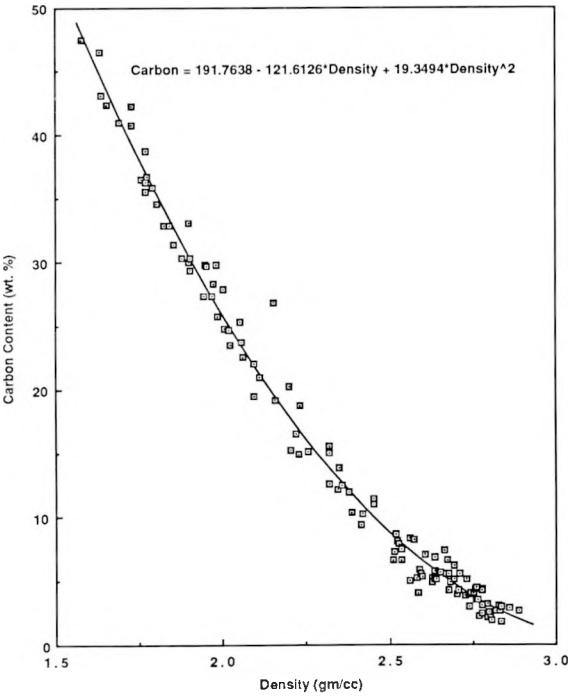

Figure 14. Relationship Between Density and Carbon Content Eastern Oil Shales (All Samples)

Relationship of New Albany Shale (Devonian-Mississippian) and Rockford Limestones (Mississippian to Silurian) in Greene County, Indiana

by

Nancy R. Hasenmueller
Indiana Geological Survey
Bloomington, Indiana 47405

Abstract

The structure on top of the carbonate rocks of the Muscatatuck Group (Middle Devonian) indicates two small isolated Silurian pinnacle-type reefs, the Dixon Reef and the Lyons West Reef, and one larger coalesced reef, the Switz City Reef in Greene County. The localized thinning of the New Albany Shale (Devonian-Mississippian) above these buried reefs indicates that the reefs affected younger overlying stratigraphic units.

On the crests of the three reef-associated structures the New Albany thins by as much as 25 feet, and the Rockford Limestone (Mississippian) is absent in most places. Where the Rockford is absent the New Providence Shale of the Borden Group (Middle Mississippian) directly overlies the New Albany Shale. The change in thickness of the New Albany over reef structures is significant and is probably the result of thinning in two ways: (1) loss distributed throughout the entire shale interval may be the result of differential sedimentation and (or) subaqueous erosion of New Albany sediments above the buried reefs, and (2) loss largely confined to the uppermost part of the formation may be the result of subaqueous erosion of the shale during post-Rockford and pre-New Providence (Mississippian) time. The absence of the Rockford above the reef-associated structures may also have been caused by post-Rockford and pre-New Providence erosion.

The continued growth of reef-induced drape structure during a period of extremely slow sedimentation, which existed during the Late Devonian and Early Mississippian, could have resulted in topographic expression on the sea floor above the buried reefs. Differential sedimentation over these topographic highs could have caused variations in the thicknesses of sediments deposited during New Albany time. Scouring of the topographic highs by currents during Middle Mississippian time could have resulted in subaqueous erosion of lithologic units on the crests and caused the unconformity between the New Albany and New Providence over the reef structures.

1989 Eastern Oil Shale Symposium November 15-17, 1989 Institute for Mining and Minerals Research, University of Kentucky

Laboratory Furnace Design for Programmed Temperature Pyrolysis of Fossil Fuels

by

Kenneth G. Foster, Eugene J. Frohwien, Robert W. Taylor and David W. Bowen
Lawrence Livermore National Loaboratory
University of California
Livermore, California 94550

ABSTRACT

For the last several years at Lawrence Livermore National Laboratory, we have been looking for a laboratory furnace for programmed-temperature pyrolysis of fossil fuels. Not completely satisfied with those found in the commercial market, we have taken many ideas and requirements to develop a furnace for laboratory use.

The furnace must have the following features: (1) It must be reliable and safe to use. (2) It must have insulation which gives a good linear temperature profile (uniform vertical heating) and quick cool down. It also has to be asbestos-free. (3) It must be able to be mounted both horizontally and vertically. (4) It must have modest energy requirements so that it can be used with various controllers.

We developed a vermiculite-insulated tube furnace heated by helically wound resistance wire positioned within helical grooves on the surface of a ceramic cylinder. This in turn surrounds a doubly slotted stainless steel cylindrical liner. For uniform heating, the pitch of the helix is shorter over the two end portions of the ceramic cylinder. The furnace can be designed to accommodate either large- or small- diameter reactors. It provides uniform temperature, offers an extremely precise programmed heating capability, features rapid cool-down, and has modest power requirements.

Now in the final stages of development, the prototype meets the criteria above. We are obtaining uniform temperature profiles and believe it is a good design.

Characterization of Particulates in Oil Sands Processing Streams

by

R.J. Mikula, W.W. Lam, and V.A. V.A. Munoz
Department of Energy, Mines and Resources, CANMET
Devon, Alberta CANADA T0C 1E0

ABSTRACT

The Clark hot water process is used in the industrial extraction of bitumen from Alberta oil sands. The goal of the extraction process is to remove bitumen from the solids and water of the oil sands, which becomes feed in the upgrading processes to produce synthetic crude oil. Characterization of solids at various conversion stages is critical to the efficient operation of the downstream processes. For example, it has been shown that high proportions of fine clays contribute to poor initial extraction of bitumen from the oil sands. Further downstream, the presence of particulates above a certain size range might indicate failure of a fine mesh screen in a unit process, or the source of particulates in a certain recycle or feed stream.

The combination of scanning electron and optical microscopy, and image analysis has been utilized to determine both the nature and size distribution of oil sands particulates. Electron and optical microscopy are complimentary techniques in that the former is most useful in determining the chemical composition of mineral components, and the latter is used for the determination of coke and other organic solids.

Microscopic Techniques for Identification of Coke

by

V.A. Munoz, R.J. Mikula, and W.W. Lam
Department of Energy, Mines and Resources, CANMET
Devon, Alberta CANADA T0C 1E0

ABSTRACT

In the production of synthetic crude oil from oil sands, bitumen and heavy oils, the goal is to maximize production of liquid fuels and to minimize production of carbonaceous solids and gases. Coke formation is an undesirable result of catalytic cracking. Aside from reducing potential liquid yields, the deposition of coke can produce problems such as fouling of catalysts and a decrease in the heat transfer capacity of reactors, possibly leading to complete failure of the conversion system. The identification of coke, organic and inorganic solids suspended in process streams is therefore of importance as a monitoring tool.

Electron microscopy is used mainly for the characterization of mineral components. The unequivocal determination of organic phases such as cokes, semicokes and heavy oils is acheived by optical microscopy using both white and blue light. The fluorescence characteristics in certain organic components allows their discrimination from coke and inorganic solids, which do not exhibit fluorescence under blue light. In turn, coke particles can be distinguished from inorganic solids using polarized and cross-polarized light, and by other optical parameters such as reflectance, color, isotropy or anisotropy.

Application of Synchrotron Radiation for Analysis of Oil Shale and Shale Derived Products

by

Muthu S. Sundaram
Brookhaven National Laboratory
Upton, L.I., New York 11973
Lawrence J. Shadle
U.S. Department of Energy
Morgantown Energy Technology Center
Morgantown, West Virginia 26507

ABSTRACT

Exended x-ray absorption fine structure (EXAFS) spectroscopy, in combination with x-ray absorption near edge structure (XANES) analysis, is an advanced analytical technique for investigation of the molecular structure of the materials and is ideally suitable for studying the oil shale chemistry. Some advantages of EXAFS are that is is (1) atom specific, (2) insensitive to long-range disorder and (3) a bulk technique. From XANES, one can obtain the electronic oxidation state of the absorber and detect mixed valence states. By comparison with standards and via computer simulation and curve-fitting techniques, one can determine the actual bond length, type and number of neighboring atoms and other important data.

A Kentucky oil shale and its pyrolysis products, which included the spent shale, heavy oil and light oil fractions, were analyzed at beam line X-19A at the National Synchrotron Light Source (NSLS). In order to compare the absorption features of various iron compounds in these samples, iron K-edge XANES/EXAFS spectra were recorded in the fluorescence mode. The iron K-edge spectra of the oil fractions were similar to each other and the spent shale contained much larger quantities of iron bearing components. The oxidation state of iron in the spent shale was characteristically different from that of the oil products. Furthermore, an independent synchrotron-radiation induced x-ray emission (SRIXE) analysis of the products showed the light oil fraction to contain significant quantities of As, Ni and Fe compounds. The trace element distribution in the spent shale was similar to that of the original shale and certain elements such as Ti, Mn, Cu and Zn tend to concentrate on the spent shale. The implications of these findings on oil shale processing will be presented.